

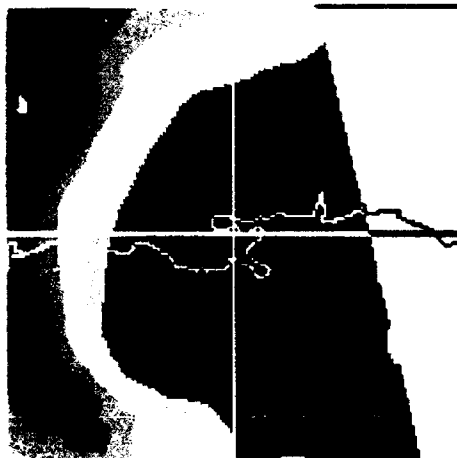
AD-A265 817



# DMSP F11 SSM/T-2 Calibration and Validation



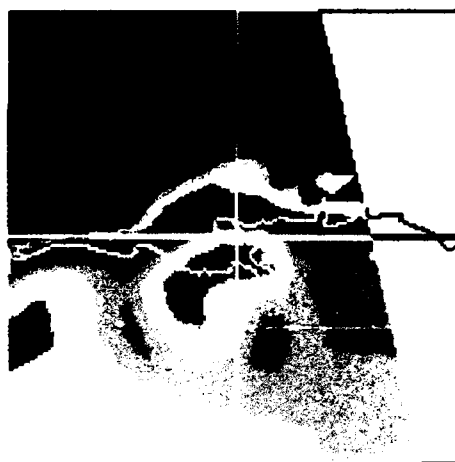
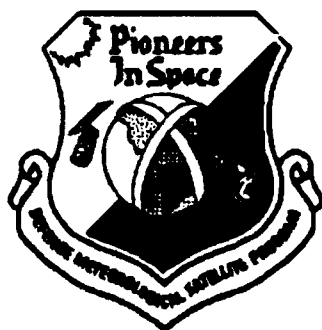
## Hurricane Andrew



SSM/T-2 183 GHz



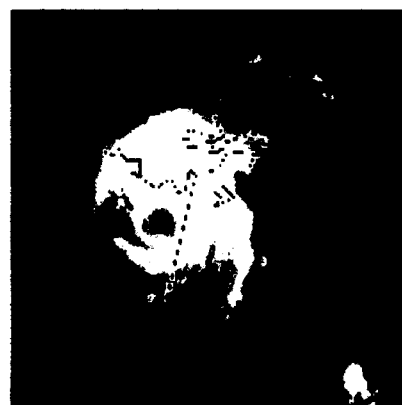
SSM/T-2 150 GHz



SSM/T-2 91 GHz



OLS Visible



OLS Infrared

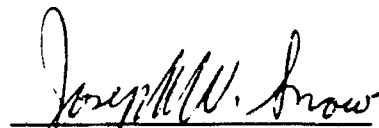
93 6 14 020

STRATEGY STATEMENT  
Approved for public release  
Distribution Unlimited

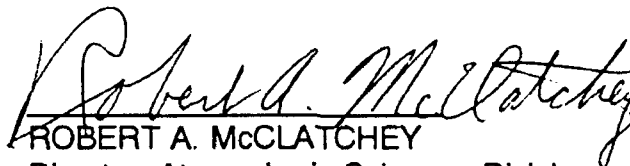
93-13194



This technical report has been reviewed and is approved for publication.



JOSEPH W. SNOW  
Chief, Satellite Meteorology Branch  
Atmospheric Sciences Division



ROBERT A. McCLATCHEY  
Director, Atmospheric Sciences Division

This report has been reviewed by the ESC Public Affairs Office (PA) and is releasable to the National Technical Information Service (NTIS).

Qualified requestors may obtain additional copies from the Defense Technical Information Center. All others should apply to the National Technical Information Service.

If your address has changed, or if you wish to be removed from the mailing list, or if the addressee is no longer employed by your organization, please notify PL/TSI, Hanscom AFB, MA 01731-5000. This will assist us in maintaining a current mailing list.

Do not return copies of this report unless contractual obligations or notices on a specific document requires that it be returned.

**PL-TR-92-2293**

**Environmental Research Papers, No. 1111**

## **SSM/T-2 CALIBRATION AND VALIDATION DATA ANALYSIS**

**V. J. Falcone  
M. K. Griffin  
R. G. Isaacs  
J. D. Pickle  
J. F. Morrissey  
A. J. Jackson  
A. Bussey**

**R. Kakar  
J. Wang  
P. Racette  
D. J. Boucher  
B. H. Thomas  
A. M. Kishi**

**29 October 1992**

**DTIC QUALITY INSPECTED 2**

Accession For	
NTIS CRA&I	<input checked="checked" type="checkbox"/>
DTIC TAB	<input type="checkbox"/>
Unannounced	<input type="checkbox"/>
Justification	
By	
Distribution /	
Availability Codes	
Dist	Avail and/or Special
<b>A-1</b>	

**APPROVED FOR PUBLIC RELEASE; DISTRIBUTION UNLIMITED**



**PHILLIPS LABORATORY  
Directorate of Geophysics  
AIR FORCE MATERIEL COMMAND  
HANSCOM AIR FORCE BASE, MA 01731-5000**

REPORT DOCUMENTATION PAGE			Form Approved OMB No 0704-0188	
Public reporting burden for this collection of information is estimated to average 1 hour per response, including the time for reviewing instructions, searching existing data sources, gathering and maintaining the data needed, and completing and reviewing the collection of information. Send comments regarding this burden estimate or any other aspect of this collection of information, including suggestions for reducing this burden, to Washington Headquarters Services, Directorate for Information Operations and Reports, 1215 Jefferson Davis Highway, Suite 1204, Arlington, VA 22202-4302, and to the Office of Management and Budget, Paperwork Reduction Project (0704-0188), Washington, DC 20503.				
1. AGENCY USE ONLY (Leave blank)	2. REPORT DATE 29 October 1992	3. REPORT TYPE AND DATES COVERED Final Report JAN 92 - NOV 92		
4. TITLE AND SUBTITLE SSM/T-2 Calibration and Validation Data Analysis		5. FUNDING NUMBERS PE: 35160F PR 6670 TA GR WU 88		
6. AUTHOR(S) V. J. Falcone, M. K. Griffin, R. G. Isaacs <sup>1</sup> , J. D. Pickle <sup>1</sup> , J. F. Morrissey, A. J. Jackson, A. Bussey, R. Kakar <sup>2</sup> , J. Wang <sup>3</sup> , P. Racette <sup>3</sup> , D. J. Boucher <sup>4</sup> , B. H. Thomas <sup>4</sup> , A. M. Kishi <sup>4</sup>				
7. PERFORMING ORGANIZATION NAME(S) AND ADDRESS(ES) Phillips Laboratory (GPAS) Hanscom Air Force Base, MA 01731-5000		8. PERFORMING ORGANIZATION REPORT NUMBER PL-TR-92-2293 ERP, No. 1111		
9. SPONSORING / MONITORING AGENCY NAME(S) AND ADDRESS(ES) SMC/CI Los Angeles AFB, CA 90009		10. SPONSORING / MONITORING AGENCY REPORT NUMBER		
11. SUPPLEMENTARY NOTES <sup>1</sup> AER, 840 Memorial Drive, Cambridge, MA 02139; <sup>2</sup> NASA Hq, 300 E St, S.W., Washington, DC; <sup>3</sup> NASA Goddard Space Flight Center, Greenbelt, MD 20771; <sup>4</sup> The Aerospace Corp, Defense Meteorological Satellite Program, El Segundo, CA				
12a. DISTRIBUTION / AVAILABILITY STATEMENT Approved for public release; distribution unlimited.		12b. DISTRIBUTION CODE		
13. ABSTRACT (Maximum 200 words) The Phillips Laboratory (PL/GPAS) is the principal investigator for the calibration and validation of the Defense Meteorological Satellite Program (DMSP) Special Sensor Microwave Water Vapor Sounder (SSM/T-2). The objective of the effort is to obtain simultaneous independent measurements of microwave radiance, water vapor mass, specific humidity and relative humidity to quantitatively measure the performance of the instrument (calibration) and to validate the ability of the SSM/T-2 to measure the water vapor parameters, i.e. the environmental data records (EDRs) of Air Force Global Weather Central (AFGWC).  Analysis of Satellite and aircraft data for calibration using both underflights and radiative transfer calculation show that the SSM/T-2 is performing within or exceeds the original contract specifications (1K). The SSM/T-2 retrieved vertical moisture profiles (EDRs) are performing within the contract specification of $\pm 30$ RH when compared with collocated radiosonde data except over certain ocean atmospheres.				
14. SUBJECT TERMS microwave, 183 Ghz, retrieval, water vapor profiler, calibration			15. NUMBER OF PAGES 432	
			16. PRICE CODE	
17. SECURITY CLASSIFICATION OF REPORT Unclassified	18. SECURITY CLASSIFICATION OF THIS PAGE Unclassified	19. SECURITY CLASSIFICATION OF ABSTRACT Unclassified	20. LIMITATION OF ABSTRACT SAR	



## TABLE OF CONTENTS

	<u>Page</u>
1. Executive Summary .....	1
1.1 Introduction .....	1
1.2 SSM/T-2 Instrument Calibration .....	5
1.3 Retrieval Algorithm Validation .....	9
1.4 Conclusions and Recommendations .....	12
2. SSM/T-2 Instrument Calibration .....	15
2.1 Introduction .....	15
2.2 SSM/T-2 Instrument .....	16
2.2.1 Instrument Sensitivity .....	21
2.2.2 Instrument Stability .....	22
2.3 MIR Instrument .....	23
2.4 Description of Aircraft Campaigns .....	27
2.4.1 West Coast Aircraft Campaign .....	27
2.4.2 East Coast Aircraft Campaign .....	34
2.5 SSM/T-2 to MIR Co-locations .....	44
2.6 Comparison of SSM/T-2 and MIR Data .....	45
2.6.1 SSM/T-2 / MIR Comparisons Stratified by Topographic Background .....	45
2.6.2 SSM/T-2 / MIR Comparisons as a Function of Scan Angle and Direction .....	55
2.6.3 Variation of MIR Within Each Co-located SSM/T-2 FOV .....	65
2.6.4 SSM/T-2 / MIR Comparisons as a Function of Time Difference .....	68
2.7 Calibration of the SSM/T-2 using Radiative Transfer Calculations .....	70
2.7.1 Radiative Transfer Models .....	70
2.7.2 SSM/T-2 Comparison Results .....	71
3. SSM/T-2 Validation .....	88
3.1 Introduction .....	89
3.2 Ground Processing at AFGWC .....	89
3.2.1 On-Line Software: Sensor Data Record Processor (SDRP) .....	90
3.2.2 On-Line Software: Environmental Data Record Processor (EDRP).....	91

## TABLE OF CONTENTS (continued)

	Page
3.2.3 Off-Line Software: Verification Processor (VERP) .....	93
3.2.4 Off-Line Software: D-Matrix Update (DMUP) .....	93
3.3 Expected Level of Performance of the D-Matrix Retrieval Algorithm .....	94
3.4 Data Collection and Database Description .....	95
3.5 Quantitative Comparison of Radiosonde versus SSM/T-2 .....	96
3.6 Qualitative Comparison of Model Analyzed Moisture versus SSM/T-2 .....	103
4. Conclusions .....	104
5. Possible Further Analysis. ....	106
6. References .....	107
Appendix A Abbreviations and Acronyms .....	A-1
Appendix B Distributions of radiosondes stations and measurements using to to calibrate the SSM/T-2. ....	B-1
Appendix C Displays of the SSM/T-2 FOV topographic classification and the TBs for the five SSM/T-2 channels measured over the west coast region on May 14 and 15, 1992 and over the east coast region on July 29 and 30 and August 6, 1992. ....	C-1
Appendix D Listing of data collected by Aerospace for the SSM/T-2 Cal/Val study. ....	D-1
Appendix E Display of selected radiosonde and SSM/T-2-retrieved RH profiles. ....	E-1
Appendix F Land and ship observations are plotted separately with the quantity (Radiosonde - SSM/T-2) RH and Q plotted on the ordinate, and the index of the co-locations on the abscissa. ....	F-1
Appendix G For the atmosphere types 1 through 5 with ocean backgrounds, the quantity (Radiosonde - SSM/T-2) RH and Q plotted on the ordinate, and the index of the co-locations on the abscissa. ....	G-1
Appendix H For symmetric beam pairs about nadir, the quantity (Radiosonde - SSM/T-2) RH and Q plotted on the ordinate, and the index of the co-locations on the abscissa. ....	H-1
Appendix I For variable spatial co-location criteria, land and ship observations are plotted separately with the quantity (Radiosonde - SSM/T-2) RH and Q plotted on the ordinate, and the index of the co-locations on the abscissa. ....	I-1
Appendix J SSM/T-2 channel TB imagery and HIRAS model-generated fields. ...	J-1

## LIST OF TABLES

	<u>Page</u>
Table 1.2-1. RMS difference / bias between the mean of the co-located MIR TBs and the observed SSM/T-2 TBs at the five SSM/T-2 channels. ....	6
Table 1.2-2. RMS difference / bias between the calculated TBs generated by the Eyre RT simulation model using a global set of radiosondes and co-located SSM/T-2 TBs at the five SSM/T-2 channels. ....	7
Table 1.3-1. Expected RMS performance of the SSM/T-2 D-matrix retrieval algorithm. ....	9
Table 1.3-2. RMS / bias between radiosonde measurements and SSM/T-2-derived RH and Q. ....	10
Table 1.3-3. SSM/T-2 validation of all ocean-type radiosondes versus the the expected RMS performance. ....	11
Table 2.2-1. SSM/T-2 channel characteristics. ....	16
Table 2.2-2. Antenna subassembly beam efficiency of the SSM/T-2 B5 unit aboard F-11. ....	17
Table 2.2.1-1. Calibration test results of the SSM/T-2 B5 unit aboard F-11. ....	22
Table 2.3-1. MIR receiver characteristics. ....	24
Table 2.3-2. MIR half-power beamwidths and first side-lobe levels. ....	24
Table 2.6.4-1. RMS difference between the mean of the co-located MIR TBs and the observed SSM/T-2 TBs at the five SSM/T-2 channels. ....	69
Table 2.7.2-1. Pressure levels required by the Eyre radiative transfer model and height levels used in the Enhanced RADTRAN model. ....	74
Table 2.7.2-2. RH correction factors used to determine the maximum limit of moisture that the sounding could have passed through and still reported the moisture profiles that it did (Brousailles and Morrissey, 1974). Pressure levels are those used in the Eyre radiative transfer program. ....	75
Table 3.2.2-1. Atmospheric types over ocean surfaces stratified by MV and temperature. ....	91
Table 3.3-1. Expected RMS performance of the SSM/T-2 D-matrix retrieval algorithm. ....	94
Table 3.5-1. Operational error checks on radiosondes at AFGWC. ....	96

# LIST OF TABLES (continued)

	<u>Page</u>
Table 3.5-2. RMS / bias between radiosonde measurements and SSM/T-2-derived RH and Q. ....	98
Table 3.5-3. RMS of SSM/T-2 retrievals by atmospheric types over ocean surfaces.....	98
Table 3.5-4. RMS of SSM/T-2 retrievals as a function of beam positions. ....	99
Table 3.5-5. RMS of SSM/T-2 retrievals by heavy cloud-type atmospheres over ocean surfaces. ....	100
Table 3.5-6. RMS of SSM/T-2 retrievals by non-heavy cloud-type atmospheres over ocean surfaces. ....	100
Table 3.5-7. RMS of SSM/T-2 retrievals stratified by spatial co-location criteria. ....	101

## LIST OF FIGURES

	<u>Page</u>
Figure 1.1-1. 24-hour global composite of 3 channels of the SSM/T-2 for May 15, 1992. The 91, 150 and $183 \pm 7$ channels are associated with the green, blue and red image colors, respectively, with bright colors representing higher moisture amounts and dark colors representing low water vapor amounts. ....	3
Figure 1.1-2. The absolute stability of the SSM/T-2 sensor based on the hot load - cold load differences versus sample number for Rev. #2774 (June 11, 1992). ....	3
Figure 1.1-3. The total noise (thermal and electronic) of the SSM/T-2 over the calibration period of 8 consecutive scans. ....	4
Figure 1.2-1. Diagram of the afternoon ascending passes of the DMSP F-11 satellite over the west coast of the U.S. on May 14 and 15, 1992. Also shown is the NASA ER-2 flight path. ....	8
Figure 1.2-2. Diagram of the morning descending passes of the DMSP F-11 satellite over the east coast of the U.S. on July 29 and 30 and August 6, 1992. Also shown is the NASA ER-2 flight path. ....	8
Figure 2.2-1. Comparison of SSM/T-1 and SSM/T-2 FOV patterns. ....	18
Figure 2.2-2. SSM/T-2 scan diagram. ....	18
Figure 2.2-3. The configuration of the SSM/T-2 and its location of the DMSP spacecraft (F-11). ....	19
Figure 2.2-4. A photograph of the SSM/T-2 unit with the thermal blanket and cover plates removed to disclose the interior construction. ....	19
Figure 2.2-5. SSM/T-2 183.3 GHz antenna pattern. ....	20
Figure 2.3-1. Photographs of the MIR, which is mounted in the fore body of the super wing pod on board the NASA ER-2 high altitude (~20 km) research aircraft. ....	25
Figure 2.3-2. The typical E-plane MIR antenna pattern measured at 89 GHz. ....	26
Figure 2.3-3. The typical E-plane MIR antenna pattern measured at 183.3 GHz. ..	26
Figure 2.4.1-1. Positions and topographic distributions of SSM/T-2 FOVs that have co-located MIR data for roughly 0100 UTC May 15, 1992. ....	29
Figure 2.4.1-2. Positions and topographic distributions of SSM/T-2 FOVs that have co-located MIR data for roughly 0100 UTC May 16, 1992. ....	31

## LIST OF FIGURES (continued)

	<u>Page</u>
Figure 2.4.1-3. Visible GOES imagery at 2330 UTC May 14, 1992. ....	33
Figure 2.4.1-4. Visible GOES imagery at 0030 UTC May 16, 1992. ....	33
Figure 2.4.2-1. Positions and topographic distributions of SSM/T-2 FOVs that have co-located MIR data for roughly 1041 UTC July 29, 1992. ....	36
Figure 2.4.2-2. Positions and topographic distributions of SSM/T-2 FOVs that have co-located MIR data for roughly 1028 UTC July 30, 1992. ....	38
Figure 2.4.2-3. Positions and topographic distributions of SSM/T-2 FOVs that have co-located MIR data for roughly 1040 UTC August 6, 1992. ...	40
Figure 2.4.2-4. Visible GOES imagery at 1230 UTC July 29, 1992. ....	42
Figure 2.4.2-5. Visible GOES imagery at 1230 UTC July 30, 1992. ....	42
Figure 2.4.2-6. Visible GOES imagery at 1230 UTC August 6, 1992. ....	43
Figure 2.6.1-1. Comparison of SSM/T-2 TBs to the mean co-located MIR TBs for the five SSM/T-2 channels for the west coast flights. ....	46
Figure 2.6.1-2. Comparison of SSM/T-2 TBs to the mean co-located MIR TBs for the five SSM/T-2 channels for the east coast flights. ....	49
Figure 2.6.1-3. Standard deviation of the co-located MIR TBs for each of the SSM/T-2 FOVs that are classified as water during west coast and east coast flights. ....	52
Figure 2.6.2-1. Based on the west coast data, the effect of the scan angle of the SSM/T-2 sensor on the difference between SSM/T-2 TBs and the mean of the co-located MIR TBs for the five SSM/T-2 channels. ....	56
Figure 2.6.2-2. For the west coast data, the effect of the MIR scan direction on the difference between SSM/T-2 TBs and the mean of the co-located MIR TBs for the five SSM/T-2 channels. The SSM/T-2 sensor was looking westward. ....	59
Figure 2.6.2-3. For the west coast data, the effect of the MIR scan direction on the difference between SSM/T-2 TBs and the mean of the co-located MIR TBs for the five SSM/T-2 channels. The SSM/T-2 sensor was looking eastward. ....	62
Figure 2.6.3-1. Based on the west coast data, RMS of the MIR TBs within each of the co-located SSM/T-2 FOVs for the five SSM/T-2 channels. ....	65

## LIST OF FIGURES (continued)

	<u>Page</u>
Figure 2.7.2-1. Global locations of radiosondes that were used to calibrate the SSM/T-2. ....	76
Figure 2.7.2-2. Calculated TBs using the Eyre RT simulation model versus SSM/T-2 TBs for the five SSM/T-2 channels. ....	77
Figure 2.7.2-3. Comparison of Eyre model results to Enhanced RADTRAN model results for the five SSM/T-2 channels using a global set of radiosondes. ....	80
Figure 2.7.2-4. Distribution of optimal surface emissivities for 91 and 150 GHz, iteratively calculated using a global set of radiosonde profiles (all over land) from late March, 1992 in the Eyre RT model. ....	83
Figure 2.7.2-5. Calculated TBs using radiosondes from India and the United States in the Eyre RT simulation model versus SSM/T-2 SDRs for $183.3 \pm 7$ GHz. ....	84
Figure 2.7.2-6. Calculated TBs using radiosondes from England, Germany, Scandinavia and Russia in the Eyre RT simulation model versus SSM/T-2 SDRs for $183.3 \pm 7$ GHz. ....	84
Figure 2.7.2-7. Changes in TBs calculated using the Eyre RT simulation model relative to the changes in precipitable water caused by modifying the humidity profiles by the correction factors presented in Table 5.2-2 (see Brousaides and Morrissey, 1974 for discussion) for the five SSM/T-2 channel frequencies. ....	85
Figure 3.2.2-1. Aerojet's heavy cloud flag over ocean using the 50.5 and 53.2 GHz channels. ....	92
Figure 3.2.2-2. Radiosonde data set verification of Figure 3.2.2-1. ....	92
Figure 3.5-1. Geographic distribution of the locations of radiosondes that were used in the SSM/T-2 validation study. ....	102

## FOREWORD TO SSM/T-2 CAL/VAL REPORT, VOLUME 1

The launch of DMSP F-11 on 28 November 91 marked several milestones. First, it marked the first flight of the Special Sensor Microwave Water Vapor Sounder (SSM/T-2). Second, it marked the first on-orbit microwave instrument containing 183.3 GHz channels. Finally, it marked the beginning of the calibration and validation to determine the accuracy of all the engineering and science behind the SSM/T-2.

As we write this report, the SSM/T-2 on-orbit performance has met or exceeded specifications. The instrument has been electrically and thermally stable since initial turn-on.

On the ground, the algorithms that convert microwave TBs into moisture parameters are exceeding specified requirements (best effort with goal of  $\pm 30$  percent). In fact, our statistical retrieval approach, using multiple linear regression, is meeting predicted performance for most atmospheric types and surface backgrounds. In the few cases where we are not meeting predicted performance, we expect algorithm coefficient updates to improve accuracy to the predicted levels. At Air Force Global Weather Central, the software is operating within throughput and memory allocations.

We express our respect for those visionaries of the past who conceived of the idea of an SSM/T-2 and worked to make the project a reality. We express our thanks to all those who worked so hard to design, develop, and test the SSM/T-2 hardware and software. Finally, we express our thanks to the CAL/VAL team members whose data collection and analysis set the stage for operational use of SSM/T-2 data and a quantum leap in weather forecasting.

We look forward to the weather forecasters and scientific community finding ways to exploit the SSM/T-2 data and increase moisture retrieval accuracy.

Michael J. LaPointe, Capt. USAF  
Chief, Sensor Development Branch  
Defense Meteorological Satellite Program



### Acknowledgements

The authors wish to thank Col. John Goyette, Program Director; Lt. Col. Nelson B. James, III, Program Manager, Current Satellite Systems; Lt. Col. Edwin Arrance, AWS Liaison; Capt. John Cadou, Deputy Program Manager, Capt. Thomas Piatkowski, Chief Sensor Development (1987-1990) and Capt. Michael J. LaPointe, Chief Sensor Development of the Defense Meteorology Satellite Program Office; Dr. Neil Baker, Aerospace Corporation - DMSP; Dr. John Theon, NASA Headquarters, Chief Atmospheric Dynamics, Radiation and Hydrology Branch; and Dr. Robert A. McClatchey, Phillips Laboratory, Director Atmospheric Sciences Division, for their direction and strong support throughout the calibration/validation effort. A sincere thanks to Dr. Joseph W. Snow, Phillips Laboratory, Branch Chief, Satellite Meteorology, without whose help and support this report would not have been possible. We appreciate the support from the Air Force Global Weather Central personnel Capt. Don Rhudy for project management, Capt. Tom Neu and Staff Sgt. Keith Hopkins for software support. Special thanks to Ms. Elizabeth Stenhouse who processed this report.

### Cover Picture

Hurricane Andrew making landfall on the coast of Louisiana, August 25, 1992. Displayed are the visible and infrared radiances from the Operational Linescan System (OLS) and the raw radiances of the SSM/T-2.



**Millimeter Wave Moisture Sounder (SSM/T-2) Calibration/Validation Program**

**SSM/T-2 CALIBRATION AND VALIDATION DATA ANALYSIS**

**VOLUME I**

**Calibration Contributors:**

V. J. Falcone, M. K. Griffin, R. G. Isaacs<sup>1</sup>, J. D. Pickle<sup>1</sup>, J. F. Morrissey, A. J. Jackson,  
A. Bussey, R. Kakar<sup>2</sup>, J. Wang<sup>3</sup>, P. Racette<sup>3</sup>

**Validation Contributors:**

D. J. Boucher<sup>4</sup>, B. H. Thomas<sup>4</sup>, A. M. Kishi<sup>4</sup>

Phillips Laboratory - Geophysics Directorate  
Atmospheric Sciences Division  
Satellite Meteorology Branch  
Hanscom AFB, MA 01731

<sup>1</sup>Atmospheric and Environmental Research, Inc.  
840 Memorial Drive  
Cambridge, MA 02139

<sup>2</sup>NASA Headquarters  
300 E Street, S.W.  
Washington, DC

<sup>3</sup>NASA Goddard Space Flight Center  
Greenbelt, MD 20771

<sup>4</sup>The Aerospace Corporation  
Defense Meteorological Satellite Program  
El Segundo, CA

## 1. Executive Summary

### 1.1 Introduction

The Phillips Laboratory Geophysics Directorate (PL/GP) presented a proposal to the Defense Meteorological Satellite Program (DMSP) to formulate, initiate and conduct a program to calibrate the Special Sensor Microwave Water Vapor Sounder (SSM/T-2) and to validate the retrieved water vapor profiles (Cal/Val). DMSP (SMC/CI) appointed PL/GPAS the principal investigator to lead the SSM/T-2 Cal/Val program. The objective of this effort is to obtain simultaneous, independent measurements of microwave radiance, water vapor mass, specific humidity and relative humidity to quantitatively measure the performance of the instrument (calibration) and to validate the ability of the SSM/T-2 to measure the water vapor parameters, i.e. environmental data records (EDRs) of Air Force Global Weather Central (AFGWC). Phillips Laboratory organized a team of experts from government and industry to undertake the study. The team members and responsibilities are:

Phillips Laboratory - program management, sensor calibration

Aerospace Corporation - product validation

NASA Headquarters and Goddard Space Flight Center - sensor calibration and ER-2 aircraft underflights of F-11

Atmospheric and Environmental Research, Inc. - sensor calibration, database and analysis

The importance of relative humidity is that it determines the spatial and vertical distribution of clouds. Indeed cloud forecast model initialization is intimately tied to accurate specification of moisture fields. Satellite remote sensing of meteorological parameters such as temperature, moisture and clouds helps to provide the initial conditions for NWP forecasts (Isaacs et al., 1986). Specification of sufficiently accurate moisture fields from satellite data in data sparse regions can improve the analysis and forecast of relative humidity (Hoffman et al., 1990). One note of caution: recent literature (Lindzen and Fox-Rabinowitz, 1989) indicates that numerical models may not fully benefit from high horizontal resolution satellite observations unless the vertical resolution is also high. Most satellites today can sense mesoscale weather features with their given horizontal resolution, but do not have the necessary vertical resolution to detect the vertical detail and extent of these features. This may be one contributing factor to the mixed success of satellite data assimilation to date. Operational use of satellite data in global forecast models has shown little or no skill increase for the Northern Hemisphere, where many other data sources are available. However, satellite data has proved important in improving forecast skill in the Southern Hemisphere, where little else is available.

The first SSM/T-2 was launched November 28, 1991 aboard the DMSP Block 5D-2 Spacecraft F-11. The SSM/T-2 is a cross-track scanning, five channel, passive, total power microwave radiometer system which measures microwave radiance at  $183.3 \pm 1$ ,  $\pm 3$ ,  $\pm 7$ ; and at 150.0 and 91.655 GHz. The nadir resolution of the SSM/T-2 is on the order of 48 km at 183.3 GHz, with a swath width of 1400 km. The SSM/T-2 was built by Aerojet Electronic Systems Division under the direction of SMC/CI. SSM/T-2 is the first operational microwave water vapor sounder to be placed on orbit.

The F-11 spacecraft is in a sun-synchronous polar orbit at an altitude of 833 kilometers with an inclination of 98.4 degrees and an orbital period of 101 minutes. F-11 completes 14.25 full orbit revolutions per day and has a local ascending nodal crossing time of 1714 hours. Figure 1.1-1 shows a global color composite of three of the SSM/T-2 channels for all passes on May 15, 1992.

The SSM/T-2 consists of a single, self-contained module with a step-scan motion in the cross-track direction  $\pm 40.5^\circ$ . During each scan period, and for all five channels, twenty-eight discrete earth viewing positions, four discrete calibration measurements of a hot-load target ( $\sim 300$  K), and cosmic background radiation (cold load  $\sim 3$  K) are monitored. The beams of the five SSM/T-2 channels have coincident centers.

An examination of the stability of the SSM/T-2 electronics has shown the instrument to be very stable. Figure 1.1-2 shows the absolute stability of the SSM/T-2 sensor. The differences are almost constant throughout the orbit.

Figure 1.1-3 shows the total noise (thermal and electronic) of the instrument over the calibration period of 8 consecutive scans.  $183.3 \pm 7$  and 150 GHz are the noisiest with standard deviations of 5 counts. The sensitivity ( $\Delta T$ ) is the "minimum detectable" signal of a radiometer. Meteorological radiometer systems detectability or sensitivity is defined in terms of the radiometer output when referred to the input of the antenna collecting aperture, defined as the Noise Equivalent Temperature Difference (NE $\Delta T$ ). From Figure 1.1-3,  $\Delta T$  is approximately 0.45 K. All these measurements are raw data with no thermal variations applied, thus both thermal and electronic noise variations are included. This approach assumes the worst case scenario for SSM/T-2 sensitivity.



*Figure 1.1-1. 24-hour global composite of 3 channels of the SSM/T-2 for May 15, 1992. The 91, 150 and  $183 \pm 7$  GHz channels are associated with the green, blue and red image colors, respectively, with bright colors representing higher moisture amounts and dark colors representing low water vapor amounts.*

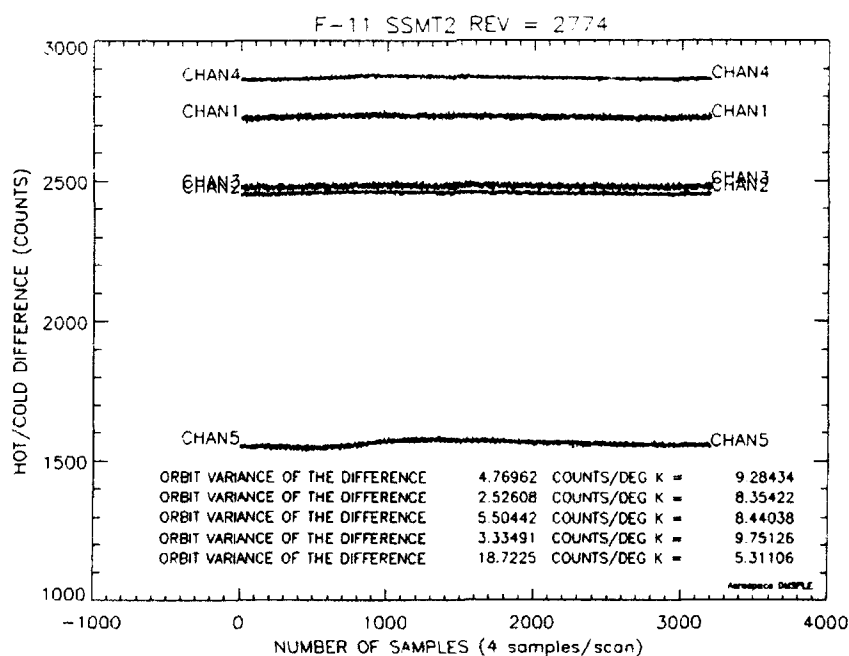


*Figure 1.1-2. The absolute stability of the SSM/T-2 sensor based on the hot load - cold load differences versus sample number for Rev. #2774 (June 11, 1992).*

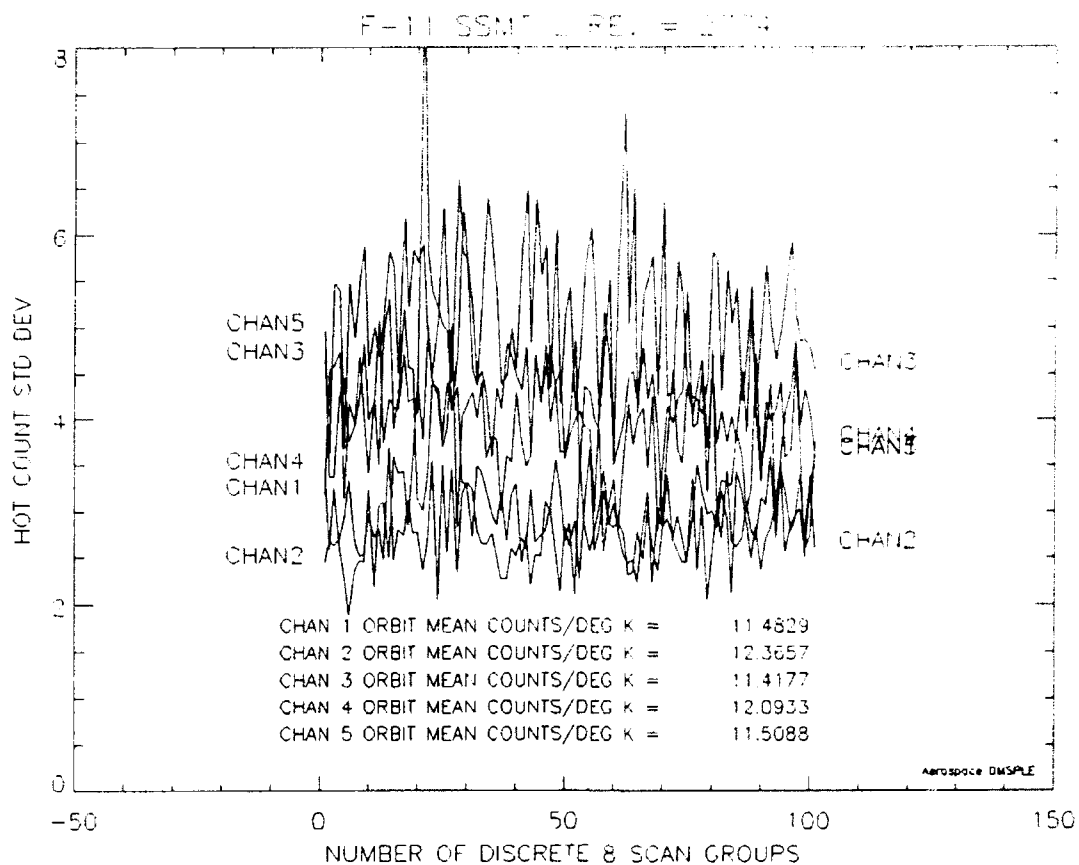


**Figure 1.1-3.** *The total noise (thermal and electronic) of the SSMIT-2 instrument over the calibration period of 8 consecutive scans for Rev. #2774 (June 11, 1992).*

## 1.2 SSM/T-2 Instrument Calibration

Of primary importance to the success of any satellite instrument is its calibration. Without a fully calibrated instrument there is no way to guarantee that the operational product is accurate. The ground calibration performed by Aerojet showed that the instrument performed as contracted, i.e., within design specifications. On orbit, that calibration has to be recalibrated to insure that the instrument has not changed due to launch forces or mechanical or electronic problems.

Two independent approaches were taken to calibrate the SSM/T-2: (a) SSM/T-2 TB data were compared with contemporaneous NASA Millimeter-wave Imaging Radiometer (MIR) data from NASA ER-2 underflights, and (b) available upper air temperature and moisture profile data (radiosondes) were used in radiative transfer models to calculate the outgoing microwave radiance for the SSM/T-2 channels.

Two aircraft campaigns were planned, one along the west coast and the other along the east coast of the United States (see Figures 1.2-1 and 1.2-2). The MIR has four channels in common with the SSM/T-2 ( $183.3 \pm 1$ ,  $\pm 3$ ,  $\pm 7$  and 150 GHz) and a fifth channel at 89 GHz which differs slightly from the SSM/T-2 91.655 GHz channel. The small frequency difference between 89 and 91.655 GHz does not appreciably effect their comparison since the atmospheric and earth surface properties vary little over this frequency range.

Aircraft MIR - SSM/T-2 comparisons were stratified according to background (land, ocean, coast) and RMS differences and biases were computed. Weather during the west coast aircraft campaign was characterized by stable atmospheric conditions. For the west coast data, water vapor absorption line (i.e., 183.3 GHz) channels over water surfaces produced SSM/T-2 - mean MIR RMS differences of 0.7 - 1.3 K with biases of a few (up to 0.7 K) tenths of a degree (see Table 1.2-1). The RMS variation for these channels is larger for coastal FOVs (up to 1.7 K) with the largest variation for land backgrounds (up to 3.8 K). The RMS differences are slightly greater for the three 183 GHz channels over the Atlantic Ocean. The window channels (e.g. 91 and 150 GHz) show larger RMS variation and bias, especially for the mixed (e.g., coastal) FOVs. This increased RMS is caused by there being large variation in the surface emissivity within the SSM/T-2 FOV which is less well represented by the limited area scanned by the MIR. Over the ocean, the surface emissivity is more homogeneous, allowing the MIR's smaller areal measurement to be more representative of the average surface emissivity affecting the SSM/T-2's FOV. The RMS difference for the window channels for the east coast data were roughly comparable in magnitude to the west coast data.

The second method used to calibrate the SSM/T-2 was the comparison of operational satellite data records (SDRs) with model calculated TBs using co-located radio-

sondes as input into radiative transfer models. The criteria for co-location in time and space is  $\pm 1$  hour and 100 km. Radiosonde profiles consisting of significant and mandatory levels were only used if the moisture measurements extended up to at least 300 hPa. Radiosonde data span the time period between January 31 to August 7, 1992. Radiative transfer calculations based on co-located radiosondes are generally in good agreement with SSM/T-2 TBs. Discrepancies are noted for the window channels which see the surface, for which mean emissivities were used in the simulations. This resulted in an underestimation of the SSM/T-2 observations over land and an overestimation for ocean surfaces. Other sources of discrepancies between the forward calculated TBs and the satellite-measured values are the lack of consideration of clouds and/or precipitation within the radiative transfer model, uncertainties of low RH radiosonde measurements, errors in radiative transfer modeling, varying abilities of the different types of radiosonde instruments to measure temperature and moisture, different reporting procedures of radiosonde data used by different countries (Garand et al., 1992), and the addition of estimated high altitude ( $> 300$  hPa) moisture data for input into the radiative transfer models. This document describes the results of a 6-month effort. Due to time constraints, the Cal/Val team has not been able to explore all the areas of question with the radiosonde data. Further data analyses will be undertaken in the Volume II Cal/Val report.

*Table 1.2-1. RMS difference / bias between the mean of the co-located MIR TBs and the observed SSM/T-2 TBs at the five SSM/T-2 channels. Frequency of SSM/T-2 FOVs follows the RMS difference in parentheses. Bias is based on the mean of the co-located MIR TBs - the SSM/T-2 TBs. The scan angle of the MIR data matched that of the co-located SSM/T-2 FOV. The time between the SSM/T-2 and the MIR measurements was  $\pm 1$  hour.*

WEST COAST FLIGHTS					
SSM/T-2 FOV TOPOGRAPHY	91 GHz	150 GHz	183 $\pm$ 7 GHz	183 $\pm$ 3 GHz	183 $\pm$ 1 GHz
WATER	3.4 / -1.5 (40)	2.4 / 0.5 (26)	0.7 / -0.3 (23)	0.8 / 0.2 (23)	1.3 / 0.7 (23)
LAND	3.5 / 0.5 (40)	4.3 / 1.1 (28)	3.8 / -0.1 (25)	2.9 / 1.5 (25)	3.2 / 2.1 (25)
COAST	9.1 / 4.1 (36)	3.8 / 1.5 (20)	1.2 / 0.0 (17)	1.1 / 0.2 (17)	1.7 / 0.0 (17)
EAST COAST FLIGHTS					
SSM/T-2 FOV TOPOGRAPHY	91 GHz	150 GHz	183 $\pm$ 7 GHz	183 $\pm$ 3 GHz	183 $\pm$ 1 GHz
WATER	3.7 / 0.2 (54)	3.6 / 2.7 (35)	1.2 / -0.6 (29)	2.1 / -1.8 (29)	1.2 / 0.2 (29)
LAND	4.7 / -1.1 (18)	2.6 / 1.2 (11)	1.9 / -1.4 (10)	2.6 / -2.5 (10)	1.2 / -0.5 (10)
COAST	10.9 / -1.2 (81)	4.5 / 1.2 (53)	1.6 / -0.8 (41)	2.4 / -1.9 (41)	1.8 / 0.3 (41)



*Table 1.2-2. RMS difference / bias between the calculated TBs generated by the Eyre RT simulation model using a global set of radiosondes and co-located SSM/T-2 TBs at the five SSM/T-2 channels. Bias is based on SSM/T-2 TBs - co-located Eyre-calculated TBs. co-location criteria are  $\pm 1$  hour and 100 km. Frequency follows the RMS difference in parentheses.*

<u>Precipitable Water (kg/m<sup>2</sup>)</u>	<u>91 GHz</u>	<u>150 GHz</u>	<u>183 <math>\pm</math> 7 GHz</u>	<u>183 <math>\pm</math> 3 GHz</u>	<u>183 <math>\pm</math> 1 GHz</u>
0 - 10	18.5 / 6.4 (296)	16.4 / 6.5 (296)	10.3 / 4.4 (296)	5.9 / 0.0 (296)	5.3 / -1.4 (296)
10 - 20	22.6 / 15.4 (343)	13.5 / 9.1 (343)	4.5 / -0.4 (343)	4.0 / -0.7 (343)	5.6 / -0.8 (343)
20 - 30	20.9 / 13.8 (204)	9.1 / 3.8 (204)	5.9 / -1.7 (204)	4.9 / -0.6 (204)	6.6 / 0.9 (204)
30 - 40	17.2 / 5.8 (176)	9.0 / -0.8 (176)	8.8 / -2.1 (176)	7.4 / -0.7 (176)	8.8 / 1.3 (176)
40 - 50	13.6 / -4.0 (110)	10.3 / -3.3 (110)	8.3 / -3.3 (110)	6.0 / -2.2 (110)	6.6 / -0.2 (110)
50 - 60	12.3 / -7.0 (80)	6.9 / -3.2 (80)	6.5 / -2.4 (80)	5.7 / -1.2 (80)	6.6 / 1.1 (80)
60 - 70	10.8 / -4.8 (16)	22.2 / -13.6 (16)	17.0 / -10.2 (16)	12.5 / -4.1 (16)	12.5 / 1.7 (16)
70 - 80	11.9 / -3.9 (2)	6.3 / 1.4 (2)	7.0 / 2.3 (2)	4.1 / 1.3 (2)	2.6 / 2.1 (2)
TOTAL	19.2 / 8.1 (1227)	12.7 / 4.0 (1227)	7.8 / -0.2 (1227)	5.7 / -0.7 (1227)	6.5 / -0.1 (1227)

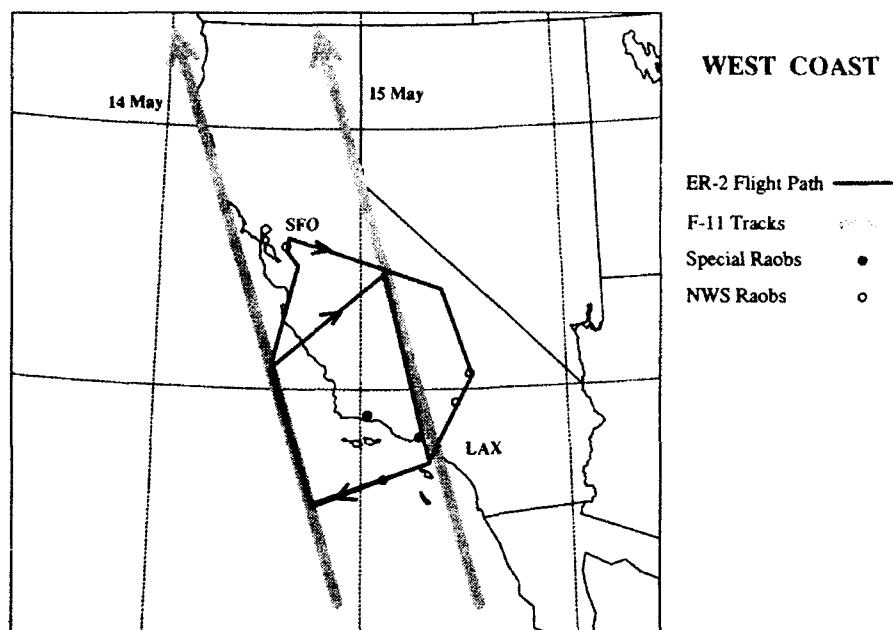


*Figure 1.2-1. Diagram of the afternoon ascending passes of the DMSP F-11 satellite over the west coast of the U.S. on May 14 and 15, 1992. Also shown in the NASA ER-2 flight path.*

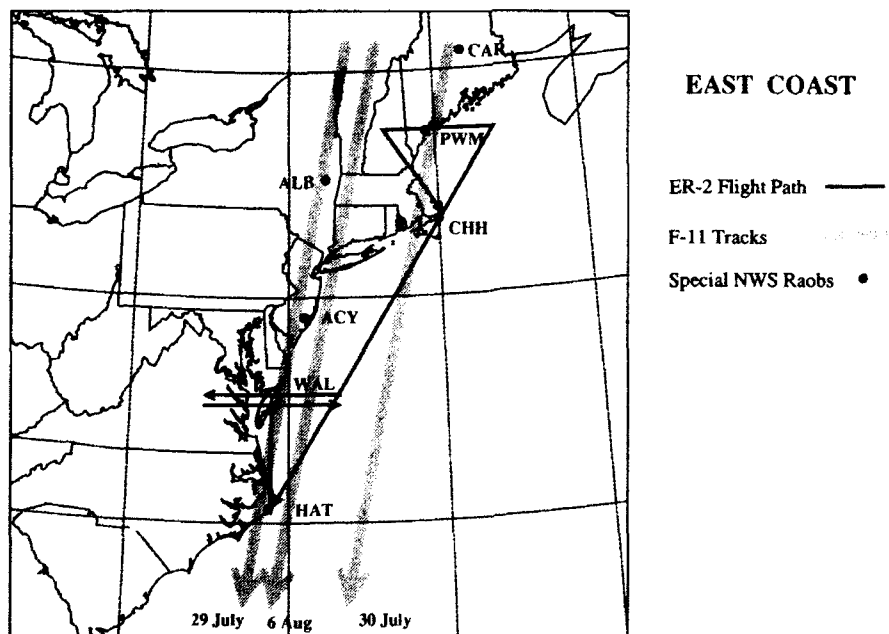


*Figure 1.2-2. Diagram of the morning descending passes of the DMSP F-11 satellite over the east coast of the U.S. on July 29 and 30 and August 6, 1992. Also shown is the NASA ER-2 flight path.*

### 1.3 Retrieval Algorithm Validation

The required derived parameters of the SSM/T-2 are relative (RH) and specific humidity (Q) at 1000, 850, 700, 500, 400, and 300 hPa. In addition, water vapor mass in seven layers (surface to 1000 hPa if available, 1000-850, 850-700, 700-500, 500-400, 400-300, 300 on up to the top of the atmosphere) is retrieved. It should be kept in mind that the accuracy of the SSM/T-2 moisture retrievals were to be on a "best effort" with a goal of  $\pm 30\%$  basis by the contractor.

The expected RMS performance of the SSM/T-2 D-matrix retrieval algorithm via radiative transfer theory is given in the Table 1.3-1.

*Table 1.3-1. Expected RMS performance for the SSM/T-2 D-matrix retrieval algorithm.*

Parameter	Units	Ocean	Land	Coast
RH @ 1000 hPa	%	13.5	20.3	16.5
RH @ 850 hPa	%	13.9	20.5	22.6
RH @ 700 hPa	%	16.0	19.4	19.6
RH @ 500 hPa	%	12.5	17.3	13.4
RH @ 400 hPa	%	11.8	15.1	13.5
RH @ 300 hPa	%	11.8	12.9	12.4
Q @ 1000 hPa	g/kg	1.41	2.79	2.71
Q @ 850 hPa	g/kg	1.09	1.88	2.32
Q @ 700 hPa	g/kg	.942	1.14	1.26
Q @ 500 hPa	g/kg	.319	.428	.391
Q @ 400 hPa	g/kg	.149	.200	.183
Q @ 300 hPa	g/kg	.054	.059	.059

Retrievals over the ocean were anticipated to have the better overall RMS performance compared to those for either the land or coast backgrounds. Ice retrievals are not listed since the database collected for this study contained no ice radiosondes versus SSM/T-2 co-locations.

A large radiosonde database has been collected from the AFGWC operational systems in support of this study. Ten thousand radiosondes pairs of co-located SSM/T-2 and radiosonde profiles were used in this study. co-location criteria were set to data within  $\pm 1$  hour in time, and 100 km in distance. Note one radiosonde profile may be co-located to multiple SSM/T-2 measurements. Table 1.3-2 displays the results of comparing the radiosonde measurements RH and Q as calculated from dew-point depression, to the SSM/T-2 derived RH and Q.

*Table 1.3-2. RMS/bias between radiosonde measurements and satellite-derived RH and Q.*

Parameter @ Level	Units	Ocean	Land	Coast
RH/Bias @ 1000 hPa	%	15.7 / 4.2	16.1 / 5.6	16.2 / -0.6
RH/Bias @ 850 hPa	%	22.7 / -3.1	24.2 / -3.7	25.1 / -7.4
RH/Bias @ 700 hPa	%	22.8 / -6.8	22.6 / -2.6	21.7 / -3.6
RH/Bias @ 500 hPa	%	25.1 / -12.2	21.8 / -4.8	20.1 / -2.0
RH/Bias @ 400 hPa	%	22.6 / -14.1	22.1 / -10.4	18.9 / -4.0
RH/Bias @ 300 hPa	%	23.2 / -13.2	19.6 / -2.5	17.4 / 0.2
Q/Bias @ 1000 hPa	g/kg	3.80 / 0.37	2.74 / -1.47	2.86 / -0.21
Q/Bias @ 850 hPa	g/kg	3.13 / -0.43	3.04 / -0.02	2.47 / -0.31
Q/Bias @ 700 hPa	g/kg	3.15 / -1.07	1.87 / 0.16	1.46 / 0.04
Q/Bias @ 500 hPa	g/kg	2.54 / -1.04	0.88 / -0.10	0.64 / 0.01
Q/Bias @ 400 hPa	g/kg	1.00 / -0.45	0.46 / -0.16	0.34 / -0.06
Q/Bias @ 300 hPa	g/kg	0.24 / -0.13	0.14 / -0.01	0.24 / -0.13

In general, the SSM/T-2 derived RH and Q have larger than predicted RMS. The RMS over ocean backgrounds are larger than either land or coast which is an unanticipated result. It has subsequently been discovered that of the five categories of SSM/T-2 ocean atmospheres, the very moist atmospheres are clearly the major contributors to the RMS. The cause could be as simple as a coding error in the generation of the a-priori regression coefficients, or more fundamental in nature. It is possible that there are physical processes that the SSM/T-2 algorithms have not properly modeled, or perhaps the shape of the absorption curve at 150 GHz is not adequately modeled. Work in this area will continue until the problem is understood and corrected.

The SSM/T-2 ocean background soundings that are flagged as contaminated by heavy cloud are removed from the statistics, and RMS are re-calculated. The heavy cloud flag over the ocean is constructed using a scatter plot of the SSM/T-1 50.5 GHz and the 53.2 GHz channels. Table 1.3-3 lists the RMS performance of all observed (i.e. in the Validation database) ocean type atmospheres against the expected RMS performance. Type 2 atmospheres are relatively dry, whereas Type 5 atmospheres are very moist. As mentioned previously, the RMS for the Type 5 (very moist) ocean atmosphere, and the Type 3 at two levels, are still larger than anticipated, however, all remaining types show significant improvement.

*Table 1.3-3. RMS of all observed ocean-type atmospheres versus the expected RMS performance.*

Parameter @ Level	Expected	Type 2	Type 3	Type 4	Type 5
RH (%) @ 1000 hPa	13.5	16.5	11.6	8.0	11.1
RH (%) @ 850 hPa	13.9	16.0	28.1	14.0	20.3
RH (%) @ 700 hPa	16.0	16.3	25.4	12.9	24.3
RH (%) @ 500 hPa	12.5	14.6	19.6	9.1	24.7
RH (%) @ 400 hPa	11.8	11.0	14.9	6.4	18.2
RH (%) @ 300 hPa	11.8	13.3	12.4	9.5	18.5
Q (g/kg) @ 1000 hPa	1.41	1.11	1.27	1.43	2.92
Q (g/kg) @ 850 hPa	1.09	.578	3.11	1.75	3.01
Q (g/kg) @ 700 hPa	.942	.393	2.99	1.64	2.54
Q (g/kg) @ 500 hPa	.319	.107	.346	.411	1.47
Q (g/kg) @ 400 hPa	.149	.040	.094	.141	.557
Q (g/kg) @ 300 hPa	.054	.014	.030	.067	.189

Overall, the performance of the SSM/T-2 moisture retrievals is promising. The reader is reminded that these statistics have been calculated using the original a-priori coefficients and a radiosonde database screened by very simple error checks. Updated coefficients will eliminate the observed system biases and most certainly bring down the RMS. As a follow-on to this initial study, SSM/T-2 derived layered water vapor mass will be compared to the total water vapor mass retrieved from the SSM/I.

## 1.4 Conclusions and Recommendations

Over water, measurements of SSM/T-2 channels in the vicinity of 183.31 GHz water vapor absorption line produce RMS deviations from the mean of the co-located MIR-measured TBs of 0.7 - 2.1 K with biases of up to 1.8 K in magnitude. RMS variation for these frequencies is larger for coastal FOVs (up to 2.4 K) with the largest variation for land backgrounds (up to 3.8 K). For the surface channels, 91 and 150 GHz, show larger RMS and bias, especially for the mixed (i.e. coastal) FOVs.

Radiative transfer calculations based on co-located radiosondes are generally in good agreement with SSM/T-2 TBs considering that there was no consideration of clouds and weather conditions within the SSM/T-2 FOV which could also affect the TBs measured within the SSM/T-2 FOV as well as the forward-calculated TBs. The three 183.3 GHz channels had RMS differences of up to 7.8 K. The larger discrepancies for the transparent channels are a result of the channels sensing the surface, for which mean emissivities used in the RT simulations underestimate the SSM/T-2 observations over land and overestimate them over the ocean.

Studies of the variations of the on-orbit calibration performed by Aerospace indicate the instrument is very stable. The analysis of the underflights indicate that the SSM/T-2 is performing within or exceeds the original specifications. This calibration study has shown that for operational utilization there are no apparent or consistent instrument biases.

The SSM/T-2 retrieved vertical moisture profiles (excluding observations contaminated by heavy cloud) compare within  $\pm 30\%$  RH with co-located radiosonde data except over certain ocean atmospheres. The radiosonde database included Asian continent stations where high altitude stations may have questionable observation accuracies. These stations were not removed from the database for this study, therefore the results should be considered as a worst case scenario. The linear biases that were observed between the SSM/T-2 versus radiosonde comparisons will be eliminated when the a-priori regression coefficients are updated. The improvement in retrieval accuracy via the update of regression coefficients is a high priority task and will be pursued as soon as possible.

The SSM/T-2 has not been advertised as an imager; however, this study indicates that the SSM/T-2 is capable of yielding high quality EDR imagery. The detailed imagery should motivate the modeling community to consider assimilating the SSM/T-2 data into operational analysis as well as using the imagery itself as a means of rapid quality control of the data prior to assimilation in the numerical models. In addition, the SSM/T-2 TBs rendered as multichannel imagery are interesting. Work to date includes combining the 91, 150 and the  $183.3 \pm 1$  GHz channels. This particular choice of channels and colors brings out the structure of small scale storms very effectively. The interpretation of the

multichannel data is, at times, very complex. The 183.3 GHz channel is the most difficult to deal with since both absorption, re-emission and scattering are occurring.

This initial validation study has the following set of recommendations: (1) detailed analysis of the a-priori ocean atmosphere Types 3 and 5, (2) careful inspection of the radiative transfer code implementation, (3) detailed analysis of the inferred heavy cloud flag over ocean, and finally (4) a careful update to the a-priori D-Matrices.

In summary, the experience that the user community gains by working with the SSM/T-2 data as both a point measurement and a volume averaged variable in the numerical weather prediction models, will simplify the transition to the higher resolution SSMIS soundings. It is imperative that proper attention be given to the fine tuning of the SSM/T-2 during a follow-on effort since all lessons learned will be directly applicable to the SSMIS system.

**Millimeter Wave Moisture Sounder (SSM/T-2) Calibration/Validation Program**

**SSM/T-2 CALIBRATION DATA ANALYSIS**



## **2. SSM/T-2 Instrument Calibration**

### **2.1 Introduction**

The Phillips Laboratory (PL/GPAS) is the principal investigator for the calibration and validation (Cal/Val) of the Defense Meteorological Satellite Program (DMSP) Special Sensor Microwave Water Vapor Sounder (SSM/T-2). The calibration portion of this study is a cooperative PL/NASA/AER program. The aim of this research project is to calibrate the SSM/T-2. The first calibration technique is to underfly the DMSP F-11 satellite with a NASA ER-2 high-altitude aircraft which is outfitted with the NASA MIR and compare the co-located measurements. MIR measured TBs are accurate to less than 1 K (Wang, personal communication, 1992). The second calibration method compares SSM/T-2 TBs to co-located TBs calculated using radiosonde profiles in radiative transfer models.

Two specific air campaigns were planned: 1) on the west coast of the U.S. during the 14th and 15th of May 1992; and 2) over the east coast of the U.S. on the 29th and 30th of July 1992 and/or the 6th and 7th of August 1992. The ascending pass of the F-11 parallels the west coast of the U.S. (Figure 1.2-1) whereas the descending pass closely parallels the east coast of the U.S. (Figure 1.2-2). These campaign choices allowed water vapor measurements under varying weather conditions and atmospheric air masses.

The aircraft flight paths were designed to maximize the variety of land and ocean background measurements for the calibration process. Figure 1.2-1, displaying the west coast ER-2 flight path and F-11 subsatellite track, illustrates this strategy. On 14 May, the ER-2 flew along the subtrack and along the side of the SSM/T-2 swath looking away from the sun (eastern side). On 15 May the ER-2 flew along and on both sides of the SSM/T-2 subtrack which looked toward and away from the sun. These measurements were examined to identify solar effects on the instrument.

The second method used to calibrate the SSM/T-2 was the comparison of operational satellite TBs with model-calculated TBs using co-located radiosondes as input into radiative transfer models. The criteria for co-location in time is  $\pm 1$  hour, and in space, 100 km. Radiosonde profiles were only used if measured moisture profiles extended up to at least 300 hPa. Radiosonde data span the time period between January 31 to August 7, 1992. Two radiative transfer models were used: (a) the Enhanced RADTRAN model (Falcone et al., 1979, 1982 and Isaacs et al., 1989), and (b) the Eyre microwave simulation model (Eyre and Woolf, 1988).

## 2.2 SSM/T-2 Instrument

The SSM/T-2 is a five-channel, total power, microwave radiometer. It has three channels situated symmetrically about the 183.31 GHz water vapor resonance line, at  $183.31 \pm 1, \pm 3, \pm 7$  GHz, and two window channels at 150.0 and 91.655 GHz (see Table 2.2-1). Throughout section 2 the SSM/T-2 channels are referred in the text by their frequency rather than the Aerojet channel numbering system. The SSM/T-2 instrument consists of a single, self-contained module with a step-scan motion in the cross-track direction of  $\pm 40.5^\circ$ . The SSM/T-2 scan mechanism is synchronized with the SSM/T-1 so that the beam cell patterns of the two sensors coincide as shown in Figure 2.2-1. During each scan period, and for all five channels at twenty-eight discrete earth viewing positions, four discrete calibration measurements of a hot-load target ( $\sim 300$  K), and cosmic background radiation ( $\sim 3$  K) are monitored. Figure 2.2-2 shows the scan diagram of the SSM/T-2. The beams of the five SSM/T-2 channels have coincident centers (see Figure 2.2-3). A photograph of the SSM/T-2 unit with the thermal blanket and cover plates removed to disclose the interior construction is shown in Figure 2.2-4. The antenna aperture is covered with a protective cover which is removed upon installation of the unit on the spacecraft.

The SSM/T-2 employs a single offset parabolic reflector with a 2.6-inch diameter projected aperture. The reflector is shrouded to eliminate the possibility of rays from the sun striking either of the calibration paths and causing unwanted thermal gradients. The feedhorn is a corrugated pyramidal horn with a flare designed to minimize phase center separation over the bandwidth (91 to 183.3 GHz), while providing a spherical wave illumination of the reflector. Figure 2.2-5 shows the antenna pattern. For 183.3 GHz, the

*Table 2.2-1. SSM/T-2 channel characteristics.*

Center Frequency (GHz)	IF (GHz)	Nadir Field-of-View (km)	Beamwidth (degrees)	Peak Altitude (hPa)
91.665	1.5	84	6.0	surface
150.0	1.5	54	3.7	1000
$183.3 \pm 7$	1.5	48	3.3	800
$183.3 \pm 3$	1.0	48	3.3	650
$183.3 \pm 1$	0.5	48	3.3	500

antenna efficiency is greater than 94%. Table 2.2-2 shows the antenna subassembly beam efficiency. A 3.3° beamwidth is achieved for the 183.3 GHz channels and larger beamwidths of approximation 3.7° and 6.0° for 150 and 91.655 GHz, respectively. These correspond to the following FOV diameters at nadir of ~48 km at 183.3 GHz, ~54 km at 150 GHz and 84 km at 91.655 GHz.

To achieve the cross-track scanning, the reflector alone rotates. The rotation of the reflector produces a rotation of the plane of polarization of the upwelling scene TBs which is permitted provided that the polarization remains identical for the two window channels and 183.3 ± 7 GHz. These channels must have the same polarization characteristics because they measure contributions from both the atmosphere and the surface. Note that all SSM/T-2 channels possess the same polarization.

The SSM/T-2 inflight warm-load calibration target is a derivative of the SSM/T-2 warm load calibration target. The warm load (~300 K) is shrouded to improve RF coupling of energy to the reflector/feedhorn antenna. This minimizes potential calibration errors arising from the reception of extraneous energy due to scattering of earth or solar radiation off of the spacecraft. The cold path shown in Figure 2.2-4 (lower right of instrument) is a cylindrical oversized waveguide tube which permits a direct view of the cosmic background (~3 K) by the antenna reflector during calibration (see Aerojet reports, June, 1990; January, 1991; and April, 1988)

*Table 2.2-2. Antenna subassembly beam efficiency of the SSM/T-2 B5 unit aboard F-11.*

Beam Position	Specified Beam Efficiency	Measured Beam Efficiency
1	≥93%	94.29%
14	≥93%	94.43%

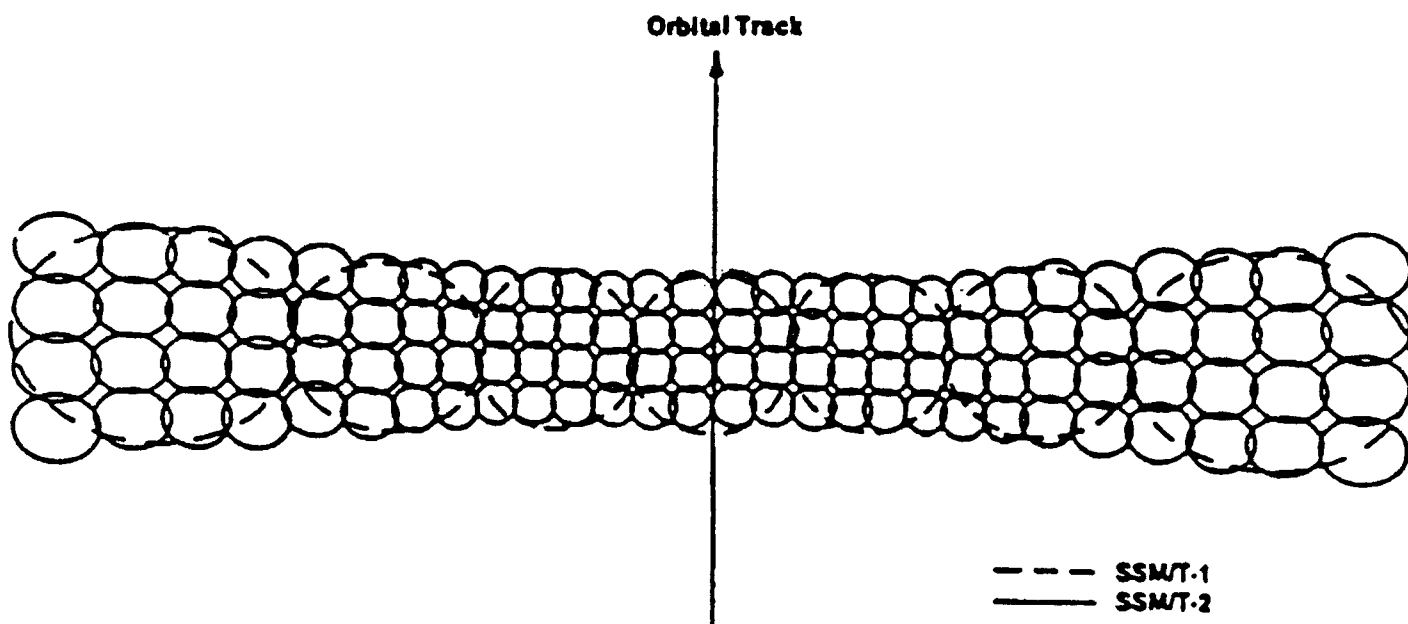


Figure 2.2-1. Comparison of SSM/T-1 and SSM/T-2 FOV patterns.

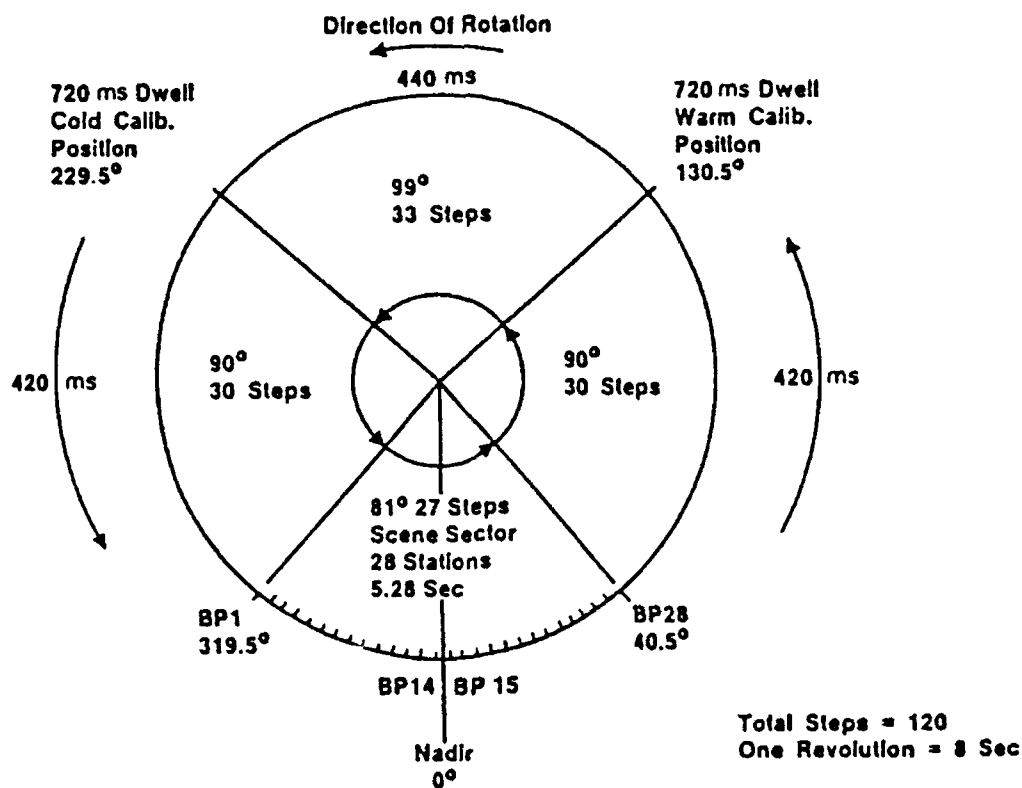
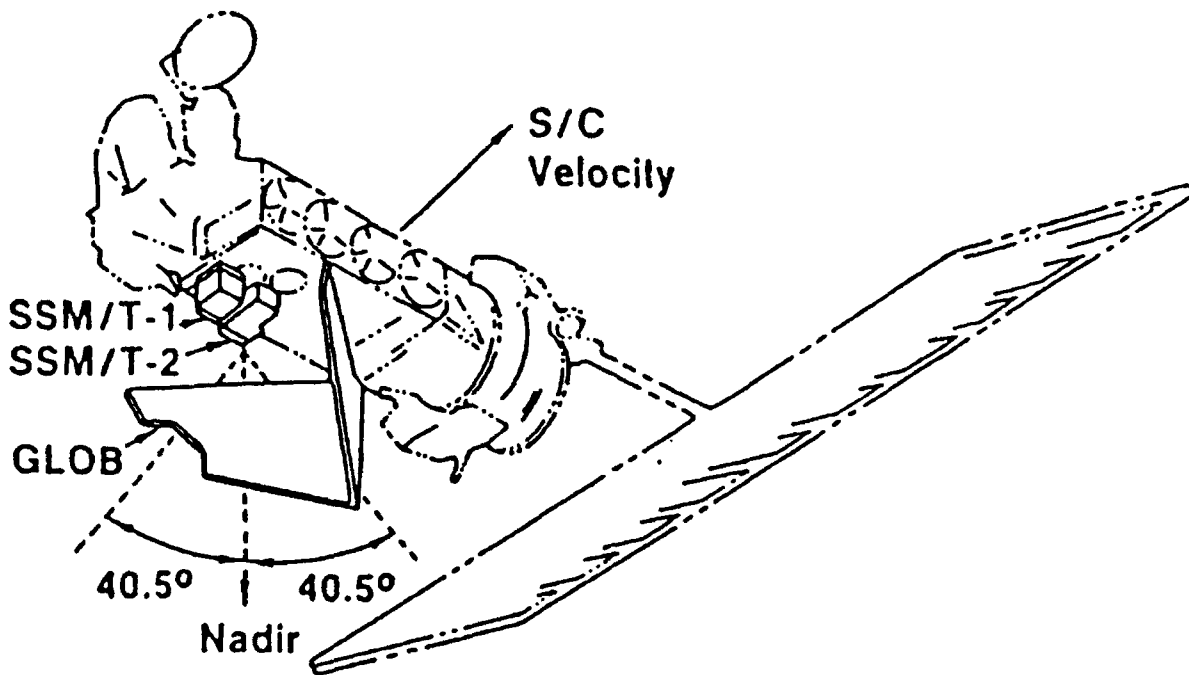
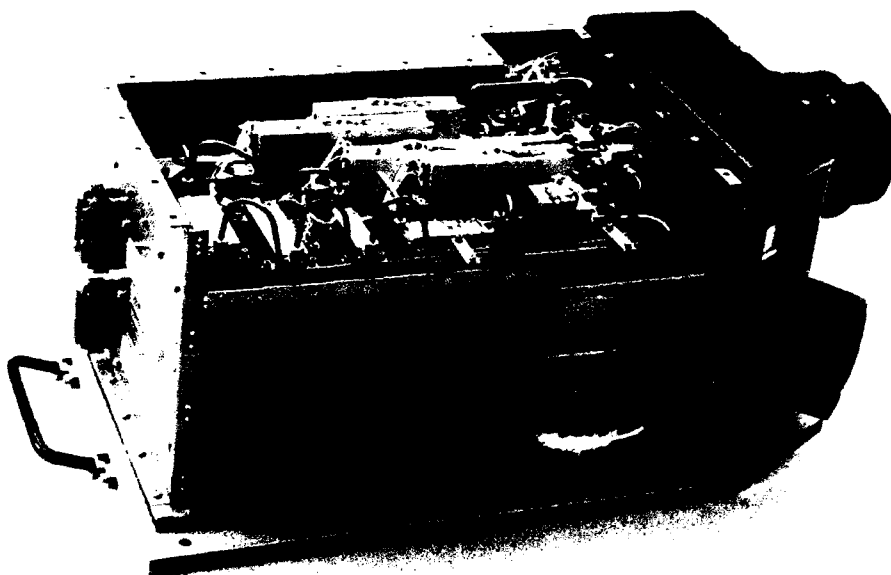


Figure 2.2-2. SSM/T-2 scan diagram.



*Figure 2.2-3. The configuration of the SSM/T-2 and its location of the DMSP spacecraft (F-11).*



*Figure 2.2-4. A photograph of the SSM/T-2 unit with the thermal blanket and cover plates removed to disclose the interior construction. The antenna aperture is covered with a protective cover which is removed upon installation of the unit on the spacecraft.*

DATE: 19 Jan 1990  
TIME: 12: 17: 00

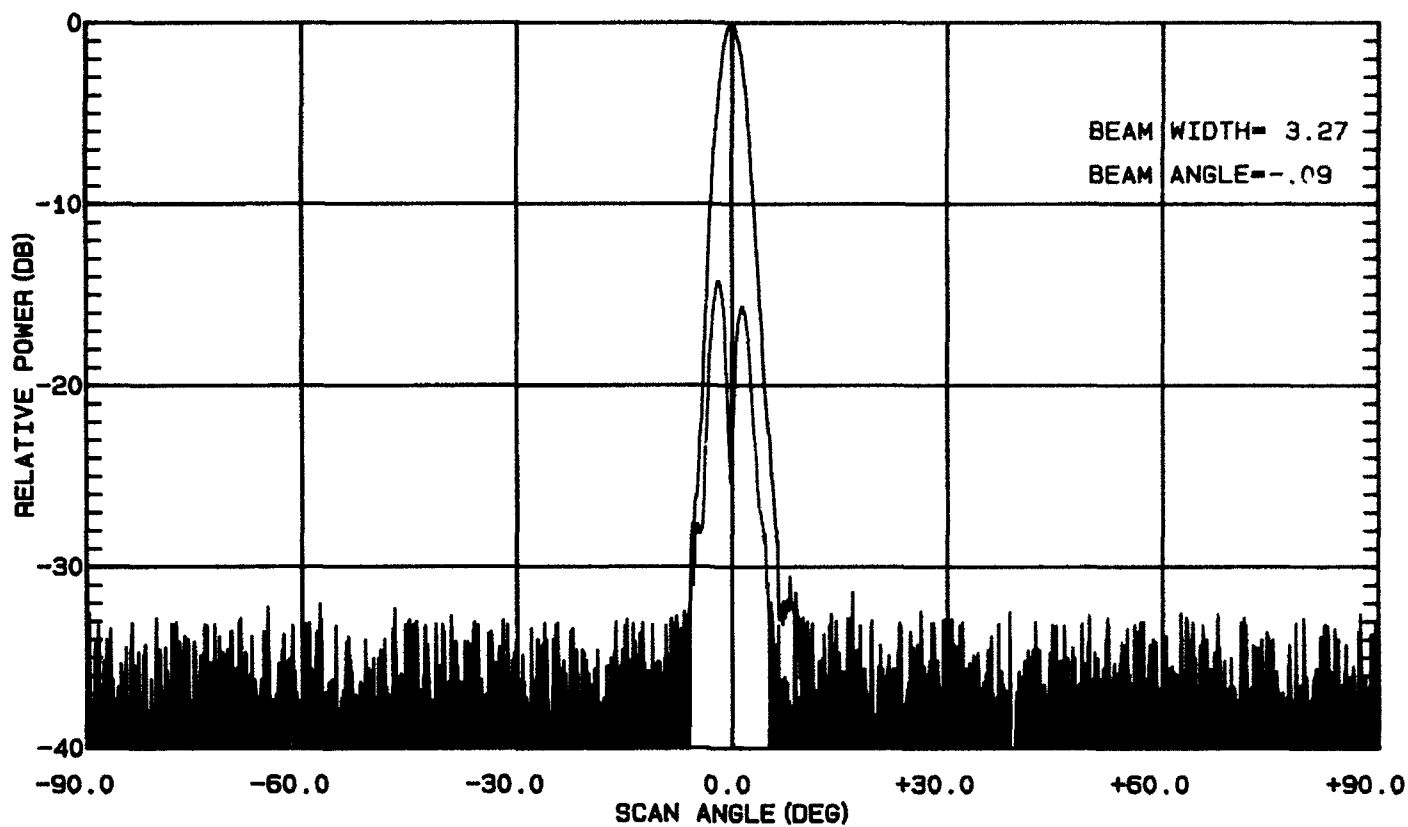


Figure 2.2-5. SSM/T-2 183.3 GHz antenna pattern.

### 2.2.1 Instrument Sensitivity

Since the SSM/T-2 has a total power radiometer receiver configuration, the radiometer sensitivity, i.e. the minimum detectable change in the radiometric antenna temperature  $\Delta T$  of the observed system is:

$$\Delta T = T_{sys} \left[ \frac{1}{B\tau} + \left( \frac{\Delta G}{G} \right)^2 + \left( \frac{\Delta T_v}{T_{sys}} \right)^2 + \left( \frac{\Delta T_q}{T_{sys}} \right)^2 \right]^{\frac{1}{2}}$$

where  $T_{sys}$  =  $T_A + T_{REC}$  (the system noise temperature),  
 $\Delta T$  = noise equivalent temperature difference,  
 $T_A$  = the scene TB incident on the antenna aperture,  
 $T_{REC}$  = the receiver input noise temperature,  
 $B$  = the predetection bandwidth,  
 $\tau$  = radiometer scene integration time,  
 $\frac{\Delta G}{G}$  = effects of characteristics associated with total power radiometer,  
i.e. gain fluctuations,  $\frac{1}{f}$  type electronic noise, power supply variations, etc.,  
 $\Delta T_v$  = RMS video electronic noise,  
 $\Delta T_q$  = RMS quantization noise.

By design the contributions to the  $\Delta T$  from the video and quantization noise are much smaller than the wide-band thermal noise term (i.e., the  $1/B\tau$  term). The contribution of  $\Delta G/G$  are minimized by employing stable components and frequent radiometer calibrations at the input to the antenna aperture.

The SSM/T-2 employs a calibration period of 8 seconds in which four samples are taken of a warm-load calibration target along with four samples of the cosmic background. The periodic calibration data are modeled by a linear transfer function to characterize the state of the total power radiometer and remove time variations of the receiver gain and offset for frequencies less than half the reciprocal of the calibration period. As a consequence relatively large temperature-related receiver gain drifts are taken into account in the periodic construction of the transfer function.

Ground based calibration estimates of the  $\Delta T$  are obtained by operating the SSM/T-2 in a thermal/vacuum chamber in a configuration that resembles actual orbital conditions. Two primary standard calibration targets operating in the range of 300 K and 80 K are sequentially viewed by the SSM/T-2 every 8 seconds for a duration of 4

samples. The warm primary standard is subsequently viewed for 28 samples which corresponds to the number of earth viewed scenes on orbit. This procedure is repeated until eight scans of data are collected. At this point the warm and cold calibration data are fitted by a linear transfer function to characterize the state of the radiometer over the eight scans. The sampled variance of the 224 samples ( $8 * 28$ ) of raw output counts is computed next and referenced to the input of the antenna aperture using the slope of the transfer function. This procedure is repeated many times, averaged and the square root taken to obtain an estimate of the  $\Delta T$ . Table 2.2.1-1 shows the  $\Delta T$ .

*Table 2.2.1-1. Calibration test results of the SSM/T-2 B5 unit aboard F-11.*

All Values K Baseplate Temperatures - Nominal 10 C, Low 5 C, High 25 C						
GHz	Channel	$\Delta T$ Nominal	$\Delta T$ High	$\Delta T$ Low	$\Delta T$ Required	Accuracy Required
$183.3 \pm 3$	1	0.50	0.53	0.50	$\leq 0.6$	$\leq 1.5$
$183.3 \pm 1$	2	0.44	0.43	0.49	$\leq 0.8$	$\leq 1.5$
$183.3 \pm 7$	3	0.64	0.60	0.63	$\leq 0.6$	$\leq 1.5$
91.655	4	0.43	0.43	0.41	$\leq 0.6$	$\leq 1.5$
150	5	0.49	0.50	0.47	$\leq 0.6$	$\leq 1.5$

### 2.2.2 Instrument Stability

An examination of the stability of the SSM/T-2 electronics has shown the instrument to be very stable. Figure 1.1-2 shows the absolute stability of the SSM/T-2 sensor. The differences are almost constant throughout the orbit.

Figure 1.1-3 shows the total noise (thermal and electronic) of the instrument over the calibration period of 8 consecutive scans.  $183.3 \pm 7$  and 150 GHz are the noisiest with standard deviations of approximately 5 counts (where 11 counts = 1 K). This translates to a "minimum detectable" temperature difference ( $\Delta T$ ) of 0.45 K. All these measurements are raw data with no thermal variations applied, thus both thermal and electronic noise variations are included. This approach assumes the worst case scenario for SSM/T-2 stability.



### 2.3 MIR Instrument

This section describes the MIR that has recently been developed by NASA Goddard Space Flight Center. The MIR is a 9-channel total power radiometer developed for atmospheric research. Three dual-pass band channels are centered about the strongly opaque 183.3 GHz water vapor absorption line; the frequencies are  $183.3 \pm 1$ ,  $\pm 3$ , and  $\pm 7$  GHz. Another channel is located on the wing of this line at 150 GHz. These four channels have varying degrees of opacity from which the water vapor profile can be inferred. In addition, there are two window channels located at 89 GHz and 220 GHz. The design includes three additional channels centered about the 325 GHz water vapor line which are to be supplied by Georgia Institute of Technology. The 325 GHz channels were not available for these campaigns and the 220 GHz channel was not utilized in this study.

The MIR is designed using total power radiometric principles. Low receiver noise temperature, wide bandwidth, stable temperature, and frequent through-the-lens calibration (every 3s) yield single-pixel temperature sensitivities of less than 1 K for all the channels. There are five lens/feedhorn antennas, each immediately followed by a double-side band mixer. The 89 GHz and 150 GHz channels use balanced mixers; the 183.3 GHz, 220 GHz, and 325 GHz use subharmonic mixers. Gain fluctuations and drifts in oscillator frequency are minimized by using proportional controllers to stabilize receiver component temperature. The IF mixer output is amplified 60 dB by a two-stage low-noise amplifier and bandpass filtered. A triplexer is used for the 183.3 GHz and 325 GHz channels to separate the received signal into three bands. Absolute calibration is performed every scan cycle by consecutively staring at the hot (~330 K) and cold (~250 K) calibration loads. The MIR is mounted in the fore body of the super wing pod on board the NASA ER-2 high altitude (~20 km) research aircraft (see photographs in Figure 2.3-1).

Table 2.3-1 summarizes characteristics of each channel (Racette et al., 1992). The sensitivity is calculated using a 75 ms integration period and gain variations factor of  $10^{-4}$ . During the SSM/T-2 underflights, the sensor was directed to view the hot and cold calibration targets sequentially on every scan and for an extended period of time every 30 minutes. Analysis of the ~360 radiometric samples from either the hot or cold calibration targets, gave an estimation of the actual temperature sensitivity ( $\Delta T$ ) of the sensor. For the three window channels at 89, 150 and 220 GHz,  $\Delta T$  is on the order of 0.2 K, which is comparable to that from theoretical calculations. For the other three channels near 183.3 GHz,  $\Delta T$  is about 0.5 K, which is somewhat higher than those given in Table 2.3-1.

The temperature distribution on the hot and cold calibration targets is measured using an array of eight resistive temperature devices (RTDs) embedded in each target.

*Table 2.3-1. MIR receiver characteristics.*

Center Frequency (GHz)	IF Pass Band (GHz)	Receiver Temperature (K)	Sensitivity (K)
89.0	1.0 ± 0.5	< 630	< 0.2
150.0	1.0 ± 0.5	< 860	< 0.2
183.0	1.0 ± 0.5	< 2000	< 0.4
	3.0 ± 1.0		< 0.3
	7.0 ± 1.0		< 0.3
220	2.5 ± 1.5	< 2000	< 0.3
325	1.0 ± 0.5	< 3500	< 0.6
	3.0 ± 1.0		< 0.5
	8.5 ± 1.5		< 0.5

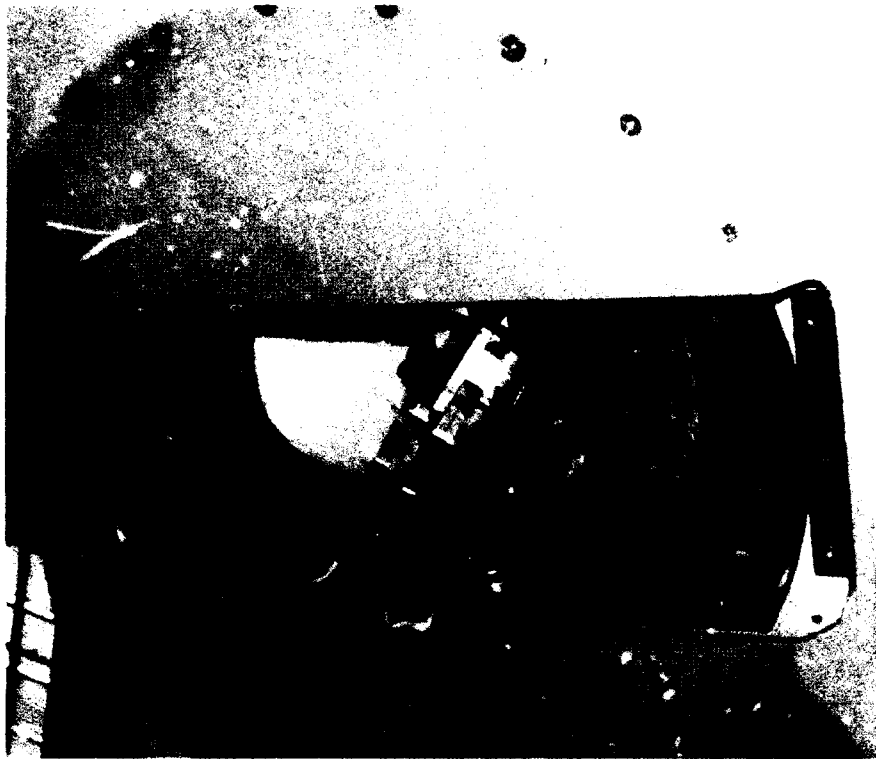
Thermal gradients during the flights were found to be no greater than  $\pm 0.5$  K across the targets. This suggests that the probable error in the calibrated MIR TB should be less than  $\pm 1$  K in the TB range of 250 - 330 K. The measured TBs for the three 183.3 GHz channels fall in this range. For the 89 GHz channel, the measured TB over the ocean surface could be as low as 200 K and the error in the radiometric measurements could exceed 1 K. The calibration accuracy of the MIR in the temperature range outside of that defined by the hot and cold calibration targets is currently under investigation.

Each of the four receiver channels (89, 150, 183.3 and 220 GHz) has its own antenna system, which consists of a corrugated feed horn and lens. All the lenses have surface-matching grooves on both sides to maximize beam efficiency. Table 2.3-2 summarizes the E- and H-plane half-power beamwidths and first side-lobe levels. Figures 2.3-2 and 2.3-3 show the typical E-plane antenna patterns measured at 89 GHz and 183.3 GHz respectively. Scanning of the beam patterns is achieved by rotating a flat gold-plated reflector. The antenna beam efficiency exceeds 92% for all four receiver channels.

*Table 2.3-2. MIR half-power beamwidths and first side-lobe levels.*

Antenna Pattern Summary	Beamwidth		1st Sidelobe	
	E-Plane	H-Plane	E-Plane	H-Plane
89 GHz	3.2°	3.6°	24 dB	25 dB
150 GHz	3.3°	3.3°	24 dB	21 dB
183.3 GHz	3.5°	3.5°	29 dB	27 dB
220 GHz	3.3°	3.4°	27 dB	30 dB

a



b

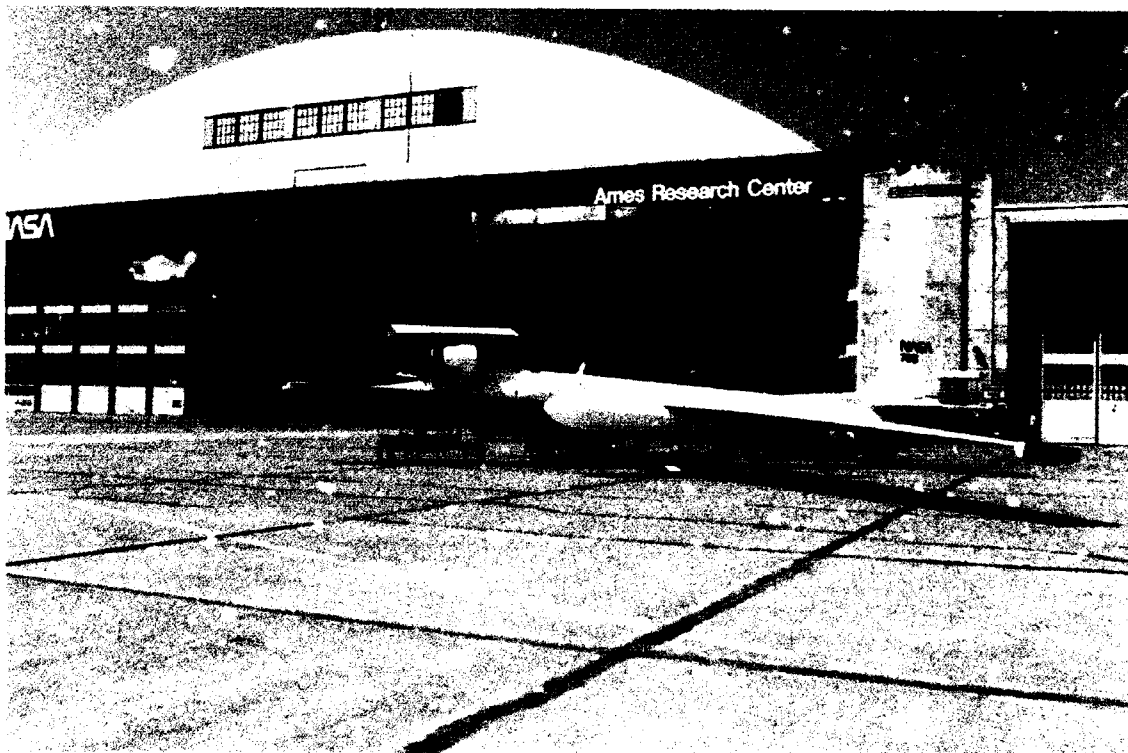


Figure 2.3-1. Photographs of the MIR (a), which is mounted in the fore body of the super wing pod on board the NASA ER-2 high altitude (~20 km) research aircraft (b).

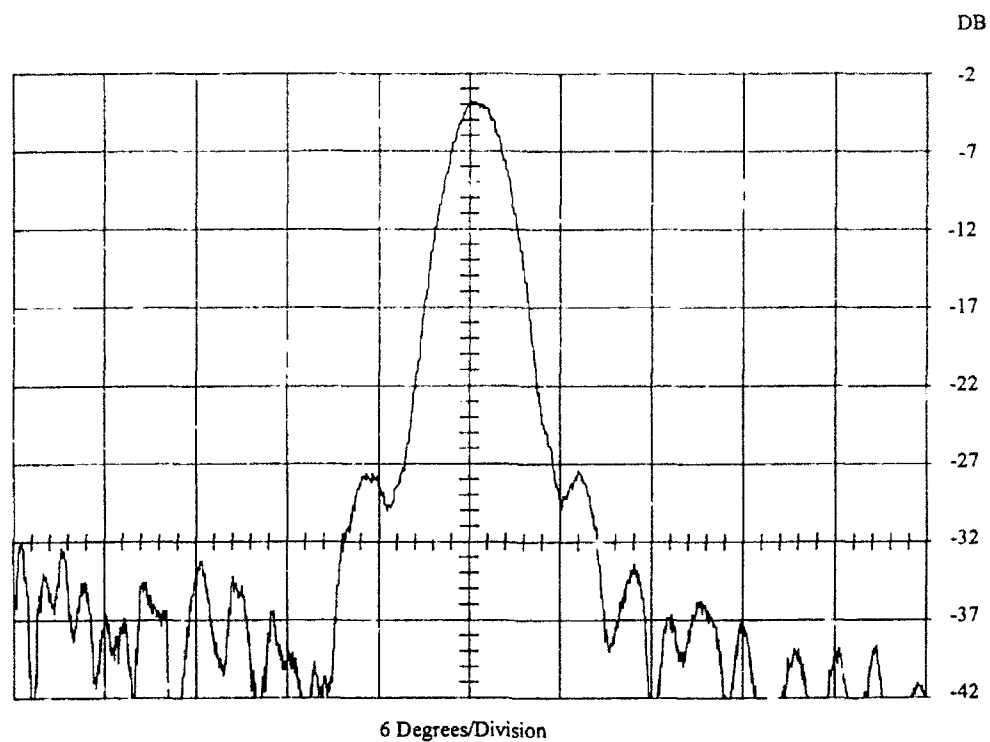


Figure 2.3-2. The typical E-plane antenna pattern measured at 89 GHz.

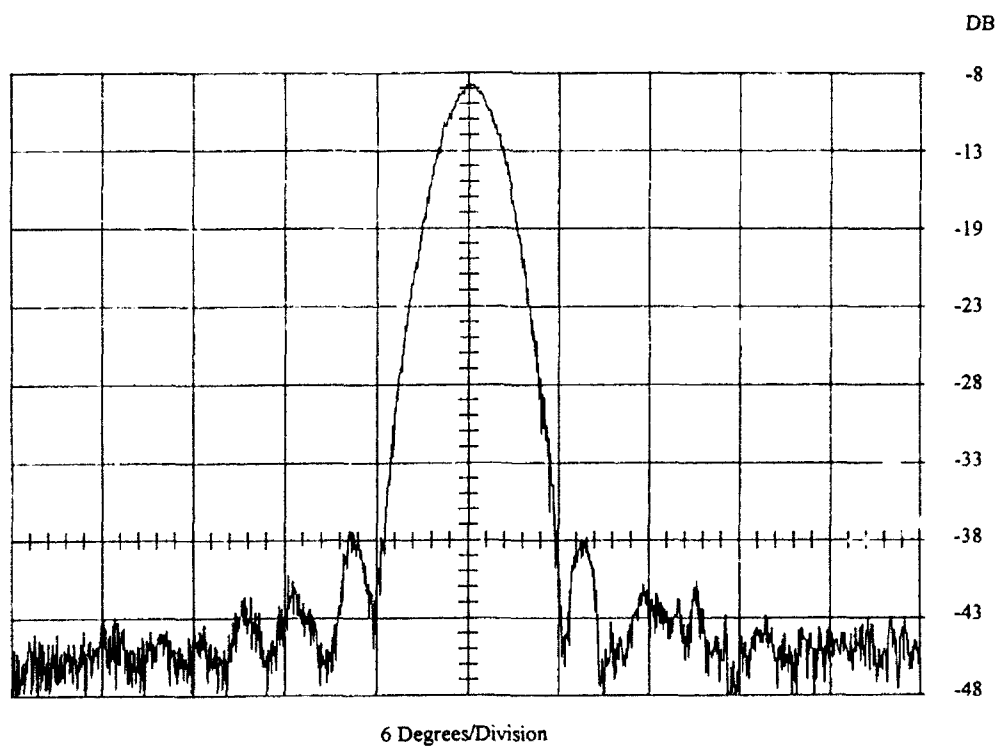


Figure 2.3-3. The typical E-plane antenna pattern measured at 183.3 GHz.

## 2.4 Description of Aircraft Campaigns

Weather support for the calibration/validation effort was critical. In calibrating the SSM/T-2 a comparison of the same scene as viewed by the satellite and by a similar instrument (MIR) on a high altitude aircraft (ER-2) are compared. Since both instruments are affected by water vapor and clouds of varying degrees, the atmospheric conditions have to be known before flights are made. In theory, what must be known before flight time is satellite track, aircraft track, cloud and earth surface properties. The latter condition of earth surface properties is required because the window channels (91 and 150 GHz) and possibly  $183.3 \pm 7$  GHz see the surface. The "best" possible flight conditions for calibration and validation are a cloudless atmosphere over a flat (no wind) ocean surface. The satellite and aircraft should view the same varied atmosphere (with the exception of a frontal system which is too inhomogeneous in water vapor and clouds within a field-of-view) and as varied an earth surface as possible.

### 2.4.1 West Coast Aircraft Campaign

The proposed flight path of the ER-2 along the west coast of California was to traverse as much dissimilar terrain as possible in order to gather data from a wide variety of atmospheric paths and underlying surfaces. Roughly half the time airborne was spent over the water due to the belief that the best calibration is over ocean surfaces. Also, in order to test the time variance of water vapor at a specific location, the flight path was to have overlapping segments. The path was chosen to pass near the sites of a number of radiosonde launch events which were coordinated with the SSM/T-2 overpass. In particular, Vandenberg AFB, Point Magu and San Nicolas Island radiosonde stations provided additional non-synoptic soundings during the two days that the ER-2 flew. The proposed flight plan along the west coast, shown in Figure 1.2-1, is given below:

- 1) Take off from Moffet Field and fly east-southeastward to Mt. Whitney,
- 2) turn southeastward to China Lake Naval Air Station,
- 3) turn south-southwestward over Los Angeles to Santa Catalina,
- 4) turn westward and fly over San Nicolas Island to the satellite subtrack point (0050 UTC for 15 May) arriving at the position 33 N 122 W at the time of the satellite overpass for that day,
- 5) turn north-northwestward, parallel to the satellite subtrack for 15 May 0050 UTC until north of 35 N,
- 6) turn northeastward and fly to Fresno,
- 7) turn southeastward to Bakersfield,
- 8) turn south-southwestward and fly over Los Angeles to Santa Catalina,
- 9) turn westward and fly over San Nicolas Island to the satellite subtrack point,

- 10) turn north-northwestward, parallel to the satellite subtrack of 15 May 0050 UTC until north of 35 N, and
- 11) return to Moffet Field.

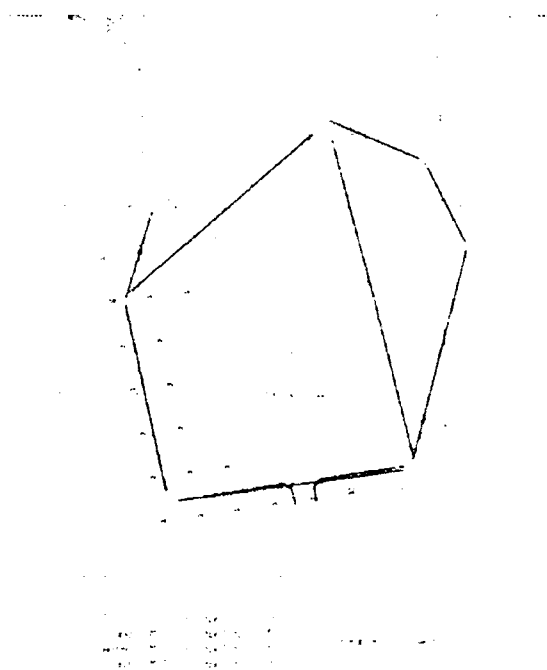
The ER-2 flights were made on May 14 and 15 (NOTE: the dates May 14 and 15 are based on local time, roughly 1700 local time; in universal time, the flights were made on May 15 and 16 at roughly 0050 UTC. For the purposes of this report, unless UTC is specified, the dates will refer to local time), with the only deviation from the above flight path arising from restricted airspace clearance not being given for a second overpass of China Lake NAS on 14 May, forcing the ER-2 to turn towards Los Angeles before reaching Bakersfield (7-8 above) (Figures 2.4.1-1 a-c and 2.4.1-2 a-c). On both days, low, thin stratus were located off the California coast, with some clear patches over water and clear over land as depicted by the visible GOES imagery (Figures 2.4.1-3 and 2.4.1-4). Also shown are the ER-2 flight tracks and SSM/T-2 FOV center locations.

On May 14, weak high pressure was located off the California coast with weak low pressure inland. This synoptic situation forced dry air southward along the California coast resulting in large areas of clear to scattered skies within 200 kilometers of the coast line. Inland was mostly clear with scattered cirrus clouds over central and southern California.

The synoptic situation on May 15 was dominated by a large ocean storm located several hundred kilometers off the California coast. The storm produced onshore flow and widespread low, thin, stratiform clouds over ocean areas. Inland sections remained mostly clear.

After the flights, NASA analyzed the MIR data, and Aerospace collected the SSM/T-2 data at AFGWC. In order to make the data more compatible with the calibration effort, NASA averaged the MIR data into 32 - 3° scan angle bins across the swath, with scan angles ranging  $\pm 48^\circ$ . The FOV of the averaged 3° values was 1 km in diameter at nadir.

**a (91 GHz)**



**b (150 GHz)**

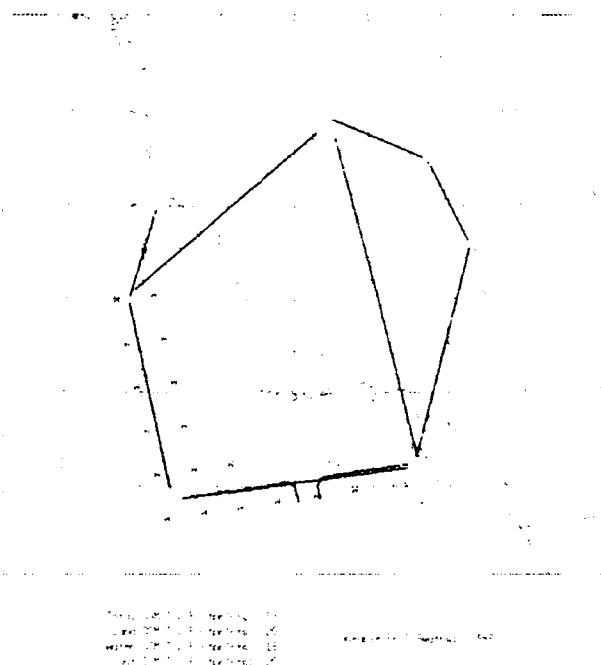
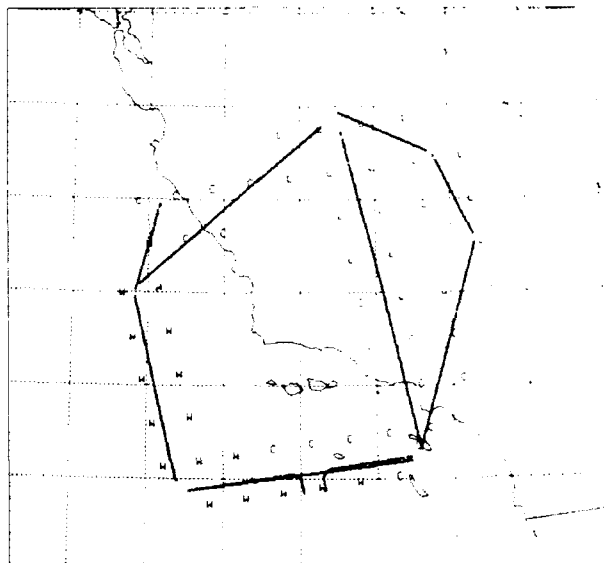


**Figure 2.4.1-1 a-c.** The positions and topographic distributions of SSM/T-2 FOVs that have co-located MIR data for roughly 0100 UTC May 15, 1992. The land (L), water (W) and coastal (C) classifications were determined by AFGWC. The fine dots represent the nadir positions of the MIR data. Usable MIR data were defined as data collected when the aircraft was above 19 km altitude and had a pitch and roll of less than 3°.

**c (183.3 GHz)**



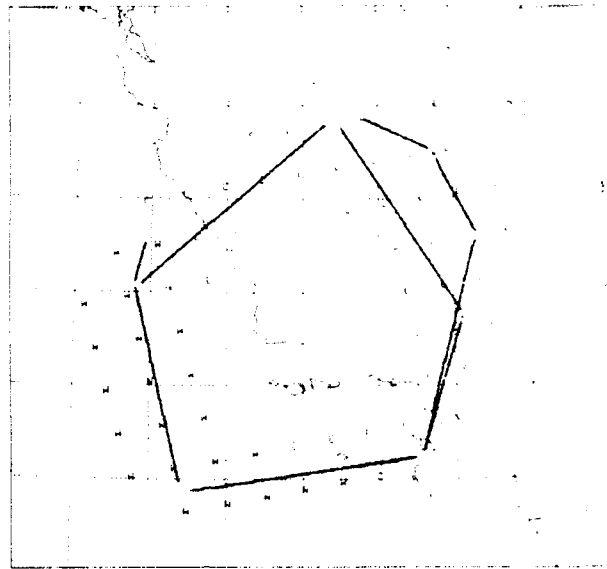
Total SSN/T-2 Footprint: 55  
Land SSN/T-2 Footprint: 19  
Water SSN/T-2 Footprint: 17  
Coast SSN/T-2 Footprint: 19

Useable EP-2 Swaths: 142

*Figure 2.4.1-1. (continued).*



**a (91 GHz)**



**b (150 GHz)**

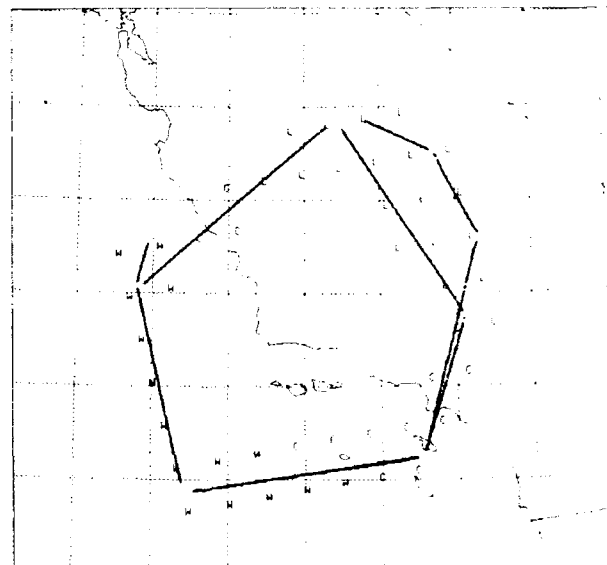


**Figure 2.4.1-2 a-c.** The positions and topographic distributions of SSM/T-2 FOVs that have co-located MIR data for roughly 0100 UTC May 16, 1992. The land (L), water (W) and coastal (C) classifications were determined by AFGWC. The fine dots represent the nadir positions of the MIR data. Usable MIR data were defined as data collected when the aircraft was above 19 km altitude and had a pitch and roll of less than 3°.

**c (183.3 GHz)**

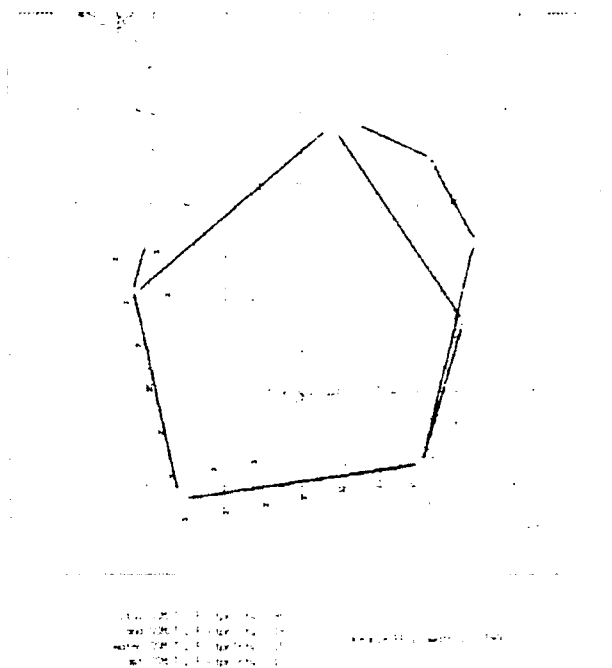


*Figure 2.4.1-2. (continued)*

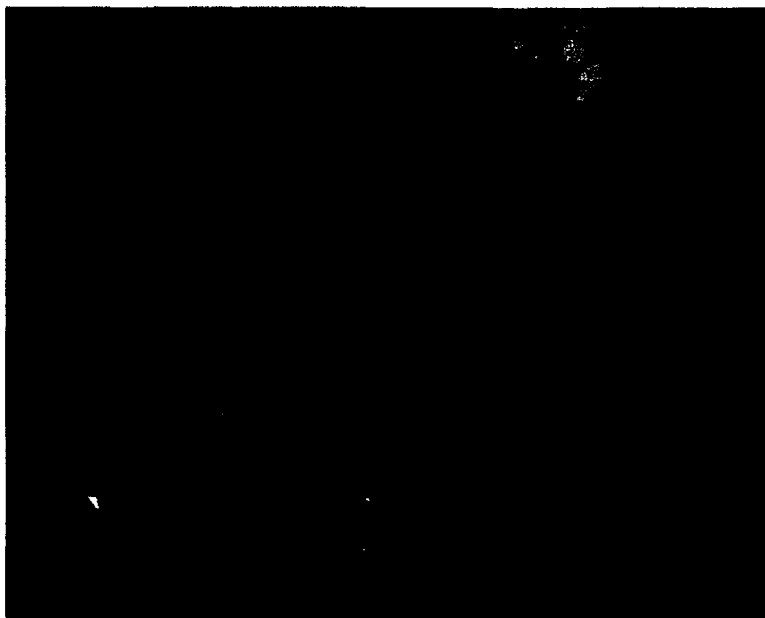


*Figure 2.4.1-3. Visible GOES imagery at 2330 UTC May 14 , 1992.*

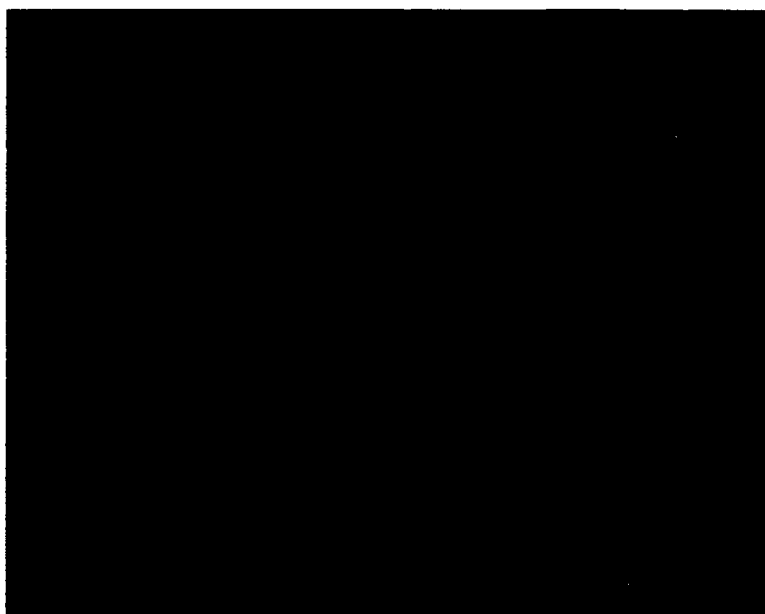


*Figure 2.4.1-4. Visible GOES imagery at 0030 UTC May 16, 1992..*

## 2.4.2 East Coast Aircraft Campaign

The two months separation between the west coast and east coast flights allowed time for some analysis of the May data set. The preliminary analysis of the west coast flights showed excellent agreement between the two instruments (SSM/T-2 and MIR) over water ( $\sim 1$  K). Data recorded by Aerospace concerning SSM/T-2 stability, showed the SSM/T-2 to be very stable (see Figure 1.1-2). These early results allowed Phillips Laboratory to declare that the SSM/T-2 was performing within or exceeding the original specifications and that for operational utilization there are no apparent or consistent instrument biases.

The early positive results allowed greater flexibility in the choice of aircraft flights on the east coast. It was decided that all weather systems be overflown with the ultimate goal of investigating atmospheric water vapor from clear to cloudy to rainy atmospheres, including frontal systems. The ER-2 flight paths of 29 and 30 July and 6 August were chosen to be the same without regard for the weather. The flight paths were chosen so as to fly over varied earth surfaces (land, ocean and coast) with emphasis on ocean surface temperature variations from 285 K in the Gulf of Maine to 297 K off Cape Hatteras and crossing the Gulf Stream. Also, as with the west coast flights, the flight path was to have overlapping segments in order to test the time variance of water vapor at a specific location. A number of National Weather Service (NWS) radiosonde launch sites provided additional non-synoptic soundings during the three days that the ER-2 flew along the east coast: Atlantic City (New Jersey), Albany (New York), Caribou (Maine), Chatham (Massachusetts), Cape Hatteras (North Carolina), and Portland (Maine). The proposed flight plan along the east coast, shown in Figure 1.2-2, is given below:

- 1) Take off from Wallops Island (37.85N 75.48W) and fly due west for 200 km during ascent,
- 2) turn and fly back across Wallops Island along a due east heading; fly past Wallops Island out over the ocean to the great circle arc intersecting Chatham (41.66N 69.96W) and Cape Hatteras (35.26N 75.55W),
- 3) turn and fly toward Chatham along the great circle arc intersecting Chatham and Cape Hatteras,
- 4) after flying over Chatham and reaching the latitude of Portland, Maine (43.65N), turn to a due west course,
- 5) fly for 200 km passing past Portland, Maine (43.65N 70.31W) along the due west heading,
- 6) turn and fly back to Chatham,
- 7) at Chatham, turn and follow the same great circle track that was initially followed to Cape Hatteras,
- 8) at Cape Hatteras, turn and fly to Wallops Island,

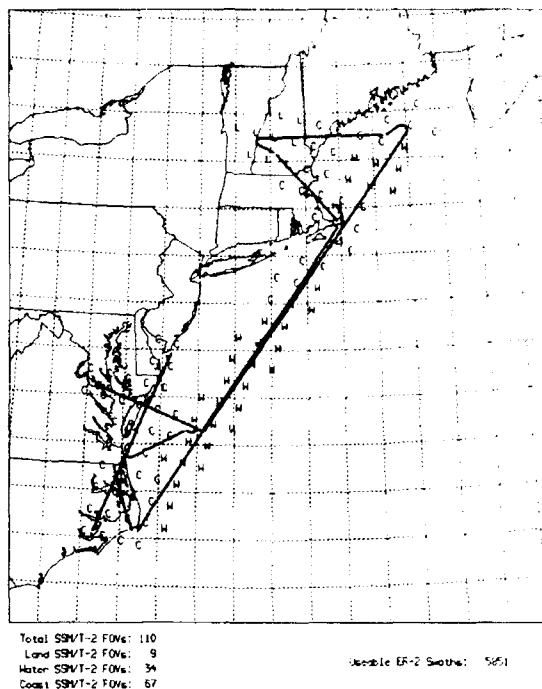
- 9) at Wallops Island, turn due east and fly to point that intersects the great circle arc between Chatham and Cape Hatteras,
- 10) at intersection, turn to a westward heading, flying back across Wallops Island, 200 km inland, and
- 11) turn and land at Wallops Island.

The only difference between the flight paths during each day of flying was the timing of the ER-2 with respect to that day's F-11 overpass. The ER-2 aircraft was required to be at roughly the halfway point of the flight (based on the total estimated flight time) at the time of the F-11 overpass. Figures 2.4.2-1 a-c through 2.4.2-3 a-c show the ER-2 flight path and SSM/T-2 FOVs for July 29 and 30 and August 6, 1992, respectively.

The ER-2 flights were made on July 29 and 30 and August 6. GOES visible imagery (Figures 2.4.2-4 through 2.4.2-6) show the cloud cover over the eastern seaboard for the three days (imagery is valid at 1230 UTC for each day). During the early morning hours of July 29, weak high pressure over the mid-Atlantic states resulted in mostly clear skies from New England to Cape Hatteras. On July 30, a cold front had passed through New England overnight and was located just offshore at daybreak. Extensive strato-cumulus clouds and fog were located over coastal sections with light rain showers just offshore. Broken clouds were present over inland sections of New England. The front was stalled along the mid-Atlantic coast where broken clouds and scattered thunderstorms were present. On August 6, high pressure was building into the New England and mid-Atlantic states, scattered clouds were present over inland areas from Maine southward to Maryland. Overcast skies and scattered showers were observed in Virginia and North Carolina. Broken clouds were present offshore from Maine to North Carolina.

The same procedure for MIR calibration and collection used for the west coast flights was followed for these flights. Again, NASA averaged the MIR data into 32-3° scan angle bins across the swath, with scan angles ranging  $\pm 48^\circ$  and FOVs of the averaged 3° values was 1 km in diameter at nadir.

**a (91 GHz)**



**b (150 GHz)**

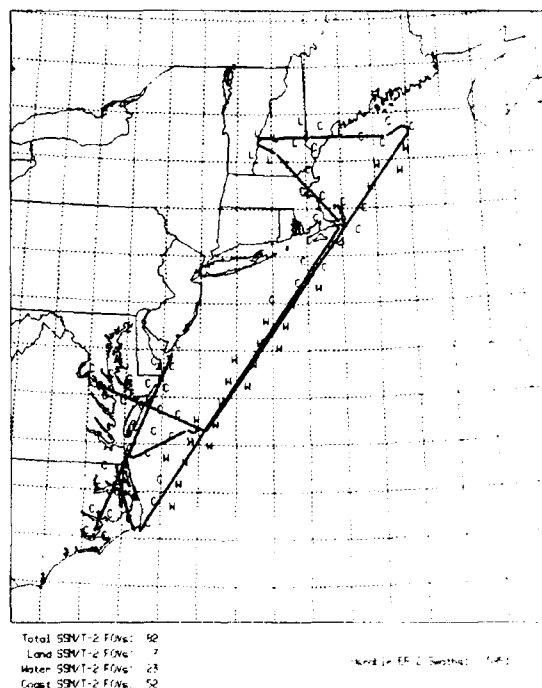
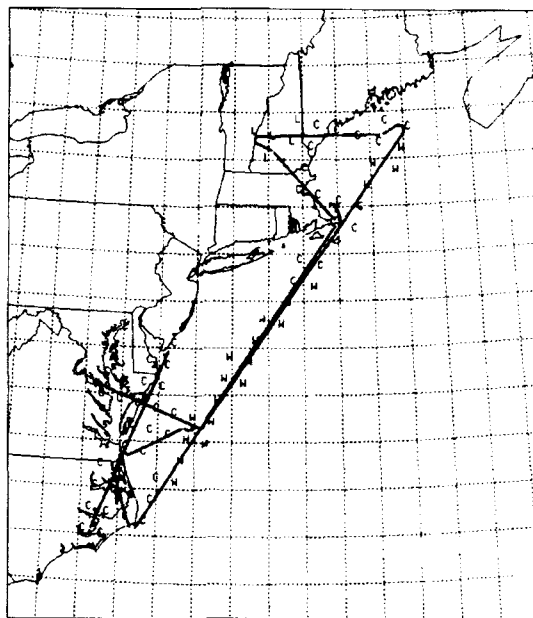


**Figure 2.4.2.1 a-c.** The positions and topographic distributions of SSM/T-2 FOVs that have co-located MIR data for roughly 1041 UTC July 29, 1992. The land (L), water (W) and coastal (C) classifications were determined by AFGWC. The fine dots represent the nadir positions of the MIR data. Usable MIR data were defined as data collected when the aircraft was above 19 km altitude and had a pitch and roll of less than 3°.

c (183.3 GHz)

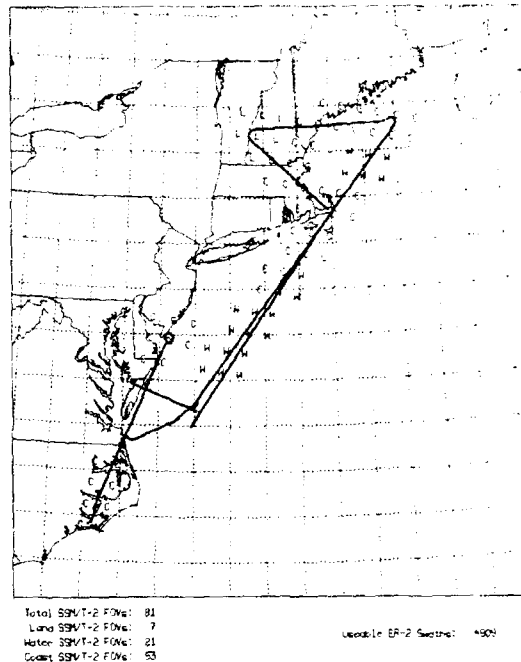


Total SSM/T-2 FOVs: 73  
Land SSM/T-2 FOVs: 6  
Water SSM/T-2 FOVs: 20  
Coast SSM/T-2 FOVs: 47

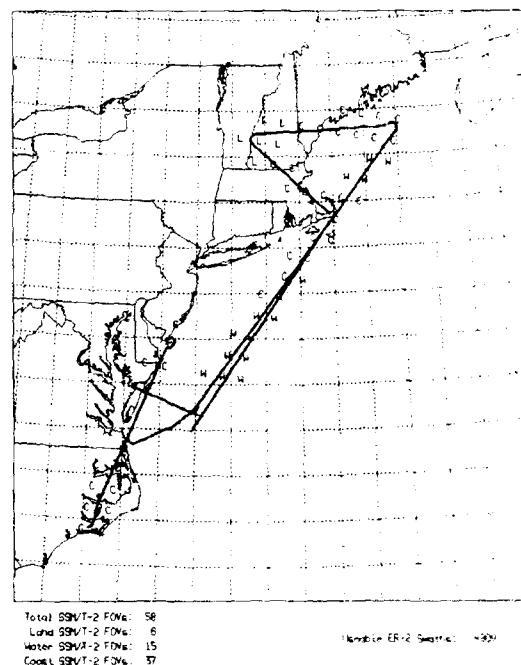
Useable ER-2 Swaths: 5851

Figure 2.4.2-1. (continued).

**a (91 GHz)**



**b (150 GHz)**



*Figure 2.4.2-2 a-c. The positions and topographic distributions of SSM/T-2 FOVs that have co-located MIR data for roughly 1028 UTC July 30, 1992. The land (L), water (W) and coastal (C) classifications were determined by AFGWC. The fine dots represent the nadir positions of the MIR data. Usable MIR data were defined as data collected when the aircraft was above 19 km altitude and had a pitch and roll of less than 3°.*



c (183.3 GHz)

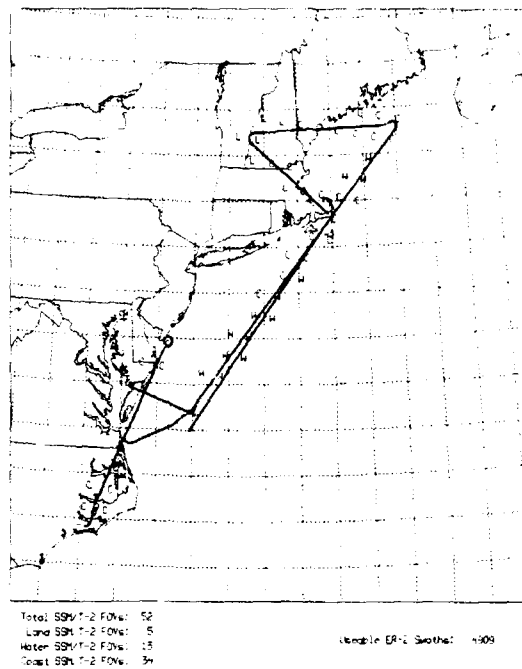
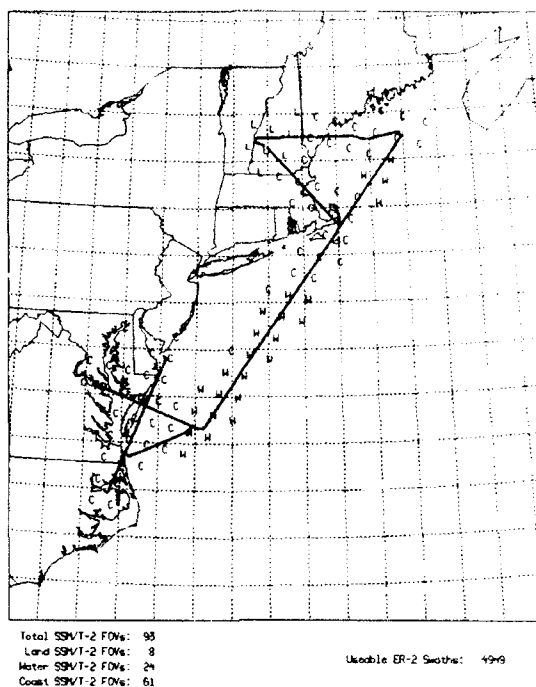
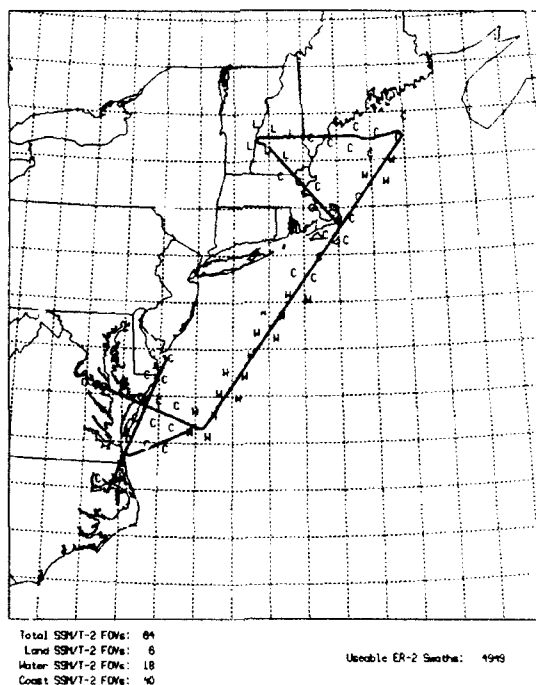


Figure 2.4.2-2. (continued).

**a (91 GHz)**



**b (150 GHz)**



**Figure 2.4.2-3 a-c.** The positions and topographic distributions of SSM/T-2 FOVs that have co-located MIR data for roughly 1040 UTC August 6, 1992. The land (L), water (W) and coastal (C) classifications were determined by AFGWC. The fine dots represent the nadir positions of the MIR data. Usable MIR data were defined as data collected when the aircraft was above 19 km altitude and had a pitch and roll of less than 3°.

c (183.3 GHz)

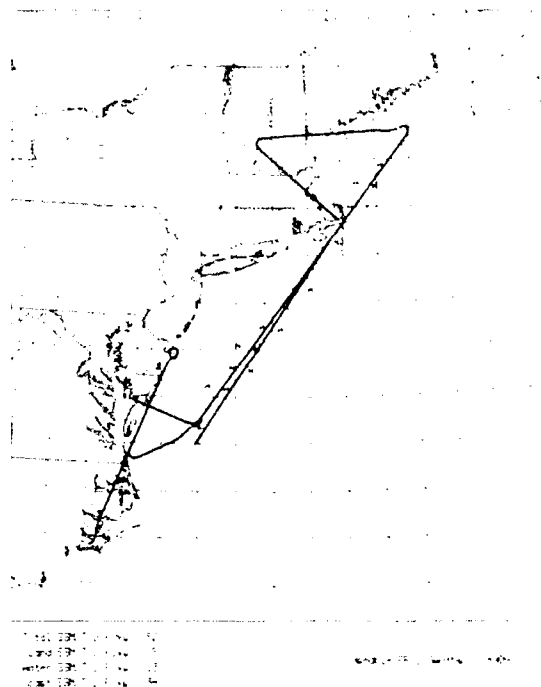
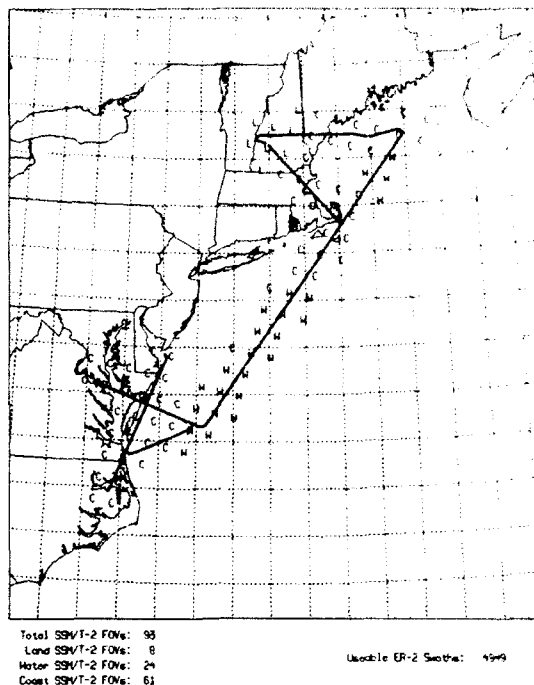
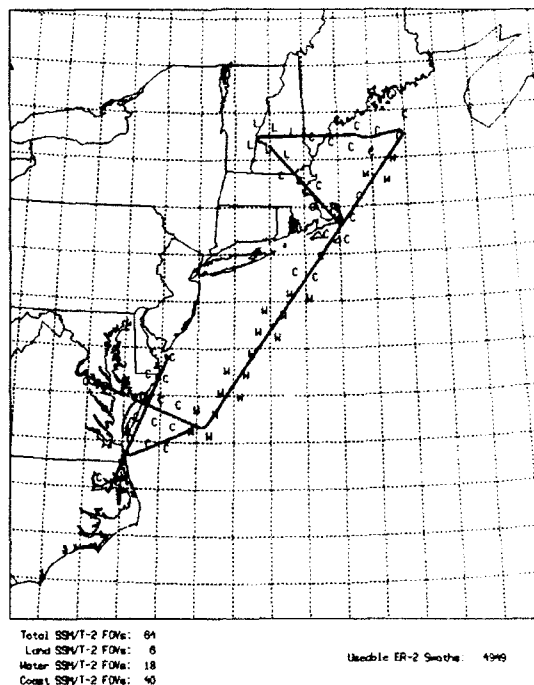


Figure 2.4.2-2. (continued).

**a (91 GHz)**



**b (150 GHz)**



**Figure 2.4.2-3 a-c.** The positions and topographic distributions of SSM/T-2 FOVs that have co-located MIR data for roughly 1040 UTC August 6, 1992. The land (L), water (W) and coastal (C) classifications were determined by AFGWC. The fine dots represent the nadir positions of the MIR data. Usable MIR data were defined as data collected when the aircraft was above 19 km altitude and had a pitch and roll of less than 3°.

c (183.3 GHz)

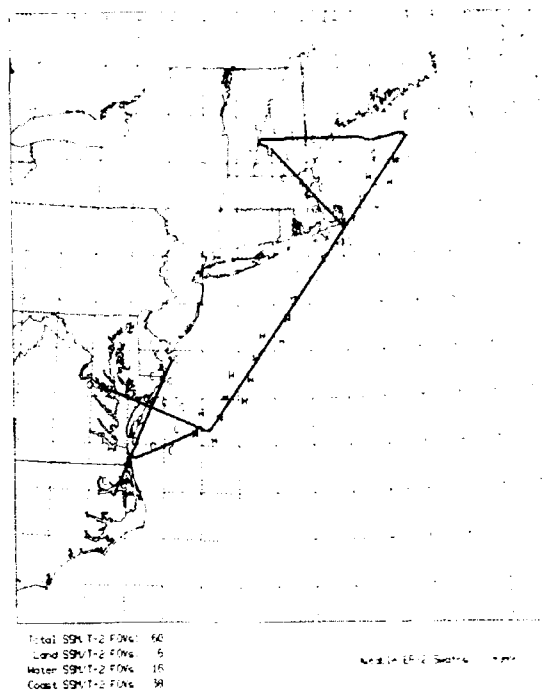
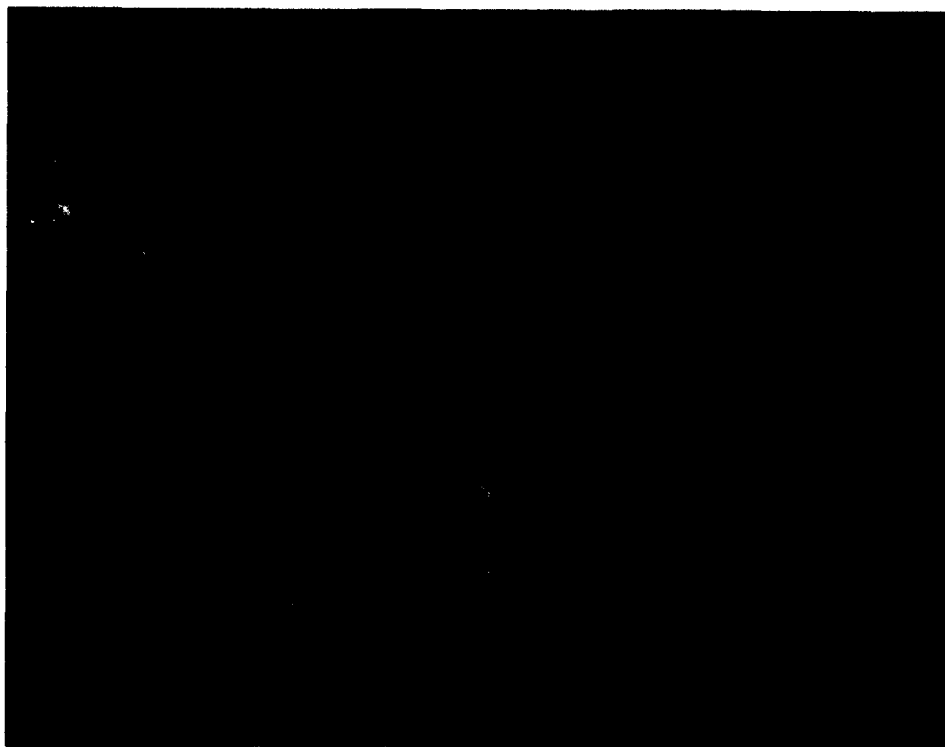
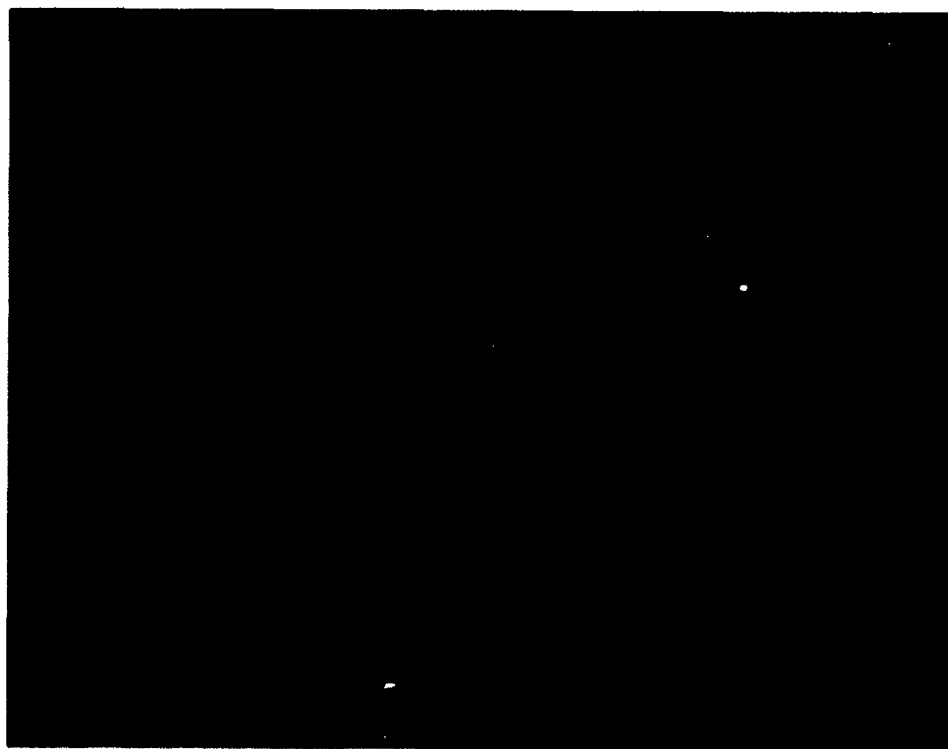


Figure 2.4.2-3. (continued).



*Figure 2.4.2-4. Visible GOES imagery at 1230 UTC July 29, 1992.*



*Figure 2.4.2-5. Visible GOES imagery at 1230 UTC July 30, 1992.*

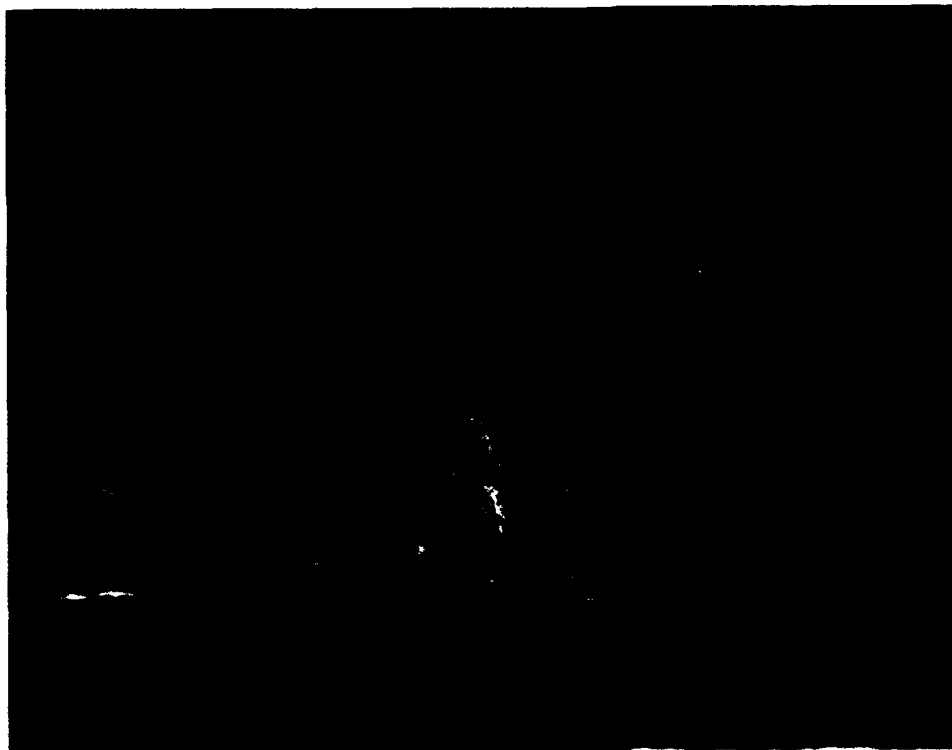


*Figure 2.4.2-6. Visible GOES imagery at 1230 UTC August 6, 1992.*

## 2.5 SSM/T-2 to MIR Co-locations

Co-locations of SSM/T-2 and MIR measurements were determined by calculating the distance between the center of the MIR FOV and the center of the SSM/T-2 FOV. co-location thresholds were defined for each channel frequency based on beamwidth for each SSM/T-2 channel (see Table 2.2-1). There was an adjustment made for the elliptical deformation of the FOV away from the SSM/T-2 subtrack (Figure 2.2-1). Since only the latitude and longitude of the ER-2 subtrack point were provided in the MIR data set, the latitude and longitude of each of the MIR FOVs across the swath had to be calculated. This was done by first calculating the heading of the ER-2 from positions during the previous 60 seconds of flight, and using this value along with the scan angle to compute the latitude and longitude of the FOVs across the swath. In order to minimize atmospheric path length effects on the MIR TB and ensure accuracy in the location of the MIR FOV, data were used only if the aircraft was at an altitude greater than 19 km with an aircraft pitch and roll less than 3°.

The SSM/T-2 data were limited to scan angles less than 28.5° due to operational processing of the SSM/T-1 and SSM/T-2 data at AFGWC. This limitation was imposed on the MIR data so that all scan angles greater than 28.5° were not used in this study. From this abbreviated database, two data sets of co-located SSM/T-2 and MIR data were created: the first containing only MIR data with the same scan angle as the co-located SSM/T-2 FOV and the second using all of the MIR data with scan angles  $\leq 28.5^\circ$  which fell within the SSM/T-2 FOVs regardless of MIR scan angle. In addition, since the ER-2 flight paths contained overlapping tracks, the time difference between the SSM/T-2 and MIR measurements was also calculated.

Figures 2.4.1-1 a-c and 2.4.1-2 a-c show the west coast ER-2 flight paths and the positions and topographic background classifications determined by AFGWC of the SSM/T-2 FOVs for the 91, 150 and 183.3 GHz channels that have co-located MIR data for May 14 and 15, respectively. The background stratification of land (L), water (W) and coast (C) is taken from the AFGWC fixed field data base (XFIX64), an eighth-mesh (48 km) gridded database (Kiess and Cox, 1988). For displays of the SSM/T-2 FOV topographic classifications for both the entire west coast and east coast regions, see Appendix C. In addition, the displays of the five SSM/T-2 channel TBs measured for both the west coast and east coast regions are shown in Appendix C. Figures 2.4.2-1 a-c, 2.4.2-2 a-c, and 2.4.2-3 a-c show the east coast ER-2 flight paths and the positions and topographic background classifications of the SSM/T-2 FOVs that have co-located MIR data for July 29 and 30 and August 6, respectively. Gaps or missing segments of the ER-2 flight paths are a result of the altitude and pitch/roll restrictions described above. The 91 GHz channel displayed more SSM/T-2 FOV co-locations than the higher frequency channels since the FOV beamwidth of the FOV is almost twice that of the higher frequencies, resulting in more overlapping fields-of-view.



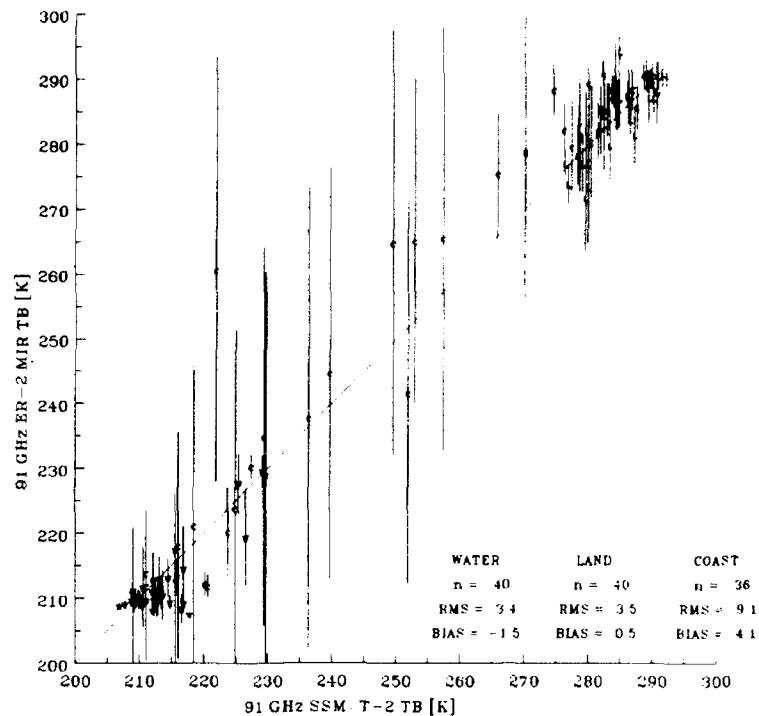
## 2.6 Comparison of SSM/T-2 and MIR Data

### 2.6.1 SSM/T-2 / MIR Comparisons Stratified by Topographic Background

SSM/T-2 data was stratified by topographic background to provide a dynamic range between low and high emissivity surfaces. For the combined west coast data, the SSM/T-2 TBs are compared to the mean co-located MIR TBs for the five channels of the SSM/T-2 sensor in Figure 2.6.1-1 a-e. The east coast data comparisons are presented in Figure 2.6.1-2 a-e. Unless stated otherwise, all MIR comparison data were limited to  $\pm 1$  hour of the time of the SSM/T-2 observations and to only those which had the same scan angle as the co-located SSM/T-2 data. The topographic backgrounds of the SSM/T-2 FOVs (land = L, water = W, and coastal = C) were determined by AFGWC and did not vary for the five sensor channel FOVs. The root mean square (RMS) and bias differences between the mean values of the co-located MIR data and the SSM/T-2 values were calculated for the three topographic backgrounds. In all cases, both the 91 and 150 GHz channels display large variations between the MIR and SSM/T-2 measurements for the coastal FOVs and considerably smaller variations for the land and water areas. This is due in part to large variations in surface emissivity (and hence observed TBs) for coastal FOVs where MIR FOVs over land and water areas are combined for comparison to a single SSM/T-2 measurement.

For the 89 GHz channel, examining the variance of MIR data within SSM/T-2 FOVs that are classified as water for both the west coast and east coast (Figures 2.6.1-3 a-e) reveals that the amount of variation of the MIR measurements within each SSM/T-2 FOV appears to be related to the distribution of clouds in the SSM/T-2 FOVs. Along the west coast and discounting the water-classified 89 GHz FOVs near Santa Catalina, the highest variance occurred where a cloud boundary appeared within the SSM/T-2 FOV. Since the GOES satellite images are 30 minutes apart and the ER-2 flights are greater than 4 hours in duration, it is difficult to precisely define the cloud boundaries within the SSM/T-2 and MIR FOVs. A more in-depth study of the relationship between the MIR and SSM/T-2 measurements of clouds in the FOVs will be considered in the near future.

**a (91 GHz)**



**b (150 GHz)**

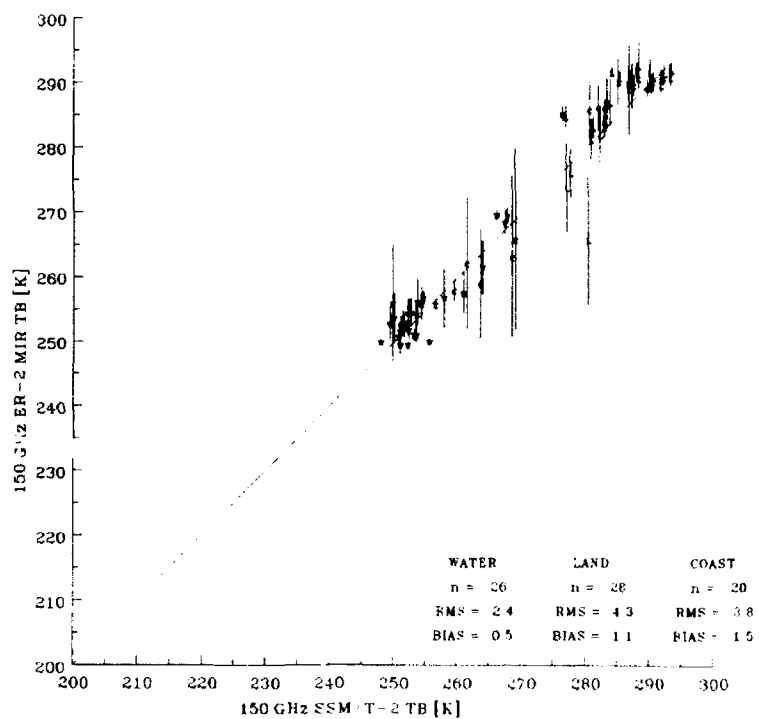
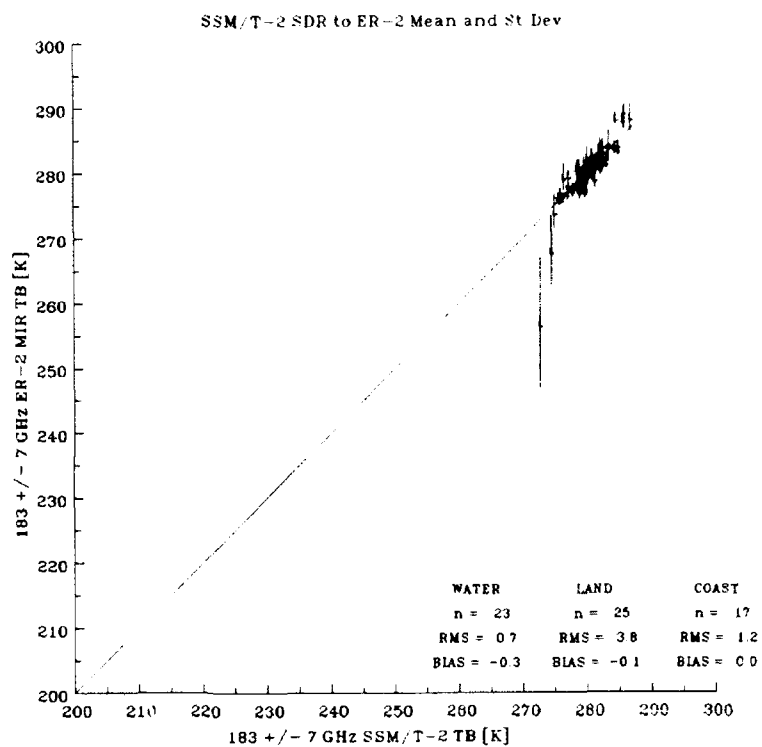


**Figure 2.6.1-1 a-e.** Comparison of SSM/T-2 TBs to the mean co-located MIR TBs for the five channels of the SSM/T-2 sensor of the west coast data. Vertical bars represent one standard deviation of the co-located MIR data in each SSM/T-2 FOV. MIR data were limited to  $\pm 1$  hour of the time of the SSM/T-2 observations and to only those which had the same scan angle as the co-located SSM/T-2 data. The topography of the SSM/T-2 FOVs is land = L, water = W, and coastal = C.

**c (183.3 ± 7 GHz)**



**d (183.3 ± 3 GHz)**

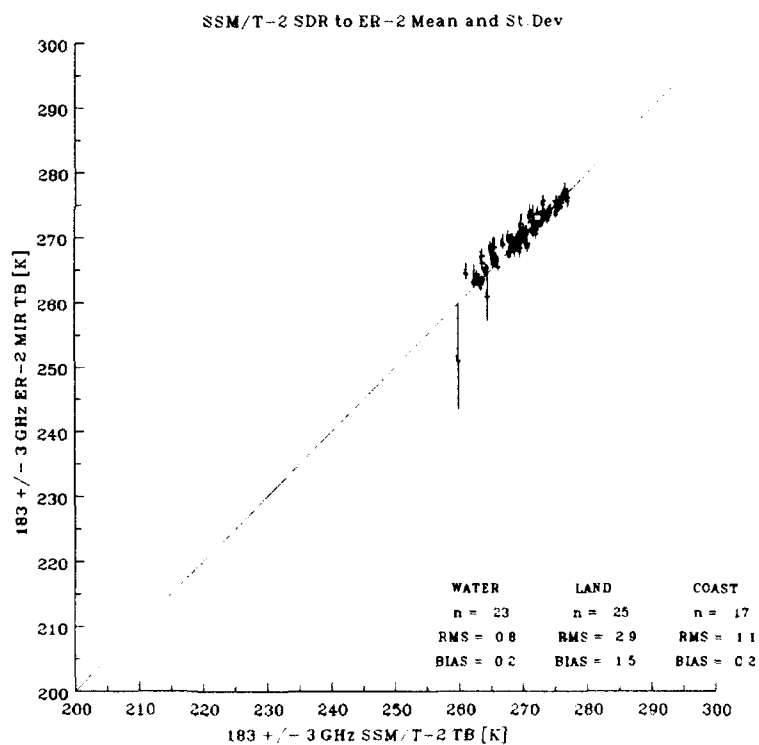
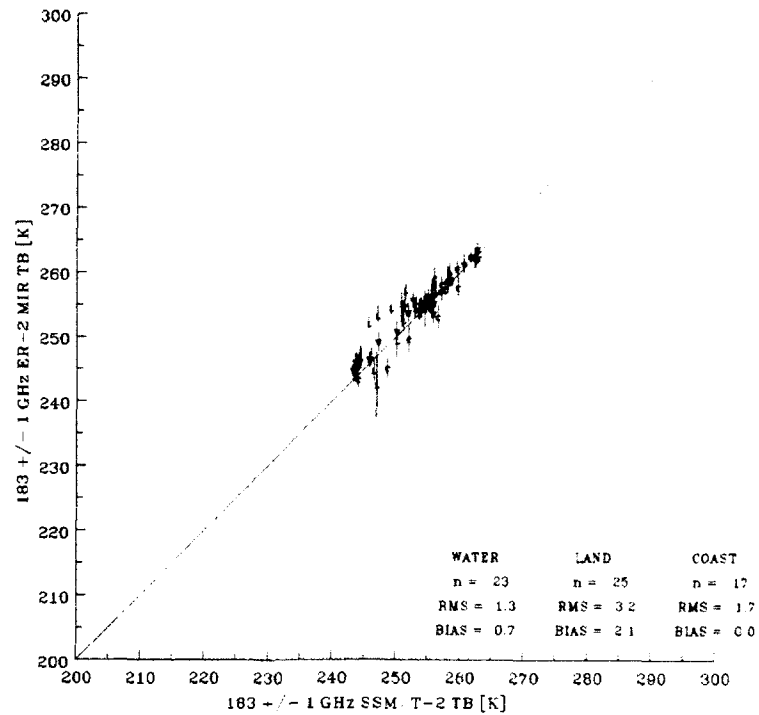


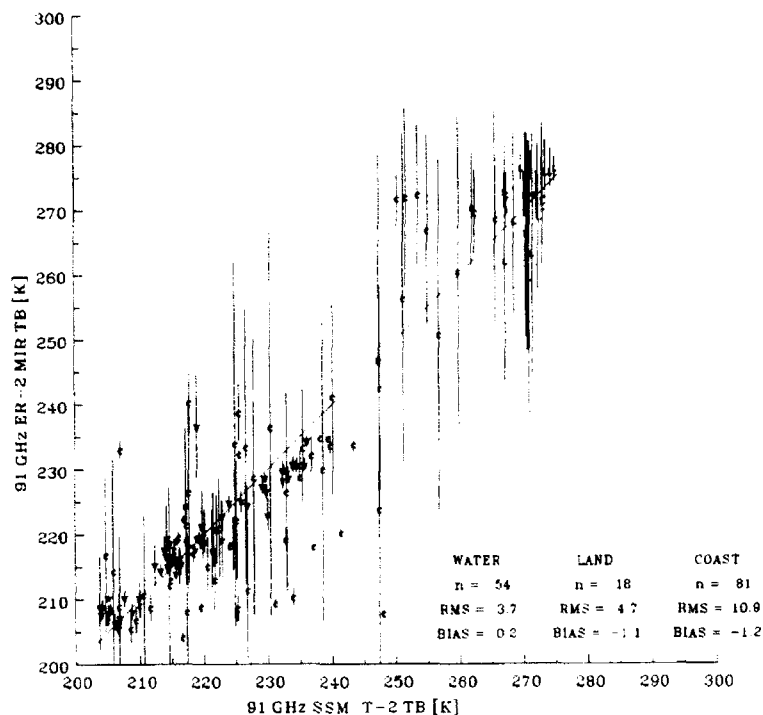
Figure 2.6.1-1. (continued).

**e (183.3 ± 1 GHz)**



*Figure 2.6.1-1. (continued).*

**a (91 GHz)**



**b (150 GHz)**

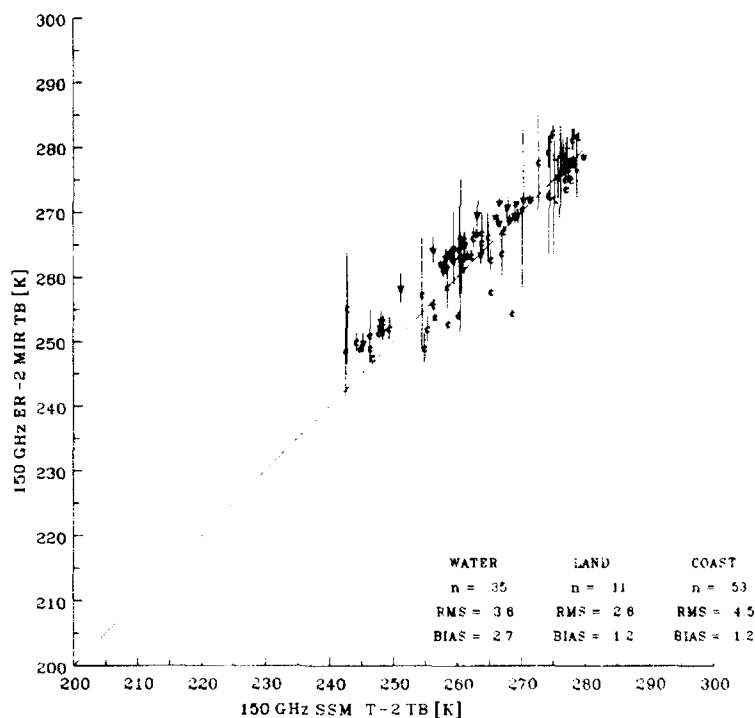
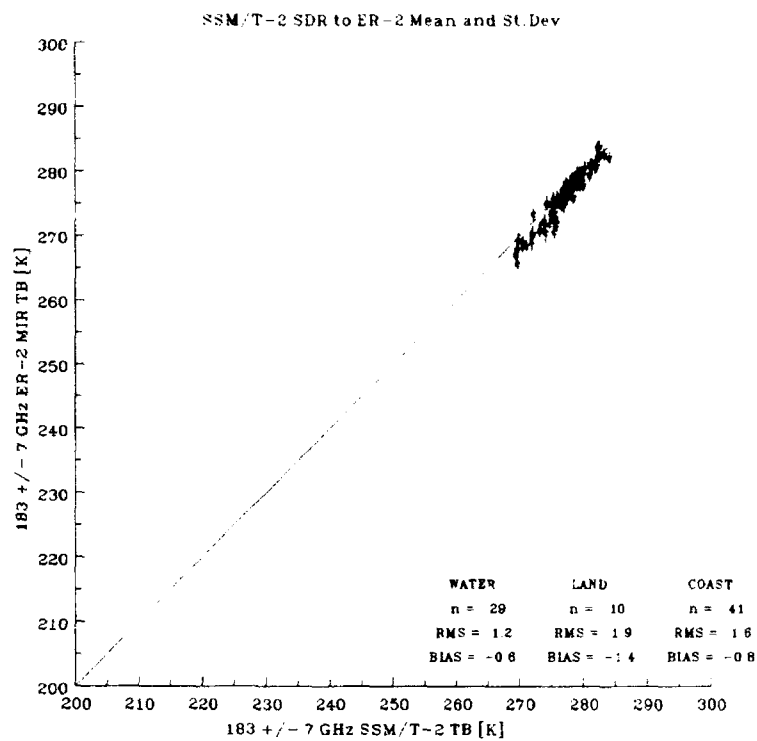


*Figure 2.6.1-2 a-e. Comparison of SSM/T-2 TBs to the mean co-located MIR TBs for the five channels of the SSM/T-2 sensor of the east coast data. Vertical bars represent one standard deviation of the co-located MIR data in each SSM/T-2 FOV. MIR data were limited to  $\pm 1$  hour of the time of the SSM/T-2 observations and to only those which had the same scan angle as the co-located SSM/T-2 data. The topography of the SSM/T-2 FOVs is land = L, water = W, and coastal = C.*

**c**  $(183.3 \pm 7 \text{ GHz})$



**d**  $(183.3 \pm 3 \text{ GHz})$

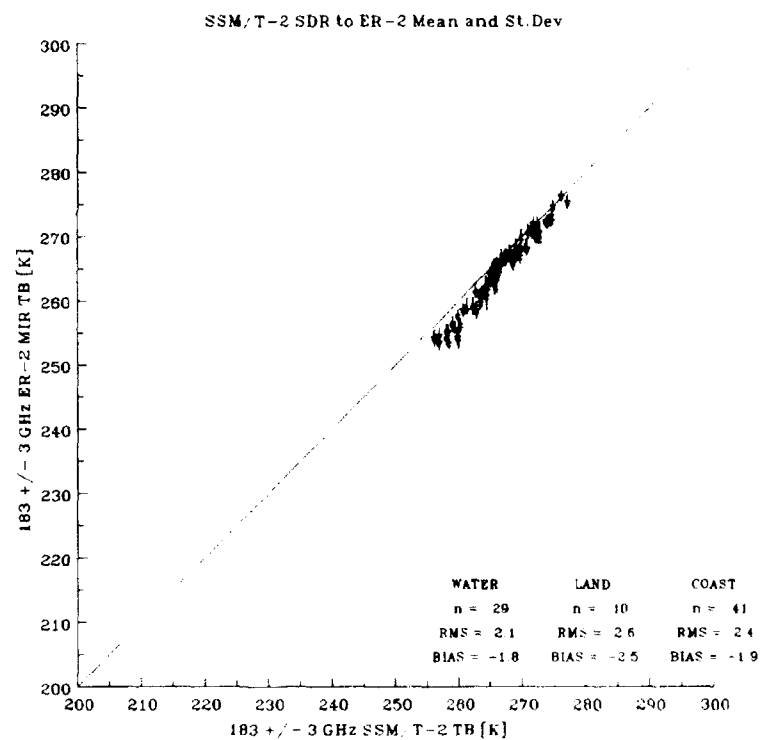
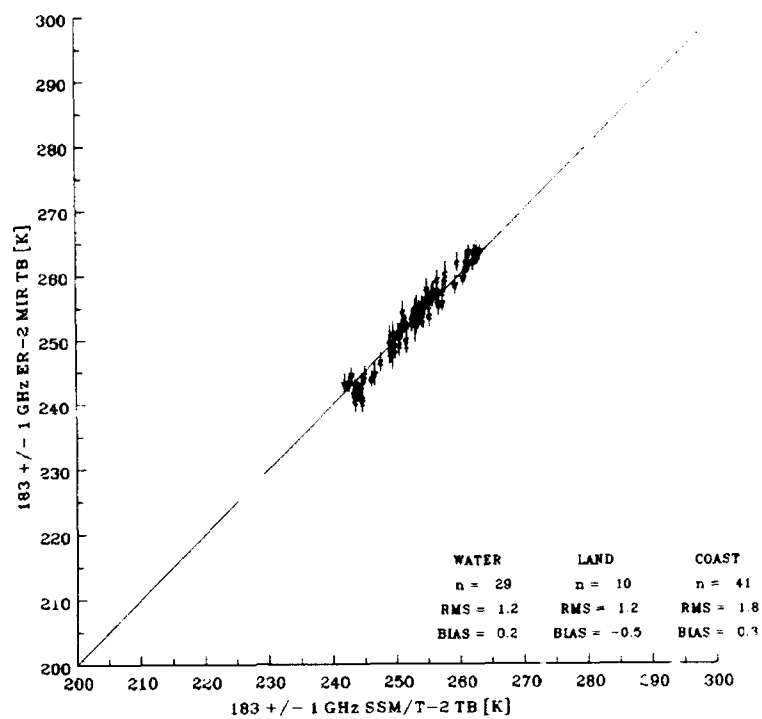


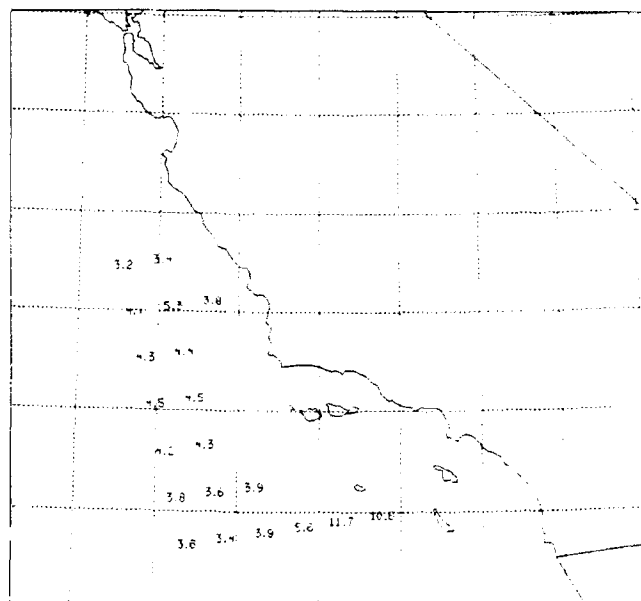
Figure 2.6.1-2. (continued).

**e (183.3 ± 1 GHz)**



*Figure 2.6.1-2. (continued).*

**a (May 14, 1992)**



**b (May 15, 1992)**

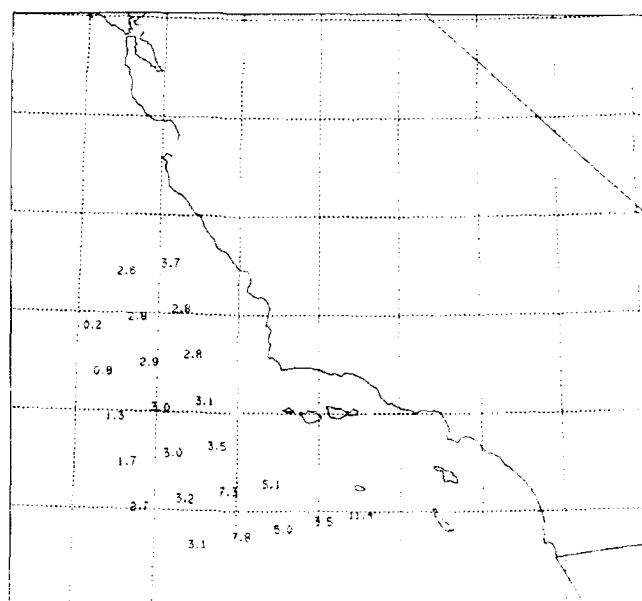
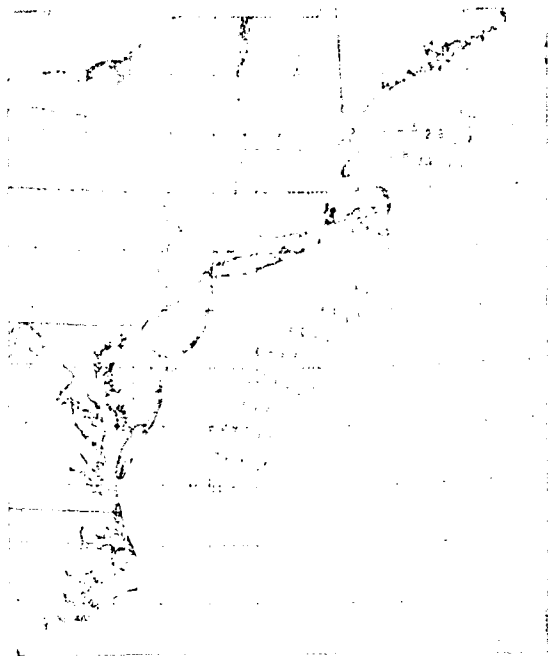


*Figure 2.6.1-3 a-e. Standard deviation of the co-located MIR TBs within each of the SSM/T-2 FOVs that are classified as water during the a) west coast May 14, 1992 flight, the b) west coast May 15, 1992 flight, the c) east coast July 29, 1992 flight, the d) east coast July 30, 1992 flight, and e) the east coast August 6, 1992 flight. Only the MIR data that was  $\pm 1$  hour of the SSM/T-2 measurements were used.*



**c (July 29, 1992)**



**d (July 30, 1992)**

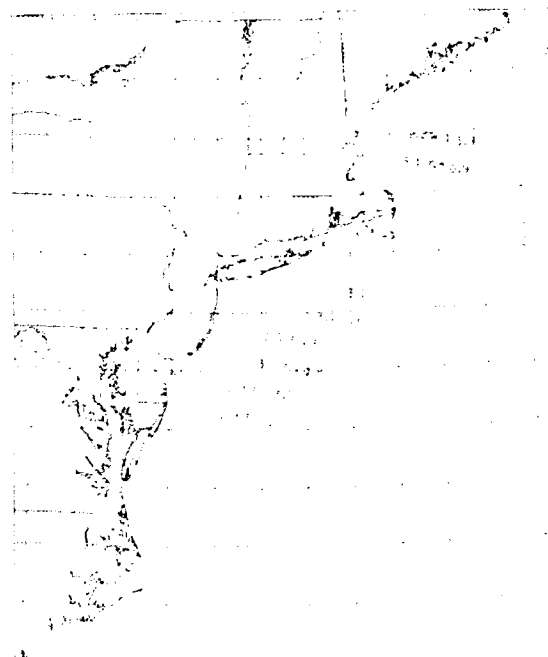


*Figure 2.6.1-3. (continued)*

e (August 6, 1992)

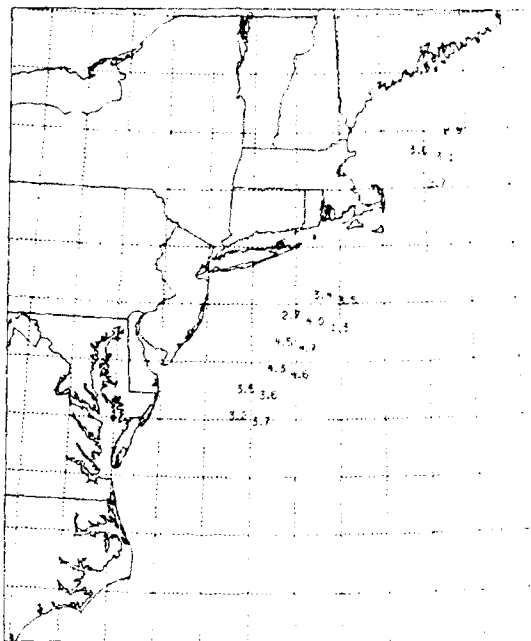


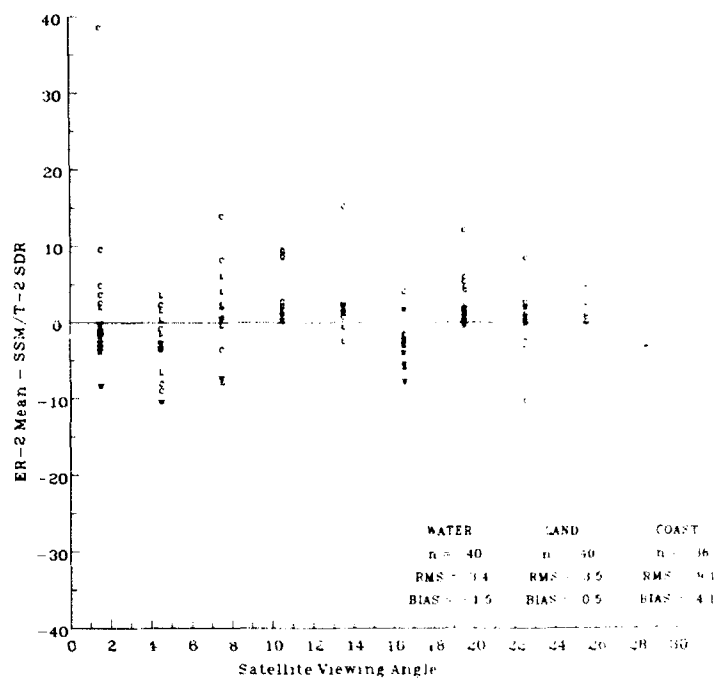
Figure 2.6.1-3. (continued)

## 2.6.2 SSM/T-2 / MIR Comparisons as a Function of Scan Angle and Direction

For the west coast data, the effect of variations in the scan angle and viewing direction (east or west) of the SSM/T-2 sensor on the difference between SSM/T-2 and mean co-located MIR TBs for the five channels of the SSM/T-2 sensor is presented in Figures 2.6.2-1 a-e through 2.6.2-3 a-e. Only SSM/T-2 FOVs that were classified as water were used in the directional study. The MIR data were limited to  $\pm 1$  hour from the time of the SSM/T-2 observations and to only those which had the same scan angle as the co-located SSM/T-2 data. In studying the effect of scan angle, both scan directions of the MIR, if contained within the SSM/T-2 FOV were used; whereas, when studying the effect of the scan direction, only MIR data with the same scan angle as the SSM/T-2 were used. Again, coastal locations show the largest difference for each scan angle. There appears to be no systematic variation between SSM/T-2 and MIR measurements with scan angle or direction. This implies that the two independent sensors are not biased by atmospheric path or scan angle; however, since SSM/T-2 data was recorded by AFGWC only for angles between  $\pm 28.5^\circ$ , surface polarization effects would be negligible and were not investigated.

Since the east coast weather conditions were such that strong predominant winds were not present over water, the effects of scan direction and angle on the east coast data were not examined at this time.

**a (91 GHz)**



**b (150 GHz)**

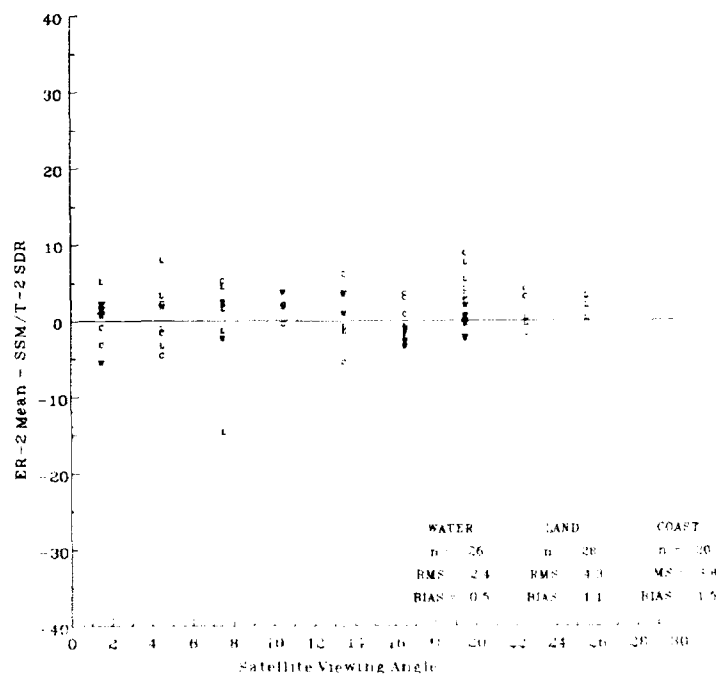
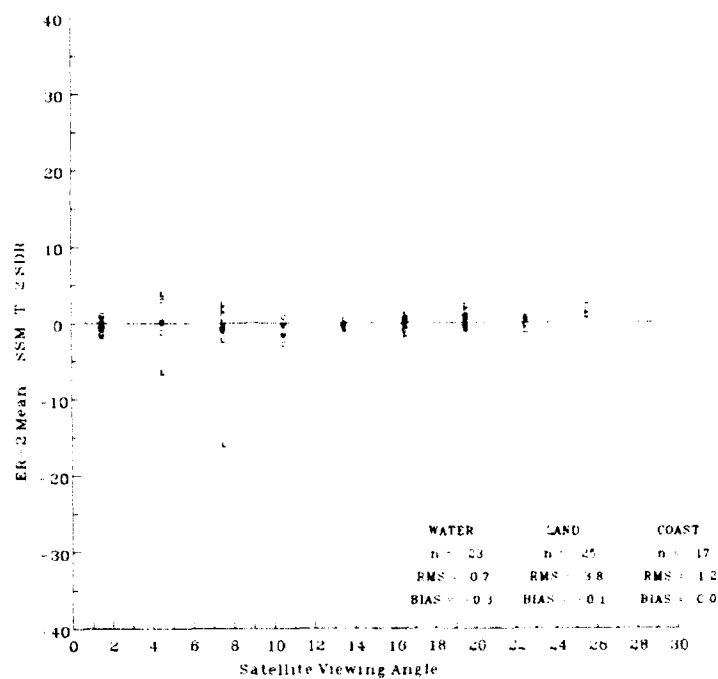


**Figure 2.6.2-1 a-e.** For the west coast data, the effect of the scan angle of the SSM/T-2 sensor on the difference between SSM/T-2 TBs and the mean of the co-located MIR TBs for the five SSM/T-2 channels. MIR data were limited to  $\pm 1$  hour from the time of the SSM/T-2 observations and to only those which had the same scan angle as the co-located SSM/T-2 data. The topography of the SSM/T-2 FOVs is land = L, water = W, and coastal = C.

**c**  $(183.3 \pm 7 \text{ GHz})$



**d**  $(183.3 \pm 3 \text{ GHz})$

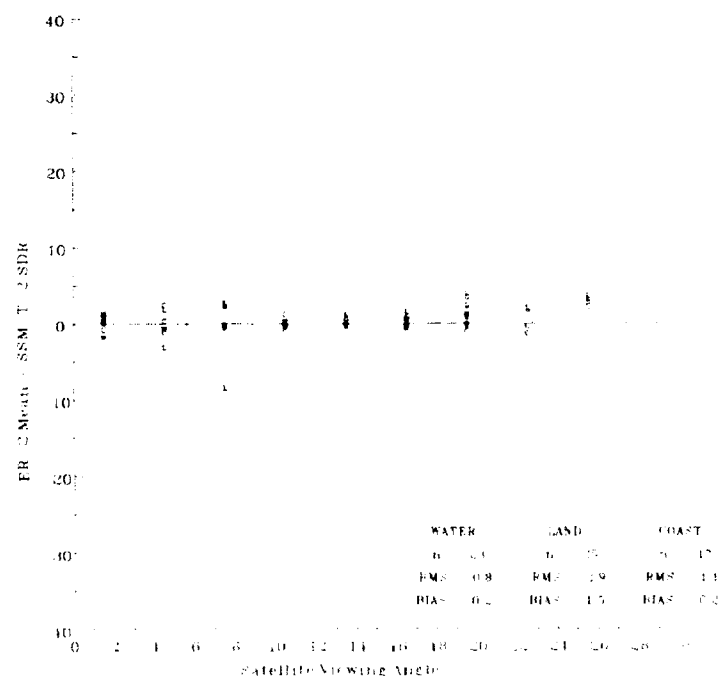


*Figure 2.6.2-1. (continued).*

e  $(183.3 \pm 1 \text{ GHz})$

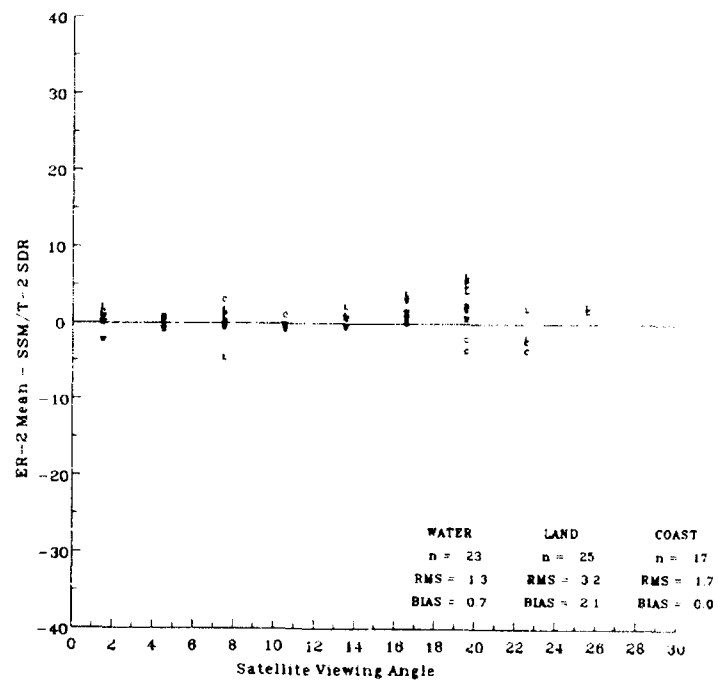
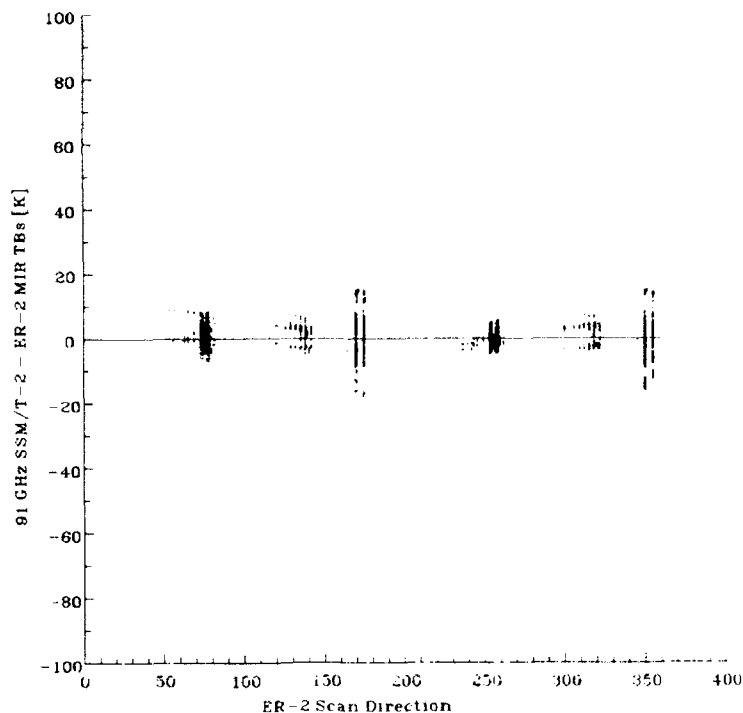
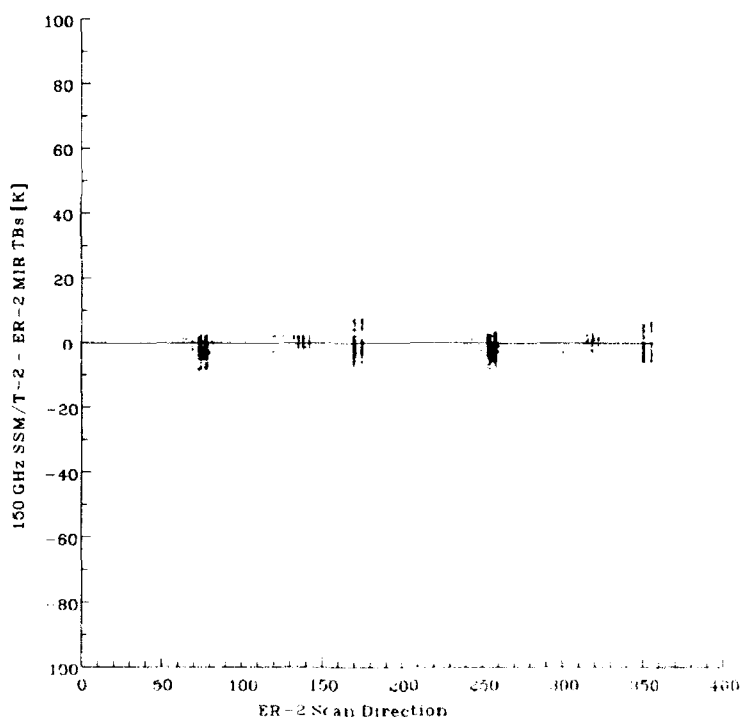


Figure 2.6.2-1. (continued).

**a (91 GHz)**

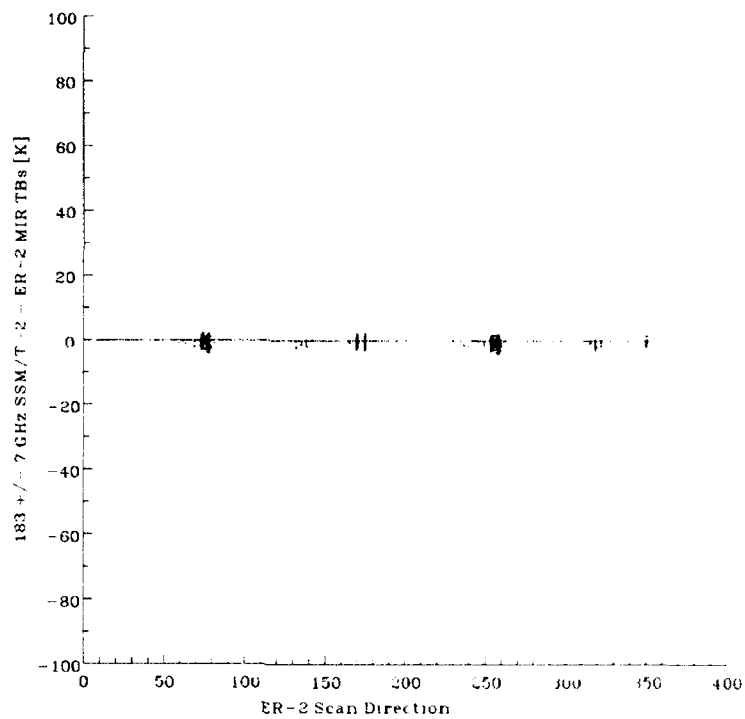


**b (150 GHz)**



*Figure 2.6.2-2 a-e. For the west coast SSM/T-2 water-classified FOVs, the effect of the scan direction of the MIR sensor on the difference between SSM/T-2 TBs and the mean of the co-located MIR TBs for the five SSM/T-2 channels. The SSM/T-2 sensor was looking westward. MIR data were limited to  $\pm 1$  hour from the time of the SSM/T-2 observations and to only those which had the same scan angle as the co-located SSM/T-2 data. The topography of the SSM/T-2 FOVs is land = L, water = W, and coastal = C.*

**c**  $(183.3 \pm 7 \text{ GHz})$



**d**  $(183.3 \pm 3 \text{ GHz})$

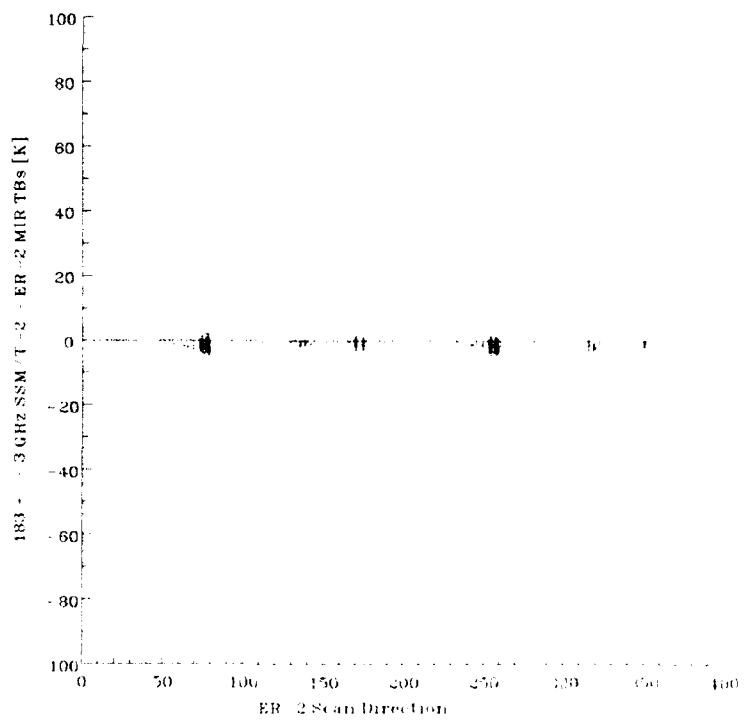


*Figure 2.6.2-2. (continued).*



**e**  $(183.3 \pm 1 \text{ GHz})$

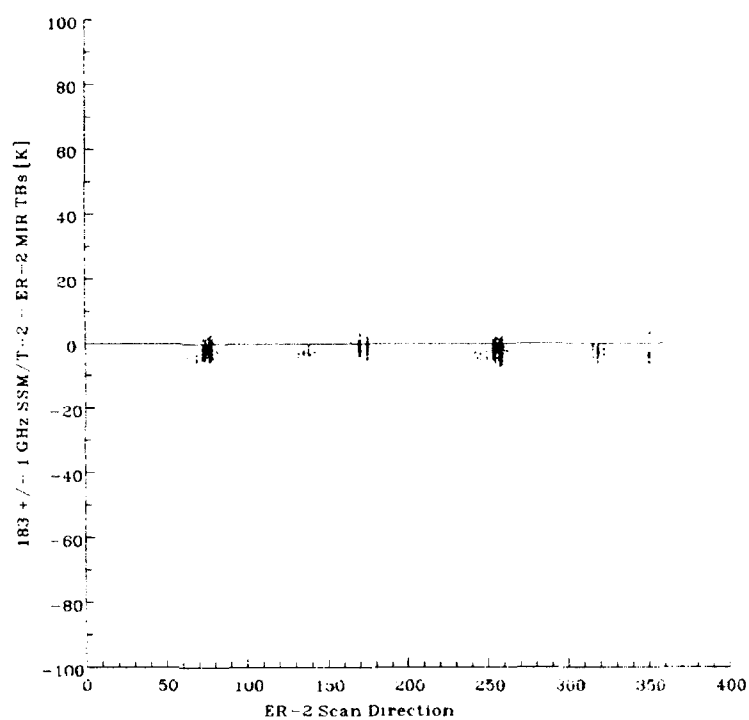
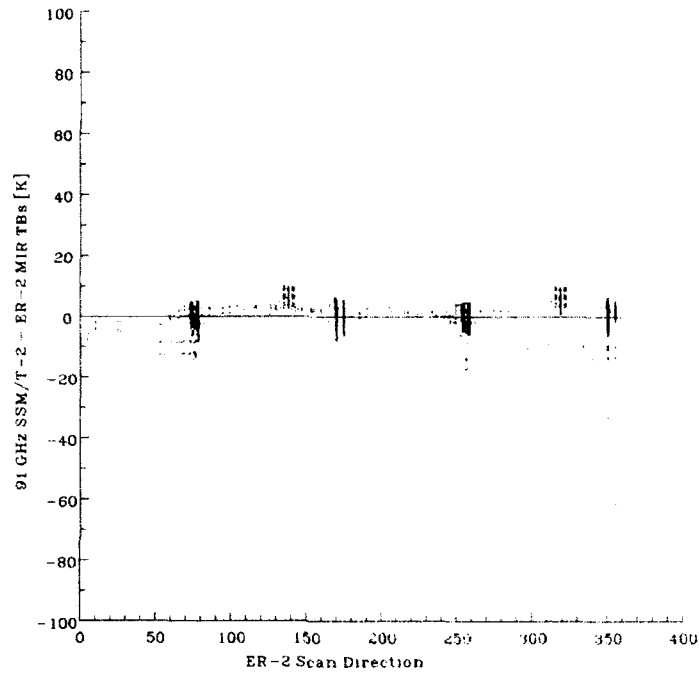


*Figure 2.6.2-2. (continued).*

**a (91 GHz)**



**b (150 GHz)**

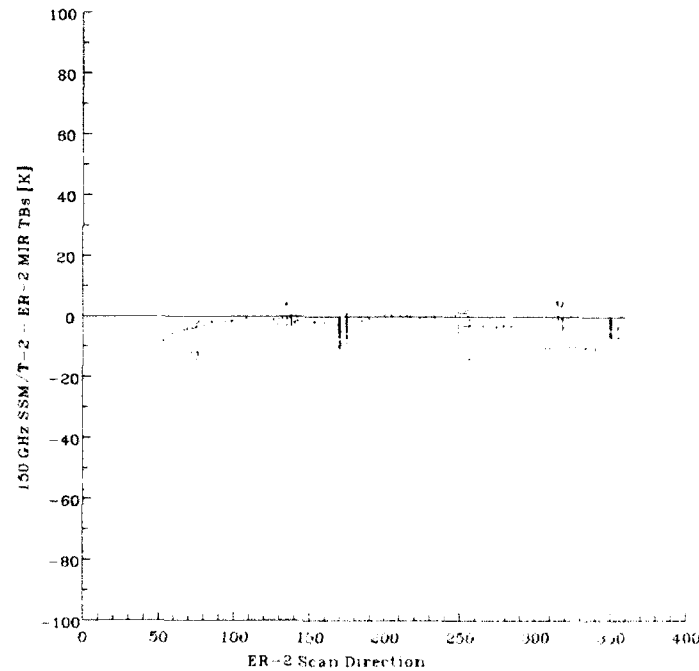
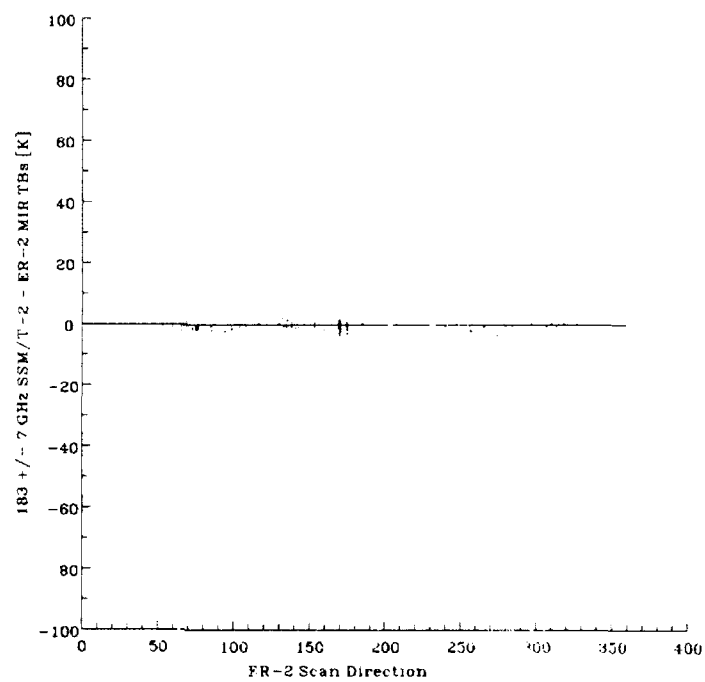


**Figure 2.6.2-3 a-e.** For the west coast SSM/T-2 water-classified FOVs, the effect of the scan direction of the MIR sensor on the difference between SSM/T-2 TBs and the mean of the co-located MIR TBs for the five SSM/T-2 channels. The SSM/T-2 sensor was looking eastward. MIR data were limited to  $\pm 1$  hour from the time of the SSM/T-2 observations and to only those which had the same scan angle as the co-located SSM/T-2 data. The topography of the SSM/T-2 FOVs is land = L, water = W, and coastal = C.

**c**  $(183.3 \pm 7 \text{ GHz})$



**d**  $(183.3 \pm 3 \text{ GHz})$

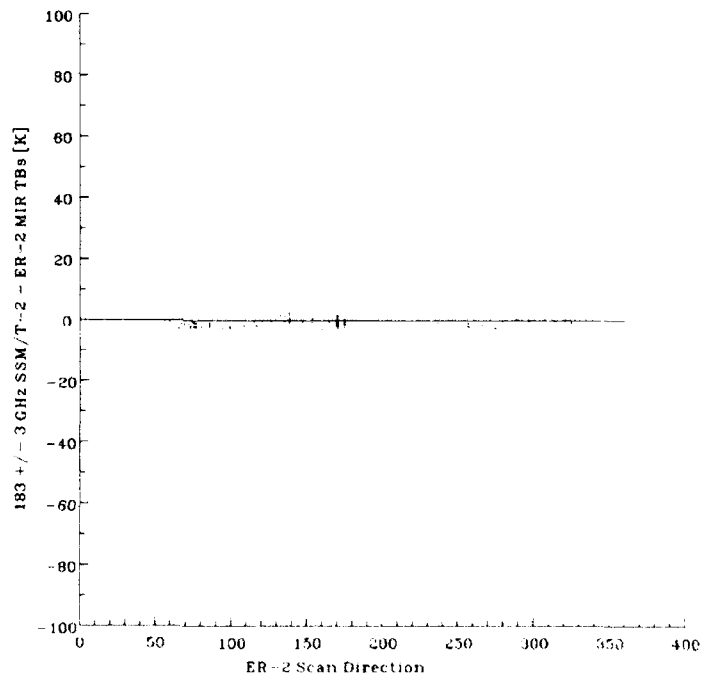


*Figure 2.6.2-3. (continued).*

**e**  $(183.3 \pm 1 \text{ GHz})$

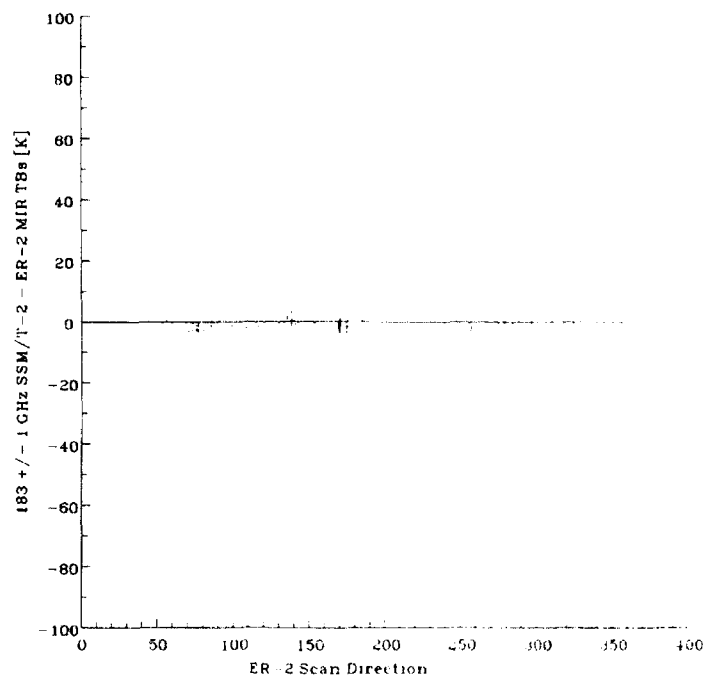
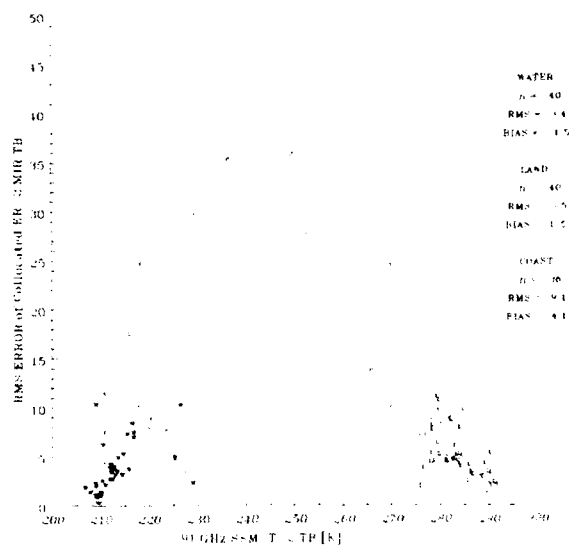


*Figure 2.6.2-3. (continued).*

### 2.6.3 Variation of MIR Within Each co-located SSM/T-2 FOV

Variation of the MIR TBs within each of the co-located SSM/T-2 FOVs for the five channels of the SSM/T-2 sensor are presented in Figure 2.6.3-1 a-e. Again, for the surface channels of 91 and 150 GHz, coastal FOVs display the largest inter-FOV variations; land and water variations are nearly all confined to 10° or less RMS. The one anomalous land FOV within the atmospheric channels occurs over the Mt. Whitney region.

**a (91 GHz)**



**b (150 GHz)**

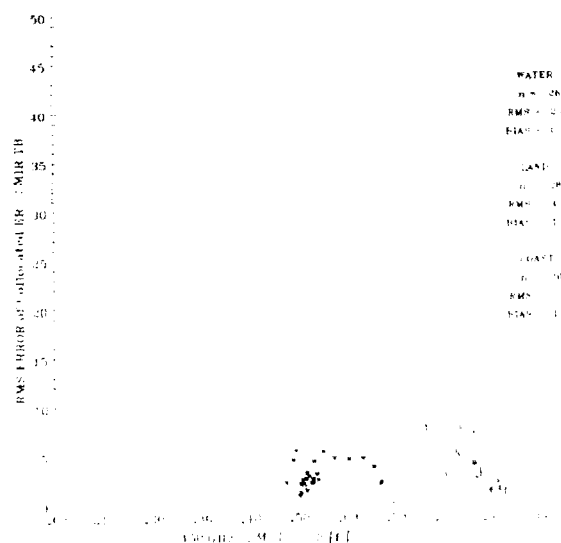
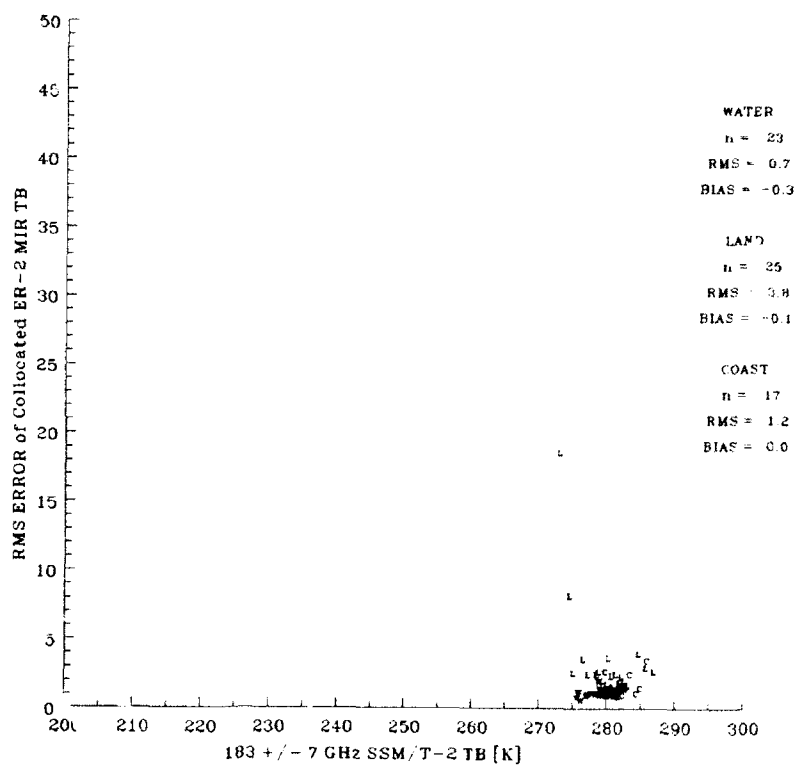


*Figure 2.6.3-1 a-e. Based on the west coast data, RMS of the MIR TBs within each of the co-located SSM/T-2 FOVs for the five SSM/T-2 channels. MIR data were limited to  $\pm 1$  hour of the time of the SSM/T-2 observations and to only those which had the same scan angle as the co-located SSM/T-2 data. The topography of the SSM/T-2 FOVs is land = L, water = W, and coastal = C.*

c  $(183.3 \pm 7 \text{ GHz})$



d  $(183.3 \pm 3 \text{ GHz})$

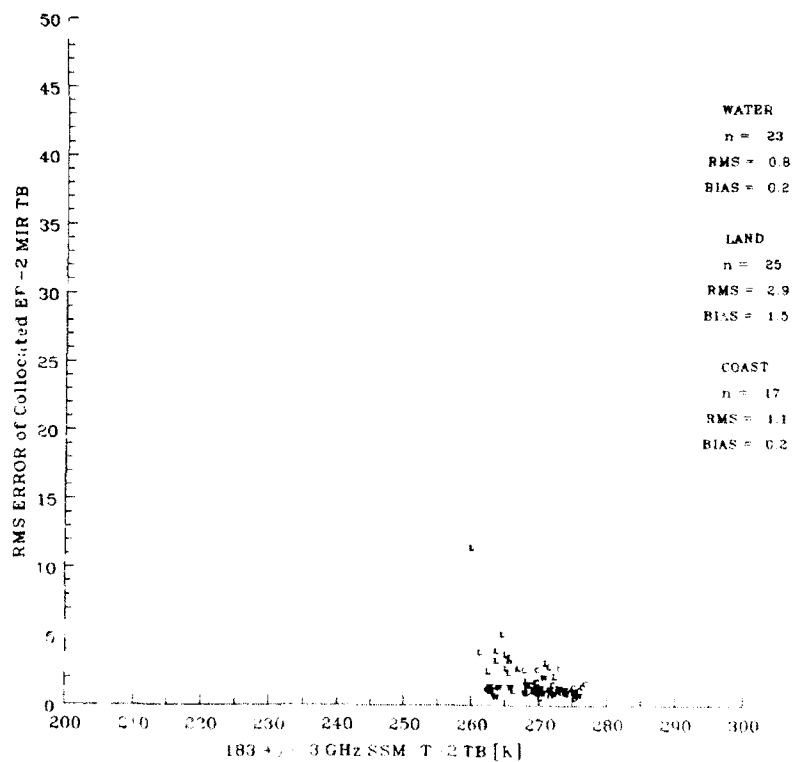


Figure 2.6.3.1. (continued).

e (183.3 ± 1 GHz)

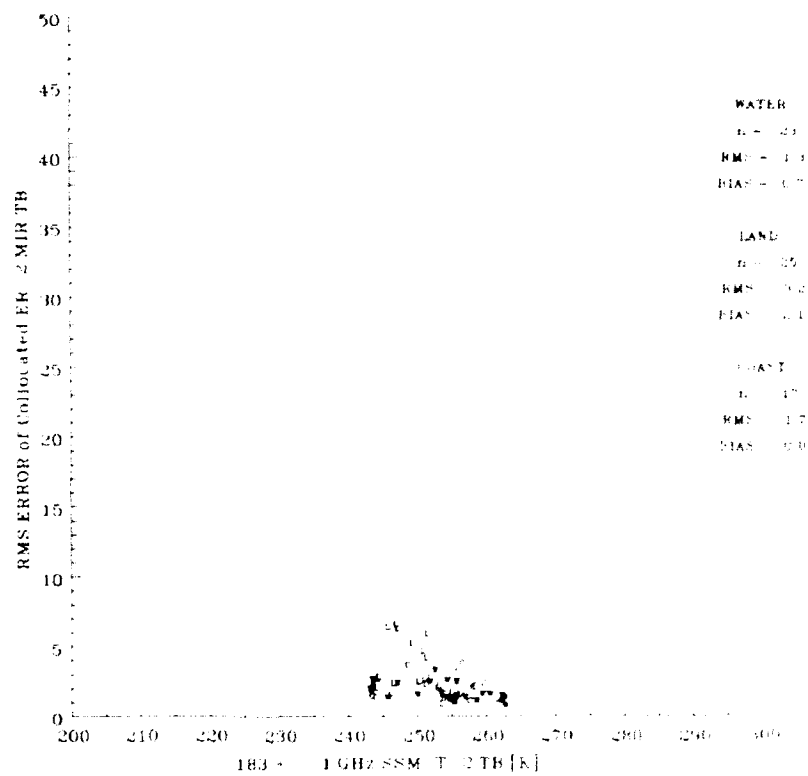


Figure 2.6.3-1. (continued).

#### 2.6.4 SSM/T-2 / MIR Comparisons as a Function of Time Difference

The separation in time between the SSM/T-2 observations (spanning 3-4 minutes along the west coast) and the MIR data (which span over four hours) are examined in Table 2.6.4-1. In each of the tables, the RMS difference between the mean of the co-located MIR data and the observed SSM/T-2 TBs are stratified by the two sets of MIR data used: one where the scan angle of the MIR data matched that of the SSM/T-2 data, and the second where all MIR data with scan angles  $\leq 28.5^\circ$  located within the SSM/T-2 FOV were used. Data are presented as a function of the time between the SSM/T-2 and the MIR data and the topographic classification of the SSM/T-2 FOV.

With the exception of coastal FOVs, the 91 and 150 GHz channels display the greatest differences between MIR and SSM/T-2 measurements as well as increasing RMS with increasing time away from the overpass time. As would be expected, the atmospheric channels display less deviation between MIR and SSM/T-2 measurements than the surface channels and also show a smaller range of variation across the three topography types. Under dry conditions or over high terrain it is possible for the atmospheric channels (183.3 GHz) to include surface contributions to its total measured radiance which could tend to increase the variance in the MIR measurements. This does not seem to be occurring for the west coast flights since the RMS differences are similar for all 3 channels, with the exception of the flight path over Mt. Whitney. Interestingly, the differences between the MIR and SSM/T-2 do not increase with the time difference of the measurement, which was not the case for the surface channels.



Same Scan Angle						
$\Delta T$ (hrs)	91	150	183 $\pm$ 7	183 $\pm$ 3	183 $\pm$ 1	WEST COAST
0-1	3.4 (40)	2.4 (26)	1.3 (23)	0.8 (23)	0.7 (23)	<u>Water</u>
1-2	3.7 (25)	2.2 (15)	1.3 (13)	0.7 (13)	0.7 (13)	
2-3	4.3 (23)	3.0 (11)	3.0 (11)	0.9 (11)	0.6 (11)	
0-1	3.5 (40)	4.3 (28)	3.2 (25)	2.9 (25)	3.8 (25)	<u>Land</u>
1-2	7.0 (25)	5.5 (13)	2.5 (10)	1.5 (10)	2.3 (10)	
2-3	---	---	---	---	---	
0-1	9.1 (36)	3.8 (20)	1.7 (17)	1.1 (17)	1.2 (17)	<u>Coastal</u>
1-2	8.8 (23)	3.8 (15)	3.2 (10)	2.0 (10)	0.8 (10)	
2-3	19.2 (4)	9.7 (2)	0.7 (1)	1.2 (1)	0.6 (1)	
EAST COAST						
0-1	3.7 (54)	3.6 (35)	1.2 (29)	2.1 (29)	1.2 (29)	<u>Water</u>
1-2	3.4 (51)	3.2 (30)	2.2 (28)	3.3 (28)	2.5 (28)	
2-3	1.9 (6)	2.1 (2)	4.3 (1)	5.8 (1)	6.8 (1)	
0-1	4.7 (18)	2.6 (11)	1.2 (10)	2.6 (10)	1.9 (10)	<u>Land</u>
1-2	1.5 (7)	1.3 (3)	5.1 (2)	5.7 (2)	2.9 (2)	
2-3	---	---	---	---	---	
0-1	10.9 (81)	4.5 (53)	1.8 (41)	2.4 (41)	1.6 (41)	<u>Coastal</u>
1-2	10.4 (65)	5.0 (37)	3.4 (35)	2.0 (35)	1.6 (35)	
2-3	12.0 (63)	5.3 (41)	3.5 (32)	2.3 (32)	2.4 (32)	
$\pm 28.5^\circ$ Scan Angle						
$\Delta T$ (hrs)	91	150	183 $\pm$ 7	183 $\pm$ 3	183 $\pm$ 1	WEST COAST
0-1	2.9 (43)	4.0 (32)	1.3 (31)	0.8 (23)	0.7 (23)	<u>Water</u>
1-2	3.3 (25)	4.5 (23)	1.3 (21)	0.8 (21)	0.8 (21)	
2-3	4.3 (25)	4.1 (13)	2.8 (11)	0.8 (11)	0.5 (11)	
0-1	4.3 (43)	4.6 (30)	3.2 (28)	2.9 (28)	3.7 (28)	<u>Land</u>
1-2	6.5 (28)	4.7 (17)	3.1 (16)	2.4 (16)	2.7 (16)	
2-3	---	---	---	---	---	
0-1	7.9 (41)	5.5 (28)	1.3 (25)	1.0 (25)	1.1 (25)	<u>Coastal</u>
1-2	6.3 (28)	4.7 (17)	3.1 (16)	2.4 (16)	2.7 (16)	
2-3	16.4 (4)	8.0 (2)	0.6 (2)	0.6 (2)	0.8 (2)	
EAST COAST						
0-1	3.7 (66)	4.6 (44)	1.7 (37)	2.5 (37)	1.3 (37)	<u>Water</u>
1-2	3.8 (57)	4.5 (39)	2.6 (35)	3.7 (35)	2.7 (35)	
2-3	3.6 (7)	4.4 (4)	3.9 (2)	7.3 (2)	8.6 (2)	
0-1	3.7 (21)	2.3 (16)	2.3 (13)	3.5 (13)	2.5 (13)	<u>Land</u>
1-2	1.3 (7)	1.4 (6)	5.4 (4)	6.1 (4)	3.1 (4)	
2-3	---	---	---	---	---	
0-1	11.1 (92)	4.2 (60)	2.3 (57)	3.2 (57)	2.0 (57)	<u>Coastal</u>
1-2	8.3 (79)	5.1 (50)	3.4 (43)	2.6 (43)	1.6 (43)	
2-3	11.5 (69)	6.7 (50)	7.0 (46)	7.2 (46)	8.7 (46)	

Table 2.6.4-1. RMS between the mean of the co-located MIR data and the SSM/T-2 TBs at the five SSM/T-2 channels. Frequency of SSM/T-2 FOVs follows in parentheses. Two sets of MIR data were used: one where the scan angle of the MIR data matched that of the co-located SSM/T-2 FOV and the second where the MIR data has a scan angle  $\leq 28.5^\circ$ .

## 2.7 Calibration of the SSM/T-2 using Radiative Transfer Calculations

### 2.7.1 Radiative Transfer Models

Radiative transfer (RT) simulations of SSM/T-2 TB observations were performed using: (a) the RADTRAN computer code which was developed by the Phillips Laboratory (GP) (Falcone et al., 1979, 1982), and (b) the Eyre microwave simulation model (Eyre and Woolf, 1988). These simulations were supported by the availability of the global set of co-located radiosonde data spanning from late January to early August, 1992. The purpose of these calculations is to examine the calibration of the sensor based on known radiative transfer properties of the atmosphere. This examination of the "forward problem" directly supports understanding of the retrieval or "inverse" problem being investigated by the validation study.

The RADTRAN code has been utilized and tested against experimental data for frequencies up to 1000 GHz. RADTRAN provides atmospheric attenuation and TB calculations for typical atmospheric paths over the frequency range from 1 to 300 GHz. It is a design tool which can readily be used to assess potential environmental impacts on microwave and millimeter wave sensors. The version we have used in our simulations is the Enhanced RADTRAN computer code which has been widely applied within the DoD and elsewhere to provide the capability to perform sensor simulation studies for satellite borne and ground based microwave and millimeter wave systems (Isaacs et al., 1989).

The Eyre simulation model essentially creates an accurate "rapid algorithm" model for the desired spectral region required using an exact line-by-line RT simulation model as a driver. The approach is described by Eyre and Woolf (1988) and is similar to that employed by NOAA/NESDIS to model passive infrared temperature channel transmittances (Fleming and McMillin, 1977). In the microwave spectral region, the rapid algorithm results in a computational savings of at least 50 times over the line-by-line method using a preselected set of microwave lines with a loss in accuracy of only 1% or less.

Modifications were required to both RT models to facilitate interfacing with the upper air data (radiosondes) in the appropriate units (for water vapor) and at the required levels (including significant levels). To accommodate missing upper-air levels, an isothermal temperature profile was added from the highest interpolated level to the top level used in both model simulations. Missing water vapor values were supplemented by an exponentially decreasing mixing ratio from 300 hPa to 70 hPa with an in Eyre's model and by a linear decrease of RH from the top of the radiosonde data to zero at the top of the Enhanced RADTRAN layer calculation. Quality control of the radiosonde data was applied to remove any soundings which did not include measured water vapor information to at least 300 hPa. In addition, the Enhanced RADTRAN required modification of the radiosonde data file to set flags and use formats required within Enhanced RADTRAN. Comparisons were made between the satellite-measured TBs and the TBs calculated by RT simulation models using co-located *in situ* radiosonde profiles.

## 2.7.2 SSM/T-2 Comparison Results

The results of the intercomparison for an ensemble of SSM/T-2 FOVs and calculated TBs using the Eyre model supplied with co-located upper air soundings (see Figure 2.7.2-1 for global locations and Appendix B for a detailed listing of contributing radiosonde stations and the time, latitude and elevation distributions of the stations and co-located profile measurements) are shown in Figures 2.7.2-2 a-e. The data span the time period from January 31 to August 7, 1992. co-locations were determined using a time limit of  $\pm 1$  hour between the release time of the radiosonde and the time of the SSM/T-2 measurement and a distance limit of 100 km. When countries reported the release time as the synoptic reporting time, e.g. the United States, the release time was assumed to be 45 minutes before the synoptic time. Note that only one SSM/T-2 measurement was finally co-located with each radiosonde, i.e., the one that was spatially closest to the radiosonde station location.

Soundings were required to have measured water vapor values up to at least 300 hPa (required by the Eyre model). Any missing dewpoint data below 300 hPa eliminated the radiosonde from further consideration. Some countries, e.g. the United States, do not report a moisture measurement when the temperature is less than -40 C or when RH is less than 20% due to uncertainties in the radiosonde's accuracy in these conditions. By limiting the data to have measured water vapor values to 300 hPa, the number of dry atmospheres and/or clear (not cloudy) cases was most likely decreased and the percentage of cloudy and/or precipitating profiles increased; however, the uncertainties of keeping these data was too large for this phase of the analysis. In this first phase of this study, the Eyre and Enhanced RADTRAN models were set to calculate TBs using clear sky conditions.

Since the Enhanced RADTRAN model produced comparable results as the Eyre model (Figure 2.7.2-3 a-e), only the Eyre model results are plotted here; however, differences range up to 4 K. One factor causing the discrepancy between the calculated outputs is the difference in vertical scale: the Eyre models requires fixed pressure coordinates from 1000 hPa to 0.1 hPa; whereas the Enhanced RADTRAN requires height coordinates (in this case, the heights were fixed from 0 to 50 km) (Table 2.7.2-1). The Eyre model log-linearly interpolated the temperature and mixing ratio sounding data to the fixed pressure values, whereas Enhanced RADTRAN linearly interpolated temperature and RH radiosonde data to the fixed height coordinates. Data being used in both radiative transfer models was not identical due to differences in interpolation schemes and due to different vertical scales which influenced how the fine structure of the sounding profile was included in the model.

Problems and discrepancies arise when temperatures and/or dewpoints are less than -50 C. The equations used to calculate the mixing ratio were developed on data with temperatures greater than -40 C, and have been extrapolated to temperatures between -50

and -40 C. When dewpoint temperature was below -50 C, the Eyre model assumed a saturated mixing ratio of 0.003 gm/kg and the Enhanced RADTRAN model assumed a RH of 20% (the cutoff of reported radiosonde RH for U. S. radiosondes). An additional factor contributing to the deviation of the models at the 91 GHz channel is that the Eyre model does not use a surface or near-surface moisture measurement as does the Enhanced RADTRAN code. A factor that increased the deviation between the two models at the  $183.3 \pm 1$  GHz (the channel sensing water vapor at the upper levels of the troposphere) compared to the lower atmospheric channels ( $183.3 \pm 7$  and  $183.3 \pm 3$  GHz) is the difference in the handling of the upper-level sounding data by both models. The Eyre model used an isothermal atmosphere above the highest sounding level up to 0.1 hPa and an exponential decay of mixing ratio from 300 hPa to 70 hPa followed by a constant mixing ratio (0.003 gm/kg) above 70 hPa to 0.1 hPa. Enhanced RADTRAN used an isothermal atmosphere above the highest interpolated level up to 50 km and a linear decay of RH with height from the highest-level of reported RH to 1% at 50 km.

The Eyre radiative transfer code described above was used to simulate SSM/T-2 TBs using co-located upper-air data on temperature and moisture profiles to provide information on atmospheric opacity. Surface temperature was estimated from the lowest atmospheric layer available in the temperature profile soundings. Surface emissivity values are required for each SSM/T-2 channel which is transparent enough to see the earth's surface. Surface emissivities were based on the mean of a set of optimal surface emissivities calculated for 91 and 150 GHz using a global SSM/T-2 radiosonde data base from early March 1992 in the Eyre RT simulation model (Figure 2.7.2-4). The optimal surface emissivity was defined to be that value which minimized the difference between the forward-calculated TB using a specific radiosonde and the co-located TB measured by the satellite. These values are intermediate between land and ocean, but weighted more toward land emissivities.

Figures 2.7.2-2 (a-e) illustrate scatter plots of the comparison of observed and calculated TBs. Total precipitable water is indicated by the plotted numbers, e.g. 0 represents a precipitable water content ranging from 0 to 10 kg/m<sup>2</sup>, 1 ranging from 10 to 20 kg/m<sup>2</sup>, and so on. Large RMS and biases are observed for the most transparent channel at 91 GHz (and to a lesser degree for the 150 GHz channel) due to the uncertainty in surface emissivity used in the simulation. Bias and RMS are reduced for the less transmissive atmospheric channels which tend to exhibit rather good agreement between the observed SSM/T-2 TBs and the RT-calculated TBs; except at the  $183.3 \pm 1$  GHz, which measures highest atmospheric water vapor, there is a slight increase in RMS compared to the lower atmospheric channels ( $183.3 \pm 7$  and  $183.3 \pm 3$  GHz).

The sounding data used in this report come from many different types of radiosonde instruments. These sonde instruments have been shown to have both random and bias differences when flown on the same balloon (Nash and Schmidlin, 1987; and

Schmidlin, 1988). A preliminary investigation was made to demonstrate that radiosonde system differences do indeed contribute to the overall scatter of the data between the observed and calculated radiation temperatures. This was done by plotting observed versus calculated temperatures for various parts of the world. In the overall data for  $183.3 \pm 7$  GHz (Figure 2.7.2-2 c), there is a significant group of relatively moist data around the computed 270 K which bulges out to the left of the calculated=observed line. Combined data from the United States and India (Figure 2.7.2-5) contribute over 60% of the points to this feature. Whereas combined data from Scandinavia, England, Germany and Russia (Figure 2.7.2-6) contributed only one point to this anomaly. This is only one item chosen to demonstrate differences due to different types of radiosondes. There are certainly many more, but more careful analysis is needed to identify biases and effects of different types of radiosondes on calculated TBs.

A second technique for examining the possible impact of radiosonde errors on the calculated radiation temperatures was tried. Using the summed errors caused by insolation and thermal lag (Brousailles and Morrissey, 1974) on the ability of radiosondes to measure water vapor at various levels of the atmosphere, maximum correction factors were determined for the pressure levels used in the Eyre radiative transfer program up to 300 hPa (Table 2.7.2-2). These correction factors were used to estimate the moistest moisture profile that the radiosonde could have passed through and still report the measurements that it did. Keeping the temperature profile and surface emissivity constant, these moister moisture profiles were used in the Eyre model to calculate the changes in TBs relative to the change in precipitable water for the five SSM/T-2 channel frequencies (Figure 2.7.2-7 a-e). The data represents the global data base of 1227 radiosondes which are predominantly land and coastal stations ranging from tropical to polar climates. Again, these calculations do not take into account weather conditions (rain, clouds, etc.) or the type of radiosonde instrument (AIR, Vaisala, VIZ, etc.). The moister profiles could produce up to a 3 K increase in 91 GHz TBs, a 1 K decrease in 150 GHz TBs, and generally a 2-3 K decrease in the  $183.3$  GHz TBs. The drier profiles tend to generate smaller positive changes in the 91 GHz TBs, and larger positive changes in the 150 and  $183.3 \pm 7$  and  $3$  GHz TBs compared to the moister profiles. Little difference is evident between the  $183 \pm 1$  GHz TBs generated by moist or dry profiles.

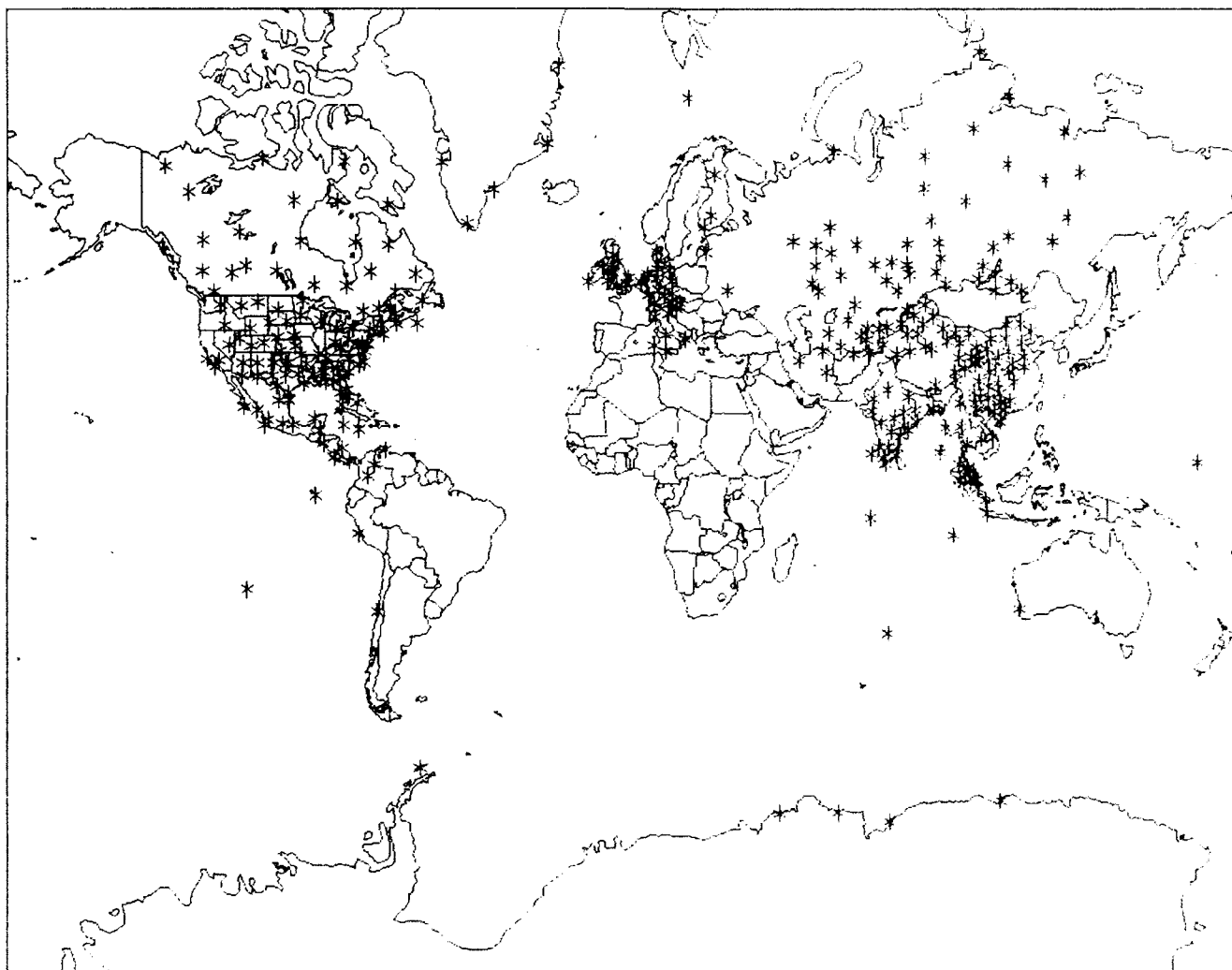
The problems associated with using a worldwide radiosonde data base to either calibrate a satellite system or to act as the basis of an empirical fit is a complex one due to the many sources of error which corrupt such a data base. A program to evaluate the sources of error and ways to improve the usefulness of a radiosonde data base for satellite application will be carried out at Phillips Laboratory over the next two years.

Table 2.7.2-1. *Pressure levels required by the Eyre radiative transfer model, and height levels used in the Enhanced RADTRAN model.*

Eyre Model Pressure Levels [hPa]	Enhance RADTRAN Height Levels [km]
0.1	50.
0.2	45.
0.5	40.
1.0	35.
1.5	30.
2.	28.
3.	26.
4.	24.
5.	22.
7.	20.
10.	19.
15.	18.
20.	17.
25.	16.
30.	15.
50.	14.
60.	13.
70.	12.
85.	11.
100.	10.
115.	9.5
135.	9.
150.	8.5
200.	8.
250.	7.5
300.	7.
350.	6.5
400.	6.
430.	5.5
475.	5.
500.	4.5
570.	4.
620.	3.5
670.	3.
700.	2.5
780.	2.
850.	1.75
920.	1.5
950.	1.25
1000.	1.0
Surface	0.75
	0.5
	0.25
	0.

*Table 2.7.2-2. RH correction factors used to determine the maximum limit of moisture that the sounding could have passed through and still reported the moisture profiles that it did (Brousaides and Morrissey, 1974). Pressure levels are those used in the Eyre radiative transfer program.*

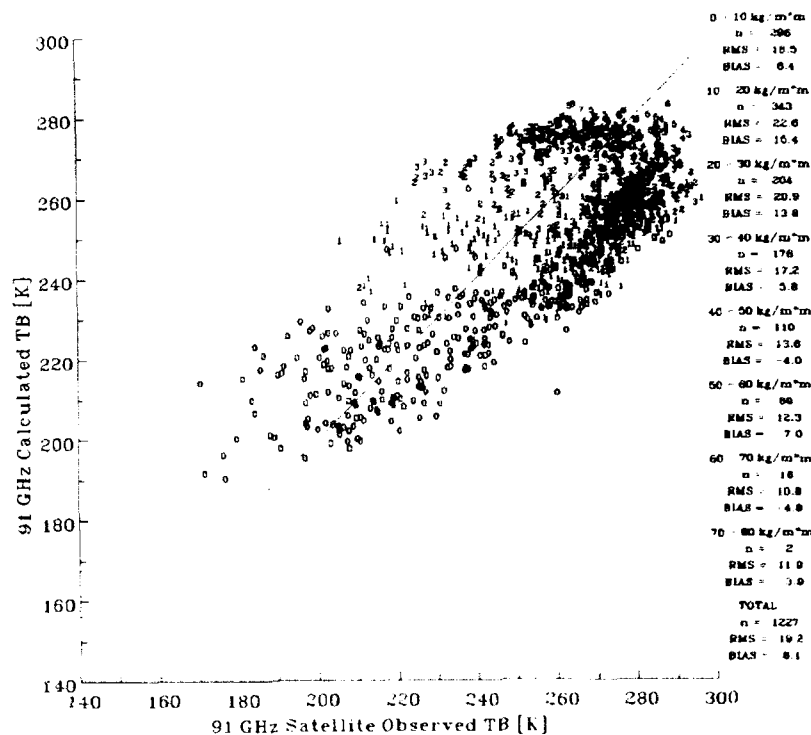
Correction Factor	Pressure Level (hPa)
.230	300
.190	350
.163	400
.148	430
.133	475
.125	500
.105	570
.095	620
.086	670
.081	700
.069	780
.060	850
.053	920
.050	950
.048	1000



*Figure 2.7.2-1. Global locations of radiosondes that were co-located with SSM/T-2 FOVs. co-locations were determined to be within  $\pm 1$  hour and 100 km of the measurements. Radiosonde profiles were used only if the measured moisture profile extended up to at least 300 hPa. Data spans the time period from January 31 to August 7, 1992.*



a (91 GHz)



b (150 GHz)

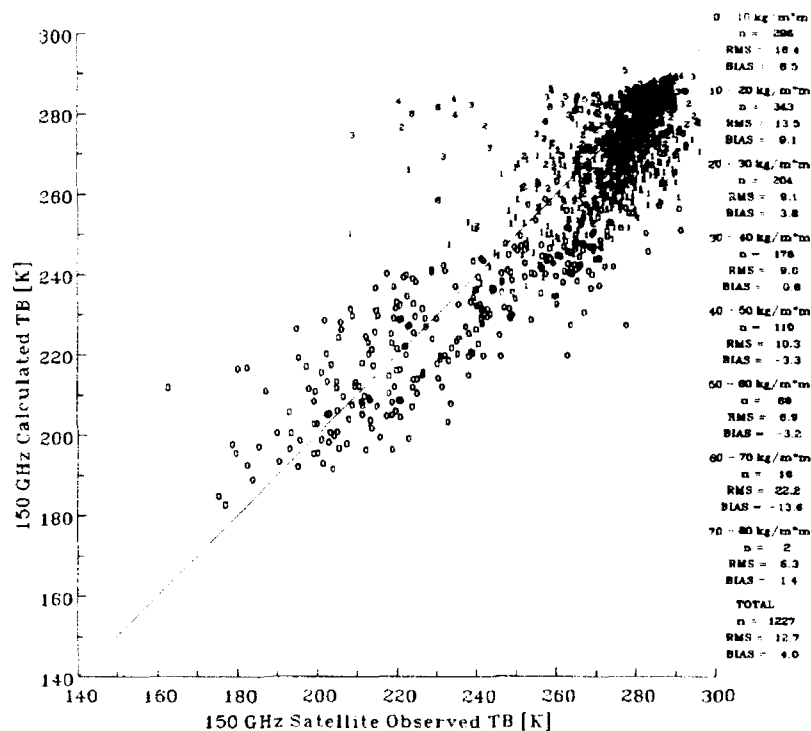
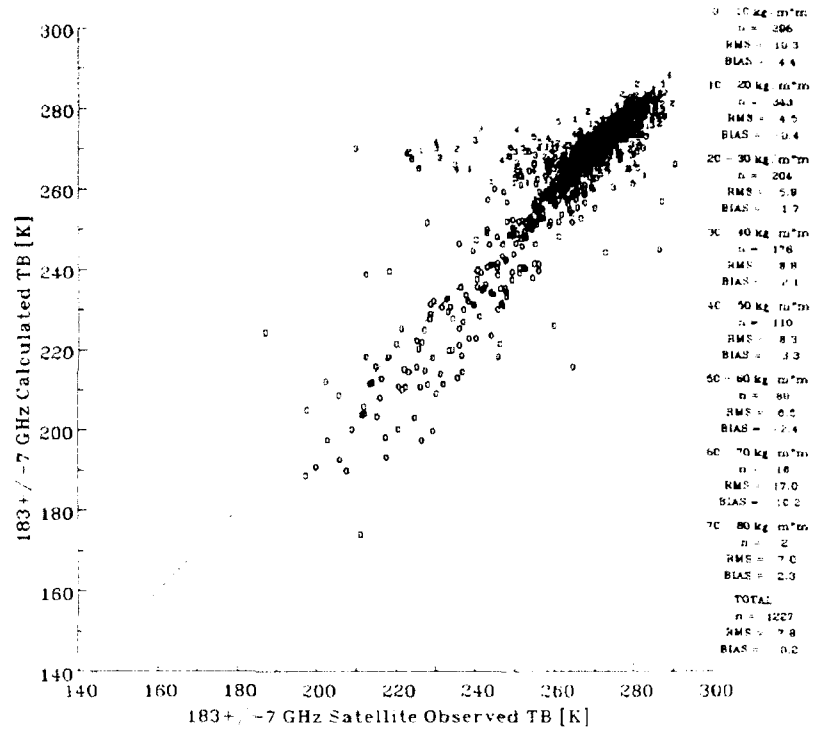


Figure 2.7.2-2 a-e. Calculated TBs using the Eyre RT simulation model versus SSM/T-2 observation for the five SSM/T-2 channels. Plotted numbers represent total precipitable water content of the radiosonde profile used in the Eyre model, e.g., 0 represents a profile with a precipitable water content ranging from 0 to 10 kg/m<sup>2</sup>, 1 represents a range from 10 to 20 kg/m<sup>2</sup>, and so on.

**c**  $(183.3 \pm 7 \text{ GHz})$



**d**  $(183.3 \pm 3 \text{ GHz})$

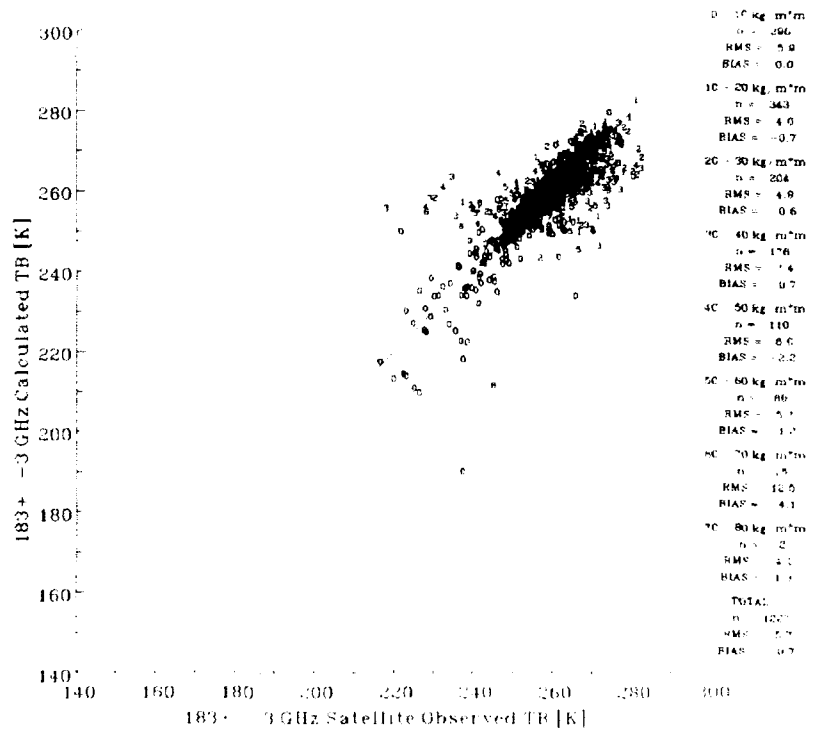


Figure 2.7.2-2. (continued).

e (183.3 ± 1 GHz)

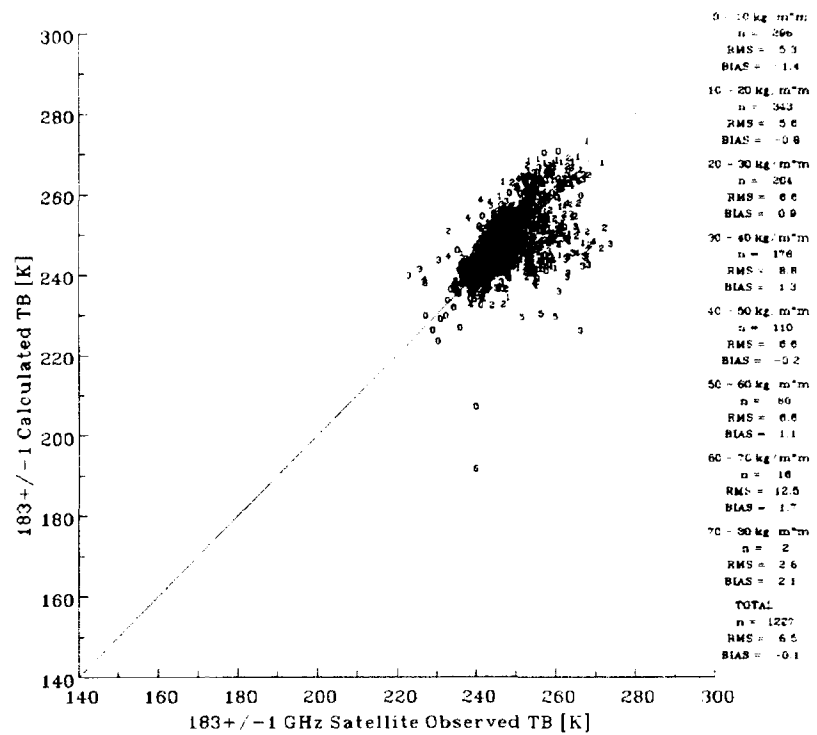
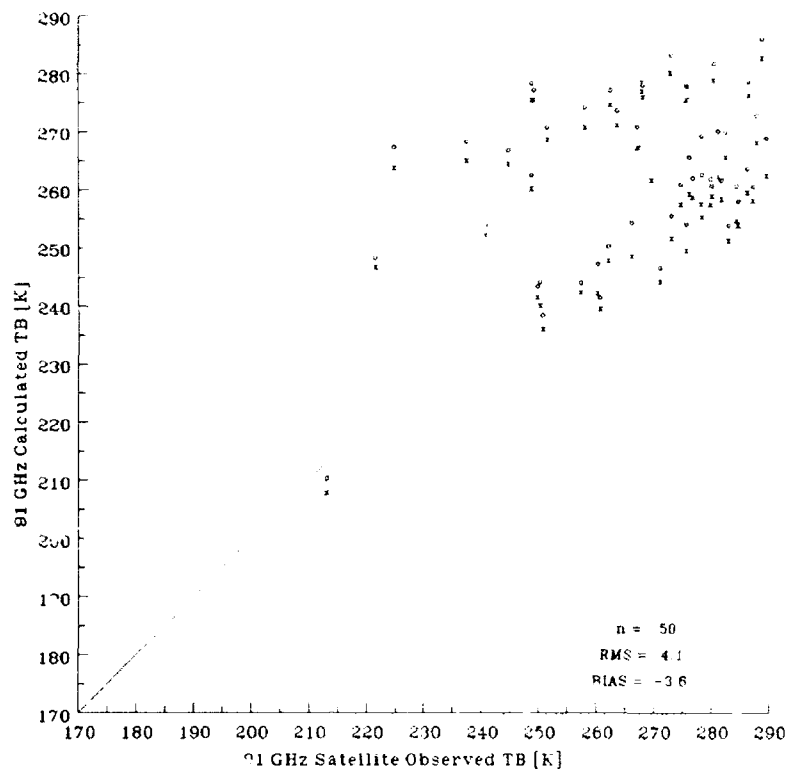
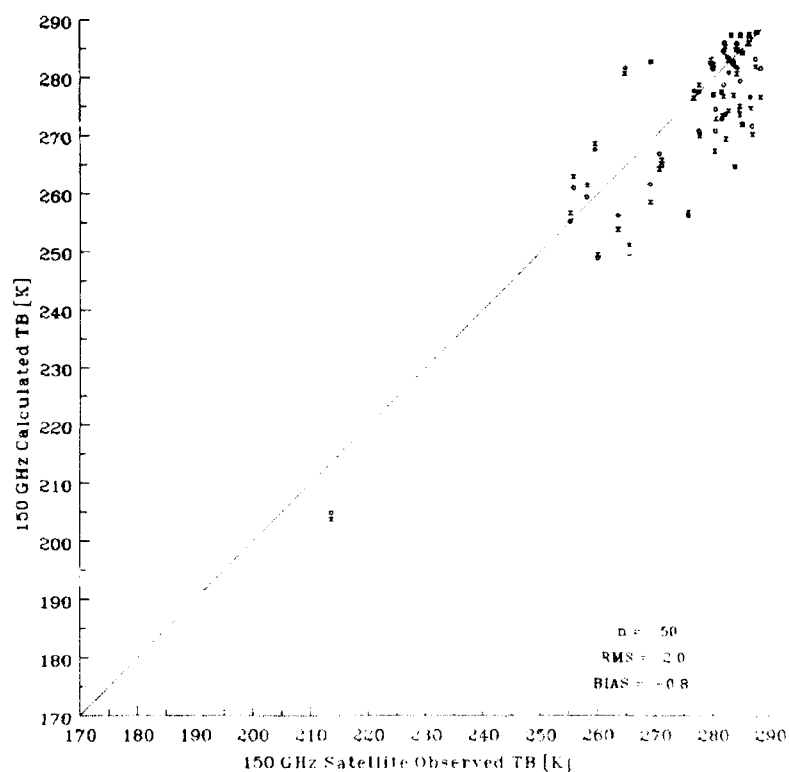


Figure 2.7.2-2. (continued).

**a (91 GHz)**

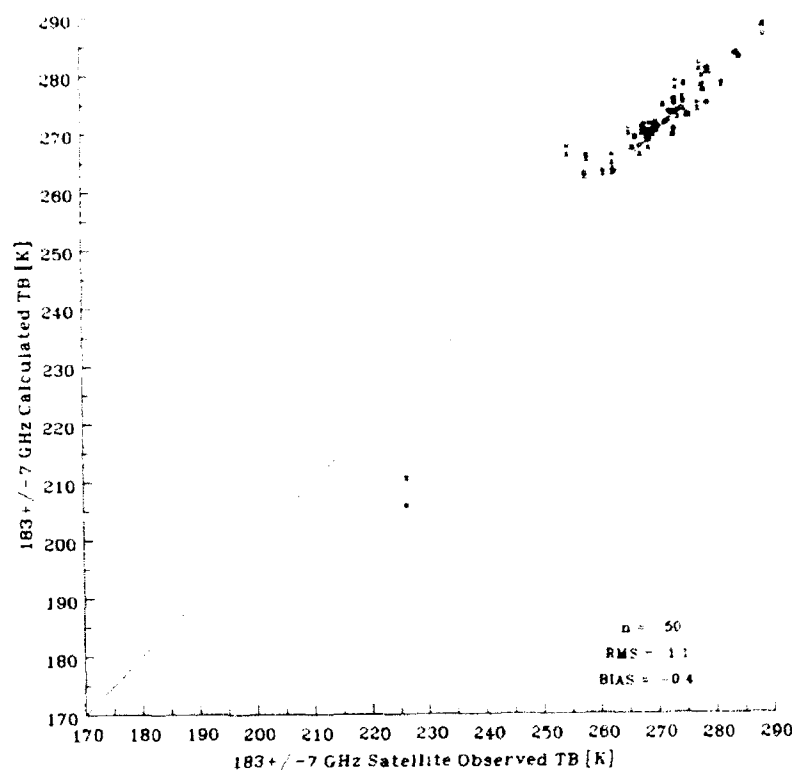


**b (150 GHz)**



**Figure 2.7.2-3 a-e.** Comparison of Eyre model results (x) to Enhanced RADTKAN model results (o) for the five SSM/T-2 channels using a global set of radiosondes.

**c**  $(183.3 \pm 7 \text{ GHz})$



**d**  $(183.3 \pm 3 \text{ GHz})$

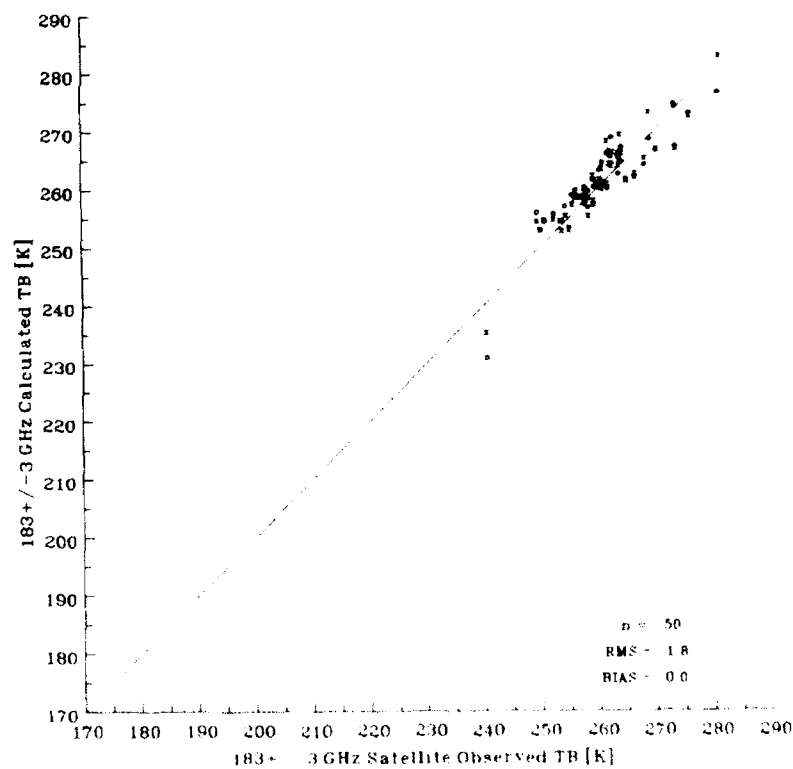


*Figure 2.7.2-3. (continued).*

**e**  $(183.3 \pm 1 \text{ GHz})$

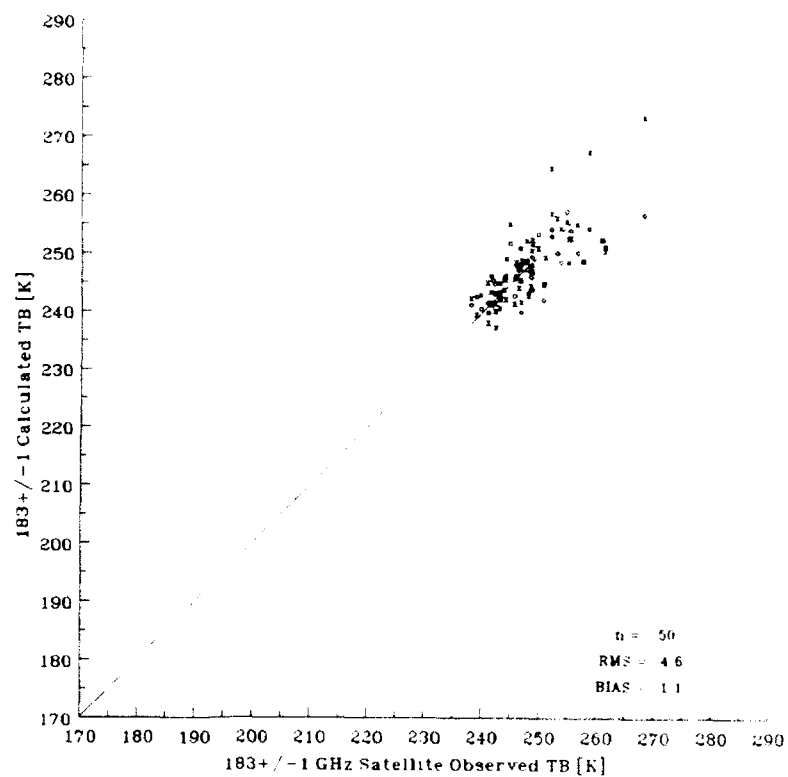


*Figure 2.7.2-3. (continued).*

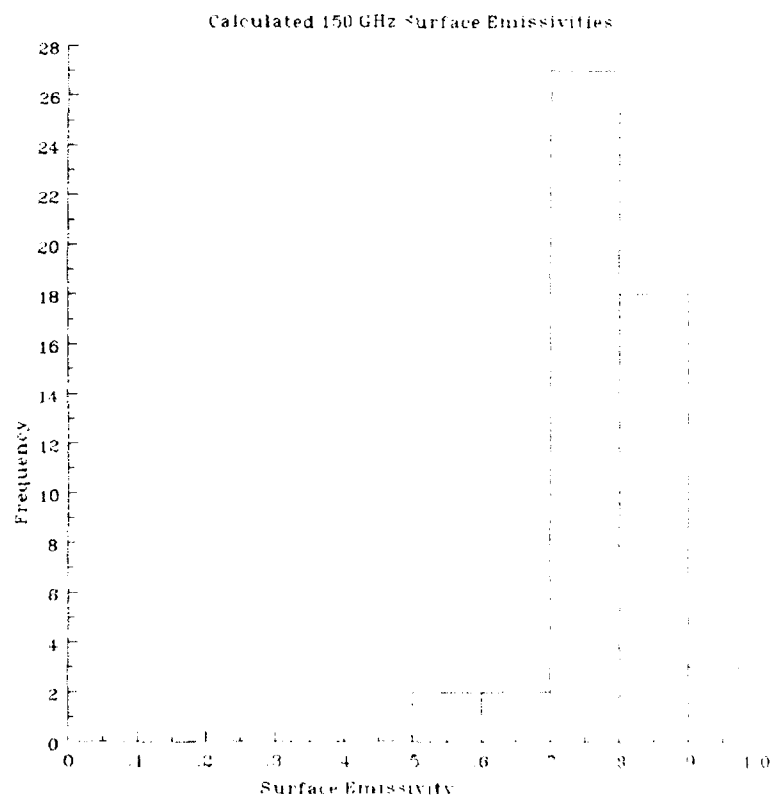
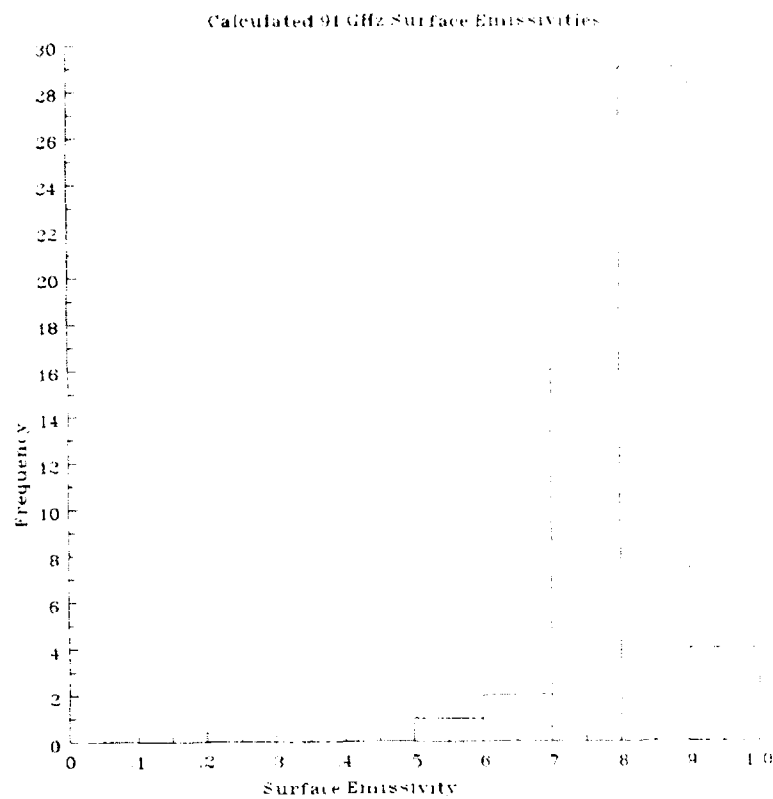


*Figure 2.7.2-4. Distribution of optimal surface emissivities for 91 and 150 GHz, iteratively calculated using a global set of radiosonde profiles (all over land) from late March, 1992.*

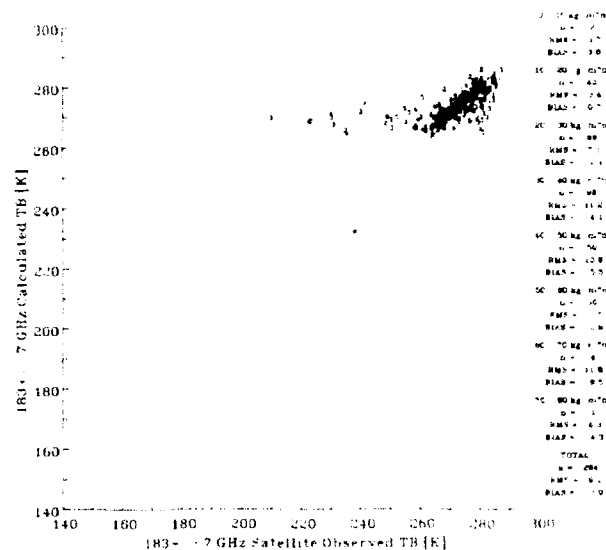


Figure 2.7.2-5. Calculated TBs using radiosondes from India and the United States in the Eyre RT simulation model versus SSM/T-2 observations for 183.3 ± 7 GHz. Plotted numbers represent total precipitable water content of the radiosonde profile used in the Eyre model, e.g., 0 represents a profile with a precipitable water content ranging from 0 to 10 kg/m², 1 represents a range from 10 to 20 kg/m², and so on.

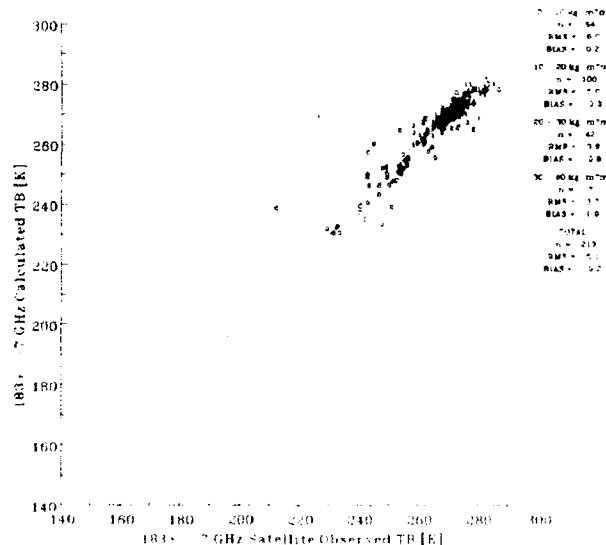
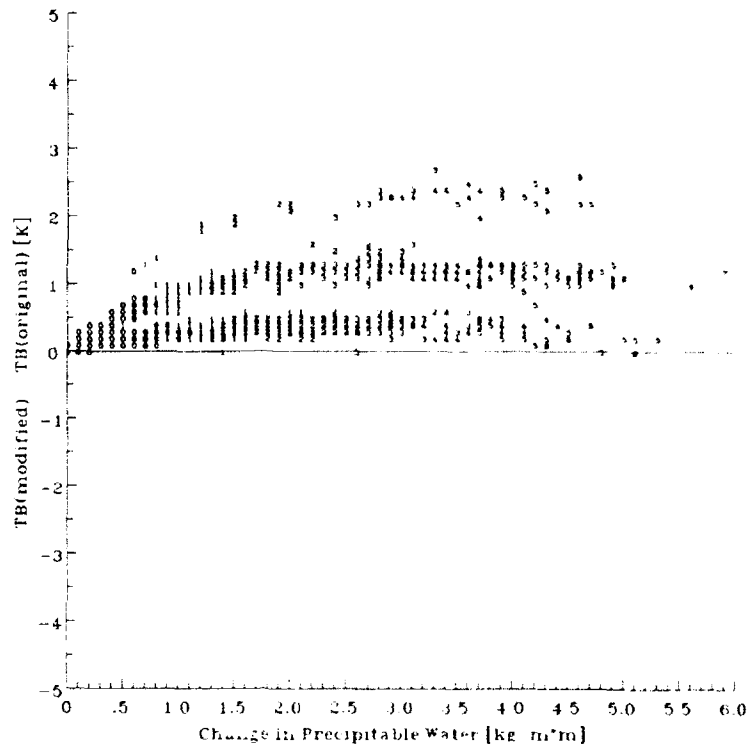


Figure 2.7.2-6. Calculated TBs using radiosondes from England, Germany, Scandinavia and Russia in the Eyre RT simulation model versus SSM/T-2 observations for 183.3 ± 7 GHz. Plotted numbers represent total precipitable water content of the radiosonde profile used in the Eyre model, e.g., 0 represents a profile with a precipitable water content ranging from 0 to 10 kg/m², 1 represents a range from 10 to 20 kg/m² and so on.



**a (91 GHz)**



**b (150 GHz)**

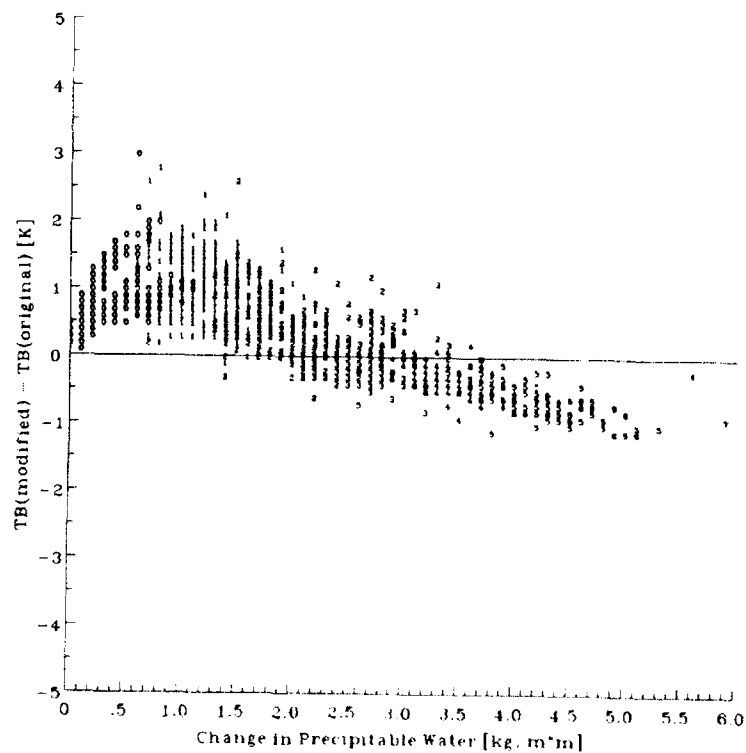
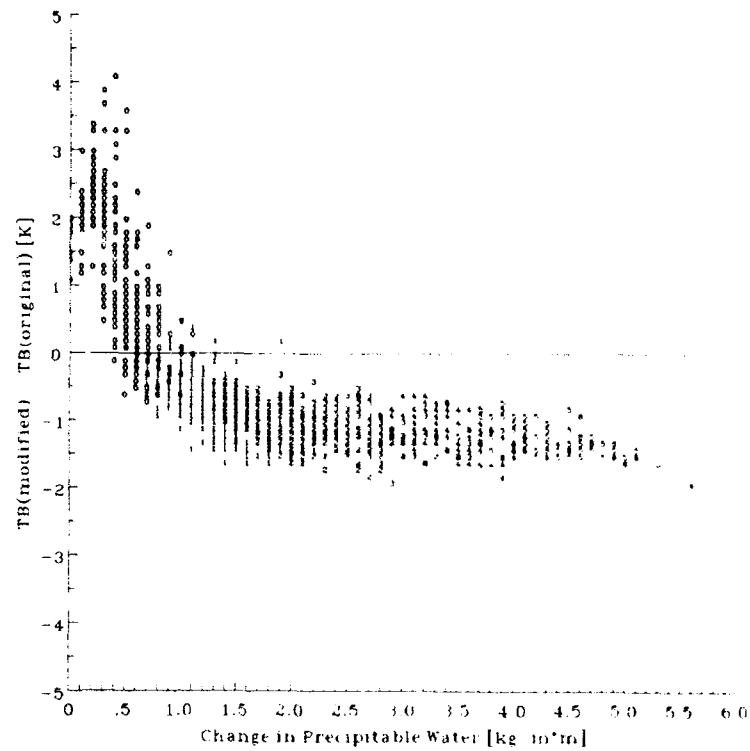
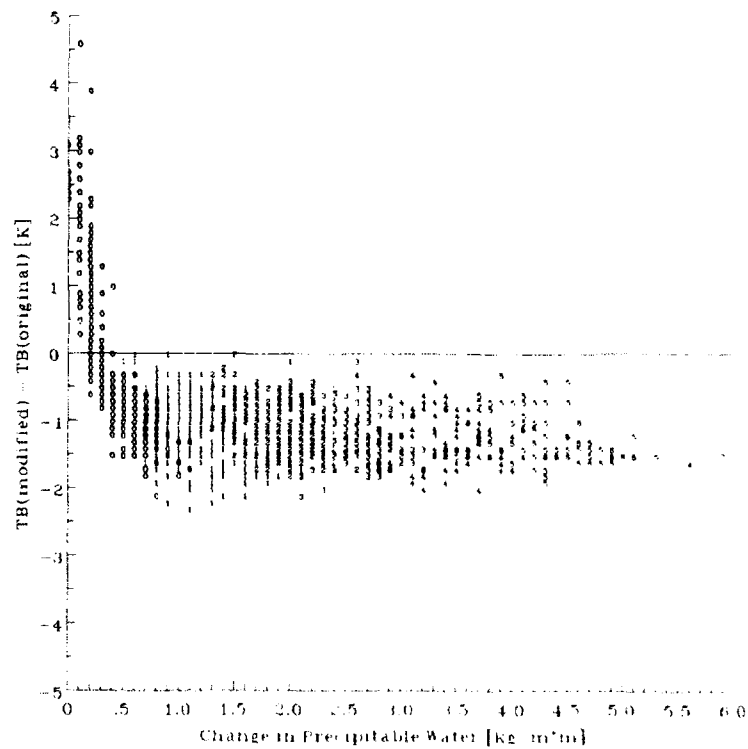


Figure 2.7.2-7 a-e. Calculated changes in TBs relative to the change in precipitable water caused by modifying the humidity profiles by the correction factors presented in Table 2.7.2-2 (see Brousaides and Morrissey, 1974 for discussion) for the five SSM/T-2 channel frequencies .

**c**  $(183.3 \pm 7 \text{ GHz})$



**d**  $(183.3 \pm 3 \text{ GHz})$



*Figure 2.7.2-7. (continued).*

e  $(183.3 \pm 1 \text{ GHz})$

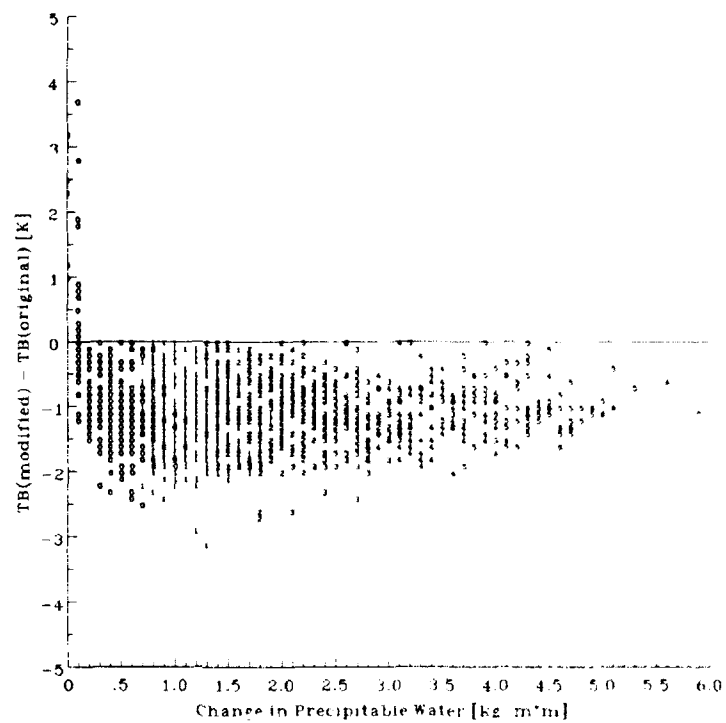


Figure 2.7.2-7. (continued).

**Millimeter Wave Moisture Sounder (SSM/T-2) Calibration/Validation Program**

**SSM/T-2 VALIDATION DATA ANALYSIS**

### 3. SSM/T-2 Validation

#### 3.1 Introduction

This section reports on the moisture retrieval performance of the first operational SSM/T-2 on DMSP F-11. The SSM/T-2 derived RH and Q are quantitatively compared to co-located radiosondes. A qualitative comparison of SSM/T-2 RH and Q to model analyzed moisture fields is also provided. The results of this study should not be taken as the final determination of the SSM/T-2 performance, but as an initial evaluation of a new sensor, and new ground processing algorithms.

No absolute error requirements were levied on the contractor for the SSM/T-2 system as a whole. The vertical moisture profile performance is on a best effort basis. With this in mind, this study will place initial RMS limits on the SSM/T-2 derived RH and Q at 1000, 850, 700, 500, 400, and 300 hPa. Water vapor mass at the seven required layers (i.e. surface-1000 hPa if available, 1000-850, 850-700, 700-500, 500-400, 400-300, and above 300 hPa) will be quantified in a follow-on effort, and compared directly to the SSM/I total water vapor mass. It should be noted that this study addresses the performance of only the first estimate (i.e. a-priori) linear regression coefficients computed by the contractor. This is not necessarily the optimal set. An update of the regression coefficients using co-located radiosonde data will most certainly improve performance.

#### 3.2 Ground Processing Software At AFGWC

The SSM/T-2 Ground Processing Software (GPS) contains four main modules, two of which are "on-line", and two "off-line". The on-line software generates SDRs, which are the calibrated TPs, and the EDRs for the RH and Q. The off-line software performs SSM/T-2 moisture sounding verification and statistically based algorithm "D-matrix" update functions. The following paragraphs will discuss in some detail both the on-line, and the off-line processing at AFGWC.

### 3.2.1 On-Line Software: Sensor Data Record Processor (SDRP)

The SDRP manipulates raw sensor data by time and data continuity checking, absolute calibration, earth location, determination of terrain type/height, retrieving numerical model 1000 hPa heights, and co-locating SSM/T-2 and SSM/T-1 SDRs.

Time checks are applied to the raw data based on time as reported by the Operational Linescan System (OLS), such that no time gaps are allowed within the data about to be calibrated. Each distinct group of four SSM/T-2 scans will be checked against the previous scans for time continuity. If all 28 SSM/T-2 scenes from each scan are not available, a time discontinuity or beam position error occurs. Should a time gap occur, the software dumps the raw data until the next contiguous four scan group is found.

Terrain types and heights are determined by utilizing the AFGWC terrain type/heights databases. For a given latitude and longitude, the relative grid points are located within the polar-stereographic database, and interpolated to the desired latitude and longitude. The terrain type is used for D-matrix selection criteria while the terrain heights are used to correct land and coastal retrievals for surface effects. The 1000 hPa heights are obtained from the AFGWC High Resolution Analysis System (HIRAS). For a given latitude and longitude, the relative grid points are located within the Mercator database, and interpolated to the desired latitude and longitude. The 1000 hPa heights are used to determine if a given atmospheric pressure surface is below the surface elevation. This information is used by the EDR generation software to properly report missing data. Co-locating SSM/T-1 SDRs to SSM/T-2 raw data is accomplished by comparing scan start time for SSM/T-1 to the SSM/T-2 four scan block time. If the time difference is less than 4 seconds, then matching scan data have been found. The matching SSM/T-1 SDR data is appended to the SSM/T-2 SDRs once calibration is complete. Should SDRP fail to match SSM/T-2 to the corresponding SSM/T-1 data, then the process is repeated for the next available four scan SSM/T-2 block. It should be noted that both SSM/T-1 and SSM/T-2 SDRs are required to process SSM/T-2 to the EDR level. All successfully processed data, along with the ancillary data, are then saved to disk for later processing.

At this point, only a qualitative evaluation of the precision of the SSM/T-2 earth location has been completed. The 91 GHz SSM/T-2 SDRs are interpolated and mapped onto a projection to include land/sea boundaries. At this frequency, the land/sea contrast is very high, and the agreement as to where the land/sea transition occurs has been found to be universally excellent. The reader is referred to SSM/T-2 Aerojet Report (1990) for a detailed discussion on the algorithms used to earth locate SSM/T-2 data. The significant change from the SSM/T-1 to the new SSM/T-2 algorithm is that the effect of earth rotation in the one minute blocks between ephemeris data points has been properly incorporated.

### 3.2.2 On-Line Software: Environmental Data Record Processor (EDRP)

The EDRP software computes RH, Q, and water vapor mass at the required levels and layers from the SDRs produced by the SDRP, relying on a stratified, multiple linear regression algorithm. A brief discussion of the retrieval scheme at AFGWC follows.

Linear regression coefficients are partitioned by background (i.e. ocean, land, coast, ice), view angle, and integrated water vapor mass (MV in  $\text{kg/m}^2$ ) in a column, and by TB (see Table 3.2.2-1 as an example of ocean background stratifications). The TB thresholding uses the SSM/T-1 54.35 and the 53.2 GHz data as well as the SSM/T-2  $183.3 \pm 1$  GHz data.

There are 25 atmospheres subdivided by surface/background type. Atmosphere Types 1-5 are for ocean background retrievals and are listed in Table 3.2.2-1. Atmospheres 6-20 are for the land, 21 and 22 are designed for the ice backgrounds, and 23-25 are for coast. Five discrete terrain height categories (0-1499 meters, 1500-2999, 3000-4499, 4500-6199, and 6200 meters and above) are used to adjust the SSM/T-2 coefficients over land backgrounds.

*Table 3.2.2-1. Atmospheric types over ocean surfaces stratified by MV and temperature.*

Type 1	MV < 10 and cold atmosphere
Type 2	MV < 10 and not cold
Type 3	MV between 10 and 26
Type 4	MV > 26, small upper level MV
Type 5	MV > 26, large upper level MV

A quality flag is also computed within EDRP for subsequent use in the verification software. It is preferable that SDRs be collected in cloud free conditions for subsequent use as input to the verification cycle since the radiative transfer calculations within the verification software will not adjust TBs for the presence of heavy cloud. The quality flag over ocean is constructed from a scatter diagram of the 50.5 GHz and 53.2 GHz channels TBs. Figure 3.2.2-1 shows this scatter plot from the contractor's radiosonde database. In order to verify the shape of this scatter plot, Figure 3.2.2-2 was generated using the dataset archived for this study. Water vapor mass and other collected cloud data will subsequently categorize the plot by clear/cloudy. Experience with co-located radiosonde data has allowed the SSM/T-2 contractor to effectively identify areas of heavy cloud over the ocean. Over non-ocean backgrounds, the quality flagging utilized SSM/T-1 temperature profiles in conjunction with the AFGWC Real-Time NEPHanalysis (RTNEPH) data. The inferred cloud type, amount, and thickness are used to determine the approximate cloud vapor mass. Should the vapor mass exceed  $0.15 \text{ kg/m}^2$ , then a quality flag is set to identify cloudy conditions.

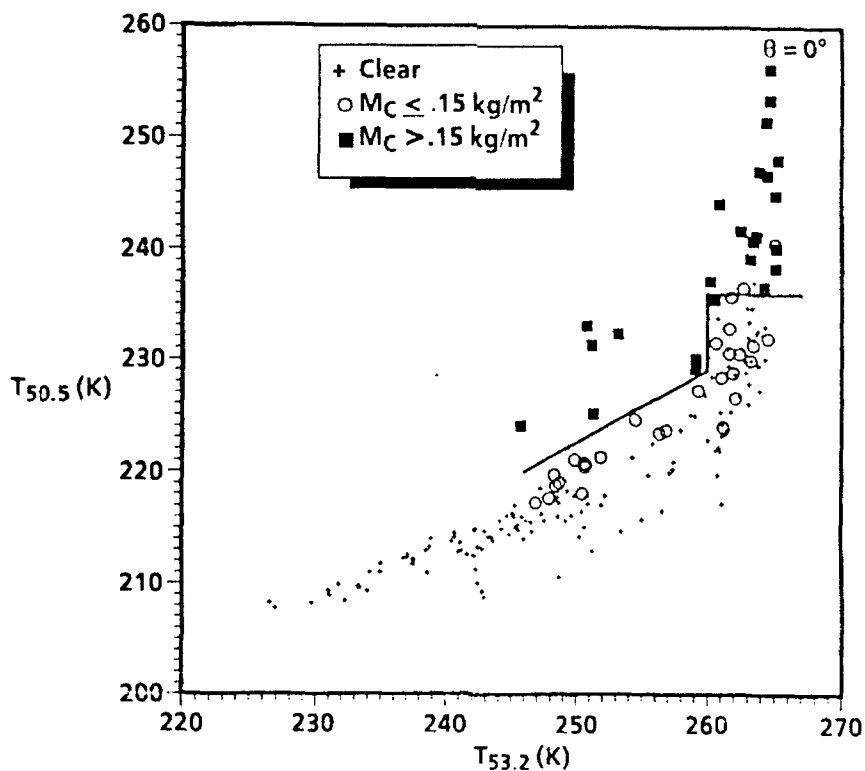


Figure 3.2.2-1. Aerojet's heavy cloud flag over ocean using the 50.5 and 53.2 GHz channels.

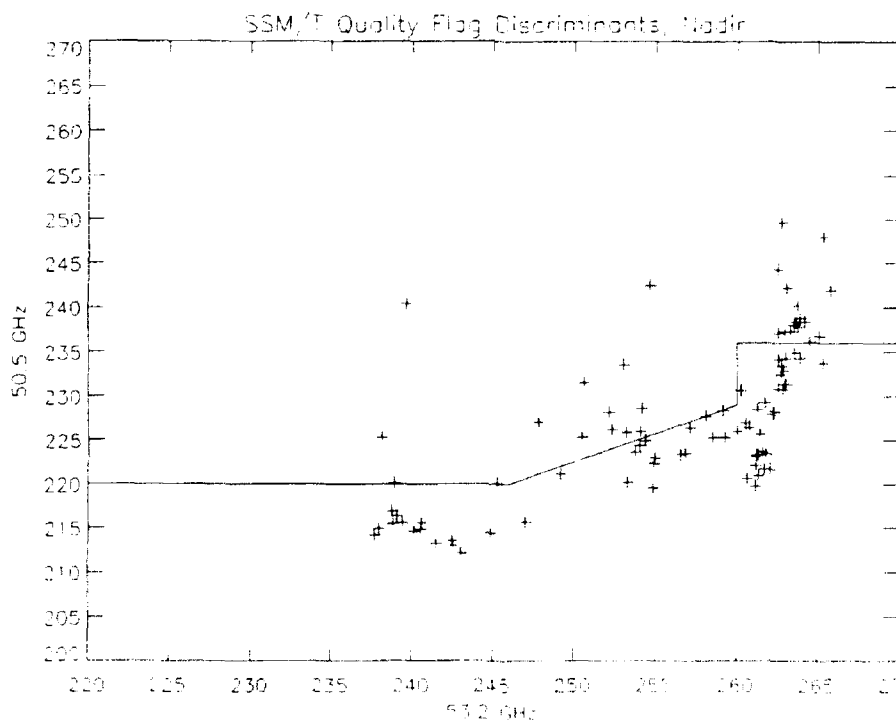


Figure 3.2.2-2. Radiosonde data set verification of Figure 3.2.2-1.



### 3.2.3 Off-Line Software: Verification Processor (VERP)

The VERP software matches SSM/T-2 EDRs to conventional radiosondes, both in time and space (co-location criteria are user selectable at run time), in order to assess quantitatively the performance of the regression coefficients. The processing flow is as follows: VERP accesses the AFGWC upper-air database directly for collection of the required radiosonde data. Approximately 650 radiosonde observations are available for each major synoptic launch time, i.e. 00 UTC and 12 UTC. The radiosonde data collected by VERP have been quality screened using the AFGWC upper-air validation criteria (a little more discussion on this will follow in a later section). For each valid SSM/T-2 versus radiosonde match, VERP will check each radiosonde reported level for useful temperature and dew point depression data. Should a value at a level be missing, VERP will reject the observation. Each radiosonde profile will be vertically interpolated to the 38 standard levels for the detailed calculations involved in the radiative transfer processing. Microwave radiances are computed from the interpolated radiosonde data and compared directly to the observed SSM/T-2 radiances. Adjustments to the regression coefficients are made in order to minimize the variance between the observed radiances, and the calculated radiances.

### 3.2.4 Off-Line Software: D-Matrix Update (DMUP)

The DMUP software utilizes the measured SSM/T-2 radiances and the calculated radiances generated in the VERP from co-located SSM/T-2/radiosonde pairs via radiative transfer theory, to statistically remove systematic error (i.e. bias) in the moisture retrievals. Due to the complexities of modeling an atmosphere containing heavy cloud (e.g. multiple scattering and re-emission), DMUP will not use SSM/T-2 versus radiosonde pairs that have been previously flagged as containing heavy cloud. Updating of the a-priori coefficients are independent of how these coefficients have been stratified. For example, the beam angle dependent coefficients can be updated independently for each set of background (ocean, land, coast, ice) coefficients. Exercising the DMUP software and updating the a-priori coefficients will be a high priority task.

The radiative transfer calculations within VERP will be tested against known standards such as Enhanced RADTRAN or the Eyre model. Accurate regression coefficient updates rely on precise radiosonde temperature to frequency dependent TB inversion.

### 3.3 Expected Level of Performance of the D-Matrix Retrieval Algorithm

Table 3.3-1 is a summary of the Aerojet expected level of RMS performance of the SSM/T-2 D-matrix retrieval algorithm via radiative transfer theory. The data have been beam averaged, with noise added for the model calculations (varying from 0.6 to 0.8 degrees Kelvin).

It is not surprising that the best retrieval statistics are expected to be over ocean backgrounds where the ocean surface emissivity is relatively uniform over a beam position. Land and especially coast background retrievals suffer from large variations in the surface emissivity within the SSM/T-2 FOV causing a correspondingly higher RMS. Ice retrievals have the difficulty of having old and new ice, and the possibility of multiphase surface water (e.g. snow or thin sheets of liquid water). Since no ice background SSM/T-2 and radiosonde co-locations have been observed to date, the ice statistics are not included in Table 3.3-1, nor is it discussed further.

*Table 3.3-1. Expected RMS performance of the SSM/T-2 D-matrix retrieval algorithm.*

Parameter @ Level	Units	Ocean	Land	Coast
RH @ 1000 hPa	%	13.5	20.3	16.5
RH @ 850 hPa	%	13.9	20.5	22.6
RH @ 700 hPa	%	16.0	19.4	19.6
RH @ 500 hPa	%	12.5	17.3	13.4
RH @ 400 hPa	%	11.8	15.1	13.5
RH @ 300 hPa	%	11.8	12.9	12.4
Q @ 1000 hPa	g/kg	1.41	2.79	2.71
Q @ 850 hPa	g/kg	1.09	1.88	2.32
Q @ 700 hPa	g/kg	.942	1.14	1.26
Q @ 500 hPa	g/kg	.319	.428	.391
Q @ 400 hPa	g/kg	.149	.200	.183
Q @ 300 hPa	g/kg	.054	.059	.059

### 3.4 Data Collection and Database Description

An extensive dataset has been collected (reference Appendix D) for this validation study. AFGWC allowed Aerospace to develop and to run data collection software on their development and production UNISYS computer systems. The software included executive control to run time sensitive batch jobs, and FORTRAN software to retrieve, reformat and write data to 9-track tape. In addition, a special computer production checklist was provided to operations staff to assist with the data collection scheduling. The detailed scheduling minimized impacts on the AFGWC operational computer systems.

In order to maximize the UNISYS computer (CPU and I/O) efficiency, the bulk of the magnetic tapes were written in UNISYS 36 bit packed format. The 36 bit word size architecture prevented direct communication of data to the Aerospace VAX and UNIX platforms. As a result, it was necessary to reload the 36 bit data collected on the operational systems, onto the development systems for post processing of the data into compatible formats. In all, some 1200 9 track tapes (approximately 108 GBytes) were written on the operational systems, post-processed on the development systems, reformatted on Aerospace computers, and archived to 8 mm tape. The following is a brief list of the data types that have been archived. (1) DMSP F-11 data to include OLS visible and infrared in the form of the Satellite Global Database (SGDB), SSM/I earth located TBs, SSM/T-1 earth located TBs, SSM/T-1 derived vertical temperature profiles, SSM/T-2 earth located TBs and vertical moisture profiles. (2) Conventional data including approximately 10,000 co-located SSM/T-2 to worldwide WMO radiosonde observations (note that more than one SSM/T-2 measurement may be co-located with each individual radiosonde observation; hence, there are not 10,000 unique soundings in this data set), and (3) data from the AFGWC Numerical Models including the RTNEPH, High Resolution Analysis System (HIRAS) RH, Winds, Temperatures, Heights, and data from the Global Spectral Model.

The reader should keep in mind that the SSM/T-2 has an artificially reduced swath width for this study. This is due to a software limitation in the SSM/T-1 processing when a glare obstructor (GLOB) is present on the spacecraft. The SSM/T-1 software eliminates the beam position that intersects the GLOB. However, not only is the GLOB obscured beam position eliminated, the symmetric beam on the other side of nadir is also eliminated. Recall that it is required to have matching SSM/T-1 and SSM/T-2 data, therefore, the missing SSM/T-1 scenes result in the loss of 8 out of 28 SSM/T-2 scenes (~28%). This extensive database can be made available to researchers in the field. Interested parties should contact one of the validation authors for further information.

### 3.5 Quantitative Comparison of Radiosonde versus SSM/T-2

The orbital geometry of F-11 and the synoptic release times (using only the 00 and 12 UTC times) of the worldwide World Meteorological Organization (WMO) radiosonde network confined the geographical distribution of co-located land-launched radiosonde and SSM/T-2 measurements. Another limiting factor is establishing SSM/T-2 versus radiosonde co-location criteria. There is no heritage in the scientific literature from which to make a choice of co-location criteria for moisture variables except for the astronomy community who deal with different horizontal correlation scales than the atmospheric sciences community. Therefore, for this initial study, 100 km in space and  $\pm 1$  hour in time was chosen primarily based on the assumption that the horizontal correlation lengths and temporal correlations for RH and Q are on this order. These criteria yield a significant set of SSM/T-2 versus radiosonde matches, on the order of 10,000. Note that there may be numerous SSM/T-2 retrieved profiles that are co-located with a single radiosonde profile. The geographical distribution of stations contributing to the matches are plotted in Figure 3.5-1. There could be a quality control problem for some of the high altitude Asian continent stations, and perhaps those over India. AFGWC does routinely reject a number of these WMO stations during the operational assimilation cycle of the HIRAS. The quality controls imposed on the radiosonde database are the first-pass error checks given in Table 3.5-1 that are used operationally at AFGWC. In addition to the WMO stations, ship-launched radiosondes are also part of the database. Unfortunately only a small number of island stations contribute to the co-location database.

For this study, radiosonde measured RH and Q are considered as "ground truth"; however, it is generally accepted that radiosonde dew point depressions are valid at the 10-15% level and can be even more suspect at low levels when launched from ships. The reader should keep this in mind when reviewing the quantitative SSM/T-2 versus radiosonde work to follow. In addition, the radiosonde observation is a "point" measurement whereas the SSM/T-2 is more appropriately a "volume" measurement. Perhaps the most

*Table 3.5-1. Operational error checks on radiosondes at AFGWC.*

Pressure (hPa)	Min. Temp (k)	Max. Temp (k)
1000.	183.2	333.2
850.	183.2	315.2
700.	183.2	305.2
500.	192.2	290.2
400.	200.2	278.2
300.	198.2	268.2

appropriate (operational) use of SSM/T-2 data would be along the lines of the European Centre for Medium Range Weather Forecasting (ECMWF) humidity analysis scheme (see "The Treatment of Humidity in ECMWF's Data Assimilation Scheme", 1980). The ECMWF analysis variable is the integrated Q between pressure levels p1 and p2 defined simply as:

$$\Delta_{1,2} = \int_{p1}^{p2} (Q) dp$$

ECMWF therefore recognizes the volumetric measurements and exploits this characteristic in the data assimilation design for the numerical weather prediction models.

Results of the radiosonde versus SSM/T-2 matches are presented in Table 3.5-2, and may be compared directly to the expected results in Table 3.3-1. The co-location criteria for Table 3.5-2 are 100 km in space and 1 hour in time. For readers who prefer to see vertical profiles in a soundings format, Appendix E is included and is a subset of the 10,000 co-located pairs. Bias is defined as (Radiosonde - SSM/T-2).

Initially, both land-launched and ship-launched radiosondes were considered as a single database. For completeness, the land and ship observations were plotted separately with surprising results (Appendix F). The quantity (Radiosonde - SSM/T-2) RH and Q is plotted on the ordinate, and index of the co-locations on the abscissa. Each four-plot panel represents one atmospheric level. In addition, the plots in Appendix F are stratified by atmosphere type. The co-location criteria are routinely annotated at the top of the plots. It is clear that the ship-launched radiosonde measurements and the SSM/T-2 derived parameters have a substantial bias. Further analysis has begun to understand the large discrepancies between the ship and SSM/T-2 data. However, as a result of this discovery, ship-launched radiosondes have been excluded from the Table 3.5-2 statistics.

The RH RMS over ocean backgrounds are certainly higher than initially predicted, and slightly higher than predicted over the land and coast backgrounds. Q RMS show similar results. In order to attempt to isolate the major contribution(s) to the variance of the data, the atmosphere types 1 through 5 with ocean backgrounds (reference Table 3.3-1) have been plotted separately in Appendix G. Ocean atmosphere 5 stands out at all levels, as well as Type 3 at several of the lower levels. Table 3.5-3 below summarizes the RMS performance of each ocean atmosphere type by level for both RH and Q. It should be noted that no Type 1 ocean atmospheres have been observed to date. Clearly, ocean atmospheres Type 5 and Type 3 (at 850 and 700 hPa) require additional investigation and will be addressed during the follow-on SSM/T-2 work. It is possible that the source of the error for the very moist Type 5 ocean atmosphere is as simple as a coding error, an error in the a-priori coefficients, or a more complex physical problem. It

*Table 3.5-2. RMS/bias of radiosonde measurements versus SSM/T-2-derived RH and Q.*

Parameter @ Level	Units	Ocean	Land	Coast
RH @ 1000 hPa	%	15.7 / 4.2	16.1 / 5.6	16.2 / -0.6
RH @ 850 hPa	%	22.7 / -3.1	24.2 / -3.7	25.1 / -7.4
RH @ 700 hPa	%	22.8 / -6.8	22.6 / -2.6	21.7 / -3.6
RH @ 500 hPa	%	25.1 / -12.2	21.8 / -4.8	20.1 / -2.0
RH @ 400 hPa	%	22.6 / -14.1	22.1 / -10.4	18.9 / -4.0
RH @ 300 hPa	%	23.2 / -13.2	19.6 / -2.5	17.4 / 0.2
Q @ 1000 hPa	g/kg	3.80 / 0.37	2.74 / -1.47	2.86 / -0.21
Q @ 850 hPa	g/kg	3.13 / -0.43	3.04 / -0.02	2.47 / -0.31
Q @ 700 hPa	g/kg	3.15 / -1.07	1.87 / 0.16	1.46 / 0.04
Q @ 500 hPa	g/kg	2.54 / -1.04	0.88 / -0.10	0.64 / 0.01
Q @ 400 hPa	g/kg	1.00 / -0.45	0.46 / -0.16	0.34 / -0.06
Q @ 300 hPa	g/kg	0.24 / -0.13	0.14 / -0.01	0.24 / -0.13

*Table 3.5-3. RMS of SSM/T-2 retrievals by atmospheric types over ocean surfaces.*

Parameter	Level	Expected	Type 2	Type 3	Type 4	Type 5
RH (%)	1000	13.5	17.0	11.6	11.4	16.3
RH (%)	850	13.9	17.1	28.1	17.4	22.5
RH (%)	700	16.0	17.5	25.6	13.1	23.2
RH (%)	500	12.5	14.9	19.8	11.0	26.4
RH (%)	400	11.8	13.1	14.9	6.6	24.5
RH (%)	300	11.8	13.7	13.2	9.8	25.2
Q (g/kg)	1000	1.41	1.44	1.34	2.23	4.10
Q (g/kg)	850	1.09	.618	3.11	1.85	3.26
Q (g/kg)	700	.942	.420	2.99	1.66	3.31
Q (g/kg)	500	.319	.201	.351	.650	2.79
Q (g/kg)	400	.149	.078	.101	.145	1.11
Q (g/kg)	300	.054	.019	.032	.069	.266

has been assumed that the line shapes at 150 and 183.3 GHz are well known and that the contribution to the absorption at these frequencies by aggregates of water vapor (e.g. dimers) is minimal. It is possible that these assumptions may not be completely valid. Follow-on work will include exercising the radiative transfer routines in the Verification Processor and calculating radiances at 183.3 GHz from the radiosonde data. In addition, considerable work is being done on the water vapor aggregates as they apply to the SSM/T-2 retrievals.

In order to assess any beam dependent RMS contributions to the statistics, RH and Q are plotted (Appendix H) by symmetric beam pairs about nadir. Recall that beam position 5 is the artificial edge of the SSM/T-2 scans due to the GLOB effects on

SSM/T-1 mentioned earlier. Beam position 24 is the symmetric beam on the opposite side of nadir. Beam positions 14 and 15 straddle nadir. The layout of Appendix H is similar to the plots of Appendix G. Table 3.5-4 summarizes the statistics.

No clear beam dependent RMS trends are observed in the analysis of the SSM/T-2 versus radiosonde comparisons in Table 3.5-4.

Heavy clouds have not been factored out of the results presented thus far. A flag for heavy cloud cover over ocean backgrounds can be estimated by examining a scatter plot of the TBs from the 50.5 GHz and 53.2 GHz channels from the SSM/T-1 (Figures 3.2.2-1 and 3.2.2-2) as mentioned earlier in the text. Results of re-computing the RMS statistics computed using only those observations tagged as heavy cloud contaminated are presented in Table 3.5-5. Only the non-cloud contaminated observation statistics are given in Table 3.5-6. Atmosphere Types 2-4 have no heavy cloud contaminated soundings as expected.

The RMS for both RH and Q are substantially reduced when cloud contamination is accounted for. The Table 3.5-2 RMS over land and coast cannot be flagged for heavy cloud contamination effectively by using the SSM/T-1 scatter plot technique due to the unknown variability in the 50.5 GHz SSM/T-1 TBs within a beam position, over the land. It is reasonable to assume that if a heavy cloud flag over land were available (and reliable), that the RMS over land and coast backgrounds would improve.

*Table 3.5-4. RMS of SSM/T-2 retrievals as a function of beam positions.*

Parameter@ Level	Ex- pected	5/24	6/23	7/22	8/21	9/20	10/19	11/18	12/17	13/16	14/15
RH@1000	13.5	17.9/12.7	15.5/15.5	15.4/19.1	15.2/17.8	15.3/18.4	16.0/17.7	15.5/15.9	15.0/17.9	15.9/13.8	15.1/13.9
RH@850	13.9	23.7/24.1	24.5/22.0	24.9/23.7	24.6/25.0	24.6/25.8	26.2/25.5	25.5/24.9	22.9/24.8	24.2/25.8	24.2/23.5
RH@700	16.0	24.5/22.4	24.1/21.0	23.2/20.8	23.1/21.8	22.9/22.8	24.1/23.5	21.2/23.5	18.4/22.9	20.3/21.7	21.5/21.9
RH@500	12.5	19.2/21.0	20.7/20.9	21.6/20.6	22.4/22.2	21.0/23.4	22.5/22.7	21.4/21.8	22.2/21.0	22.1/19.3	19.6/19.5
RH@400	11.8	19.4/20.8	19.5/19.8	19.6/19.9	19.9/22.4	20.3/22.6	21.5/21.6	22.1/22.2	21.8/20.8	21.4/20.8	20.6/22.0
RH@300	11.8	17.4/17.3	16.3/19.2	16.7/18.7	17.6/20.1	18.4/19.0	18.7/20.3	19.2/21.0	20.4/18.5	20.5/19.9	18.5/20.2
Q@1000	1.41	2.39/3.11	2.00/2.74	2.92/2.97	3.15/3.04	3.05/3.50	2.64/2.83	2.12/3.04	2.52/3.95	2.65/3.22	3.07/3.50
Q@850	1.09	2.50/2.40	3.05/2.35	3.57/2.67	3.69/2.90	3.48/2.70	2.83/2.75	2.58/2.87	2.35/2.98	2.45/2.90	2.56/2.69
Q@700	.942	1.81/2.28	1.72/1.52	1.67/1.70	1.83/2.00	1.70/2.09	1.80/2.10	1.57/1.93	1.44/1.91	1.57/1.52	1.71/1.70
Q@500	.319	.731/856	.750/752	.881/798	1.21/976	1.02/1.06	.863/874	.805/949	.809/1.07	.852/777	1.05/848
Q@400	.149	.363/447	.352/396	.383/427	.502/501	.518/492	.426/424	.429/476	.383/495	.409/461	.486/493
Q@300	.054	.114/111	.118/122	.117/121	.127/130	.149/125	.133/138	.135/151	.135/138	.140/150	.132/153

*Table 3.5-5. RMS of SSM/T-2 retrievals by heavy cloud-type atmospheres over ocean surfaces.*

Parameter @ Level	Expected	Type 2	Type 3	Type 4	Type 5
RH @ 1000 hPa	13.5	N/A	N/A	N/A	19.8
RH @ 850 hPa	13.9	N/A	N/A	N/A	24.1
RH @ 700 hPa	16.0	N/A	N/A	N/A	22.1
RH @ 500 hPa	12.5	N/A	N/A	N/A	27.5
RH @ 400 hPa	11.8	N/A	N/A	N/A	28.5
RH @ 300 hPa	11.8	N/A	N/A	N/A	29.3
Q @ 1000 hPa	1.41	N/A	N/A	N/A	4.91
Q @ 850 hPa	1.09	N/A	N/A	N/A	3.44
Q @ 700 hPa	.942	N/A	N/A	N/A	3.78
Q @ 500 hPa	.319	N/A	N/A	N/A	3.48
Q @ 400 hPa	.149	N/A	N/A	N/A	1.41
Q @ 300 hPa	.054	N/A	N/A	N/A	.314

*Table 3.5-6. RMS of SSM/T-2 retrievals by non-heavy cloud-type atmospheres over ocean surfaces.*

Parameter @ Level	Expected	Type 2	Type 3	Type 4	Type 5
RH @ 1000 hPa	13.5	16.5	11.6	8.0	11.1
RH @ 850 hPa	13.9	16.0	28.1	14.0	20.3
RH @ 700 hPa	16.0	16.3	25.4	12.9	24.3
RH @ 500 hPa	12.5	14.6	19.6	9.1	24.7
RH @ 400 hPa	11.8	11.0	14.9	6.4	18.2
RH @ 300 hPa	11.8	13.3	12.4	9.5	18.5
Q @ 1000 hPa	1.41	1.11	1.27	1.43	2.92
Q @ 850 hPa	1.09	.578	3.11	1.75	3.01
Q @ 700 hPa	.942	.393	2.99	1.64	2.54
Q @ 500 hPa	.319	.107	.346	.411	1.47
Q @ 400 hPa	.149	.040	.094	.141	.557
Q @ 300 hPa	.054	.014	.030	.067	.189

A final concern is the question as to whether a different choice of spatial co-location criteria (other than the assumed 100 km value) would substantially alter the SSM/T-2 Vs radiosonde RMS statistics. In order to address this concern, the spatial co-location criteria were changed to 25 and 50 km (keeping the temporal value of  $\pm 1$  hour), and RMS statistics were re-calculated (again stratified by the ocean, land, and coast backgrounds). The results are plotted in Appendix I and summarized below in Table 3.5-7. There are improvements in RMS at some levels, and poorer results at others when compared to the 100 km co-location statistics by background (Table 3.5-7). However the number of co-locations begin to suffer and the resulting sample size is insufficient to determine statistically significant results at the 25 km value. Overall, the 100 km spatial



co-location criteria gives consistent results compared to the 50 km data, and has a significant sample size.

These co-location results (a-priori coefficients only) are very encouraging, except for the type 3 and type 5 atmospheres over ocean, in light of the unknown quality of a large number of the radiosondes collected over the Asian continent. The errors will most certainly decrease after the a-priori coefficients are replaced by an updated set.

Perhaps the best comparison of the overall utility and versatility of the SSM/T-2 is to examine the horizontal structure of the relatively high resolution SSM/T-2 measurements. In the following Section, SSM/T-2 RH and Q imagery will be compared to the High Resolution Analysis System (HIRAS) analyzed RH and Q imagery.

*Table 3.5-7. RMS of SSM/T-2 retrievals stratified by spatial co-location criteria.*

Co-location @	Parameter @ Level	Units	Ocean	Land	Coast
25 km	RH @ 1000 hPa	%	12.4	16.2	16.1
50 km	RH @ 1000 hPa	%	12.5	15.7	14.5
25 km	RH @ 850 hPa	%	14.1	24.1	24.0
50 km	RH @ 850 hPa	%	18.1	23.5	24.3
25 km	RH @ 700 hPa	%	26.8	21.9	20.3
50 km	RH @ 700 hPa	%	21.0	22.3	20.9
25 km	RH @ 500 hPa	%	27.6	19.5	19.1
50 km	RH @ 500 hPa	%	24.5	20.2	19.7
25 km	RH @ 400 hPa	%	15.7	21.2	18.1
50 km	RH @ 400 hPa	%	16.9	20.7	18.5
25 km	RH @ 300 hPa	%	19.3	19.0	17.9
50 km	RH @ 300 hPa	%	21.1	19.0	17.8
25 km	Q @ 1000 hPa	g/kg	3.26	2.15	2.92
50 km	Q @ 1000 hPa	g/kg	3.00	2.22	2.69
25 km	Q @ 850 hPa	g/kg	2.06	2.65	2.38
50 km	Q @ 850 hPa	g/kg	2.64	2.98	2.35
25 km	Q @ 700 hPa	g/kg	2.70	1.74	1.47
50 km	Q @ 700 hPa	g/kg	2.48	1.77	1.43
25 km	Q @ 500 hPa	g/kg	1.69	.856	.565
50 km	Q @ 500 hPa	g/kg	1.64	.827	.610
25 km	Q @ 400 hPa	g/kg	.560	.443	.326
50 km	Q @ 400 hPa	g/kg	.519	.433	.318
25 km	Q @ 300 hPa	g/kg	.228	.131	.115
50 km	Q @ 300 hPa	g/kg	.209	.132	.107

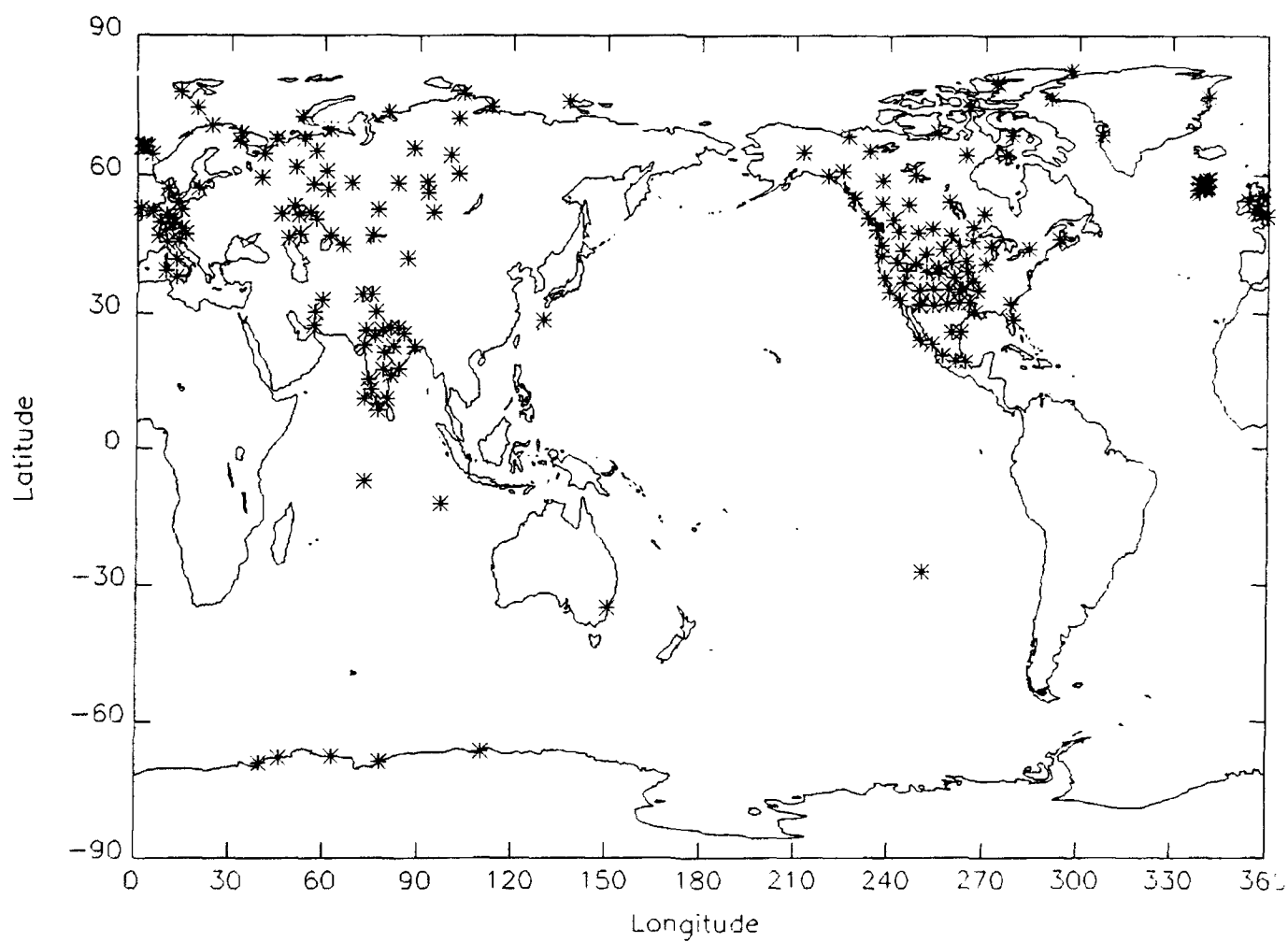


*Figure 3.5-1. Geographic distribution of the locations of radiosondes that were used in the SSM/T-2 validation study.*

### 3.6 Qualitative Comparison of Model Analyzed Moisture versus SSM/T-2

An extensive set of SSM/T-2 and model analysis imagery are available in the DMSP Library. A small subset is included in Appendix J. The purpose of including this qualitative dataset is to anticipate the use of the SSM/T-2 data in global numerical weather prediction models. The SSM/T-2 has tremendous horizontal resolution compared to existing moisture analysis at AFGWC. It is hoped that these data will encourage the users to exploit the capabilities of the SSM/T-2 system and spark new research in small-scale energy conversion processes, as well as global water vapor budgets for climate research.

The authors encourage the modeling community to examine the small dataset in Appendix J in detail. The SSM/T-2 has never been advertised as an imager; however, with proper horizontal interpolation, the SSM/T-2 may be transformed into useful imagery. Tools were written in Interactive Data Language (IDL)<sup>®</sup> to construct imagery from the SSM/T-2 and the model data. The color lookup tables are scaled consistently between the SSM/T-2 EDRs and the model analysis to permit the direct overlay of data for comparison. This dataset consists of SSM/T-2 RH and Q at several levels, as well as the corresponding HIRAS analysis. In addition, the wind analysis from HIRAS is included as well as the ground track of the analyzed F-11 SSM/T-2 orbit. Each orbit contains cyclones or convective clusters directly overflown by the SSM/T-2. Analysis of the imagery should proceed as follows: compare the F-11 ground track to the HIRAS wind field analysis in order to isolate areas of interest. Begin with RH at low levels. The signature of small scale convective activity is depletion (via convergence and entrainment) of the local moisture. Moving to the upper levels (i.e. 500 hPa), look for saturation due to the convective energy conversions, and eventual RH depletion by detrainment further aloft. Specific humidity shows similar features. A note of caution over land. Missing data appear as light purple giving the impression of very dry conditions. The larger scale synoptic features should be compared directly to the HIRAS analysis. The SSM/T-2 imagery show convection and post-frontal drying in great detail. These clearly defined physical processes have the potential to improve the moisture specification significantly.

In addition, viewing the SSM/T-2 data as imagery is a very fast means of quality control. Out of range values can be spotted by the eye very quickly, bogused out of the dataset, and past on to the data assimilation schemes. Workstations are now fast enough to handle these multidimensional datasets in a very short (processing) time.

The assimilation of SSM/T-2 data into HIRAS could begin by a judicious averaging of the RH/Q since adjacent SSM/T-2 observations appear to be reasonably well correlated. Perhaps a more rigorous interpolation scheme along the lines of Kriging (1973) would yield an optimum interpolation. What is clear after examining the SSM/T-2 RH/Q imagery compared to the HIRAS equivalent is that new research must be started in order to take advantage of the excellent horizontal resolution of the SSM/T-2, and the overall quality of the observations on a given pressure level.

#### 4. CONCLUSIONS

Over water, measurements of SSM/T-2 channels in the vicinity of 183.31 GHz water vapor absorption line produce RMS deviations from the mean of the co-located MIR-measured TBs of 0.7 - 2.1 K with biases of up to 1.8 K in magnitude. RMS variation for these frequencies is larger for coastal FOVs (up to 2.4 K) with the largest variation for land backgrounds (up to 3.8 K). For the surface channels, 91 and 150 GHz, show larger RMS and bias, especially for the mixed (i.e. coastal) FOVs.

Radiative transfer calculations based on co-located radiosondes are generally in good agreement with SSM/T-2 TBs considering that there was no consideration of clouds and weather conditions within the SSM/T-2 FOV which could also affect the TBs measured within the SSM/T-2 FOV as well as the forward-calculated TBs. The three 183.3 GHz channels had RMS differences of up to 7.8 K. The larger discrepancies for the transparent channels are a result of the channels sensing the surface, for which mean emissivities used in the RT simulations underestimate the SSM/T-2 observations over land and overestimate them over the ocean.

Studies of the variations of the on-orbit calibration performed by Aerospace indicate the instrument is very stable. The analysis of the underflights indicate that the SSM/T-2 is performing within or exceeds the original specifications. This calibration study has shown that for operational utilization there are *no apparent or consistent* instrument biases.

The SSM/T-2 retrieved vertical moisture profiles (excluding observations contaminated by heavy cloud) compare favorably with co-located radiosonde data except over certain ocean atmospheres. The radiosonde database included Asian continent stations, and high altitude stations that may have questionable observation accuracies. These stations were not removed from the database for this study, therefore the results should be considered as a worst case scenario. The linear biases that were observed between the SSM/T-2 versus radiosonde comparisons will be eliminated when the a-priori regression coefficients are updated. The improvement in retrieval accuracy via the update of regression coefficients is a high priority task and will be pursued as soon as possible.

The SSM/T-2 has not been advertised as an imager, however, this study has proved that the SSM/T-2 is capable of yielding high quality EDR imagery. The detailed imagery should energize the modeling community to consider assimilating the SSM/T-2 data into operational analysis as well as using the imagery itself as a means of rapid quality control of the data prior to assimilation in the numerical models. In addition, the SSM/T-2 TBs rendered as multichannel imagery are interesting. Work to date includes combining the 91 GHz window channel, the 150 GHz (middle atmosphere) channel, and the  $183.3 \pm 1$  GHz channel. This particular choice of channels and colors brings out the

structure of small scale storms very effectively. The interpretation of the multichannel data is, at times, very complex. The 183.3 GHz channel is the most difficult to deal with since both absorption, re-emission and scattering are occurring.

This initial validation study has the following set of recommendations:

(1) detailed analysis of the a-priori ocean atmosphere Types 3 and 5, (2) careful inspection of the radiative transfer code implementation, (3) detailed analysis of the inferred heavy cloud flag over ocean, and finally (4) a careful update to the a-priori D-Matrices.

In summary, the experience that the user community gains by working with the SSM/T-2 data as both a point measurement and a volume averaged variable in the numerical weather prediction models, will simplify the transition to the higher resolution SSMIS soundings. It is imperative that proper attention be given to the fine tuning of the SSM/T-2 during a follow-on effort since all lessons learned will be directly applicable to the SSMIS system.

## **5. POSSIBLE FURTHER ANALYSIS**

In the Cal/Val Volume II an attempt will be made to address the following areas:

- 1) weather analysis of FOV on calibration,
- 2) plot of time line of the ER-2 data and demarcation of topography (as determined by the SSM/T-2 classification),
- 3) MIR TB changes over the same location with time,
- 4) global rawinsonde comparison during this time,
- 5) compare polarization difference between SSM/T-2 and MIR, and
- 6) examine increased  $183.3 \pm 1$  GHz RMS over land and water compared to the  $183.3 \pm 3$  and  $183.3 \pm 7$  GHz,
- 7) experiment with different retrieval techniques,
- 8) research surface problems, such as cold air outbreaks and snow/ice surfaces,
- 9) examine statistics of global water vapor distribution as it impacts the D-matrix retrieval technique,
- 10) research water retrievals,
- 11) cloud impact and use in retrievals, and
- 12) earth surface polarization studies.

## 6. REFERENCES

- Aerojet Report, June, 1990: System summary report for the SSM/T-2 water vapor profiling sensor hardware segment, Air Force Contract F04701-83-C-0038, CDRL 035A2.
- Aerojet Report, January, 1991: Acceptance test report for the SSM/T-2 water vapor profiler (P/N 1328900, S/N B5), Air Force Contract F04701-83-C-0038, CDRL 040A2.
- Aerojet Report, April, 1988: SSM/T-2 ground support equipment operations manual, Air Force Contract F04701-83-C-0038.
- Brousailles, F. J., and J. F. Morrissey, 1974: Residual temperature-induced humidity errors in the National Weather Service radiosonde, Final Report, AFCRL-TR-74-0111, Instrumentation Papers, No. 215, Air Force Cambridge Research Laboratories, Mass., 40 pp.
- Eyre, J. and H. Woolf, 1988: Transmittance of atmospheric gases in the microwave region: a fast model. Applied Optics, 27, 15, 3244-3249.
- Falcone, V.J., L.W. Abreu, and E.P. Shettle, 1979: Atmospheric attenuation of millimeter and submillimeter waves: Models and computer code, AFGL-TR-79-0253. [NTIS AD A084485]
- Falcone, V.J., L.W. Abreu, and E.P. Shettle, 1982: Atmospheric attenuation in the 30-300 GHz region using RADTRAN and MWTRAN. Proc. Soc. Photo Opt. Instrum. Eng., 337, 62-66.
- Fleming, H. and L. McMillin, 1977: Atmospheric transmittance of an absorbing gas. 2: A computationally fast and accurate transmittance model for slant paths at different zenith angles. Applied Optics, 16, 5, 1366-1606.
- Garand, L., C. Grassotti, J. Hallé, and G.L. Klein, 1992: On differences in radiosonde humidity-reporting practices and their implications for numerical weather prediction and remote sensing. Bulletin American Meteorological Society, 73, 9, 1417-1423.
- Hoffman, R.N., C. Grassotti, R.G. Isaacs, J.-F. Louis, T. Nehr Korn, and D.C. Norquist, 1990: Assessment of the Impact of Simulated Satellite Lidar Wind and Retrieved Water Vapor Observations on a Global Data Assimilation System. Mon. Wea. Rev., 118, 12, 2513-2542.

- Isaacs, R.G., 1987: Review of 183 GHz Moisture Profile Retrieval Studies. Scientific Report No. 1. Air Force Geophysics Laboratory, Hanscom AFB, MA, 01731. AFGL-TR-87-0127.
- Isaacs, R.G., R.N. Hoffman and L.D. Kaplan, 1986: Satellite remote sensing of meteorological parameters for global numerical weather prediction. Review of Geophysics, 24, 4, 701-743.
- Isaacs, R.G. and G. Deblonde, 1987: Millimeter wave moisture sounding: The effect of clouds. Radio Science, 22, 3, 367-377.
- Isaacs, R.G., R.D. Worsham, B.L. Lindner, 1989: Characterizing Microwave Propagation Using the AFGL Microwave Attenuation/Transmittance/TB Code. GL-TR-89-0188, Air Force Geophysics Laboratory, Hanscom AFB, MA, 01731.
- Kiess, R. B., and W. Cox, 1988: The AFGWC Automated Real-time Cloud Analysis Model. AFGWC Technical Note 88/001, Air Force Global Weather Central, Offutt AFB, NE, 82 pp.
- Kriging, D.P., 1973, Analyse Objective du geopotential et du vent geostrophique par Krigeage universel, La Meteorologie, V-25.
- Lindzen, R. S., and Fox-Rabinovitz, M., 1989: Consistent horizontal and vertical resolution. Monthly Weather Review, 117, p. 2575-2583.
- Nash, J., and F. J. Schmidlin, 1987, WMO International Radiosonde Comparison, Final Report. World Meteorological Organization Instruments and Observing Methods Report No. 30, WMO/TD-No. 195, 103 pp.
- Racette, P.E., L.R. Dod, J.C. Shiue, R.F. Adler, D.M. Jackson, A.J. Gasiewski, D.S. Zacharias, 1992: Millimeter-wave imaging radiometer for cloud, precipitation, and atmospheric water vapor studies. IGARS-92, Houston, TX Proceedings.
- Schmidlin, F. J., 1988, WMO International Radiosonde Intercomparison Phase II, 1985. World Meteorological Organization Instruments and Observing Methods Report No. 29, WMO/TD-No. 312, 113 pp.
- The Treatment of Humidity in ECMWF's Data Assimilation Scheme, 1980, Atmospheric Water Vapor, Academic Press, pp. 497-512.



Appendix A  
Abbreviations and Acronyms

<u>Abbreviation or Acronym</u>	<u>Definition</u>
AER	Atmospheric and Environmental Research, Inc.
Aerojet	Aerojet Electronic Systems Division
AFGWC	Air Force Global Weather Central
Cal/Val	Calibration/Validation
CI	Two-letter Military Abbreviation for Defense Meteorological Satellite Program
CPU	Central Processing Unit
DMSP	Defense Meteorological Satellite Program
DMUP	D-Matrix Update
$\Delta T$	Minimal Detectable Change in Radiometer Antenna Temperature
ECMWF	European Centre for Medium Range WeatherForecasting
EDR	Environmental Data Record
ER-2	Earth Resources Aircraft (U-2)
FOV	Field-of-View
GLOB	Glare Obstructor
GPS	Ground Processing Software
HIRAS	High Resolution Analyses System
IDL	Interactive Data Language
I/O	Input/Output
MIR	Millimeter-wave Imaging Radiometer
MV	Integrated Water Vapor Mass
NAS	Naval Air Station
NASA	National Aeronautics & Space Agency
NE $\Delta$ T	Noise Equivalent Temperature Difference

Appendix A (continued)  
Abbreviations and Acronyms

<b>Abbreviation or Acronym</b>	<b>Definition</b>
NOAA/NESDIS	National Oceanic and Atmospheric Administration/National Environmental Satellite Data and Information Service
OLS	Operational Linescan System
PL/GP	Phillips Laboratory/Geophysics Directorate
PRT	Platinum Resistance Thermometer
Q	Specific Humidity (gm/kg)
RF	Radio Frequency
RH	Relative Humidity (%)
RMS	Root Mean Square
RT	Radiative Transfer
RTD	Resistive Temperature Devices
RTNEPH	Real-Time NEPH Analysis
SDR	Sensor Data Record
SDRP	Sensor Data Record processor
SGDB	Satellite Global Database
SMC	Space & Missiles Center
SSM/I	Special Sensor Microwave, Imager
SSMIS	Special Sensor Microwave Imaging Sounder
SSM/T-1	Special Sensor Microwave, Temperature
SSM/T-2	Special Sensor Microwave, Water Vapor
TB	Brightness Temperature
UTC	Universal Time Coordinated (formally Greenwich Mean Time)
VERP	Verification Processor
WMO	World Meteorological Organization

Appendix B. Distributions of radiosonde stations and measurements that were used to calibrate the SSM/T-2. Co-locations were determined by the thresholds of  $\pm 1$  hours and  $\pm 100$  km. The soundings were required to have reported moisture profiles up to 300 hPa.

#### Latitude Distribution of Radiosonde Measurements and Radiosonde Stations

<u>Latitude</u>	<u>Latitude</u>	<u>Number of RAOBs</u>	<u>Number of Stations</u>
90	80	11	2
80	70	31	7
70	60	112	24
60	50	238	67
50	40	193	62
40	30	274	76
30	20	153	37
20	10	95	25
10	0	60	15
0	-10	11	4
-10	-20	10	2
-20	-30	1	1
-30	-40	4	3
-40	-50	0	0
-50	-60	0	0
-60	-70	34	5
-70	-80	0	0
-80	-90	0	0
	TOTAL	1227	330

#### Elevation Distribution of Radiosonde Measurements and Radiosonde Stations

<u>Elevation [m]</u>	<u>Elevation [m]</u>	<u>Number of RAOBs</u>	<u>Number of Stations</u>
0	50	435	106
50	100	122	32
100	200	157	43
200	300	75	23
300	400	71	23
400	500	45	13
500	600	22	9
600	700	29	11
700	800	24	8
800	900	33	8
900	1000	36	10
1000	2000	140	32
2000	3000	24	6
3000	4000	14	6
4000	5000	0	0
5000	99999	0	0
	TOTAL	1227	330

### Time Distribution of Radiosonde Measurements

<u>Time (UTC)</u>	<u>Number of RAOBs</u>
0	410
6	104
12	675
18	38
TOTAL	1227

Individual listing of radiosonde stations (block number and station number), latitude, longitude, elevation and frequency of radiosonde profiles that were co-located with SSM/T-2 observations (using  $\pm 1$  hour and 100 km)

<u>Block &amp; Station Number</u>	<u>Latitude + North - South</u>	<u>Longitude - East + West</u>	<u>Elevation [m]</u>	<u>Frequency</u>
10280	74.51	-19.01	18.	6
28360	67.36	-26.65	178.	9
29350	62.40	-25.66	139.	7
29630	60.81	-23.50	103.	7
31700	56.43	2.86	4.	1
32130	54.31	3.40	8.	2
32400	55.41	1.60	23.	5
33220	53.55	2.91	54.	8
34960	52.68	-1.68	13.	1
35020	52.13	4.56	133.	1
36930	51.55	-0.83	2.	1
37430	51.20	1.80	132.	2
37740	51.08	0.21	143.	5
39200	54.48	6.10	37.	10
39530	51.93	10.25	9.	1
42200	68.70	52.75	40.	2
42700	61.18	45.43	4.	1
43200	76.76	18.66	14.	10
43390	70.48	21.96	65.	1
60300	57.10	-9.86	3.	1
62600	52.10	-5.18	2.	3
93930	52.21	-14.13	115.	2
95480	50.56	-10.38	450.	1
100460	54.38	-10.15	31.	2
101840	54.10	-13.40	2.	8
102000	53.35	-7.21	5.	3
102380	52.81	-9.93	70.	1
103040	52.71	-7.31	19.	2
103930	52.21	-14.11	115.	5
105480	50.56	-10.36	450.	8
106180	49.70	-7.33	376.	3
107710	49.43	-11.90	419.	3

109210	47.98	-8.90	807.	1
110110	48.23	-14.18	298.	2
110350	48.25	-16.36	200.	1
112390	47.00	-15.43	340.	1
115200	50.00	-14.45	303.	6
160440	46.03	-13.18	93.	2
160800	45.43	-9.28	107.	4
163200	40.65	-17.95	15.	2
164290	37.91	-12.50	7.	4
165600	39.25	-9.05	4.	4
200460	80.61	-58.05	20.	7
202920	77.71	-104.28	13.	1
208910	71.98	-102.46	33.	4
215040	74.66	-112.93	35.	3
218240	71.63	-128.85	8.	6
230220	69.76	-61.68	53.	11
230780	69.33	-88.10	62.	4
234720	65.78	-87.95	32.	10
238840	61.60	-90.00	63.	5
239210	60.68	-60.43	101.	12
241250	68.48	-112.43	209.	5
242660	67.55	-133.38	137.	3
243430	66.76	-123.40	84.	4
245070	64.16	-100.06	188.	6
249590	62.08	-129.75	103.	2
264220	56.96	-24.06	3.	5
271960	58.65	-49.61	164.	3
282750	58.15	-68.18	44.	8
284400	56.80	-60.63	237.	11
286980	54.93	-73.40	94.	13
287220	54.81	-56.15	104.	1
289520	53.21	-63.61	171.	3
292310	58.30	-82.90	76.	3
292630	58.45	-92.15	78.	3
295740	56.00	-92.88	215.	6
296120	55.36	-78.40	120.	3
296340	55.03	-82.90	141.	7
298380	53.33	-83.70	250.	4
298650	53.75	-91.40	256.	6
300540	59.45	-112.58	193.	1
302300	57.76	-108.11	258.	1
305210	54.80	-105.16	428.	1
306350	53.43	-108.98	457.	1
307150	52.48	-103.85	450.	1
307580	52.01	-113.33	668.	1
309350	50.36	-108.75	770.	1
309650	50.38	-116.51	684.	1
333450	50.40	-30.45	168.	1
351210	51.75	-55.10	120.	1
352290	50.28	-57.15	219.	3
356710	47.80	-67.71	345.	3
360030	52.28	-76.95	119.	3
360960	51.66	-94.38	629.	7
361770	50.35	-80.25	194.	11

368700	43.23	-76.93	847.	10
380620	44.76	-65.53	129.	3
383410	42.85	-71.38	653.	4
383530	42.83	-74.58	828.	4
383920	41.83	-59.98	88.	1
384570	41.26	-69.26	493.	10
386060	40.55	-70.95	405.	1
386870	39.08	-63.60	193.	2
388800	37.96	-58.33	304.	1
389270	37.28	-67.31	310.	1
389540	37.50	-71.51	2120.	3
407540	35.68	-51.31	1204.	1
408090	32.86	-59.20	1491.	1
421820	28.58	-77.20	211.	1
423390	26.30	-73.01	217.	1
423790	26.75	-83.36	76.	2
426470	23.06	-72.63	55.	1
427000	23.36	-85.33	612.	2
427790	22.76	-81.90	624.	1
428670	21.10	-79.05	308.	2
429710	20.25	-85.83	45.	1
430140	19.85	-75.40	582.	2
430410	19.08	-82.03	552.	1
431280	17.45	-78.46	545.	1
431500	17.70	-83.30	66.	4
431850	16.35	-81.15	3.	2
432790	13.00	-80.18	10.	2
432850	12.95	-74.83	32.	1
432950	12.96	-77.58	920.	5
433110	11.11	-72.73	3.	1
433330	11.66	-92.71	79.	2
433460	10.91	-79.83	7.	2
433530	9.93	-76.23	1.	2
480800	18.46	-94.35	9.	1
483270	18.78	-98.98	323.	4
484070	15.25	-104.86	123.	4
484550	13.73	-100.50	4.	4
485650	8.10	-98.30	3.	5
485680	7.20	-100.60	4.	7
486010	5.30	-100.26	3.	5
486150	6.16	-102.28	5.	3
486480	3.10	-101.65	46.	5
486570	3.78	-103.21	18.	2
486980	1.36	-103.98	14.	9
488550	16.03	-108.18	7.	2
510760	47.73	-88.08	737.	9
511330	46.73	-83.00	549.	3
512430	45.60	-84.85	428.	2
512880	45.36	-90.53	1651.	2
514310	43.95	-81.33	663.	7
514630	43.78	-87.61	919.	3
516440	41.71	-82.95	1100.	10
516560	41.75	-86.13	933.	1
517770	39.03	-88.16	889.	8

518280	37.13	-79.93	1375.	7
518480	37.93	-83.65	1264.	11
518860	38.35	-90.15	3139.	1
522030	42.81	-93.51	739.	1
522670	41.95	-101.06	941.	6
523230	41.80	-97.03	1770.	6
524180	40.15	-94.68	1140.	4
525330	39.76	-98.51	1478.	3
526810	38.63	-103.08	1367.	6
528360	36.30	-98.10	3192.	3
528660	36.71	-101.75	2296.	2
528890	36.05	-103.88	1518.	7
530680	43.65	-112.00	966.	5
534630	40.81	-111.68	1065.	2
535130	40.76	-107.40	1041.	1
536140	38.48	-106.21	1112.	2
537720	37.78	-112.55	779.	3
538450	36.60	-109.50	959.	3
539150	35.55	-106.66	1348.	5
542180	42.26	-118.96	572.	1
545110	39.80	-116.46	55.	2
548230	36.68	-116.98	58.	1
555910	29.66	-91.13	3650.	2
560290	33.00	-97.01	3682.	3
560460	33.80	-99.80	3968.	1
560800	34.96	-102.90	2910.	2
561370	31.15	-97.16	3307.	4
562940	30.66	-104.01	508.	7
565710	27.88	-102.30	1592.	6
566910	26.86	-104.28	2235.	5
567390	25.03	-98.48	1649.	10
567780	25.01	-102.68	1894.	8
569850	23.38	-103.38	1302.	8
570360	34.30	-108.93	398.	3
570830	34.71	-113.65	111.	2
571270	33.06	-107.03	509.	5
571780	33.01	-112.53	131.	2
574470	30.26	-109.48	466.	1
574940	30.58	-114.26	23.	1
577490	27.56	-110.00	261.	2
578160	26.48	-106.65	1222.	3
579570	25.33	-110.30	167.	2
579720	25.81	-113.01	185.	1
580270	34.28	-117.16	42.	1
592110	23.91	-106.61	245.	4
592650	23.48	-111.30	120.	1
594310	22.81	-108.35	73.	1
597580	20.03	-110.35	18.	1
619670	-7.30	-72.40	1.	1
619960	-37.80	-77.53	27.	2
690020	36.00	121.31	320.	2
691194	34.68	77.03	7.	1
710430	65.28	126.75	95.	2
710810	68.76	81.21	8.	2

710820	82.50	62.33	64.	4
711150	50.23	119.28	555.	1
711190	53.55	114.10	766.	3
711240	54.75	110.05	700.	1
716000	43.93	60.01	4.	1
717010	45.83	66.43	51.	9
717160	46.90	71.48	178.	2
717220	46.36	75.98	170.	6
718110	50.21	66.25	53.	7
718150	48.53	58.55	60.	1
718160	53.30	60.36	36.	3
718230	53.75	73.66	307.	6
718360	51.26	80.65	10.	3
718450	51.45	90.20	386.	2
718670	53.96	101.10	273.	2
718960	53.88	122.66	675.	1
719060	58.10	68.41	60.	6
719070	58.45	78.11	7.	3
719090	63.75	68.55	20.	3
719130	58.73	94.08	27.	4
719150	64.20	83.36	52.	4
719250	69.13	105.06	25.	1
719260	64.30	96.00	49.	3
719340	60.03	111.93	204.	4
719450	58.83	122.60	378.	3
722010	24.55	81.75	2.	11
722030	26.68	80.11	6.	14
722080	32.90	80.03	14.	5
722100	27.70	82.40	12.	10
722130	31.25	82.40	46.	6
722140	30.38	84.36	25.	5
722210	30.48	86.51	20.	1
722290	32.90	87.25	140.	2
722350	32.31	90.08	105.	7
722400	30.11	93.21	4.	7
722470	32.35	94.65	124.	7
722500	25.90	97.43	7.	8
722510	27.76	97.50	13.	5
722600	32.21	98.18	402.	8
722610	29.36	100.91	310.	6
722650	31.95	102.18	875.	3
722700	31.80	106.40	1206.	2
722740	32.11	110.93	802.	2
723040	35.26	75.55	2.	7
723110	33.95	83.31	246.	2
723270	36.25	86.56	180.	2
723400	34.83	92.25	172.	7
723490	36.88	93.90	437.	5
723550	34.65	98.40	360.	3
723570	35.21	97.45	357.	6
723630	35.23	101.70	1099.	6
723650	35.05	106.61	1619.	2
723740	35.01	110.73	1487.	3
723910	34.11	119.11	4.	1



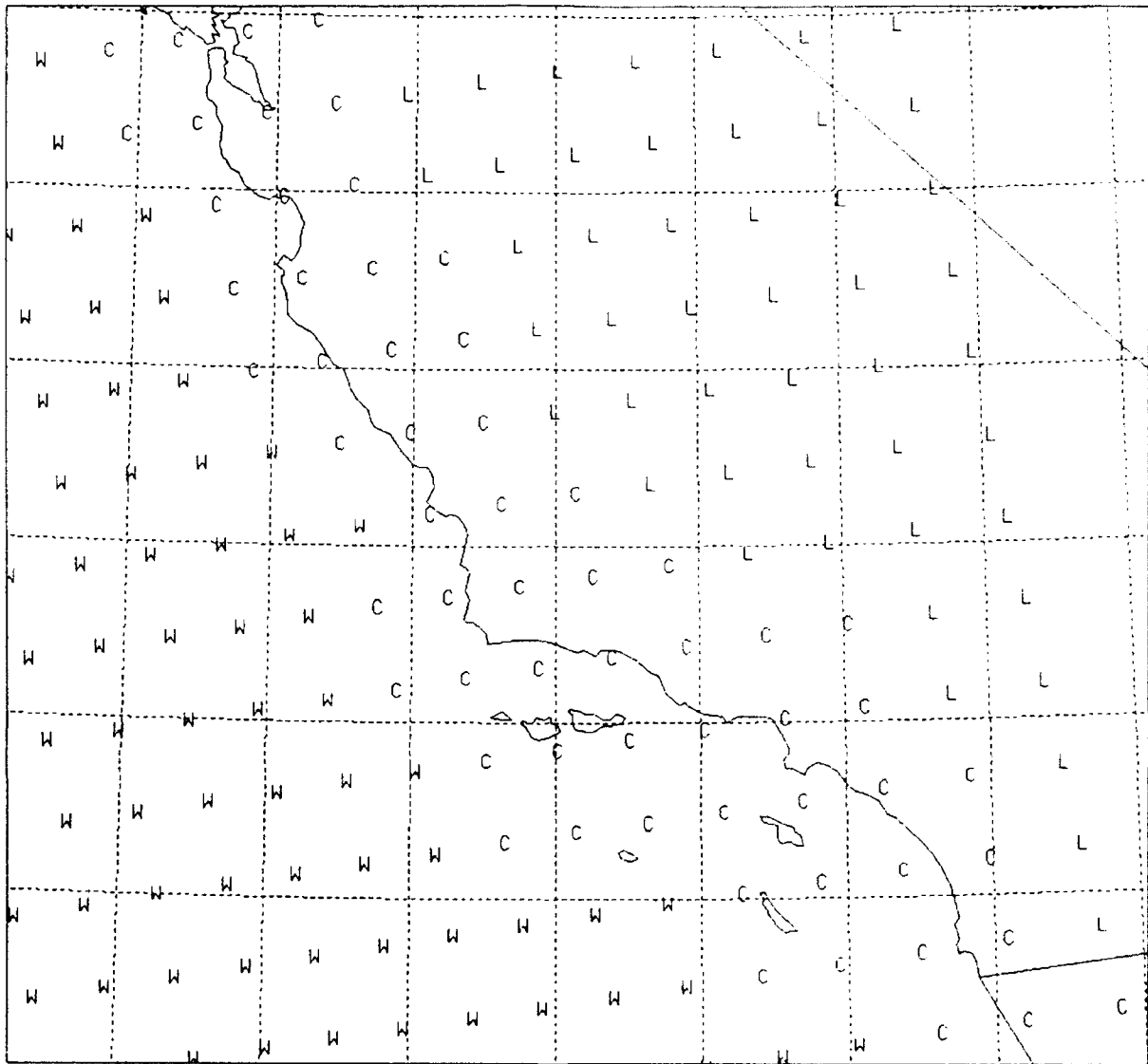
724020	37.85	75.48	4.	6
724030	38.98	77.46	95.	5
724070	39.45	74.56	21.	6
724250	38.36	82.55	252.	1
724290	39.86	84.11	298.	3
724350	37.06	38.76	126.	2
724510	37.76	99.96	791.	5
724560	39.06	95.63	268.	5
724690	39.75	104.86	1611.	3
724760	39.11	108.53	1472.	2
724860	39.28	114.85	1908.	1
725200	40.53	80.23	359.	5
725280	42.93	78.73	220.	3
725530	41.36	96.01	399.	3
725620	41.13	100.68	847.	3
725720	40.76	111.96	1288.	2
725760	42.81	108.73	1703.	2
726060	43.65	70.31	23.	2
726370	42.96	83.73	236.	1
726450	44.48	88.13	212.	1
726540	44.38	98.21	392.	2
726550	45.55	94.06	313.	2
726620	44.05	103.06	970.	3
726810	43.56	116.21	871.	2
727120	46.86	68.01	190.	1
727470	48.56	93.38	360.	2
727640	46.76	100.75	511.	1
727680	48.21	106.61	699.	1
727750	47.48	111.36	1118.	2
727850	47.63	117.53	723.	1
740010	34.60	86.63	175.	1
744940	41.66	69.96	14.	3
746120	35.68	117.68	696.	1
747940	28.46	80.55	3.	9
763940	25.86	100.20	450.	3
764050	24.16	110.30	18.	1
764580	23.20	106.41	4.	2
766120	20.68	103.38	1589.	1
766440	20.95	89.66	11.	3
766540	19.06	104.33	6.	6
766790	19.43	99.08	2231.	11
766920	19.15	96.11	13.	11
780730	25.05	77.46	3.	8
783840	19.30	81.36	3.	8
783970	17.93	76.78	3.	6
785830	17.53	88.30	5.	5
787200	14.03	87.25	999.	4
787620	9.98	84.21	920.	5
788060	8.98	79.55	69.	7
789880	12.20	68.96	62.	1
800010	12.58	81.70	0.	5
804470	7.85	72.45	378.	1
840030	-0.90	89.61	6.	8
846280	-12.01	77.03	13.	1

854690	-27.16	109.43	41.	1
855430	-32.78	71.51	8.	1
890500	-62.20	58.93	16.	1
895420	-67.66	-45.85	40.	2
895640	-67.60	-62.88	15.	9
895710	-68.58	-77.98	12.	8
896110	-66.25	-110.53	15.	14
913660	8.73	-167.73	2.	2
946100	-31.91	-115.96	20.	1
960350	3.56	-98.66	27.	3
962370	-2.16	-106.13	33.	1
967490	-6.13	-106.66	10.	1
969960	-12.18	-96.83	3.	9

Appendix C. Displays of the SSM/T-2 FOV topographic classification and the TBs for the five SSM/T-2 channels for the west coast region on May 14 and 15, 1992 and for the east coast region on July 29 and 30 and August 6, 1992.

SSM/T-2 FOOTPRINTS

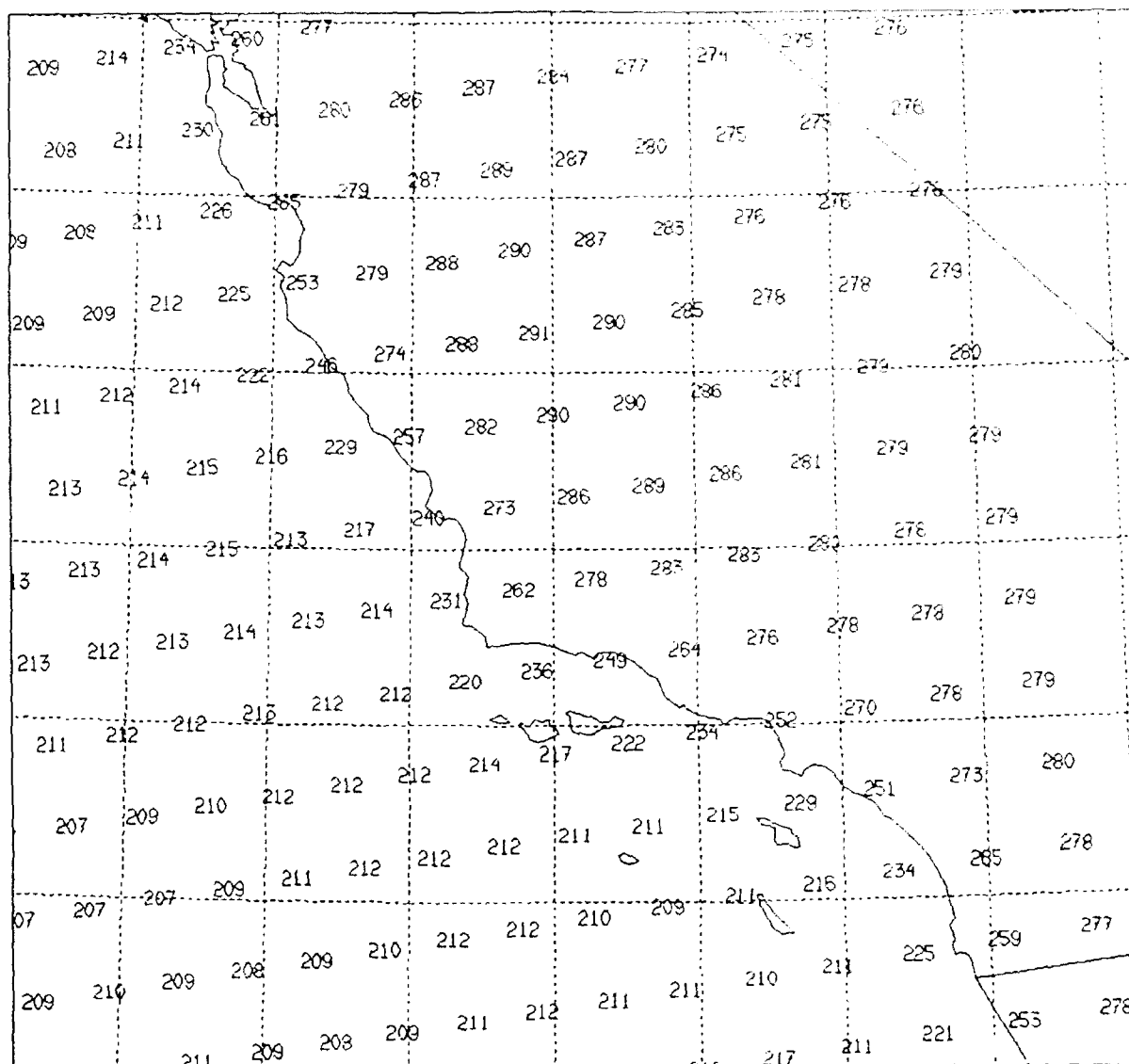
14 MAY 1992



# SSM/T-2 FOOTPRINTS

91 GHz

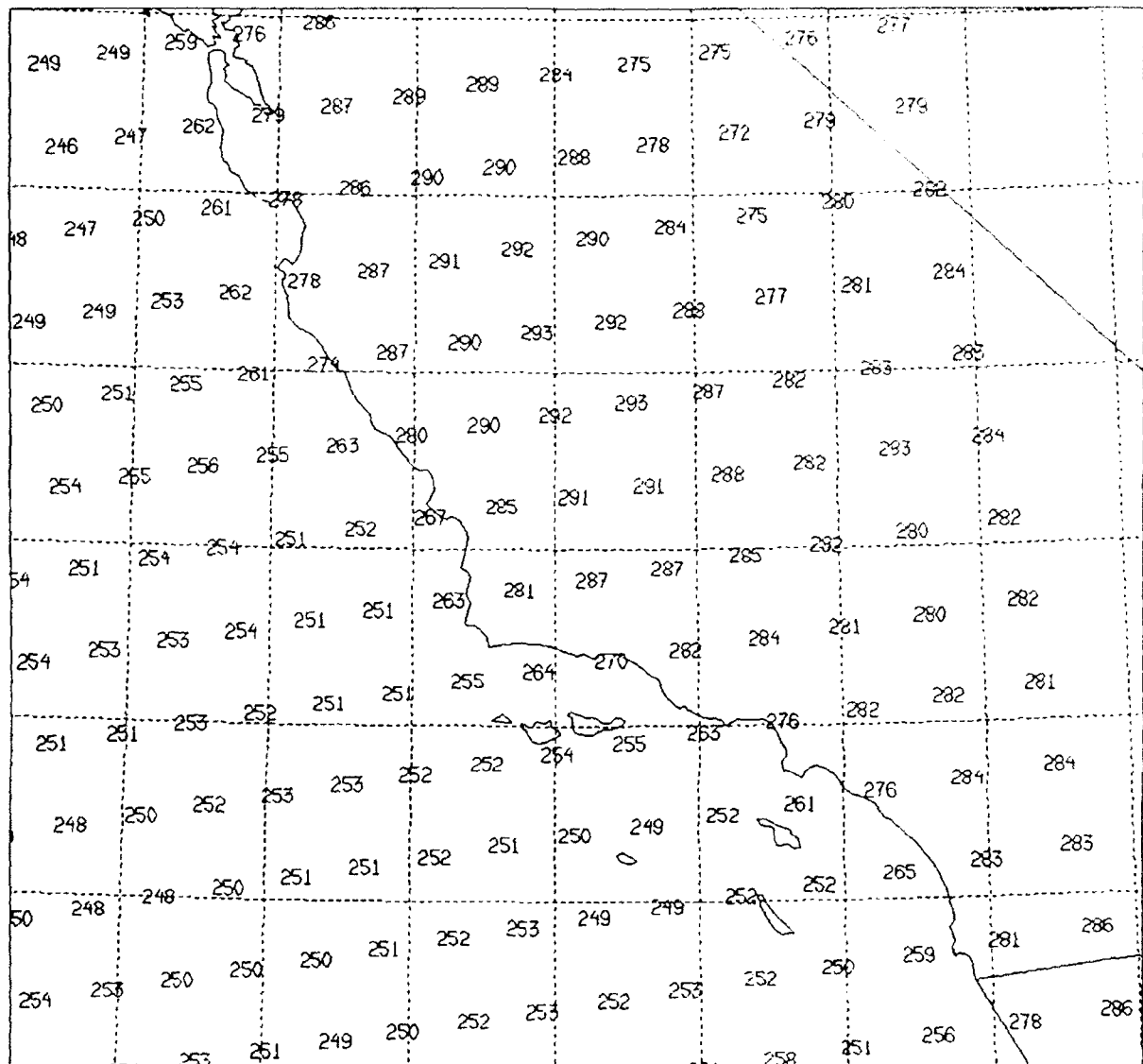
14 MAY 1992



# SSM/T-2 FOOTPRINTS

150 GHz

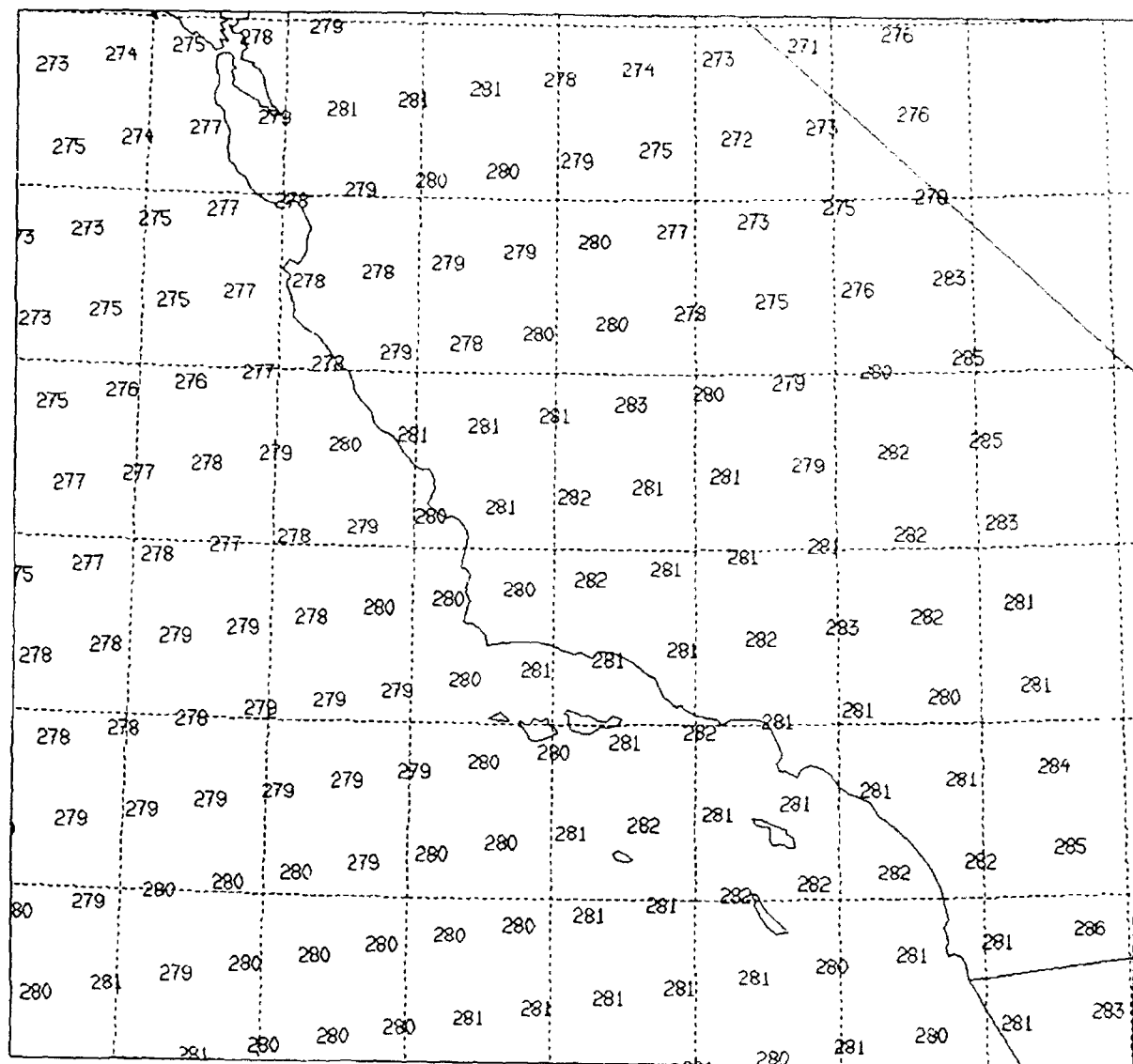
14 MAY 1992



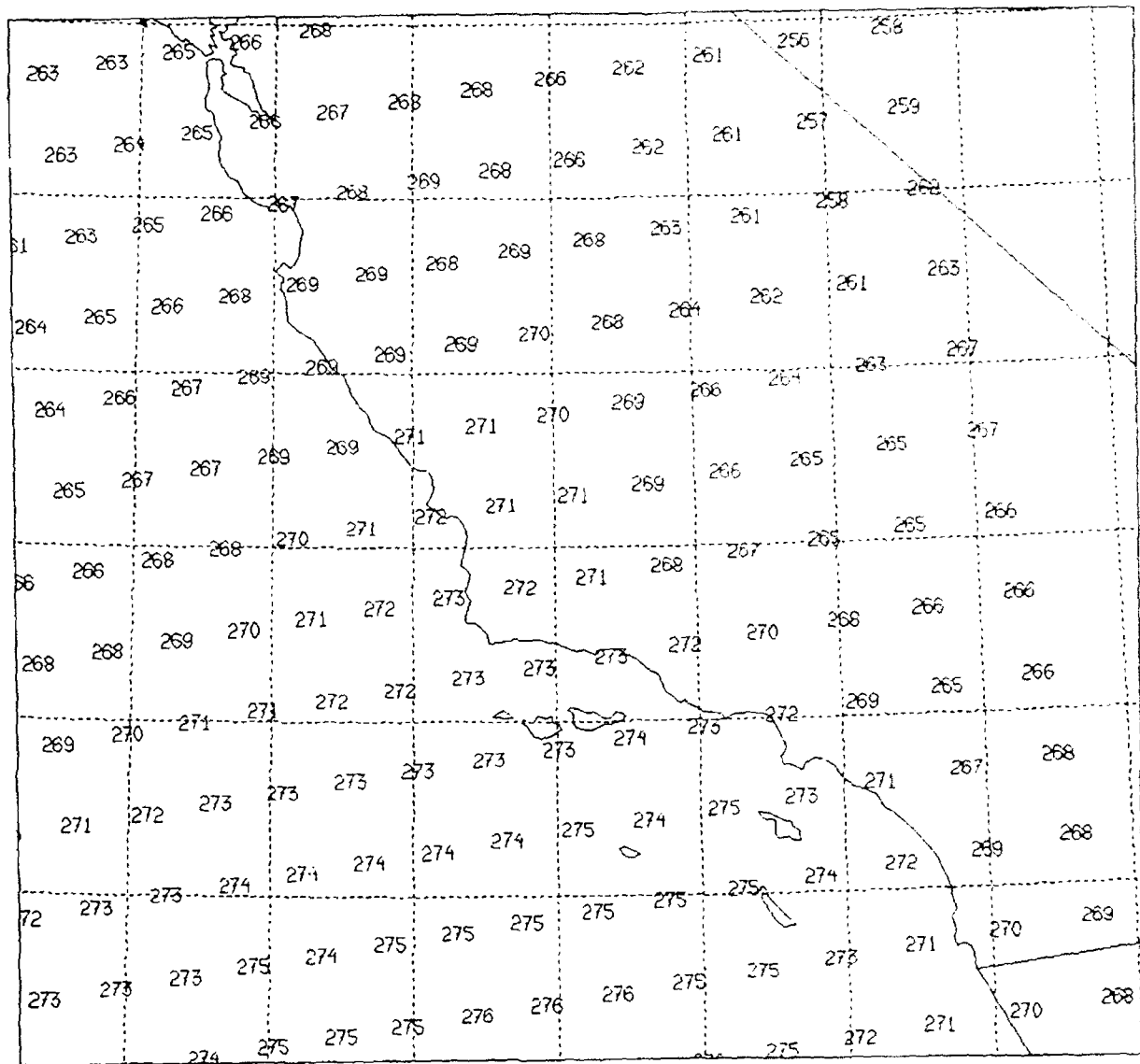
SSM/T-2 FOOTPRINTS

183 +/- 7 GHz

14 MAY 1992

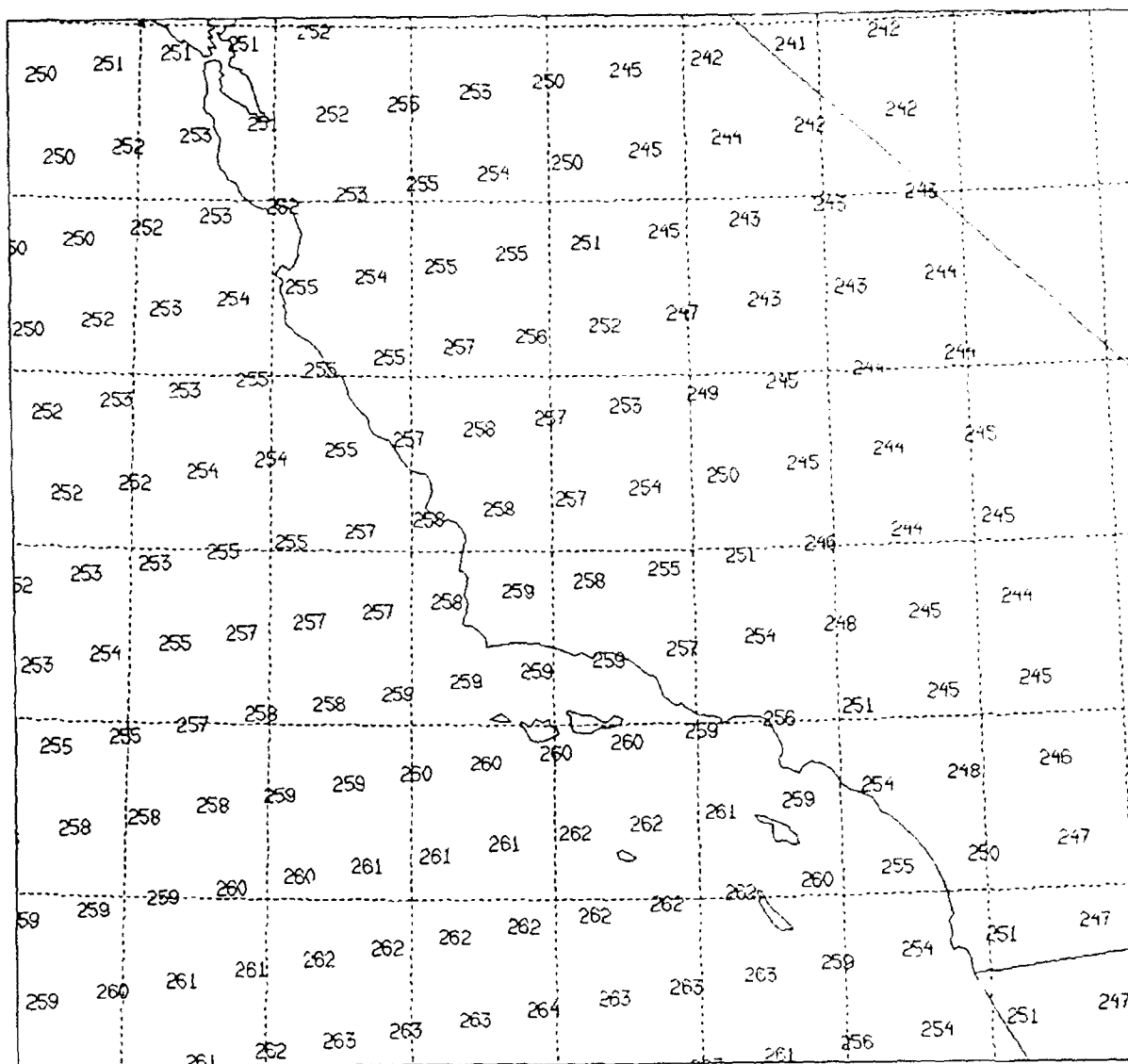


14 MAY 1992



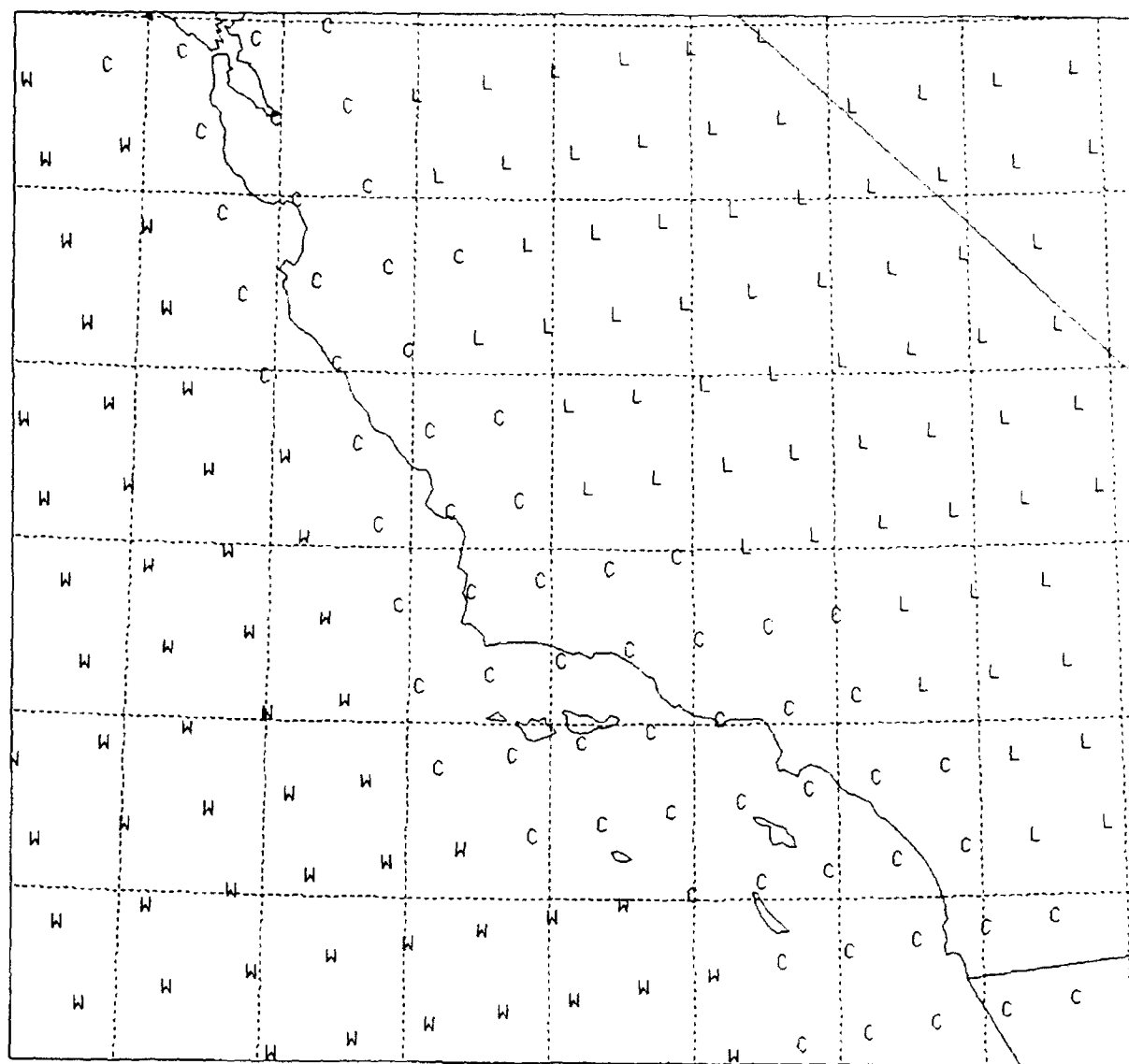


14 MAY 1992



SSM/T-2 FOOTPRINTS

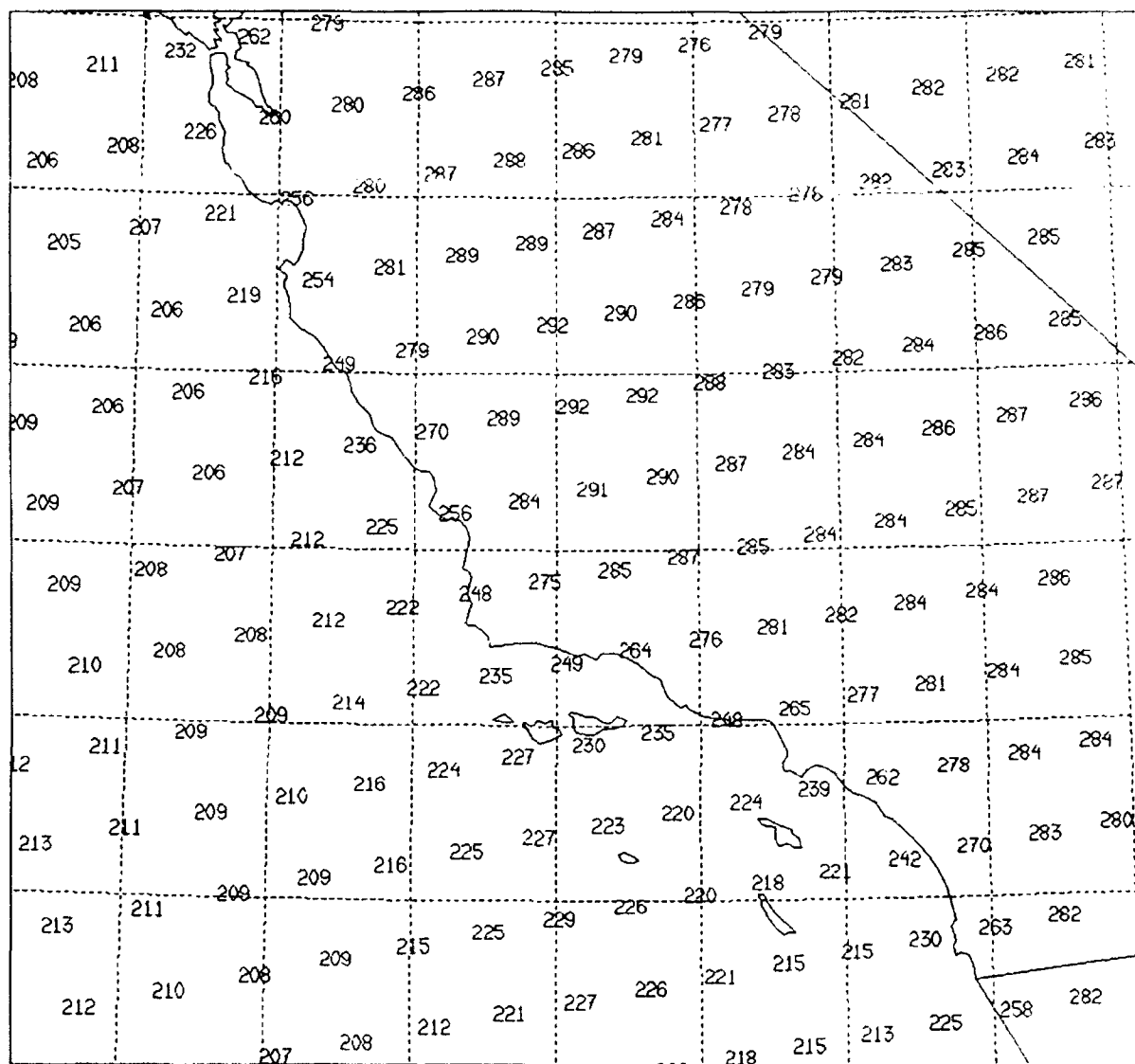
15 MAY 1992



# SSM/T-2 FOOTPRINTS

91 GHz

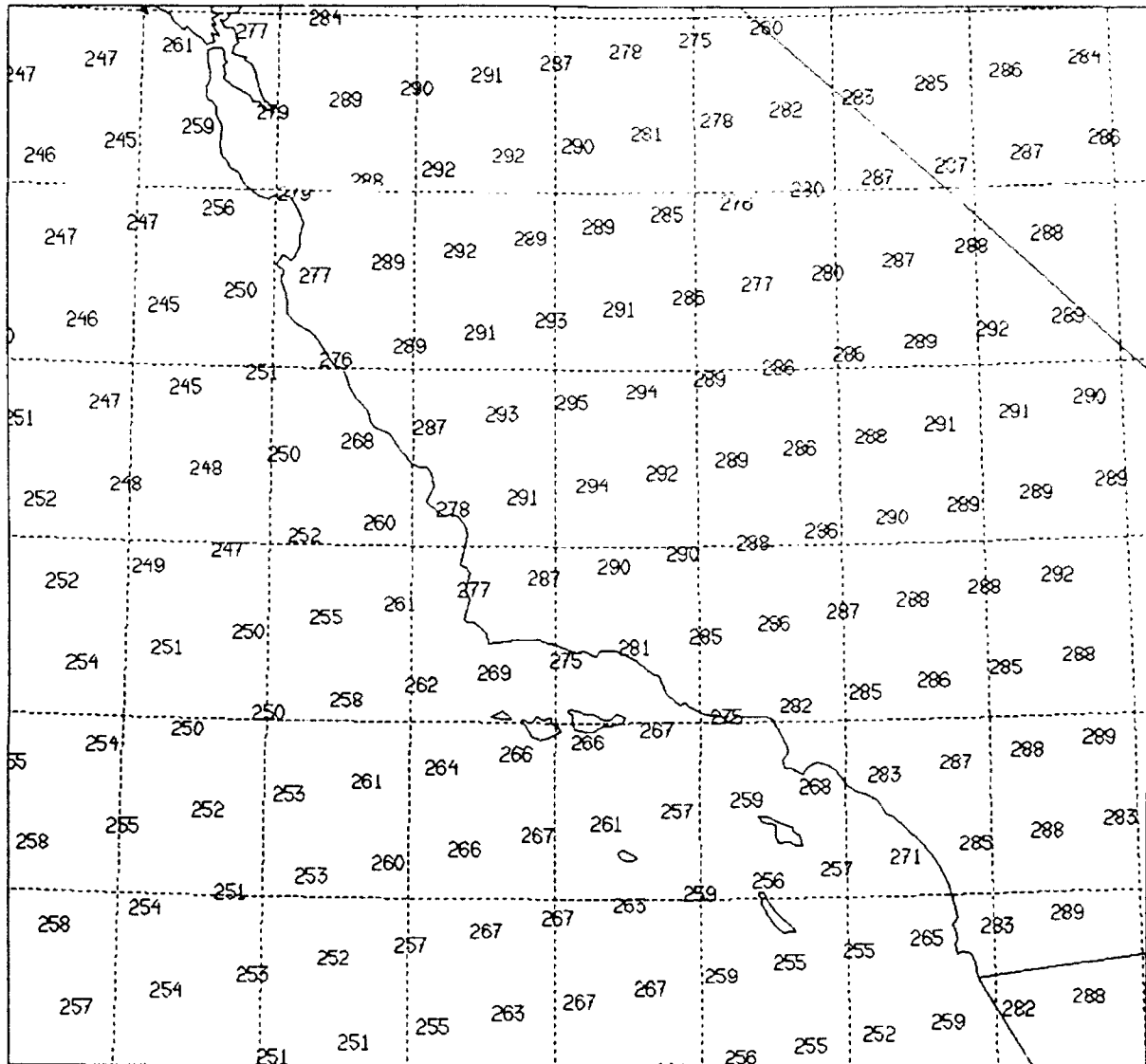
15 MAY 1992



# SSM/T-2 FOOTPRINTS

150 GHz

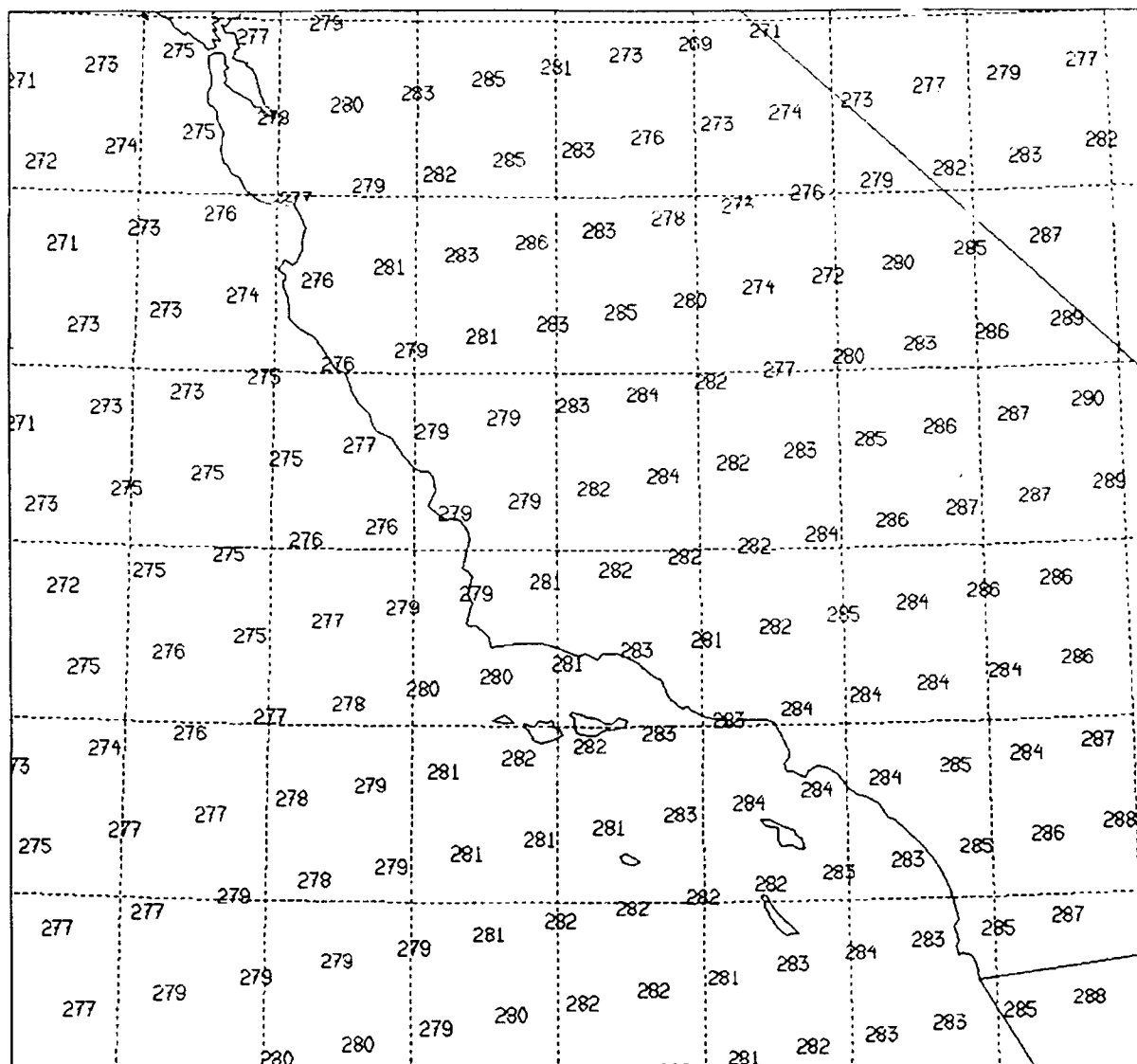
15 MAY 1992



## SSM/I-2 FOOTPRINTS

183 +/- 7 GHz

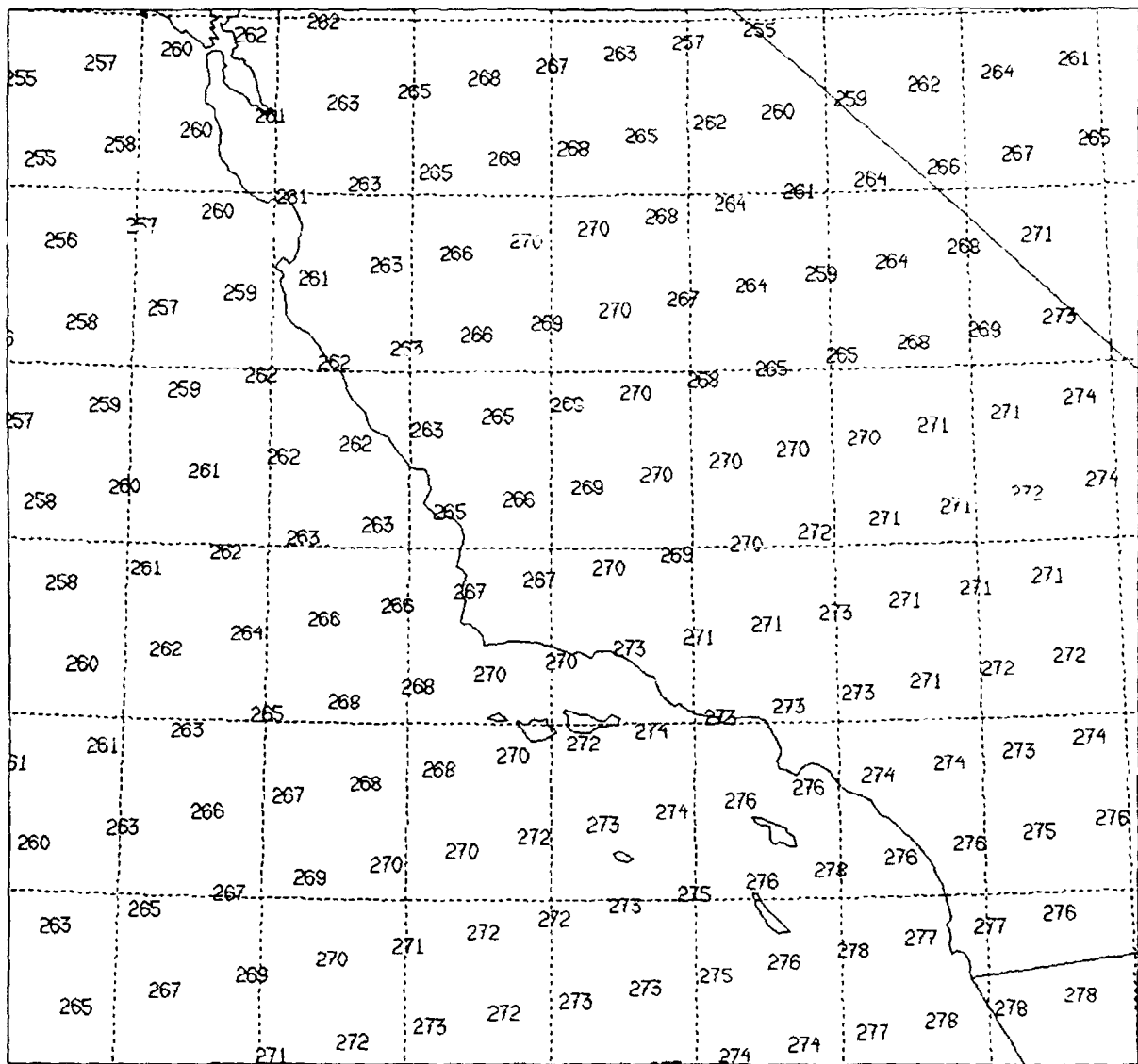
15 MAY 1992



# SSM/T-2 FOOTPRINTS

183 +/- 3 GHz

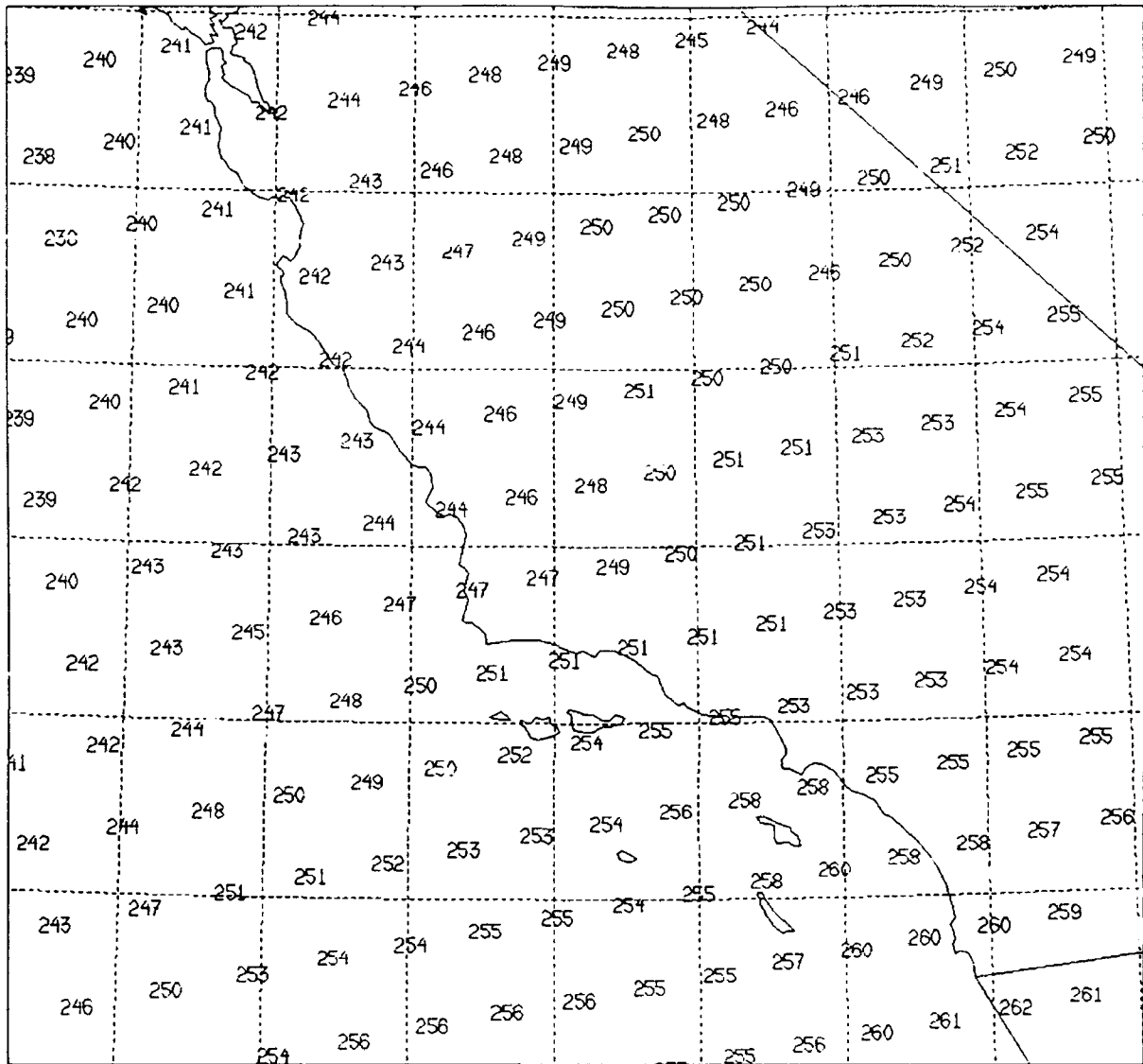
15 MAY 1992



# SSM/T-2 FOOTPRINTS

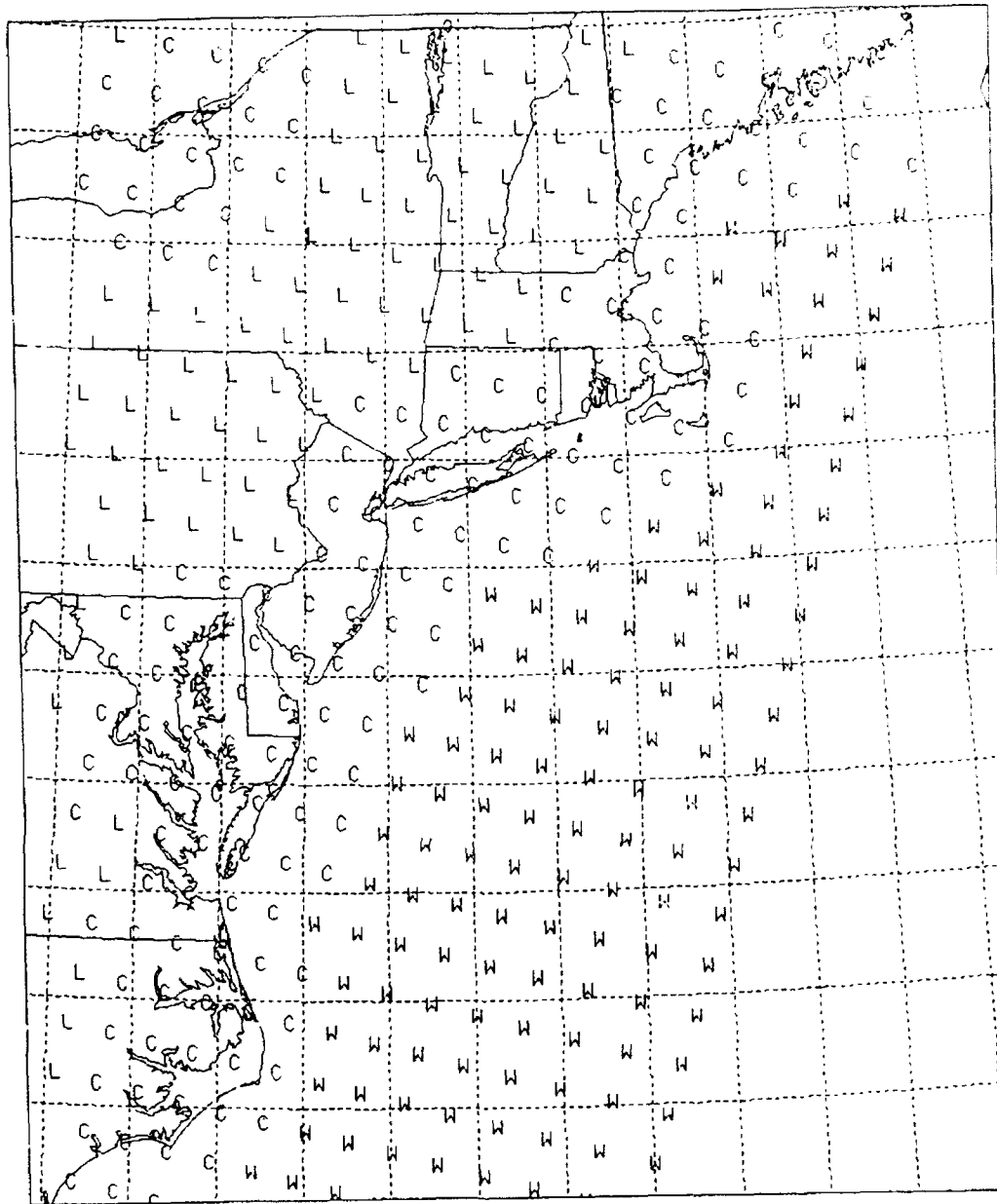
183 +/- 1 GHz

15 MAY 1992



SSM/T-2 FOOTPRINTS

29 JUL 1992

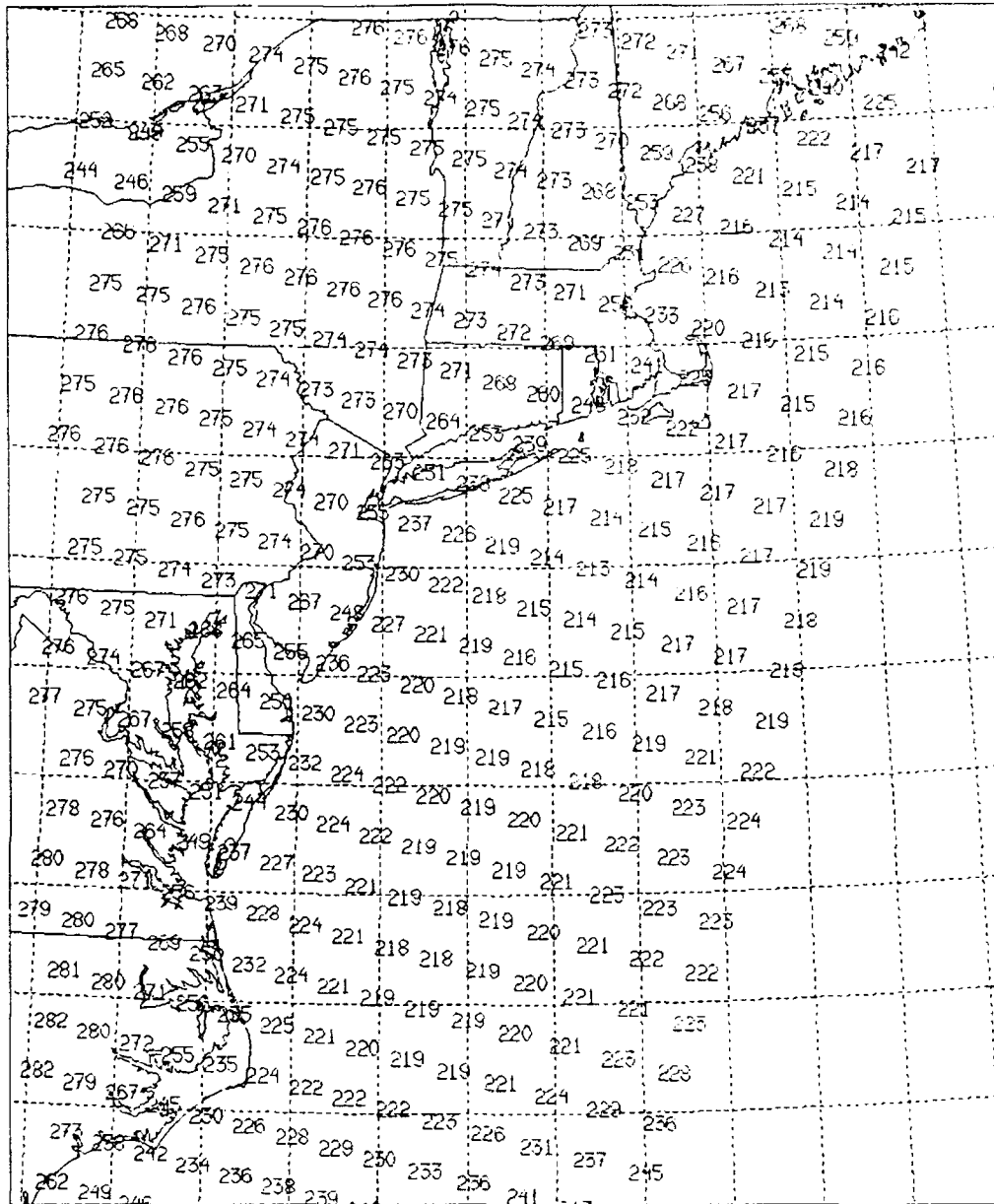




## SSM/T-2 FOOTPRINTS

91 GHz

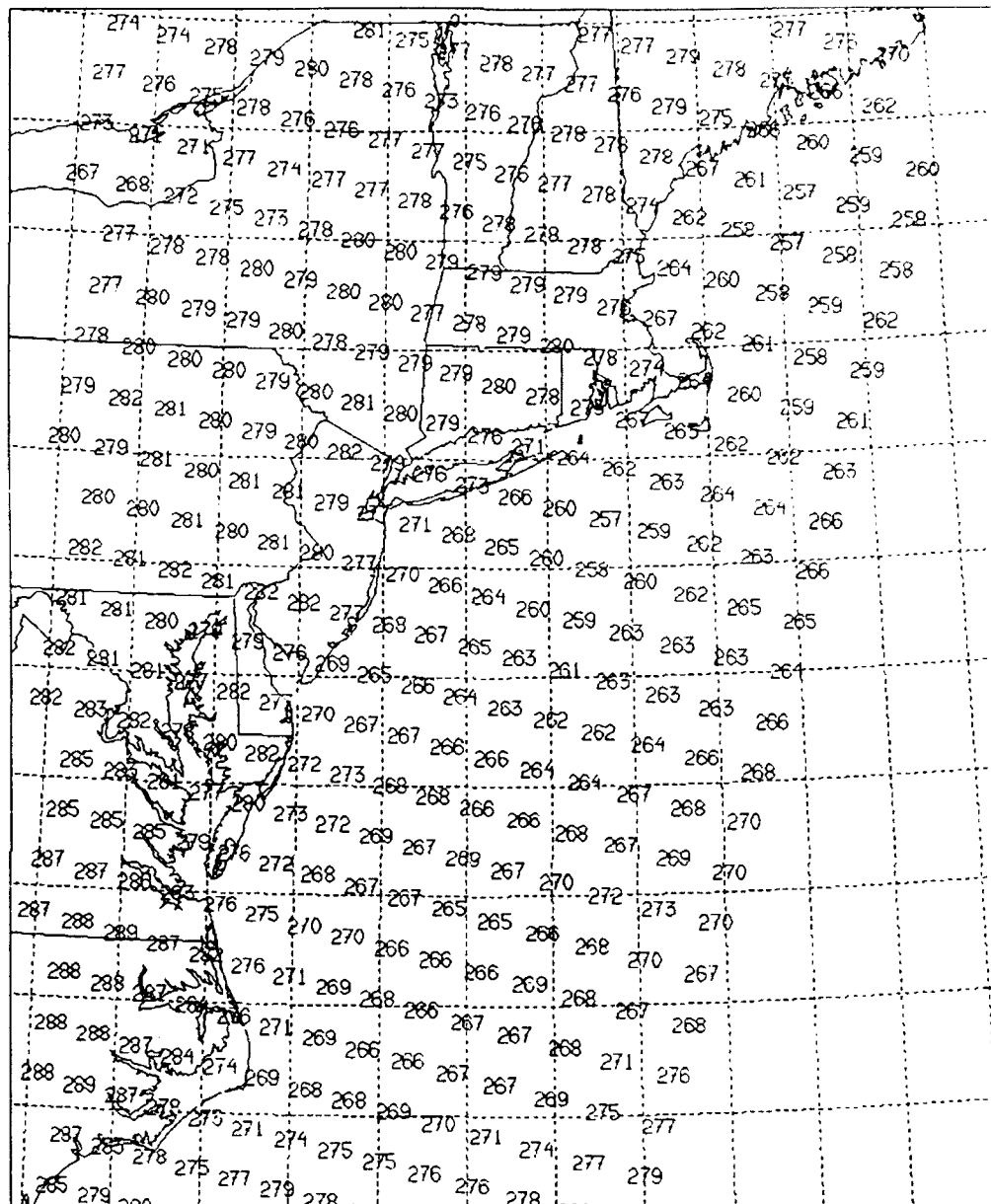
29 JUL 1992



## SSM/T-2 FOOTPRINTS

150 GHz

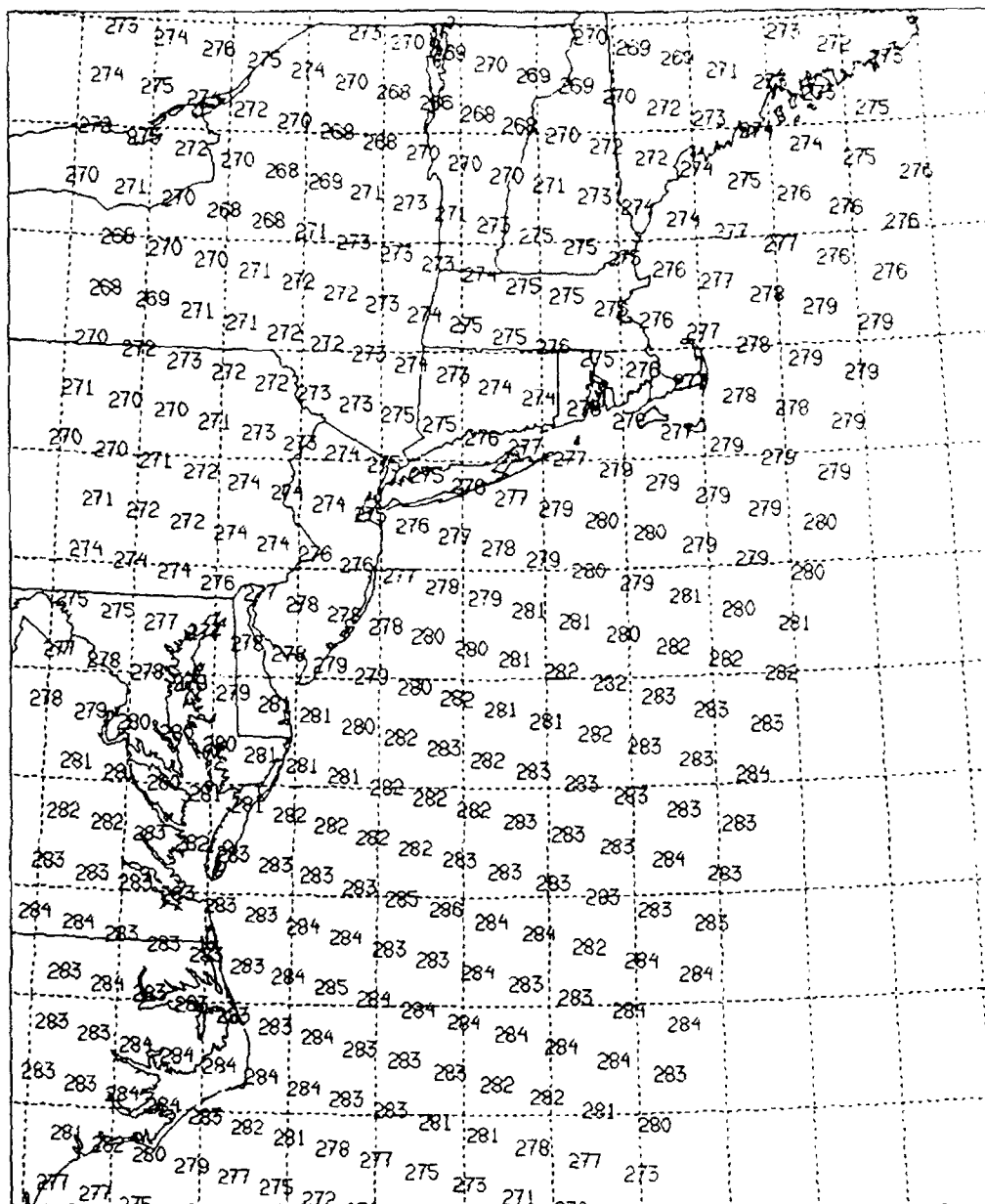
29 JUL 1992



# SSM/T-2 FOOTPRINTS

183 +/- 7 GHz

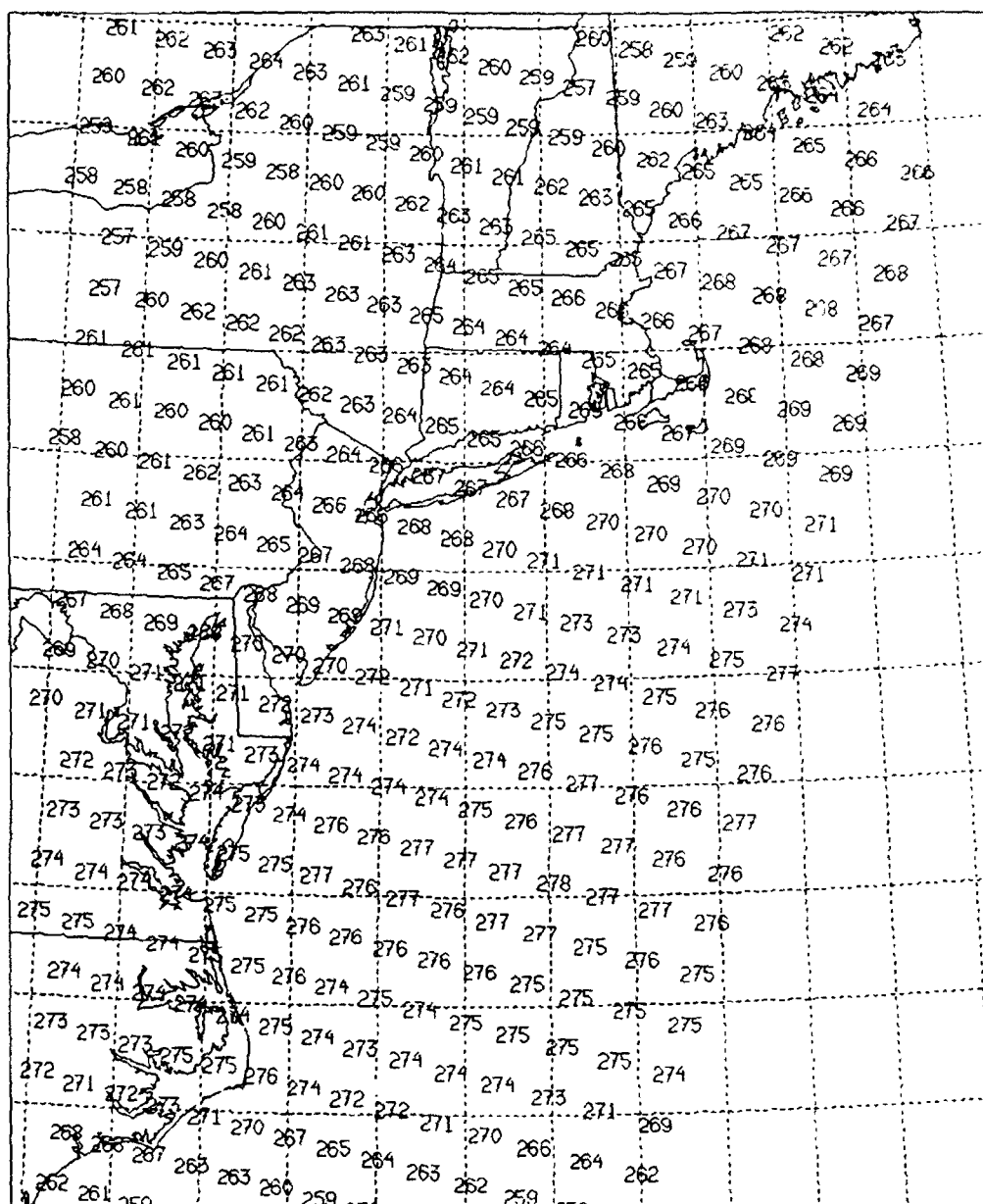
29 JUL 1992



# SSM/T-2 FOOTPRINTS

183 +/- 3 GHz

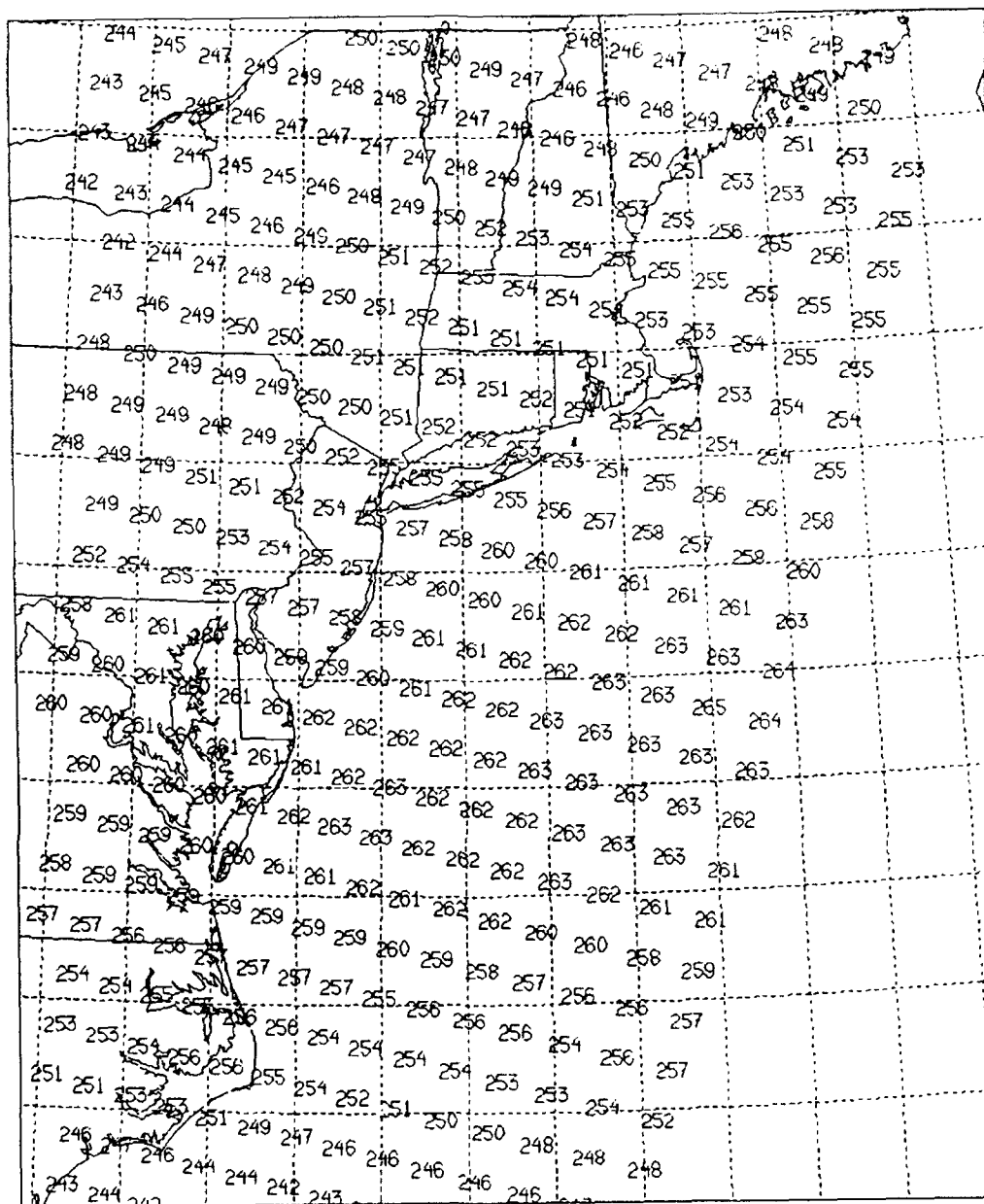
29 JUL 1992



# SSM/T-2 FOOTPRINTS

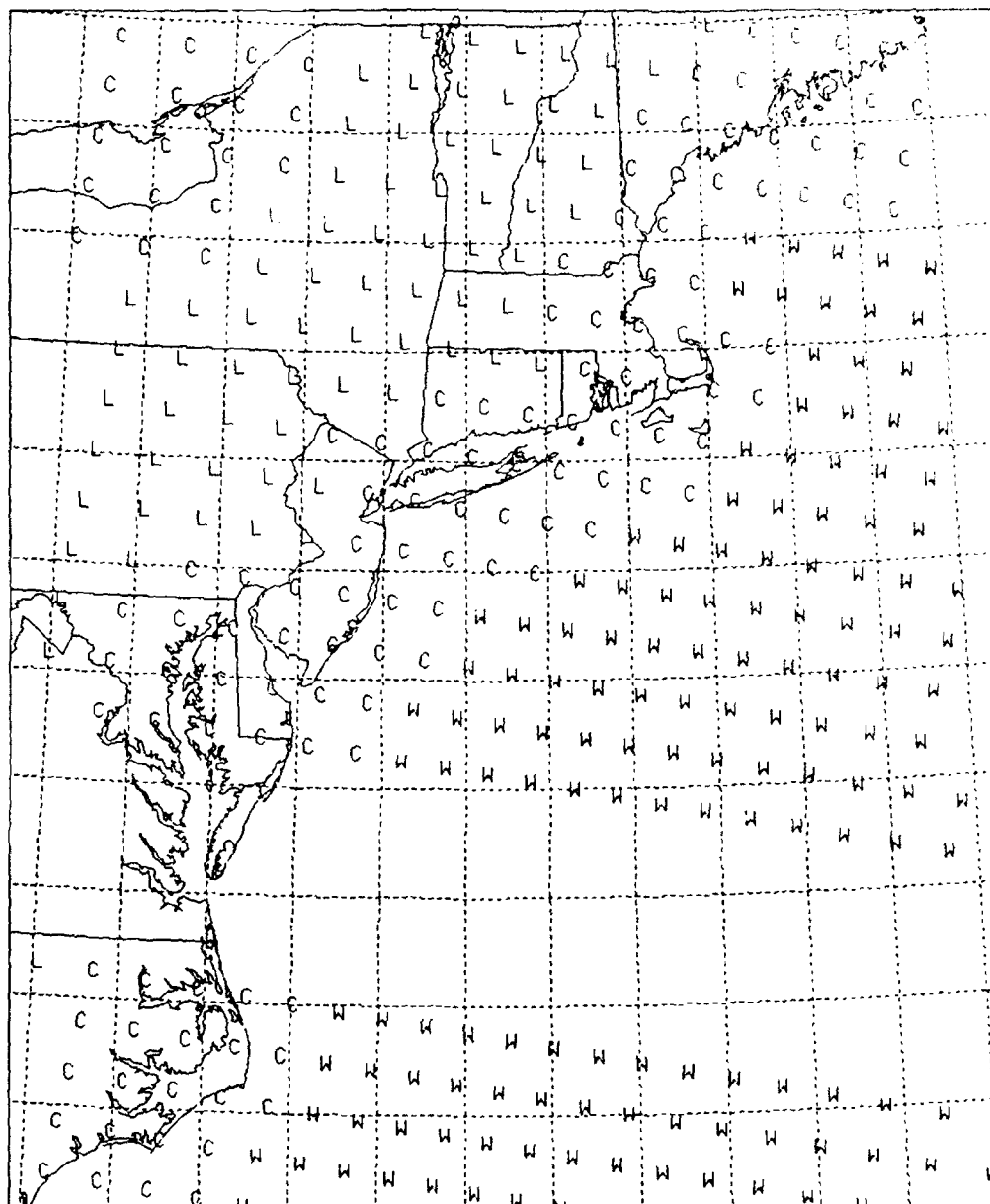
183 +/- 1 GHz

29 JUL 1992



SSM/T-2 FOOTPRINTS

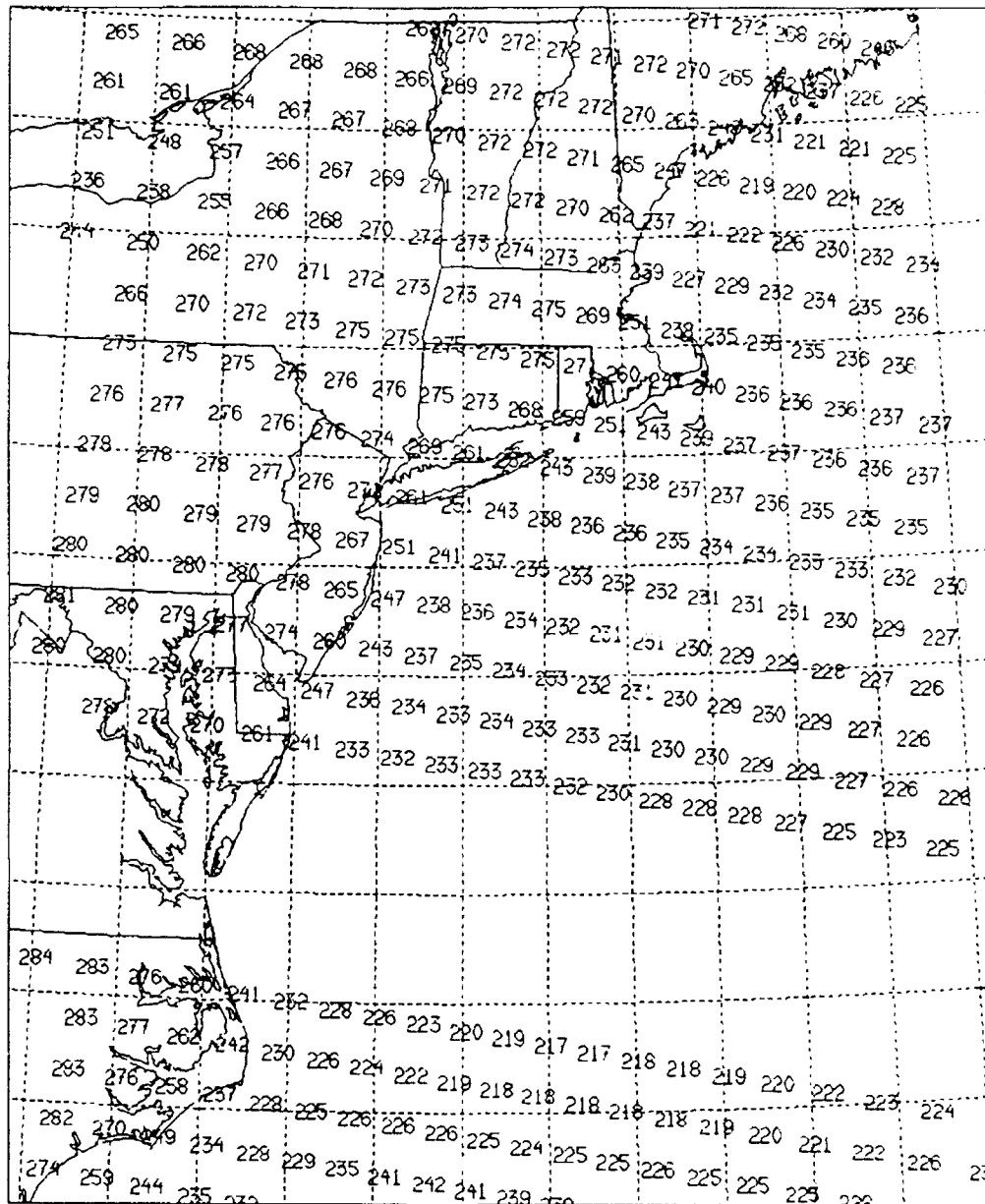
30 JUL 1992



## SSM/T-2 FOOTPRINTS

91 GHz

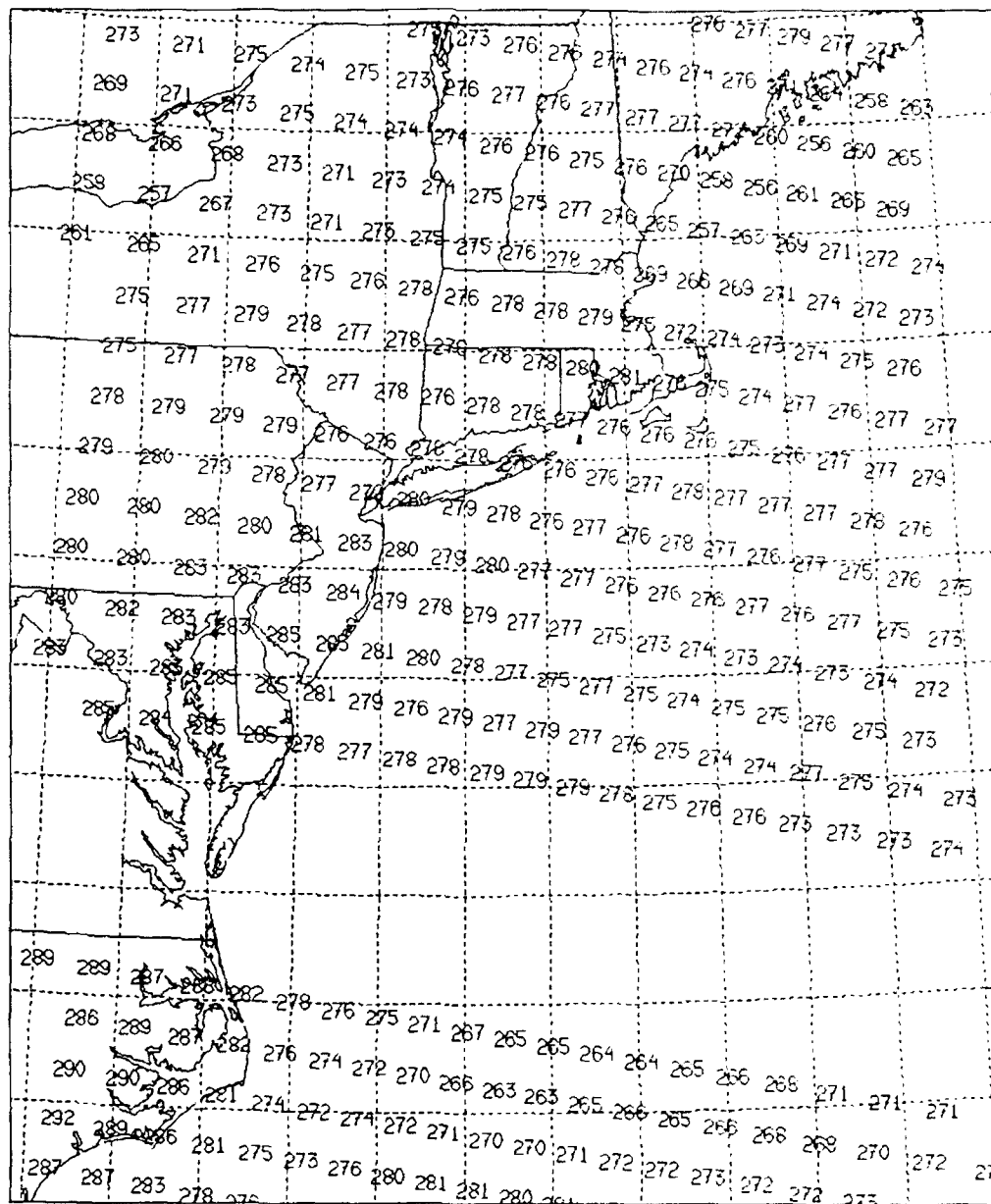
30 JUL 1992



## SSM/T-2 FOOTPRINTS

150 GHz

30 JUL 1992

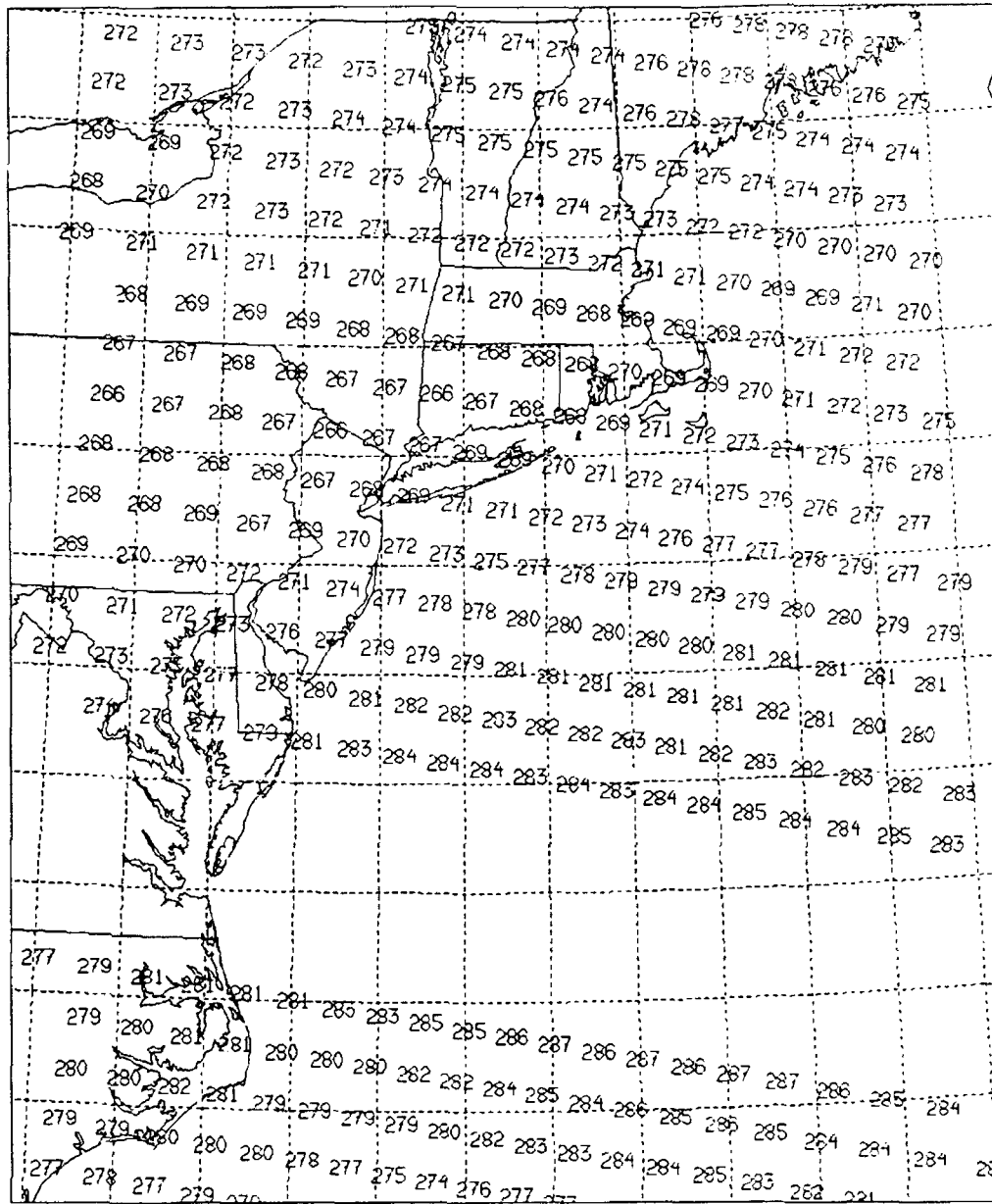




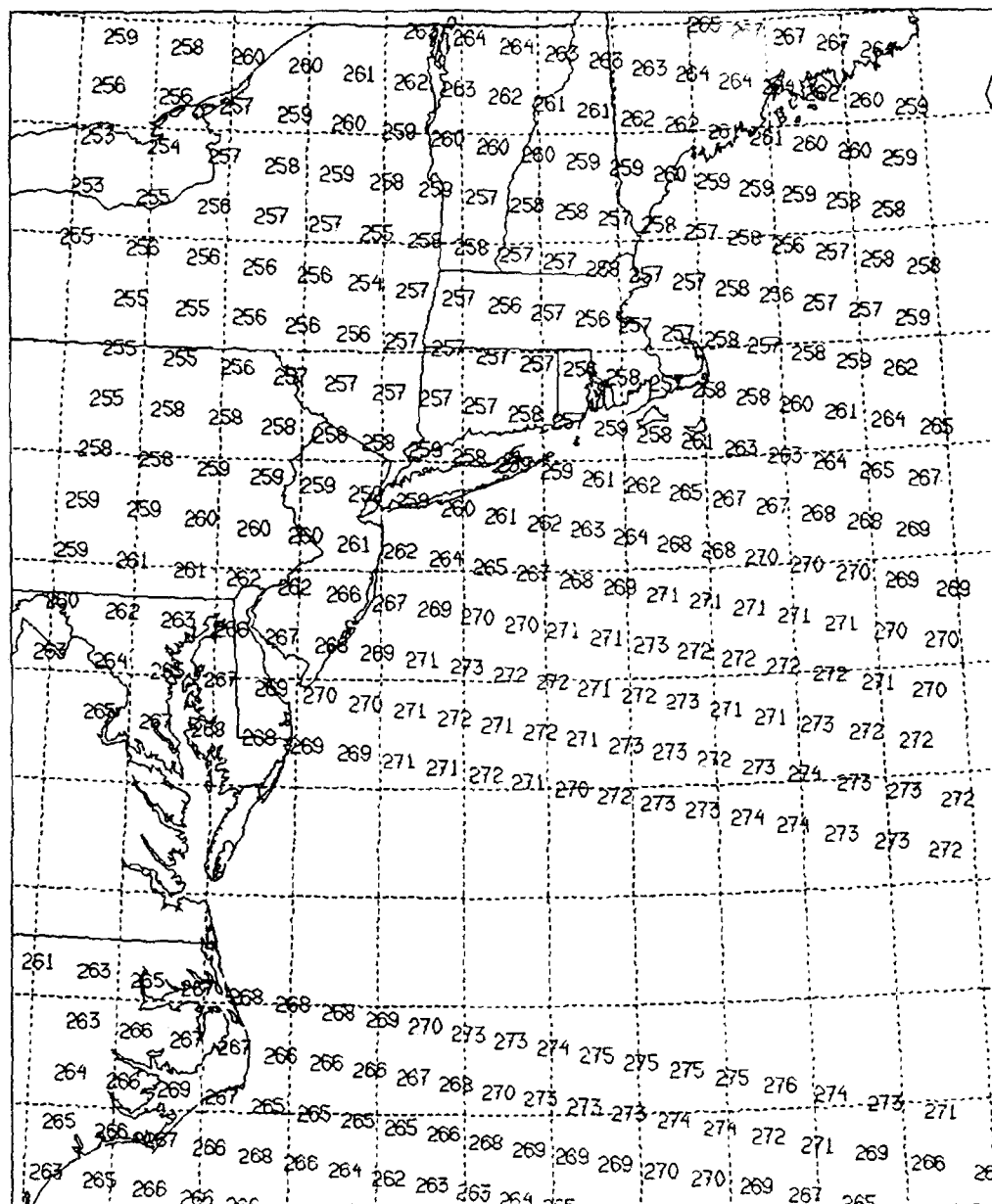
## SSM/T-2 FOOTPRINTS

183 +/- 7 GHz

30 JUL 1992



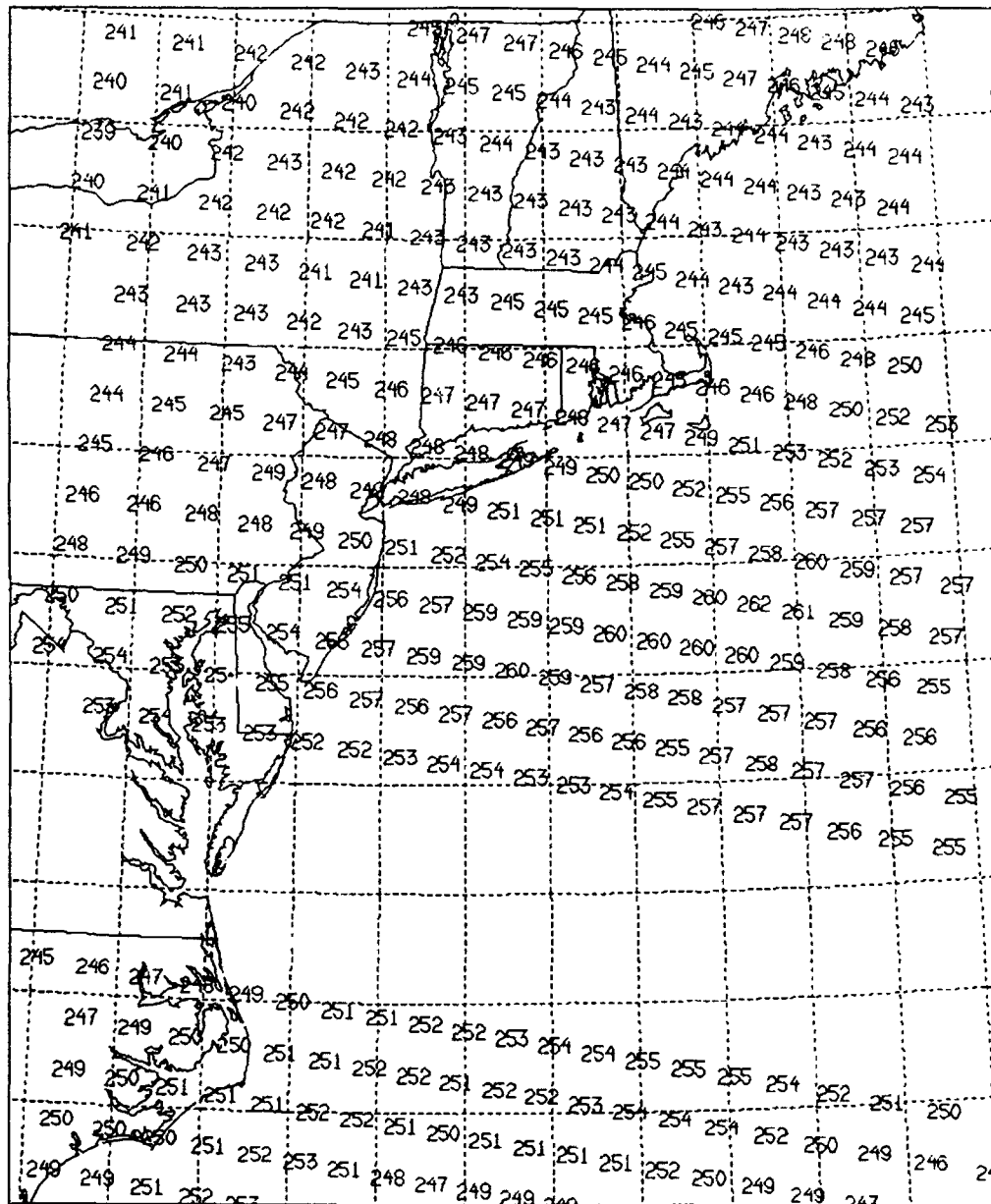
30 JUL 1992



## SSM/T-2 FOOTPRINTS

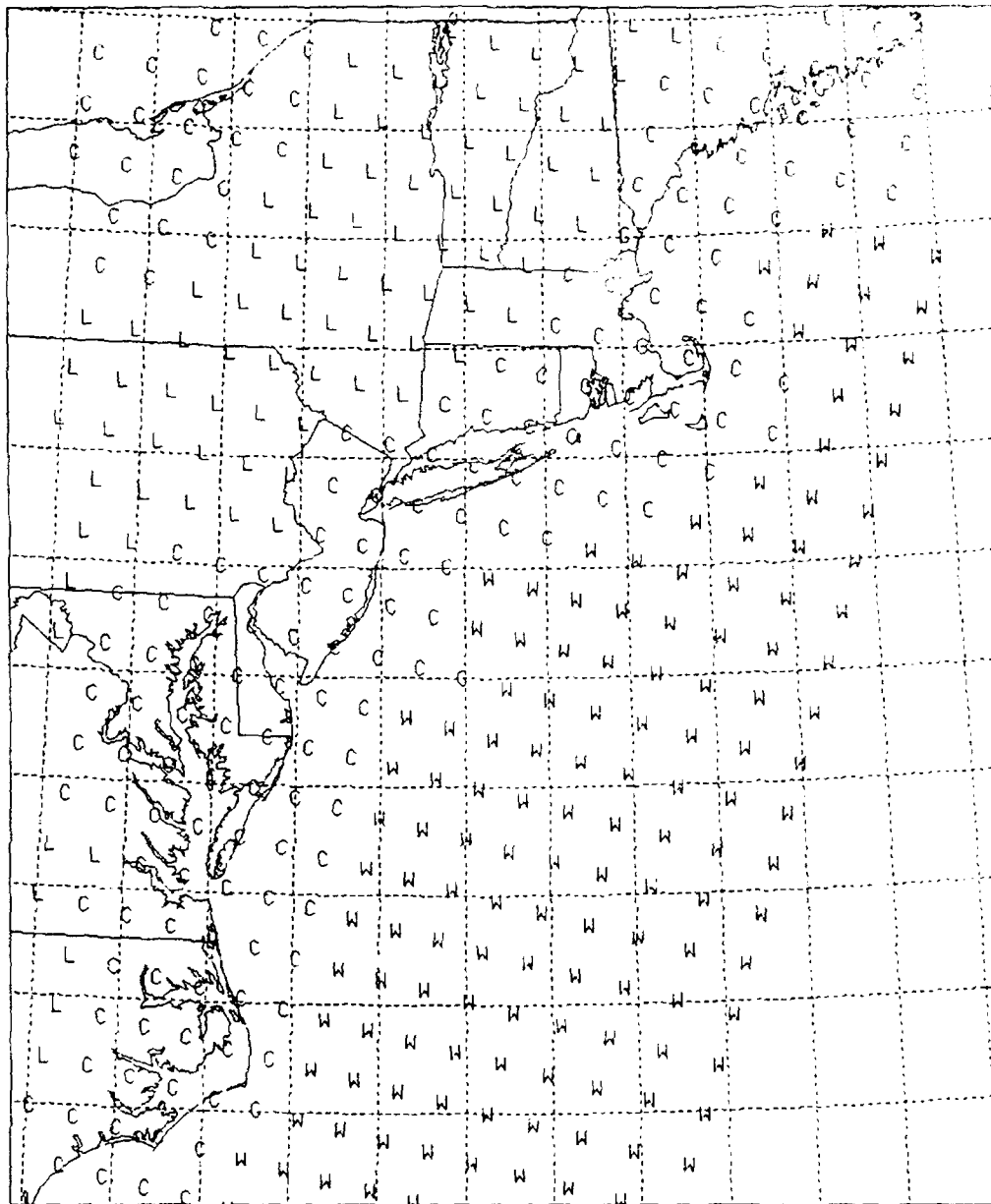
183 +/- 1 GHz

30 JUL 1992



SSM/T-2 FOOTPRINTS

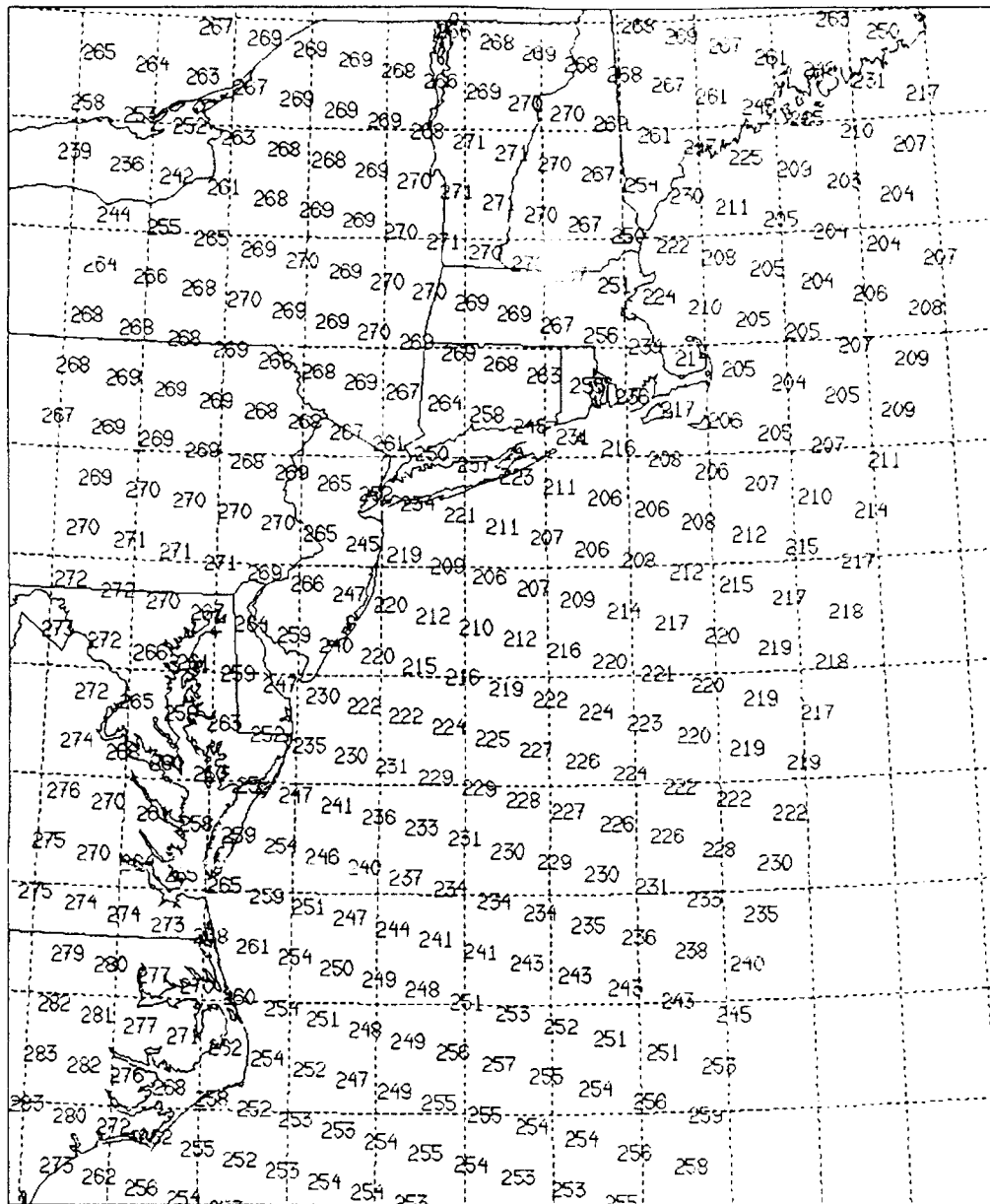
6 AUG 1992



## SSM/T-2 FOOTPRINTS

91 GHz

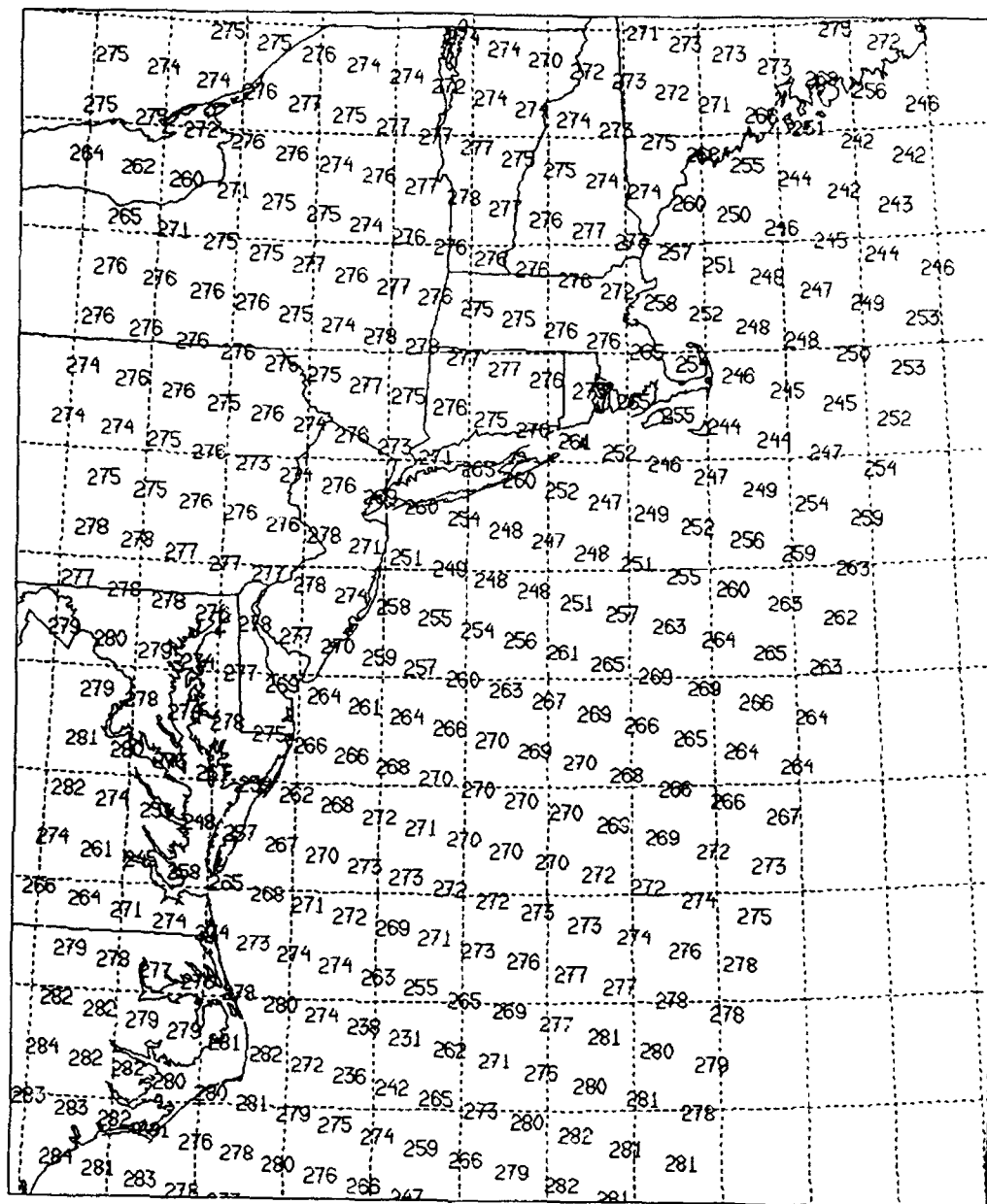
6 AUG 1992



## SSM/T-2 FOOTPRINTS

150 GHz

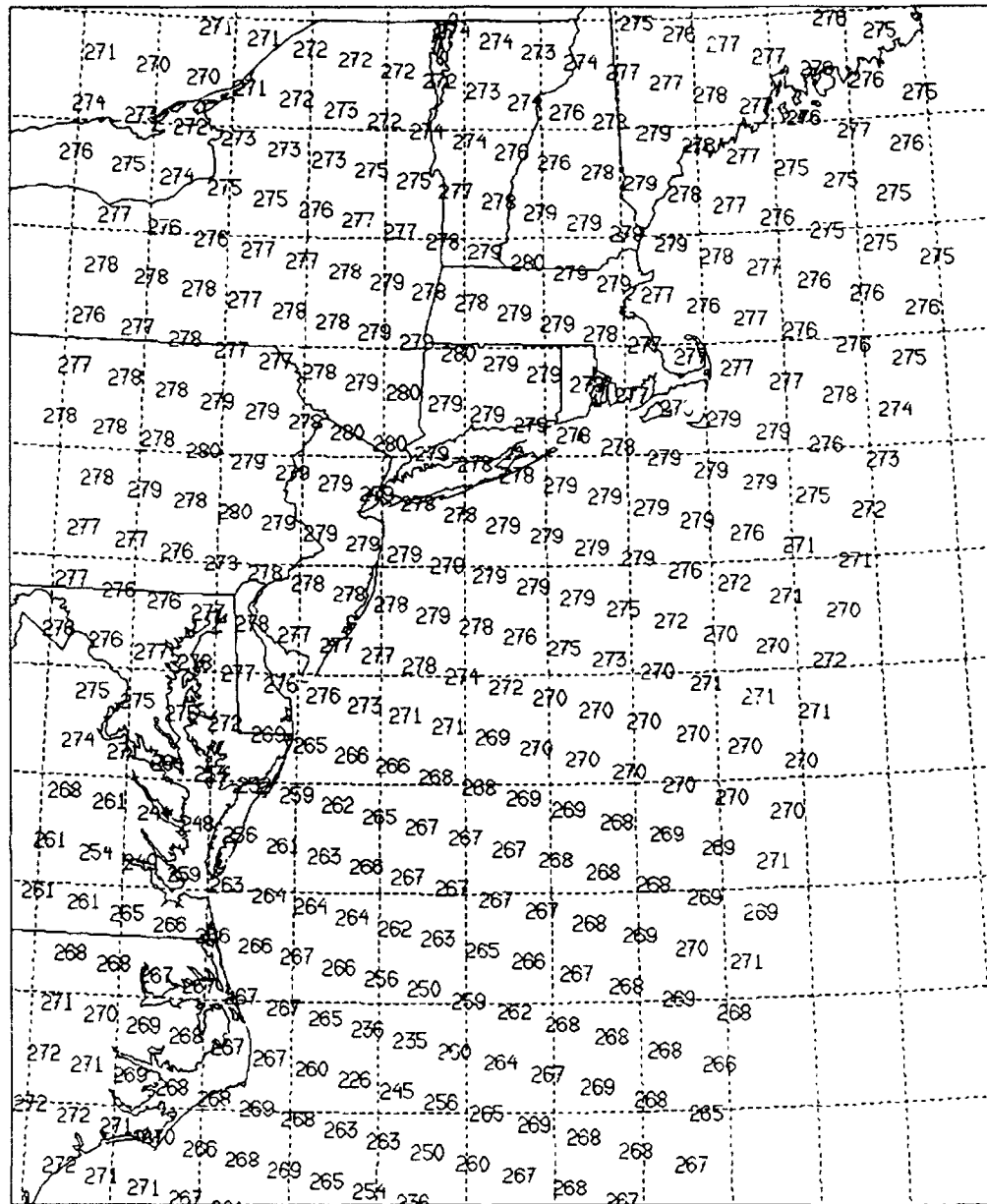
6 AUG 1992



# SSM/T-2 FOOTPRINTS

183 +/- 7 GHz

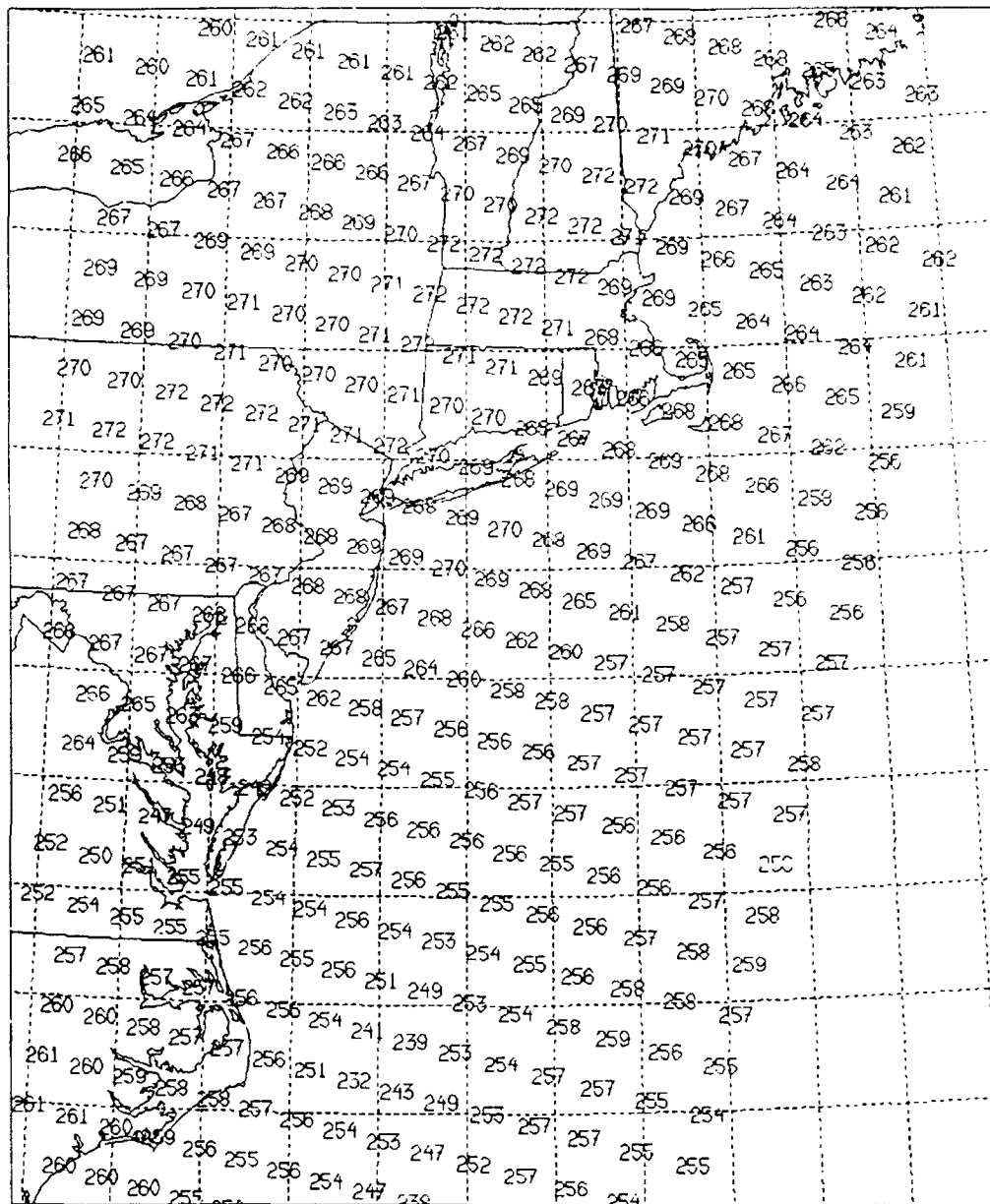
6 AUG 1992



## SSM/T-2 FOOTPRINTS

183 +/- 3 GHz

6 AUG 1992

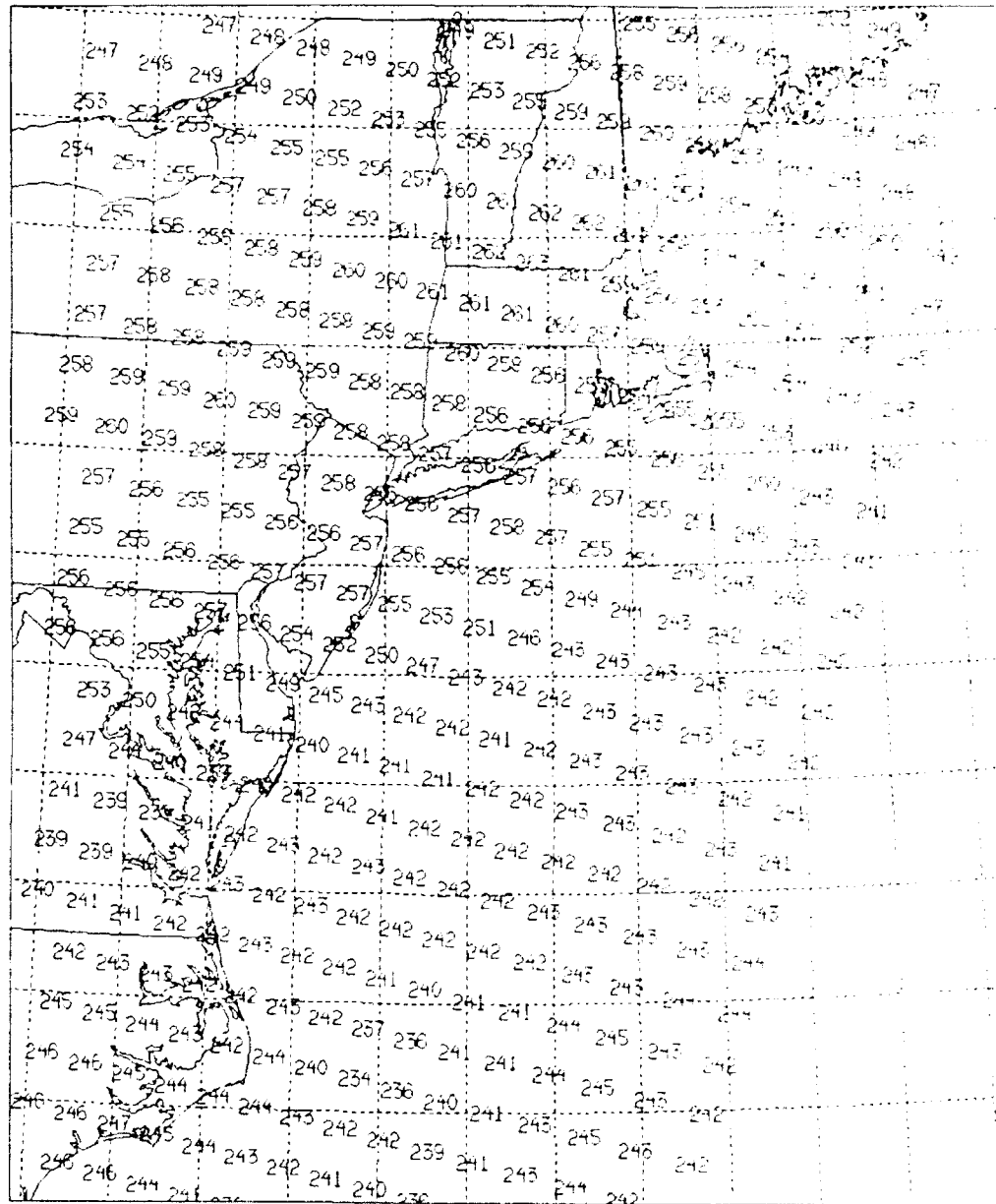




## SSM/T-2 FOOTPRINTS

183 +/- 1 GHz

6 AUG 1992



**Appendix D. Listing of data collected by Aerospace for the SSM/T-2 Cal/Val study.**

# SSMT/2 Calibration / Validation Database

REV#	ANODE DTG	MTSDRS	MTEDRS	T2SDRS	T2EDRS	MISDRS	MIEDRS	CONV	JUHR	SGDB	RTNEPH	MODEL
897	2319Z 30JAN92			YES	YES							
898	0101Z 31JAN92											
899	0243Z			YES	YES				211134			
900	0606Z			YES	YES							
901	0748Z											
902	0930Z			YES	YES				211140			
903	1112Z			YES	YES							
904	1254Z											
905	1436Z 31JAN92	YES	YES	YES	YES							
906	1618Z			YES	YES							
907	1800Z	YES	YES	YES	YES				211146			
908	1942Z			YES	YES							
909	2124Z	YES	YES	YES	YES							
910	2306Z	YES	YES	YES	YES							
911	0048Z 01FEB92	YES	YES	YES	YES				211152			
912	0230Z	YES	YES	YES	YES							
913	0412Z	YES	YES	YES	YES							
914	0554Z	YES	YES	YES	YES				211158			
915	0736Z	YES	YES	YES	YES							
916	0918Z	YES	YES	YES	YES							
917	1100Z											
918	1242Z	YES	YES	YES	YES				211164			
919	1424Z	YES	YES	YES	YES							
920	1605Z			YES	YES							
921	1748Z	YES	YES	YES	YES				211170			
922	1929Z			YES	YES							
923	2112Z	YES	YES	YES	YES							
924	2254Z	YES	YES	YES	YES							
925	0035Z 02FEB92	YES	YES	YES	YES				211176			
926	0217Z			YES	YES							
927	0359Z	YES	YES	YES	YES							
928	0541Z	YES	YES	YES	YES				211182			
929	0723Z	YES	YES	YES	YES							
930	0905Z	YES	YES	YES	YES							
931	1047Z			YES	YES							
932	1229Z	YES	YES	YES	YES				211188			
933	1411Z			YES	YES							
934	1553Z											
935	1735Z											
936	1917Z	YES	YES	YES	YES				211194			

Courtesy of The Aerospace Corporation, DMSPLE



REV# ANODE DIG MTSDRS MTEPRS T2SDRS T2EDRS MISDRS MIEDRS CONV JUHR SGDB RTNEPH MODEL

978	1839Z								211266		
979	2021Z	YES	YES								
980	2203Z	YES	YES	YES	YES						
981	2345Z	YES	YES	YES	YES						
982	0127Z 06FEB92	YES	YES	YES	YES				211272		
983	0309Z	YES	YES	YES	YES						
984	0451Z	YES	YES	YES	YES						
985	0633Z										
986	0814Z	YES	YES	YES	YES				211278		
987	0956Z	YES	YES	YES	YES						
988	1138Z	YES	YES	YES	YES						
989	1320Z	YES	YES	YES	YES				211284		
990	1502Z	YES	YES	YES	YES						
991	1644Z										
992	1826Z	YES	YES	YES	YES				211290		
993	2008Z	YES	YES	YES	YES						
994	2150Z	YES	YES	YES	YES						
995	2332Z	YES	YES	YES	YES				211296		
996	0114Z 07FEB92	YES	YES	YES	YES						
997	0256Z	YES	YES	YES	YES						
998	0438Z	YES	YES	YES	YES						
999	0620Z								211302		
1000	0802Z	YES	YES	YES	YES						
1001	0944Z										
1002	1126Z	YES	YES	YES	YES				211308		
1003	1308Z	YES	YES	YES	YES						
1004	1450Z	YES	YES	YES	YES						
1005	1630Z										
1006	1813Z	YES	YES	YES	YES				211314		
1007	1955Z	YES	YES	YES	YES						
1008	2137Z	YES	YES	YES	YES						
1009	2319Z								211320		
1010	0101Z 08FEB92	YES	YES	YES	YES						
1011	0243Z	YES	YES	YES	YES						
1012	0425Z										
1013	0607Z								211326		
1014	0749Z										
1015	0931Z										
1016	1113Z										
1017	1255Z								211332		
1018	1437Z										

Courtesy of The Aerospace Corporation, DMSPL

REV# ANODE DTG MISDRS MIEDRS T2SDRS T2EDRS MISDRS MIEDRS CONV JUHR SGDB RINEPH MODEL

1019 1619Z								211338	
1020 1801Z									
1021 1943Z									
1022 2125Z	YES								
1023 2307Z	YES	YES							
1024 0049Z 09FEB92	YES	YES	YES	YES				211344	
1025 0231Z	YES	YES							
1026 0413Z									
1027 0554Z	YES	YES						211350	
1028 0736Z	YES	YES							
1029 0918Z									
1030 1100Z									
1031 1242Z	YES	YES						211356	
1032 1424Z	YES	YES							
1033 1606Z									
1034 1748Z								211362	
1035 1930Z	YES	YES							
1036 2112Z	YES	YES							
1037 2254Z	YES	YES							
1038 0036Z 10FEB92	YES	YES	YES	YES				211368	
1039 0218Z	YES	YES	YES	YES					
1040 0400Z	YES	YES	YES	YES					
1041 0542Z	YES	YES						211374	
1042 0724Z	YES	YES	YES	YES					
1043 0906Z									
1044 1048Z									
1045 1230Z	YES	YES						211380	
1046 1412Z	YES	YES							
1047 1553Z	YES	YES							
1048 1735Z								211386	YES
1049 1917Z	YES	YES	YES	YES					YES
1050 2059Z	YES	YES	YES	YES					YES
1051 2241Z	YES	YES	YES	YES					YES
1052 0023Z 11FEB92	YES	YES	YES	YES				211392	YES
1053 0205Z									YES
1054 0347Z	YES	YES	YES	YES					YES
1055 0529Z	YES	YES	YES	YES				211398	YES
1056 0711Z	YES	YES	YES	YES					YES
1057 0853Z	YES	YES	YES	YES					YES
1058 1035Z	YES	YES	YES	YES					YES
1059 1217Z	YES	YES	YES	YES				211404	YES

Courtesy of The Aerospace Corporation, DMSPL

REV#	ANODE	DIG	MISDRS	MIEDRS	T2SDRS	T2EDRS	MISDRS	MIEDRS	CONV	JUHR	SGDB	RTNEPH	MODEL
1060	1359Z		YES	YES	YES	YES	YES						
1061	1541Z						YES						
1062	1723Z			YES	YES	YES	YES		211410				
1063	1905Z						YES						
1064	2047Z			YES	YES	YES	YES						
1065	2229Z						YES						
1066	0011Z	12FEB92					YES		211416				
1067	0153Z		YES	YES	YES	YES	YES						
1068	0334Z		YES	YES	YES	YES	YES						
1069	0516Z		YES	YES	YES	YES	YES		211422				
1070	0658Z		YES	YES			YES						
1071	0840Z		YES	YES			YES						
1072	1022Z		YES	YES	YES	YES	YES						
1073	1204Z		YES	YES	YES	YES	YES		211428				
1074	1346Z		YES	YES	YES	YES	YES						
1075	1528Z		YES	YES	YES	YES	YES						
1076	1710Z		YES	YES	YES	YES	YES						
1077	1852Z		YES	YES	YES	YES	YES						
1078	2034Z		YES	YES	YES	YES	YES		211434				
1079	2216Z		YES	YES	YES	YES	YES						
1080	2358Z		YES	YES	YES	YES	YES		211440				
1081	0140Z	13FEB92	YES	YES									
1082	0322Z			YES	YES	YES	YES						
1083	0504Z			YES	YES	YES	YES						
1084	0646Z			YES	YES	YES	YES		211446				
1085	0828Z												
1086	1010Z				YES	YES							
1087	1152Z												
1088	1334Z								211452				
1089	1515Z												
1090	1657Z												
1091	1839Z		YES	YES	YES	YES	YES		211458				
1092	2021Z		YES	YES	YES	YES	YES						
1093	2203Z												
1094	2345Z		YES	YES	YES	YES	YES						
1095	0127Z	14FEB92	YES	YES	YES	YES	YES		211464				
1096	0309Z												
1097	0451Z		YES	YES	YES	YES	YES						
1098	0633Z												
1099	0815Z		YES	YES	YES	YES	YES		211470				
1100	0957Z												
1101	1139Z		YES	YES	YES	YES	YES		211476				

Courtesy of The Aerospace Corporation, DMSPL

REV#	ANODE	DTG	MISDRS	MTEDRS	T2SDRS	T2EDRS	MISDRS	MTEDRS	CONV	JUHR	SGDB	RTNEPH	MODEL
1102	1321Z		YES	YES	YES	YES	YES						
1103	1503Z			YES	YES	YES	YES						
1104	1645Z		YES	YES	YES	YES	YES		211482		YES		
1105	1827Z		YES	YES	YES	YES	YES						
1106	2009Z		YES	YES	YES	YES	YES						
1107	2151Z		YES	YES	YES	YES	YES				YES		
1108	2333Z		YES	YES	YES	YES	YES		211488				
1109	0114Z	15FEB92	YES	YES	YES	YES					YES		
1110	0256Z		YES	YES									
1111	0438Z		YES	YES									
1112	0620Z		YES	YES					211494				
1113	0802Z		YES	YES							YES		
1114	0944Z												
1115	1126Z								211500				
1116	1308Z		YES	YES	YES	YES	YES				YES		
1117	1450Z		YES	YES									
1118	1632Z												
1119	1814Z				YES	YES	YES		211506				
1120	1956Z			YES	YES	YES	YES				YES		
1121	2138Z		YES	YES	YES	YES	YES						
1122	2320Z		YES	YES	YES	YES	YES		211512				
1123	0102Z	16FEB92		YES	YES	YES	YES						
1124	0244Z				YES	YES	YES						
1125	0426Z		YES	YES	YES	YES	YES				YES		
1126	0608Z		YES	YES	YES	YES	YES						
1127	0750Z		YES	YES	YES	YES	YES				YES		
1128	0932Z		YES	YES	YES	YES	YES						
1129	1113Z												
1130	1255Z		YES	YES	YES	YES	YES						
1131	1437Z												
1132	1619Z										YES		
1133	1801Z		YES	YES	YES	YES	YES						
1134	1943Z		YES	YES	YES	YES	YES						
1135	2125Z		YES	YES	YES	YES	YES				YES		
1136	2307Z				YES	YES	YES						
1137	0049Z	17FEB92		YES	YES	YES	YES				YES		
1138	0231Z			YES	YES	YES	YES						
1139	0413Z		YES	YES	YES	YES	YES				YES		
1140	0555Z		YES	YES	YES	YES	YES				YES		
1141	0737Z		YES	YES									
1142	0919Z		YES	YES	YES	YES	YES						
1143	1101Z		YES	YES									

Courtesy of The Aerospace Corporation, DMSPL



REV#	ANODE DTG	MISDRS	MIEDRS	T2SDRS	T2EDRS	MISDRS	MIEDRS	CONV	JUHR	SGDB	RINEPH	MODEL
1144	1243Z	YES	YES	YES	YES	YES						
1145	1425Z	YES	YES			YES				YES		
1146	1607Z					YES						
1147	1749Z			YES	YES	YES				YES		
1148	1931Z			YES	YES	YES						
1149	2112Z	YES	YES	YES	YES	YES						
1150	2254Z	YES	YES	YES	YES	YES						
1151	0036Z 18FEB92	YES	YES	YES	YES	YES					YES	
1152	0218Z	YES	YES	YES	YES	YES				YES	YES	
1153	0400Z	YES	YES	YES	YES	YES						
1154	0542Z	YES	YES	YES	YES	YES		211566			YES	
1155	0724Z	YES	YES			YES						
1156	0906Z					YES				YES	YES	
1157	1048Z	YES	YES	YES	YES	YES						
1158	1230Z	YES	YES			YES		211572			YES	
1159	1412Z					YES						
1160	1554Z					YES					YES	
1161	1736Z	YES	YES			YES		211578		YES	YES	
1162	1917Z					YES						
1163	2059Z	YES	YES	YES	YES	YES					YES	
1164	2241Z	YES	YES	YES	YES	YES						
1165	0023Z 19FEB92	YES	YES	YES	YES	YES		211584			YES	
1166	0205Z	YES	YES	YES	YES	YES						
1167	0347Z	YES	YES	YES	YES	YES					YES	
1168	0529Z	YES	YES	YES	YES	YES		211590			YES	
1169	0711Z					YES						
1170	0853Z					YES						
1171	1035Z					YES						
1172	1217Z					YES				YES	YES	
1173	1359Z					YES						
1174	1541Z					YES					YES	
1175	1723Z					YES						
1176	1905Z			YES	YES	YES						
1177	2047Z			YES	YES	YES						
1178	2229Z			YES	YES	YES				YES		
1179	0011Z 20FEB92			YES	YES	YES		211602				
1180	0152Z			YES	YES	YES						
1181	0334Z			YES	YES	YES						
1182	0516Z			YES	YES	YES					YES	
1183	0658Z			YES	YES	YES					YES	
1184	0840Z											
1185	1022Z			YES	YES	YES				YES	YES	

Courtesy of The Aerospace Corporation, DMSPL

REV#	ANODE DTG	MTSDRS	MTEDRS	T2SDRS	T2EDRS	MISDRS	MIEDRS	CONV	JUHR	SGDB	RTNEPH	MODEL
1186	1204Z					YES					YES	
1187	1346Z					YES				YES		
1188	1528Z					YES					YES	
1189	1710Z			YES		YES						
1190	1852Z			YES		YES					YES	
1191	2034Z	YES	YES	YES		YES					YES	
1192	2216Z	YES	YES	YES		YES						
1193	2358Z	YES	YES	YES		YES					YES	
1194	0140Z 21FEB92	YES	YES	YES		YES					YES	
1195	0322Z			YES		YES						
1196	0504Z	YES	YES	YES		YES					YES	
1197	0646Z			YES		YES						
1198	0828Z	YES	YES	YES		YES					YES	
1199	1009Z					YES						
1200	1151Z											
1201	1333Z	YES	YES	YES		YES						
1202	1515Z			YES		YES				YES		
1203	1657Z					YES						
1204	1839Z			YES		YES						
1205	2021Z					YES						
1206	2203Z	YES	YES	YES		YES						
1207	2345Z	YES	YES	YES		YES						
1208		YES	YES	YES								
1209		YES	YES	YES								
1210		YES	YES	YES								
1211		YES	YES	YES								
1212		YES	YES	YES								

# SSMT/2 Calibration / Validation Database

REV#	ANODE DTG	MTSDRS	MTEDRS	T2SDRS	T2EDRS	MISDRS	MIEDRS	CONV	JUHR	SGDB	RINEPH	MODEL
1277	2241Z 26FEB92			YES	YES							
1278	0023Z 27FEB92			YES	YES							
1279	0205Z			YES	YES							
1280	0347Z	YES	YES	YES	YES							
1281	0529Z	YES	YES	YES	YES							
1282	0711Z	YES	YES	YES	YES							
1283	0853Z	YES	YES	YES	YES							
1284	1035Z	YES	YES	YES	YES							
1285	1217Z	YES	YES	YES	YES							
1286	1359Z	YES	YES	YES	YES							
1287	1541Z							211794				
1288	1723Z			YES	YES							
1289	1905Z			YES	YES							YES
1290	2047Z			YES	YES							
1291	2229Z			YES	YES							YES
1292	0011Z 28FEB92			YES	YES			211800				
1293	0153Z			YES	YES							YES
1294	0334Z	YES	YES									YES
1295	0516Z	YES	YES					211806				YES
1296	0658Z	YES	YES									YES
1297	0840Z	YES	YES									YES
1298	1022Z			YES	YES							YES
1299	1204Z			YES	YES							YES
1300	1346Z	YES	YES	YES	YES							YES
1301	1528Z	YES	YES	YES	YES							YES
1302	1710Z	YES	YES	YES	YES							YES
1303	1852Z	YES	YES	YES	YES							YES
1304	2034Z	YES	YES	YES	YES							YES
1305	2216Z	YES	YES	YES	YES							YES
1306	2358Z											YES
1307	0140Z 29FEB92											
1308	0322Z											
1309	0504Z			YES	YES					YES		
1310	0646Z			YES	YES					YES		YES
1311	0828Z			YES	YES					YES		YES
1312	1010Z	YES	YES									YES
1313	1151Z											YES
1314	1333Z	YES	YES	YES	YES							YES
1315	1515Z			YES	YES							YES
1316	1657Z	YES	YES	YES	YES							YES

Courtesy of The Aerospace Corporation, DMSPL

REV#	ANODE	DTG	MISDRS	MTEDRS	T2SDRS	T2EDRS	MISDRS	MTEDRS	CONV	JUHR	SGDR	RTNEPH	MODEL
1317	1839Z		YES	YES	YES	YES	YES					YES	
1318	2021Z		YES	YES	YES	YES	YES					YES	
1319	2203Z						YES						
1320	2345Z		YES	YES	YES	YES	YES		211848			YES	YES
1321	0127Z 01MAR92		YES	YES	YES	YES	YES					YES	
1322	0309Z		YES	YES	YES	YES	YES						
1323	0451Z		YES	YES	YES	YES	YES						
1324	0633Z		YES	YES	YES	YES	YES		211854				YES
1325	0815Z						YES				YES		
1326	0957Z						YES						
1327	1139Z				YES	YES	YES		211860		YES		YES
1328	1321Z				YES	YES	YES						
1329	1503Z				YES	YES	YES						
1330	1645Z		YES	YES	YES	YES	YES		211866		YES		
1331	1826Z		YES	YES	YES	YES	YES						
1332	2008Z		YES	YES	YES	YES	YES						
1333	2150Z		YES	YES	YES	YES	YES		211872				
1334	2332Z		YES	YES	YES	YES	YES						
1335	0114Z 02MAR92		YES	YES	YES	YES	YES						
1336	0256Z		YES	YES	YES	YES	YES		211878				
1337	0438Z		YES	YES	YES	YES	YES						
1338	0620Z												
1339	0802Z		YES	YES	YES	YES	YES						
1340	0944Z		YES	YES	YES	YES	YES		211884				
1341	1126Z		YES	YES	YES	YES	YES						
1342	1308Z		YES	YES	YES	YES	YES						
1343	1450Z		YES	YES	YES	YES	YES						
1344	1632Z		YES	YES	YES	YES	YES		211890			YES	
1345	1814Z				YES	YES	YES						
1346	1956Z		YES	YES	YES	YES	YES					YES	
1347	2138Z		YES	YES	YES	YES	YES		211896			YES	
1348	2320Z		YES	YES	YES	YES	YES					YES	
1349	0102Z 03MAR92		YES	YES	YES	YES	YES						
1350	0244Z				YES	YES	YES						
1351	0425Z				YES	YES	YES						
1352	0607Z		YES	YES	YES	YES	YES		211902			YES	
1353	0749Z		YES	YES	YES	YES	YES						
1354	0931Z		YES	YES	YES	YES	YES					YES	
1355	1113Z				YES	YES	YES		211908			YES	
1356	1255Z		YES	YES	YES	YES	YES						
1357	1437Z		YES	YES	YES	YES	YES						
1358	1619Z		YES	YES	YES	YES	YES					YES	

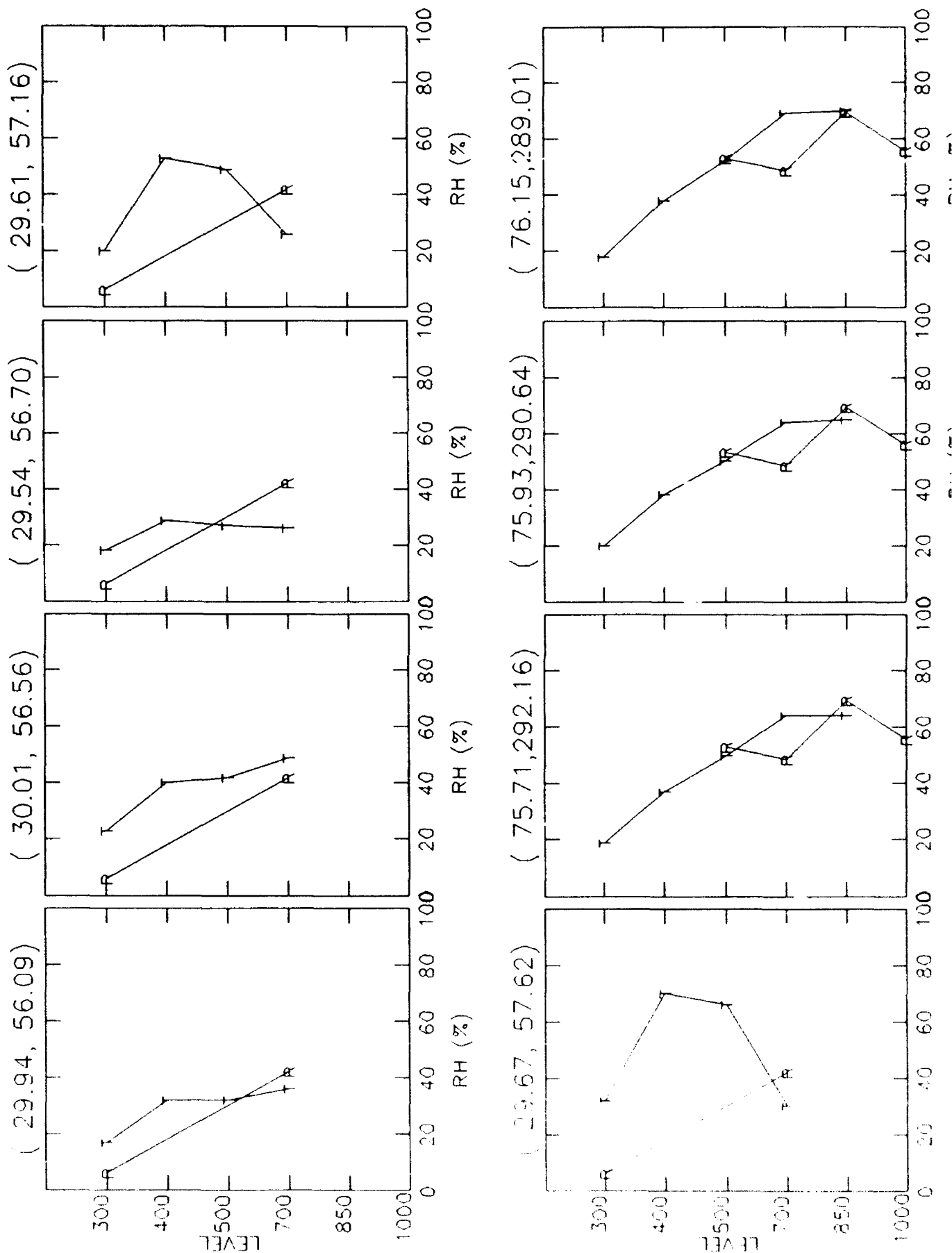
Courtesy of The Aerospace Corporation, DMSPL

REV#	ANODE DTG	MISDRS	MTEDRS	T2SDRS	T2EDRS	MISDRS	MTEDRS	CONV	JUHR	SGDB	RINEPH	MODEL
1359	1801Z	YES	YES	YES	YES	YES		211914			YES	
1360	1943Z	YES	YES			YES					YES	
1361	2125Z					YES						
1362	2307Z	YES	YES	YES	YES	YES		211920			YES	
1363	0049Z 04MAR92	YES	YES	YES	YES	YES					YES	
1364	0231Z			YES	YES	YES					YES	
1365	0413Z	YES	YES	YES	YES	YES		211926			YES	
1366	0555Z	YES	YES	YES	YES	YES					YES	
1367	0737Z	YES	YES	YES	YES	YES					YES	
1368	0919Z	YES	YES			YES						
1369	1100Z	YES	YES			YES		211932		YES	YES	
1370	1242Z	YES	YES			YES					YES	
1371	1424Z					YES						
1372	1606Z					YES		211938				
1373	1748Z					YES						
1374	1930Z					YES						
1375	2112Z					YES						
1376	2254Z					YES		211944				
1377	0036Z 05MAR92					YES						
1378	0218Z					YES						
1379	0400Z					YES		211950				
1380	0542Z					YES				YES		
1381	0724Z					YES						
1382	0906Z					YES						
1383	1048Z			YES	YES	YES		211956				
1384	1230Z	YES	YES	YES	YES	YES						
1385	1412Z			YES	YES	YES				YES		
1386	1554Z			YES	YES	YES						
1387	1736Z	YES	YES	YES	YES	YES		211962				
1388	1917Z	YES	YES	YES	YES	YES					YES	
1389	2059Z	YES	YES	YES	YES	YES					YES	
1390	2241Z	YES	YES			YES					YES	
1391	0023Z 06MAR92	YES	YES			YES		211968				
1392	0205Z	YES	YES			YES						
1393	0347Z			YES	YES	YES		211974			YES	
1394	0529Z			YES	YES	YES					YES	
1395	0711Z			YES	YES	YES					YES	
1396	0853Z			YES	YES	YES						
1397	1035Z	YES	YES	YES	YES	YES		211980		YES	YES	
1398	1217Z	YES	YES	YES	YES	YES						
1399	1359Z	YES	YES	YES	YES	YES				YES	YES	
1400	1541Z	YES	YES	YES	YES	YES					YES	

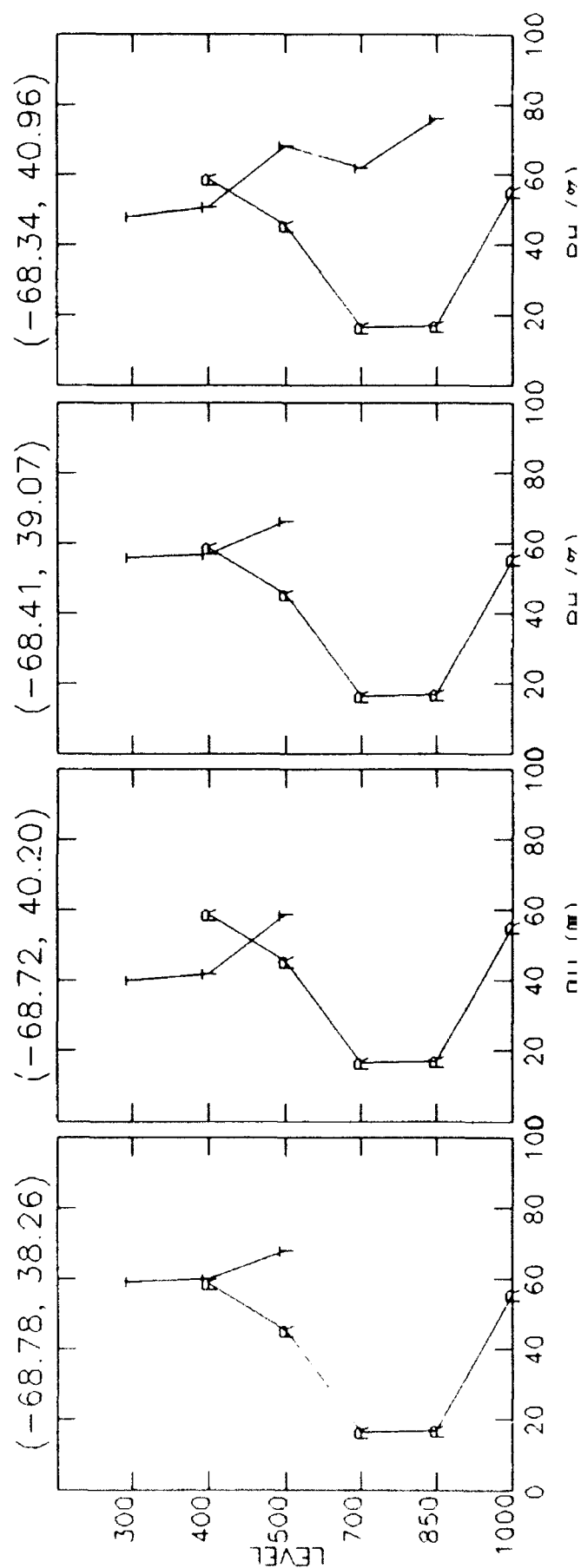
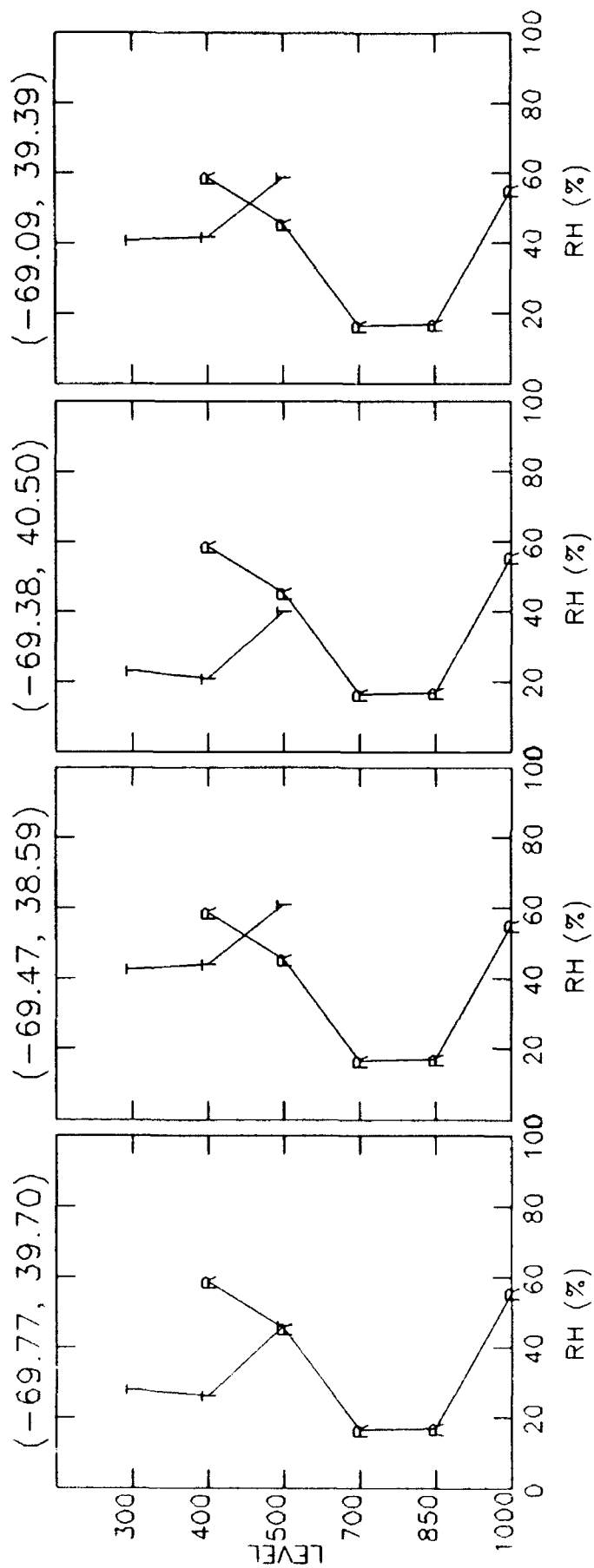
Courtesy of The Aerospace Corporation, DMSPL

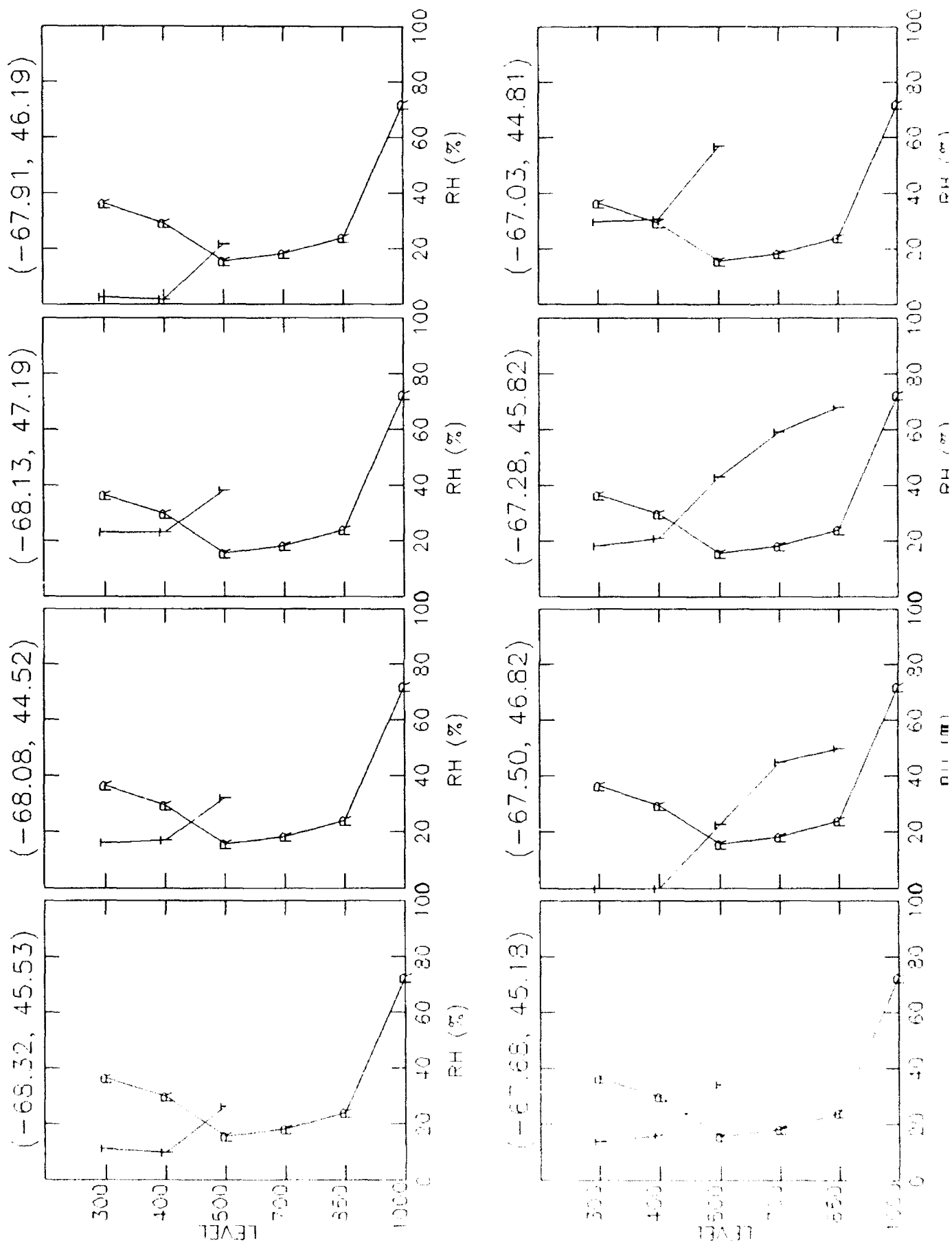
REV#	ANODE DTG	MISDRS	MTEDRS	T2SDRS	T2EDRS	MISDRS	MIEDRS	CONV JUHR	SGDB	RTNEPH	MODEL
1401	1723Z	YES	YES			YES		211986		YES	YES
1402	1905Z	YES	YES	YES	YES	YES					
1403	2047Z	YES	YES	YES	YES	YES	YES			YES	
1404	2229Z	YES	YES	YES	YES	YES					
1405	0011Z 07MAR92	YES	YES	YES	YES	YES		211992		YES	YES
1406	0152Z			YES	YES	YES					
1407	0334Z	YES	YES	YES	YES	YES	YES	211998	YES	YES	YES
1408	0516Z			YES	YES	YES					
1409	0658Z	YES	YES			YES	YES		YES	YES	
1410	0840Z	YES	YES			YES					
1411	1022Z	YES	YES			YES					
1412	1204Z		YES	YES	YES	YES		212004		YES	
1413	1346Z	YES	YES	YES	YES	YES					
1414	1528Z	YES	YES			YES	YES		YES	YES	
1415	1710Z	YES	YES	YES	YES	YES		212010		YES	YES
1416	1852Z			YES	YES	YES					
1417	2034Z	YES	YES	YES	YES	YES				YES	
1418	2216Z	YES	YES	YES	YES	YES					
1419	2358Z			YES	YES	YES		212016		YES	
1420	0140Z 08MAR92					YES			YES	YES	
1421	0322Z			YES	YES	YES	YES				
1422	0504Z			YES	YES	YES					
1423	0646Z			YES	YES	YES		212022		YES	YES
1424	0828Z			YES	YES	YES	YES			YES	
1425	1009Z			YES	YES	YES					
1426	1151Z										
1427	1333Z								YES	YES	YES
1428	1515Z										
1429	1657Z										
1430	2021Z										
1431	2203Z										
1432	2345Z										
1433	0127Z 09MAR92										
1434	0127Z						YES				
1435	0309Z								YES		
1436	0451Z										
1437	0633Z										
1438	0815Z						YES				YES
1439	0957Z										
1440	1139Z										
1441	1321Z						YES				

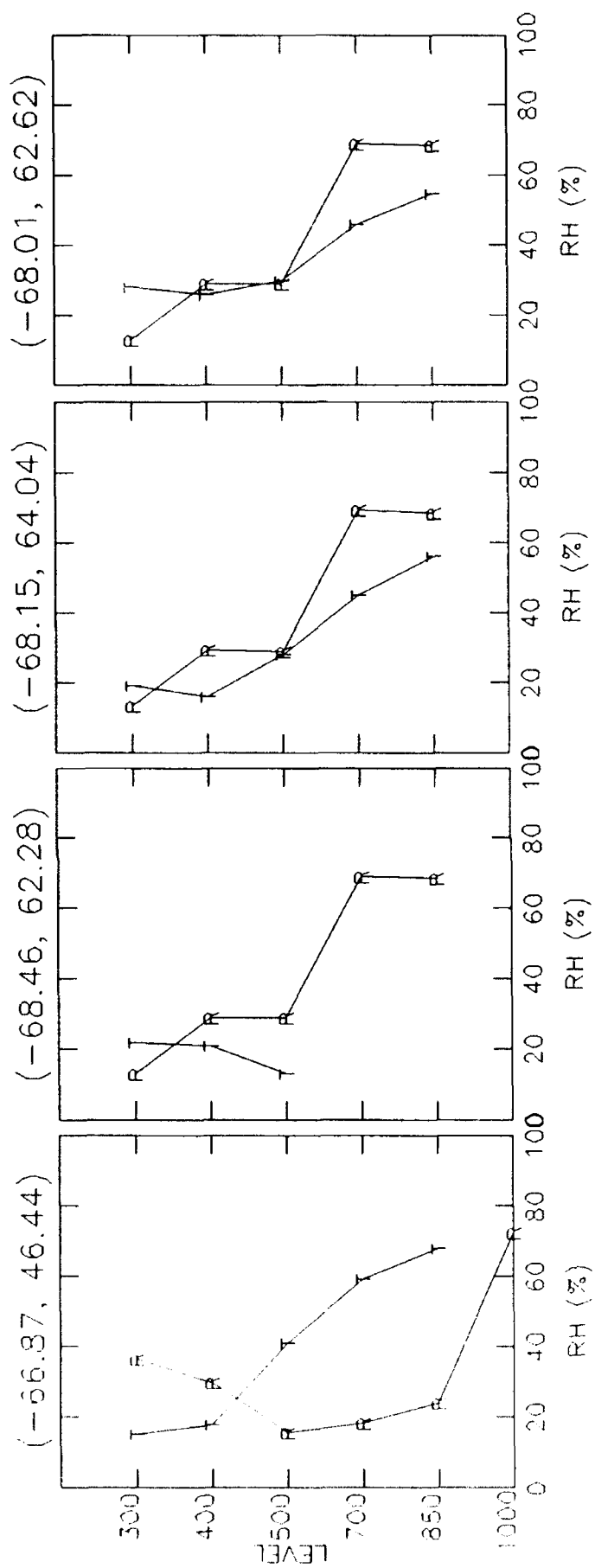
Appendix E. Display of selected radiosonde (R) and SSM/T-2-retrieved (T) RH profiles.



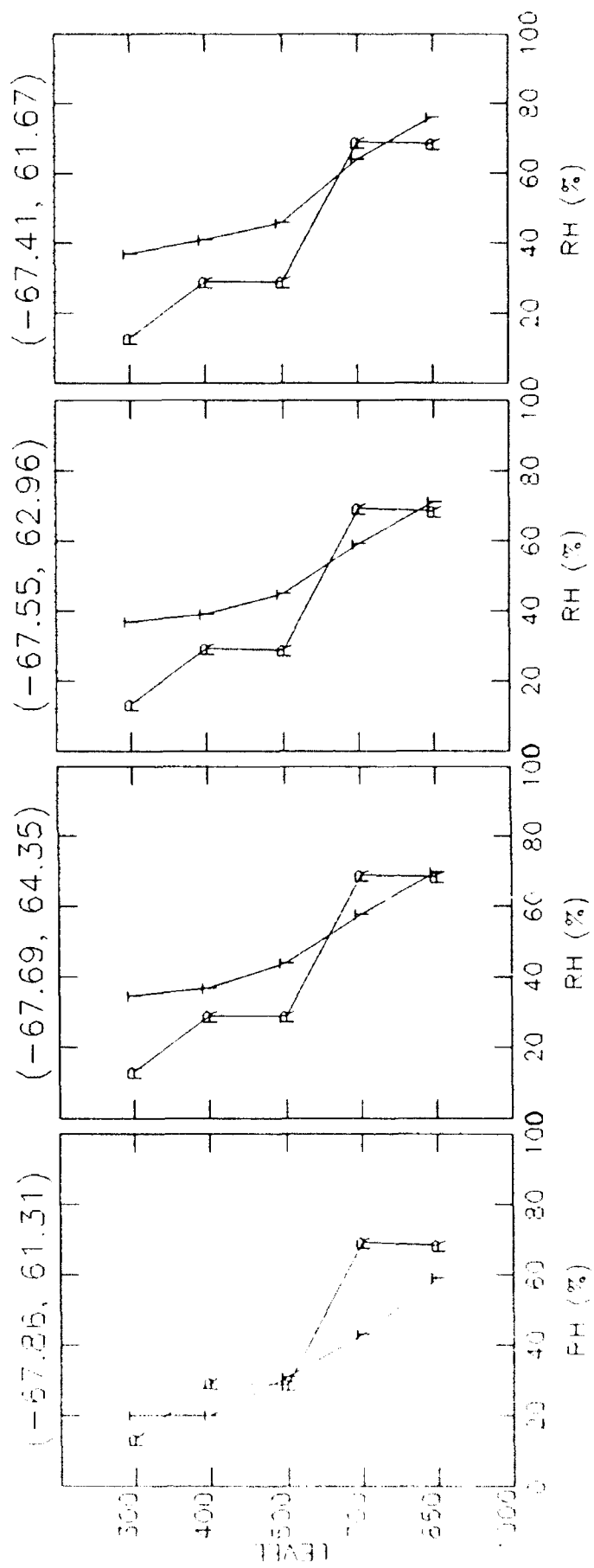


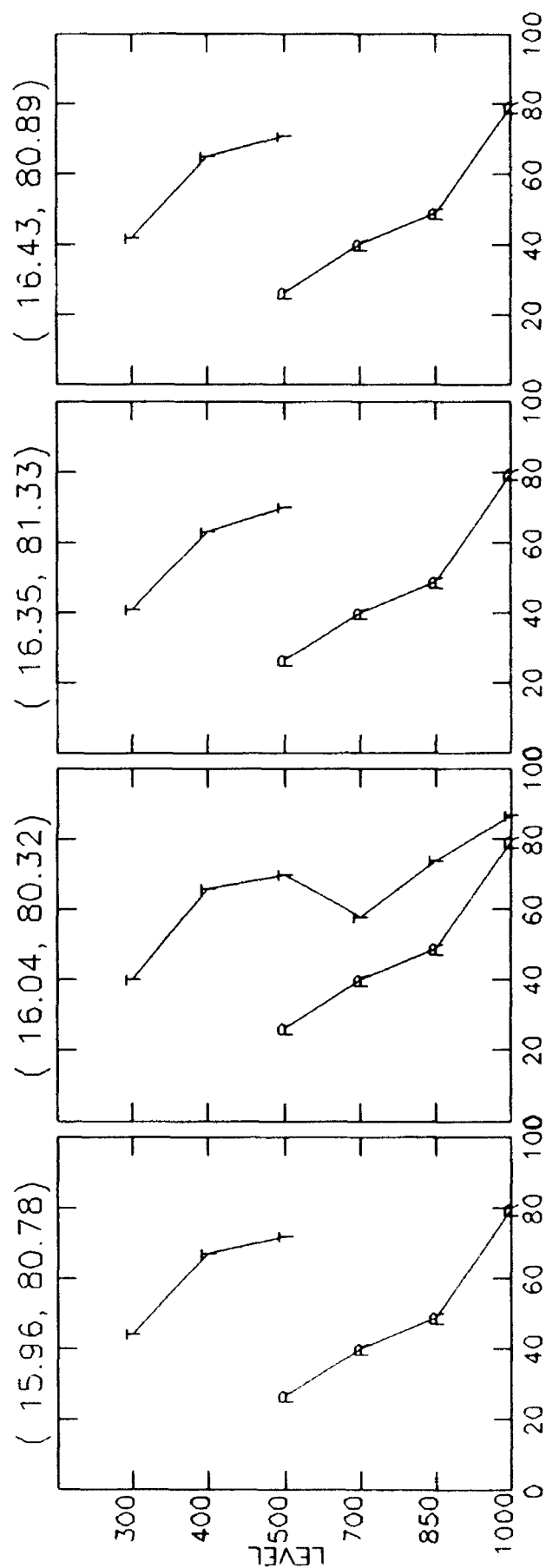
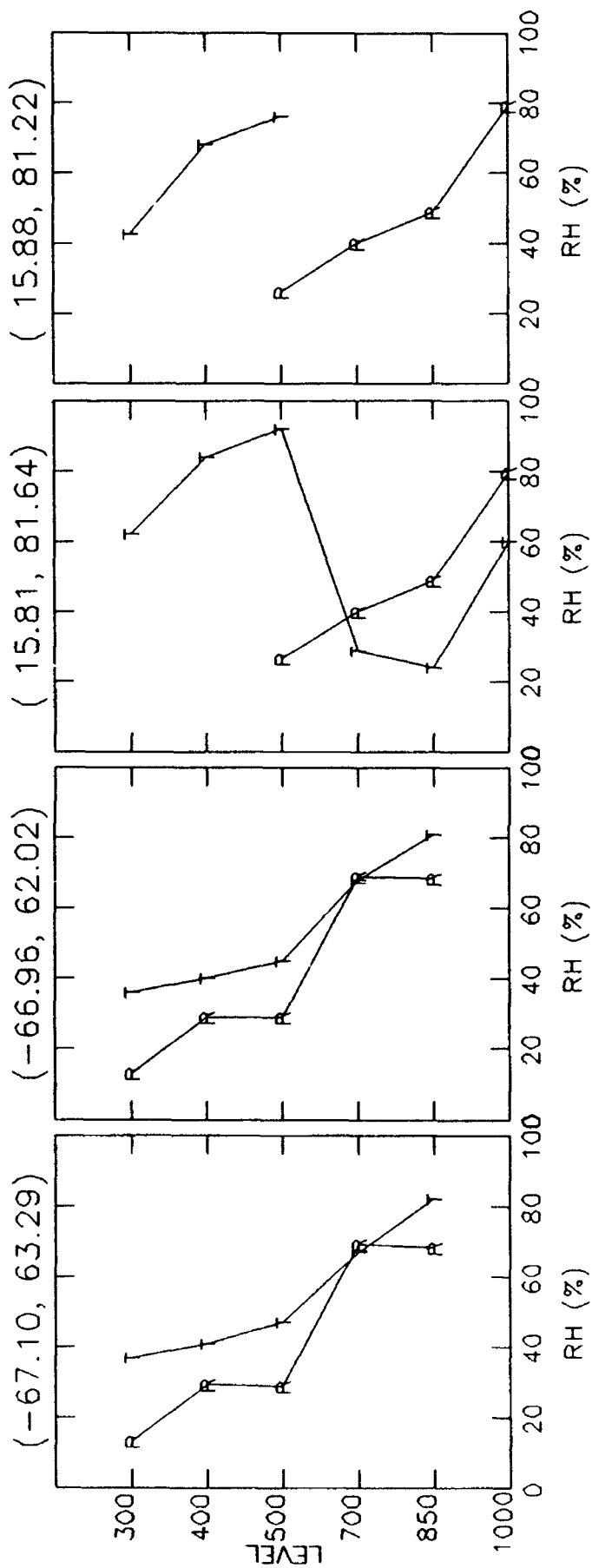


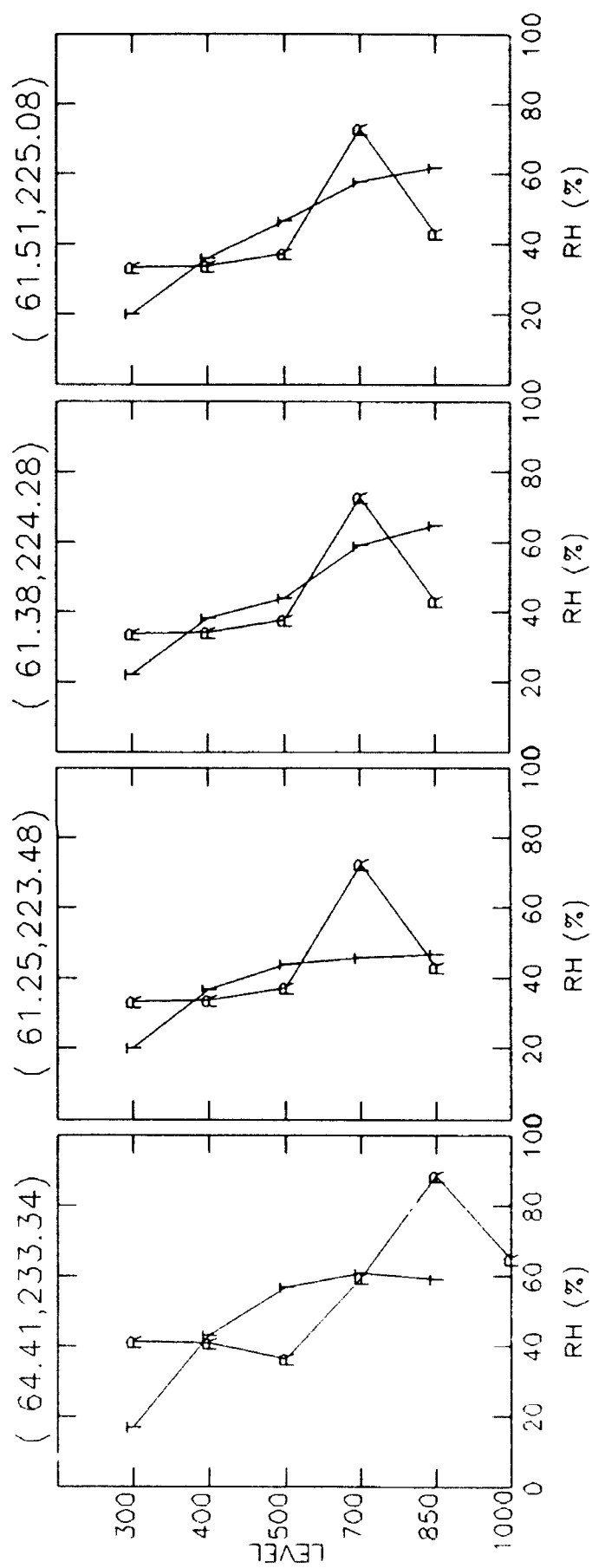
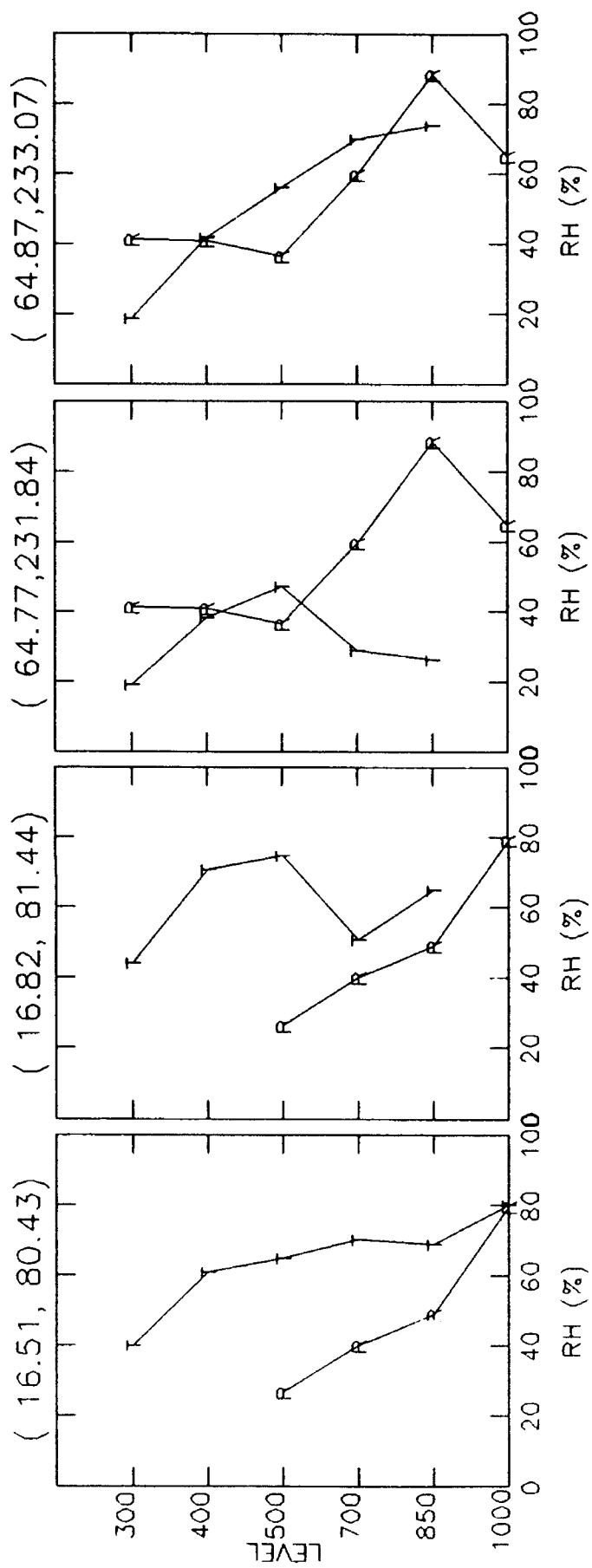


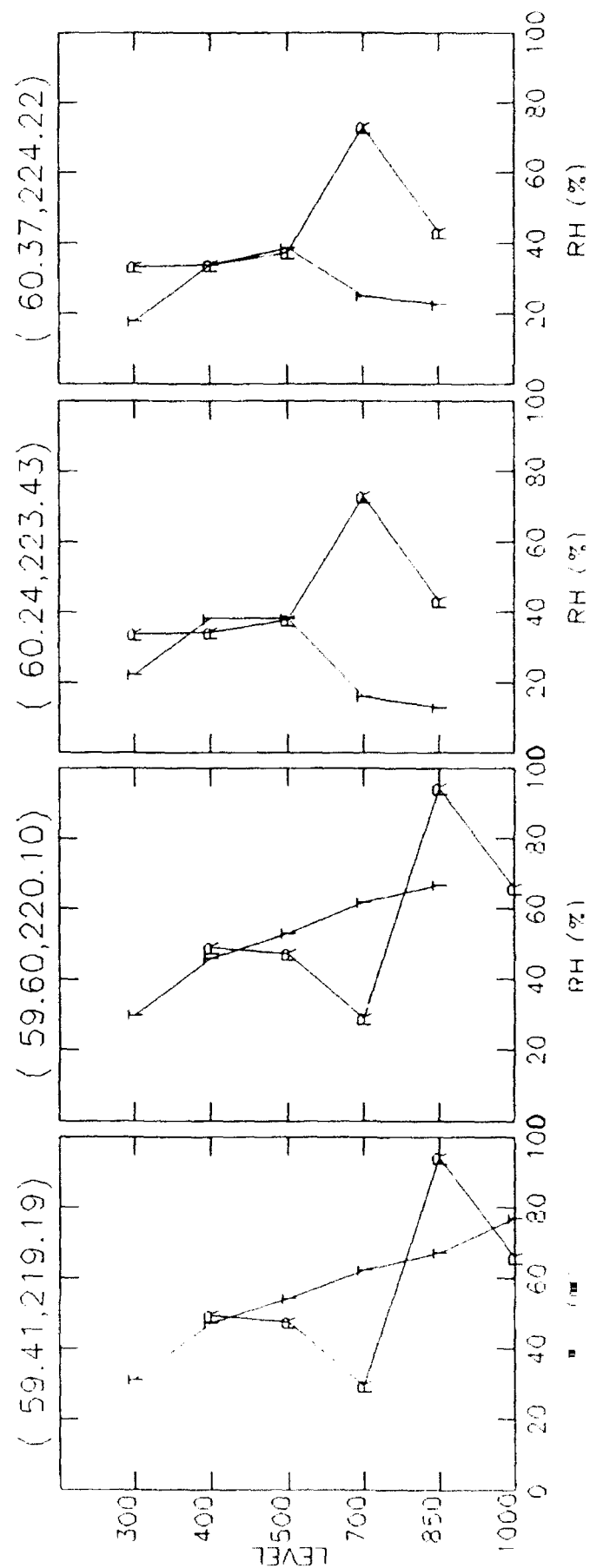
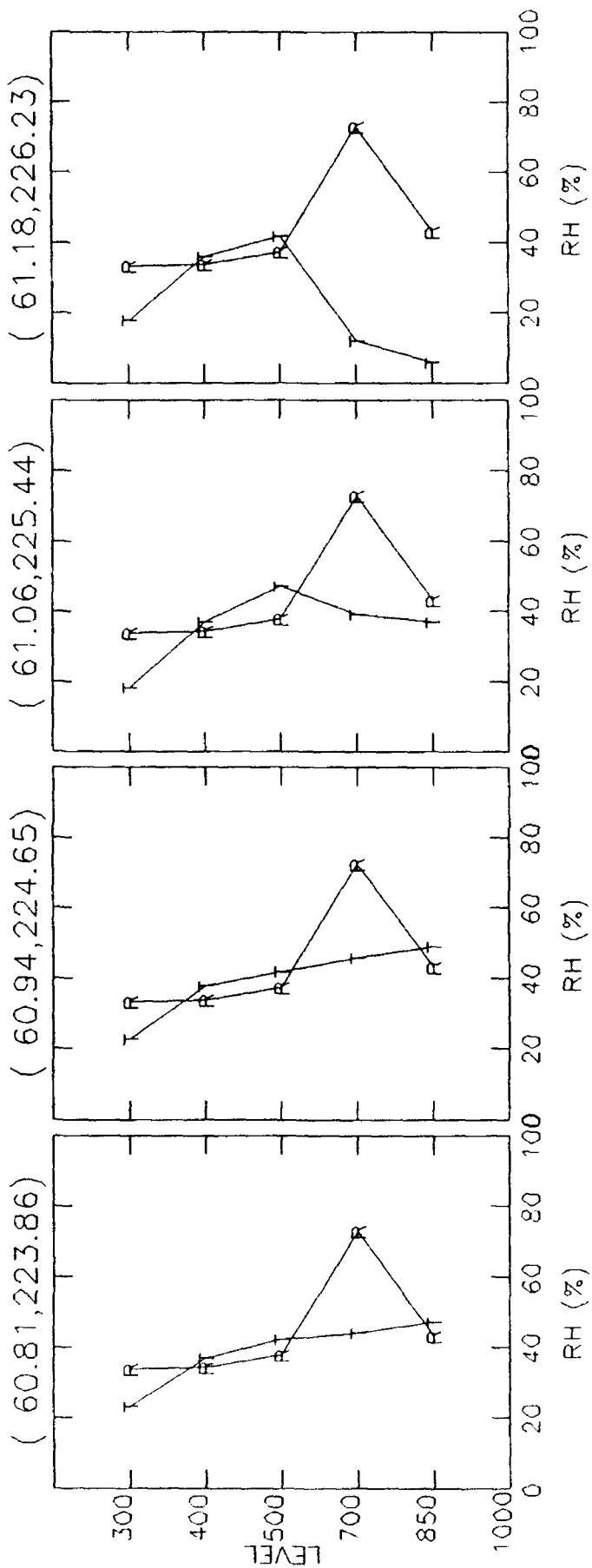


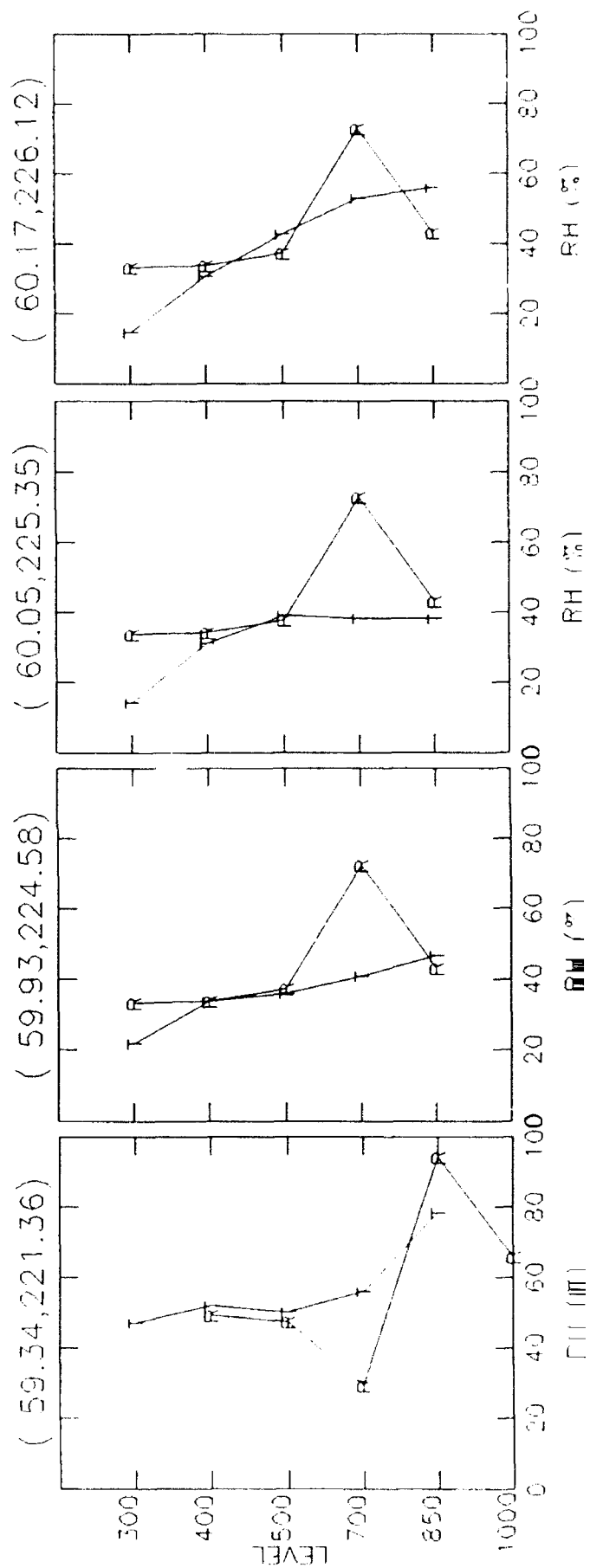
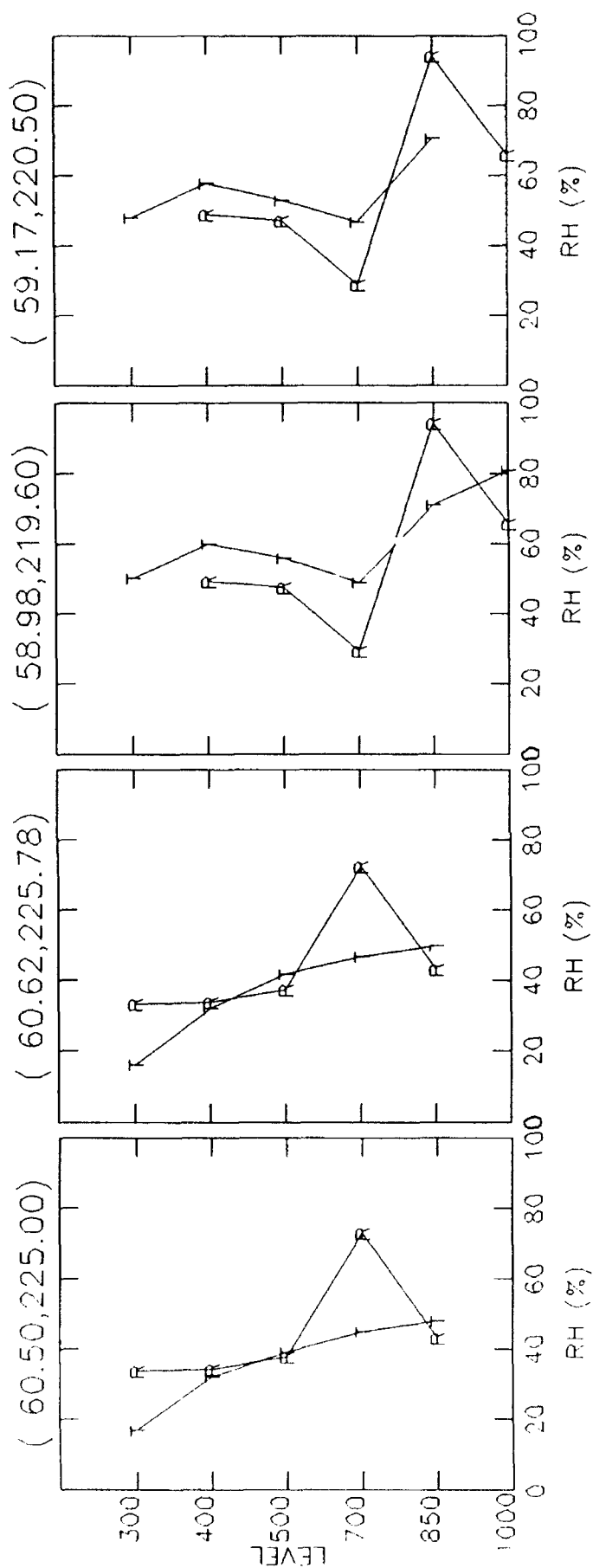
E-5

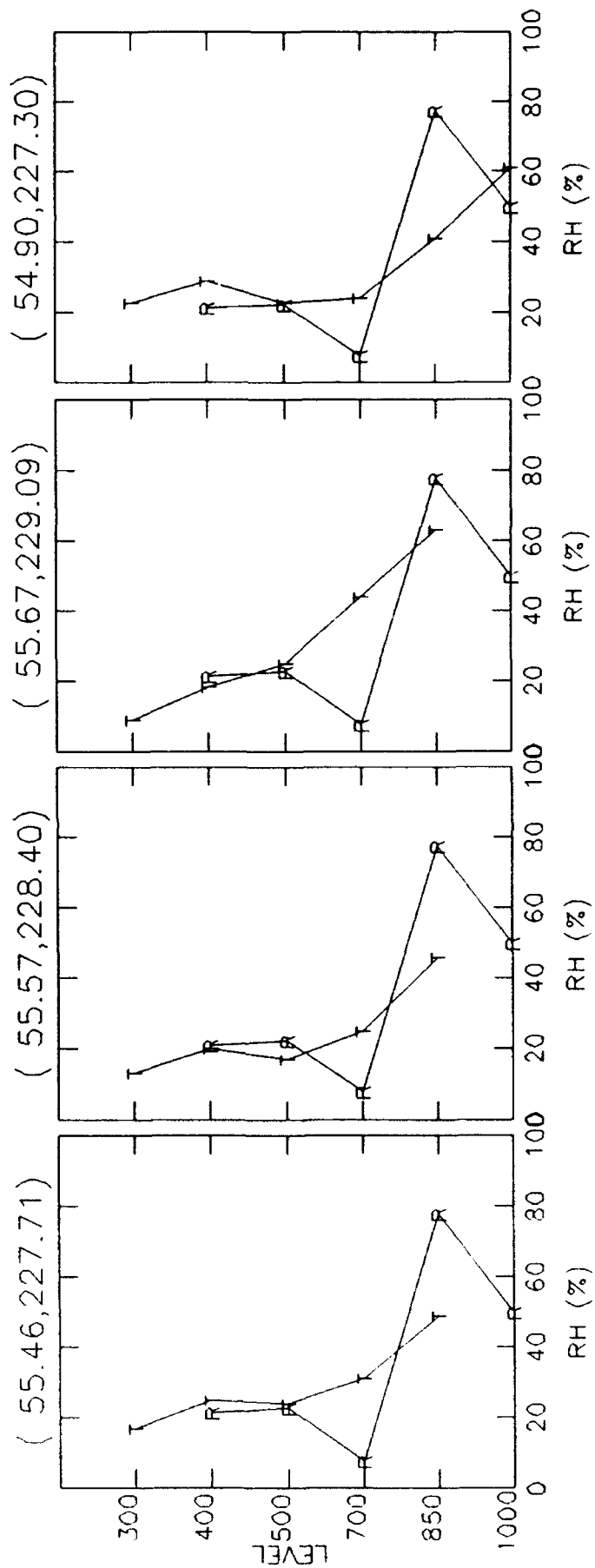
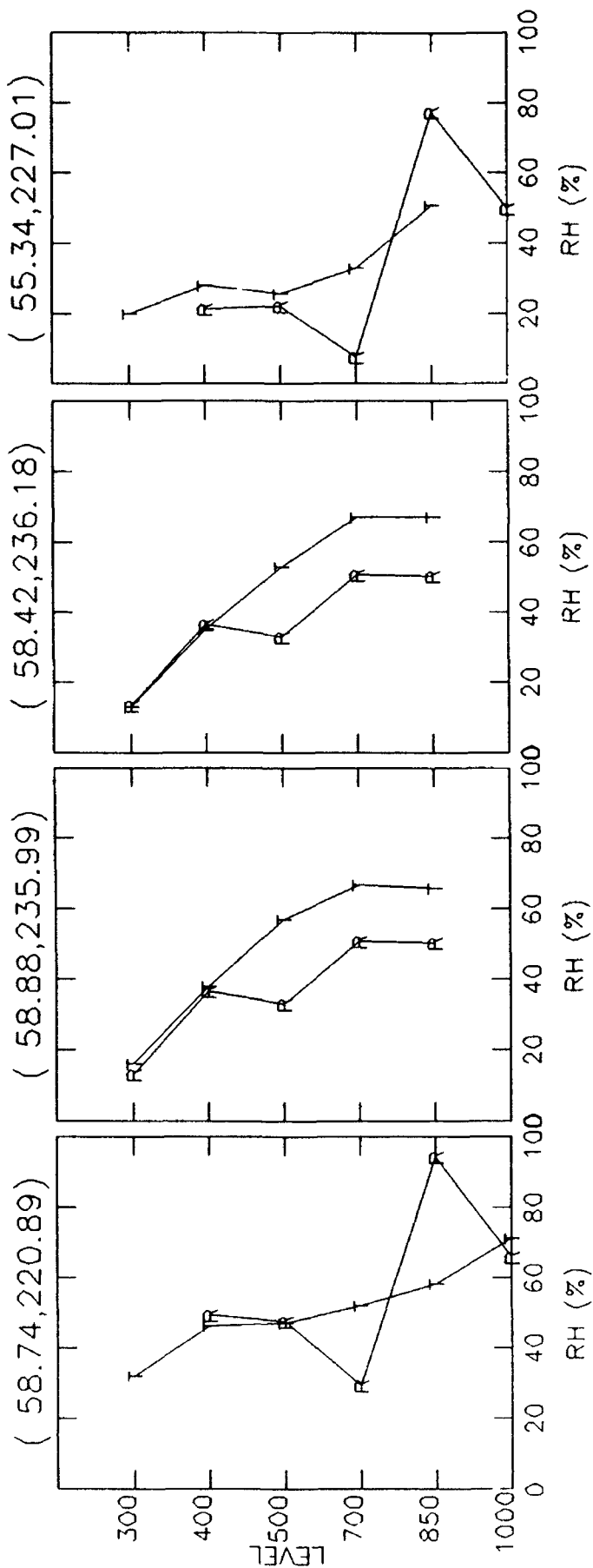




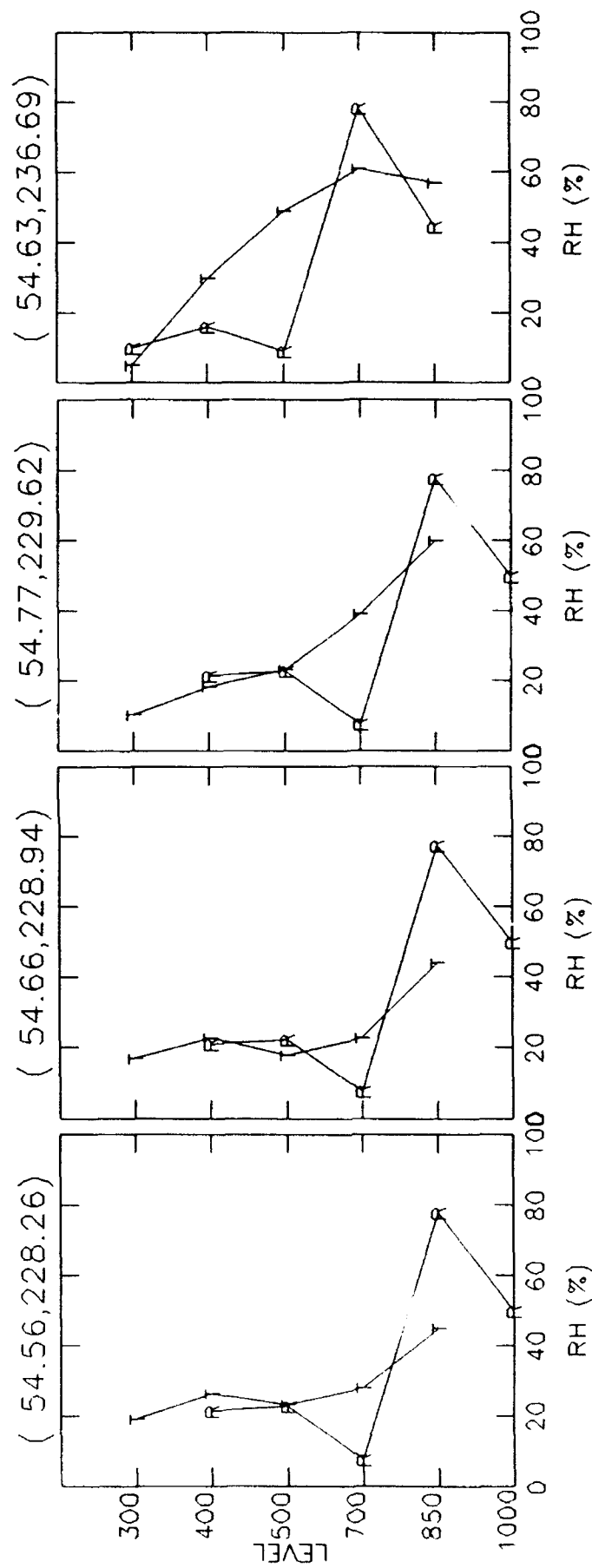
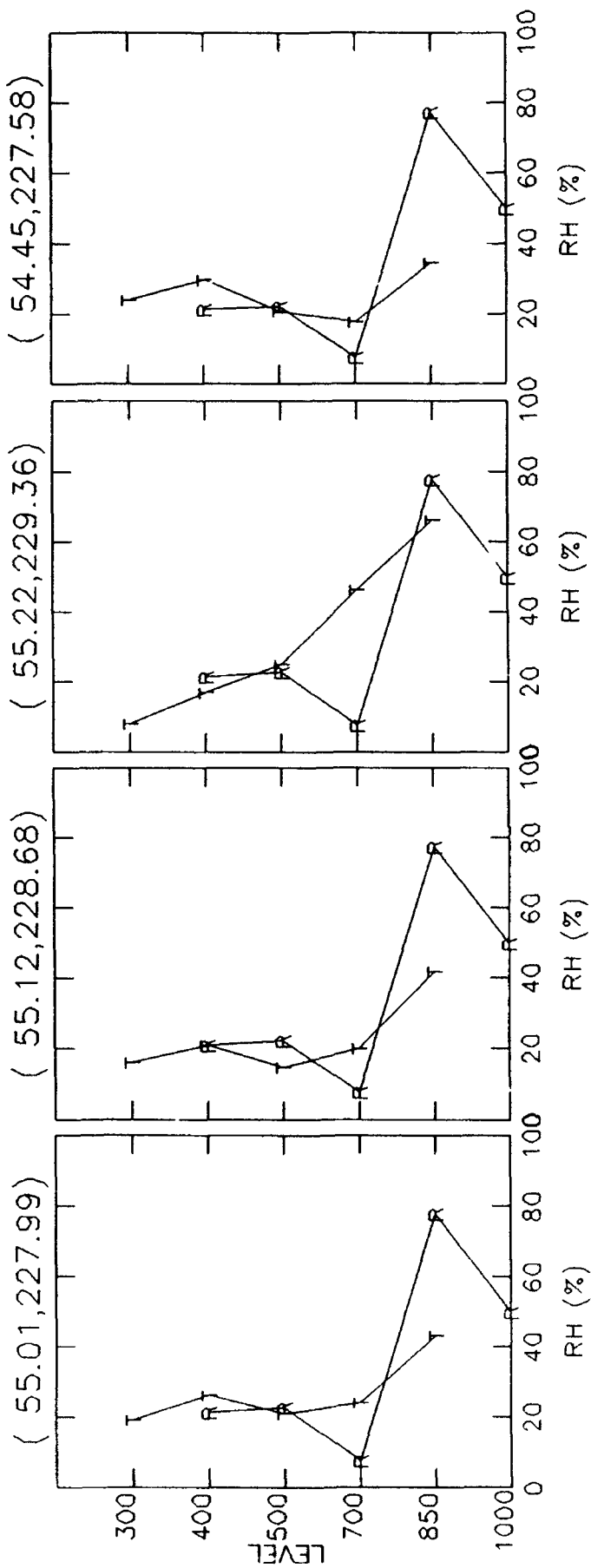


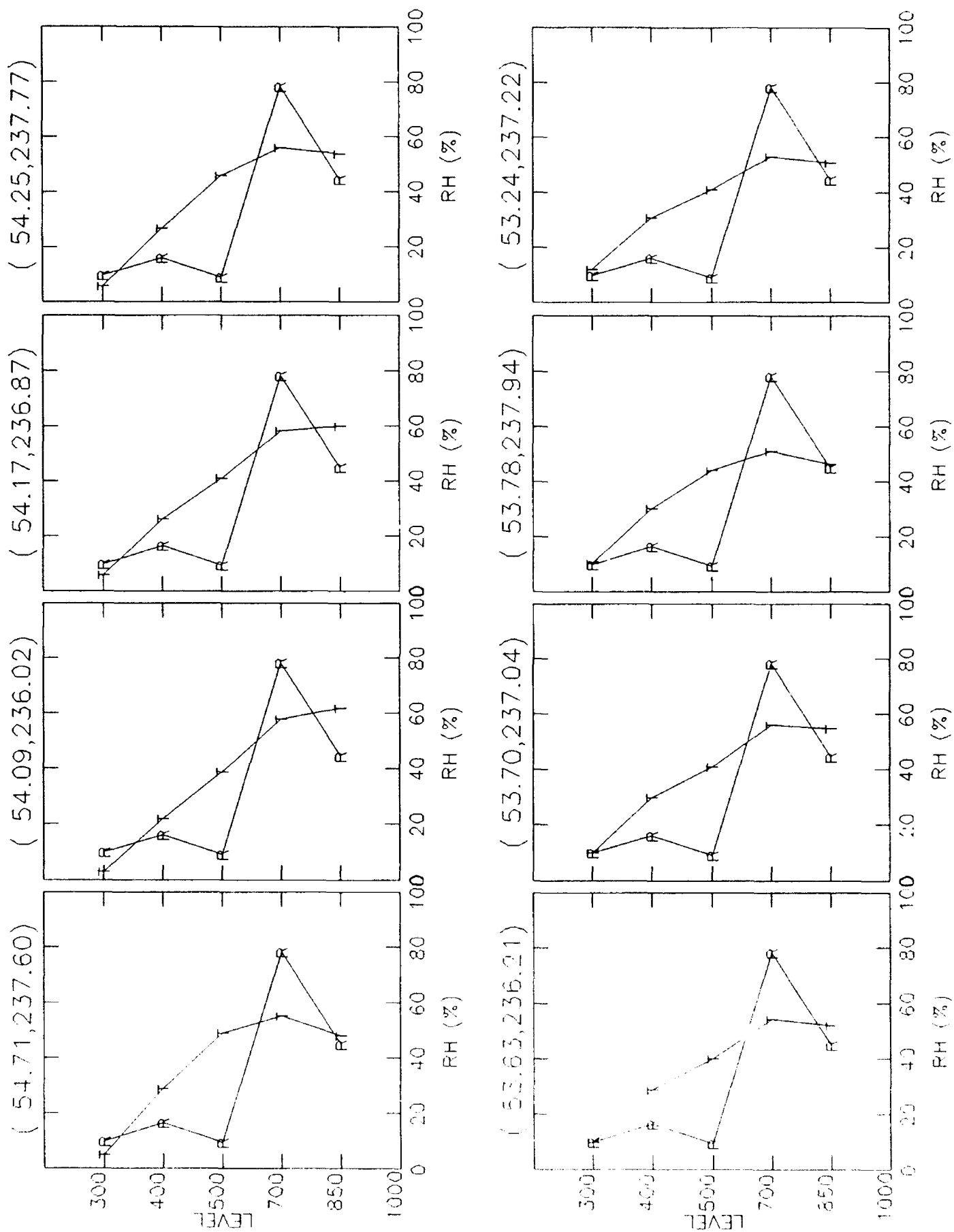


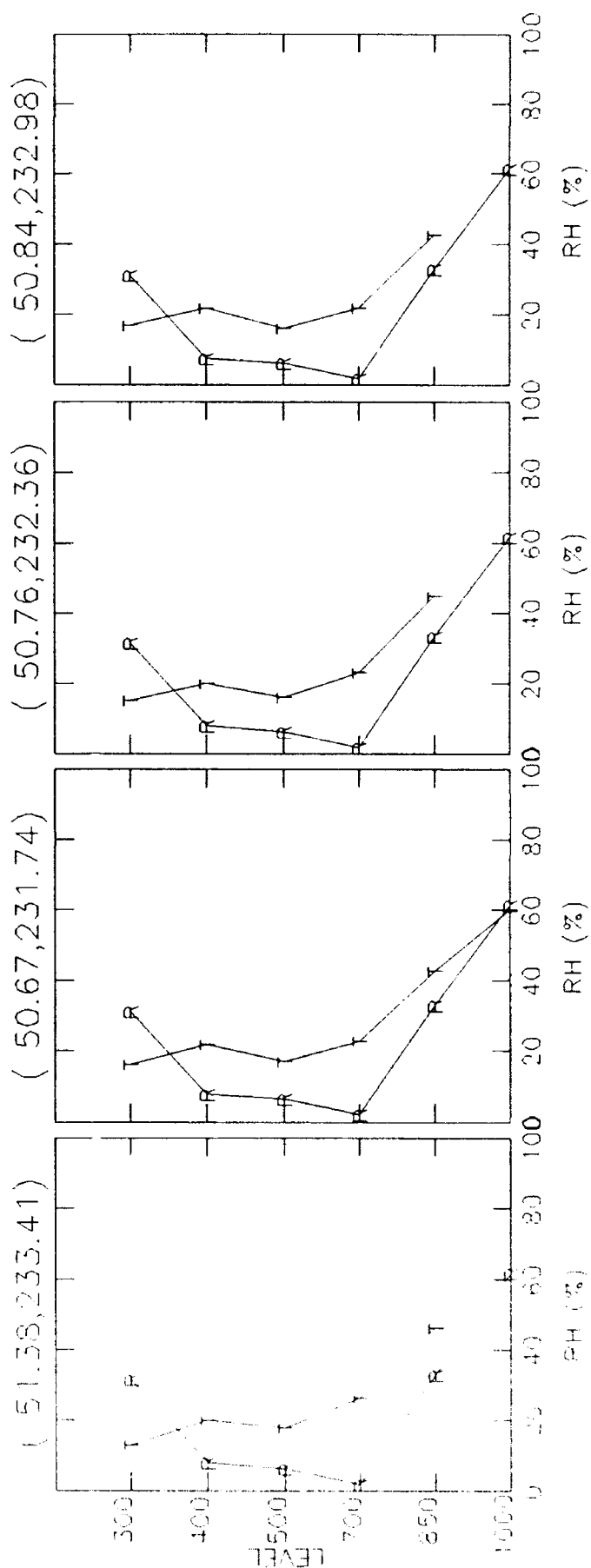
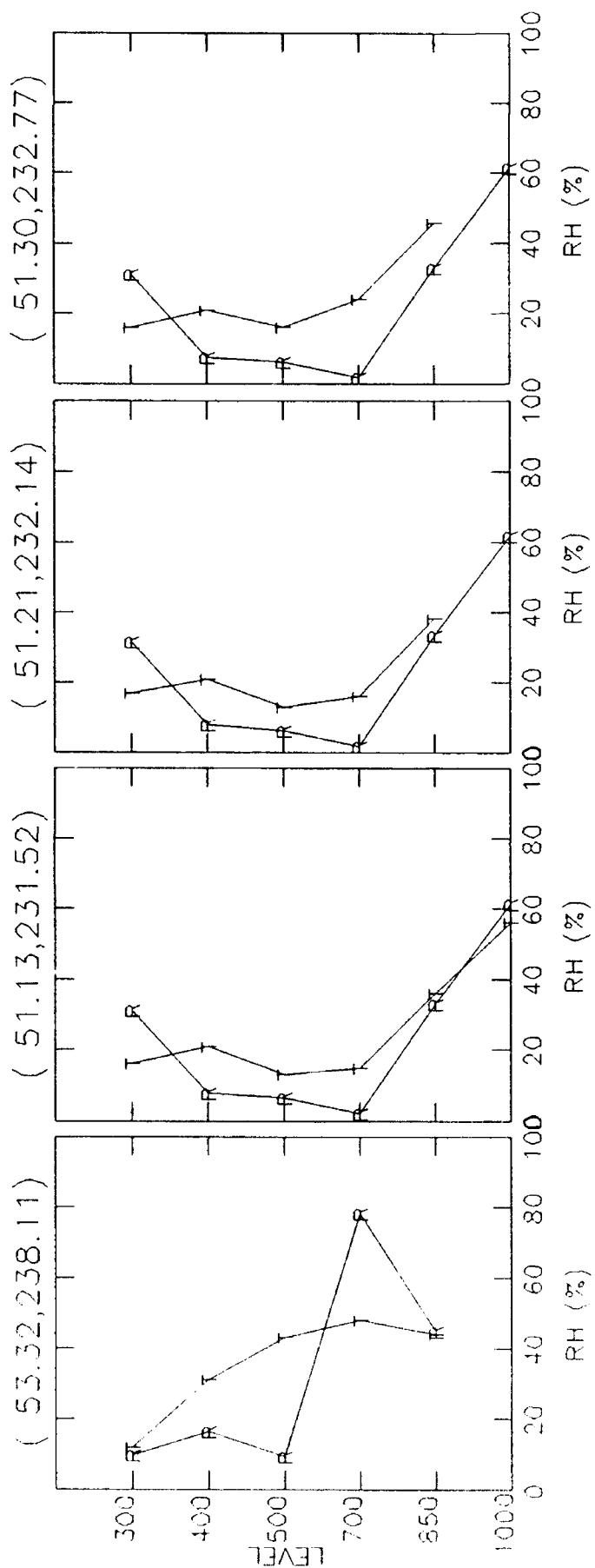


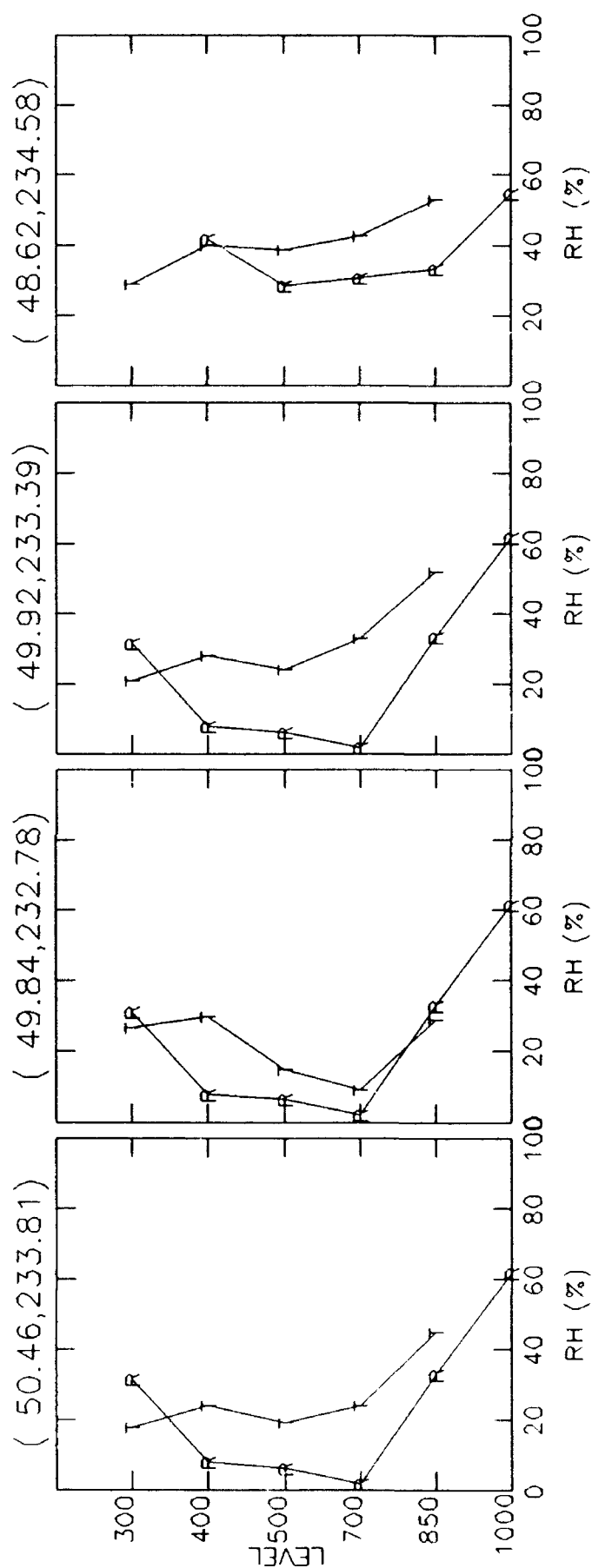
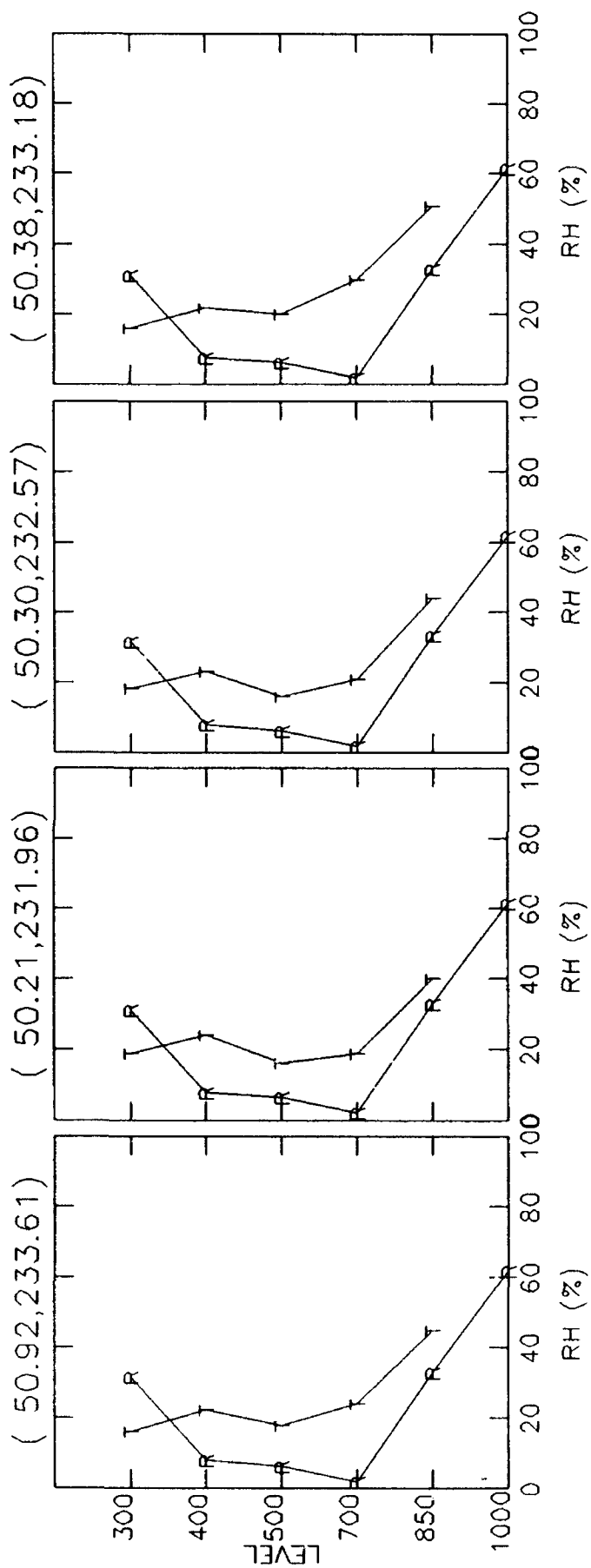


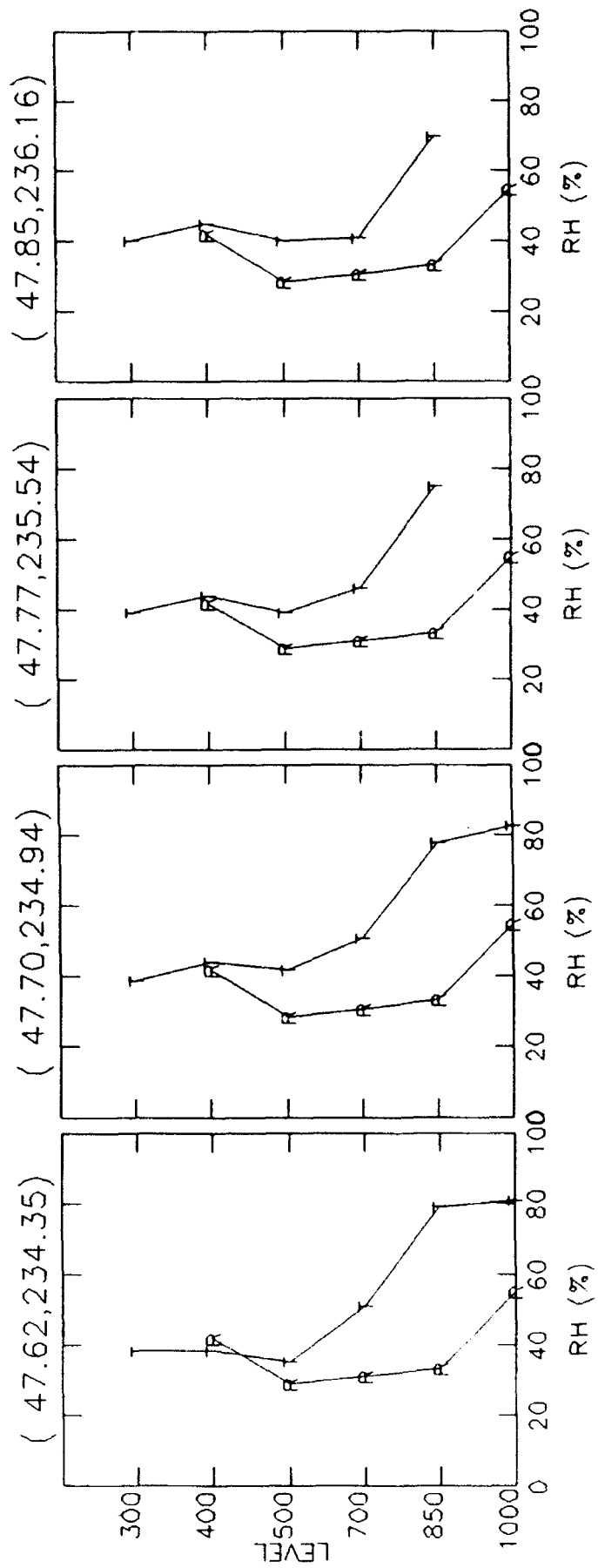
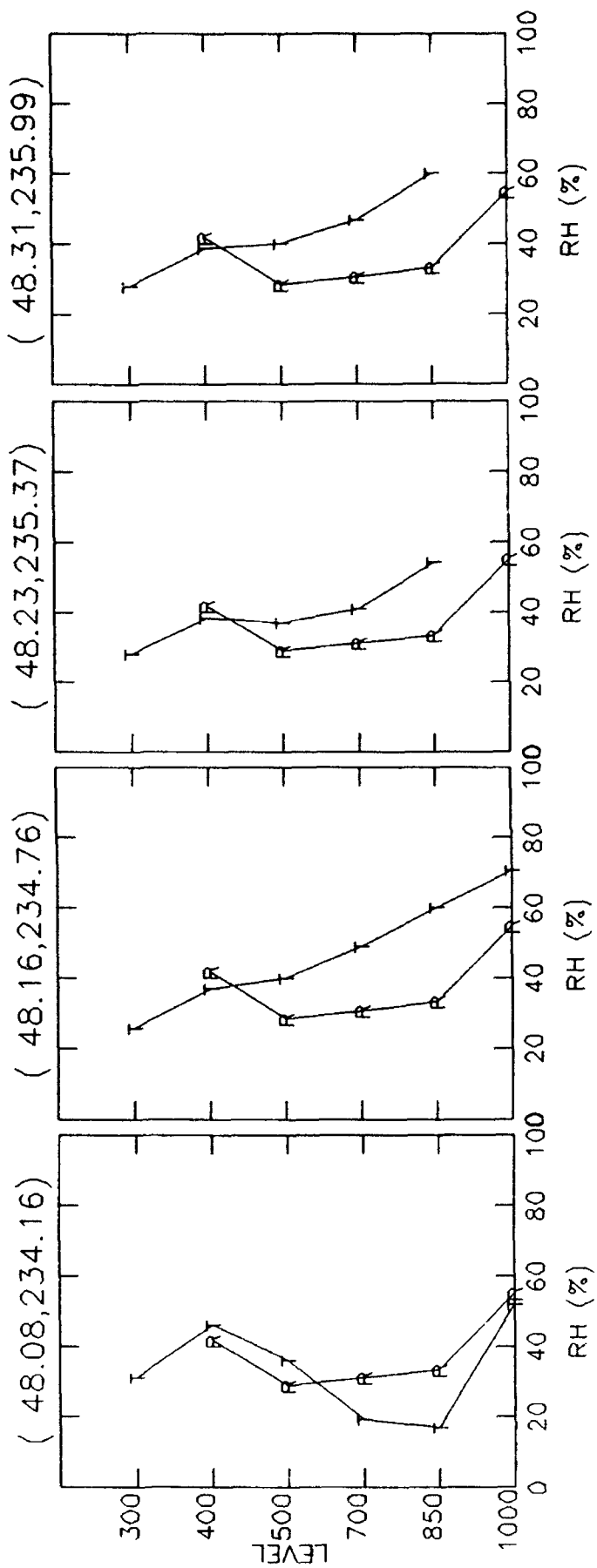


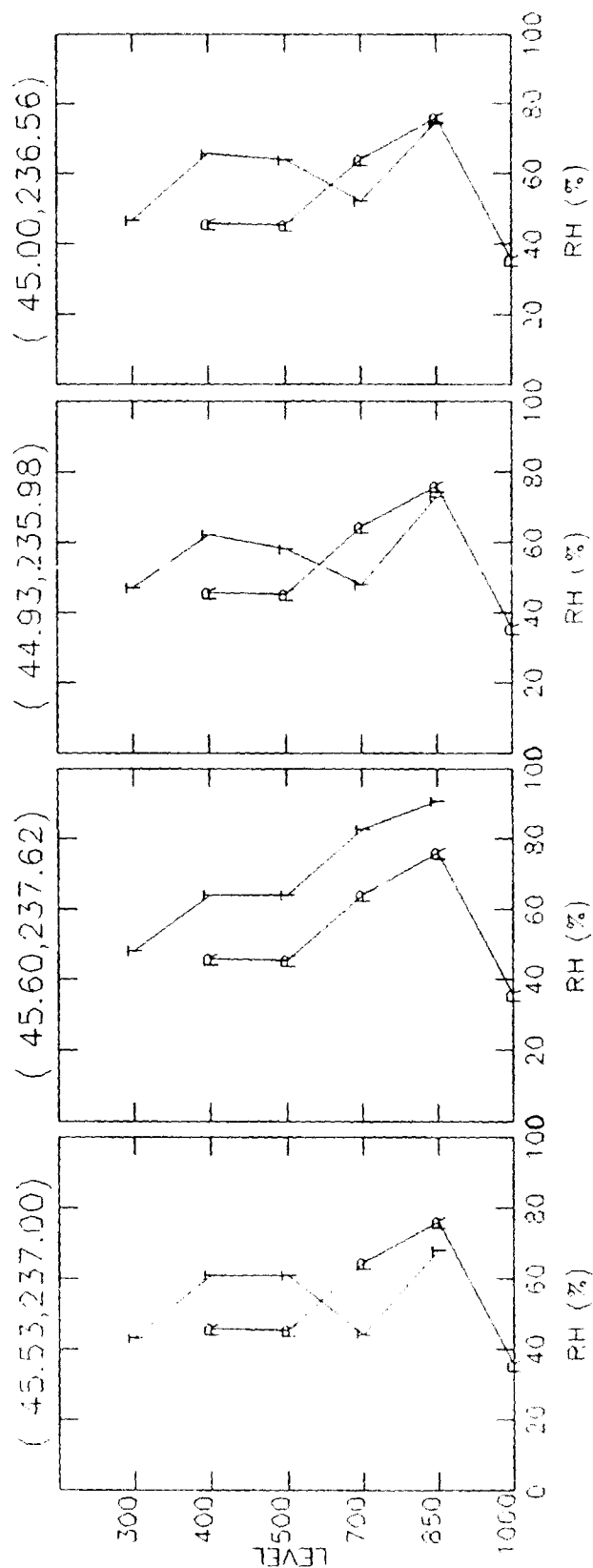
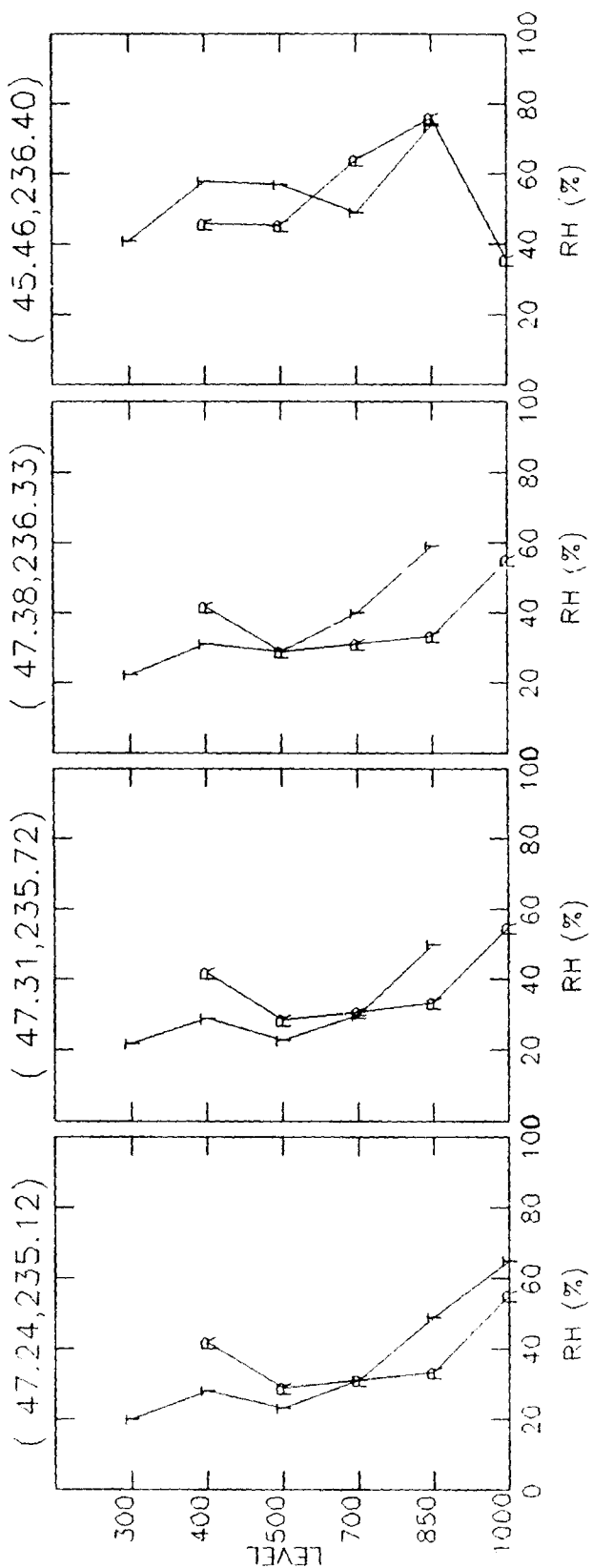


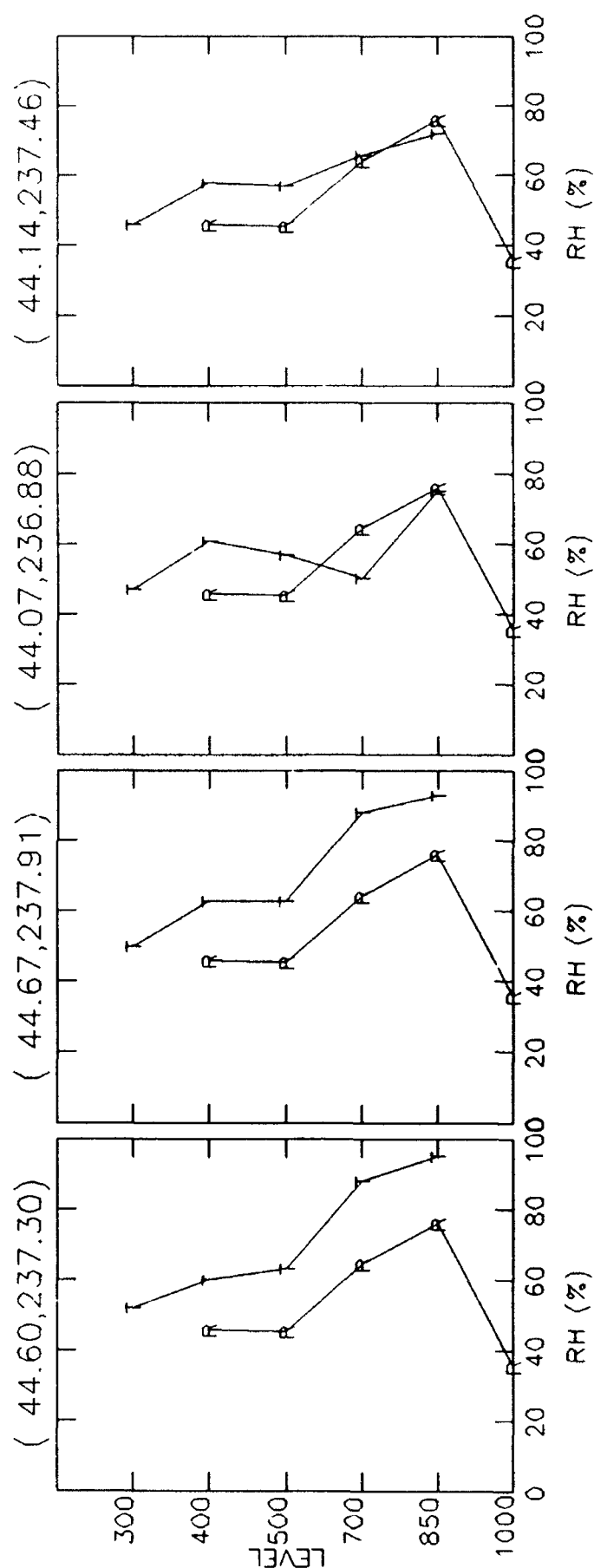
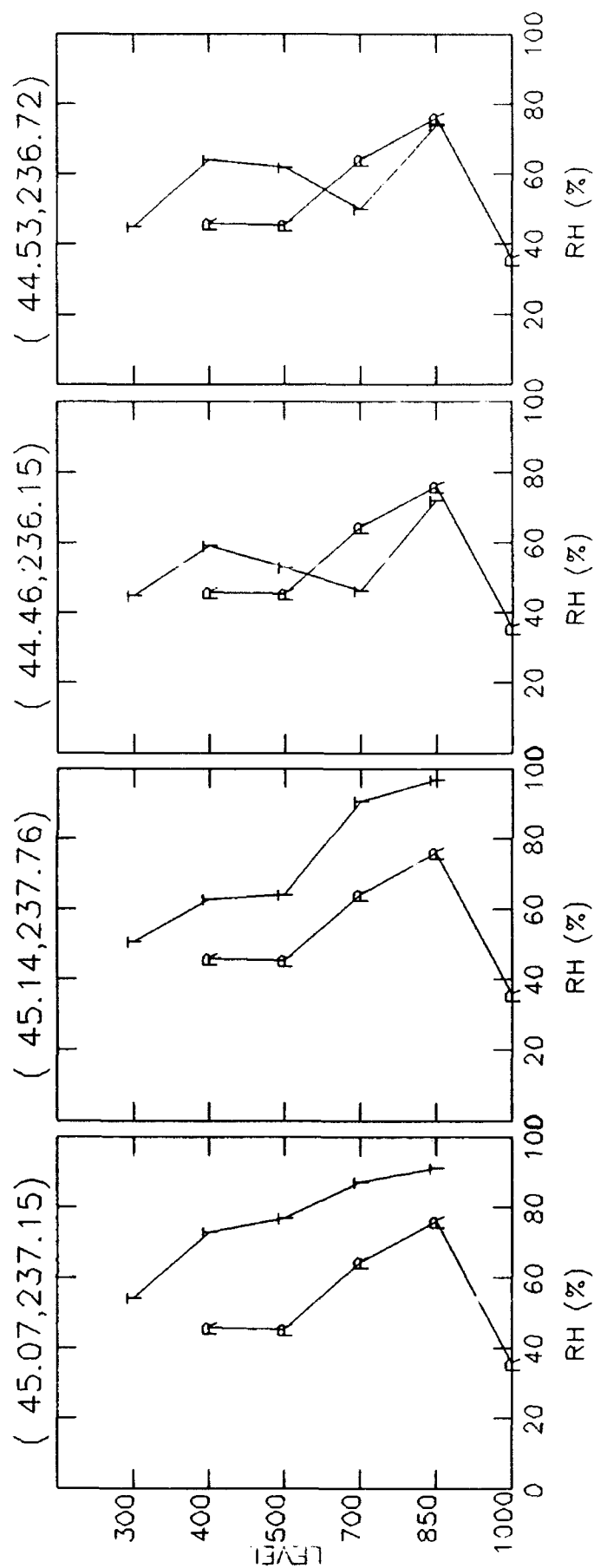


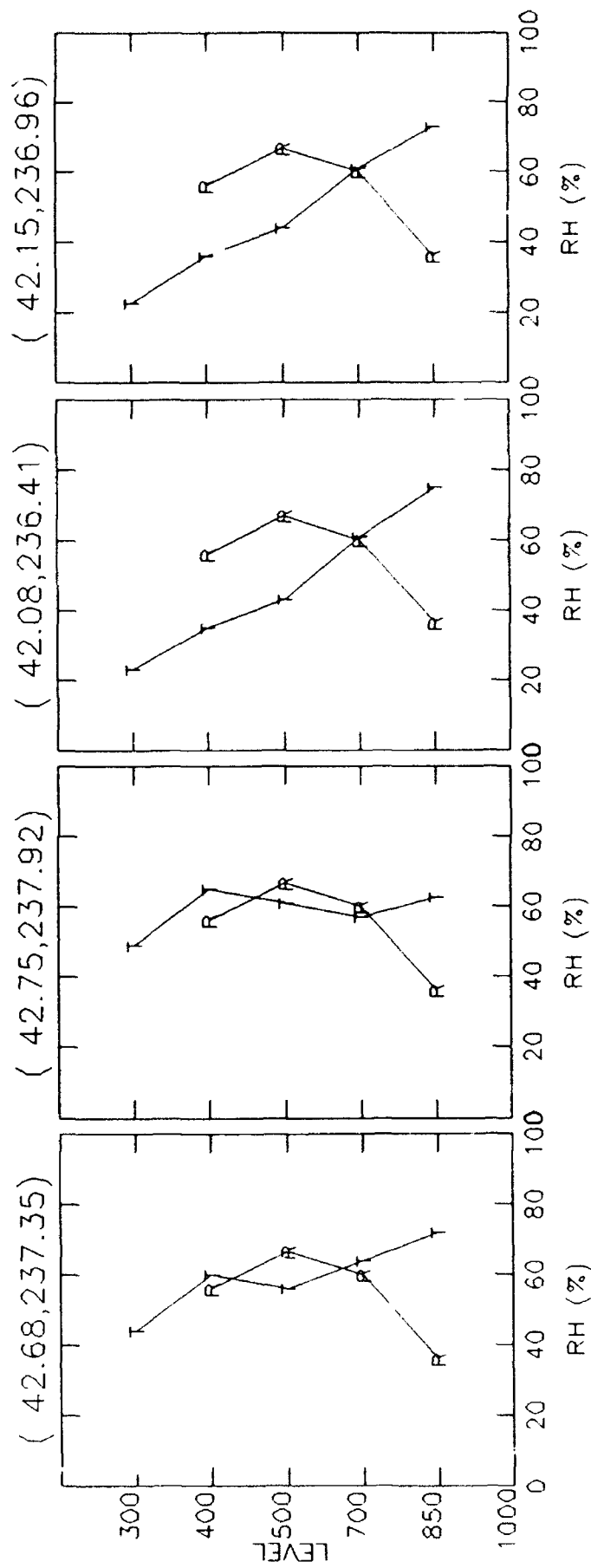
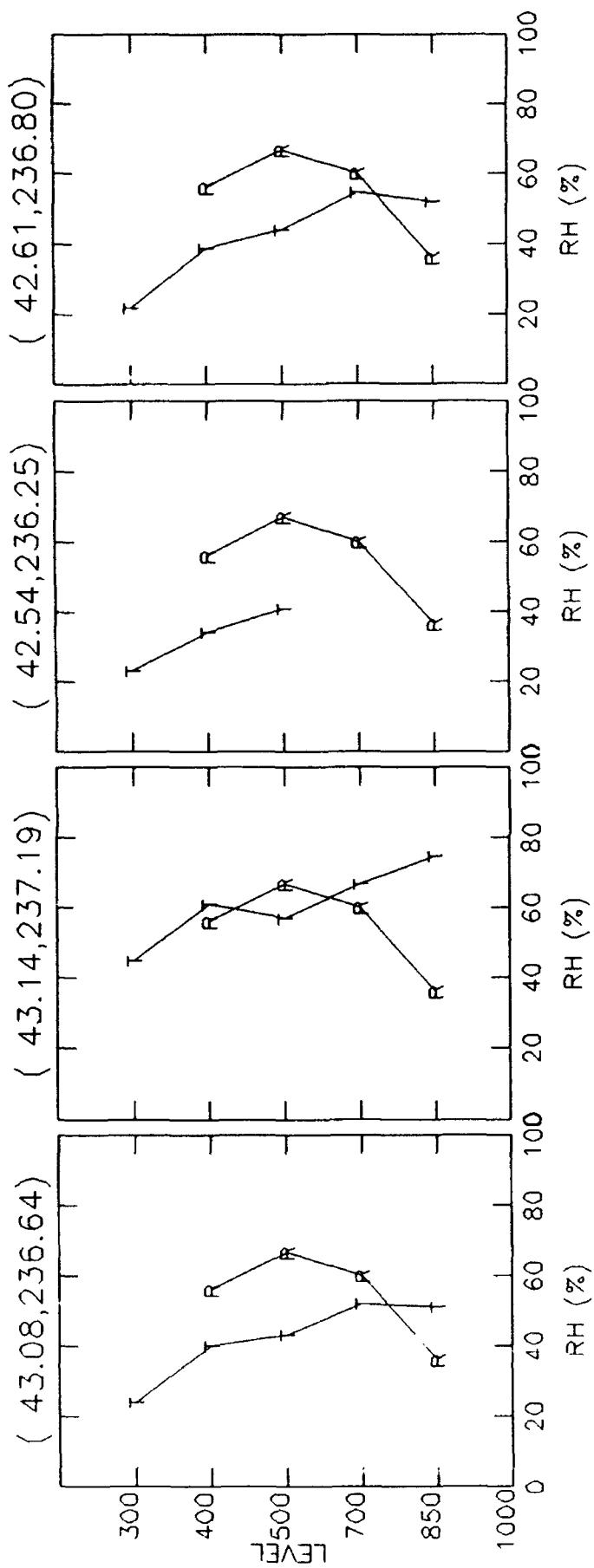




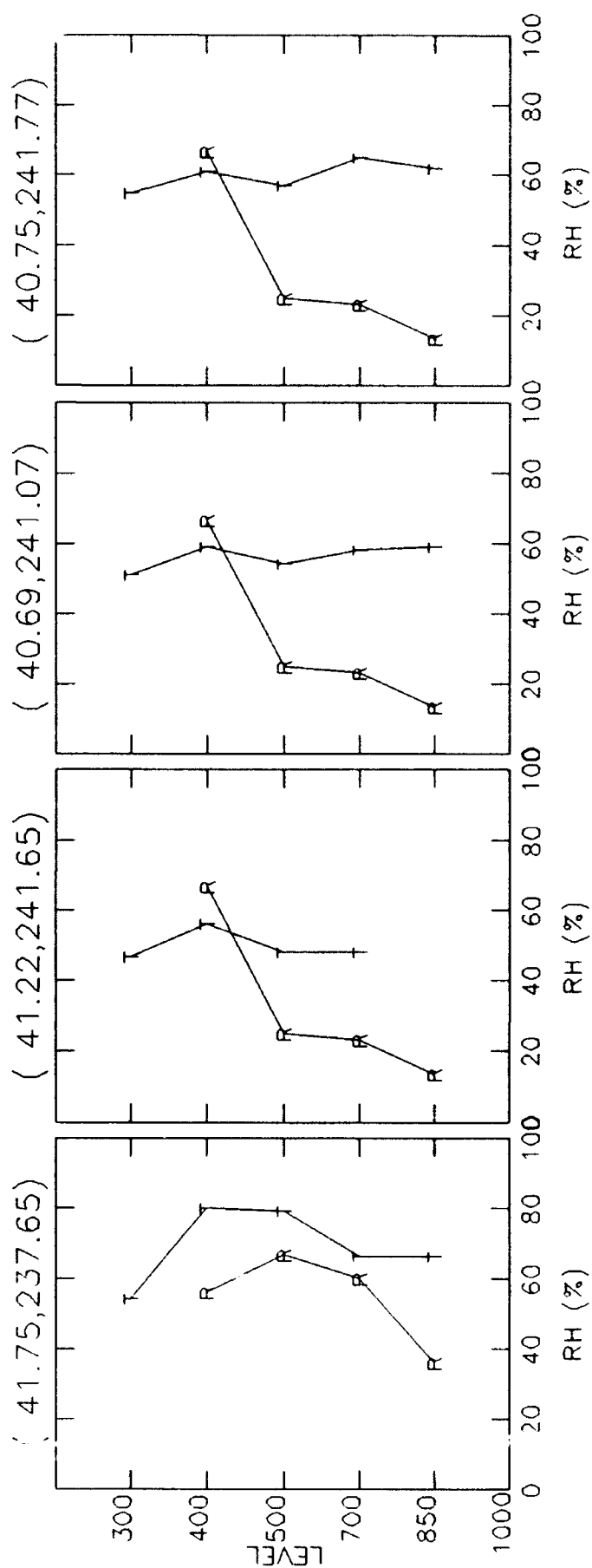
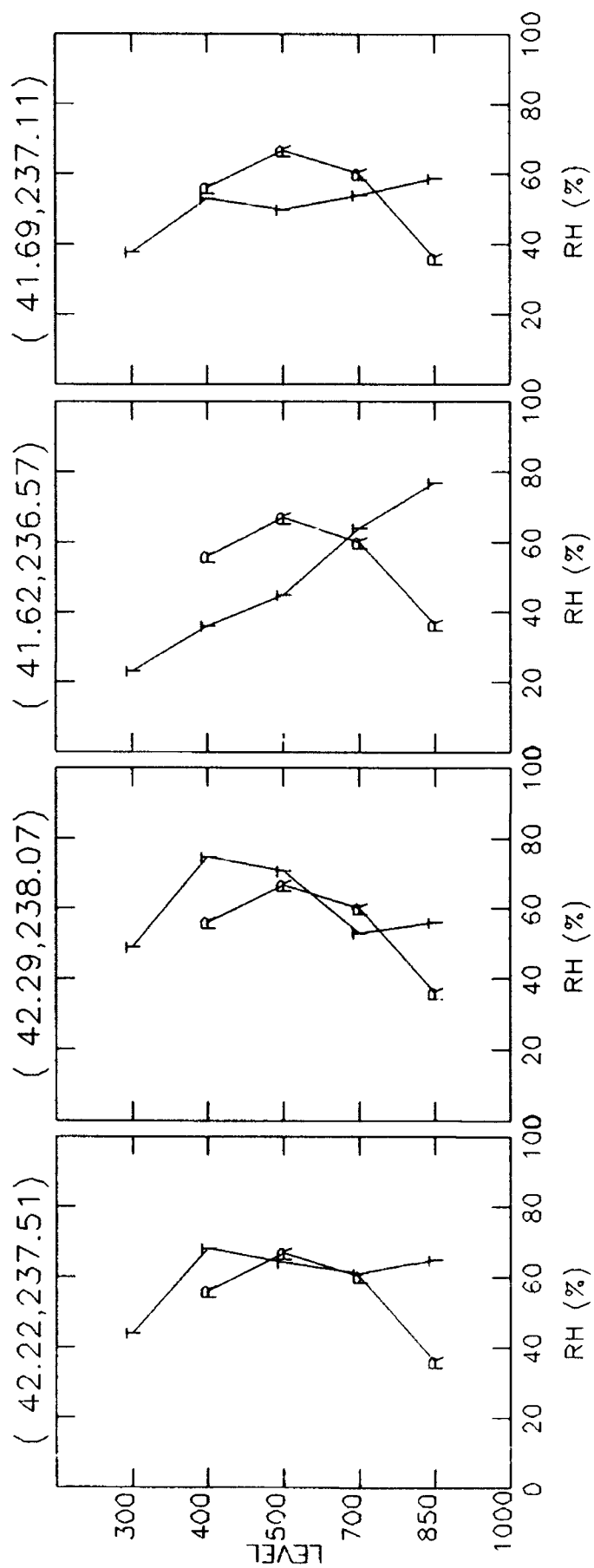


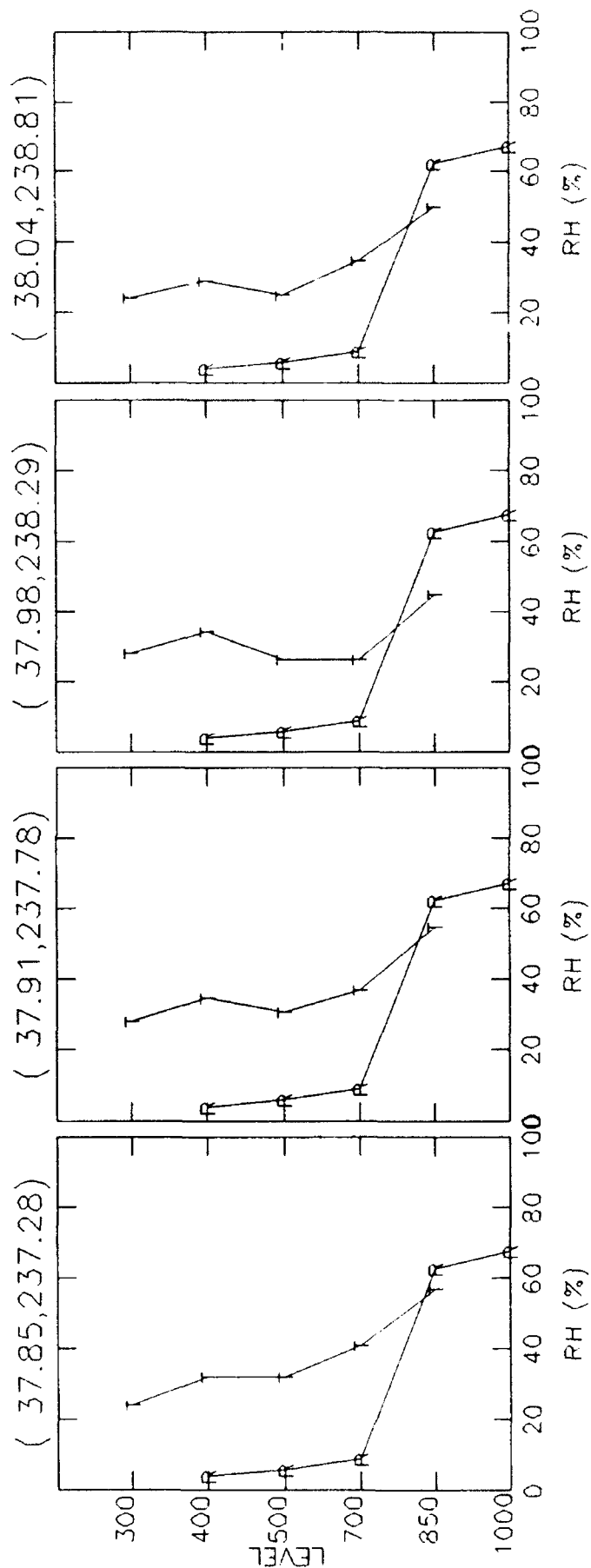
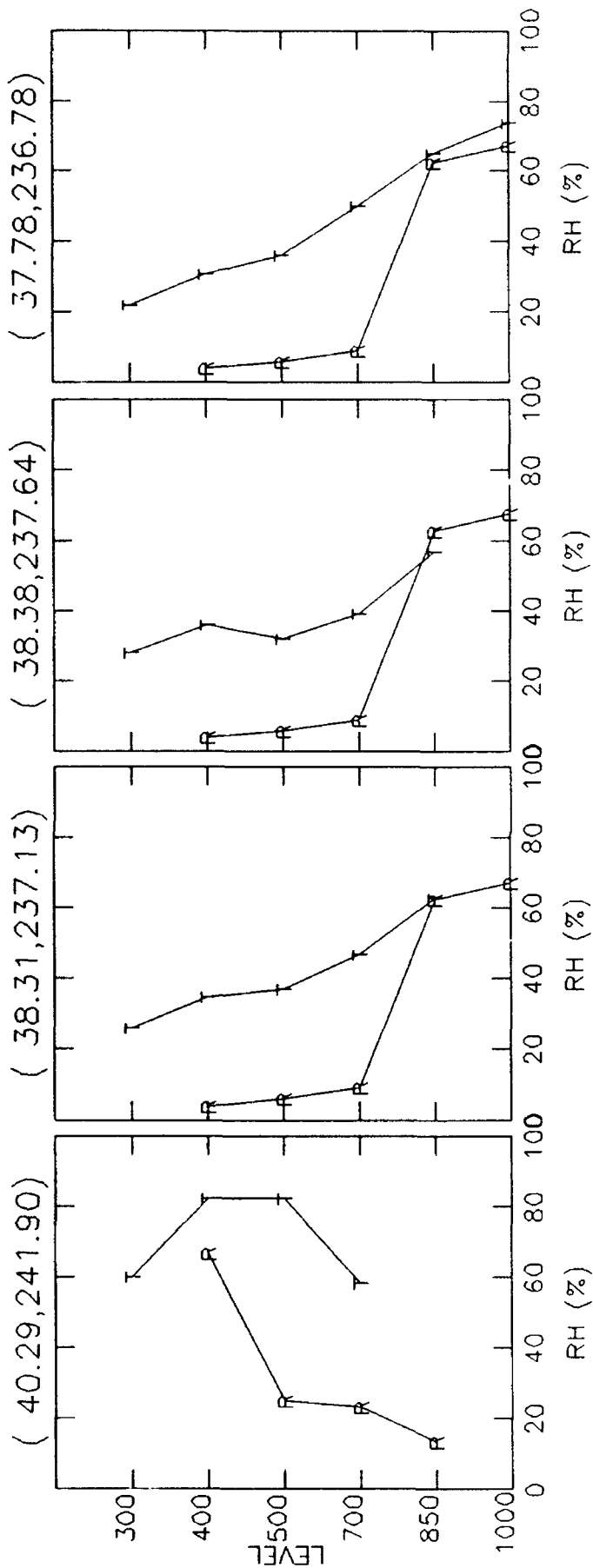


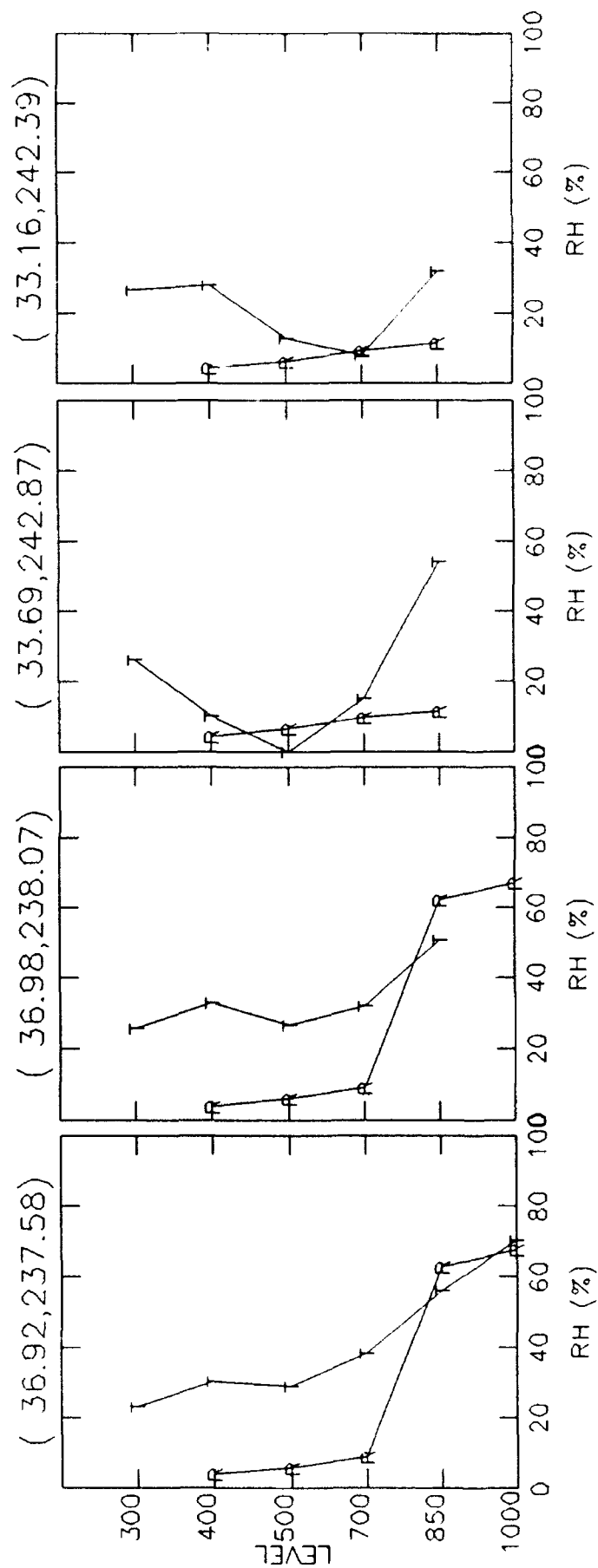
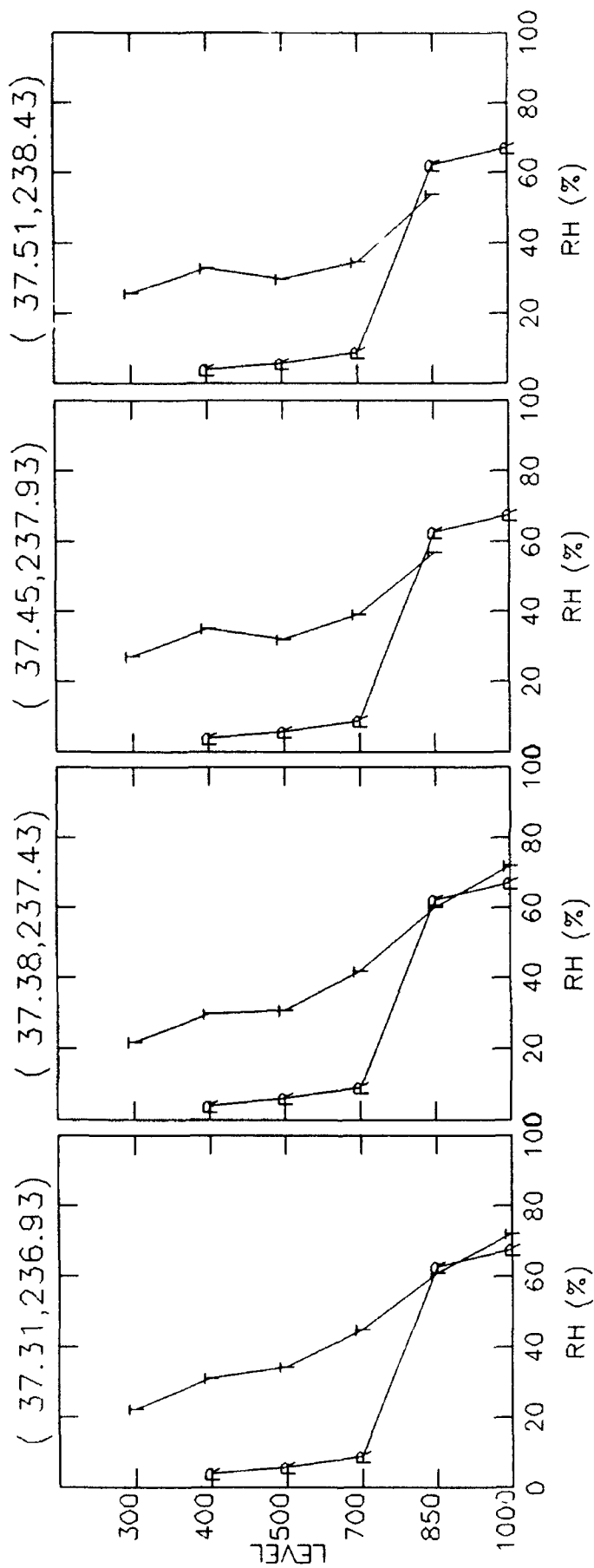


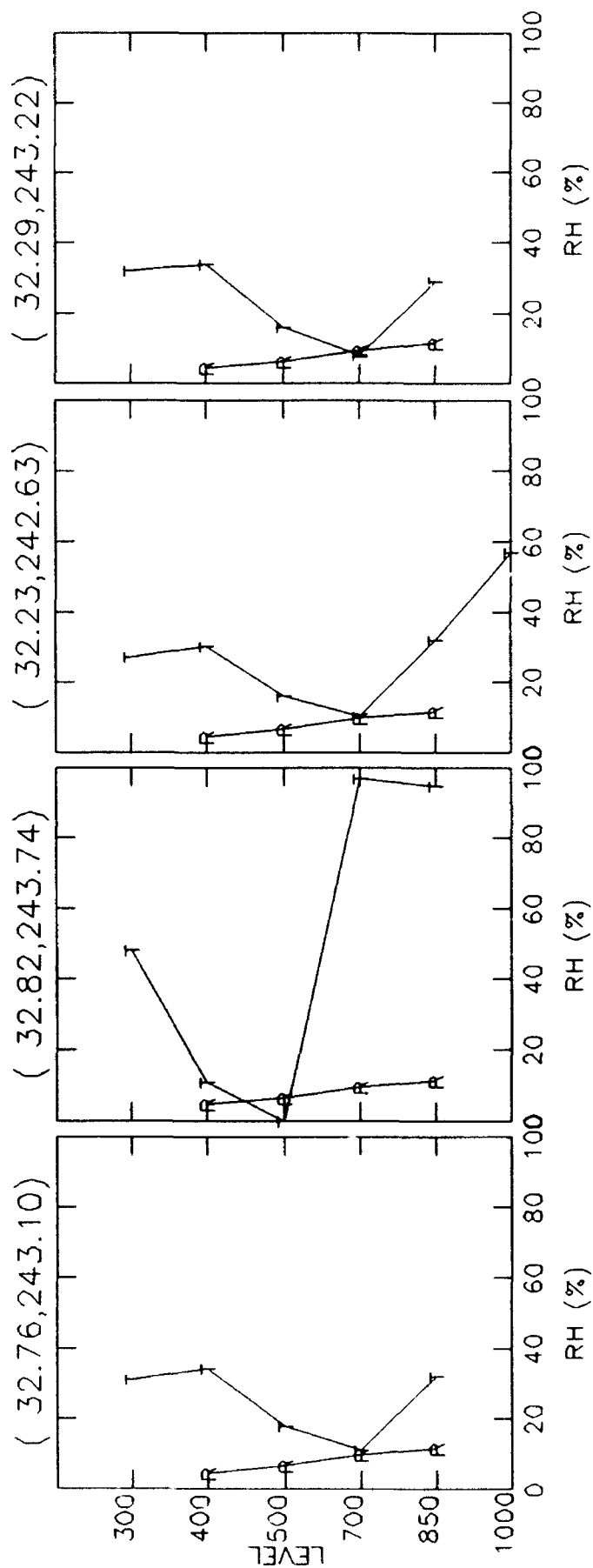
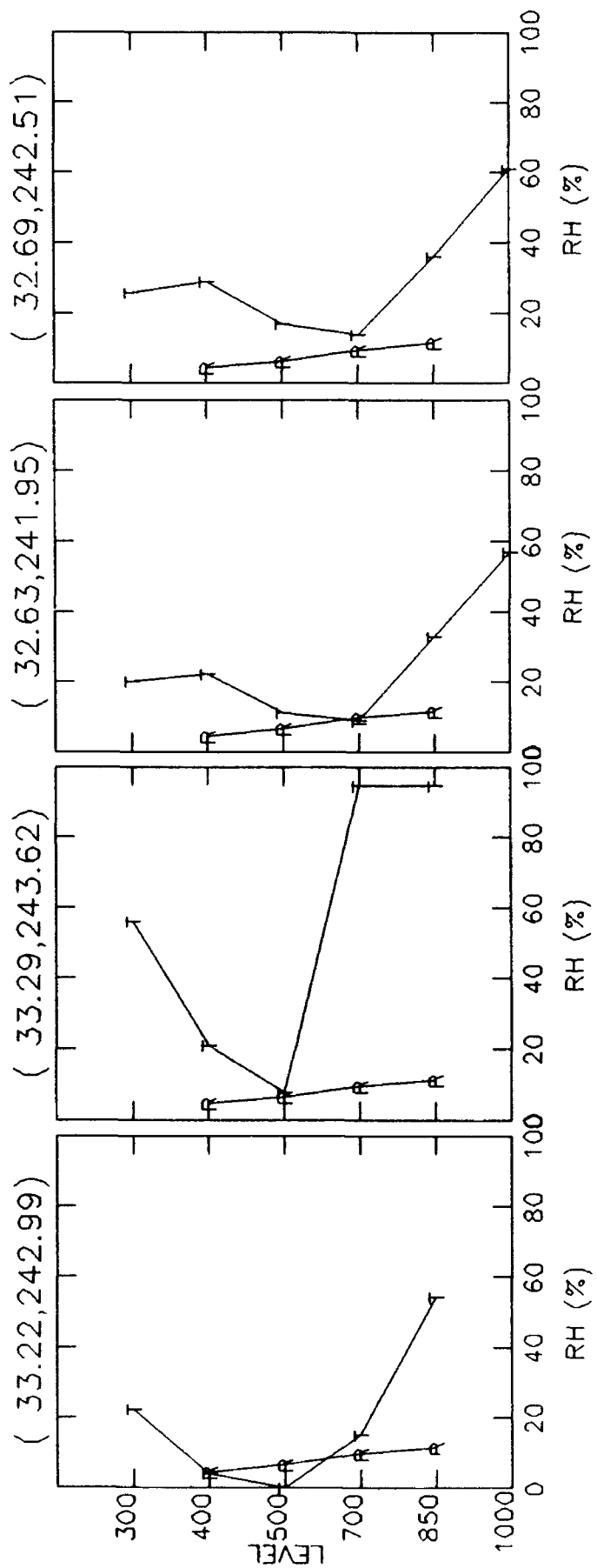


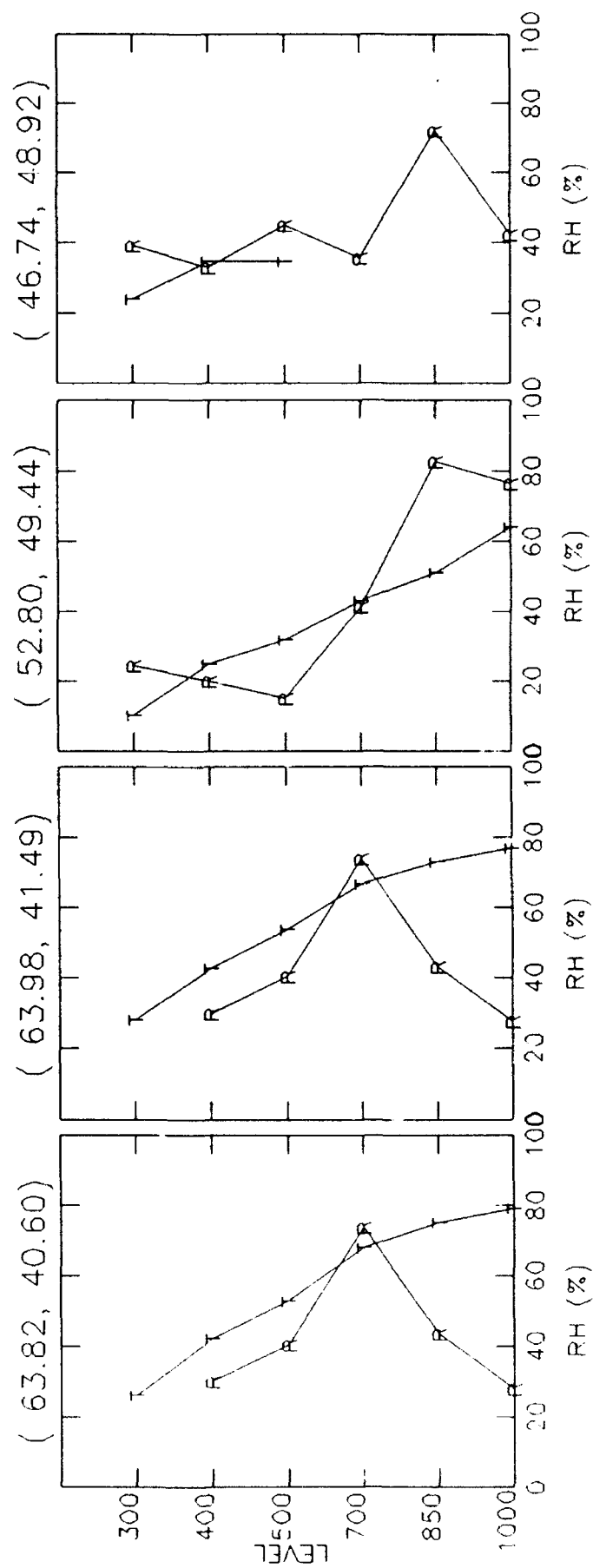
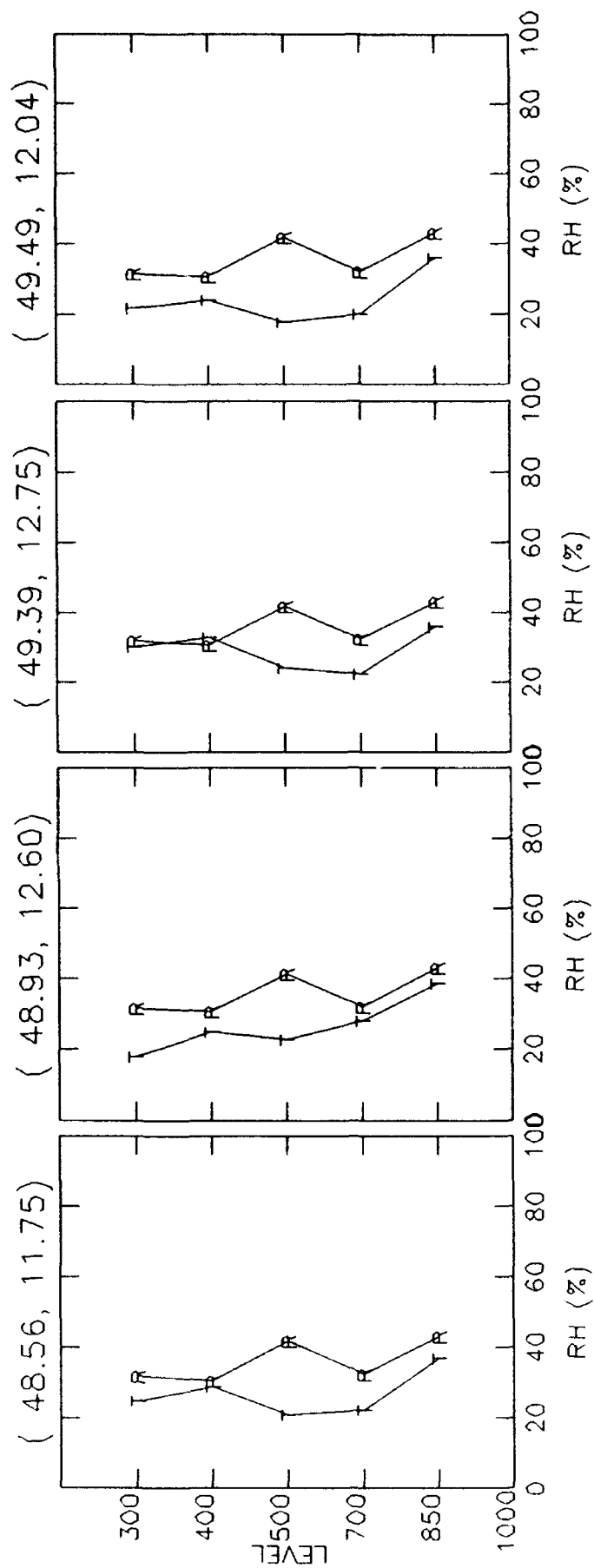


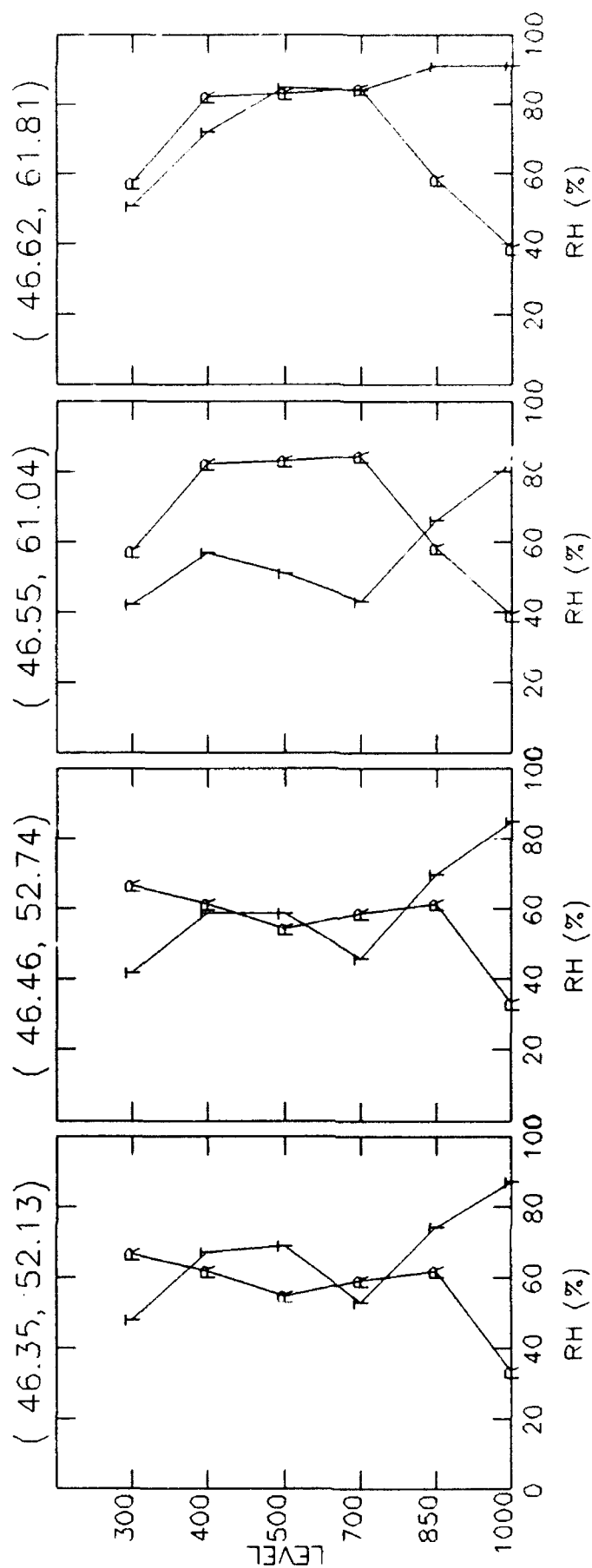
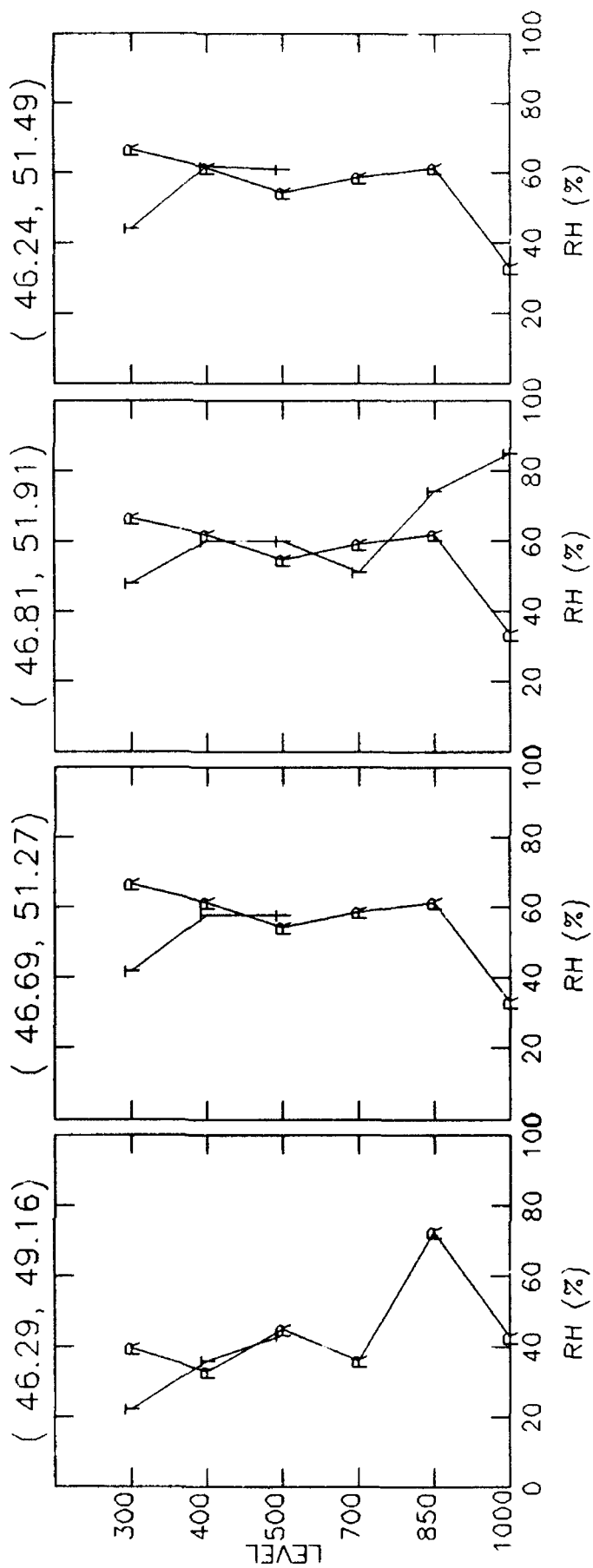


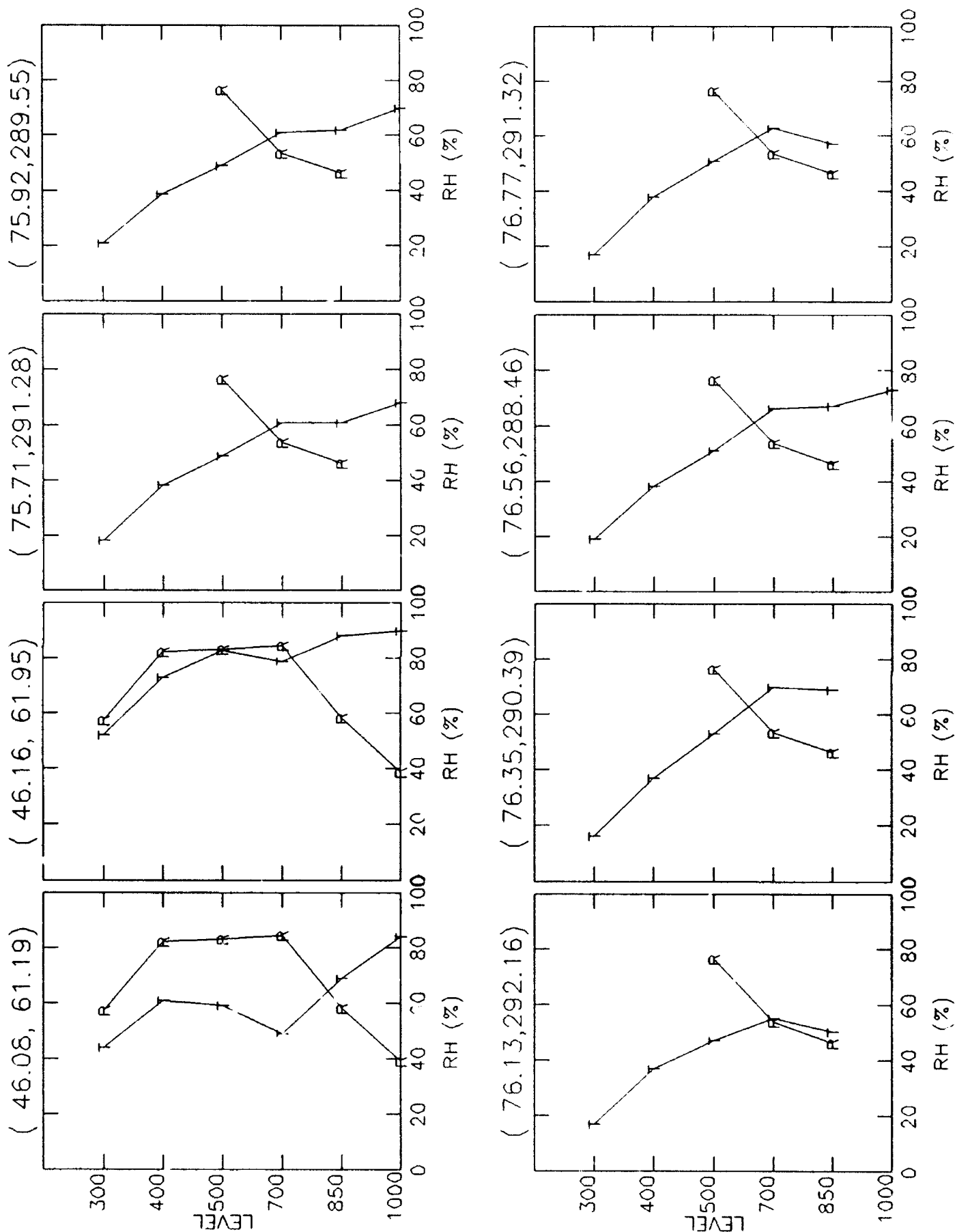


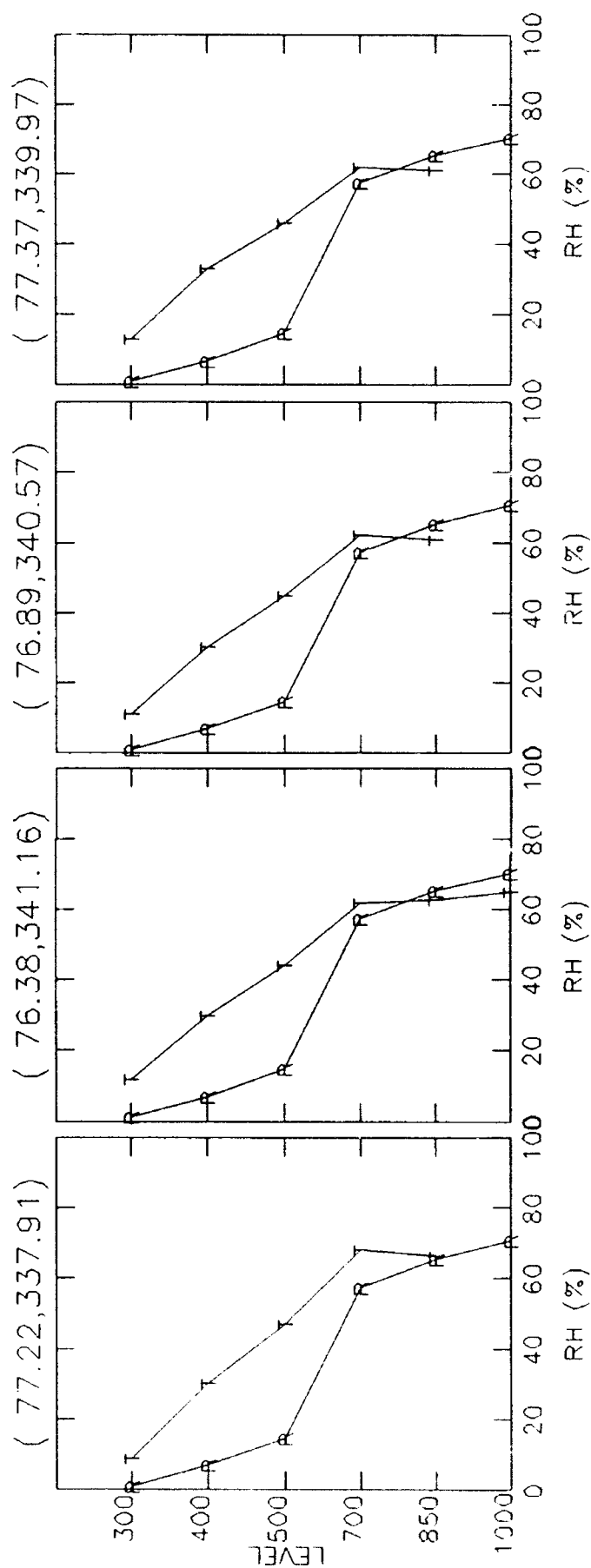
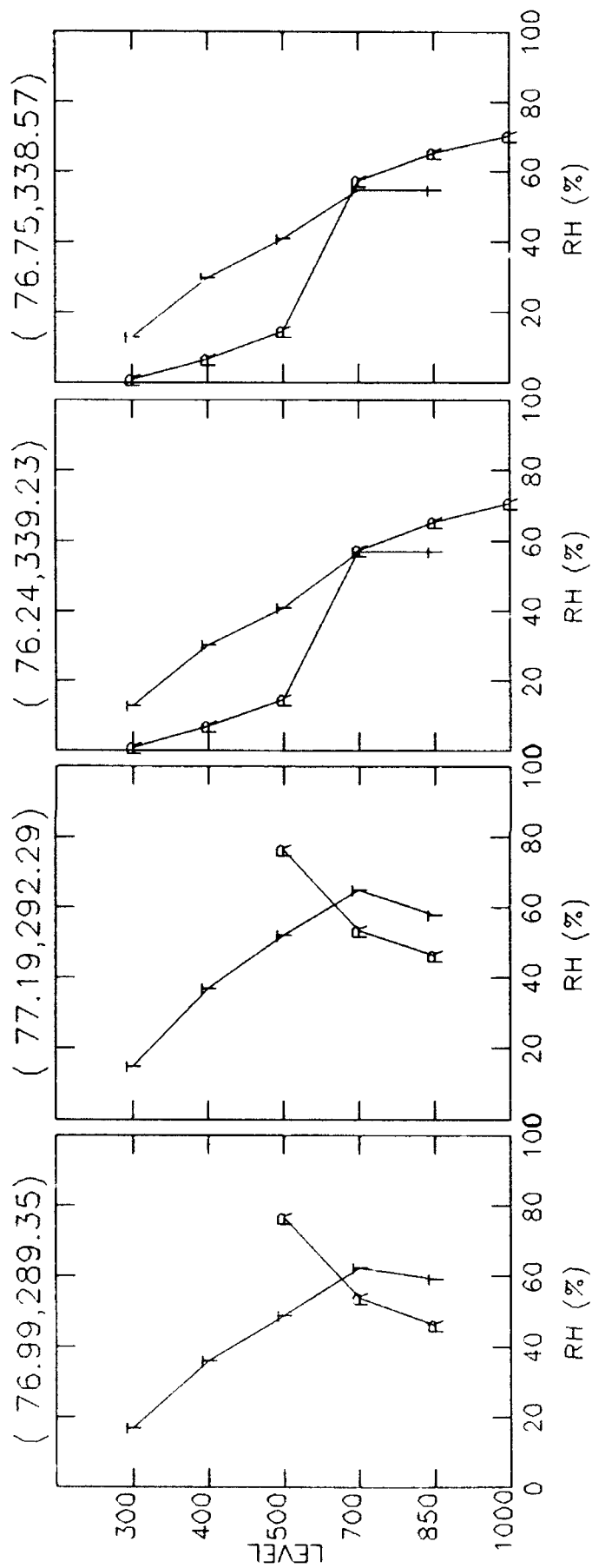




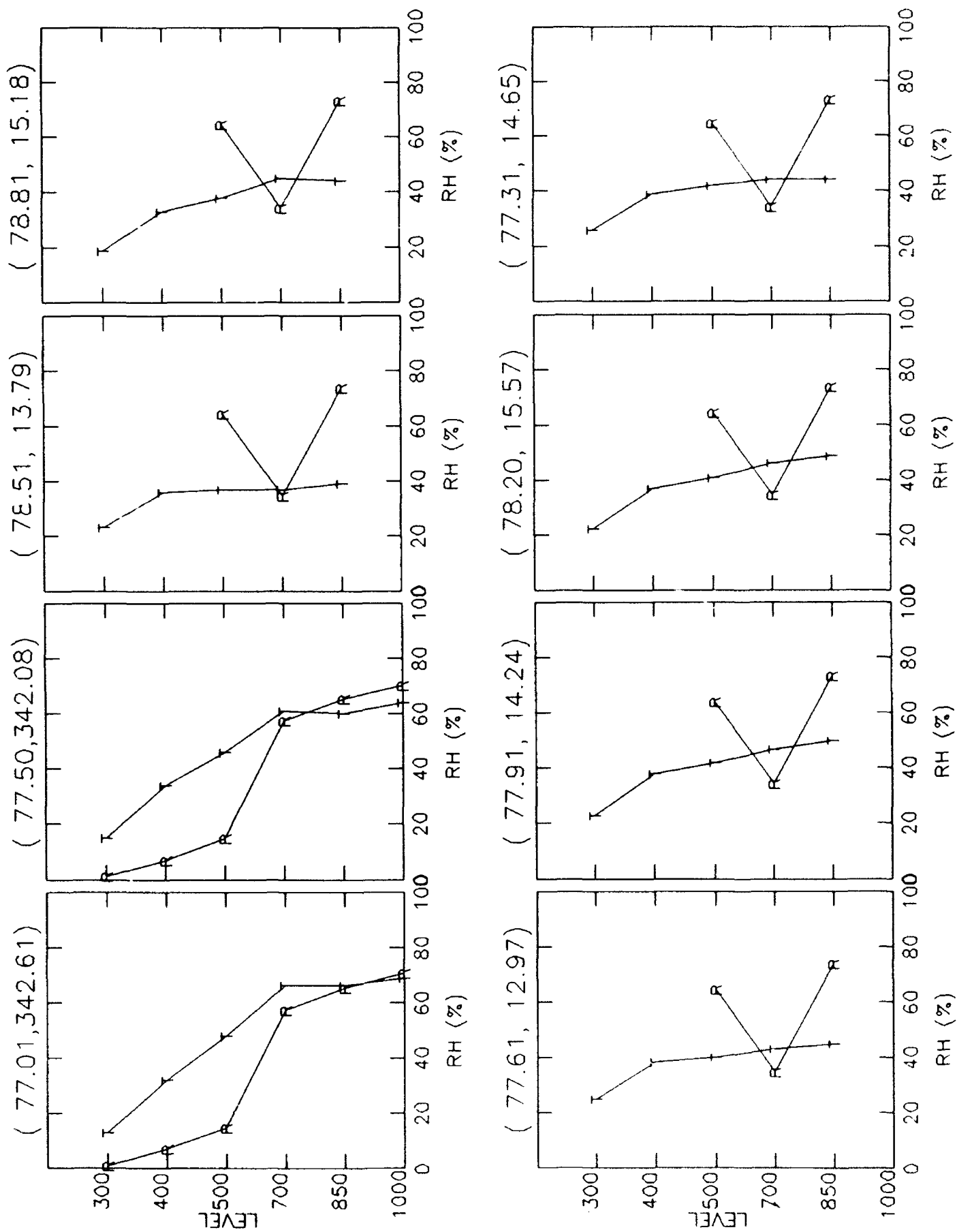


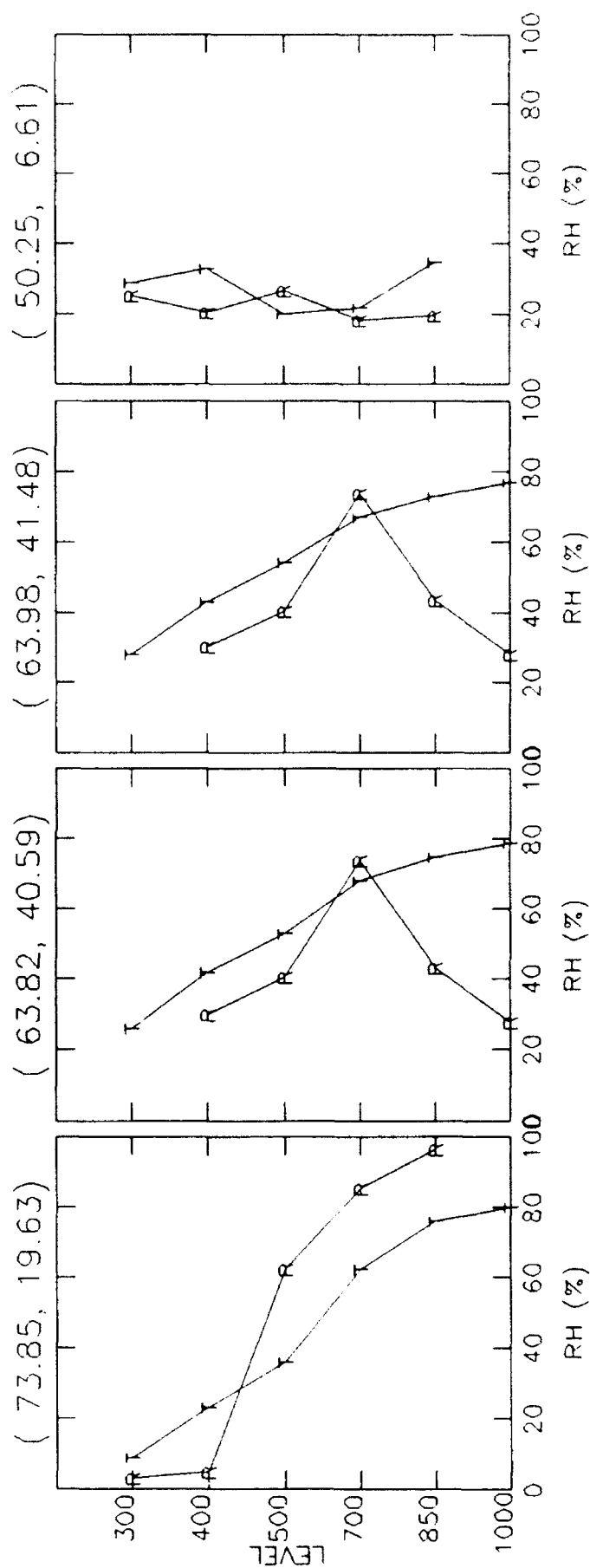
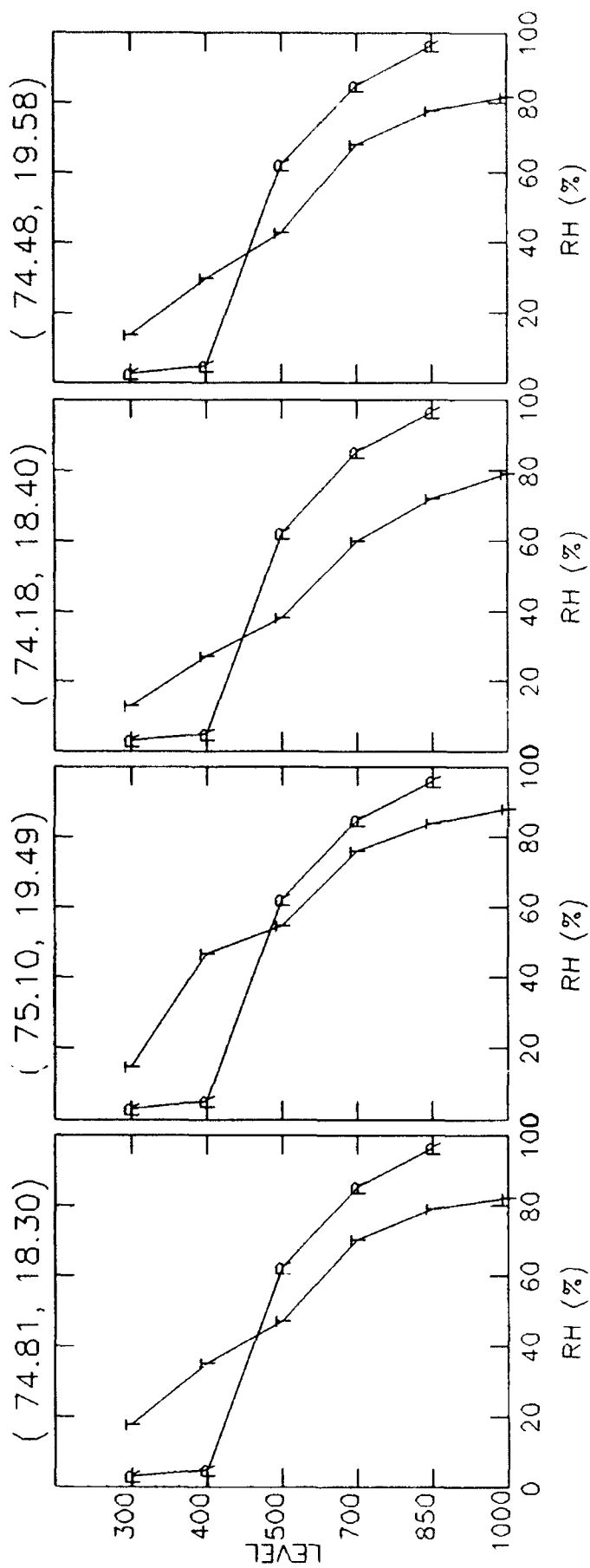


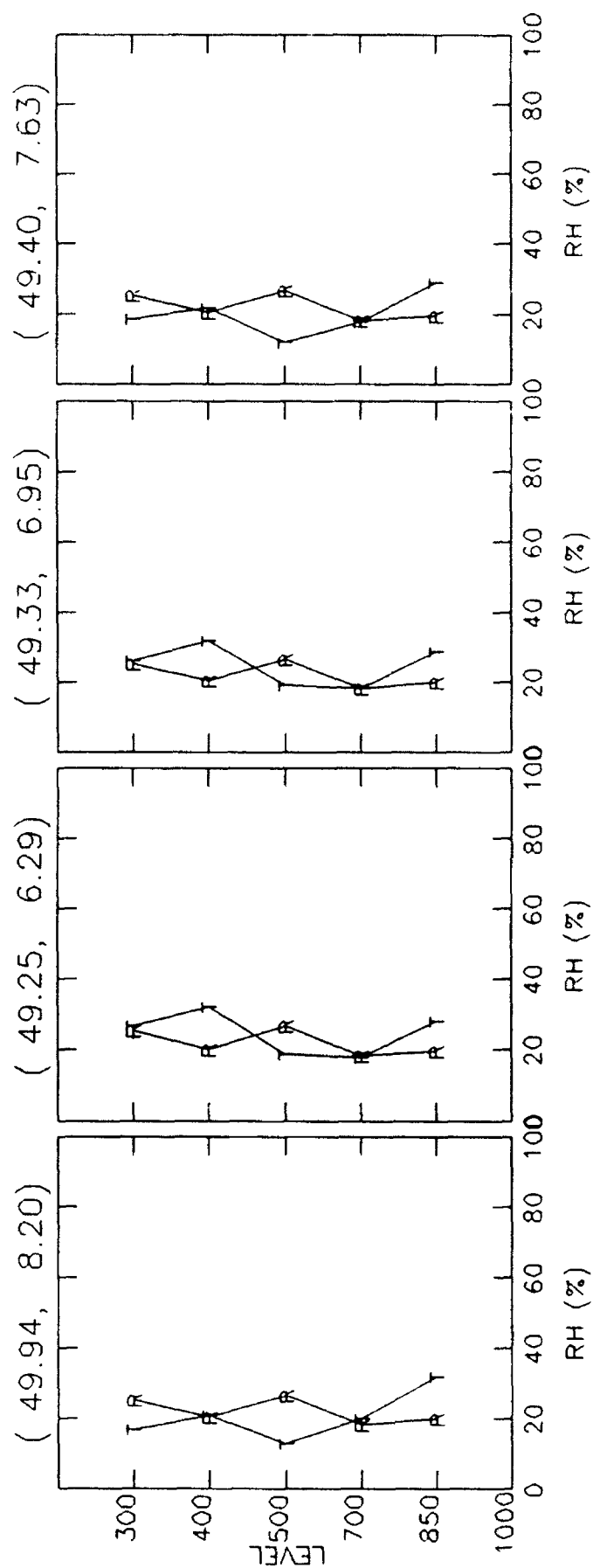
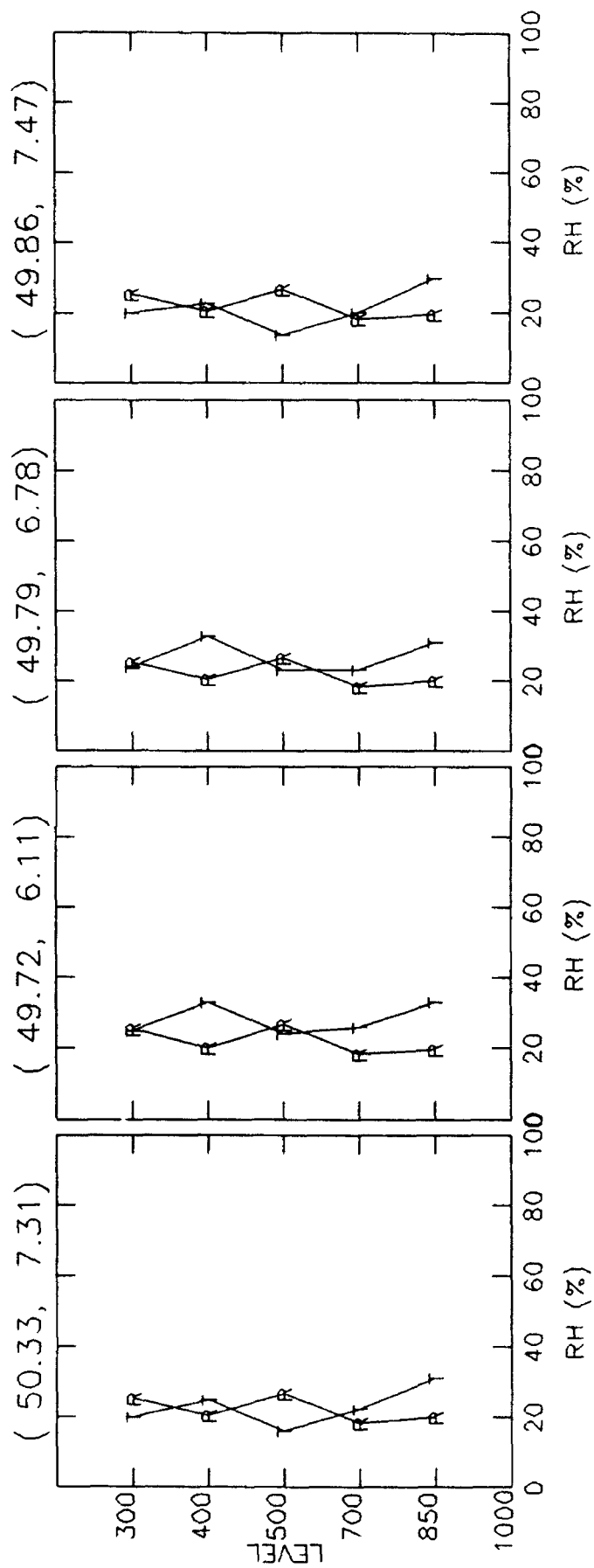


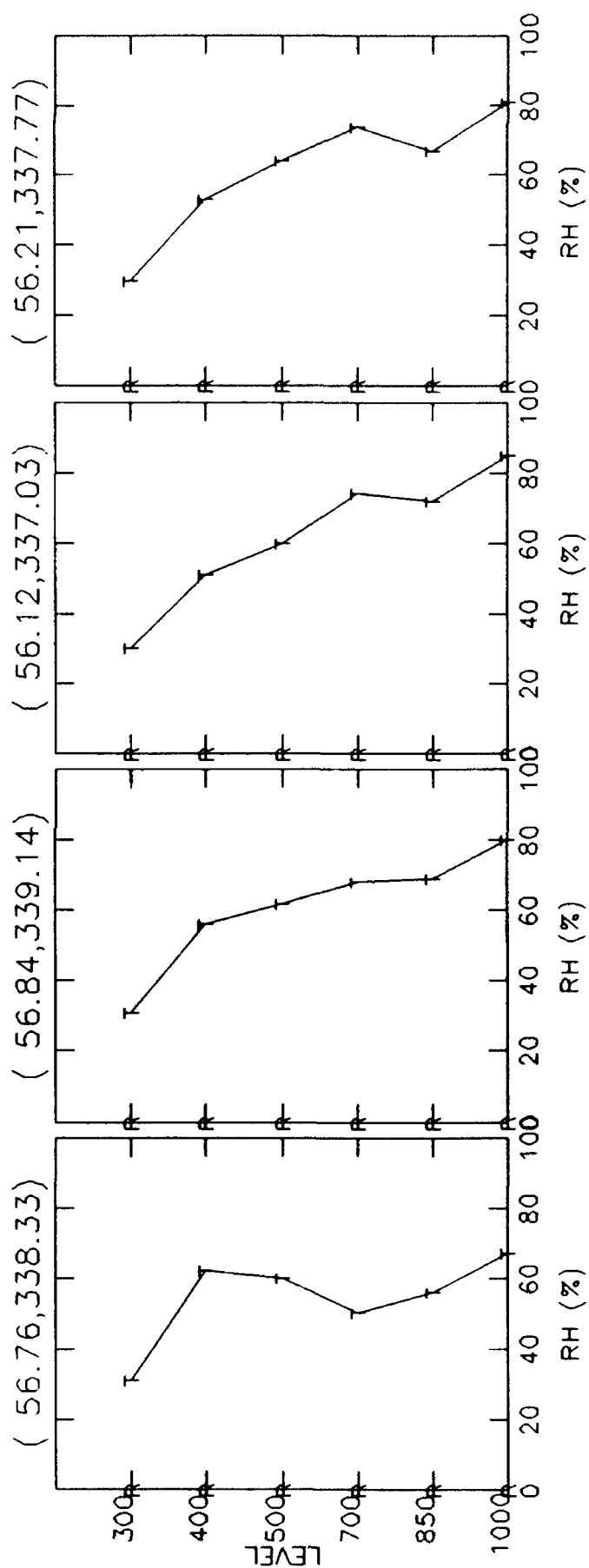
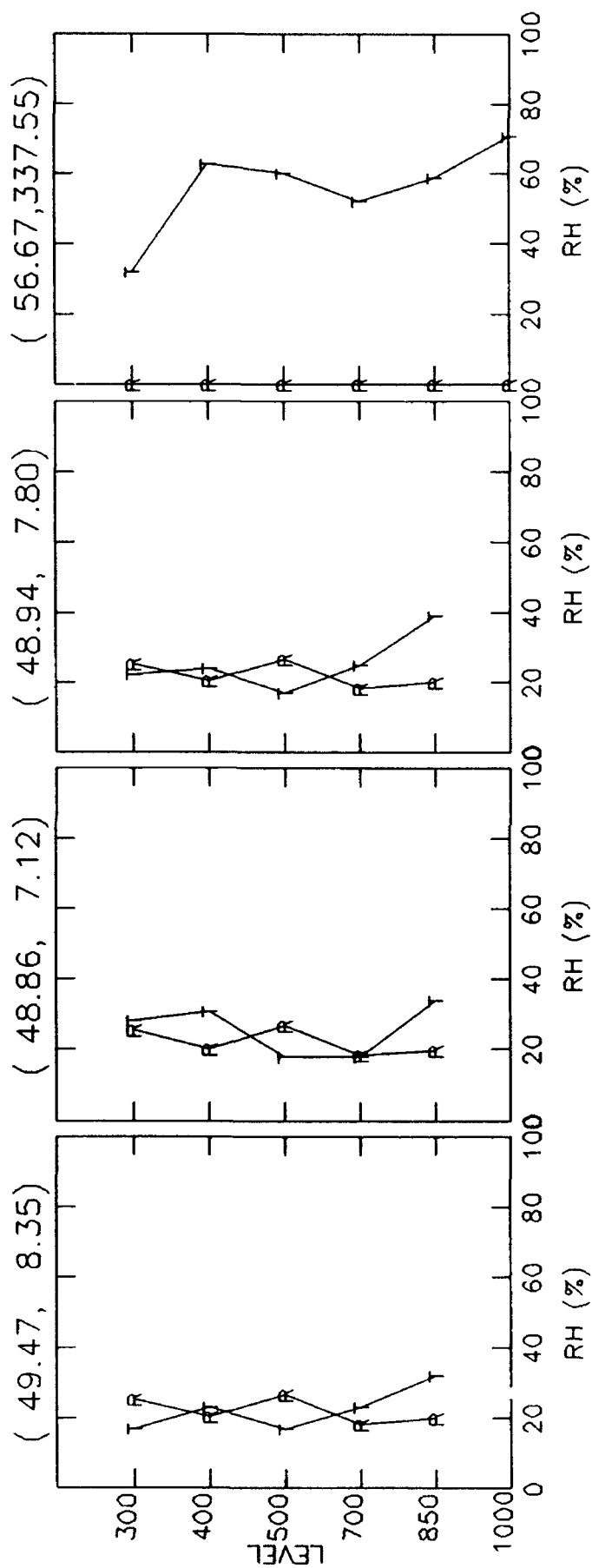


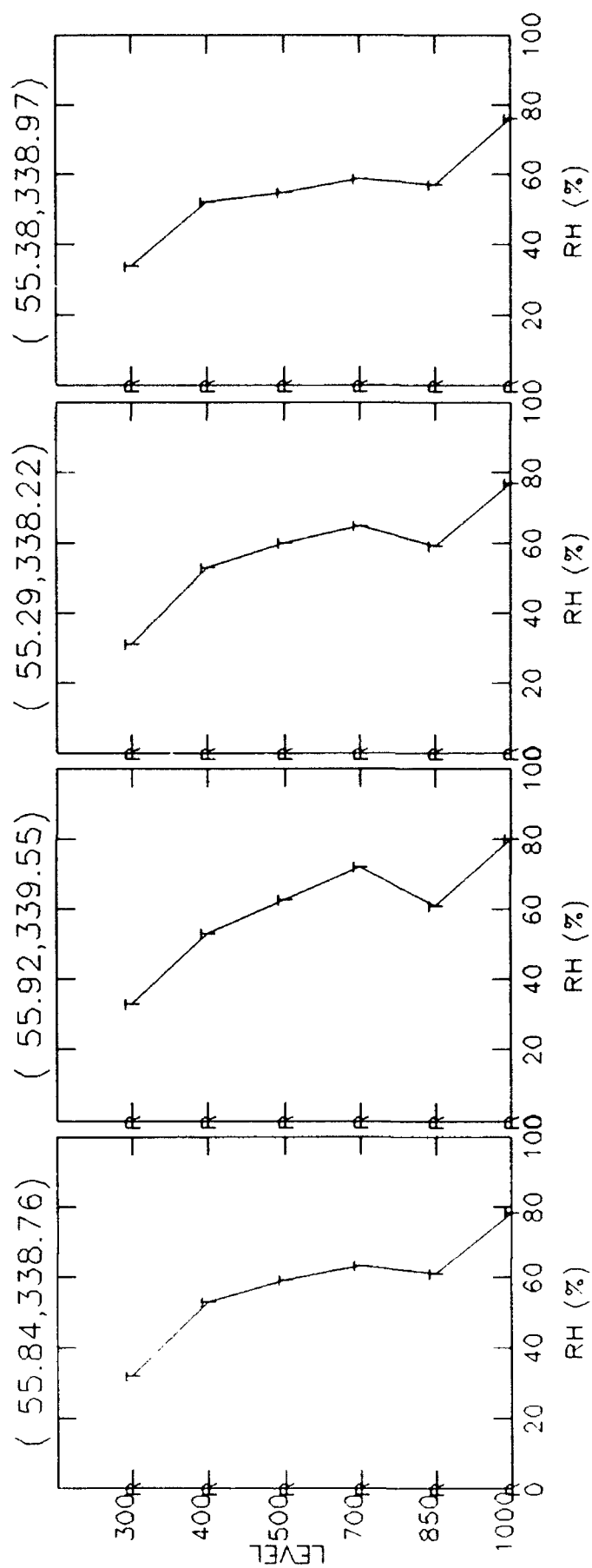
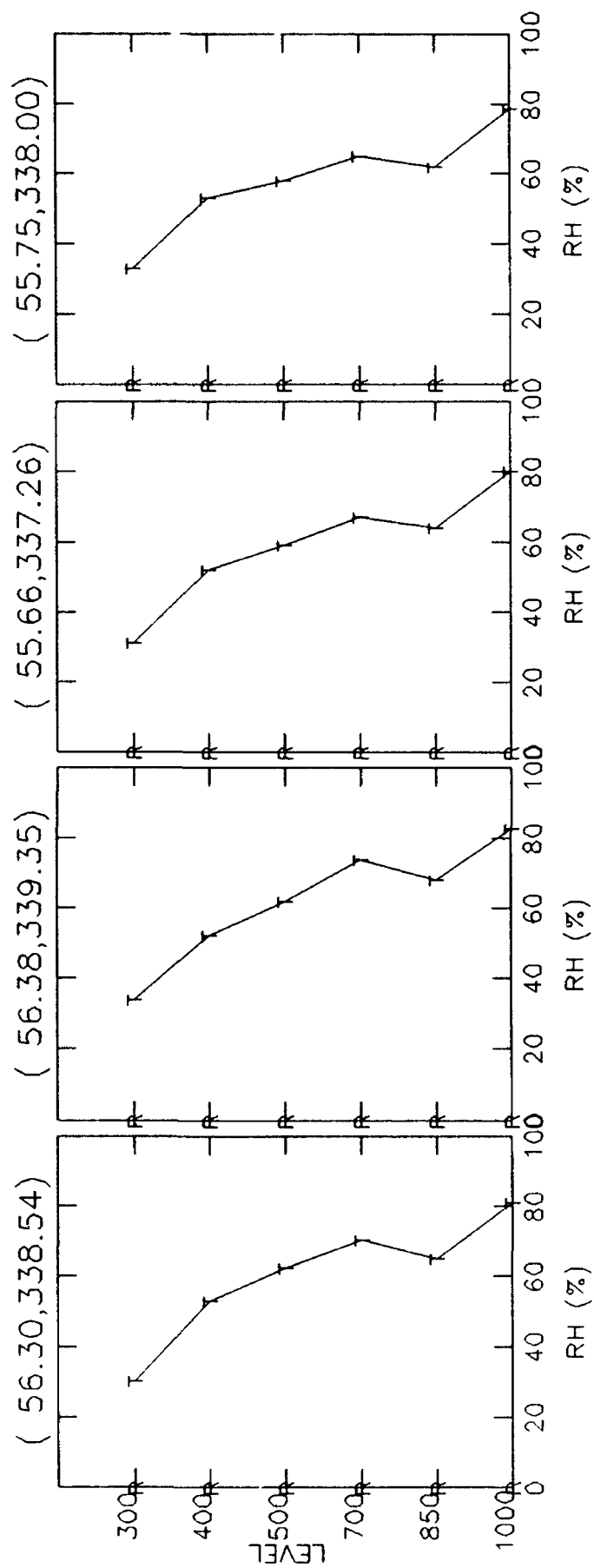


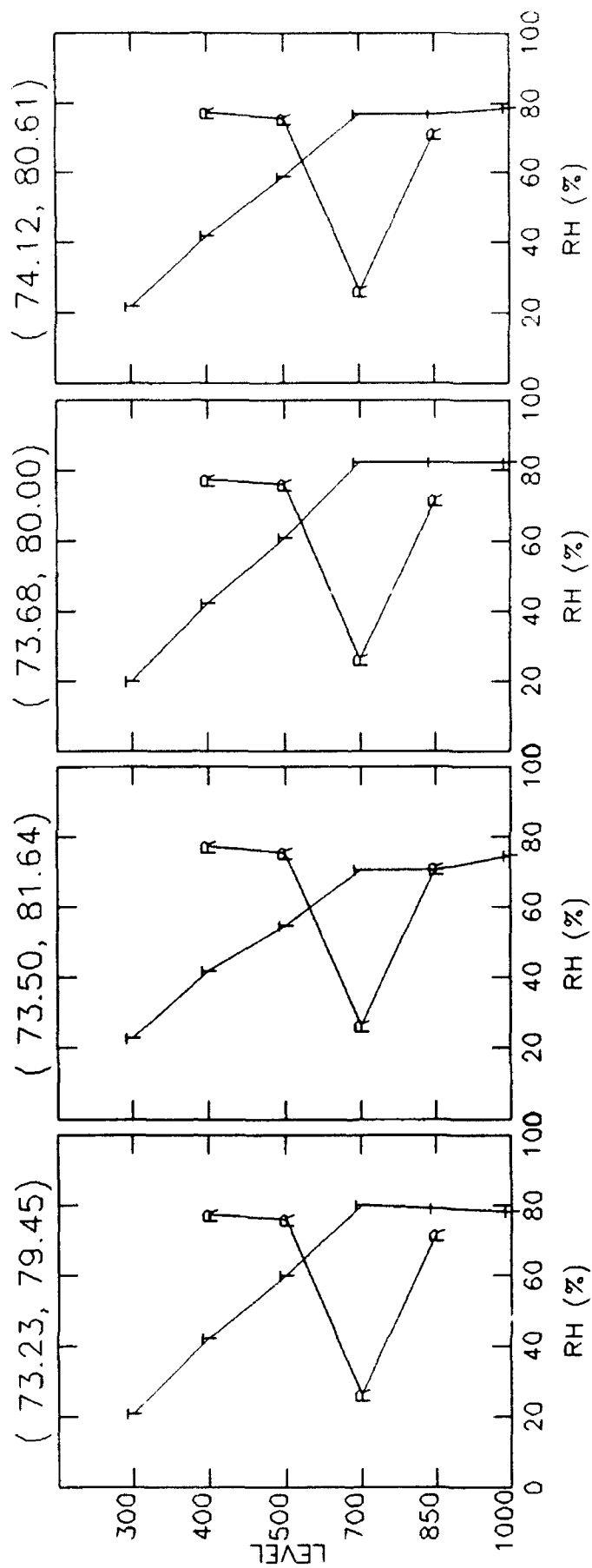
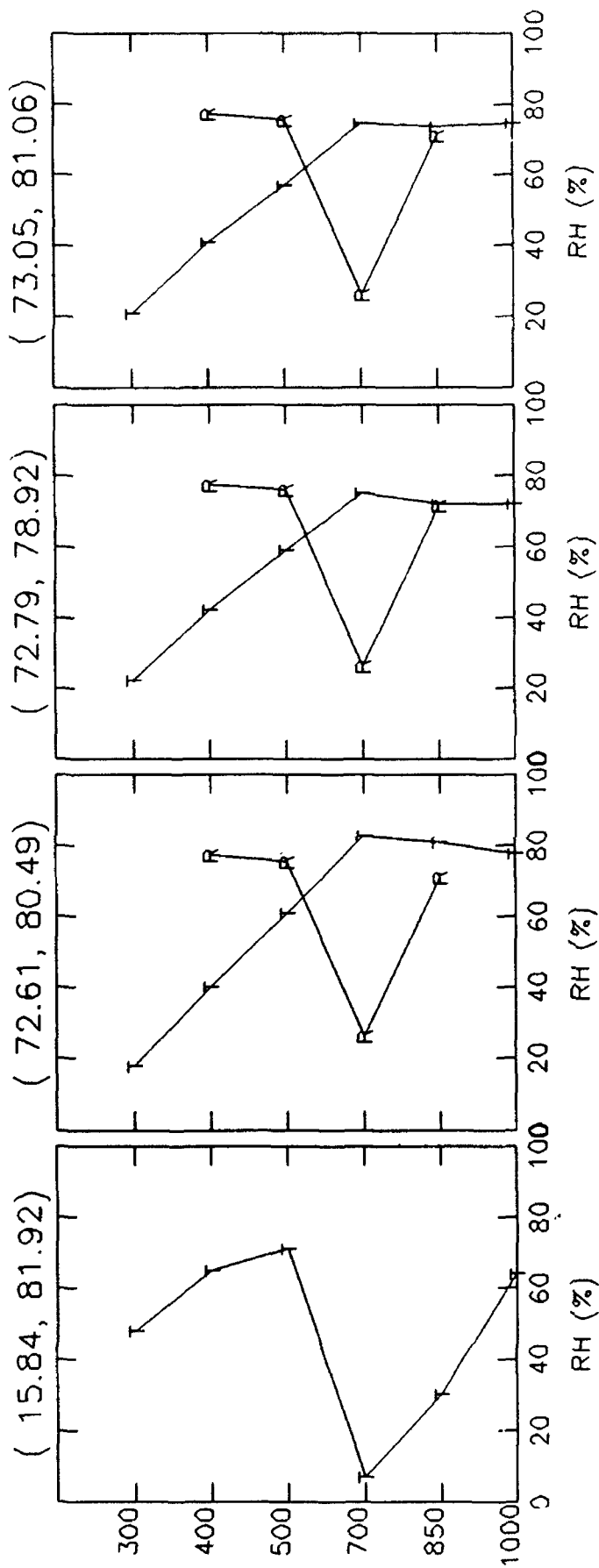


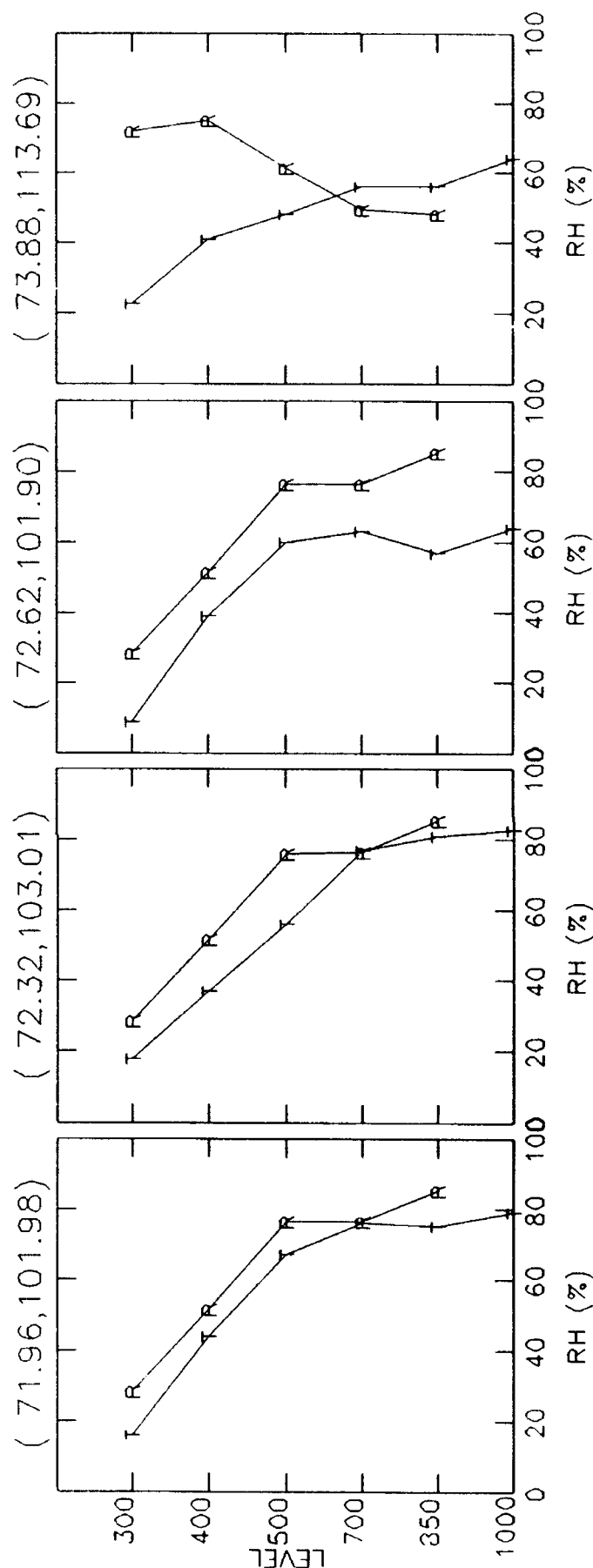
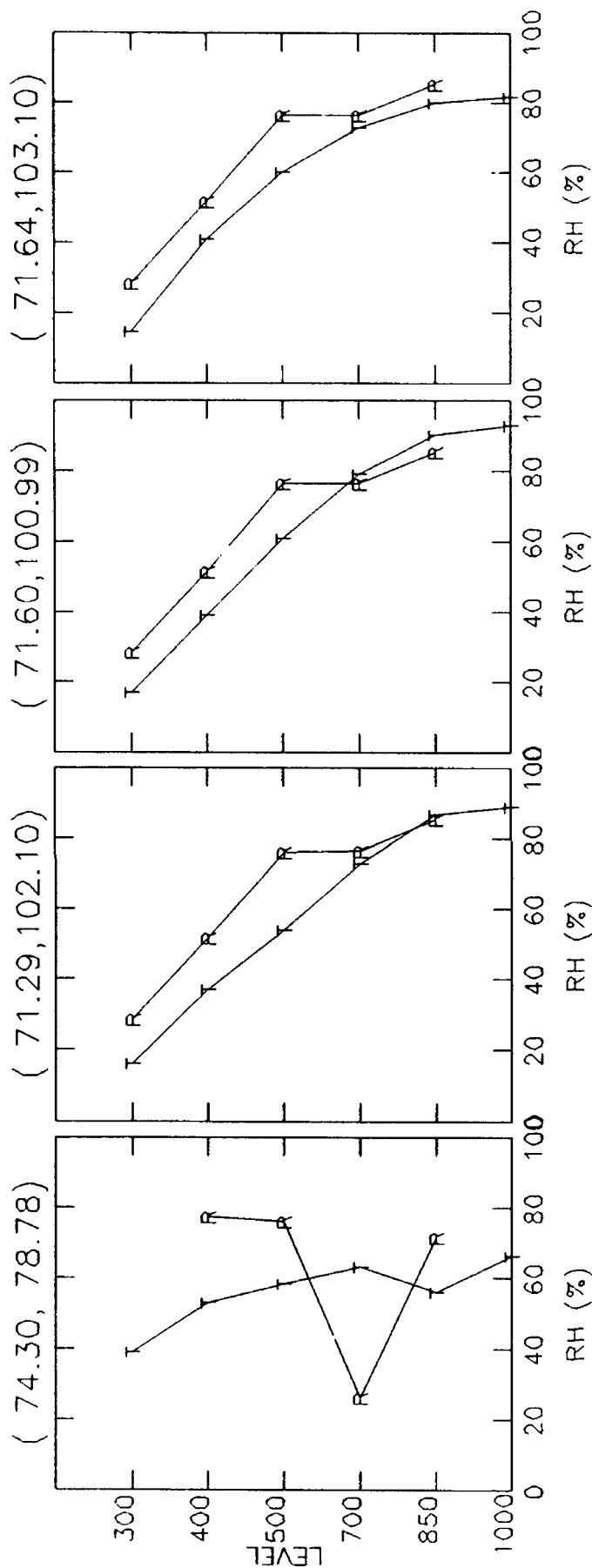


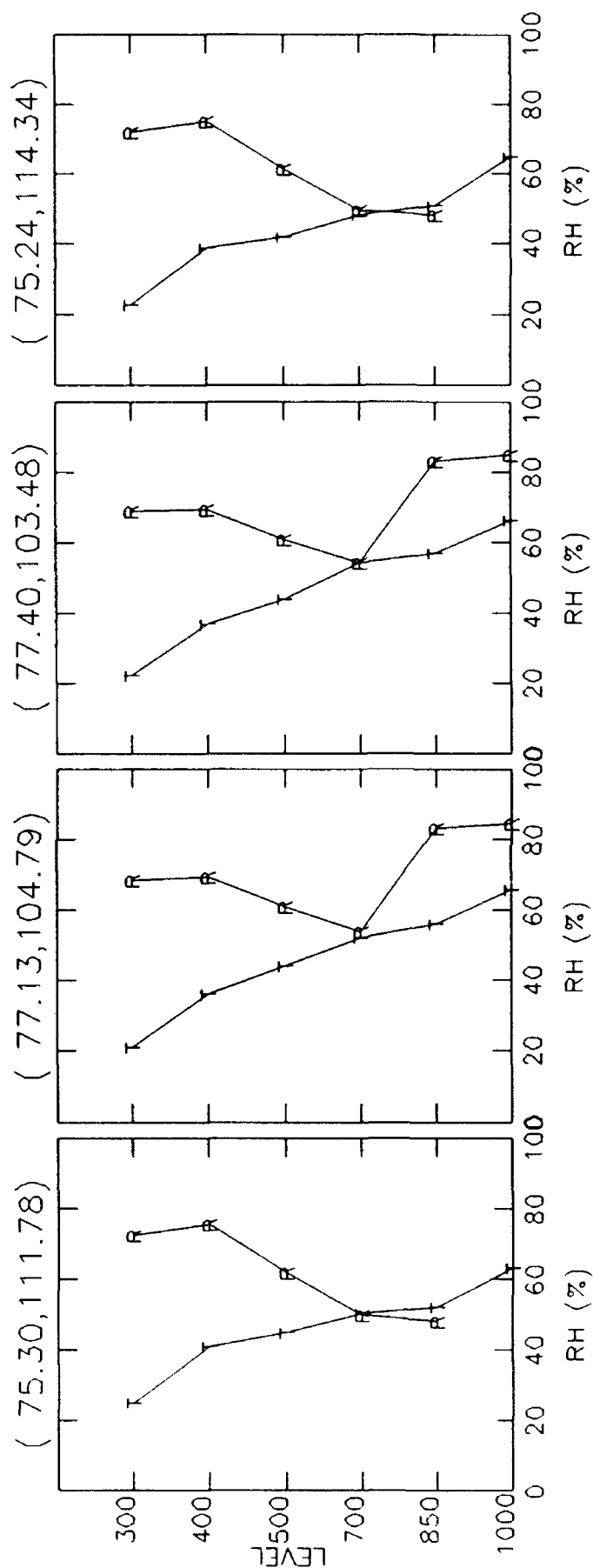
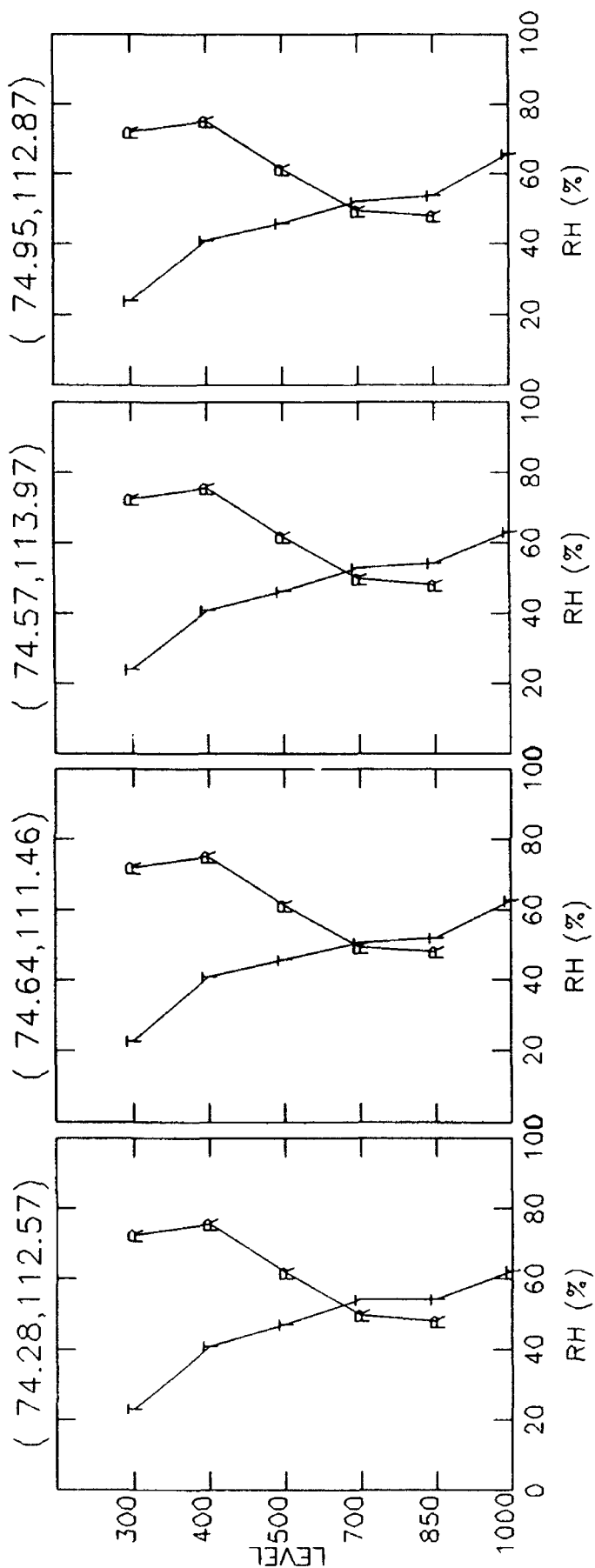




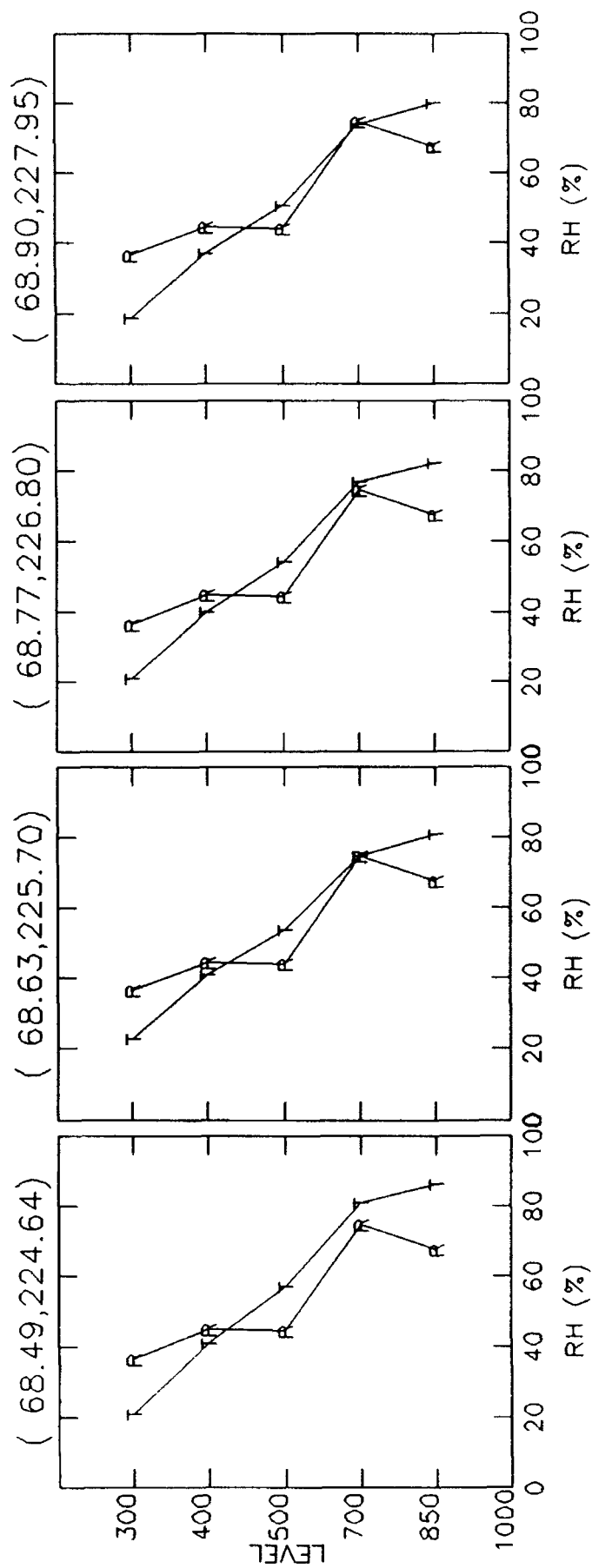
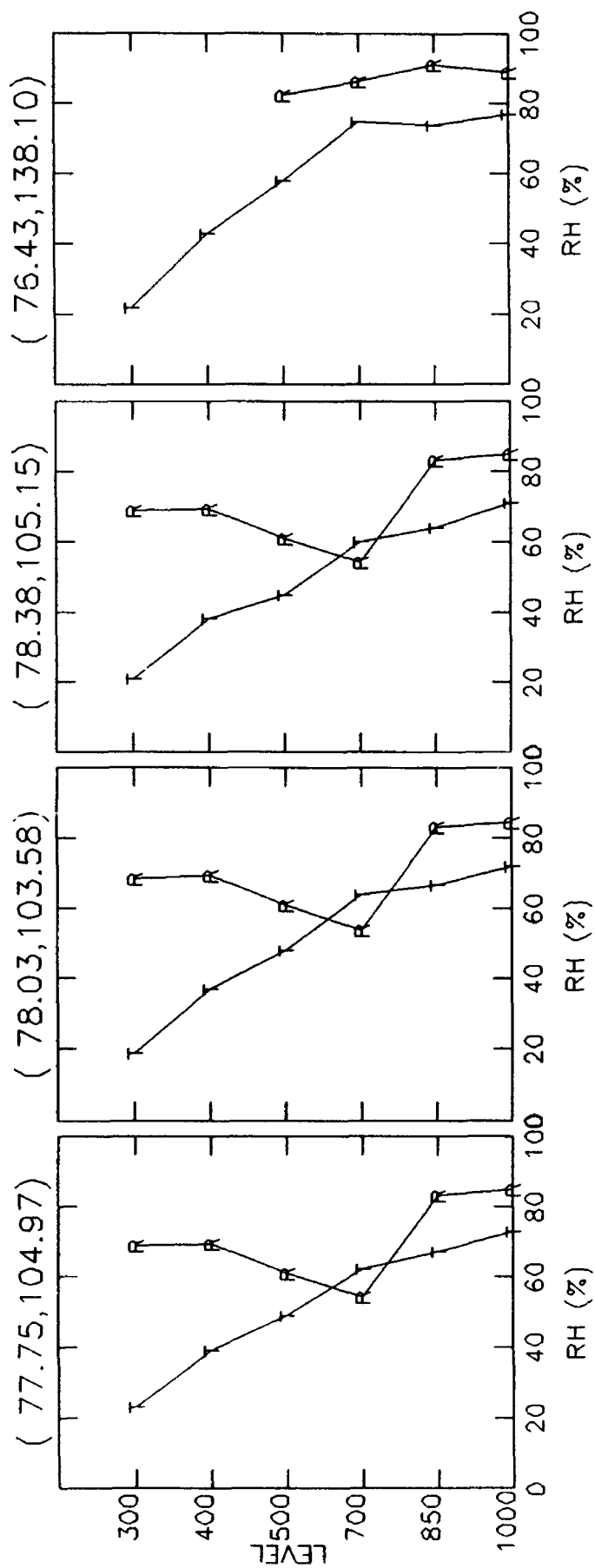


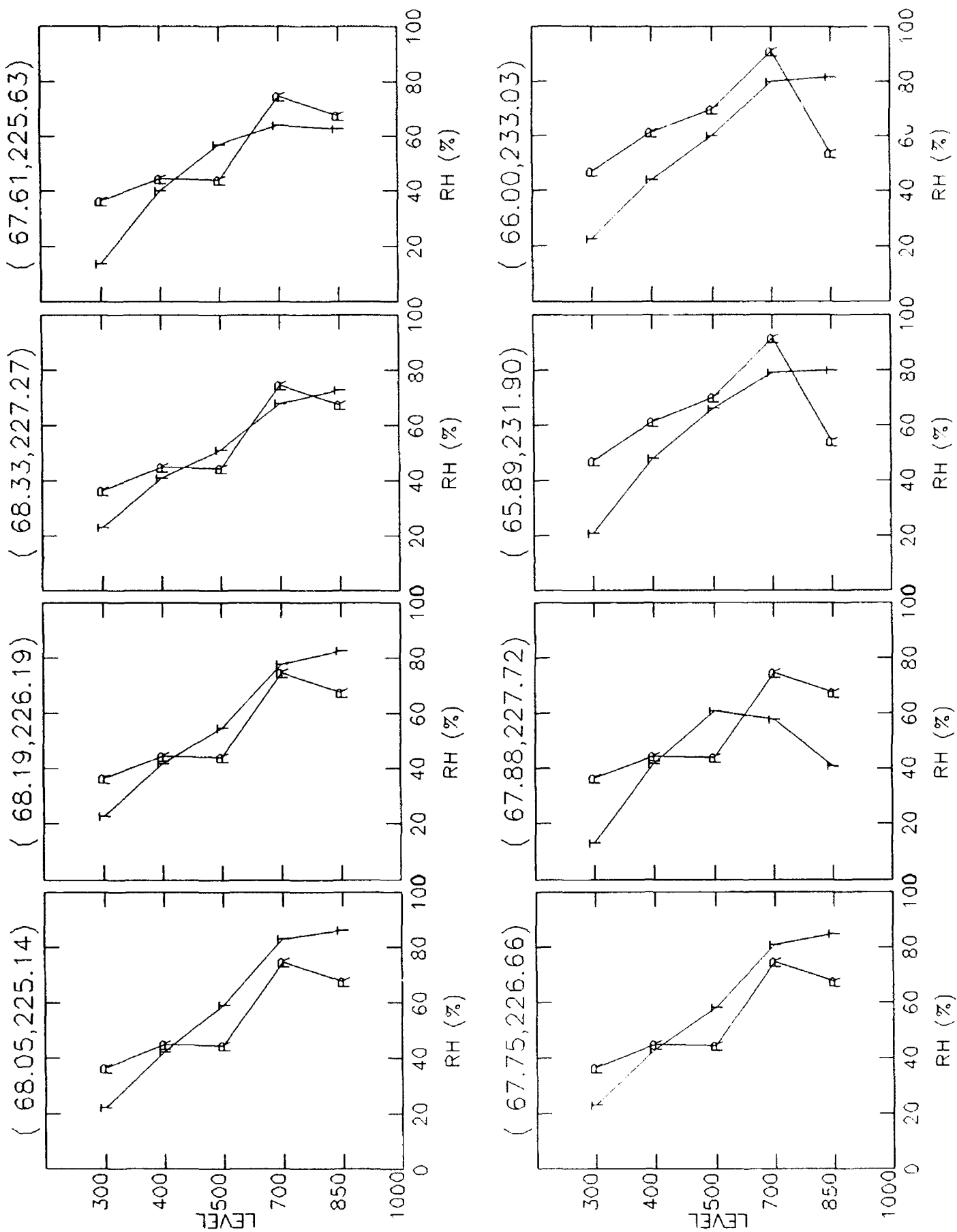


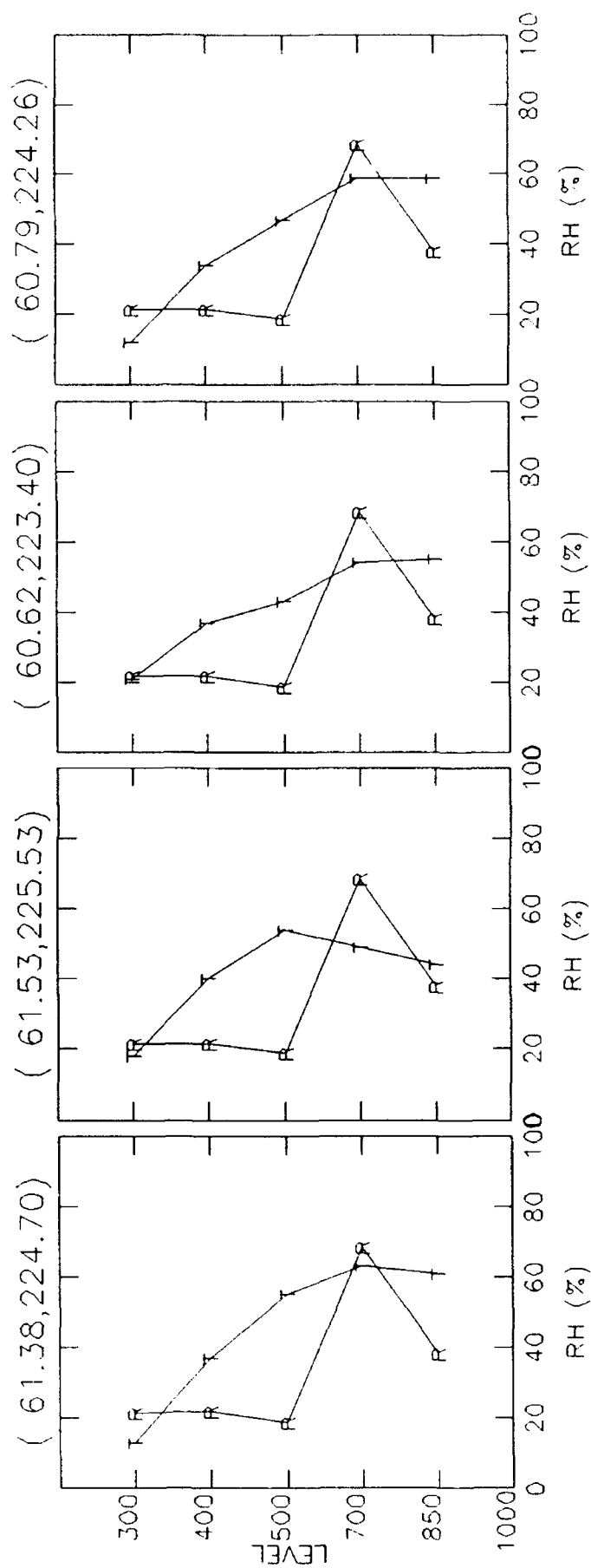
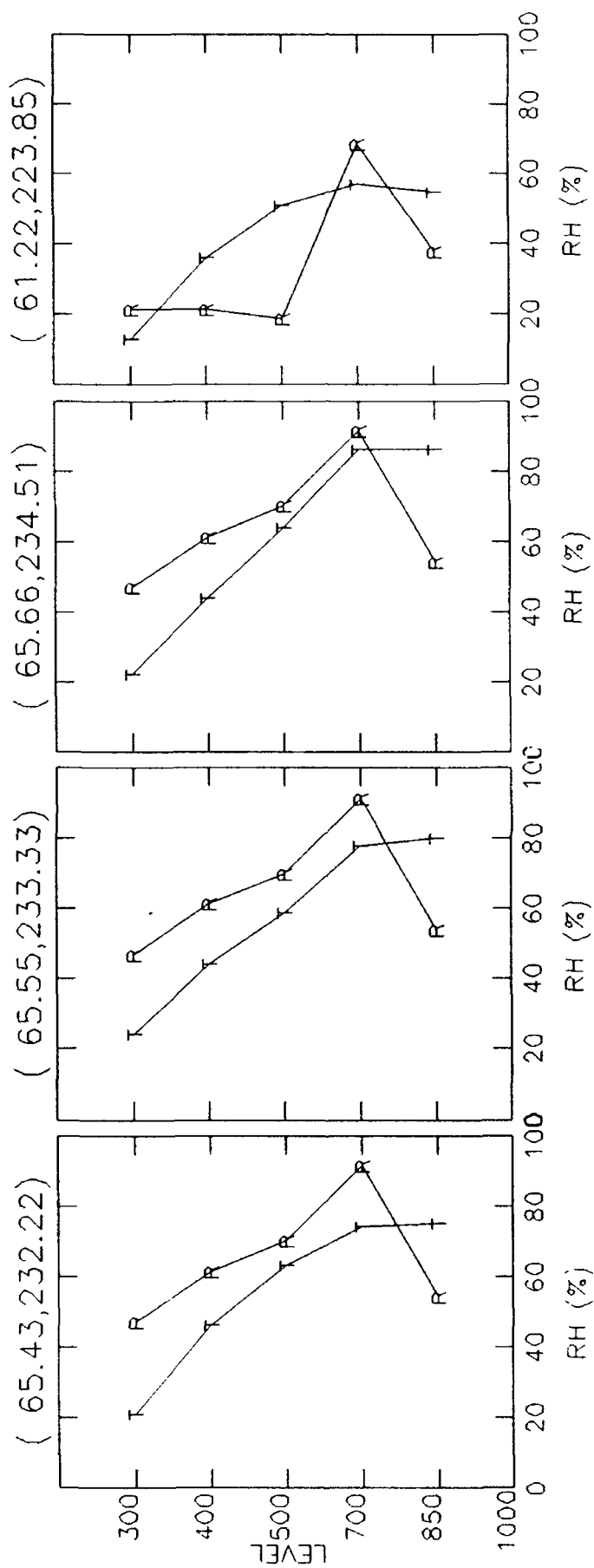


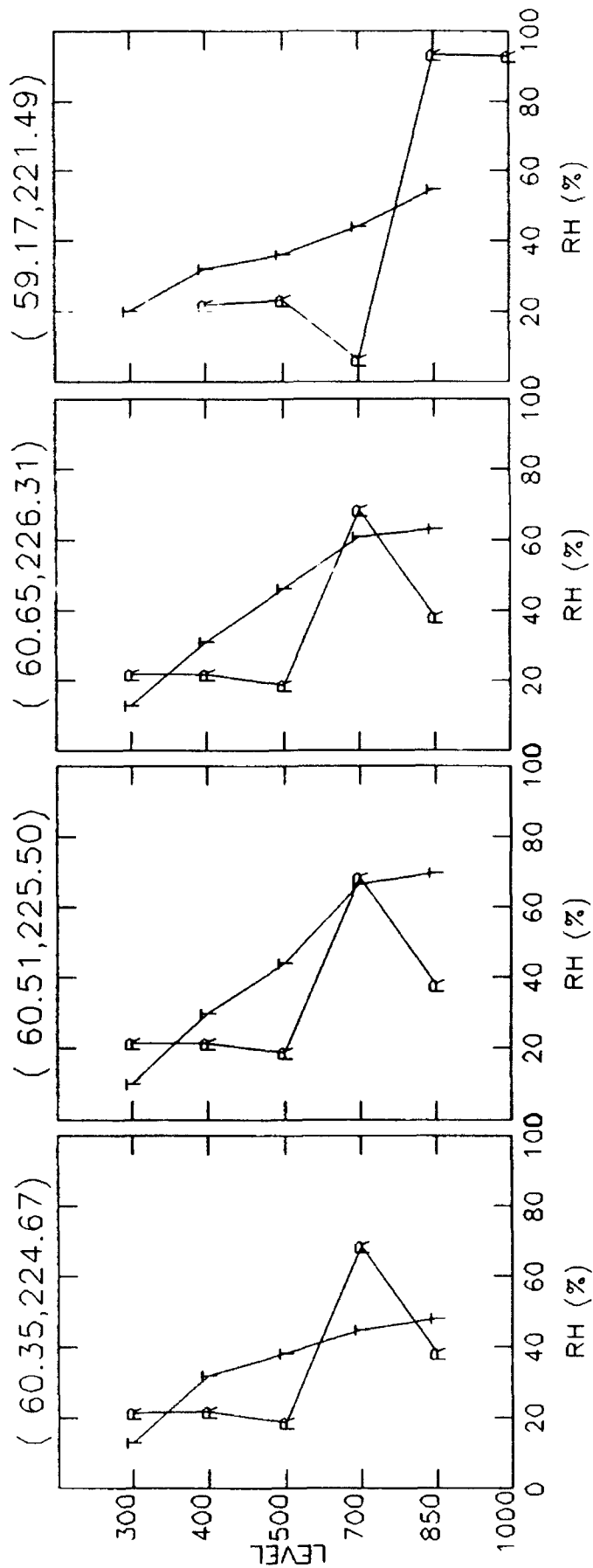
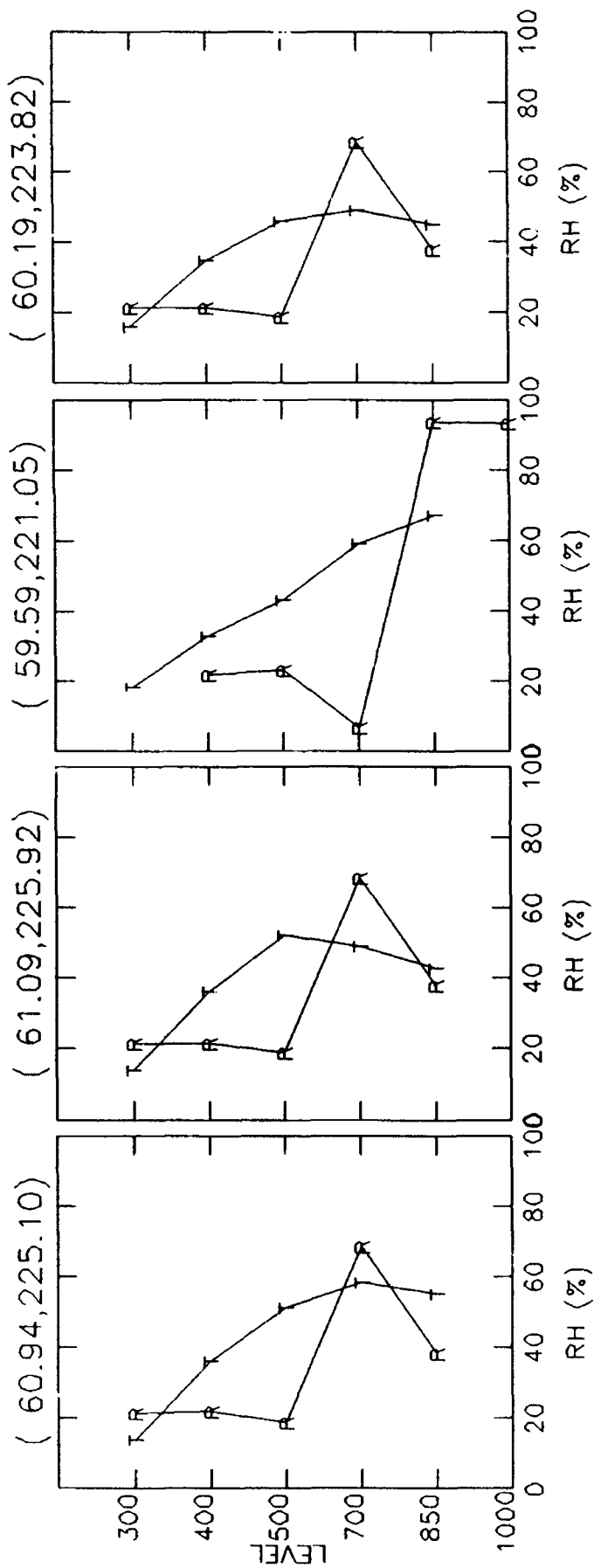


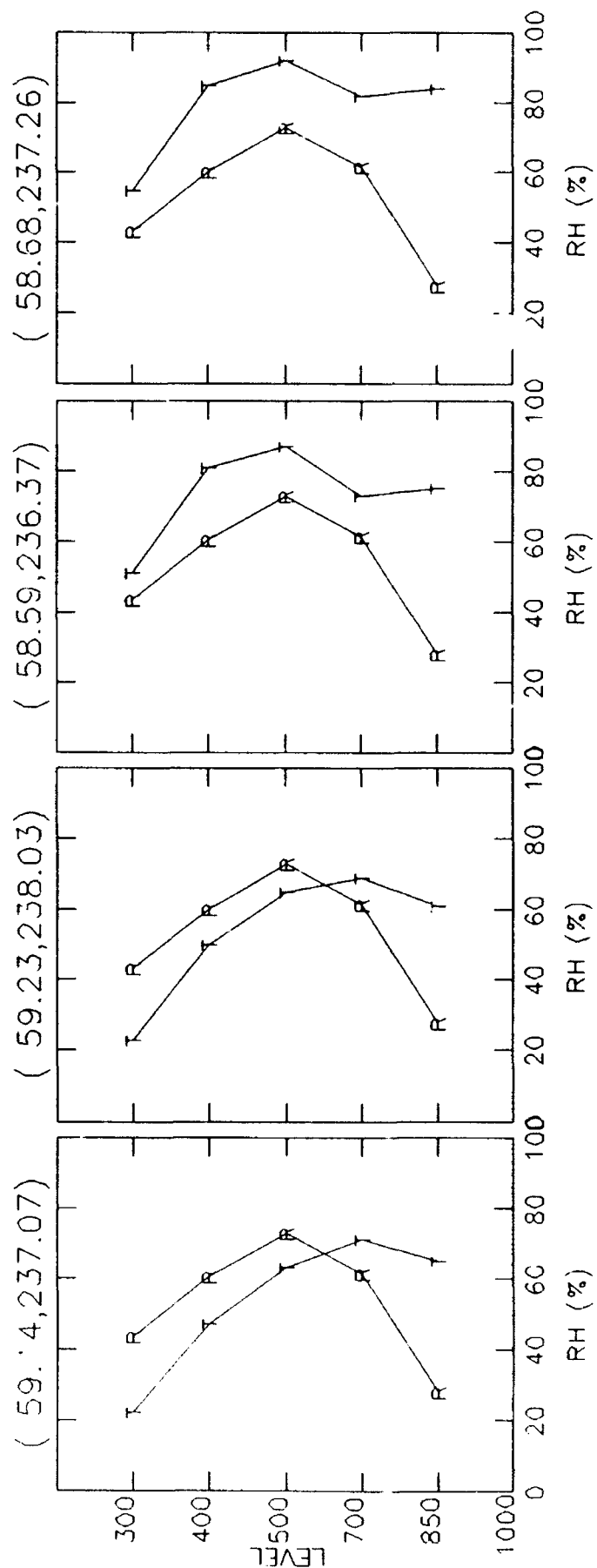
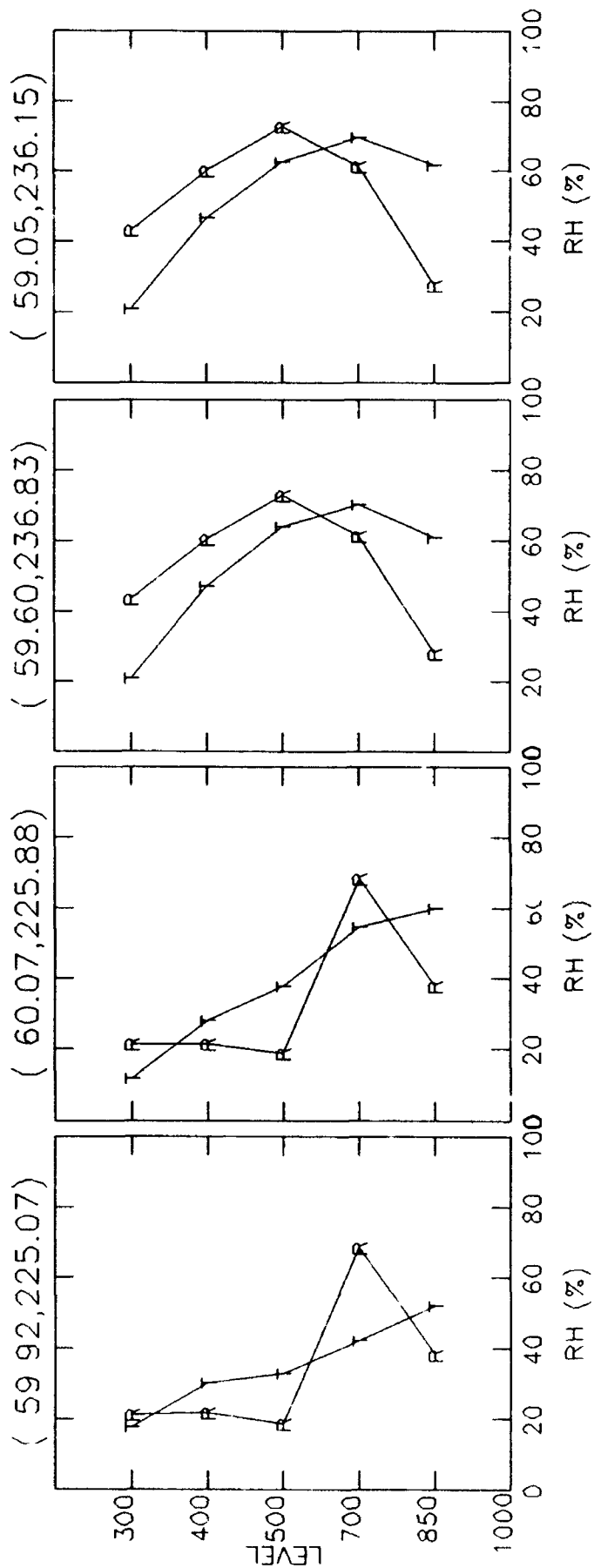


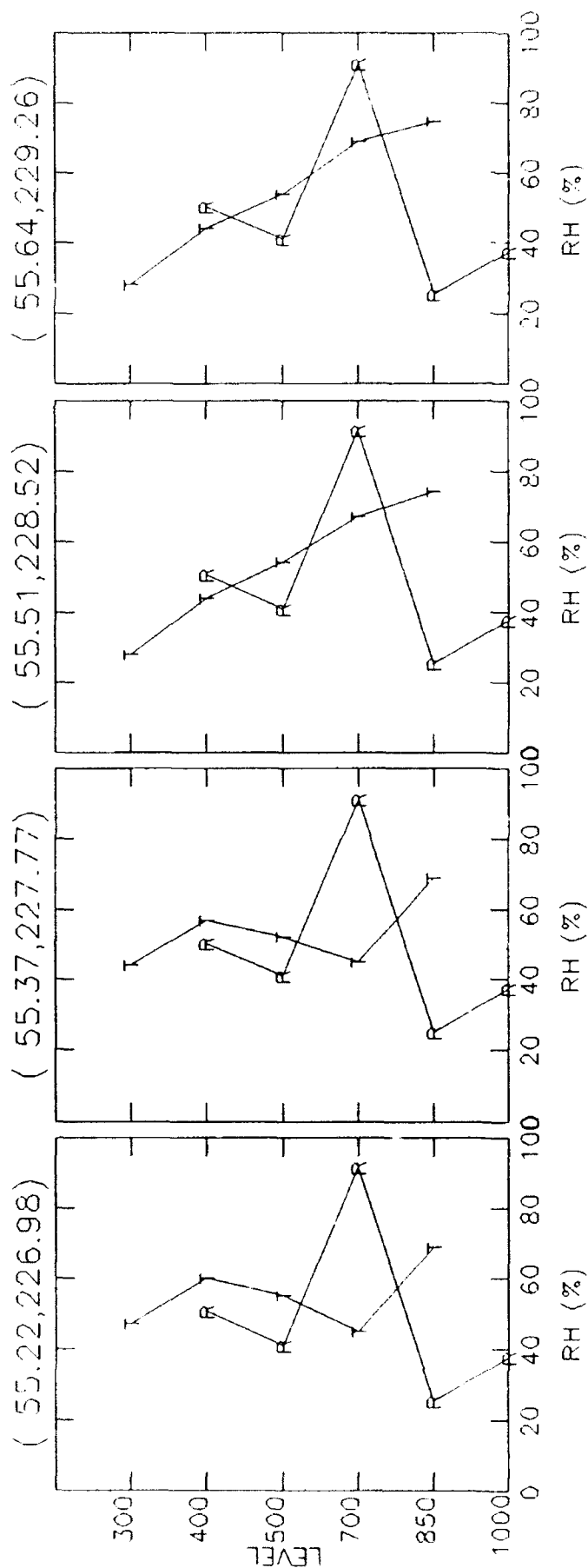
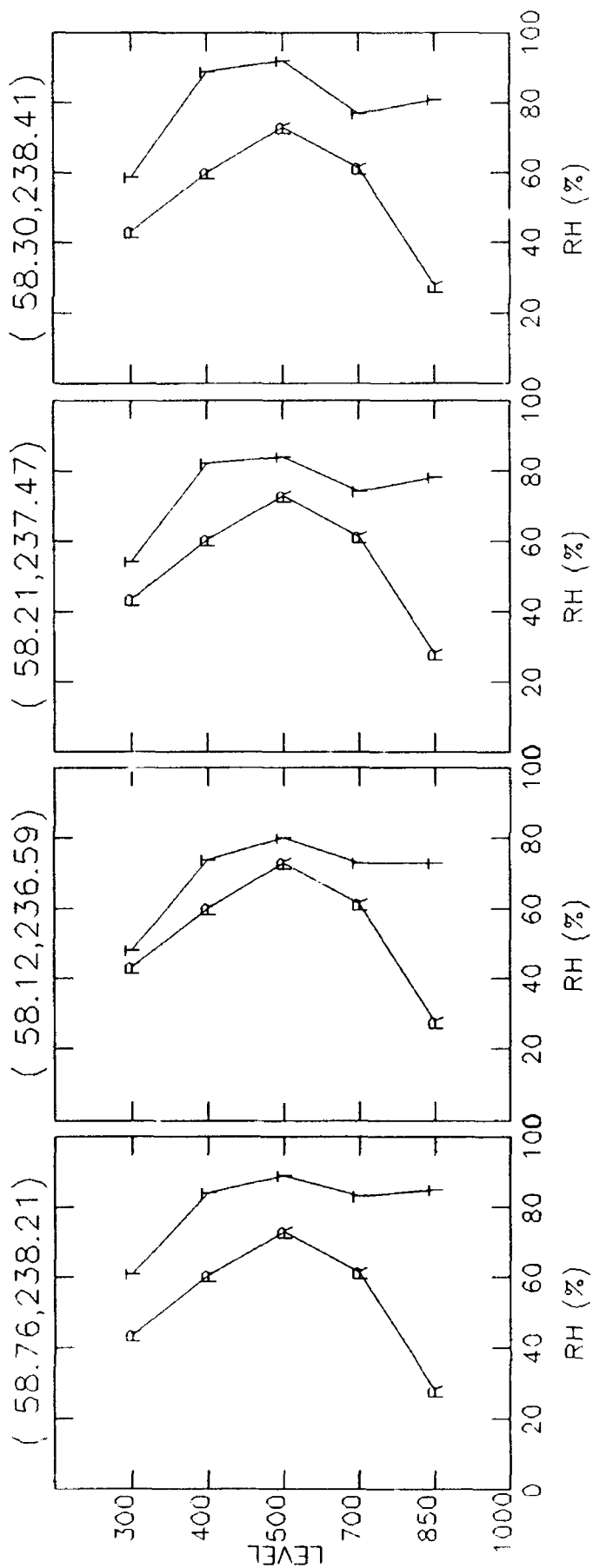


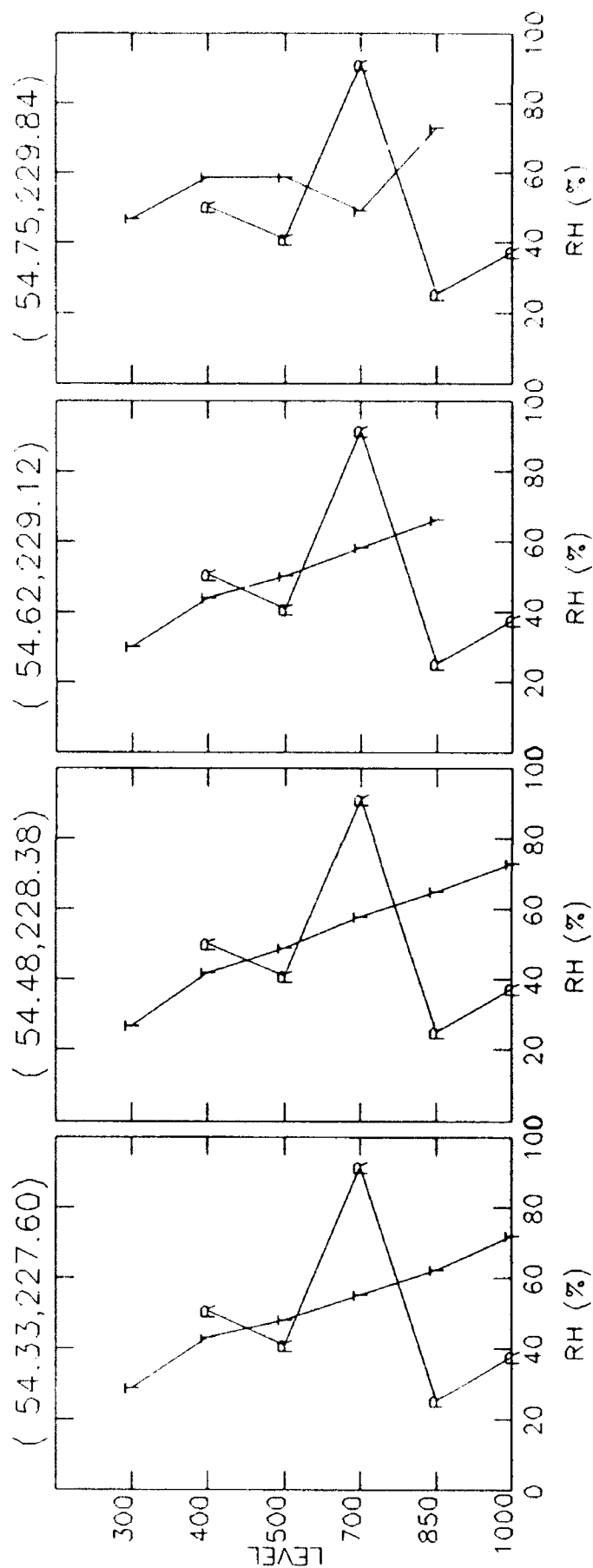
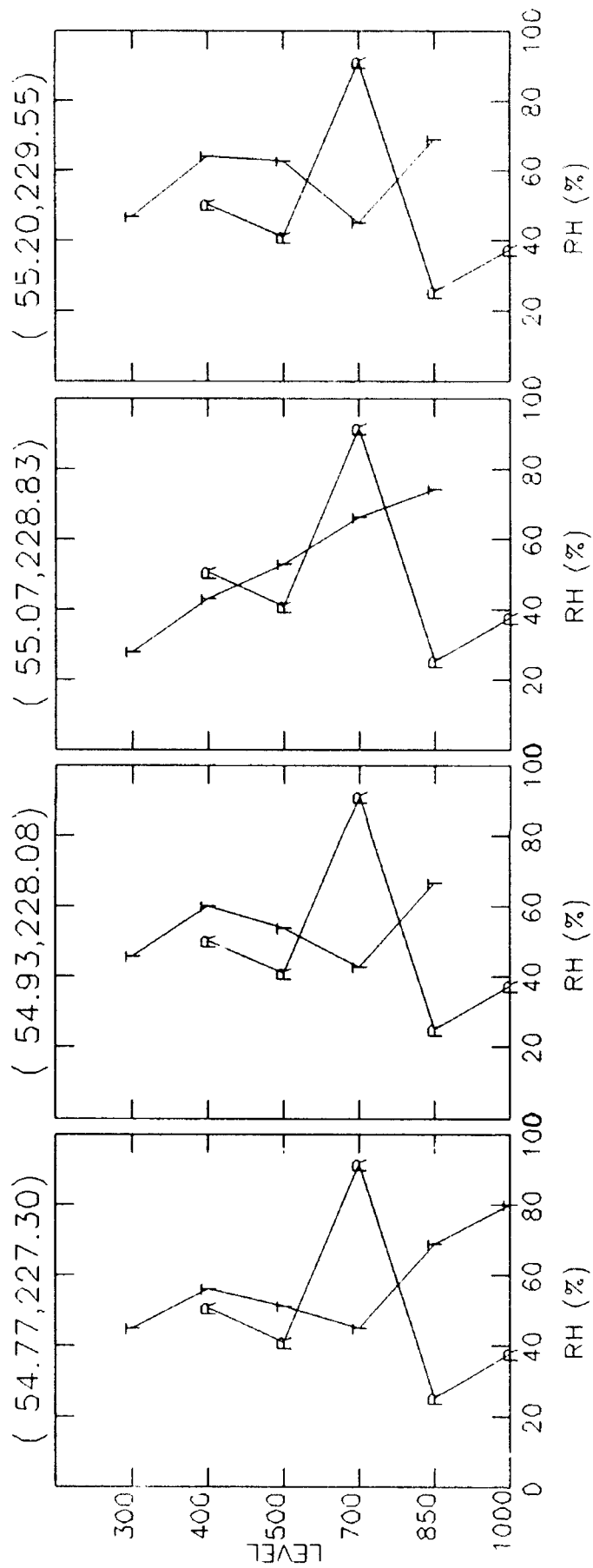


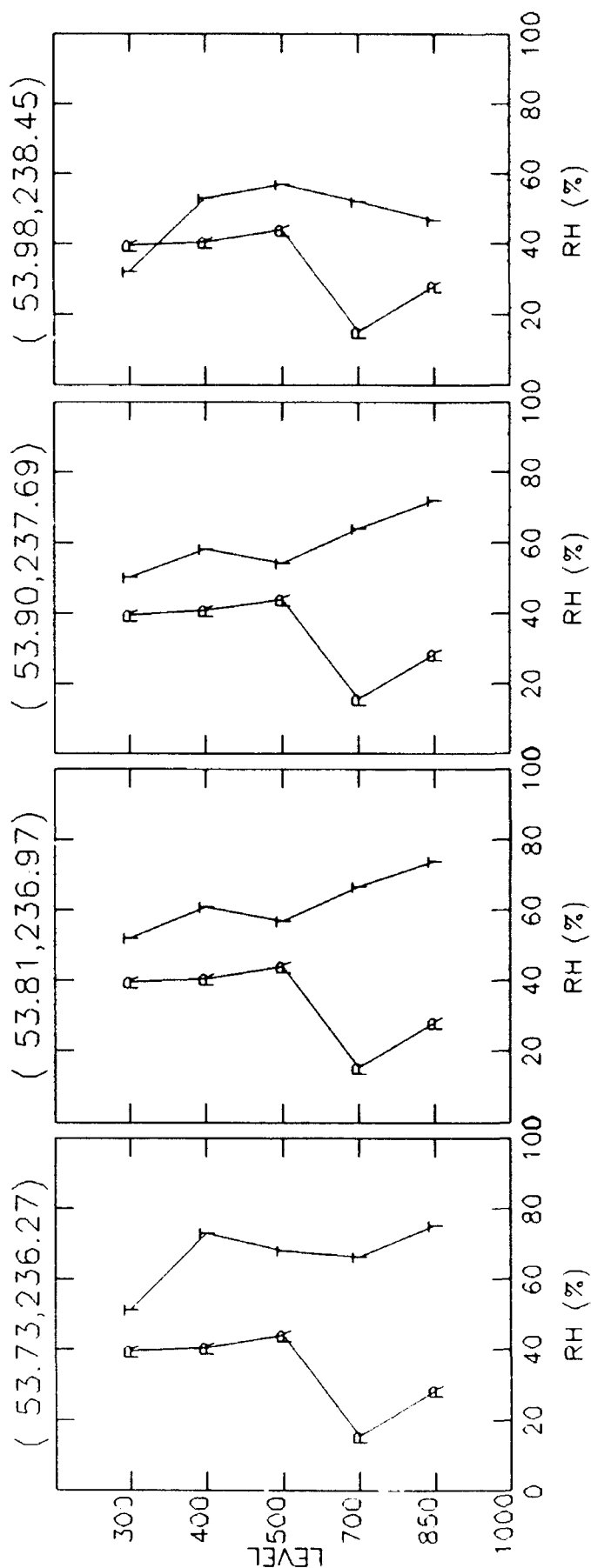
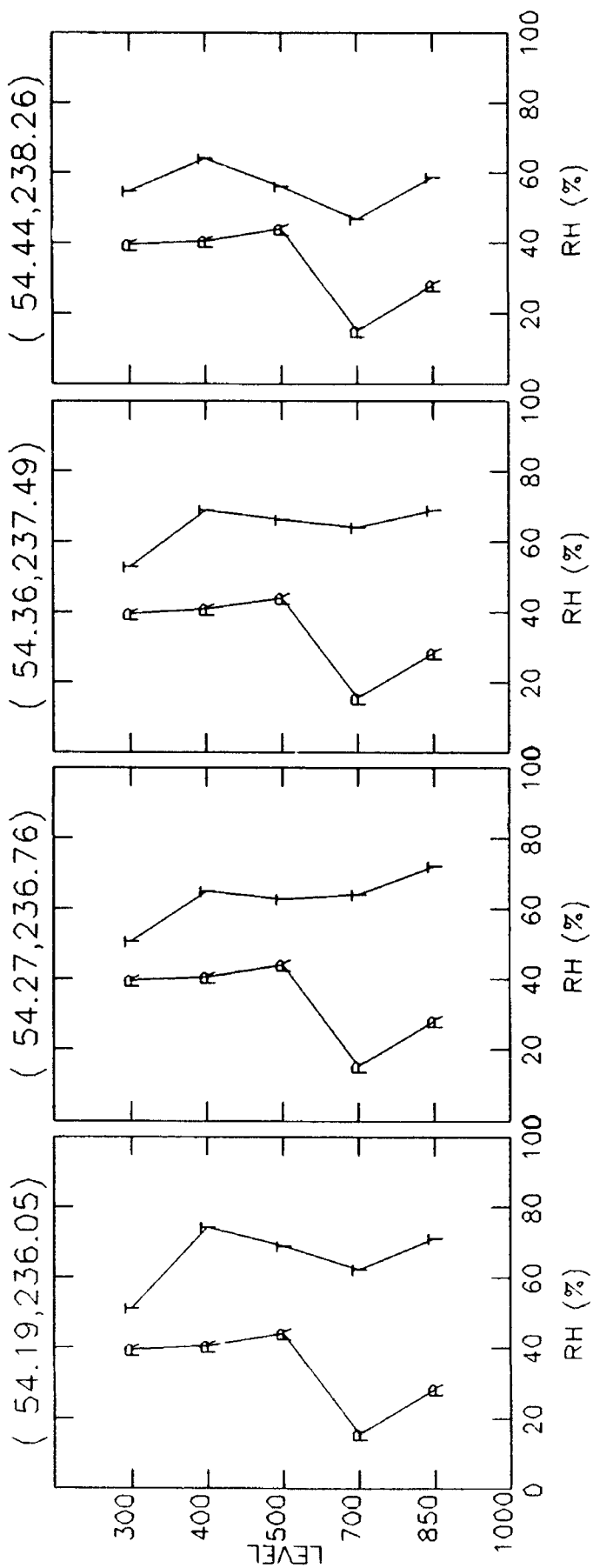




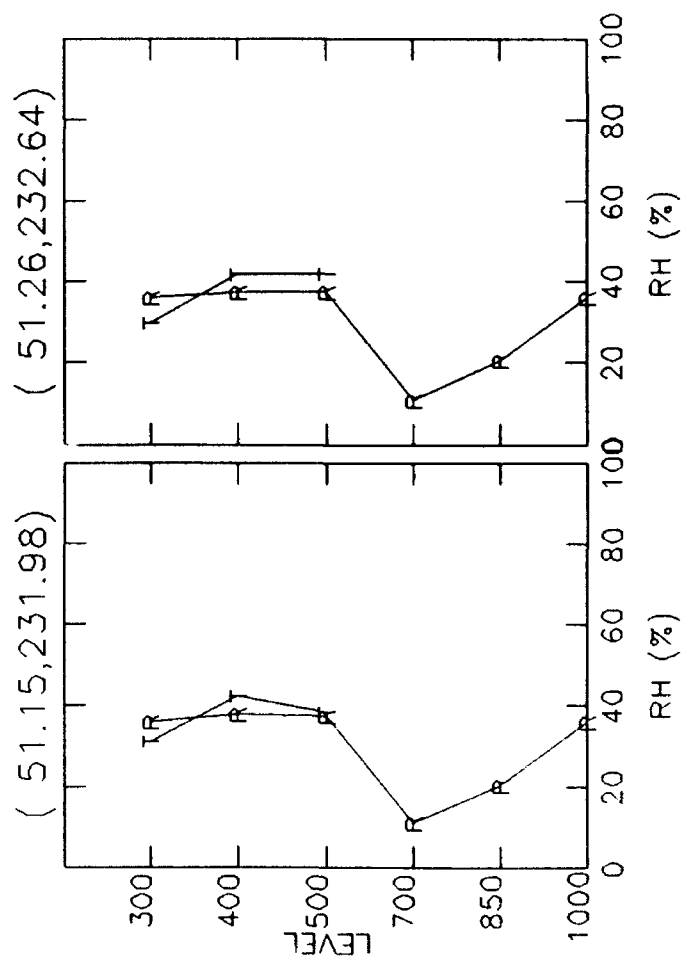
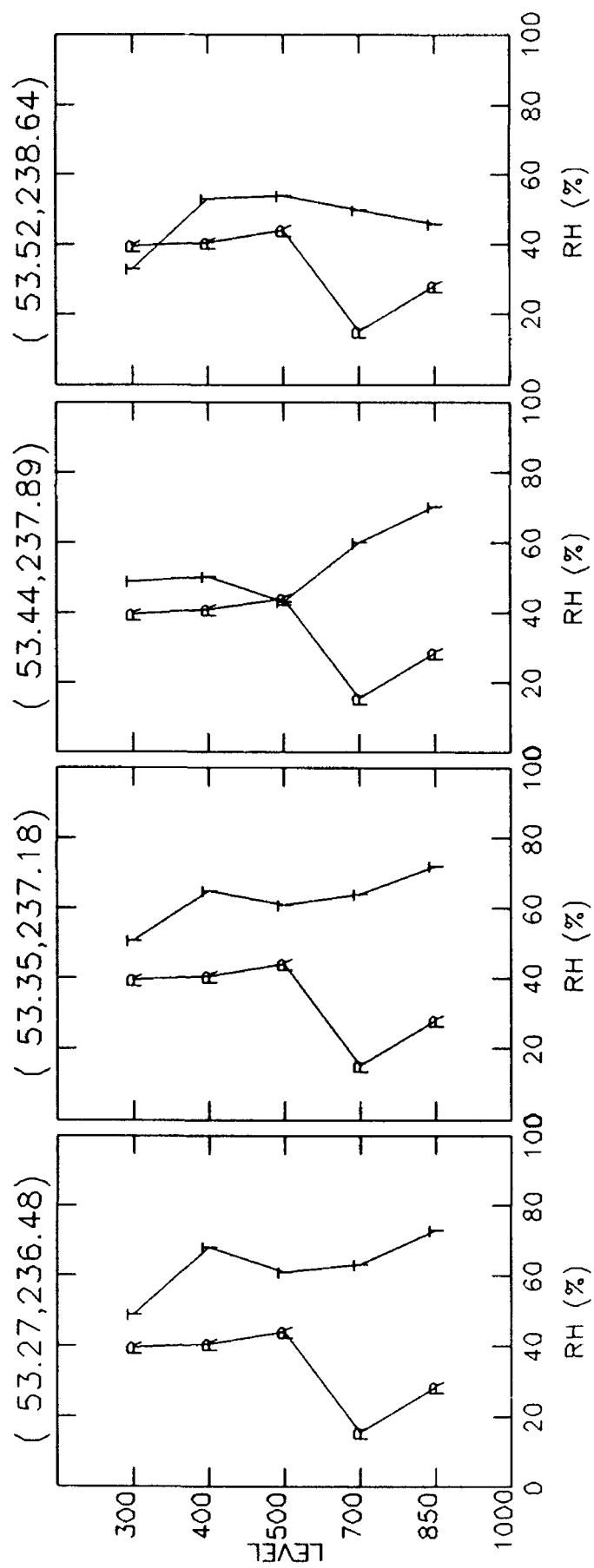




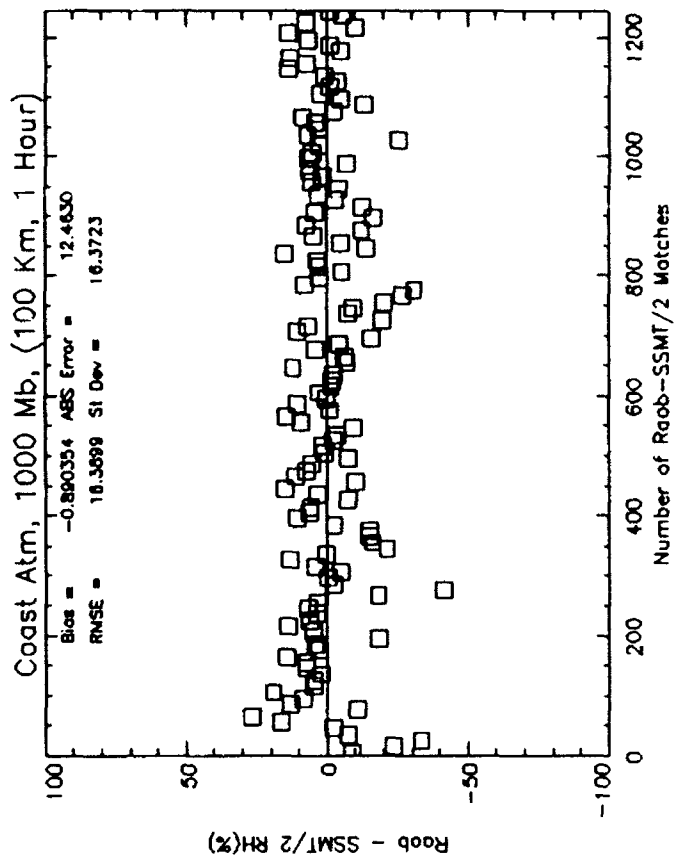
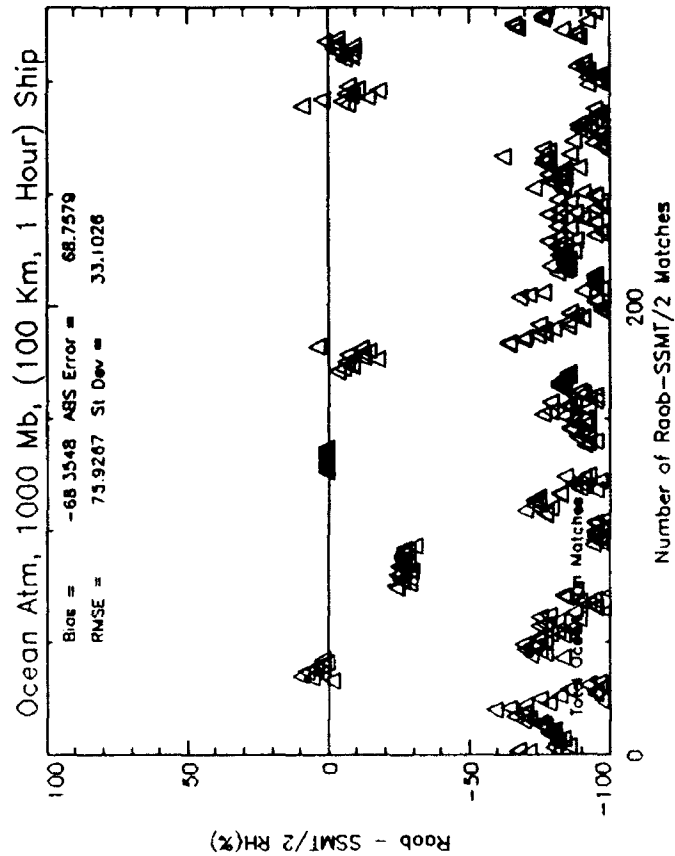
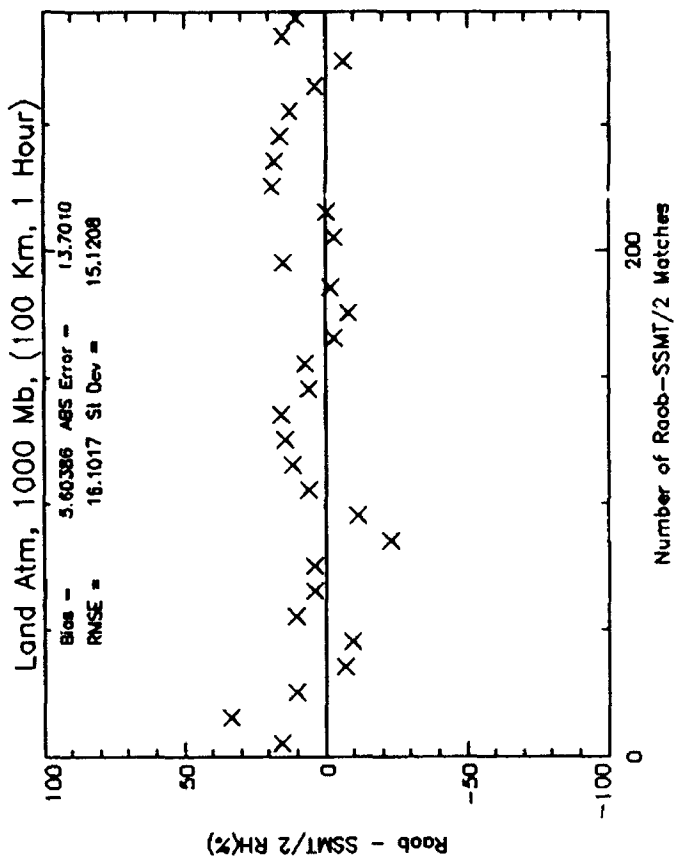
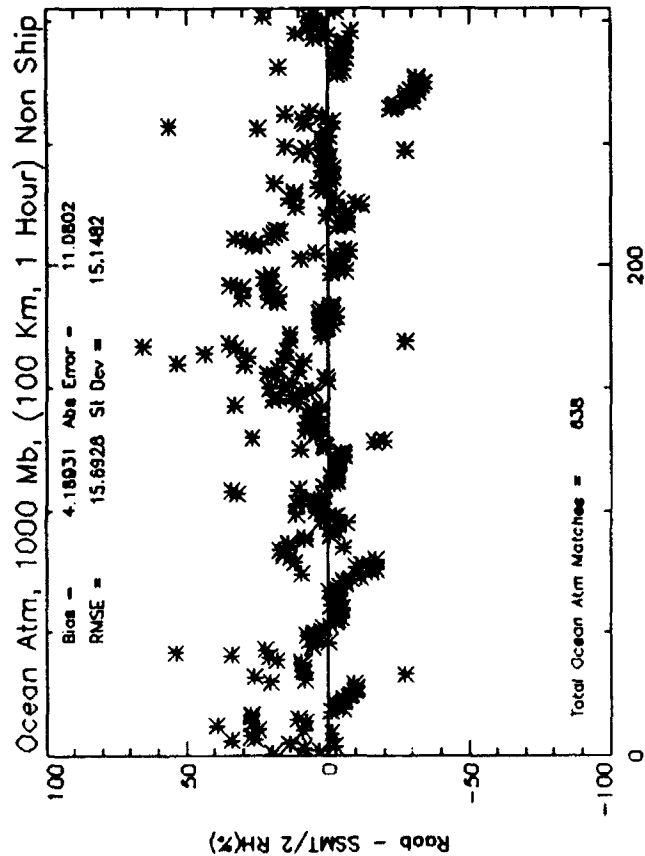


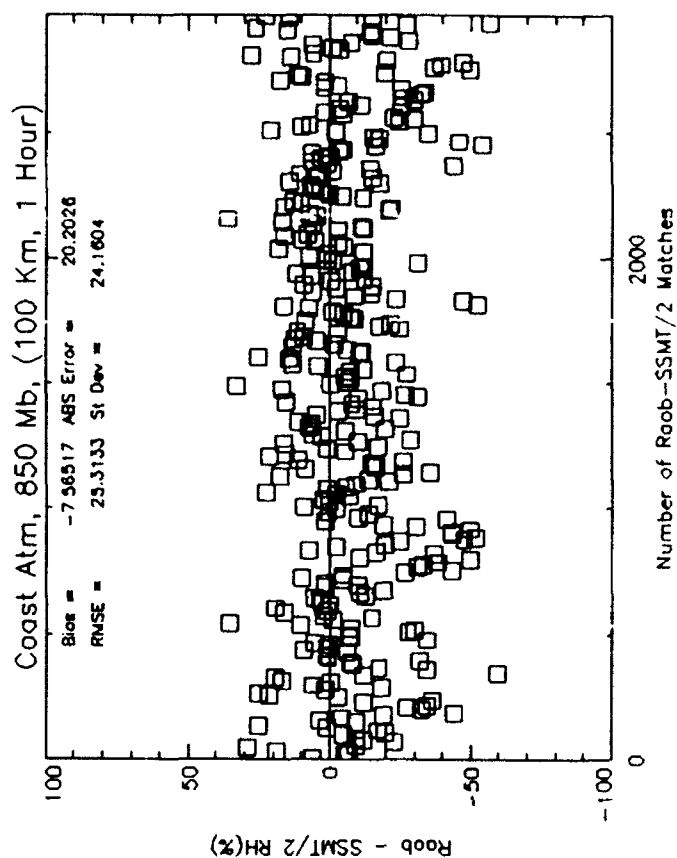
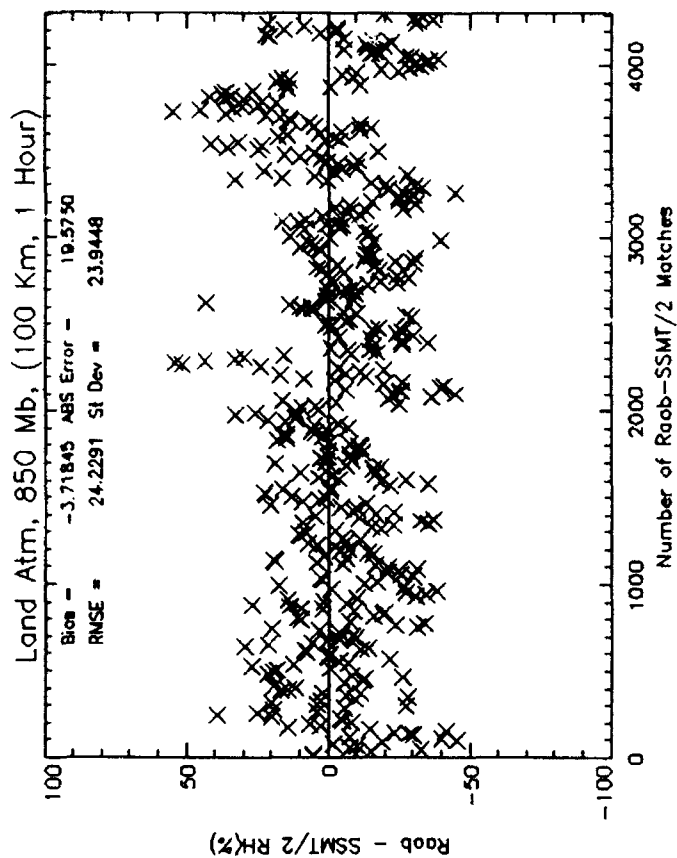
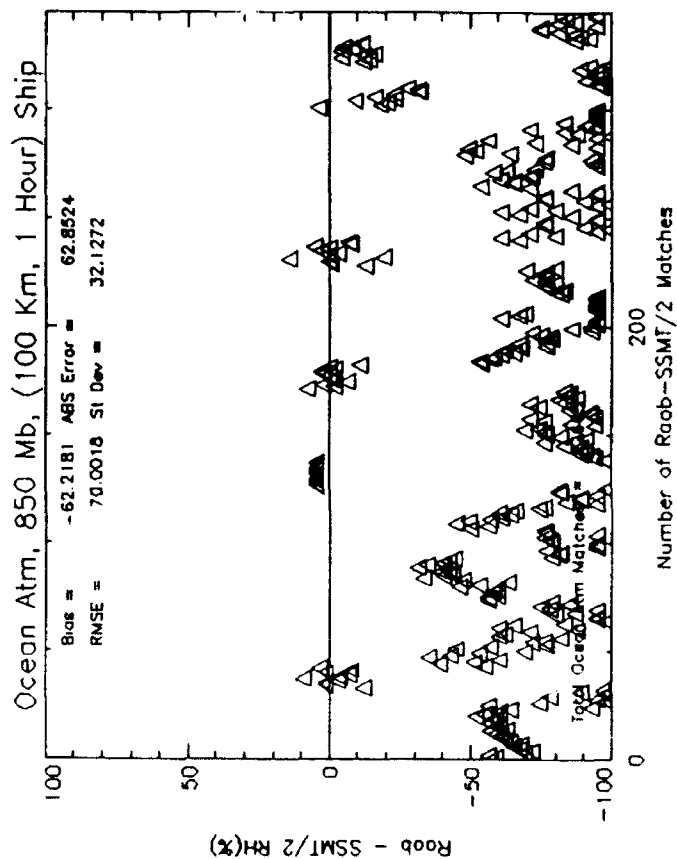
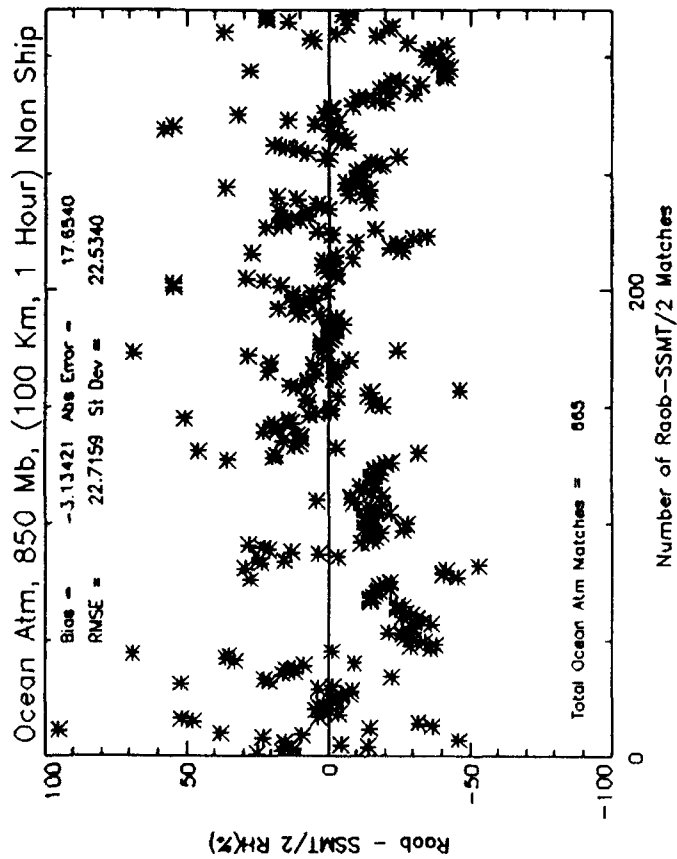


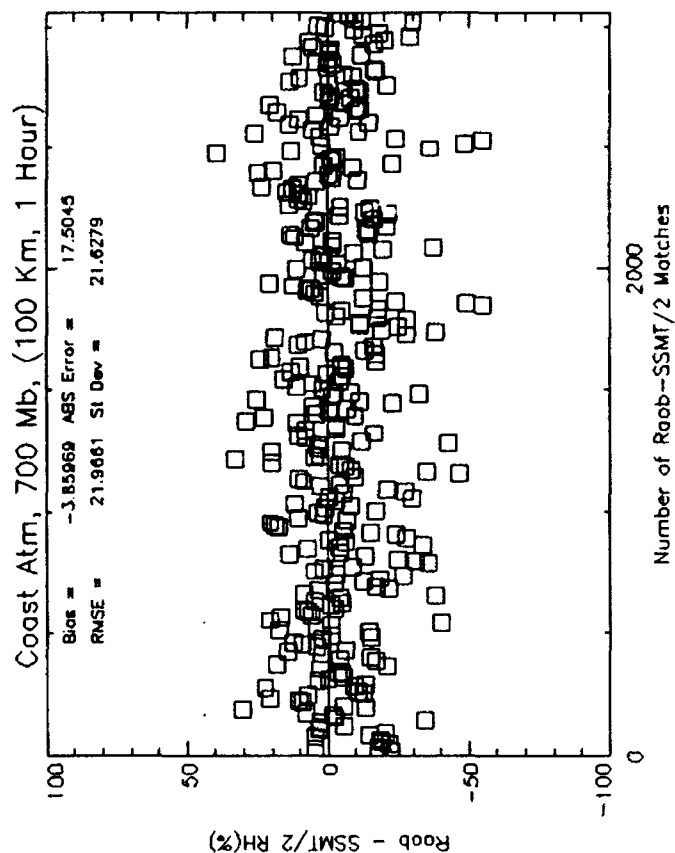
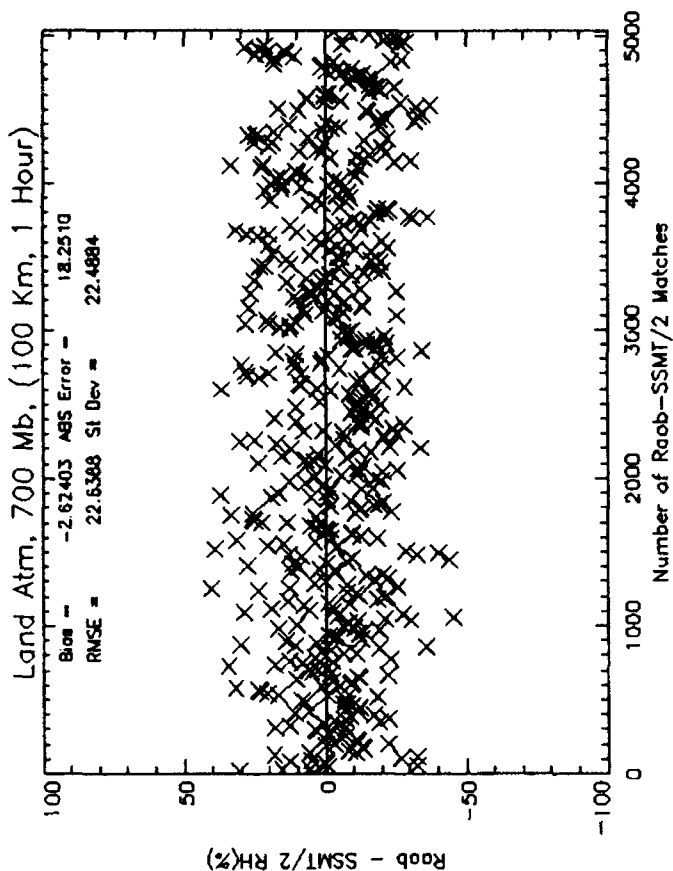
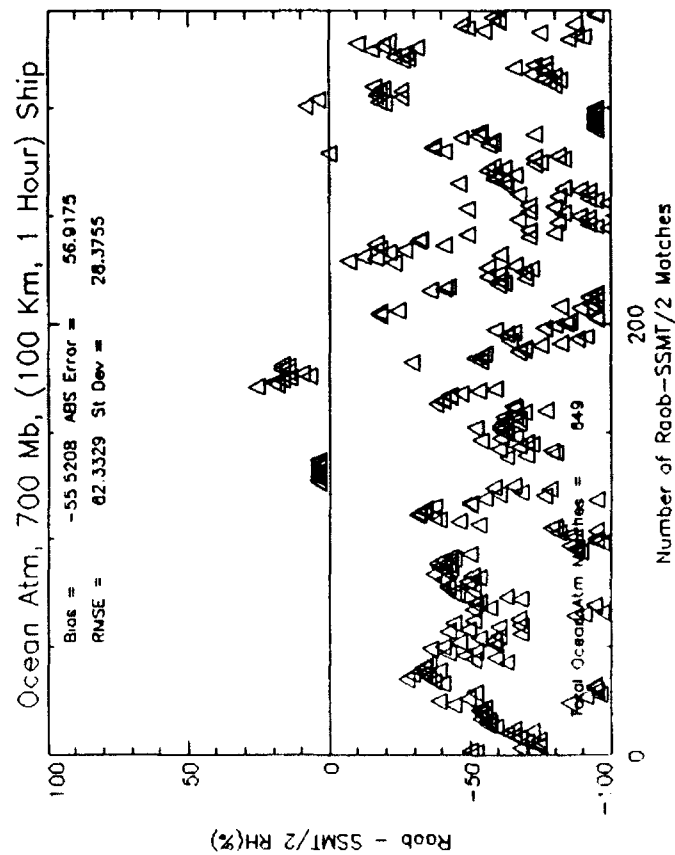
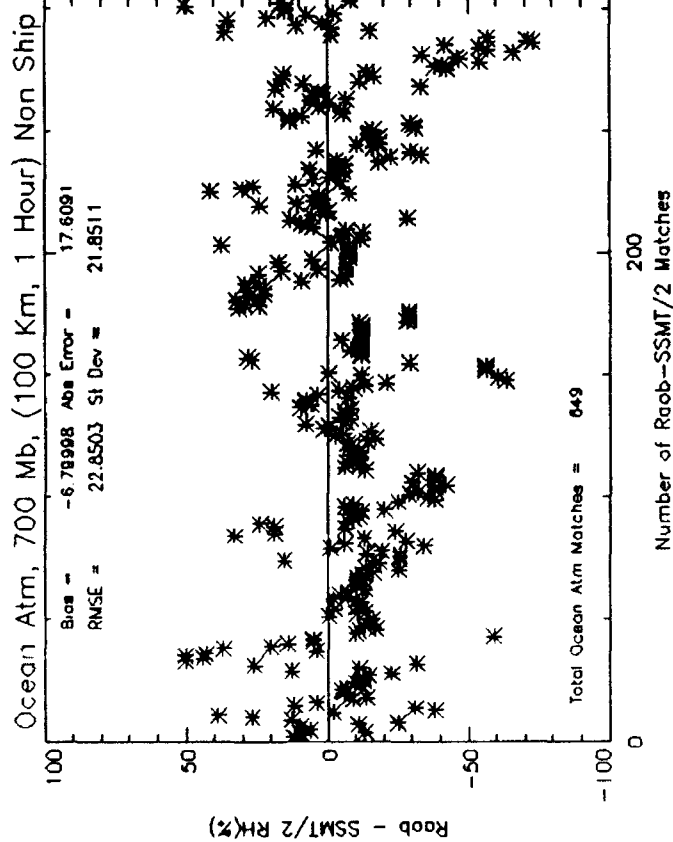


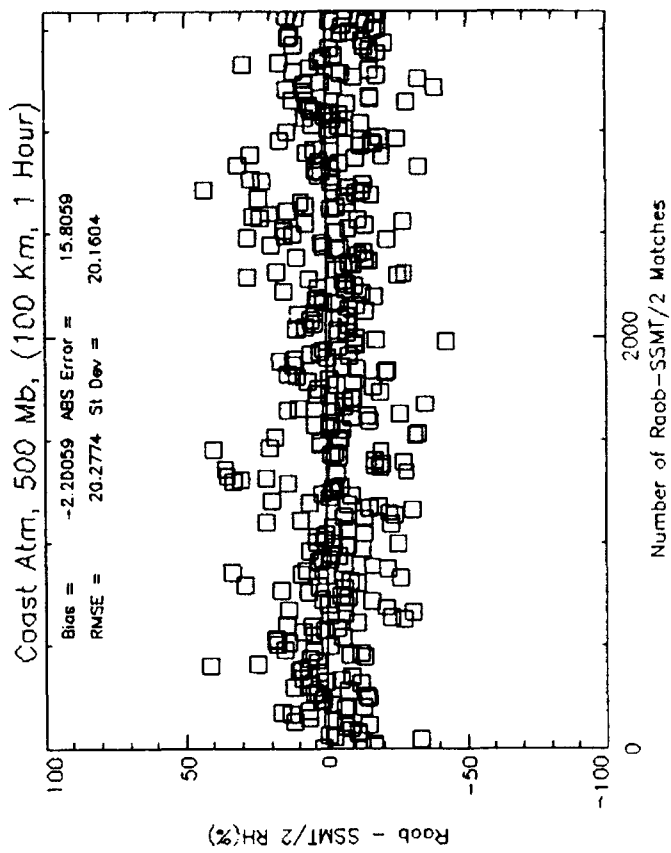
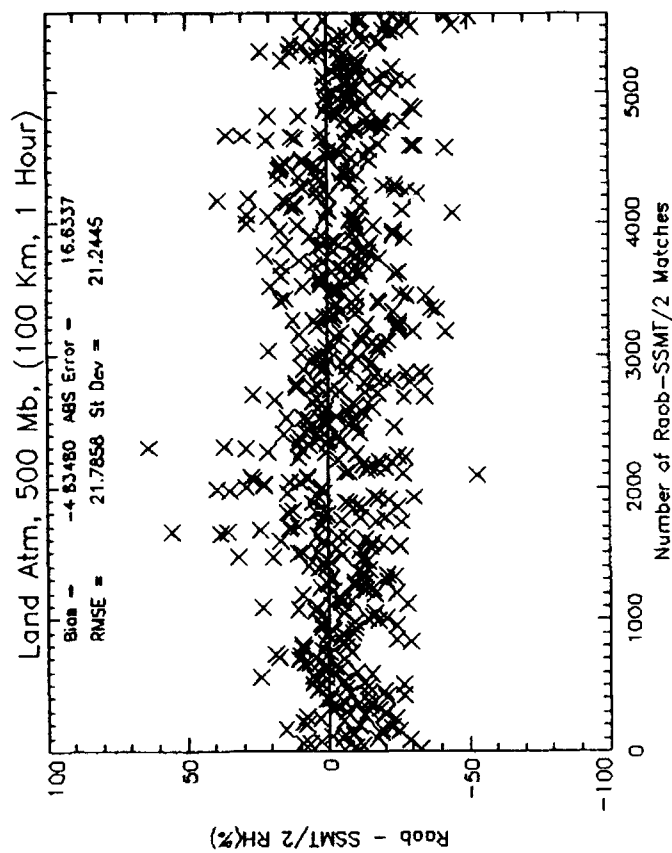
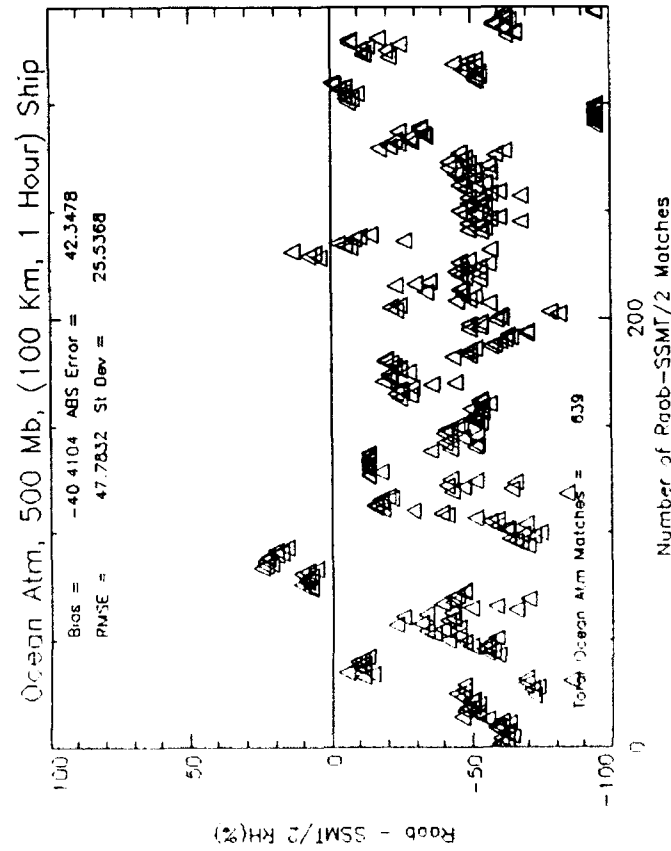
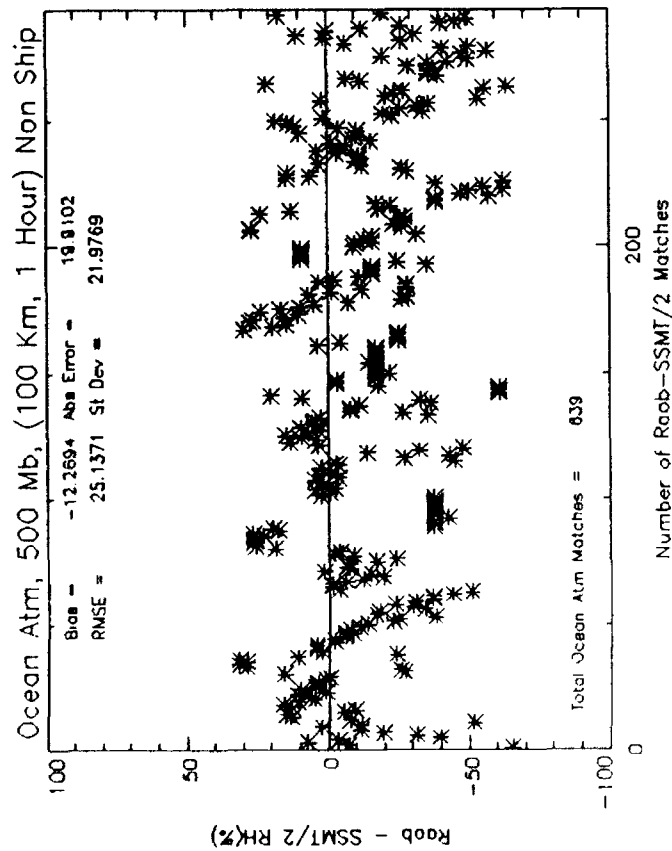


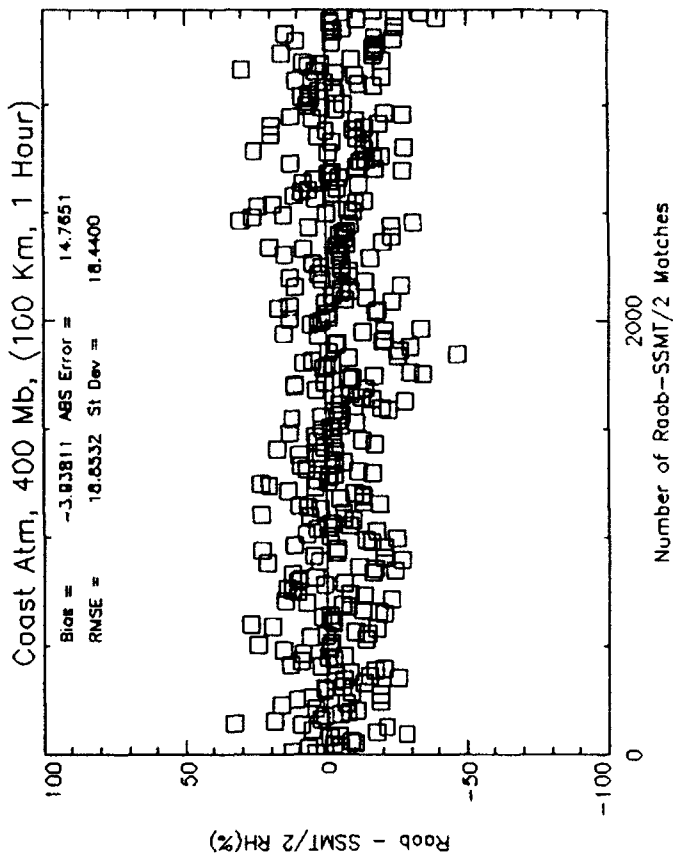
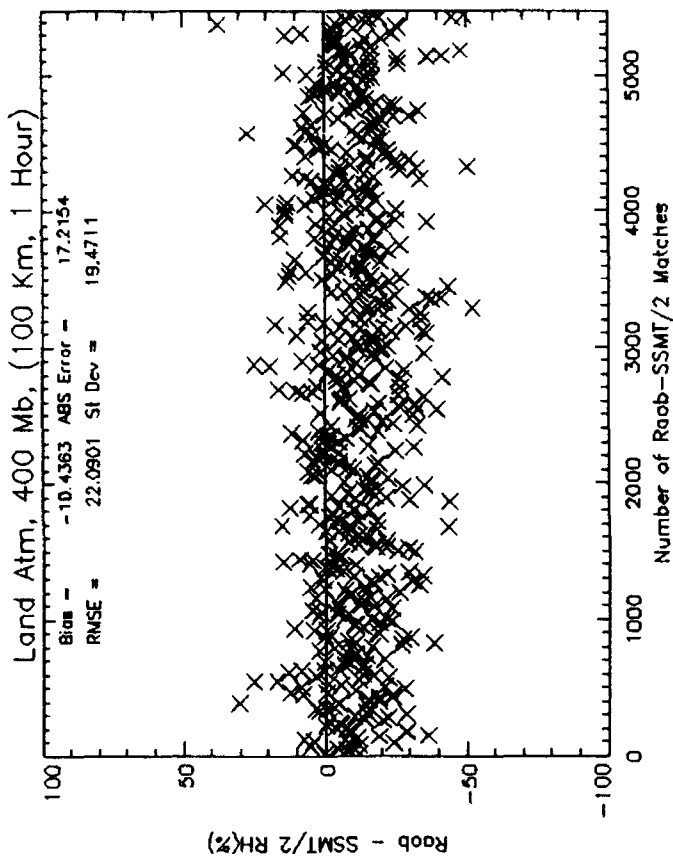
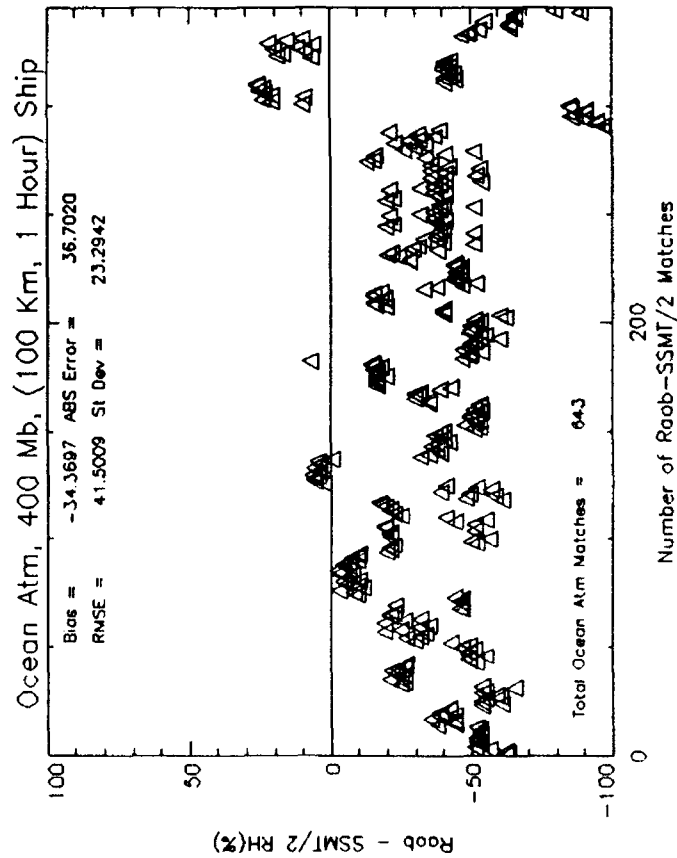
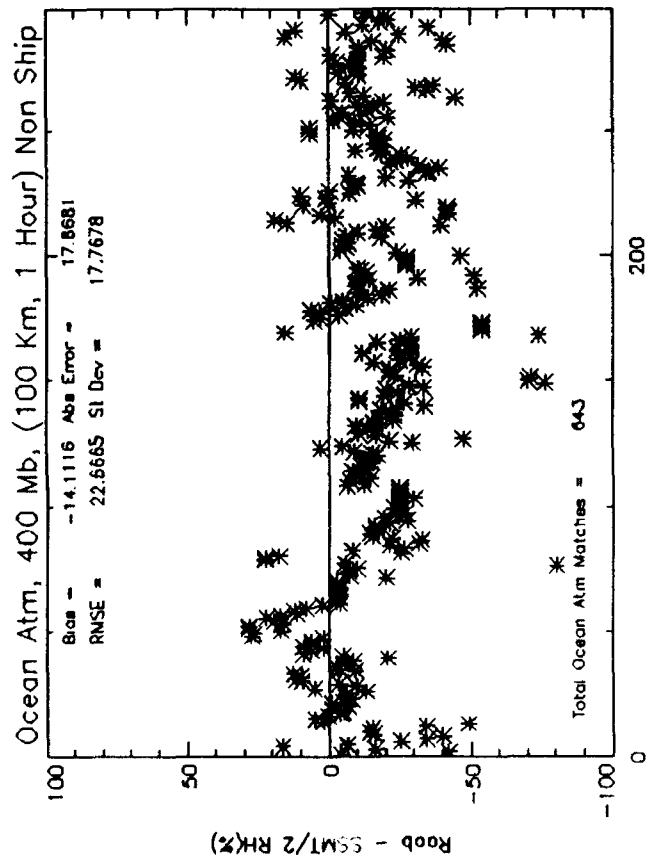
Appendix F. Land and ship observations are plotted separately with the quantity (Radiosonde - SSM/T-2) RH and Q plotted on the ordinate, and the index of the co-locations on the abscissa. Each four-plot panel represents one atmospheric level. In addition, the plots are stratified by atmosphere type. The co-location criteria are annotated at the top of the plots.

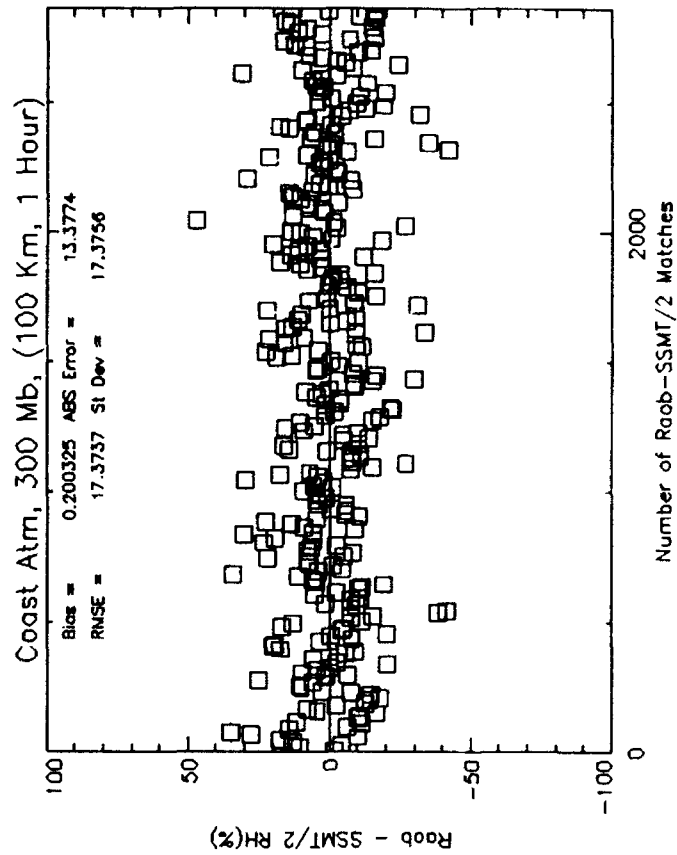
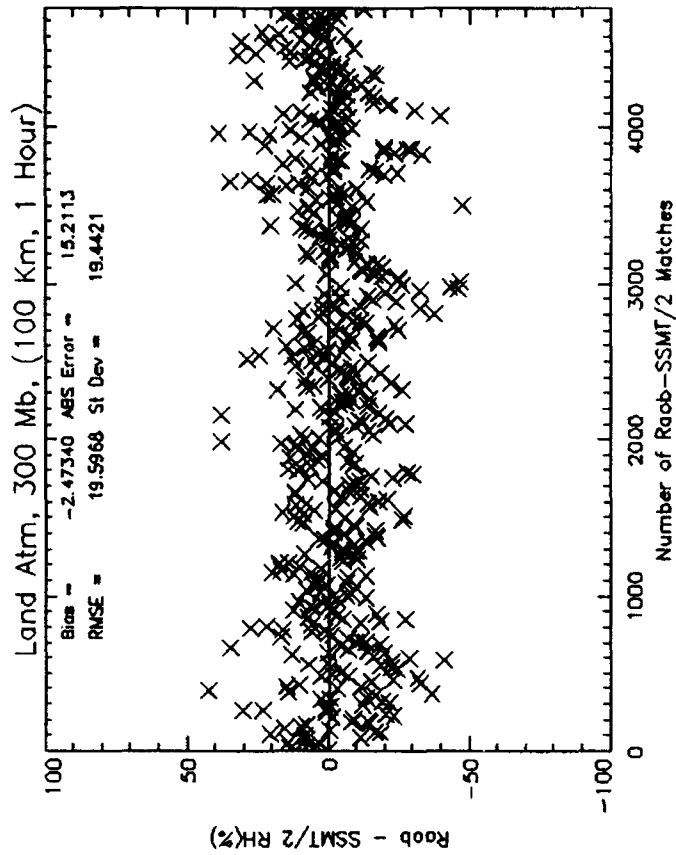
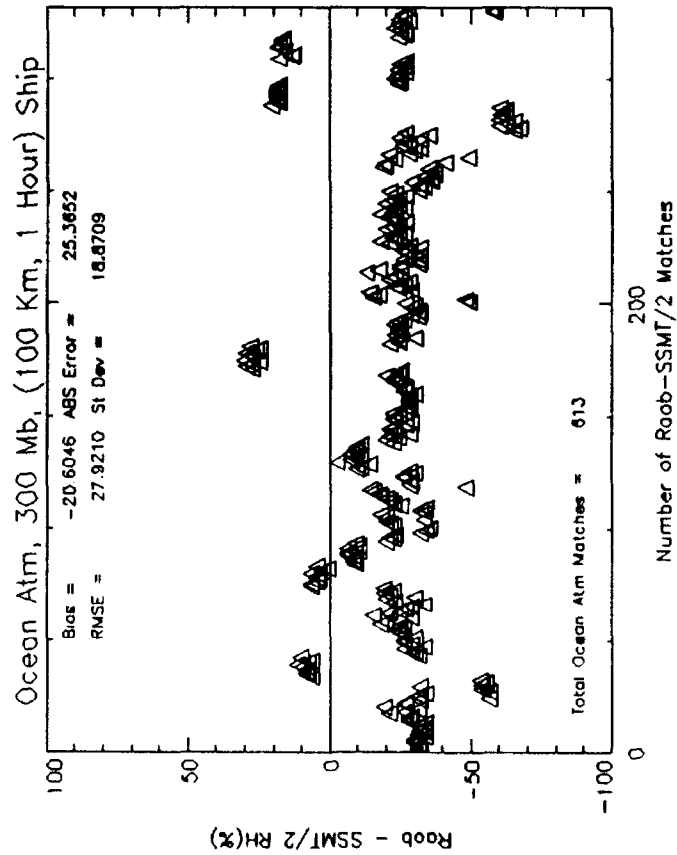
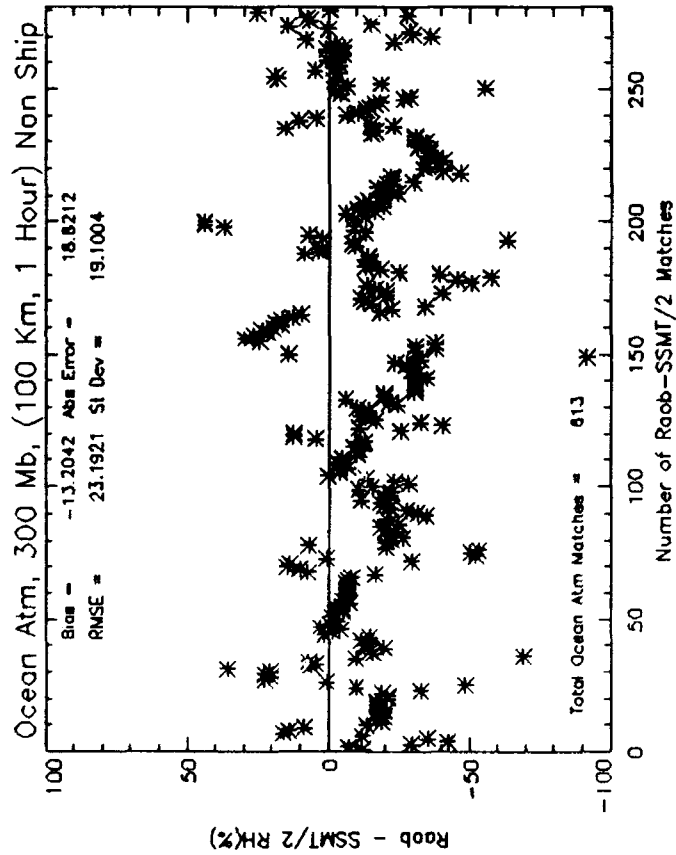




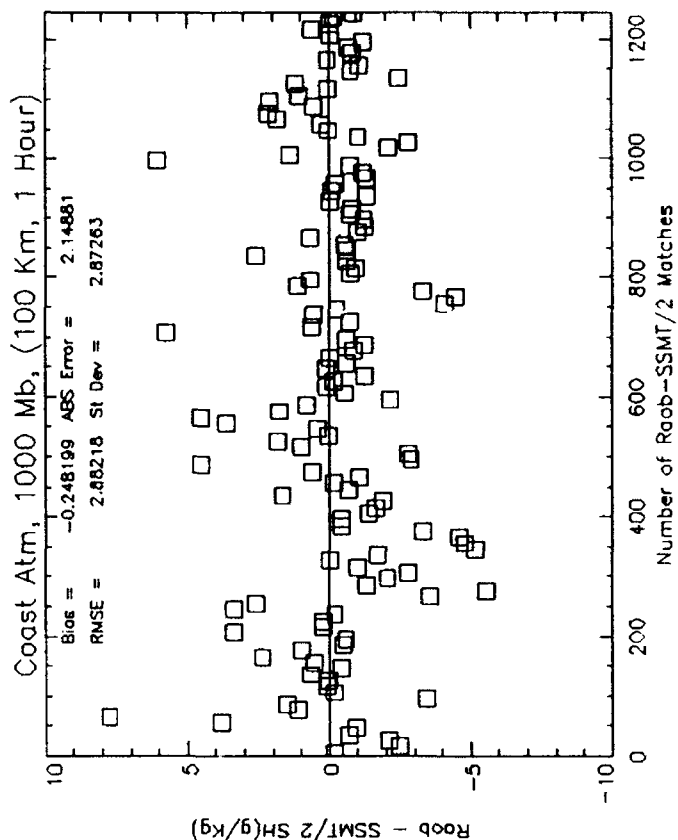
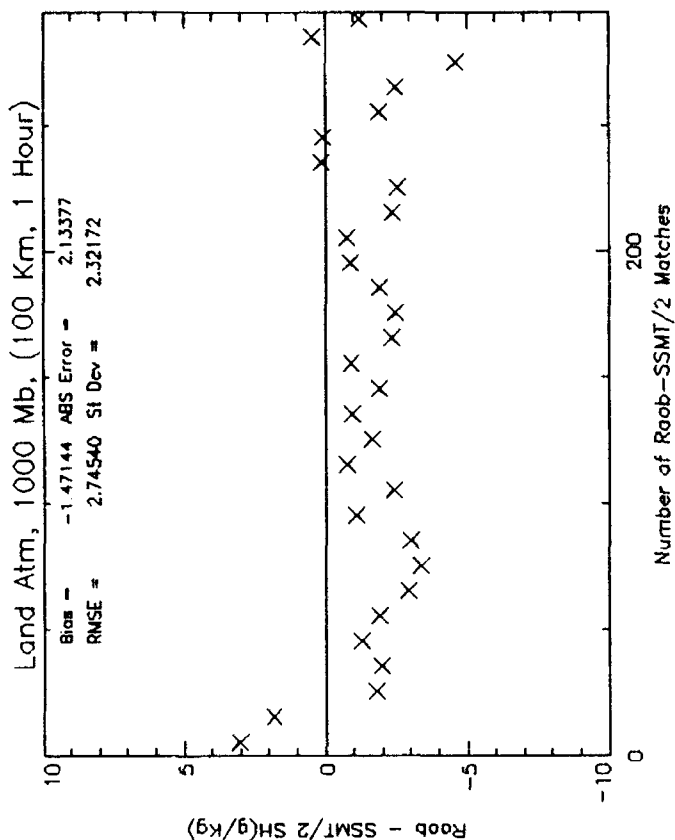
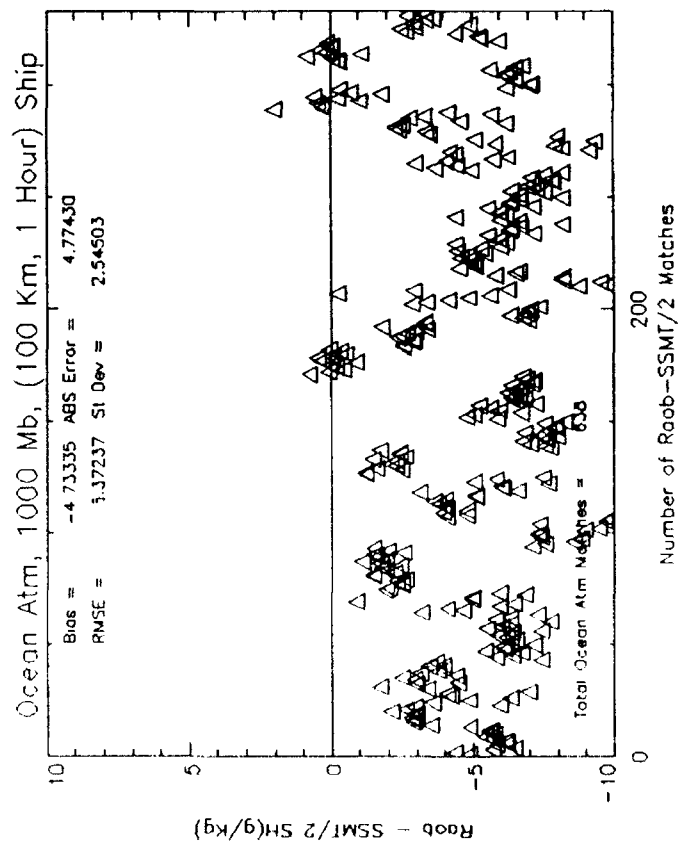
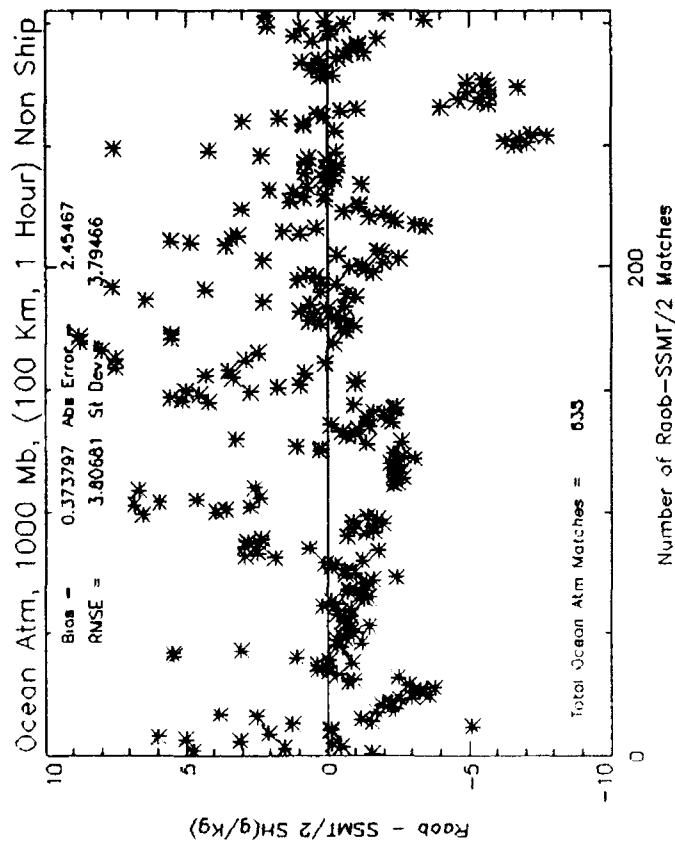


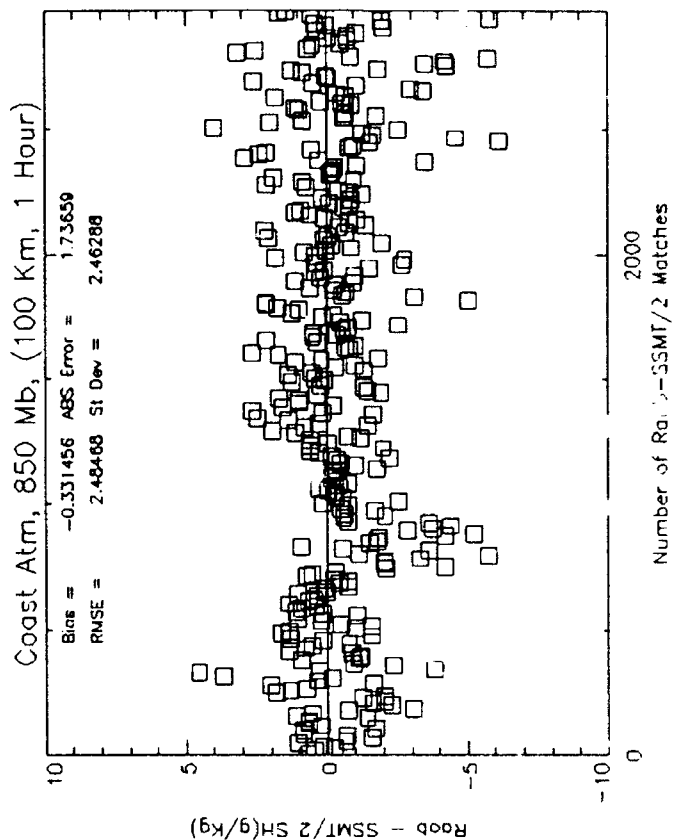
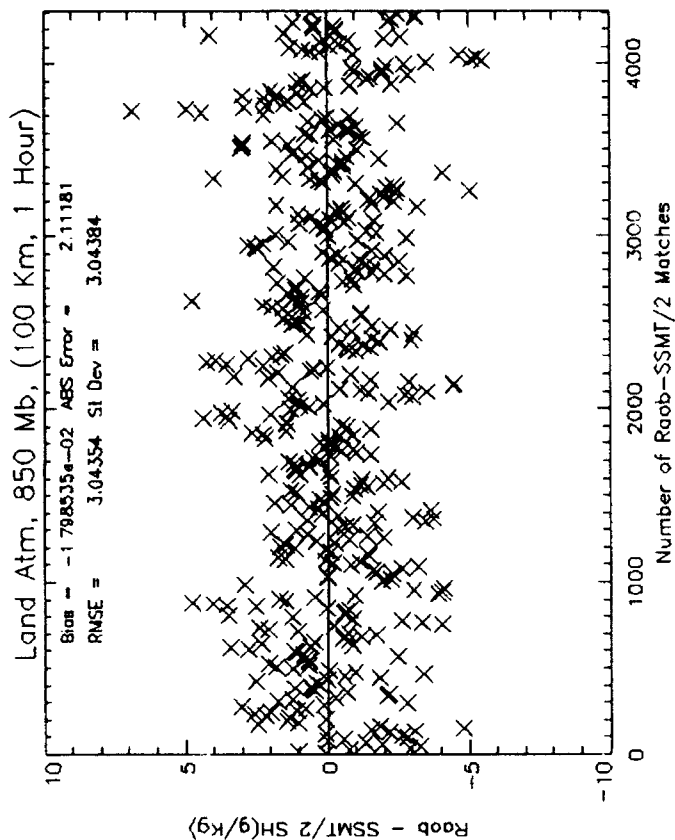
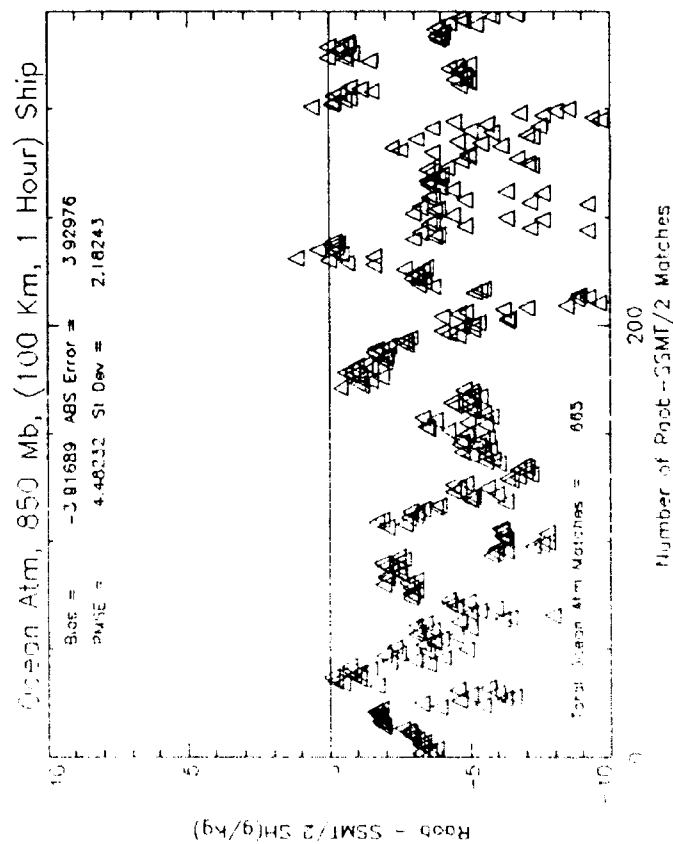
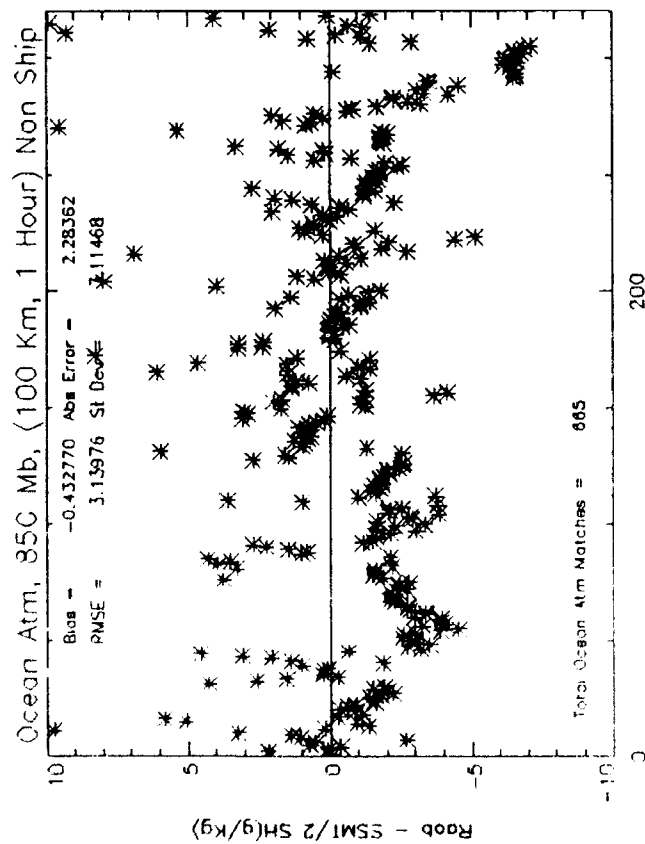


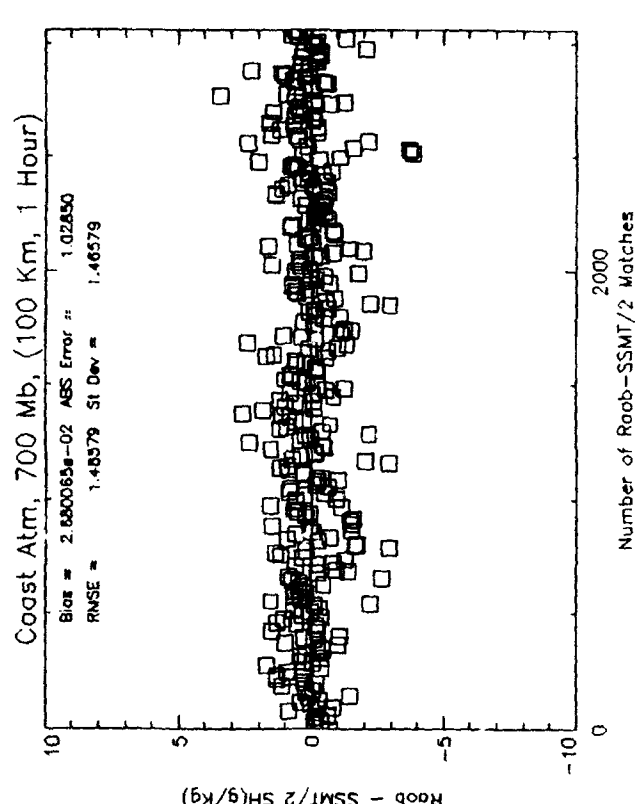
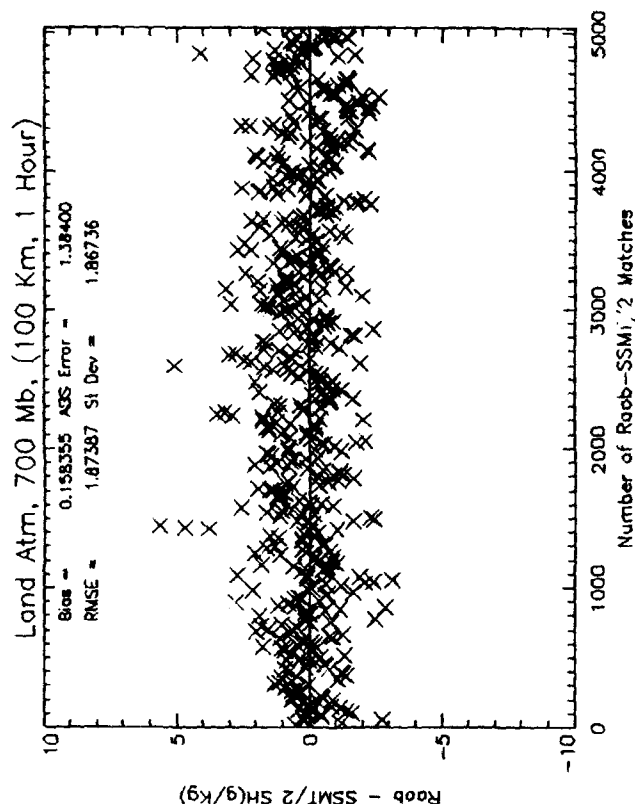
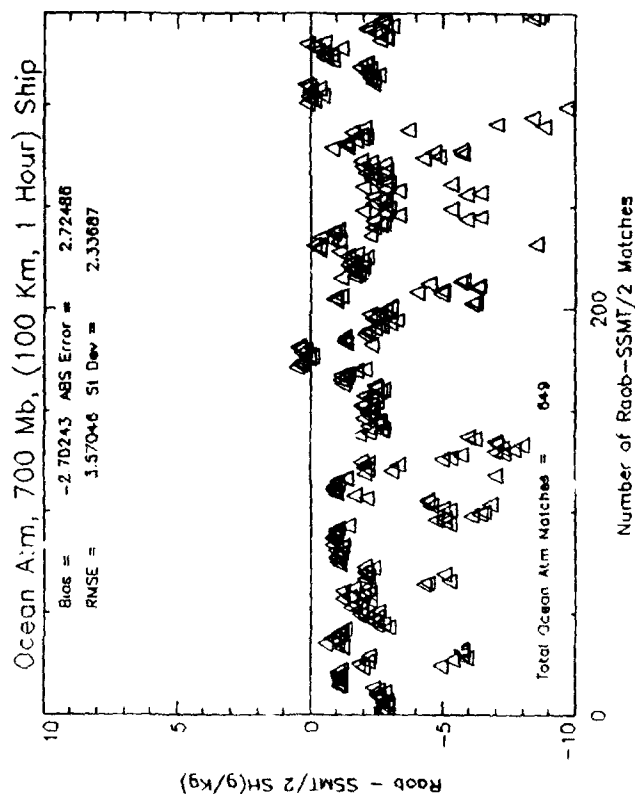
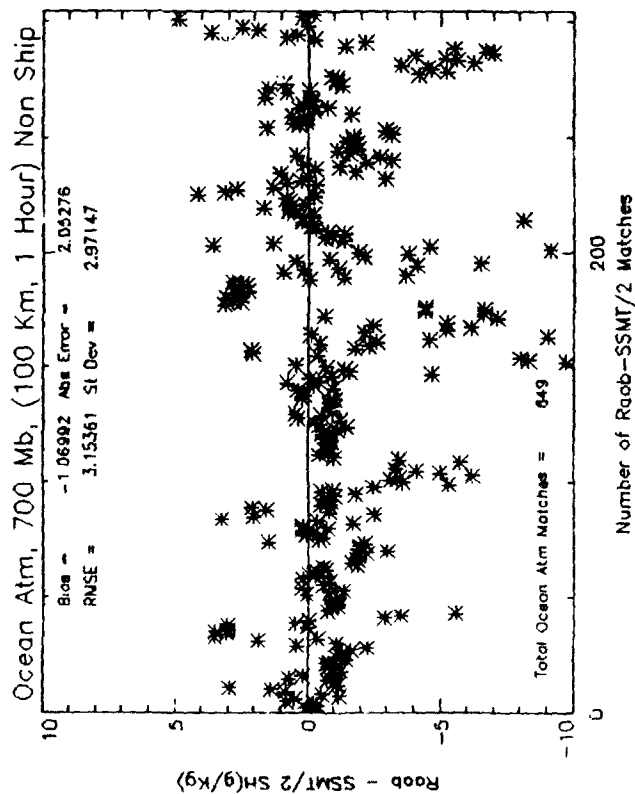


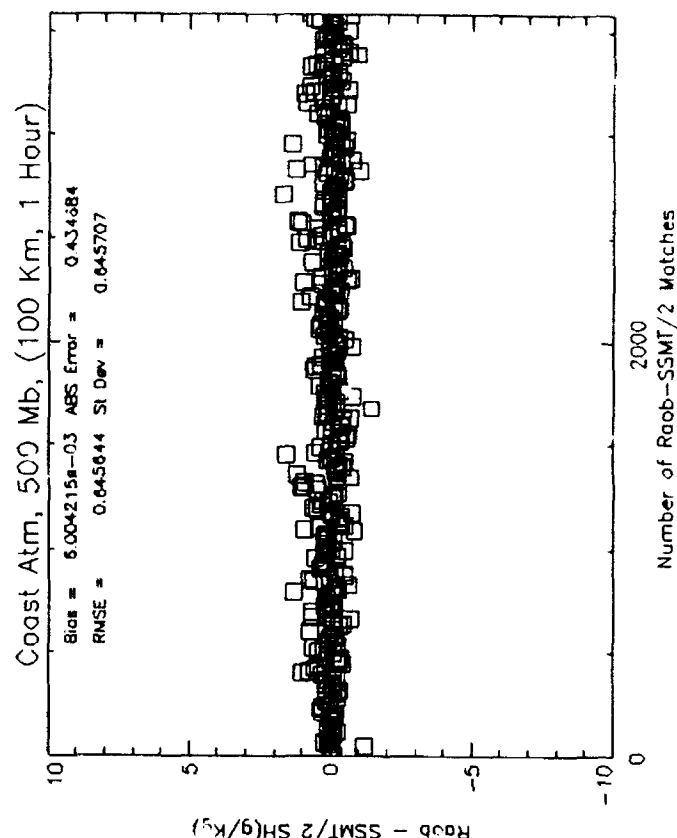
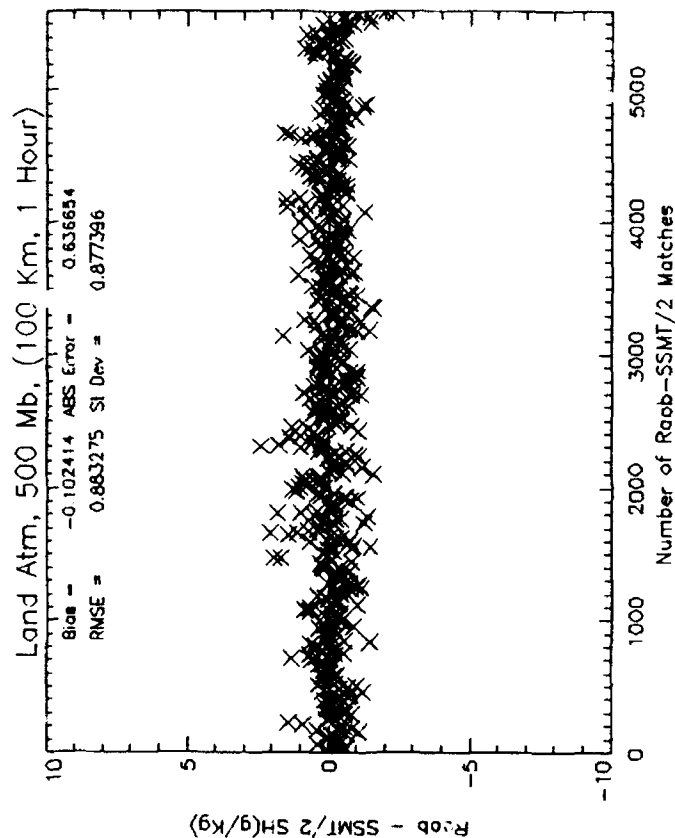
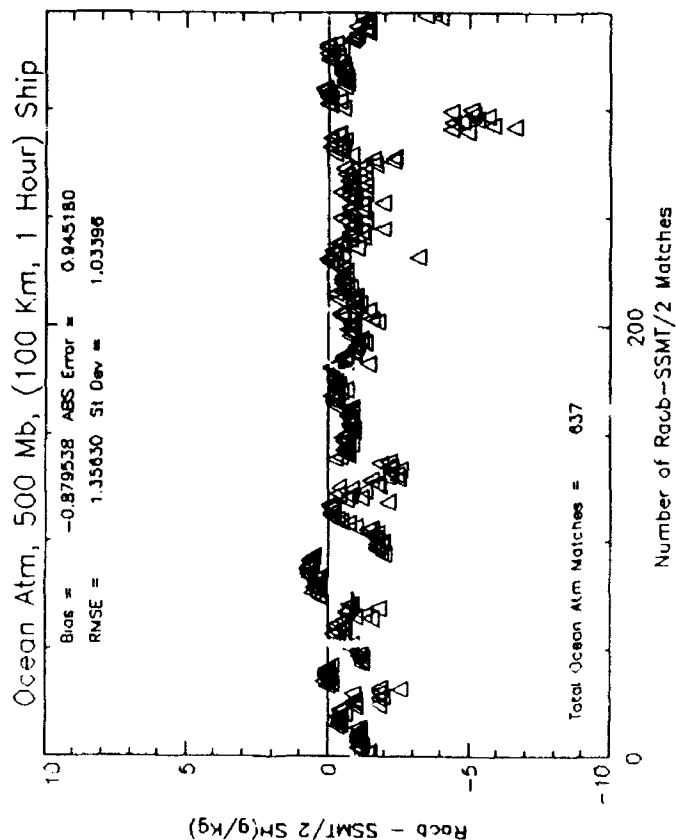
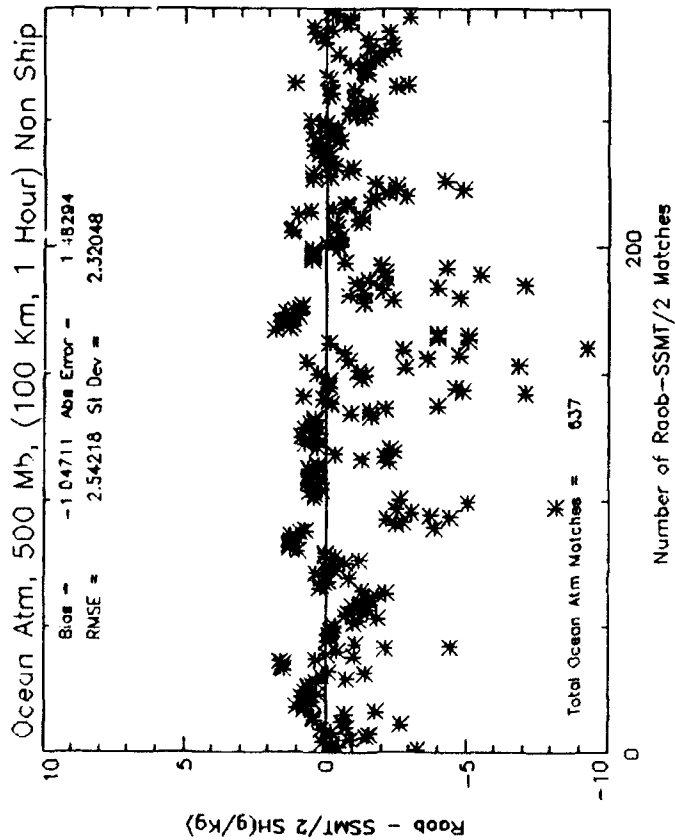


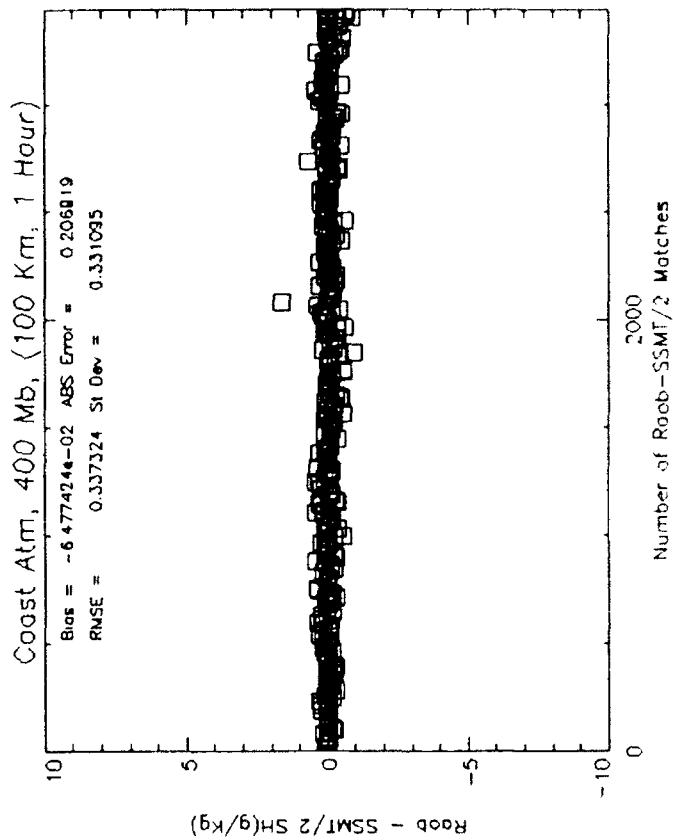
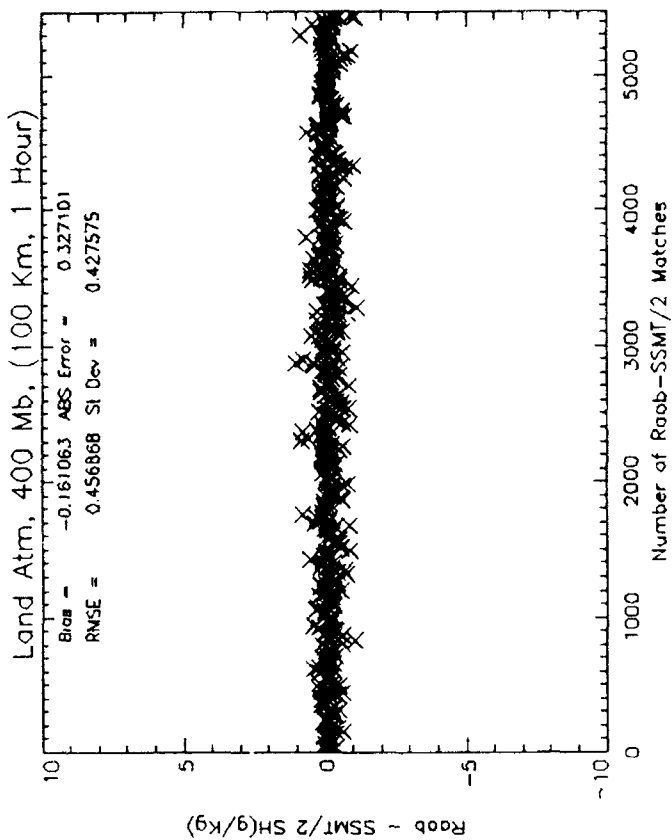
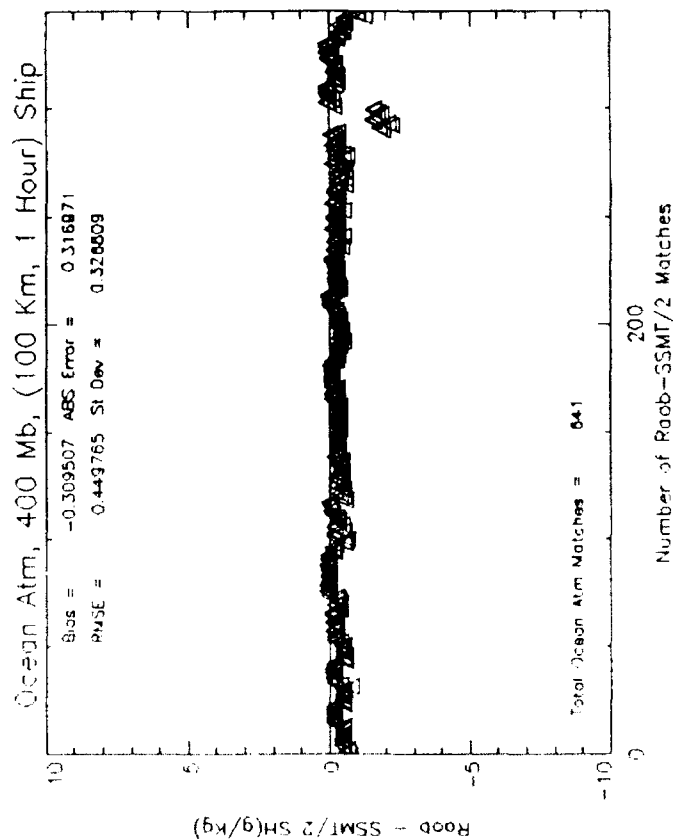
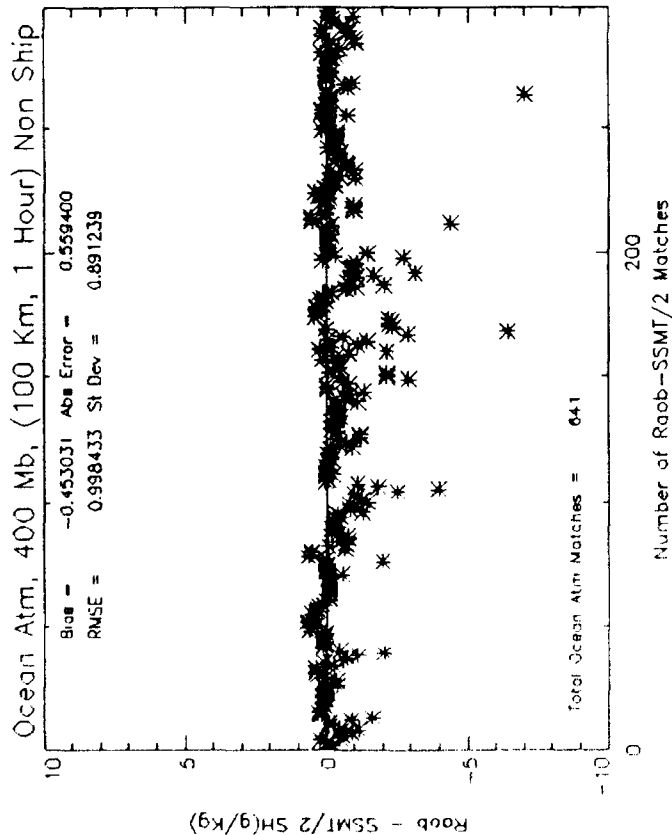


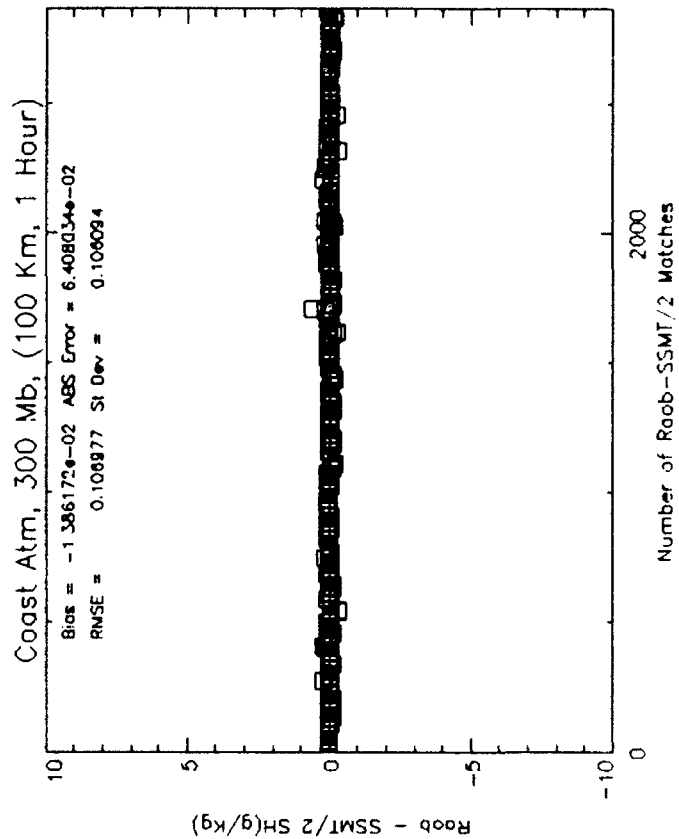
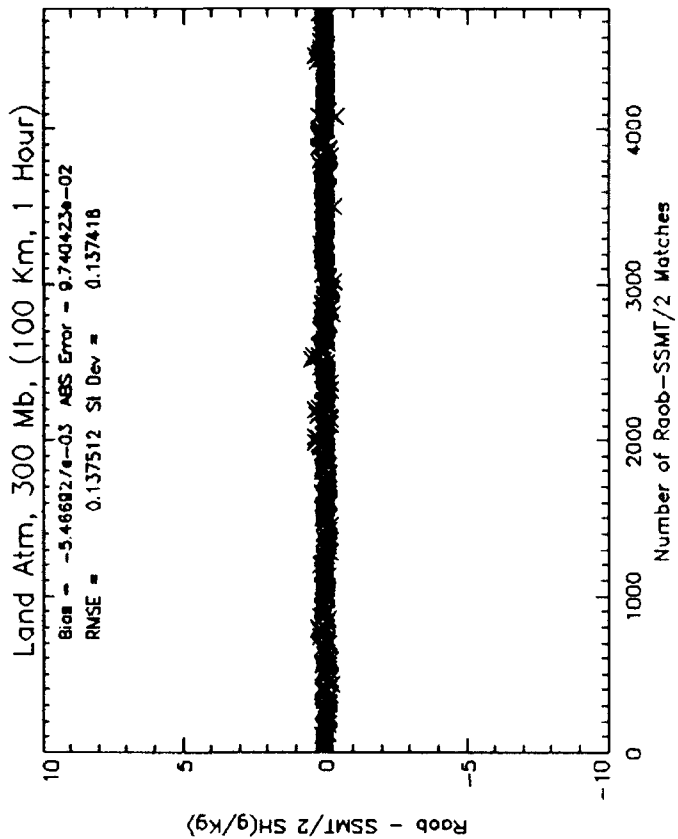
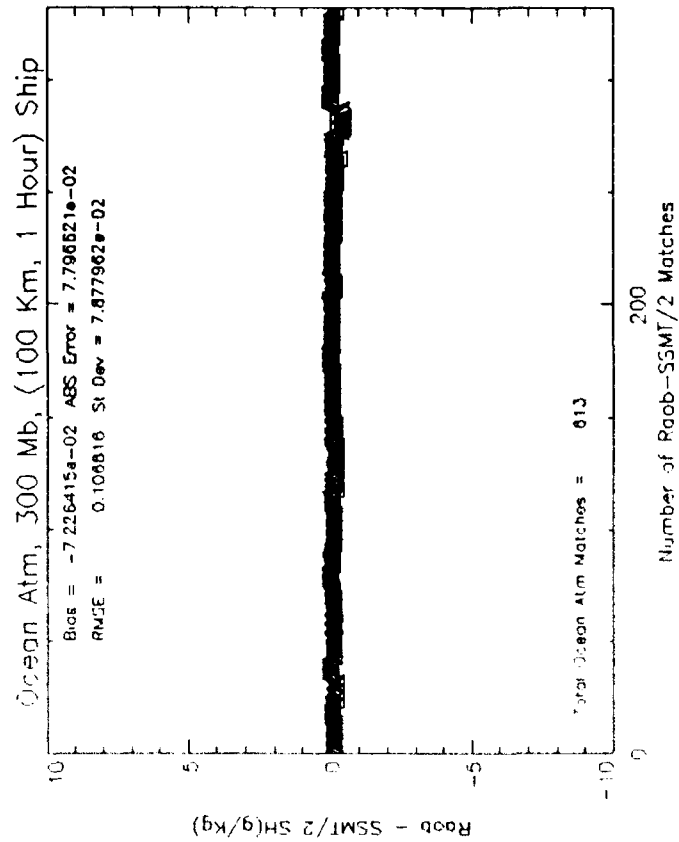
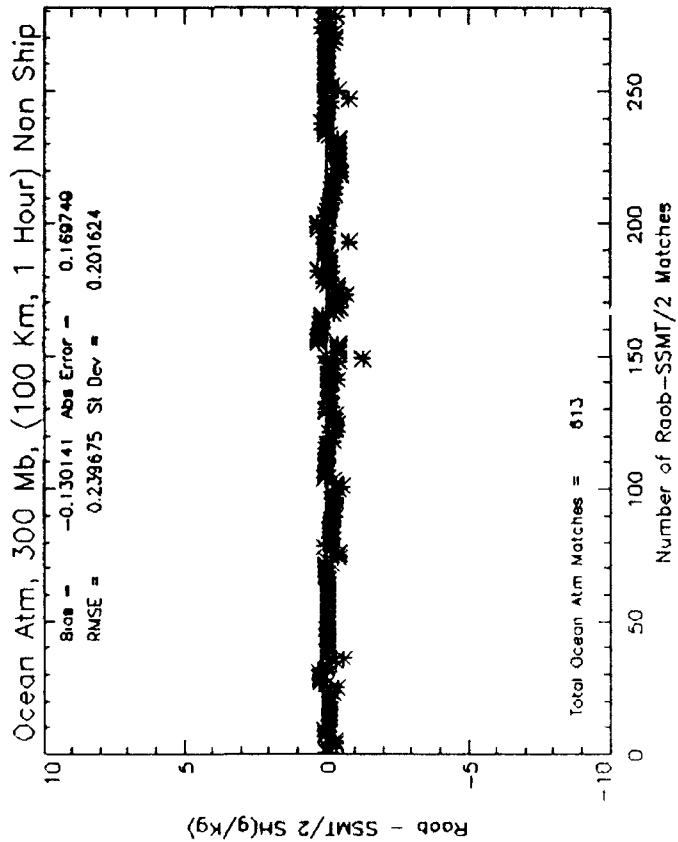




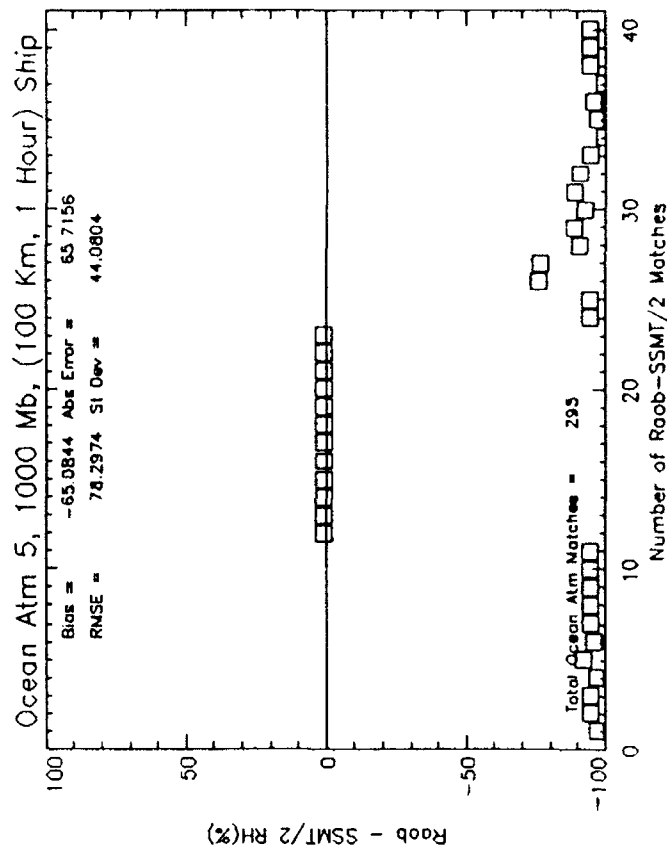
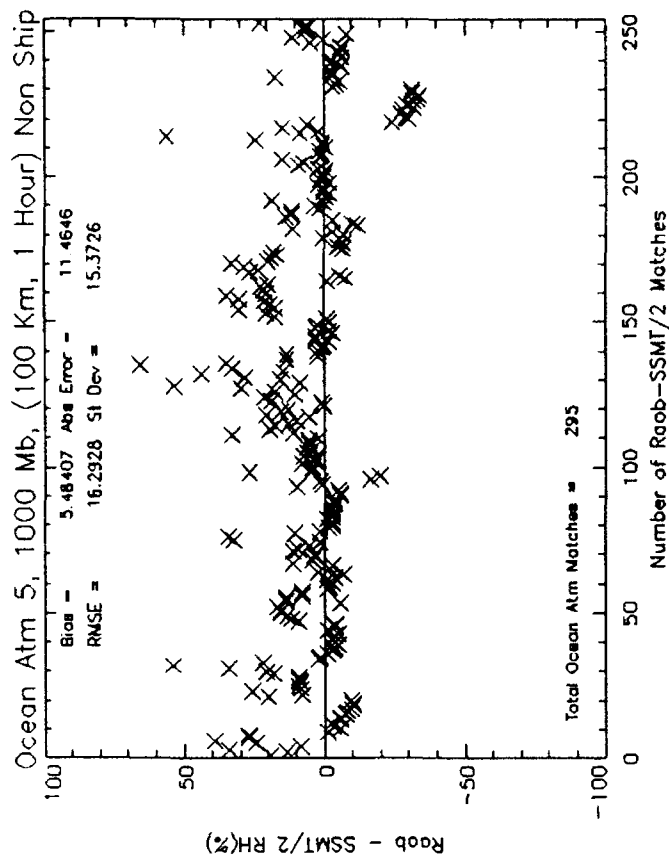
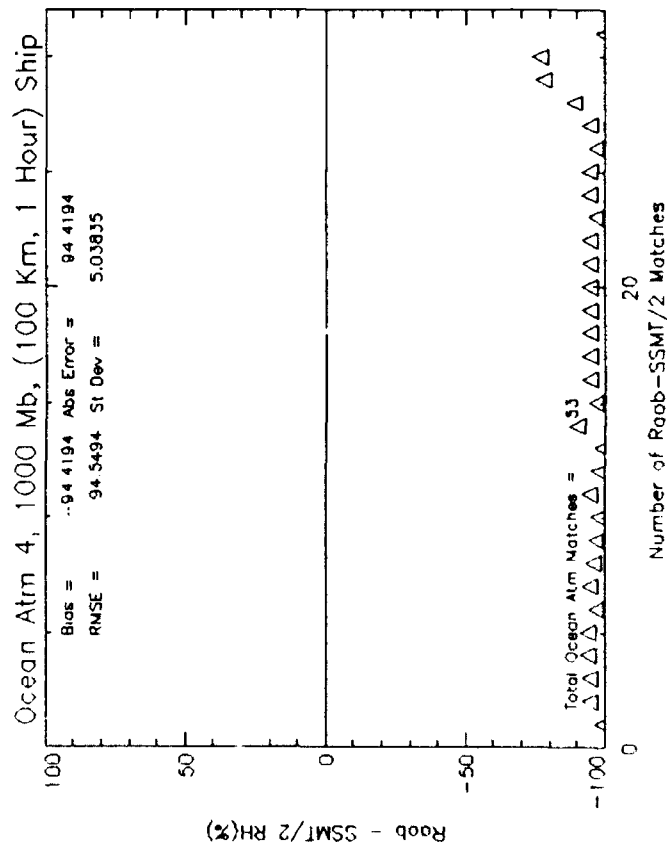
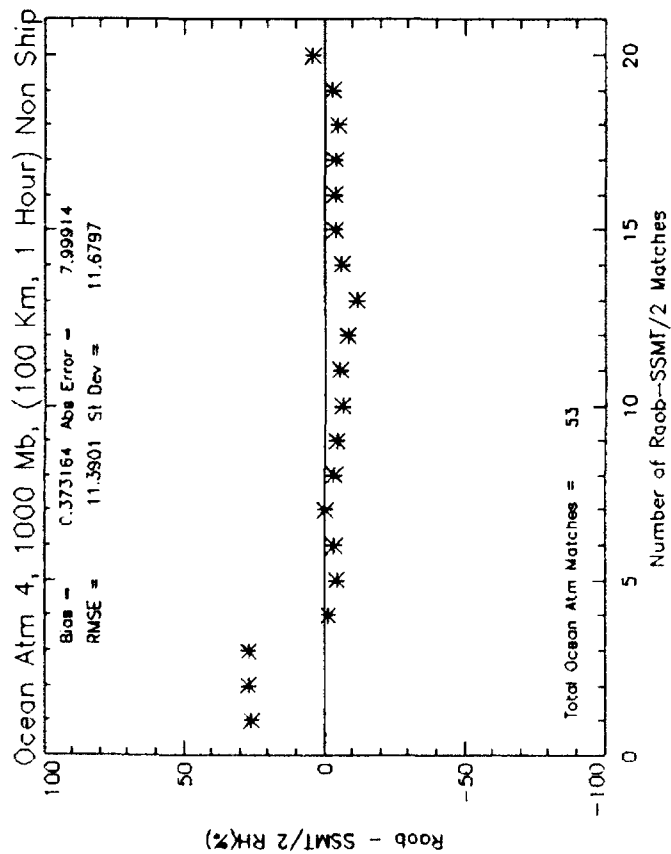




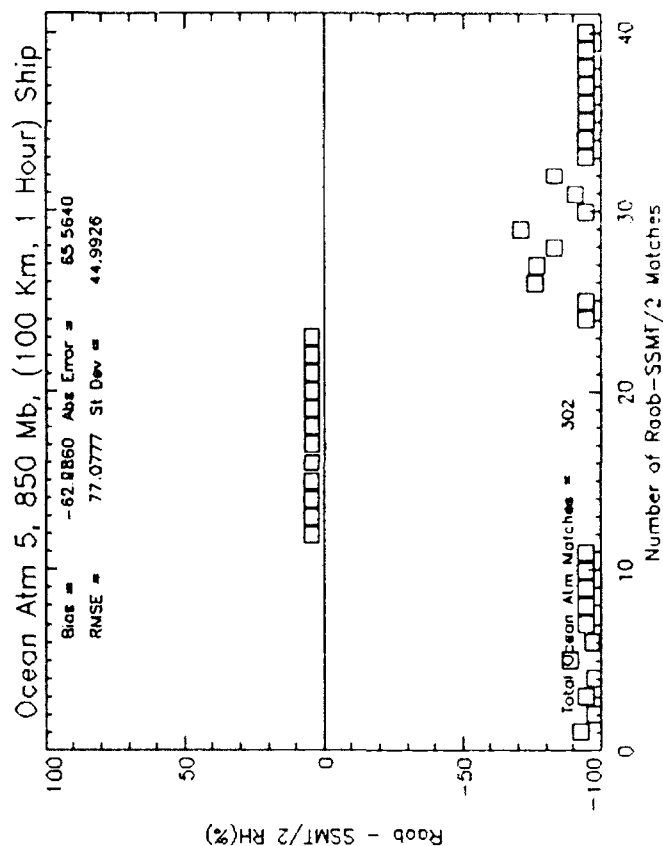
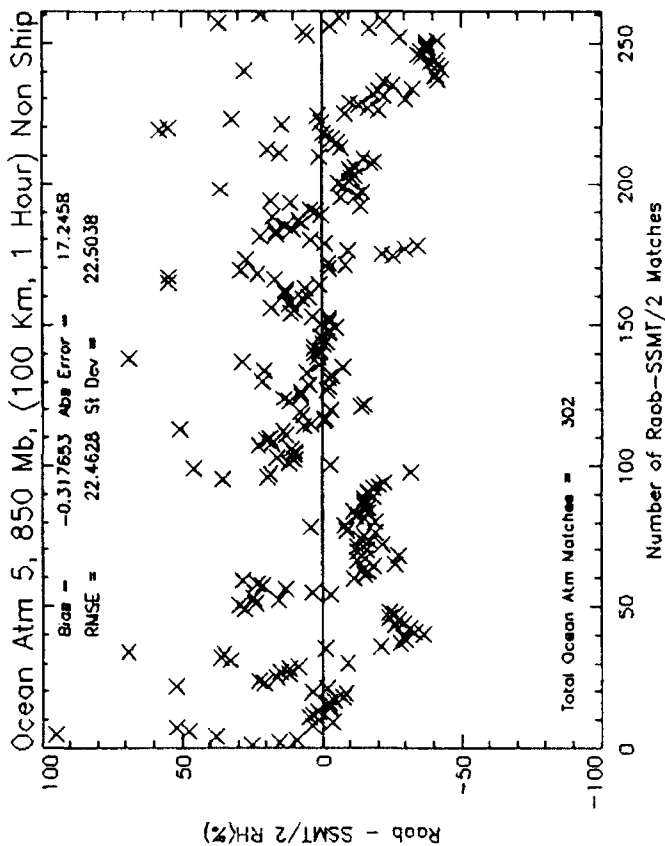
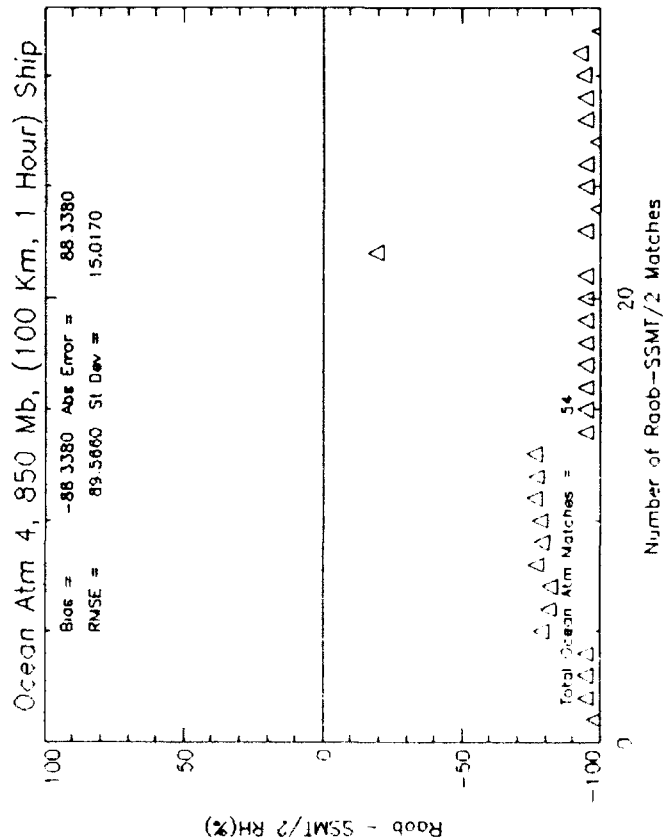
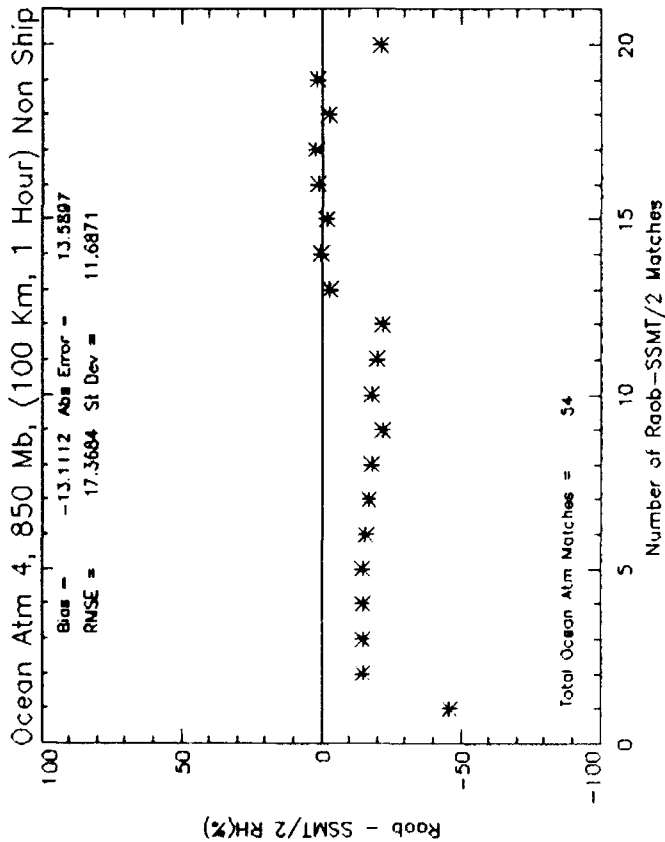


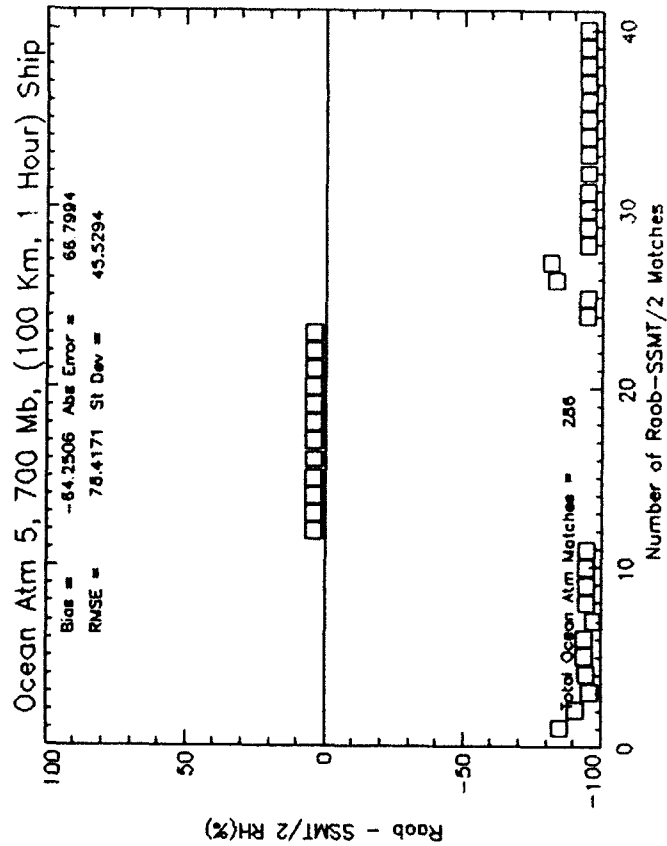
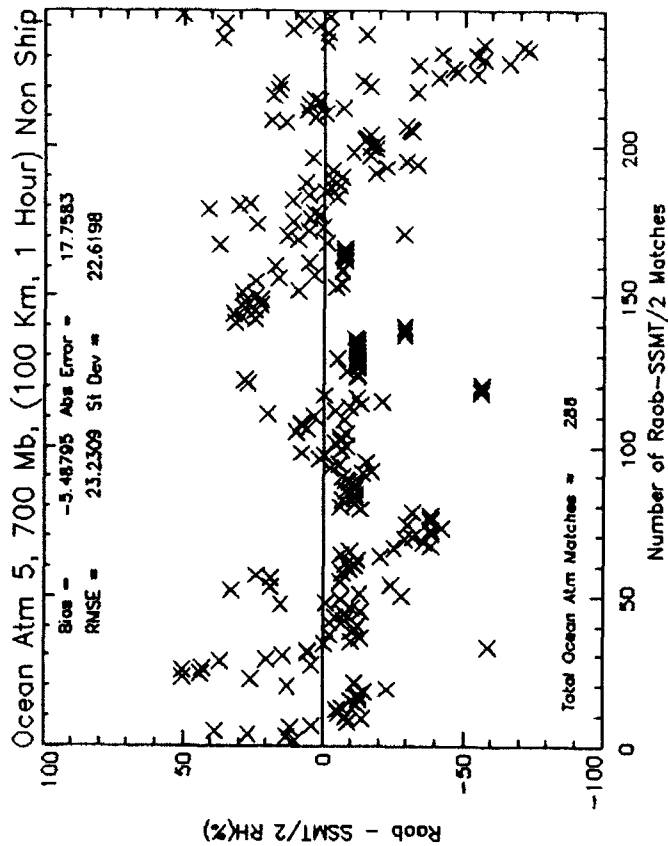
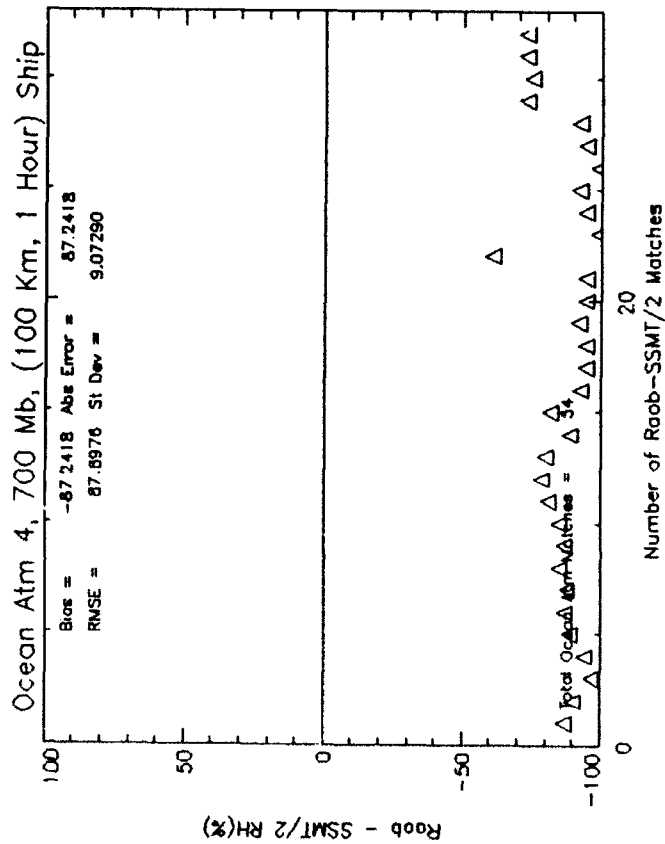
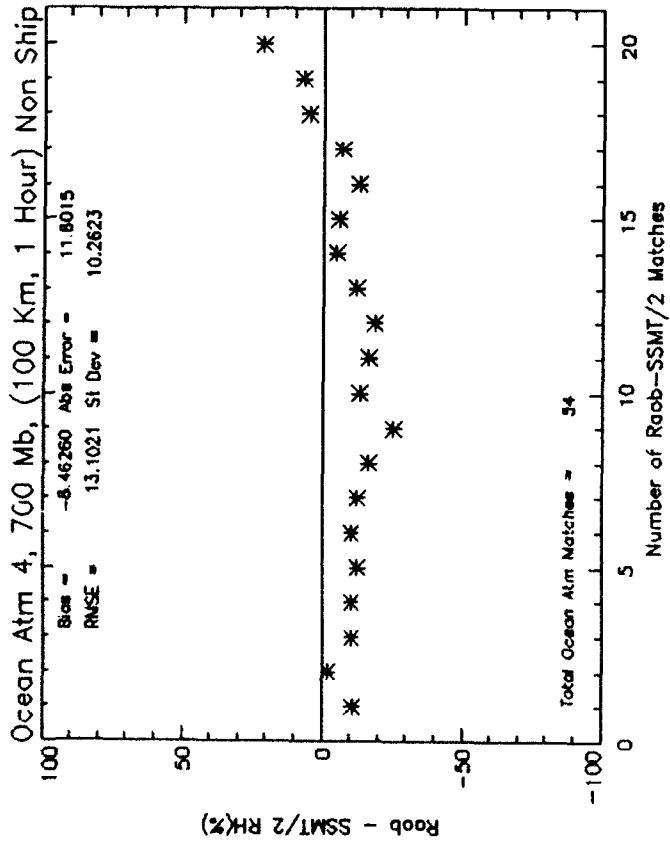


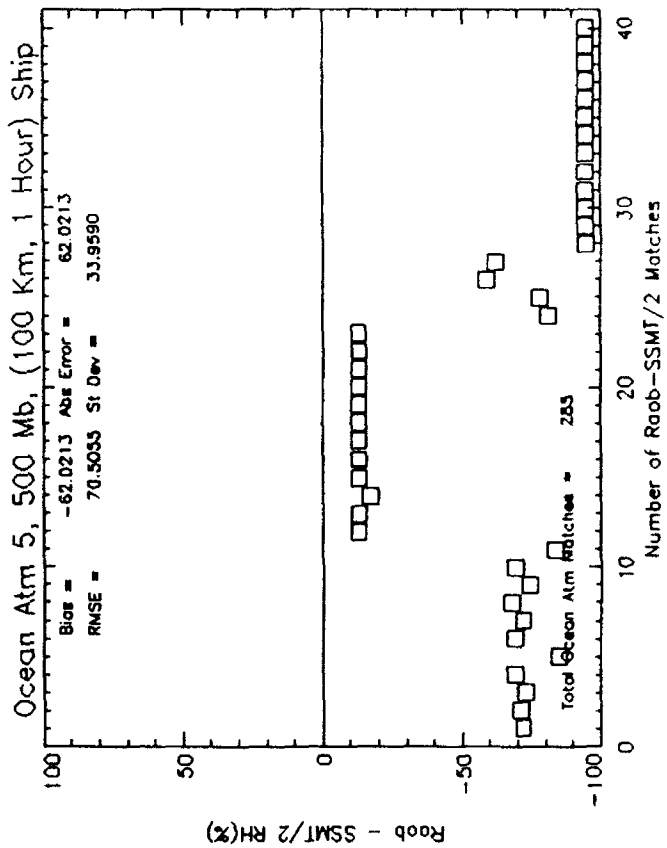
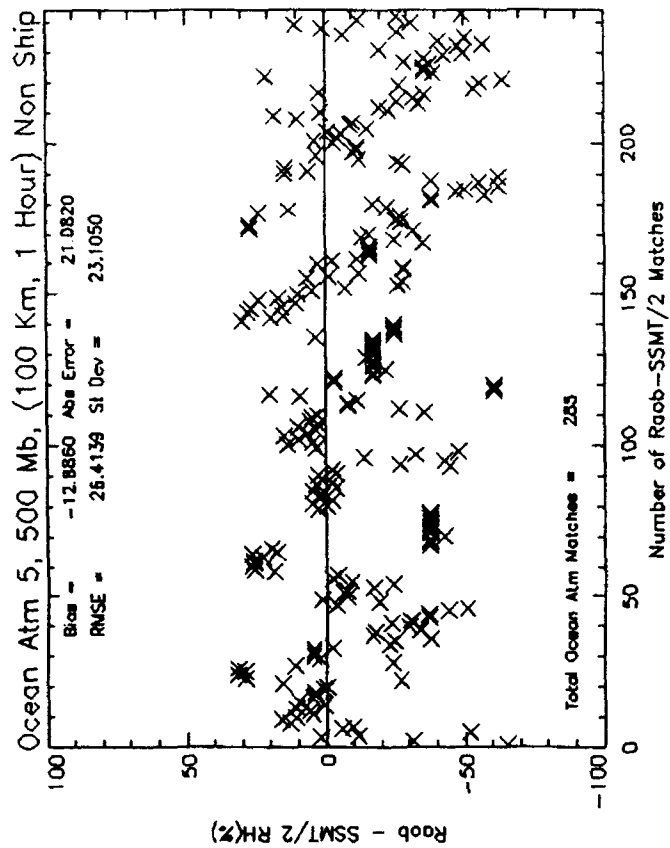
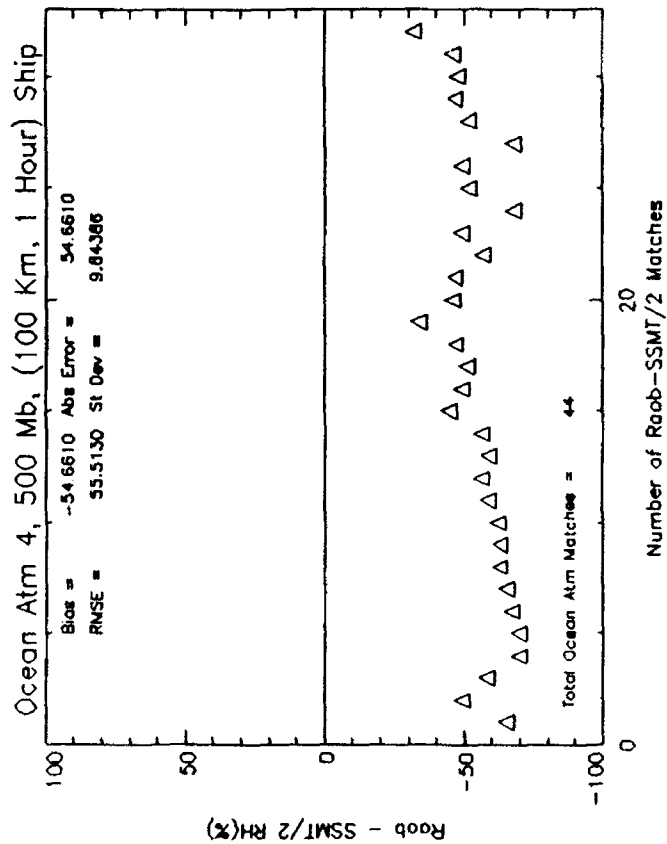
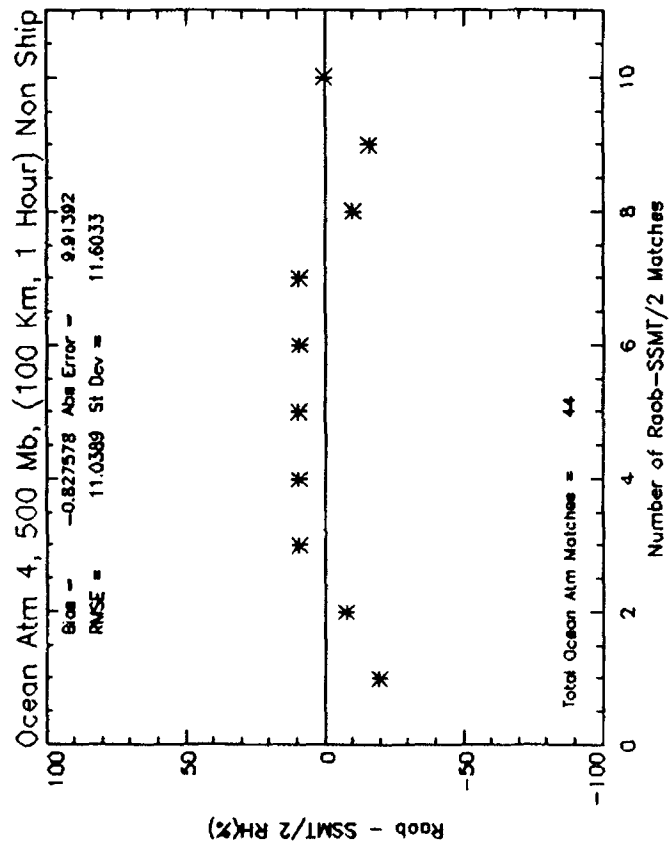
Appendix G. For the atmosphere types 1 through 5 with ocean backgrounds, the quantity (Radiosonde - SSM/T-2) RH and Q plotted on the ordinate, and the index of the co-locations on the abscissa. Each four-plot panel represents one atmospheric level. The co-location criteria are annotated at the top of the plots.

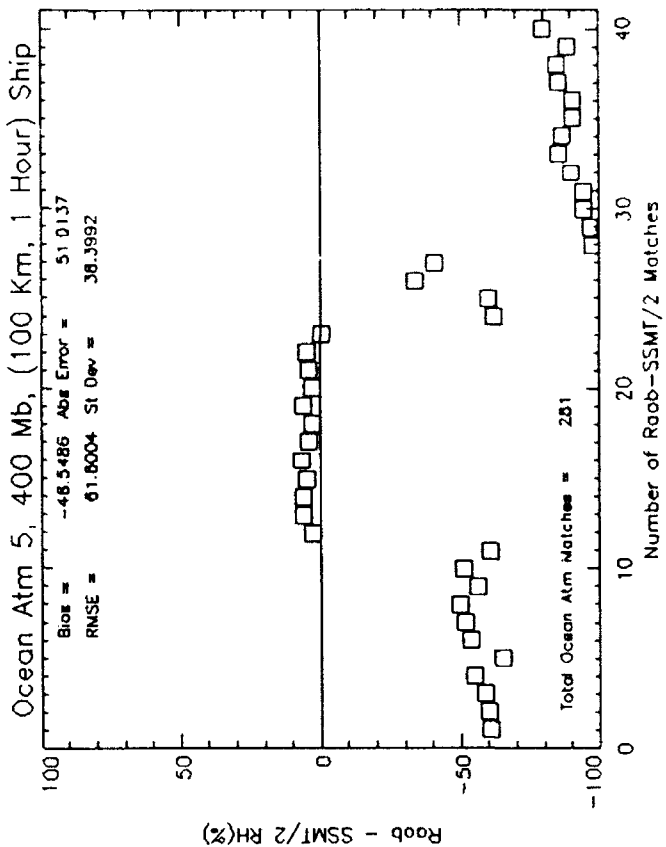
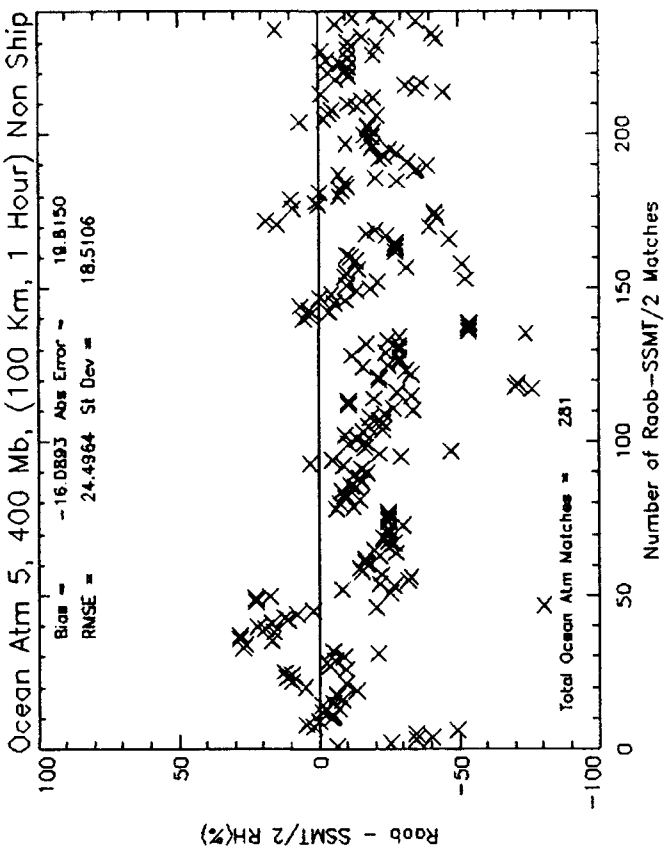
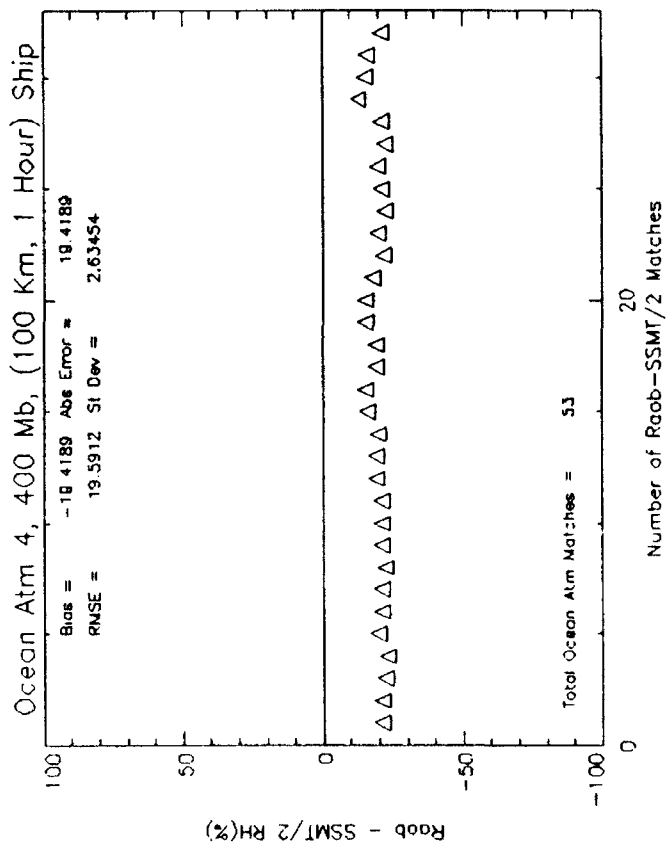
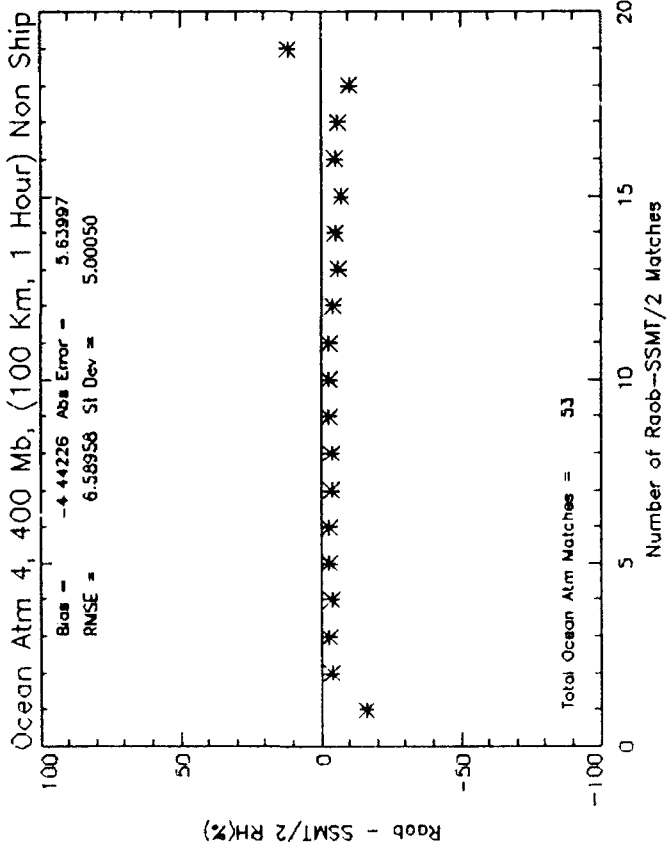


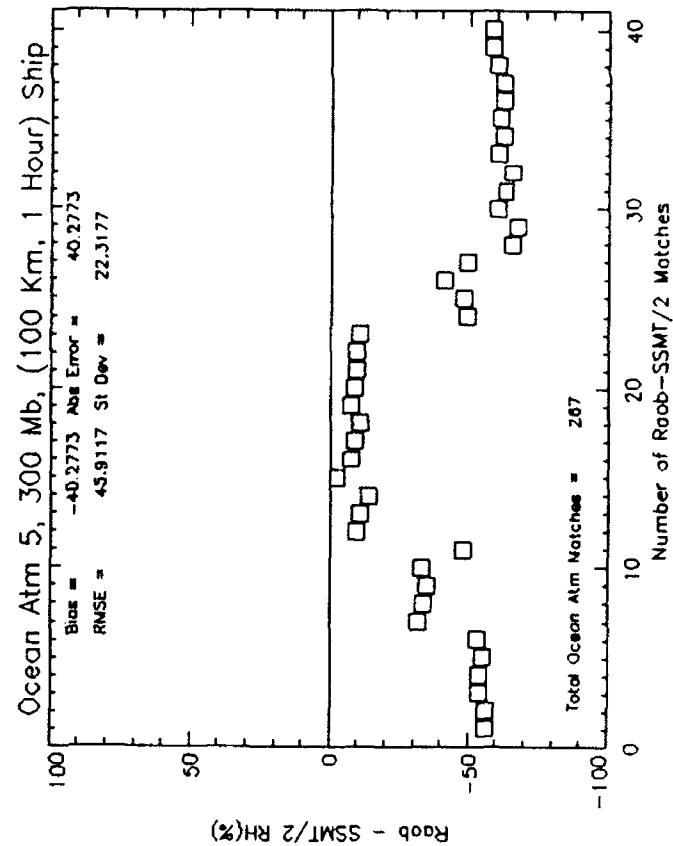
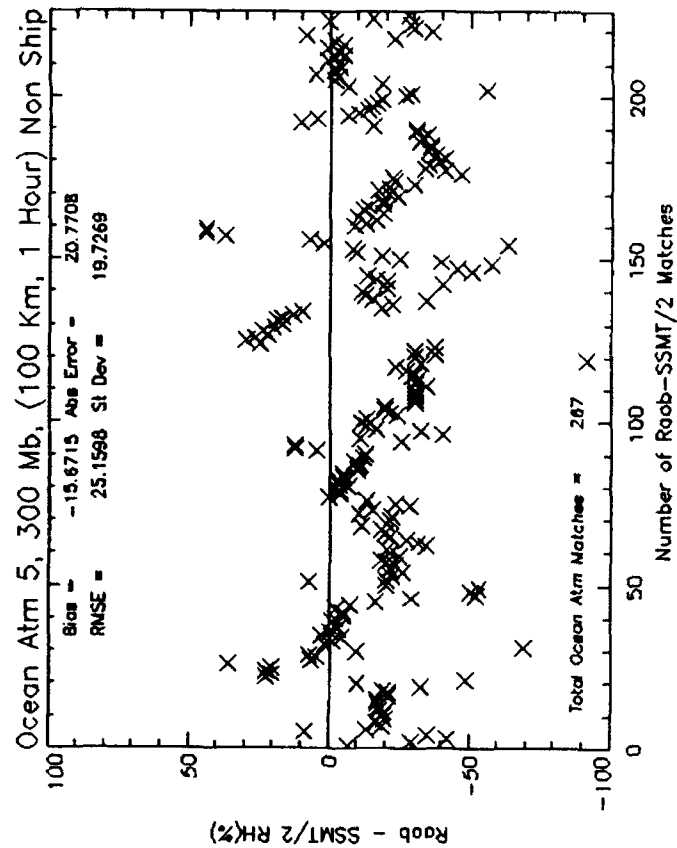
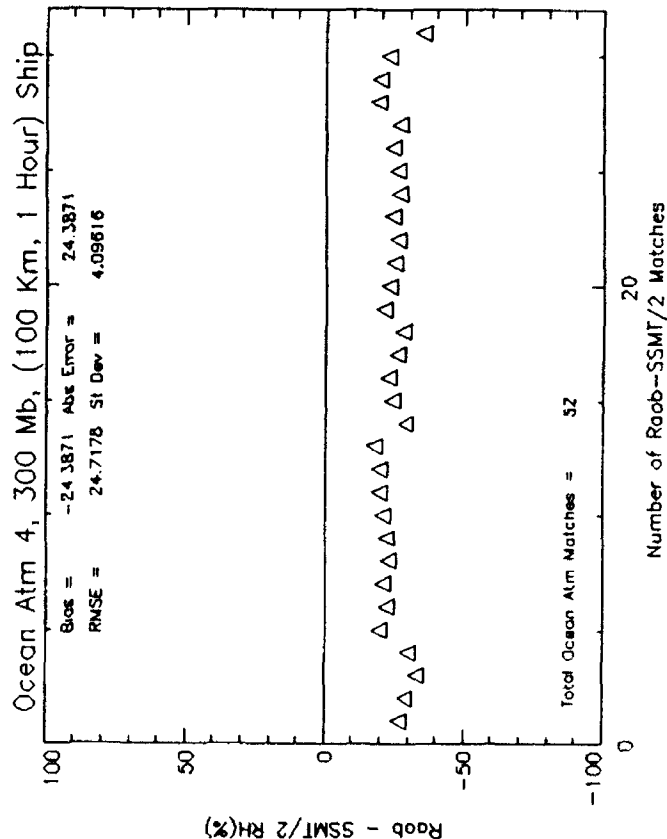
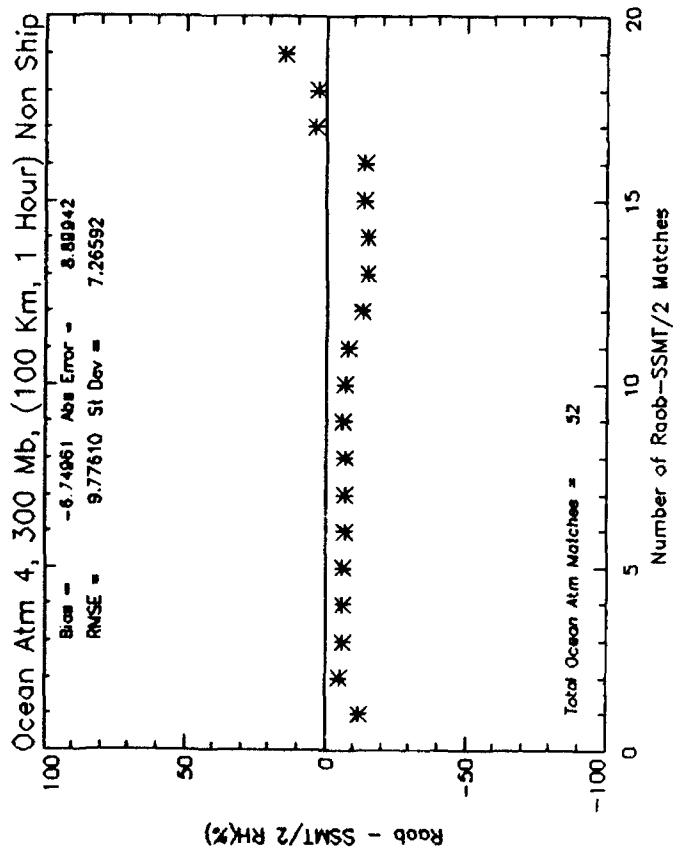


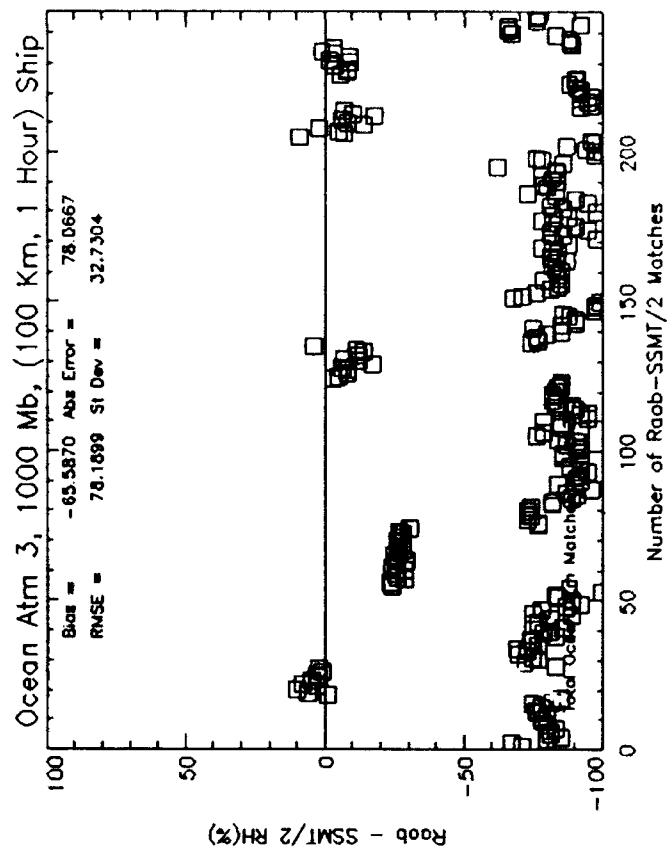
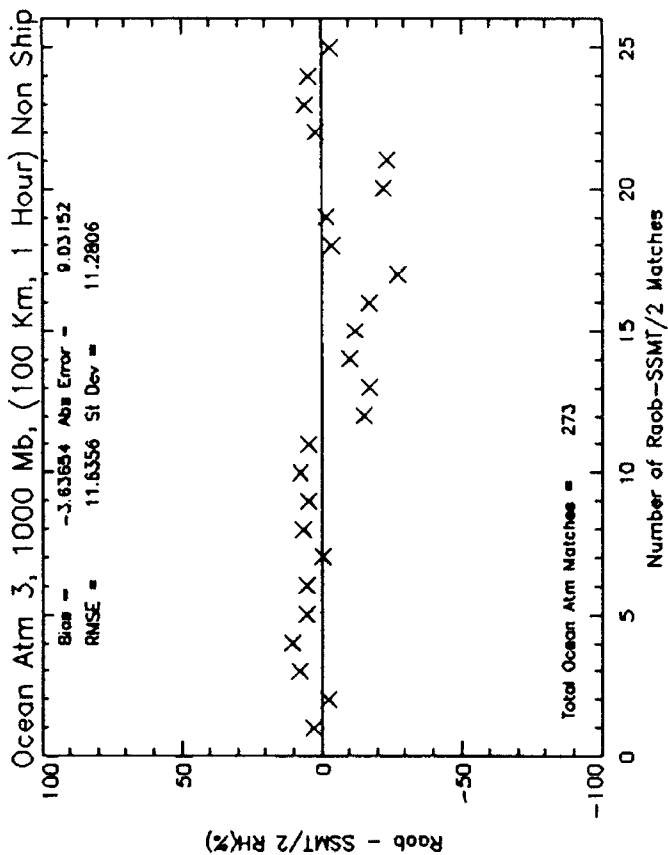
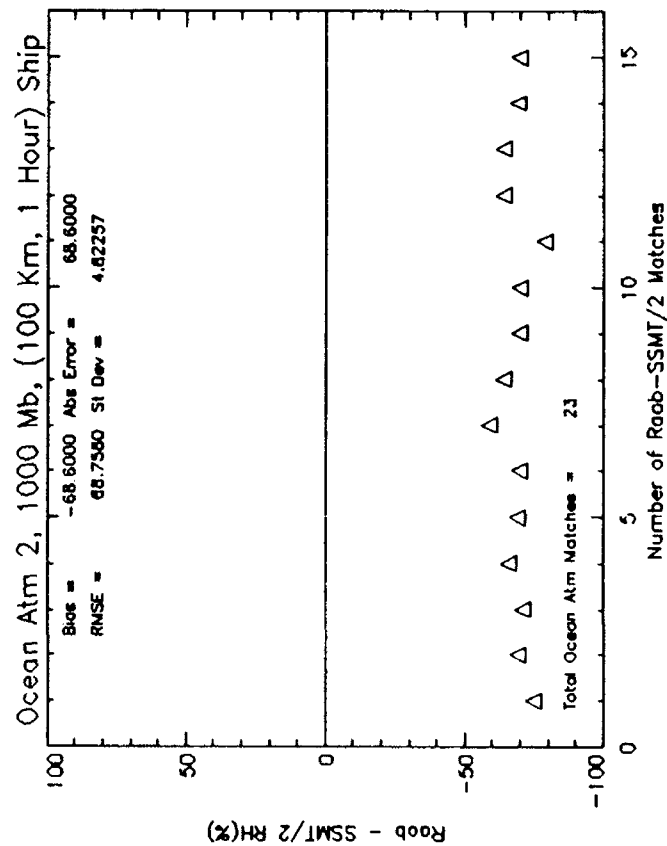
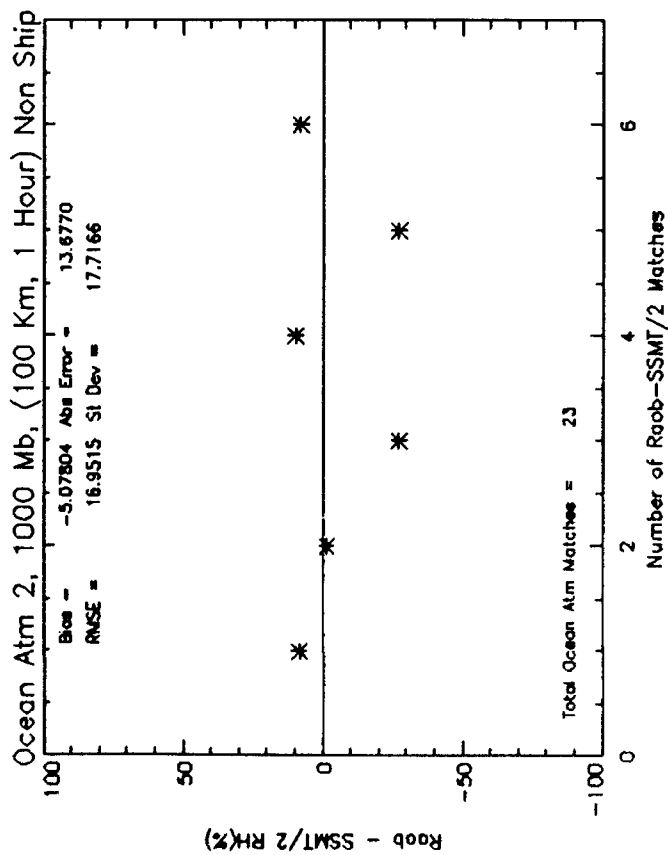


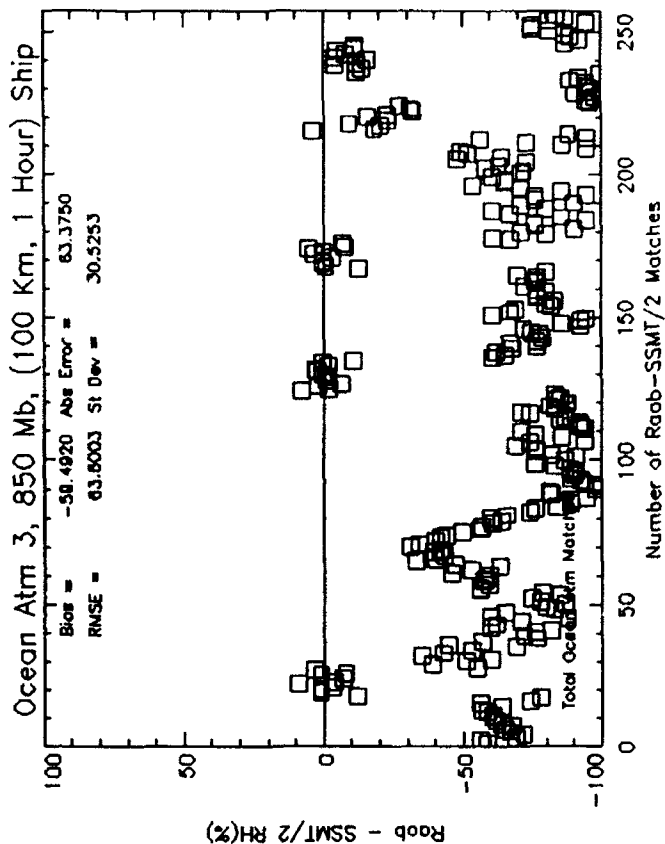
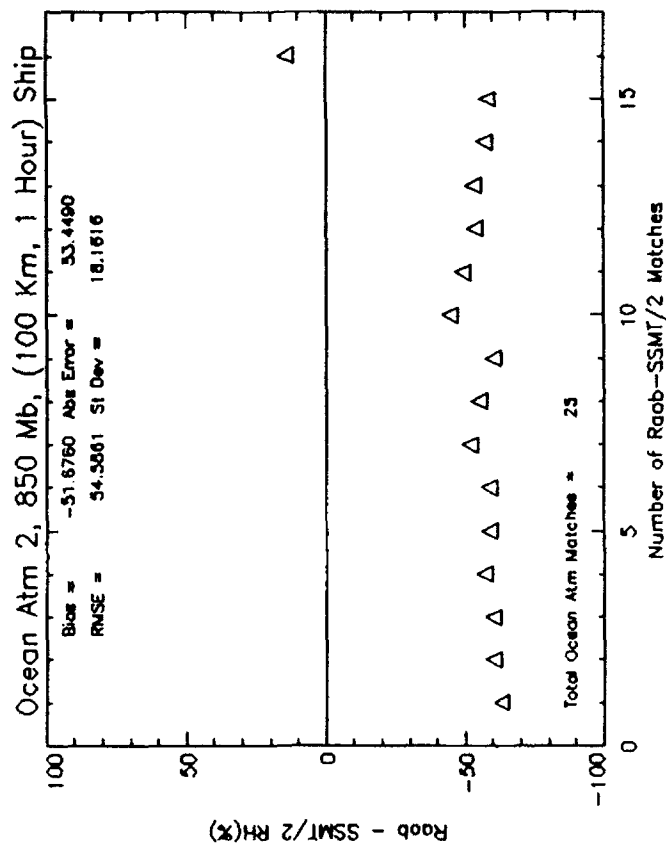
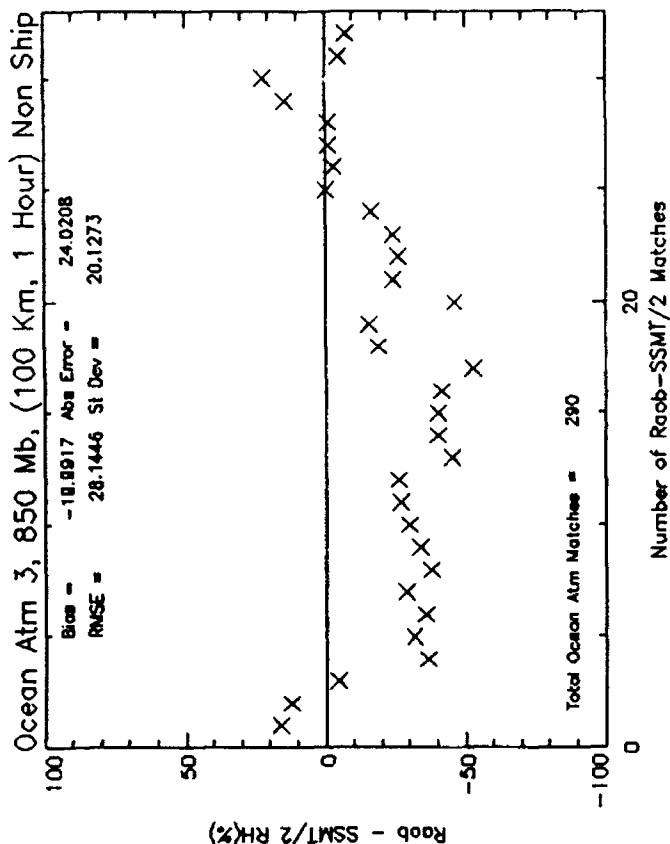
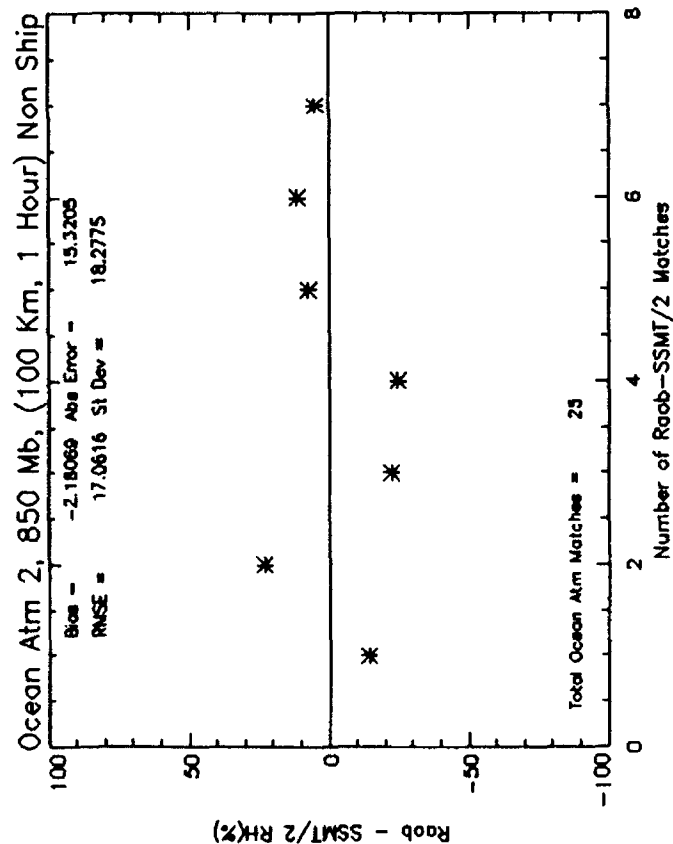


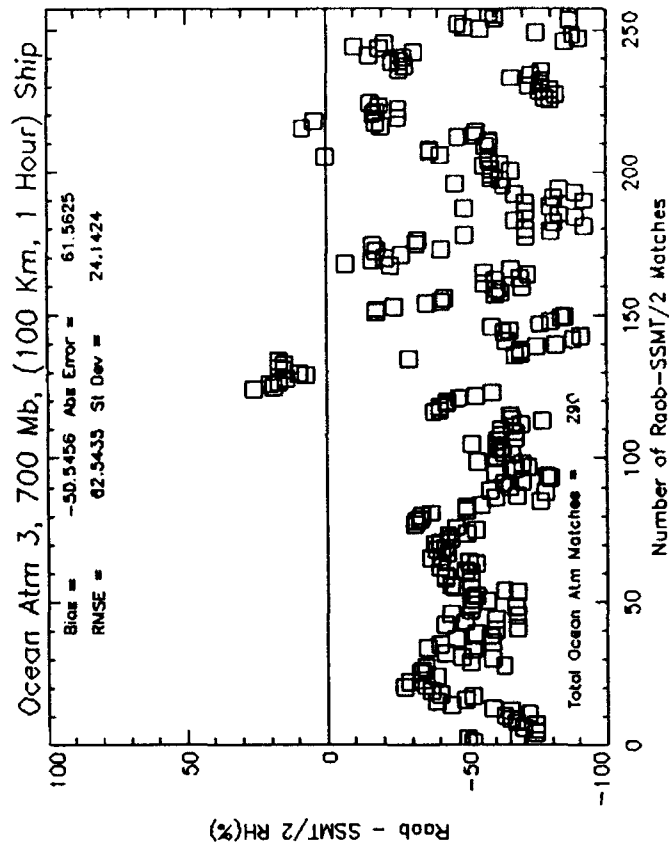
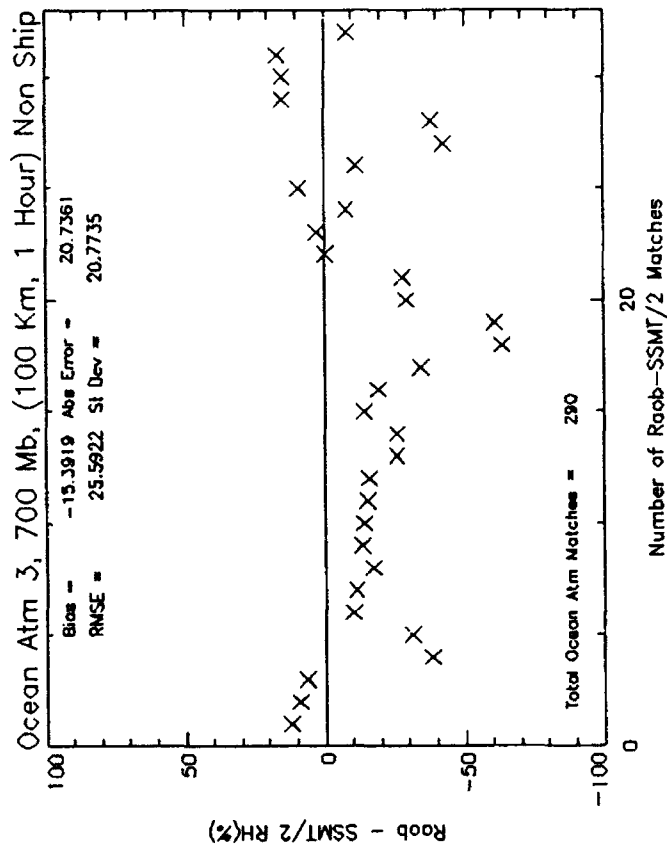
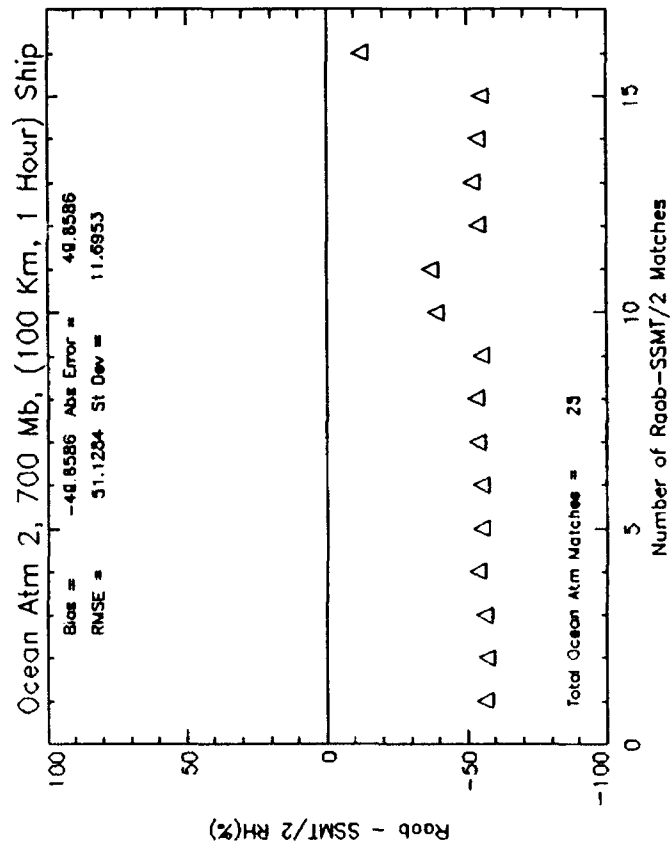
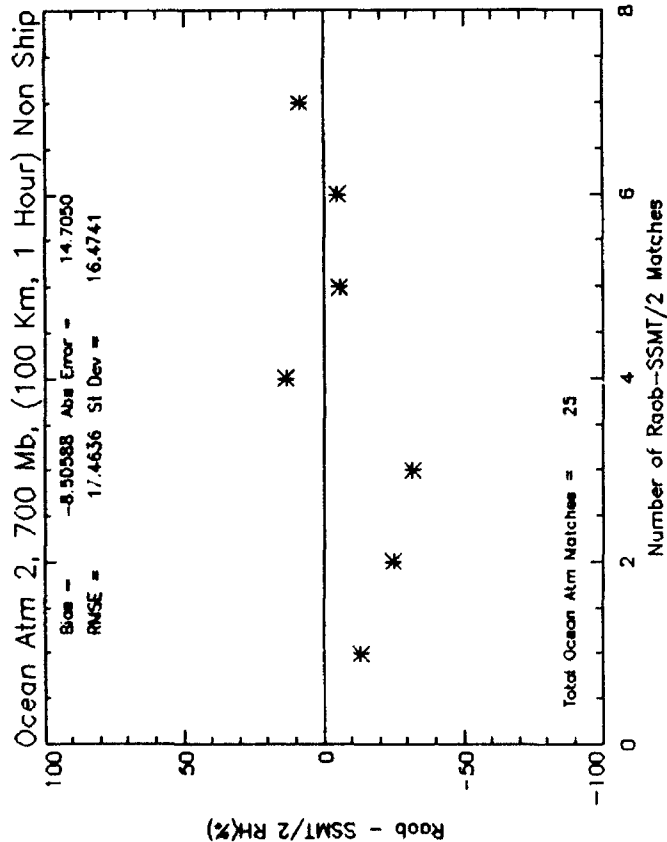




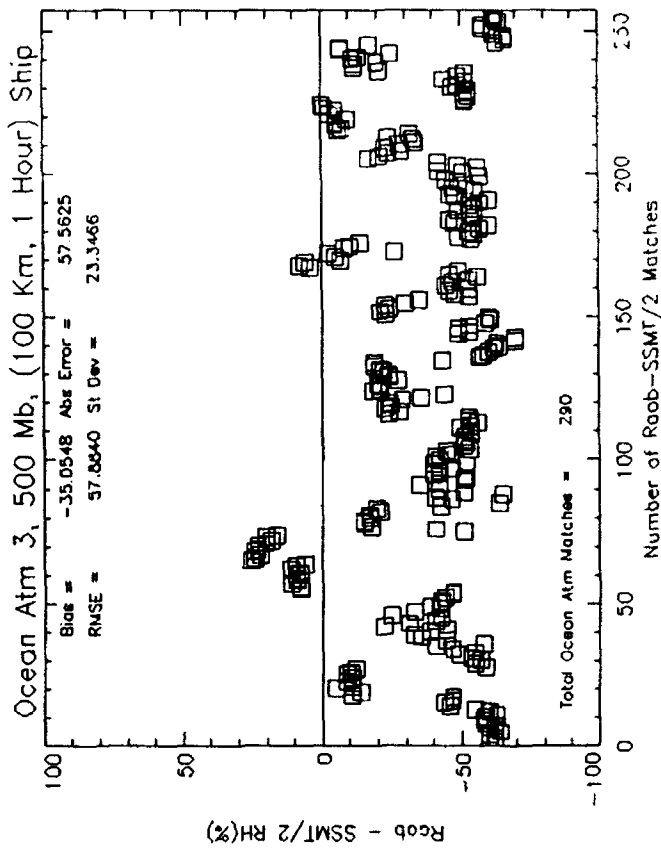
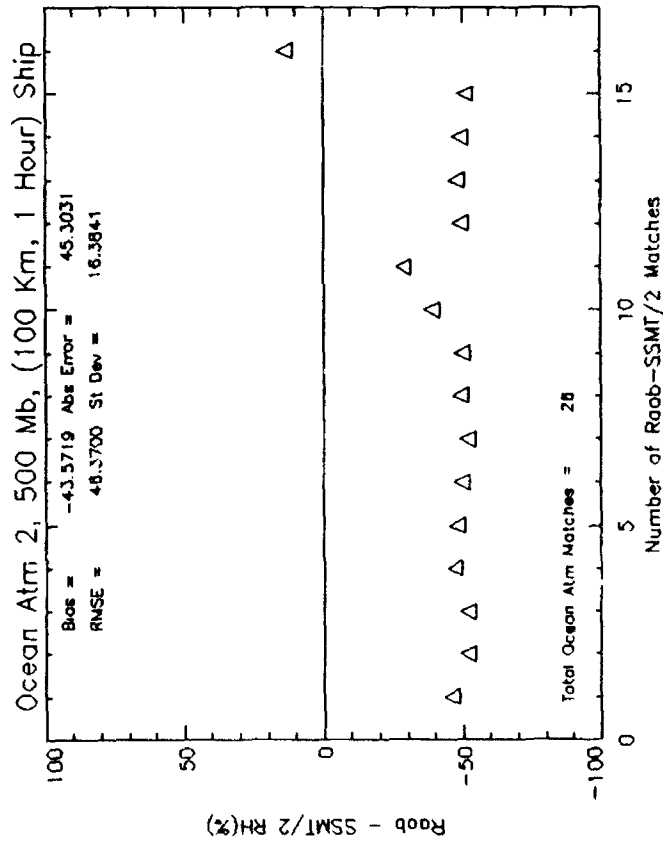
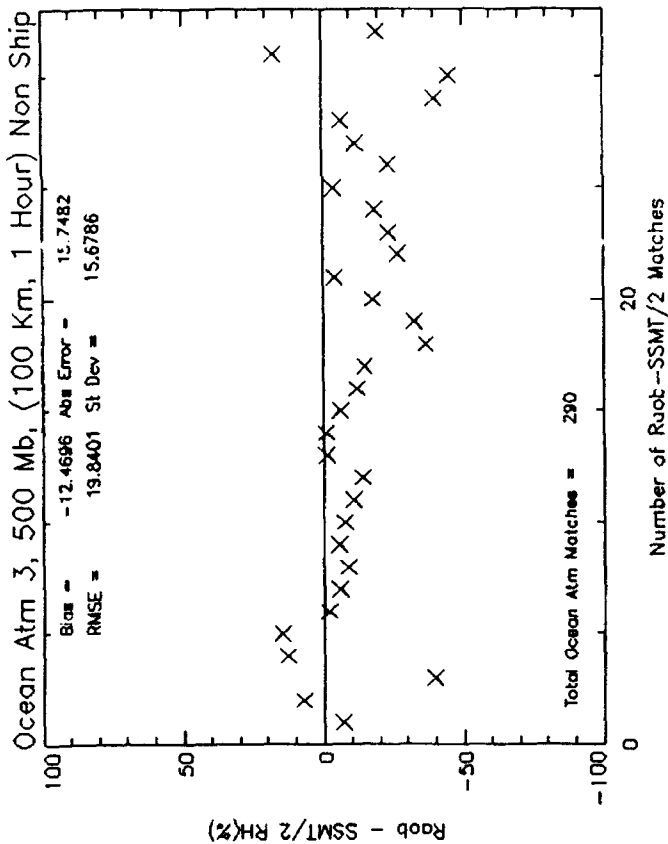
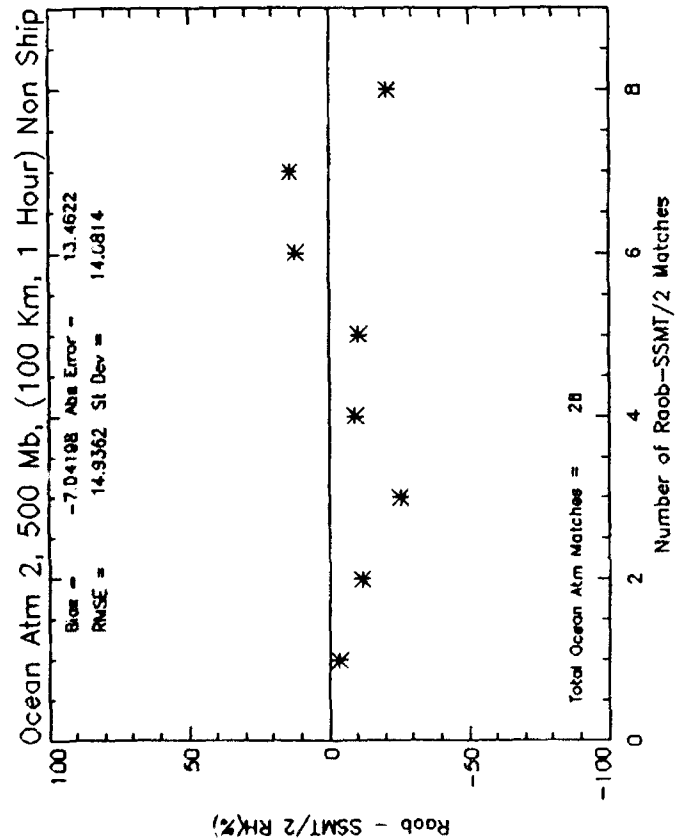


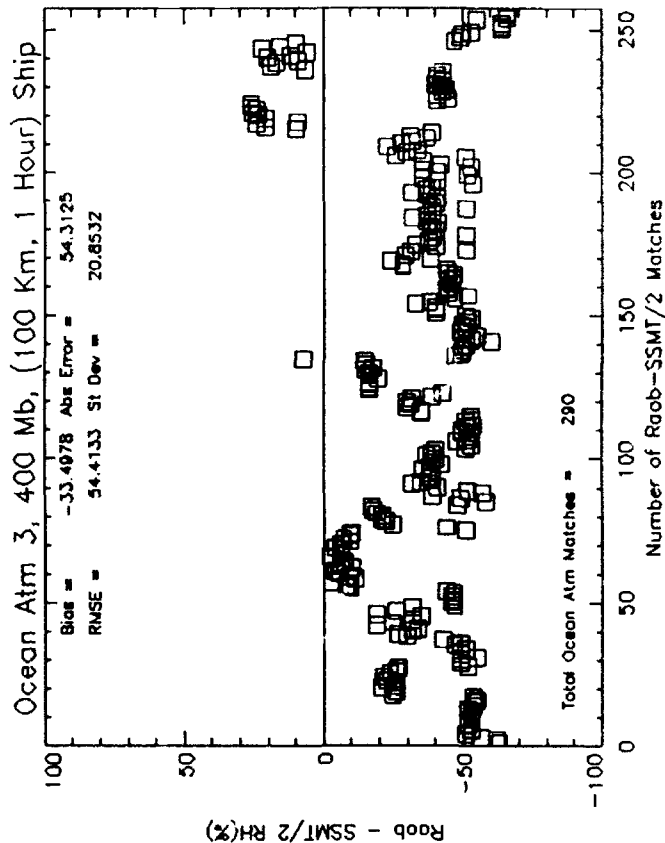
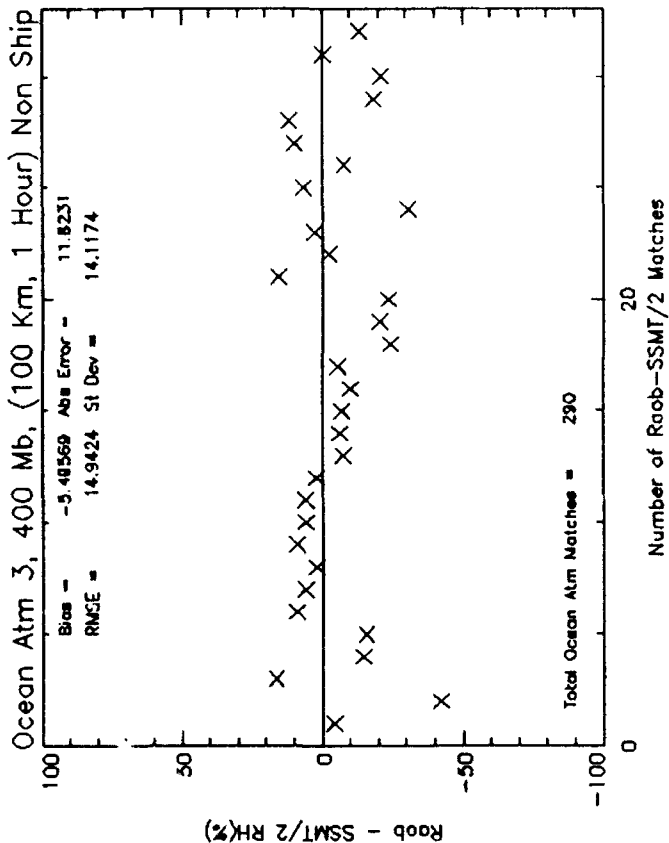
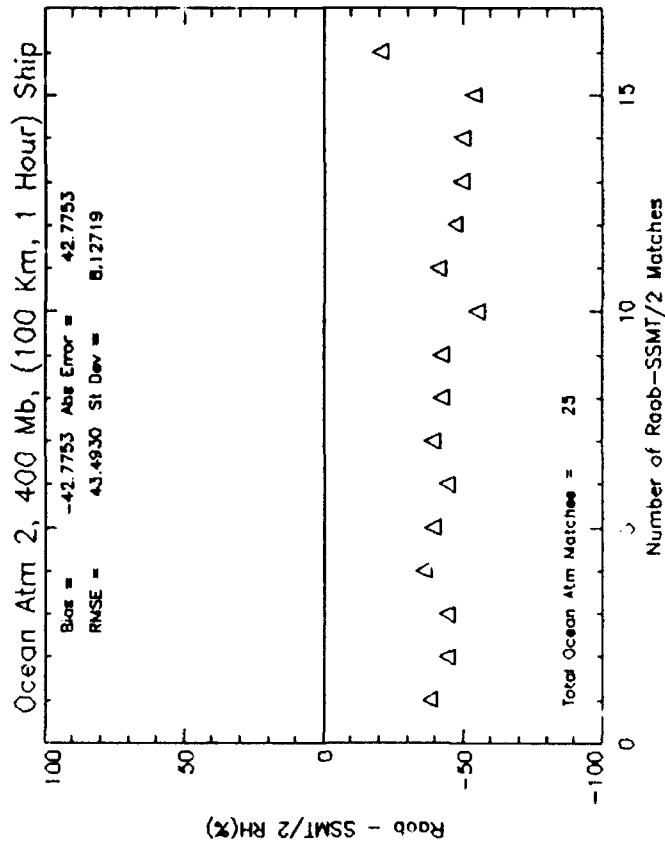
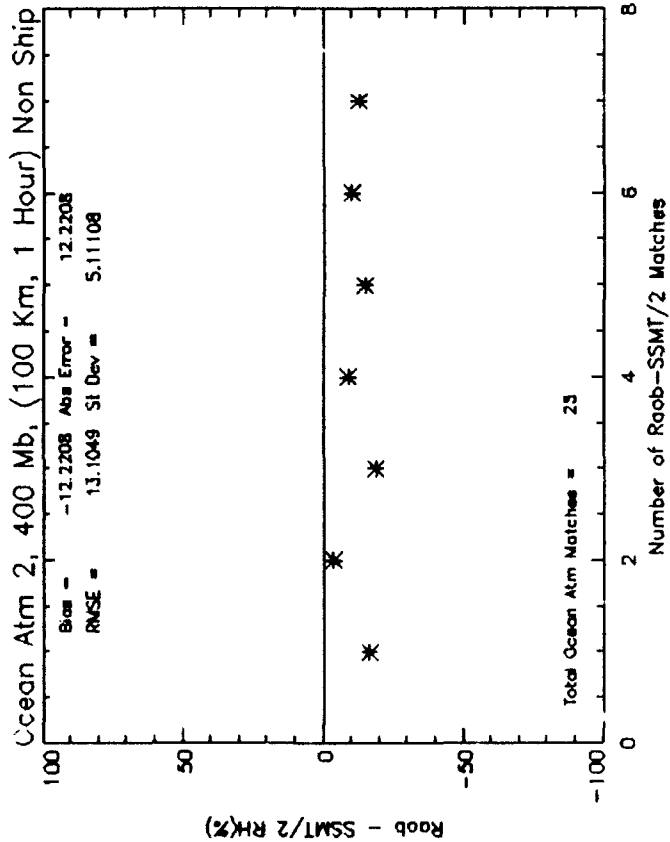


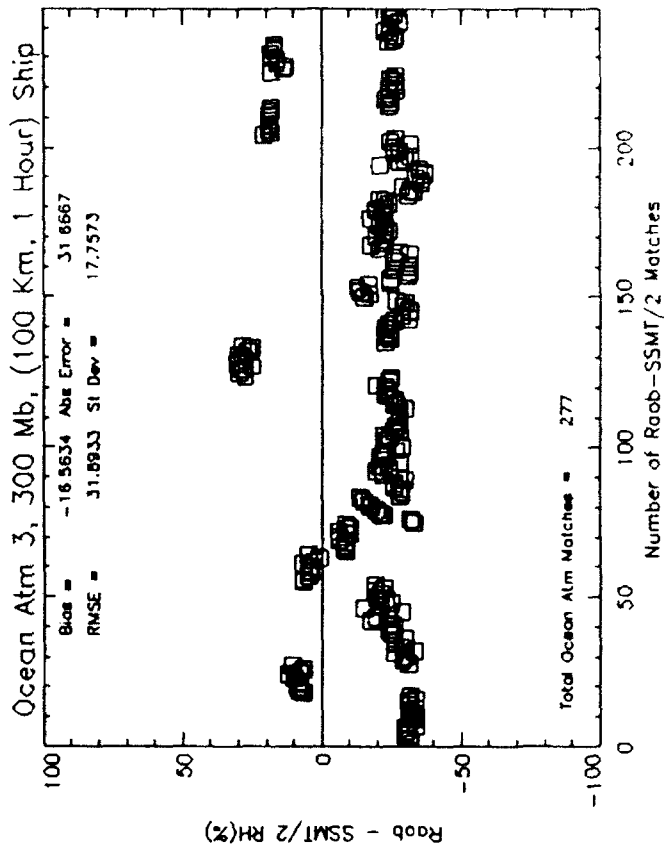
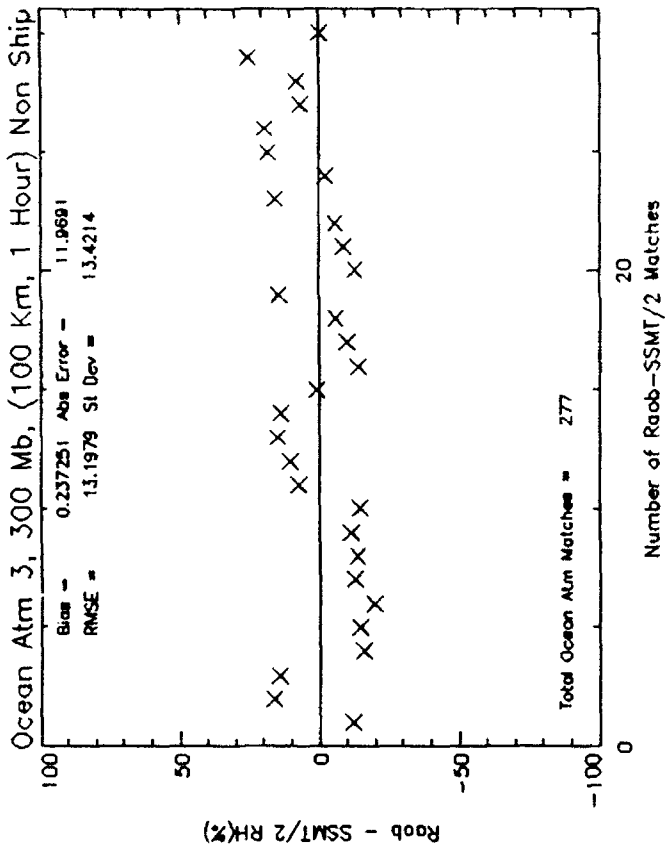
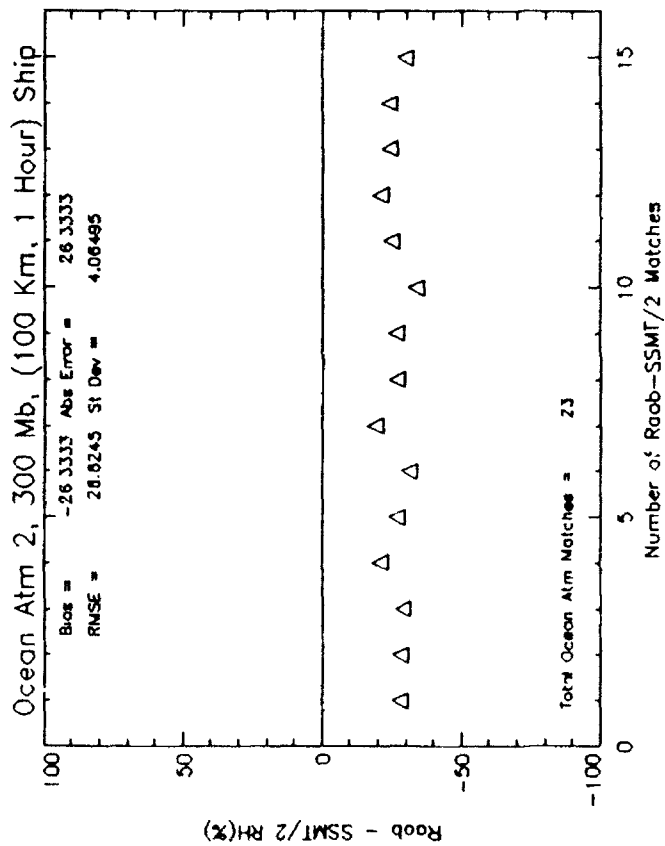
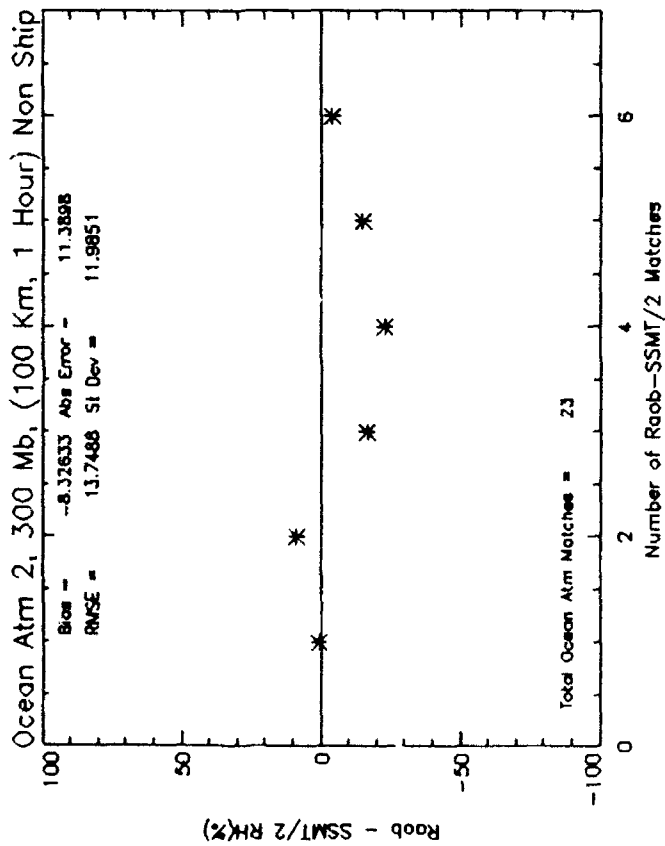


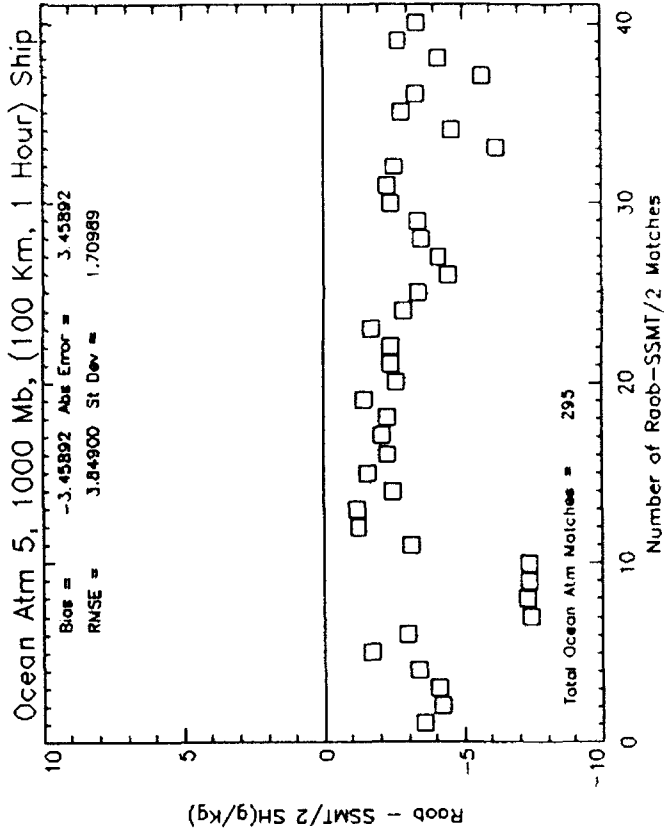
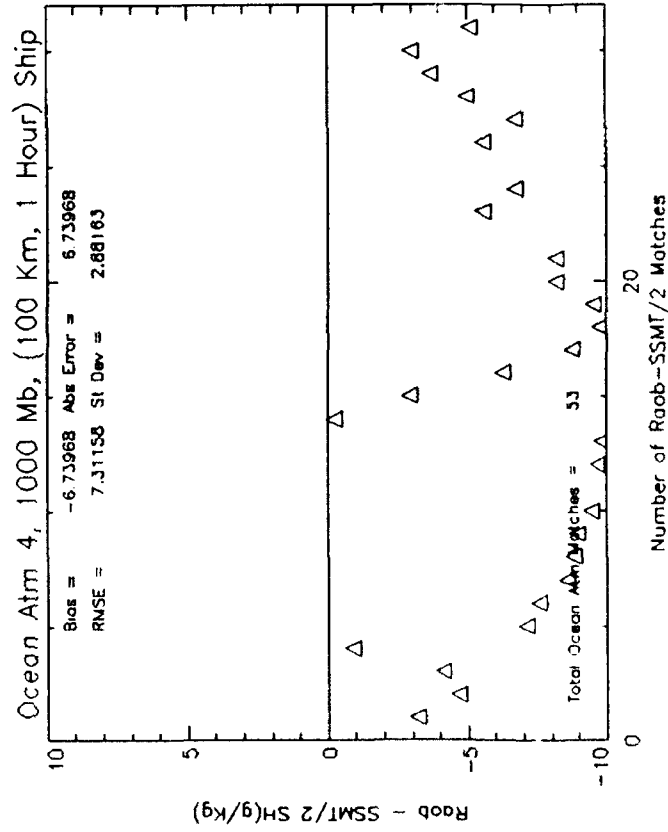
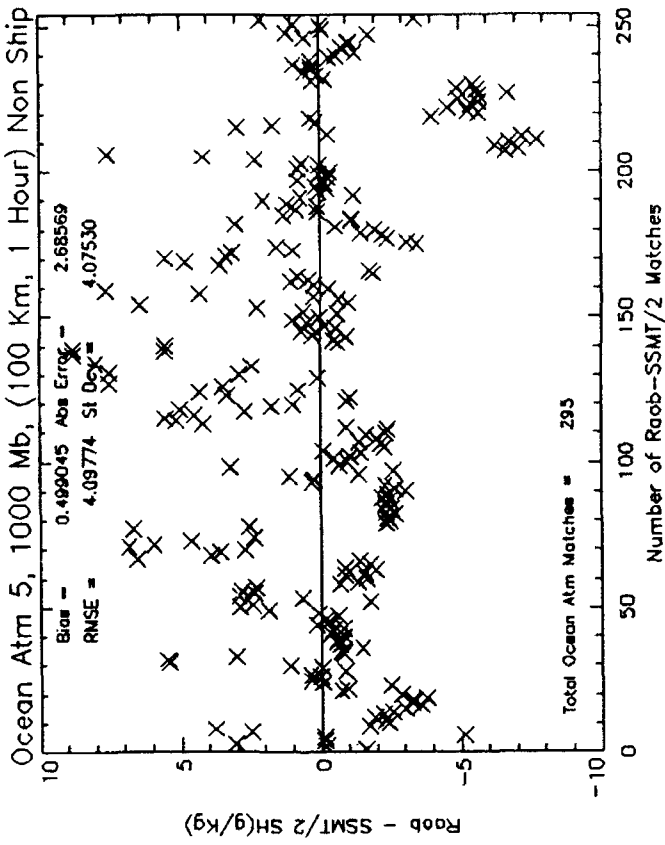
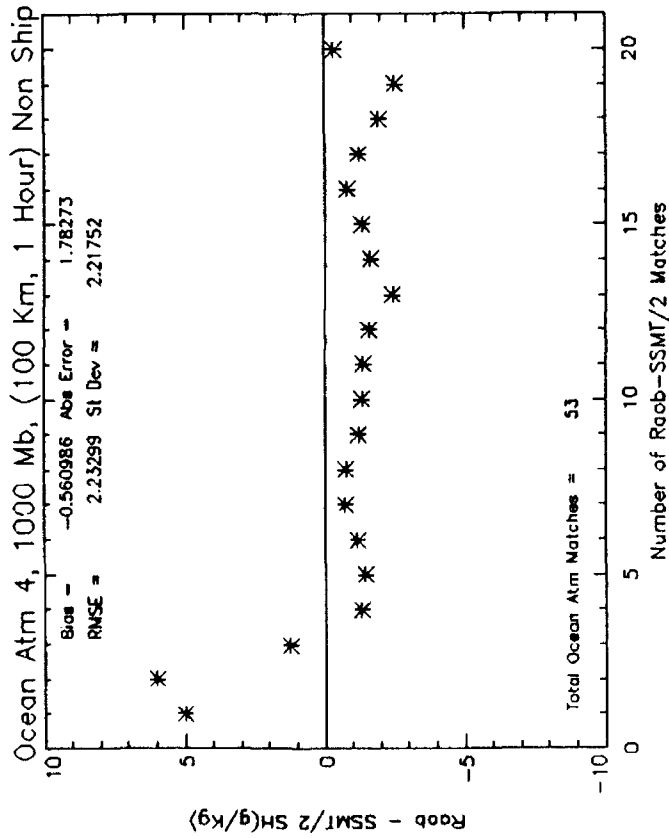


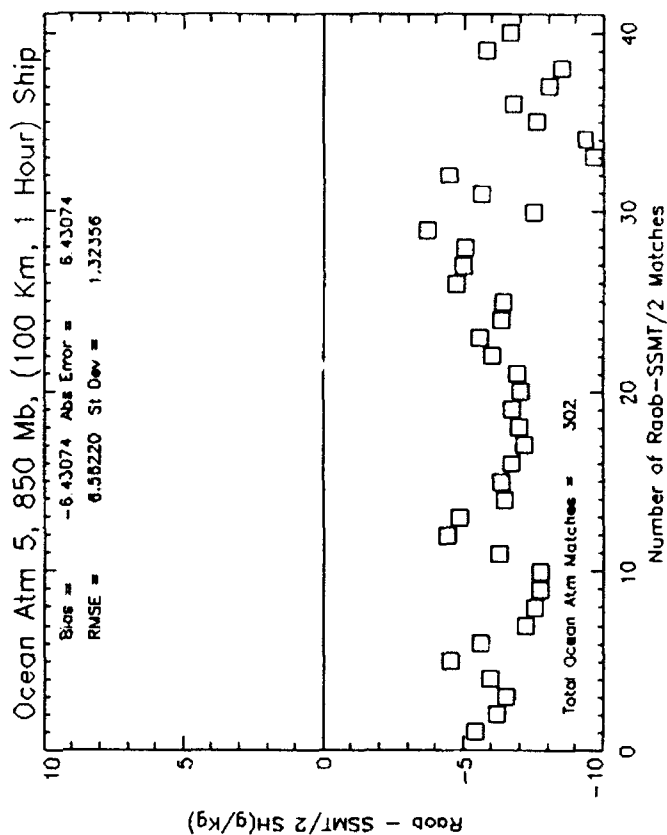
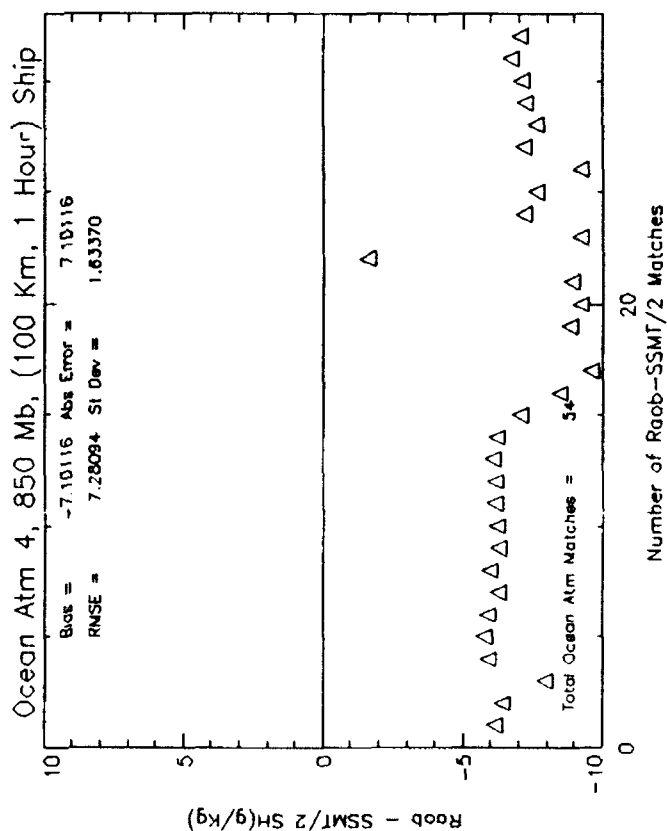
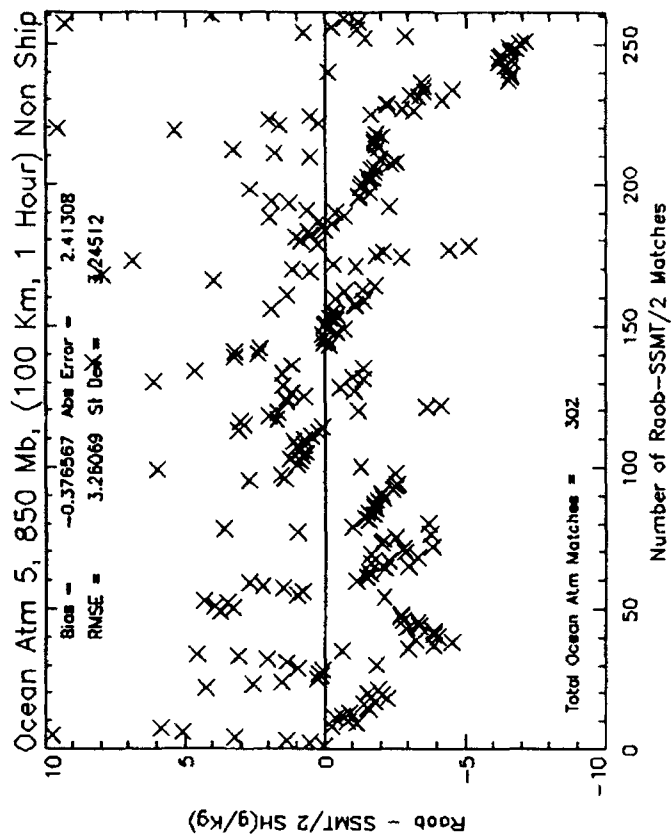
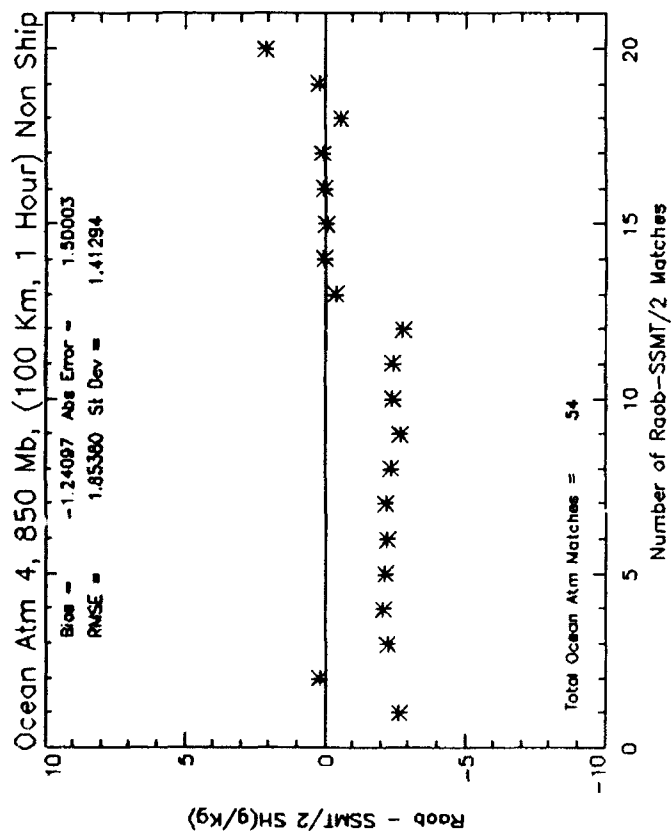


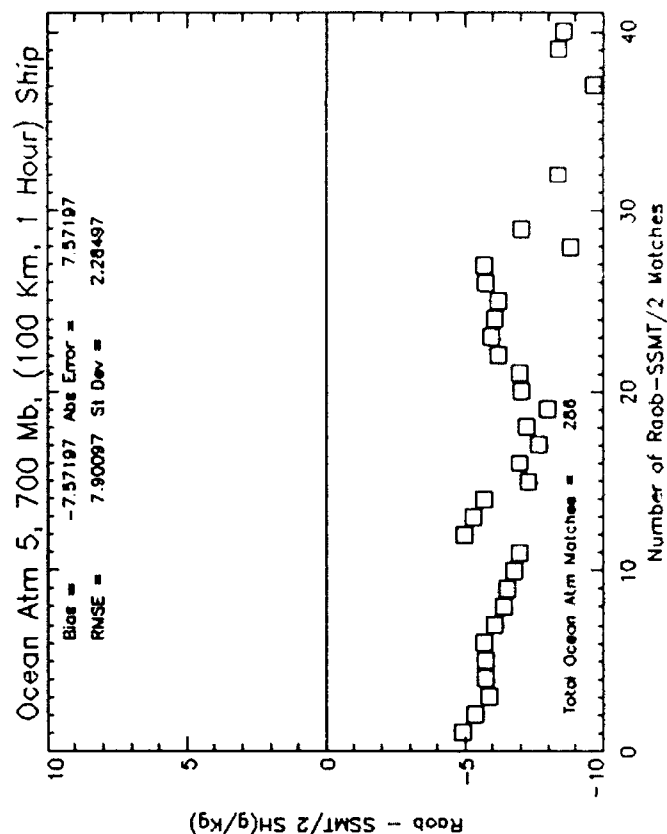
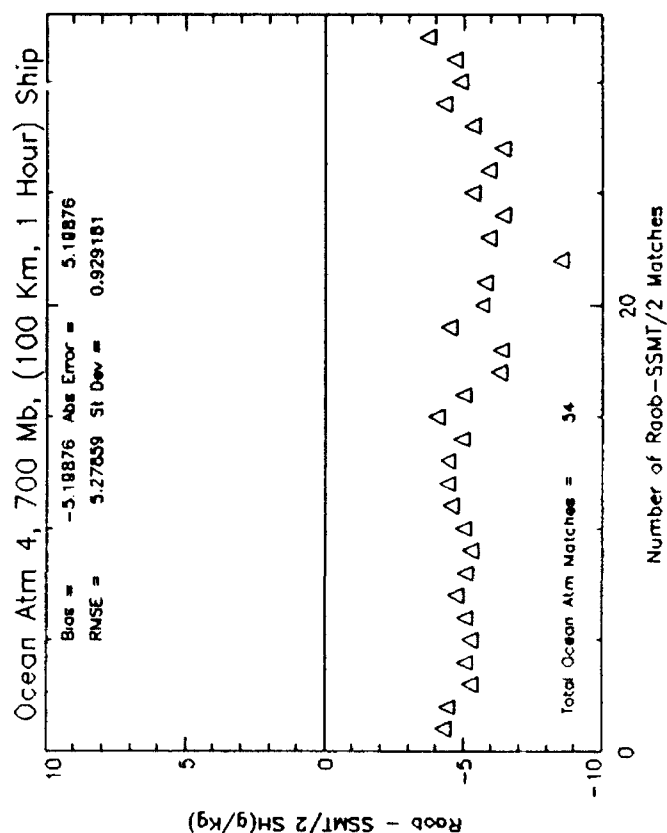
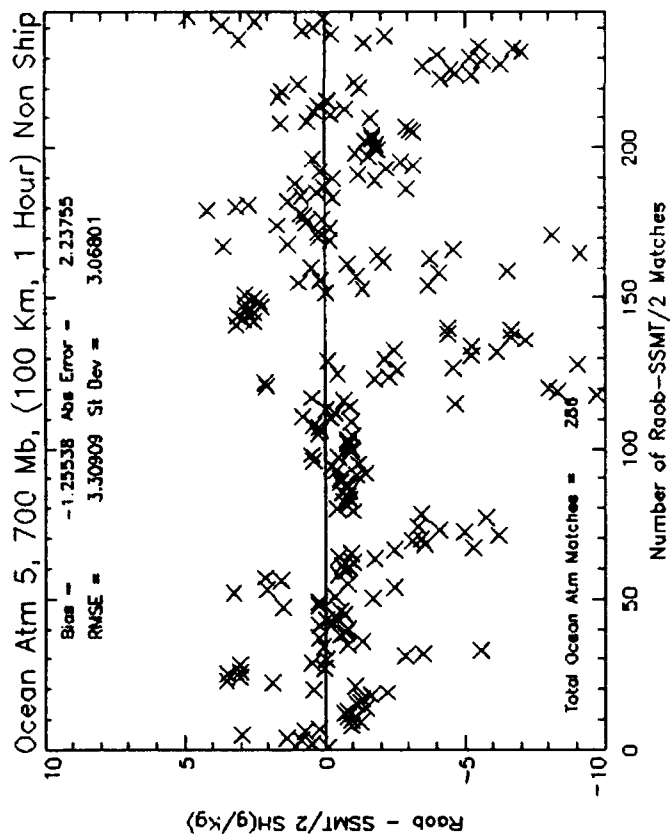
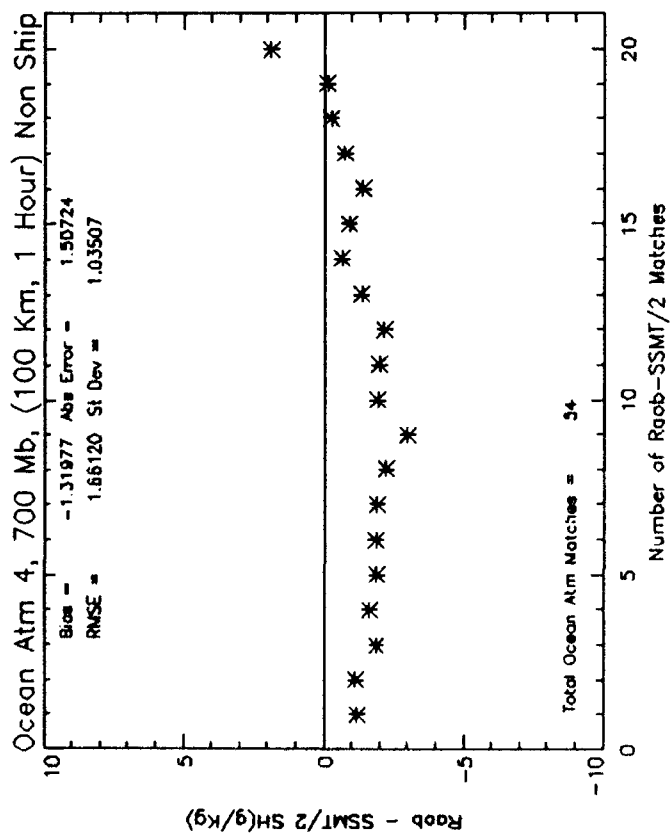


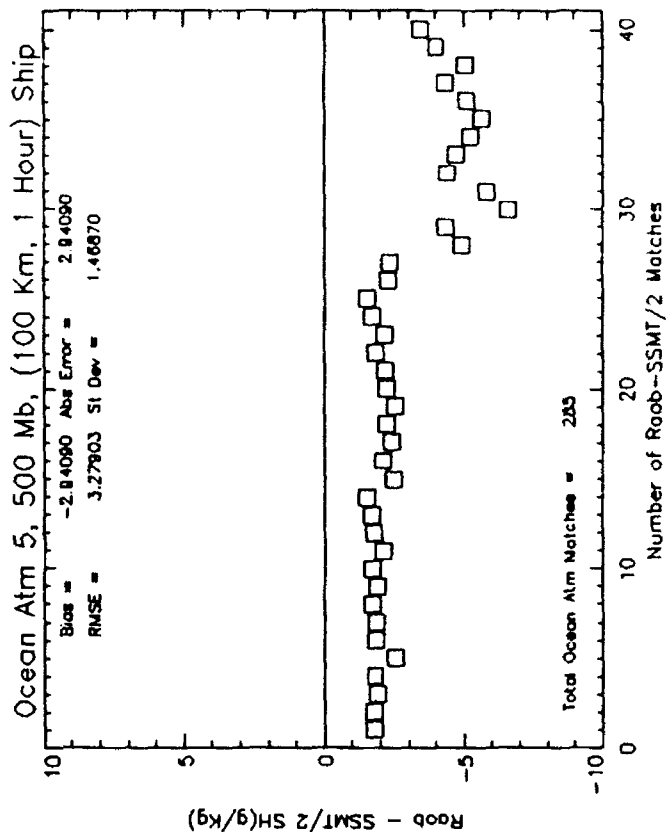
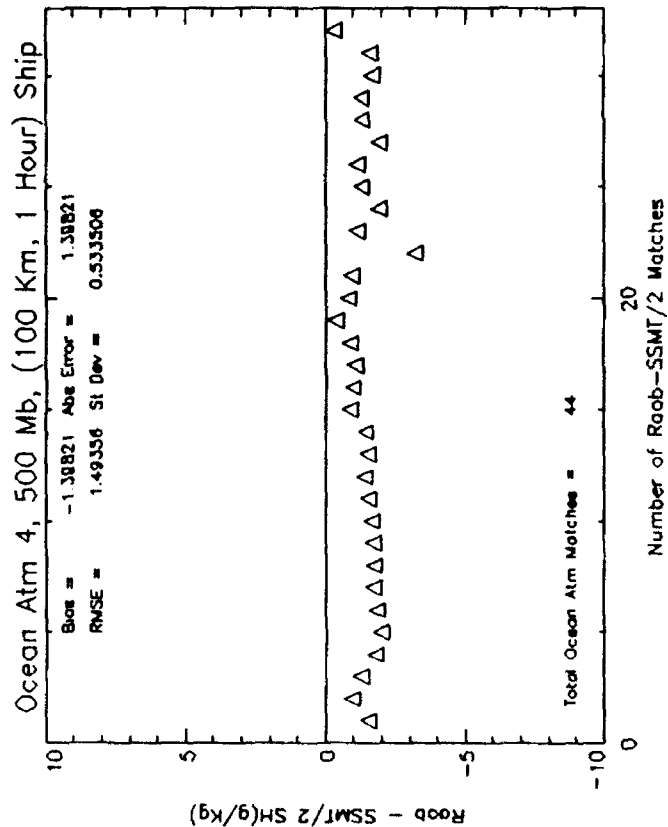
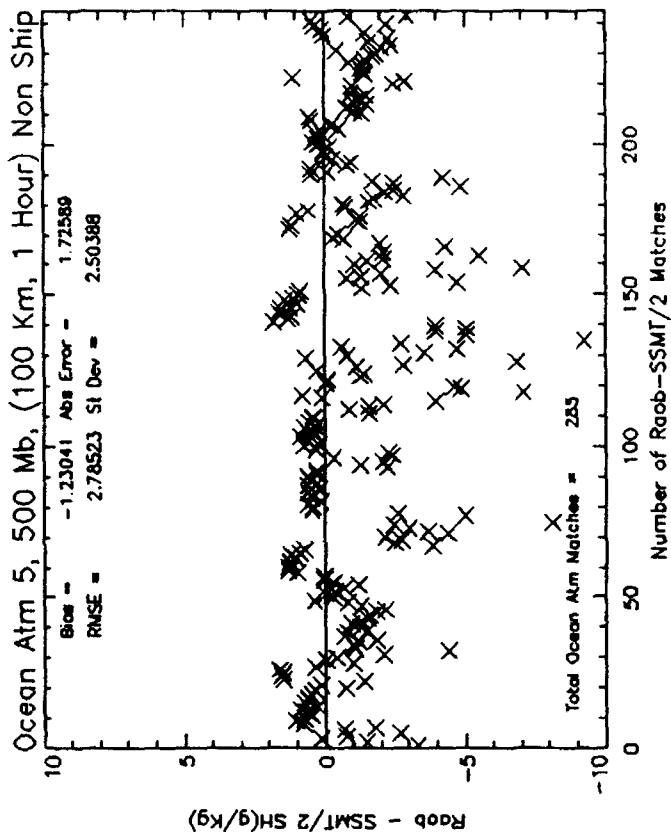
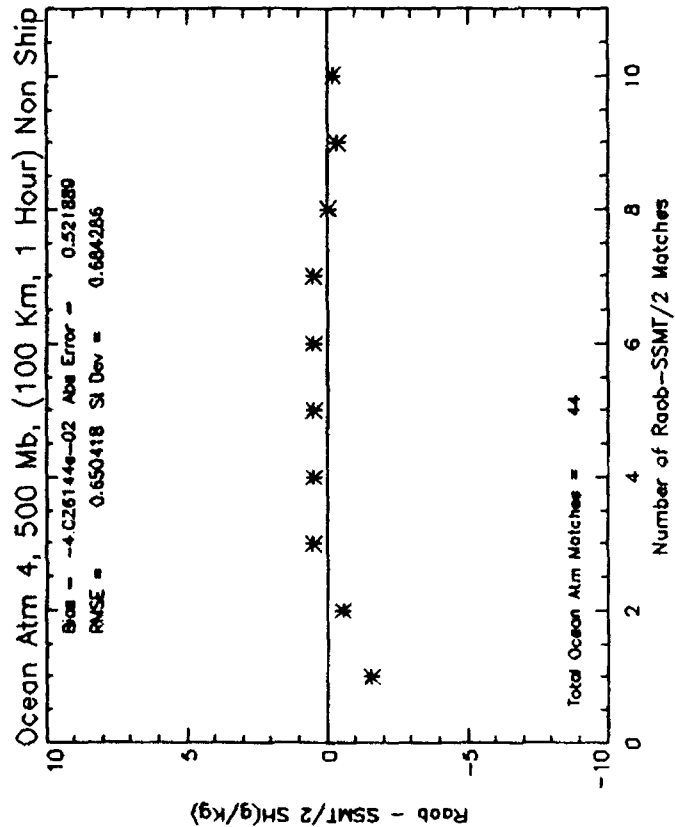


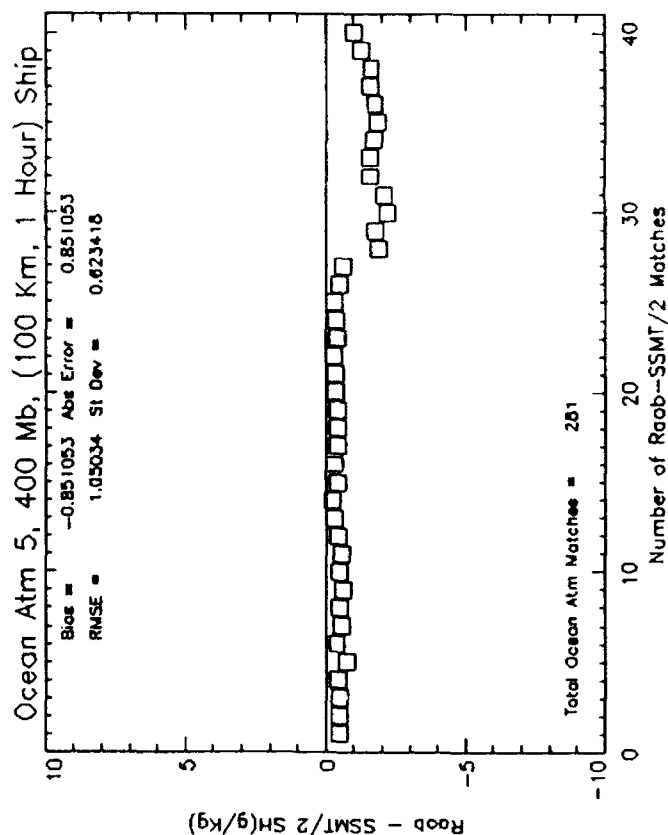
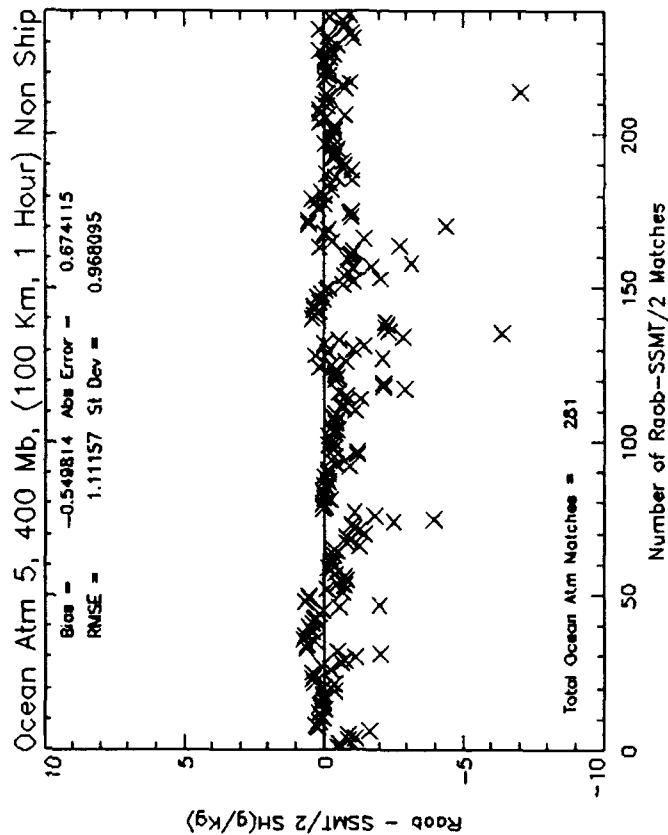
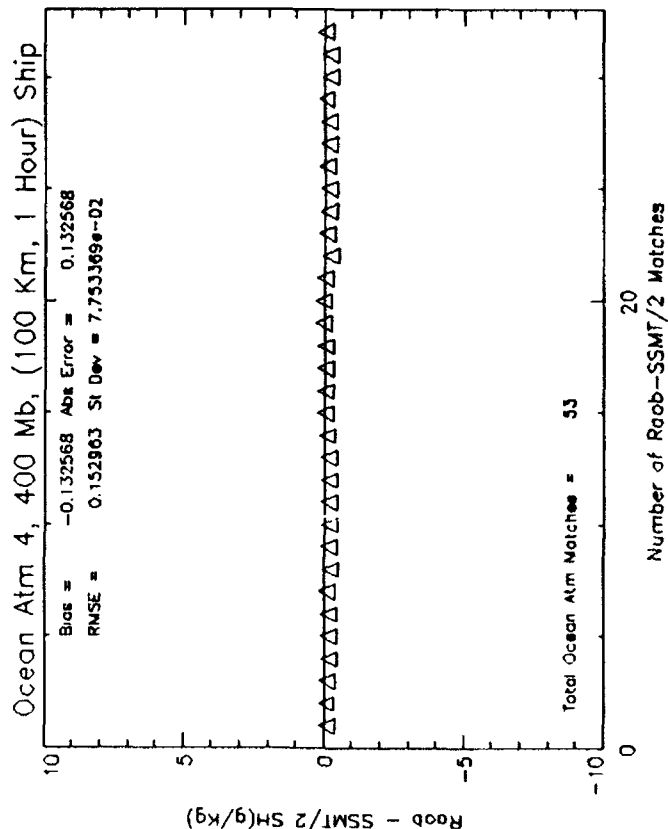
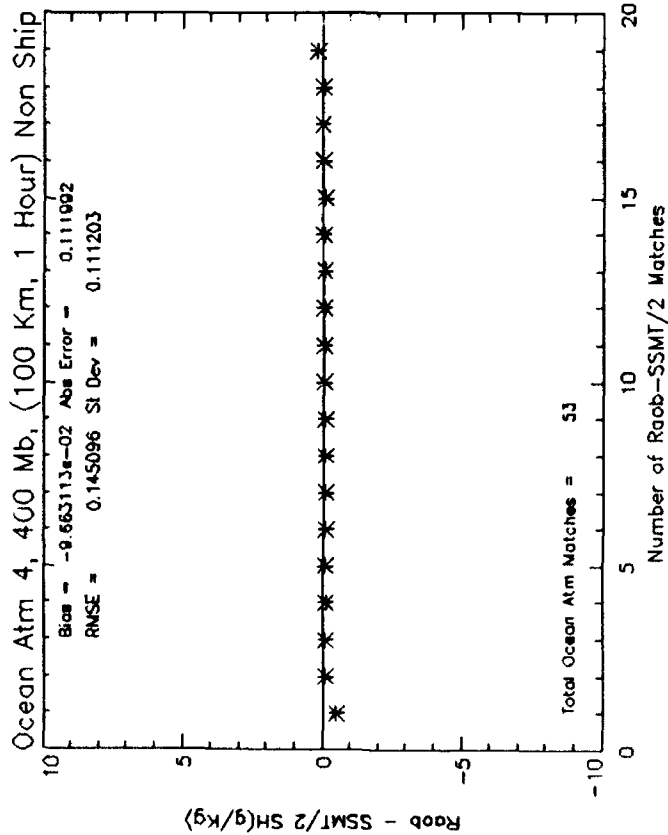




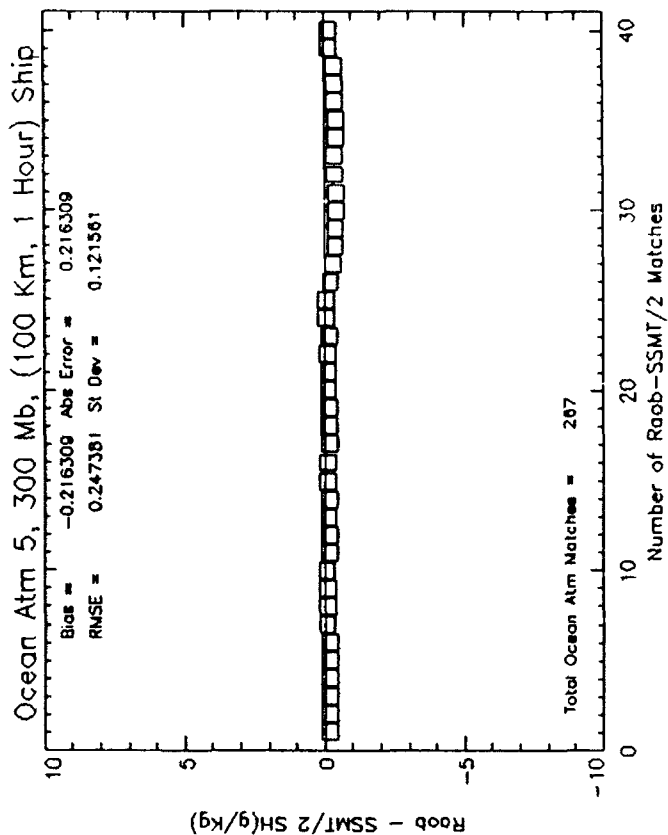
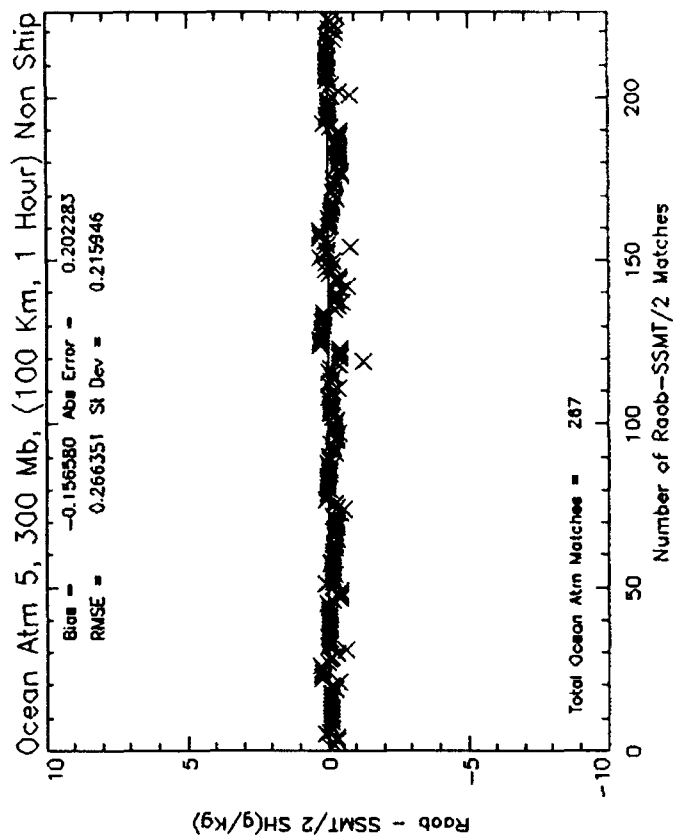
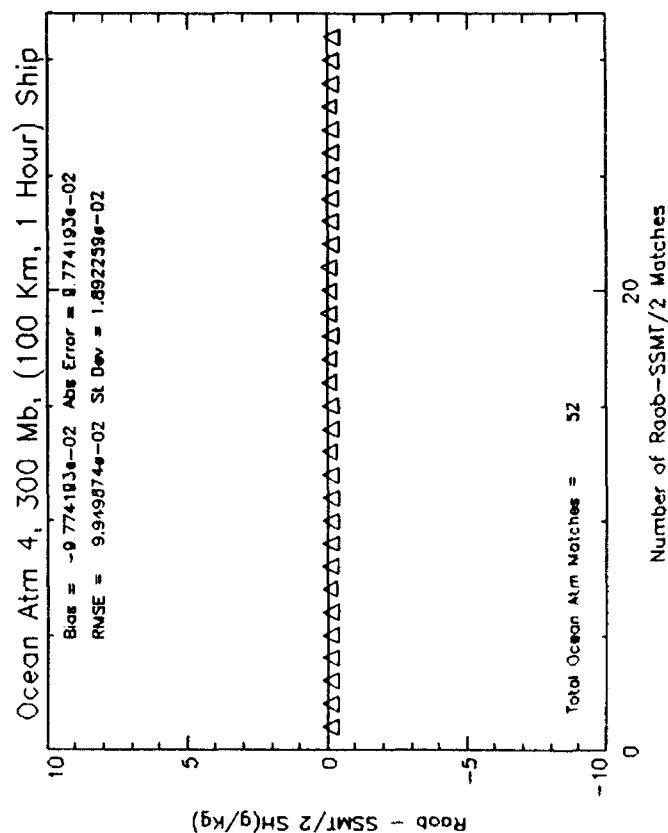
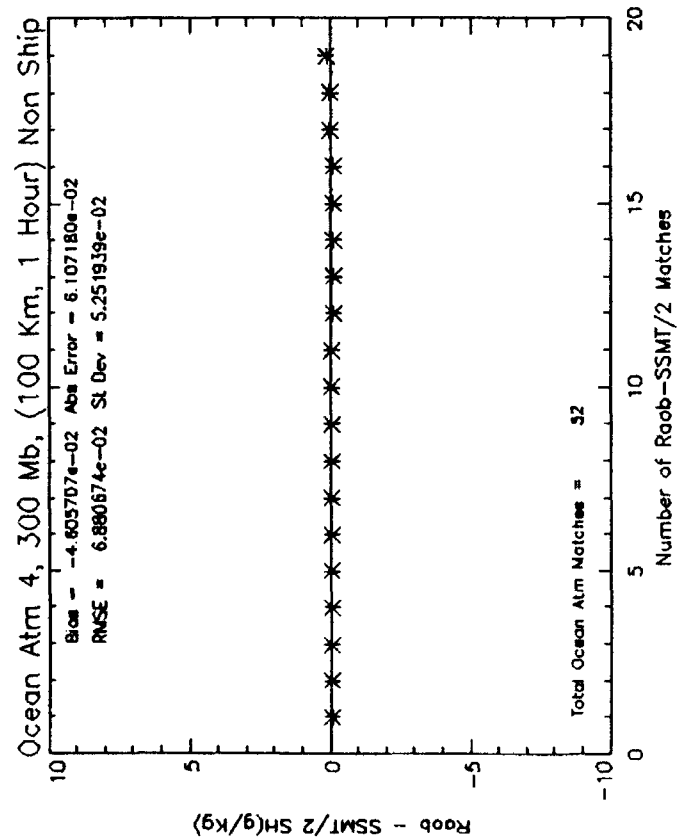




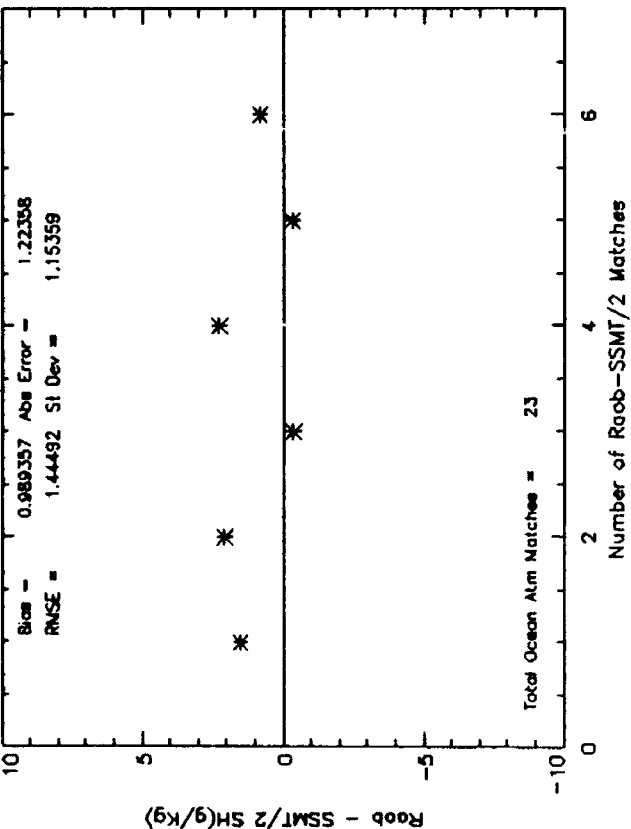




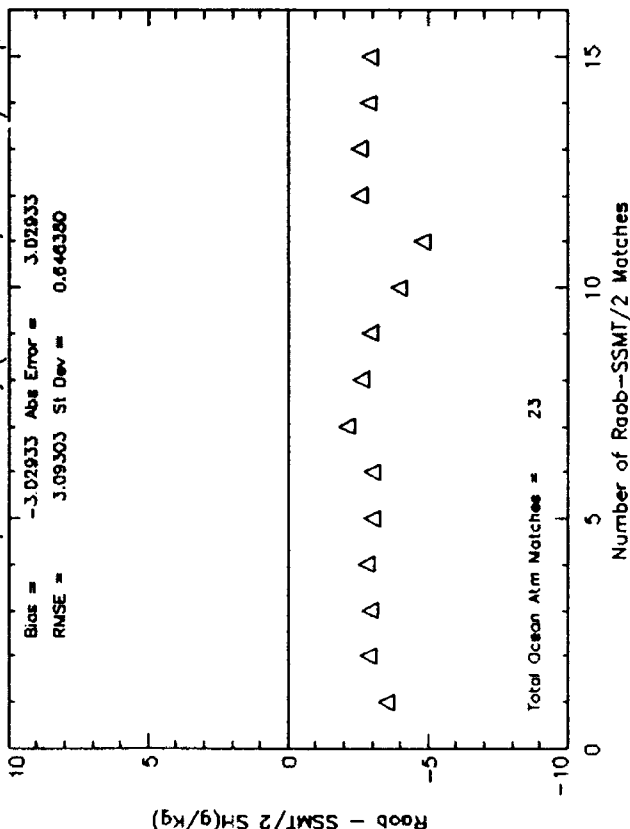




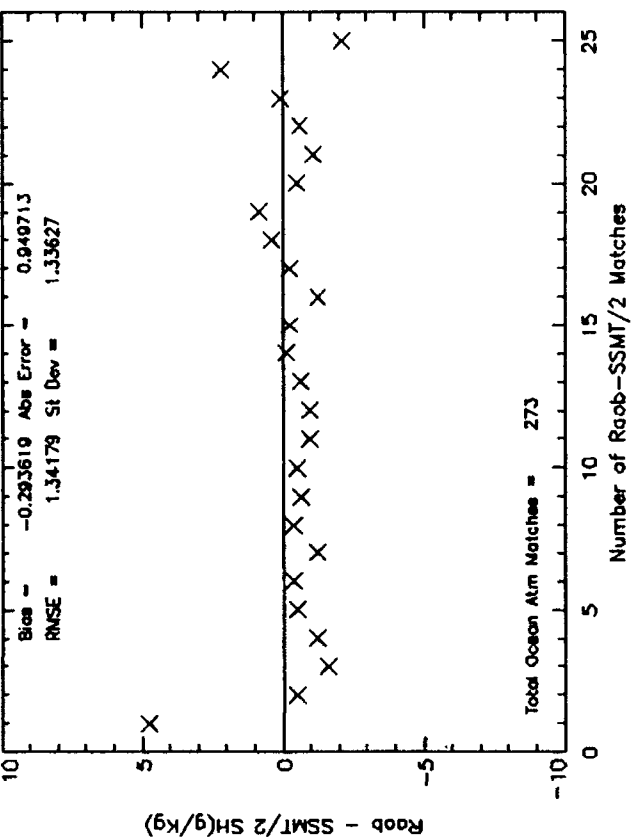
Ocean Atm 2, 1000 Mb, (100 Km, 1 Hour) Non Ship



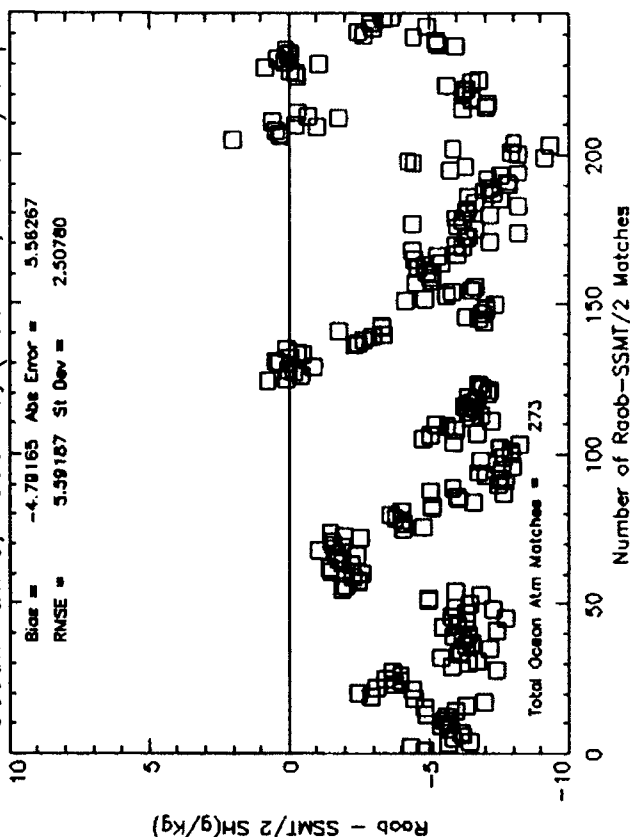
Ocean Atm 2, 1000 Mb, (100 Km, 1 Hour) Ship

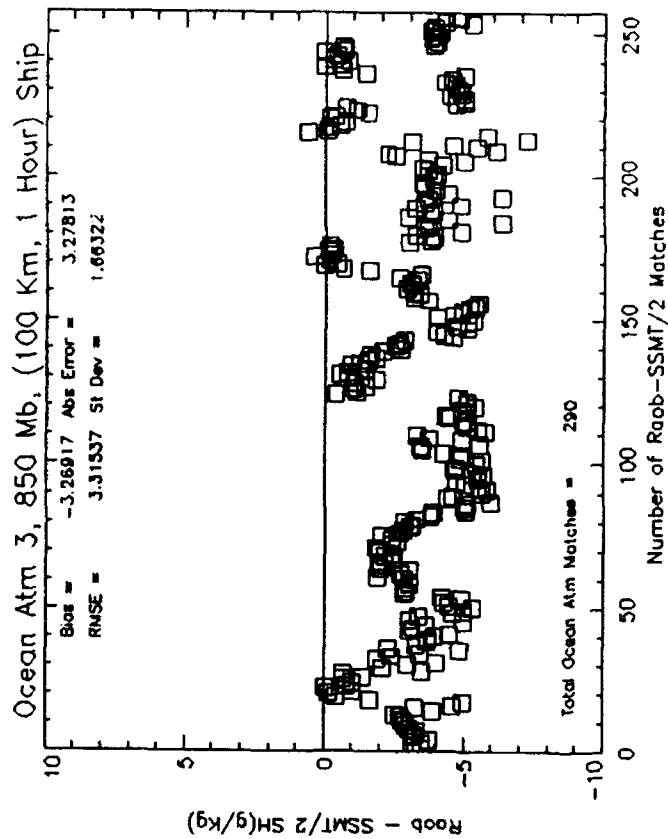
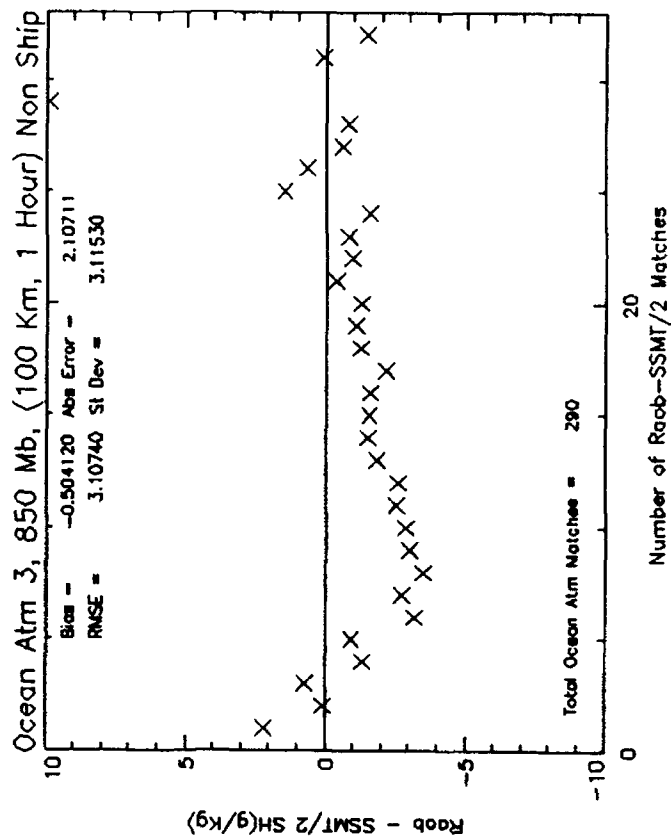
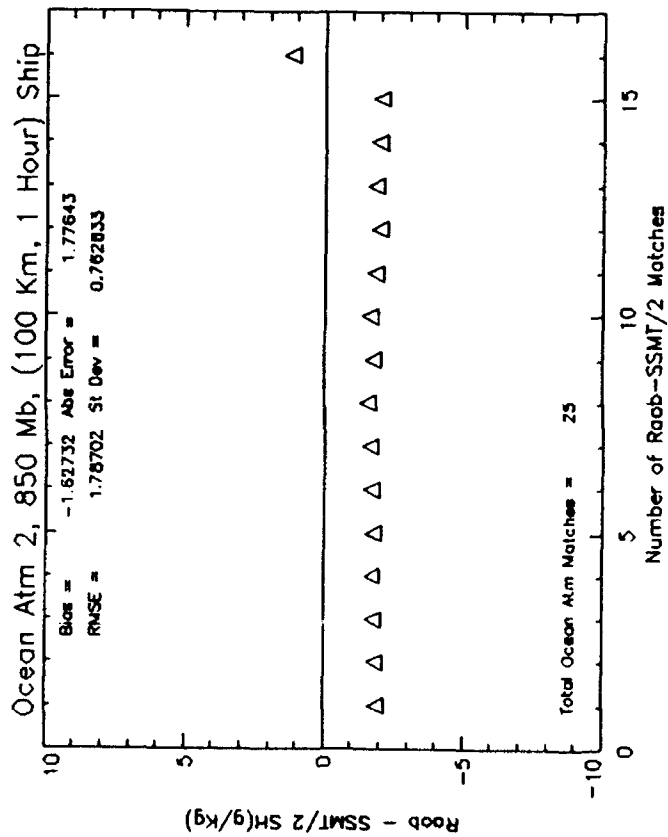
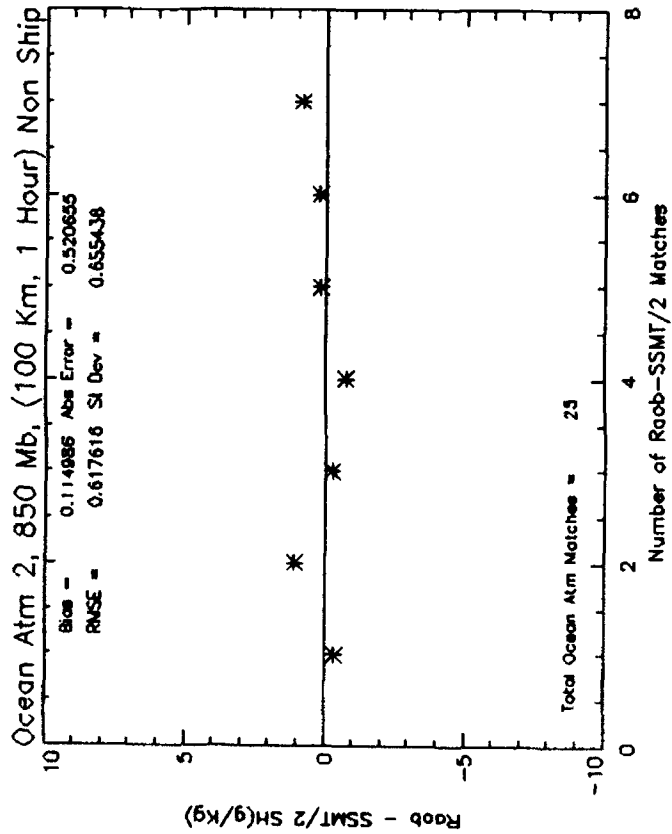


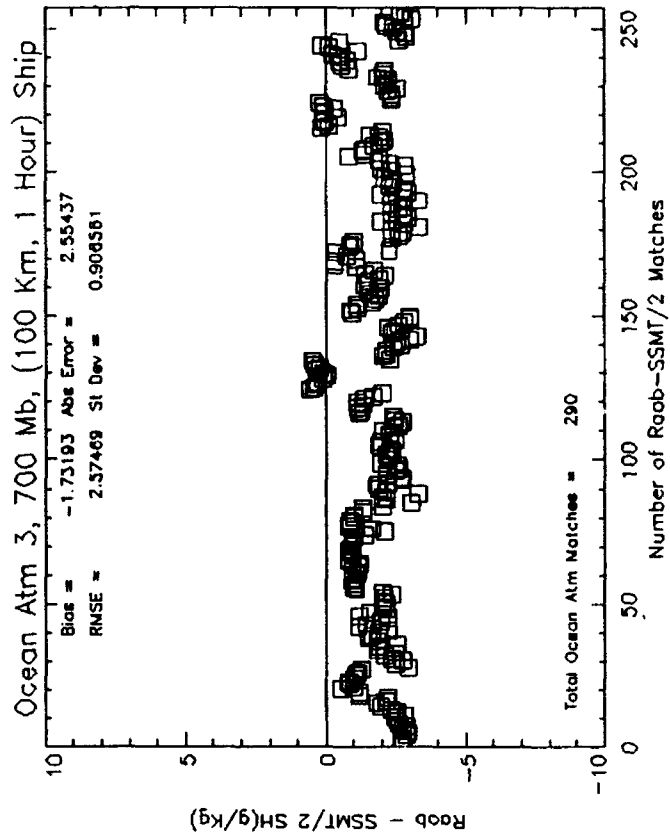
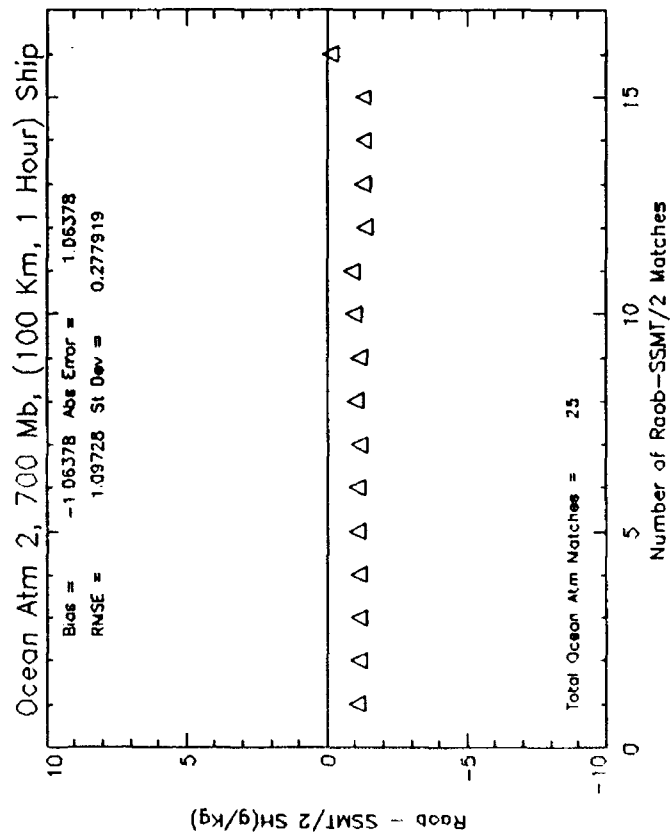
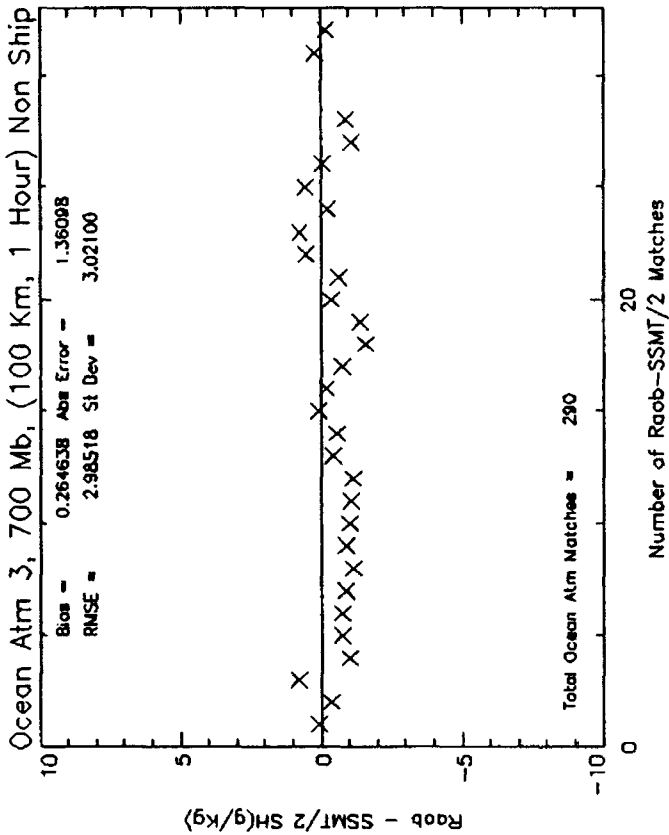
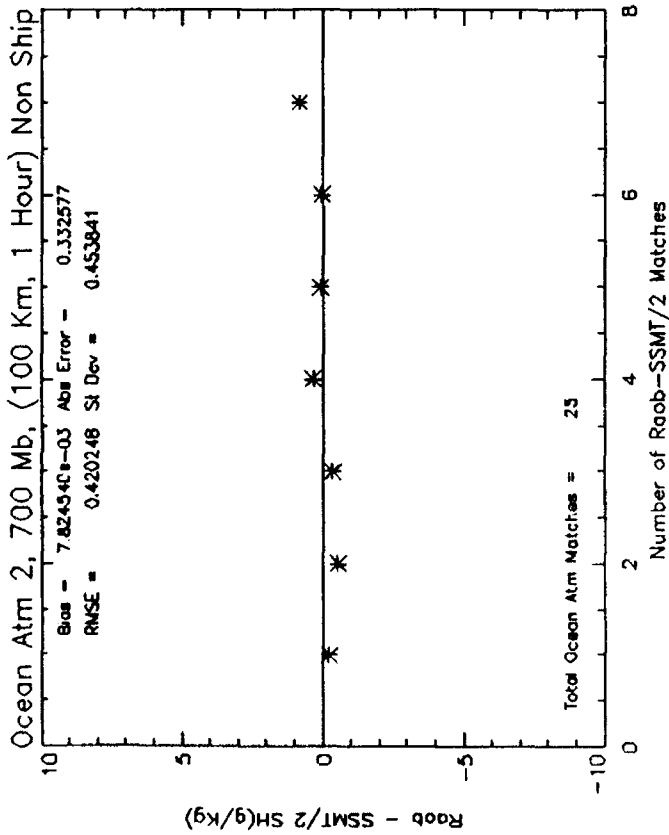
Ocean Atm 3, 1000 Mb, (100 Km, 1 Hour) Non Ship

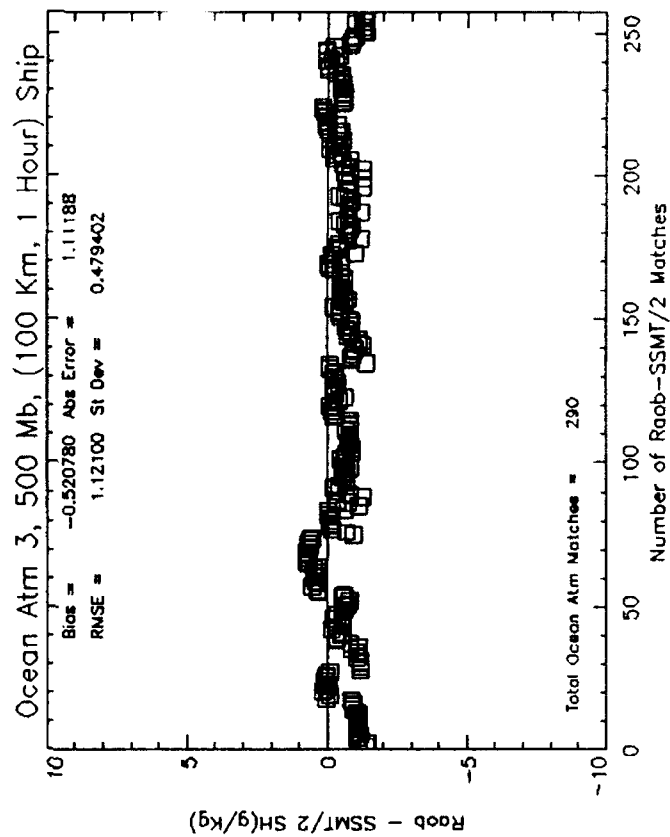
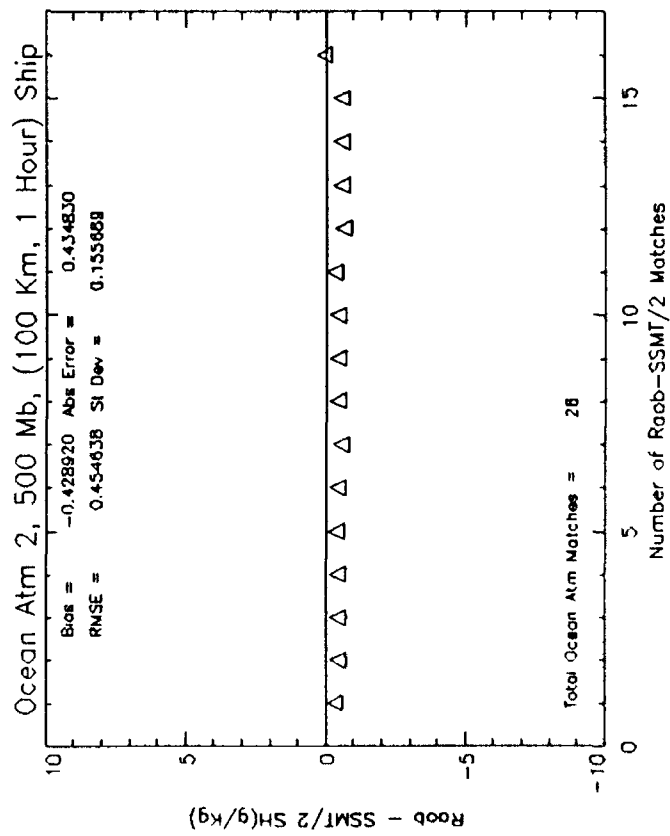
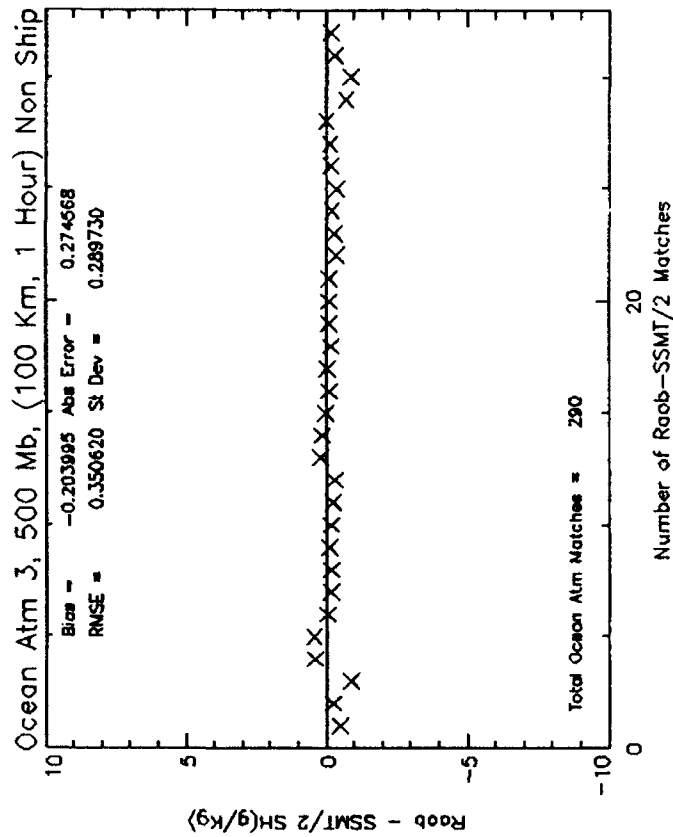
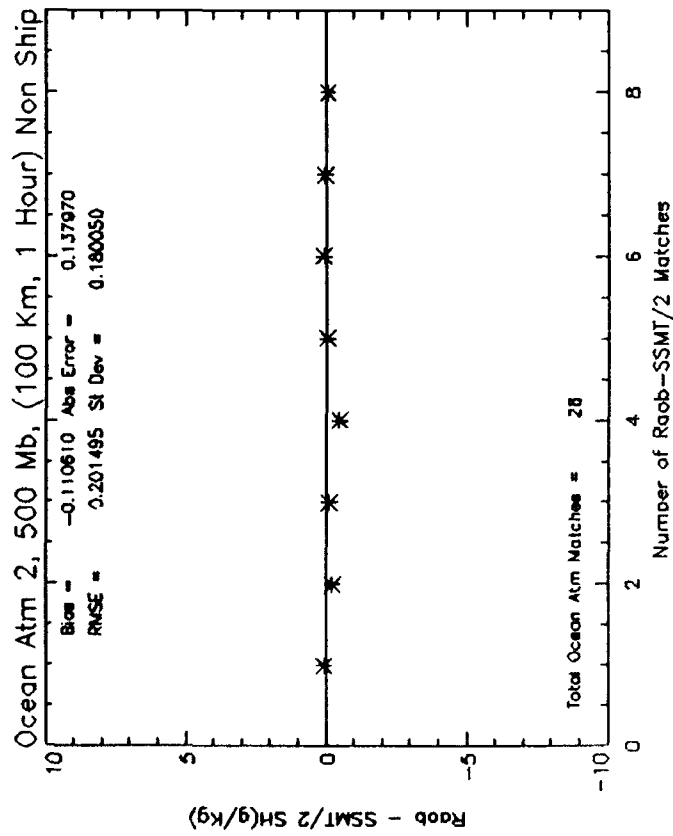


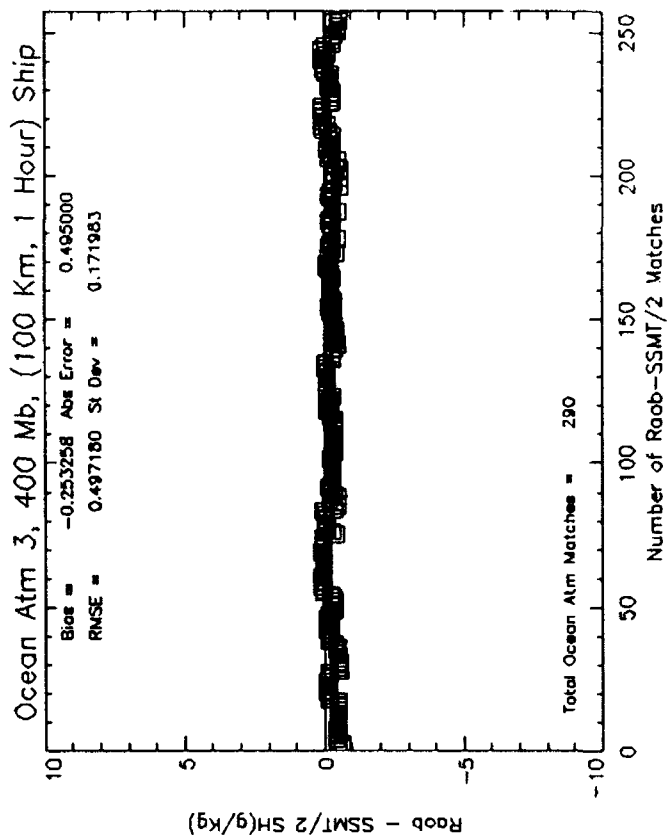
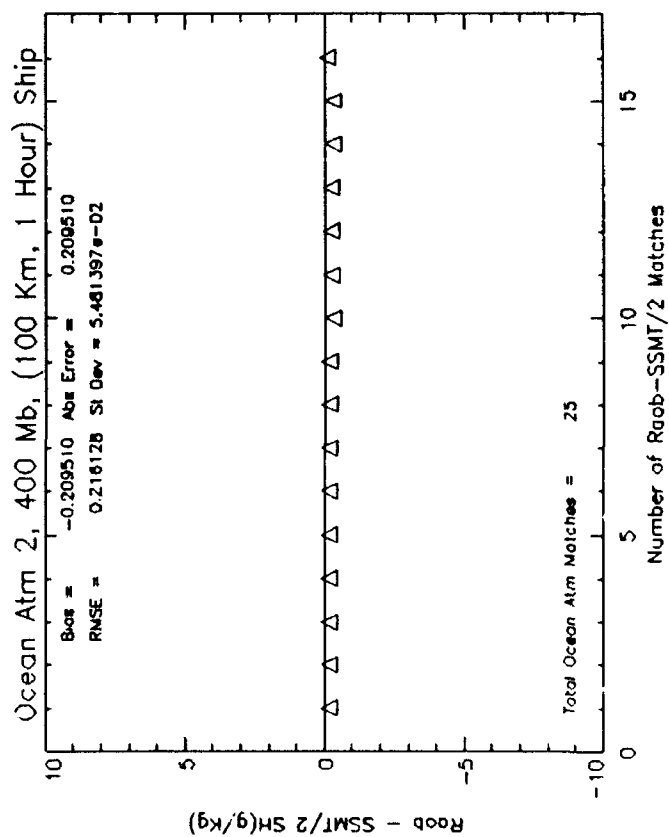
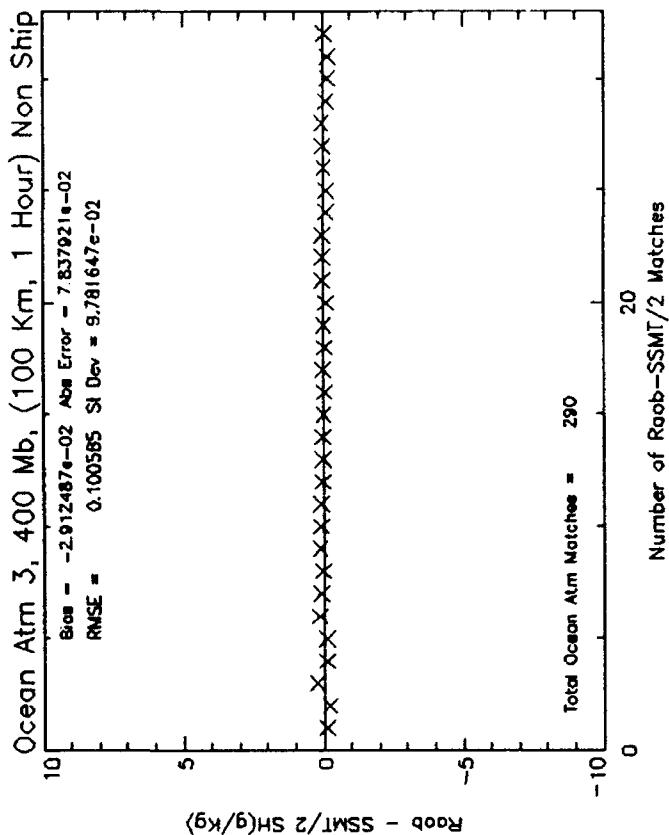
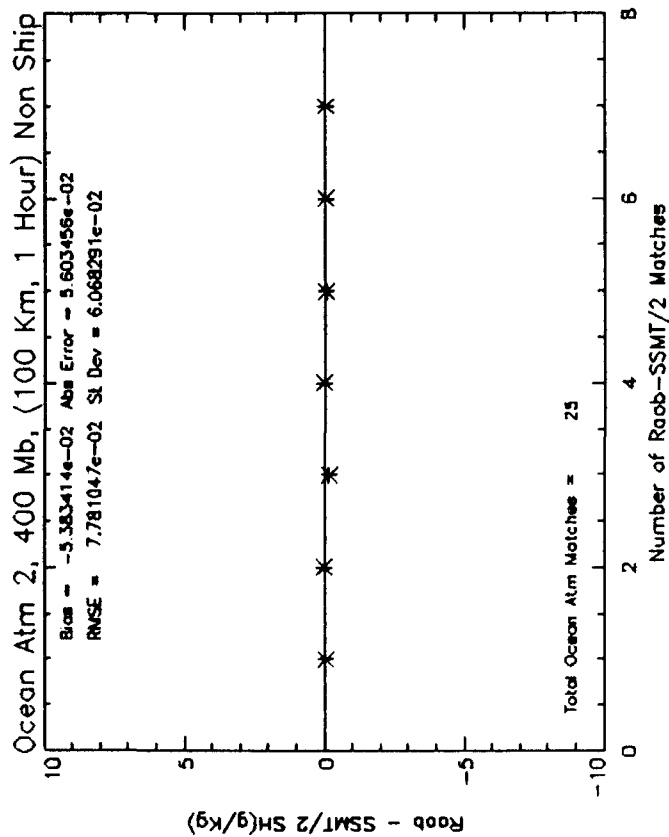
Ocean Atm 3, 1000 Mb, (100 Km, 1 Hour) Ship

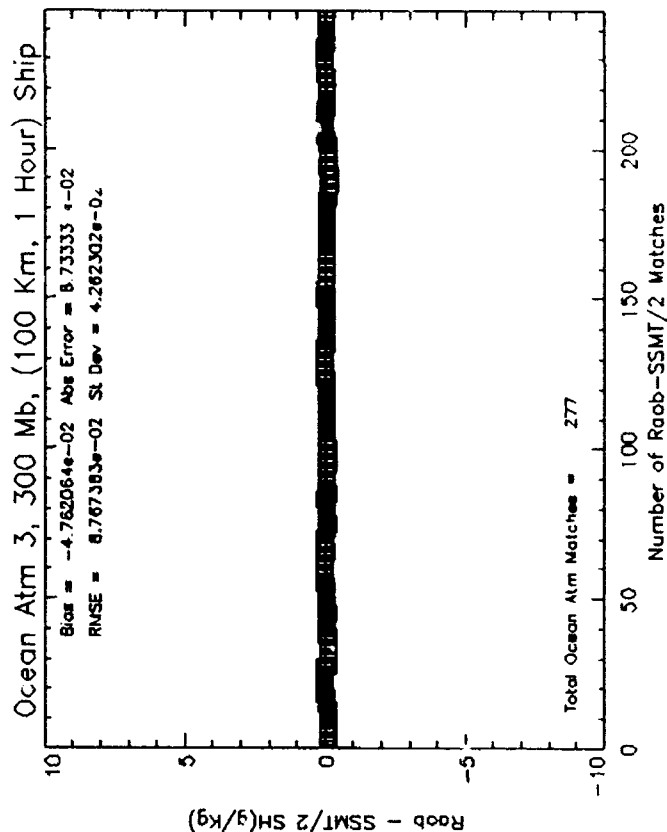
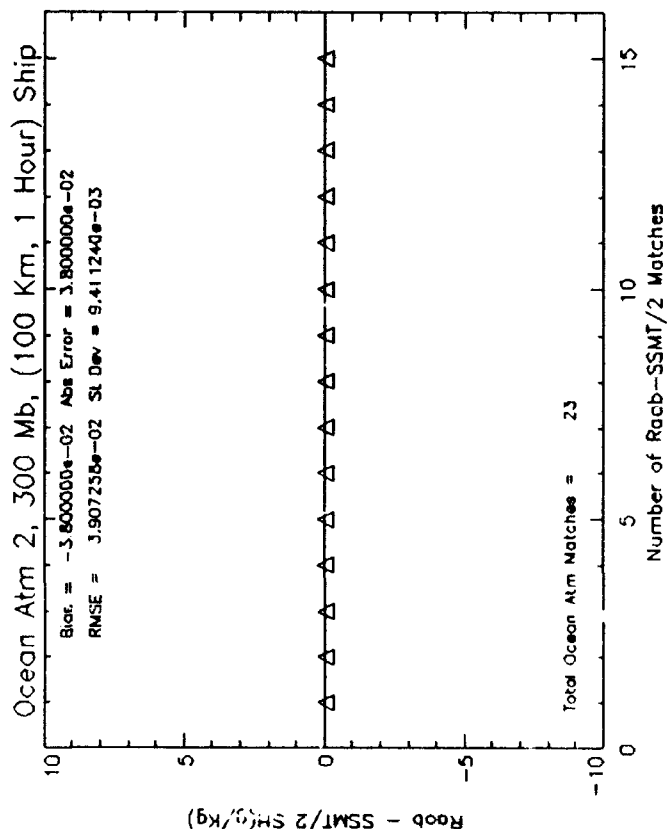
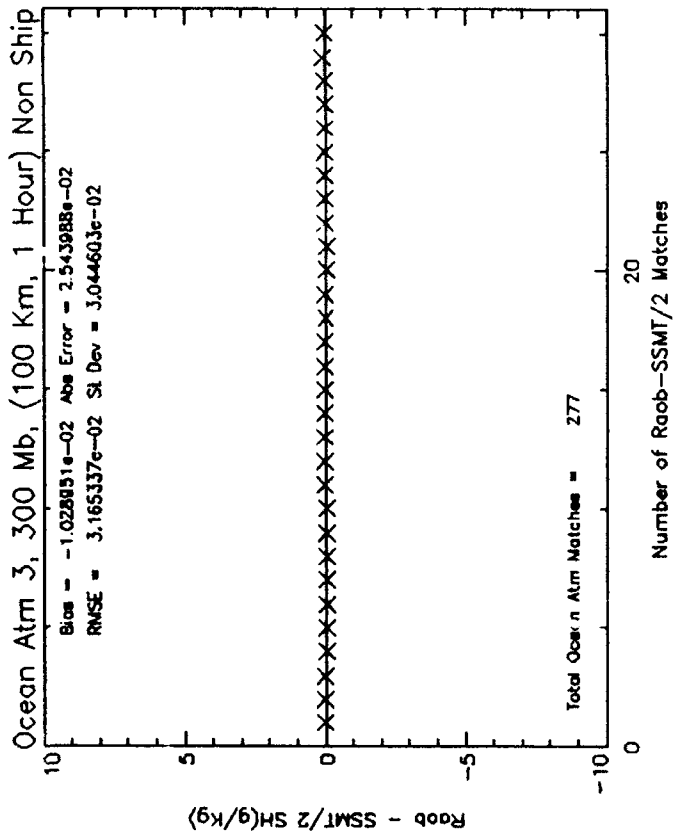
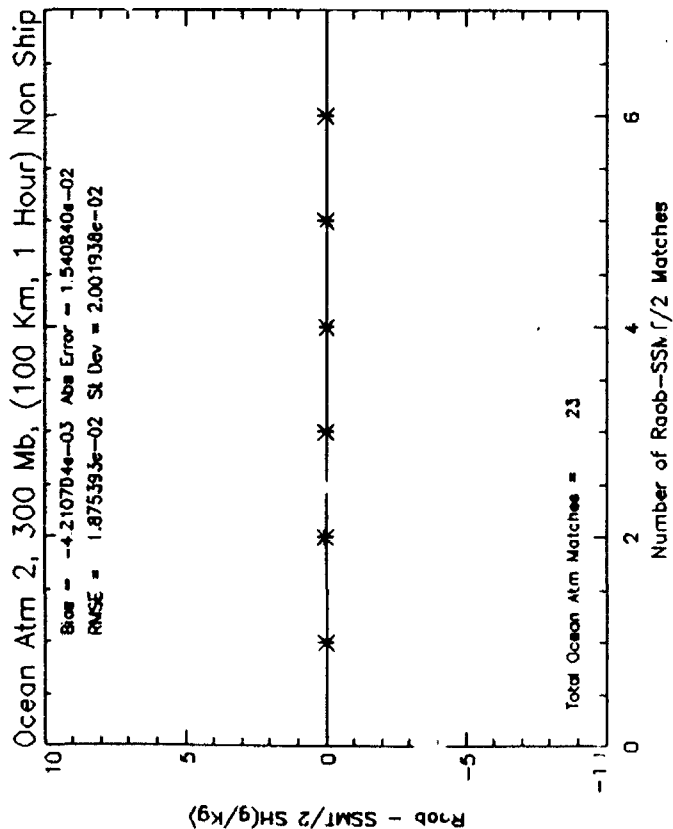






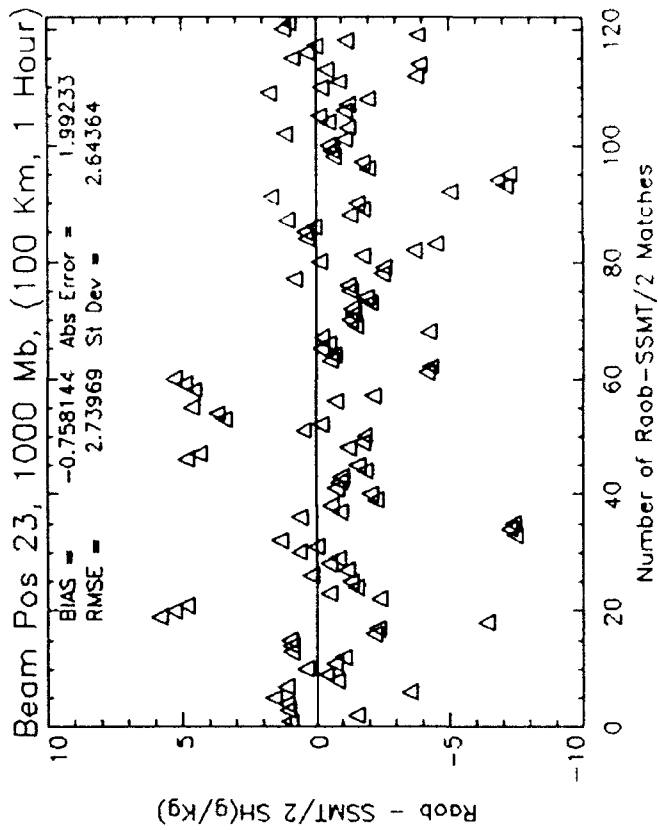
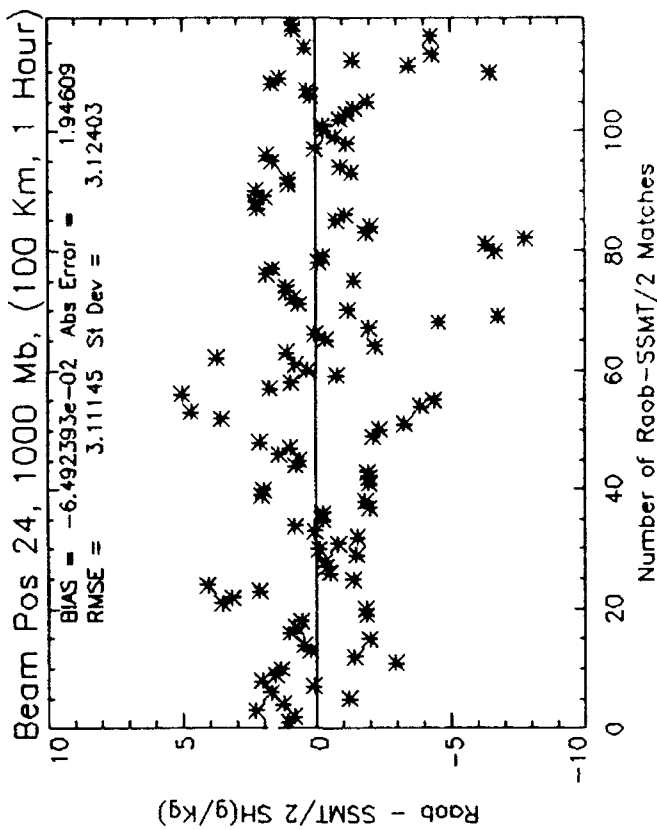
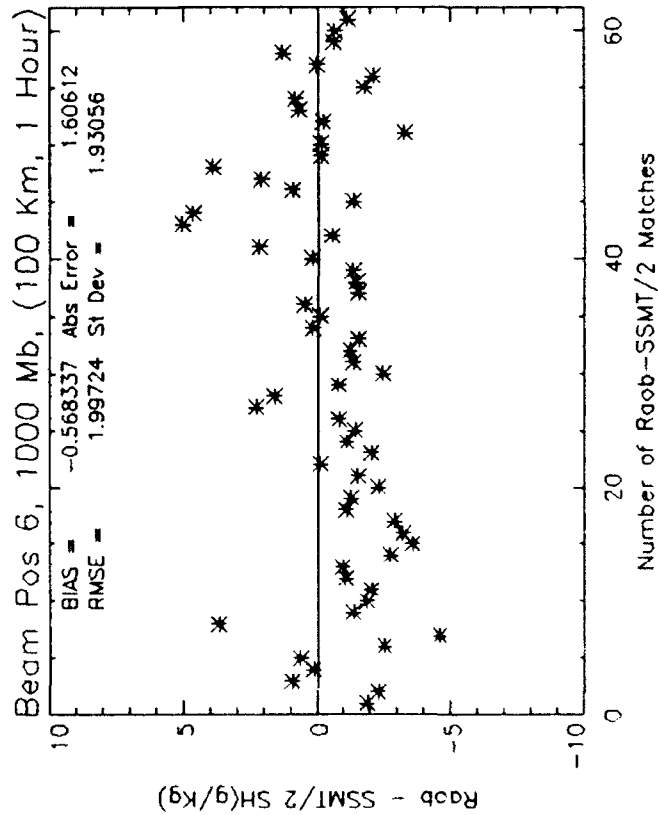
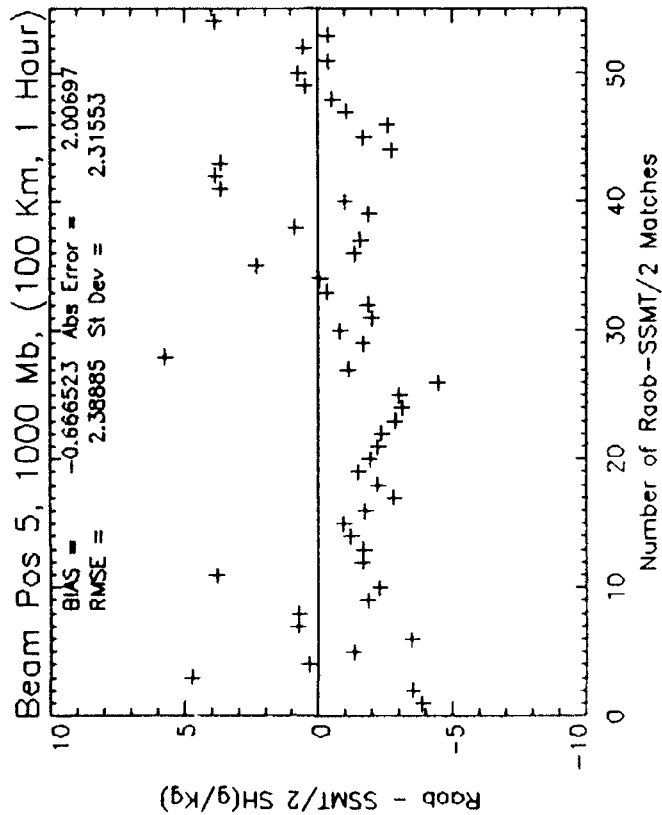


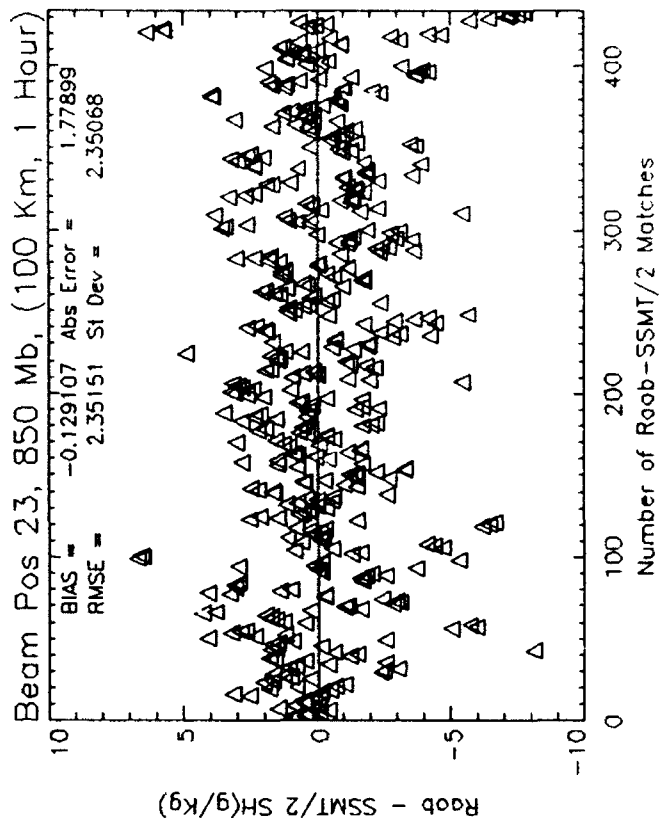
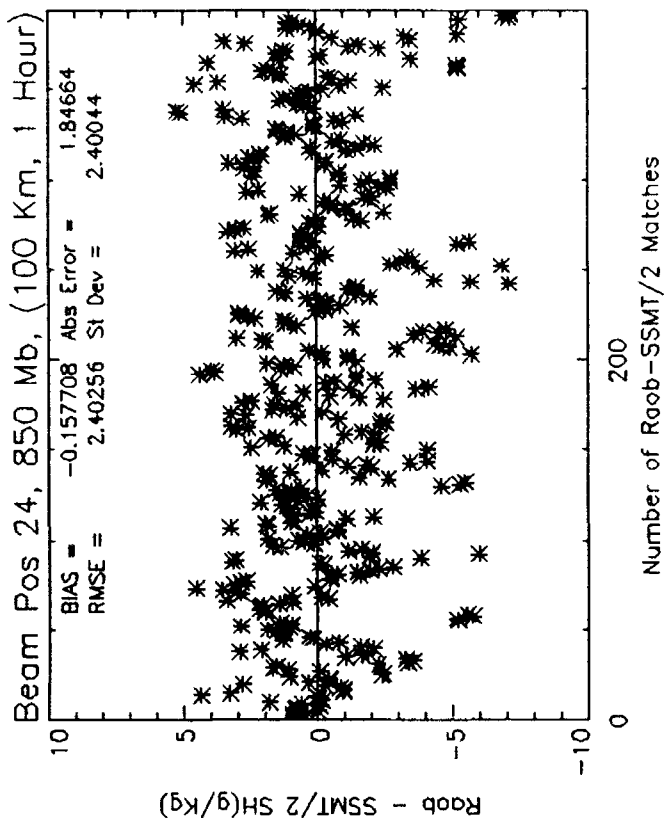
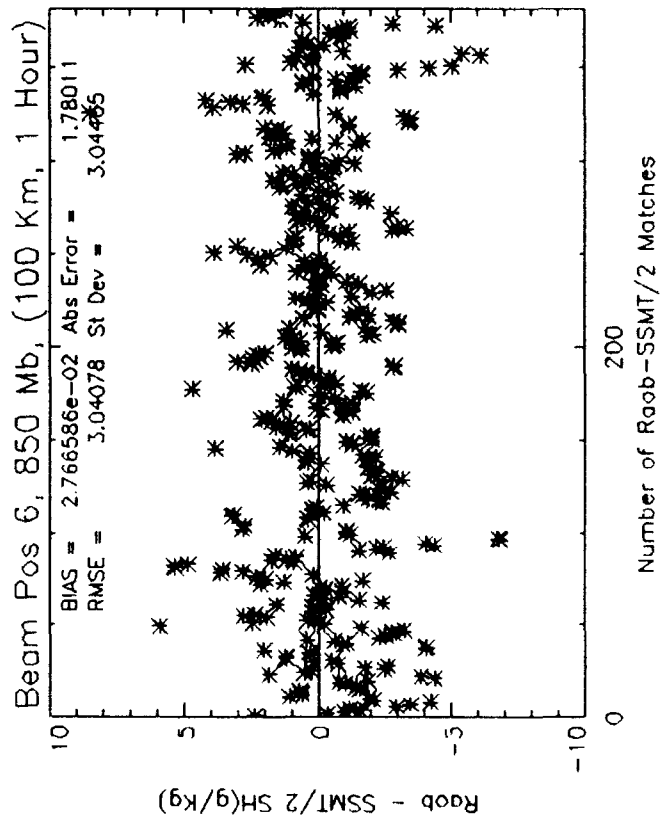
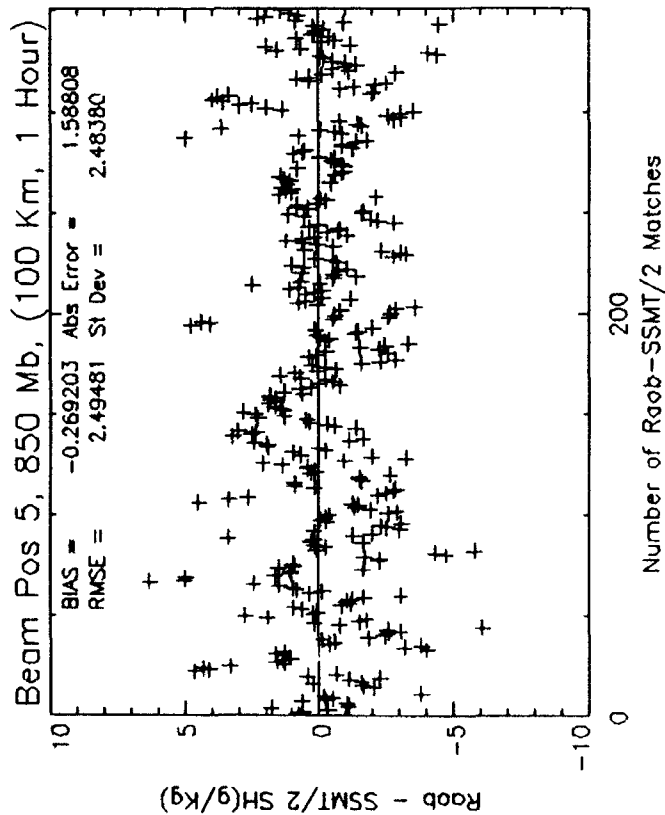




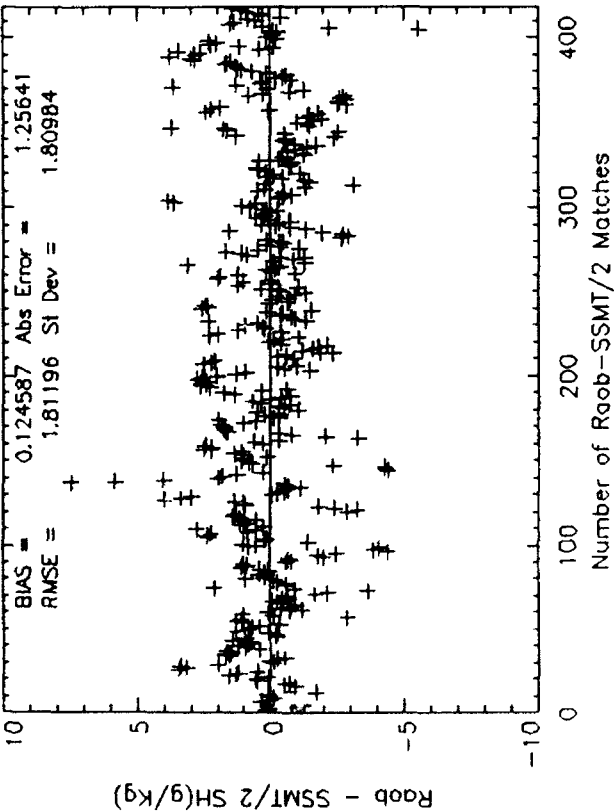
Appendix H. For symmetric beam pairs about nadir, the quantity (Radiosonde - SSM/T-2) RH and Q plotted on the ordinate, and the index of the co-locations on the abscissa. Recall that beam position 5 is the artificial edge of the SSM/T-2 scans due to the GLOB effects on SSM/T-1 mentioned earlier. Beam position 24 is the symmetric beam on the opposite side of nadir. Beam positions 14 and 15 straddle nadir. Each four-plot panel represents one atmospheric level. The co-location criteria are annotated at the top of the plots.



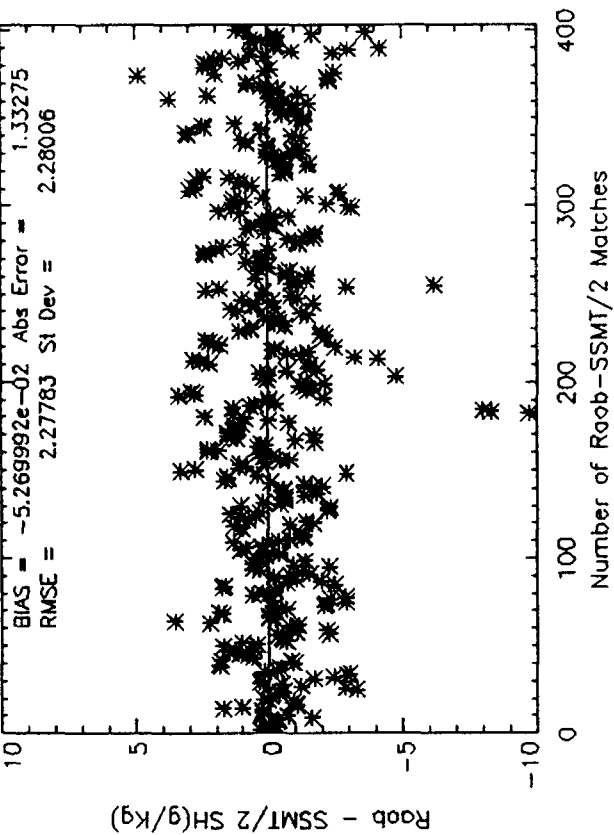




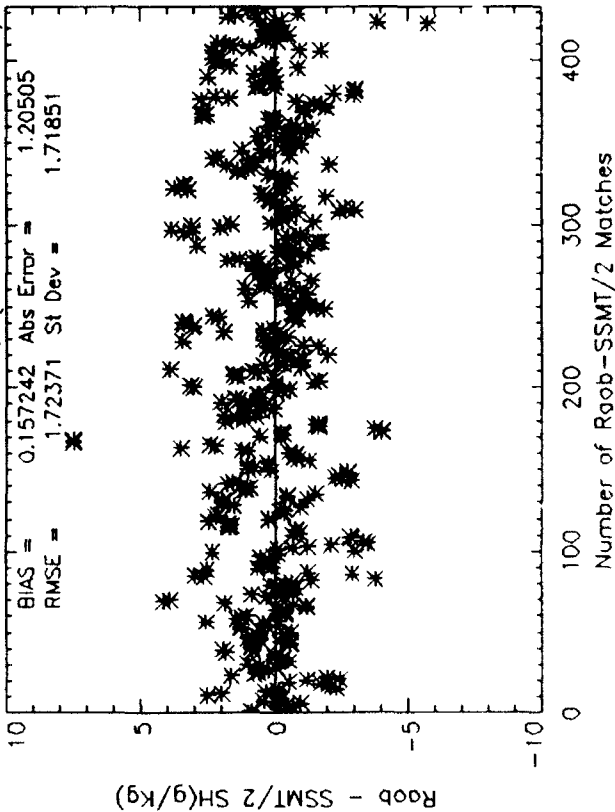
Beam Pos 5, 700 Mb, (100 Km, 1 Hour)



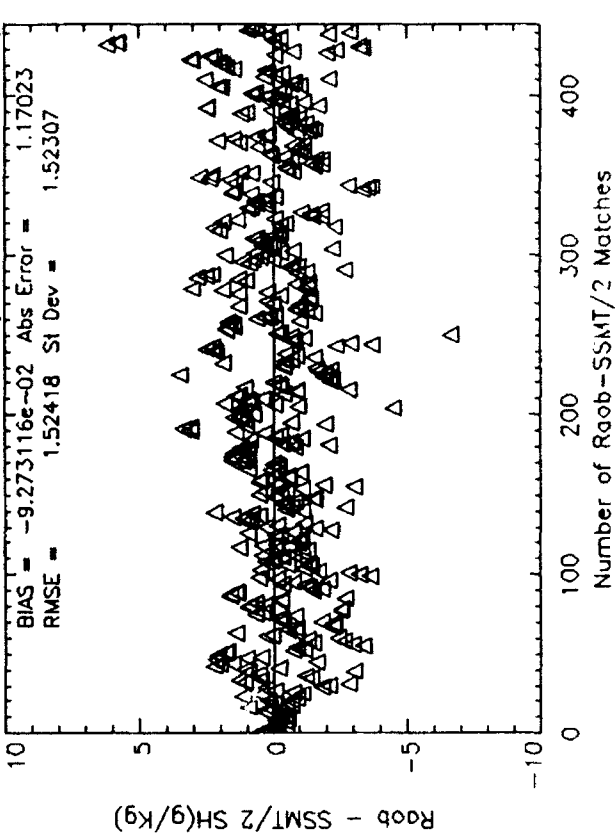
Beam Pos 24, 700 Mb, (100 Km, 1 Hour)

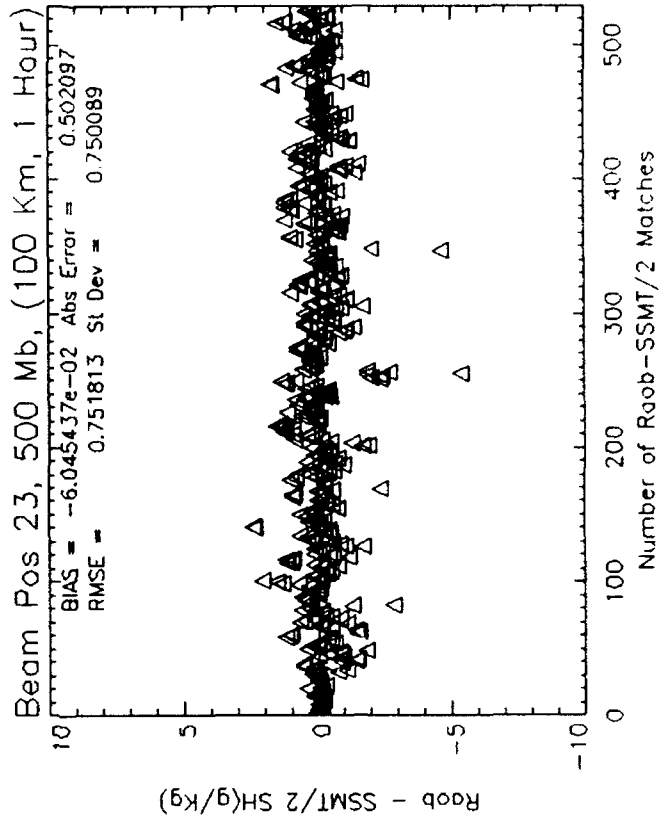
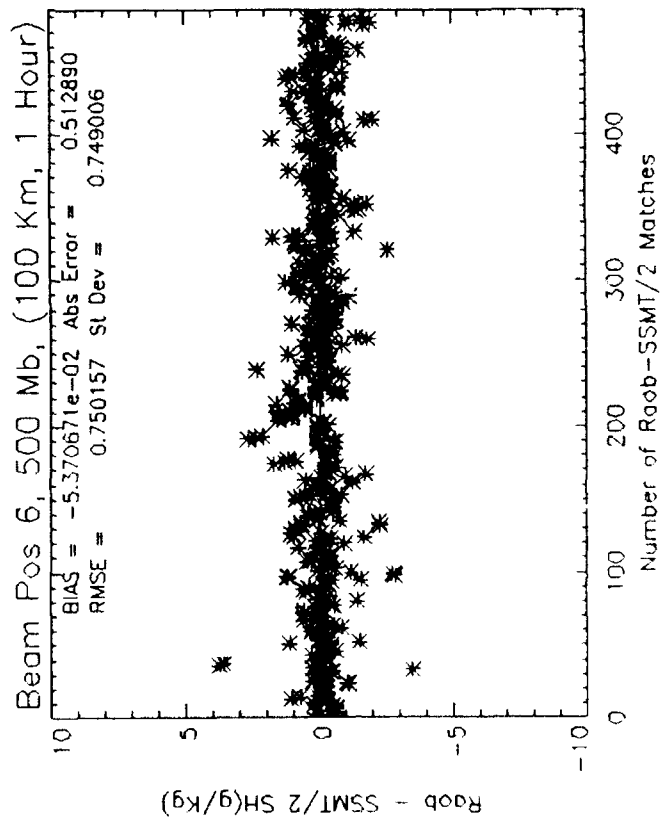
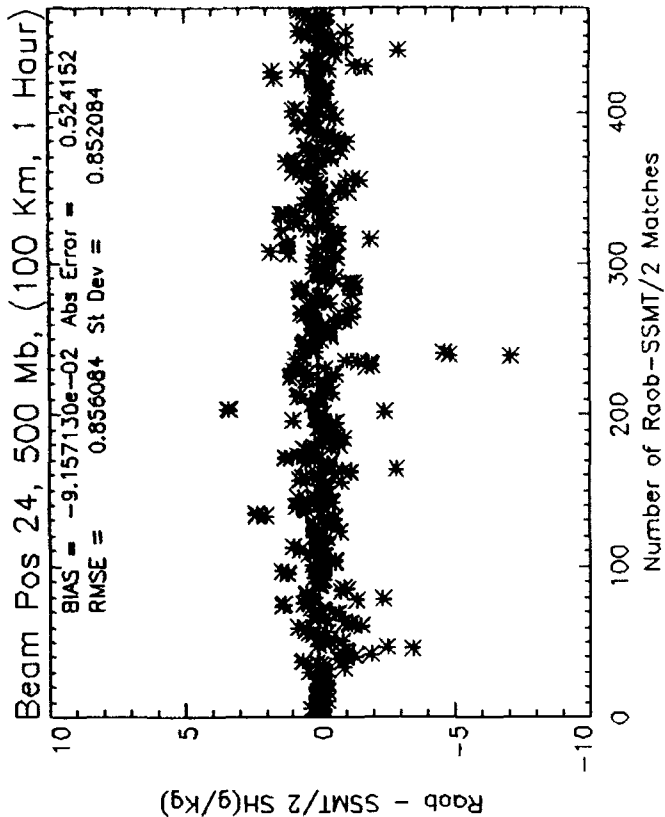
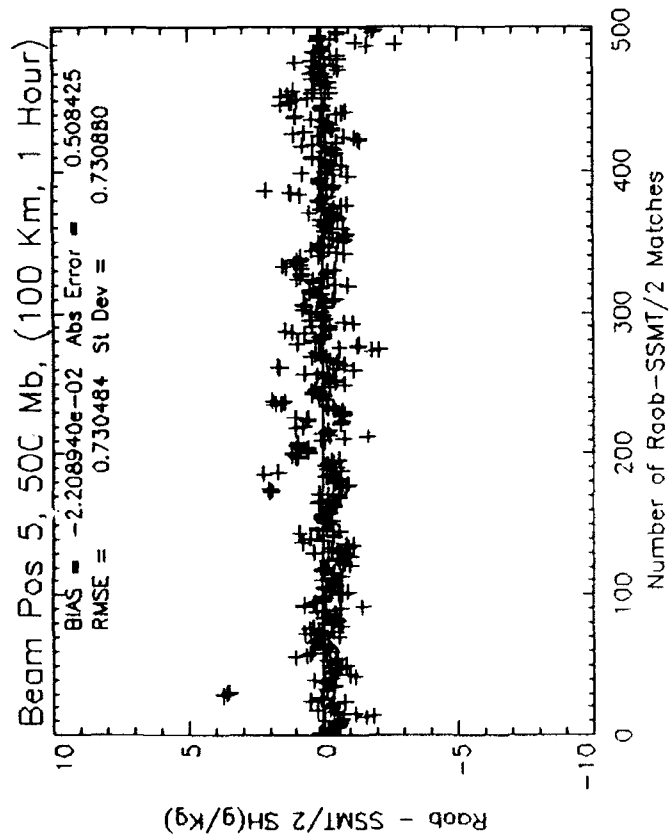


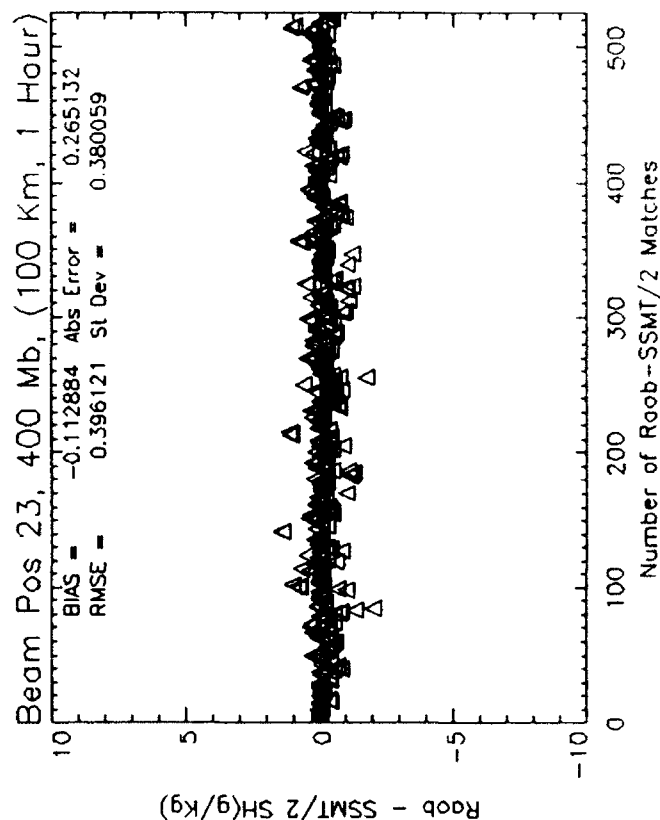
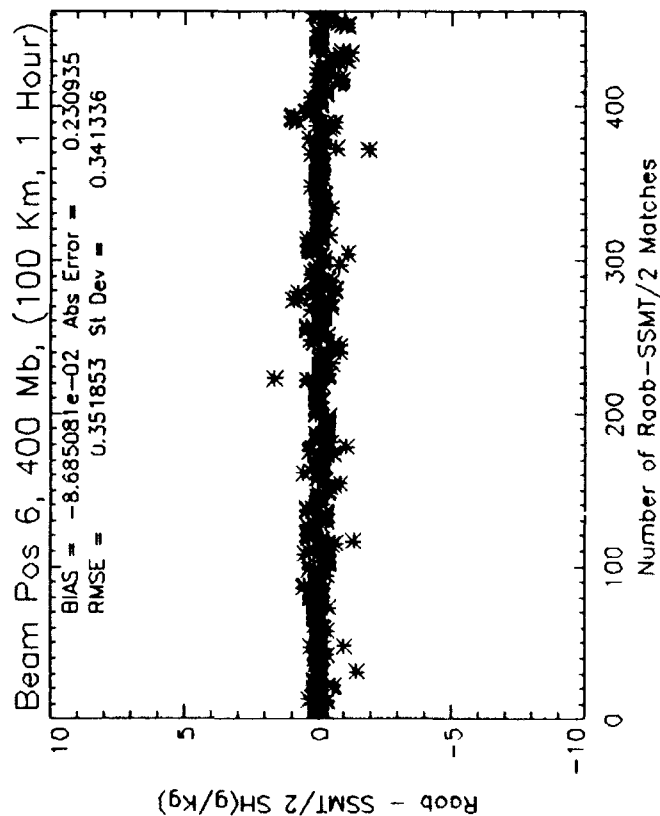
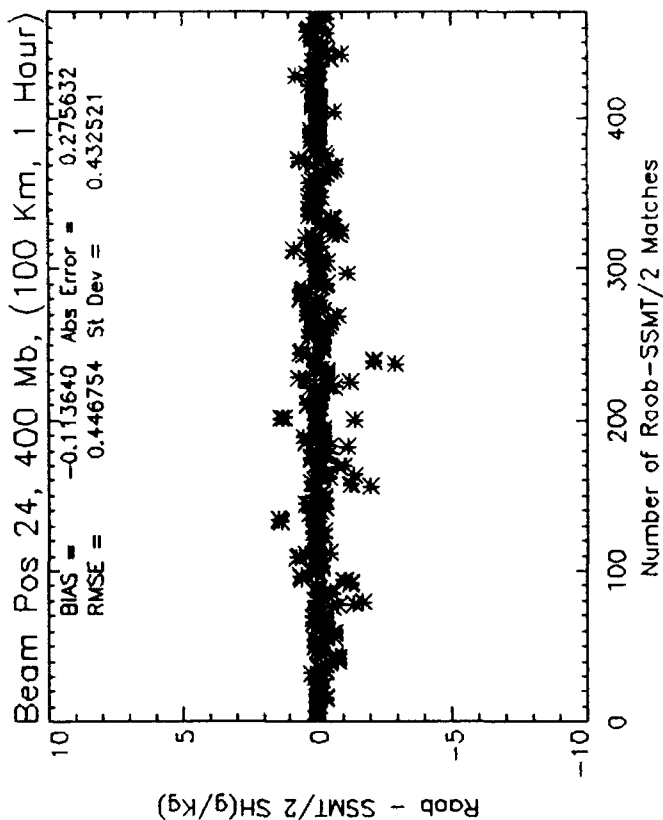
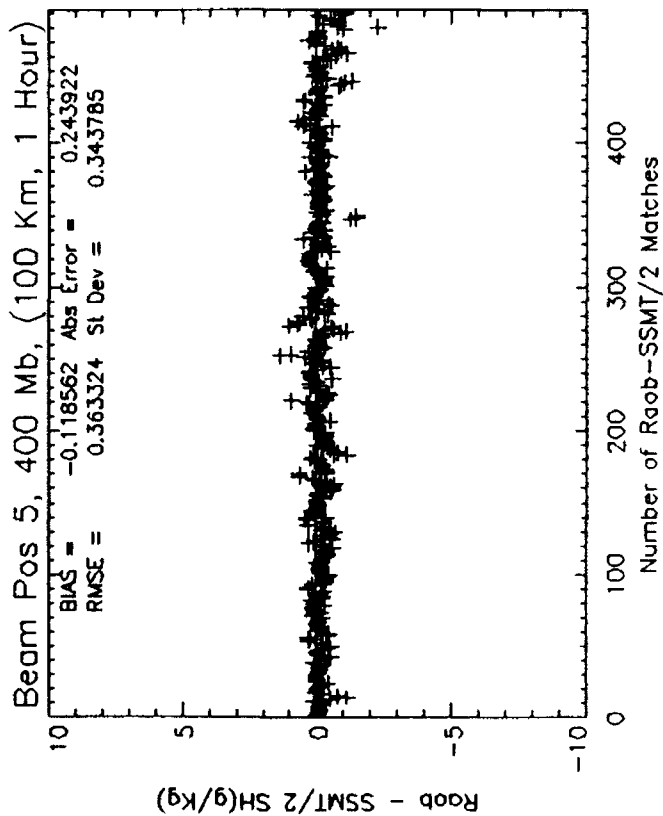
Beam Pos 6, 700 Mb, (100 Km, 1 Hour)

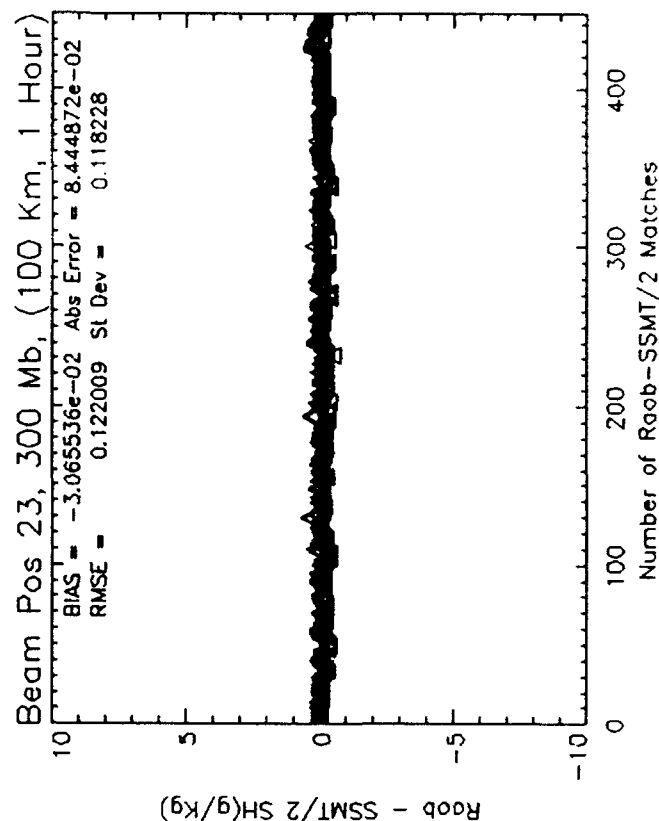
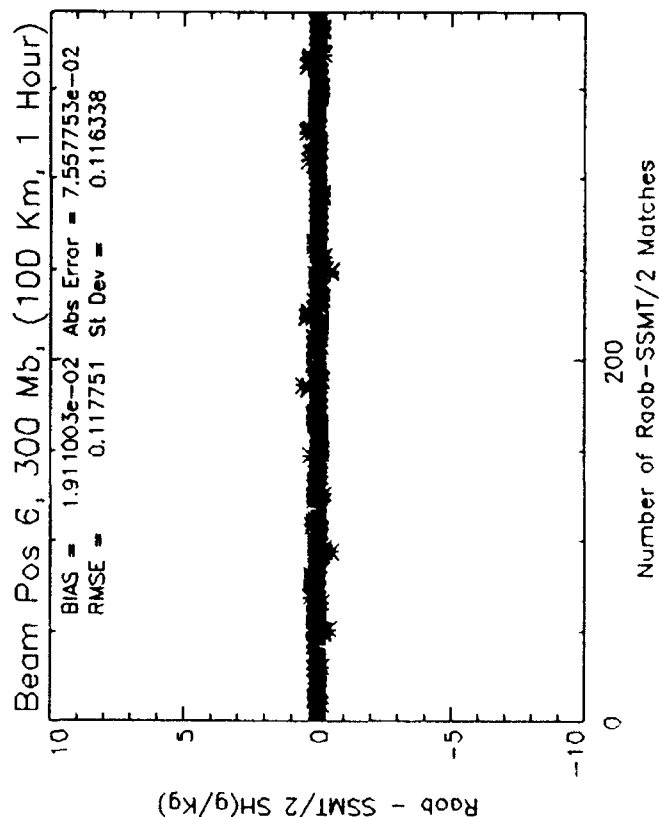
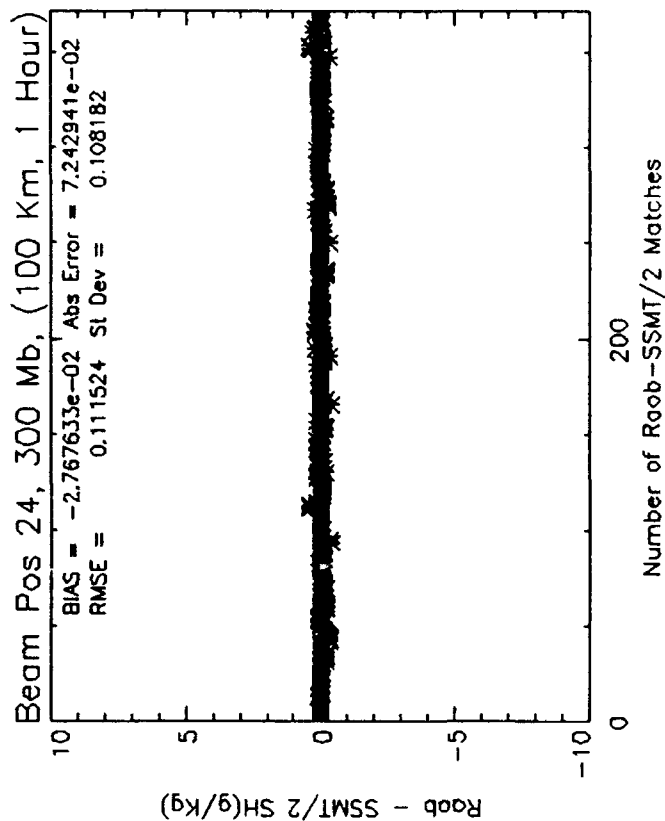
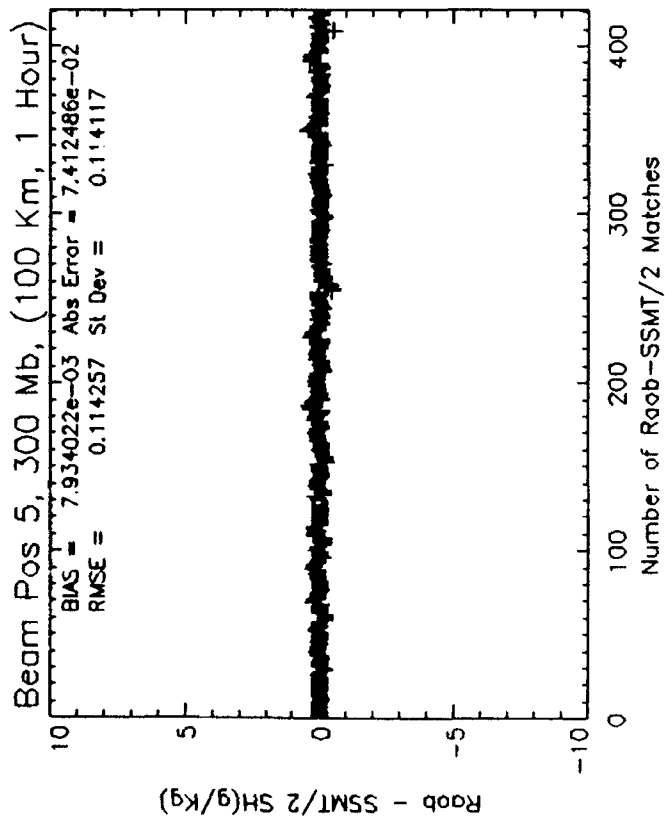


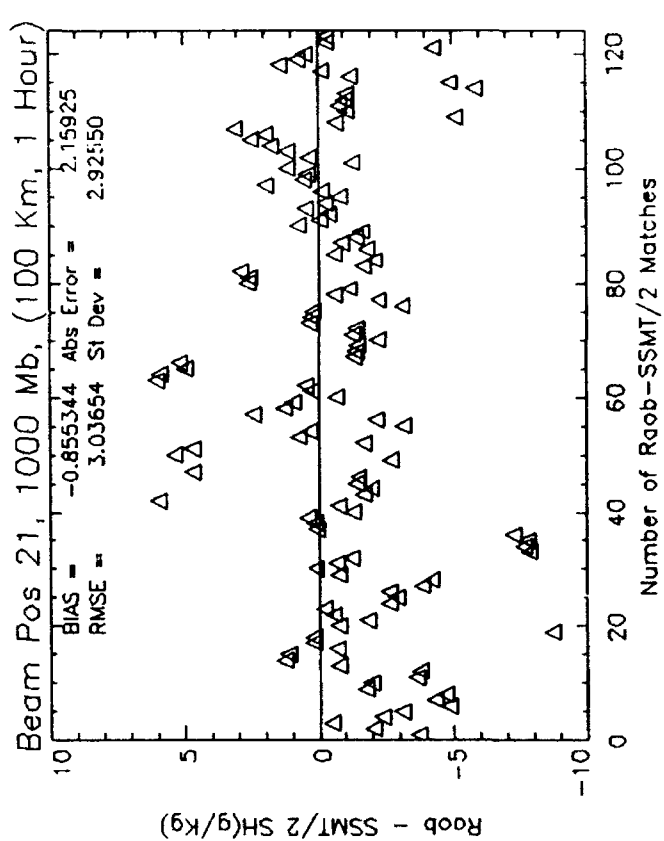
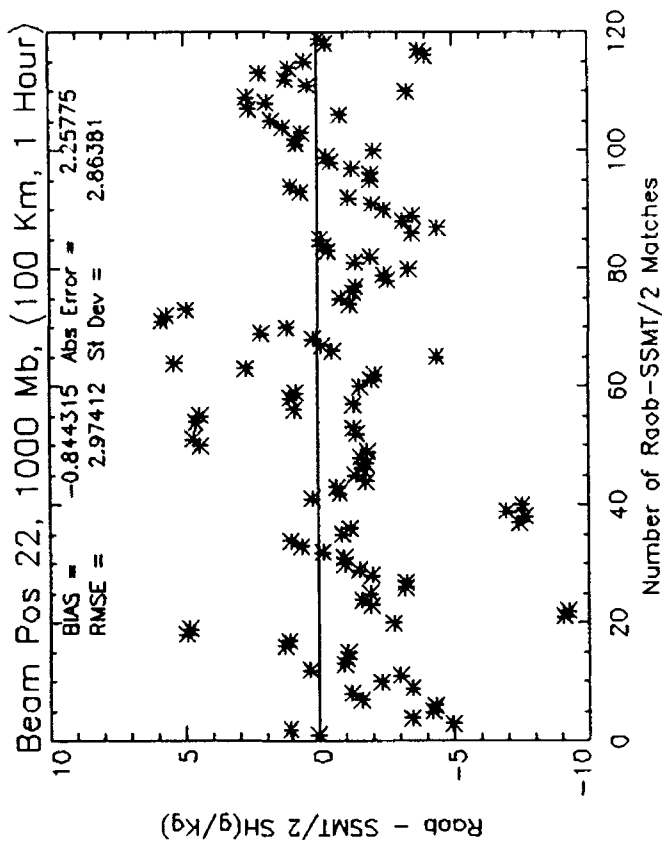
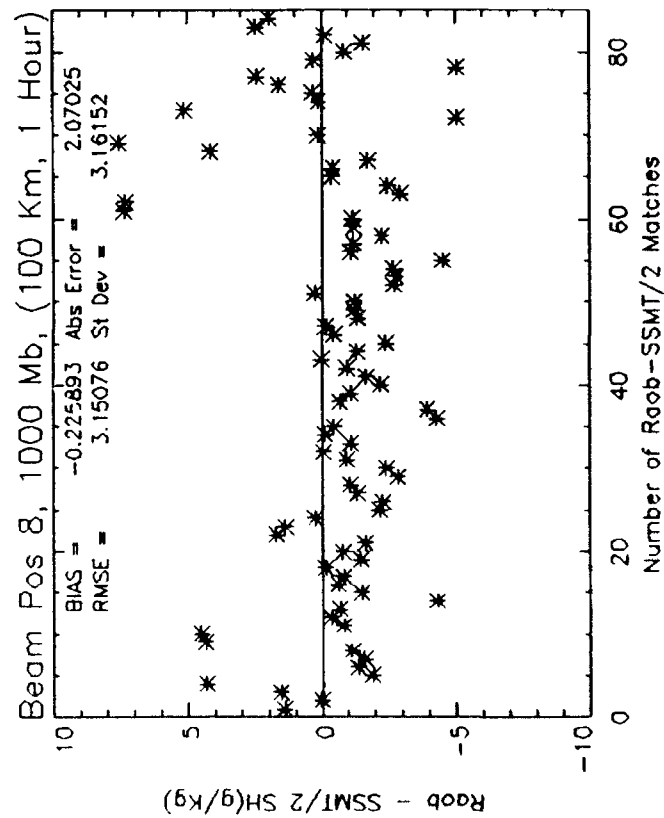
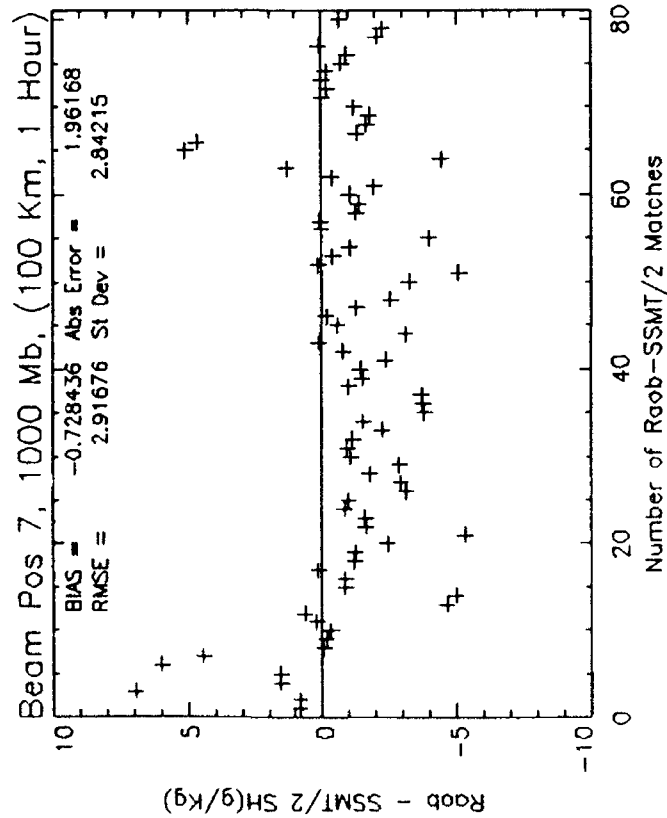
Beam Pos 23, 700 Mb, (100 Km, 1 Hour)

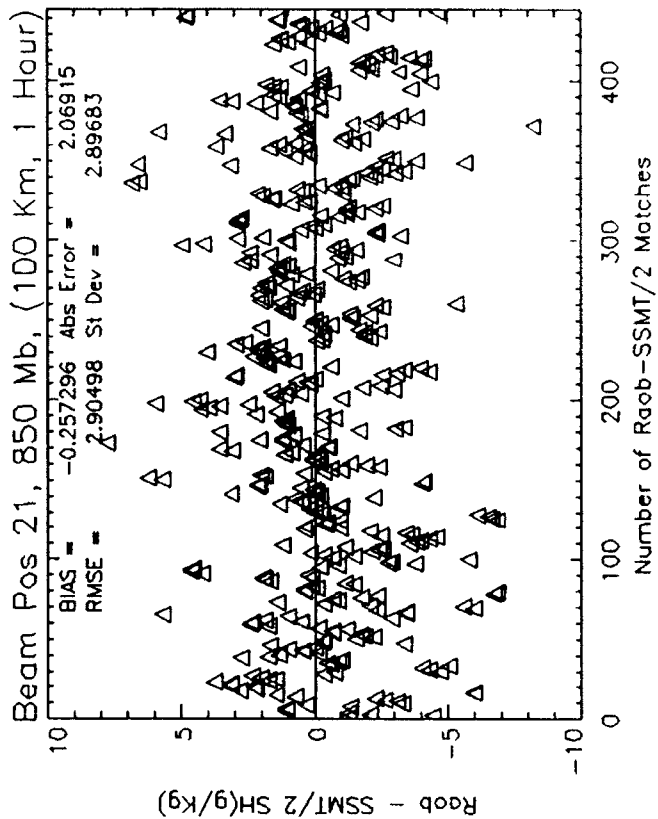
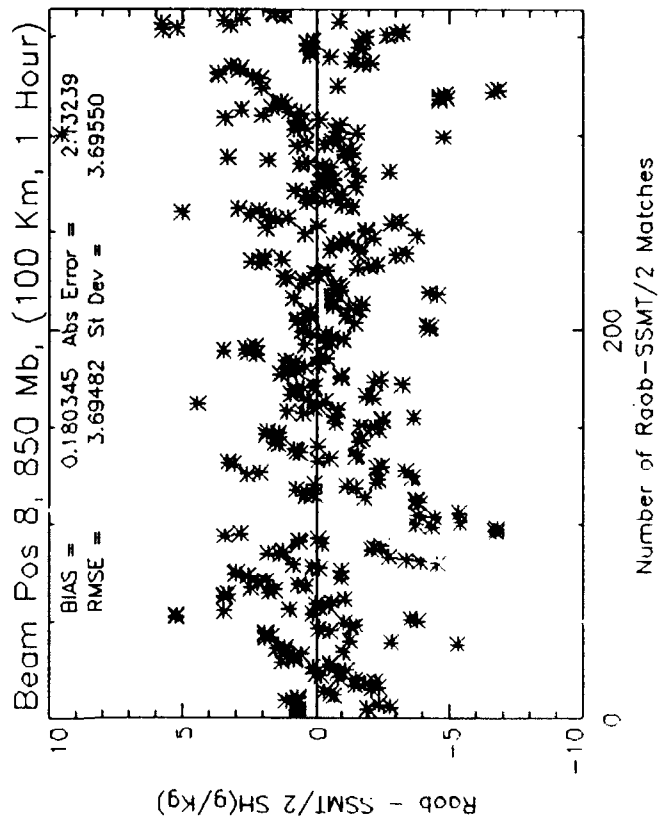
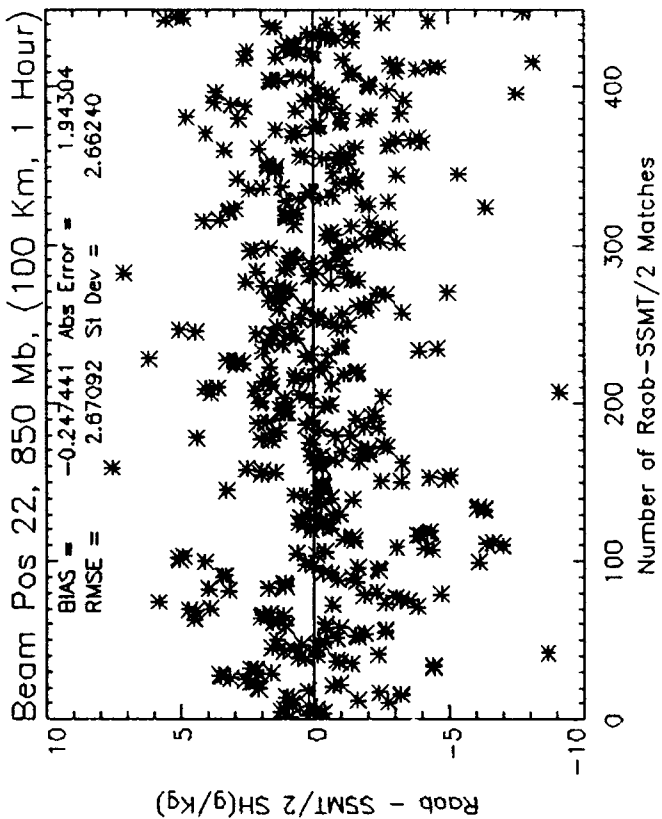
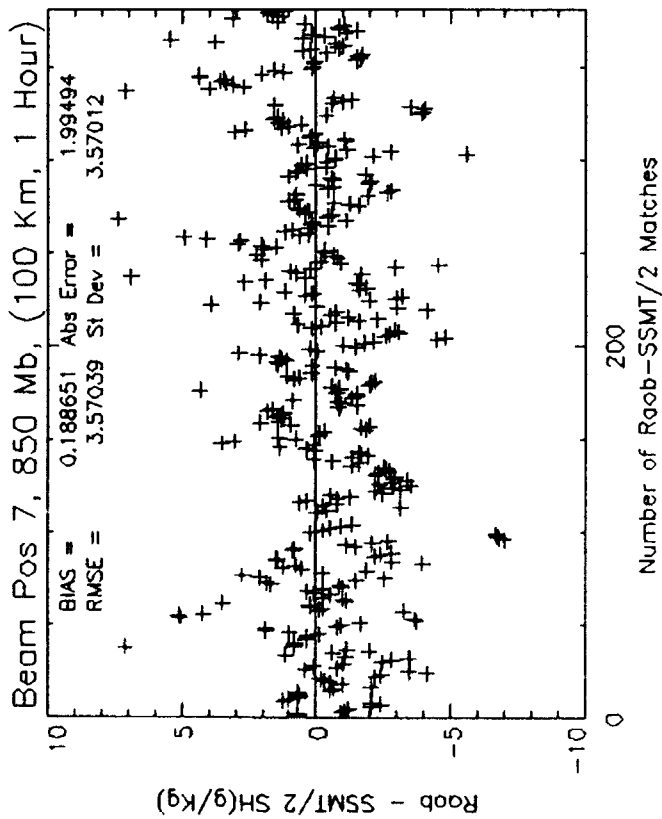




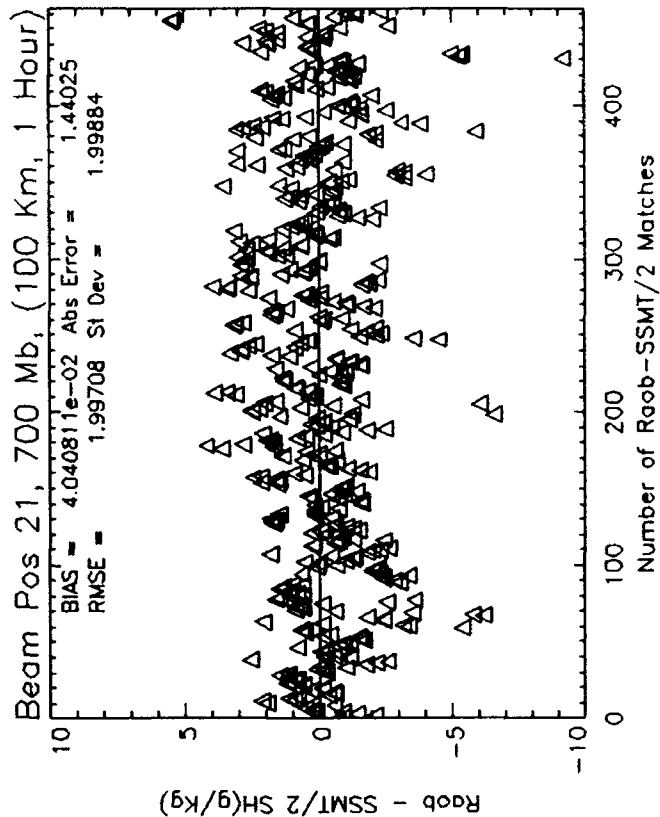
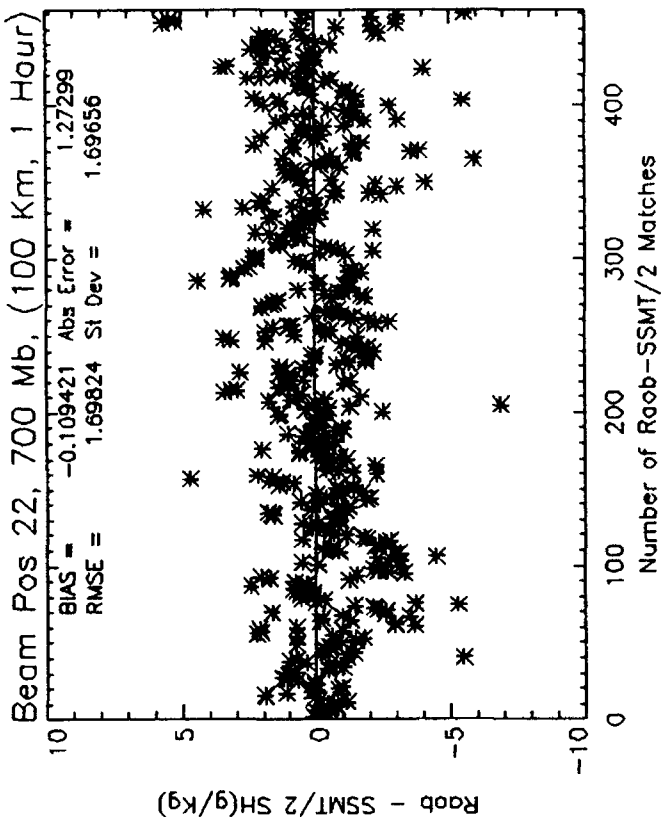
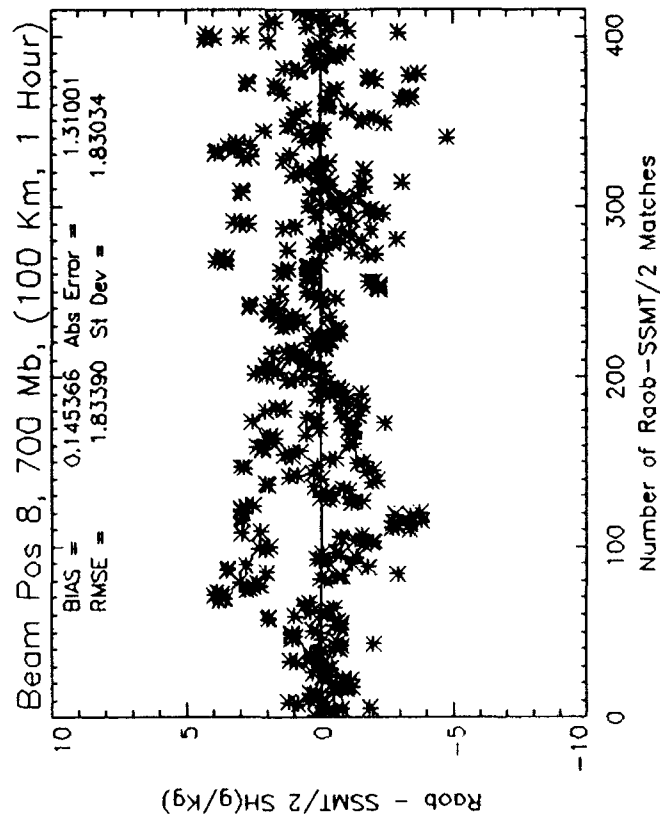
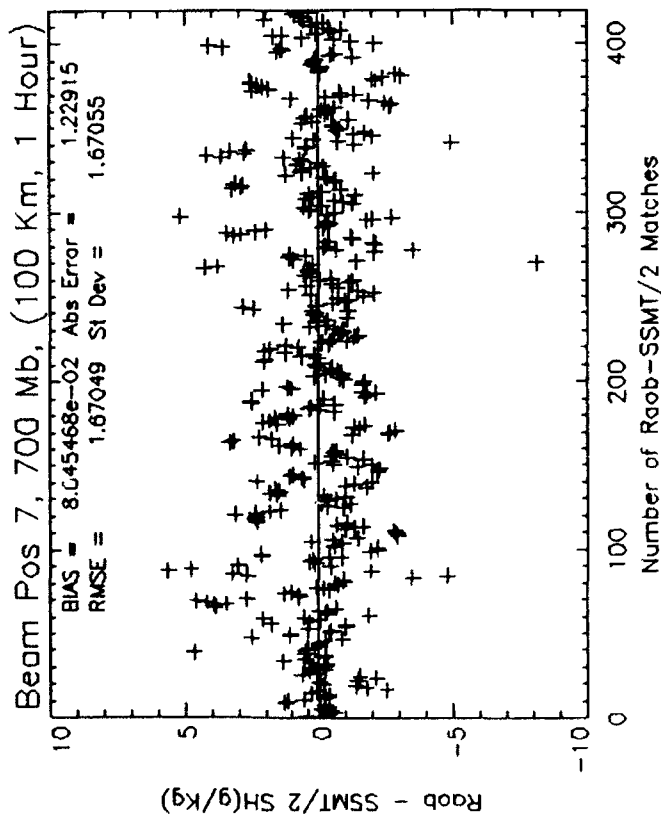


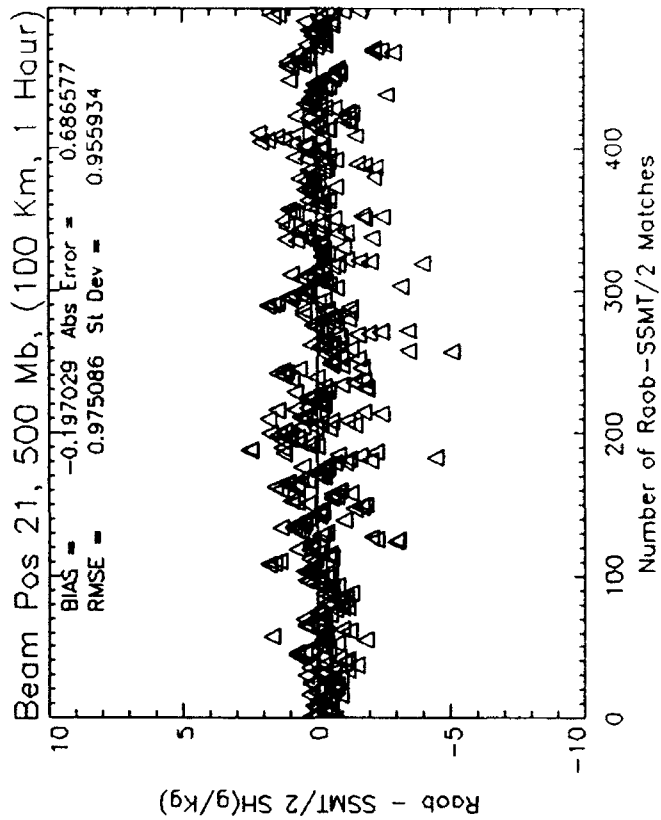
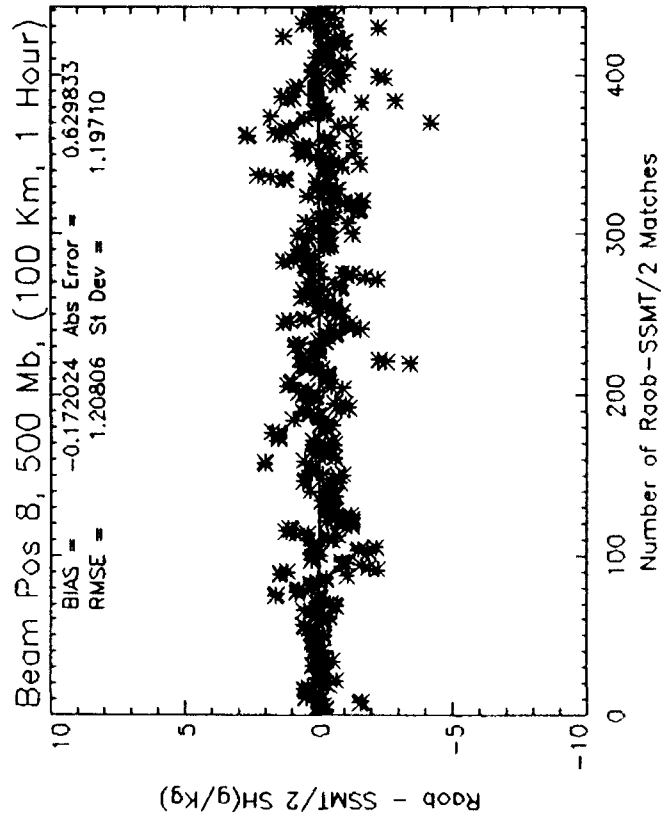
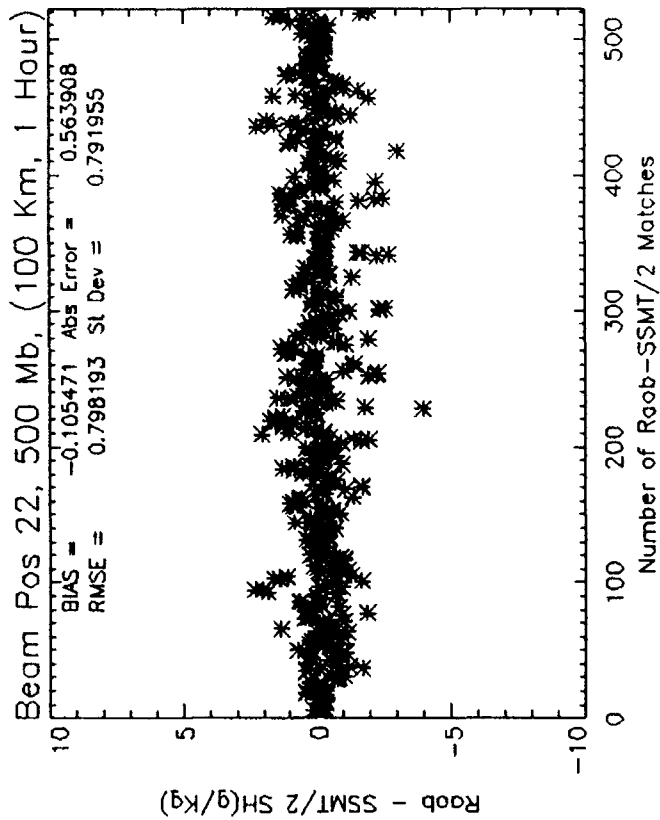
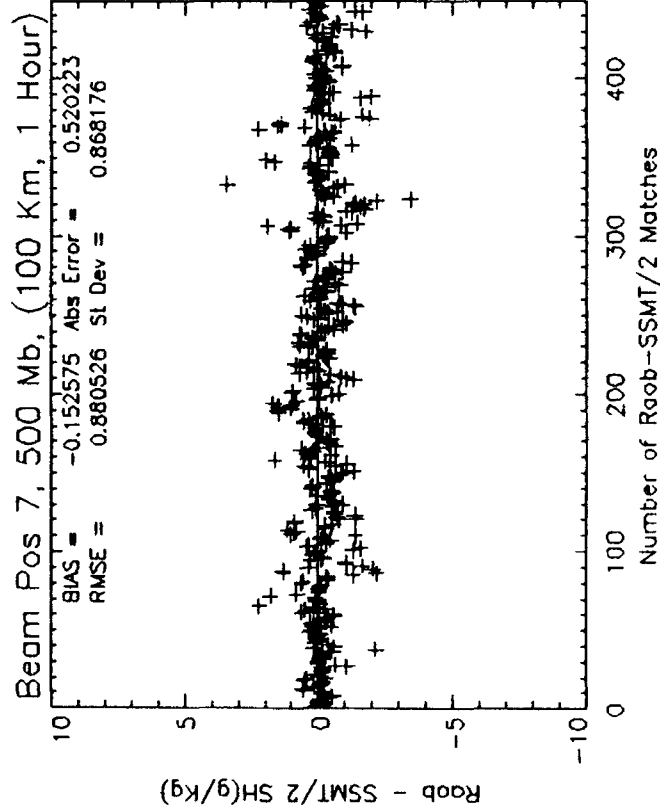


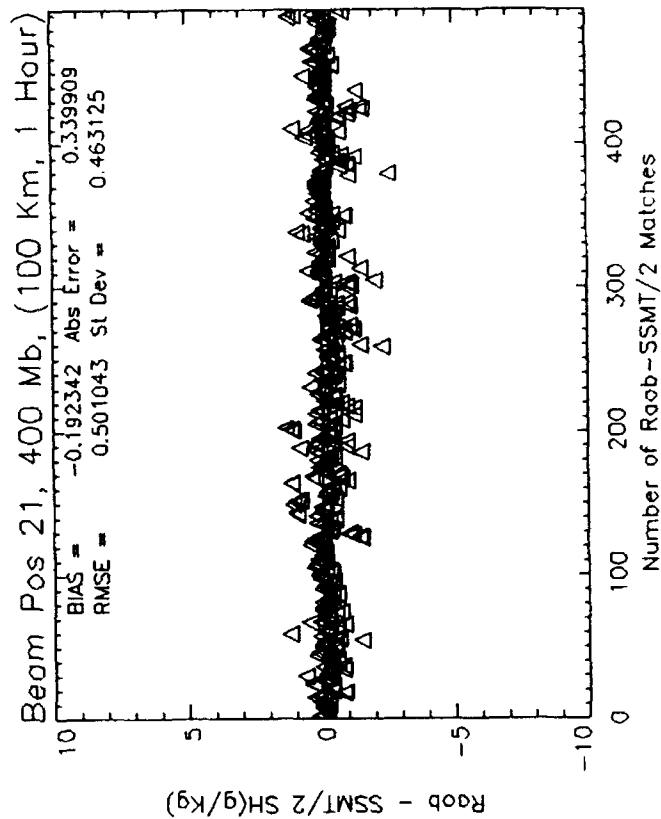
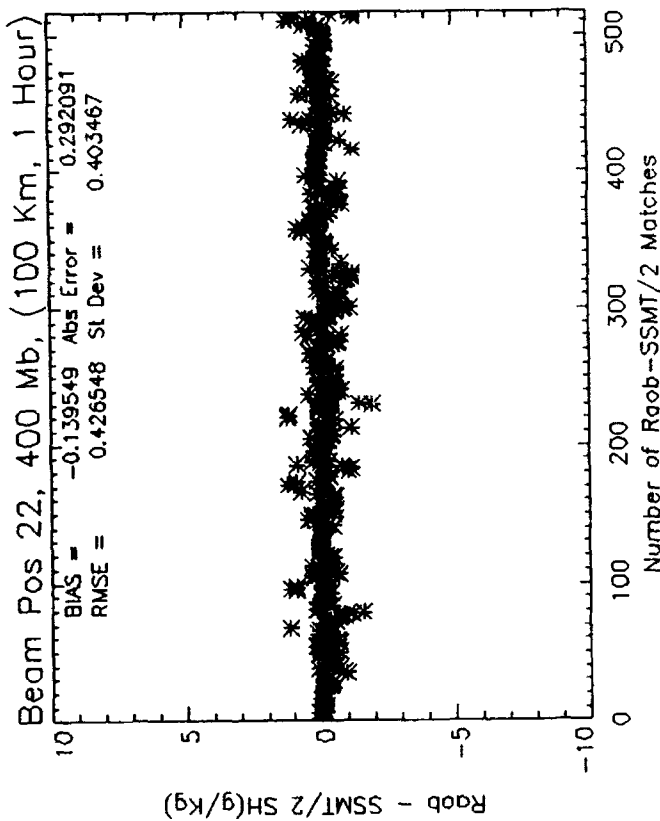
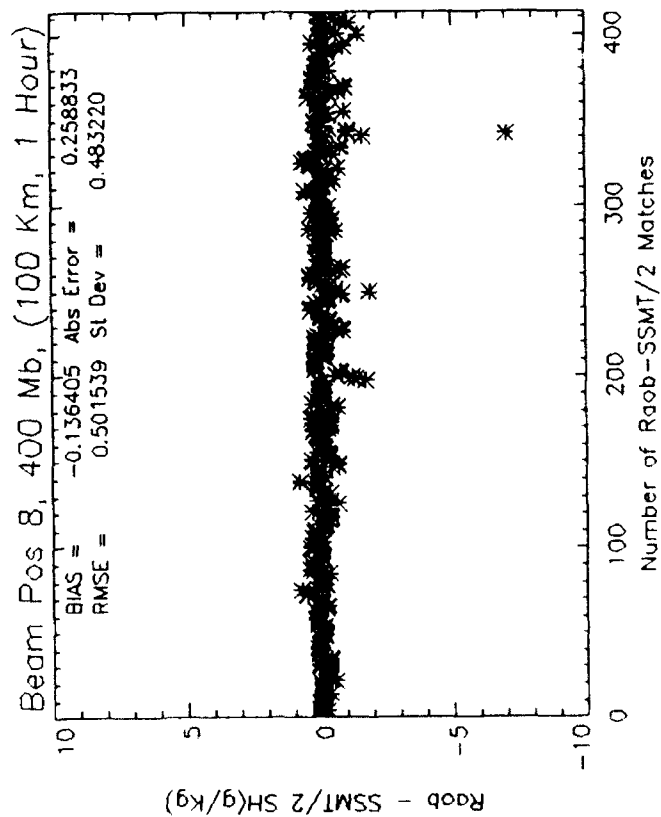
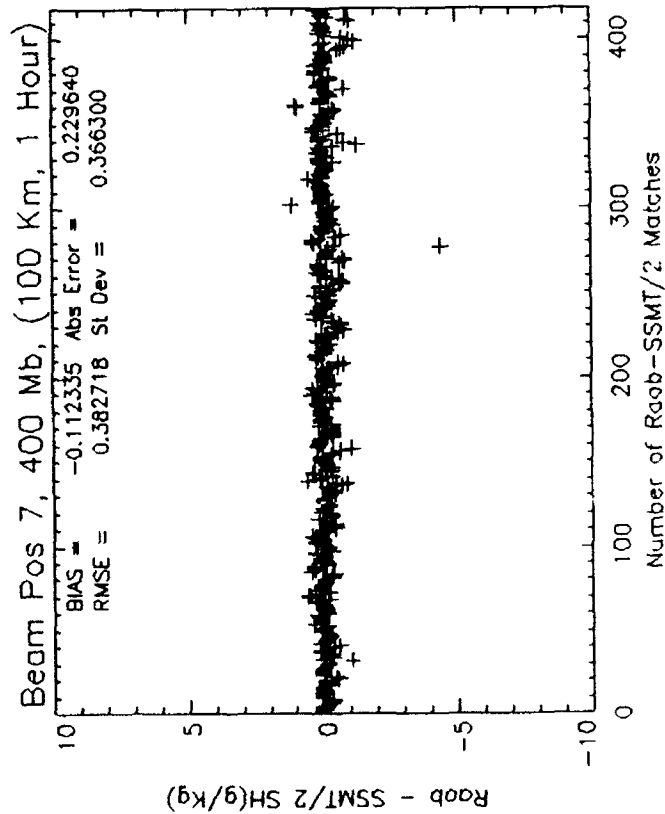


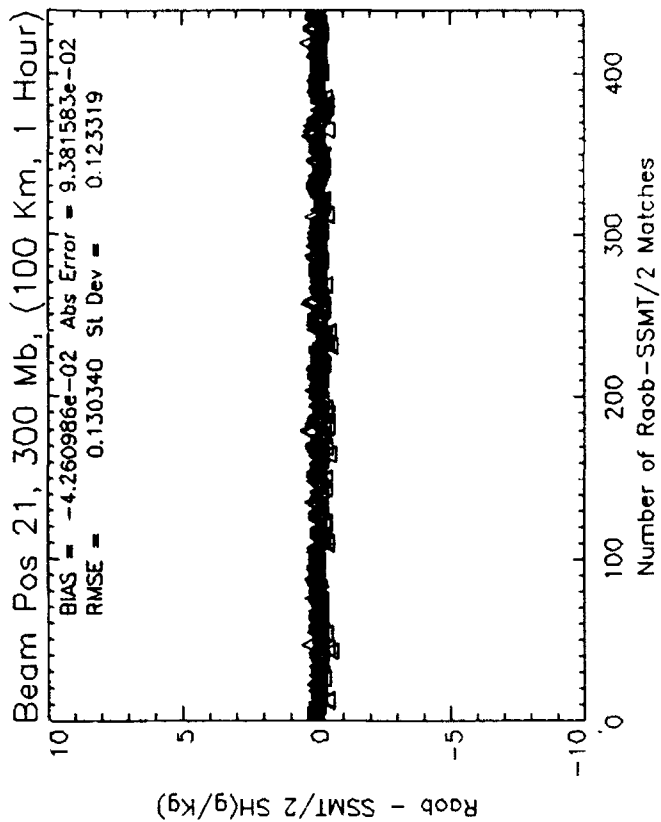
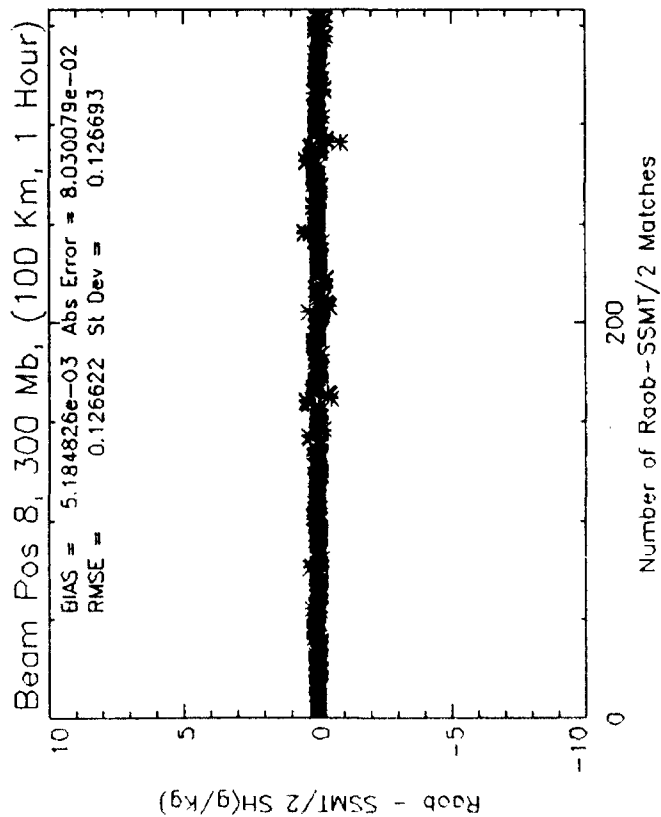
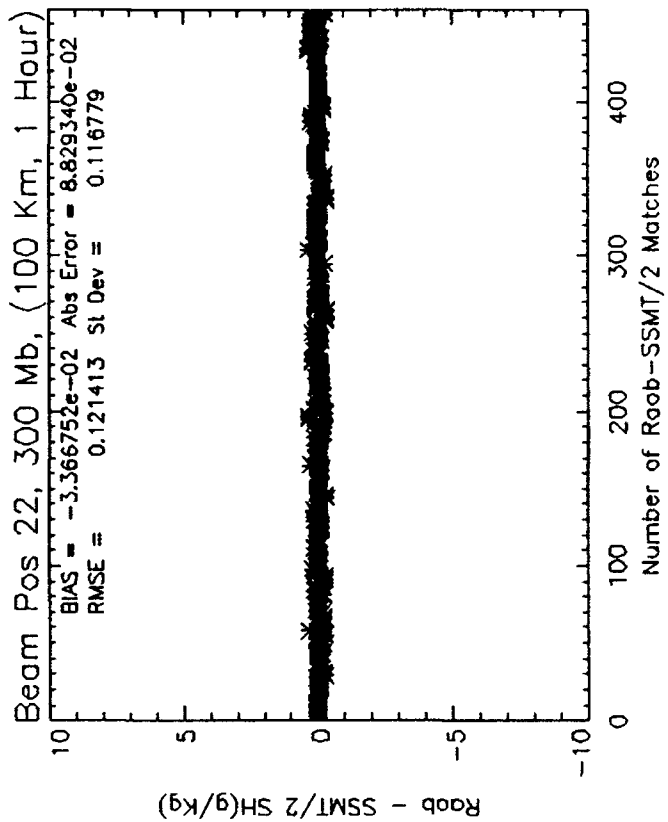
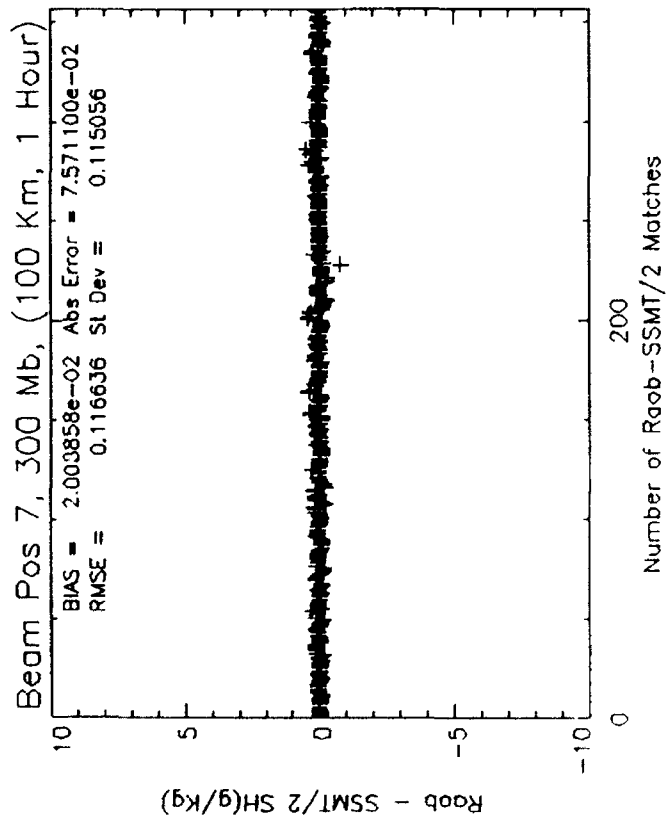


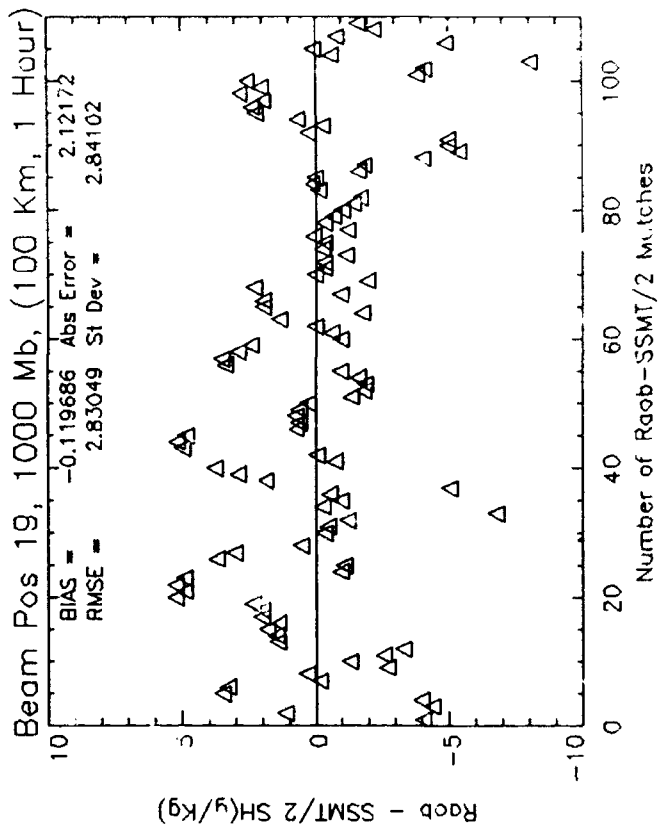
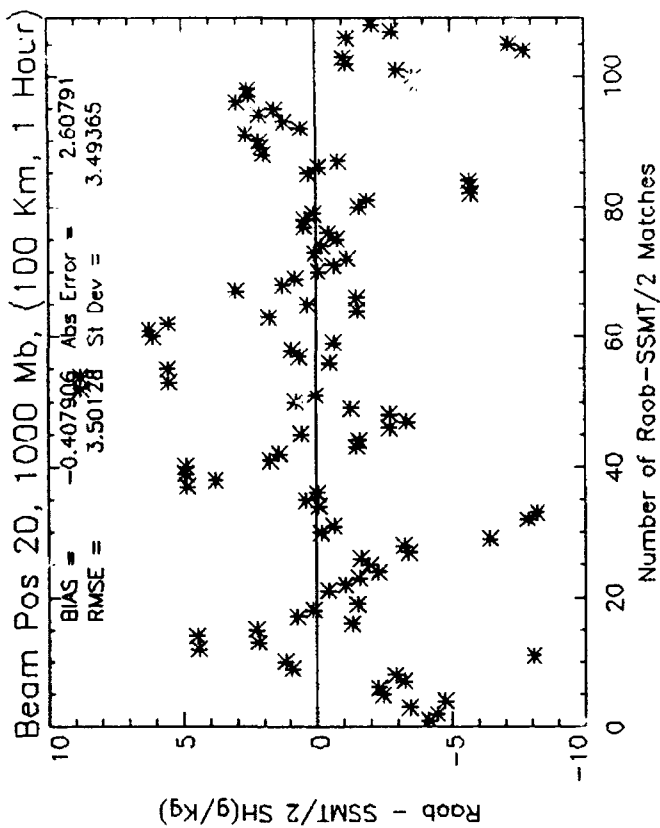
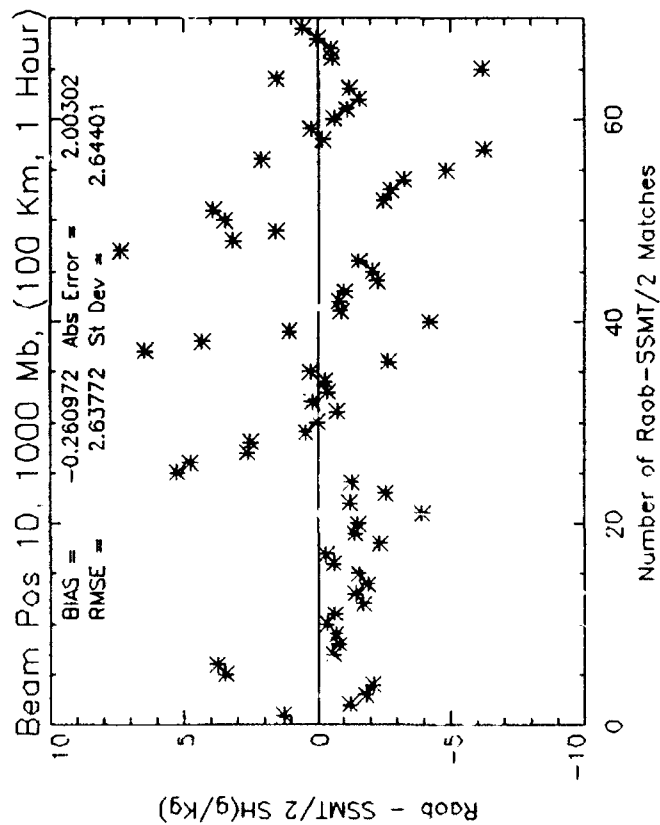
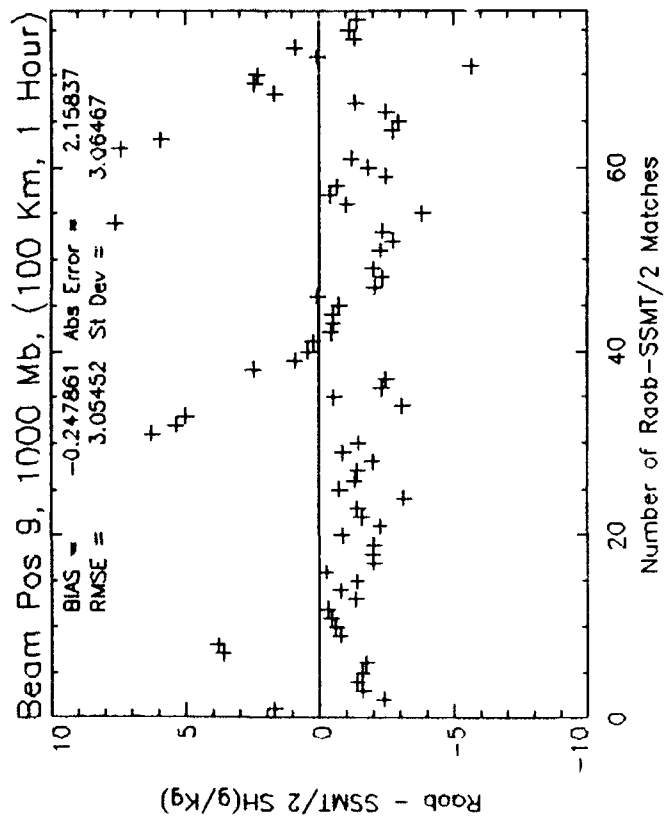


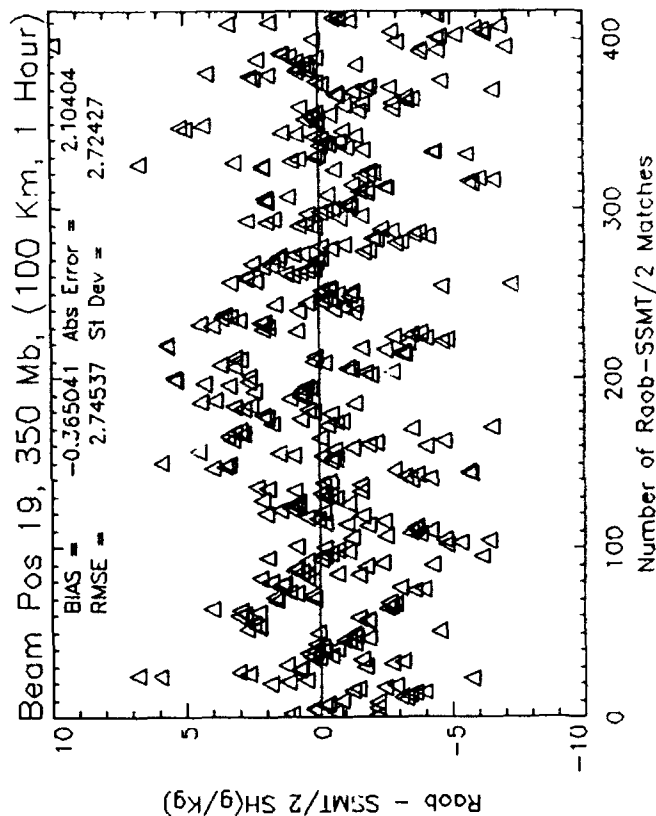
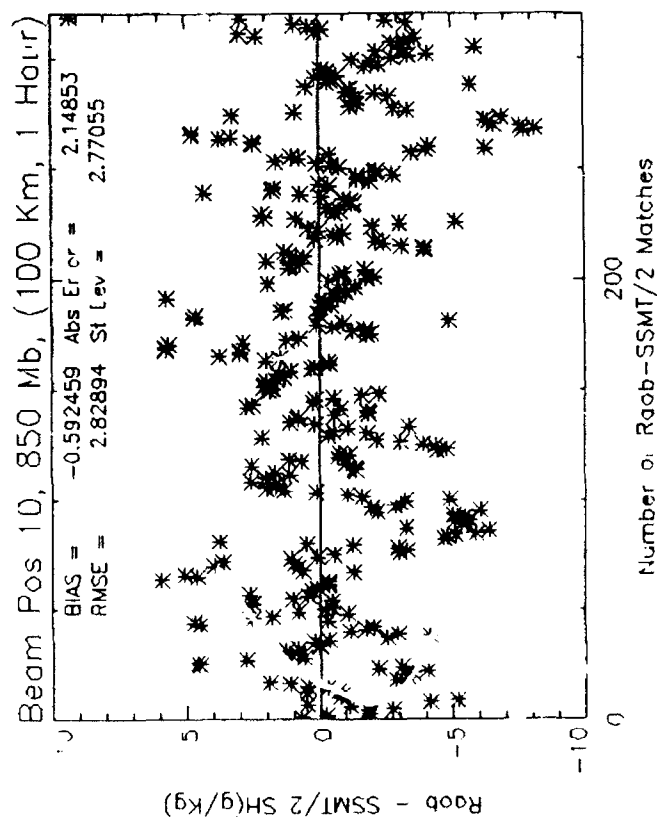
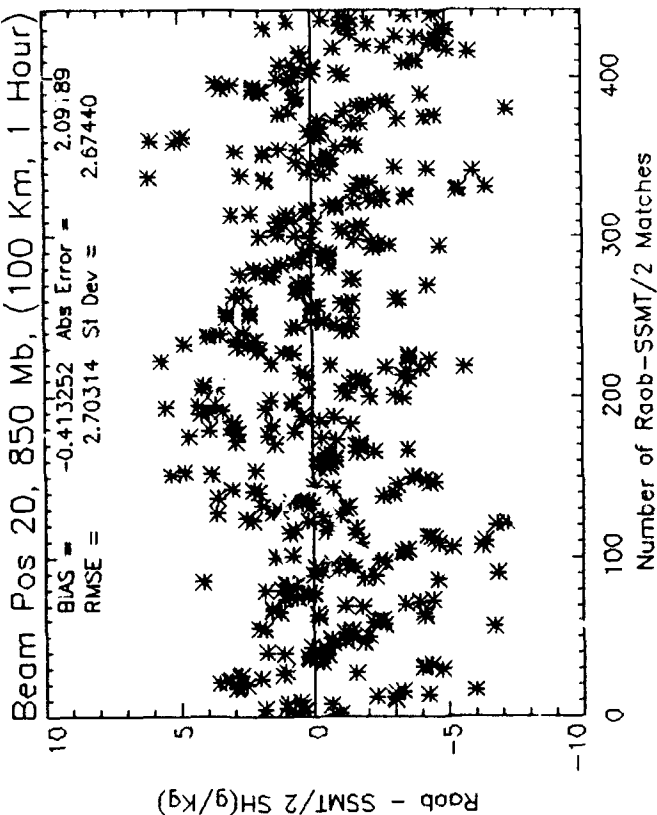
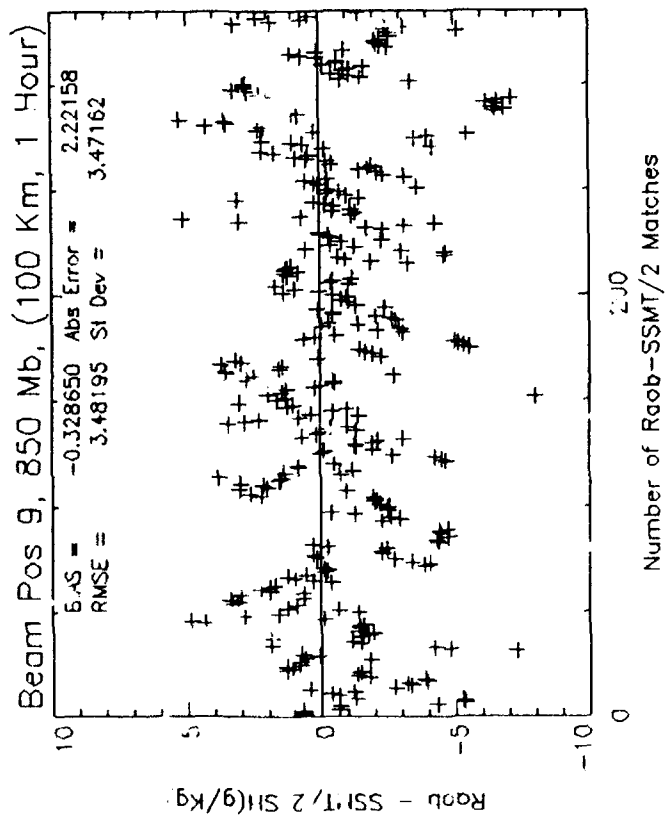


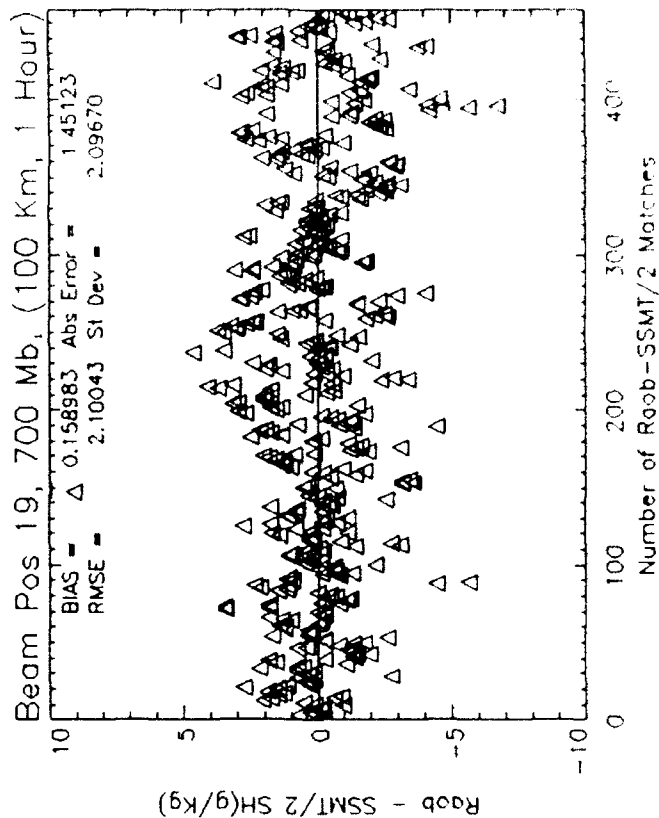
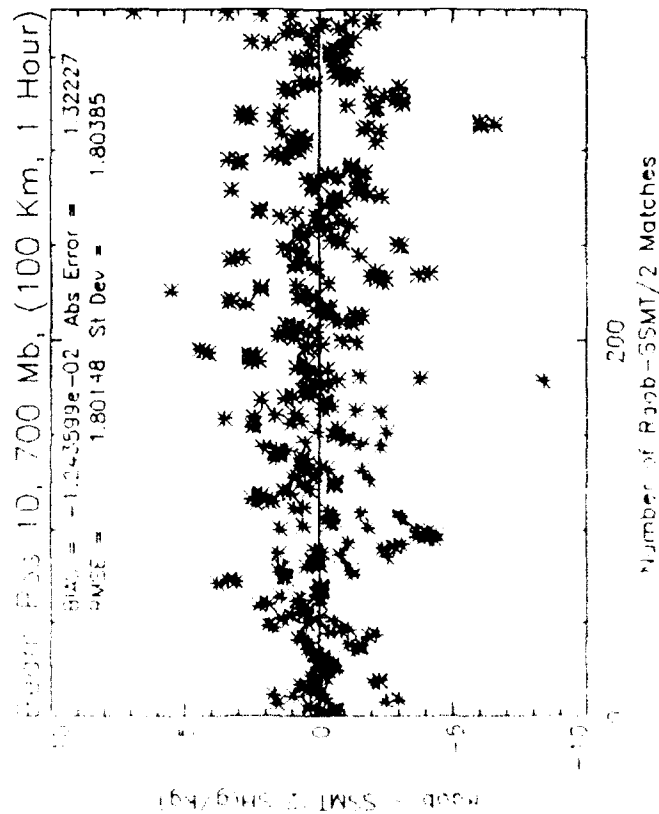
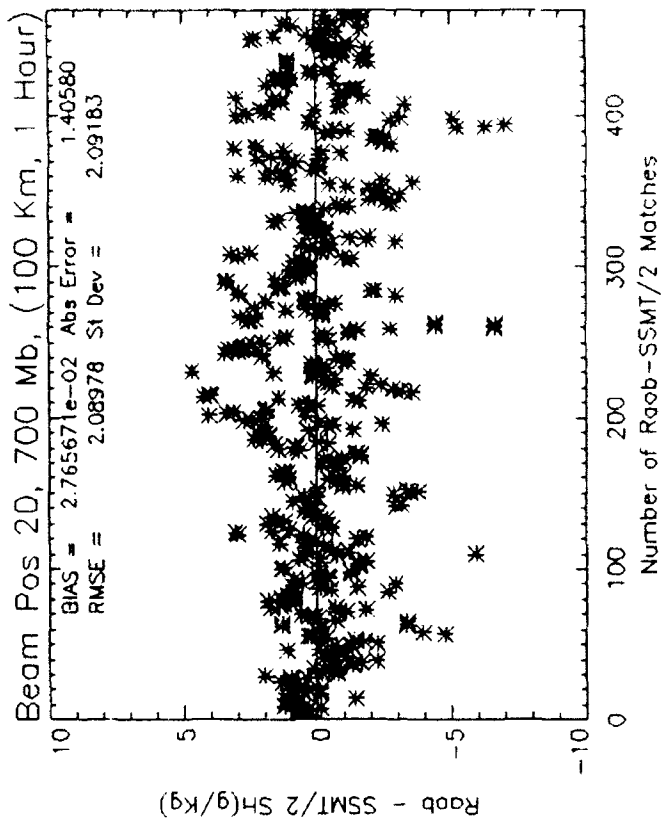
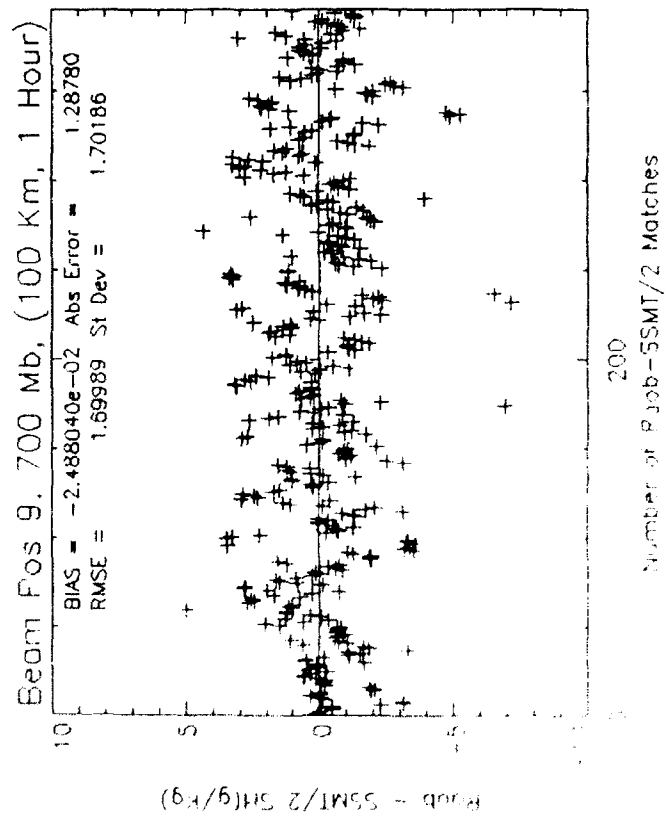


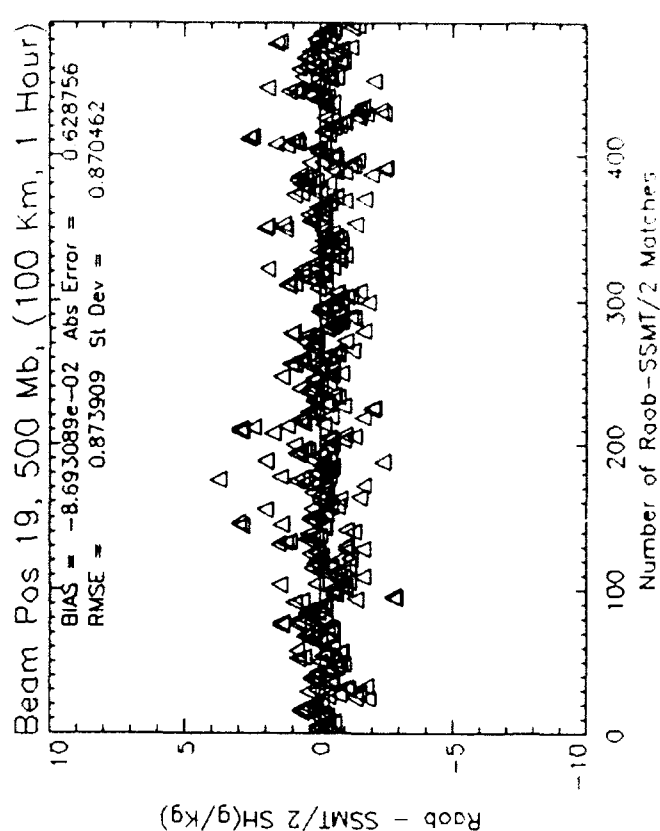
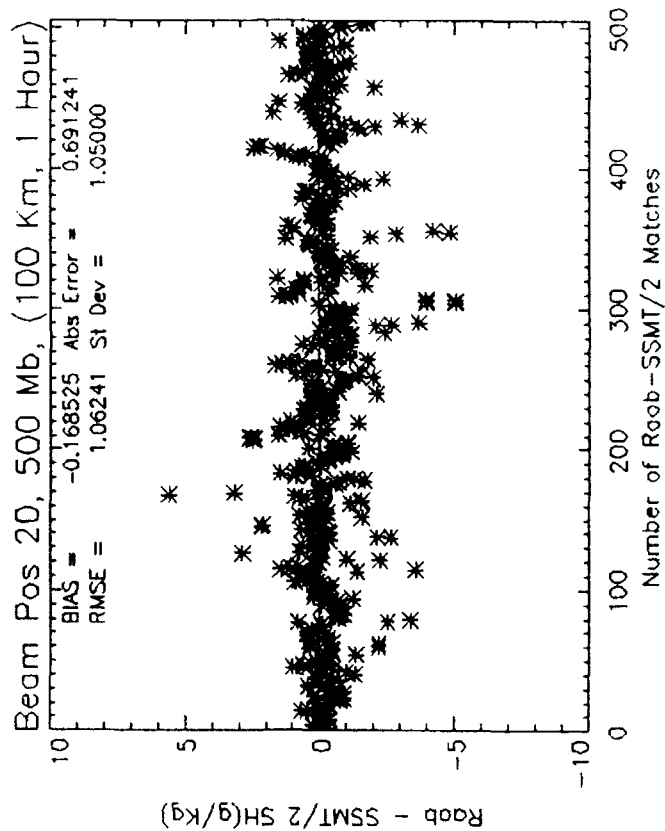
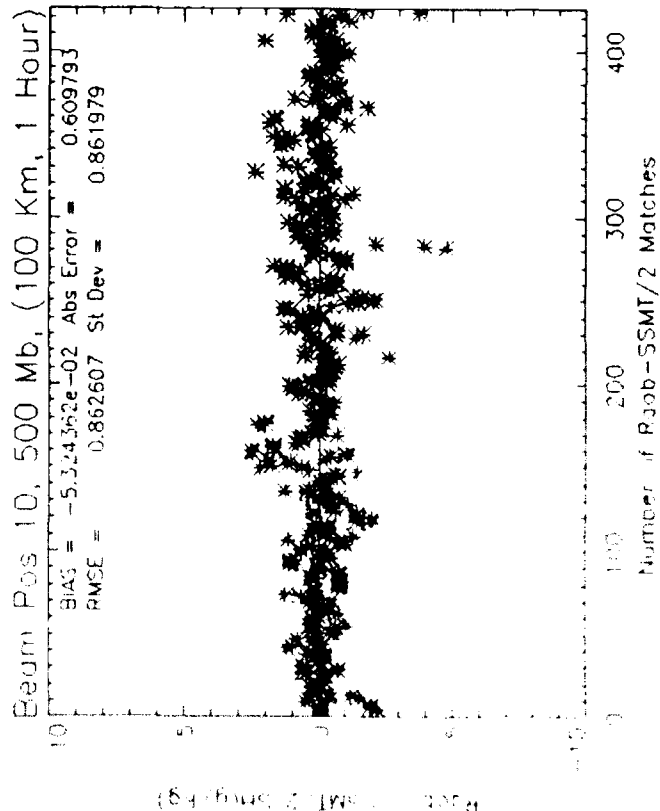
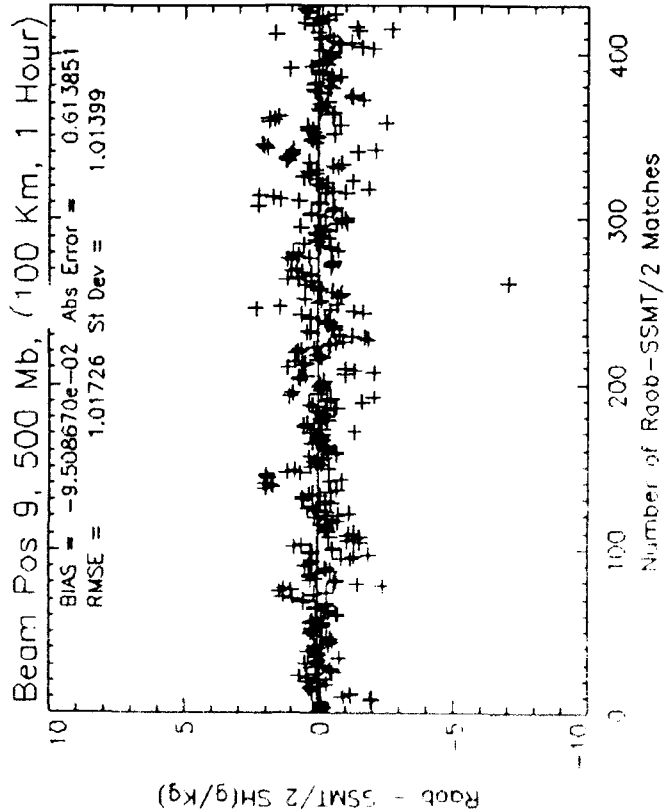




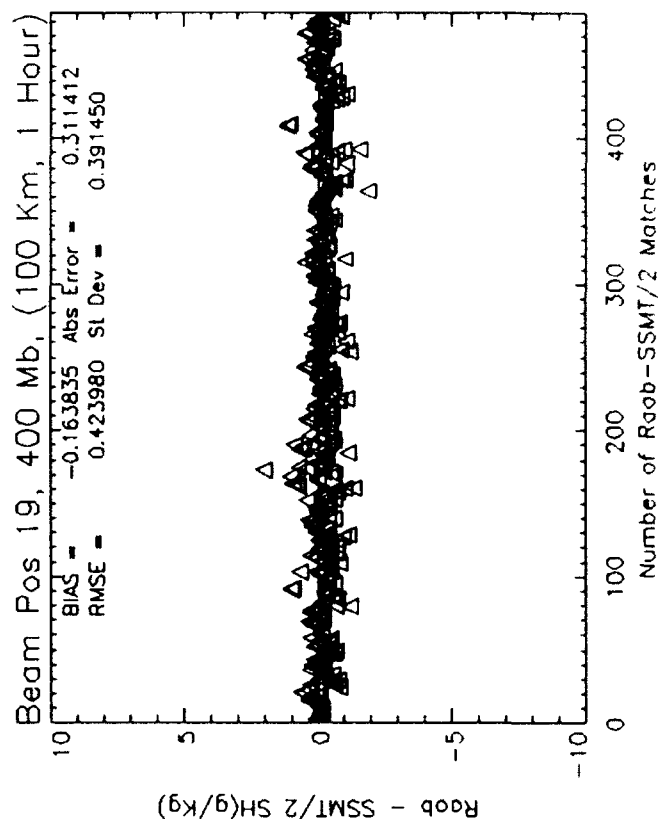
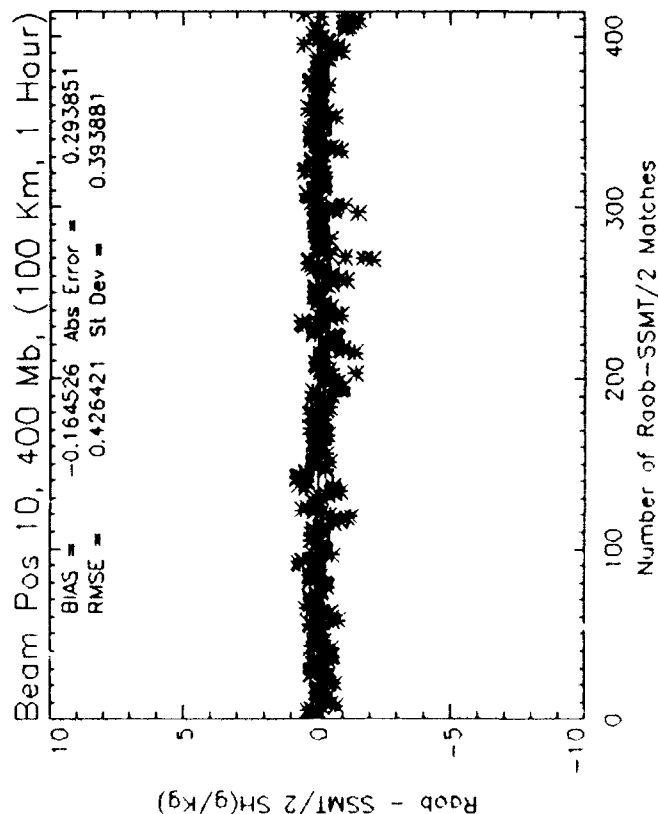
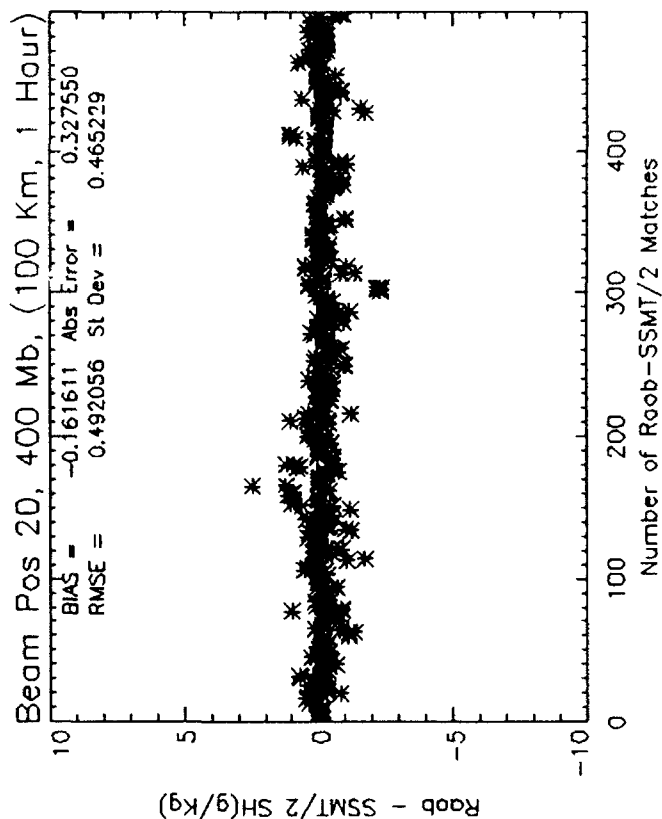
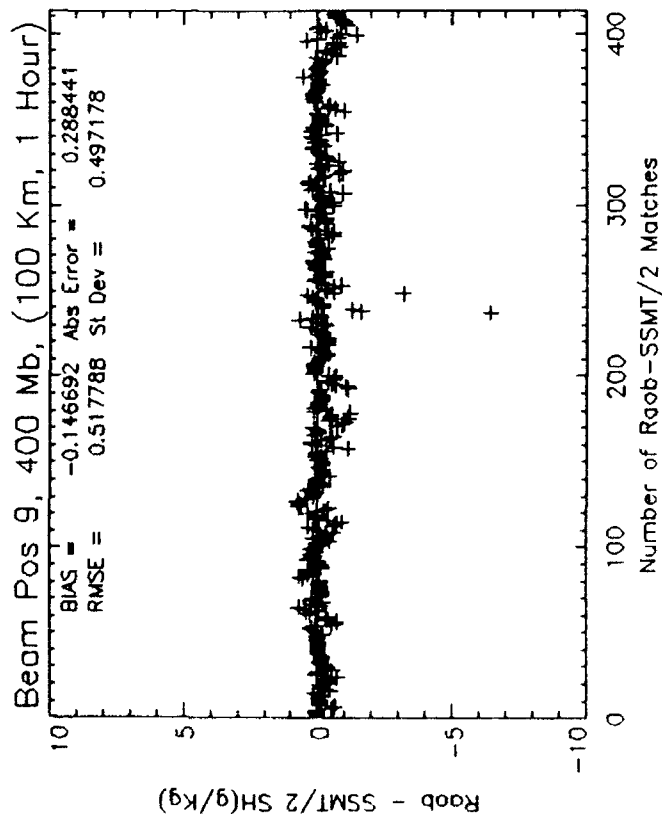


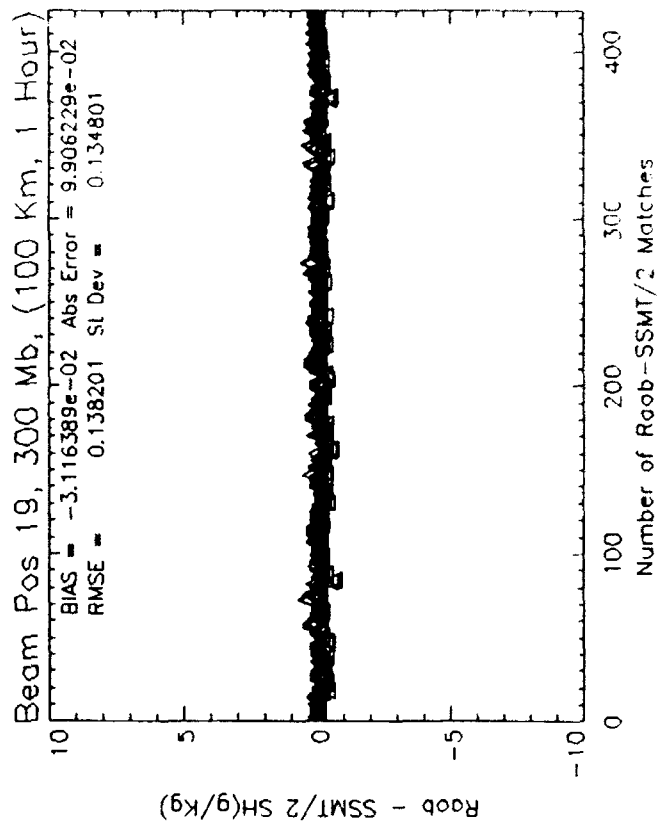
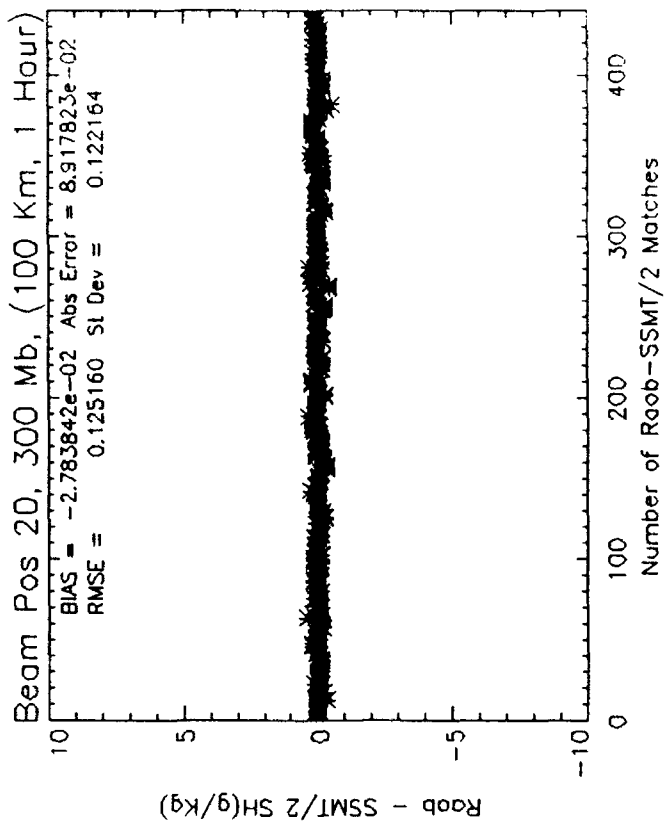
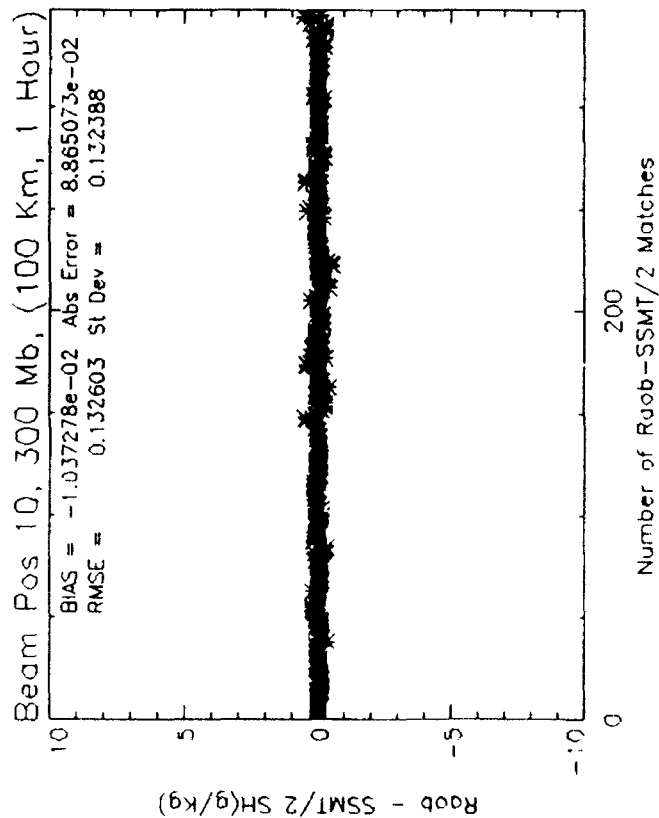
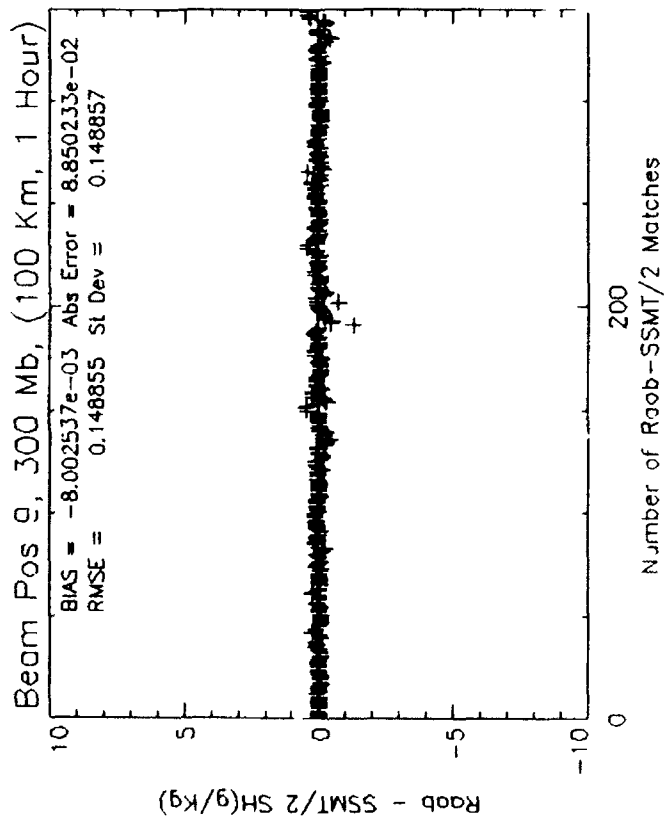


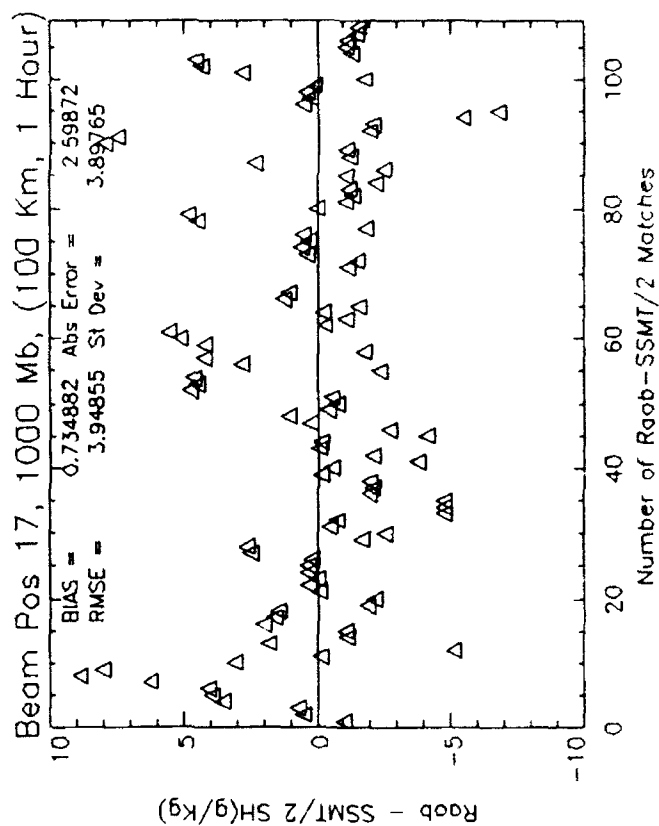
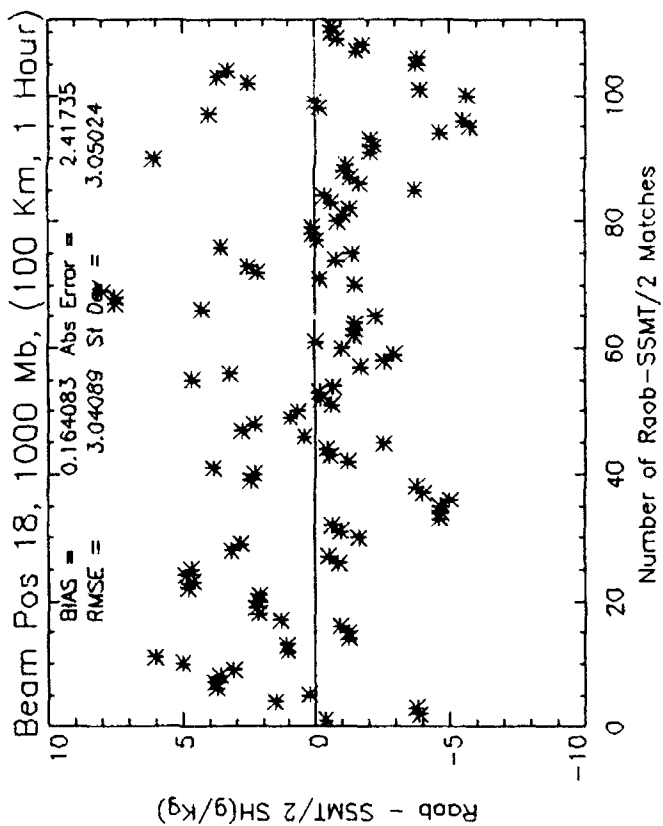
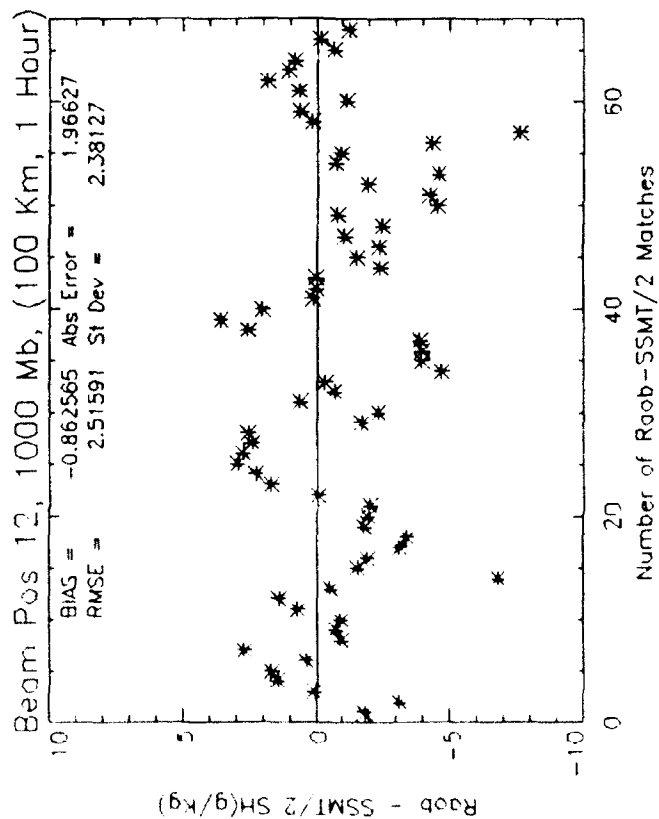
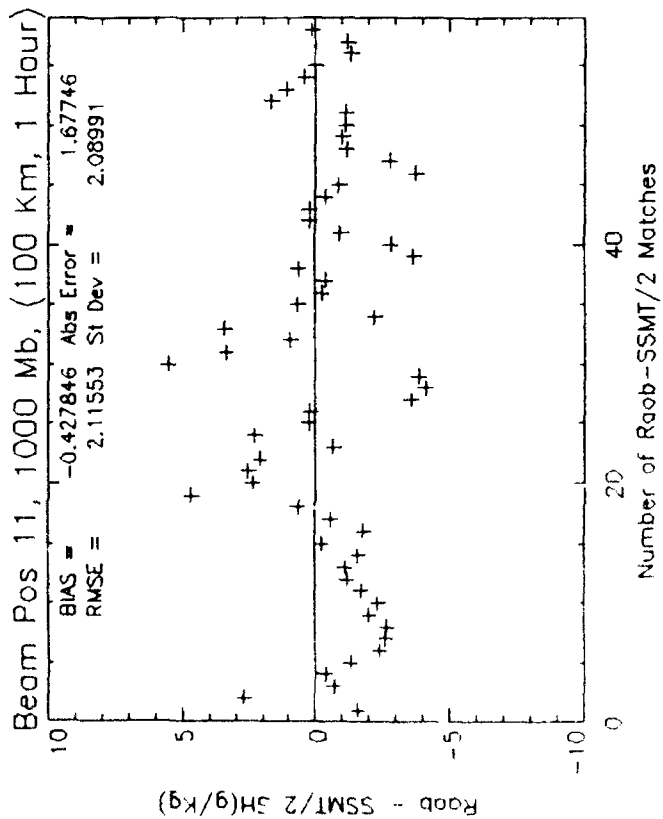


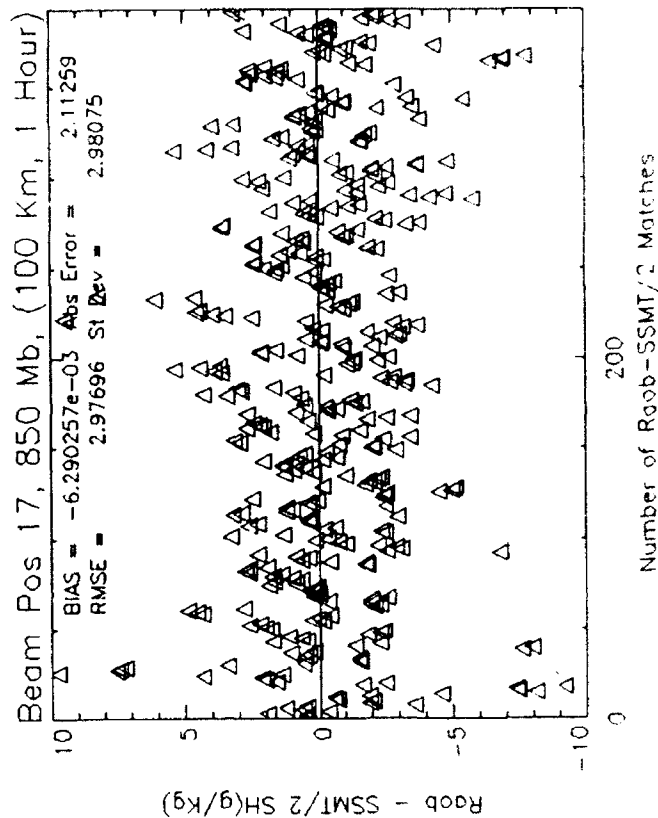
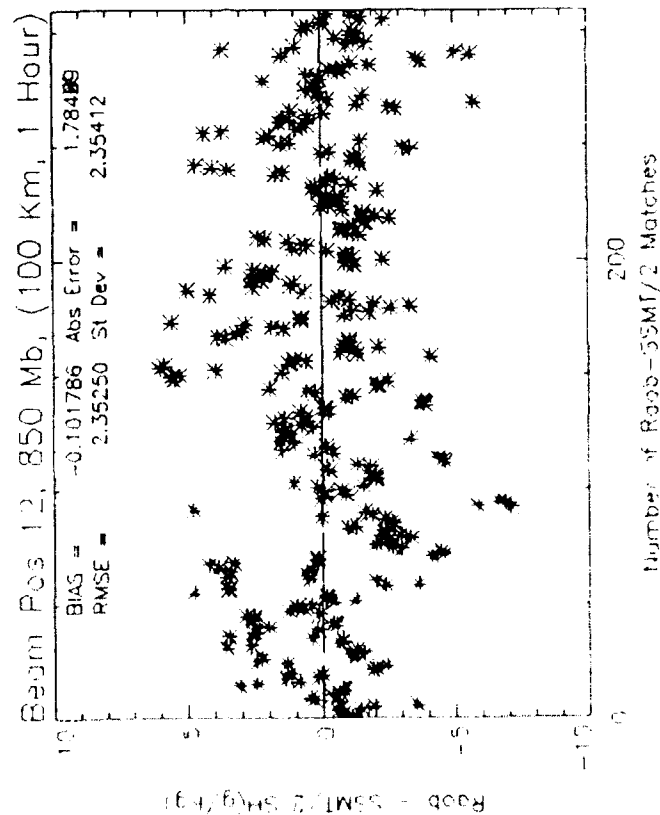
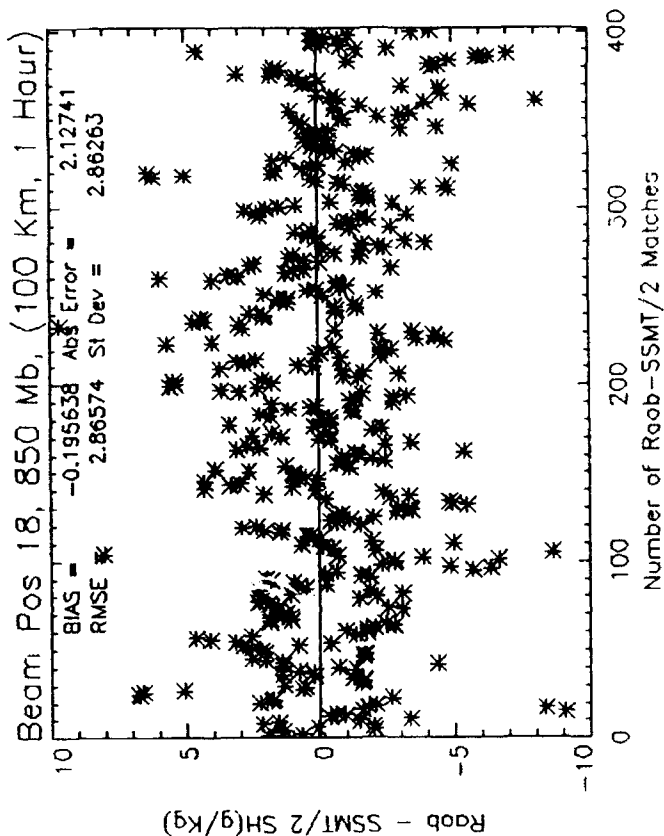
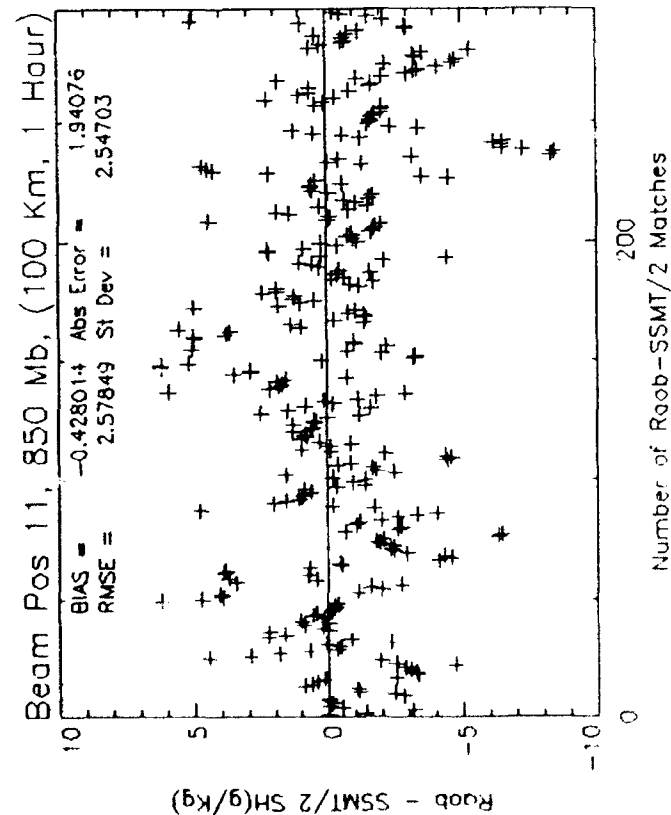


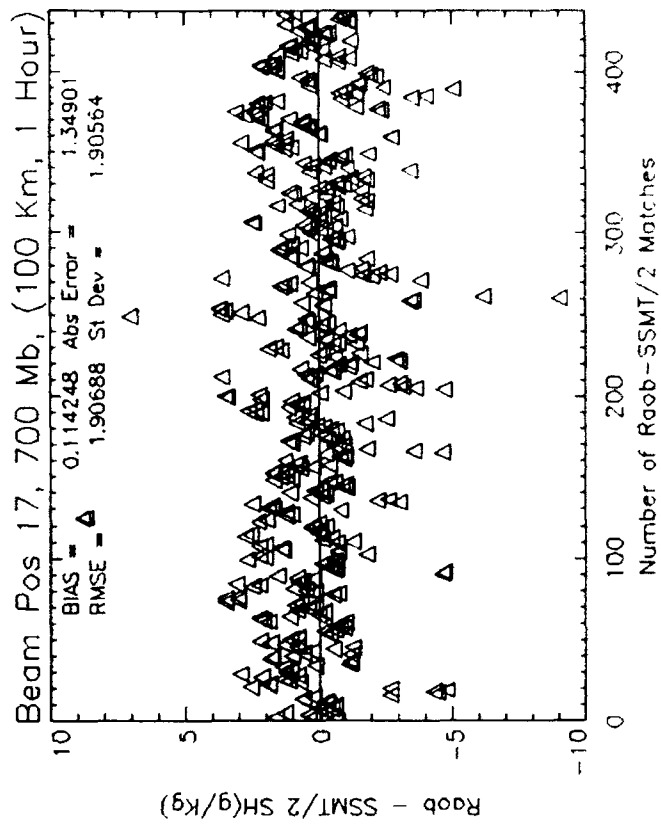
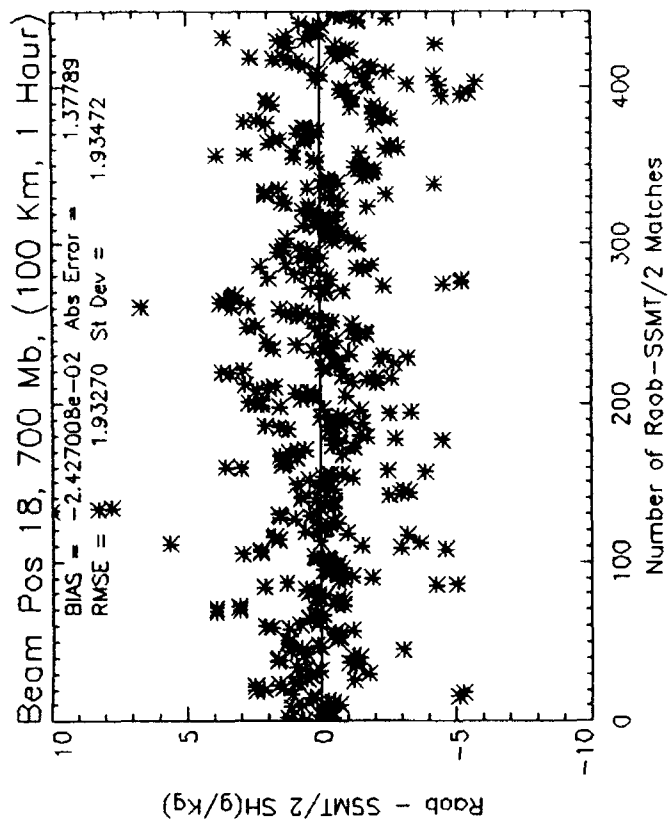
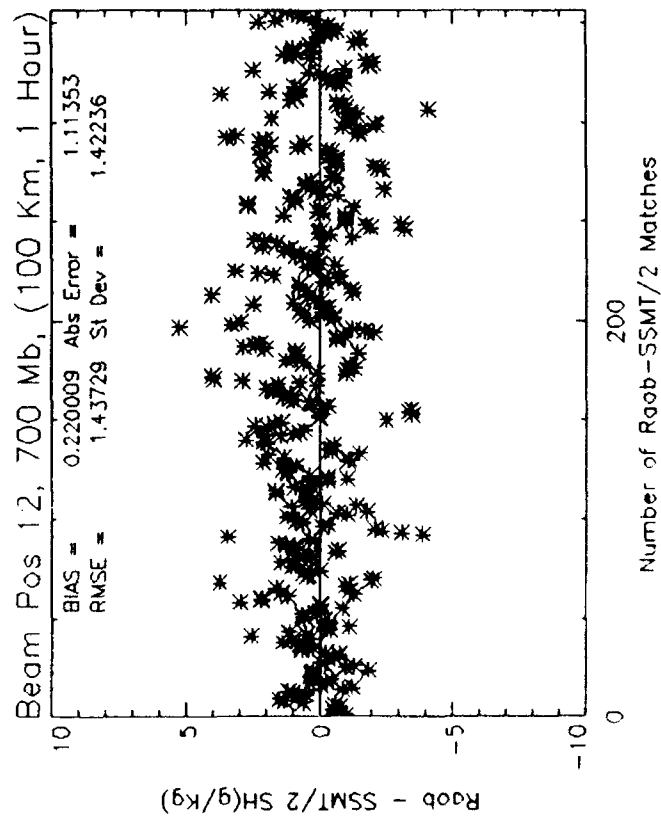
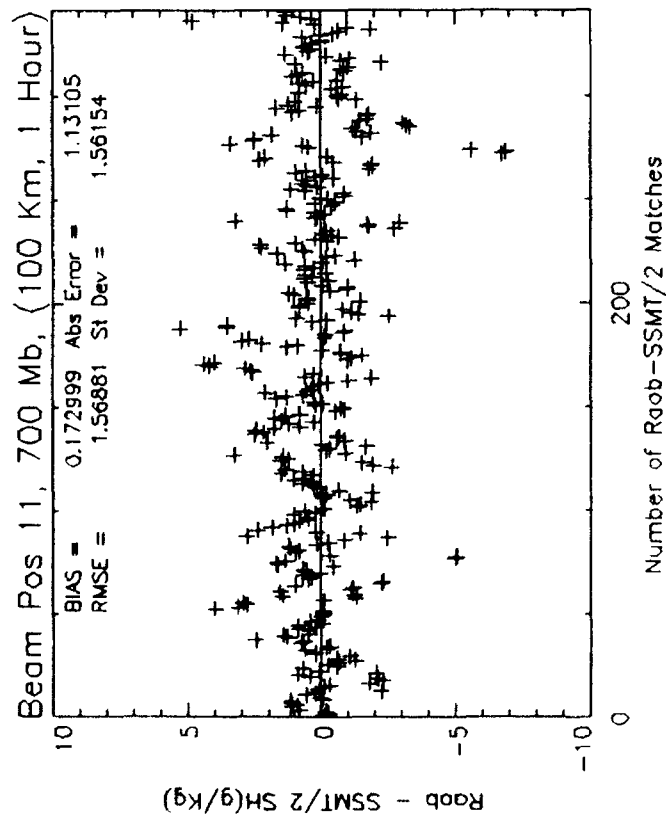


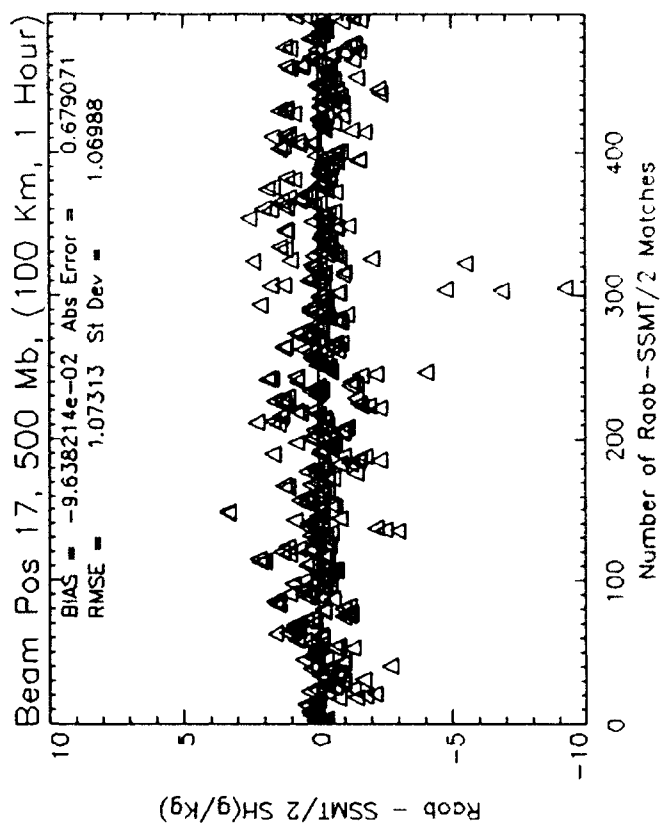
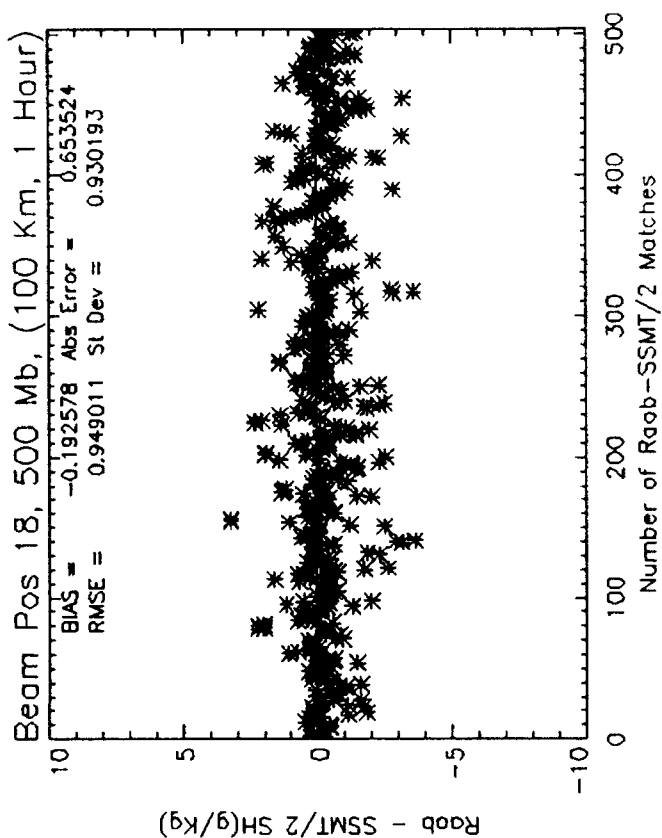
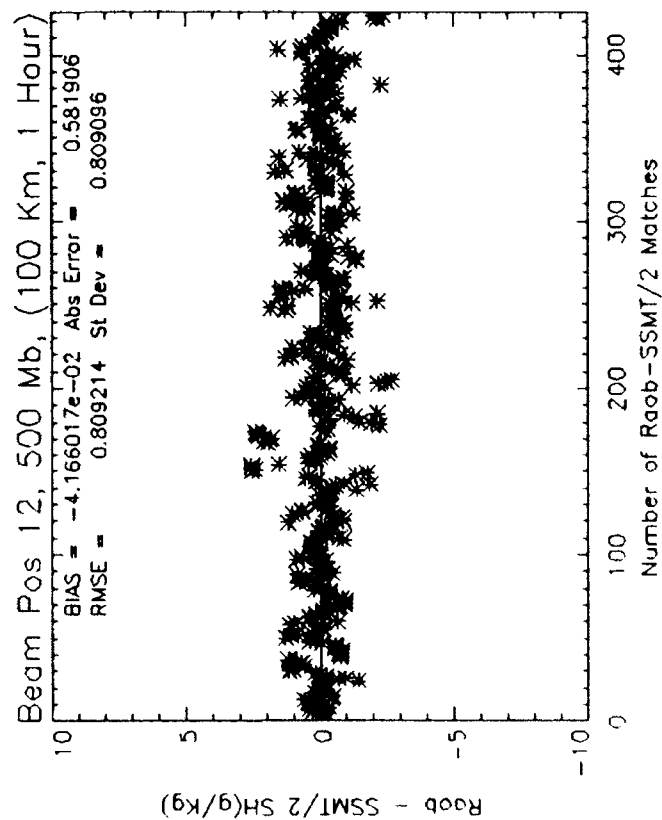
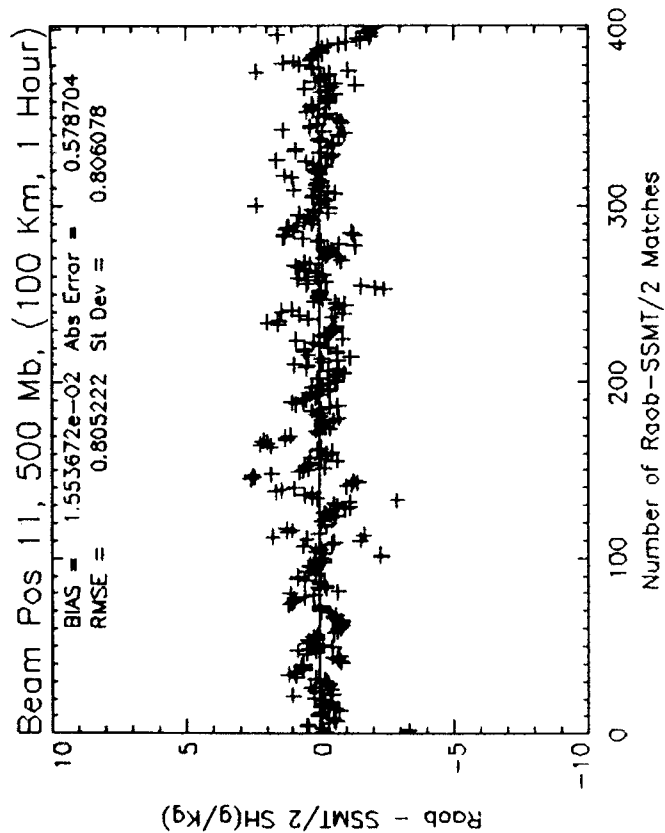


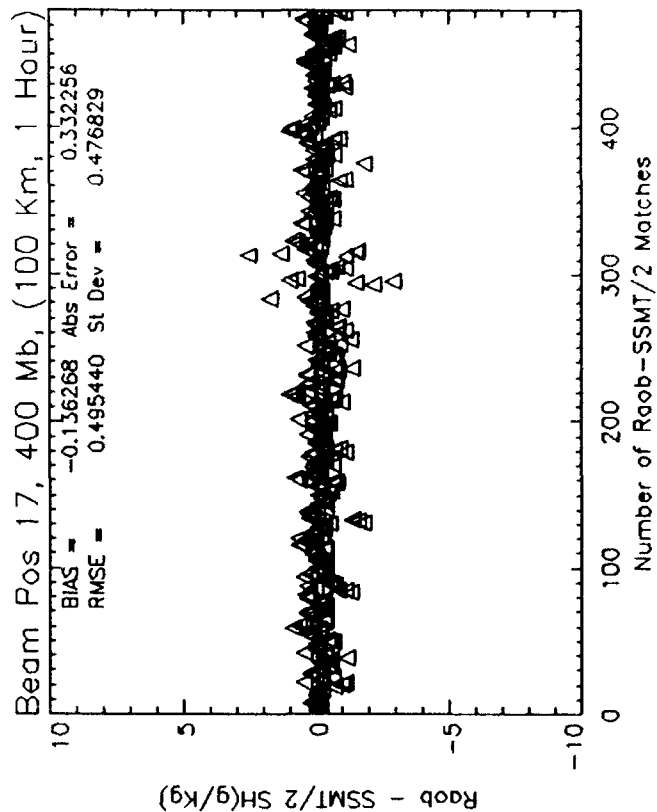
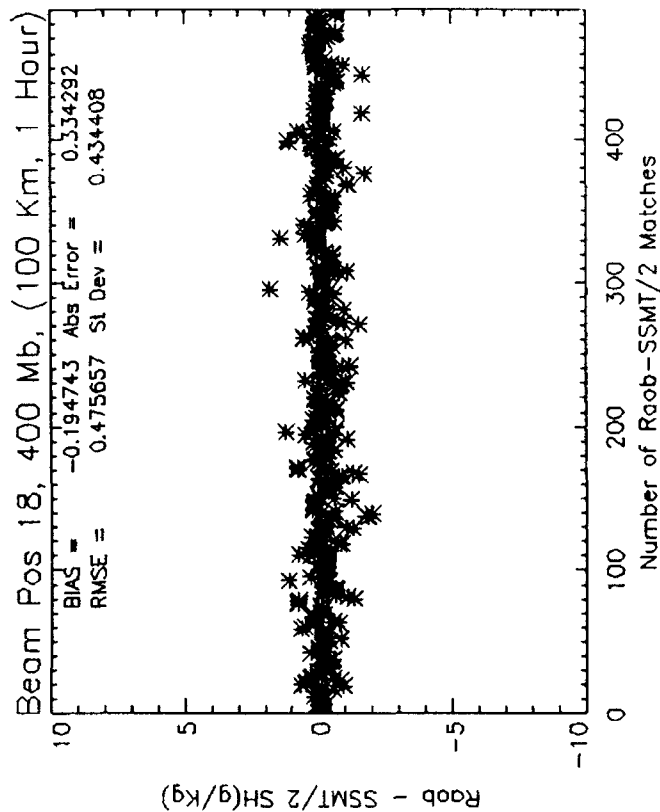
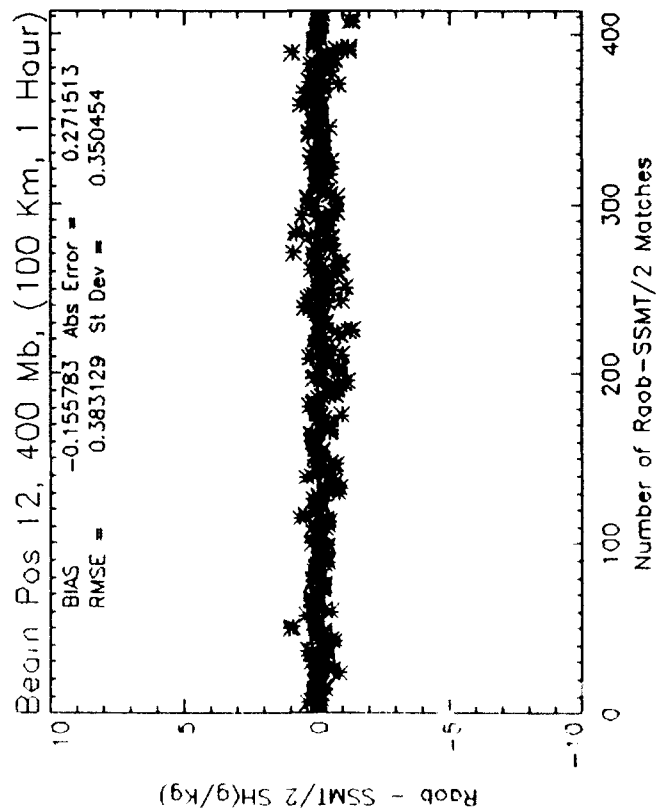
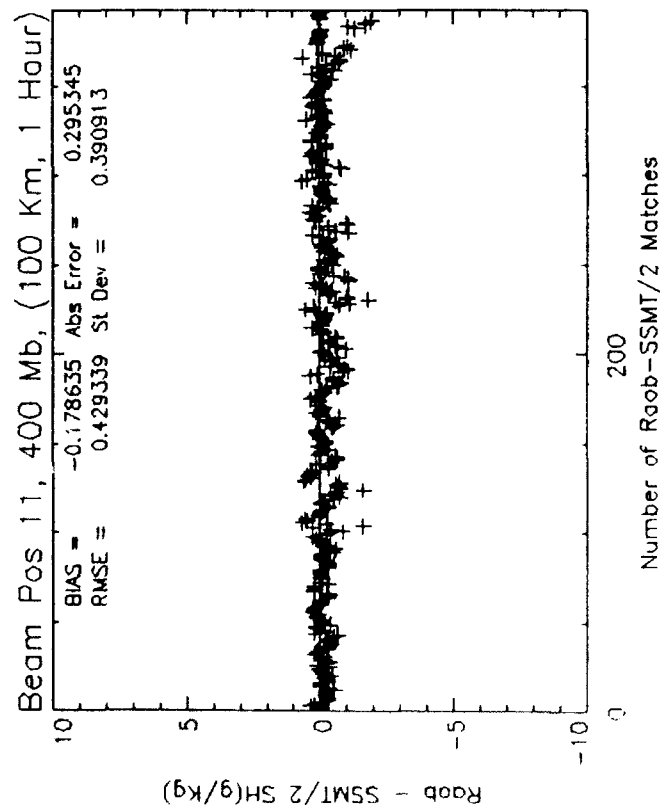


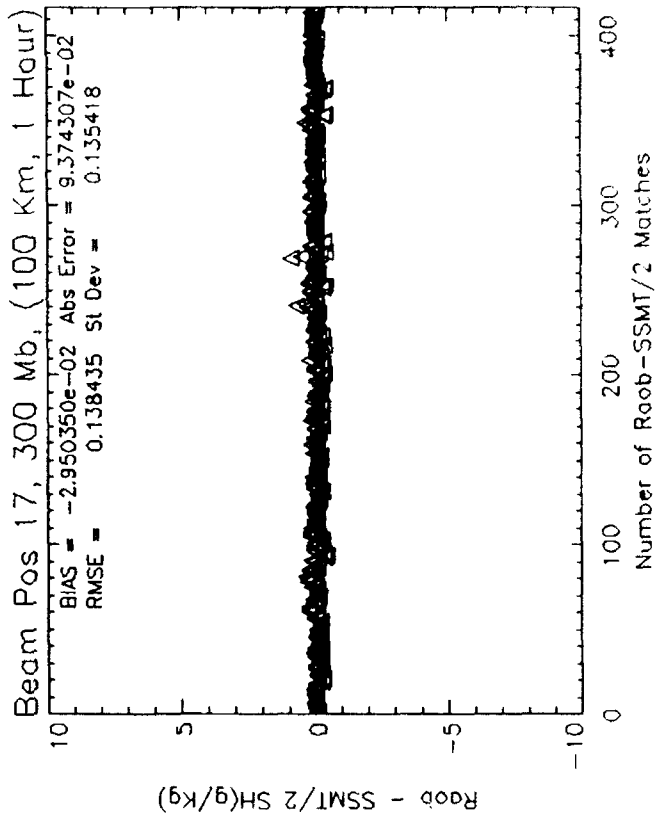
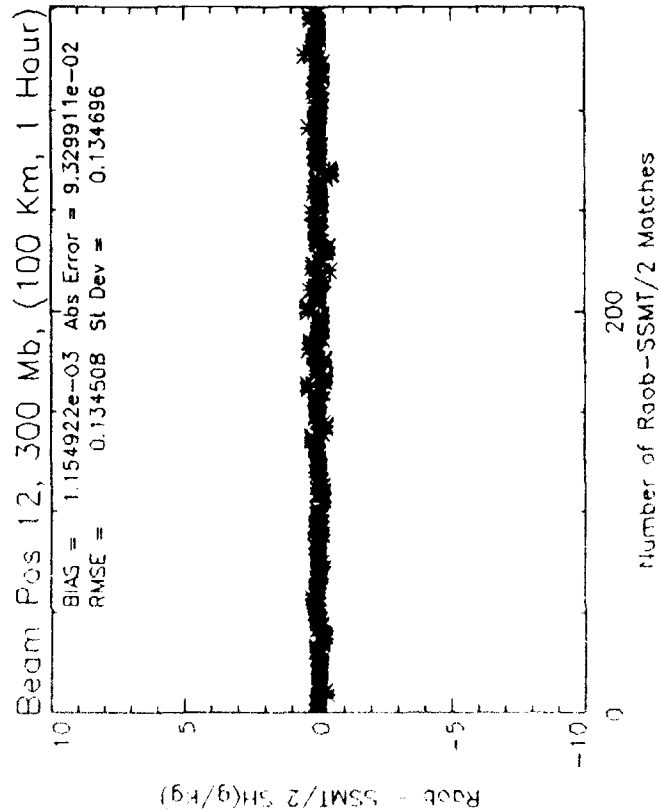
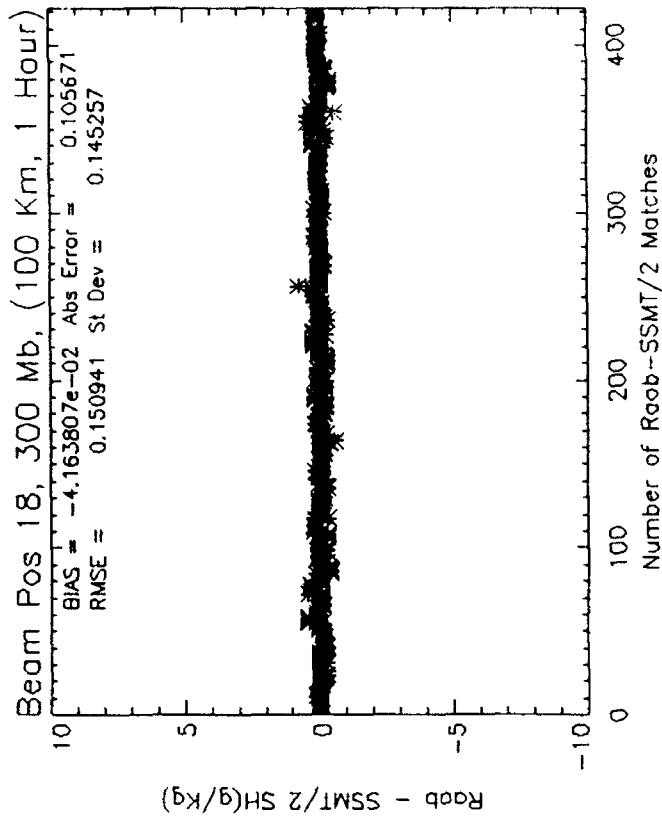
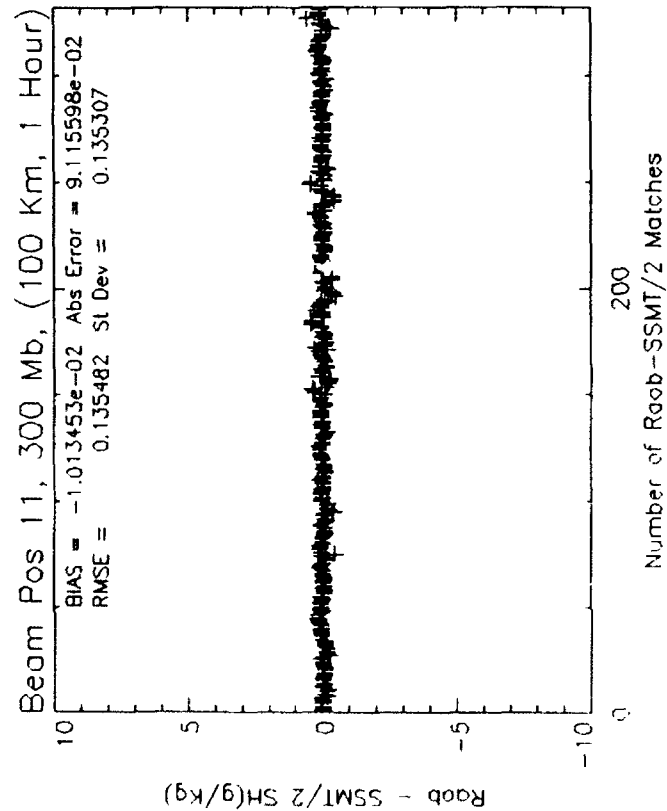




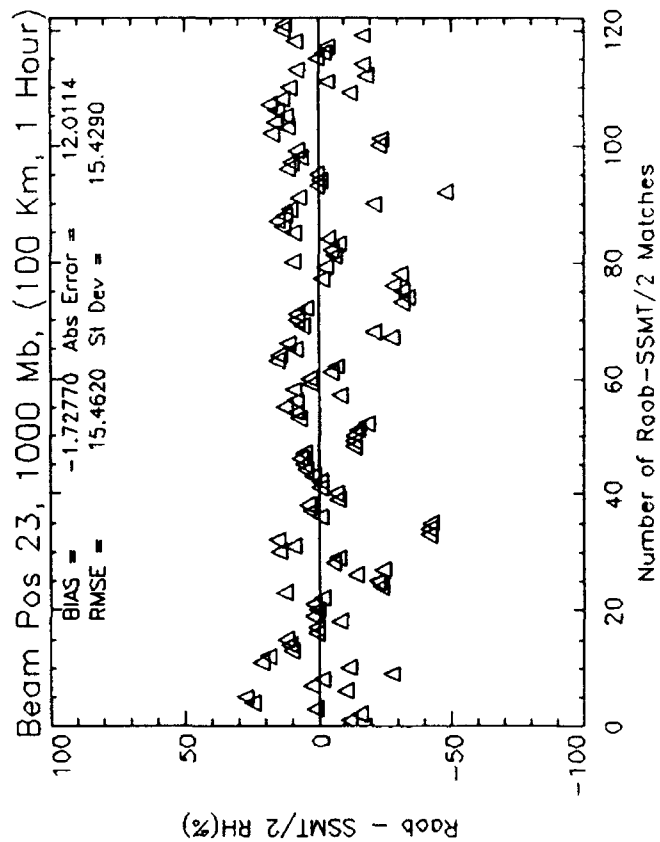
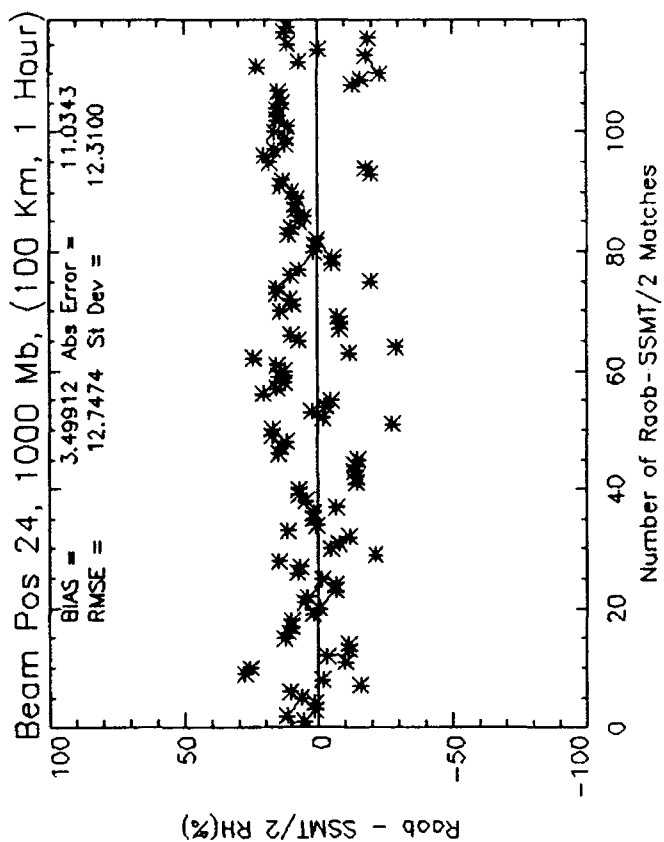
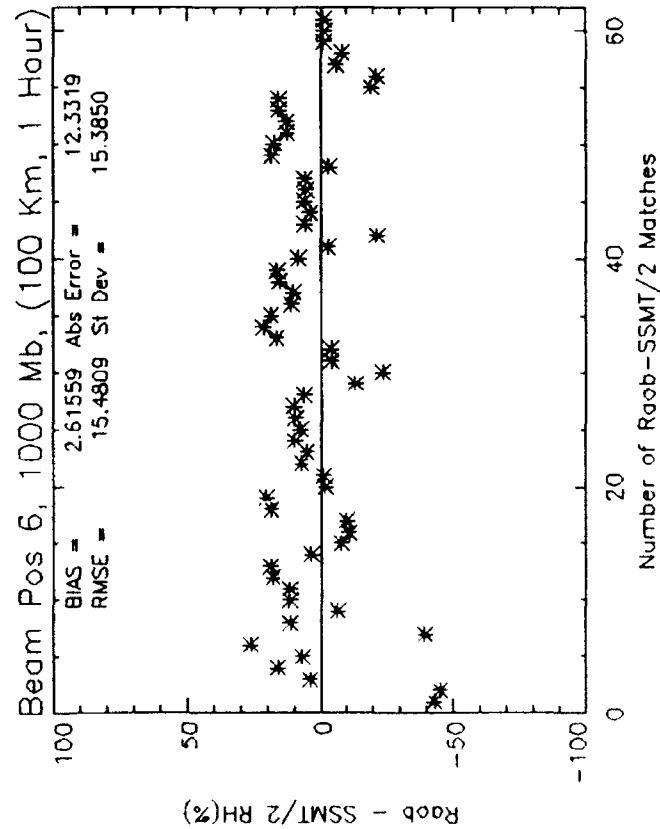
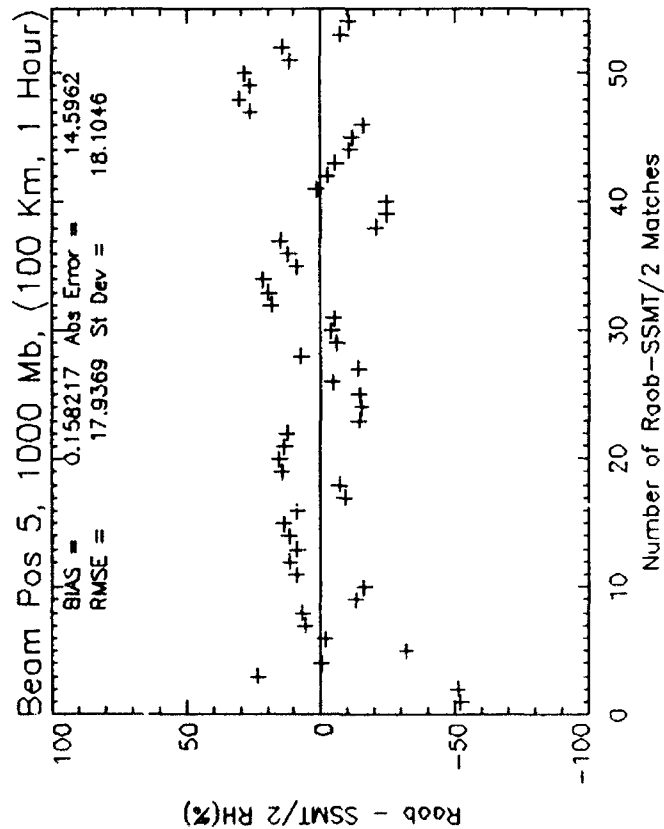


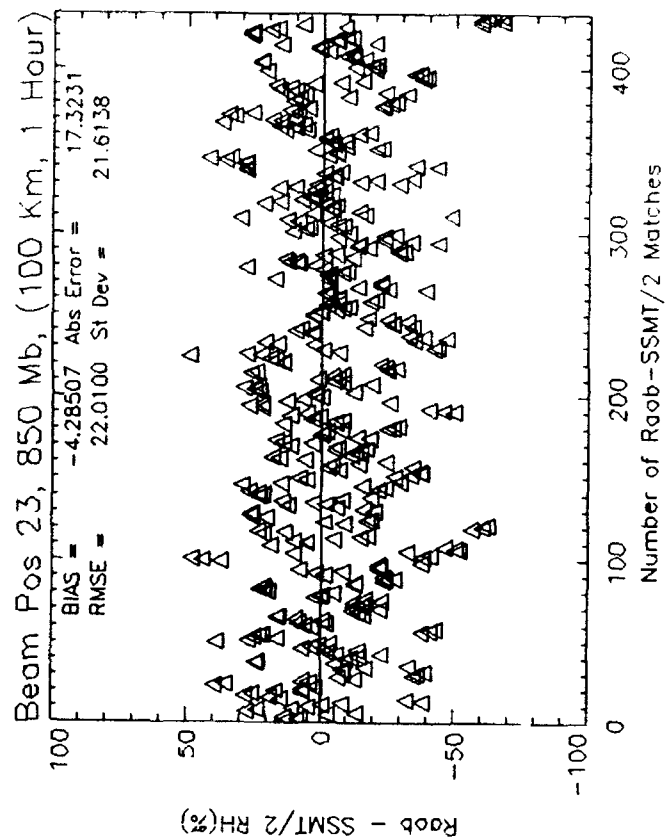
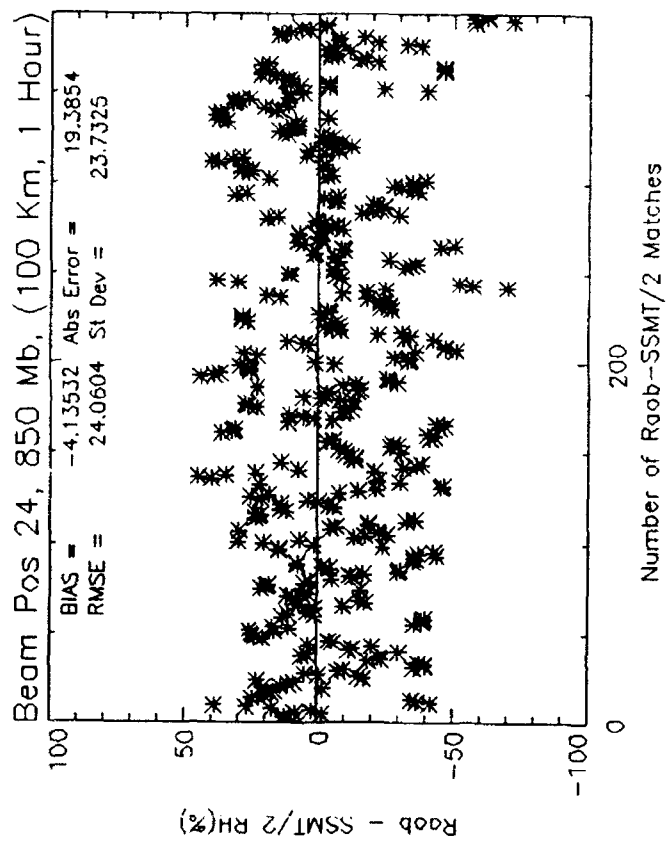
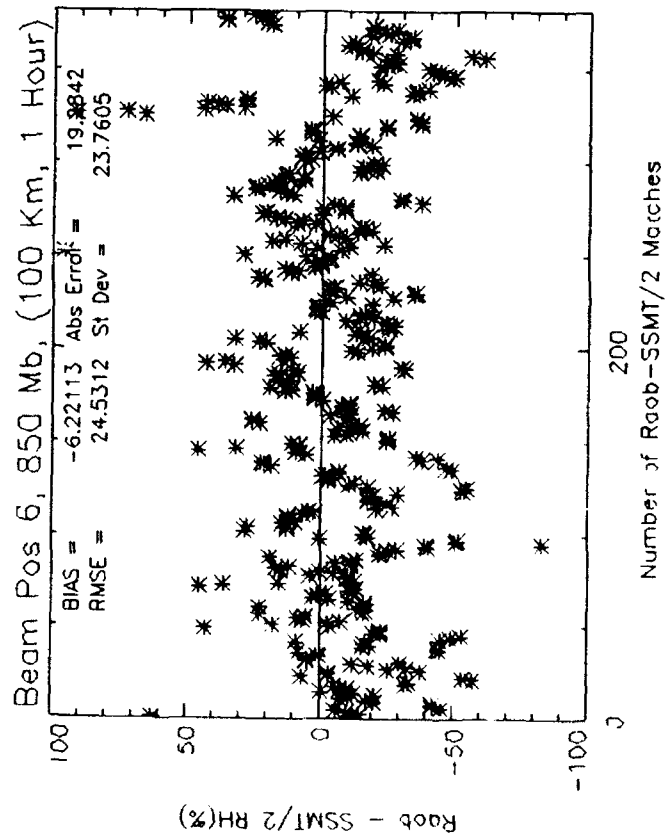
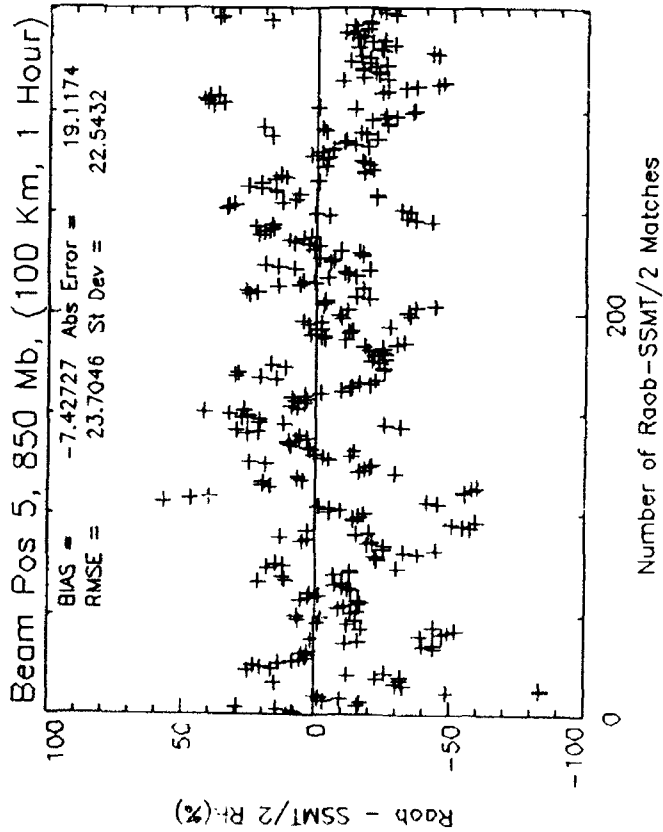


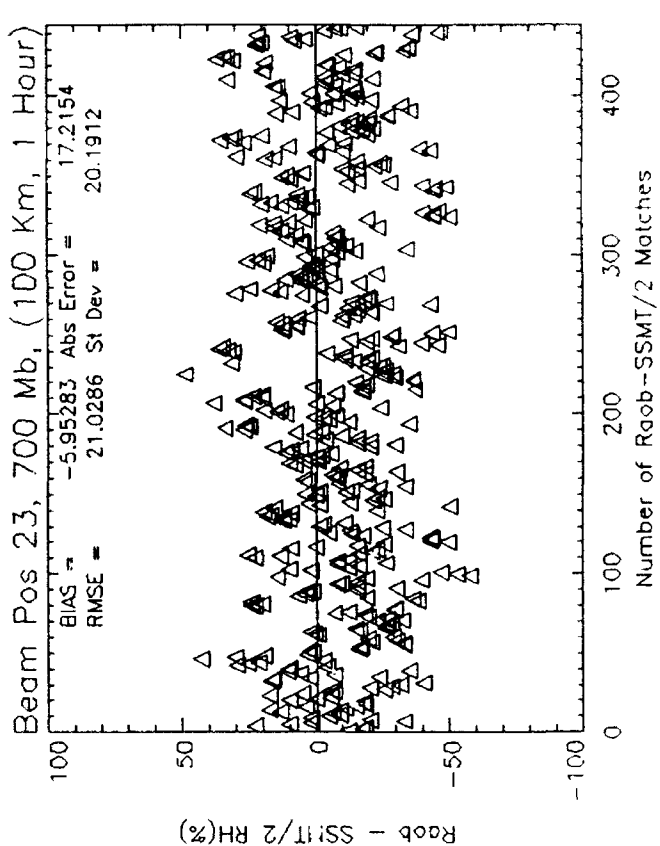
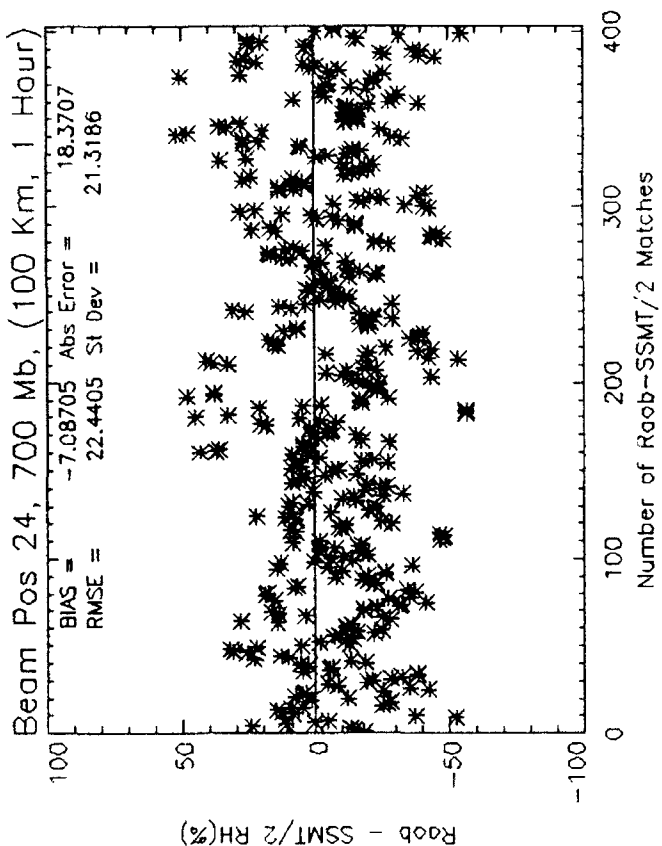
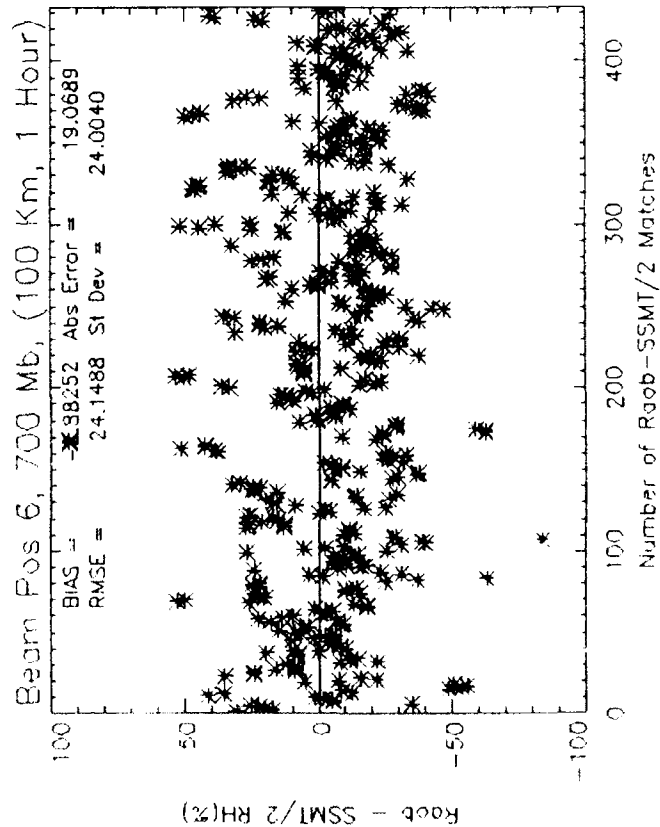
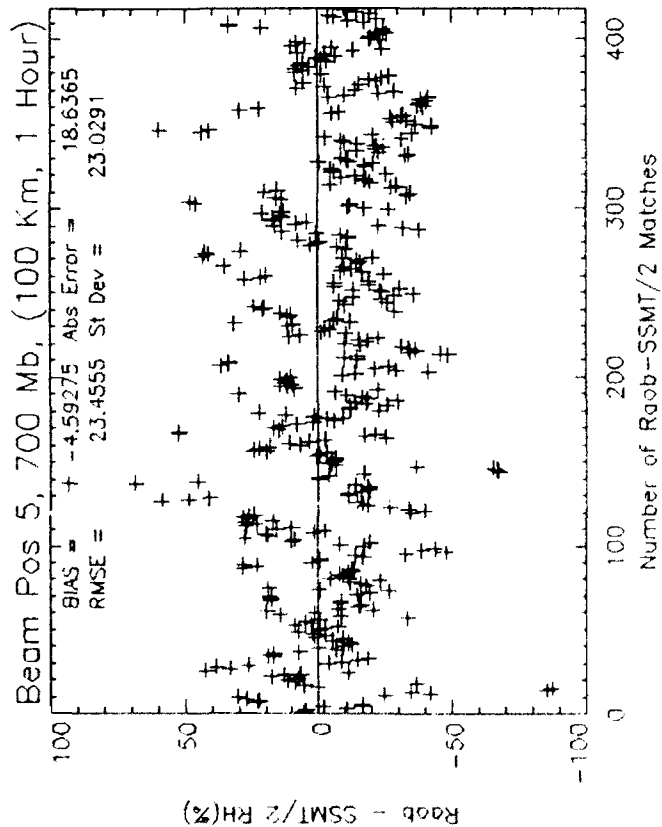


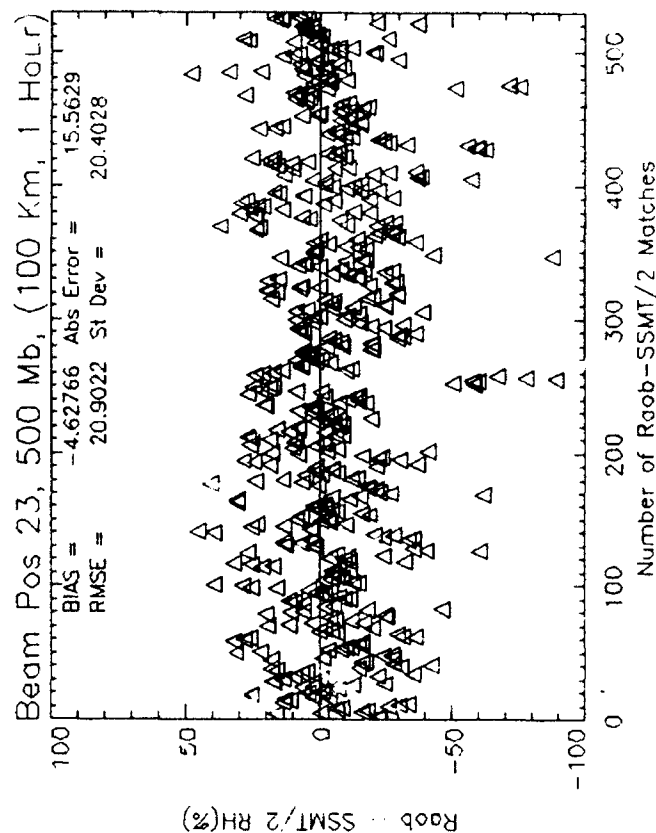
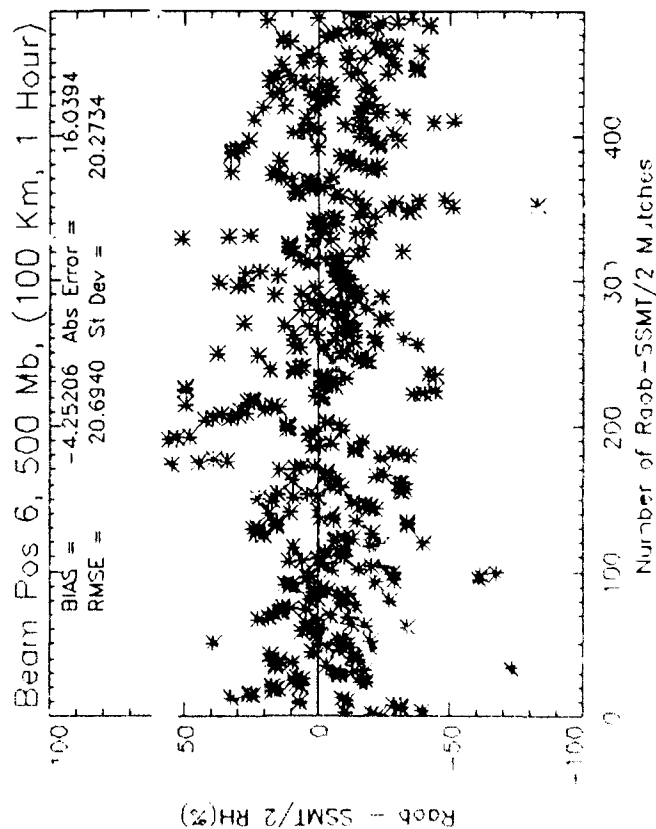
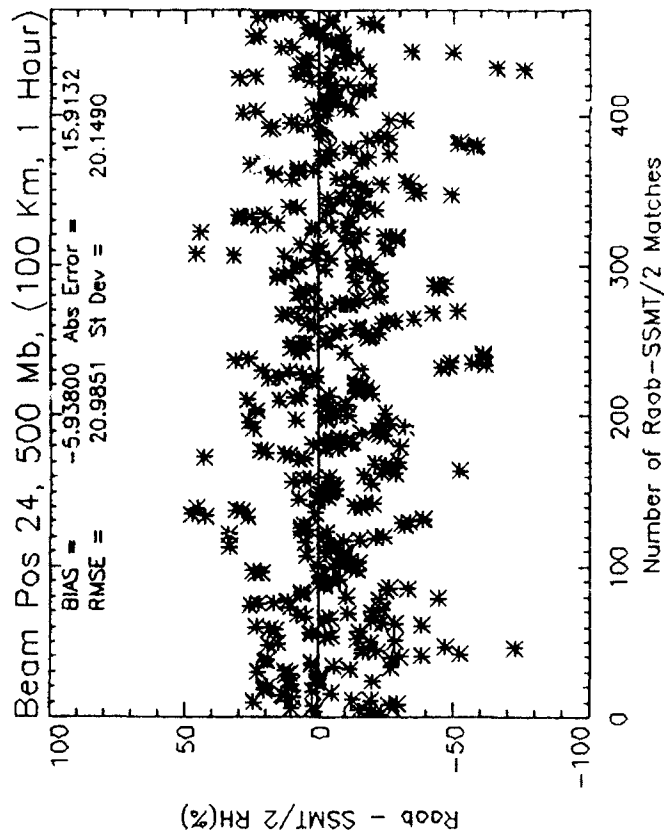
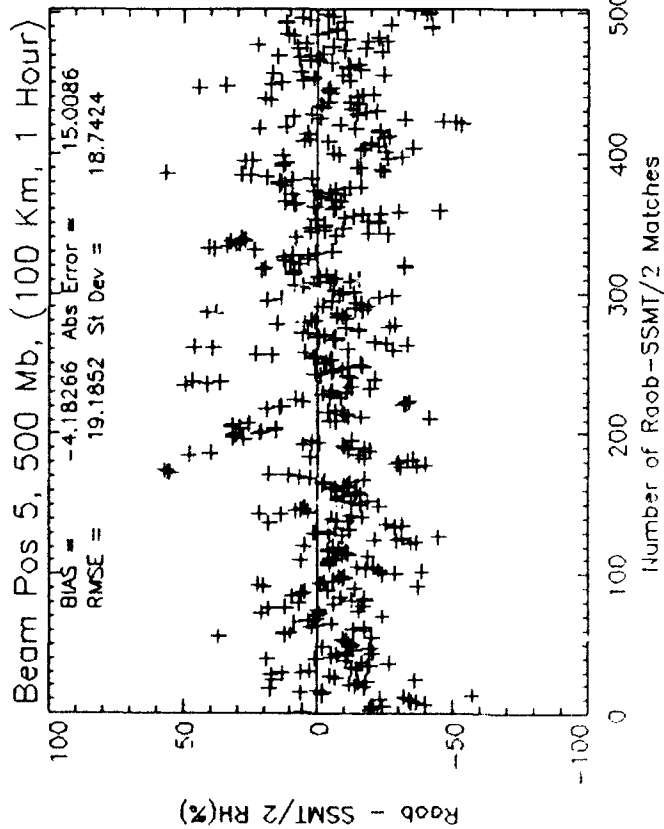


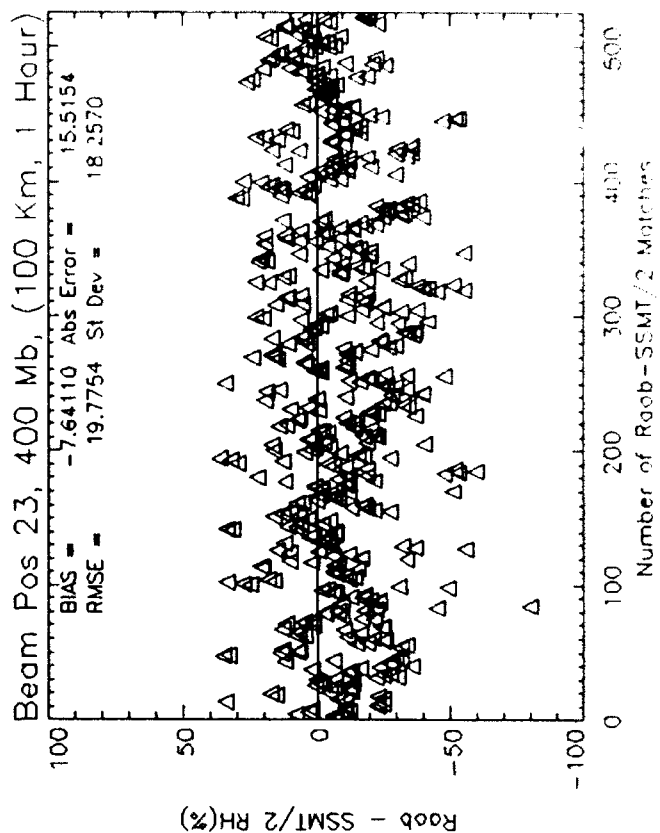
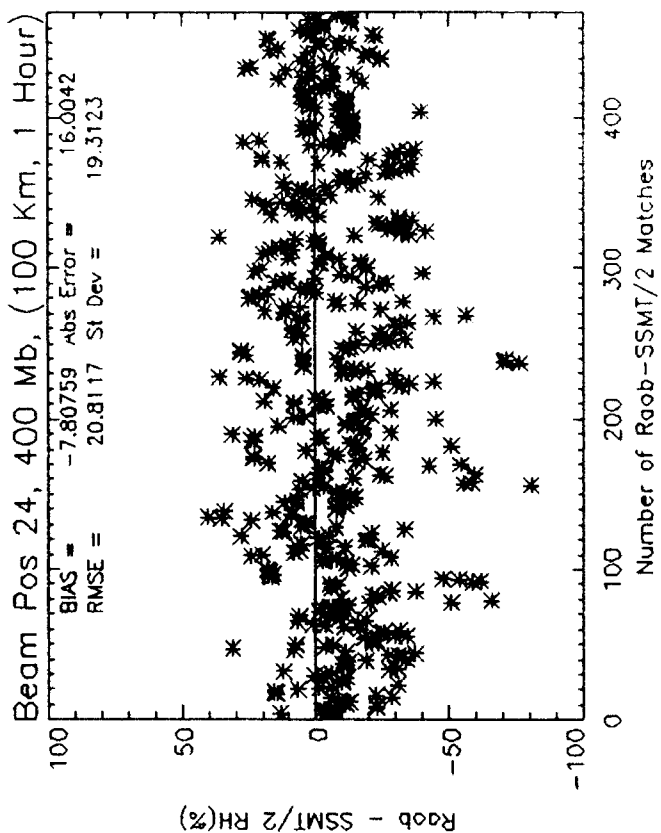
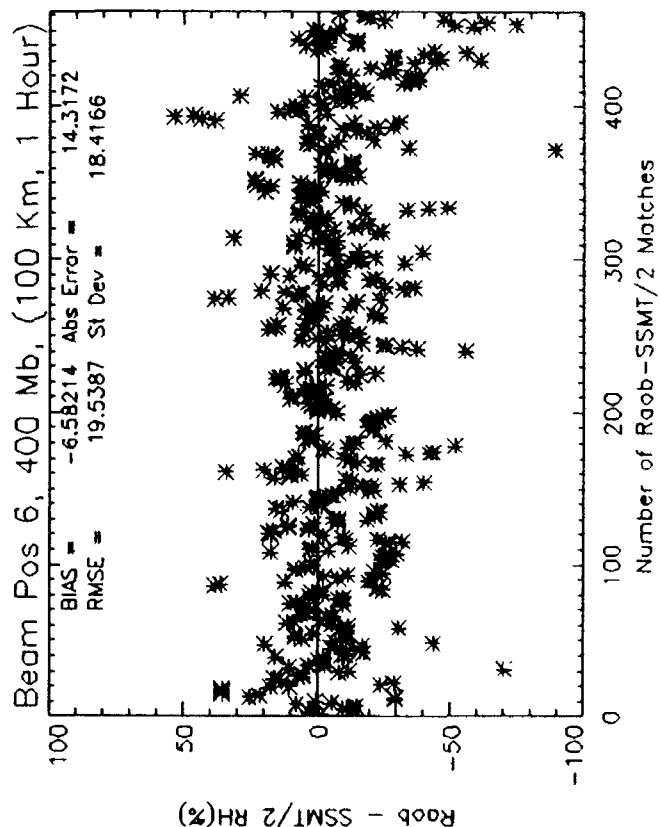
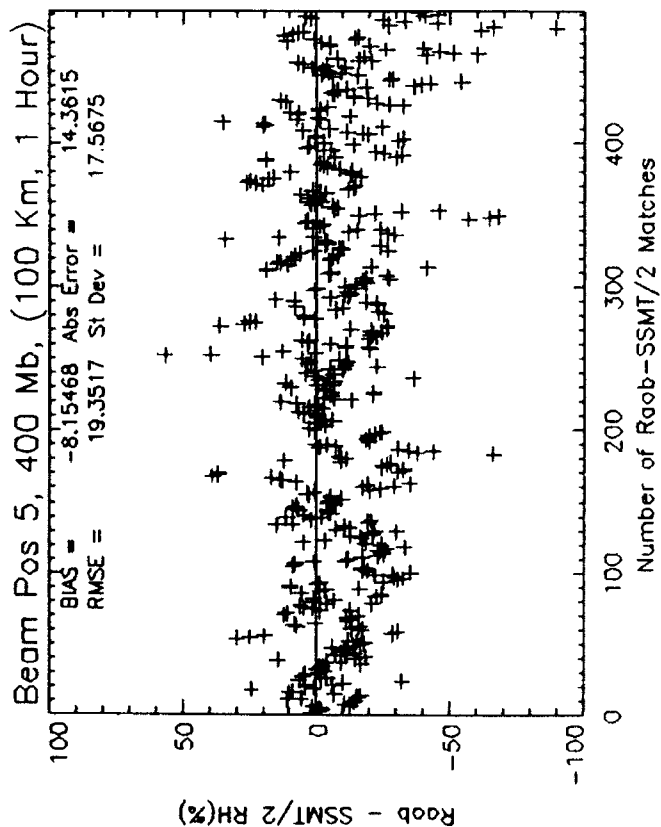


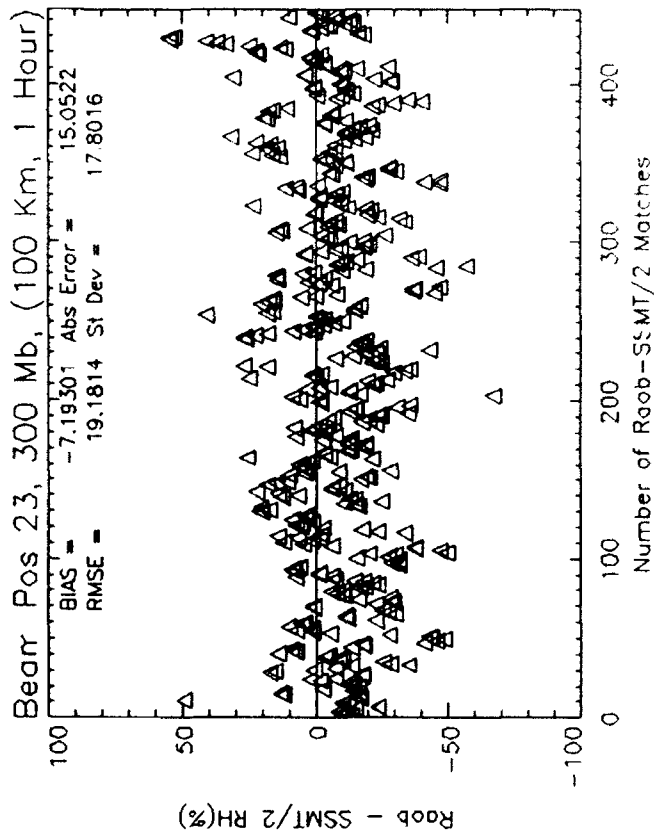
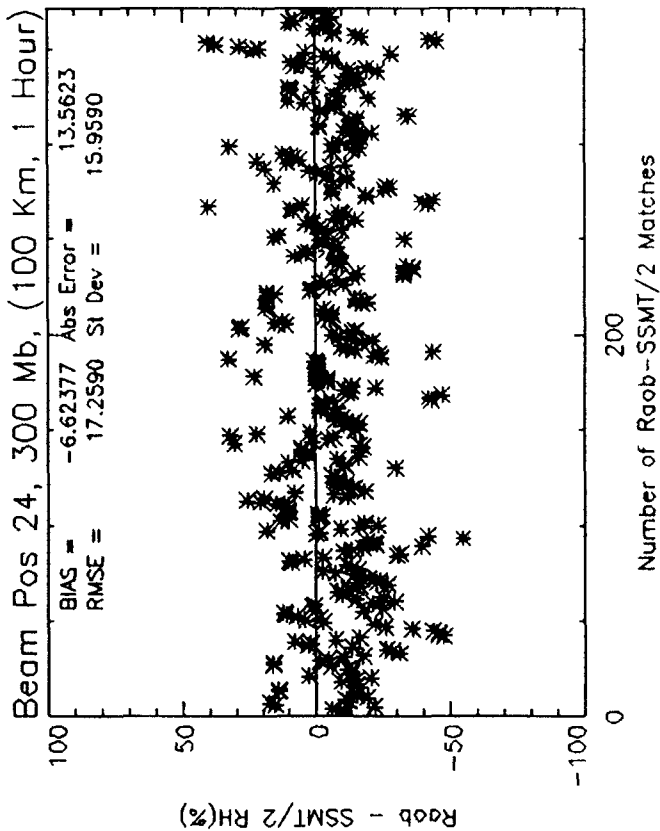
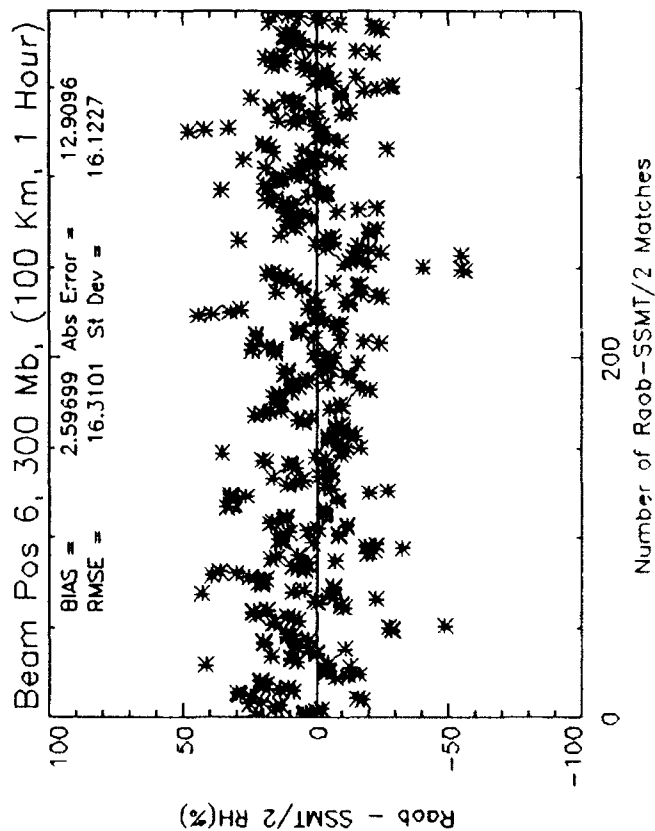
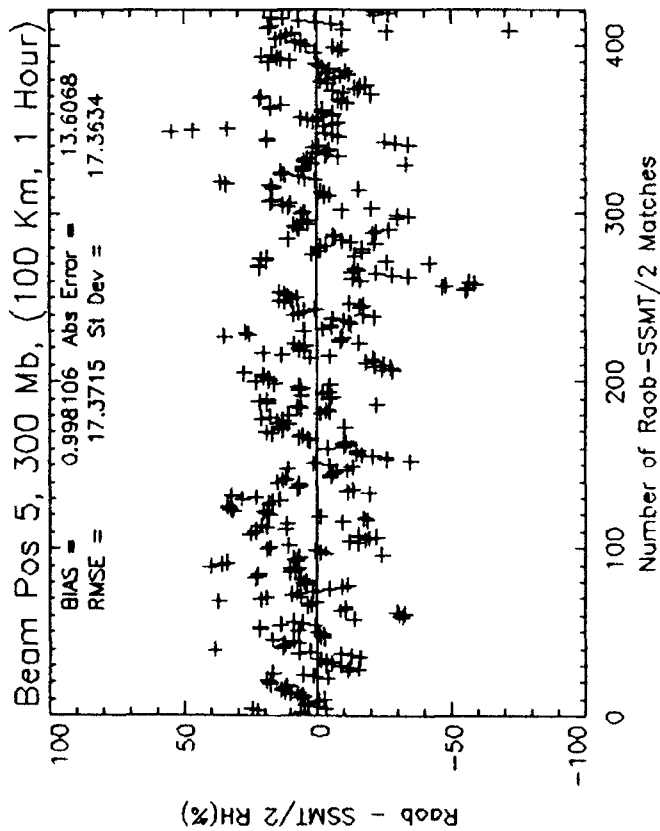


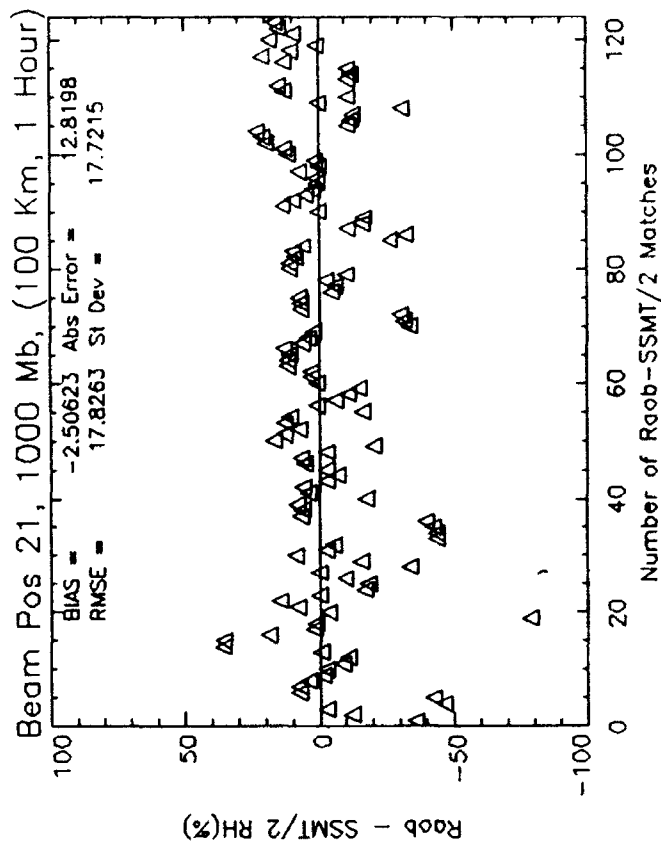
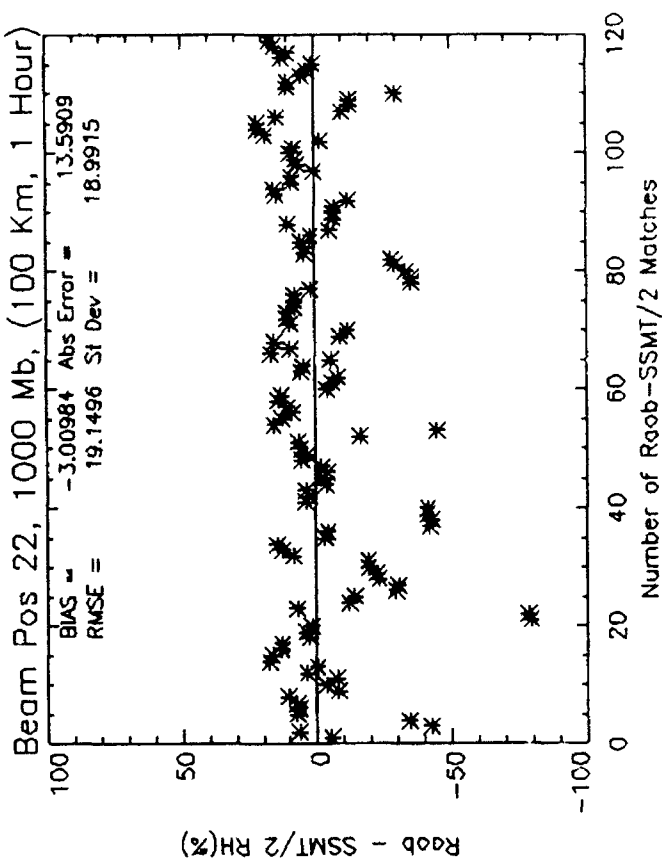
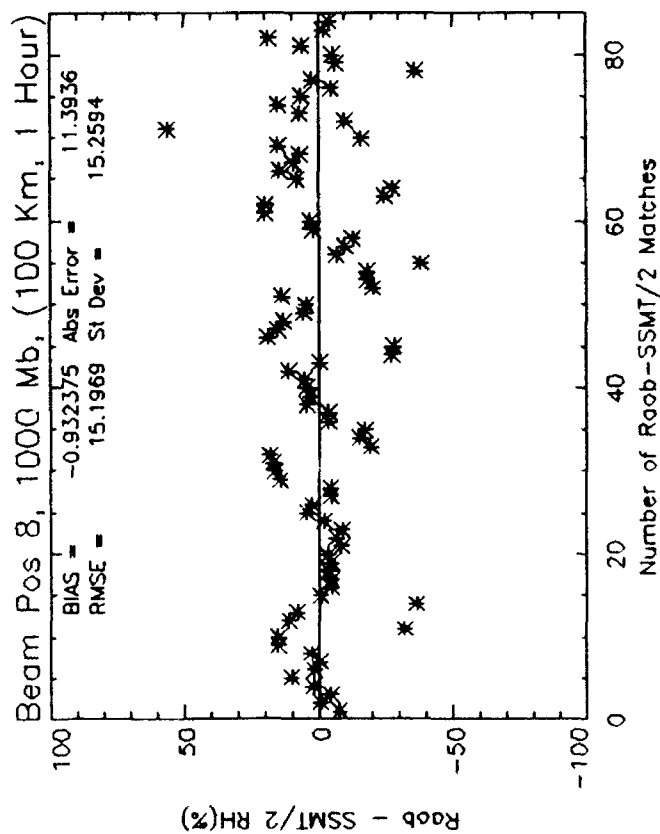
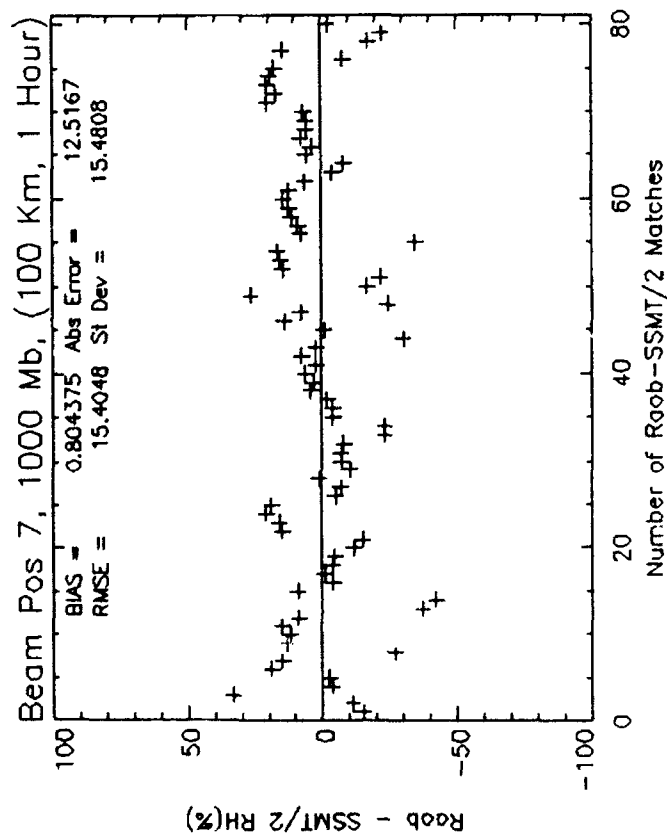


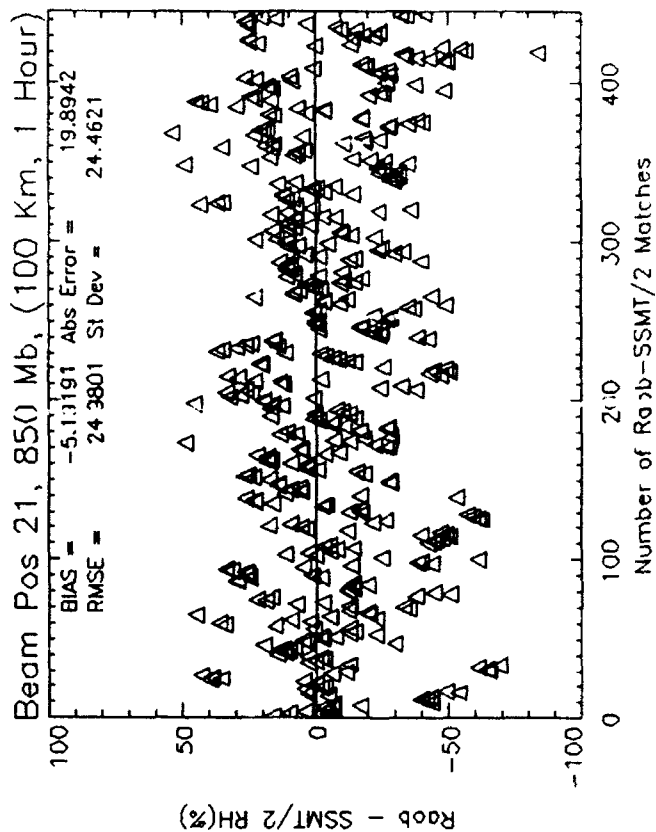
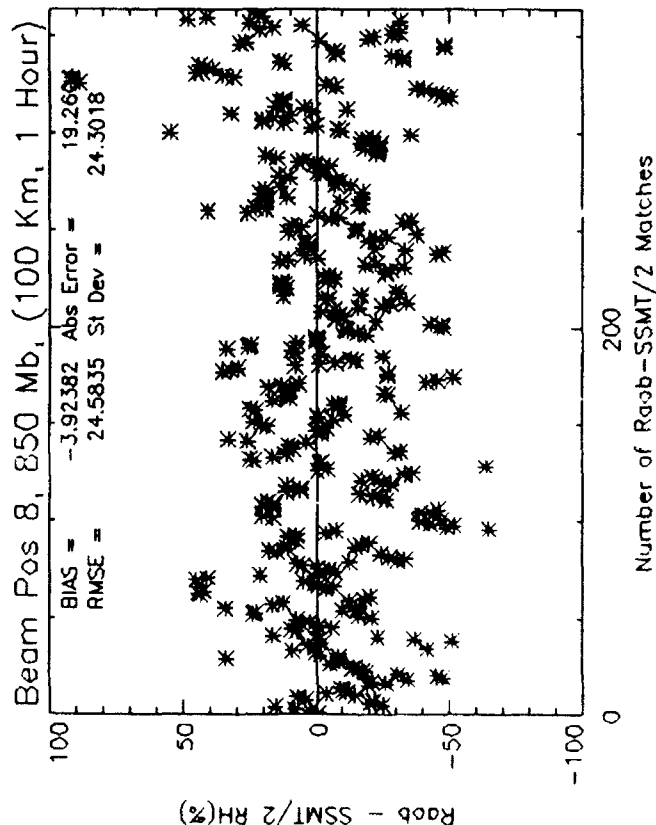
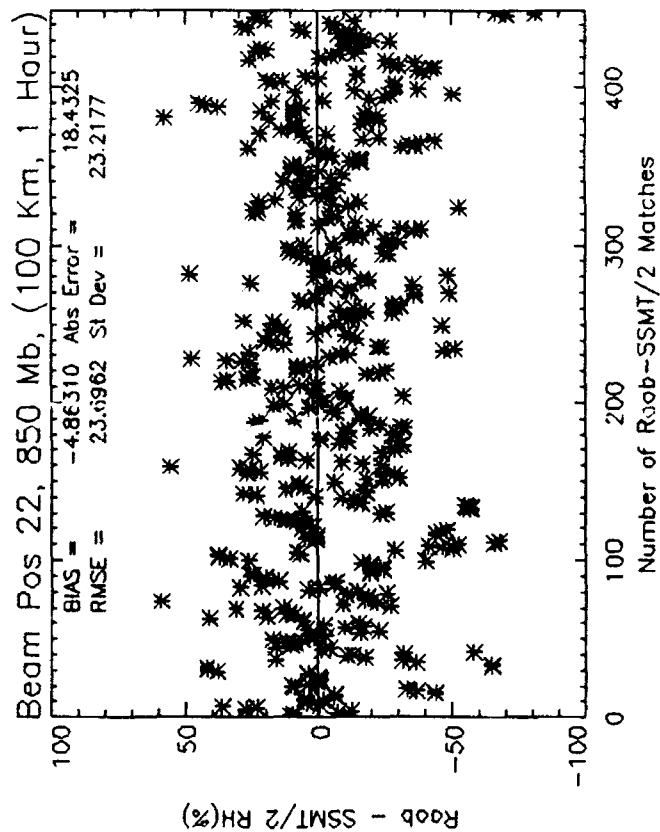
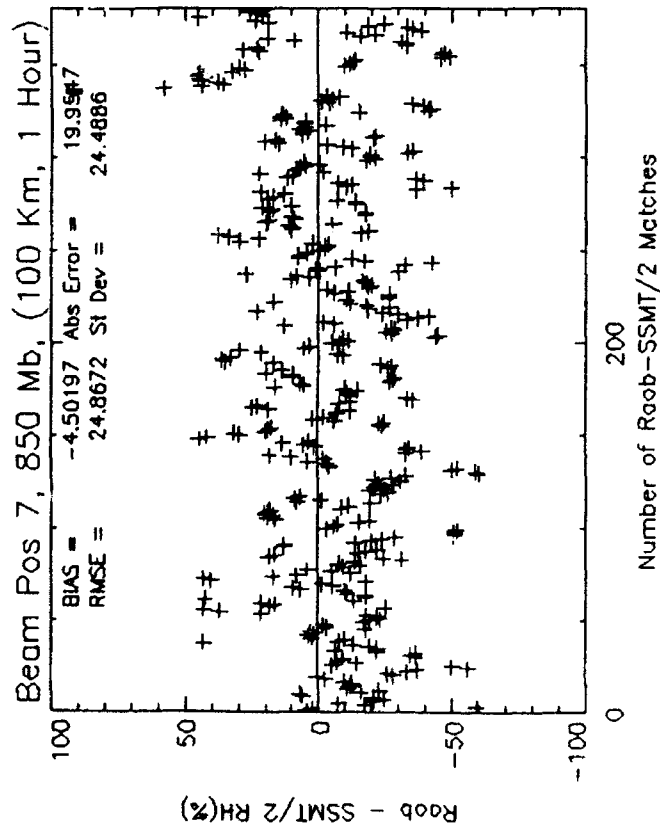




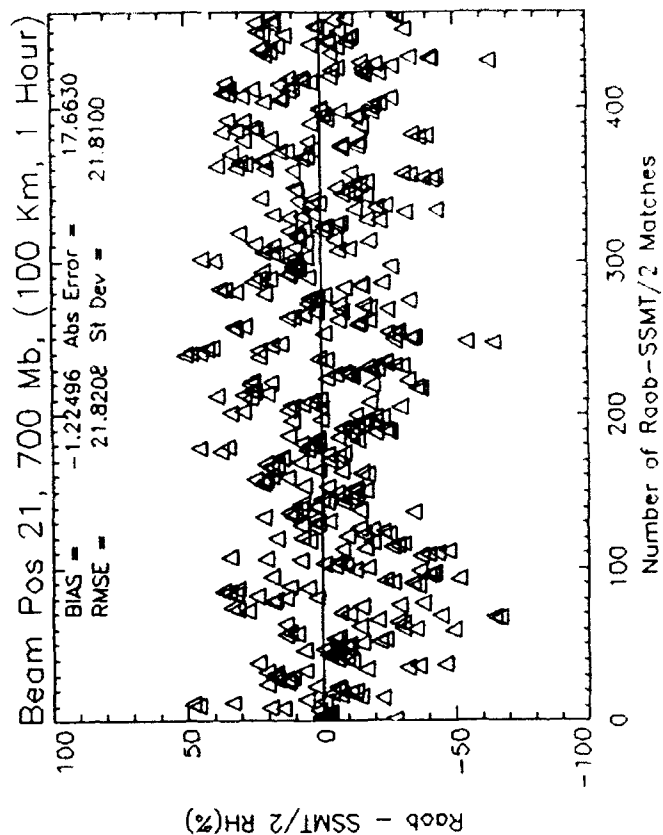
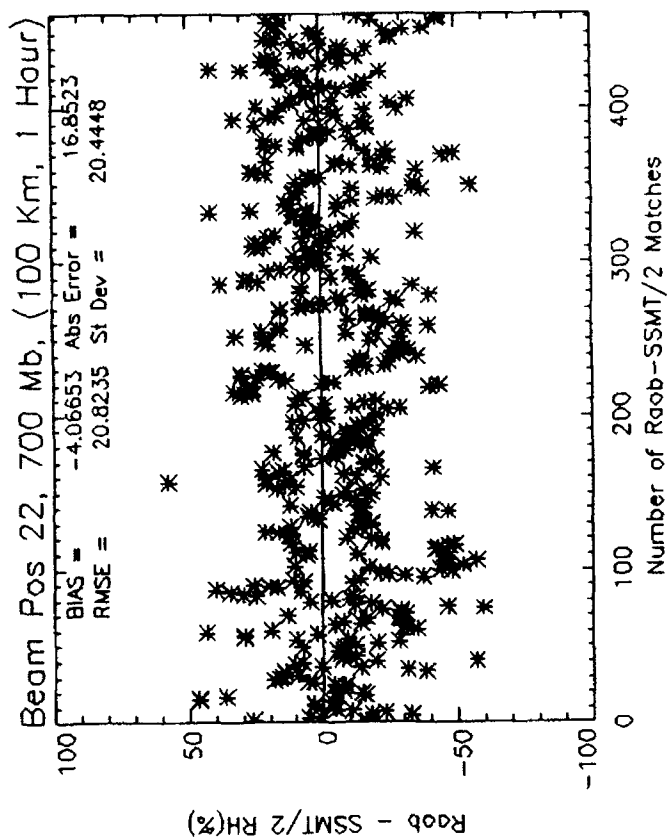
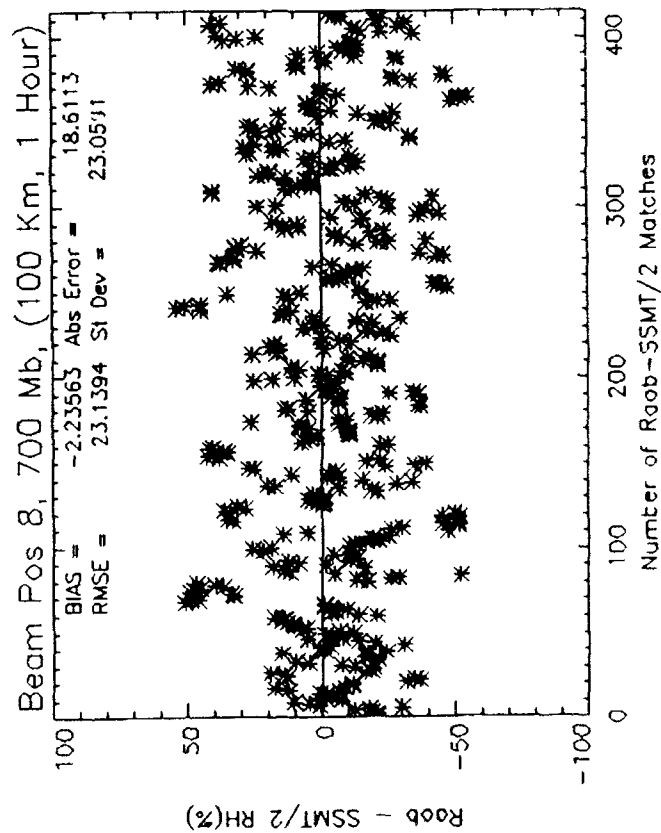
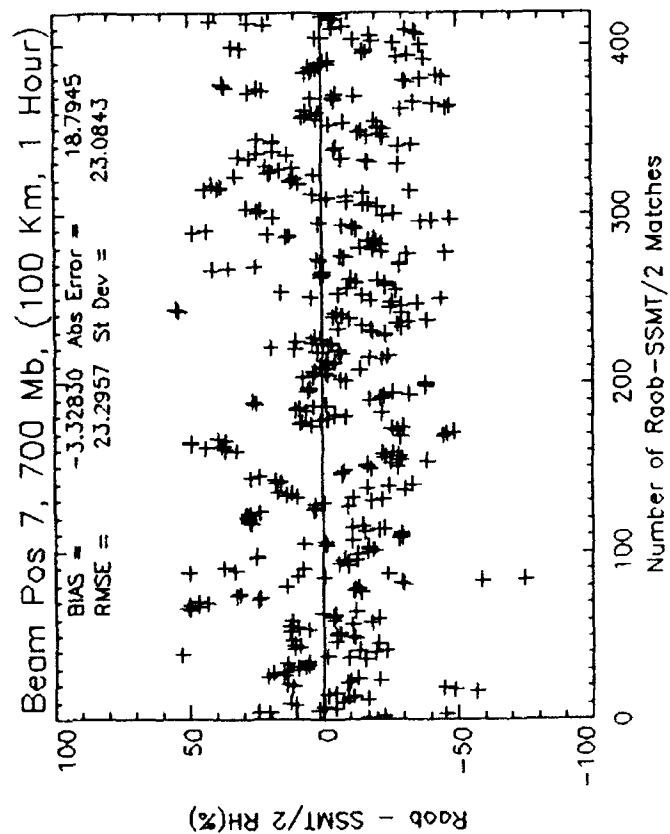


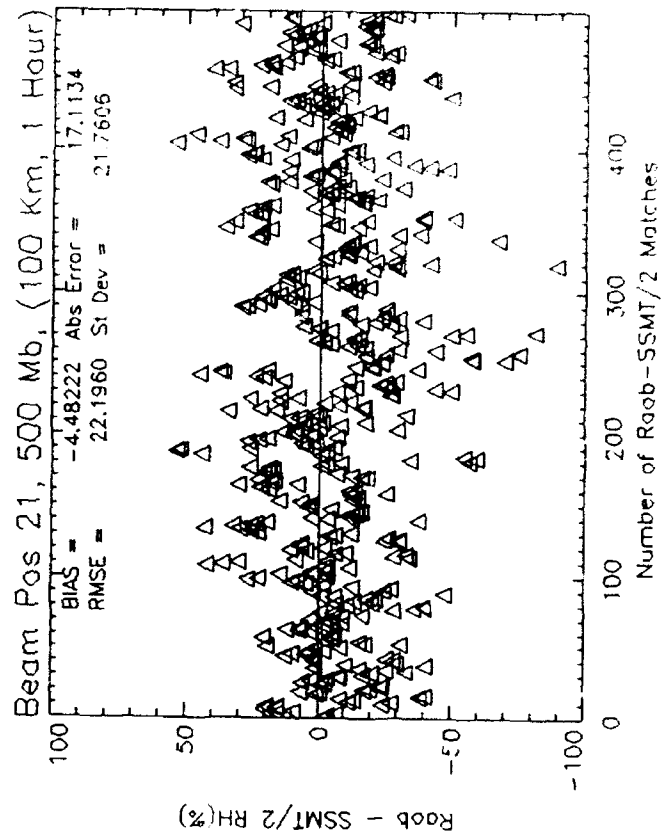
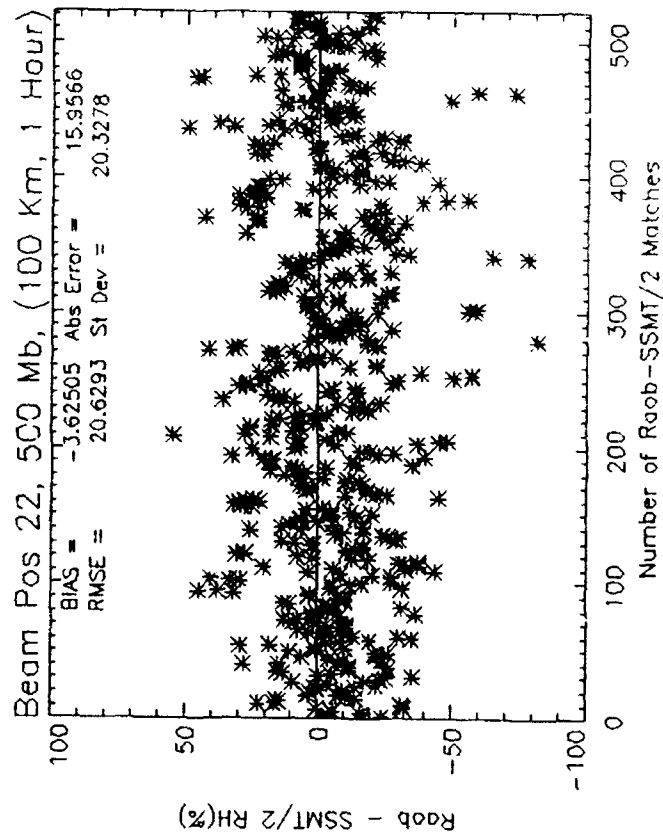
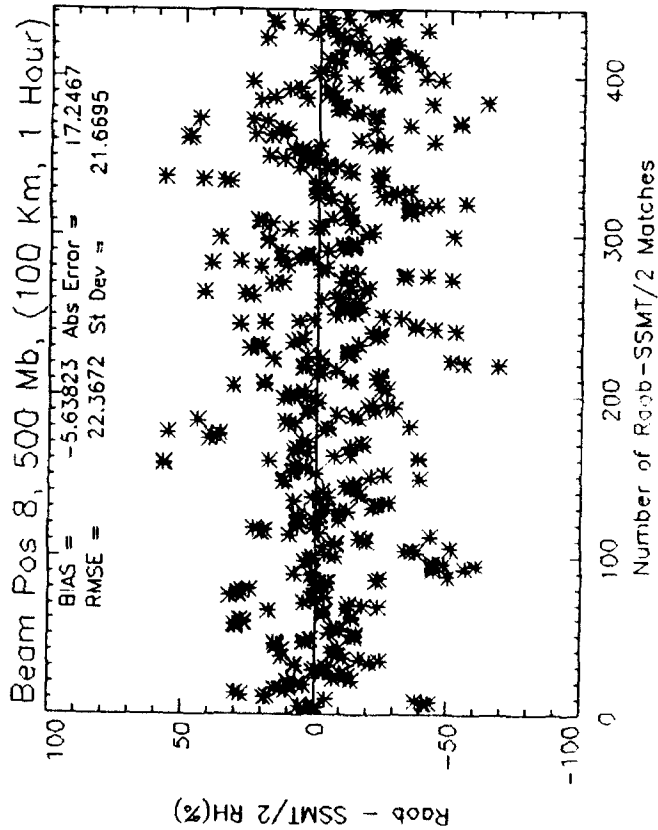
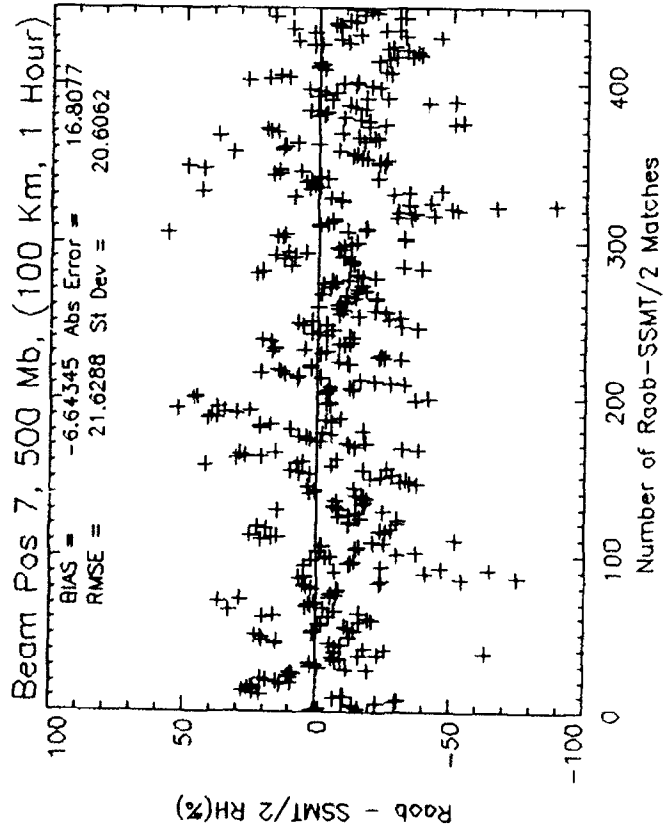


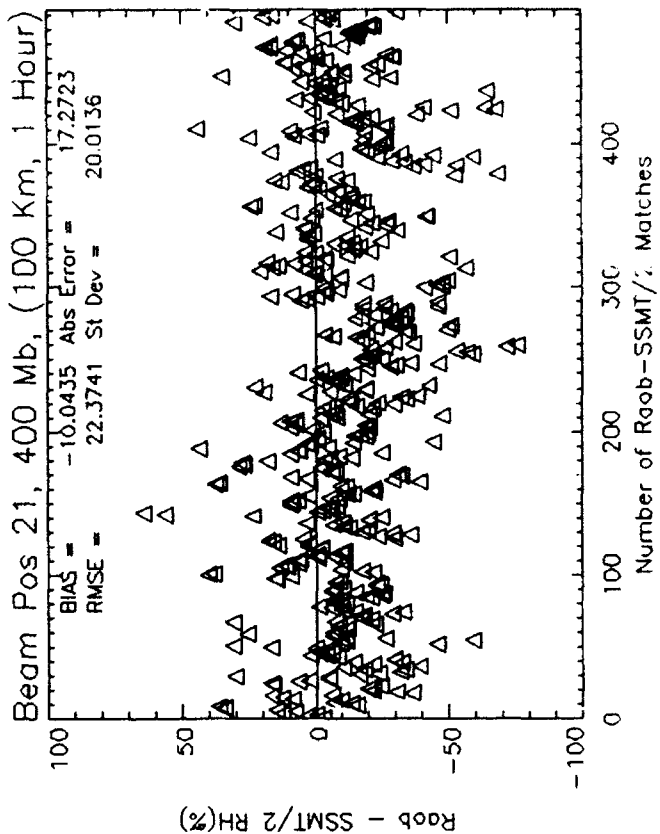
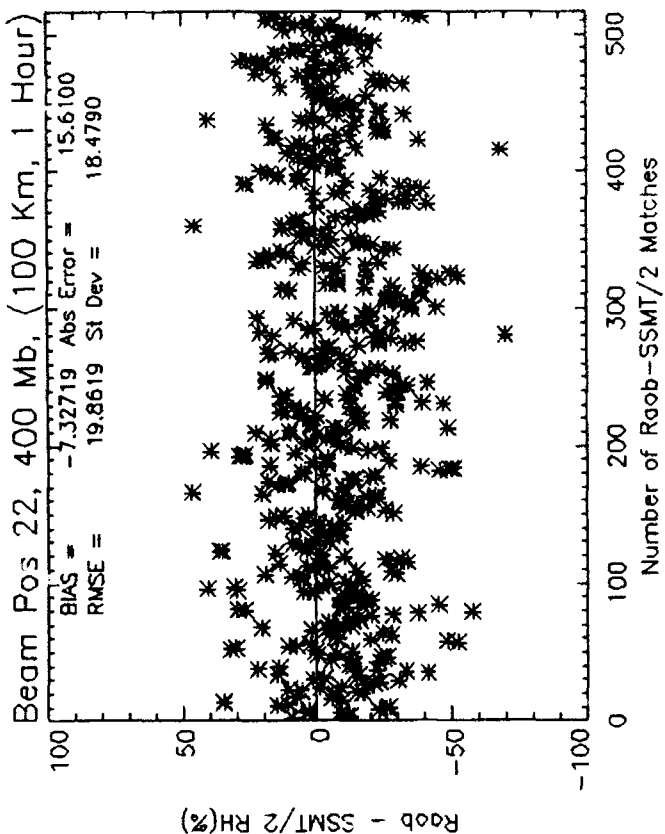
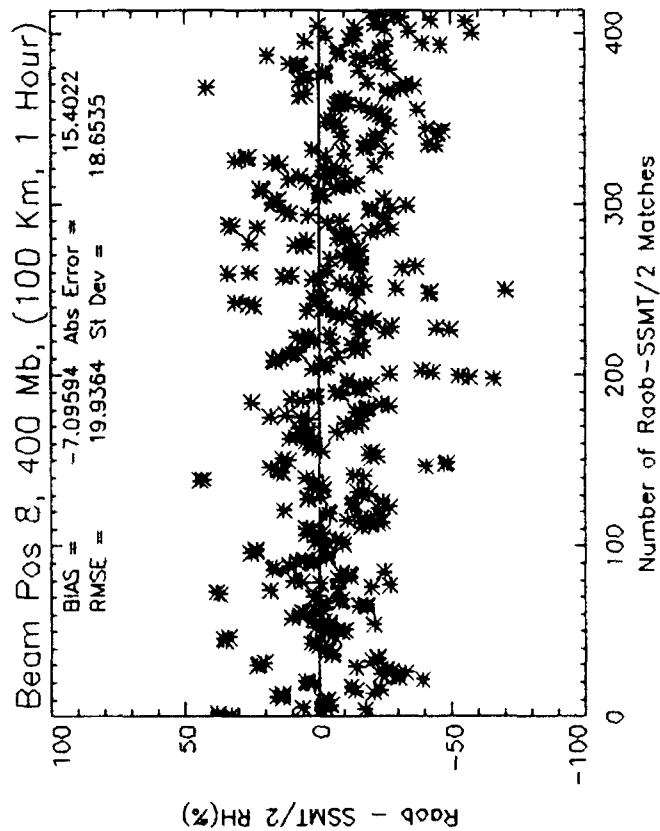
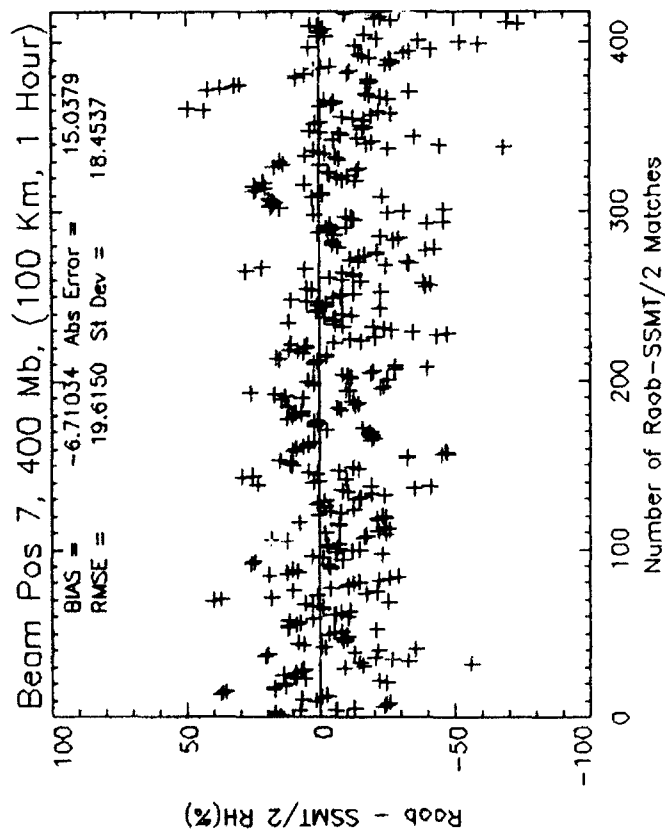


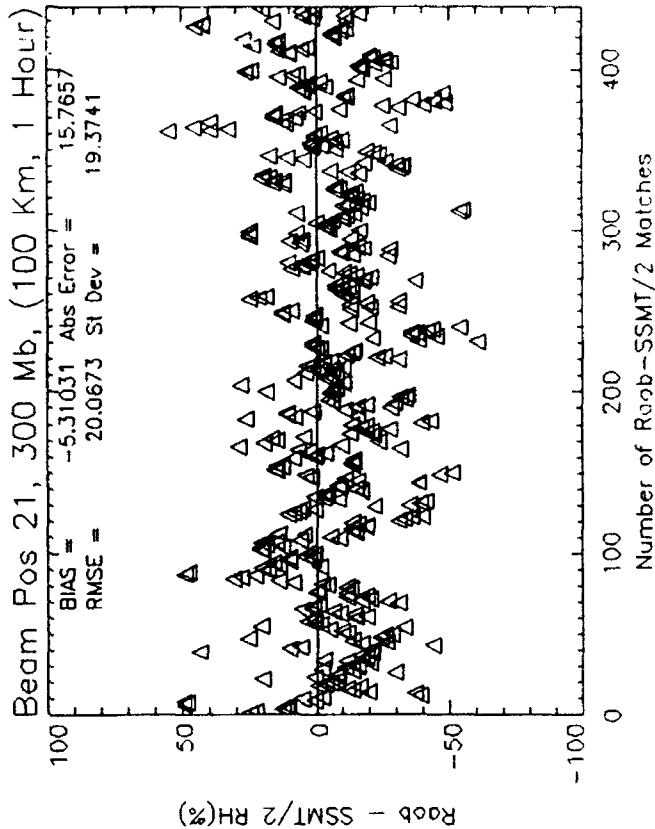
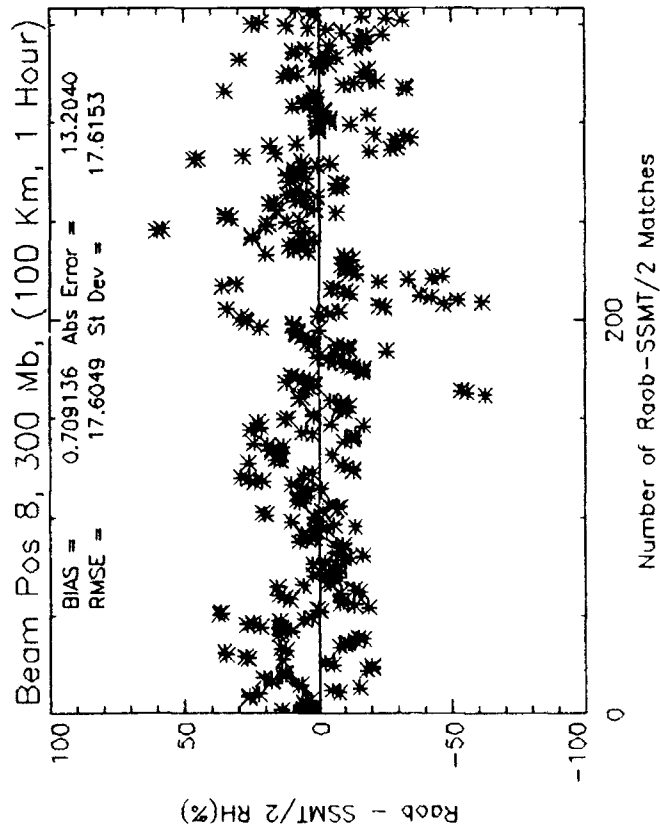
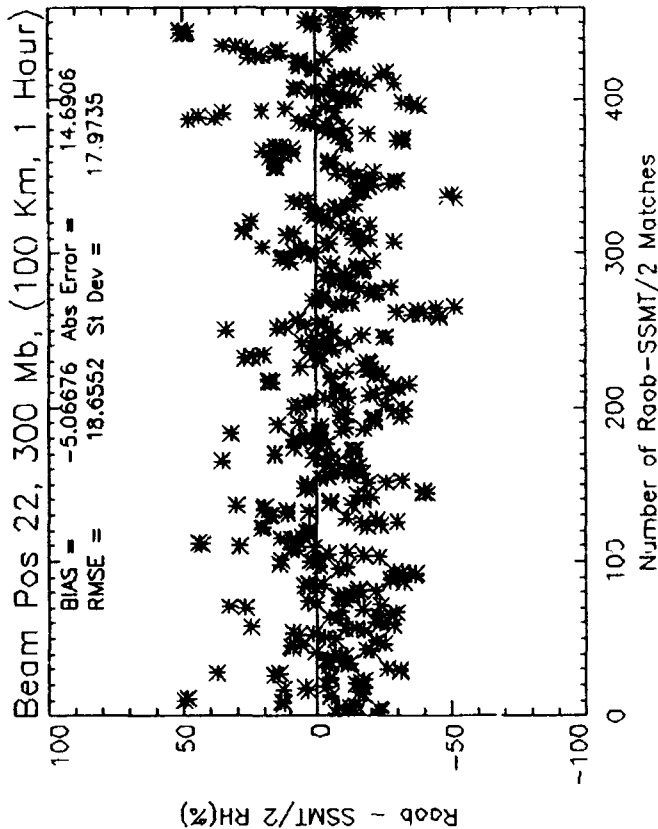
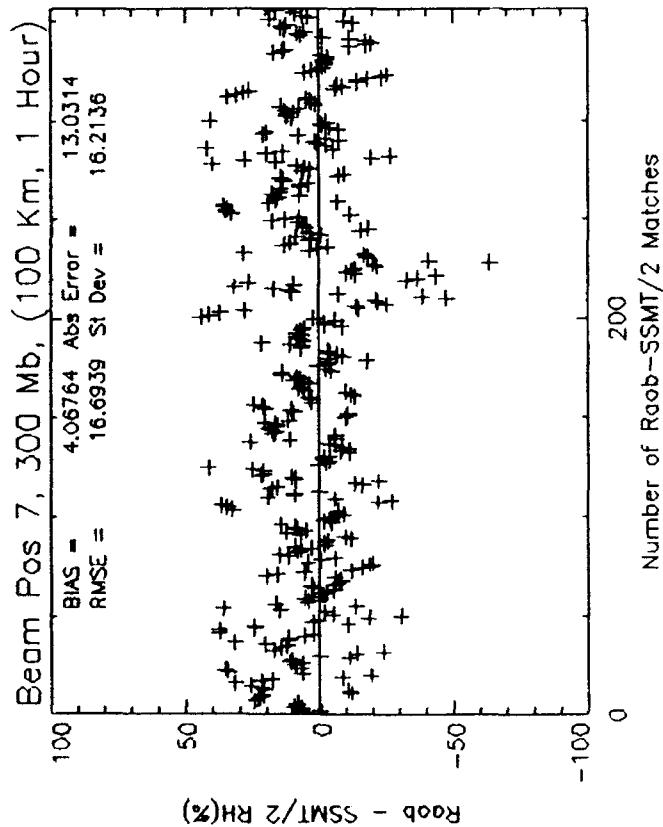


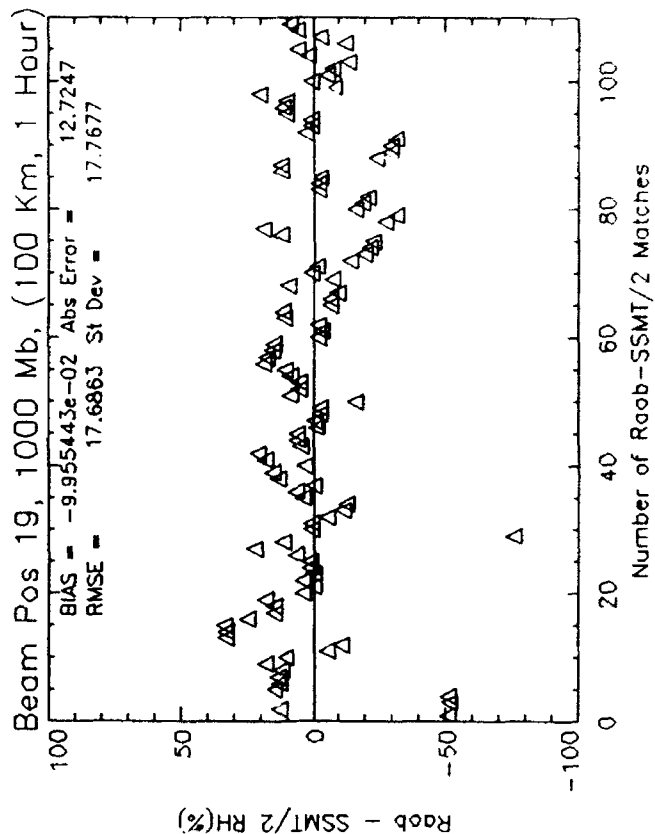
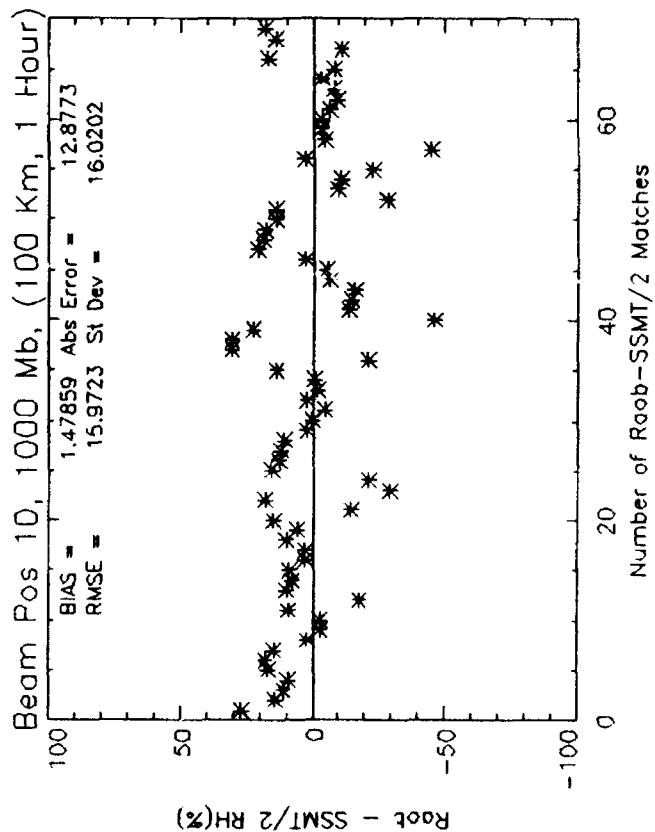
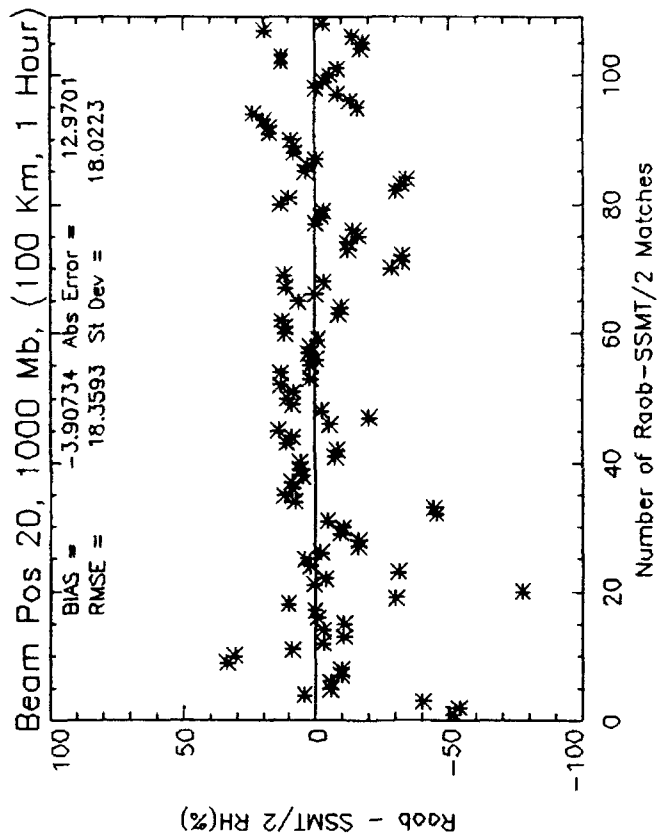
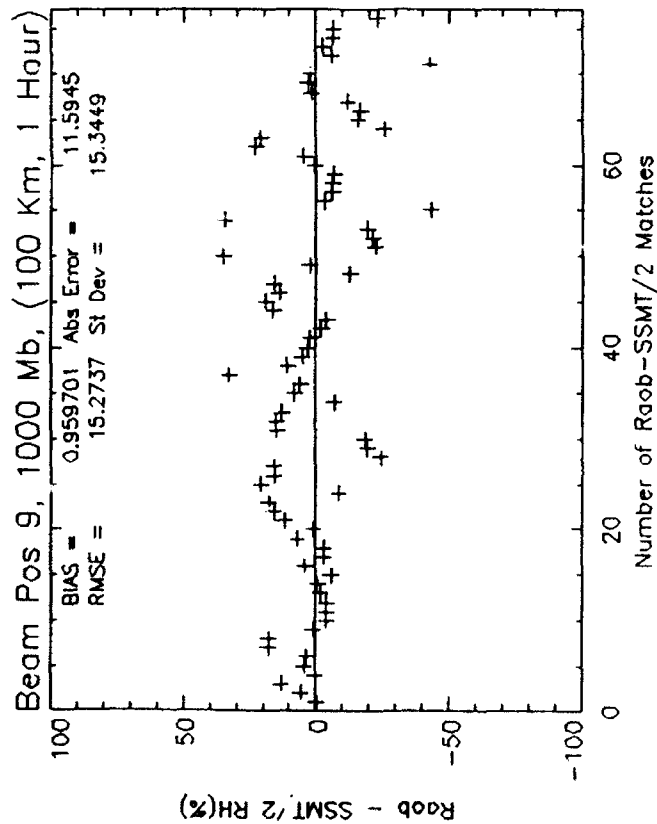


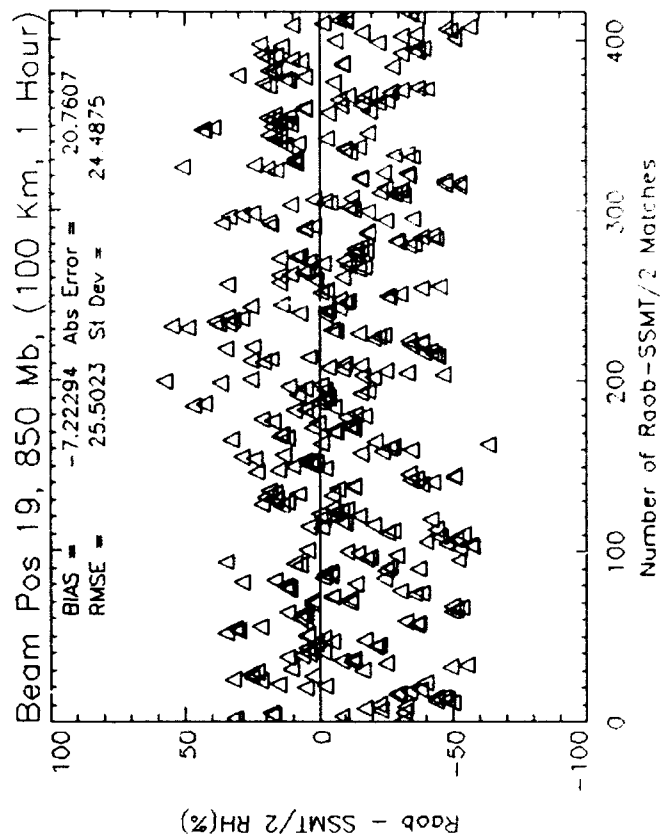
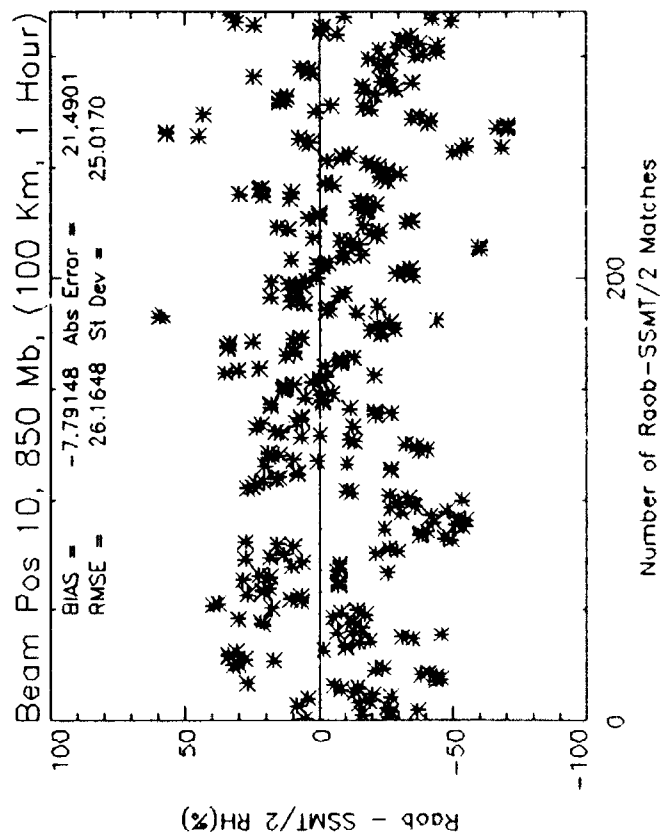
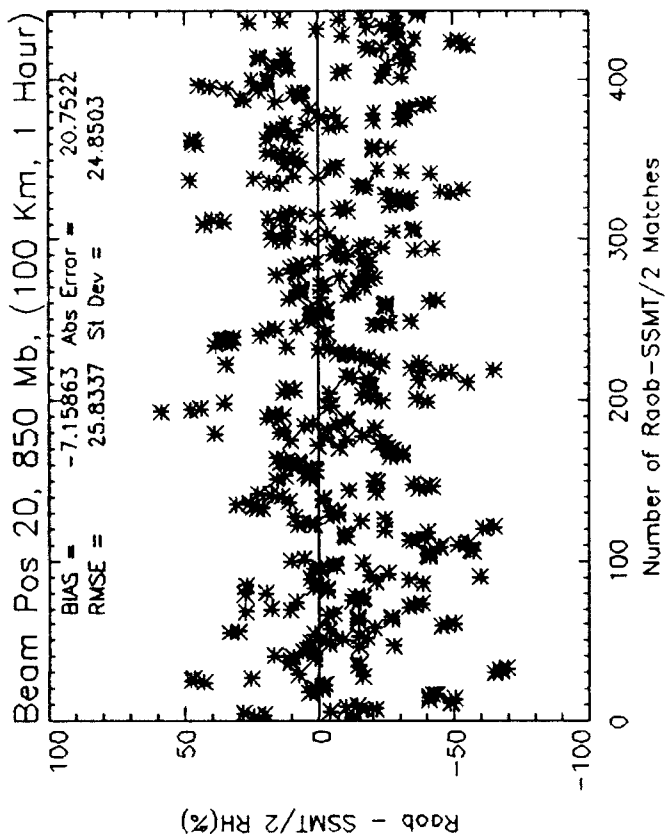
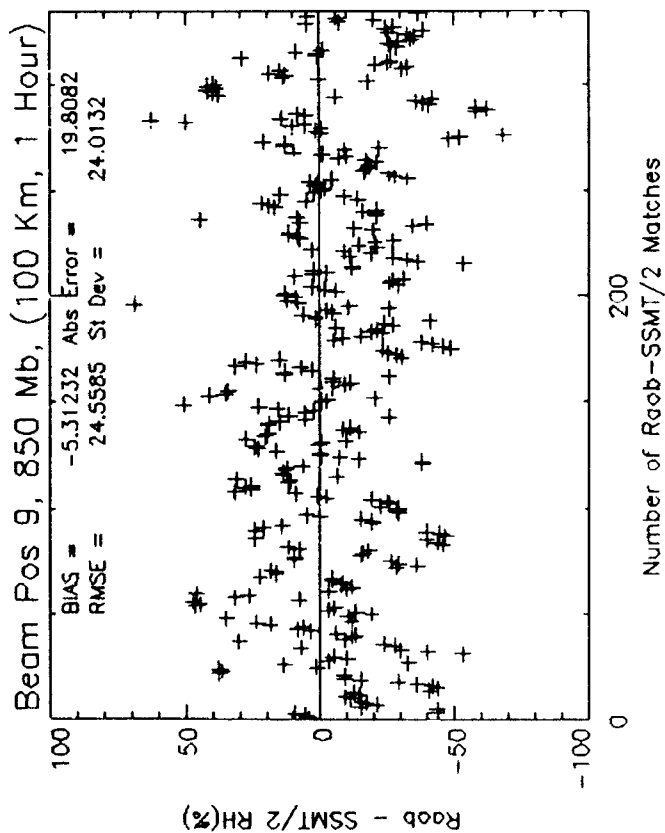


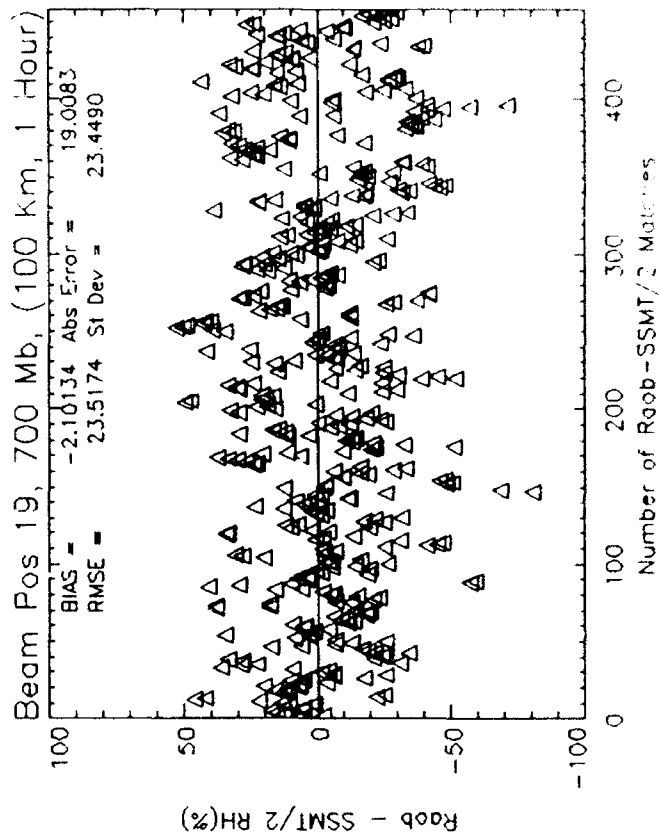
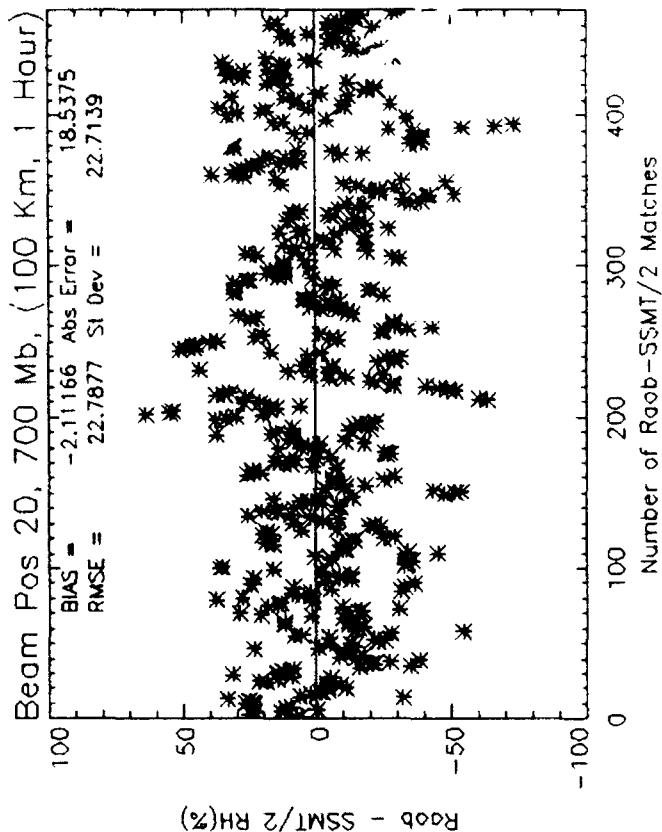
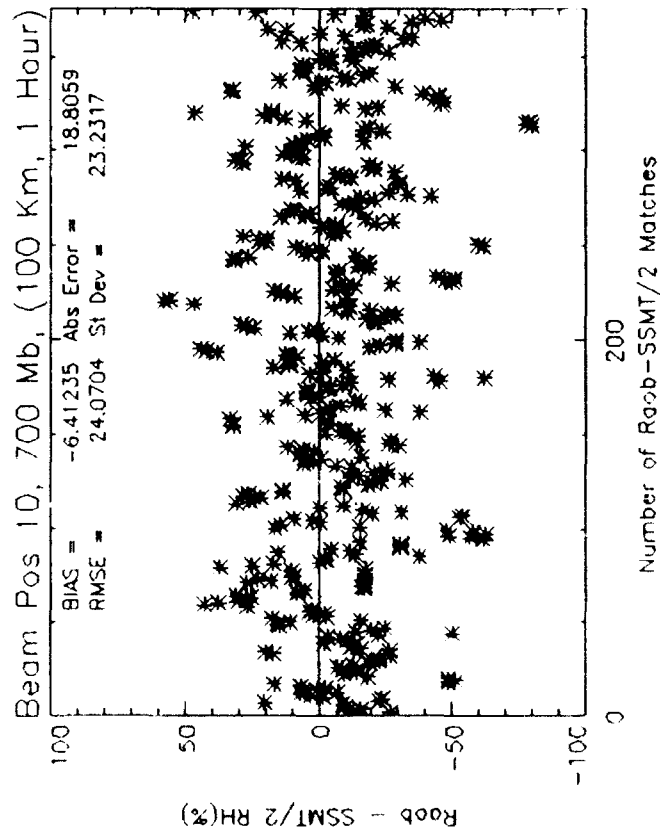
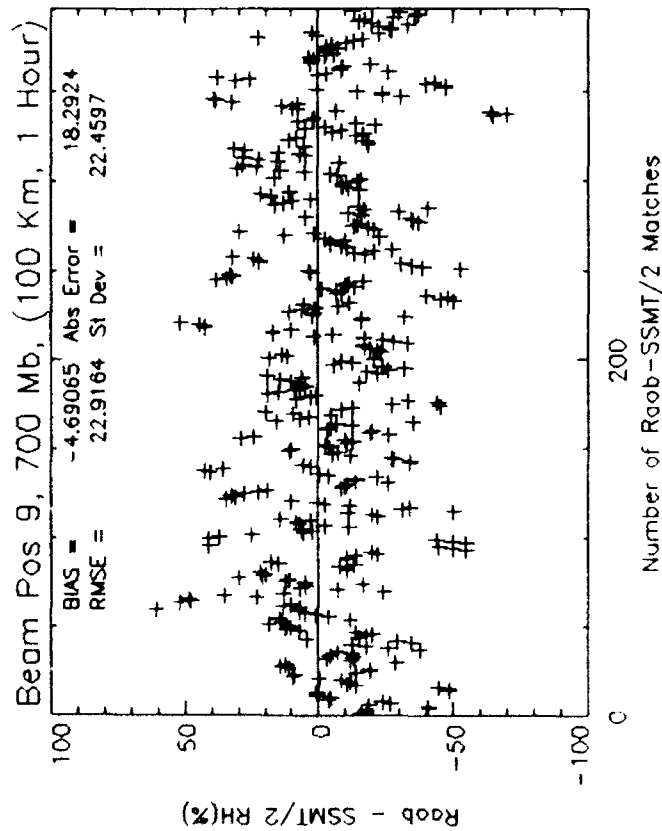


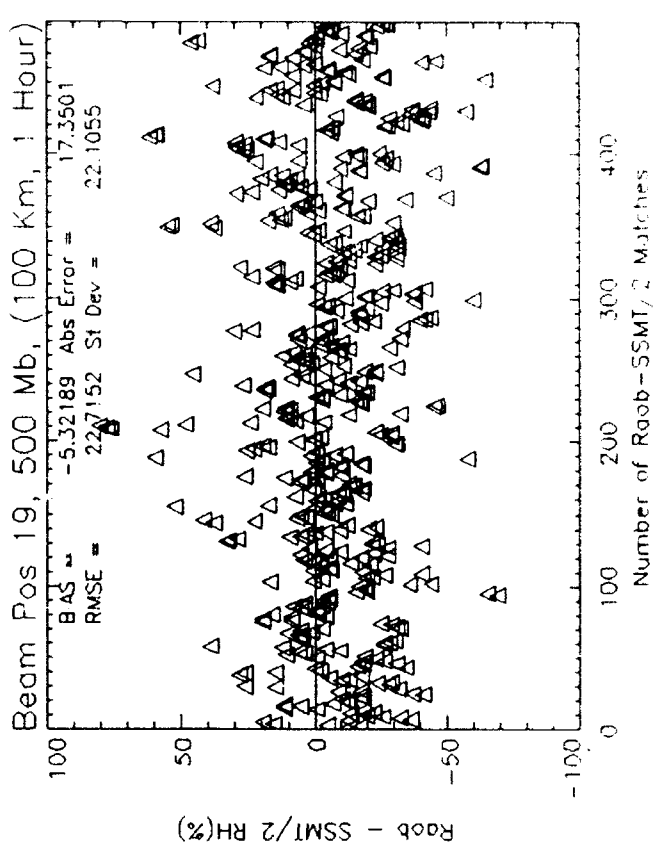
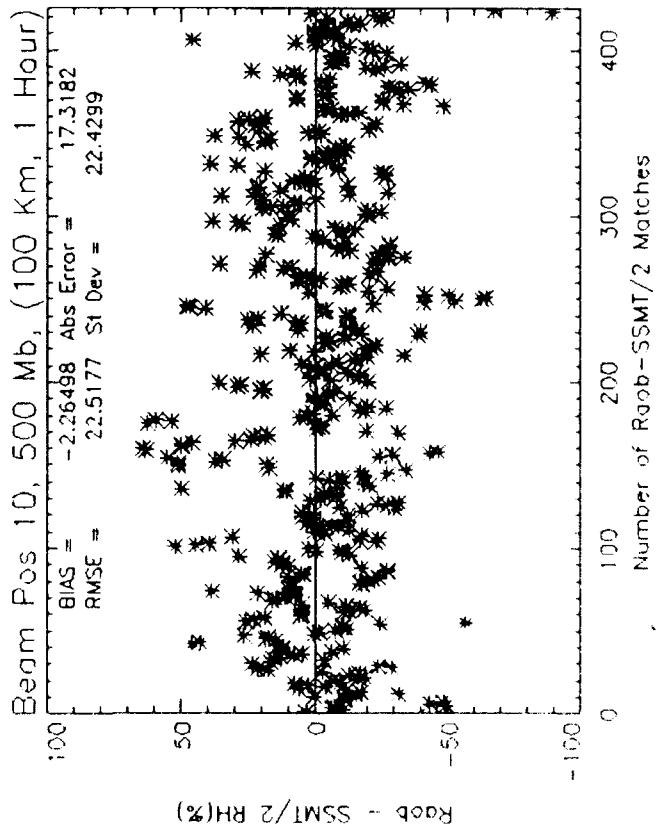
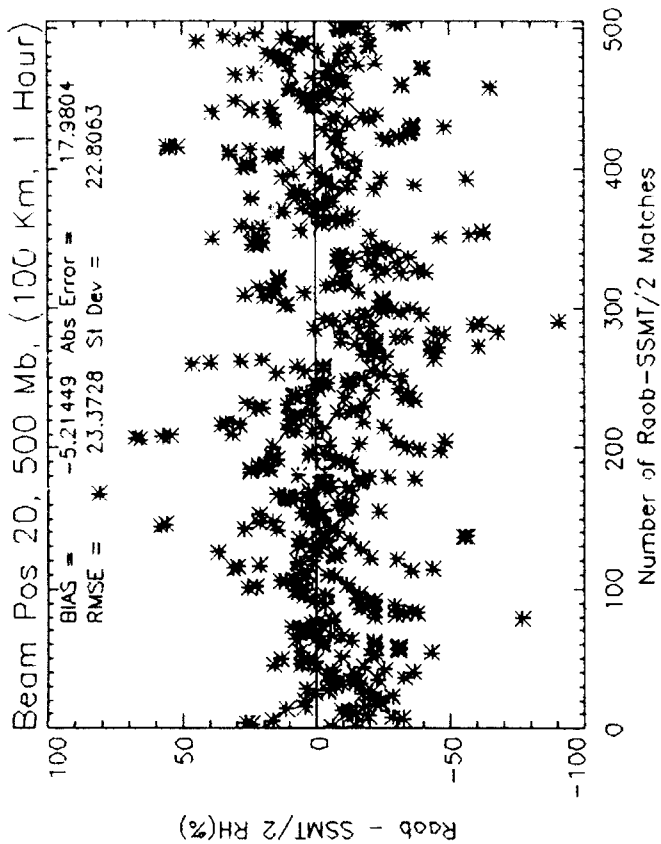
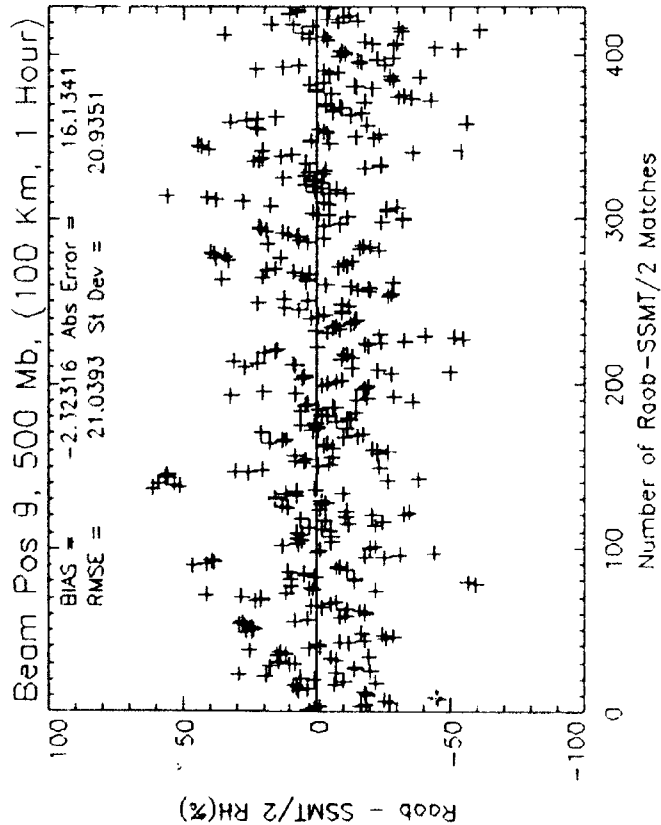




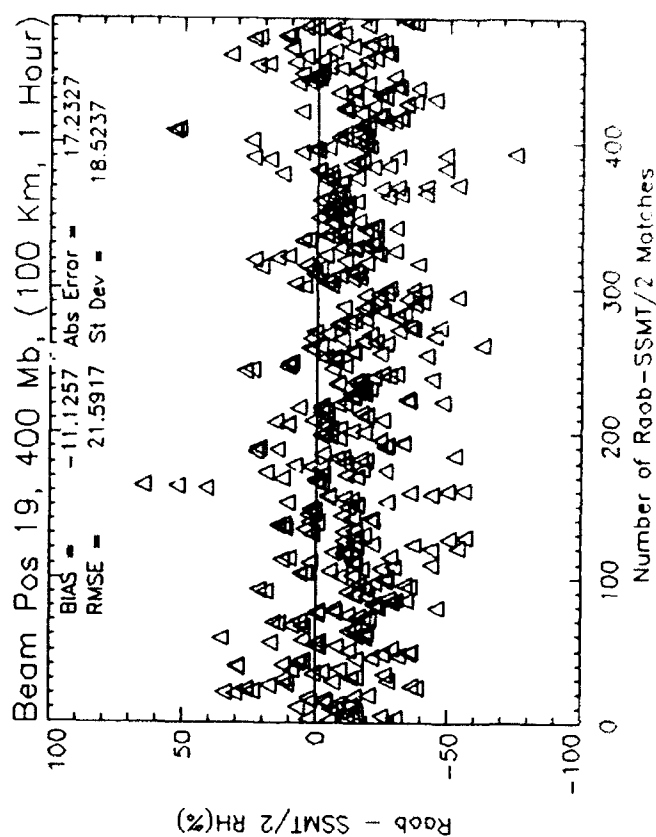
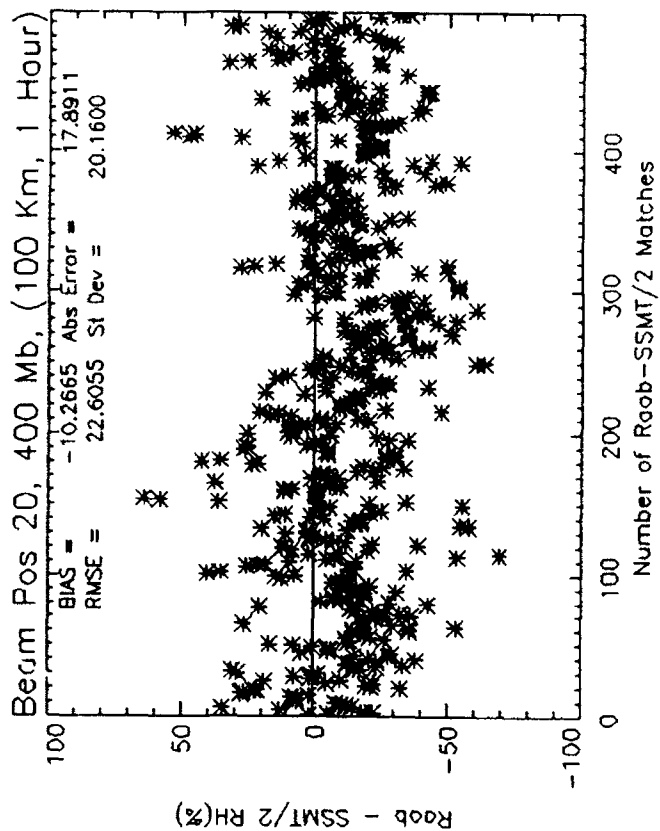
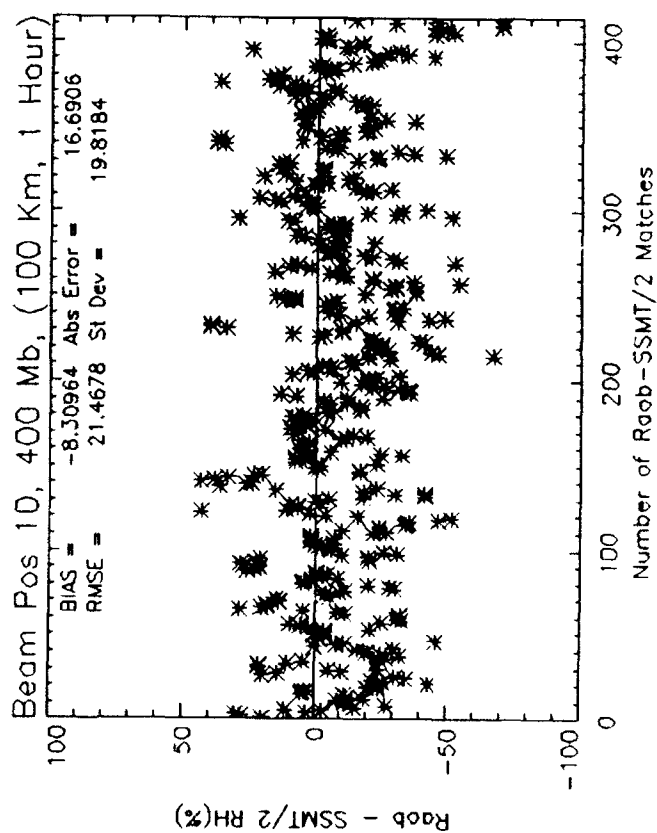
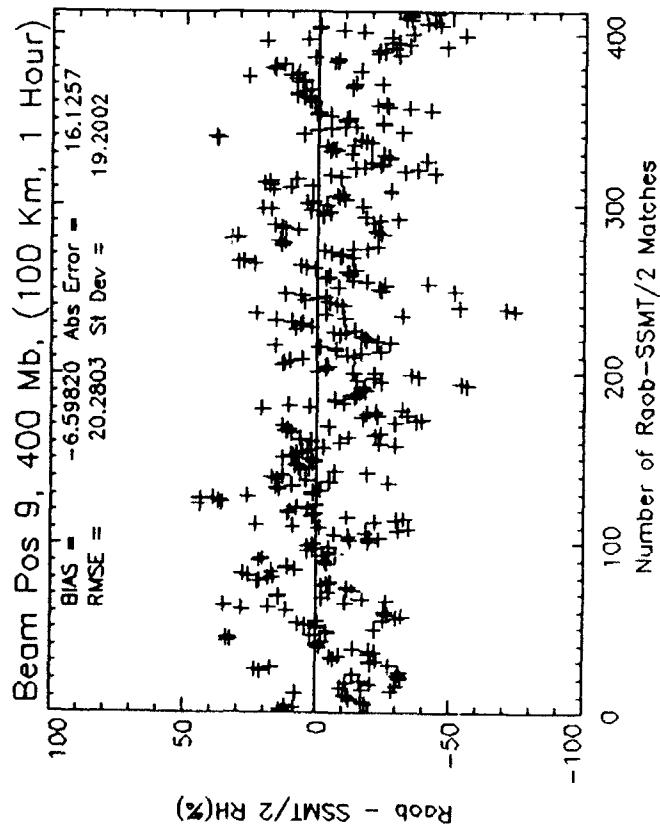


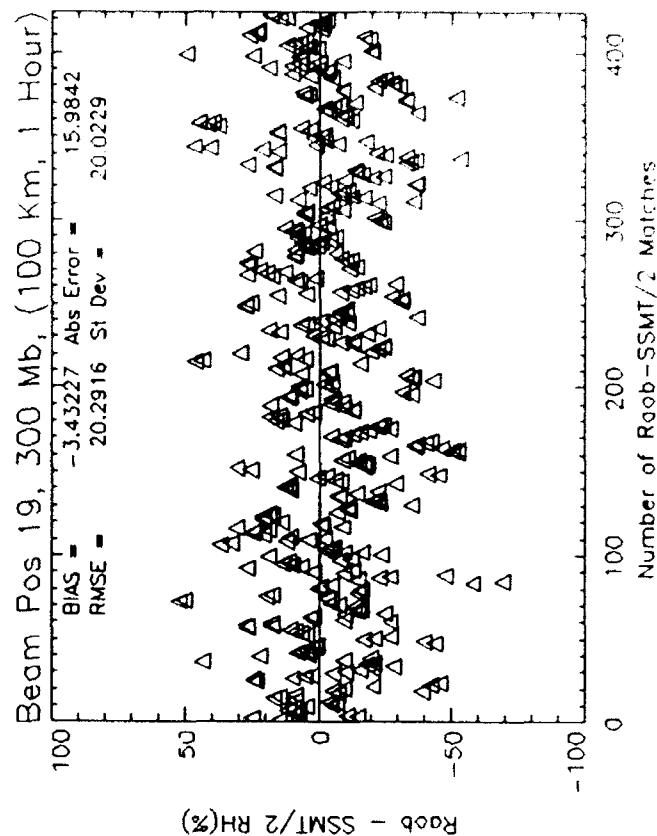
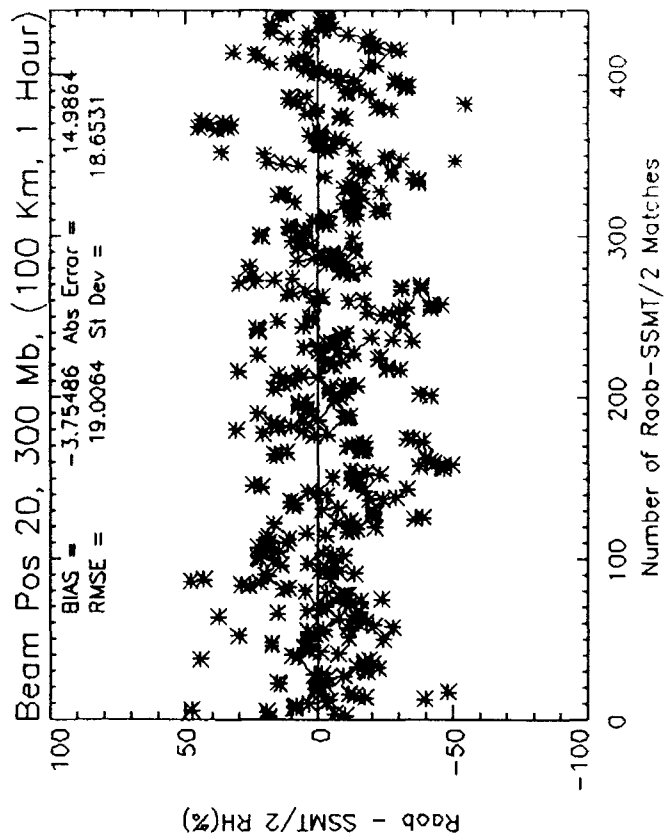
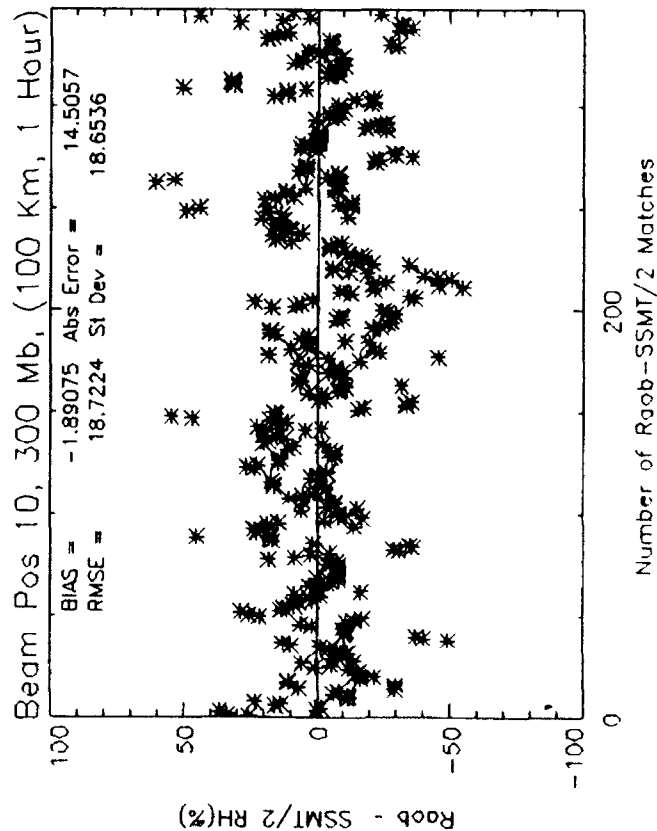
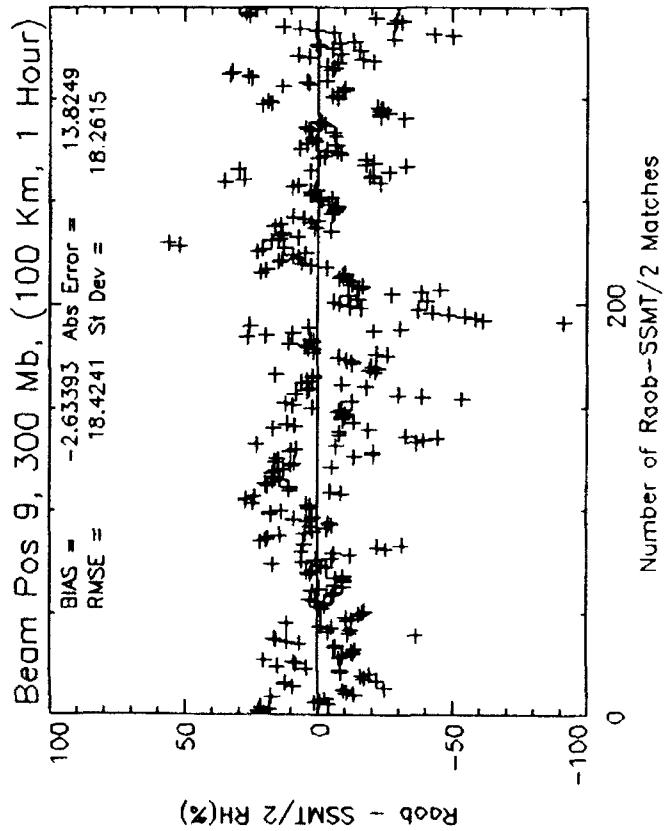


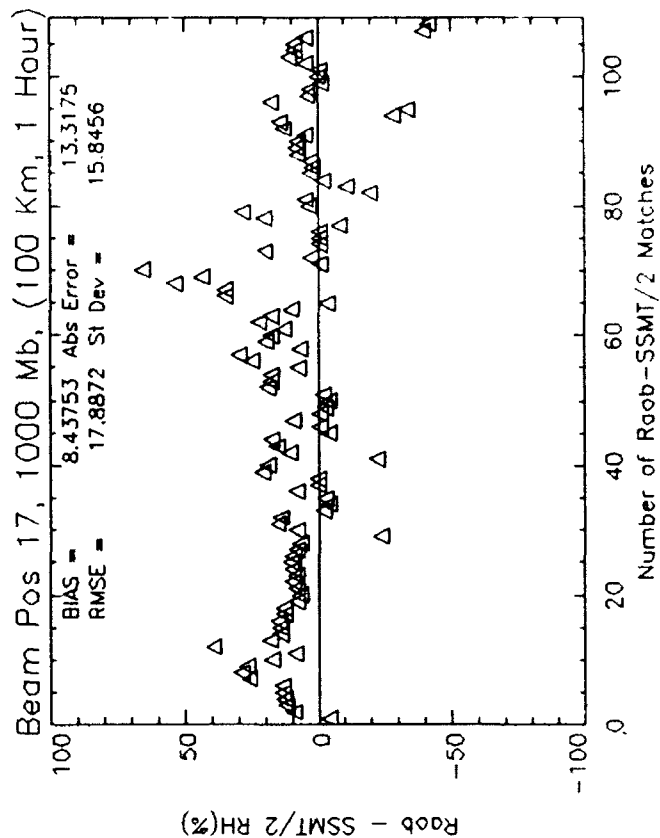
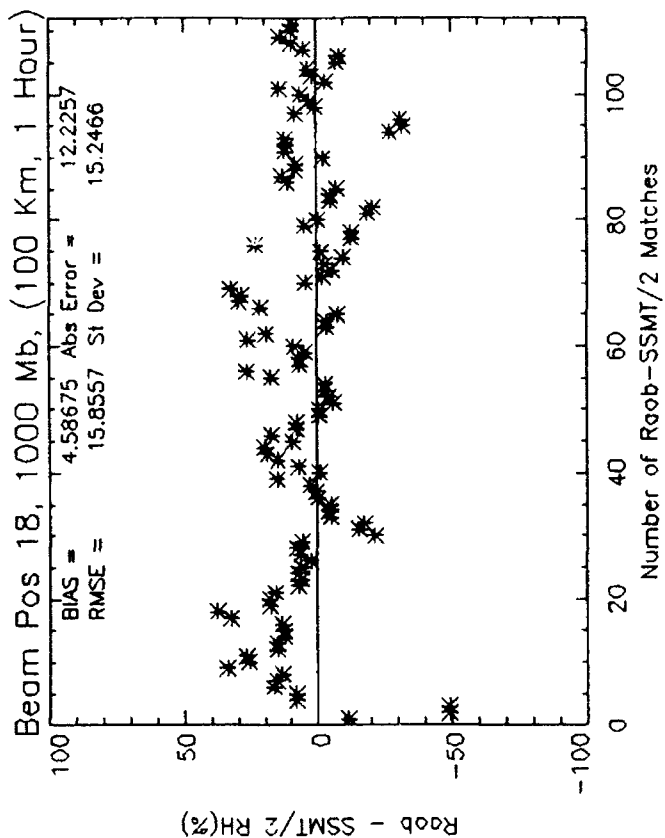
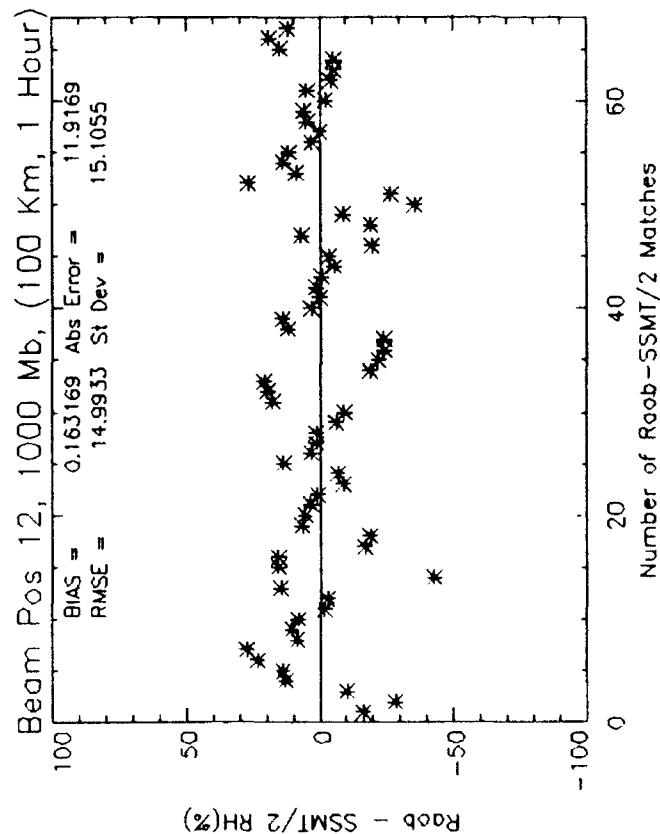
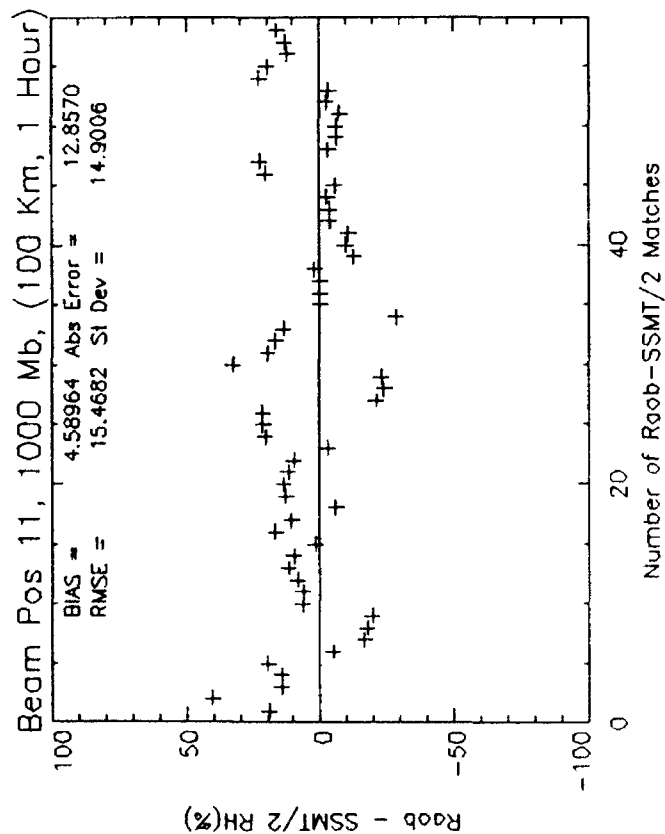


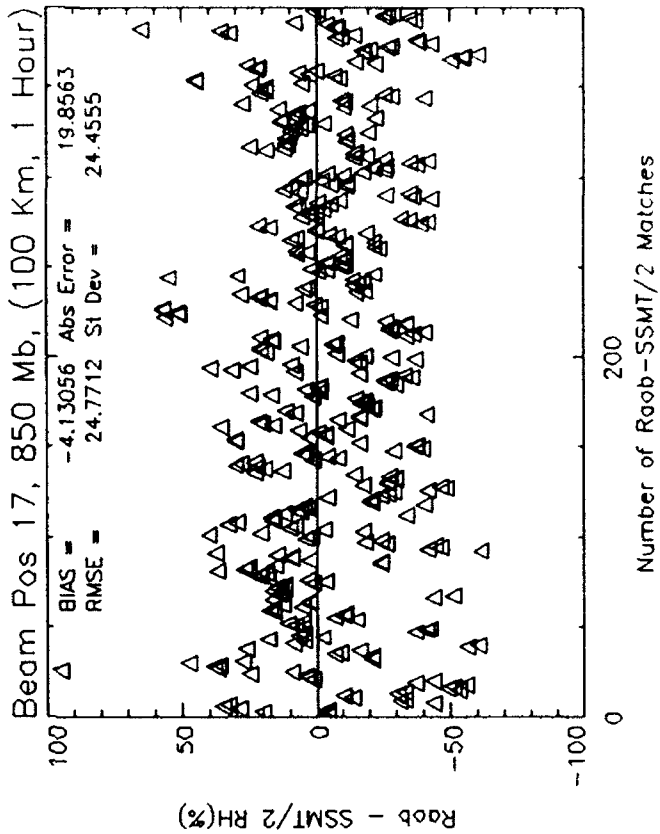
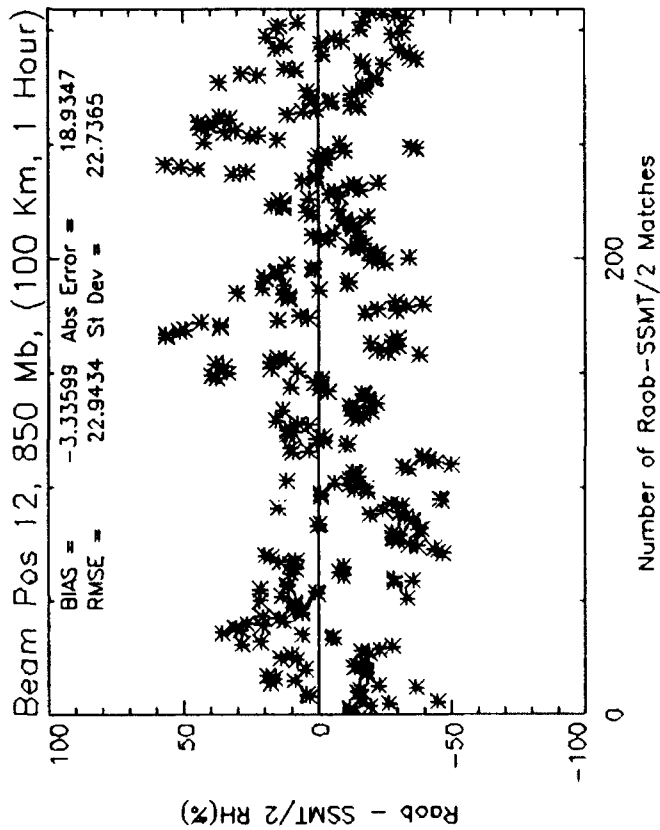
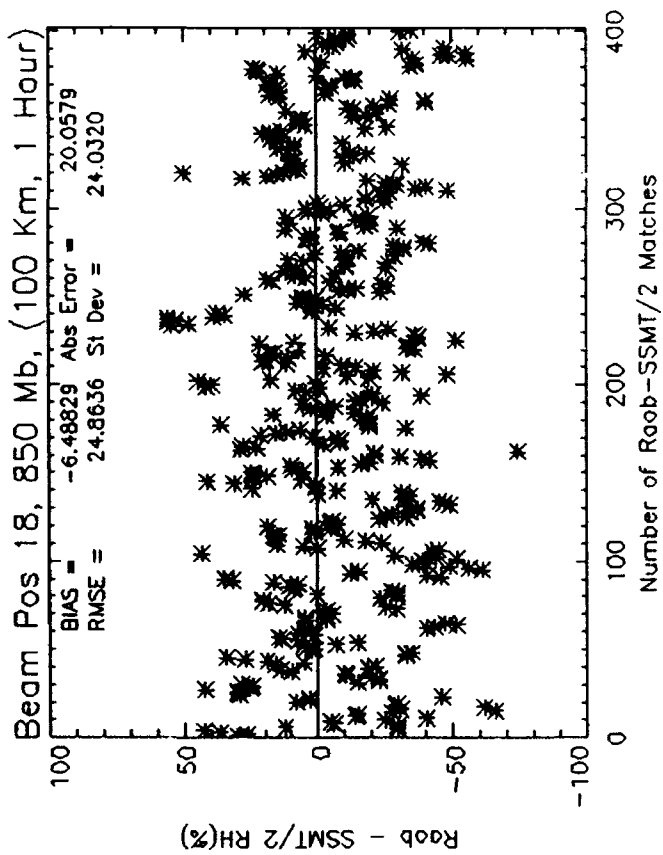
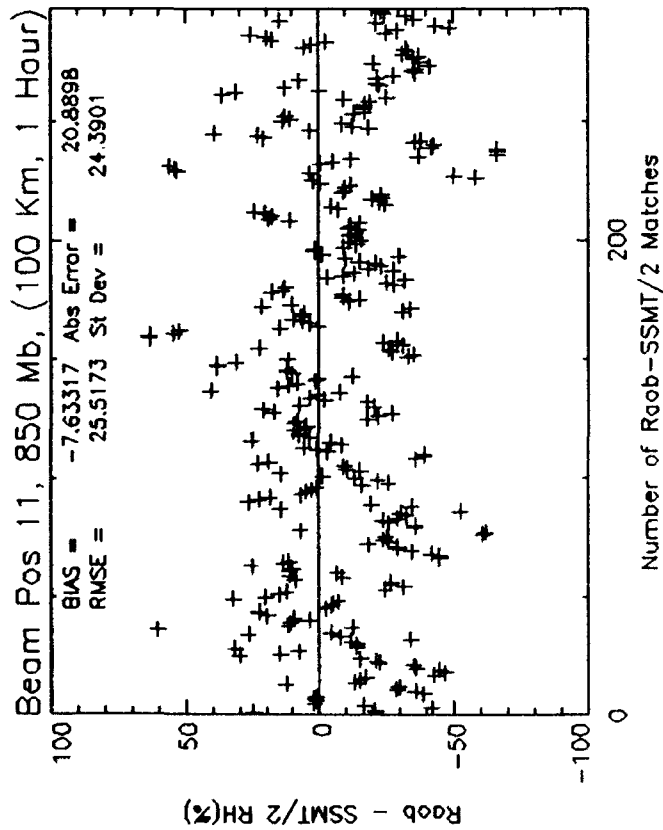


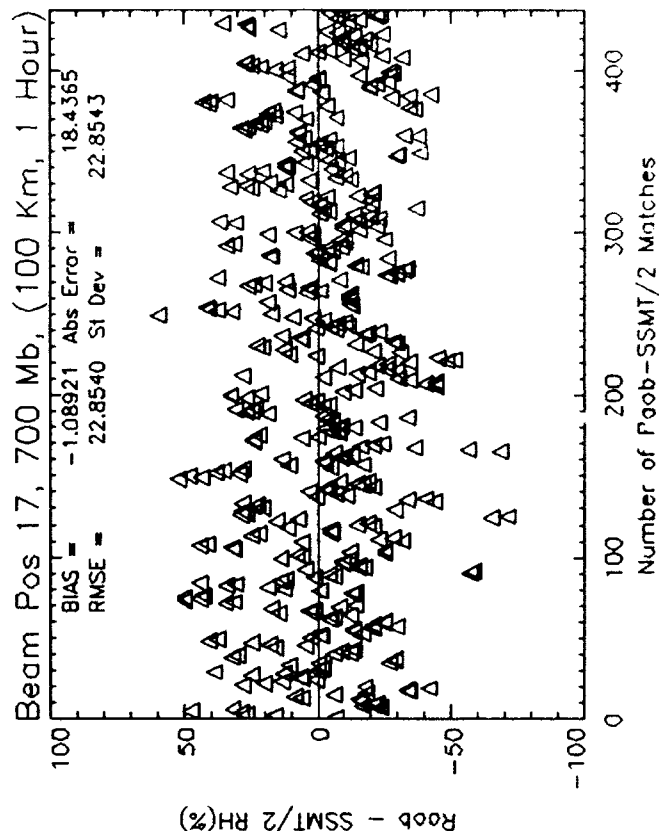
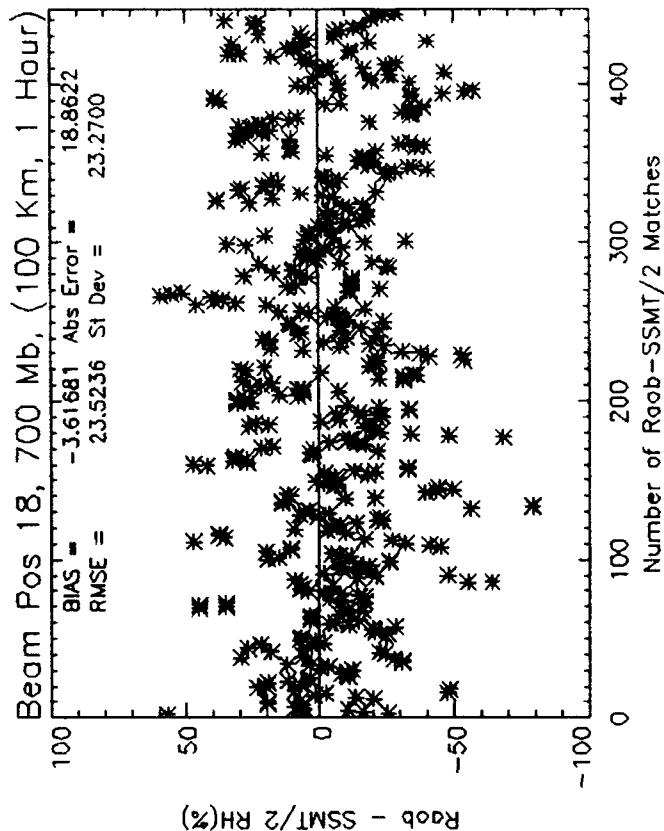
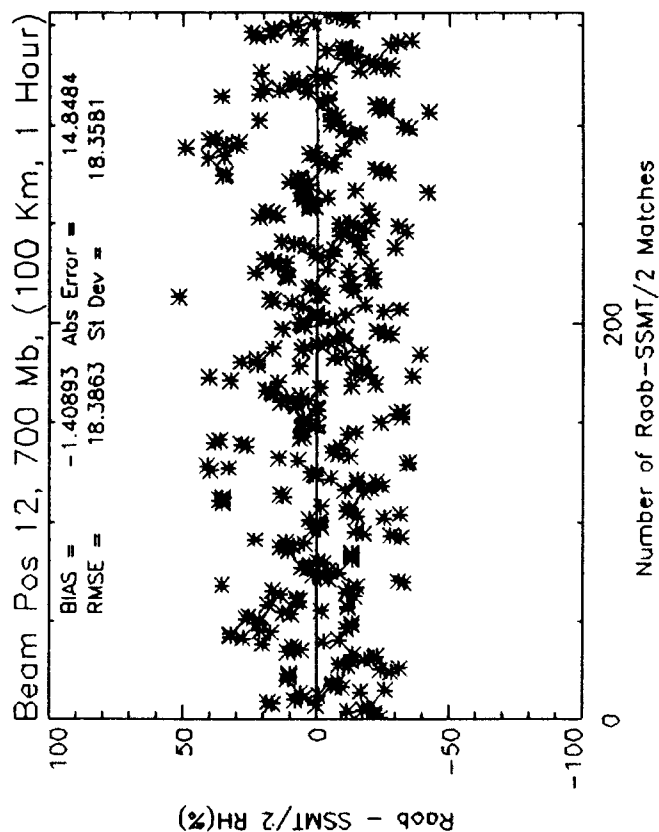
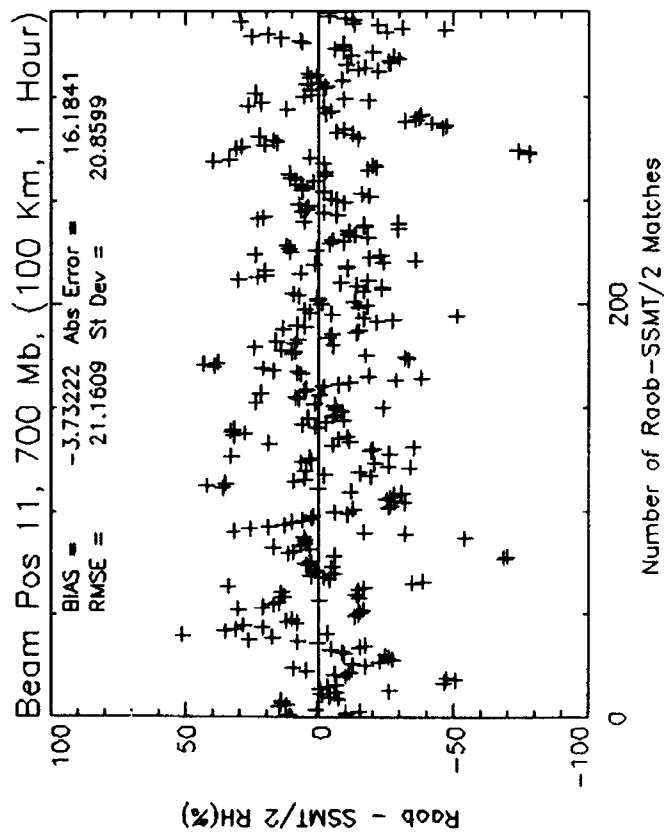


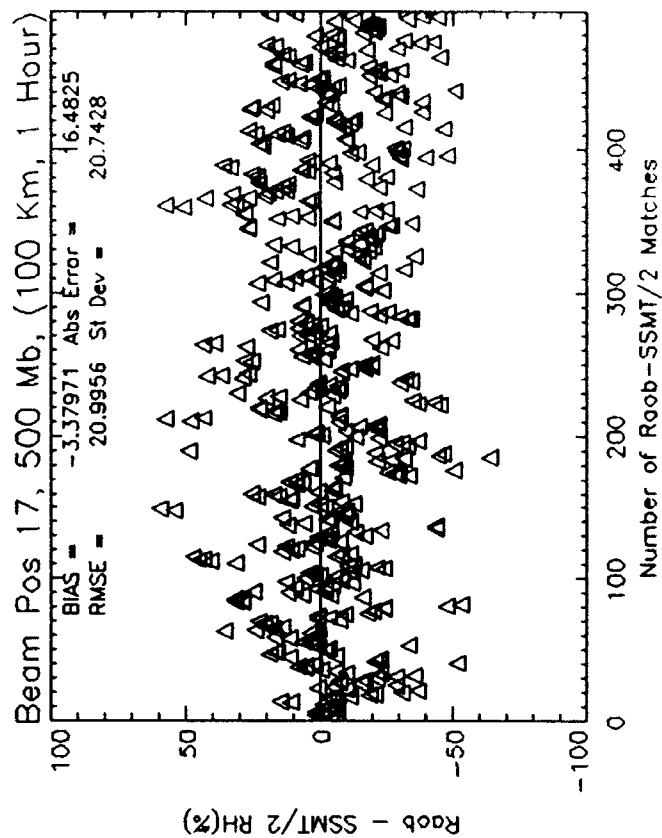
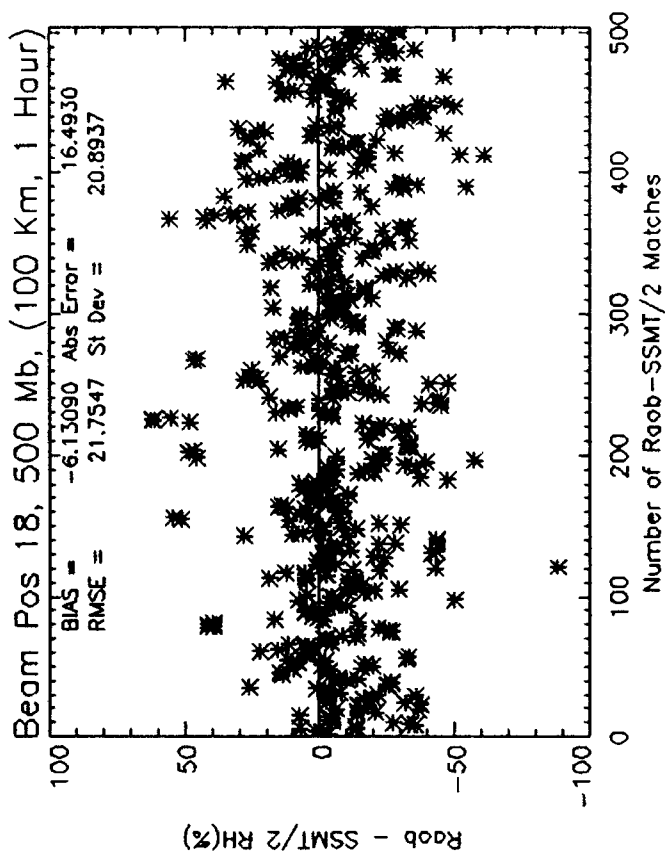
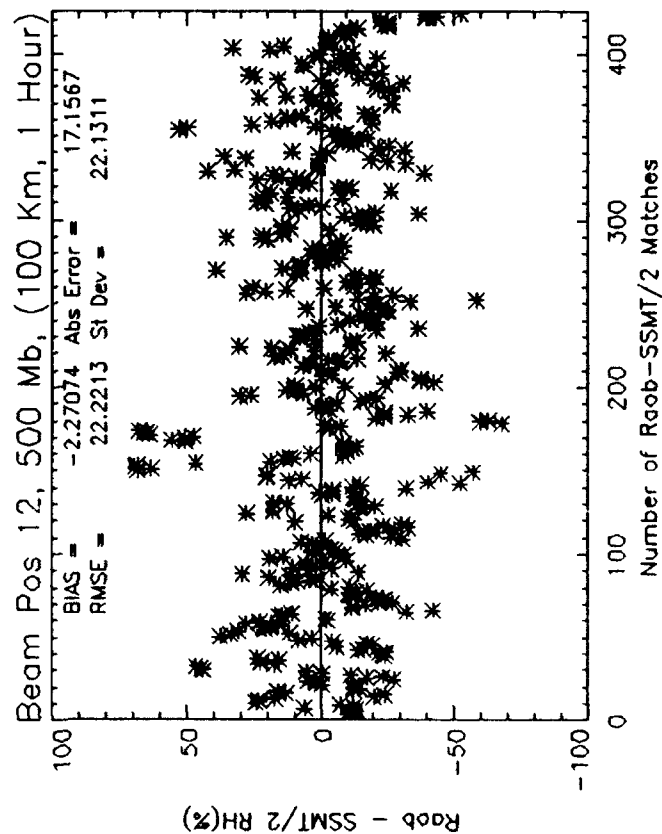
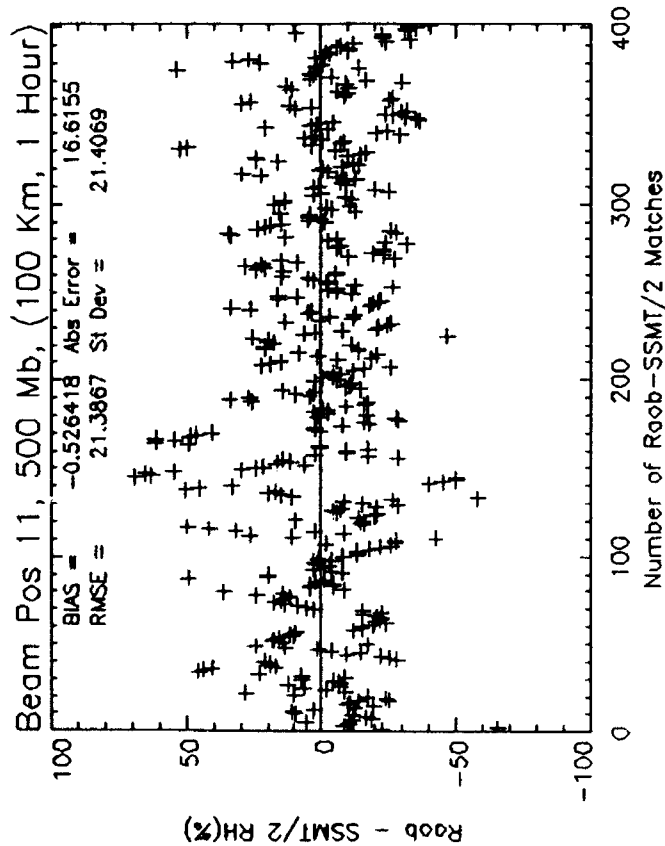


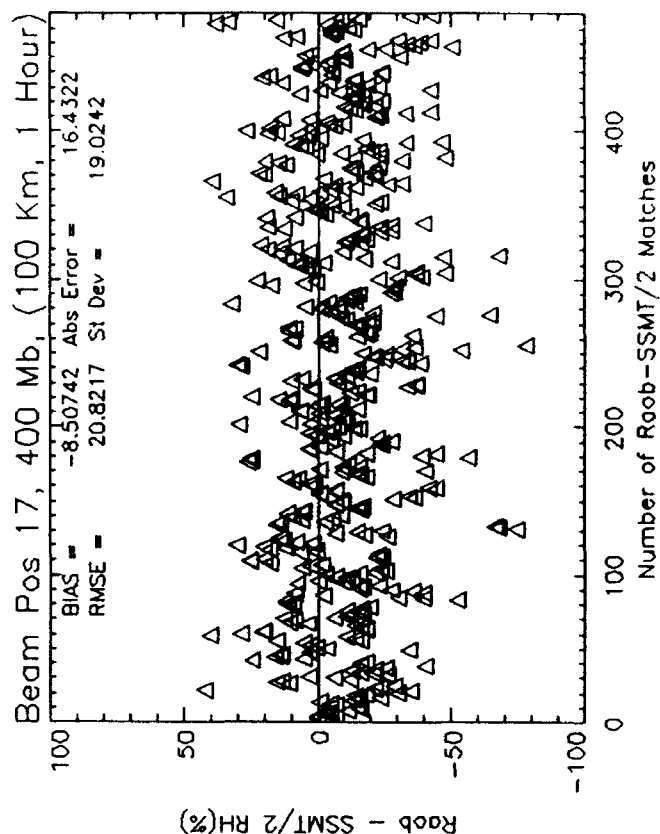
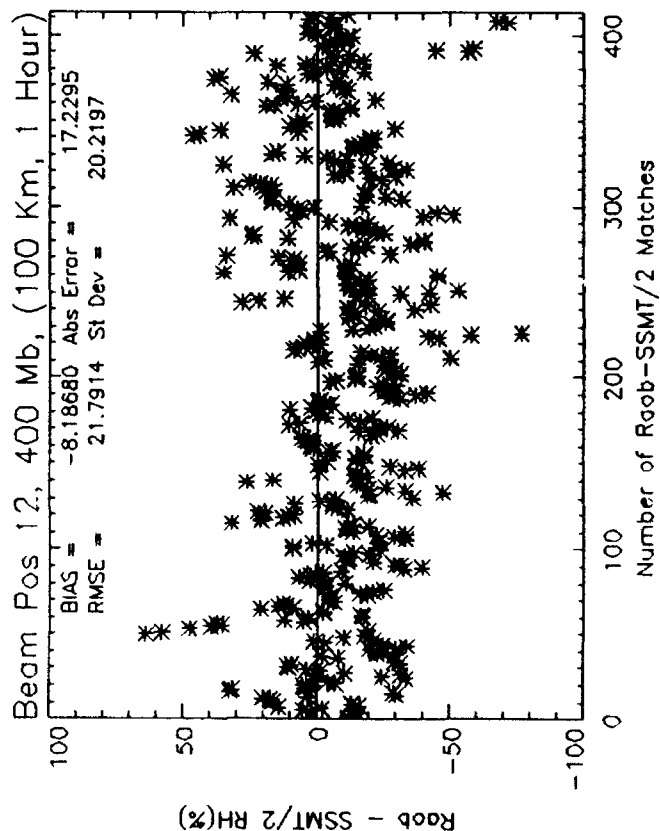
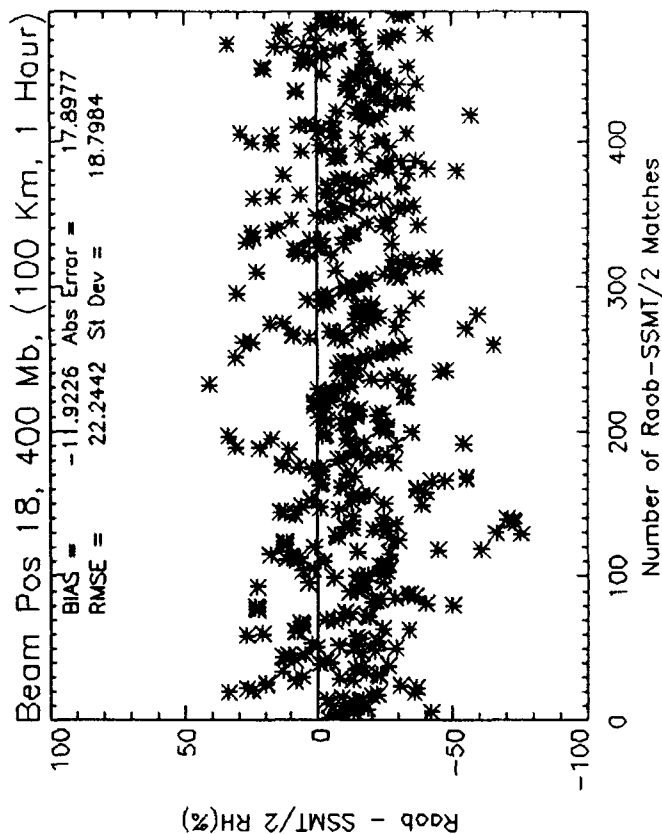
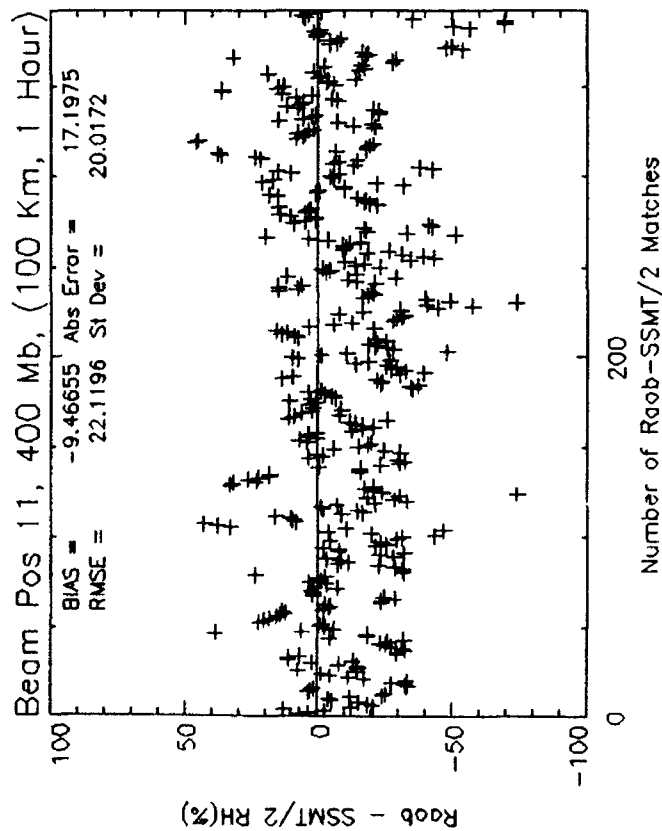


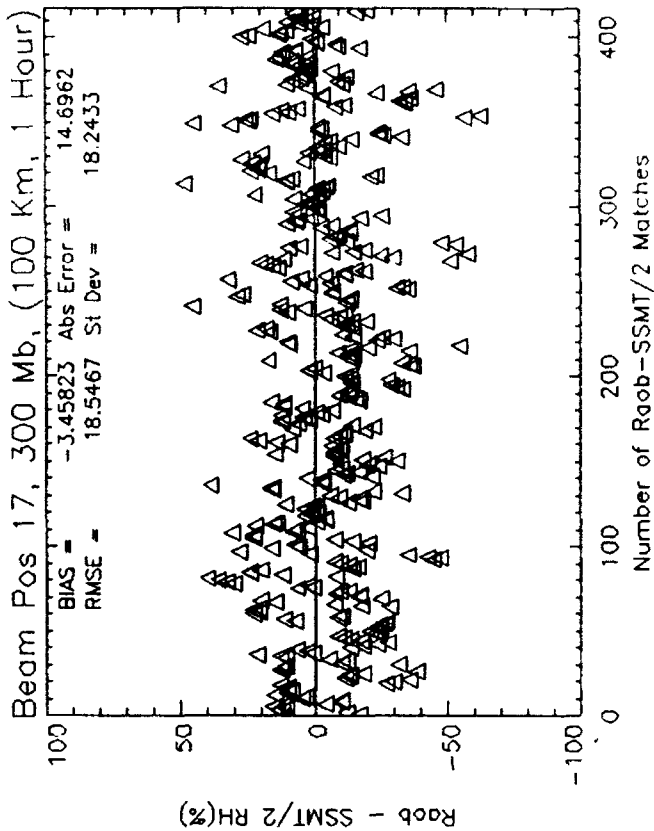
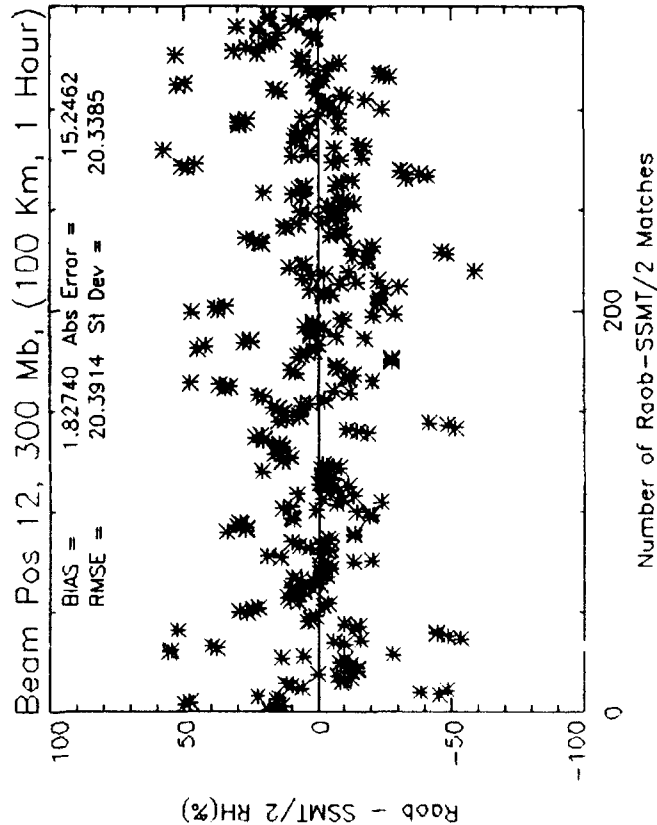
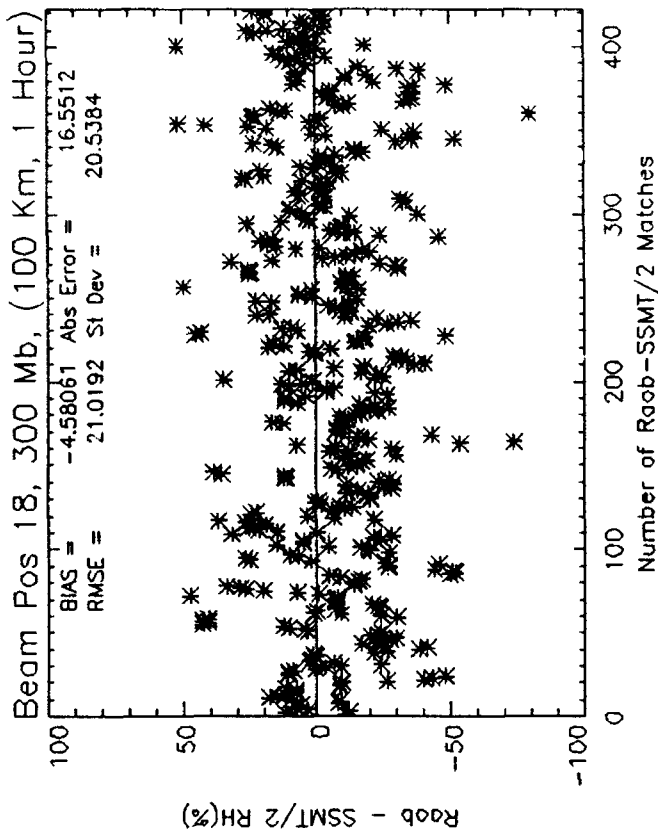
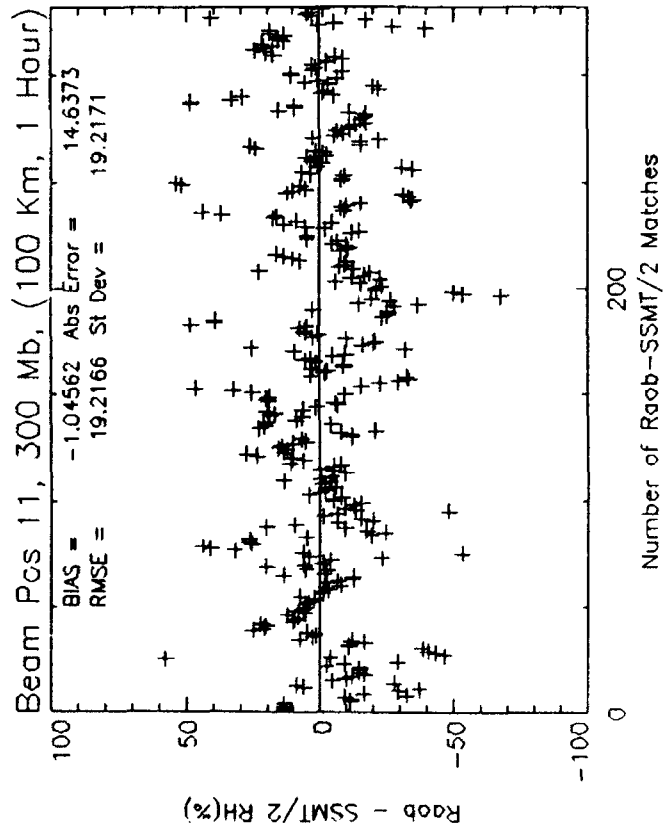




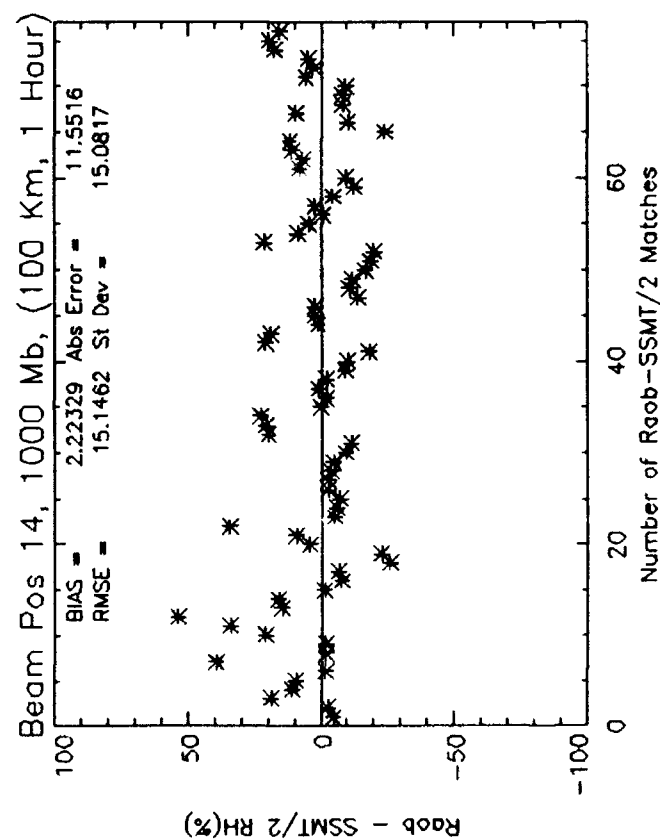
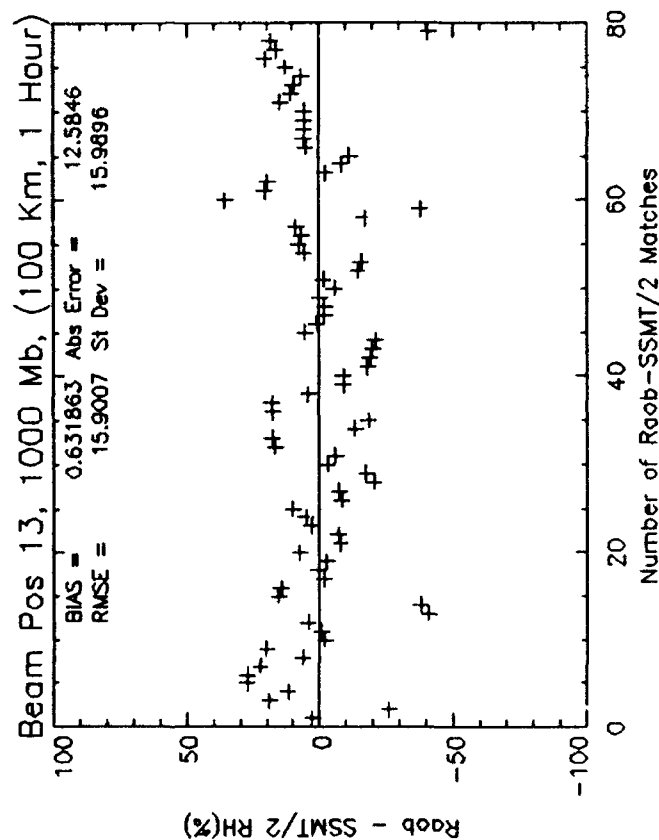
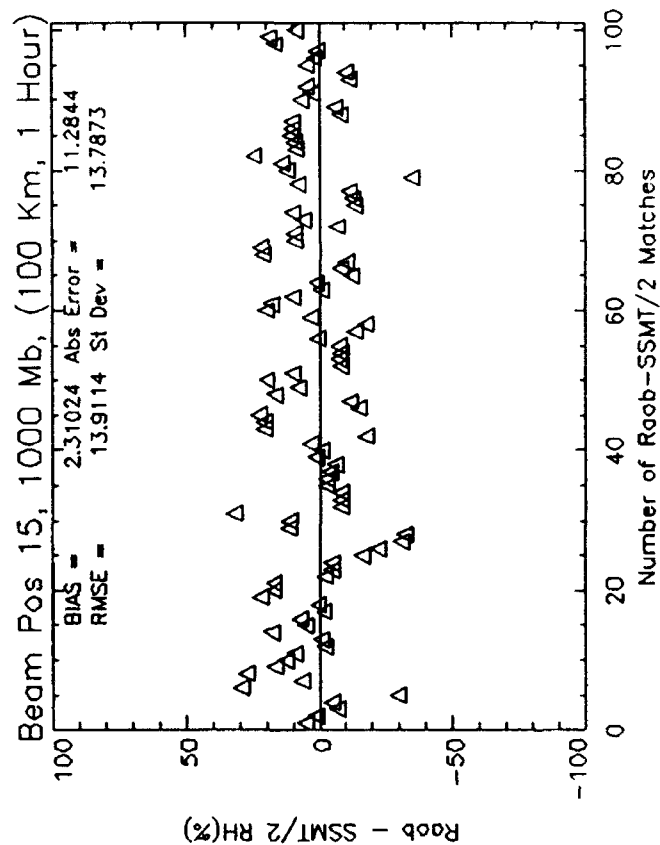
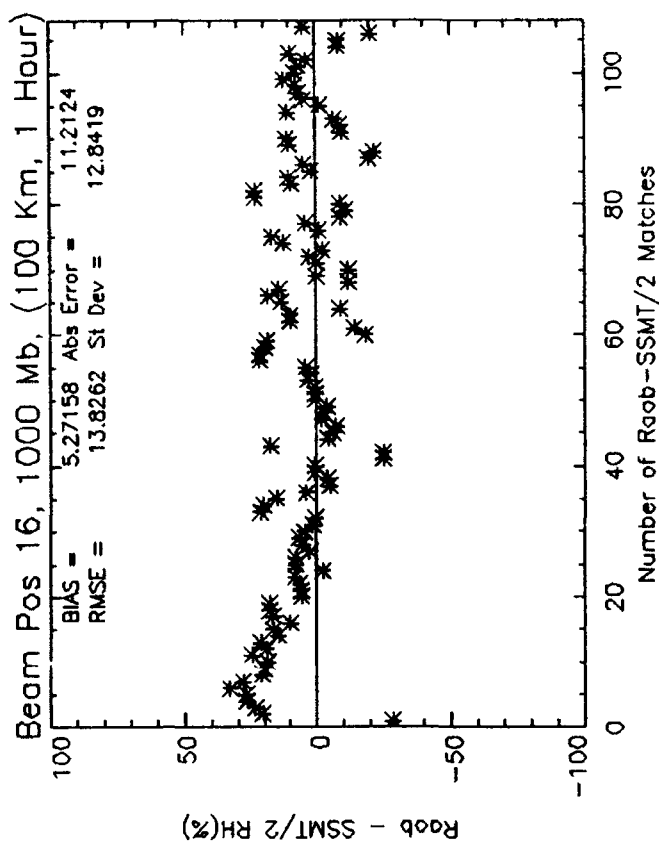


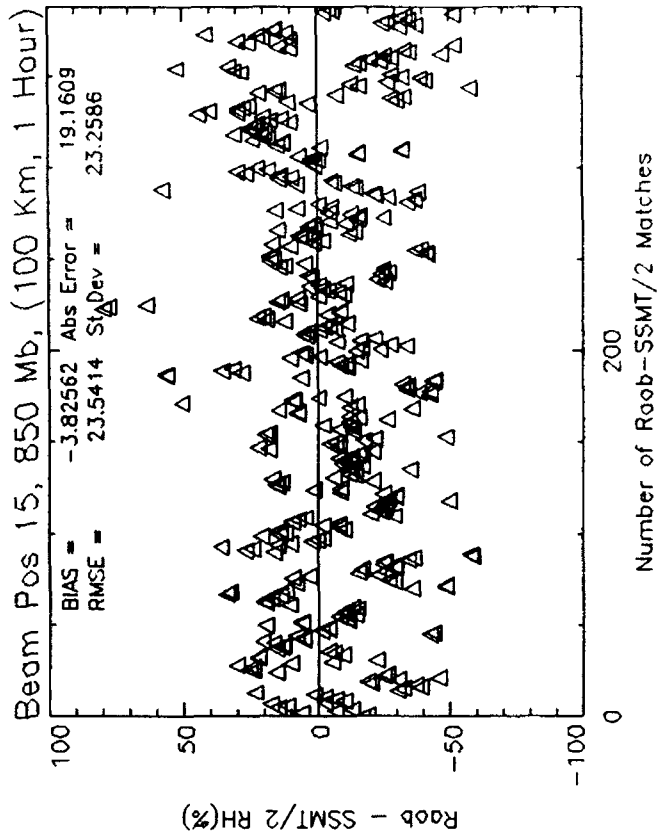
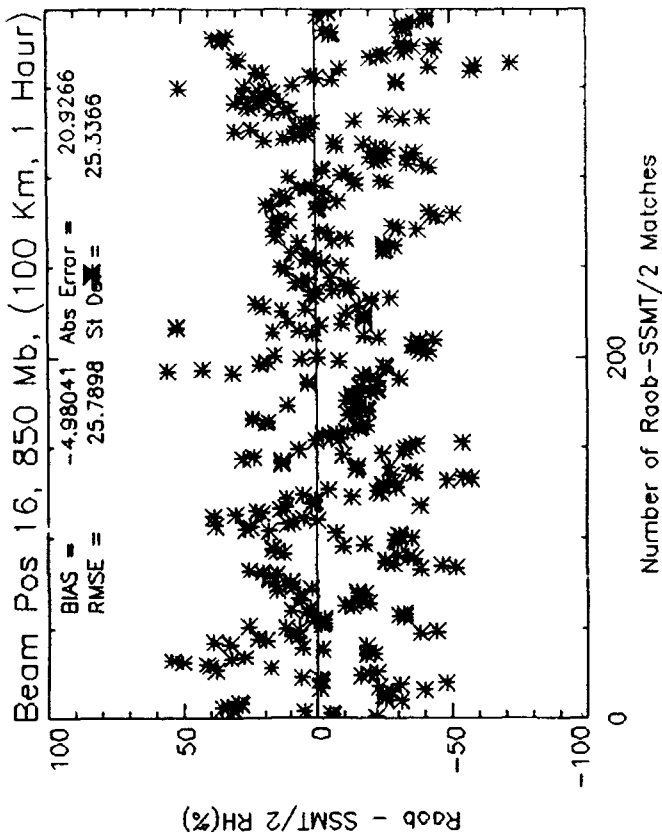
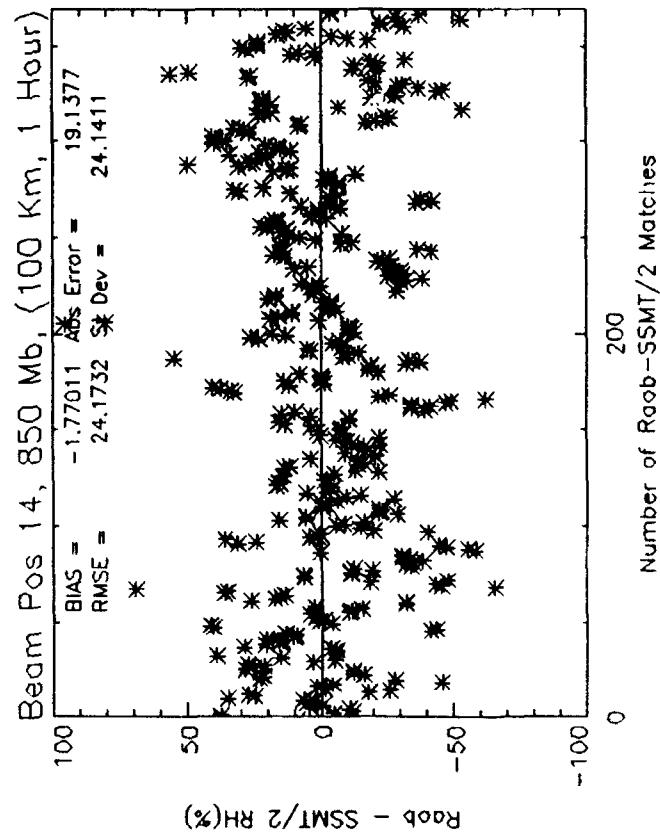
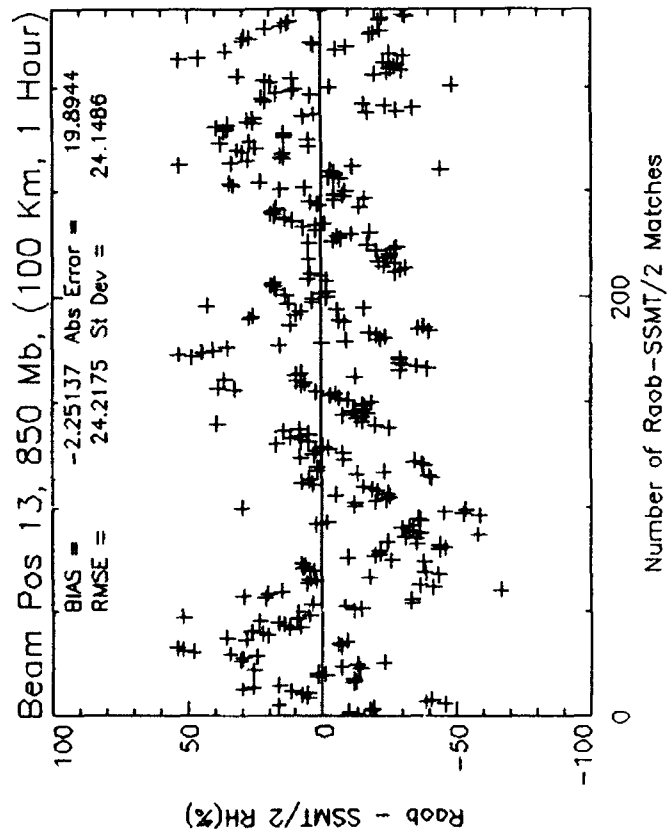


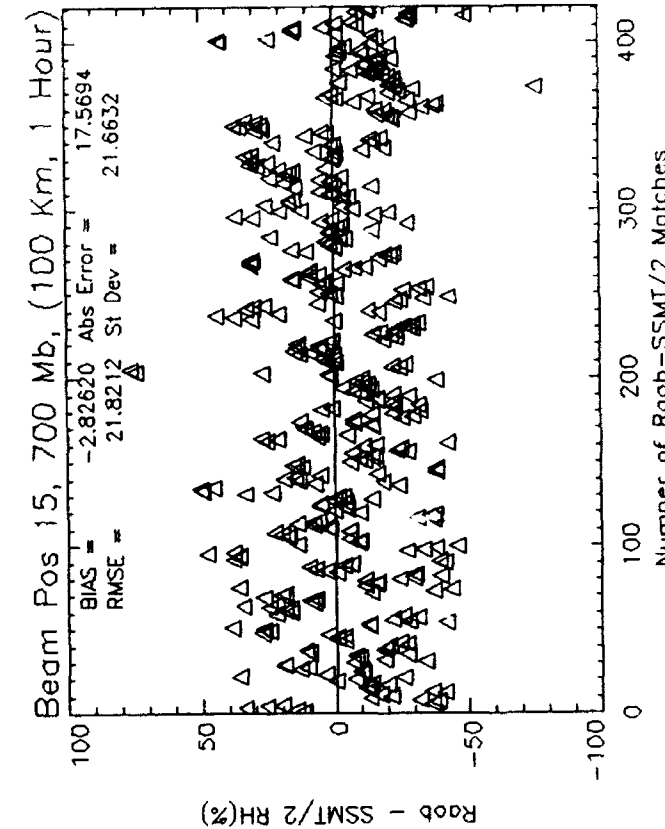
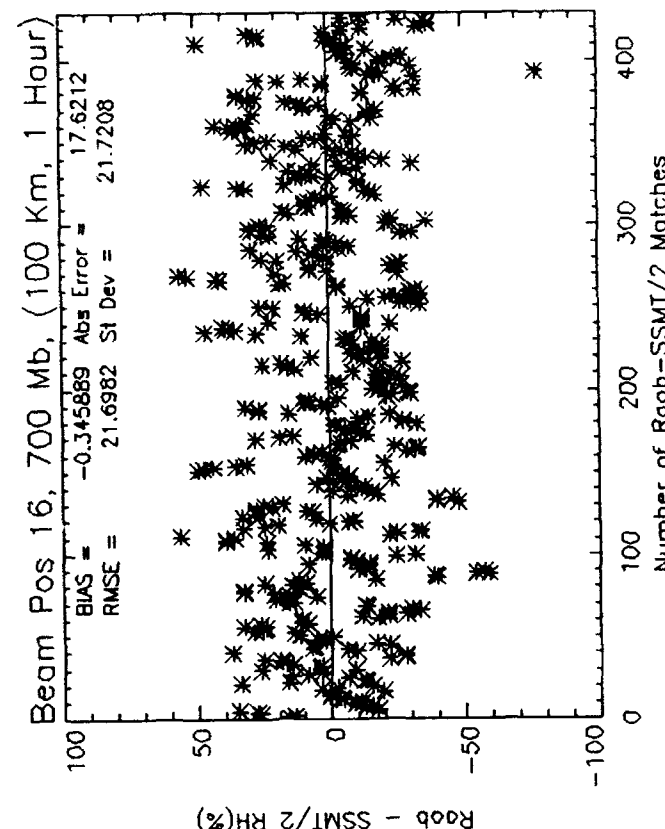
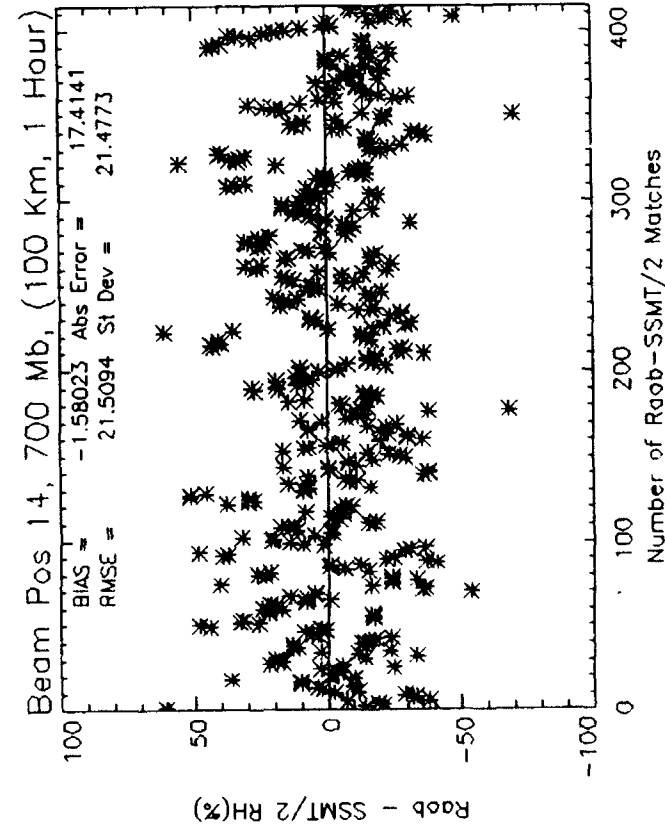
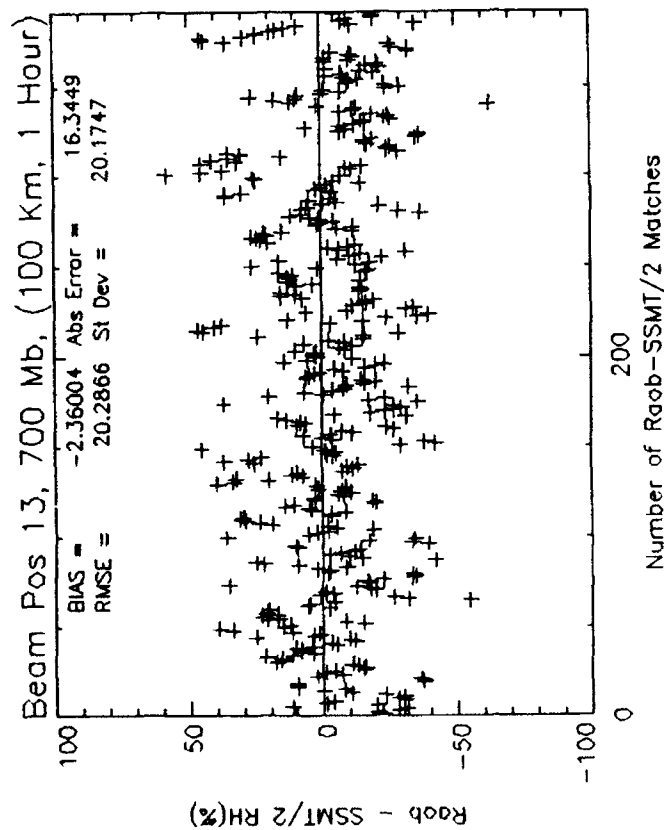


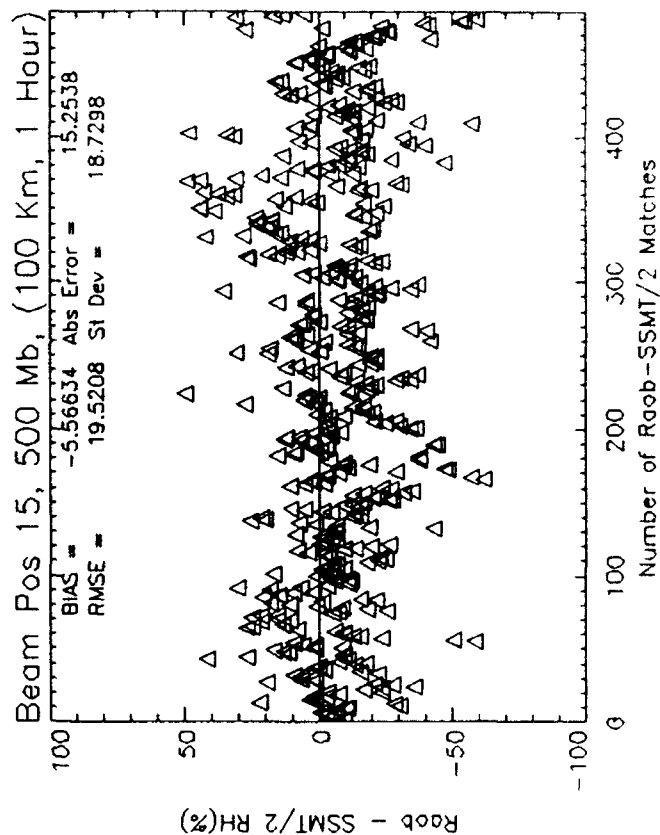
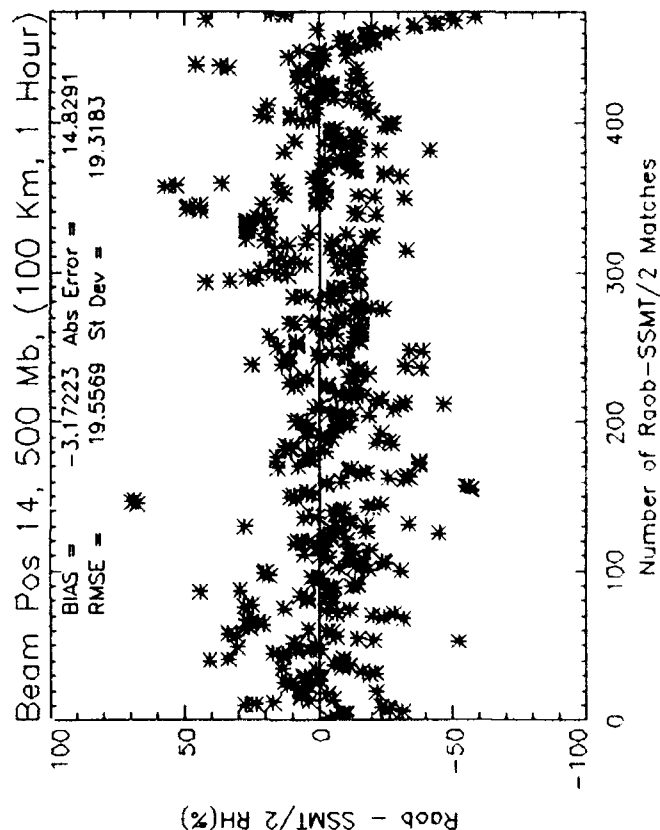
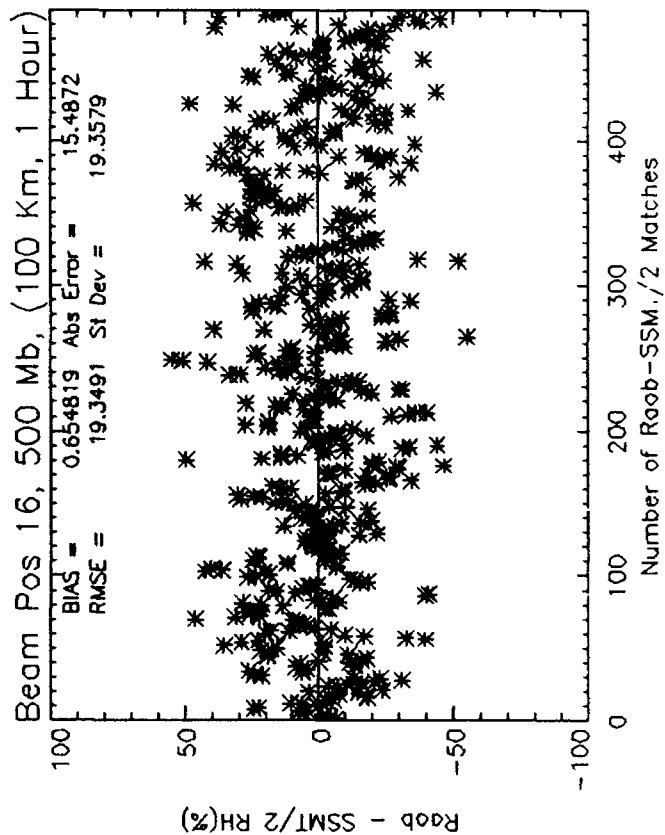
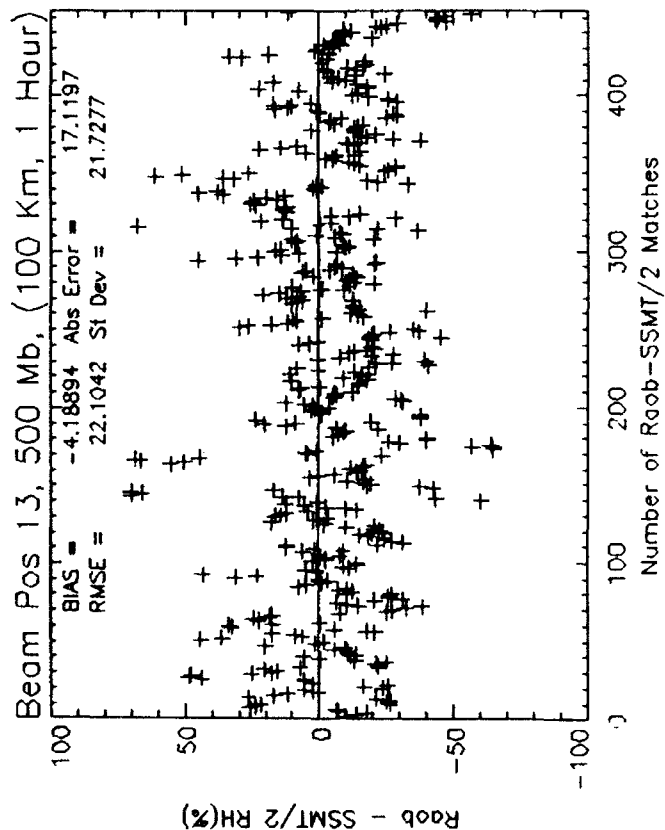


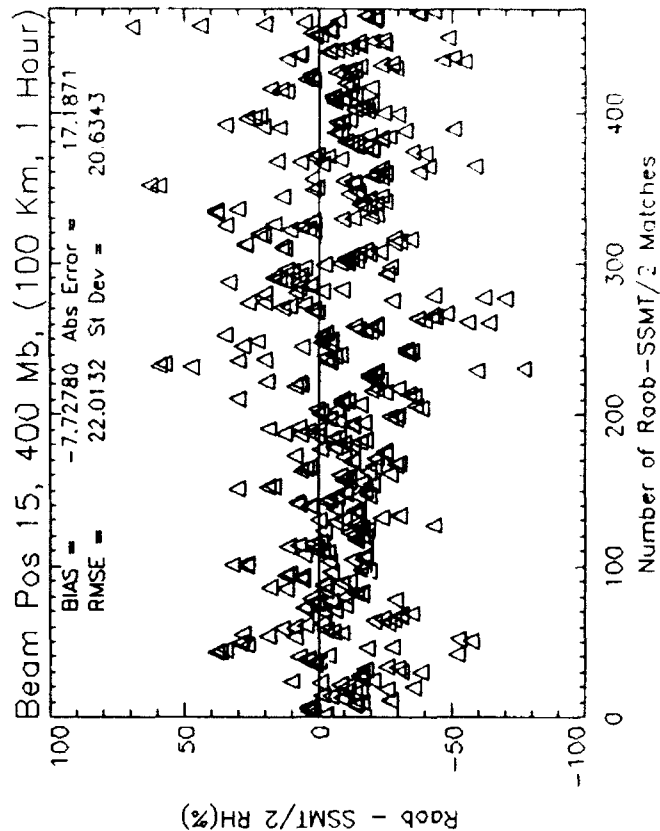
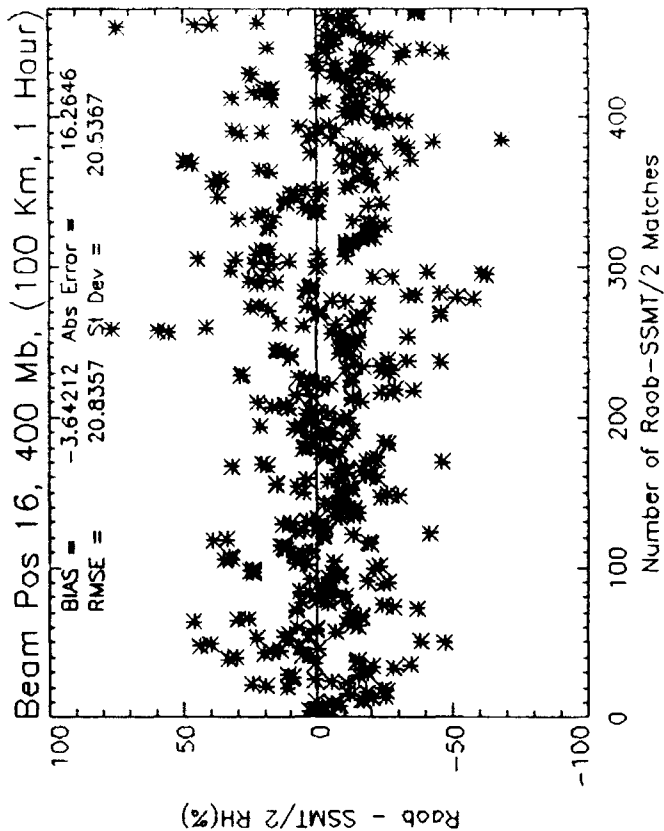
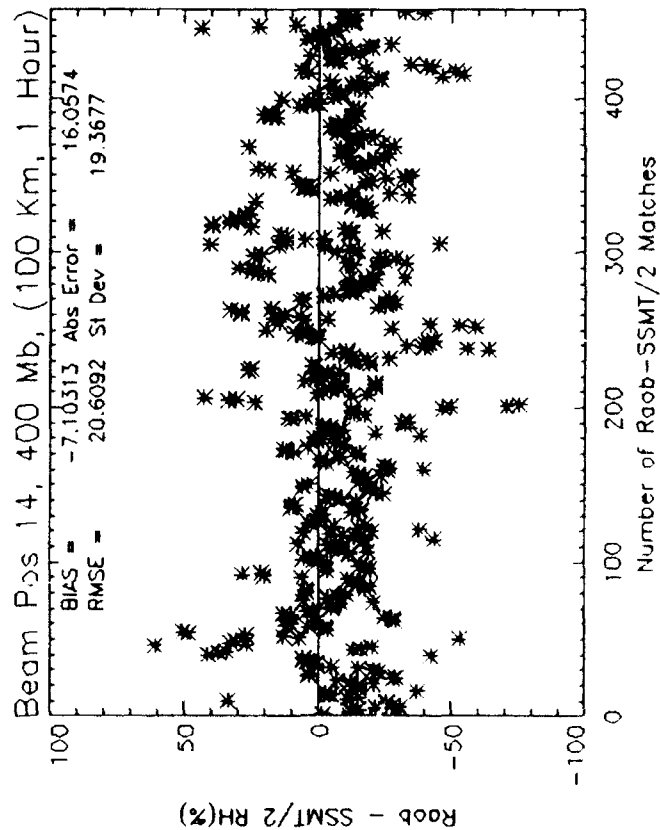
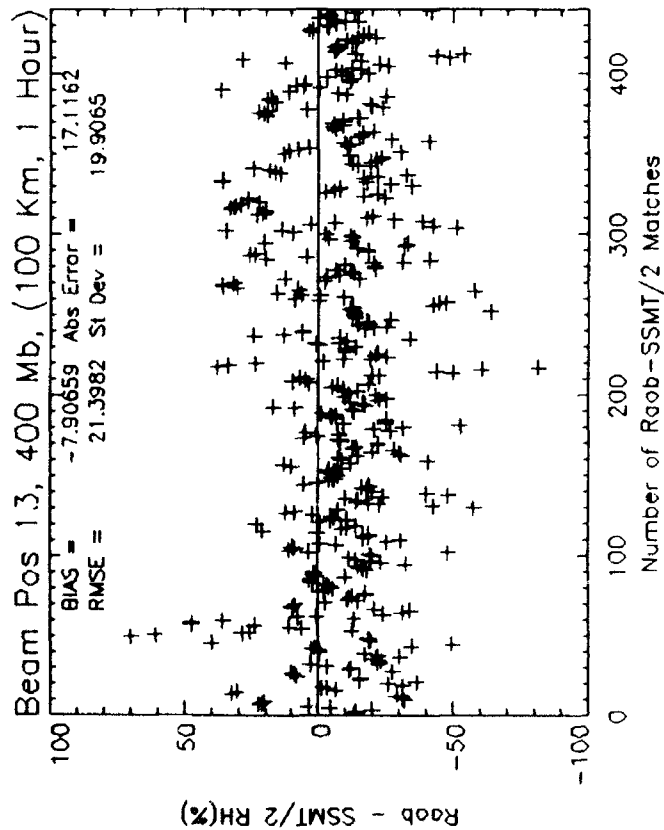


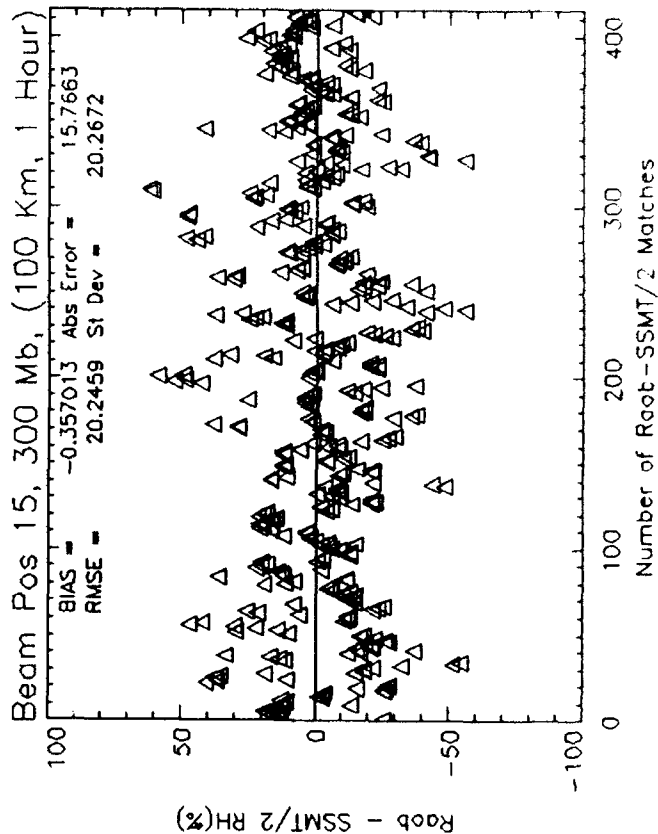
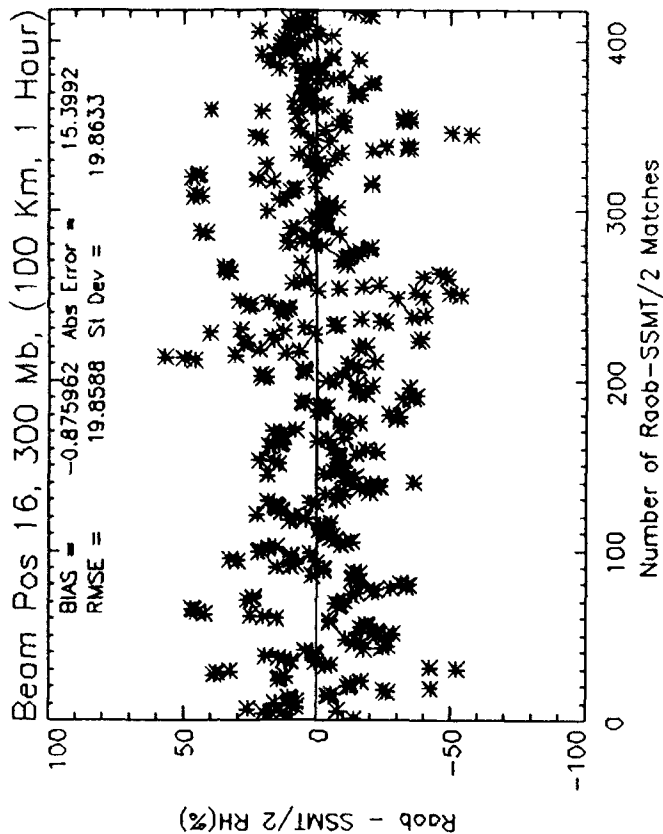
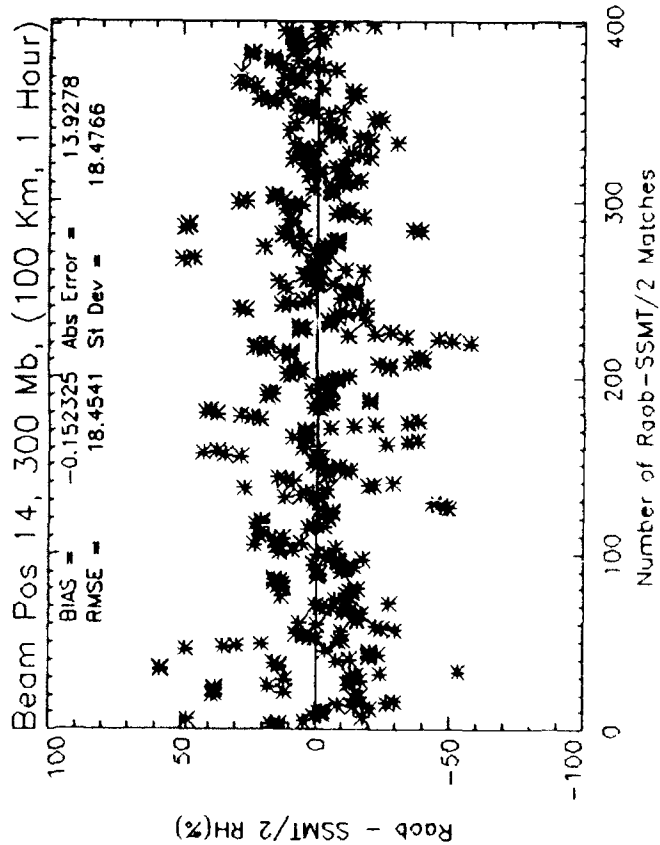
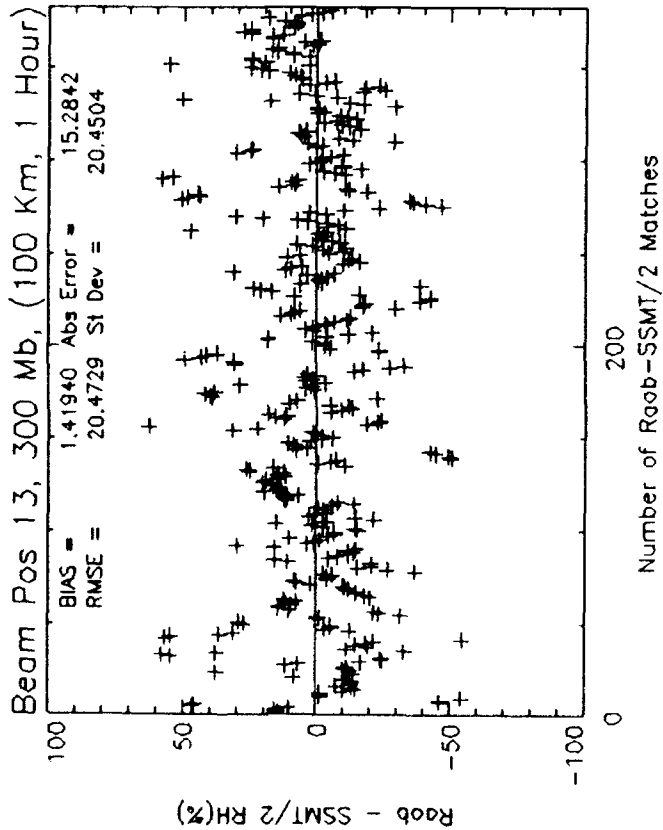


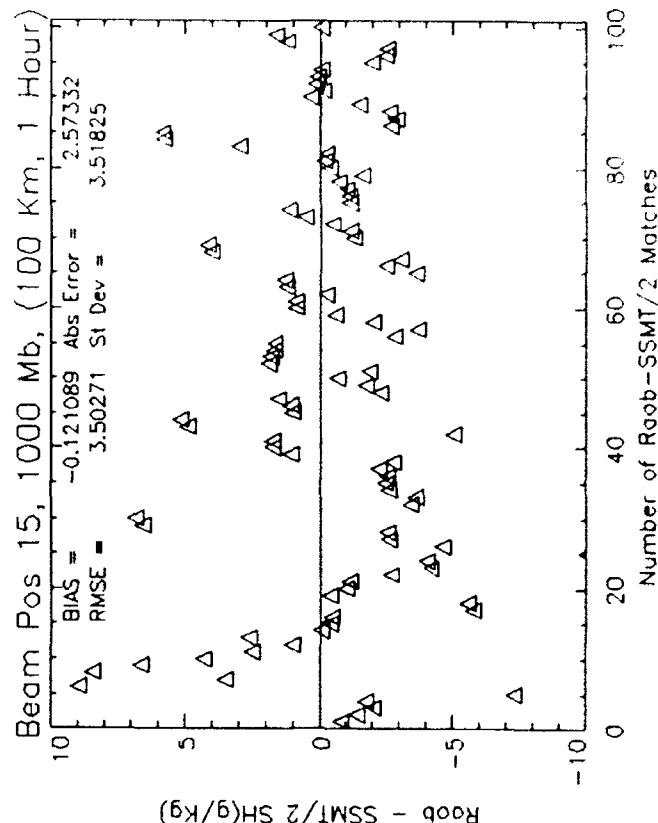
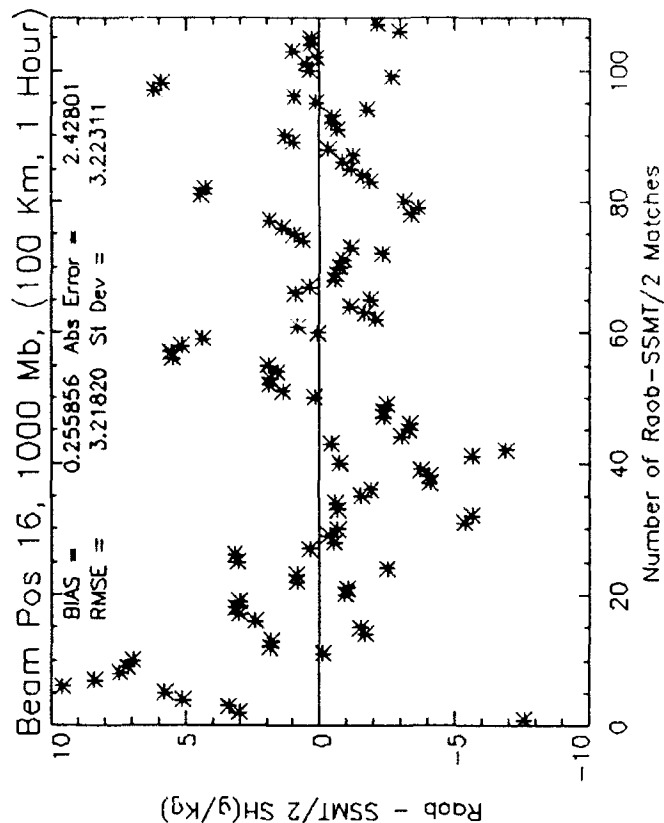
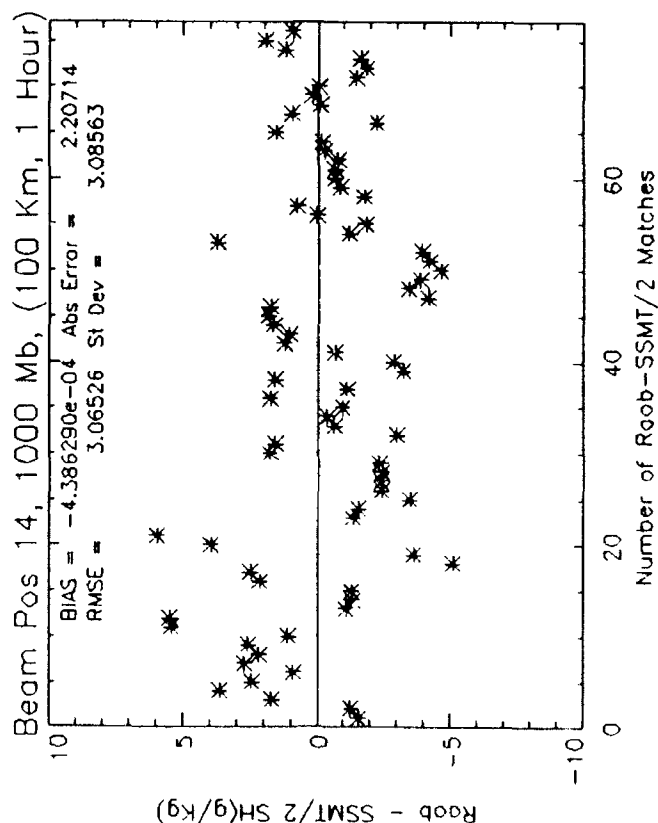
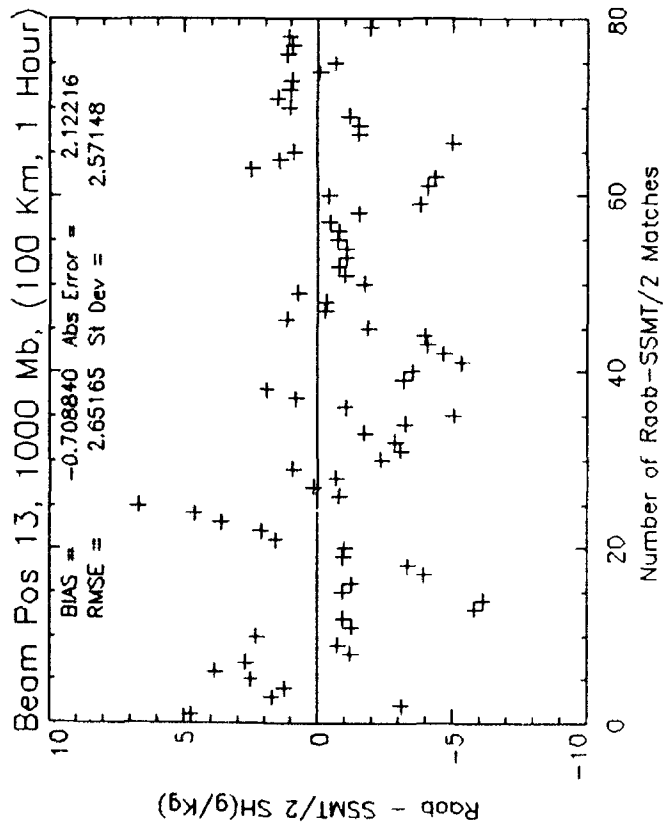


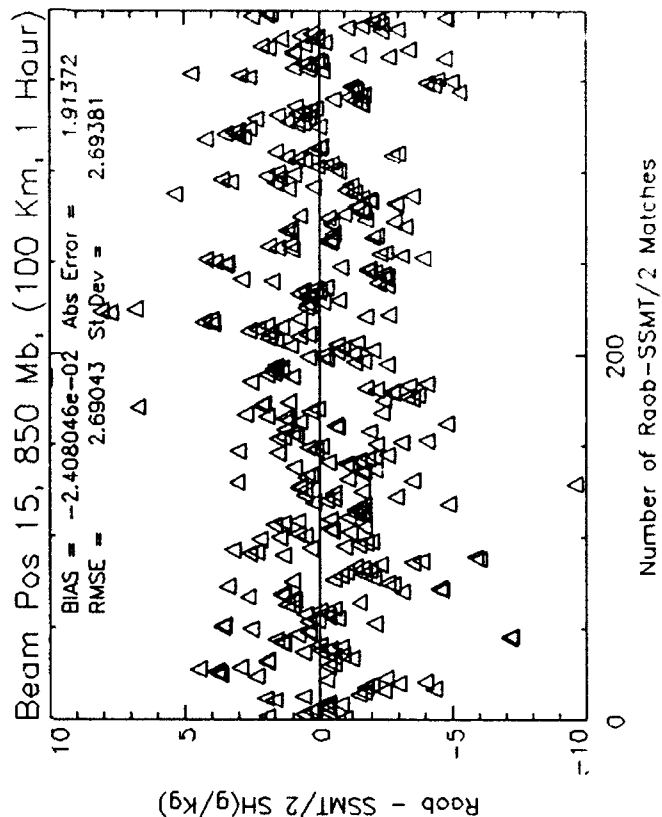
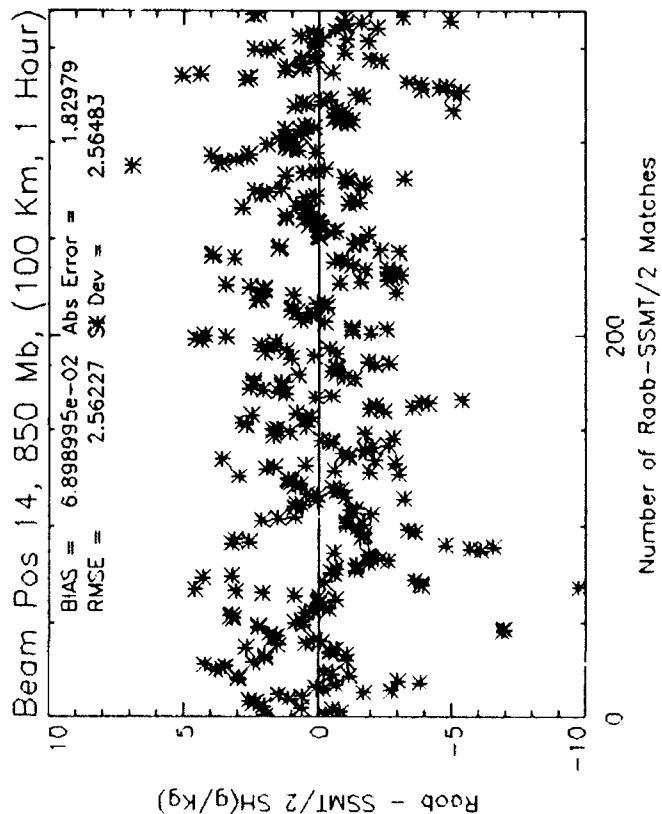
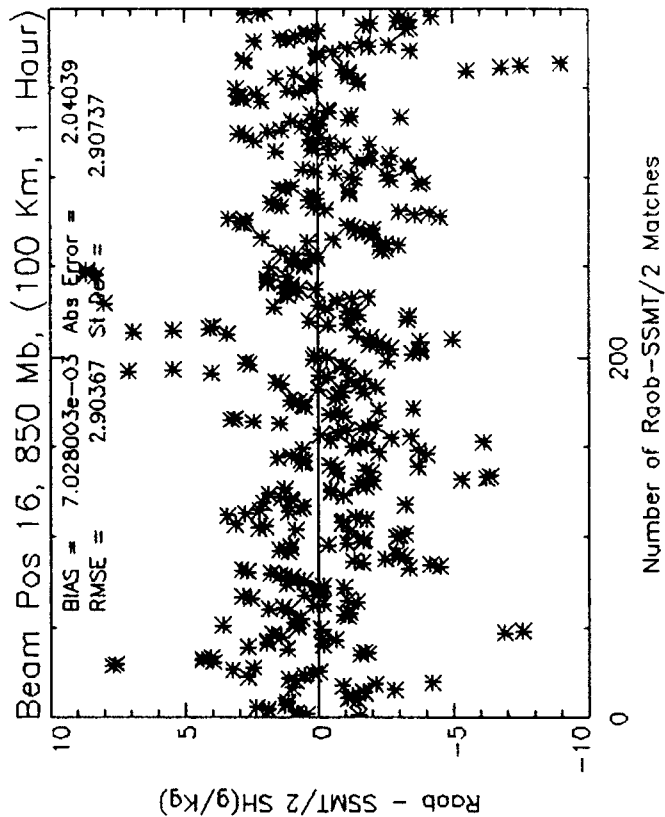
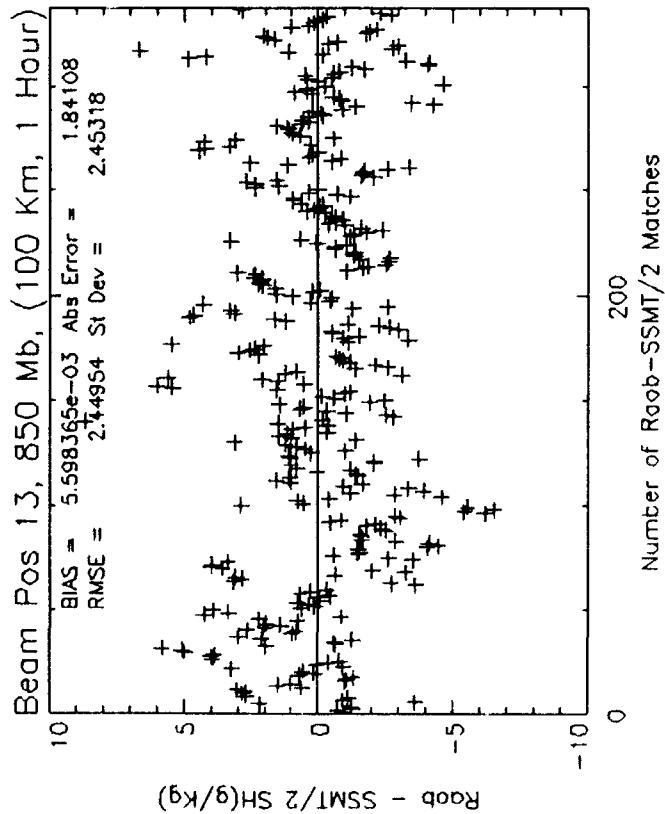




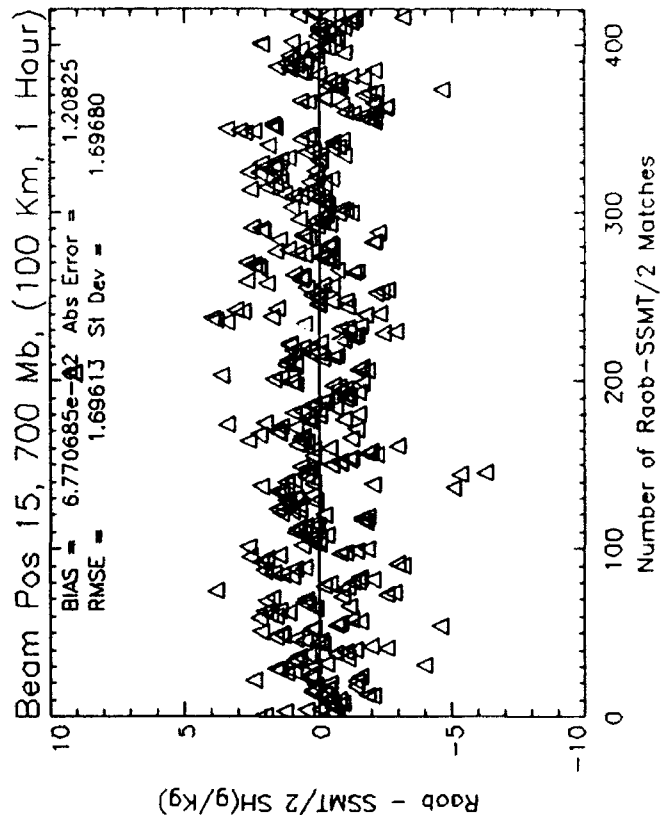
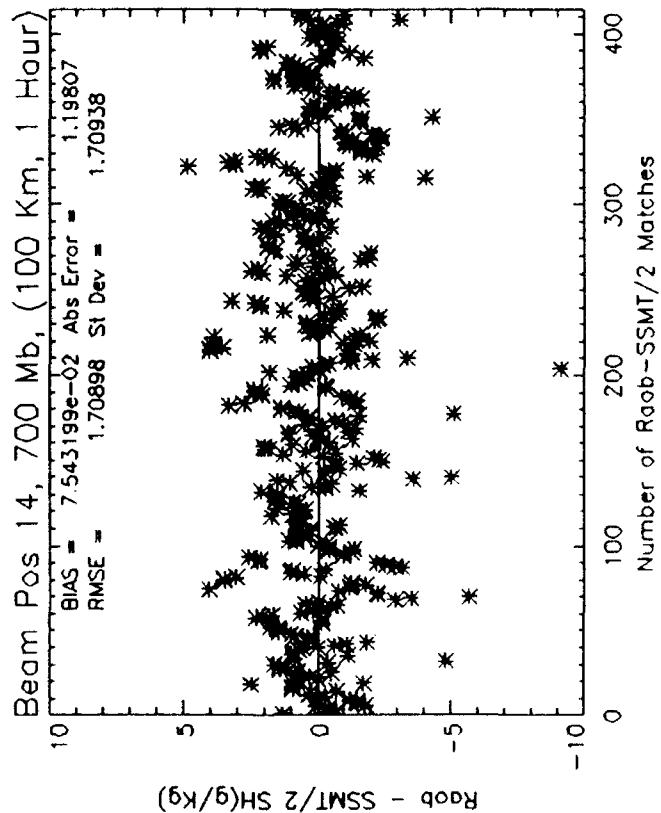
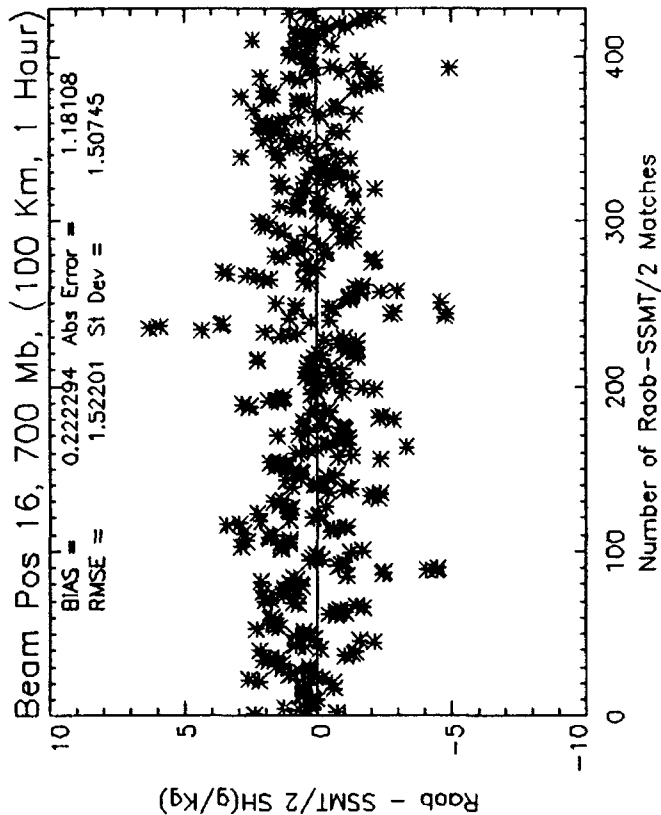
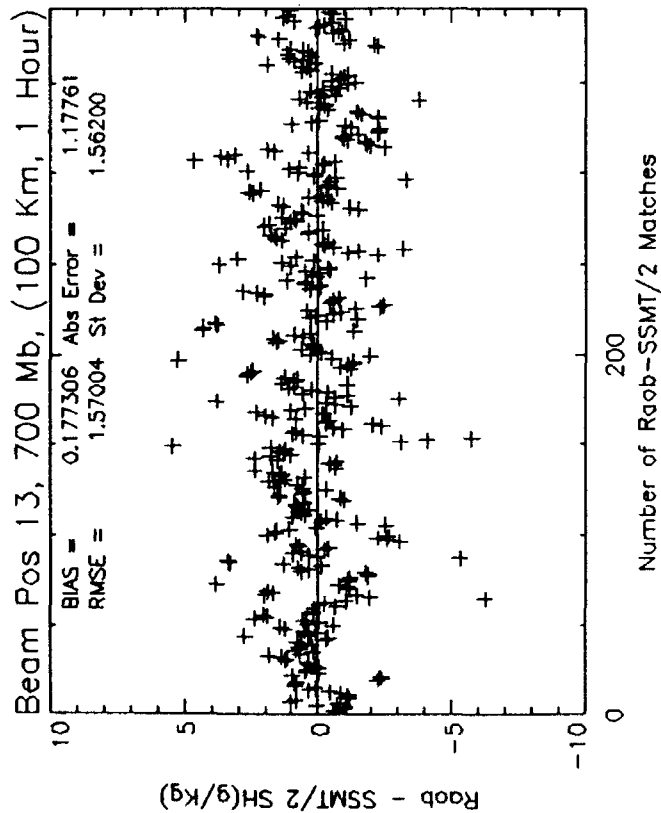


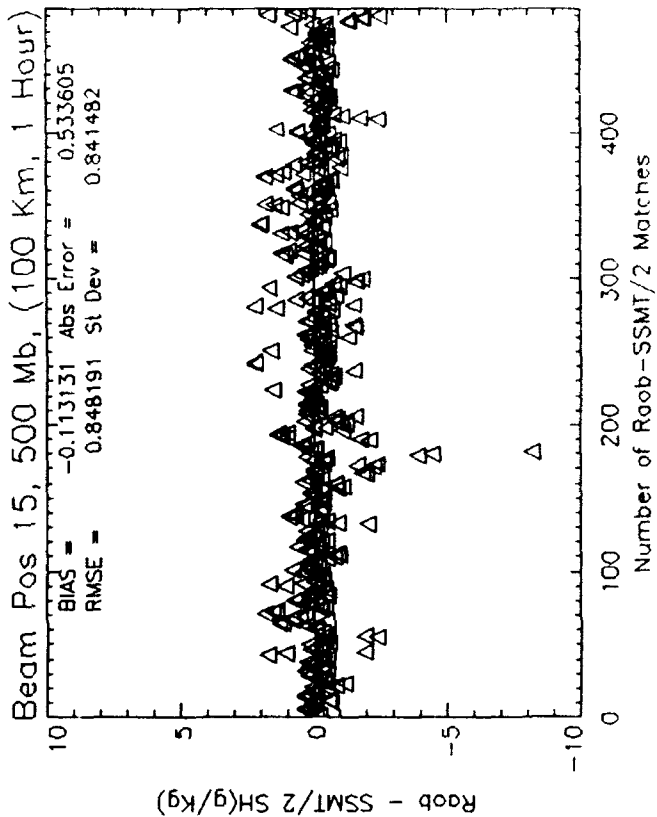
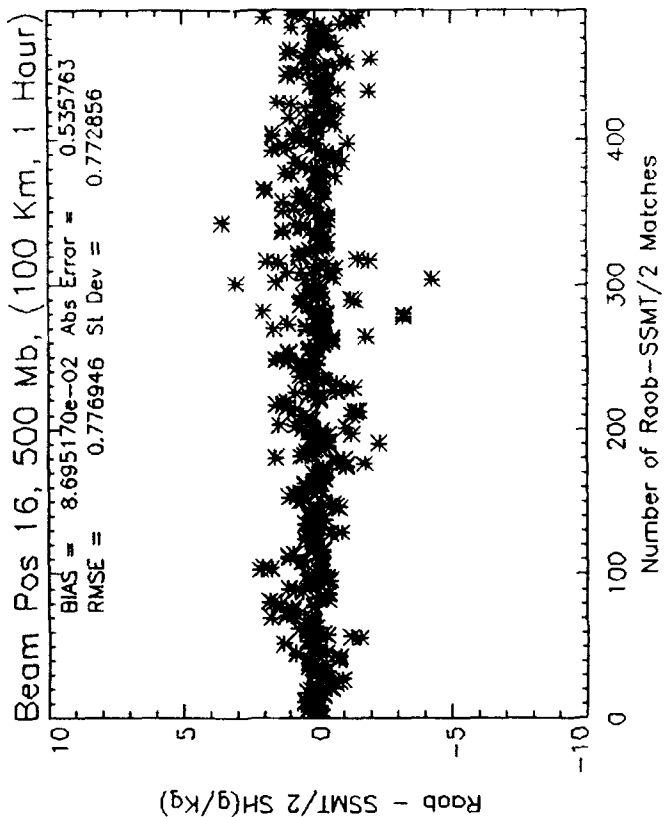
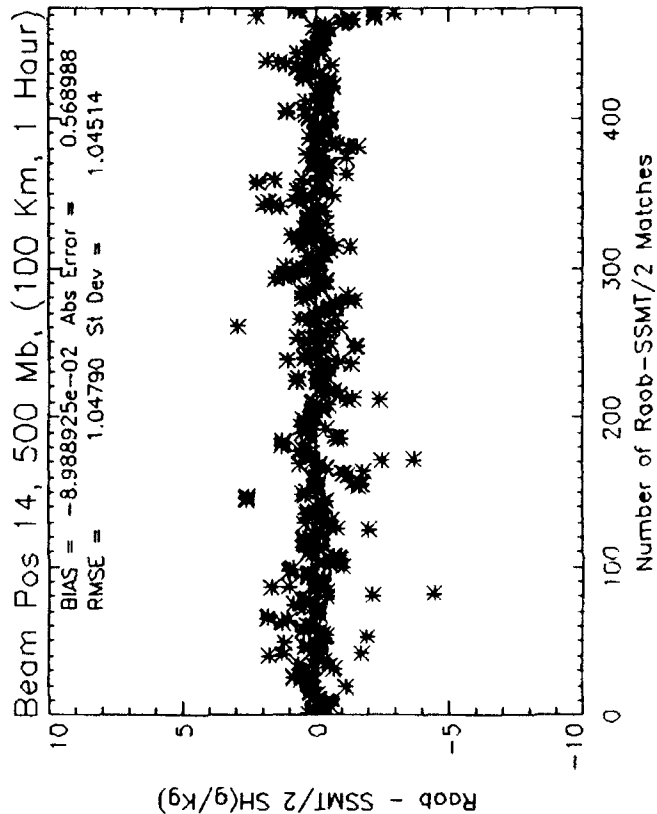
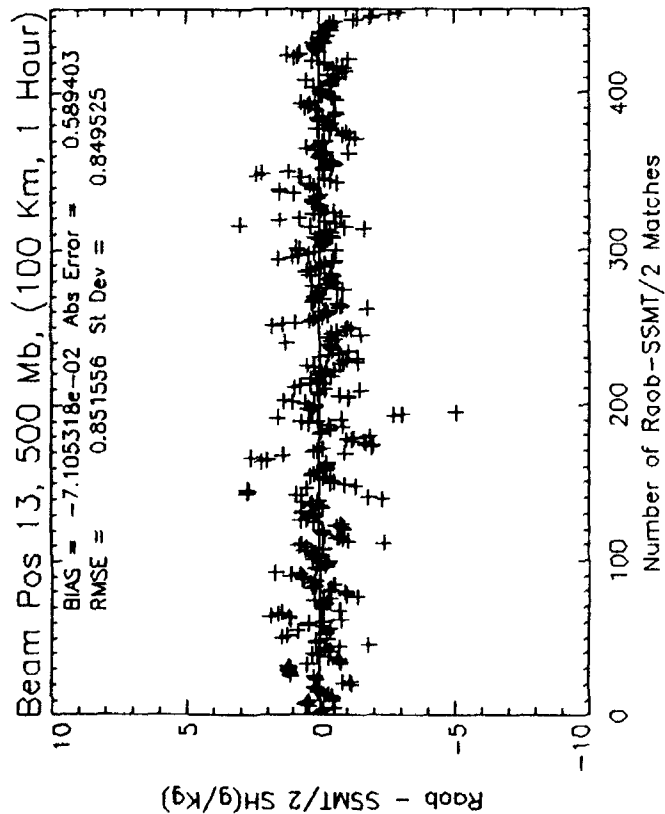


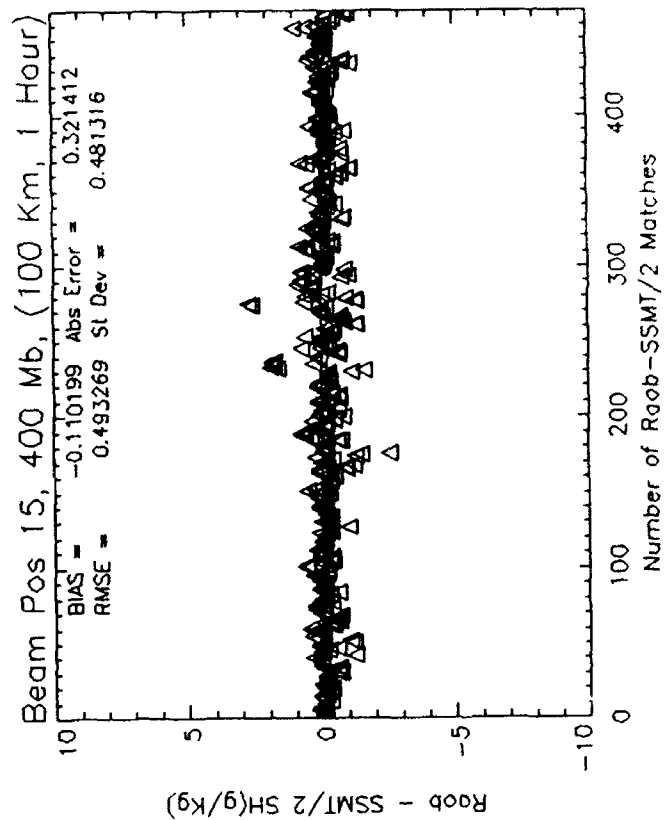
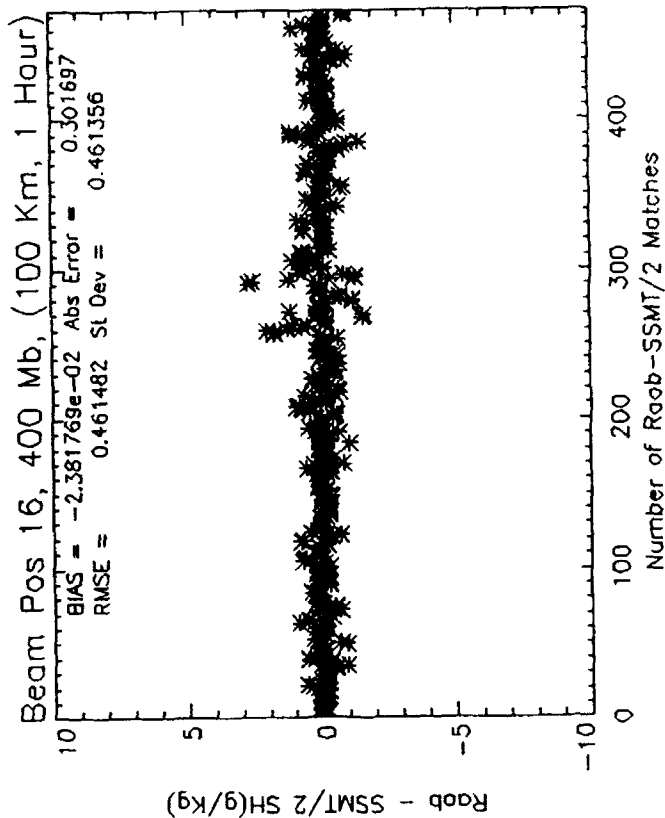
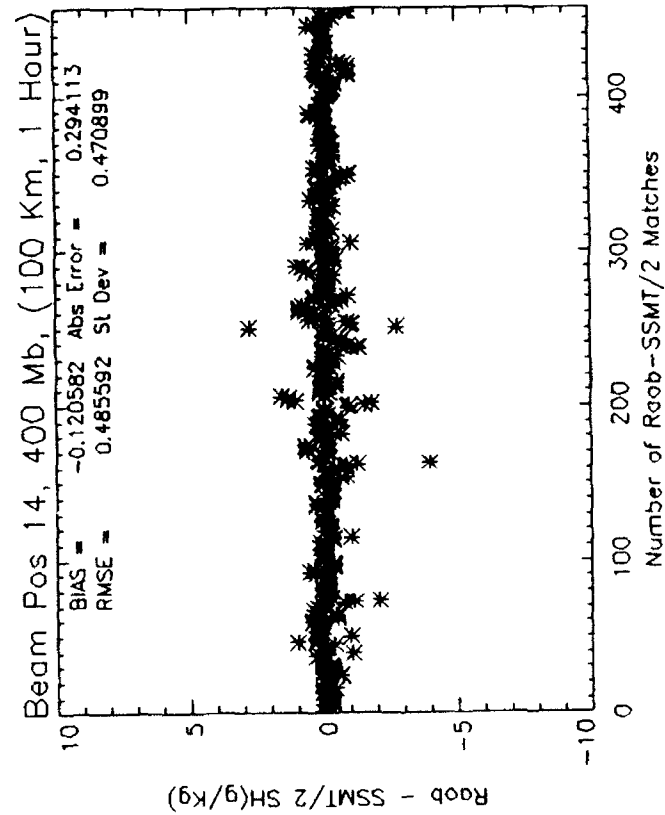
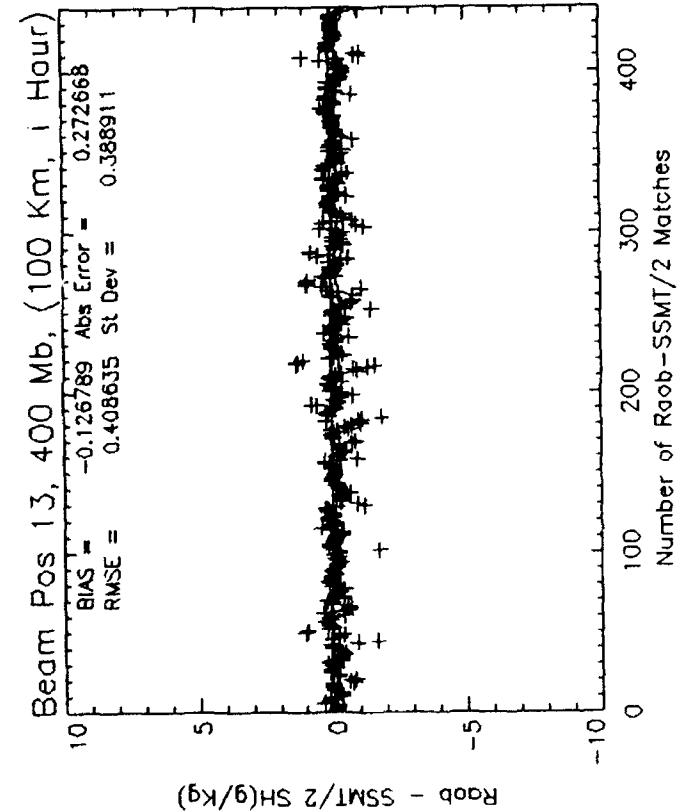


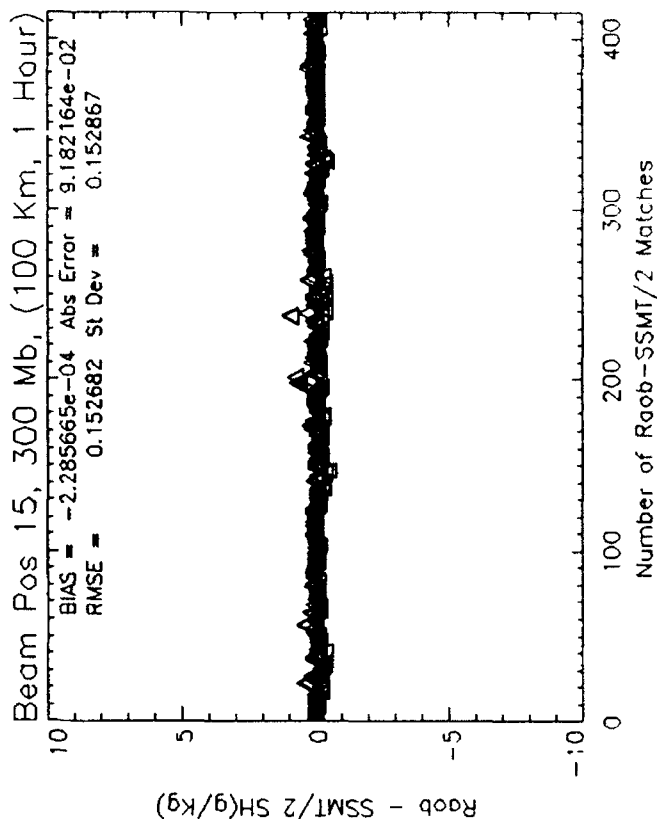
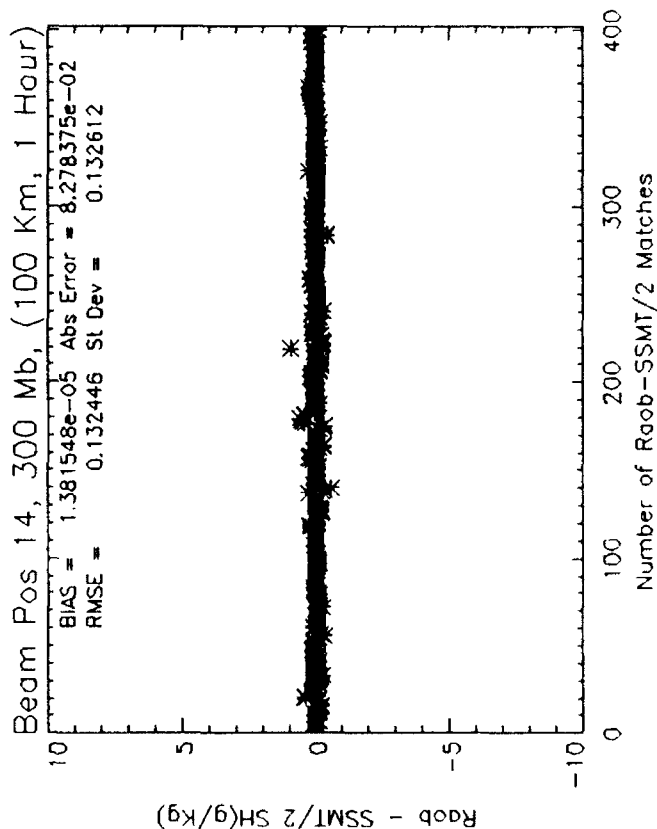
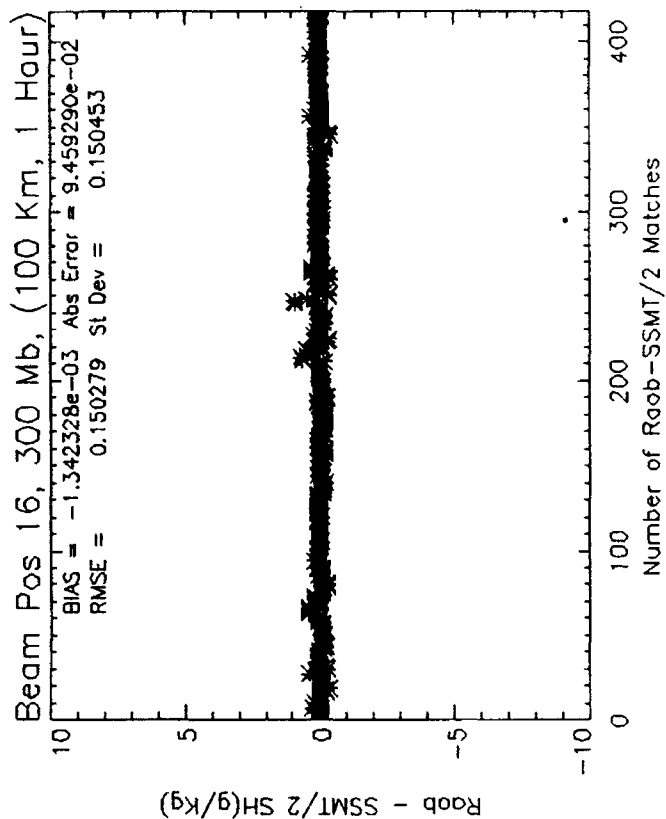
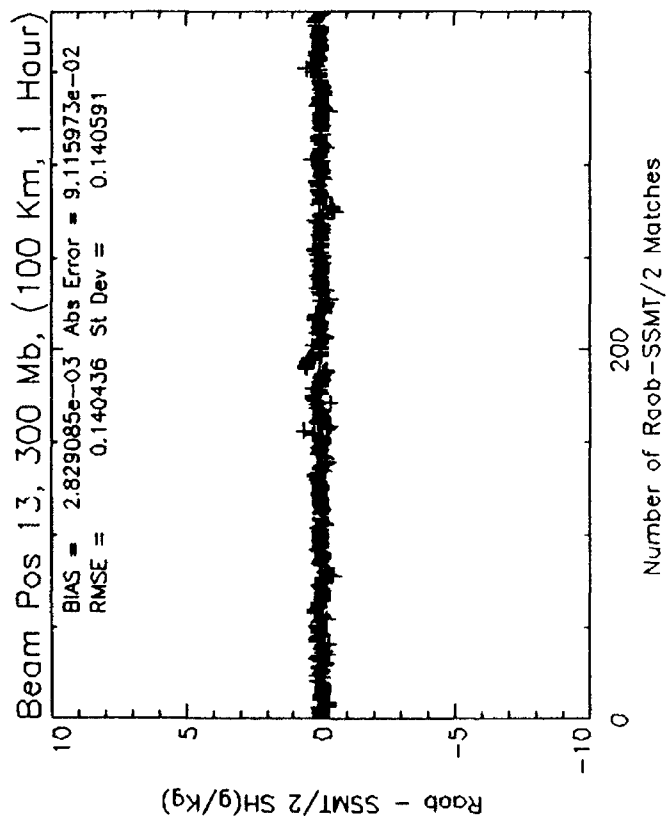




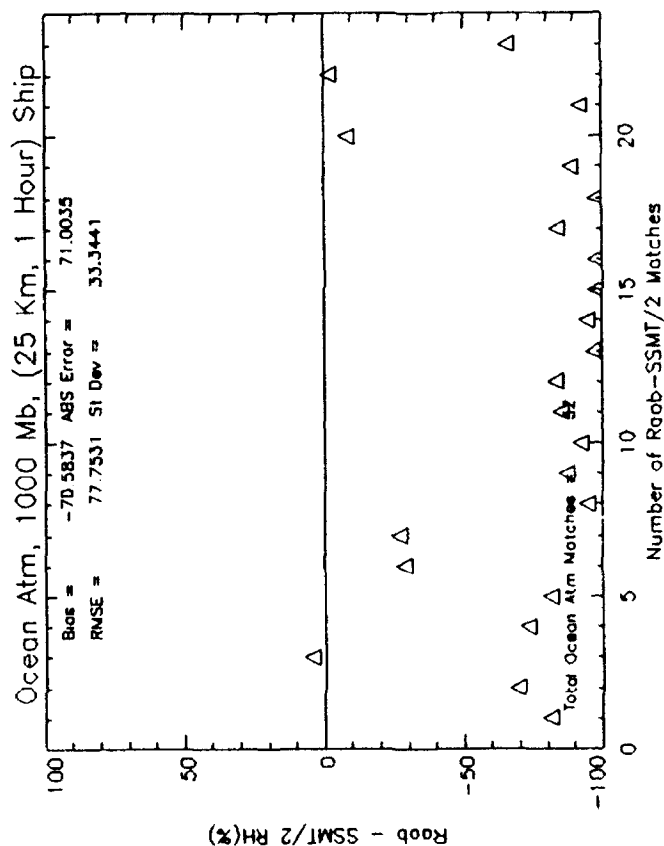
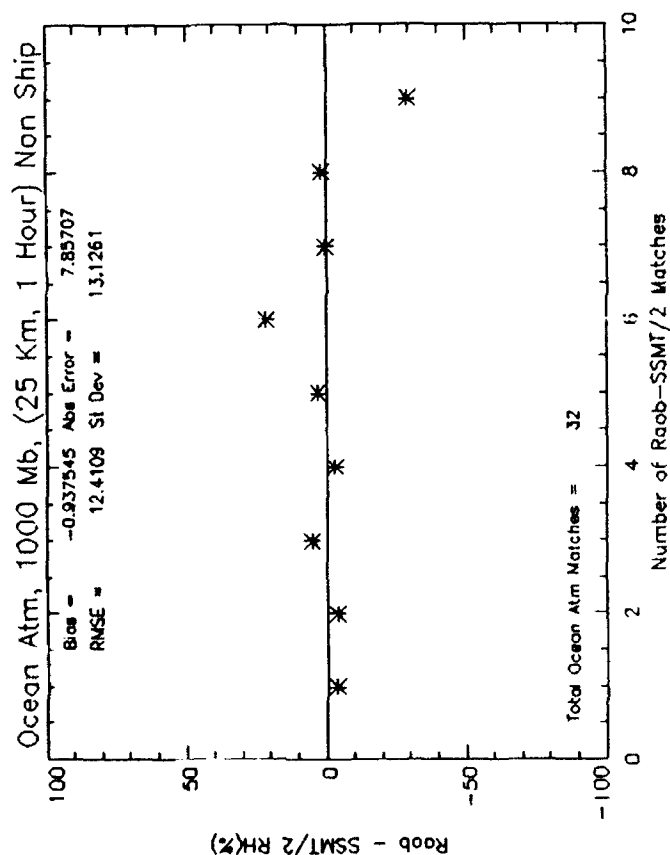
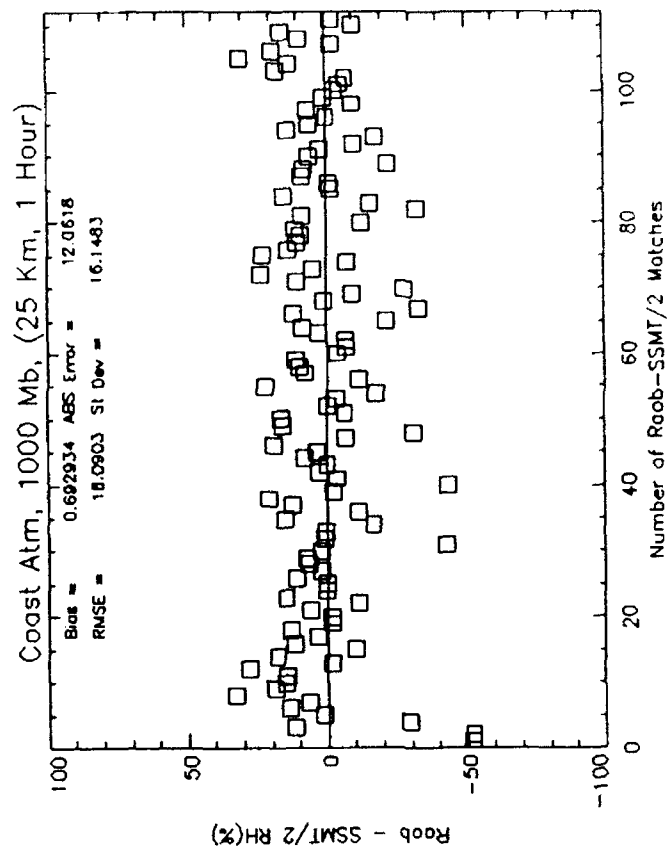
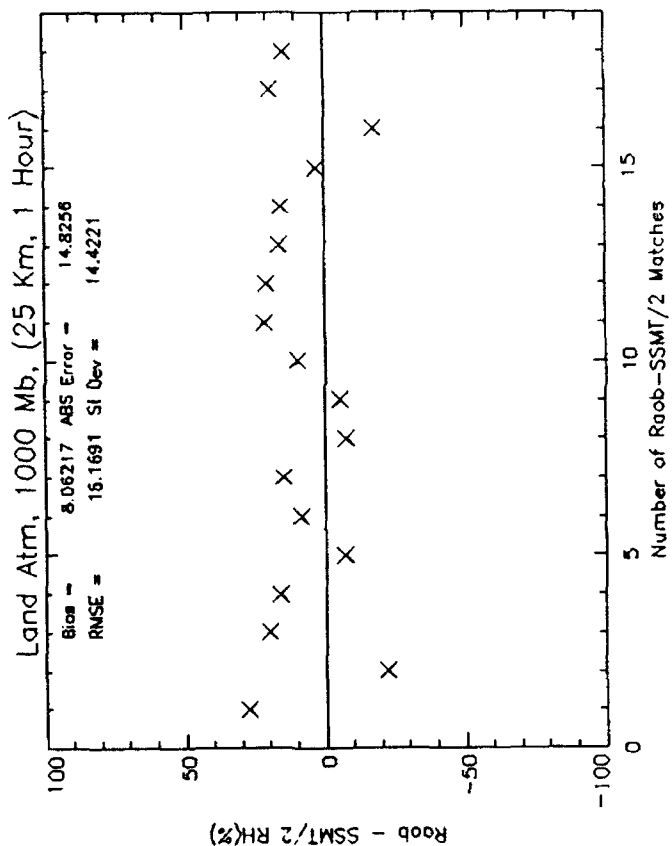


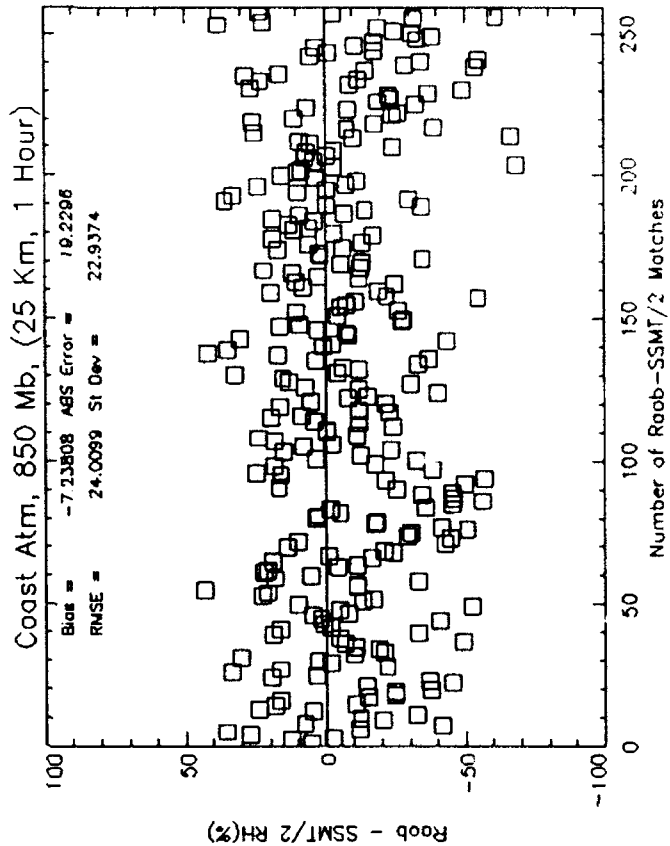
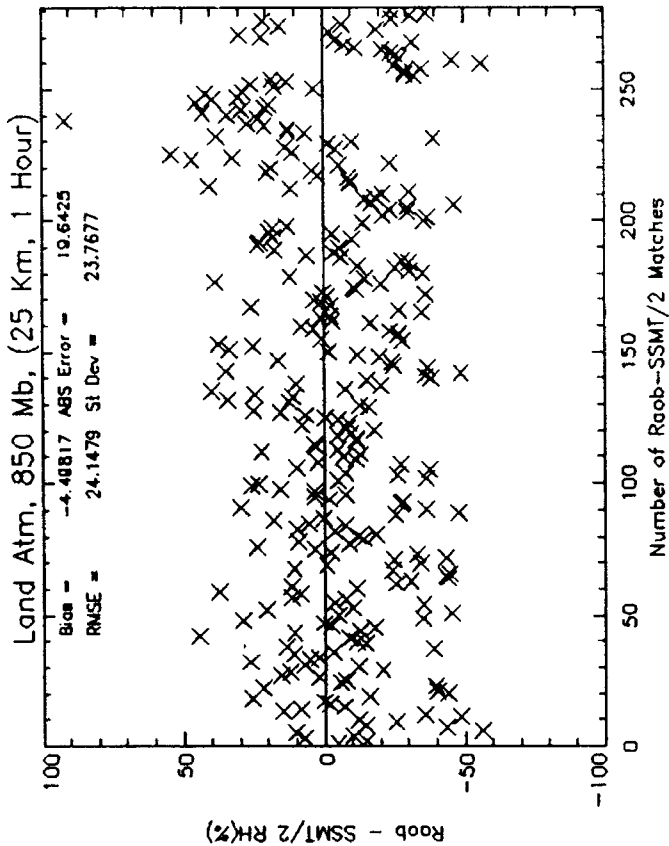
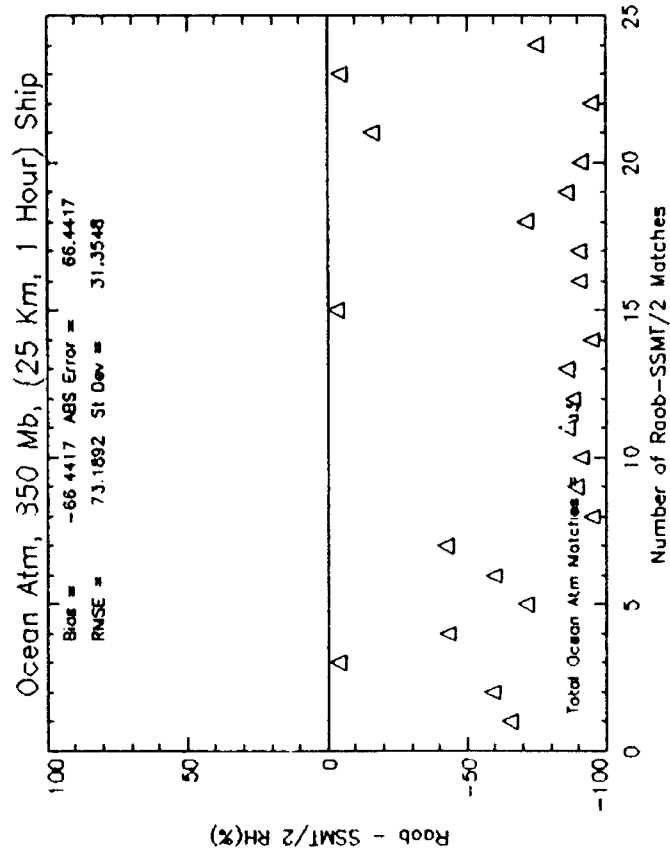
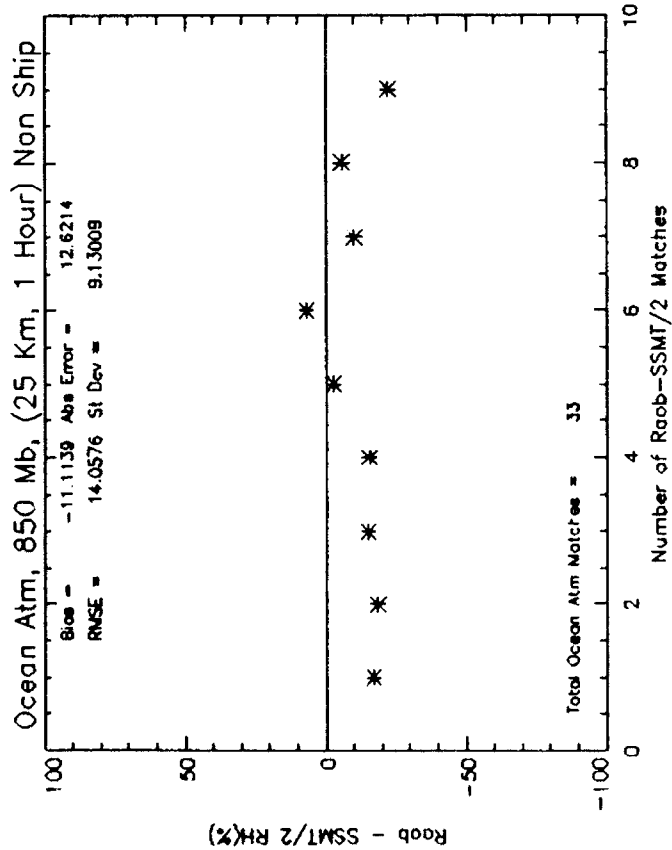


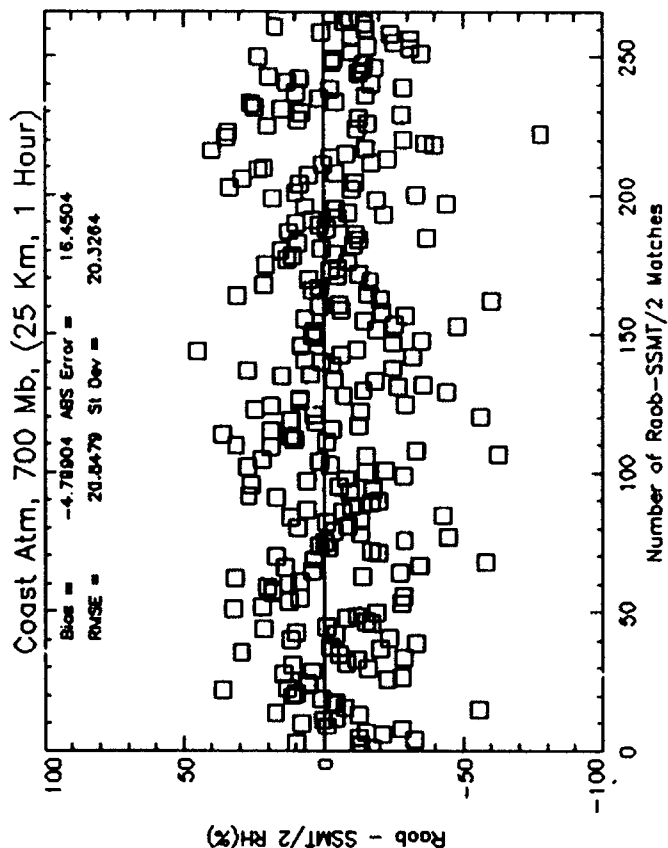
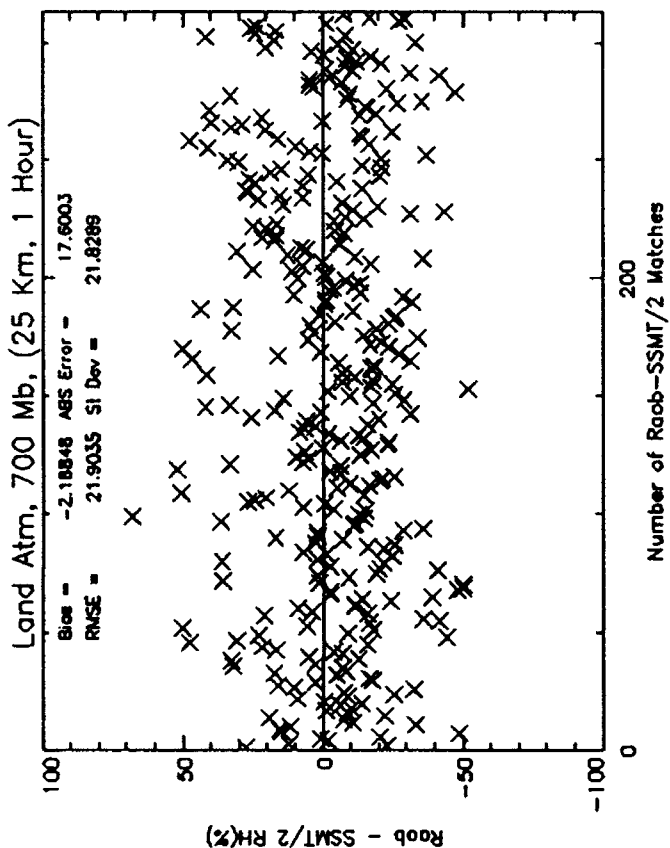
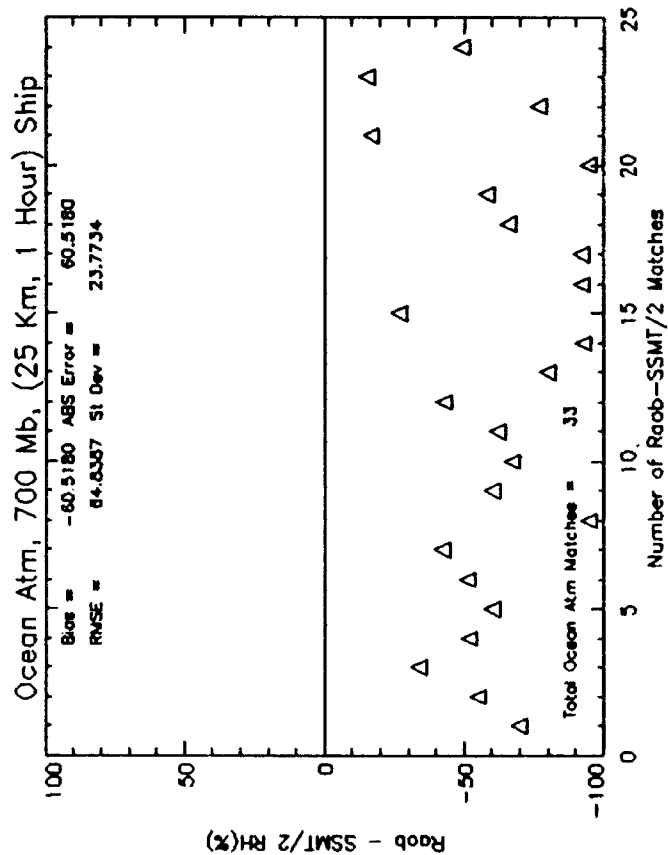
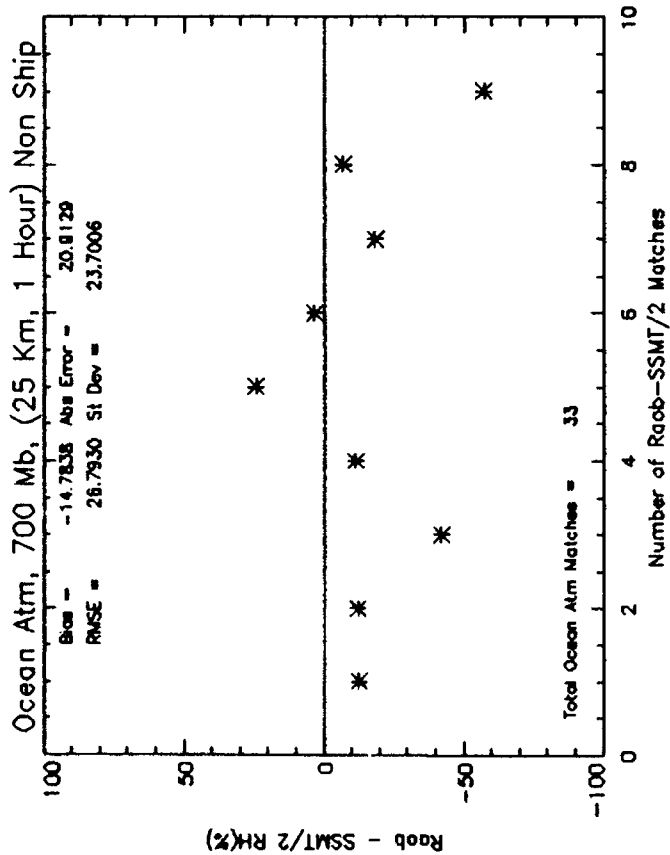




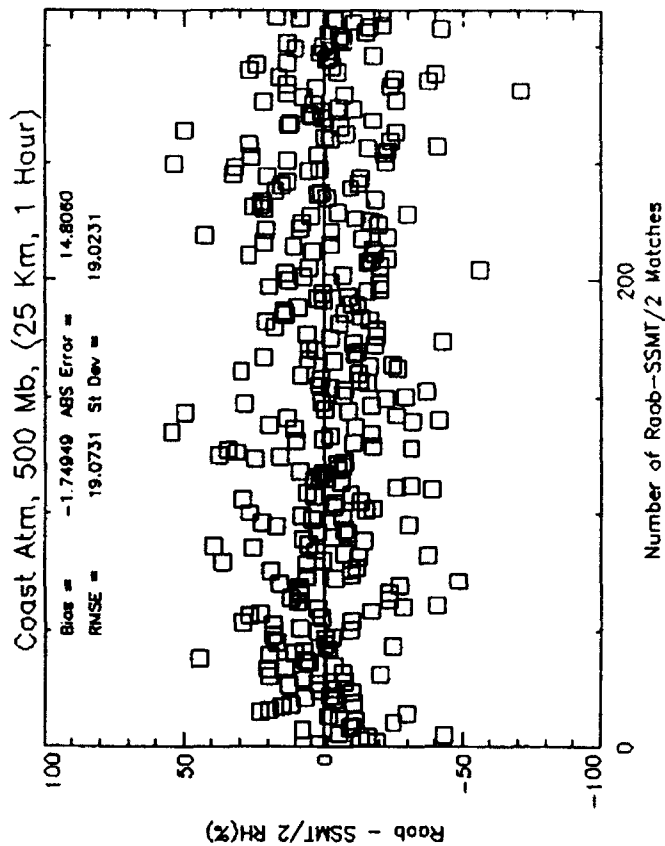
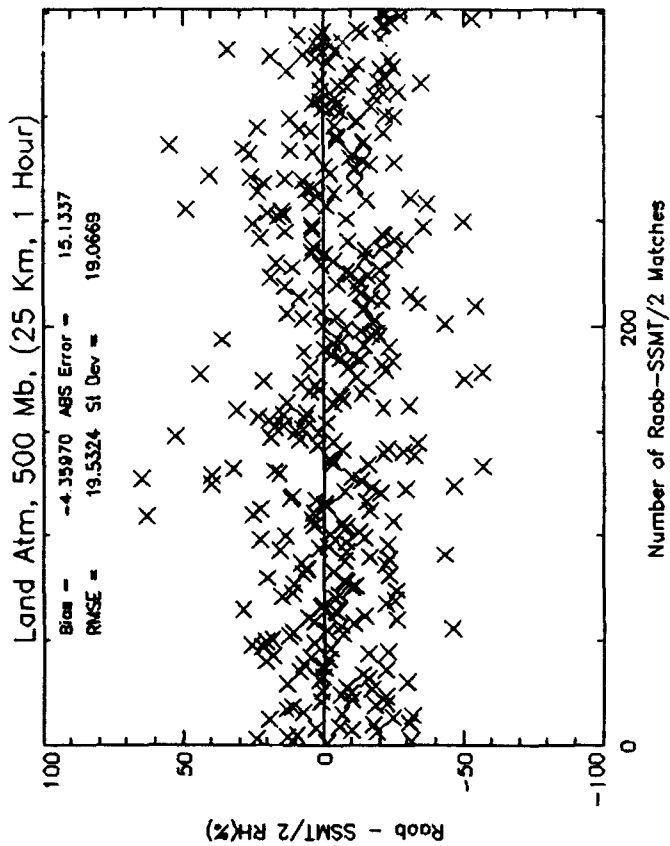
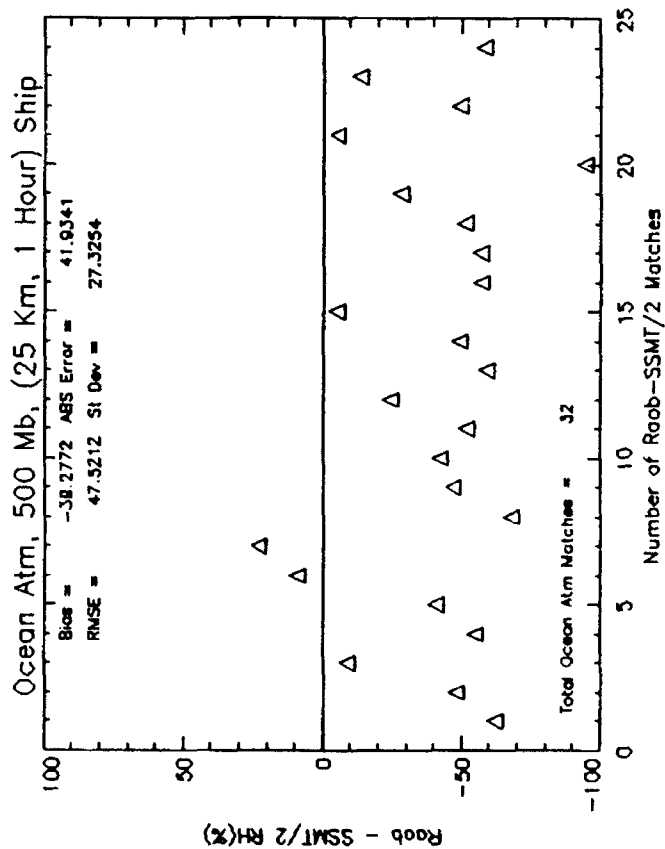
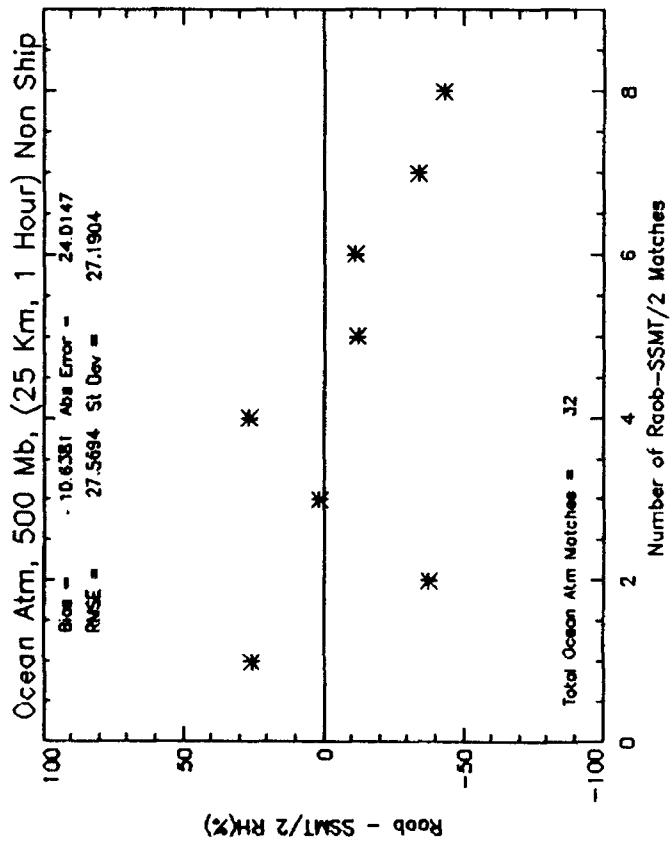
Appendix I. For variable spatial co-location criteria, land and ship observations are plotted separately with the quantity (Radiosonde - SSM/T-2) RH and Q plotted on the ordinate, and the index of the co-locations on the abscissa. Each four-plot panel represents one atmospheric level. In addition, the plots are stratified by atmosphere type. The co-location criteria are annotated at the top of the plots.



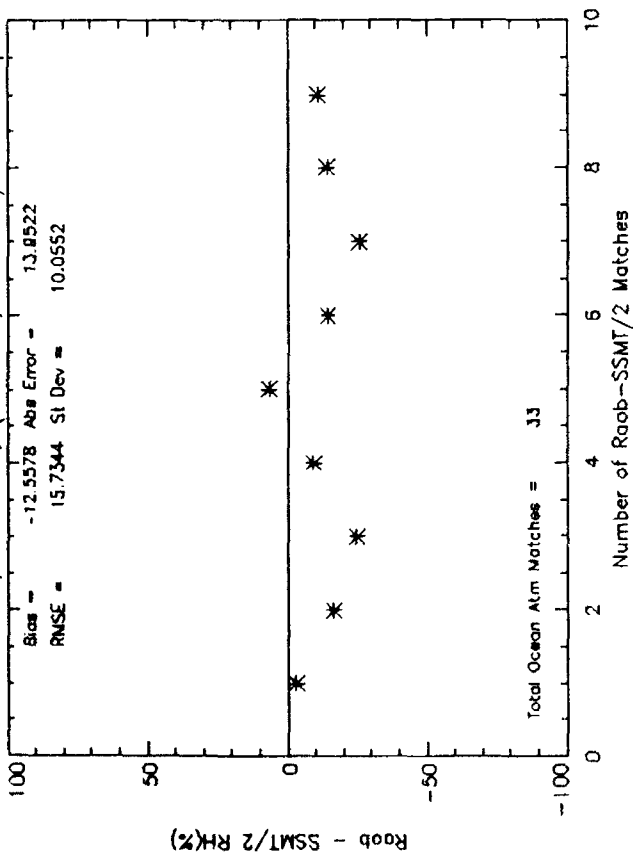




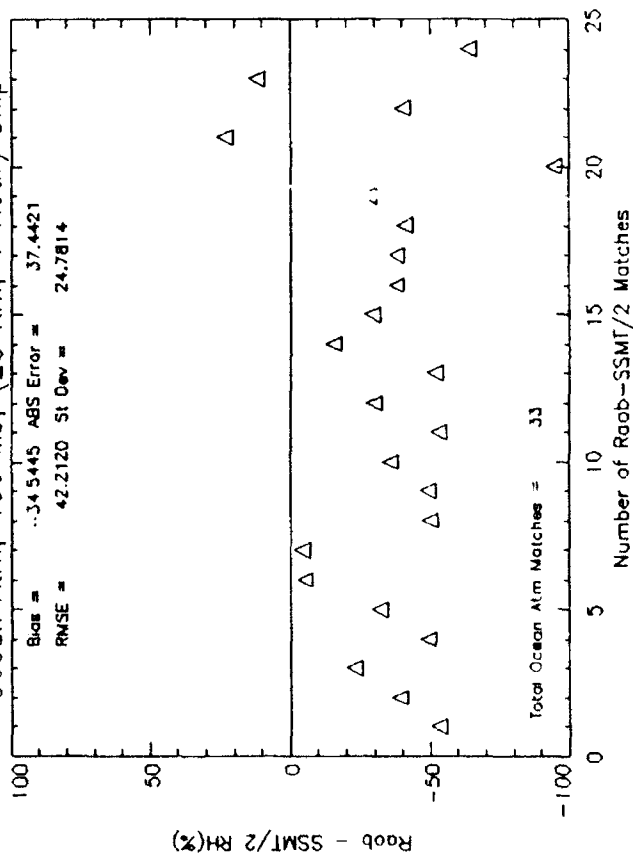




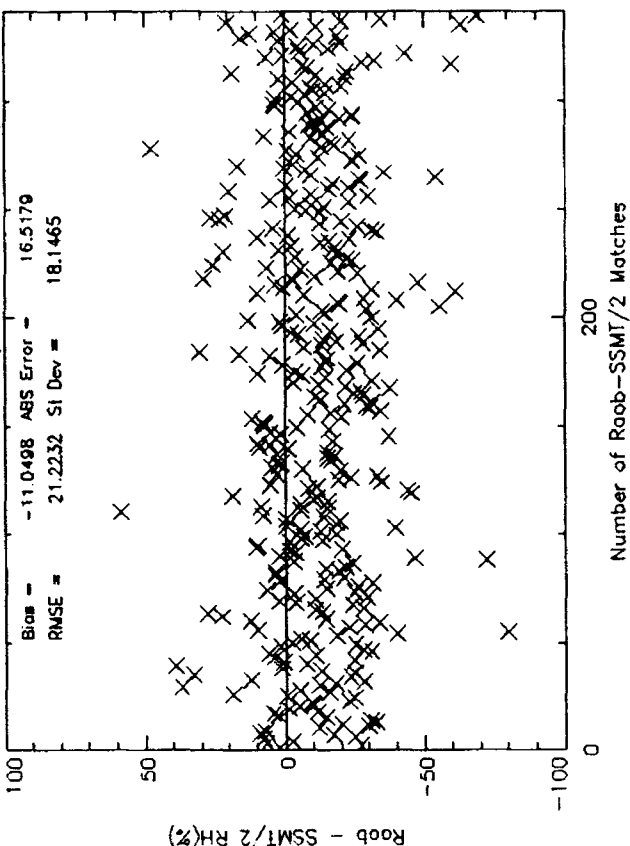
Ocean Atm, 400 Mb, (25 Km, 1 Hour) Non Ship



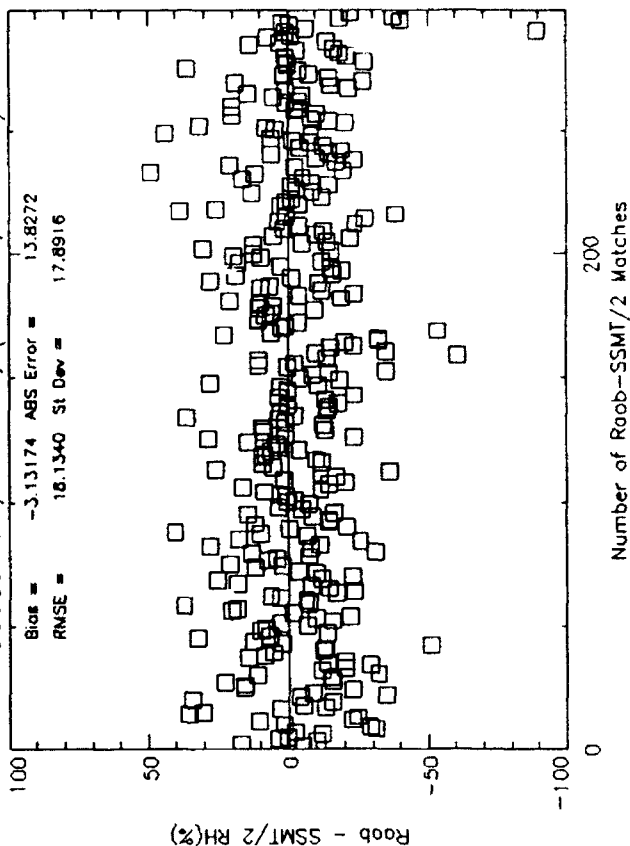
Ocean Atm, 400 Mb, (25 Km, 1 Hour) Ship

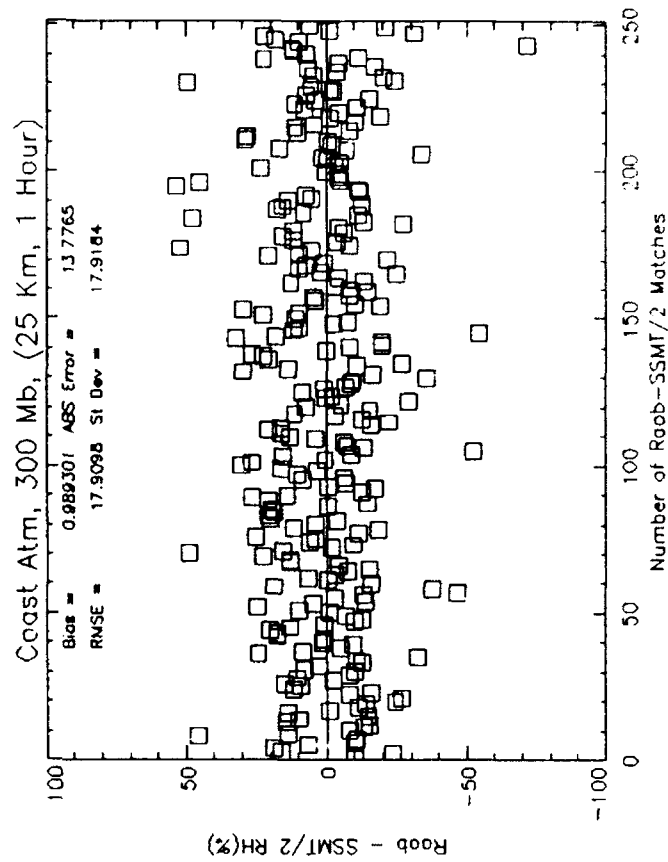
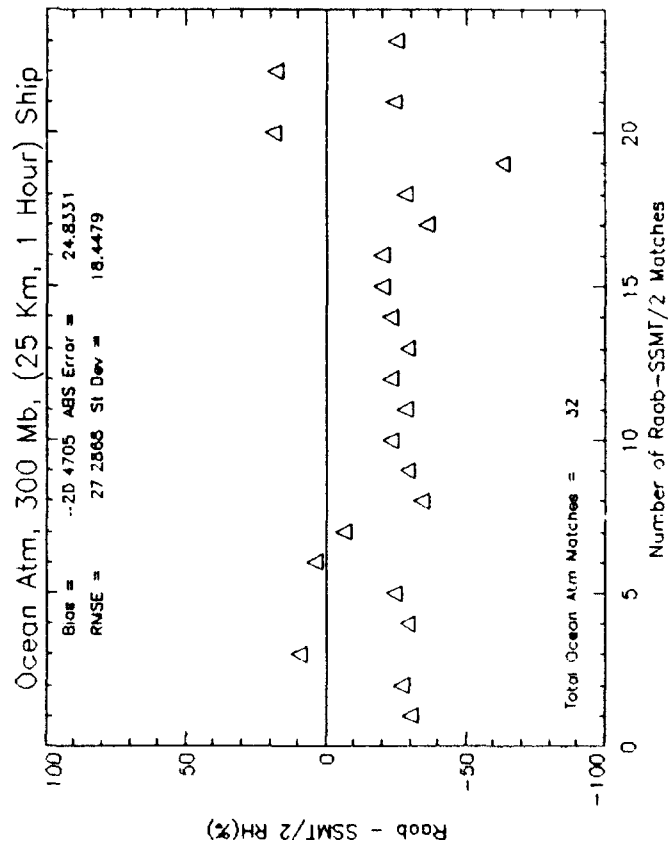
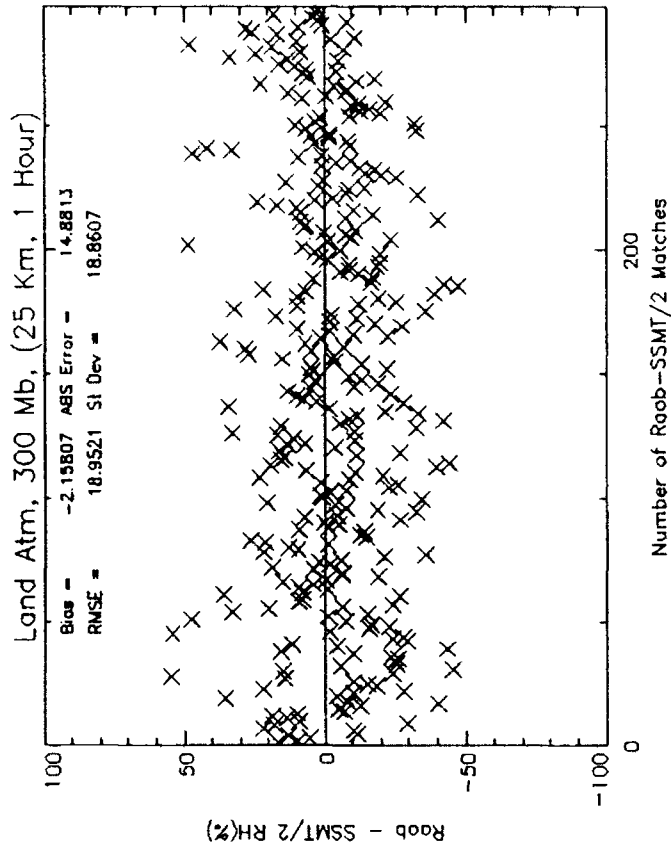
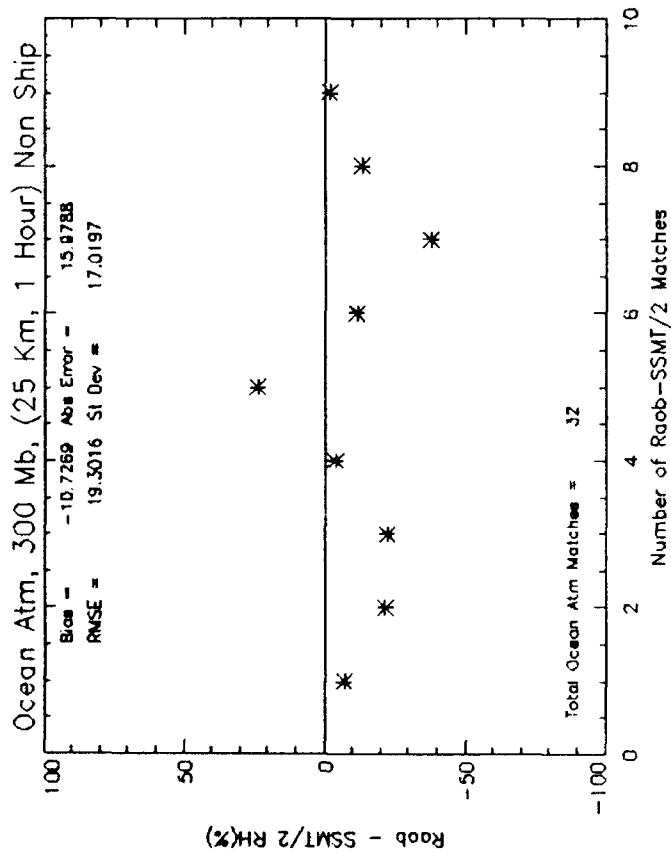


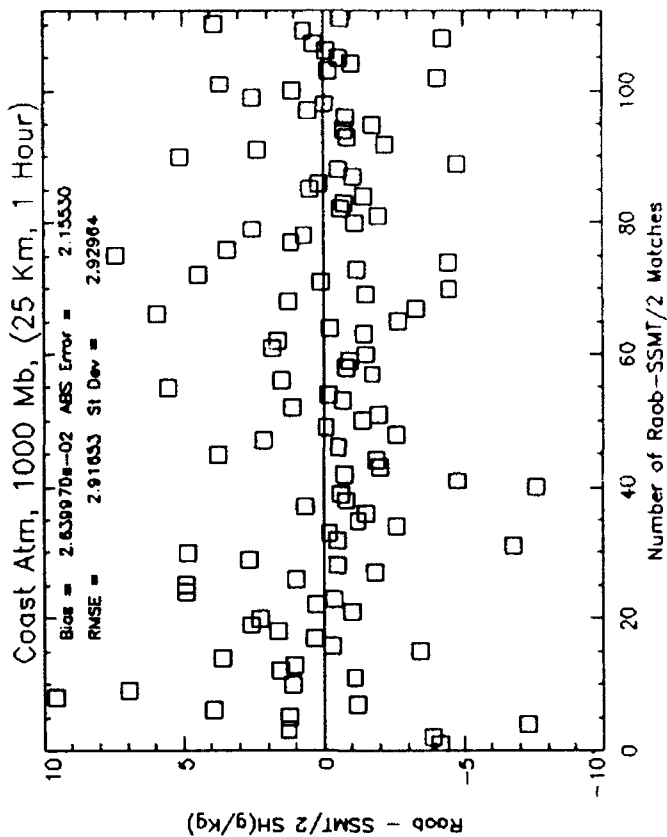
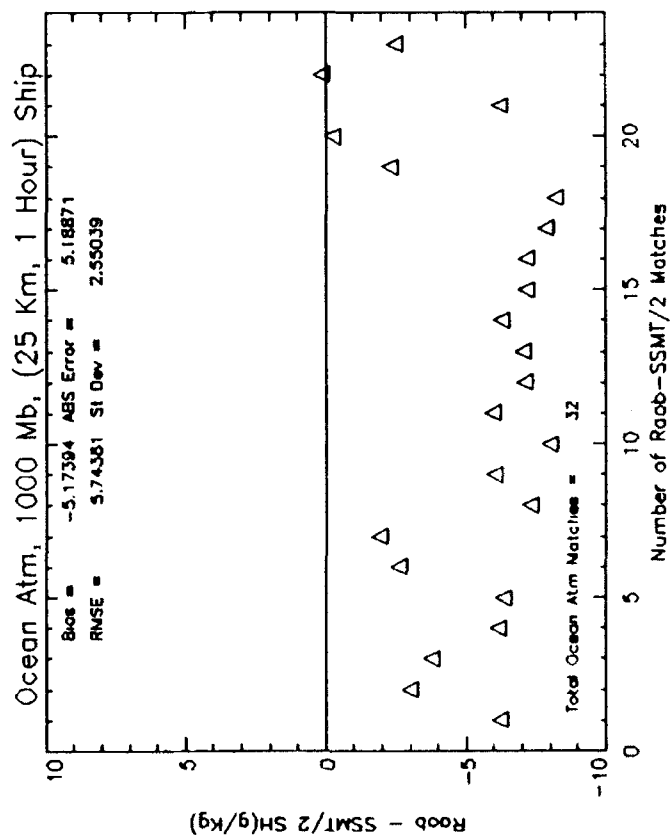
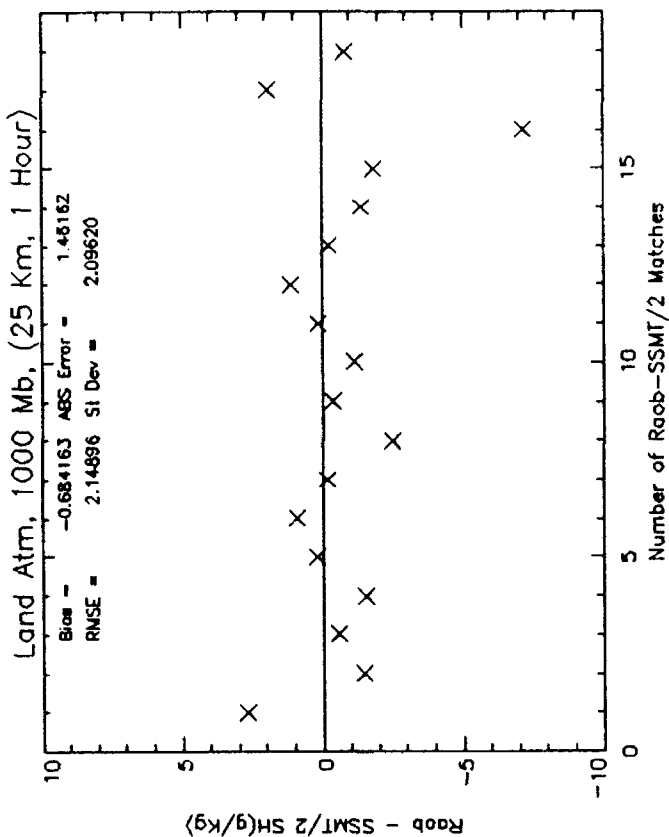
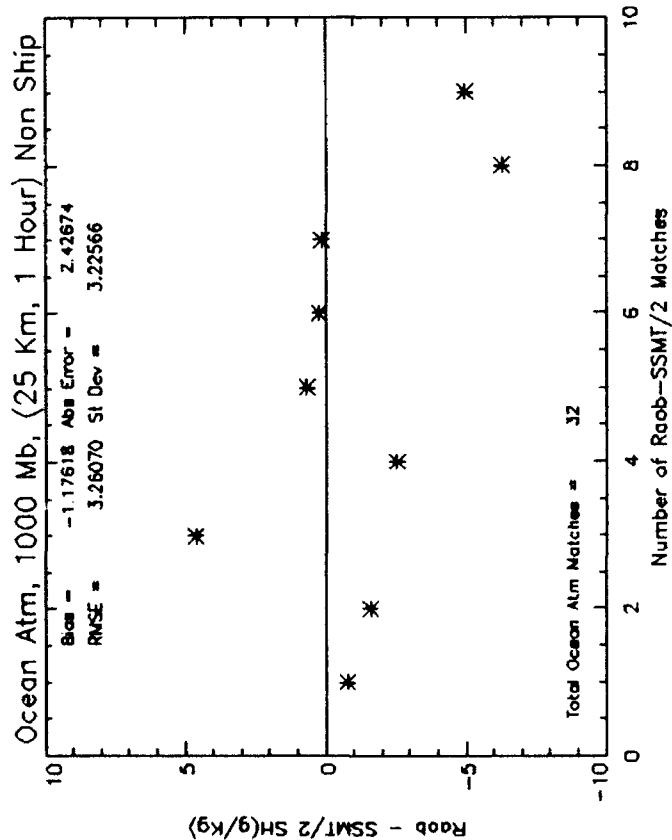
Land Atm, 400 Mb, (25 Km, 1 Hour)

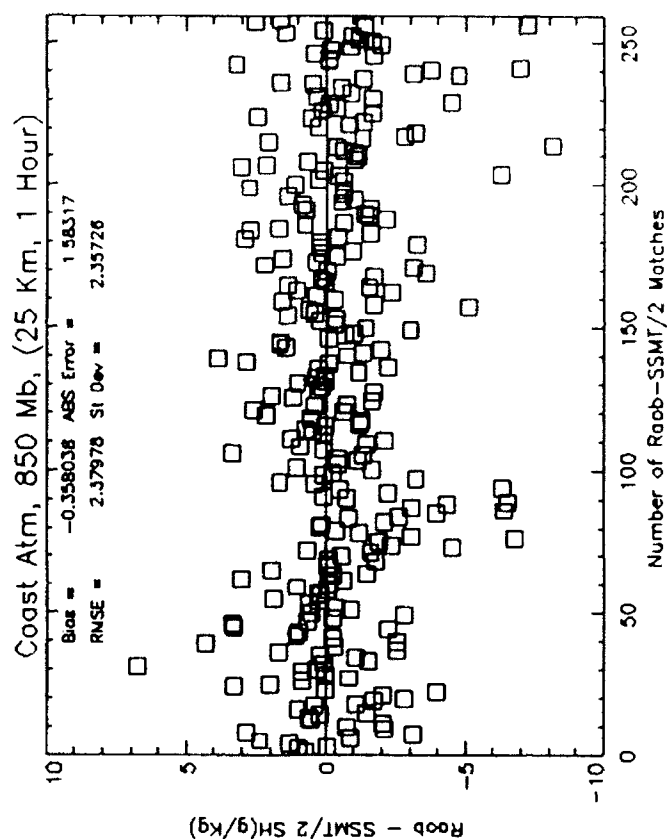
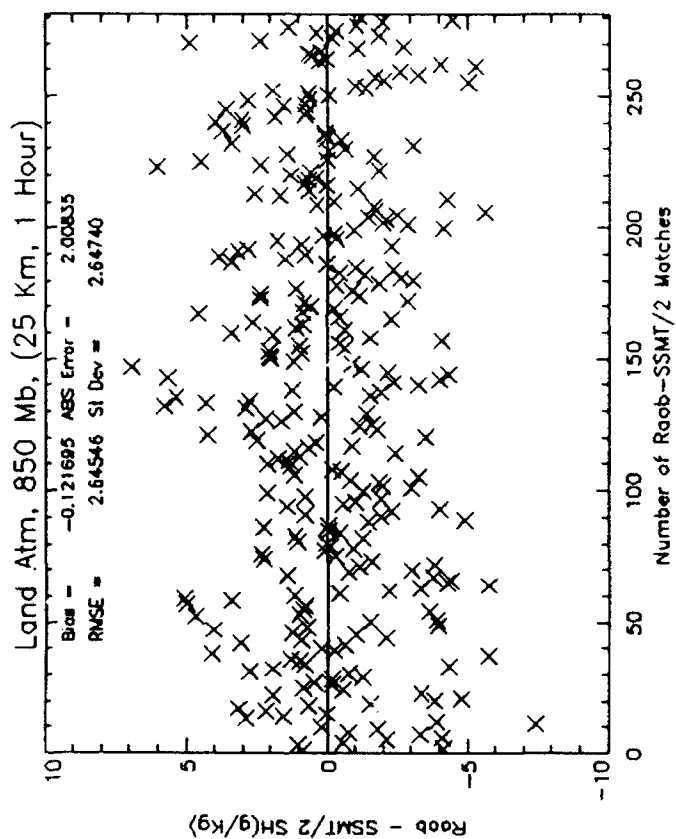
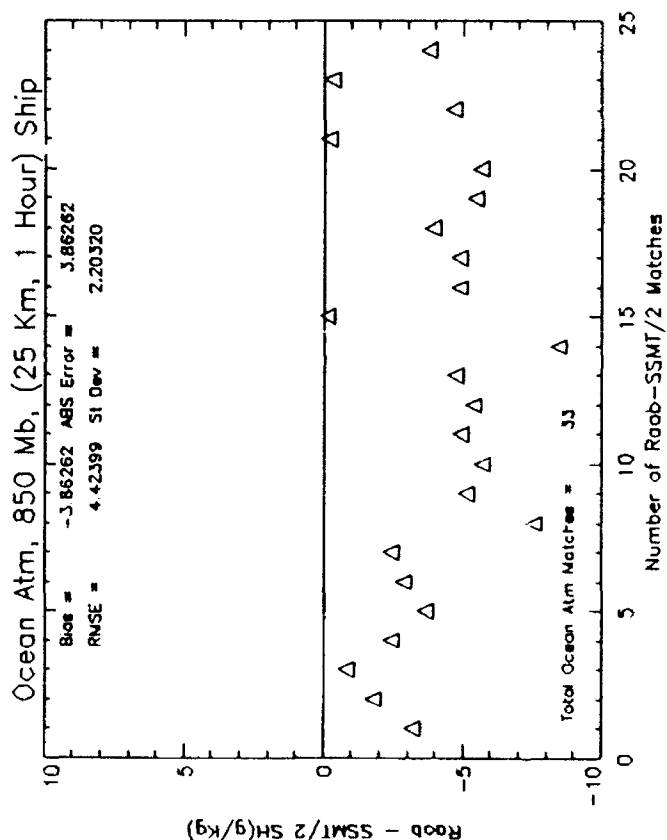
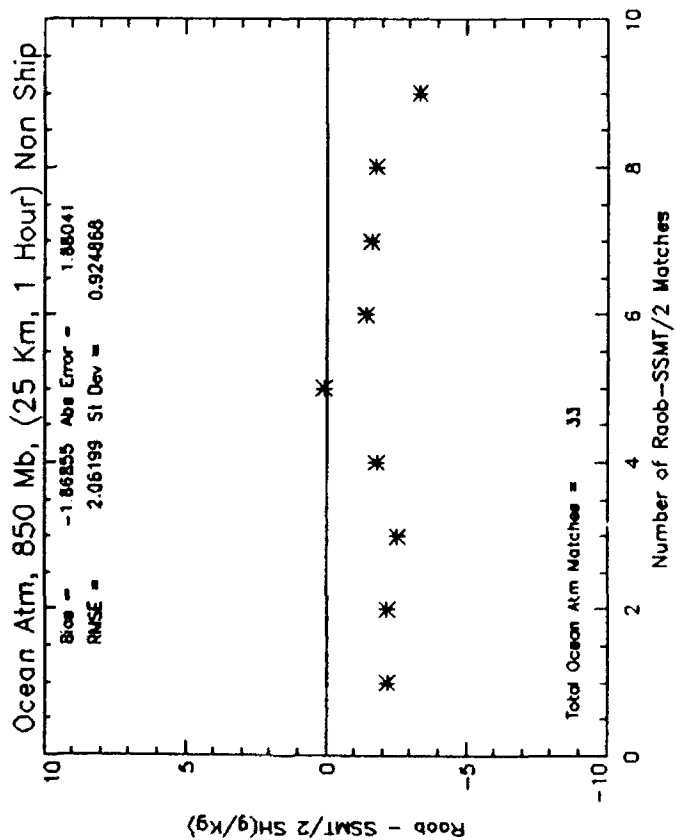


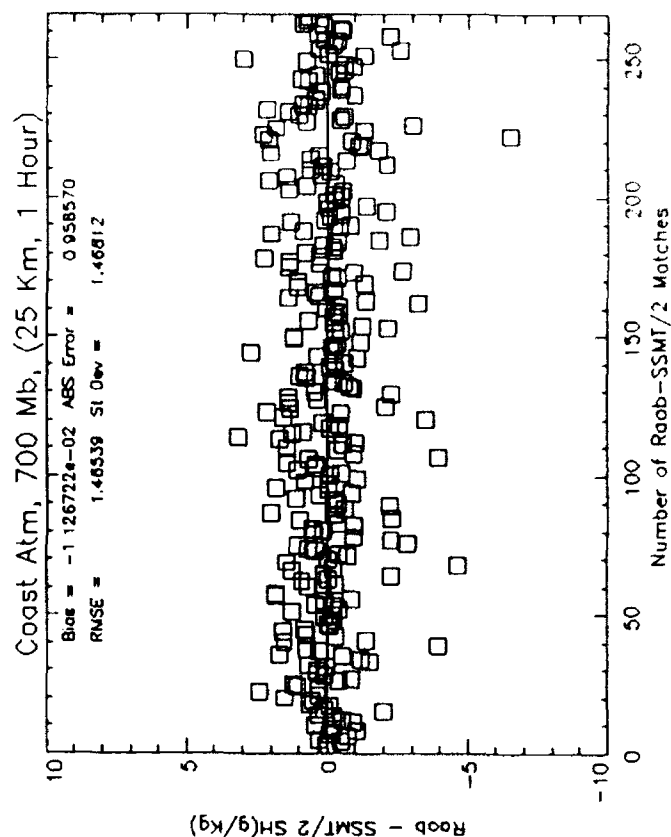
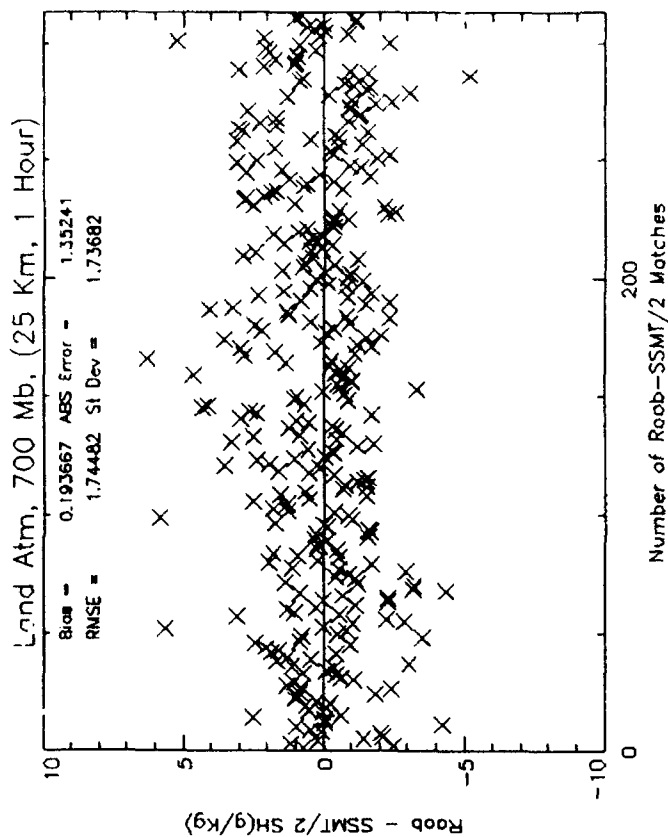
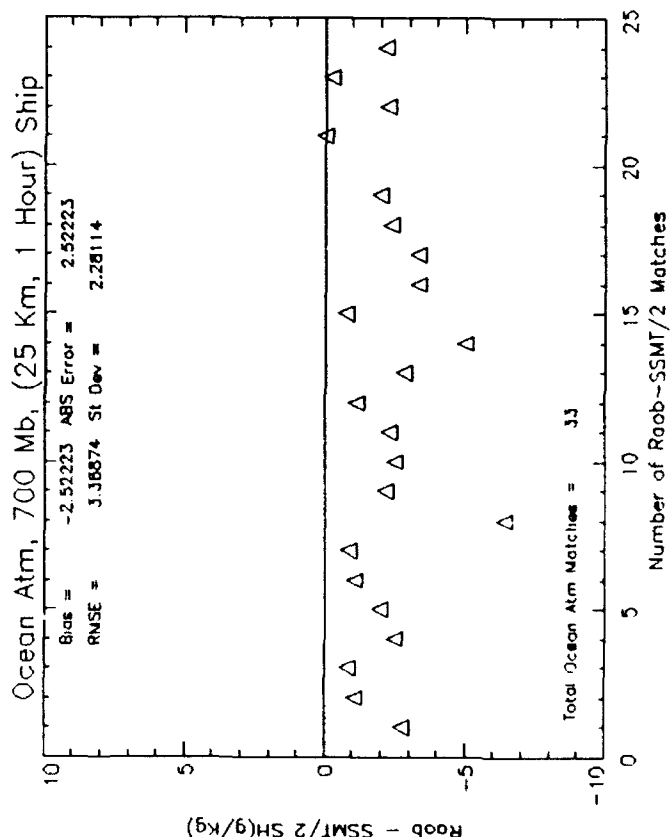
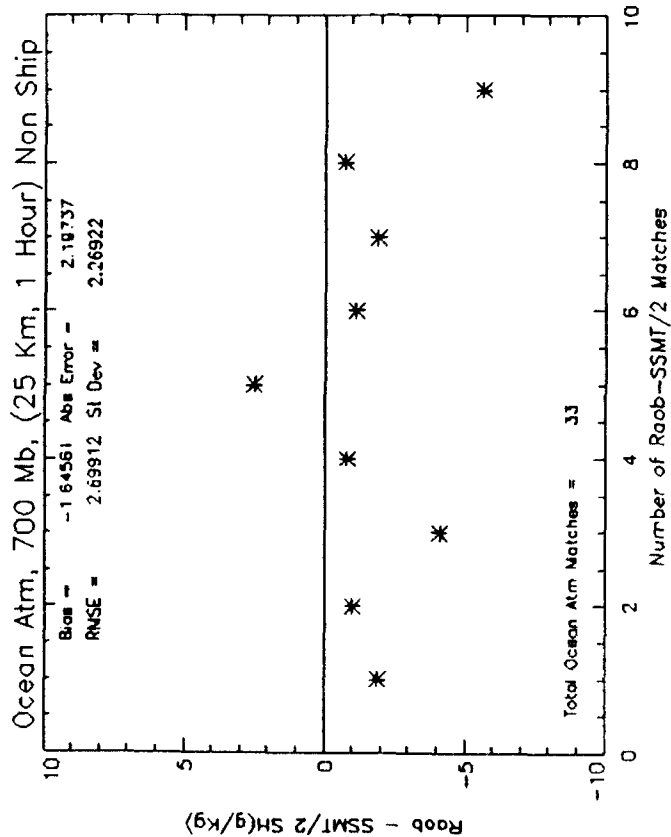
Coast Atm, 400 Mb, (25 Km, 1 Hour)

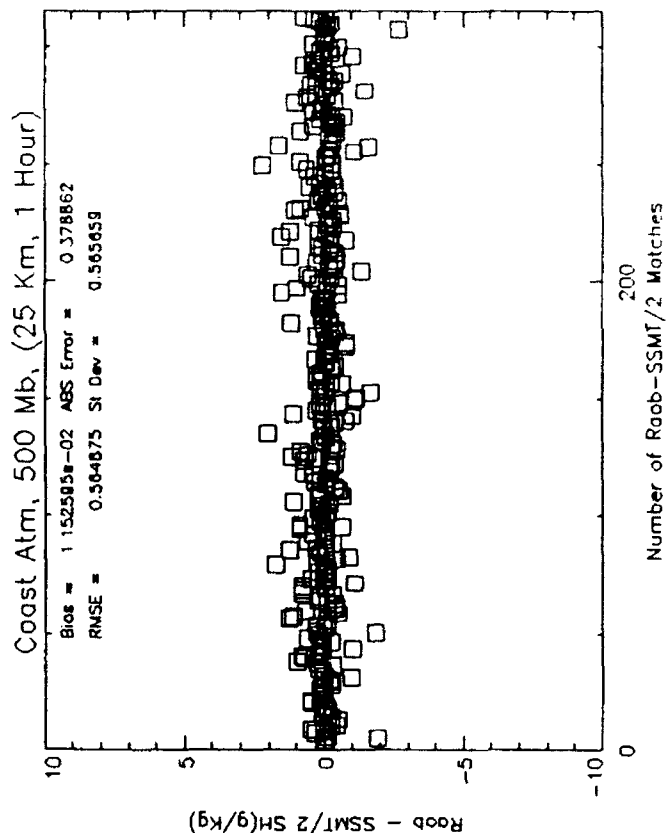
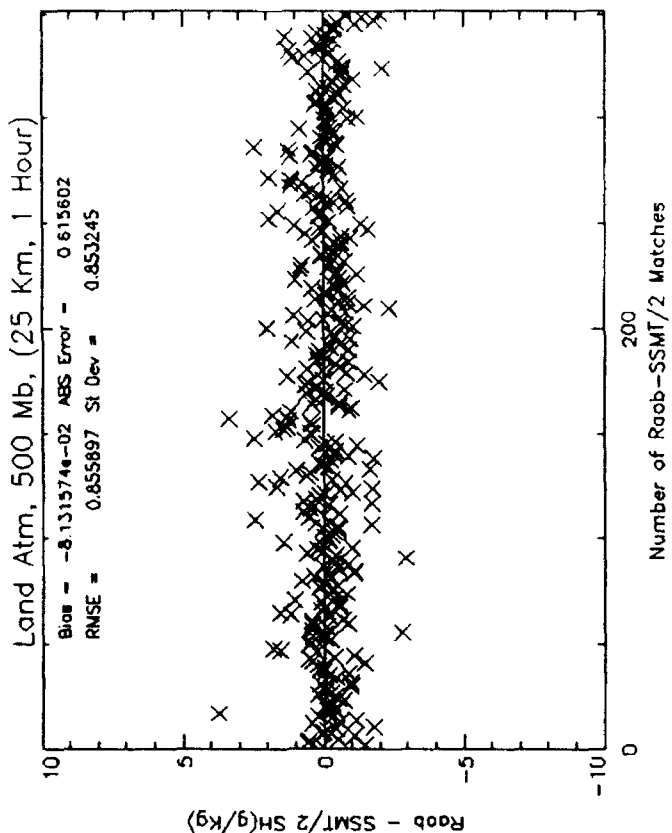
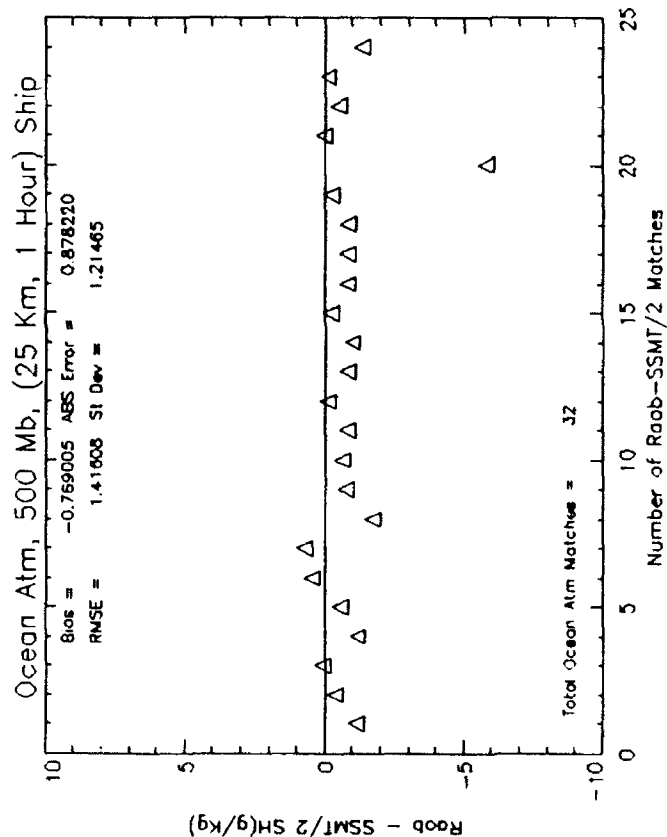
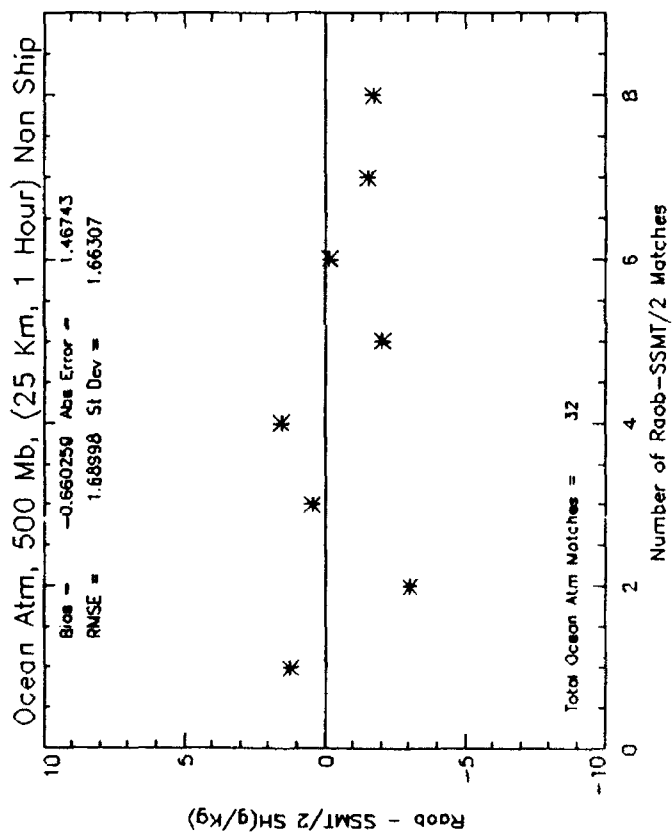




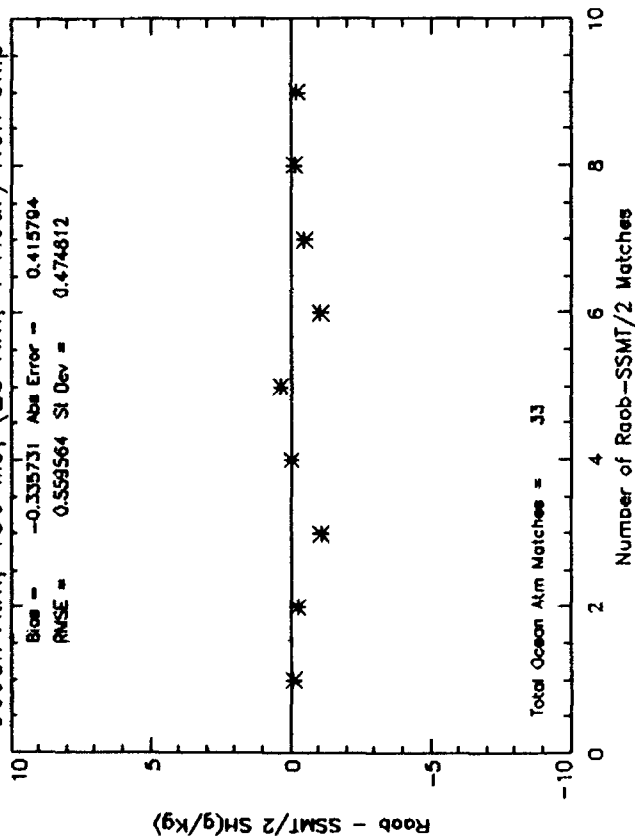




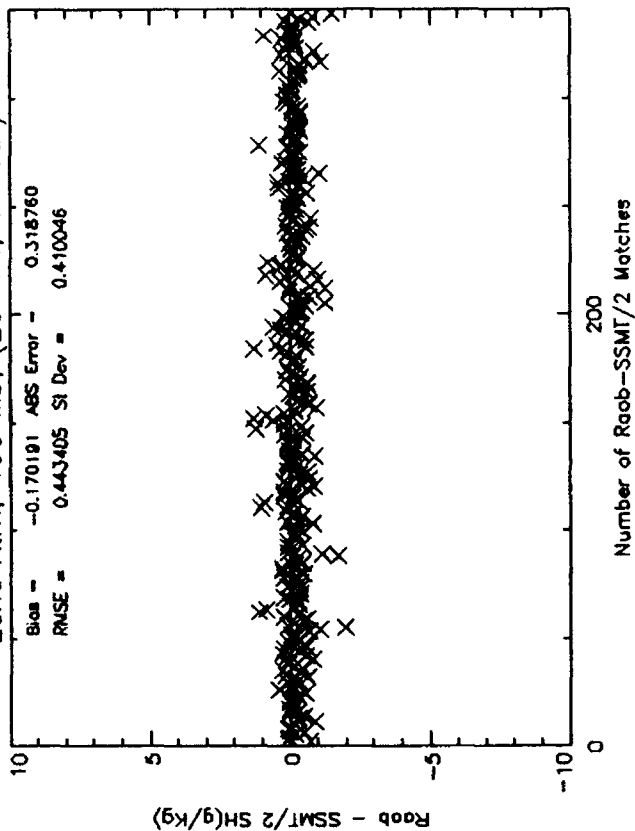




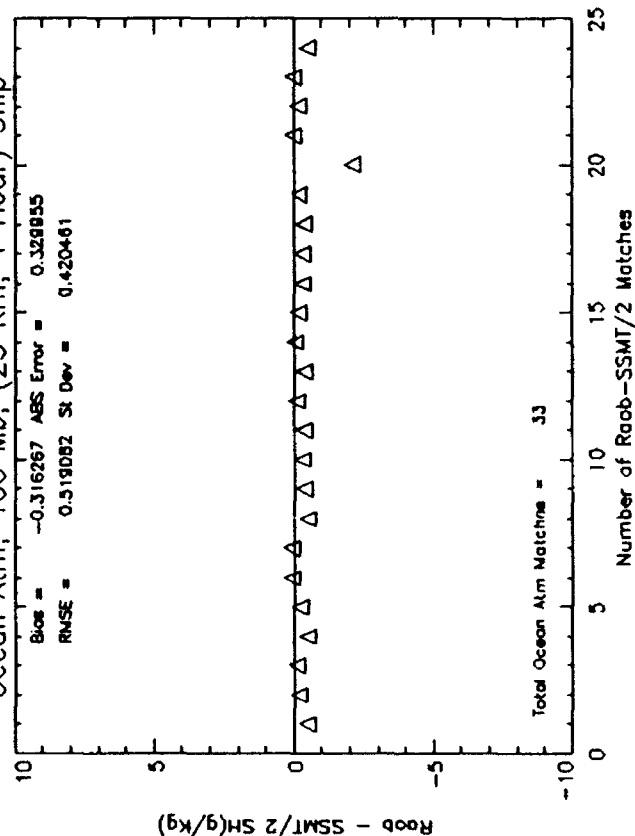
Ocean Atm, 400 Mb, (25 Km, 1 Hour) Non Ship



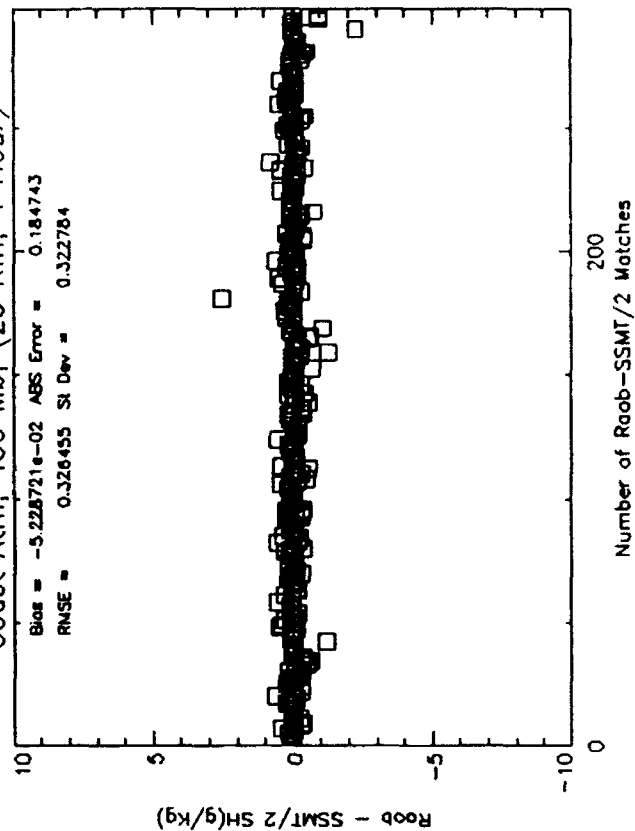
Land Atm, 400 Mb, (25 Km, 1 Hour)



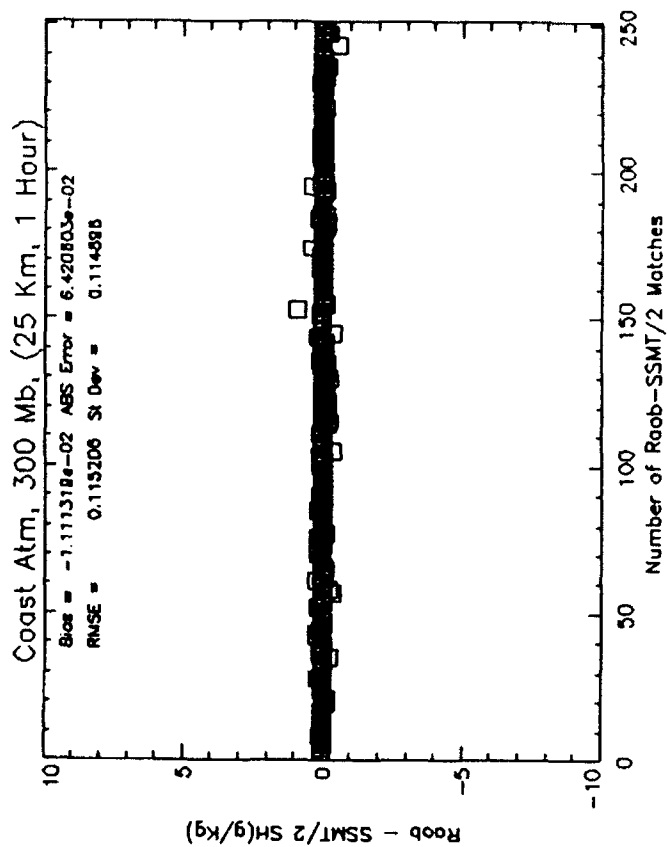
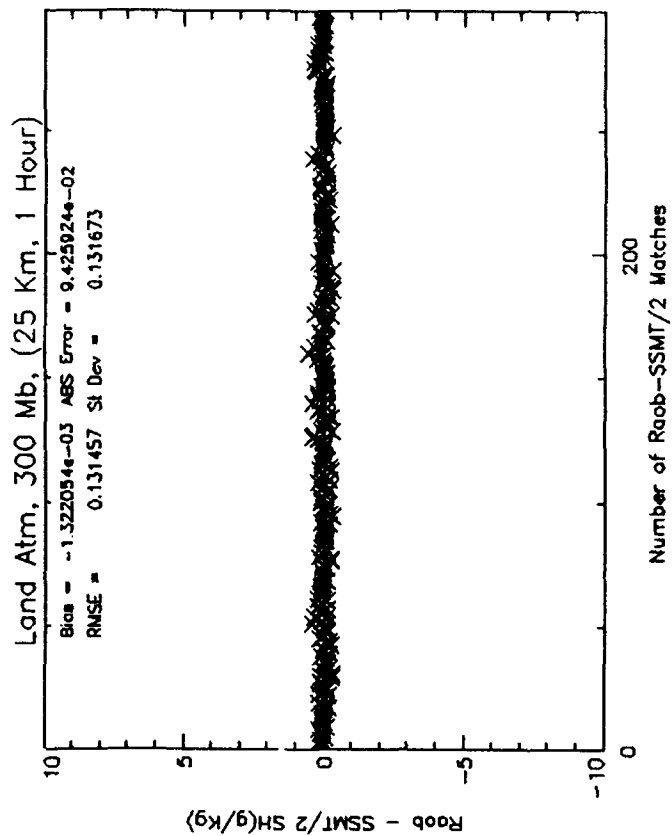
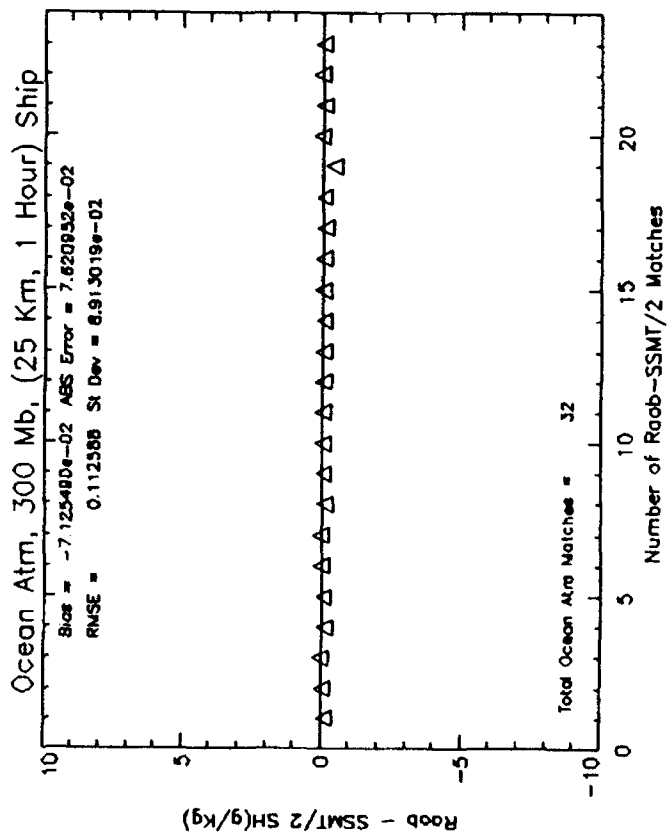
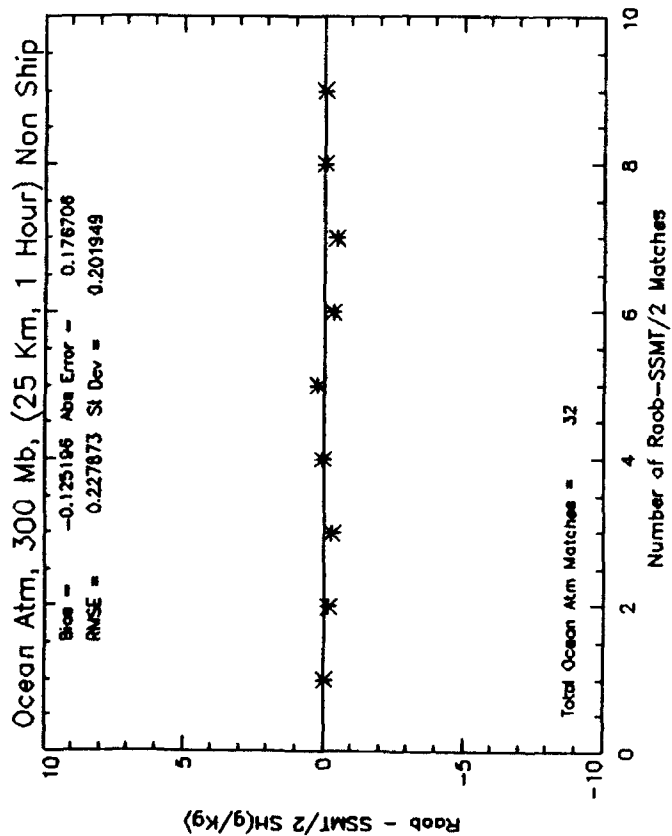
Ocean Atm, 400 Mb, (25 Km, 1 Hour) Ship

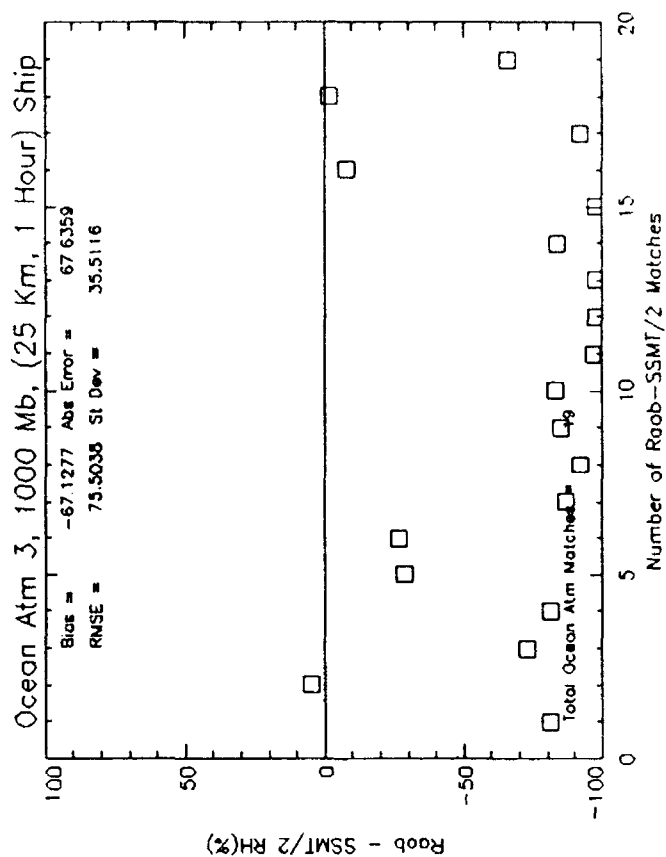
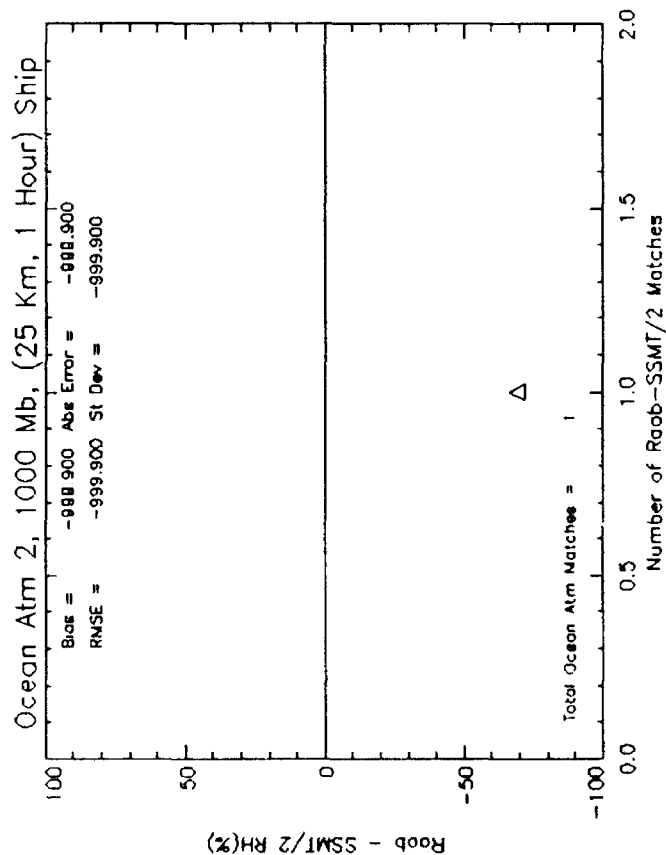
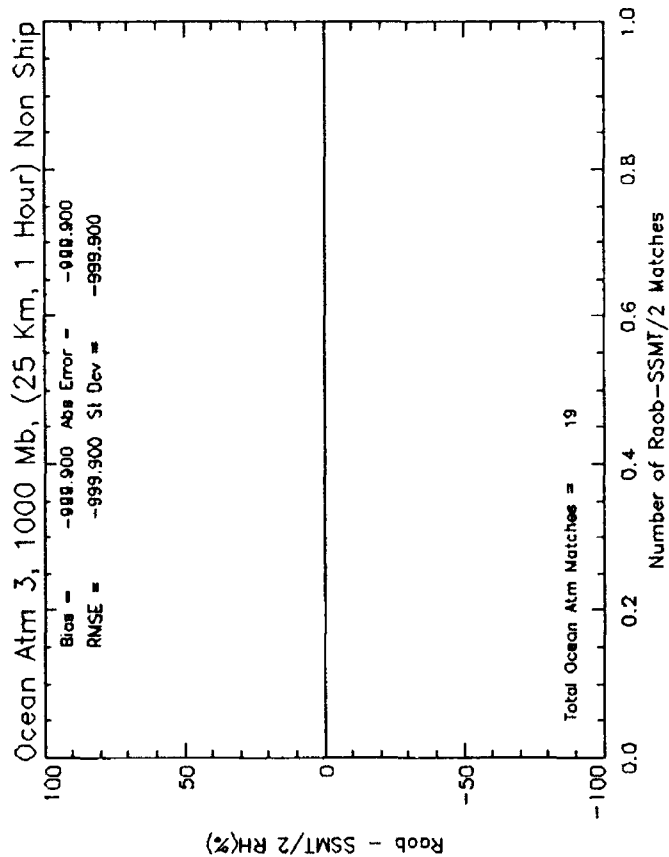
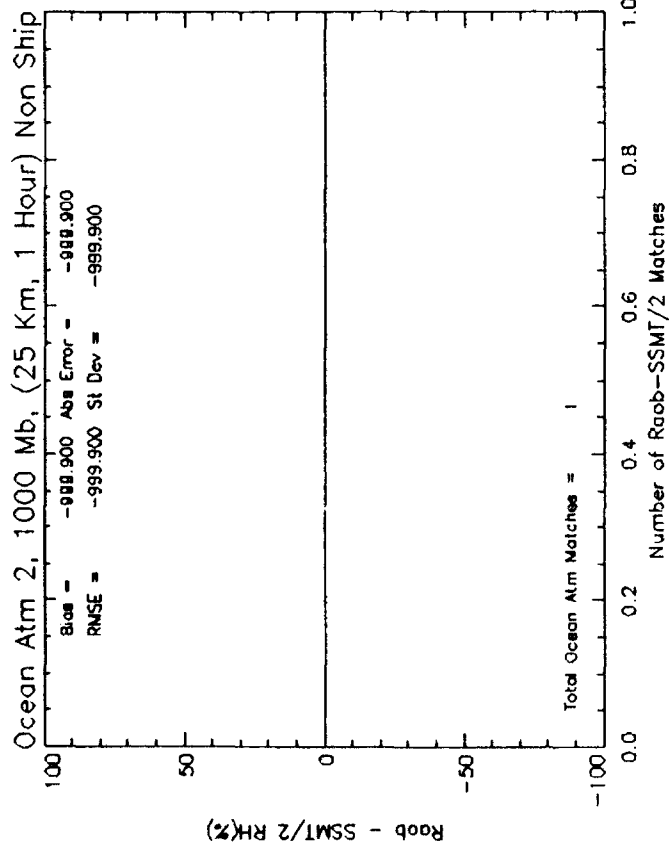


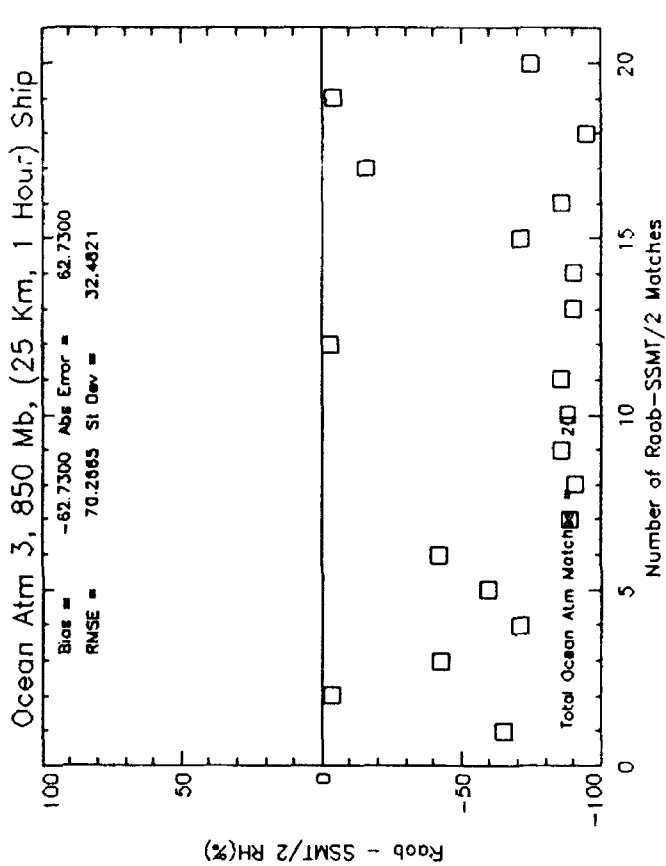
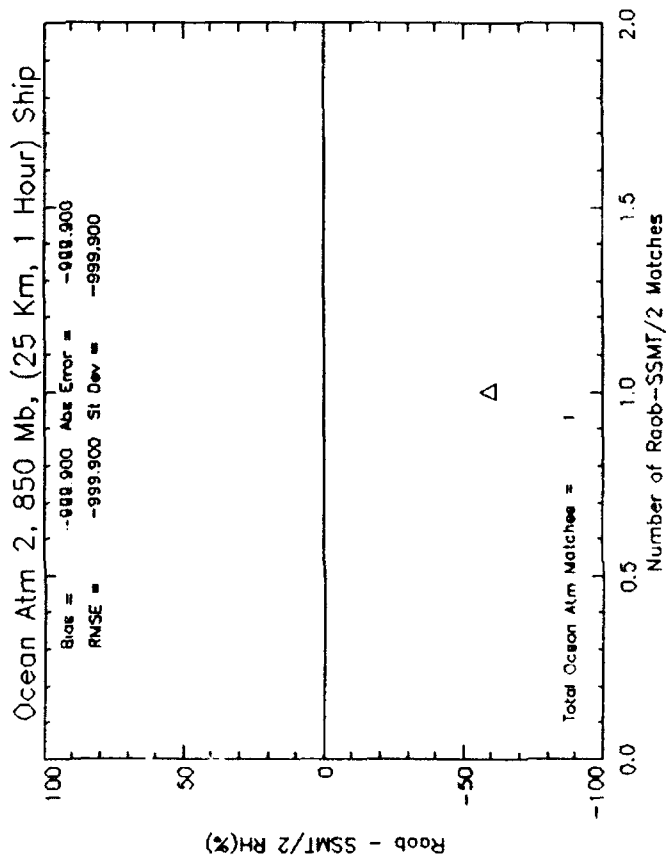
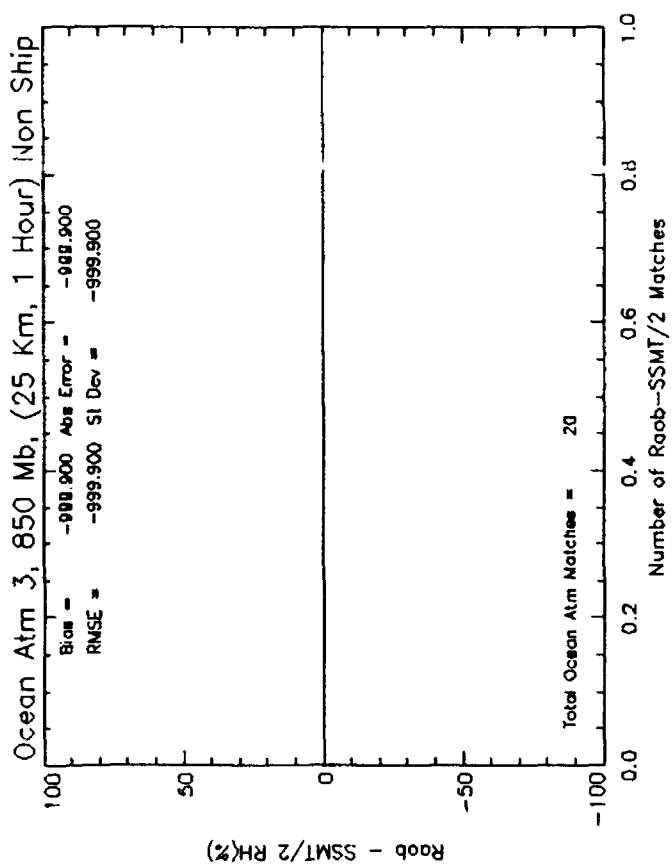
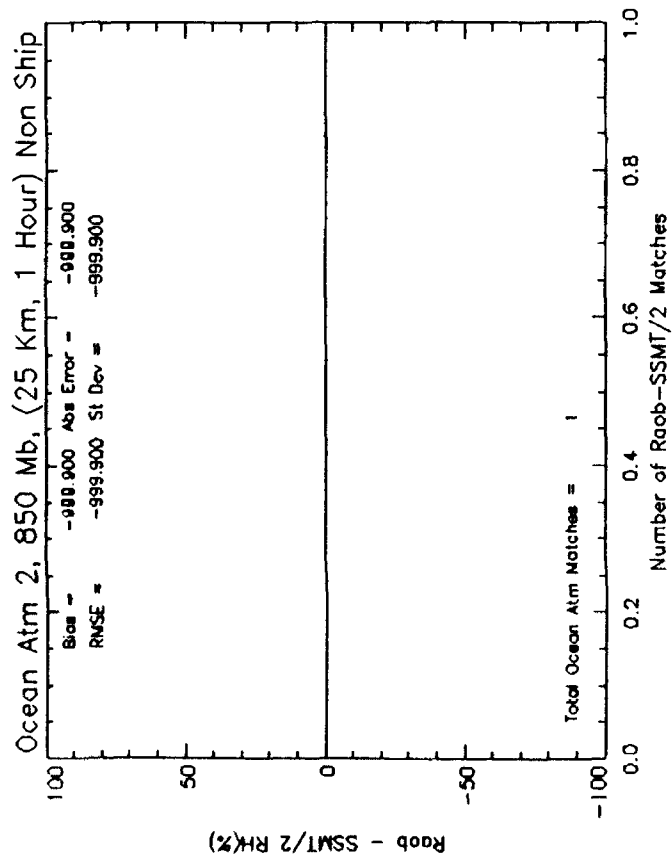
Coast Atm, 400 Mb, (25 Km, 1 Hour)

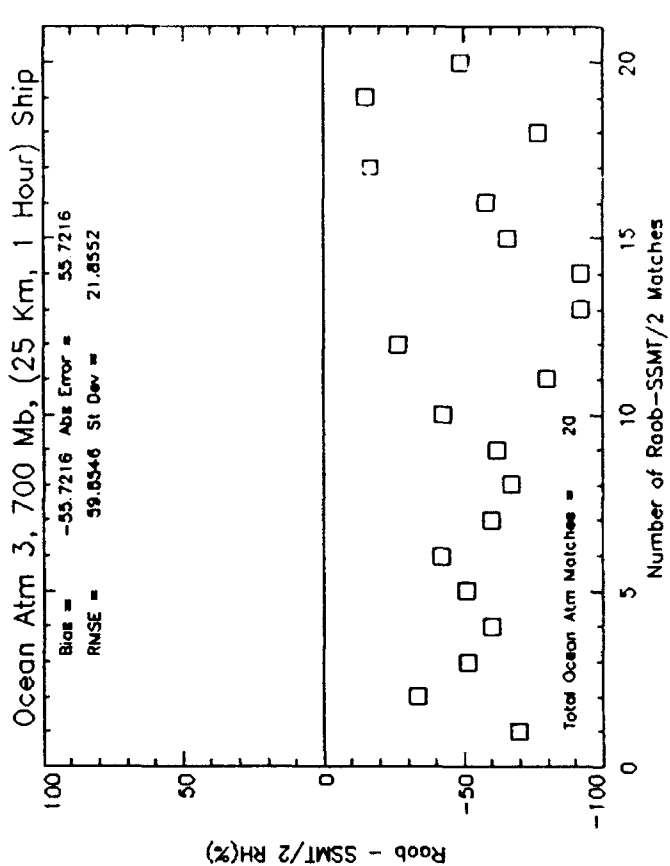
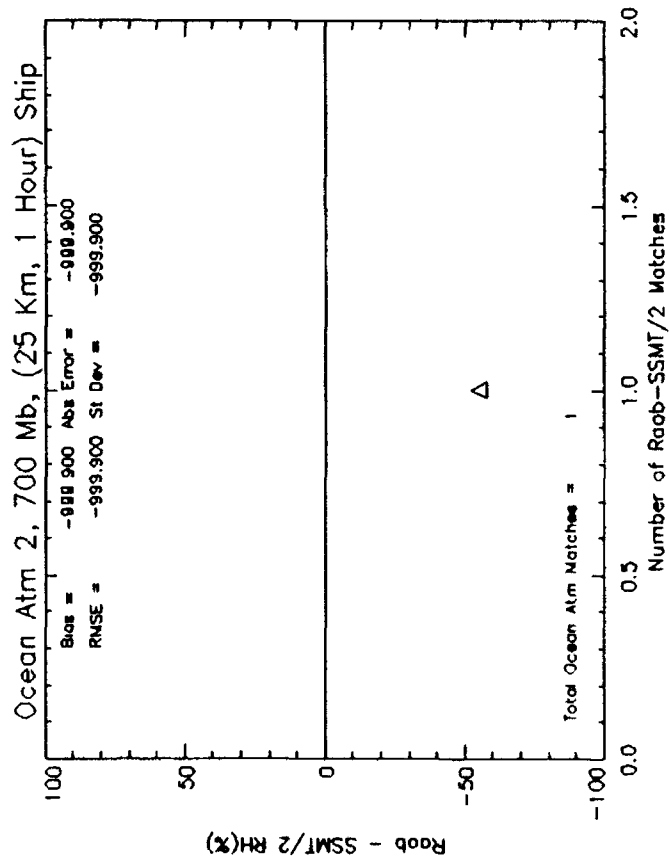
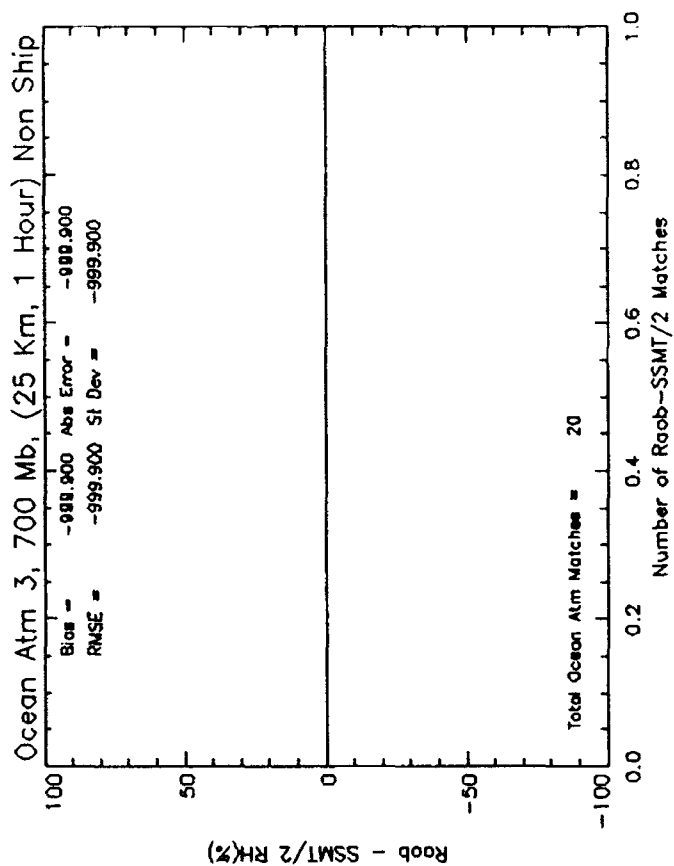
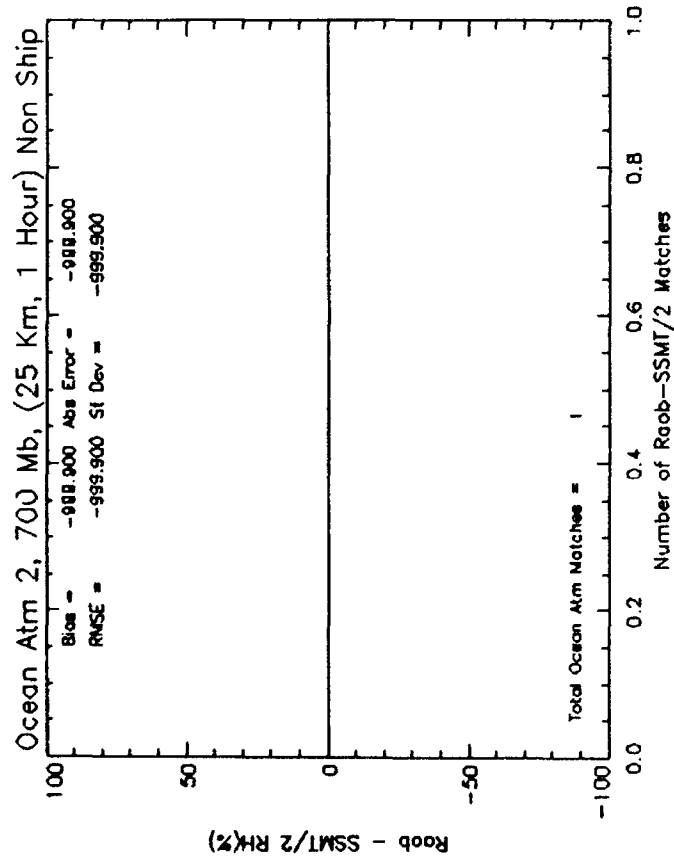


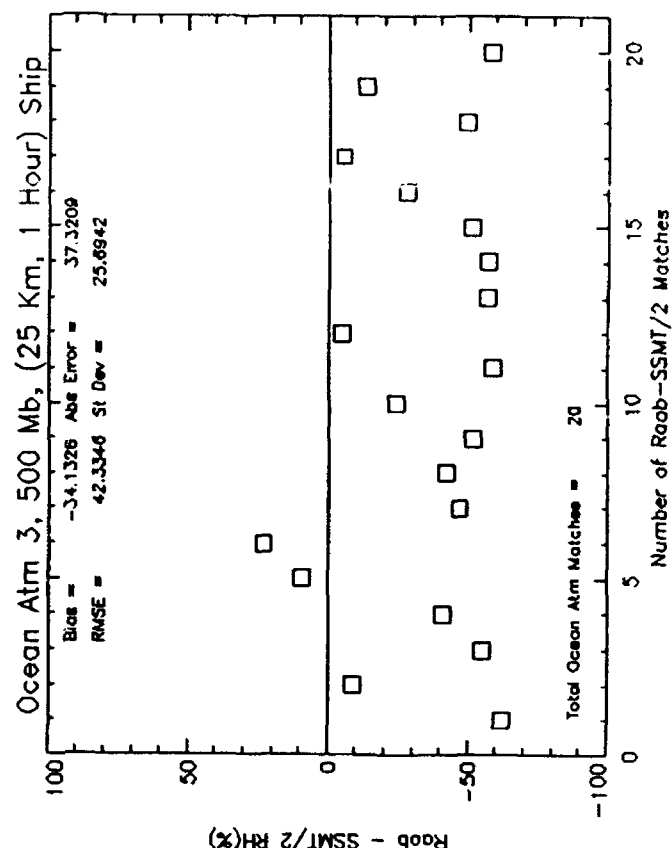
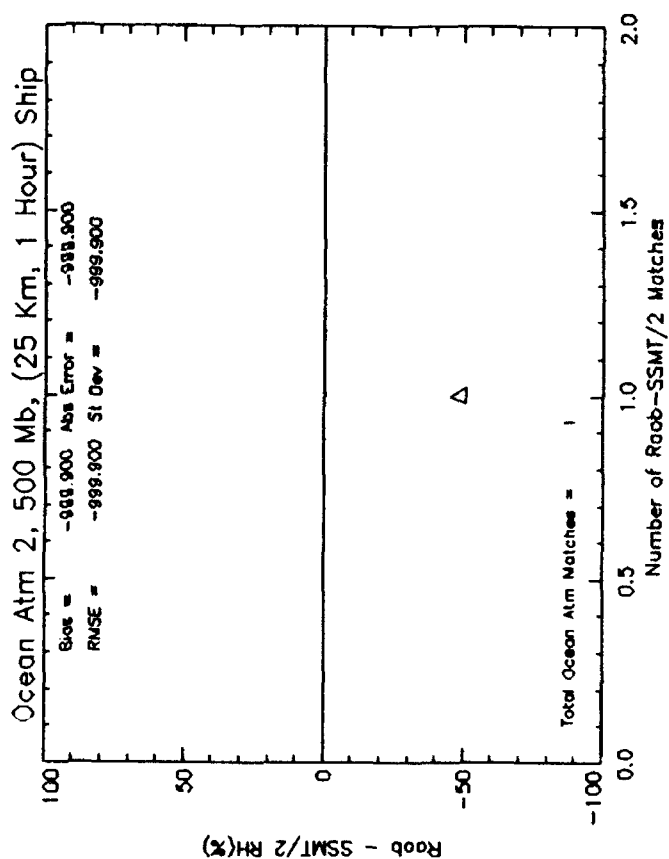
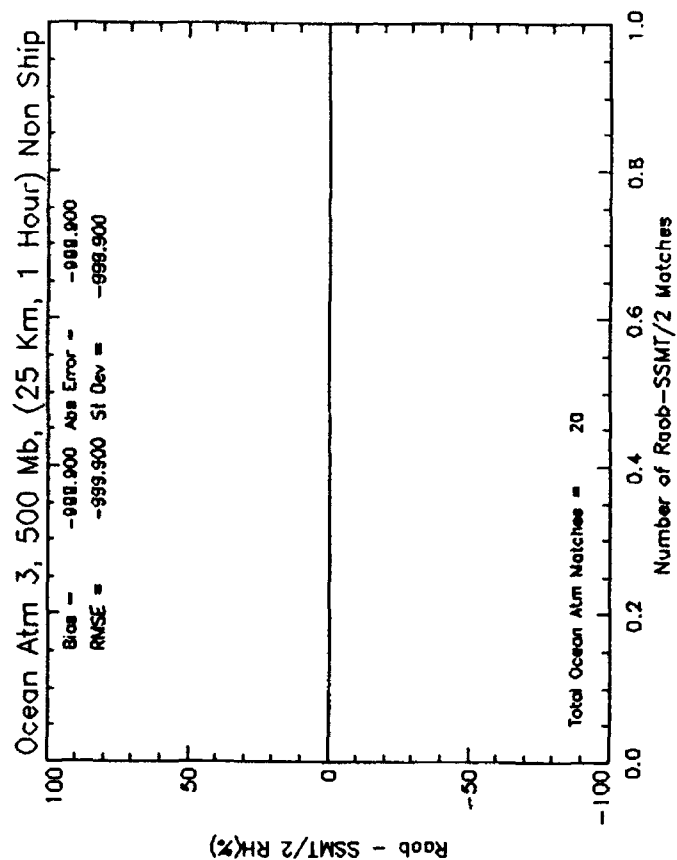
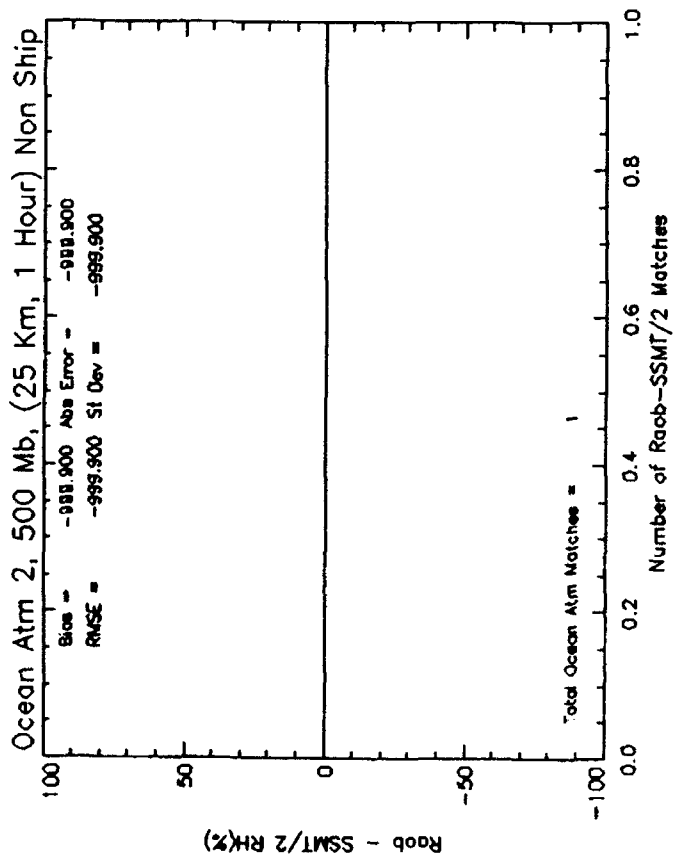


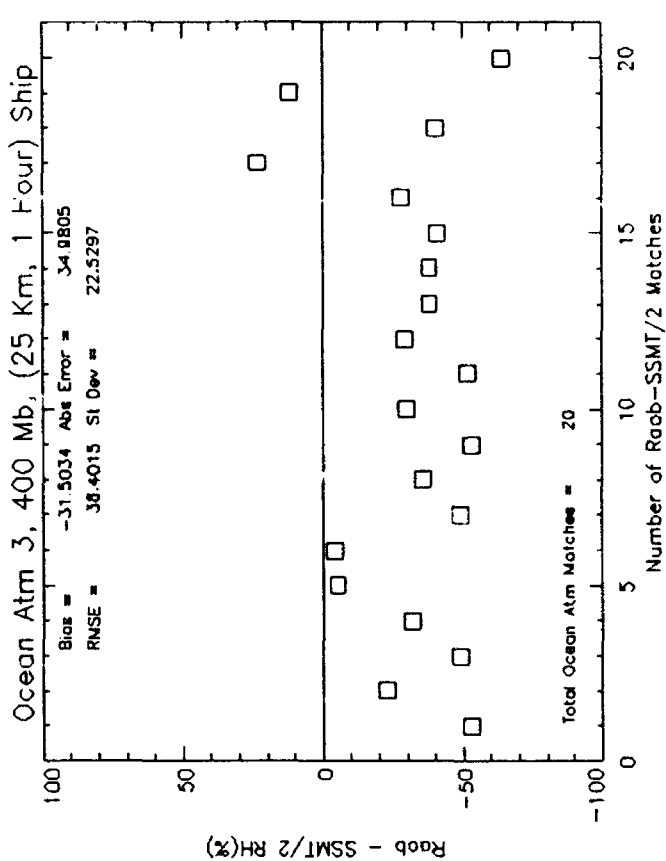
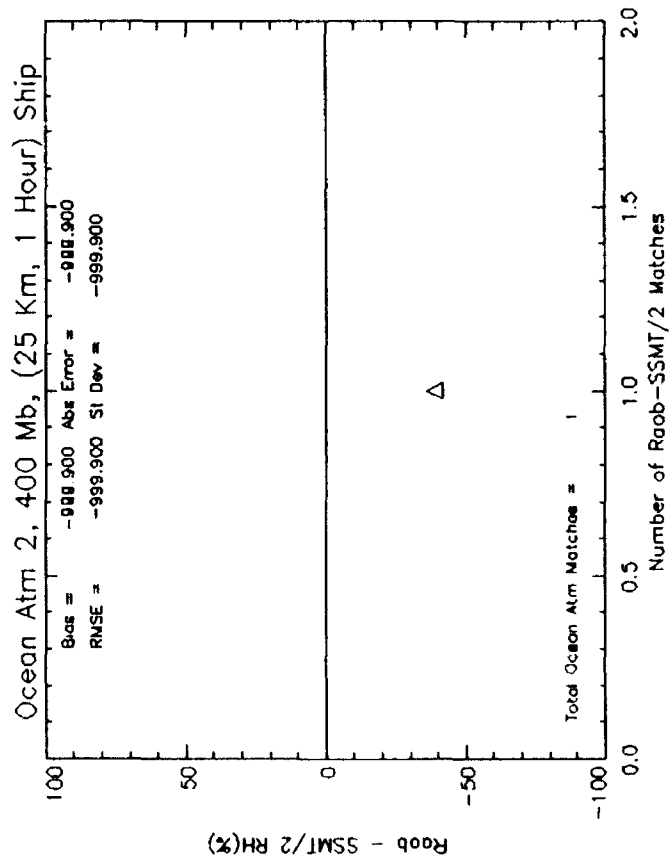
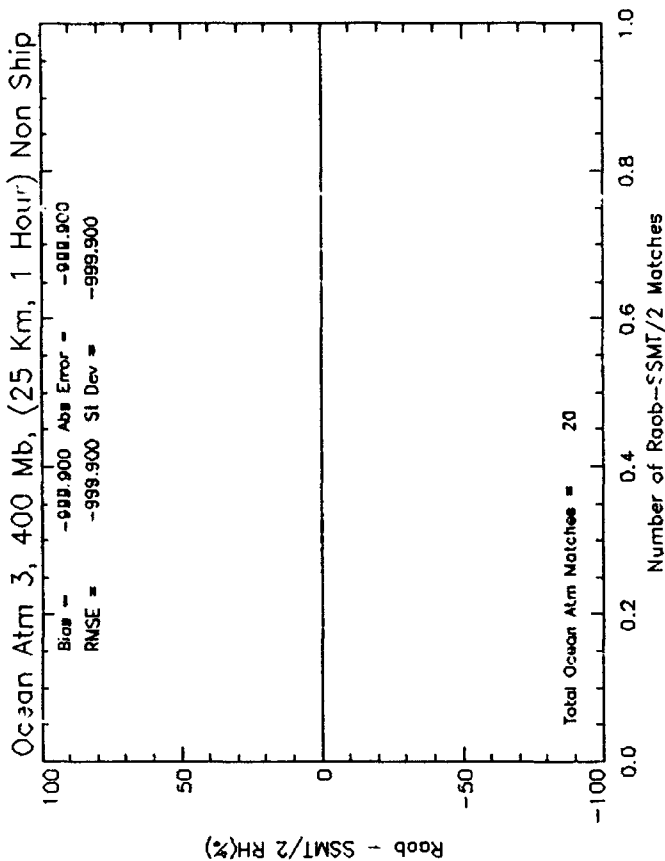
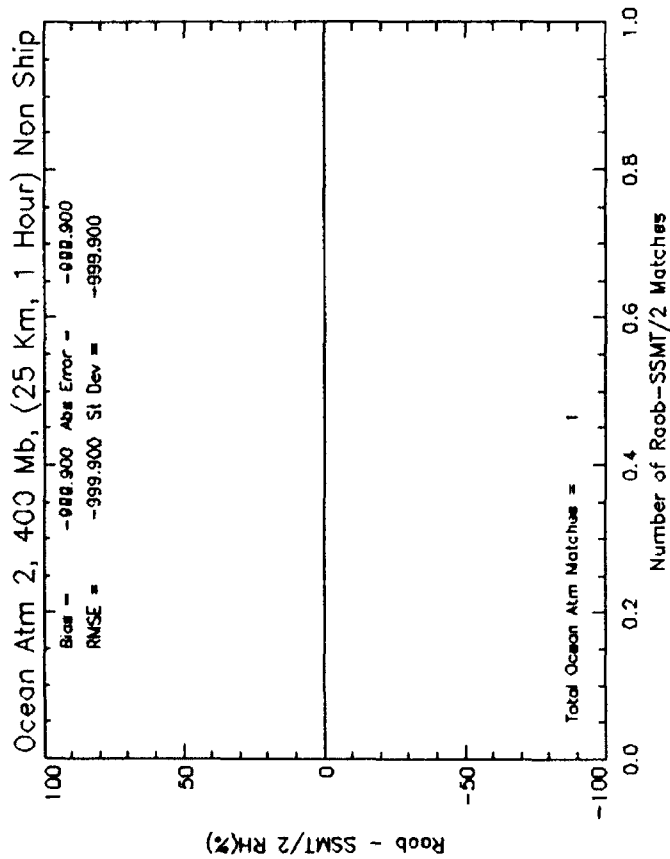


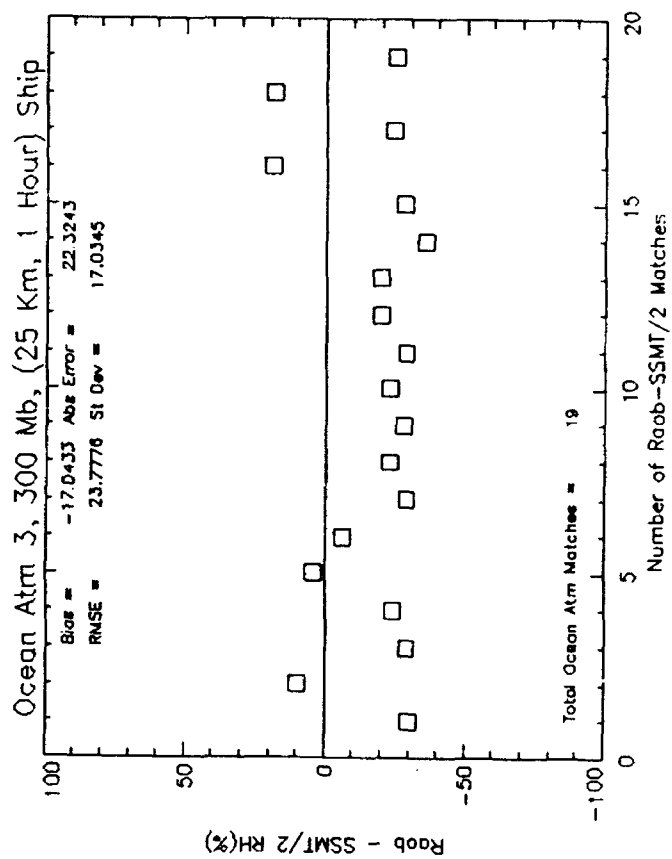
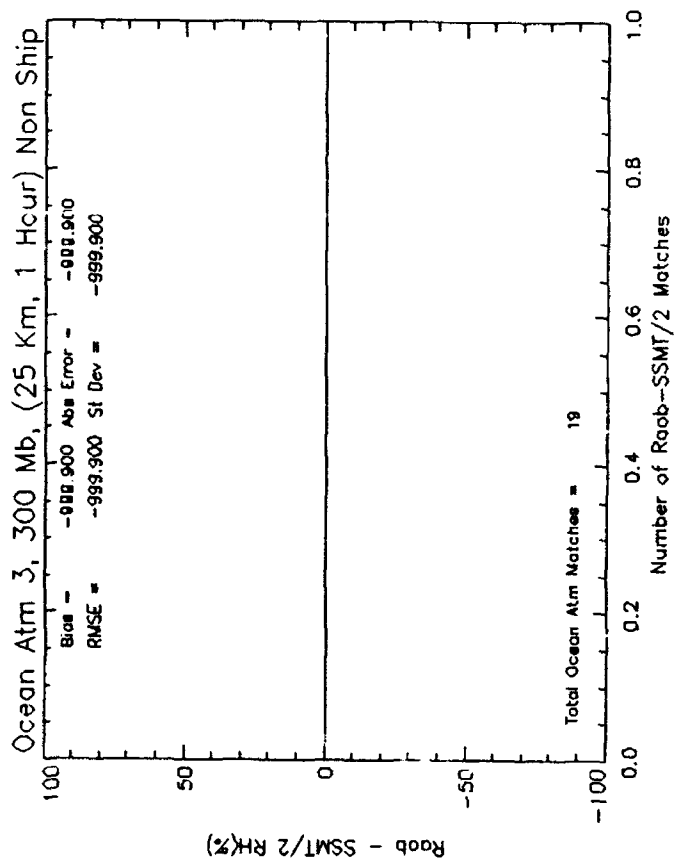
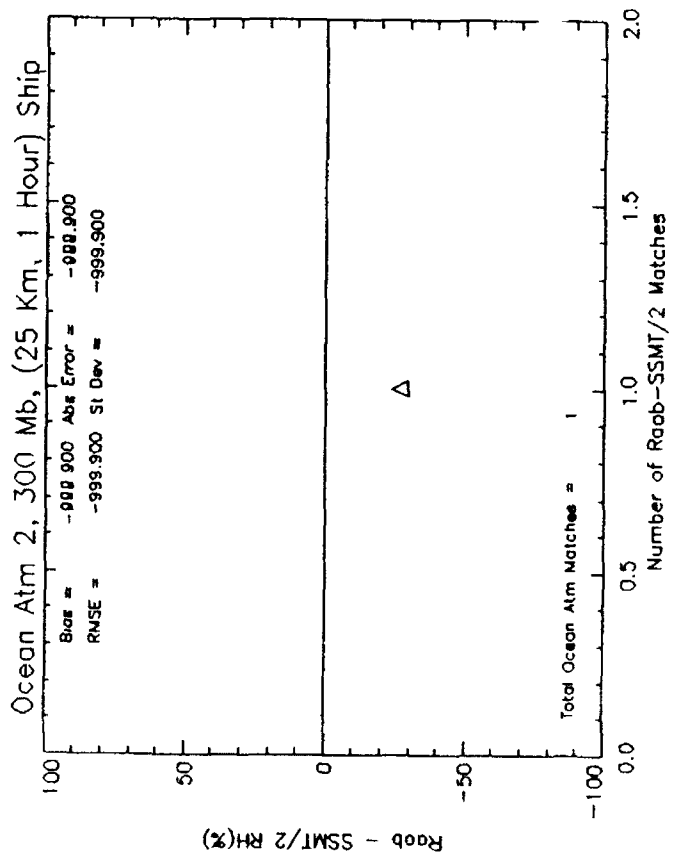
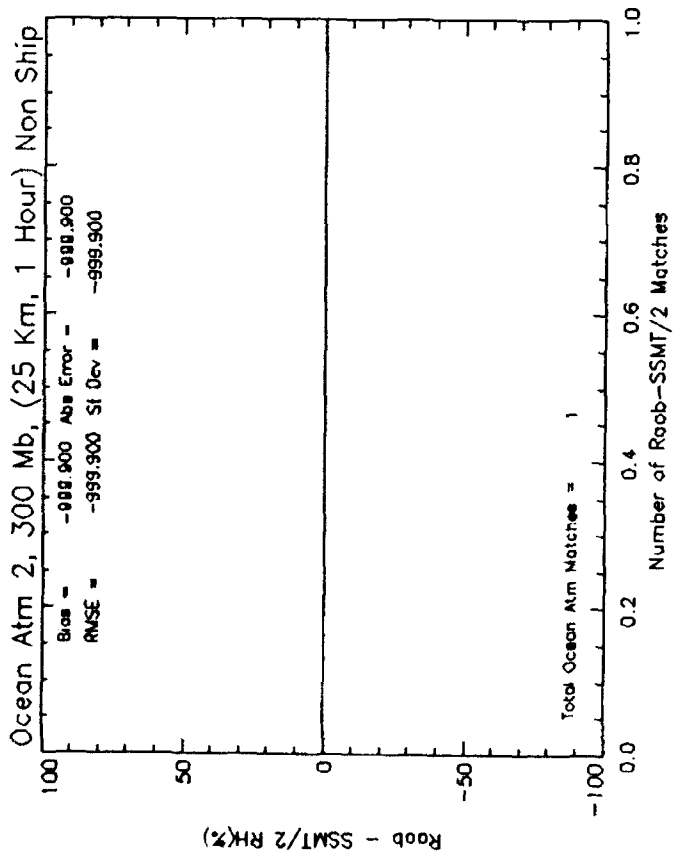


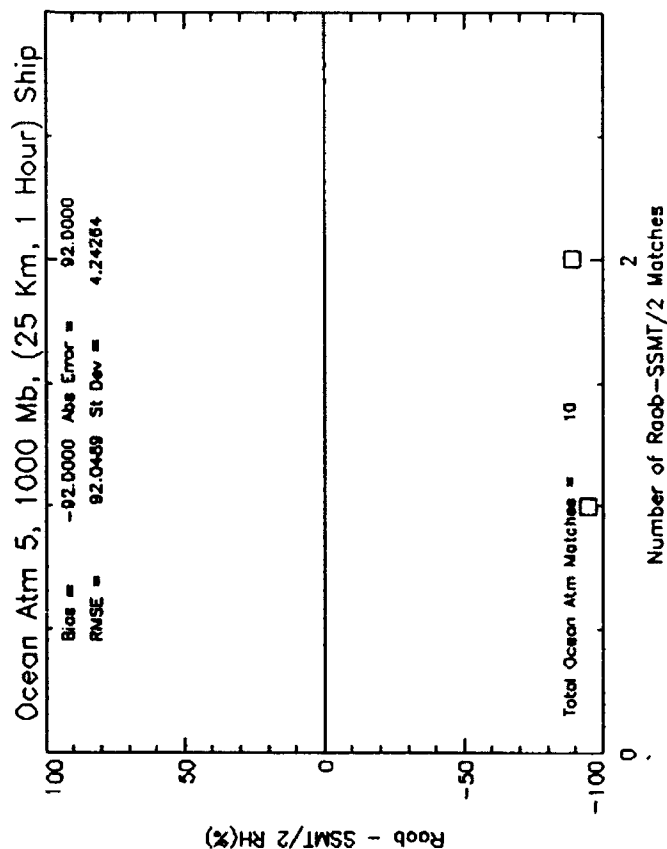
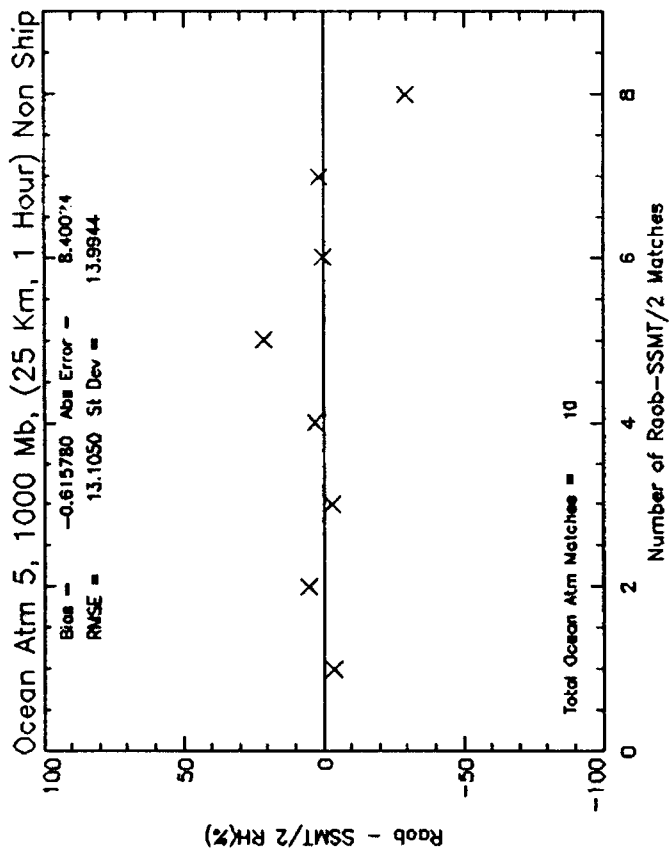
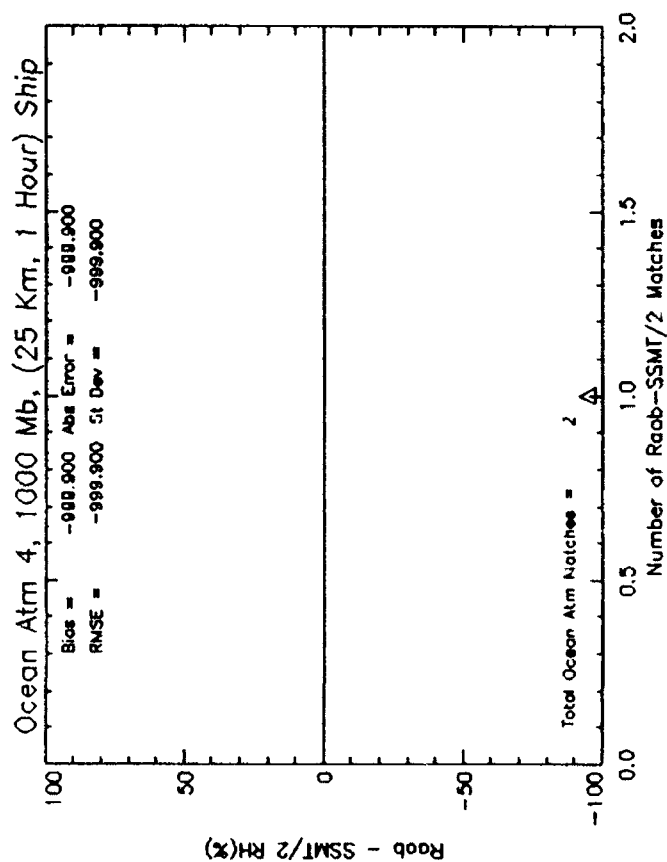
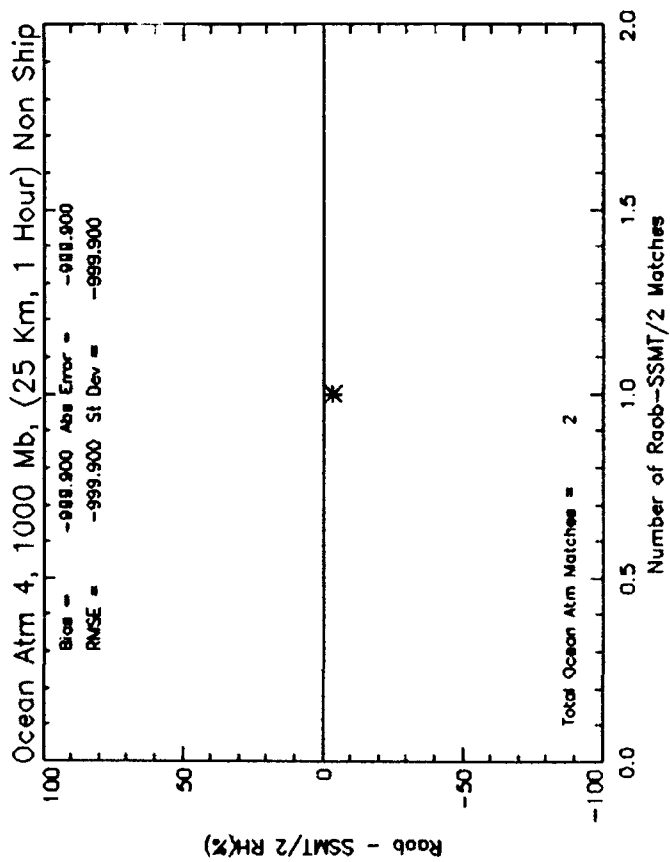




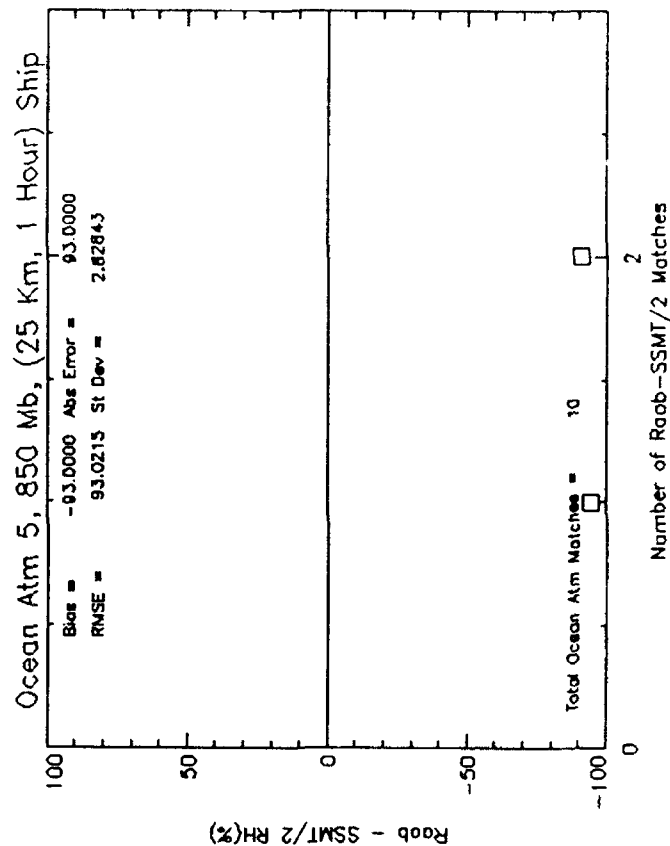
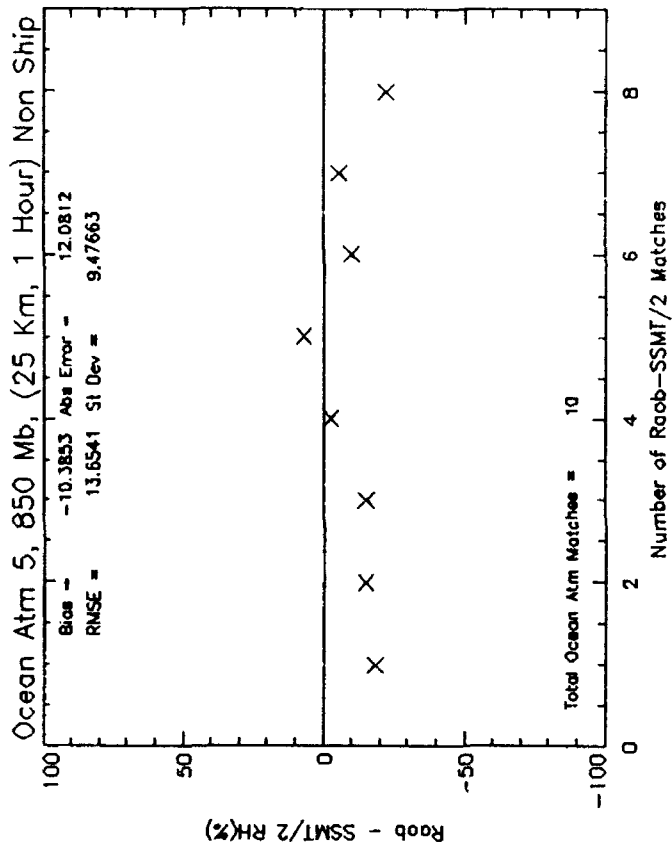
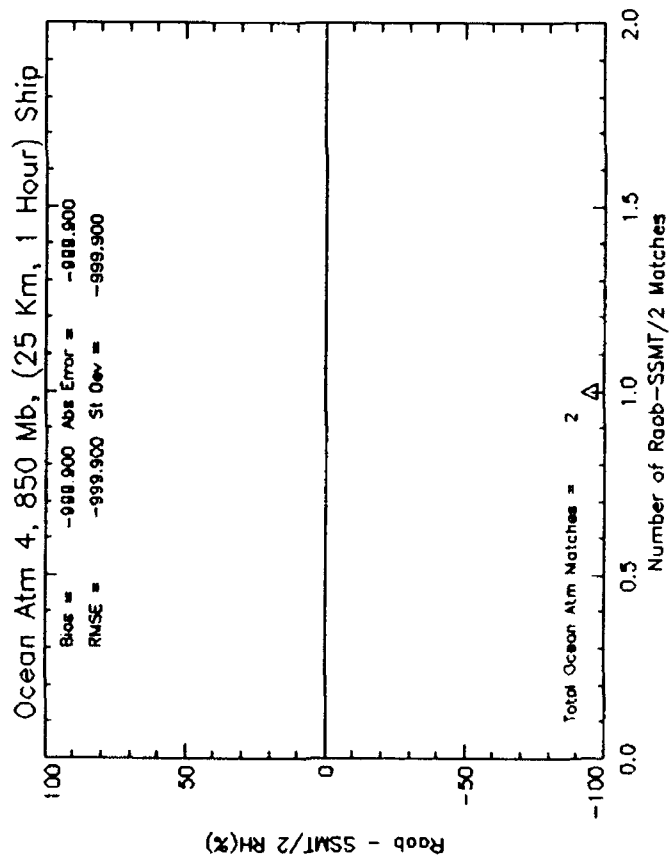
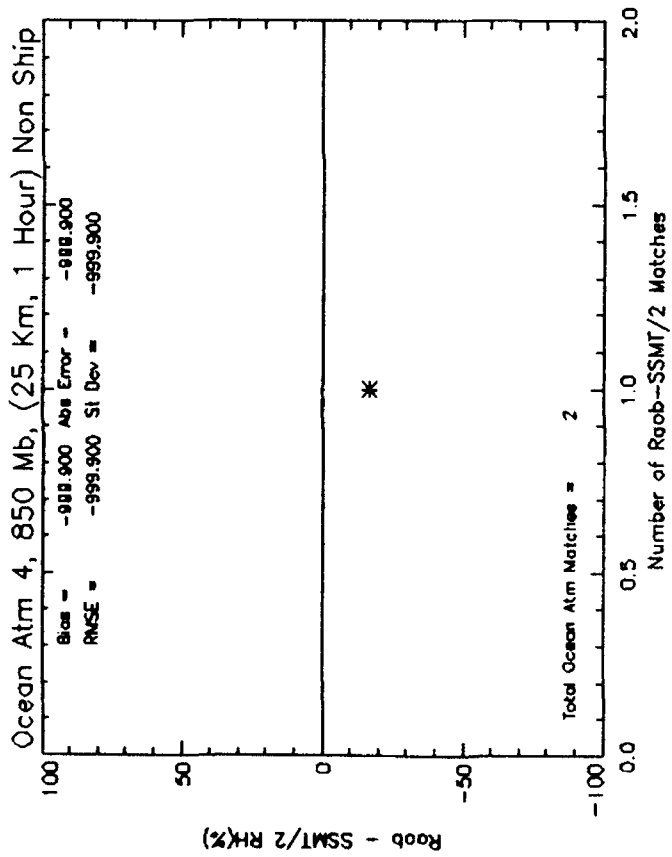


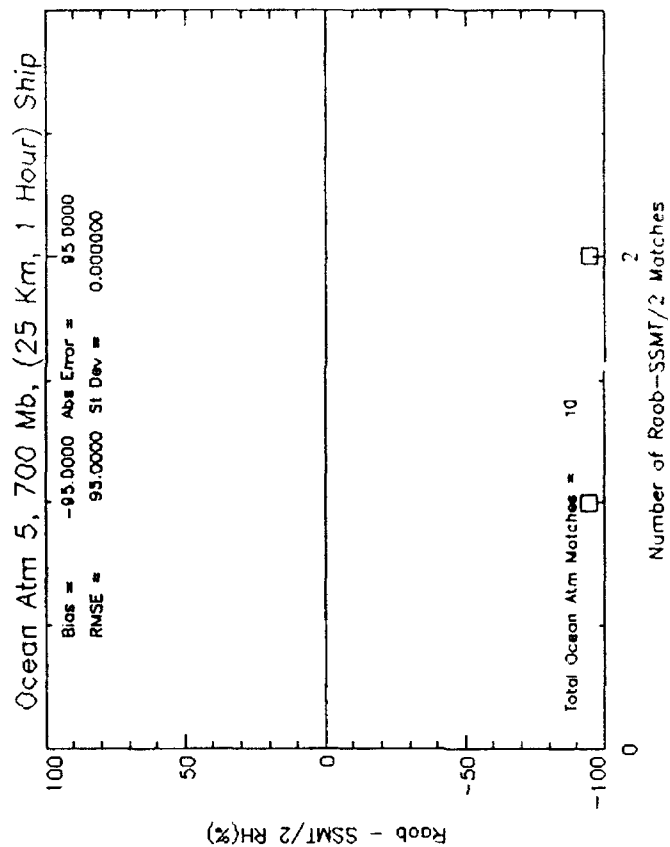
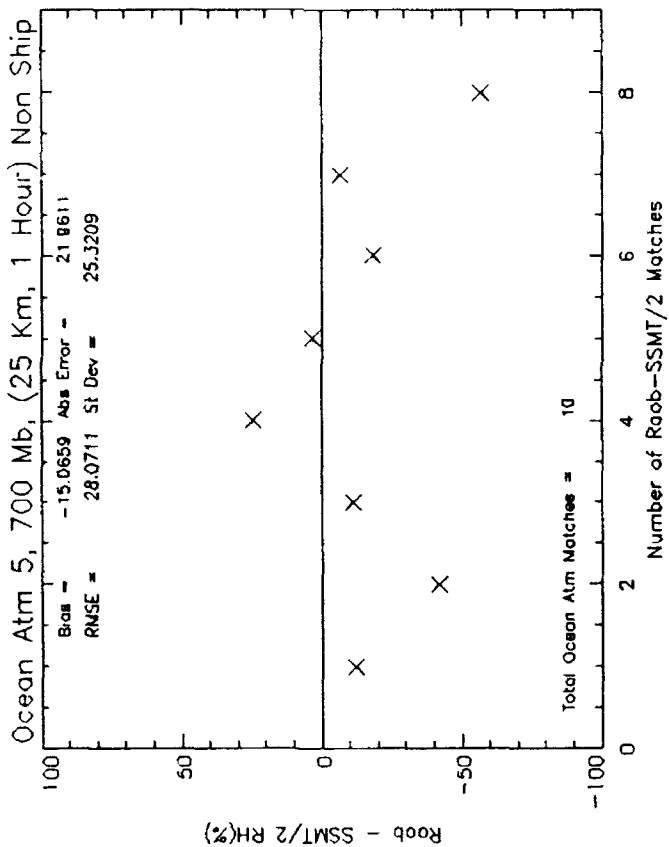
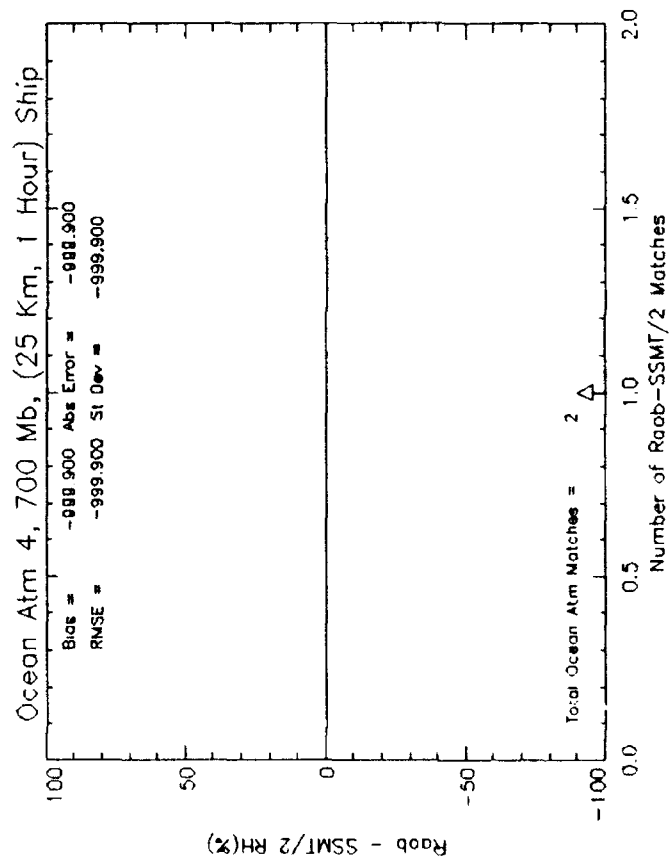
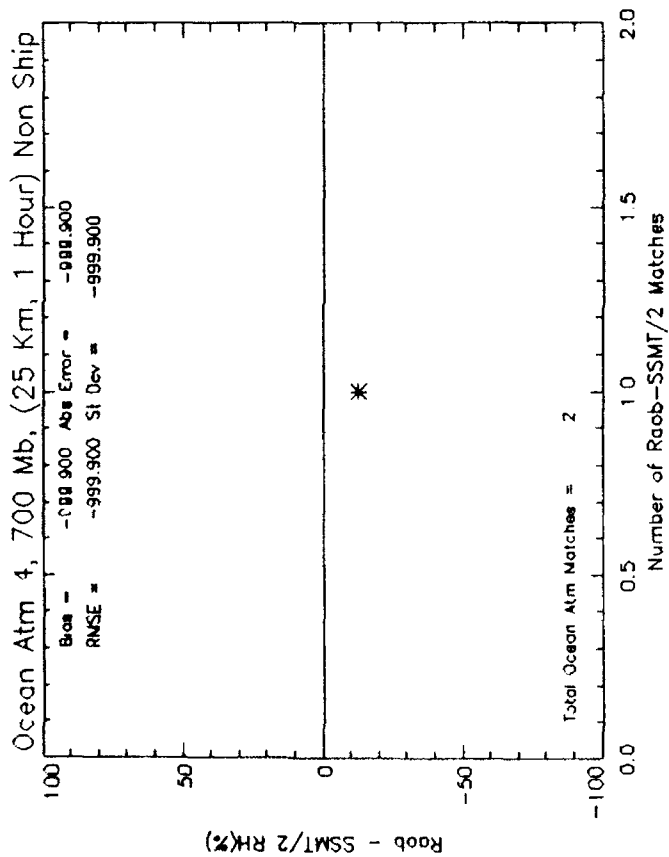


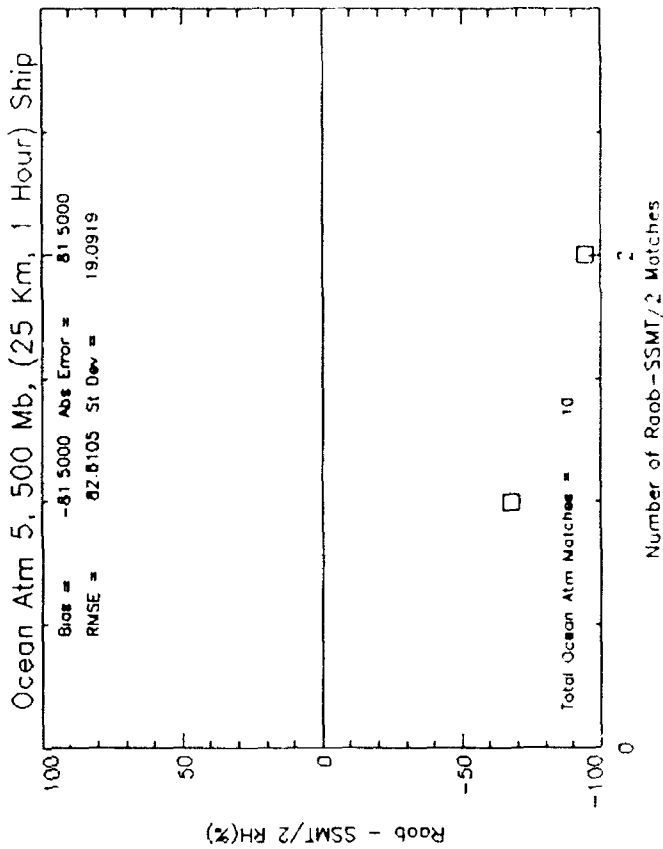
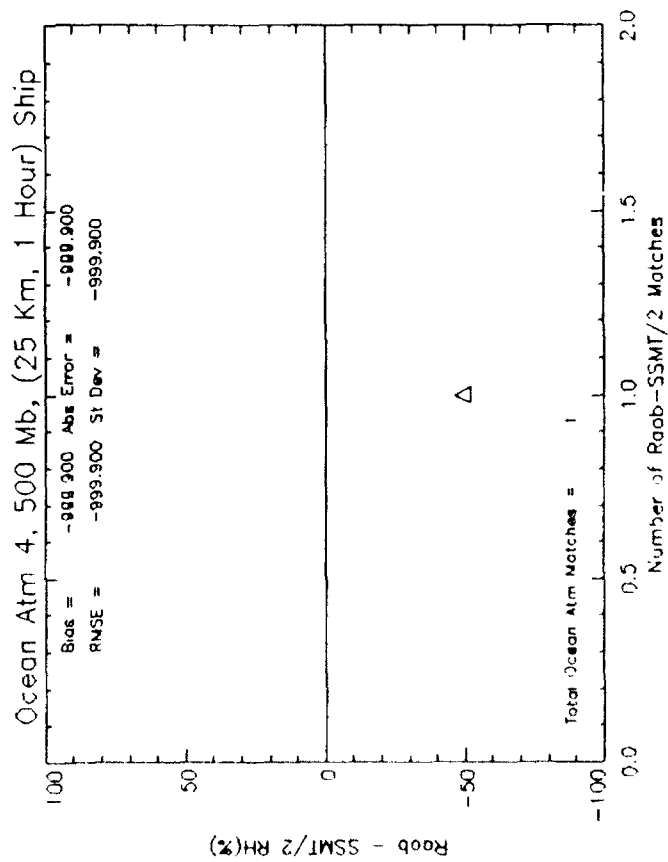
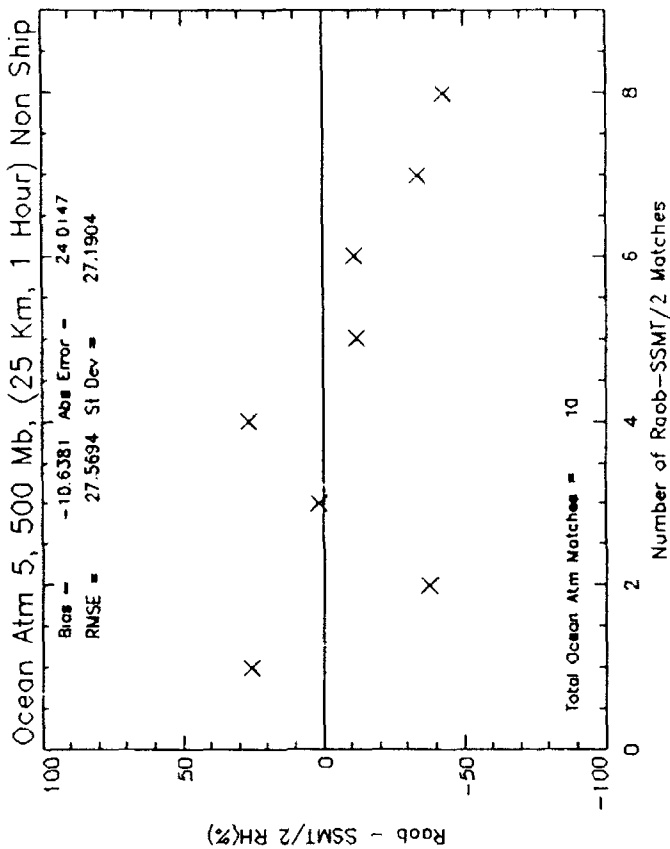
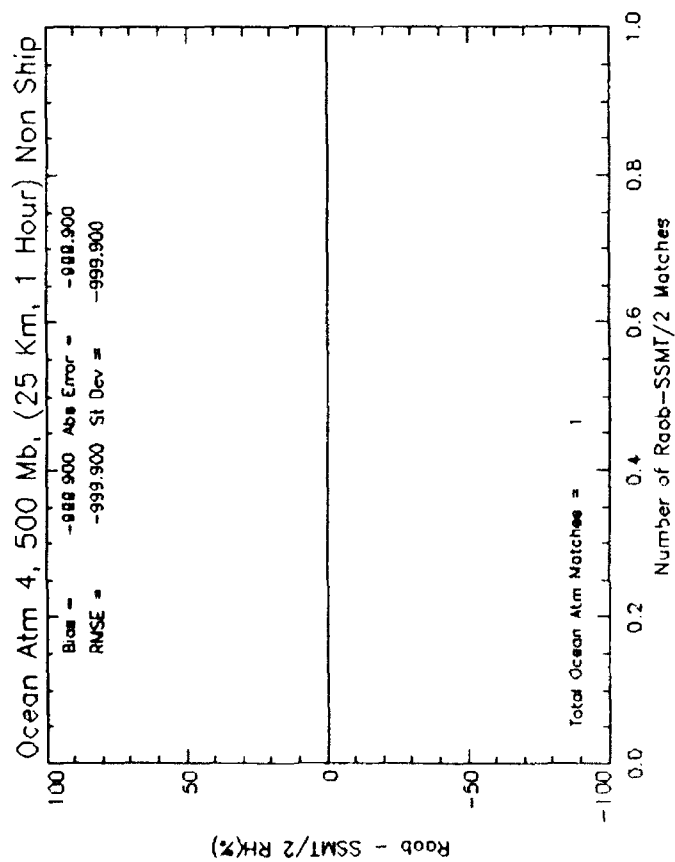


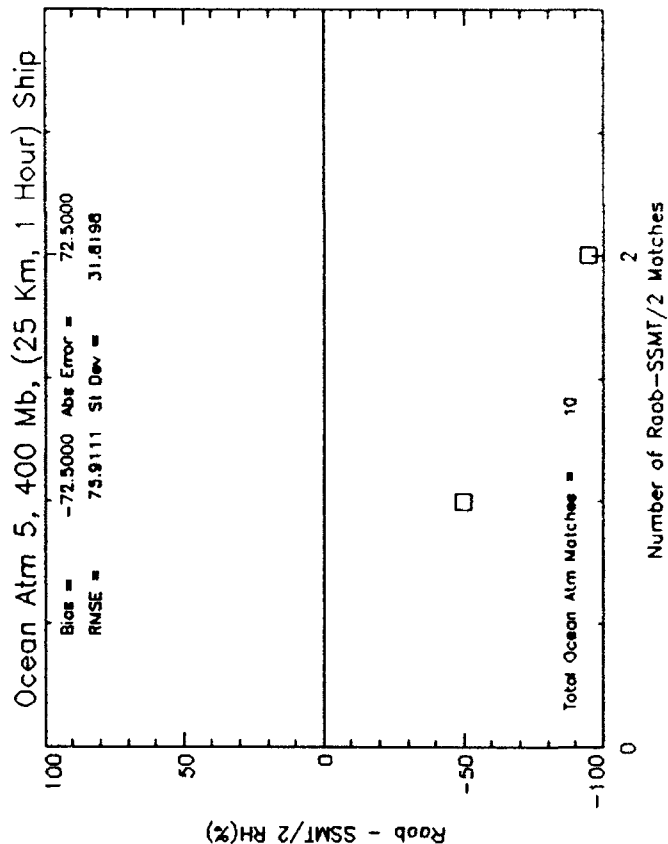
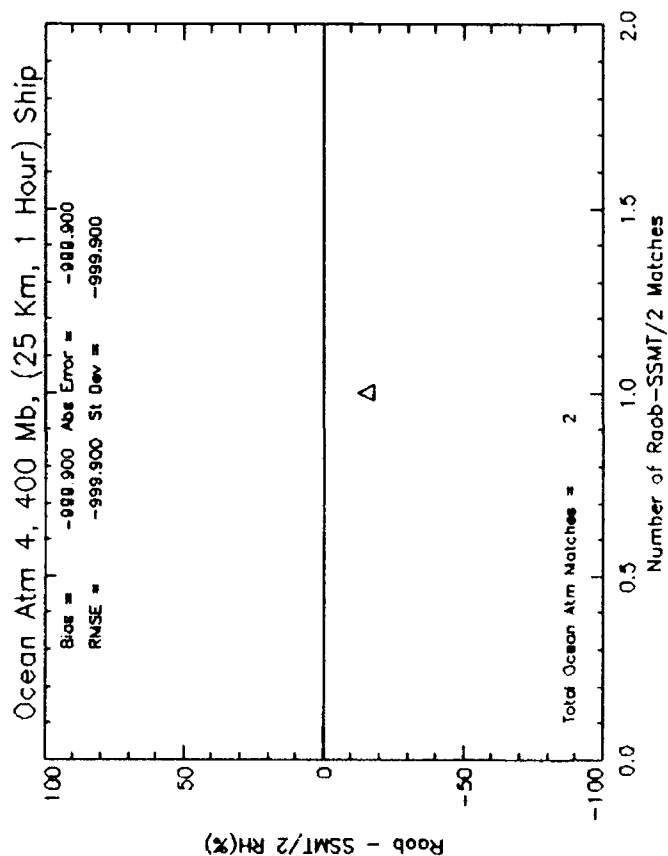
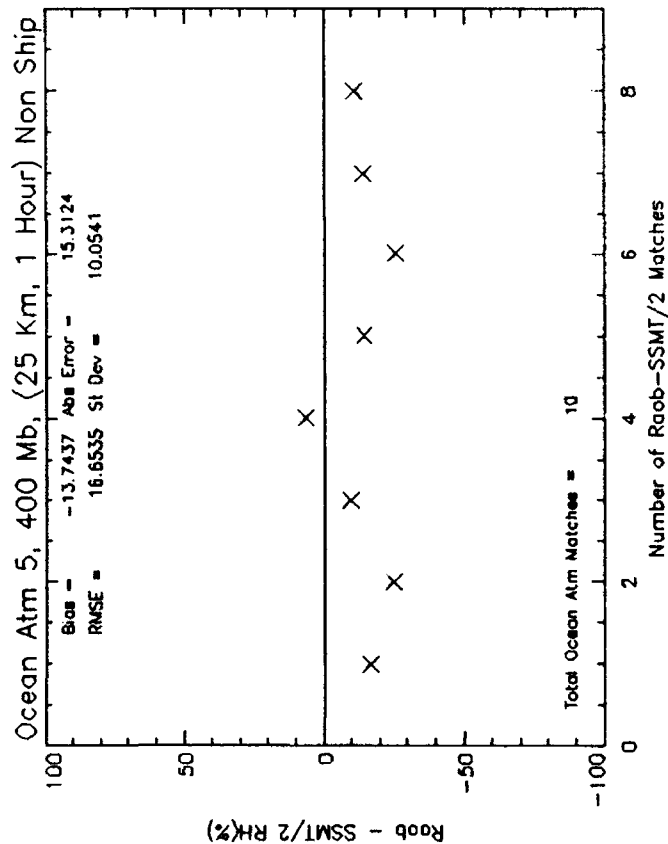
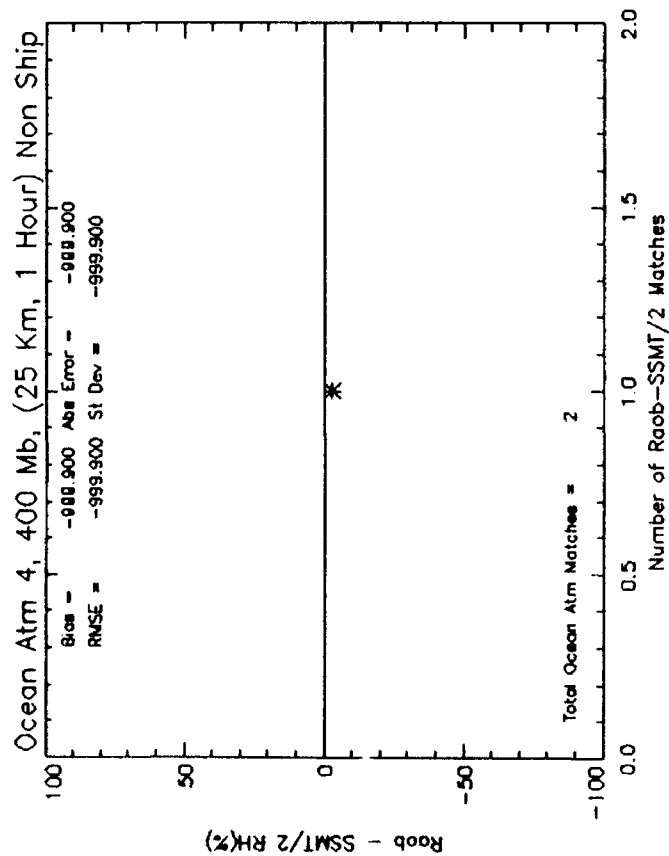


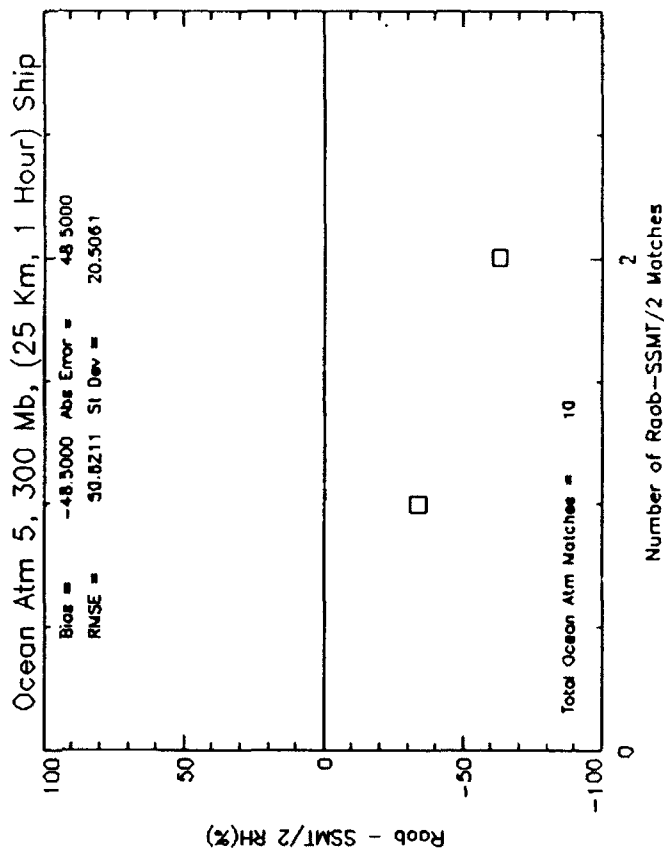
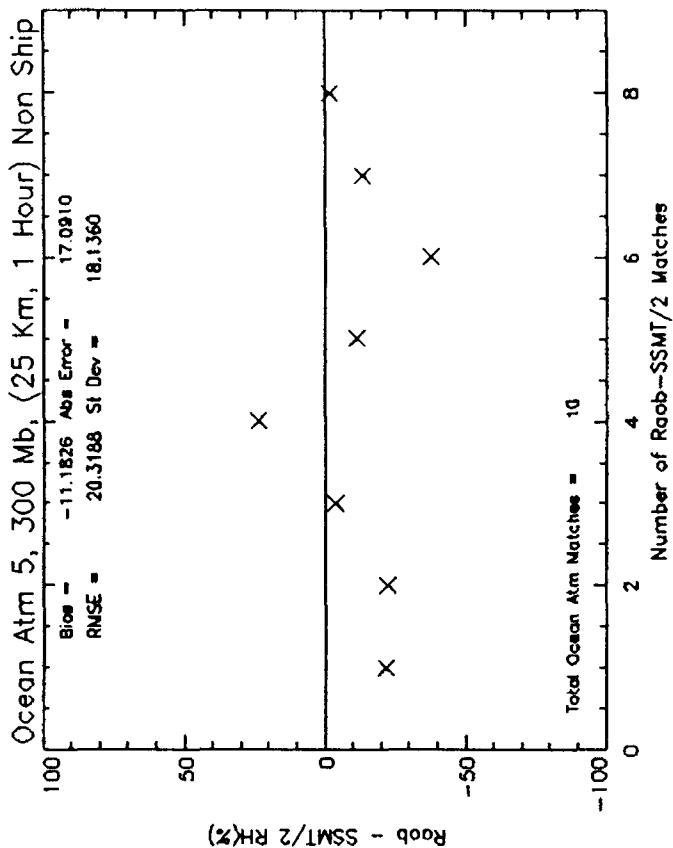
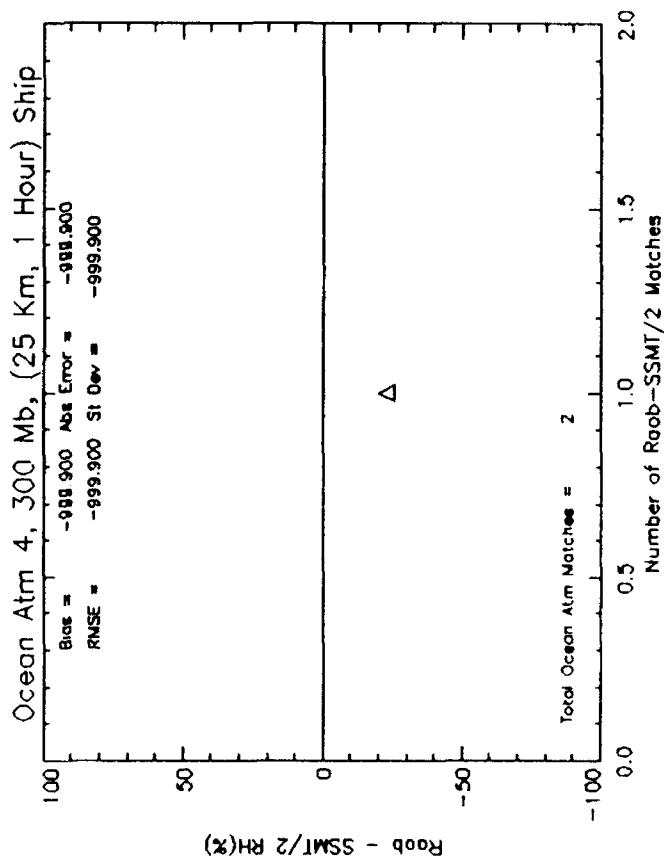
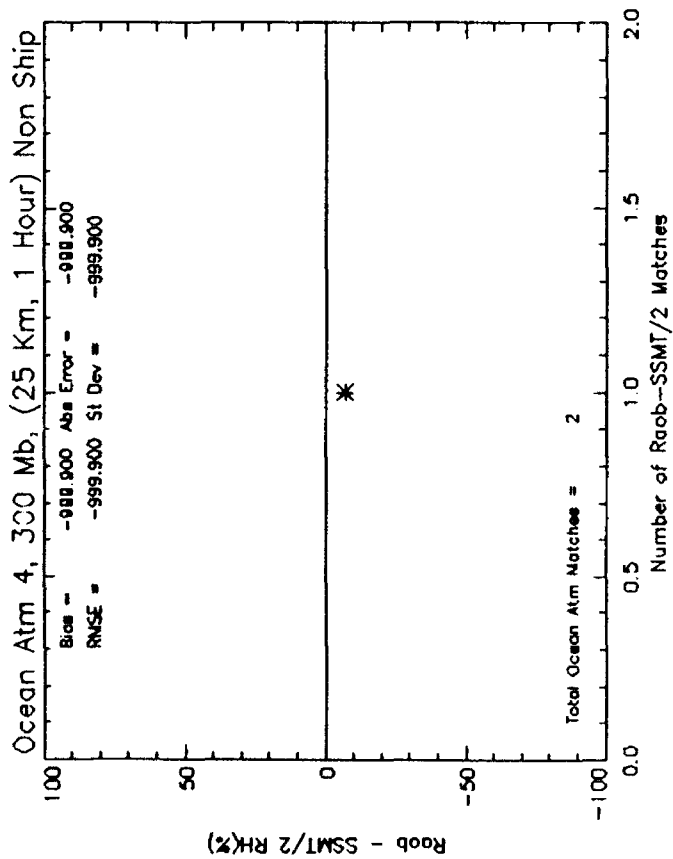


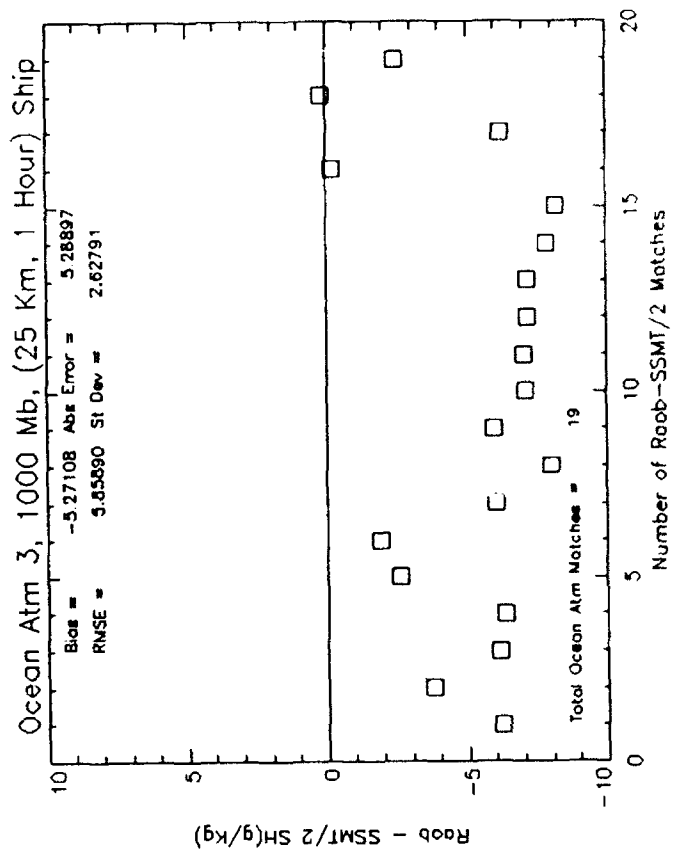
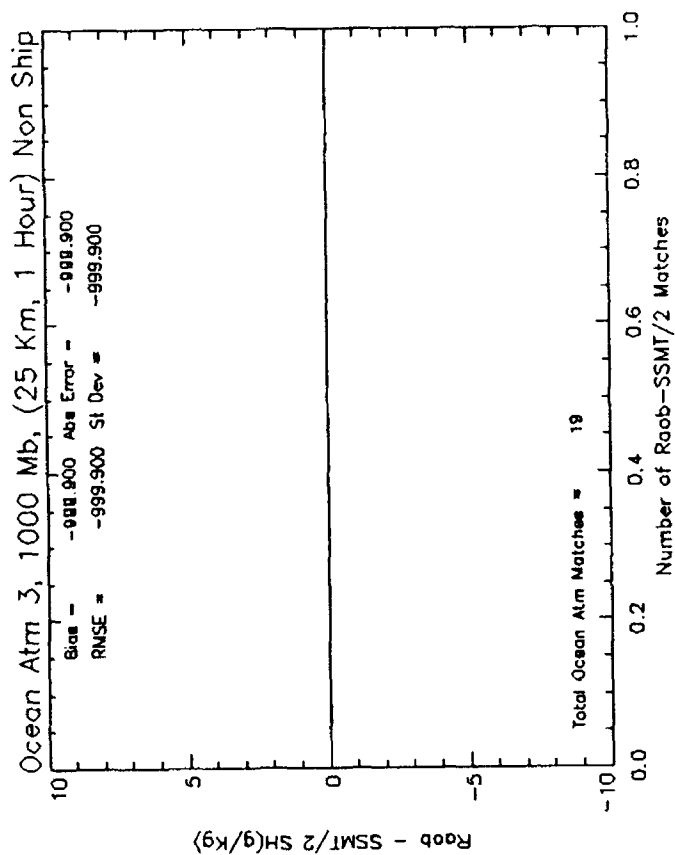
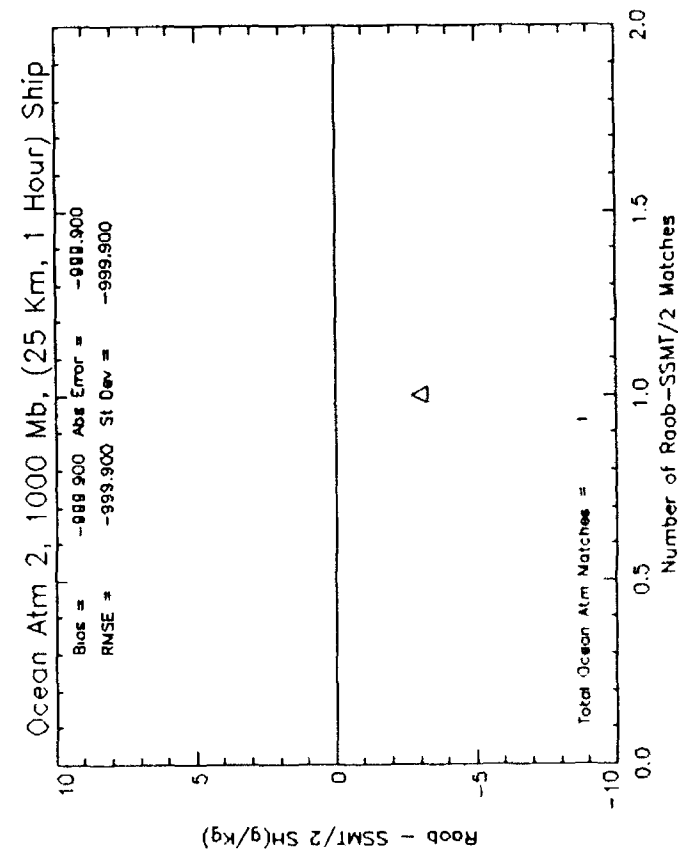
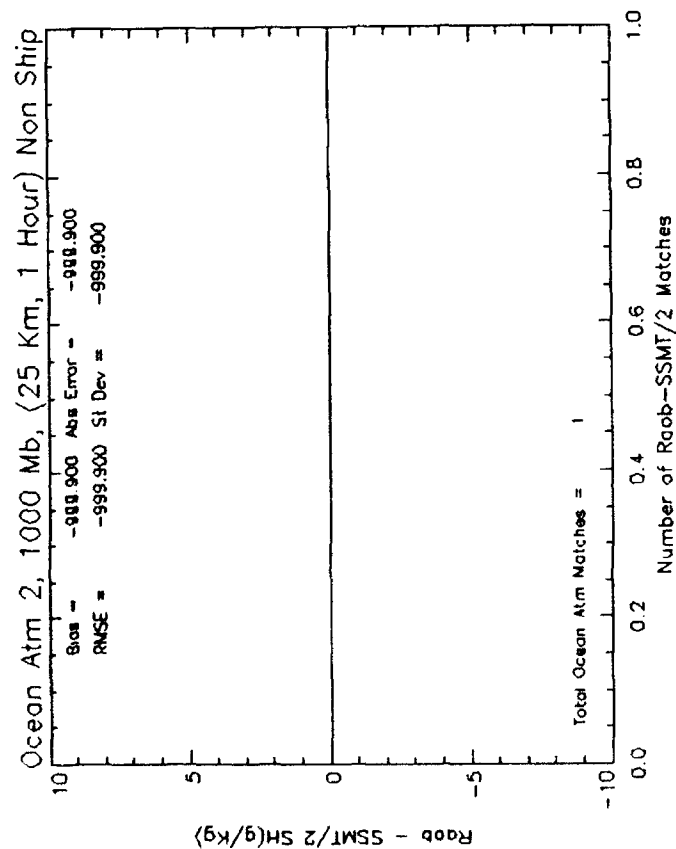


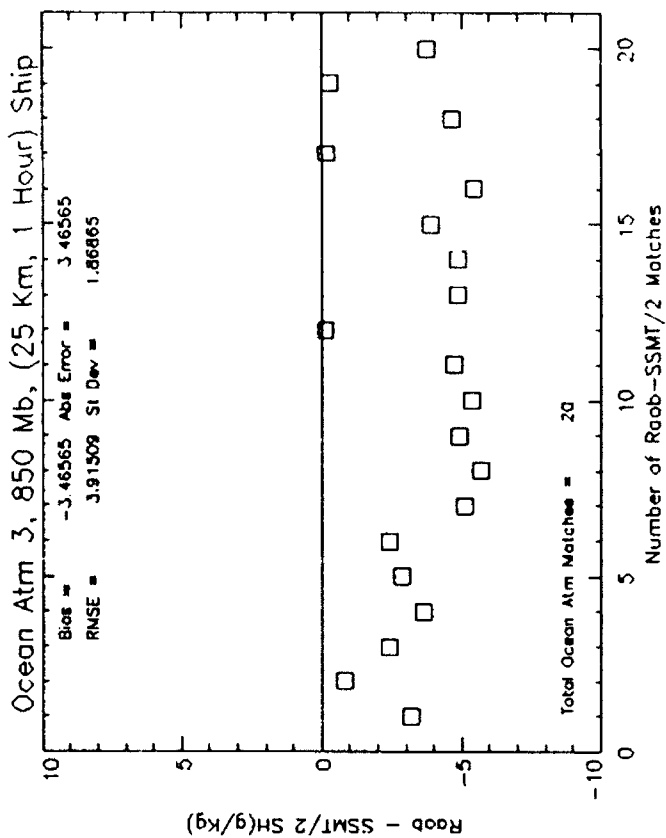
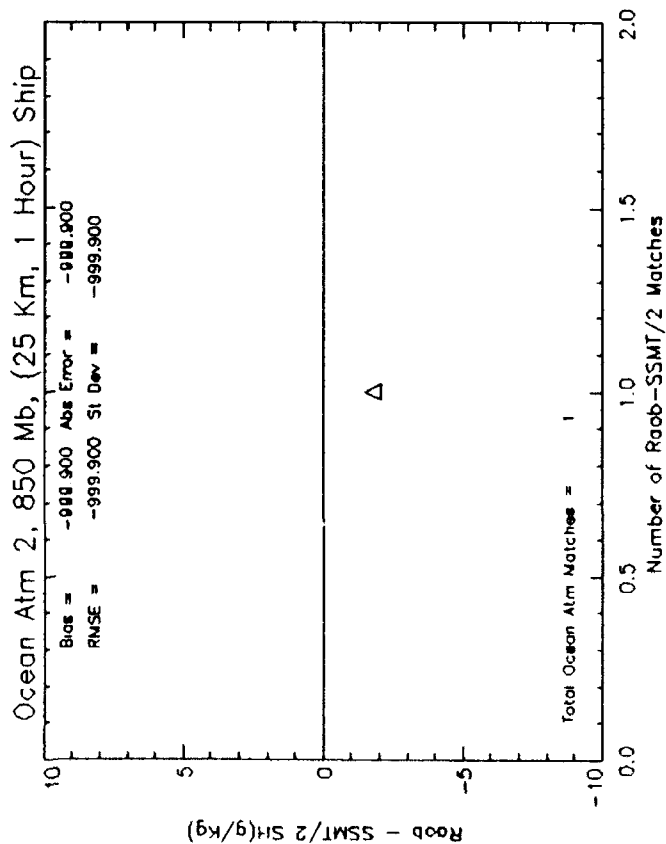
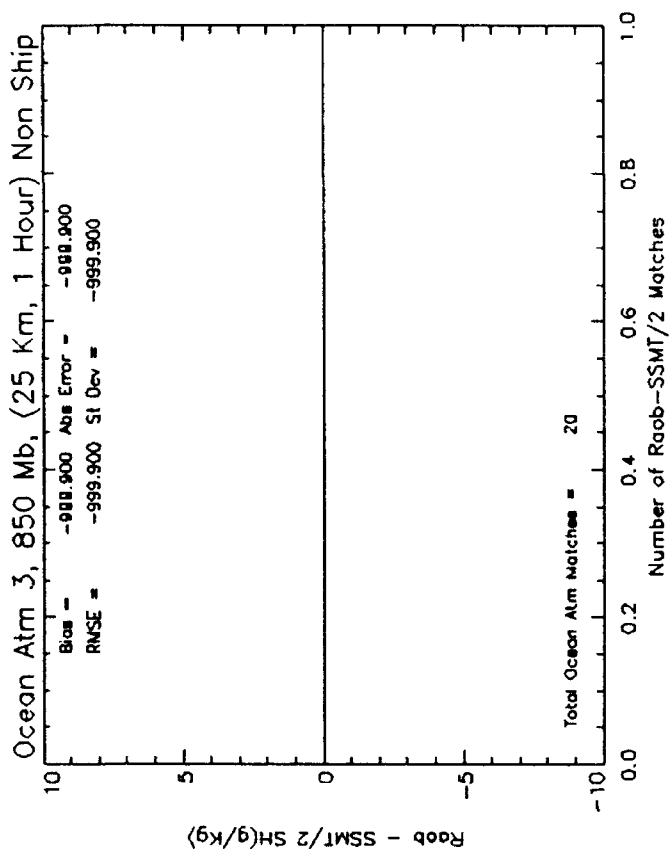
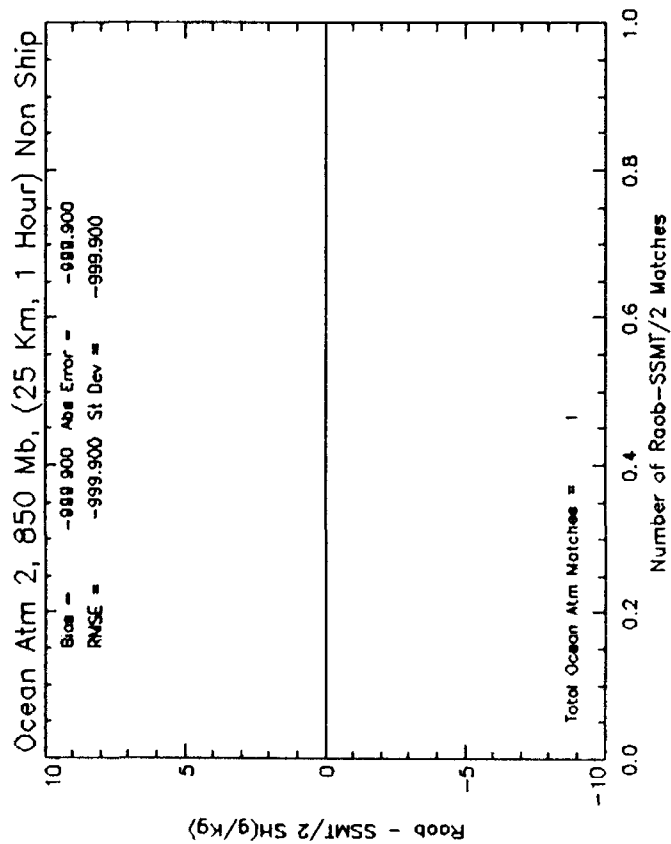


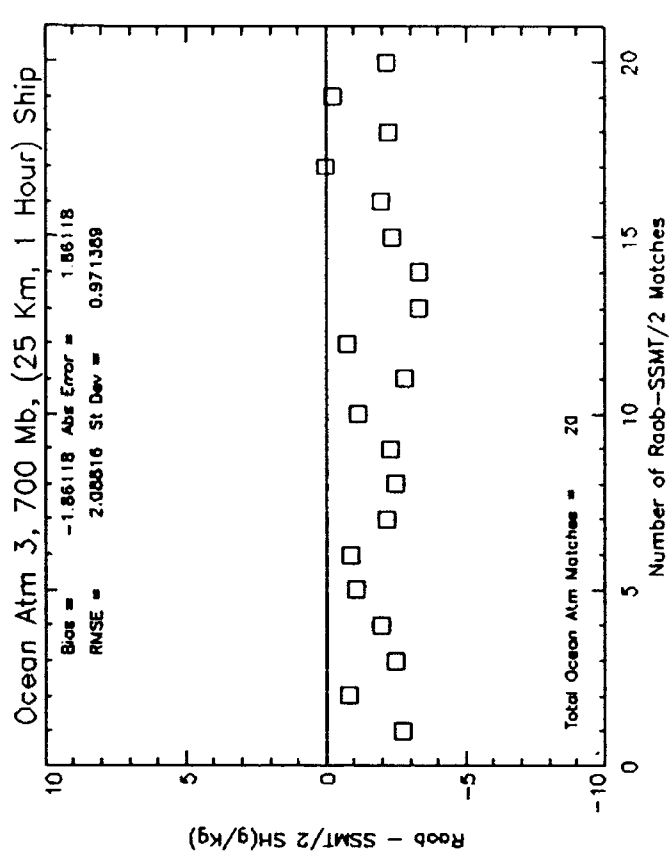
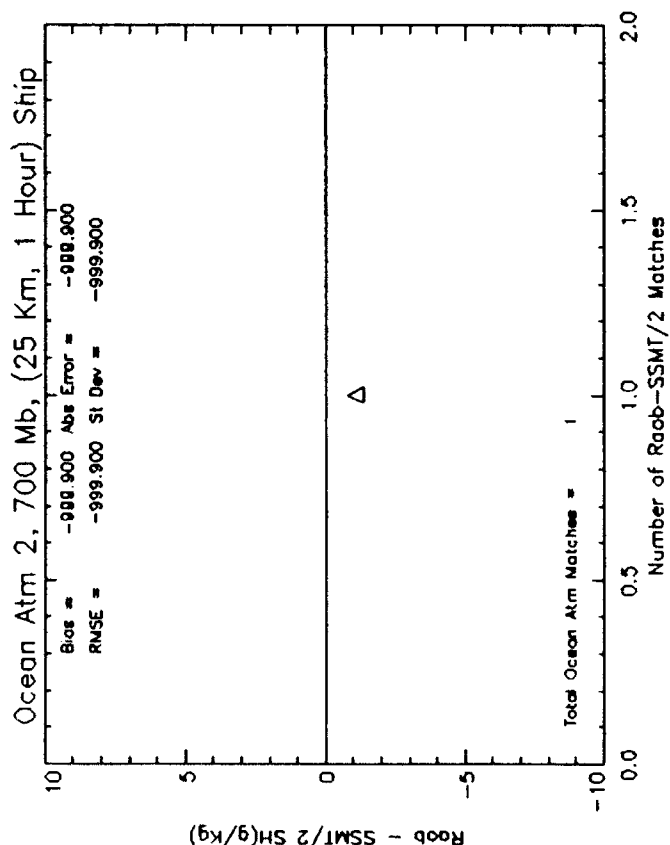
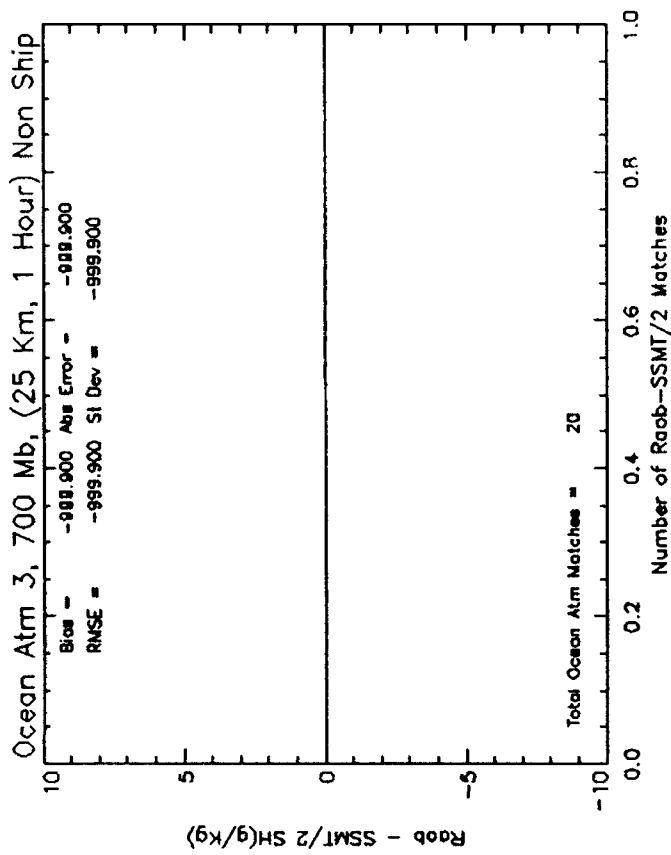
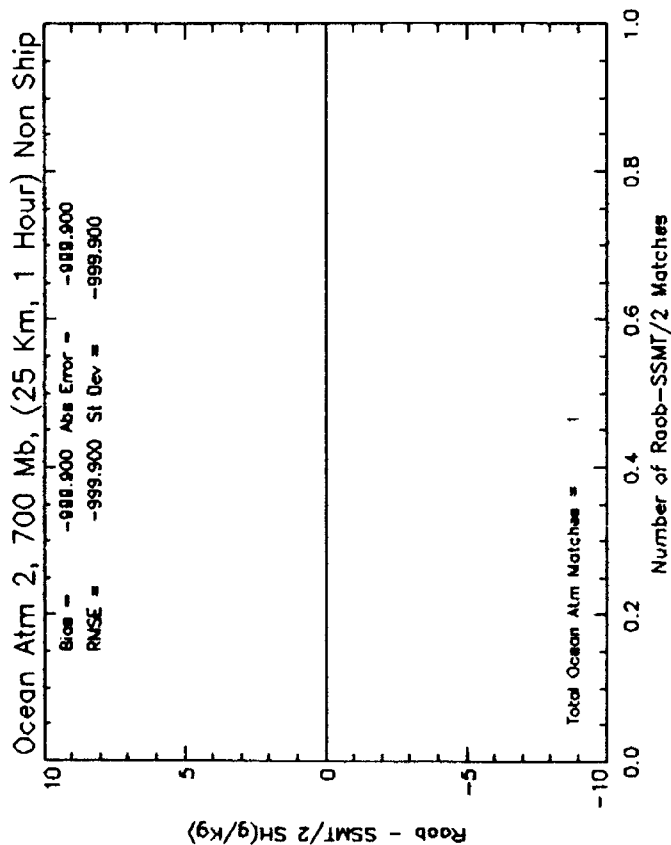




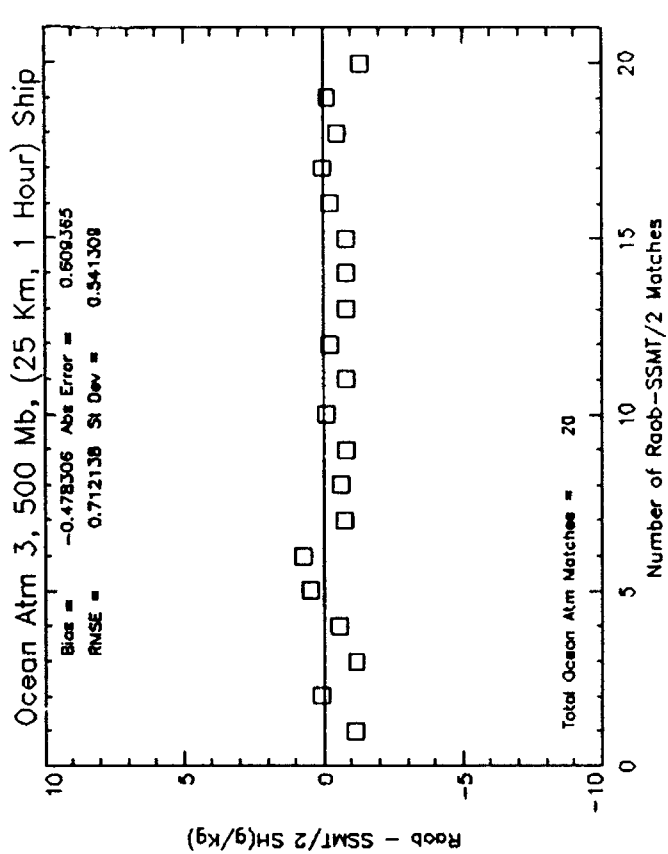
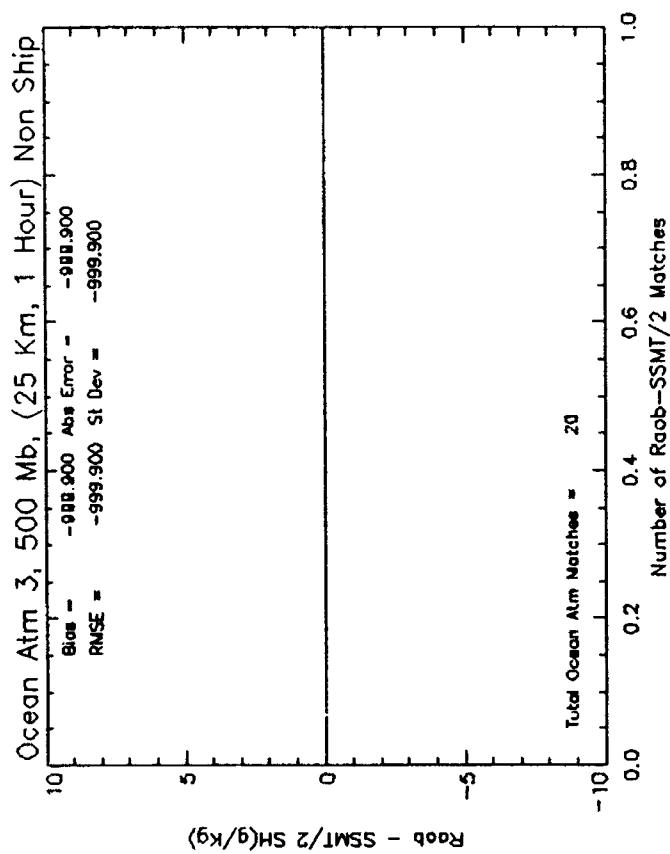
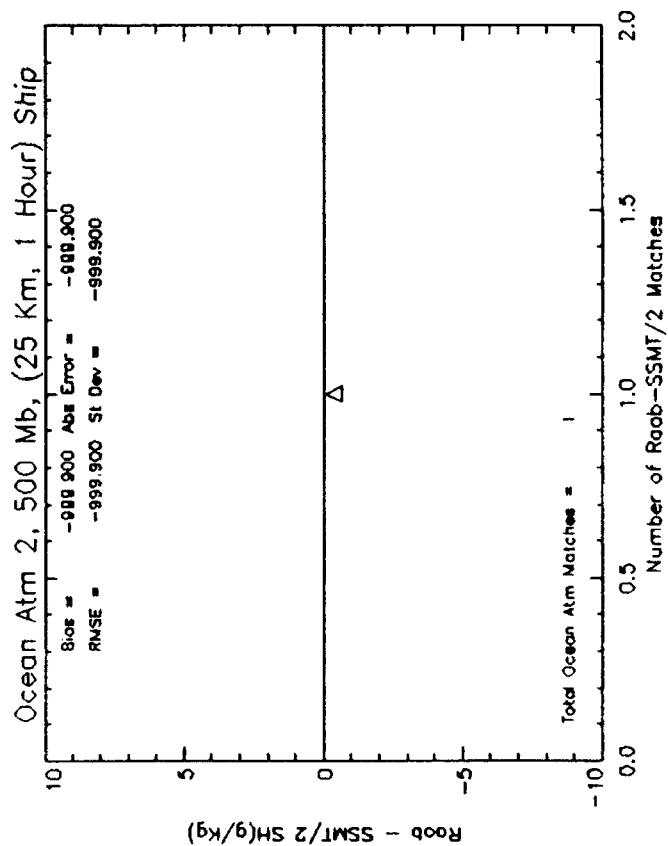
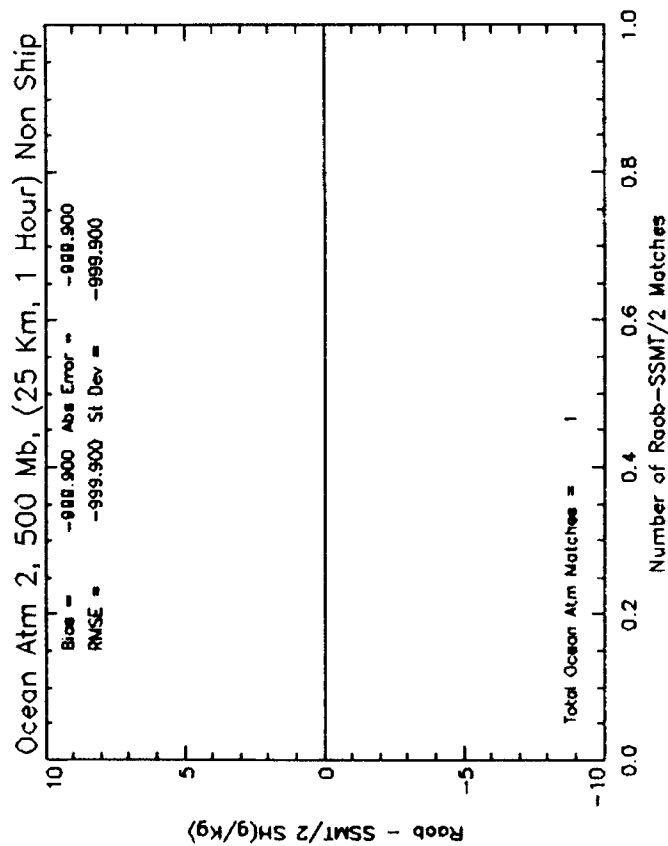


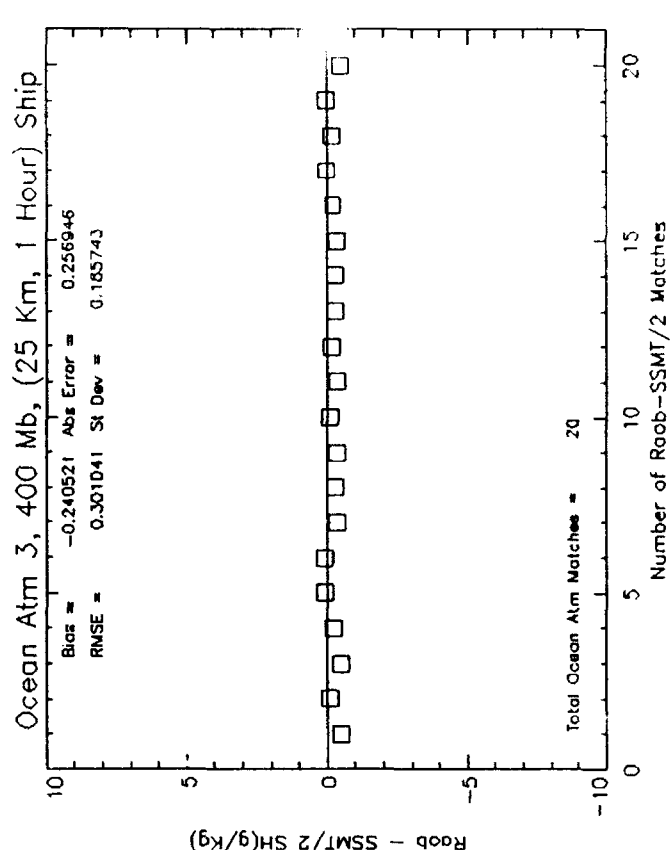
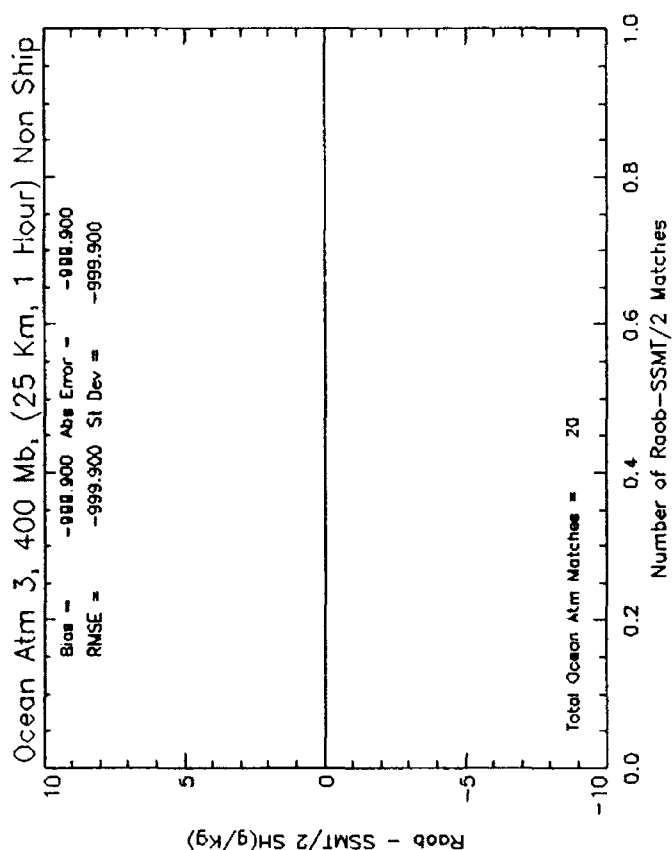
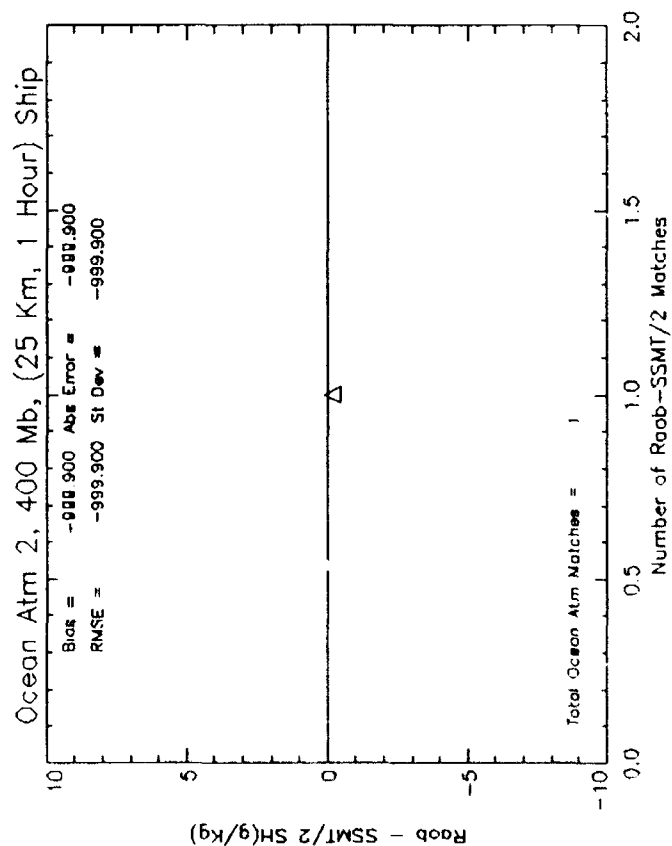
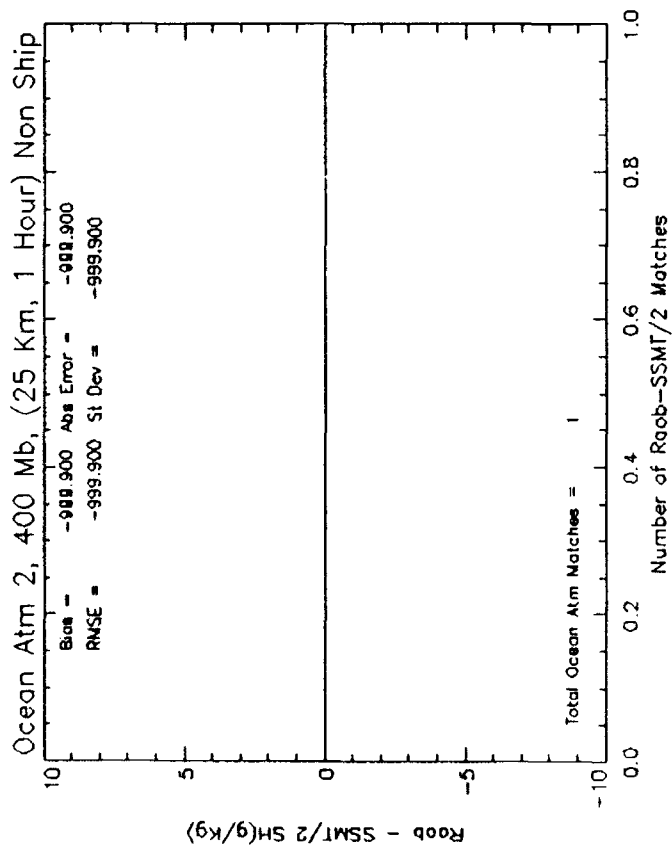


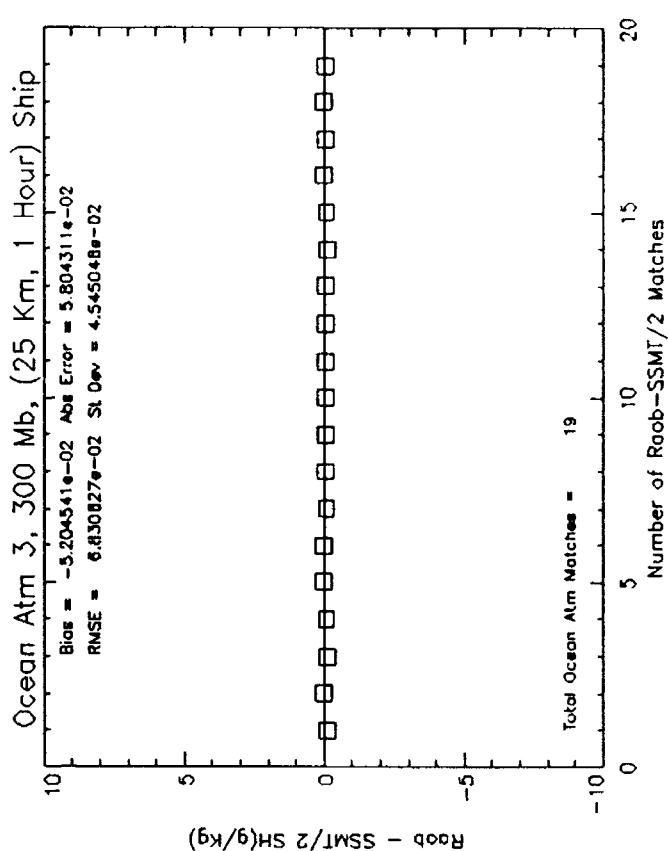
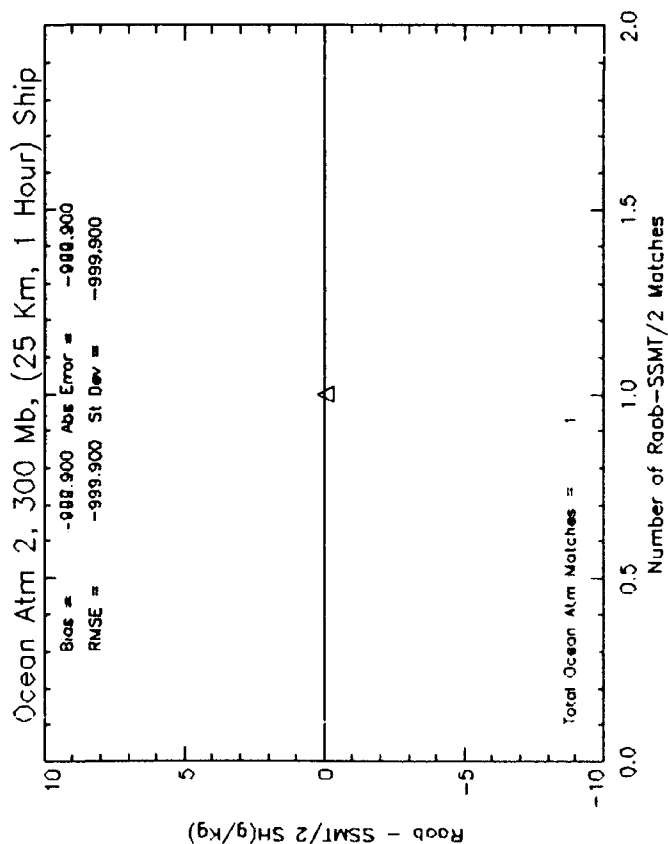
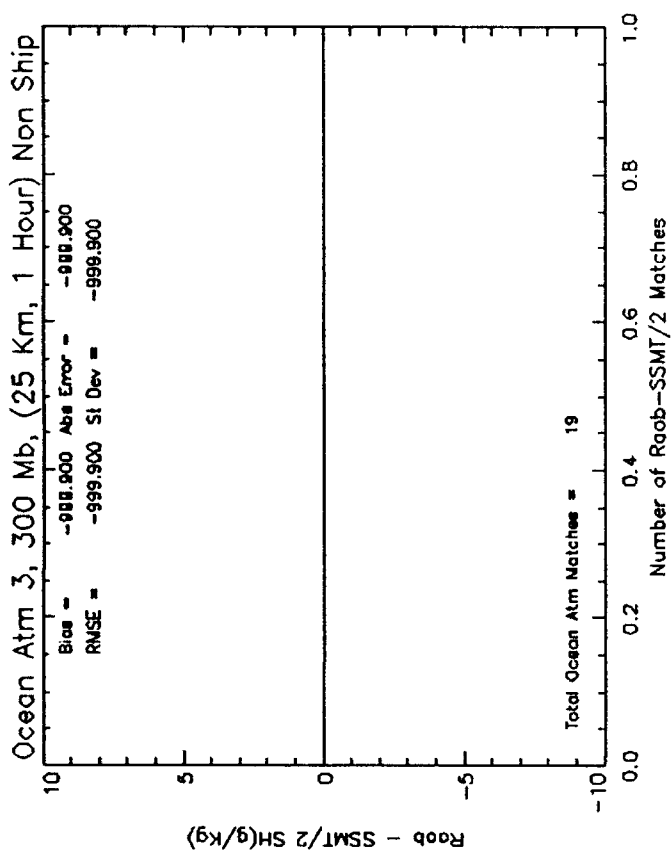
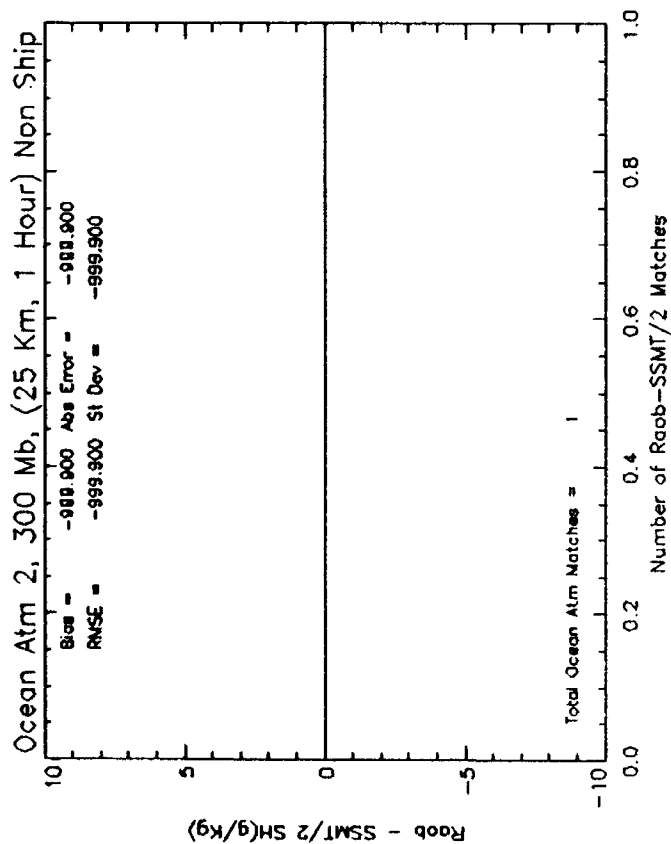


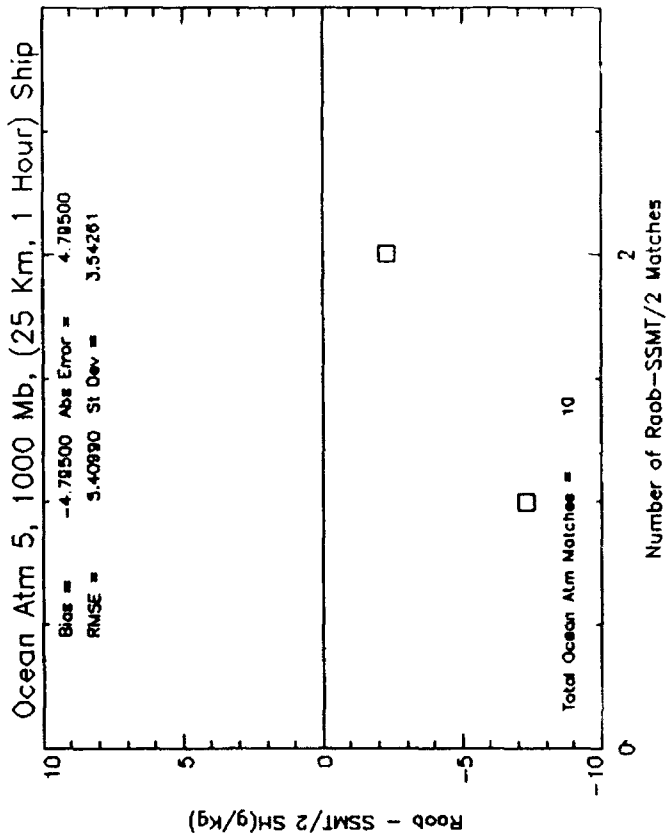
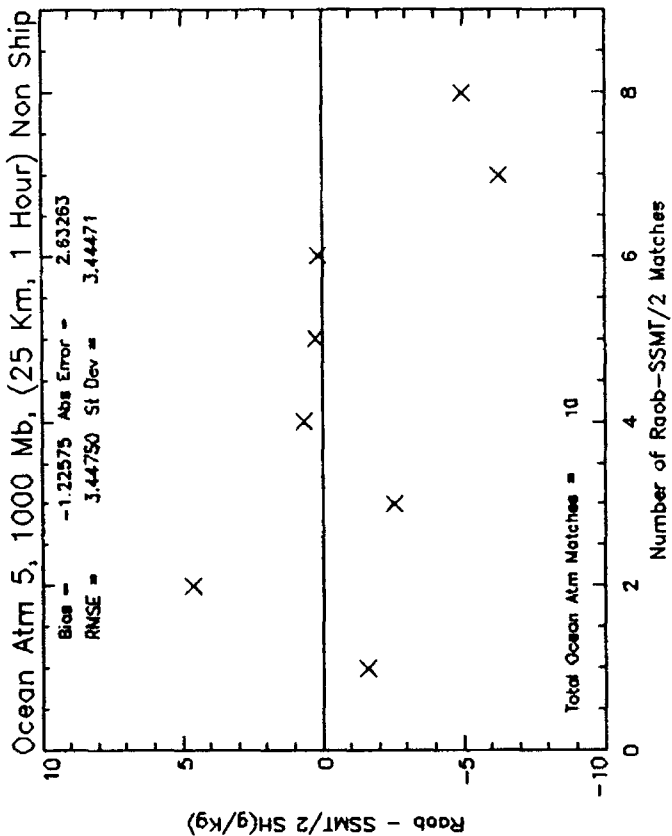
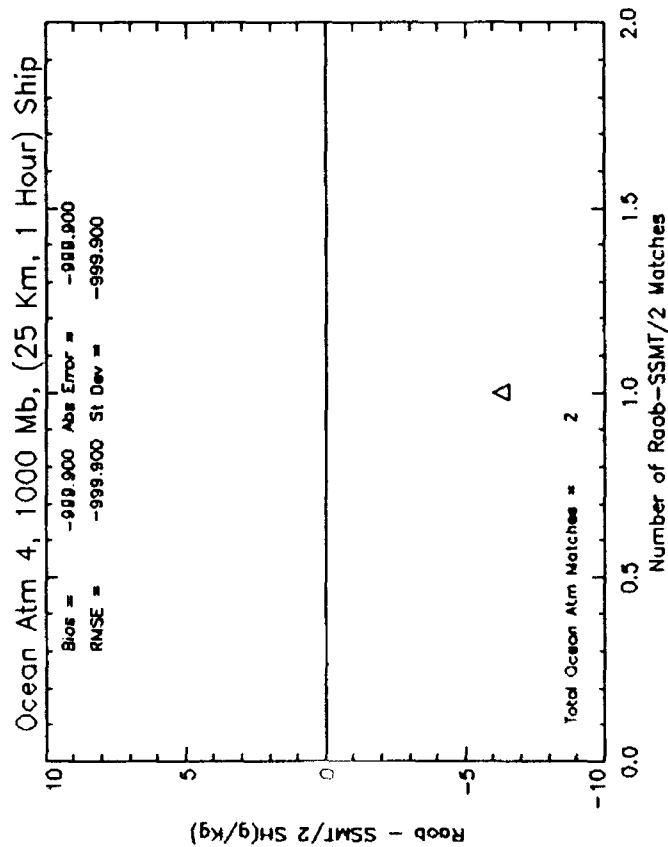
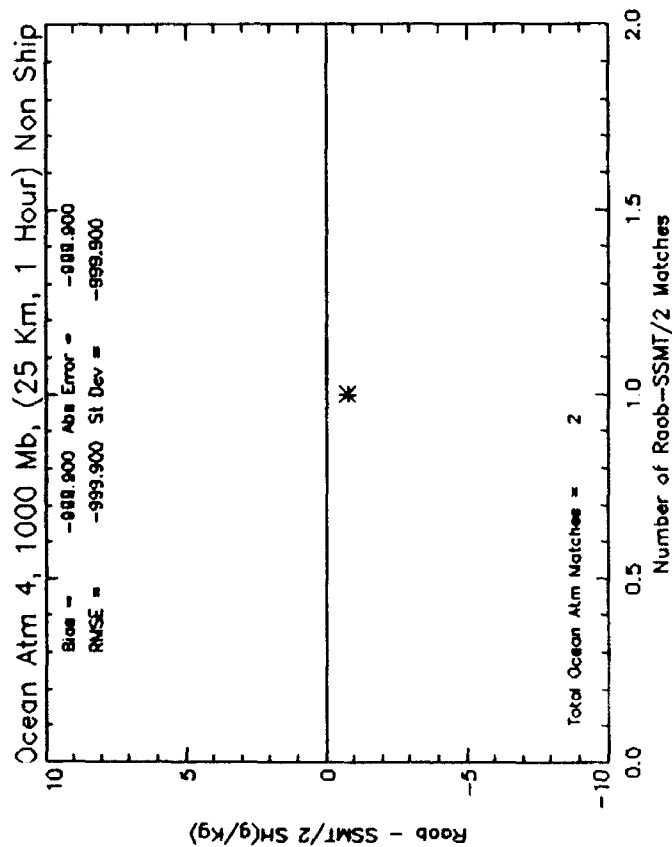


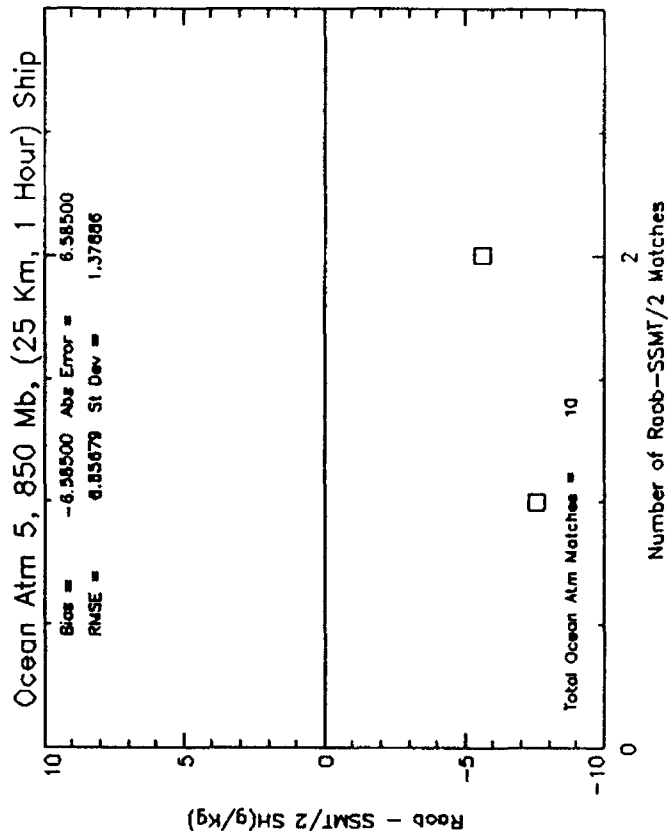
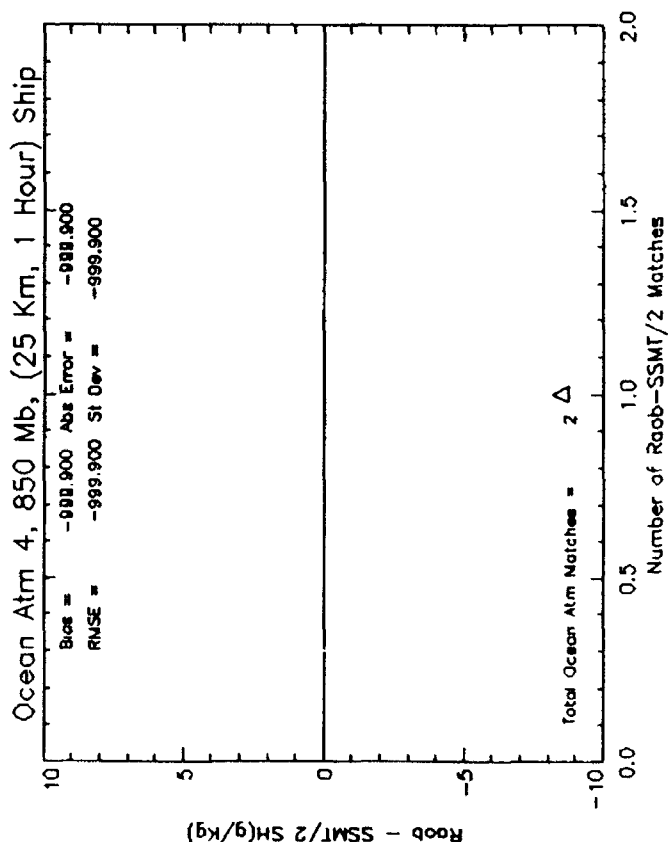
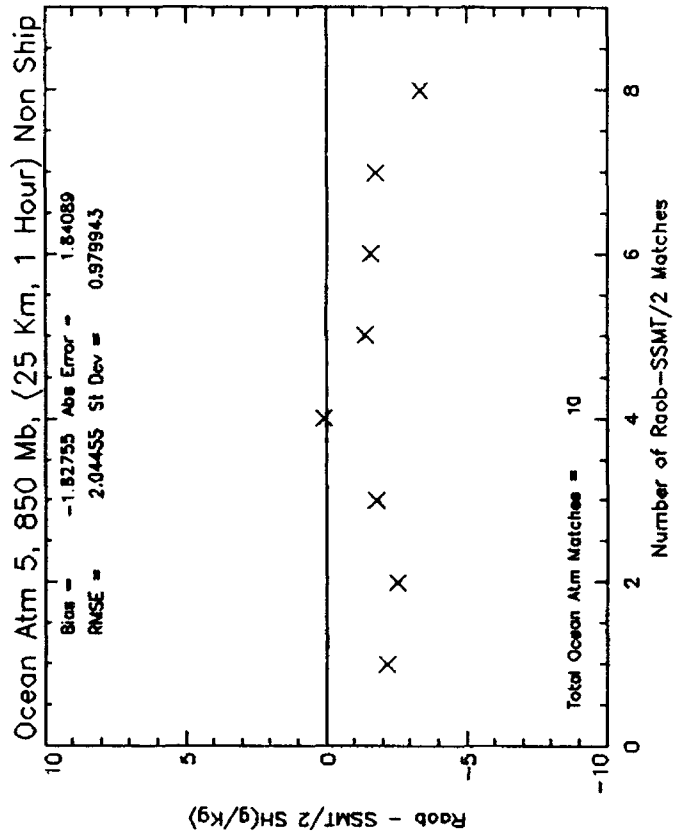
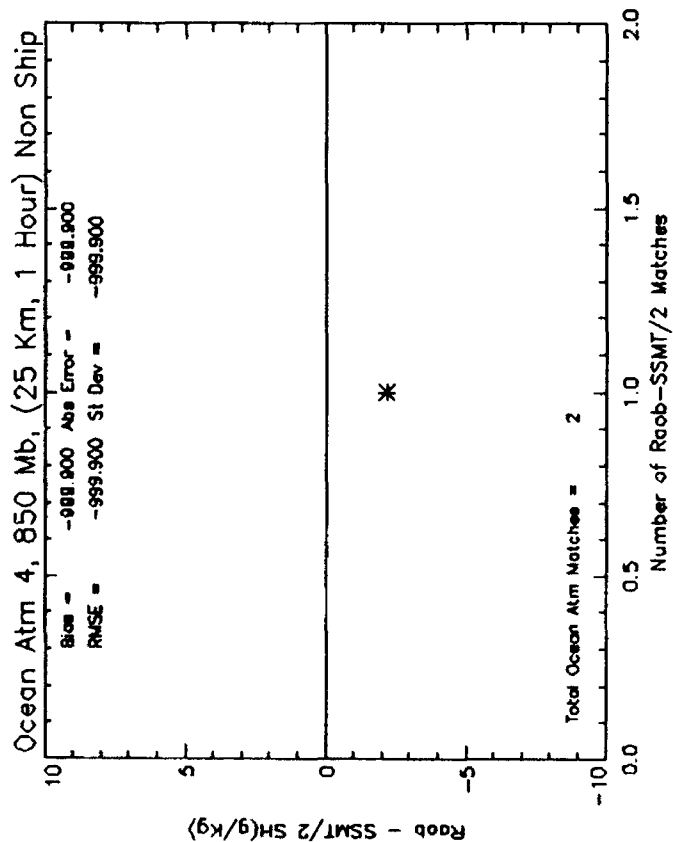


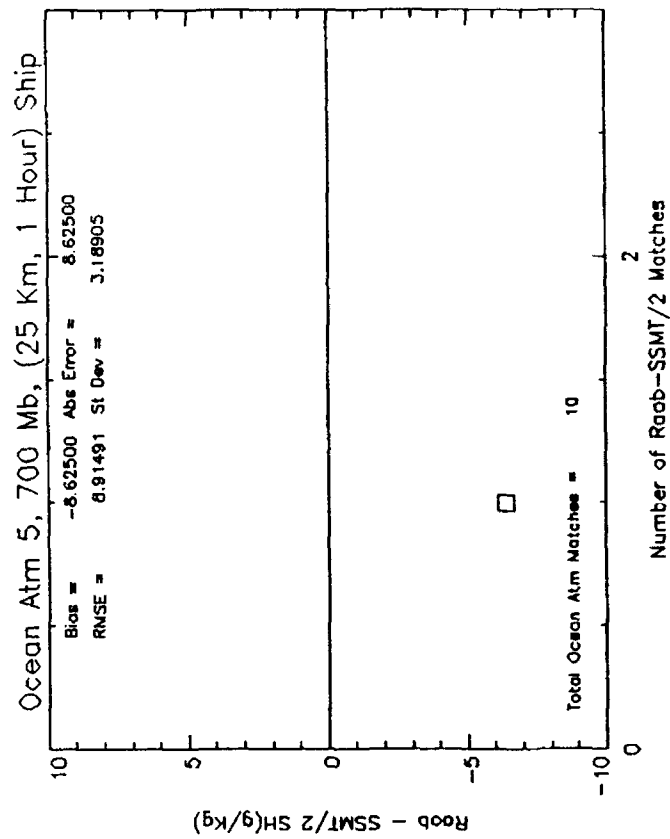
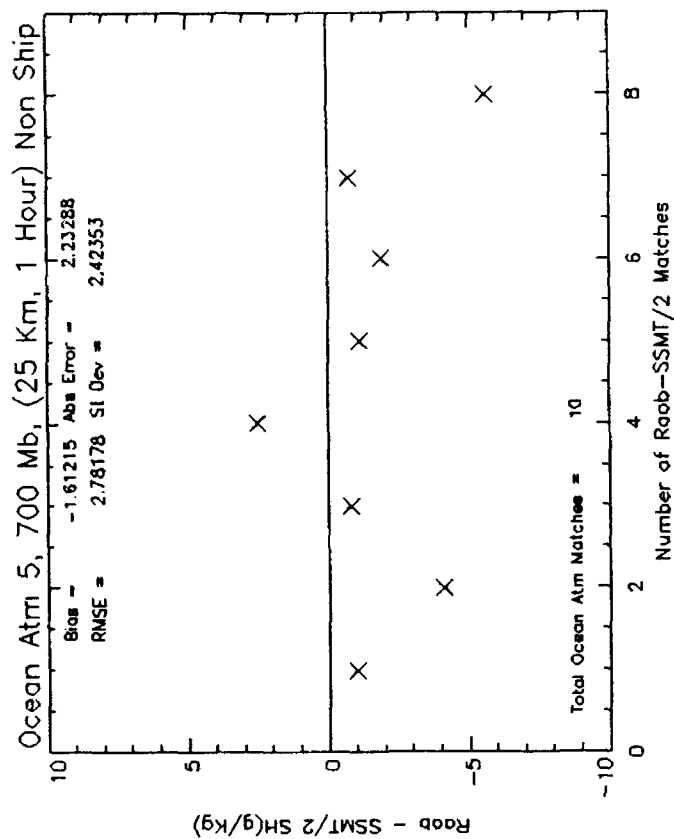
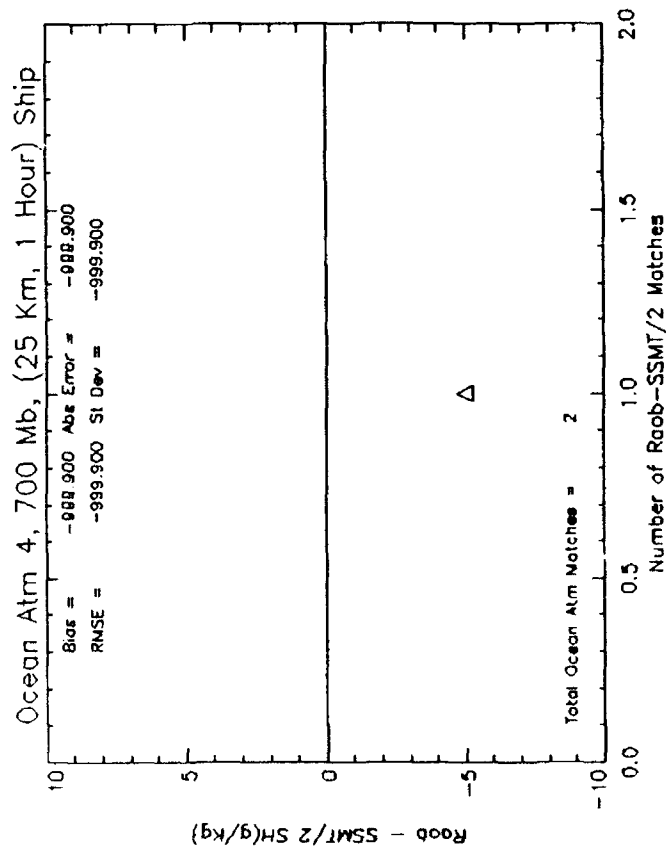
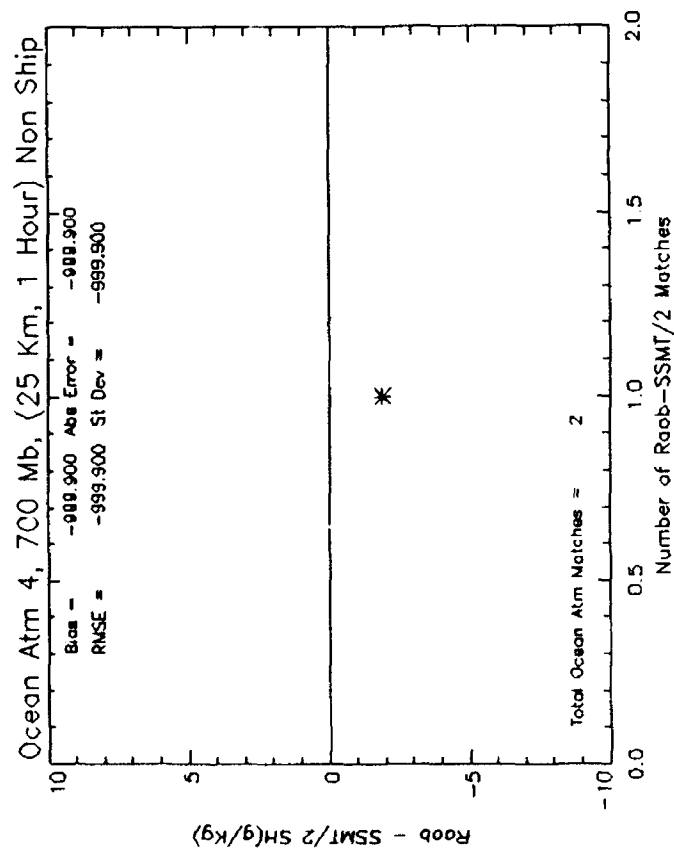


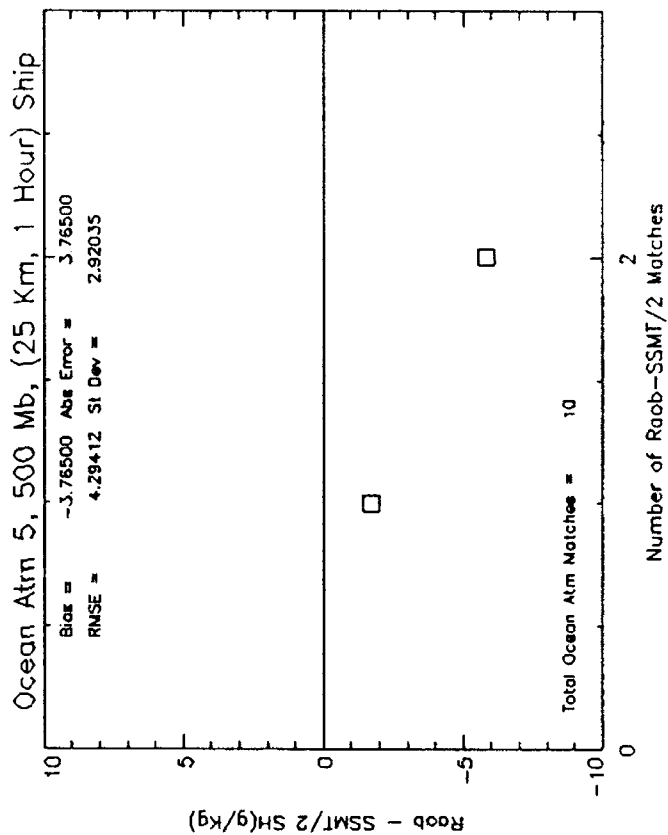
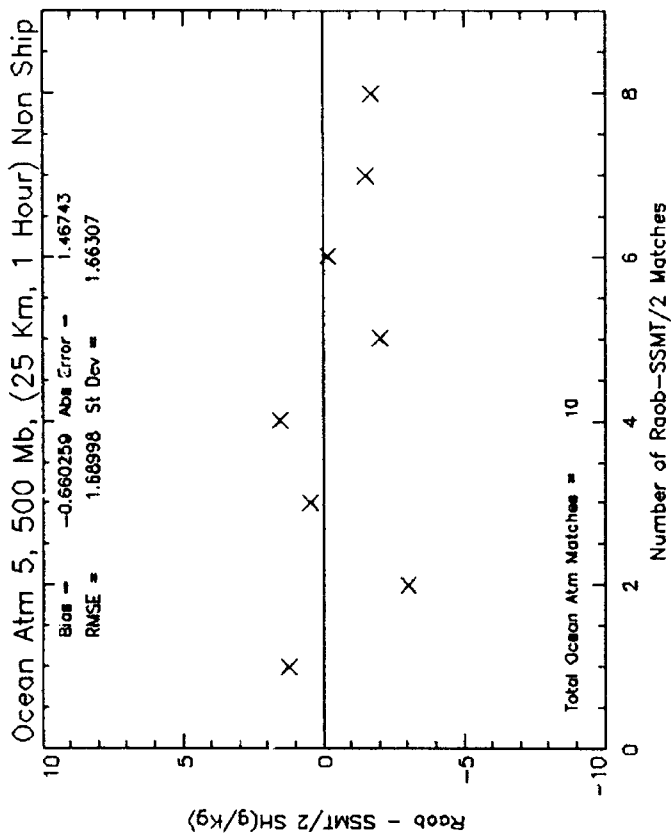
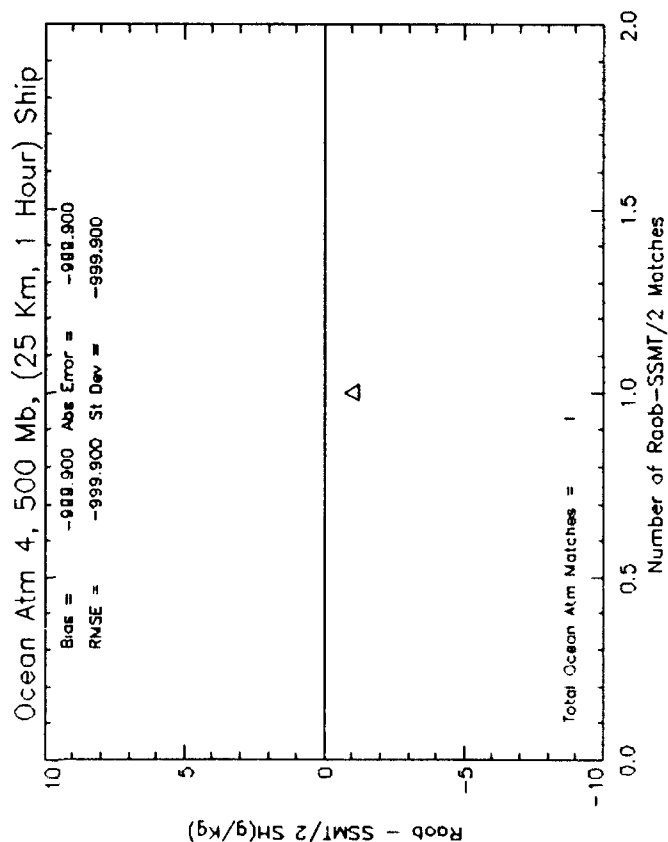
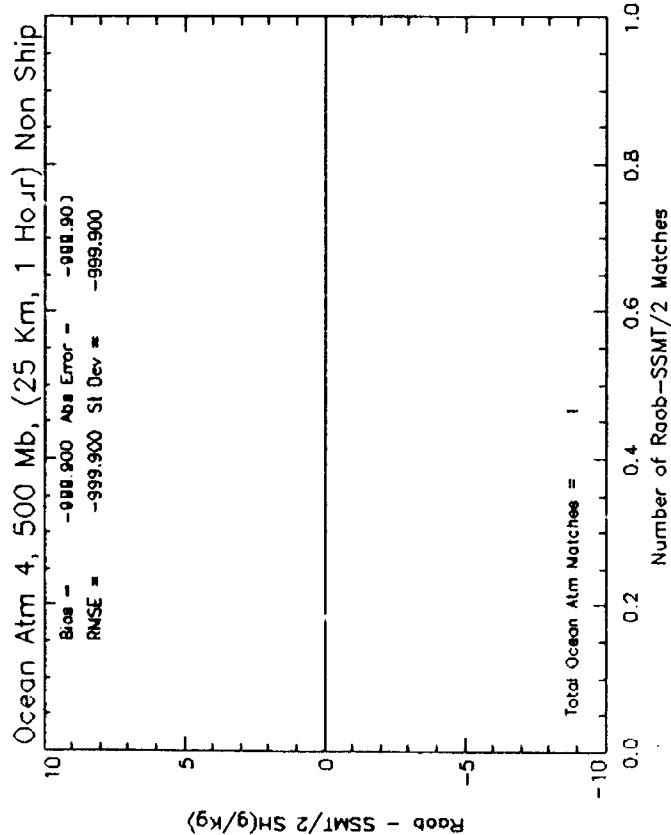


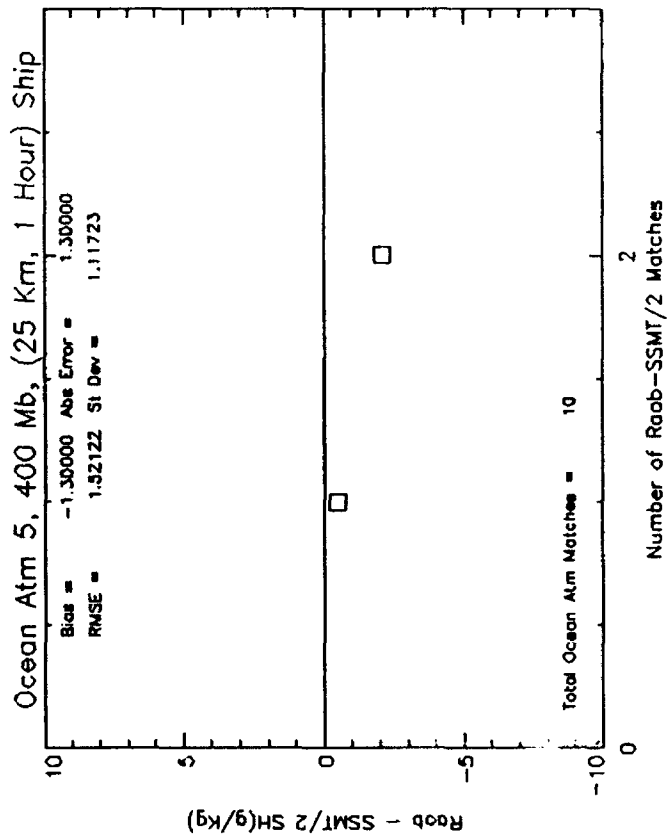
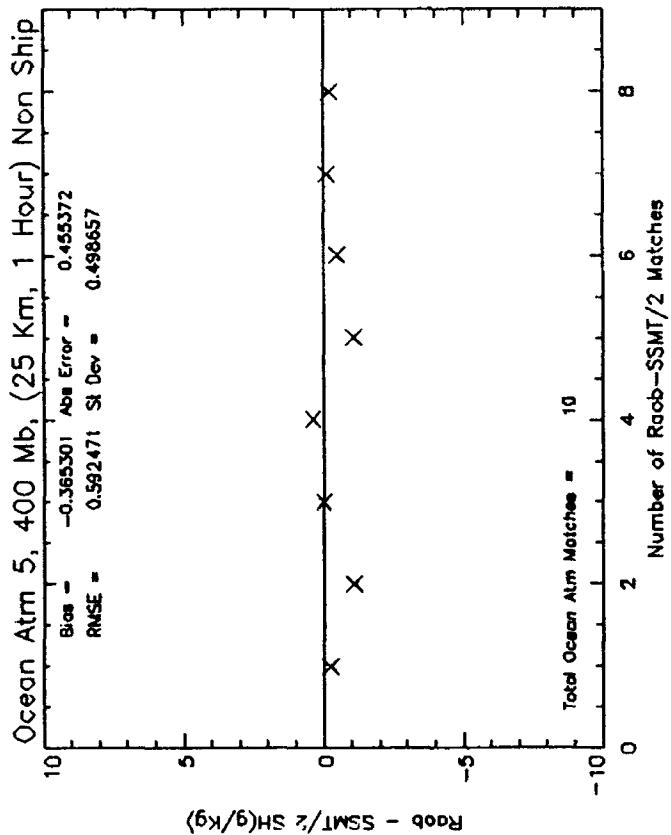
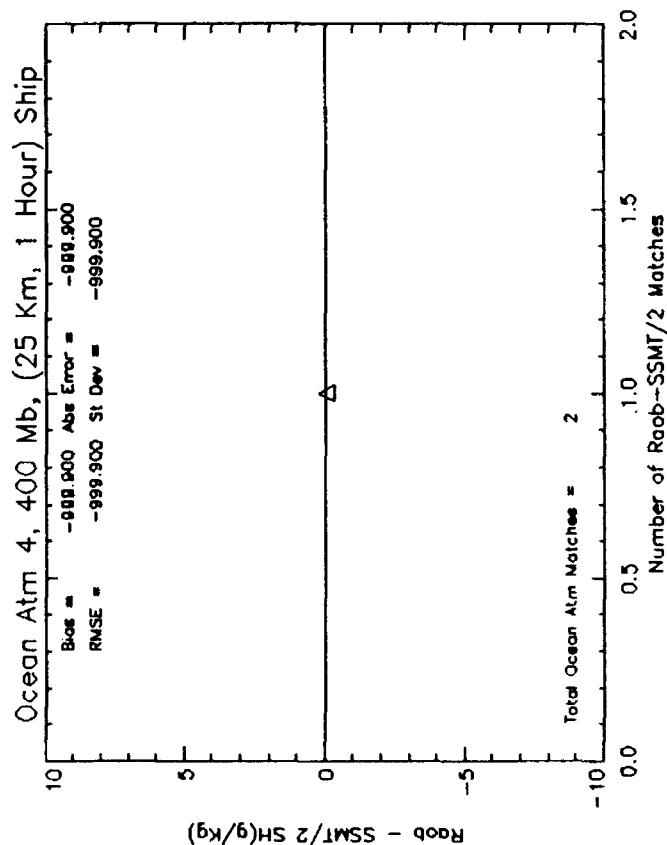
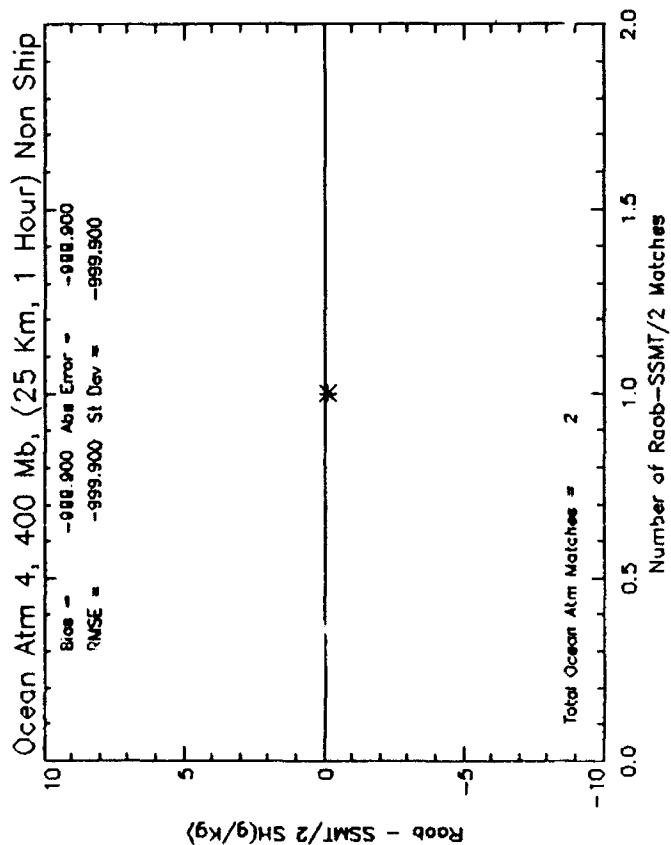




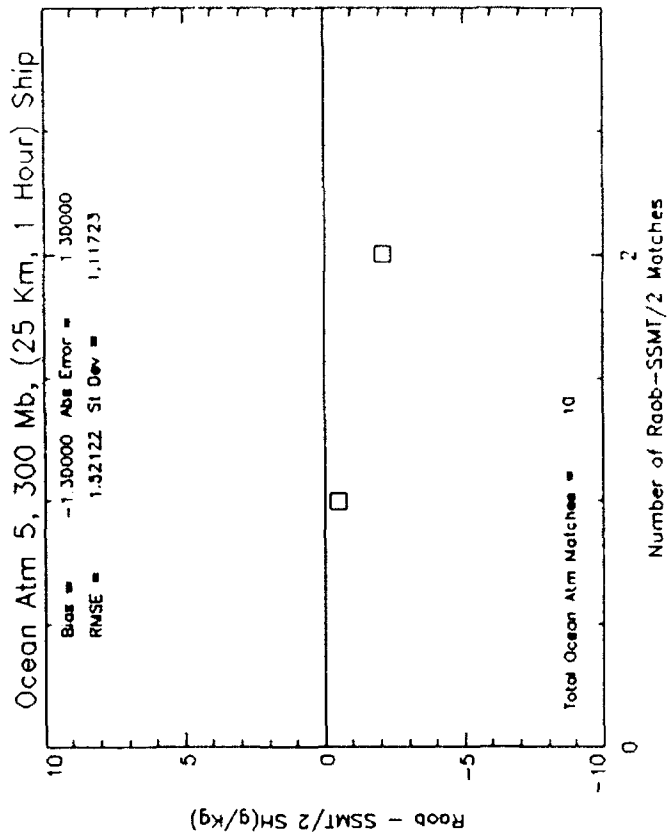
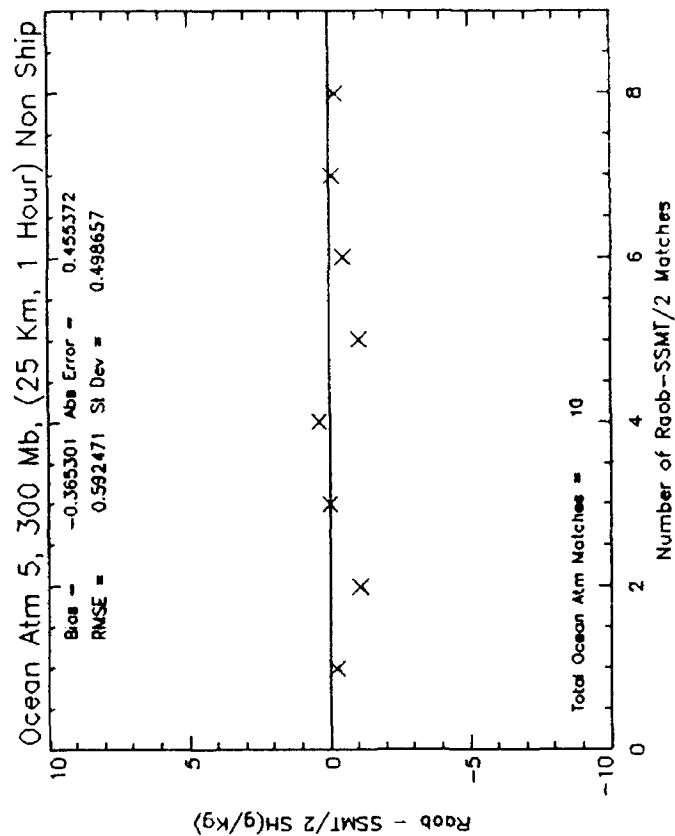
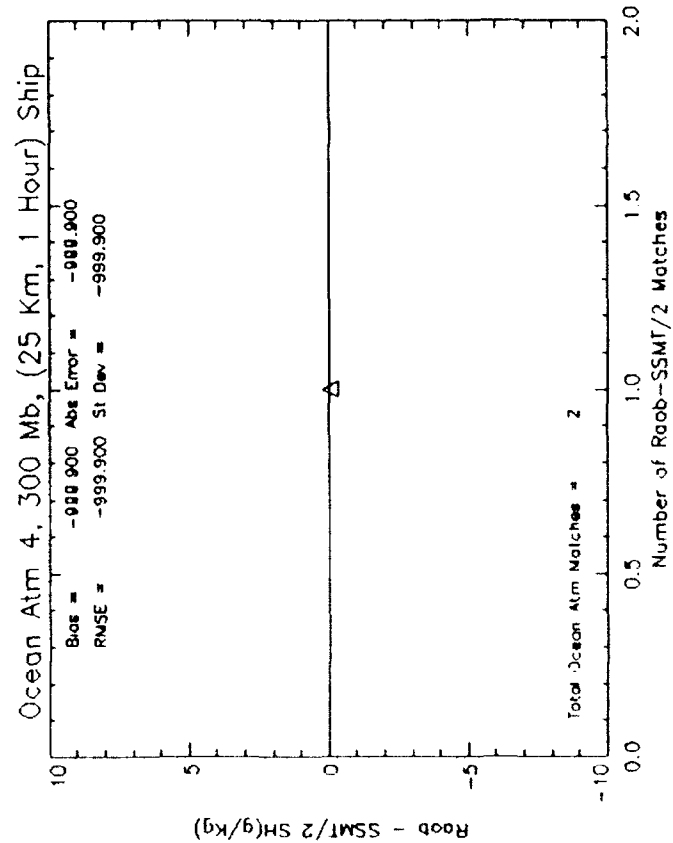
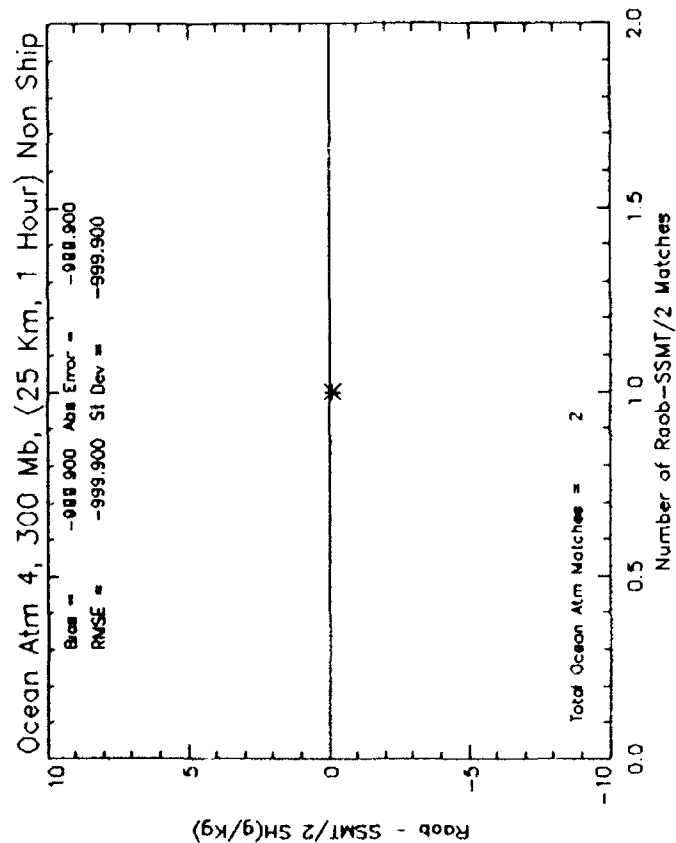


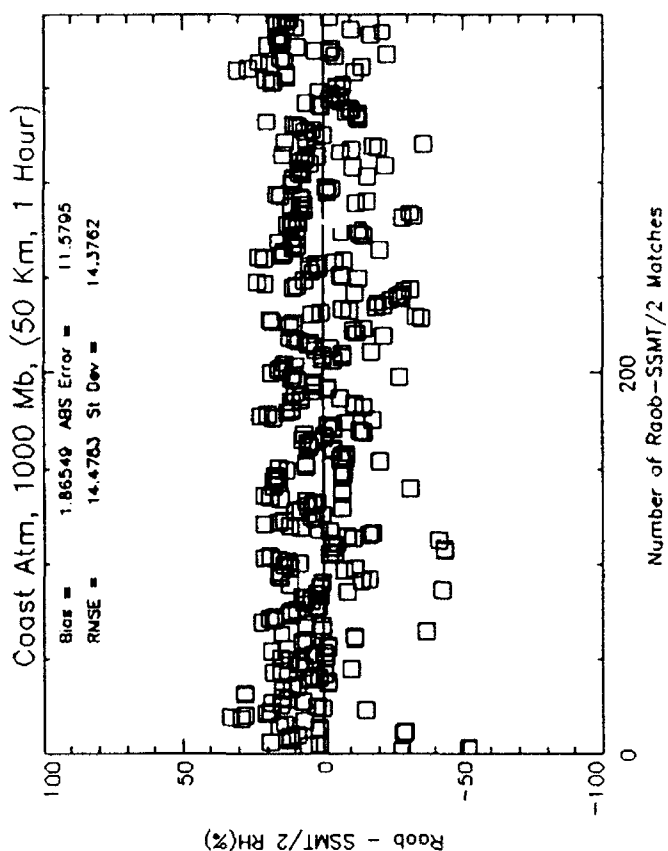
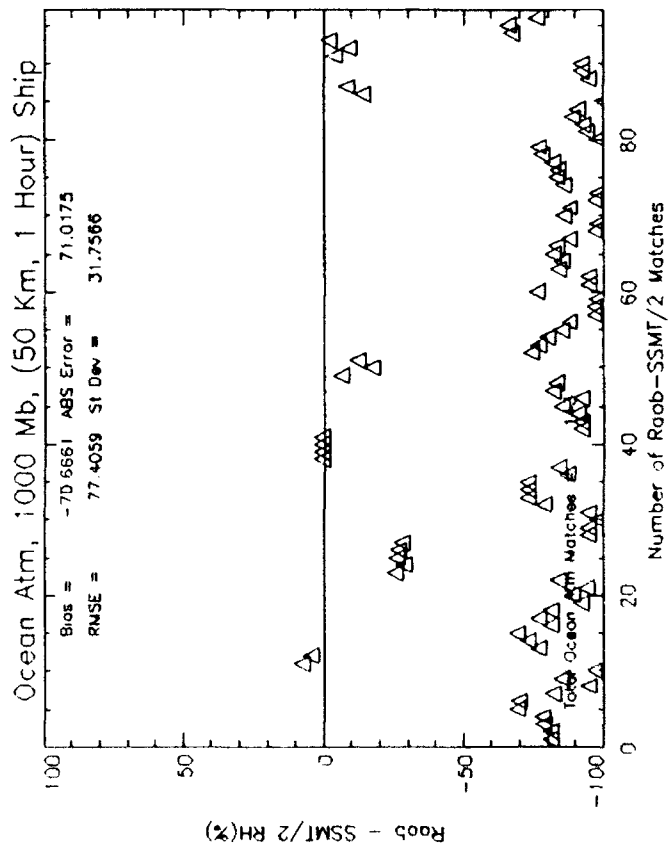
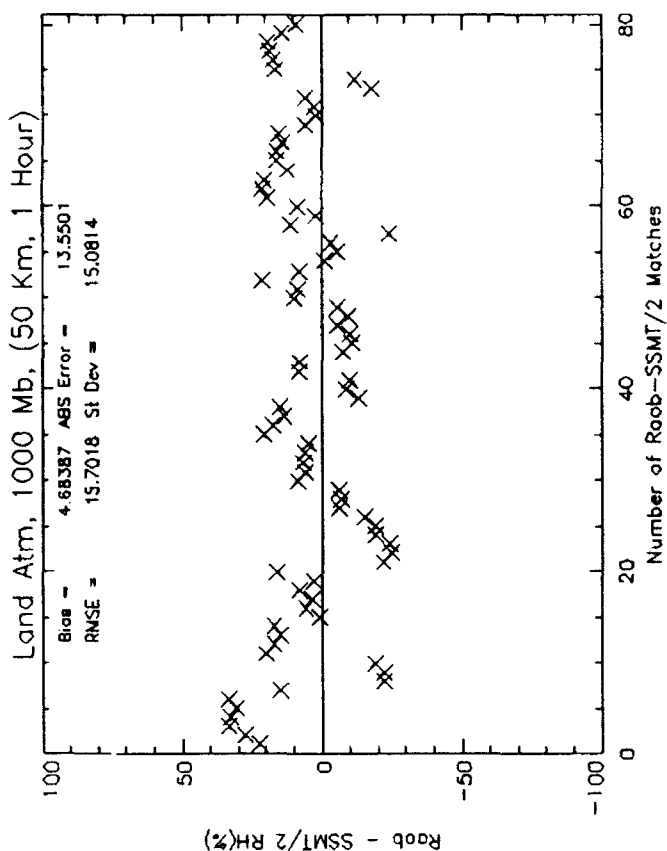
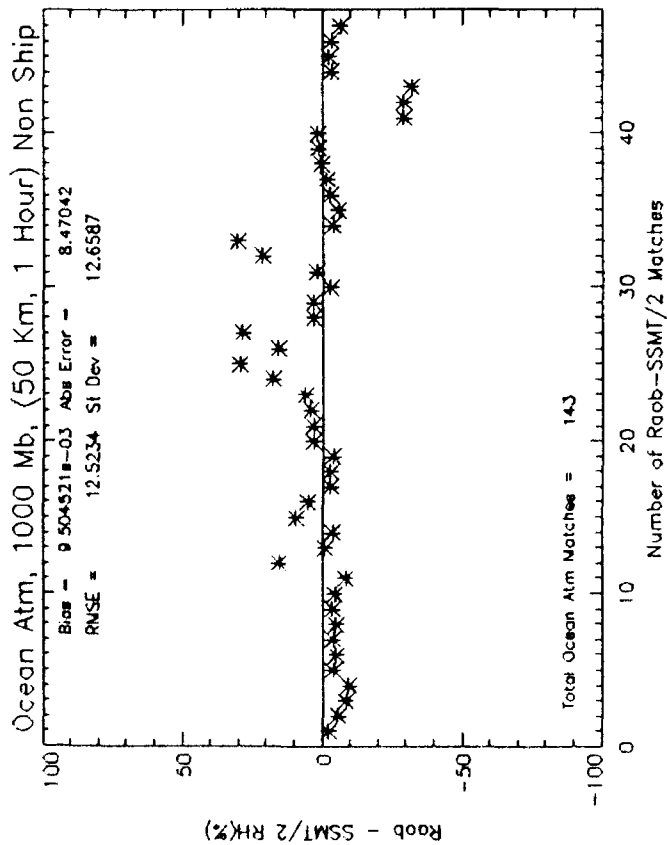


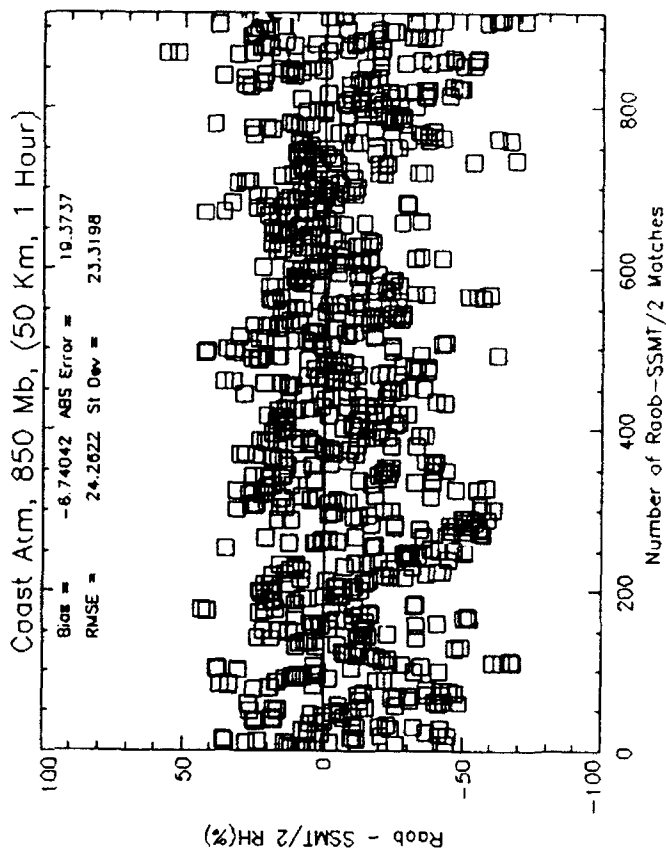
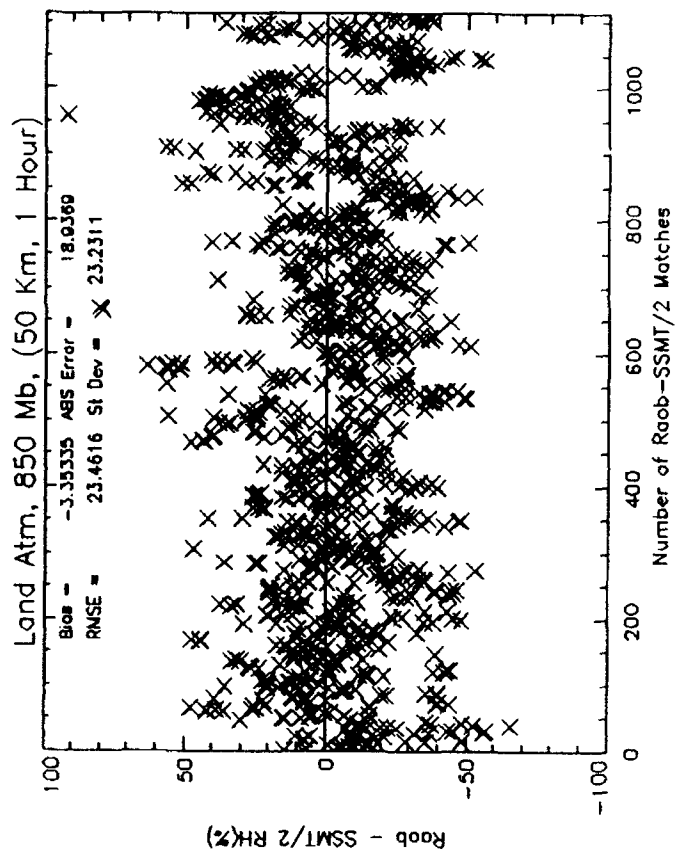
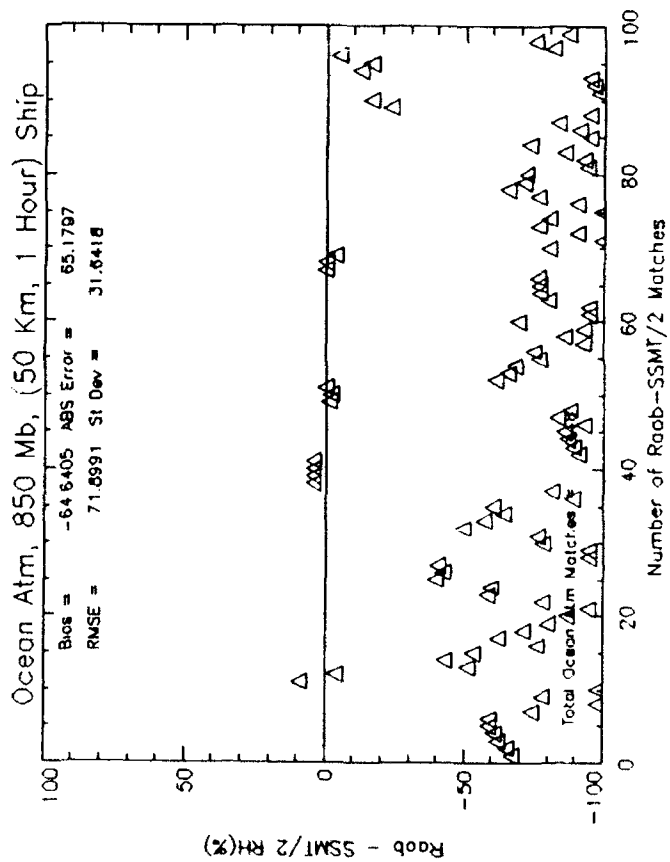
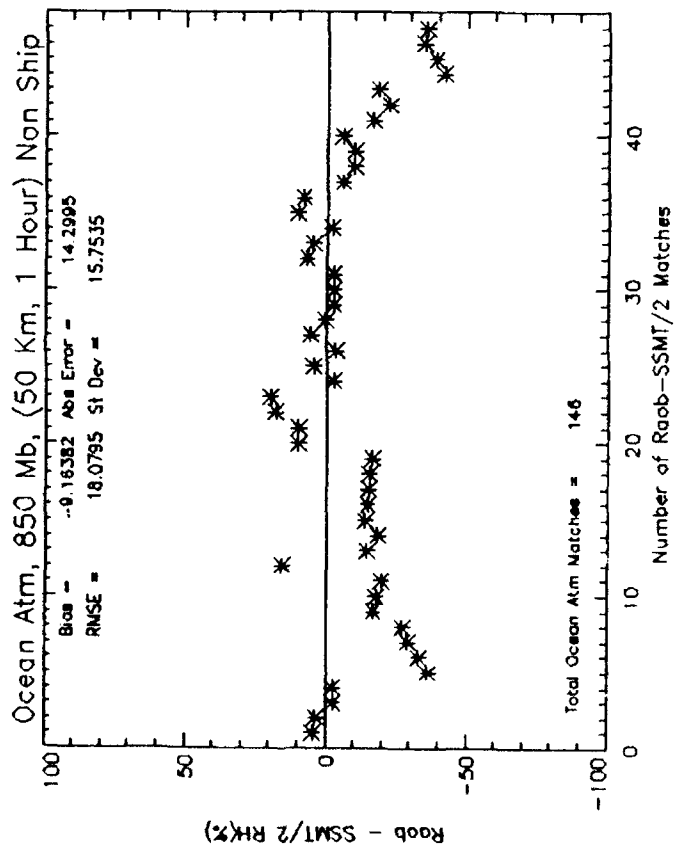


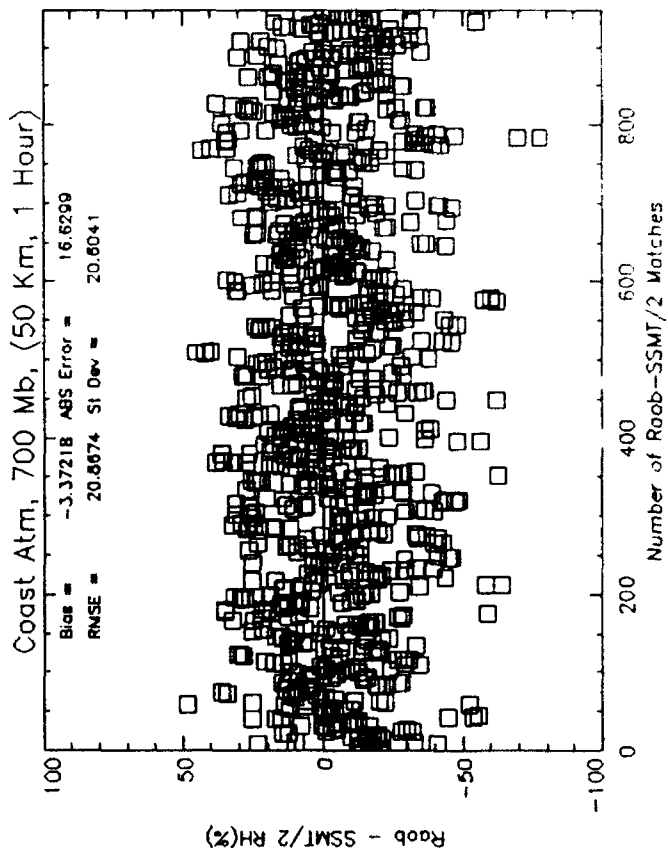
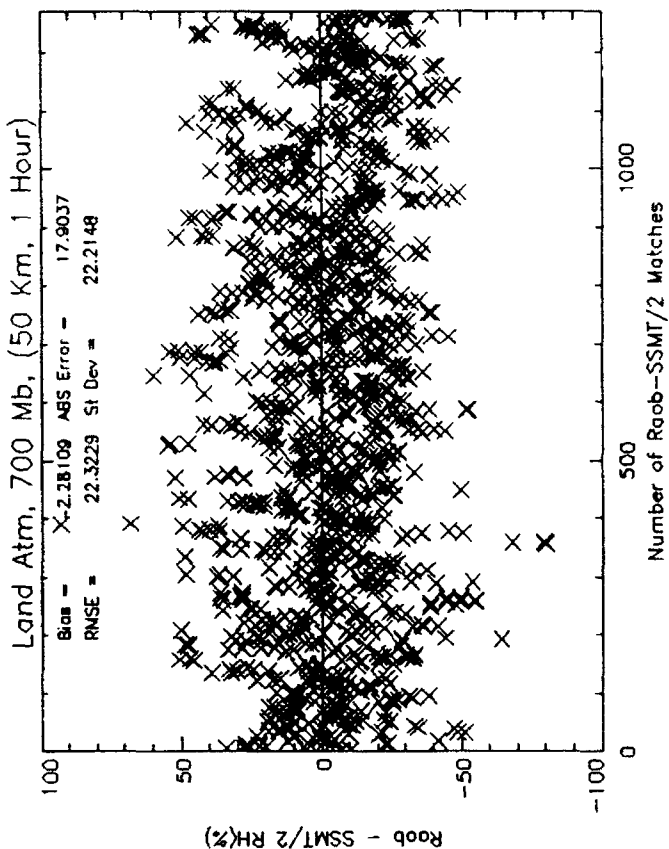
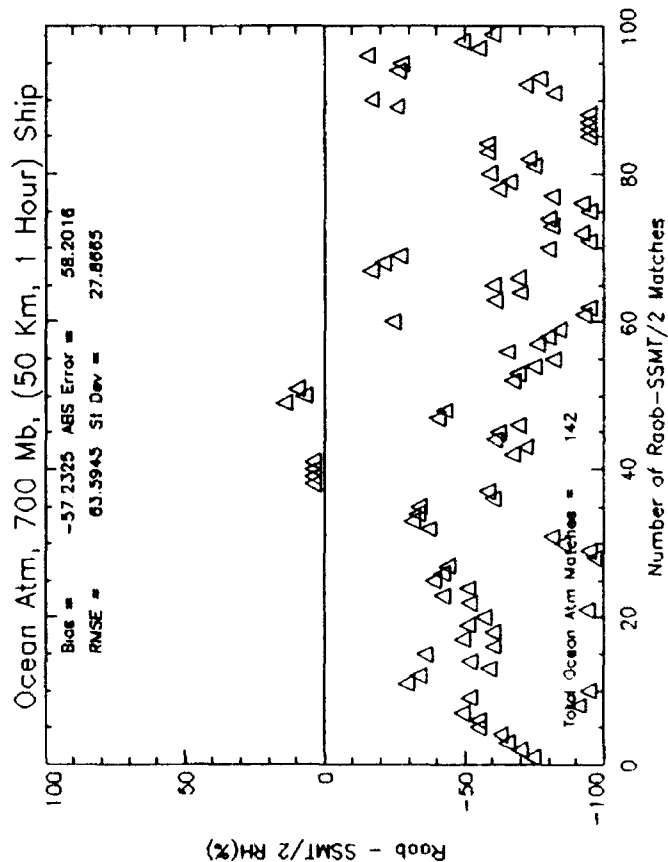
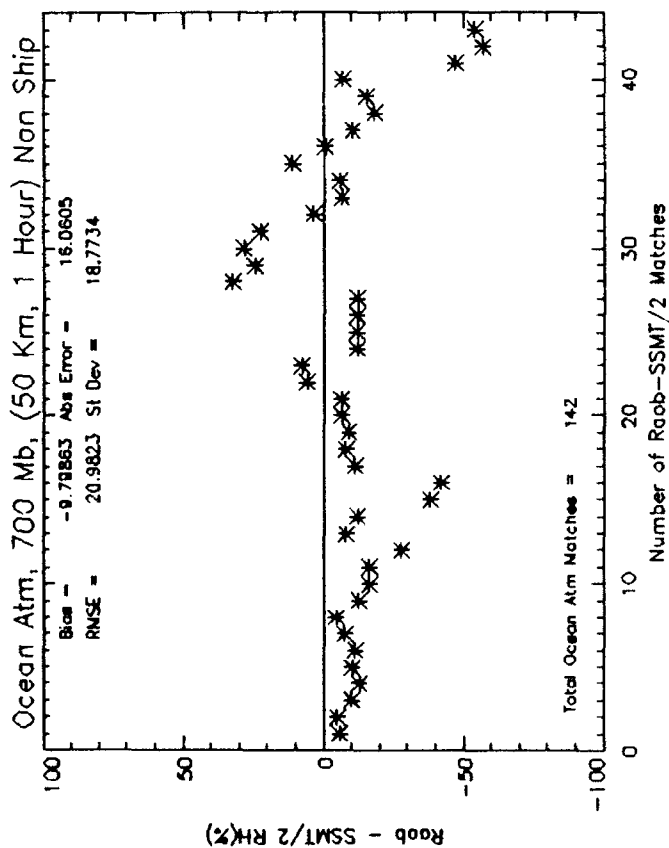


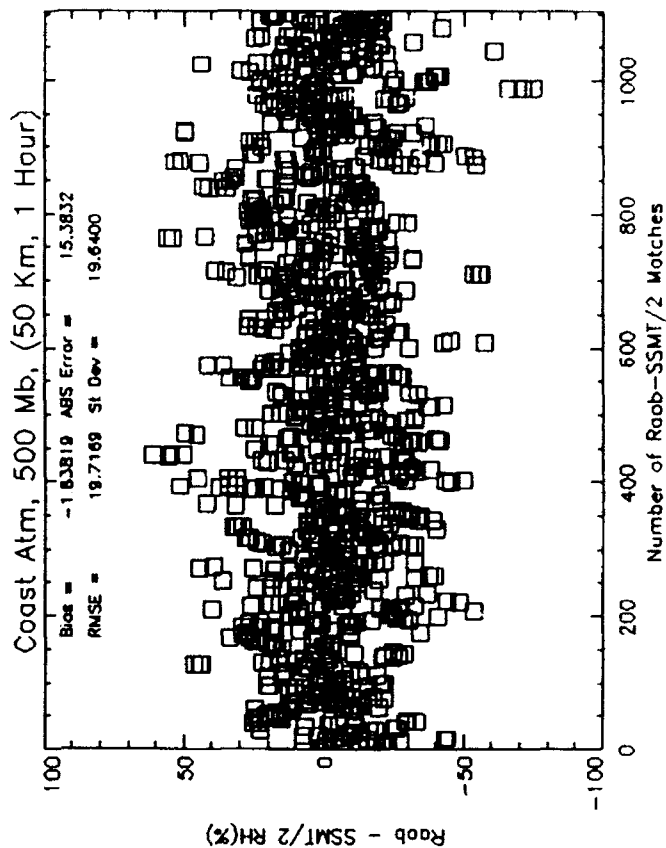
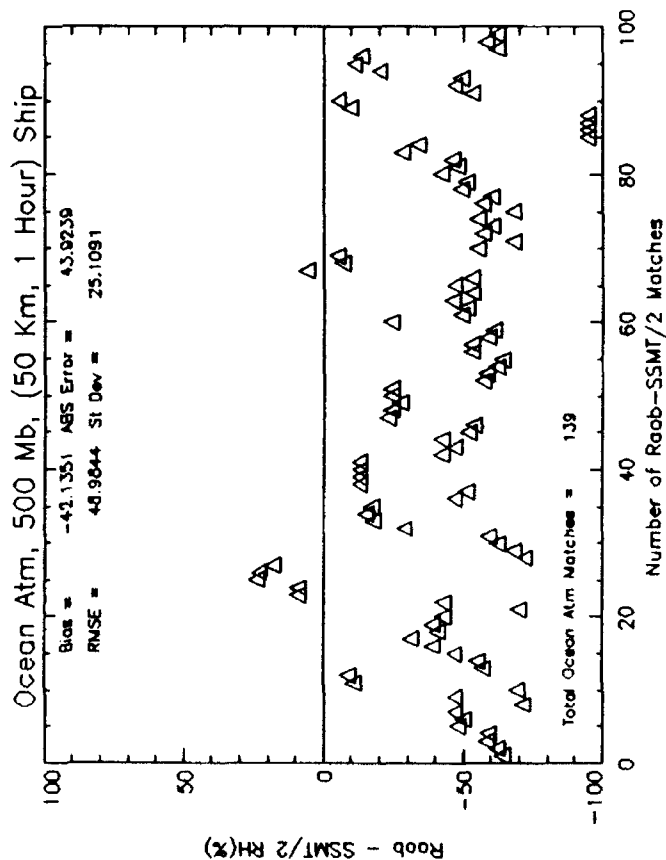
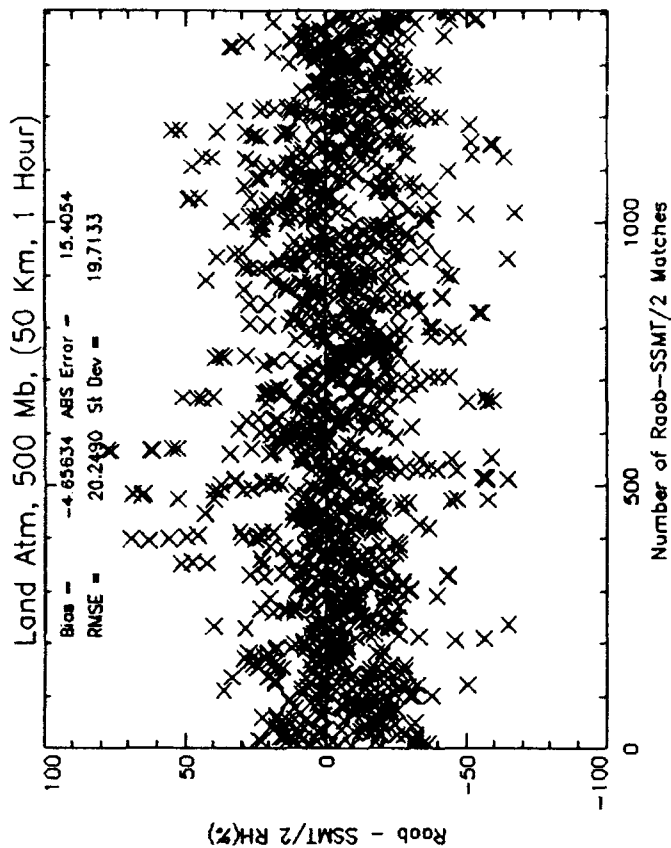
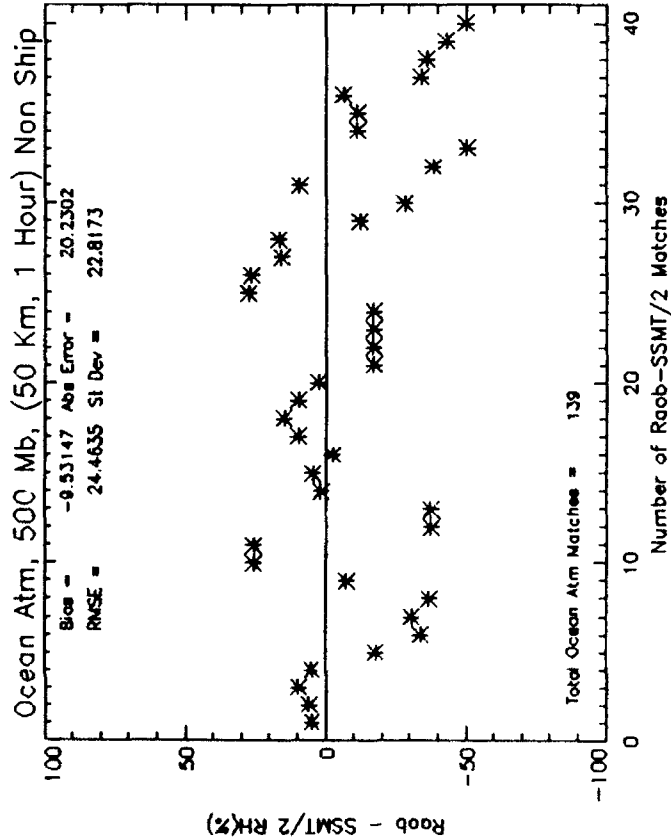


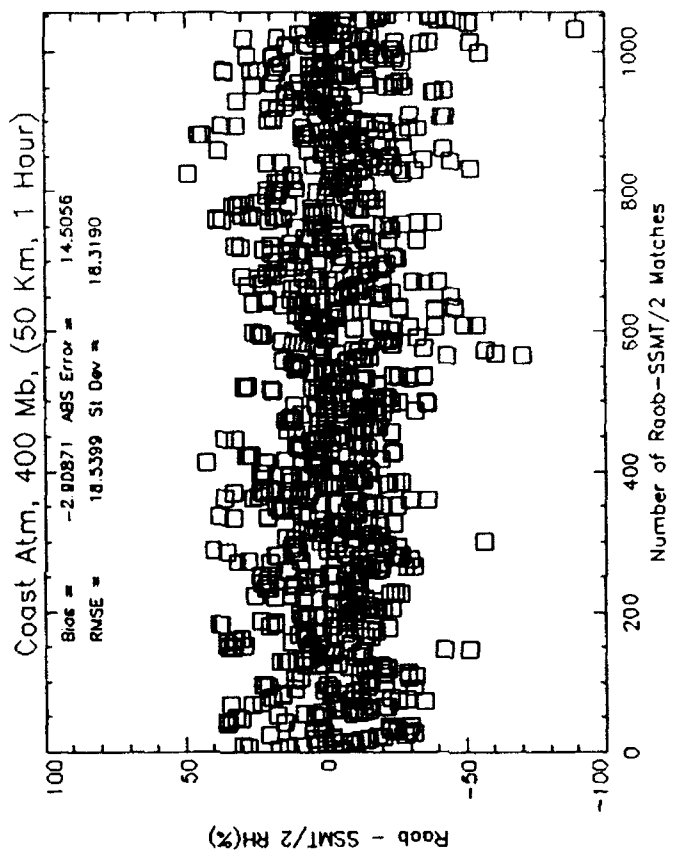
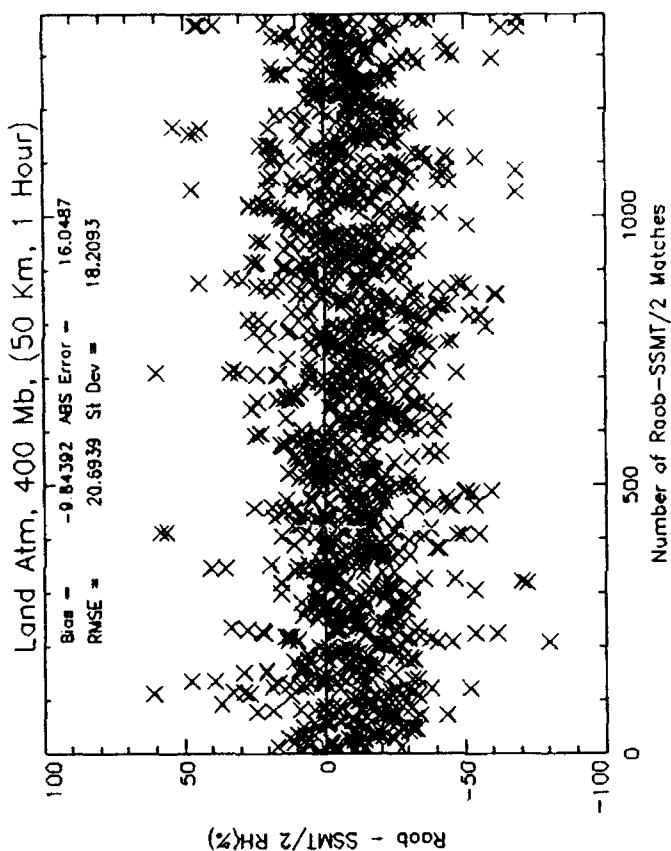
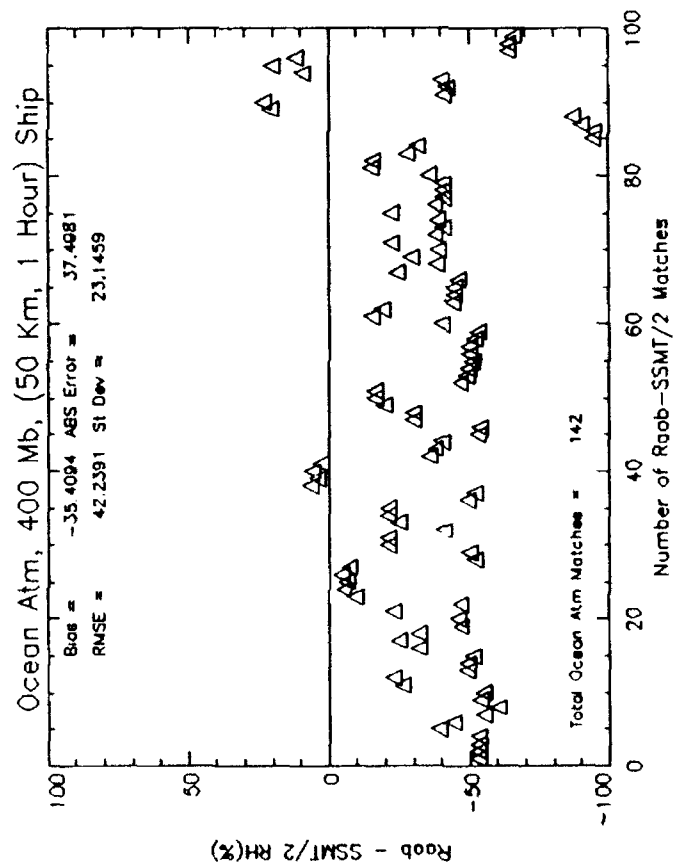
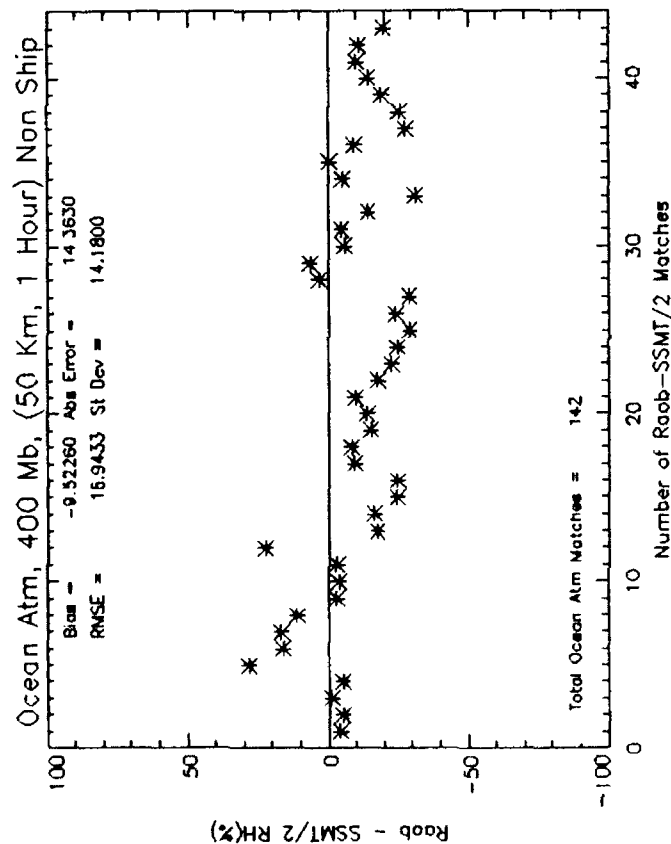


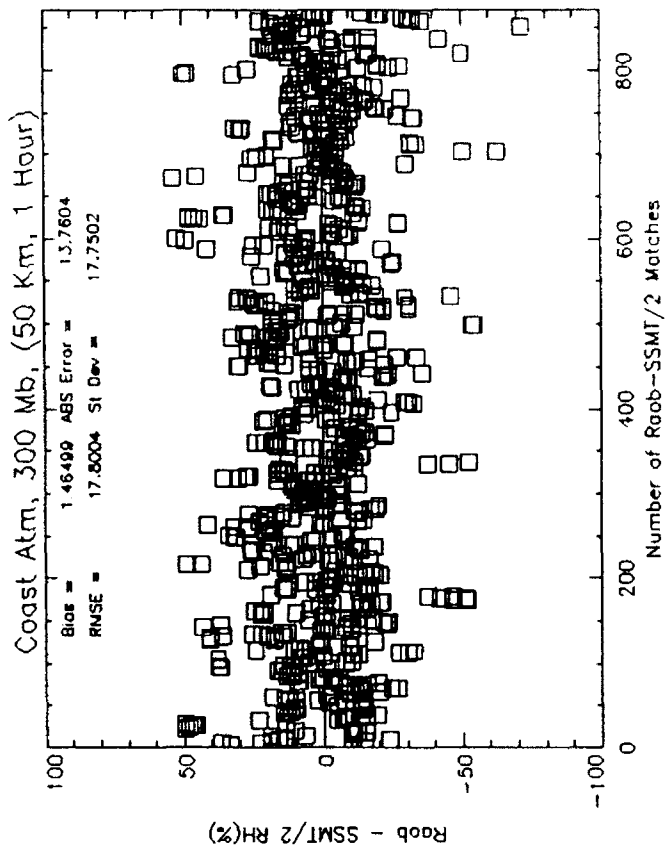
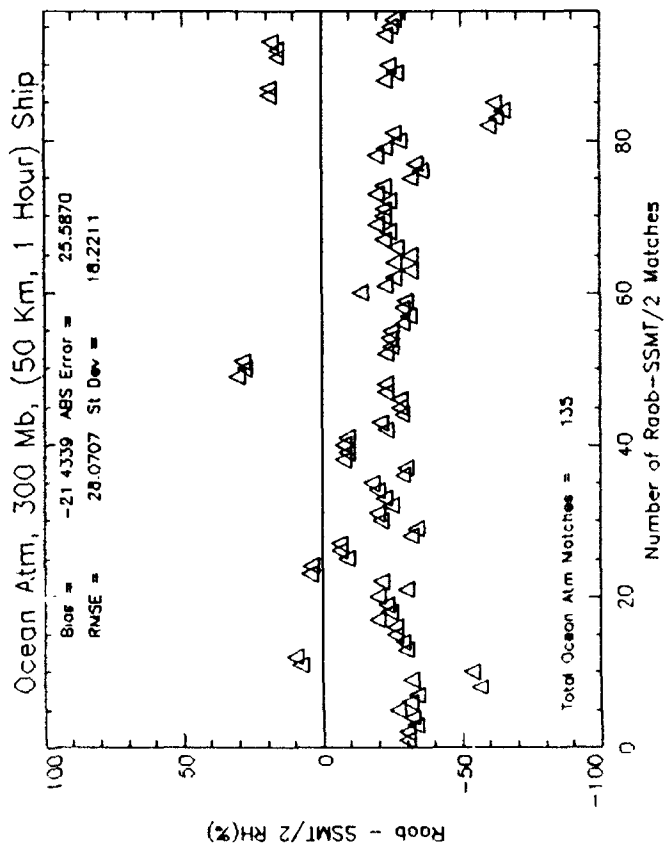
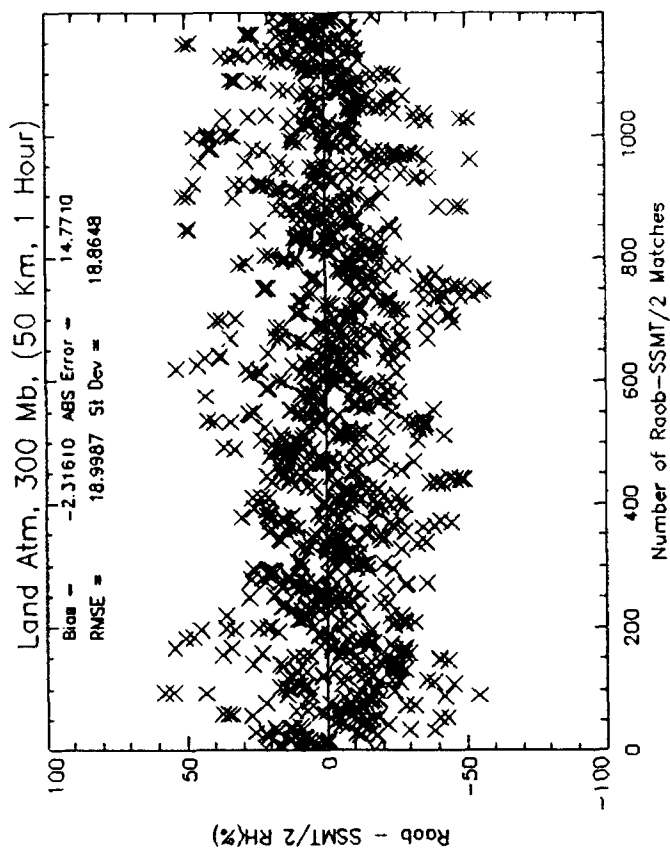
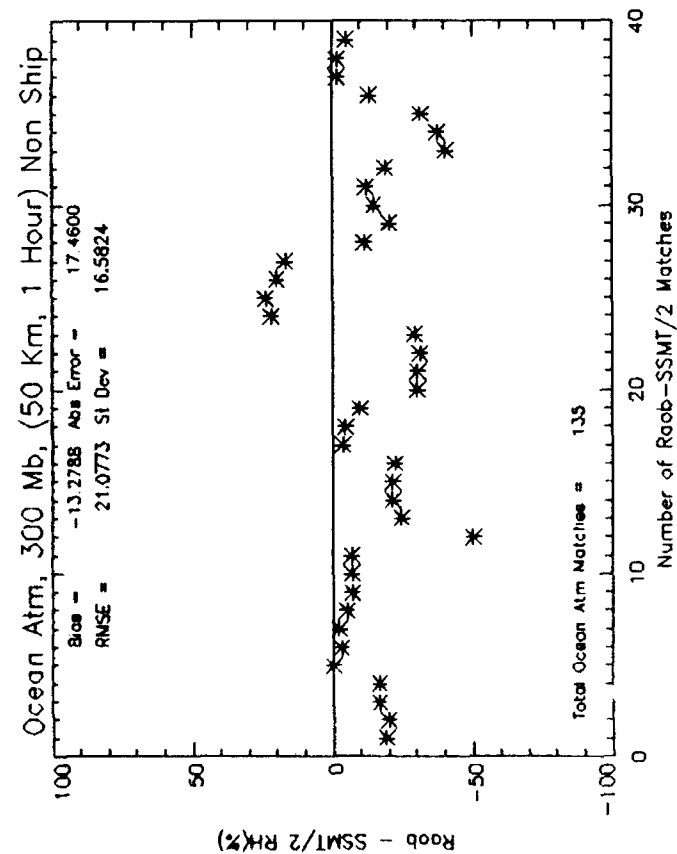


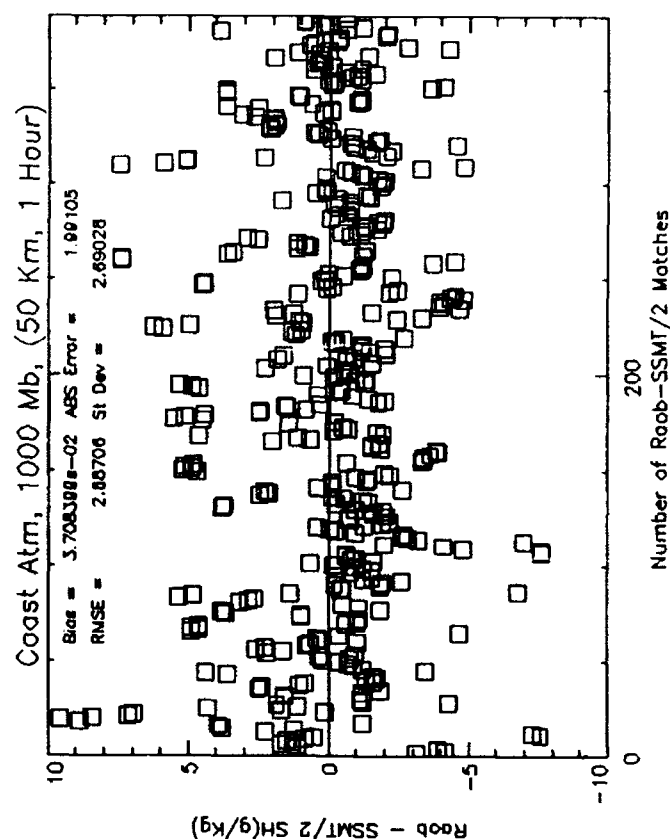
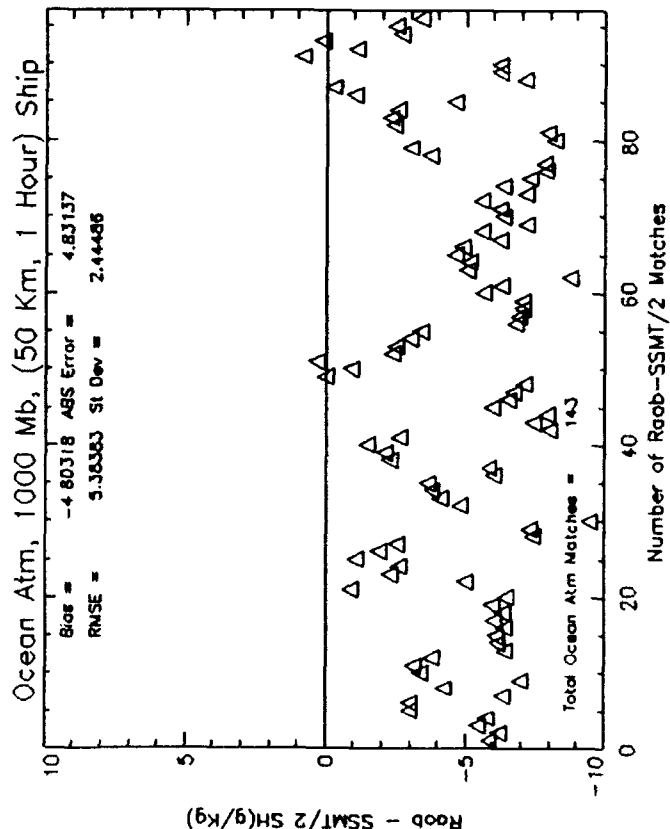
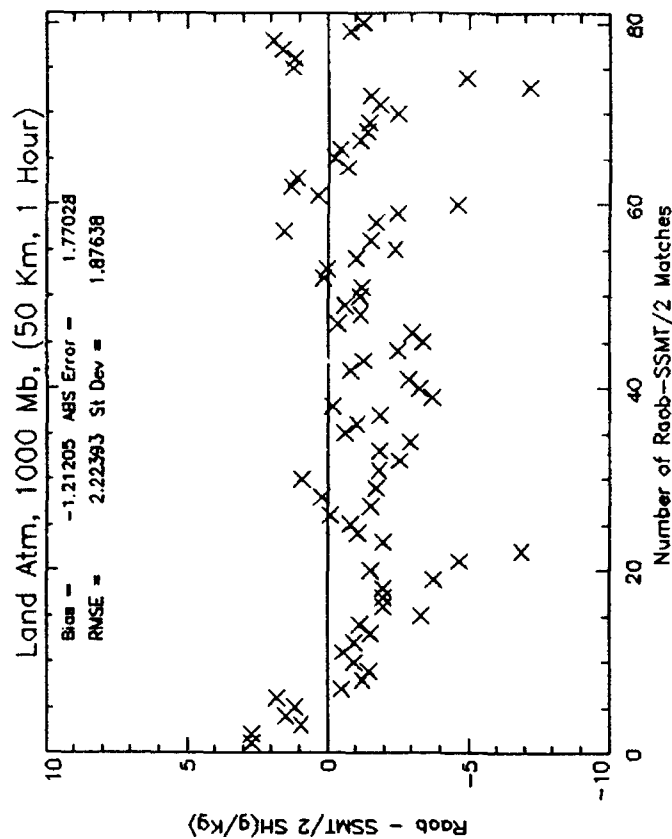
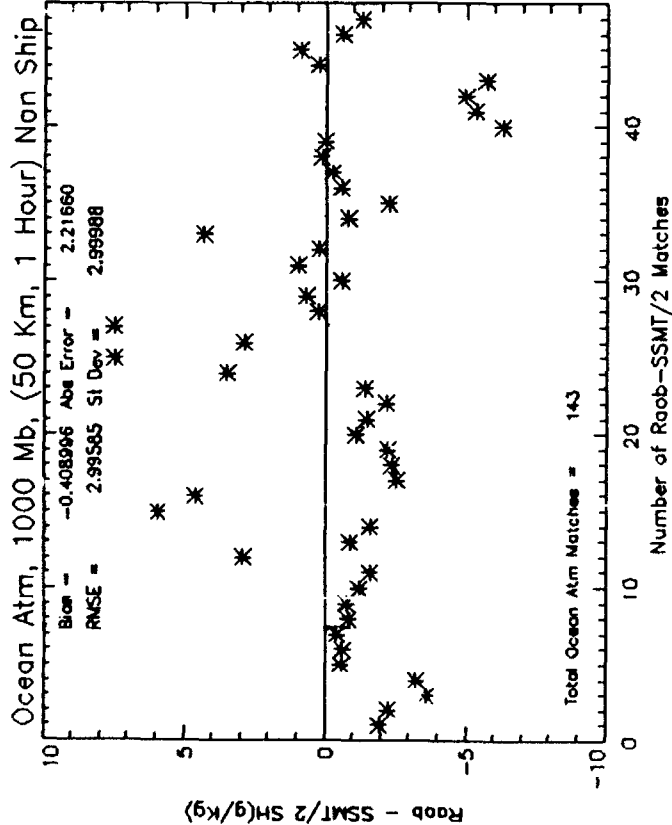




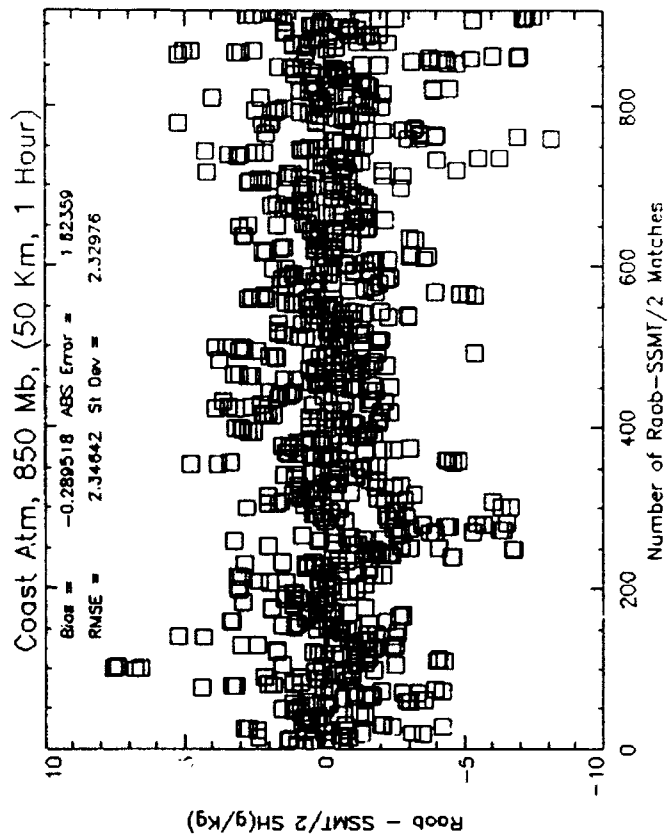
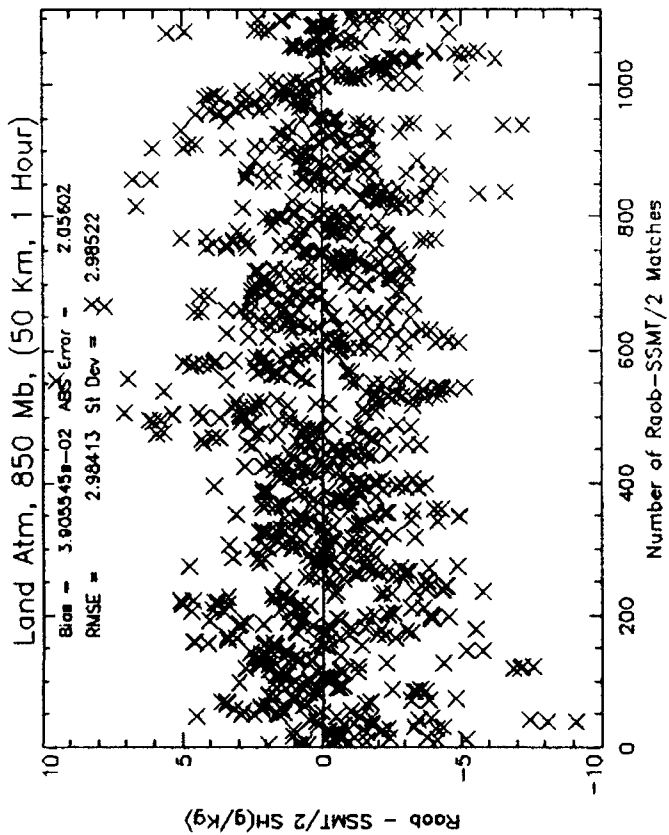
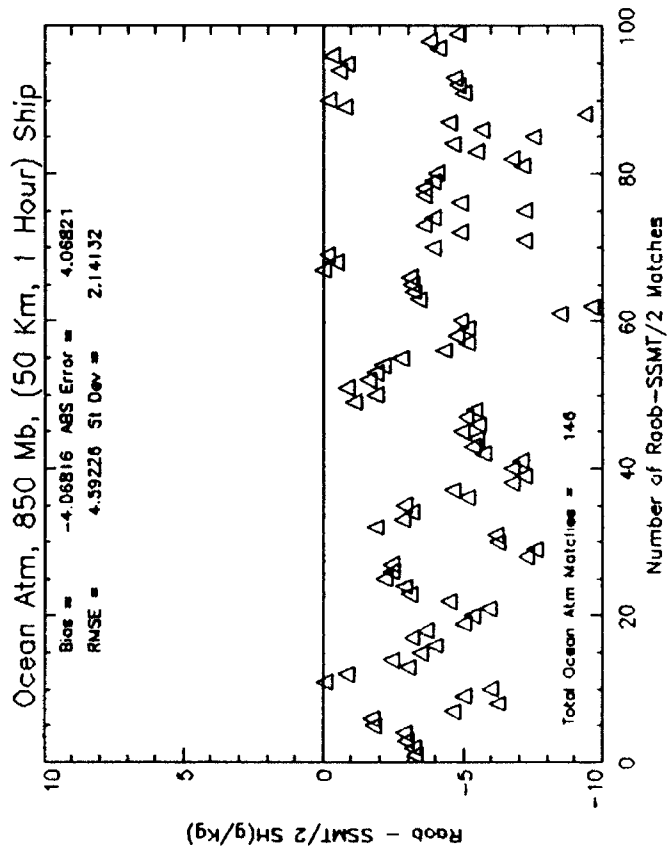
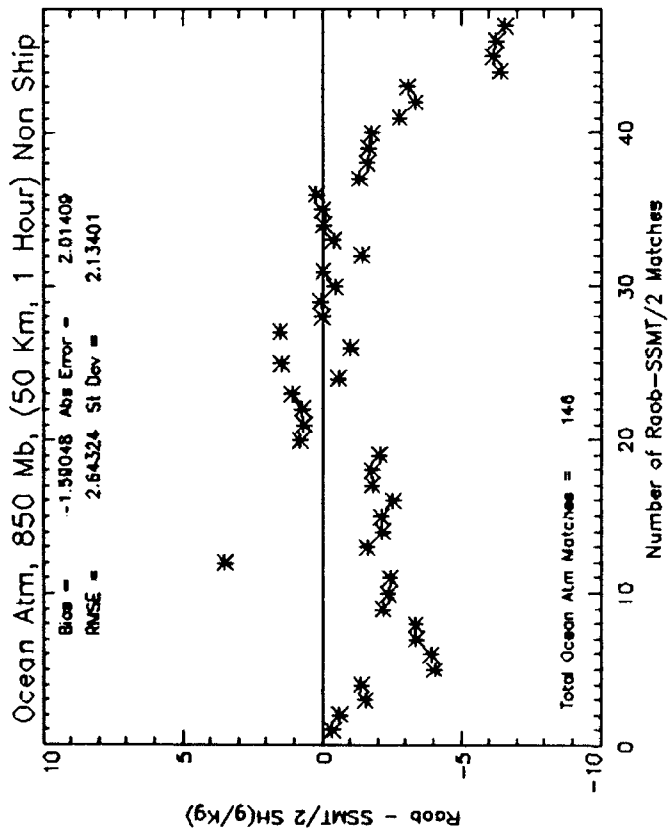


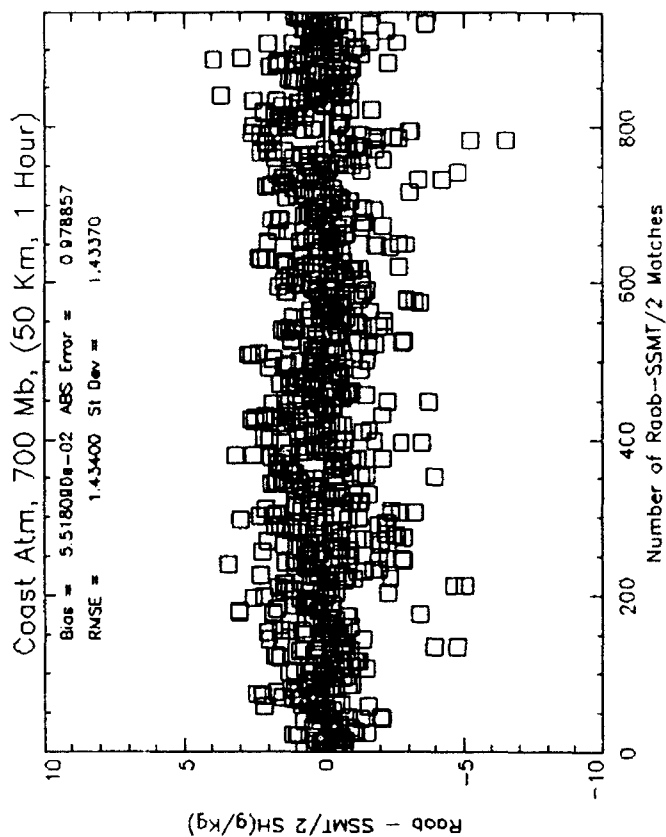
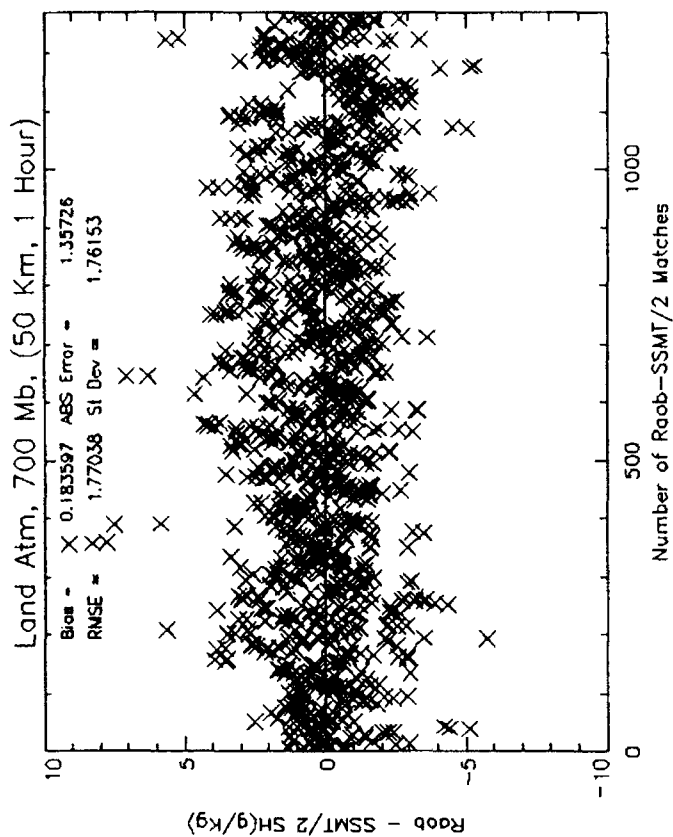
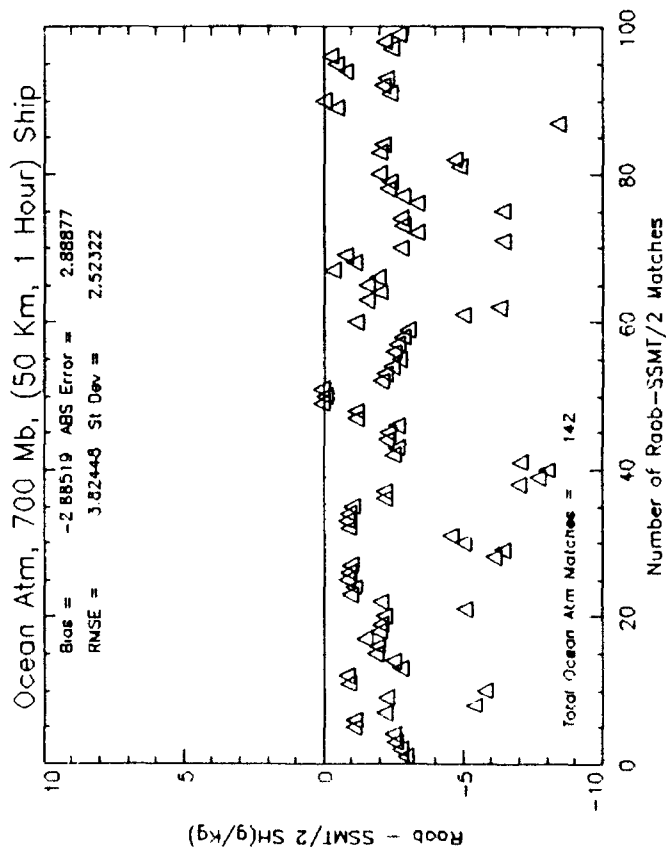
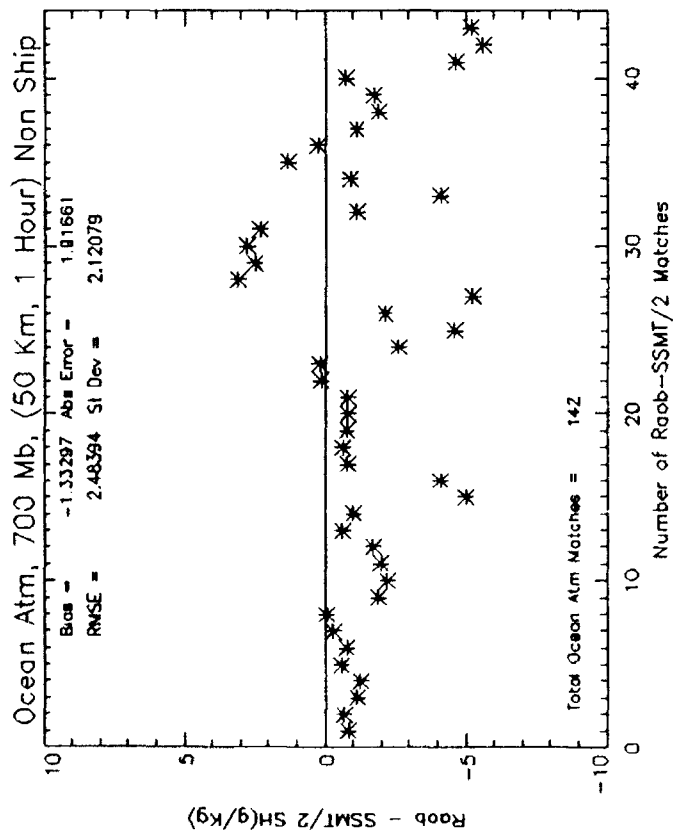


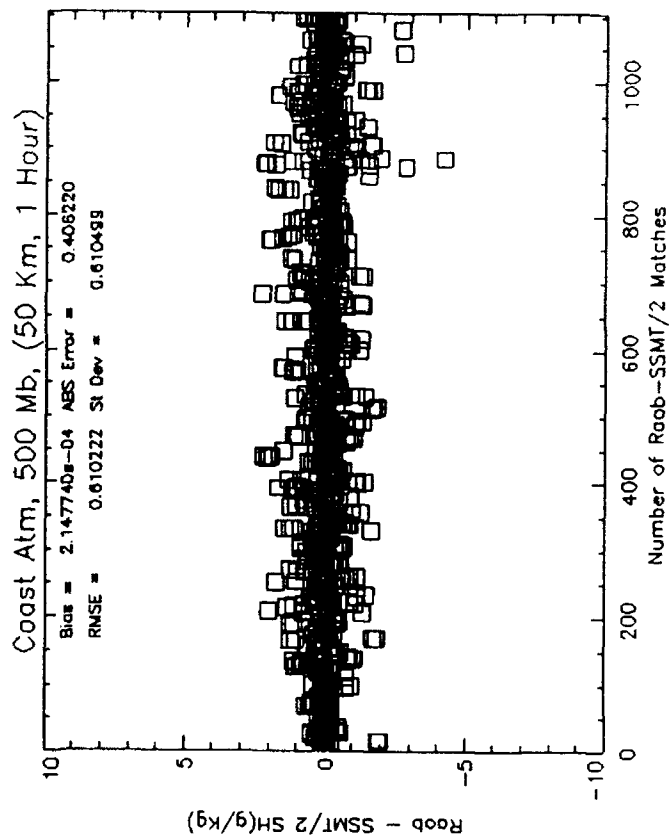
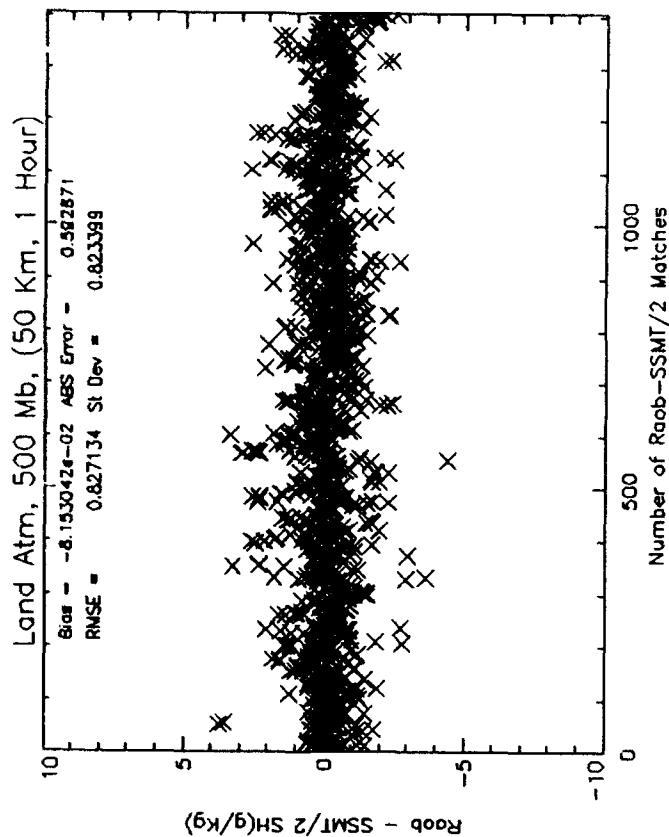
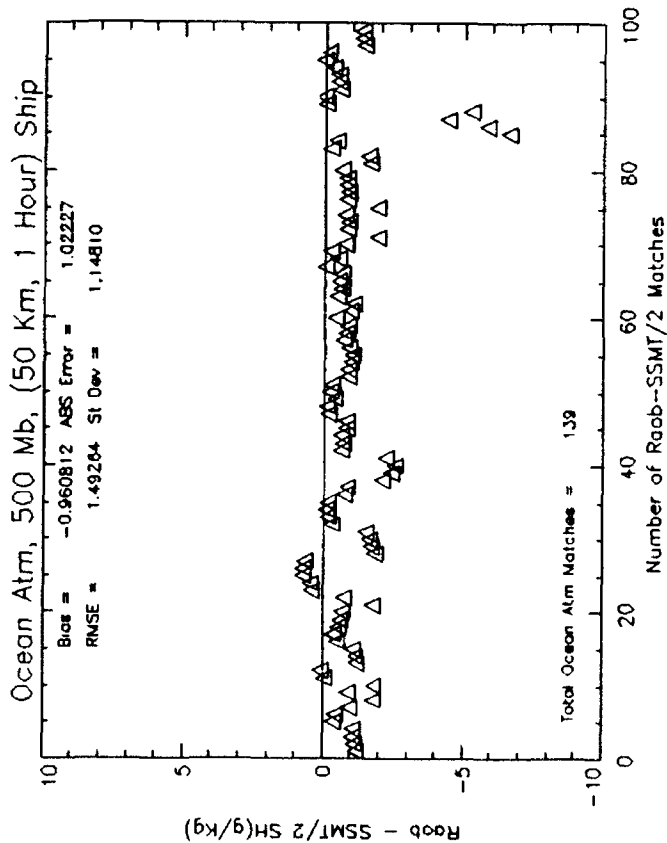
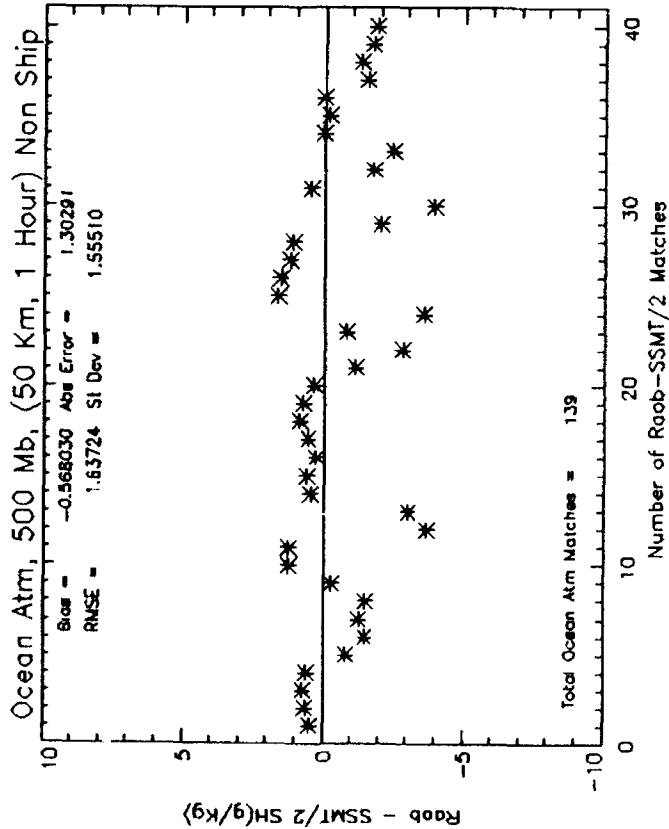


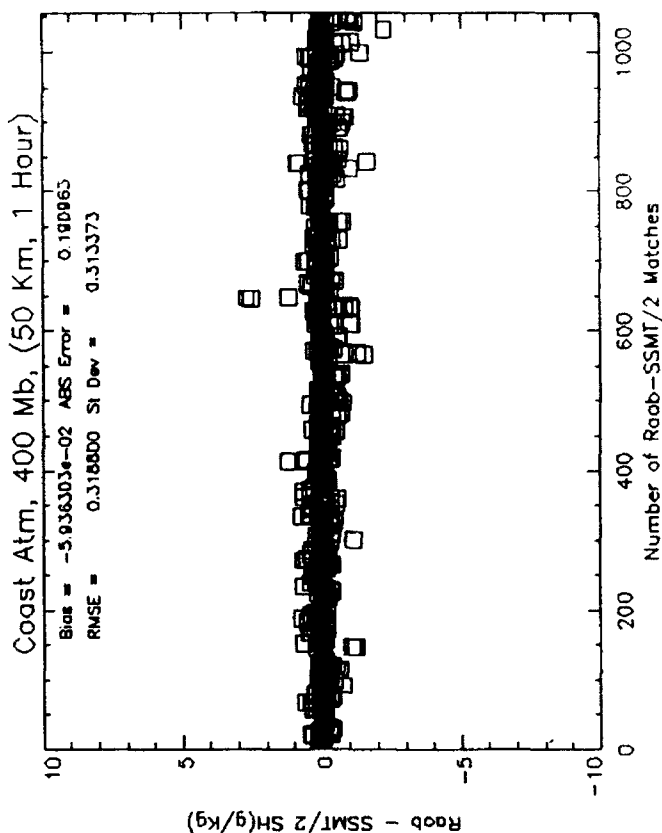
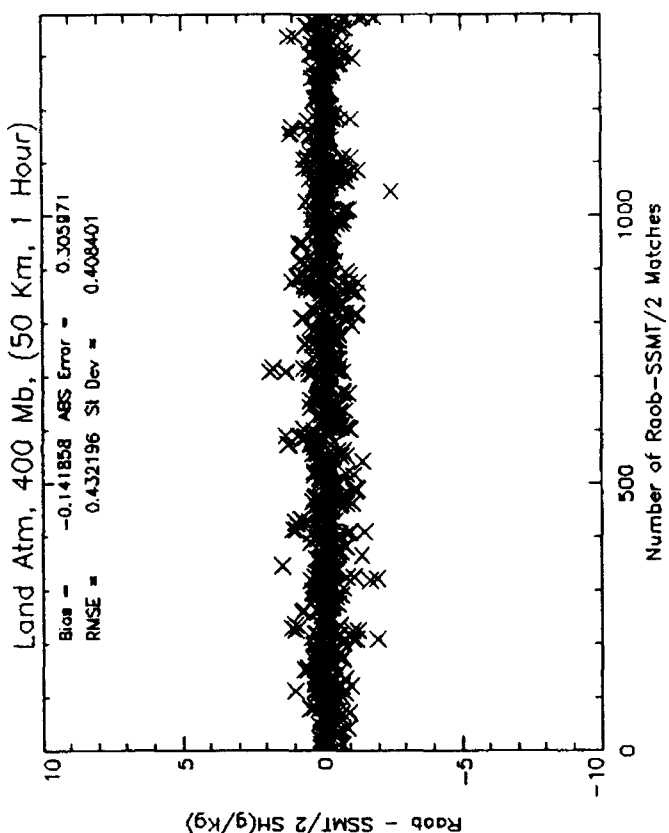
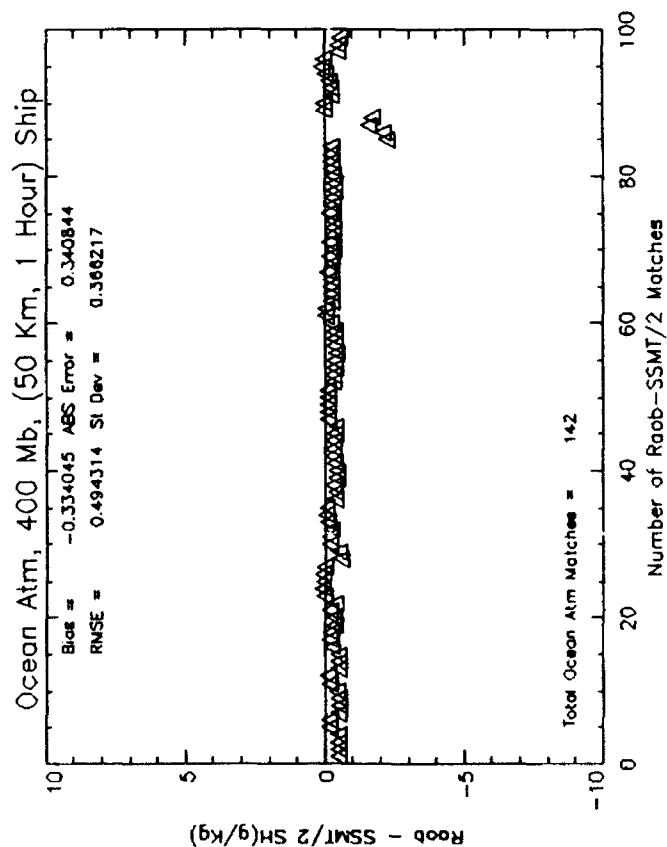
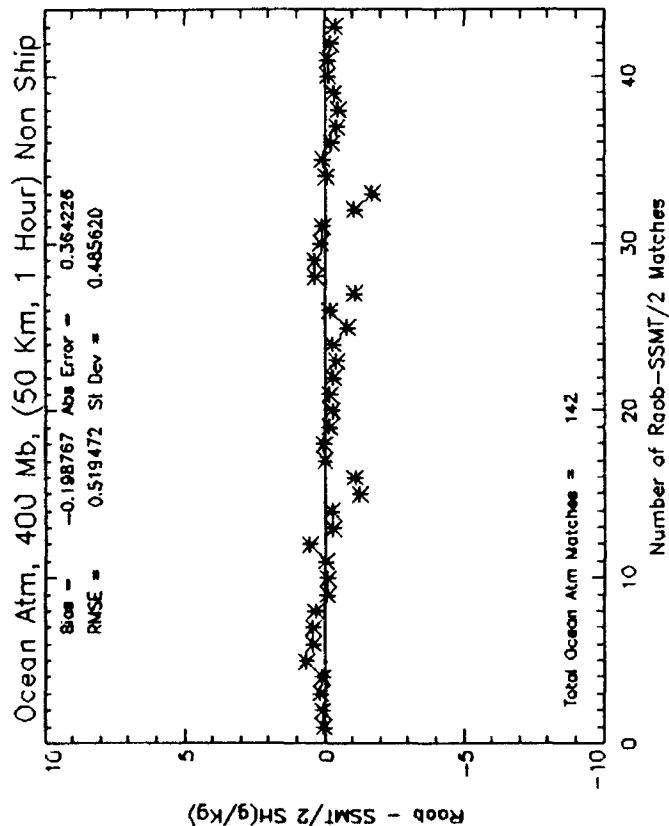


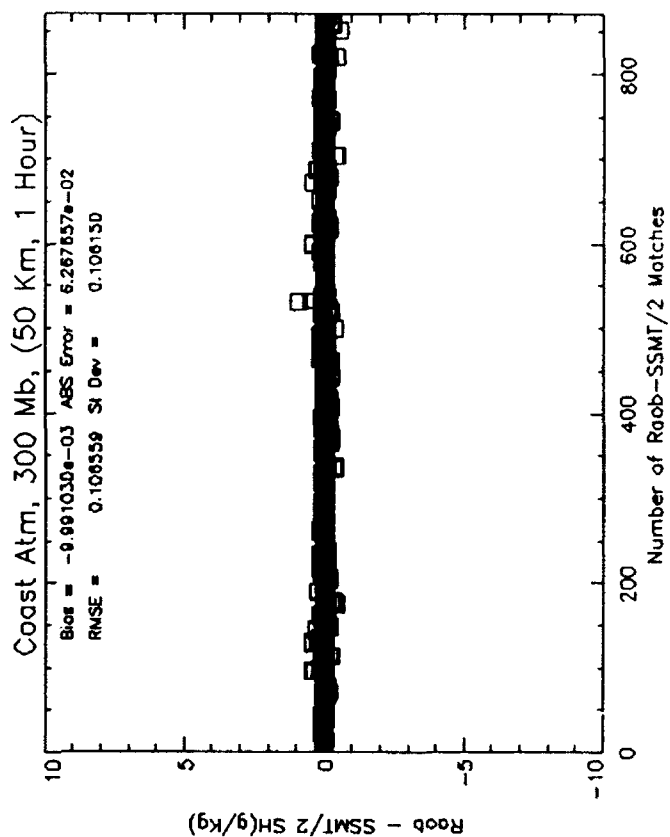
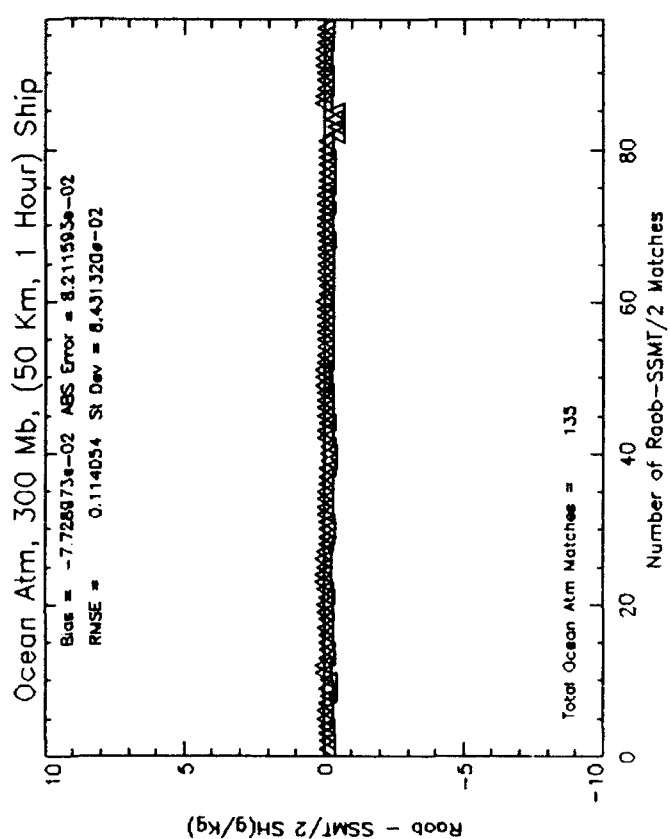
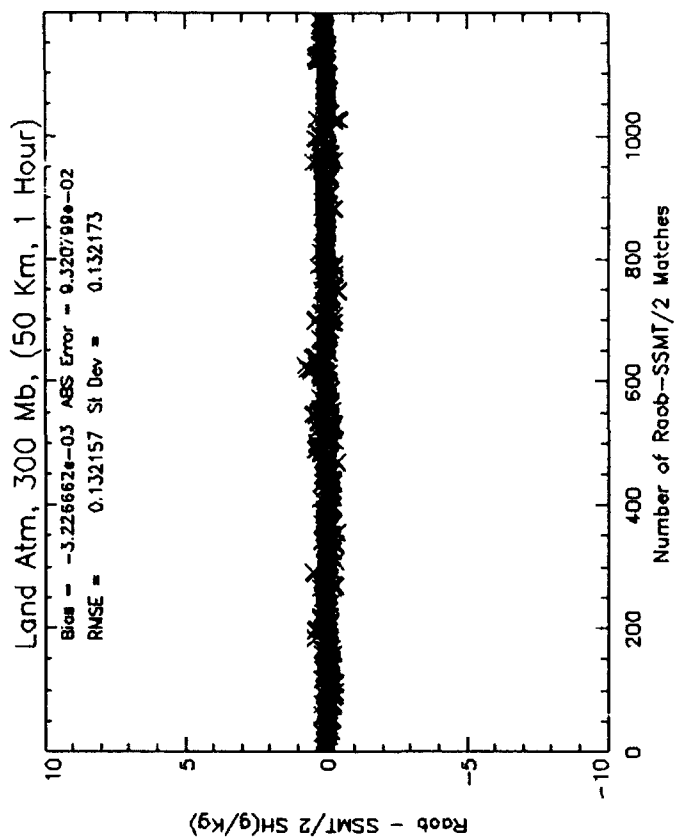
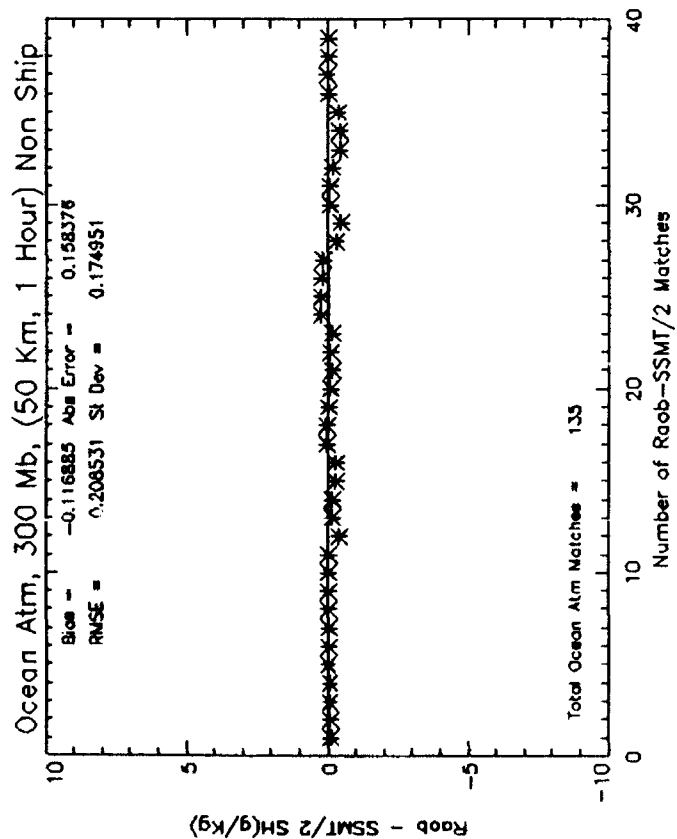


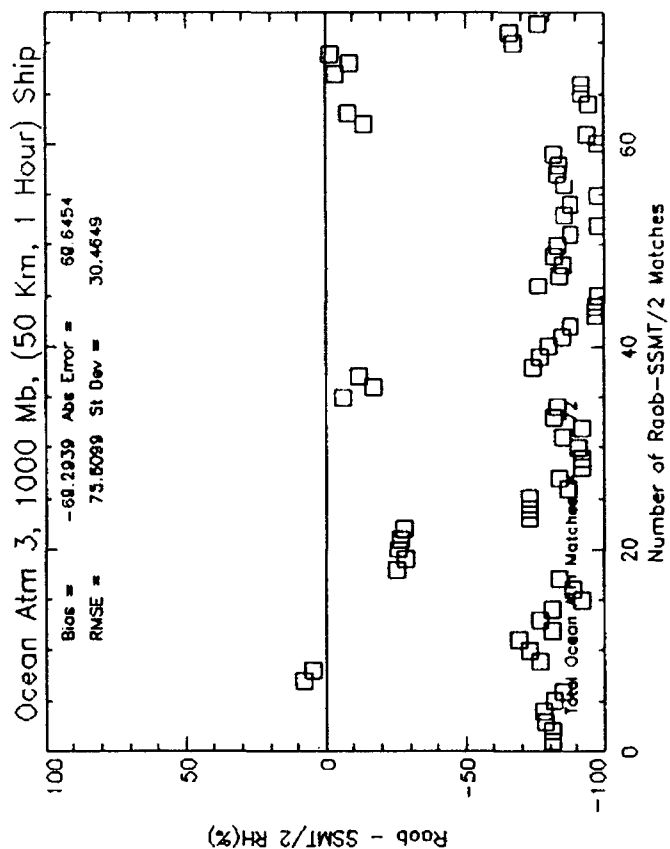
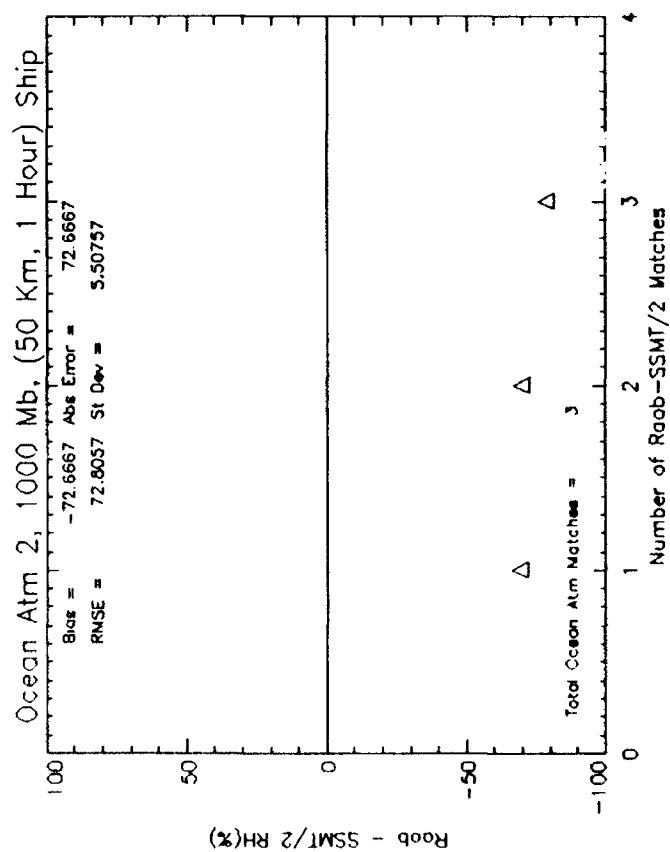
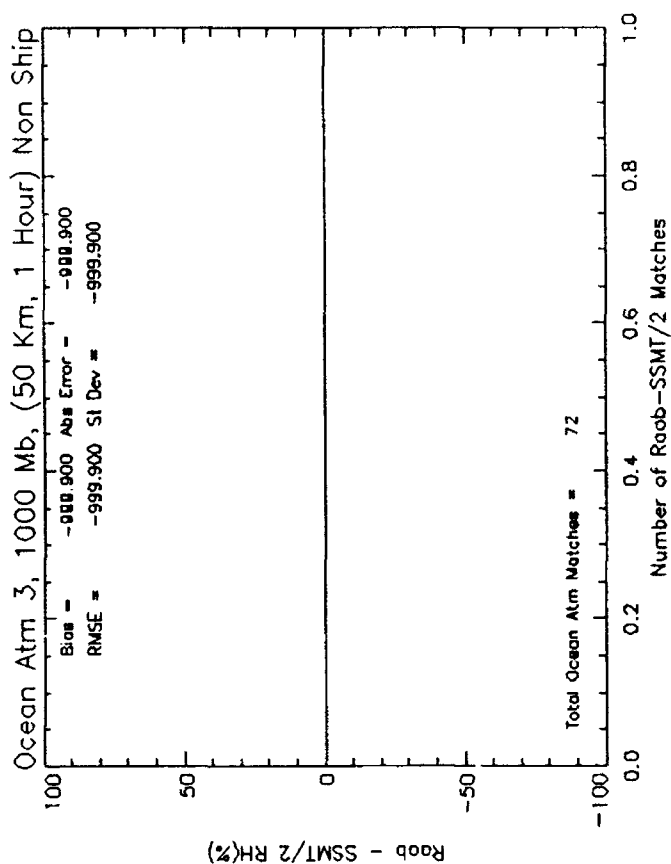
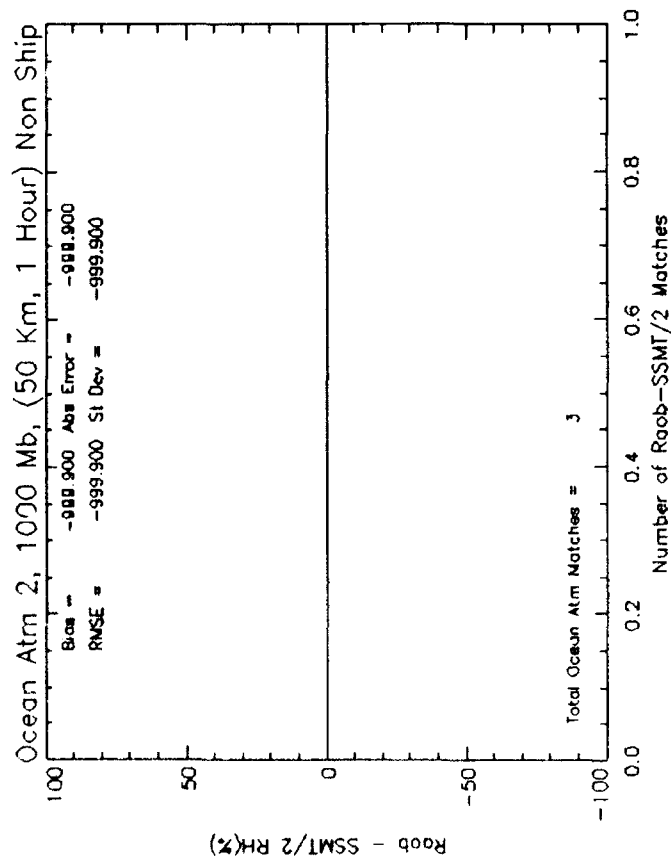


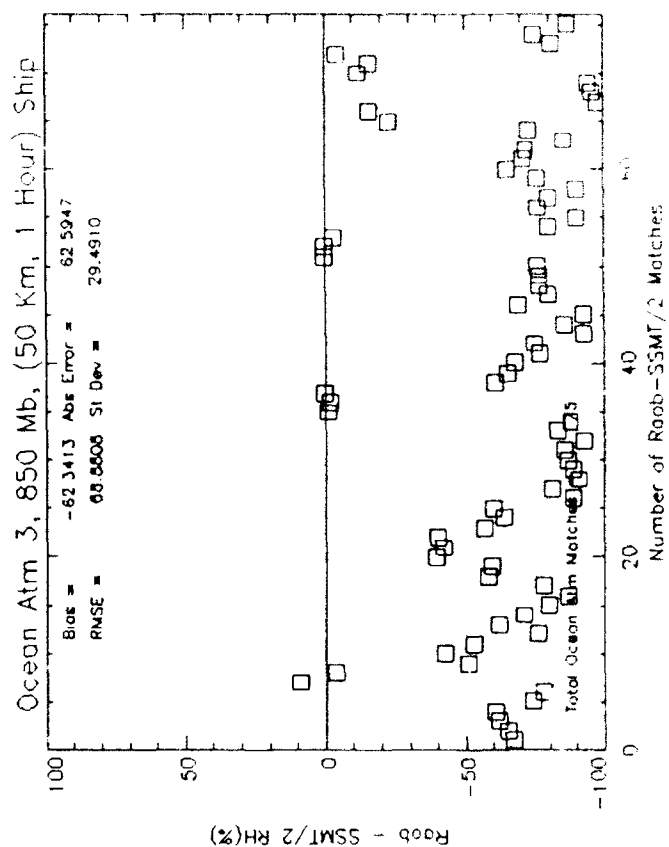
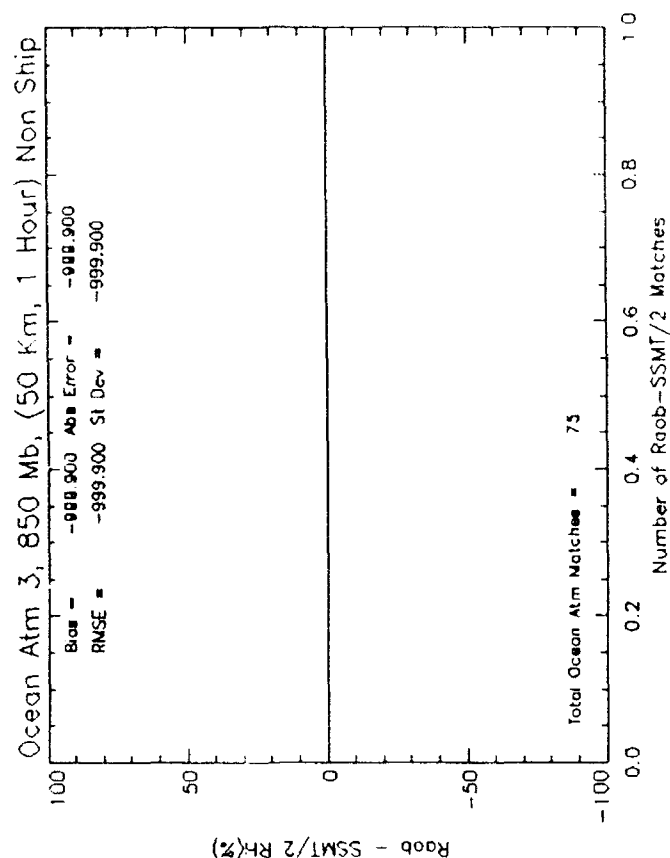
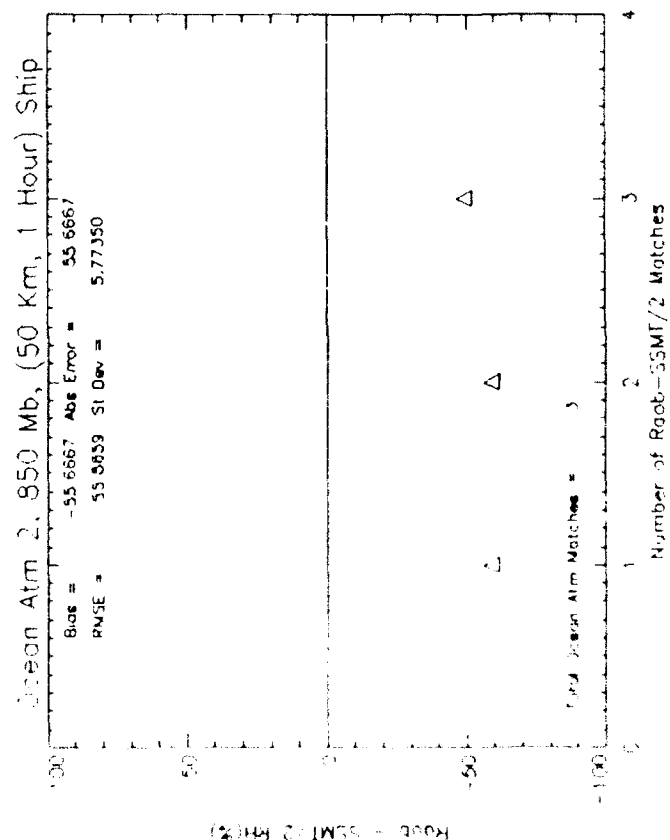
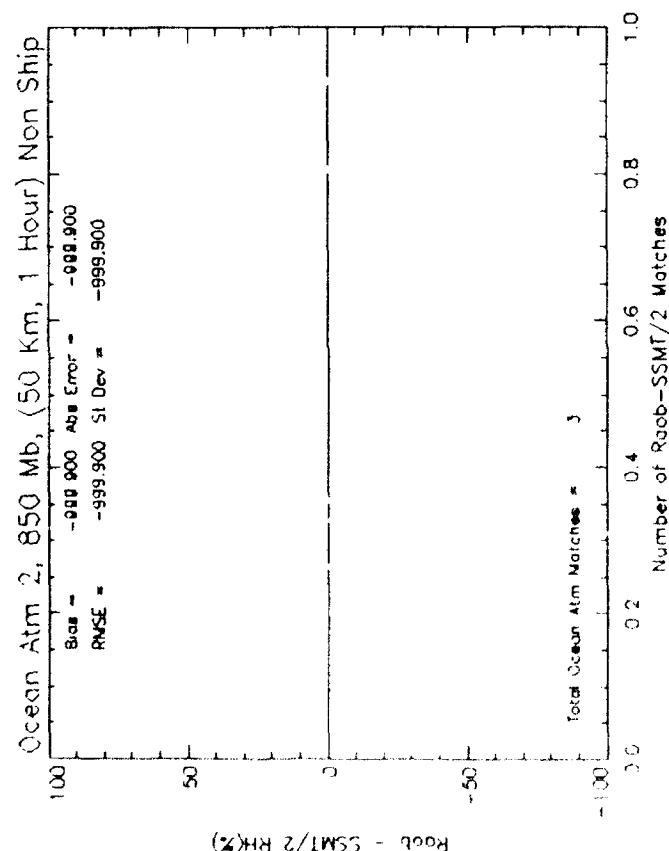


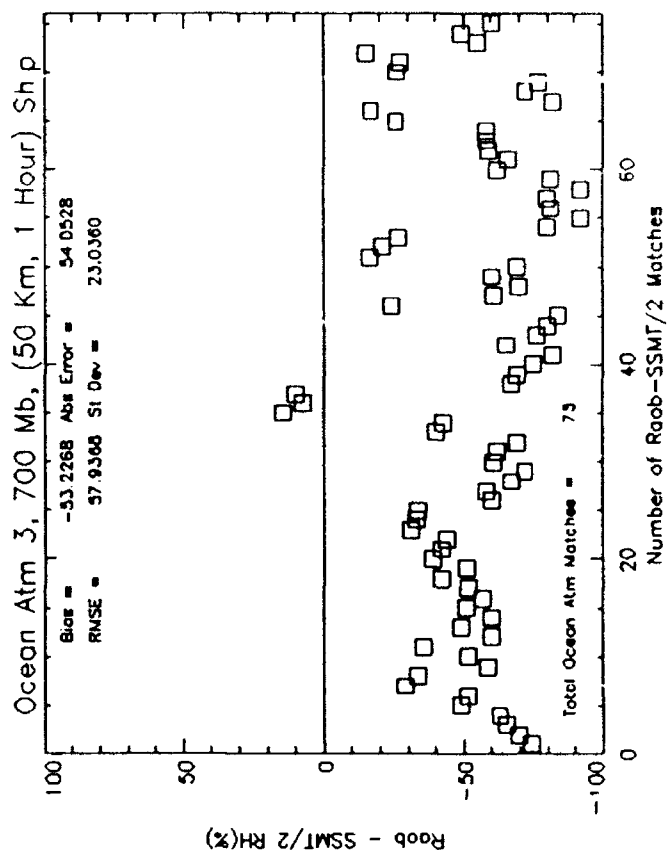
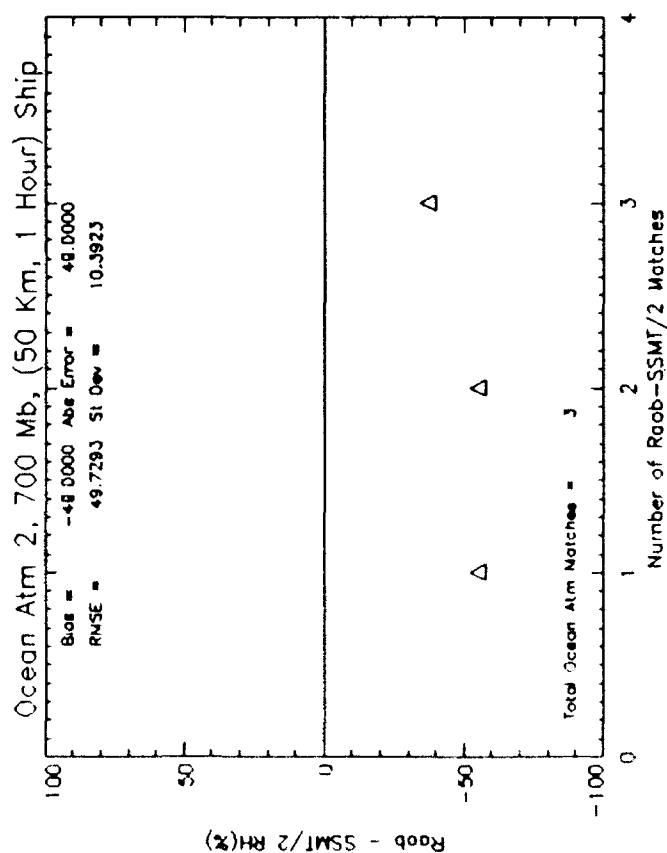
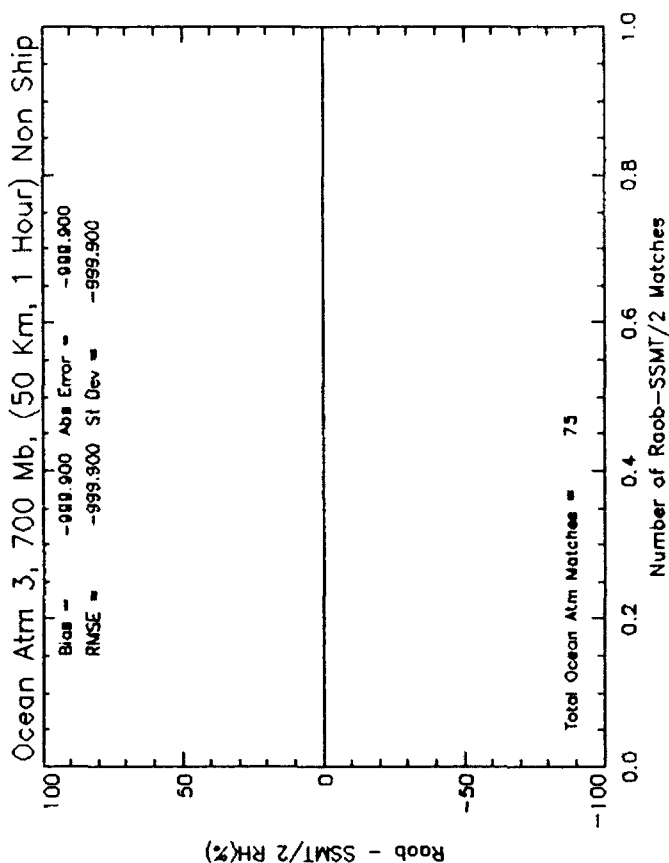
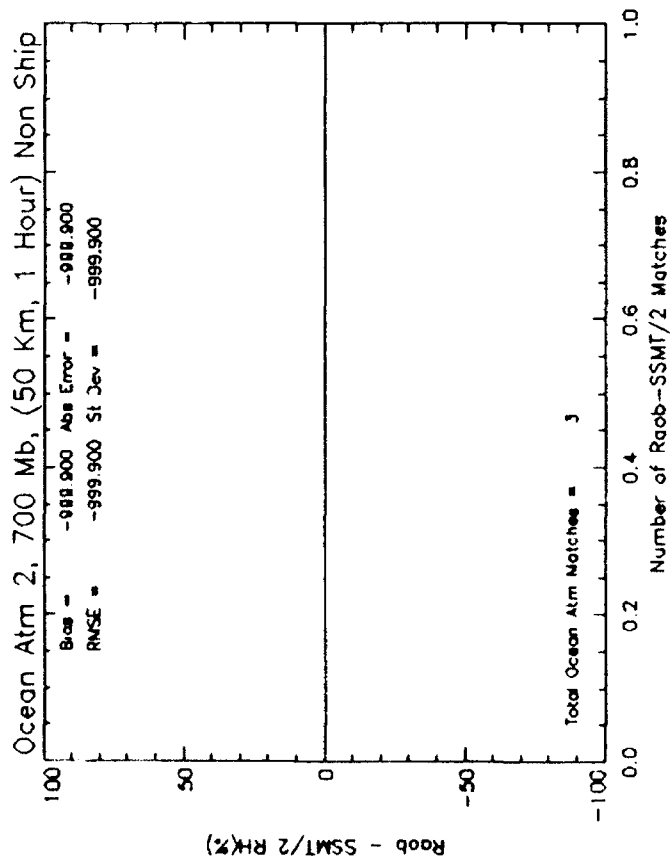




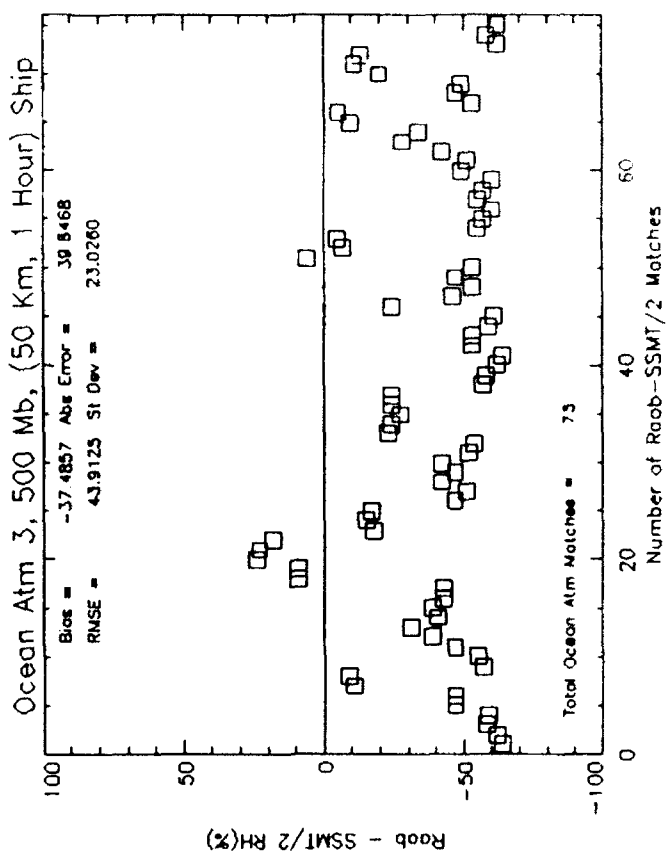
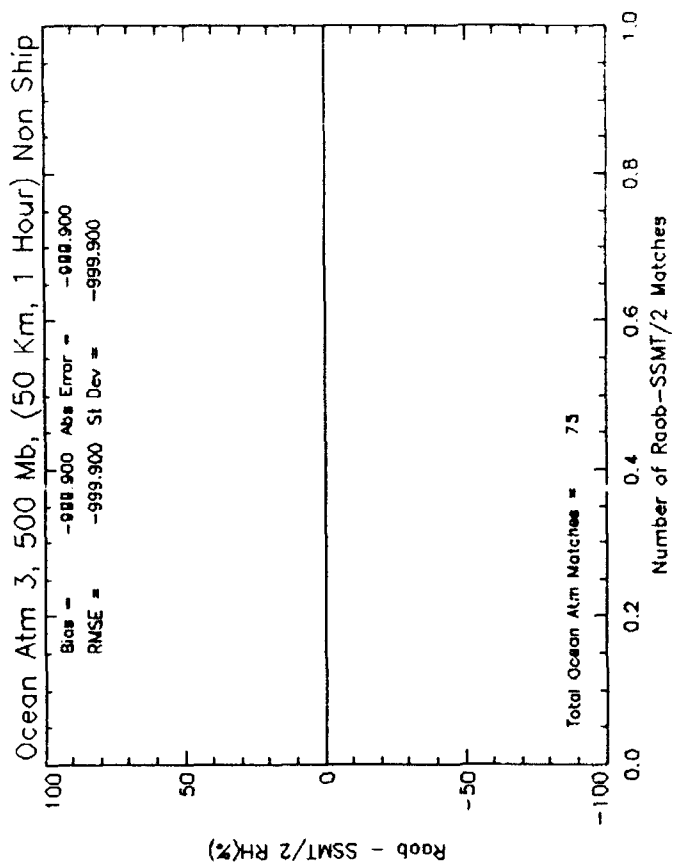
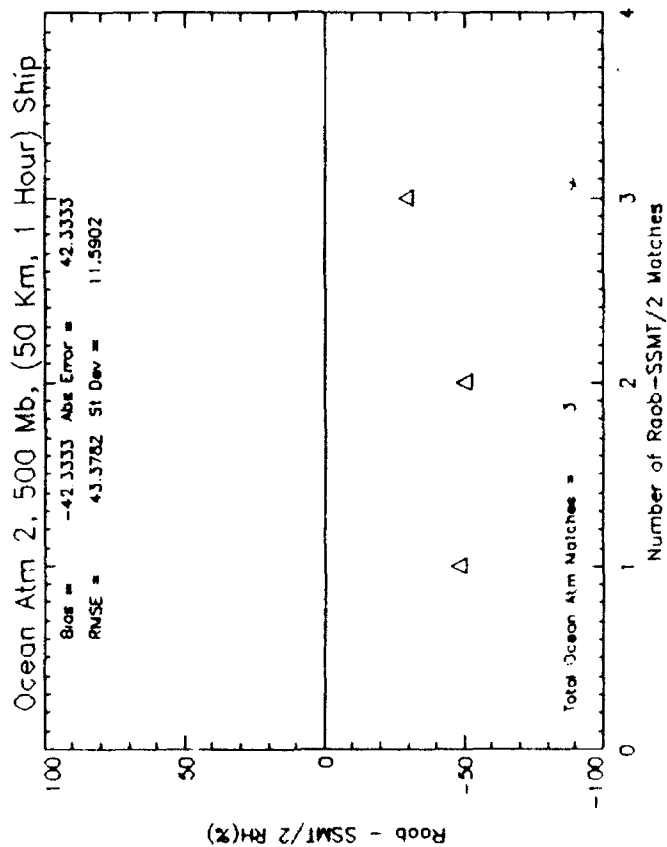
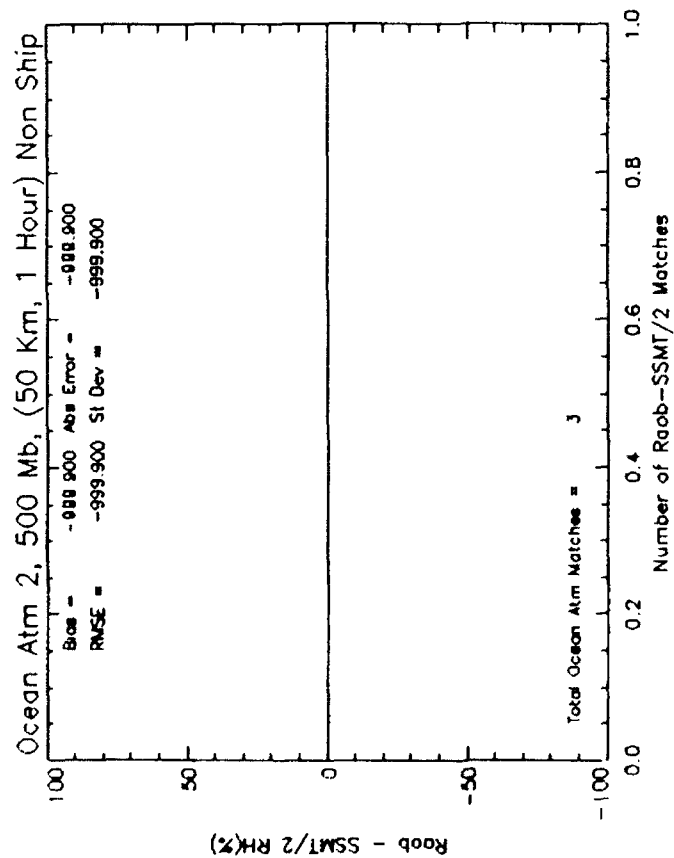


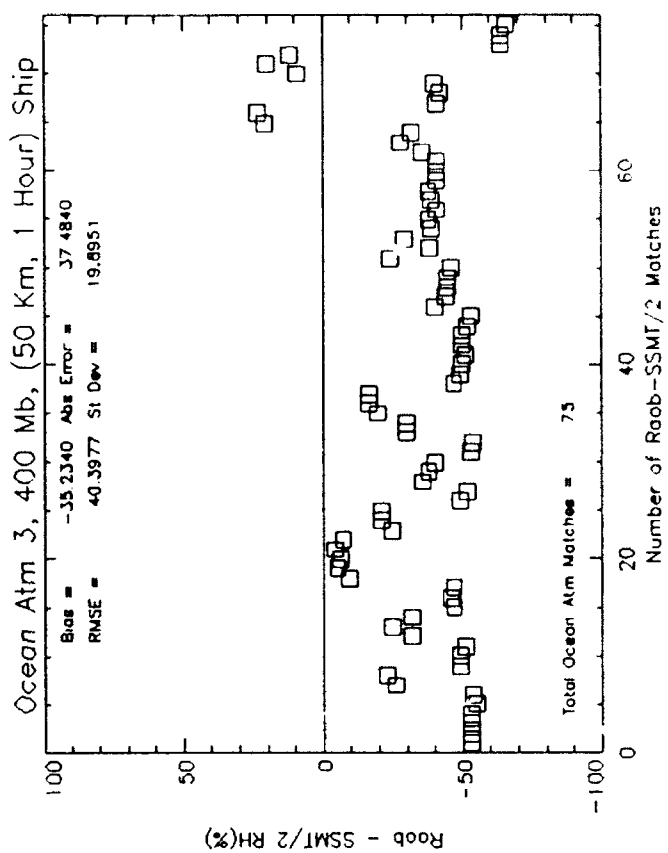
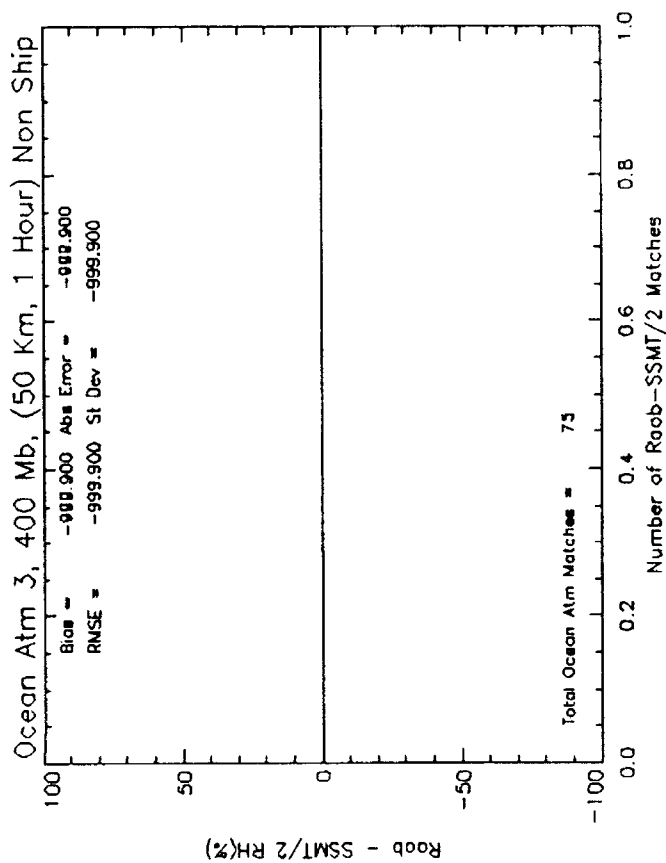
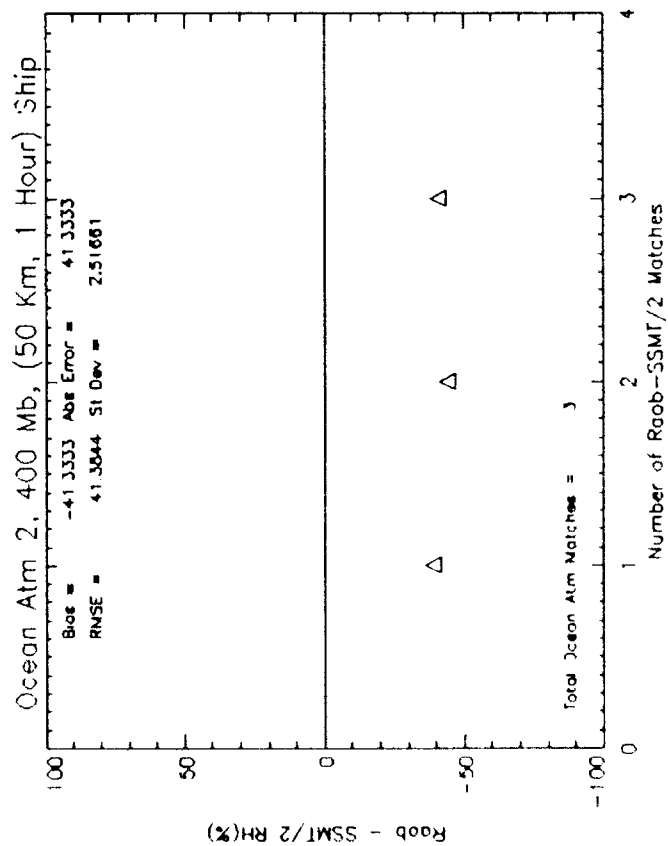
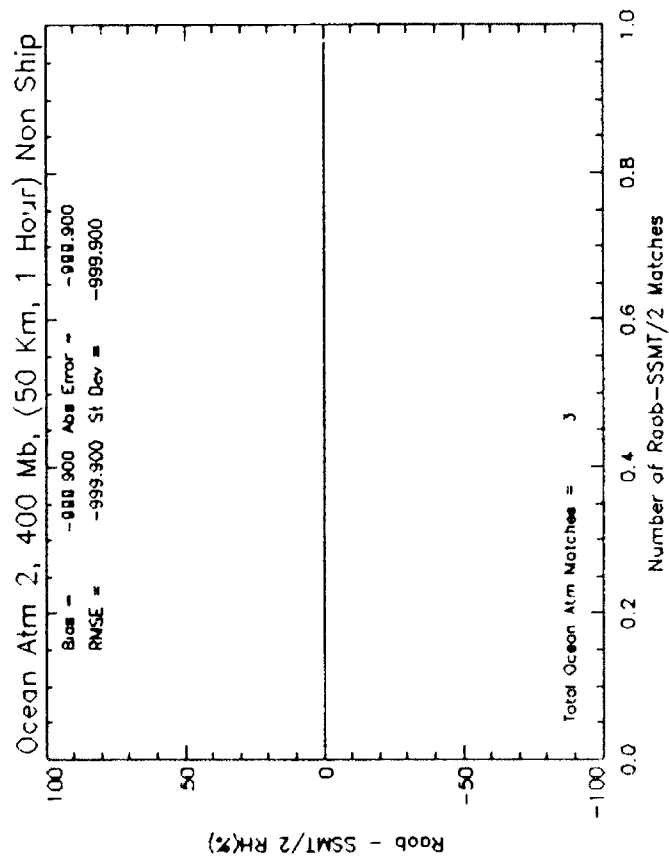


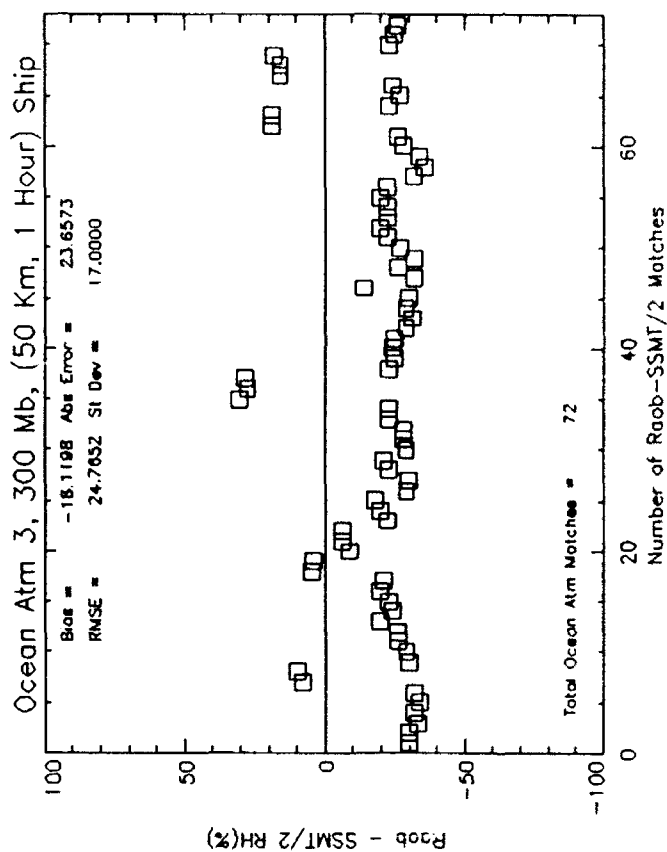
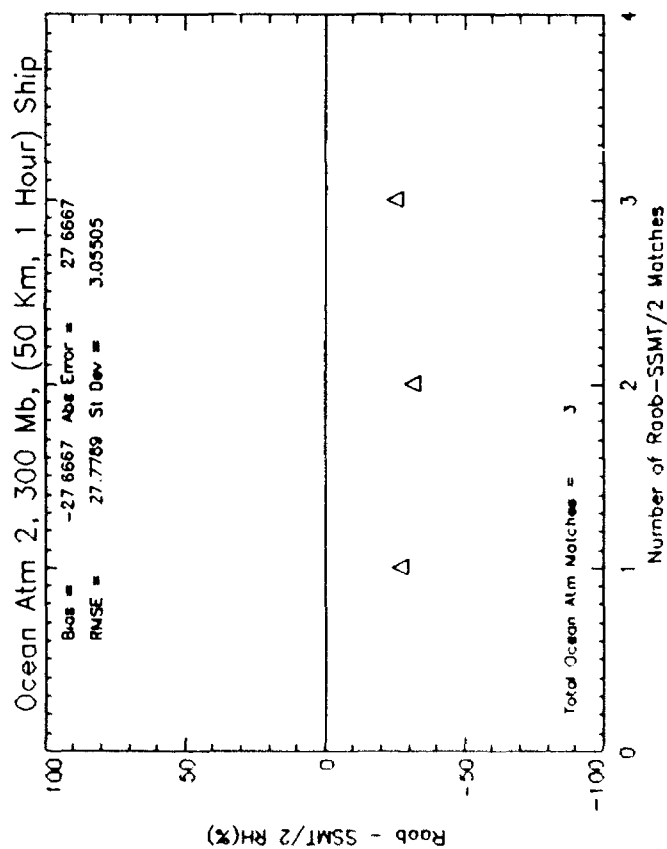
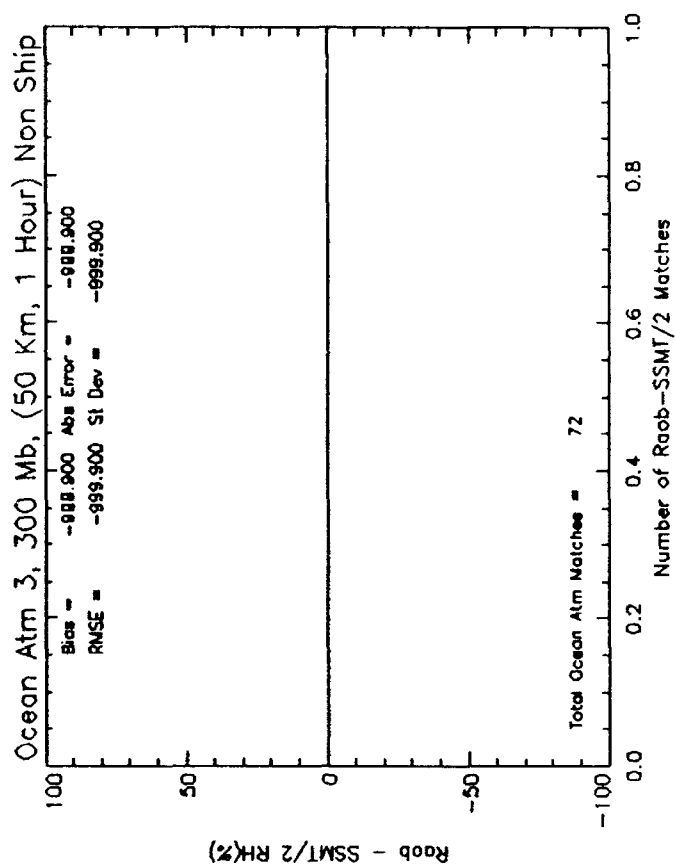
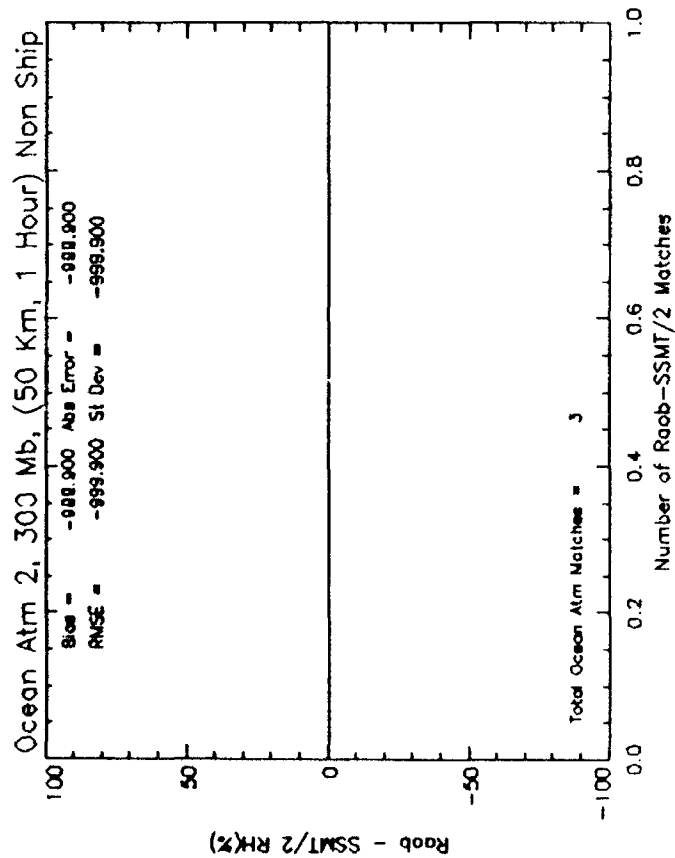


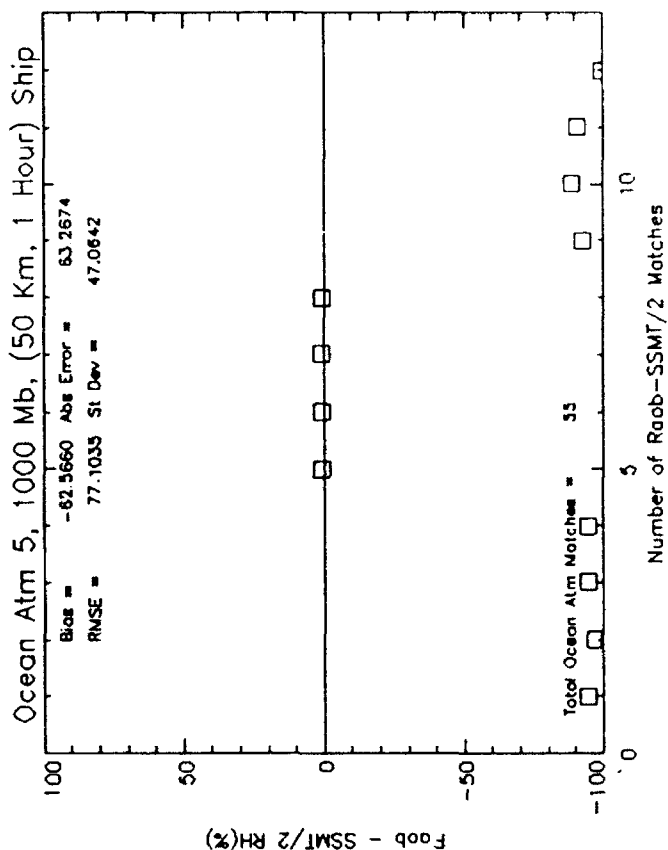
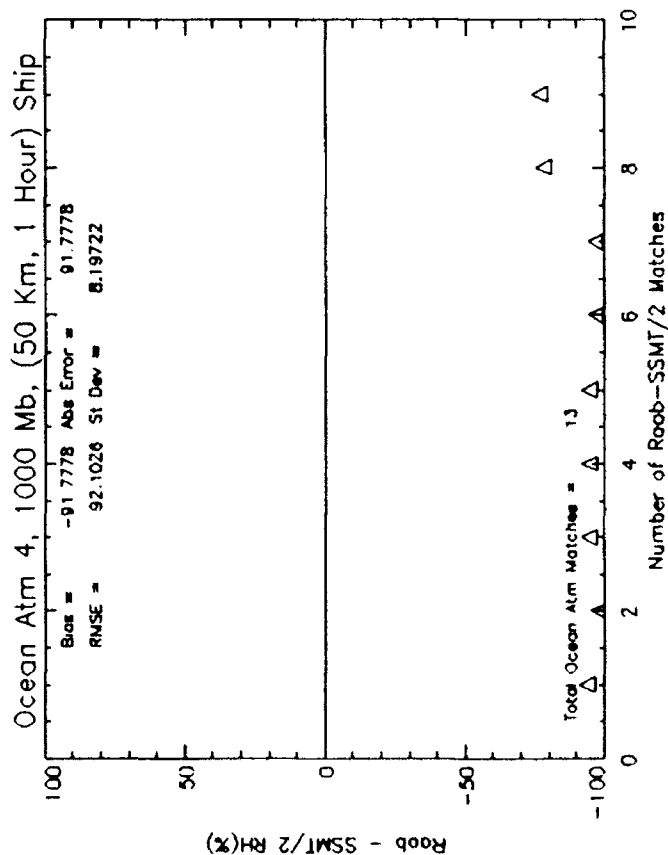
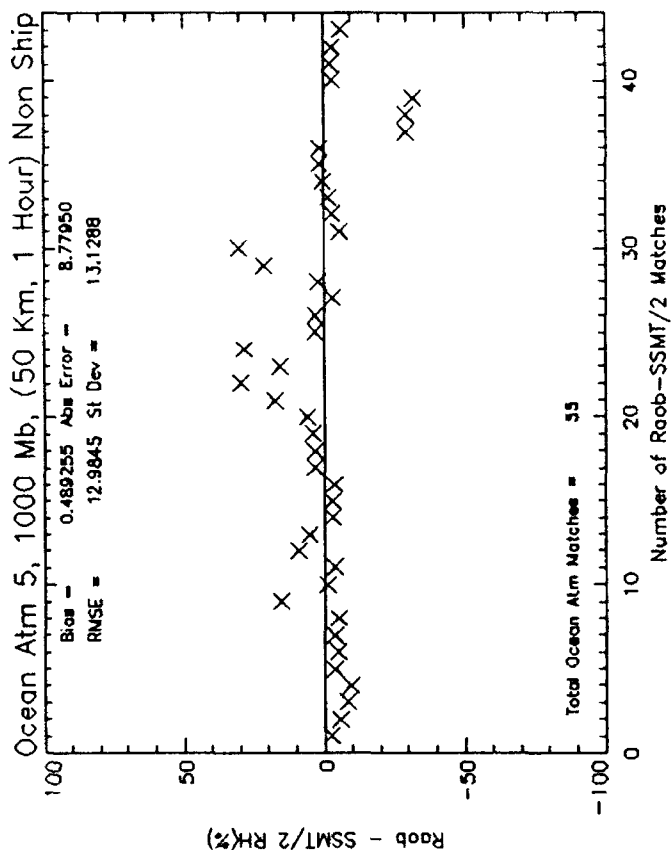
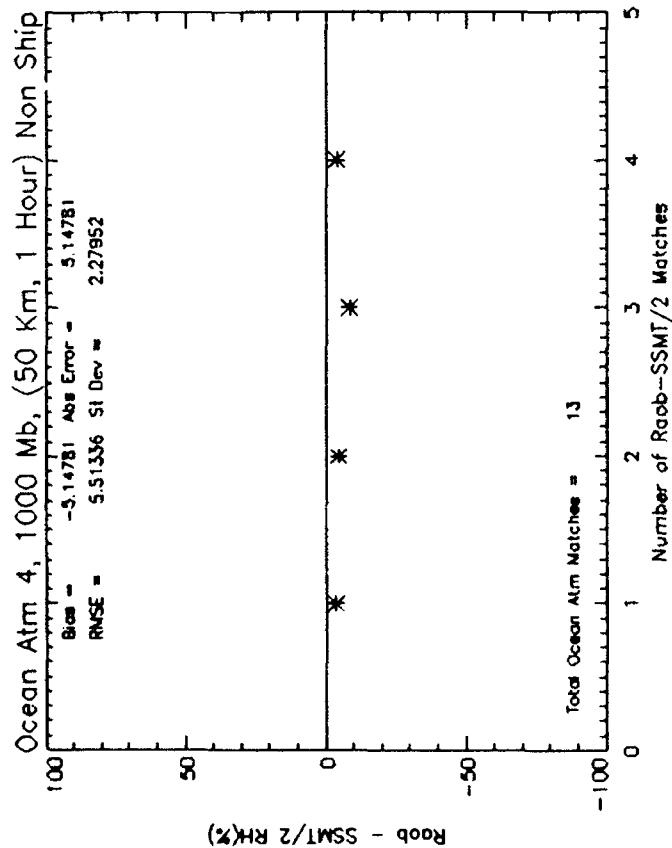


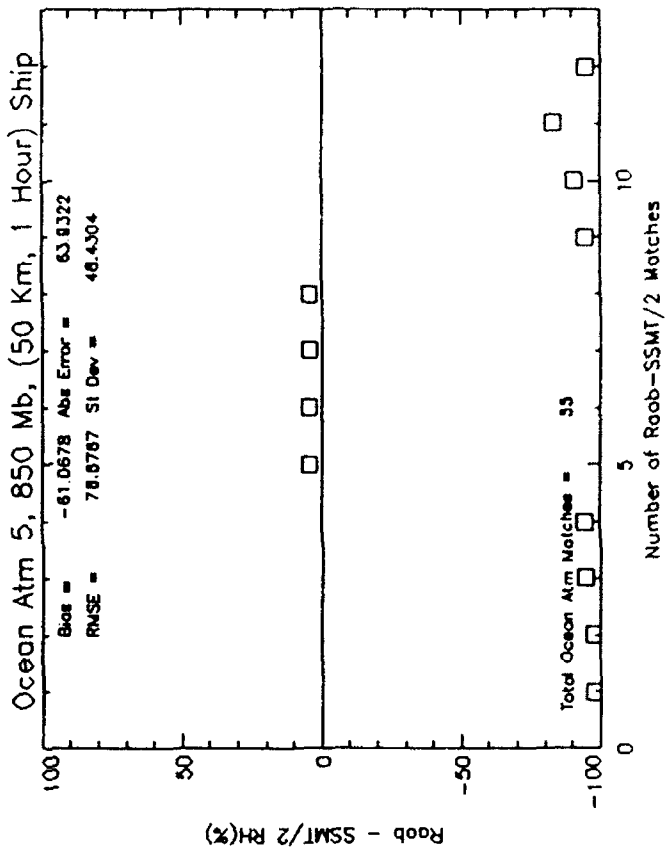
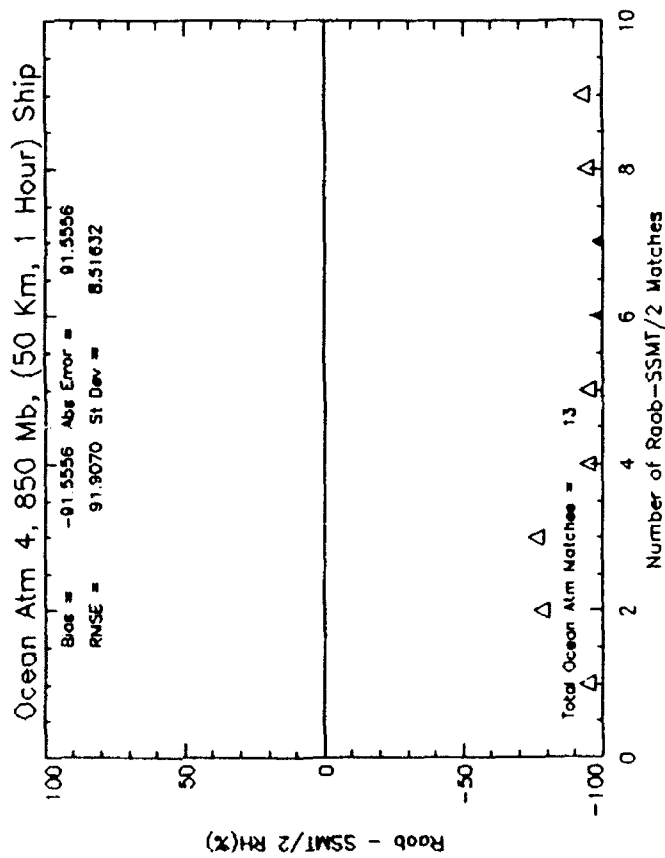
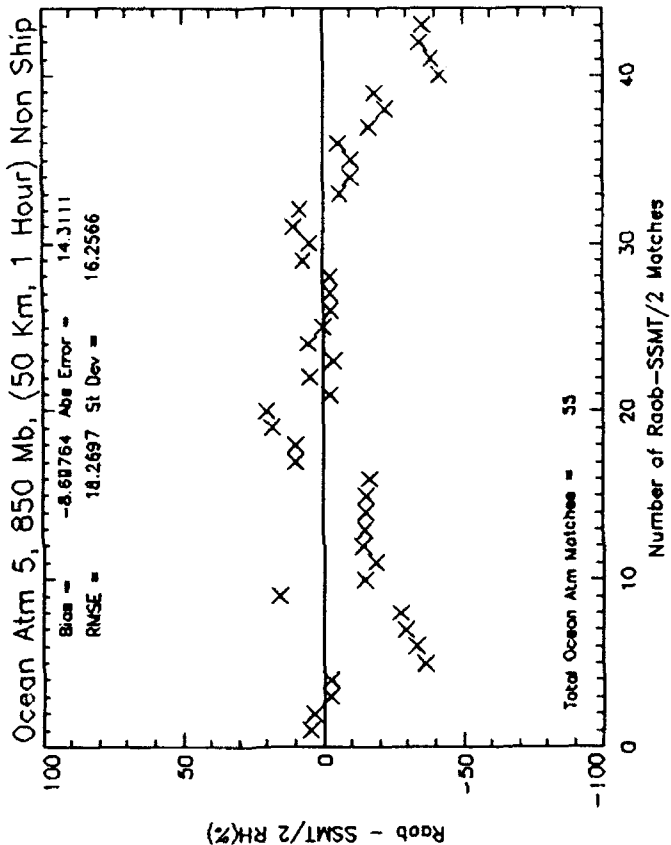
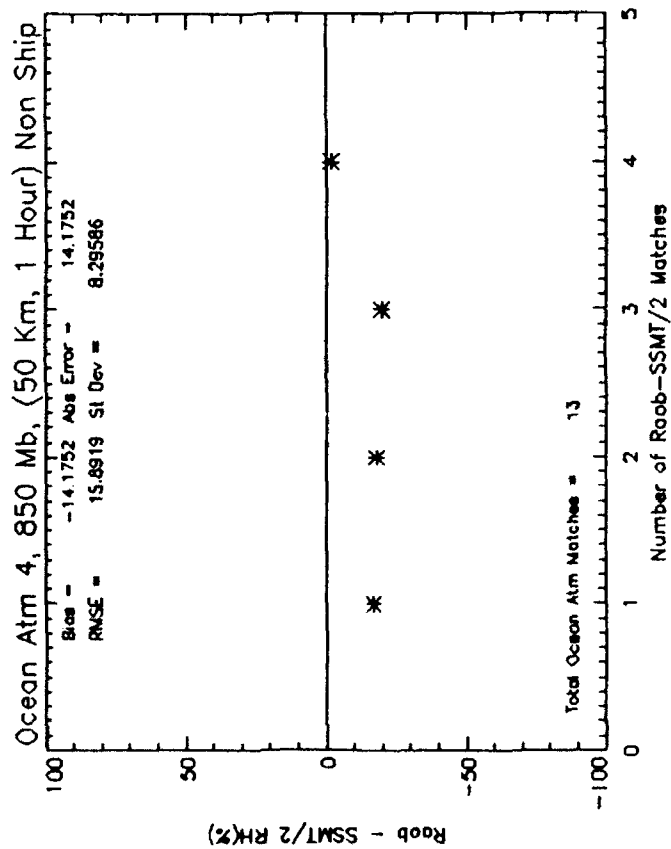


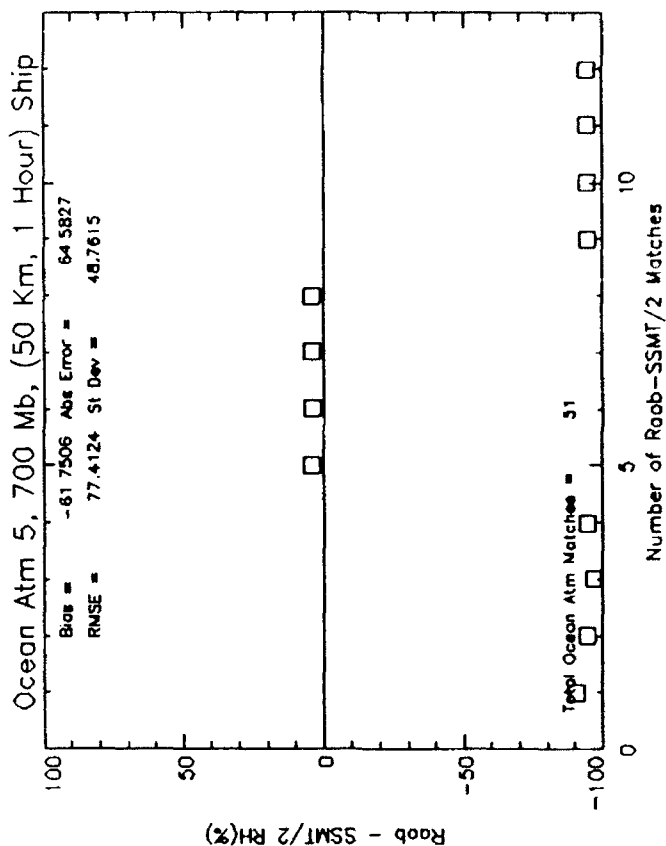
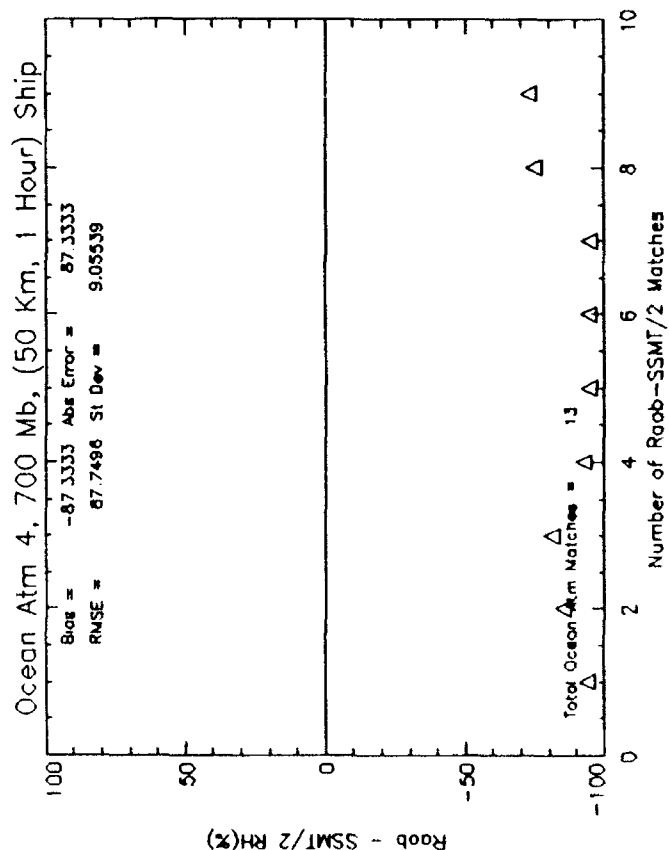
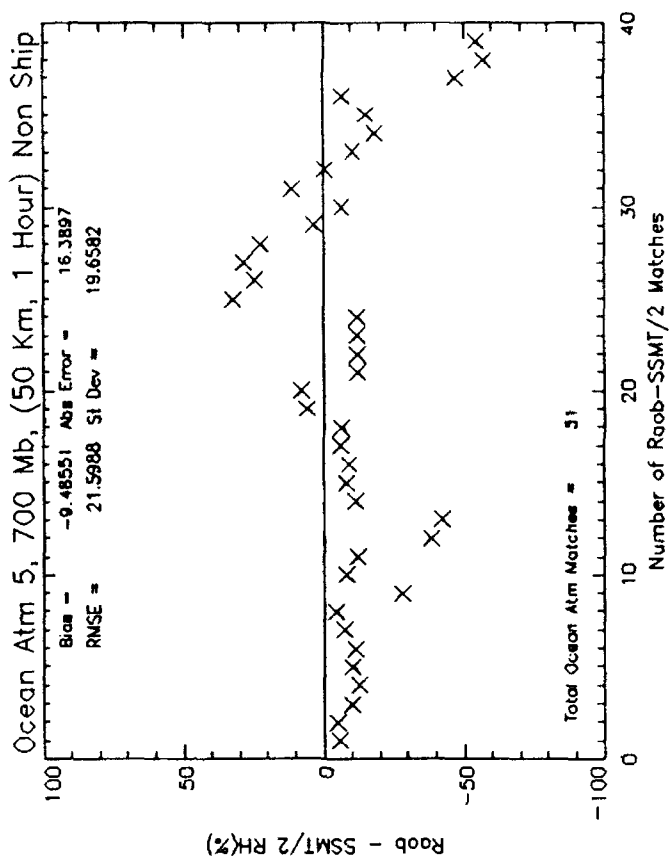
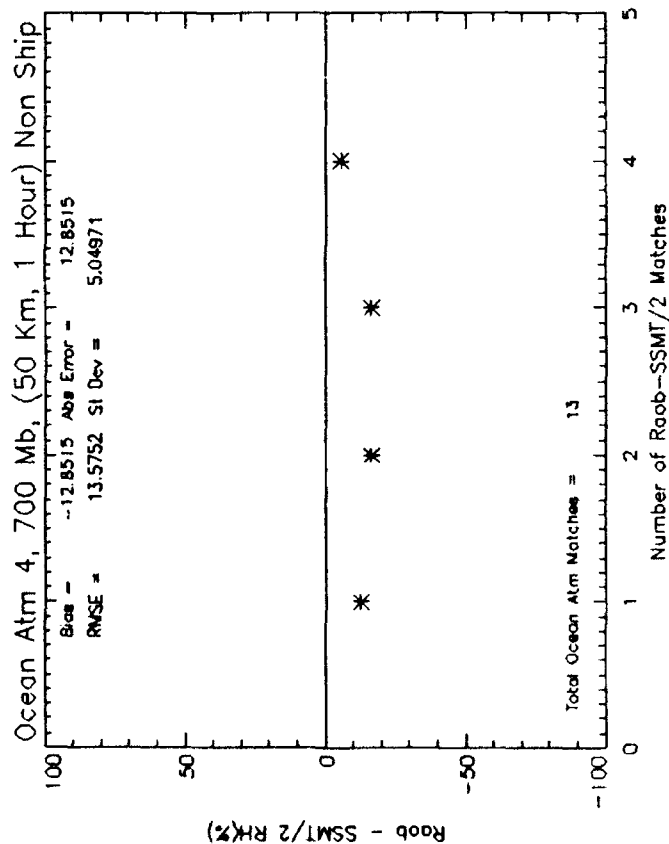


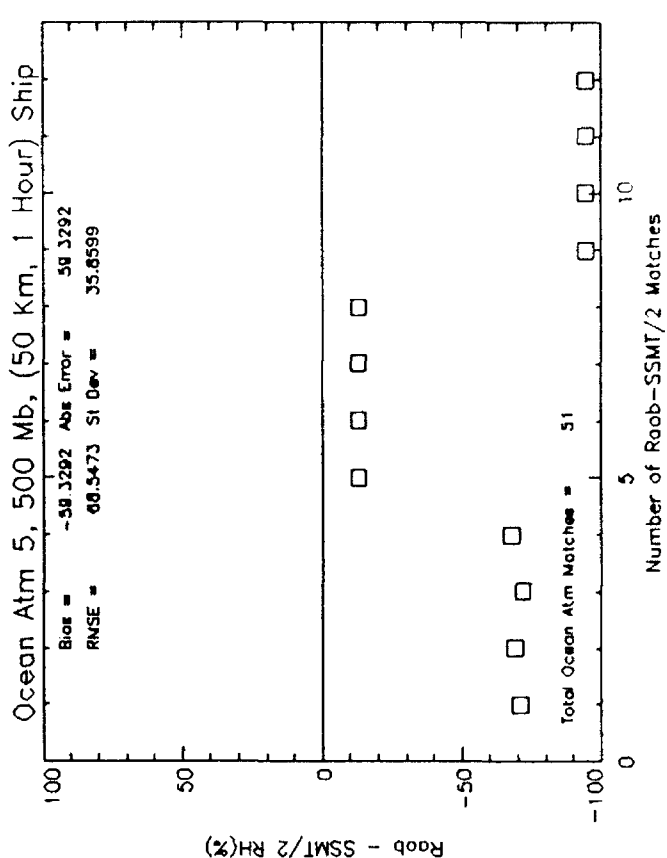
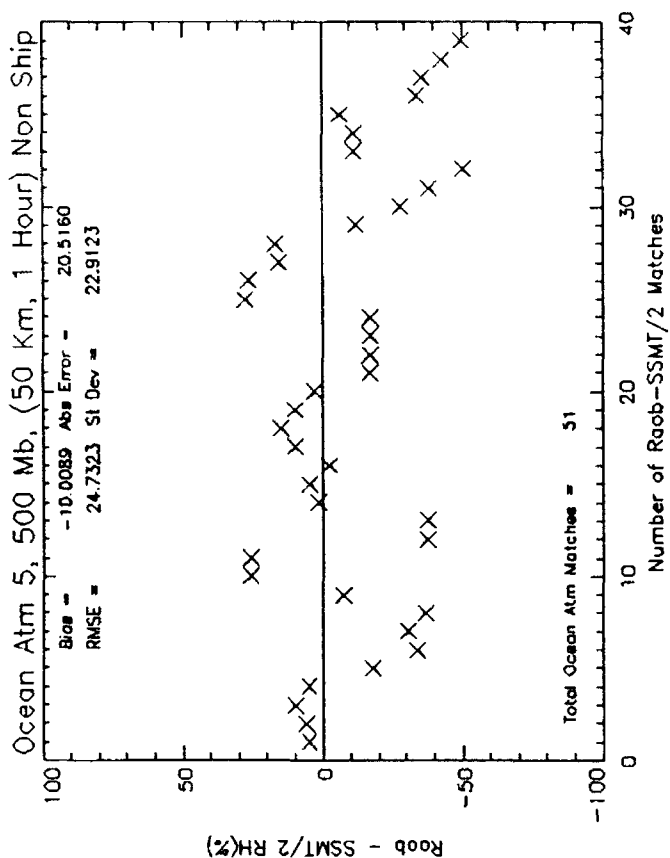
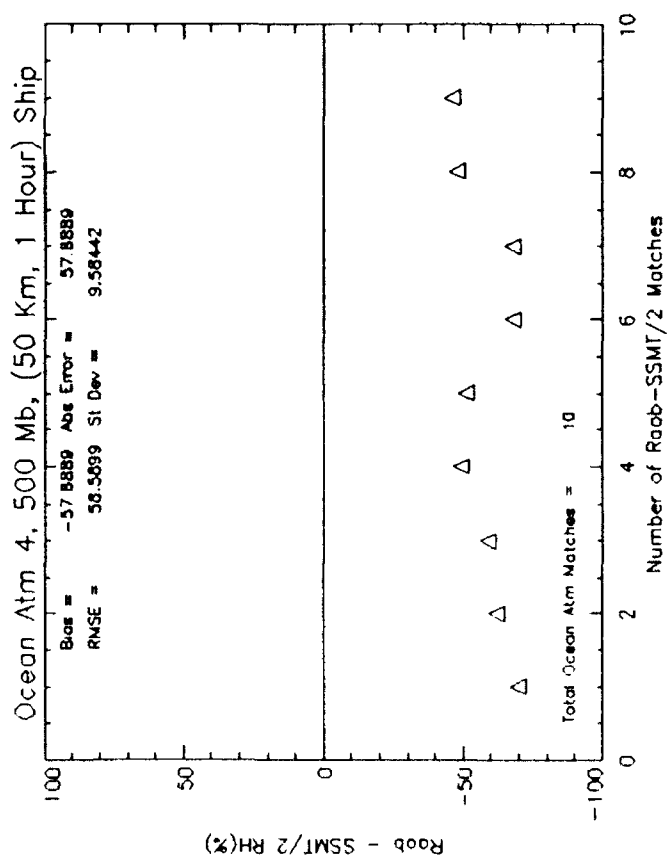
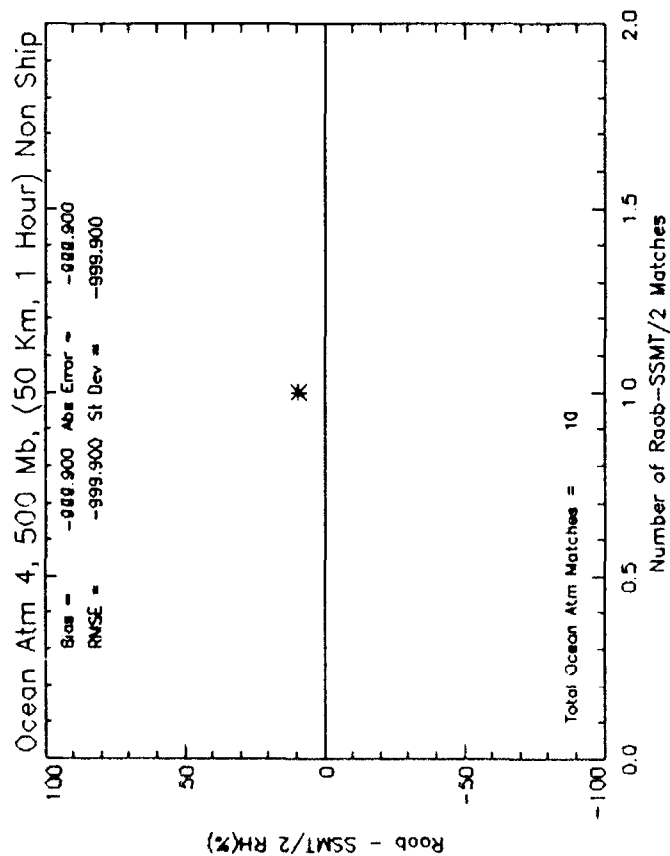


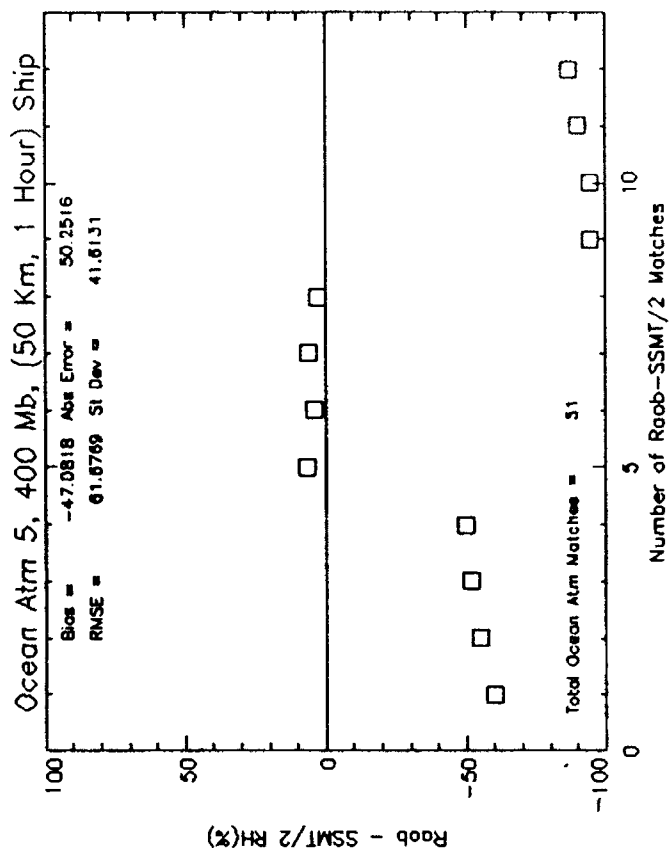
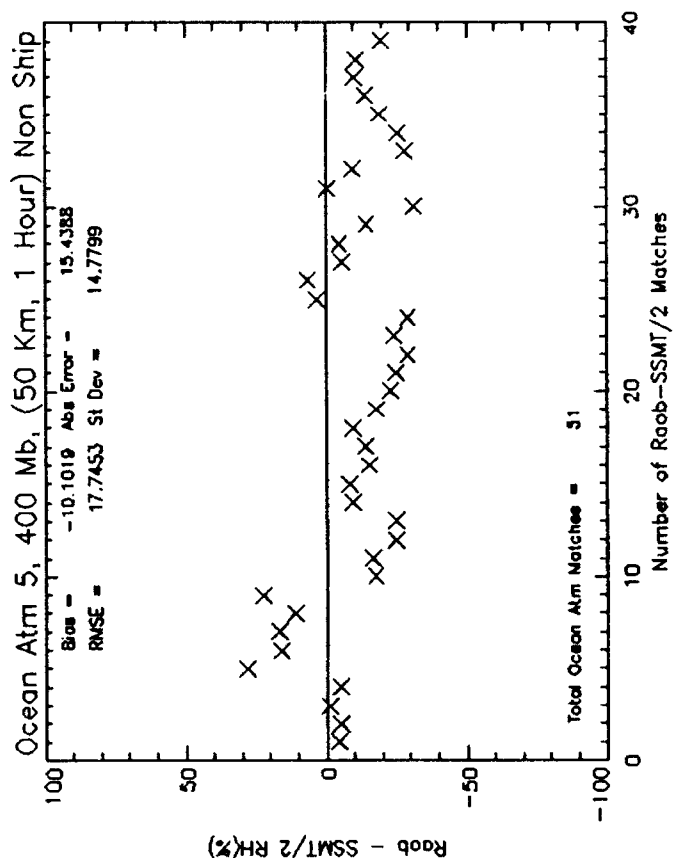
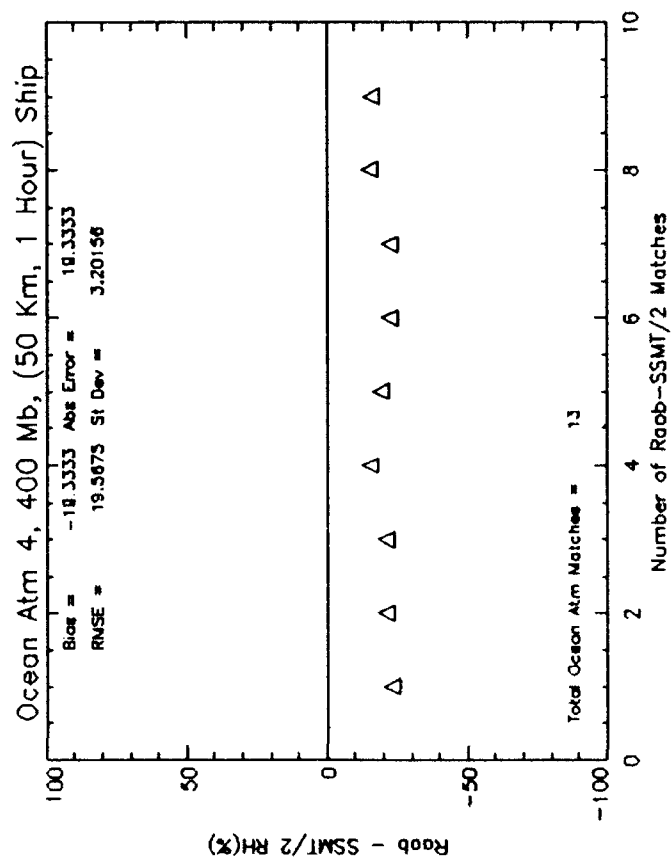
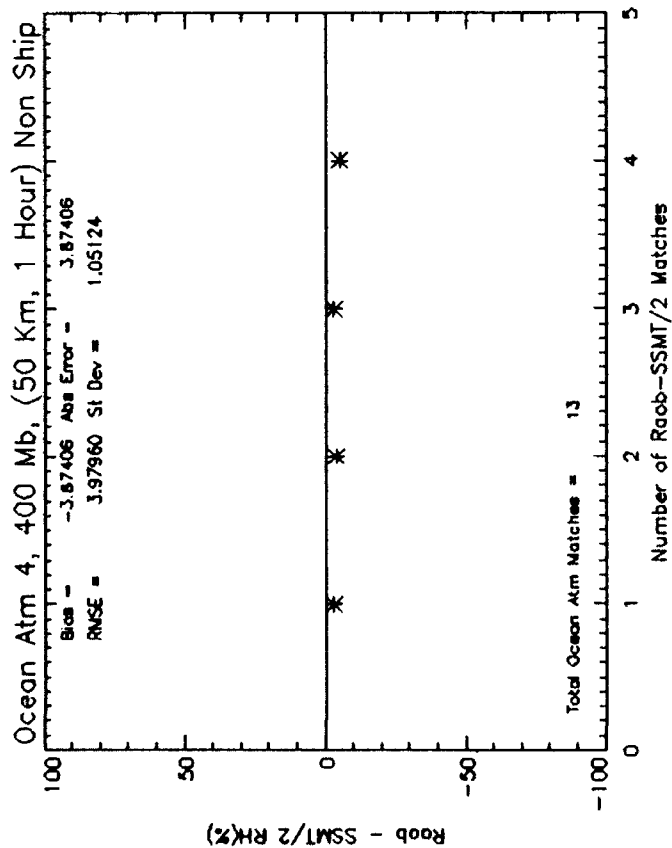




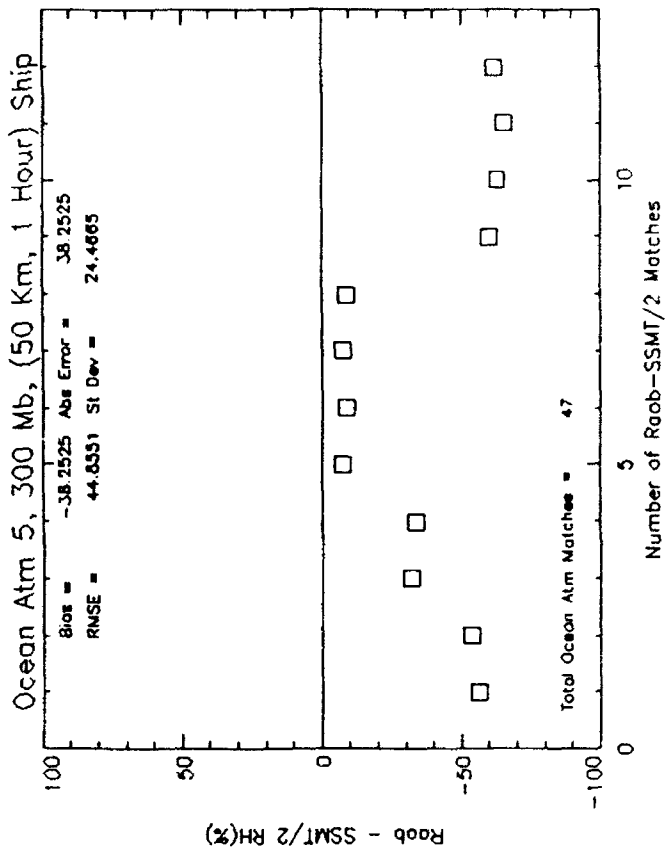
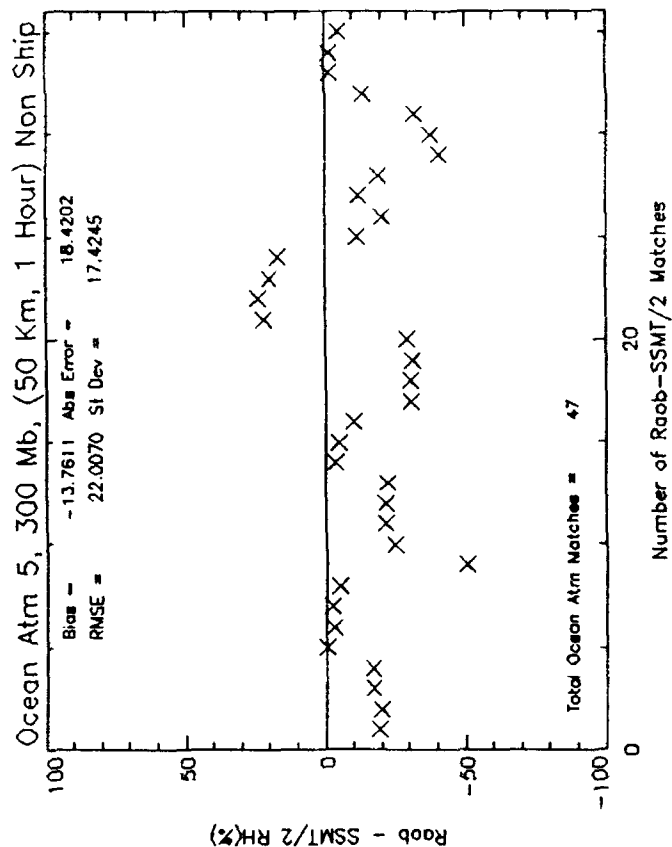
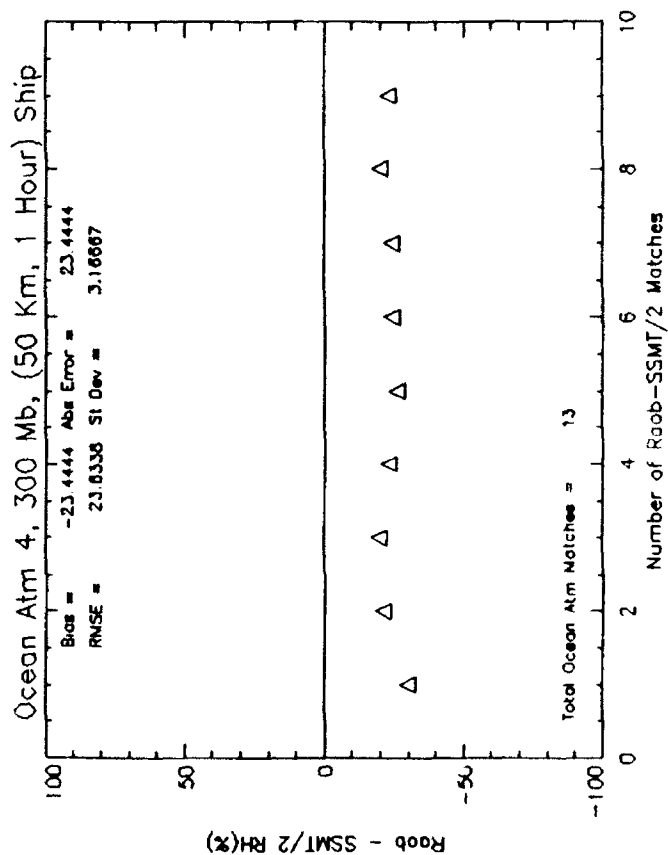
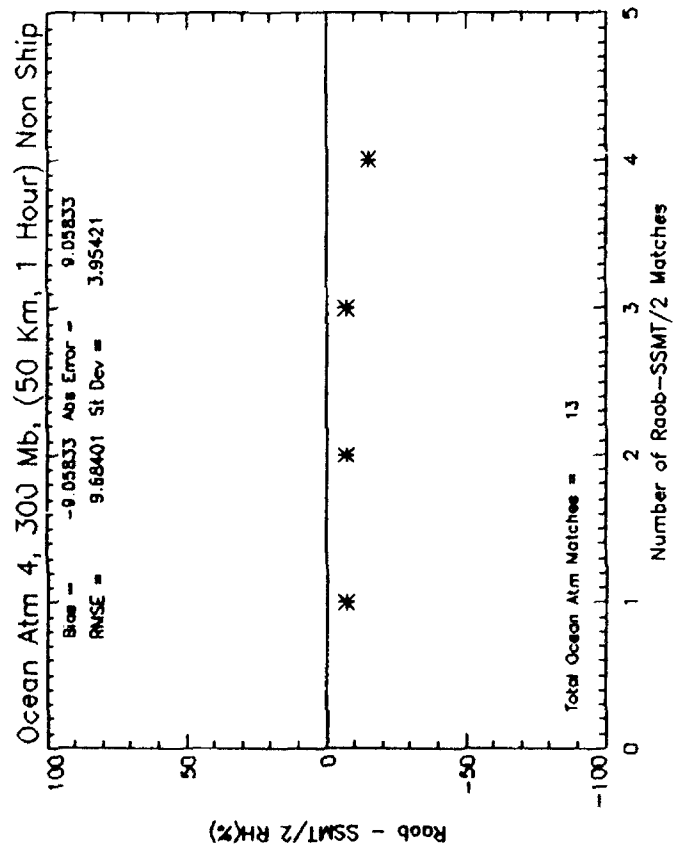


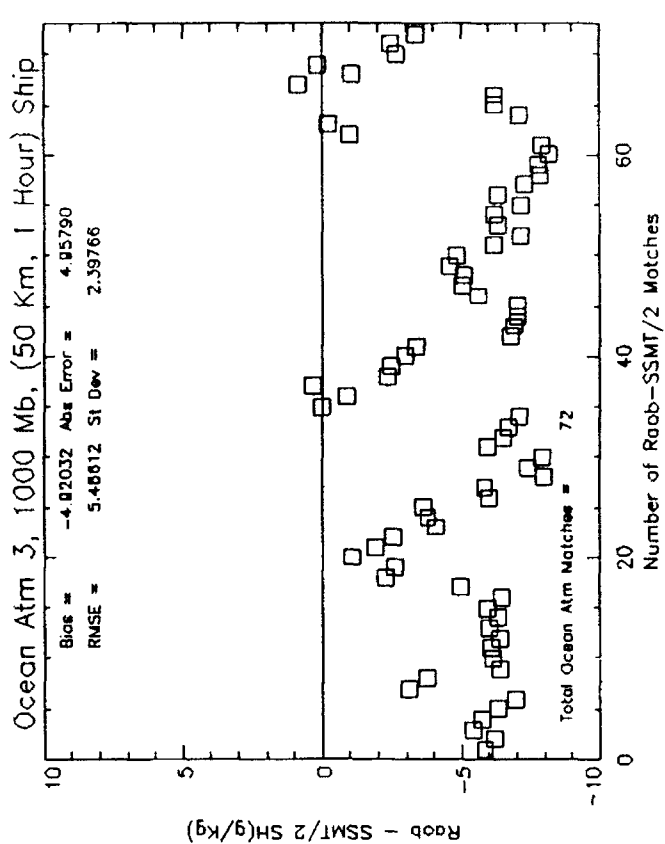
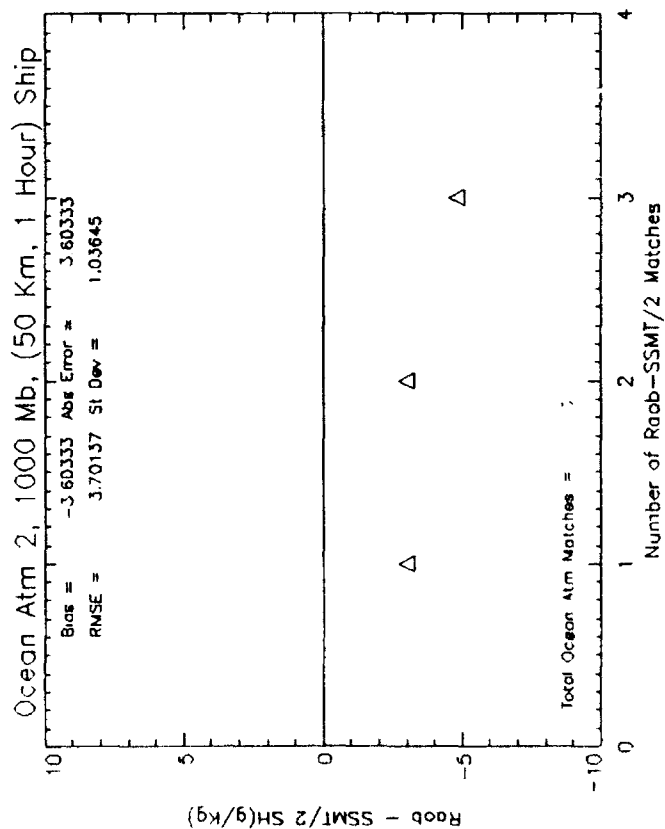
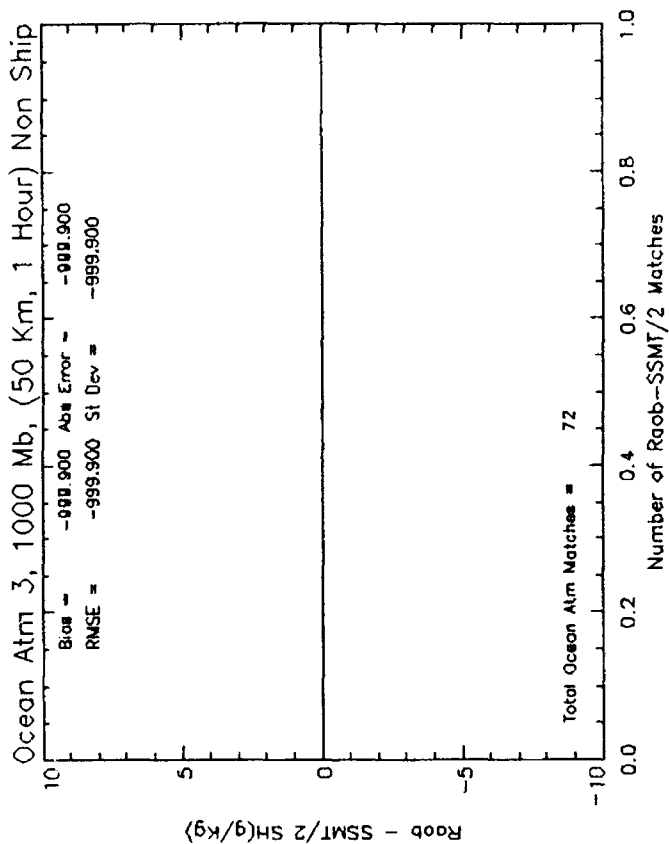
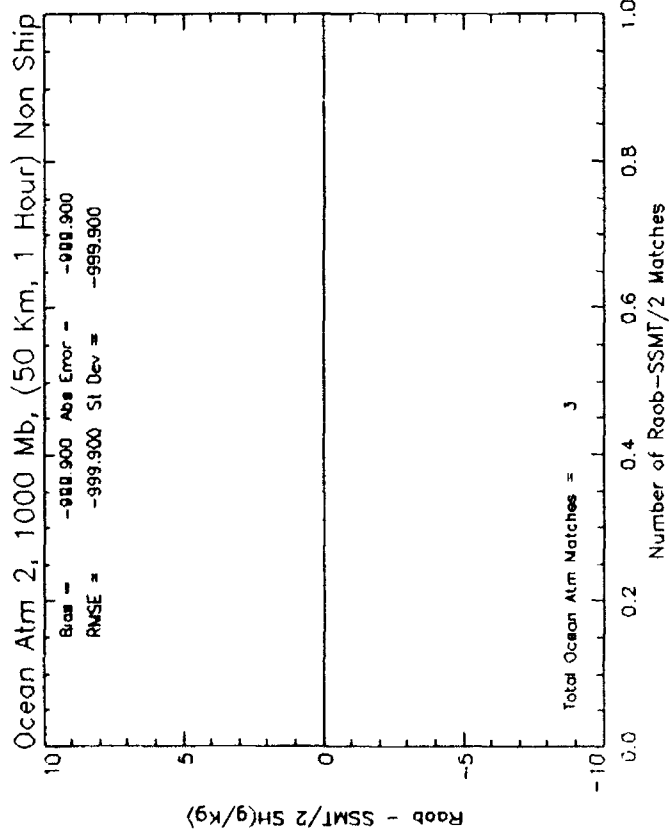


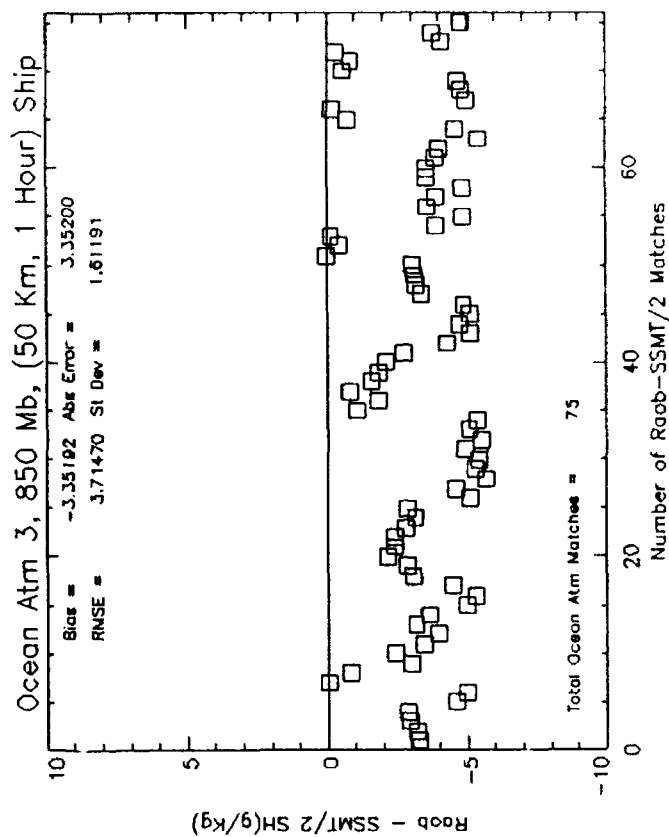
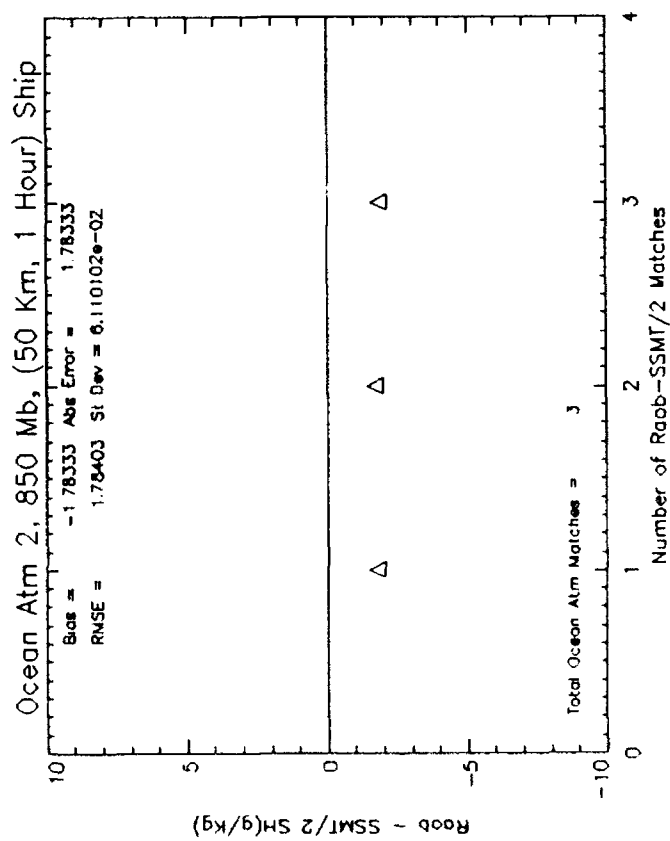
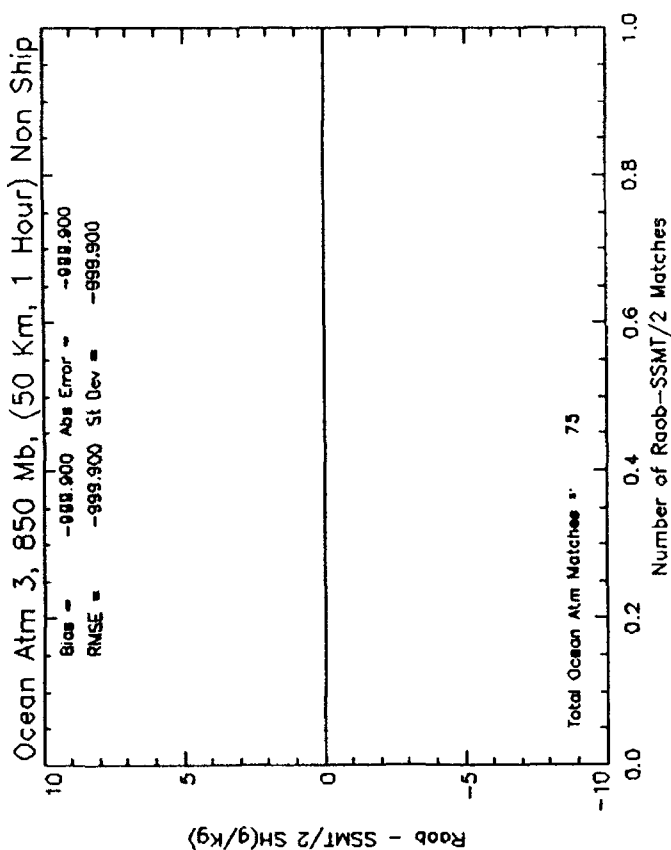
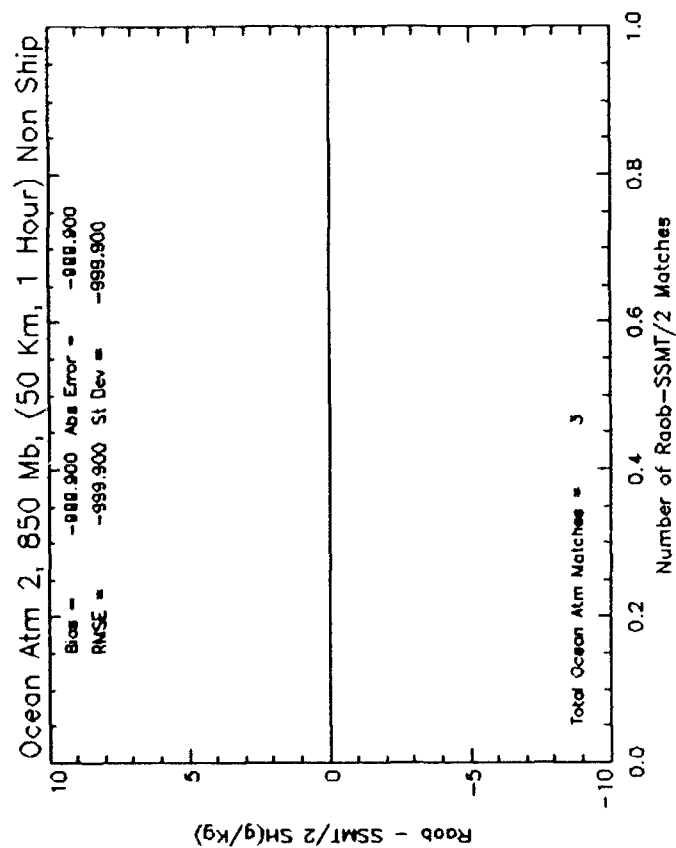


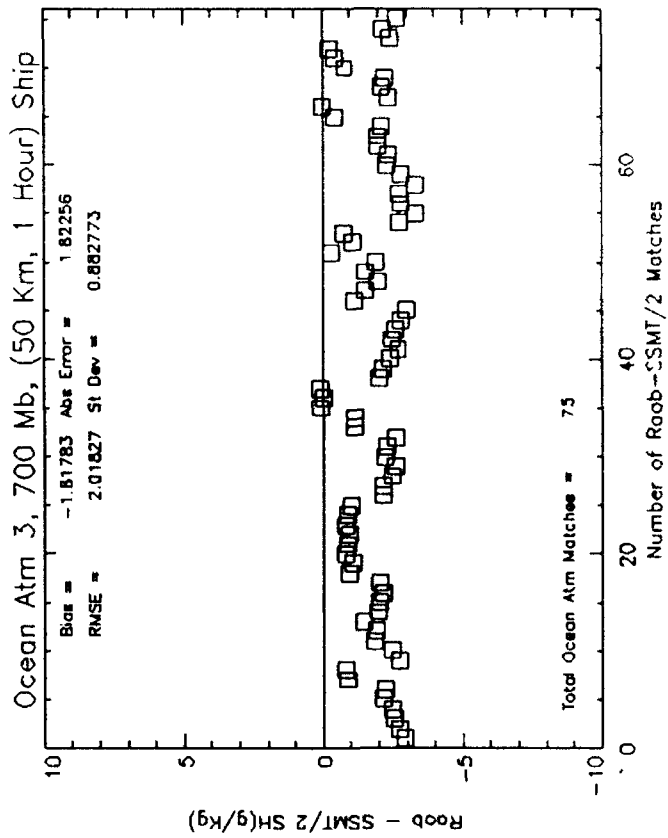
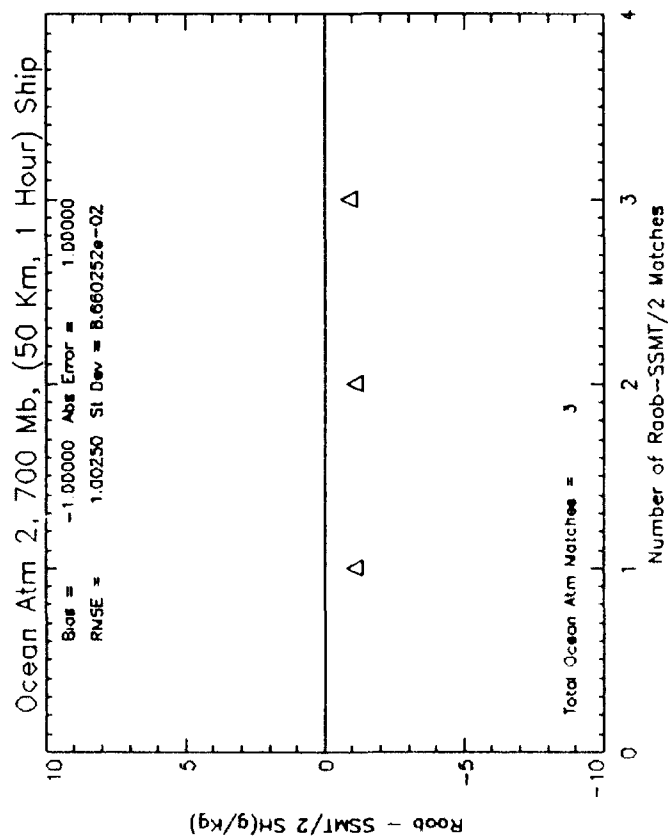
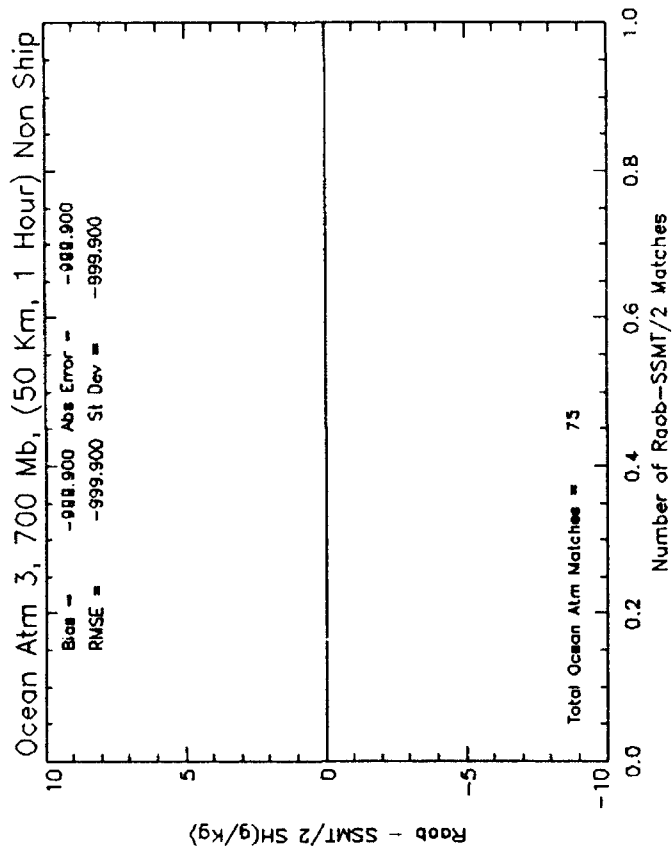
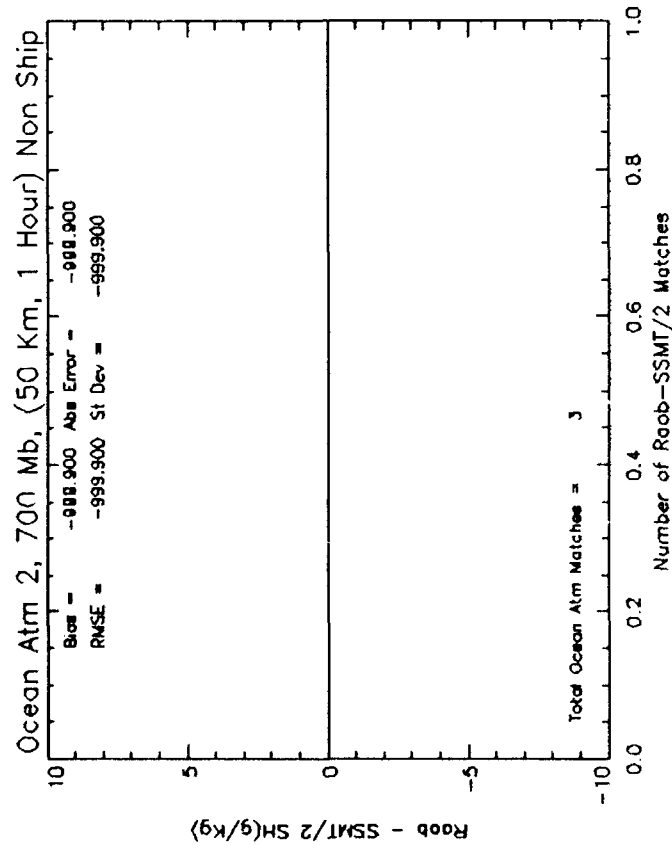








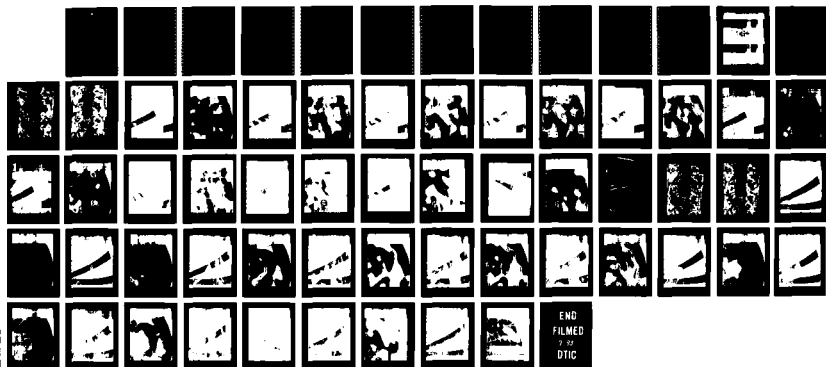




AD-A265 817 DASP F11 SSM/T-2 CALIBRATION AND VALIDATION(US) PHILLIPS 575  
LAB HANSCOM AFB MA V FALCONE ET AL. 29 OCT 92  
PL-TR-92-2293 XC-SMC

UNCLASSIFIED

NL



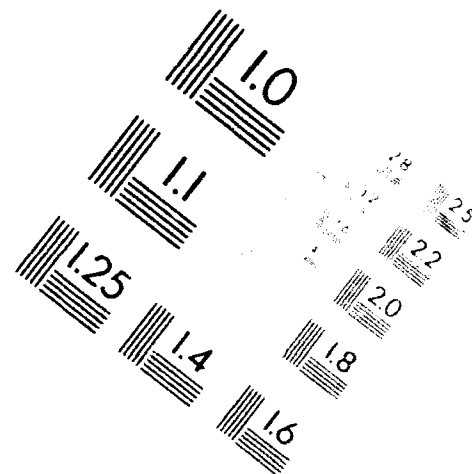
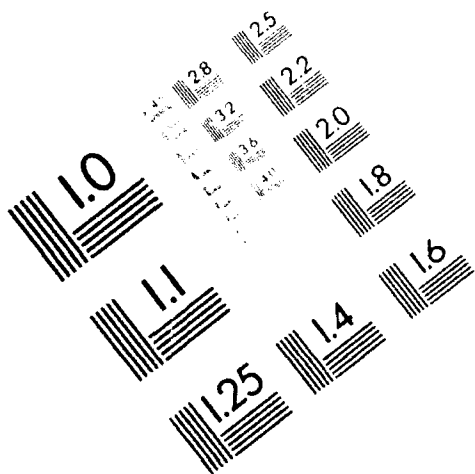


**AIM**

**Association for Information and Image Management**

1100 Wayne Avenue, Suite 1100  
Silver Spring, Maryland 20910

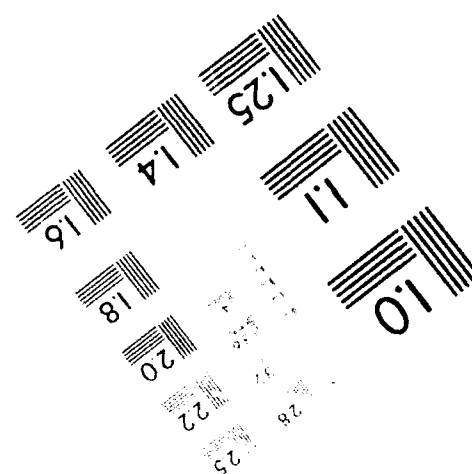
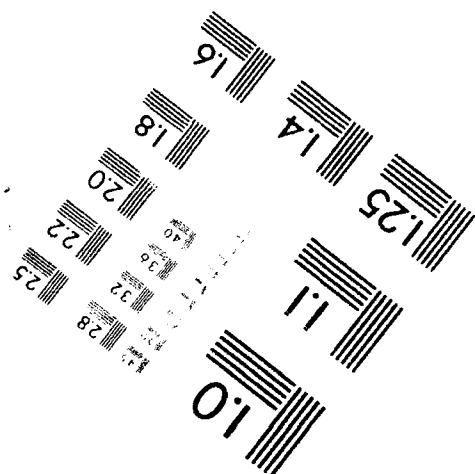
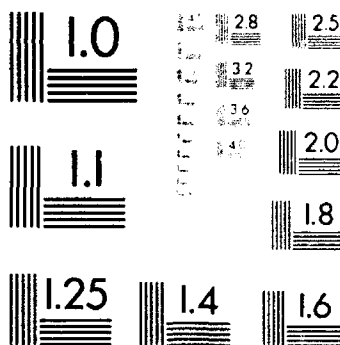
301 587-8202



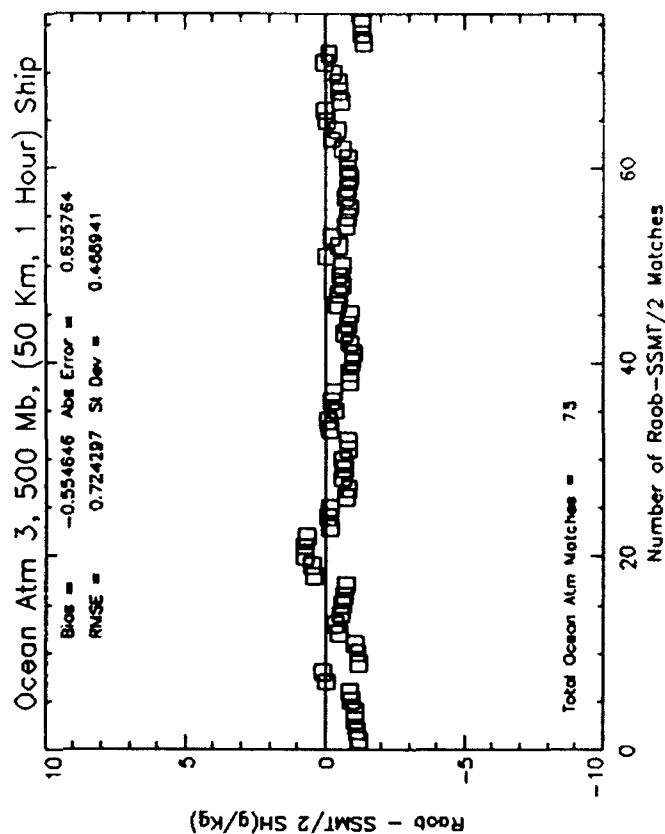
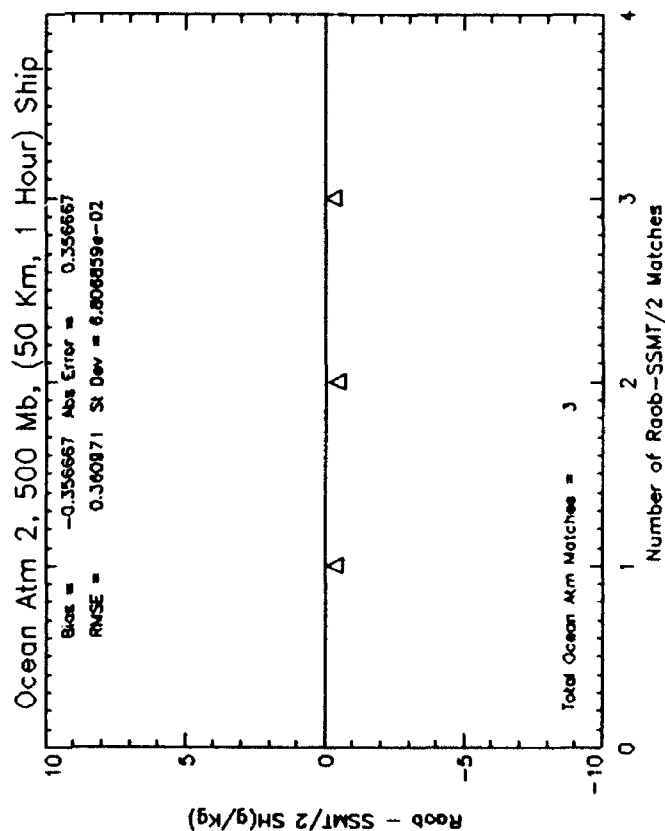
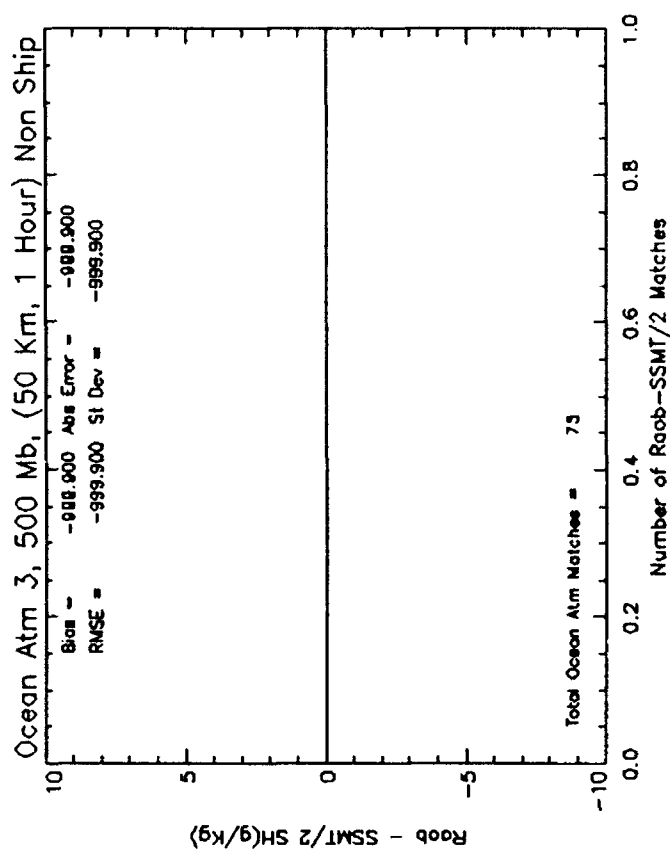
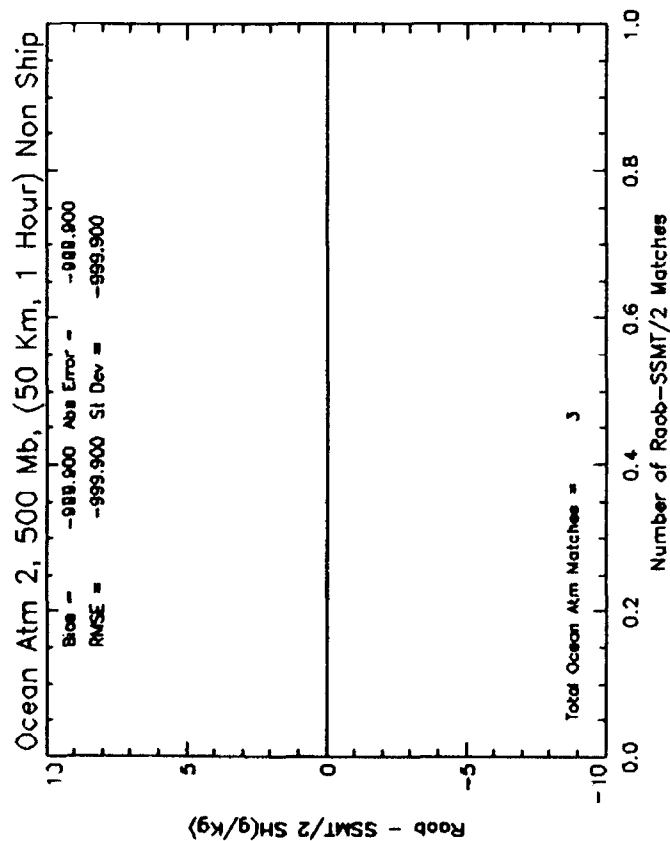
**Centimeter**

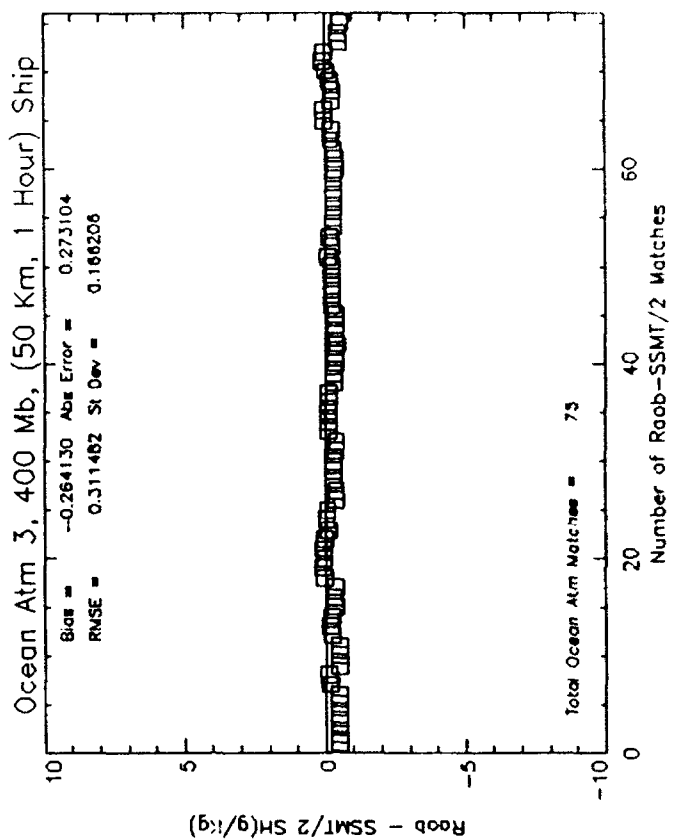
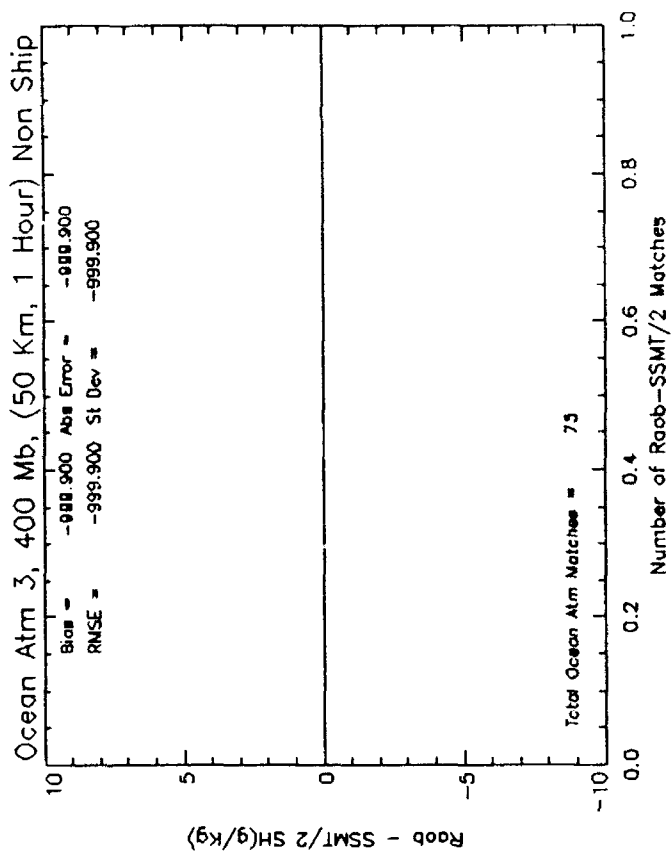
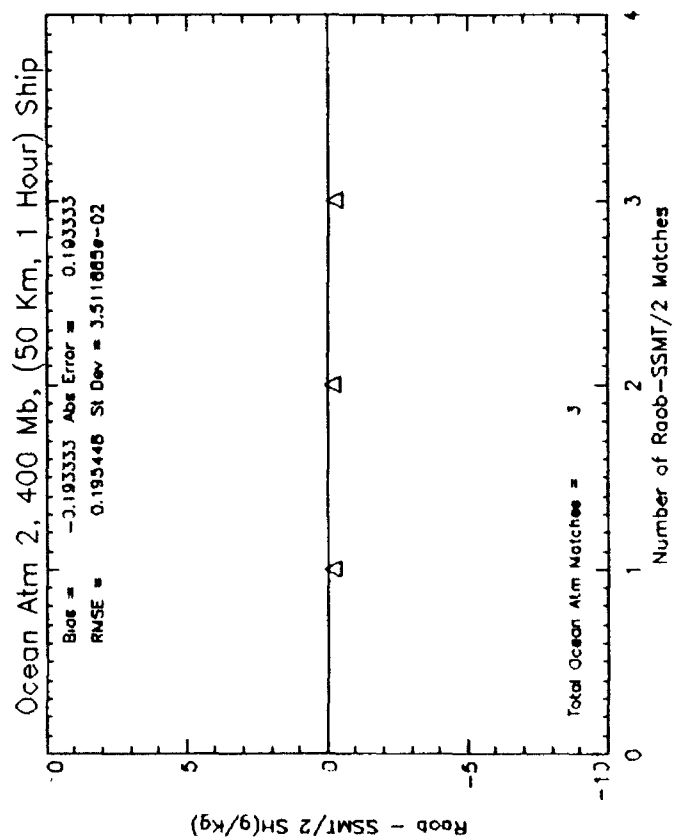
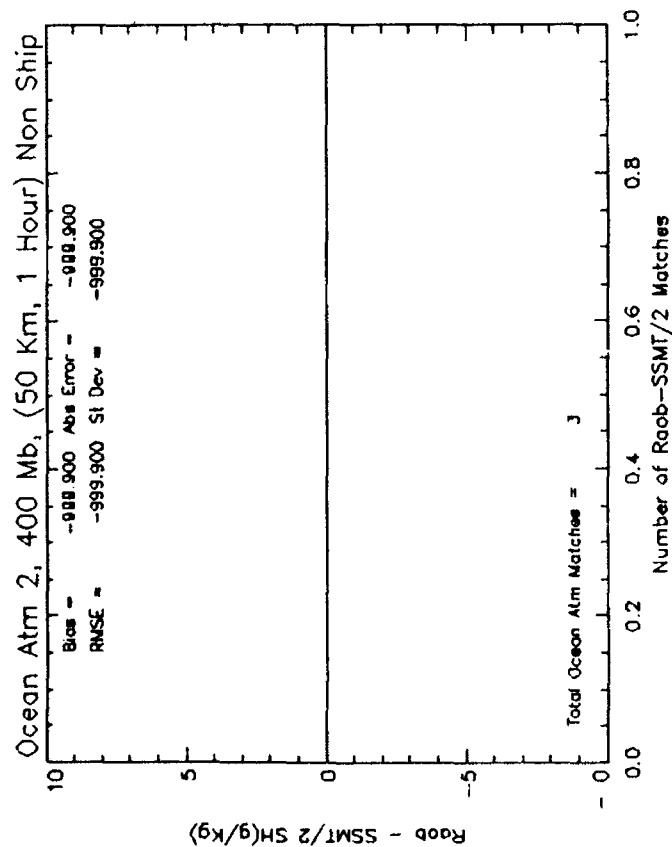


**Inches**

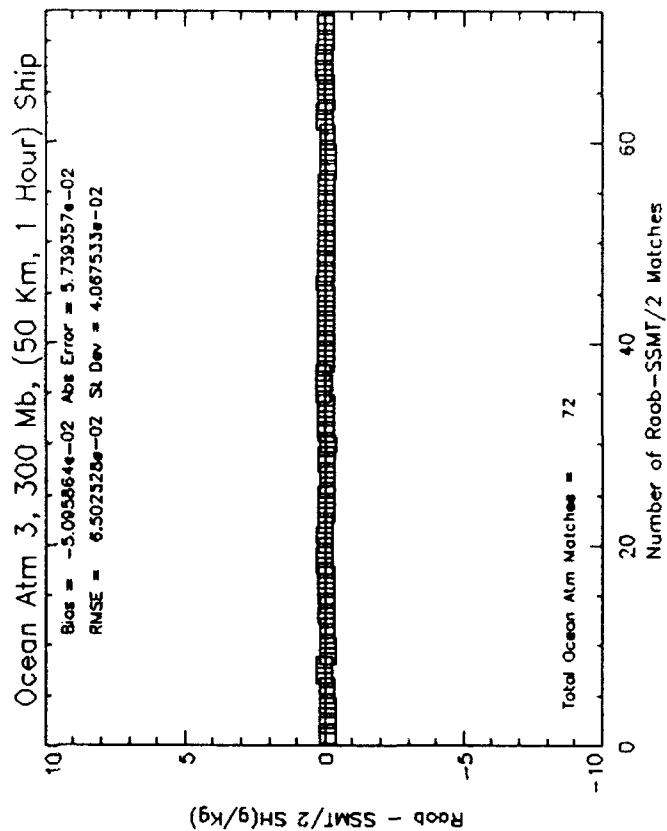
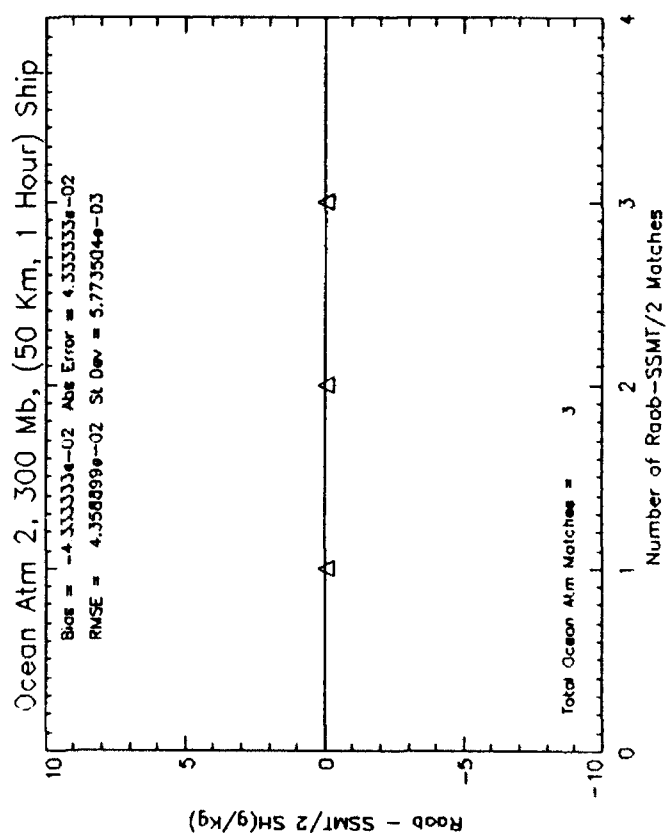
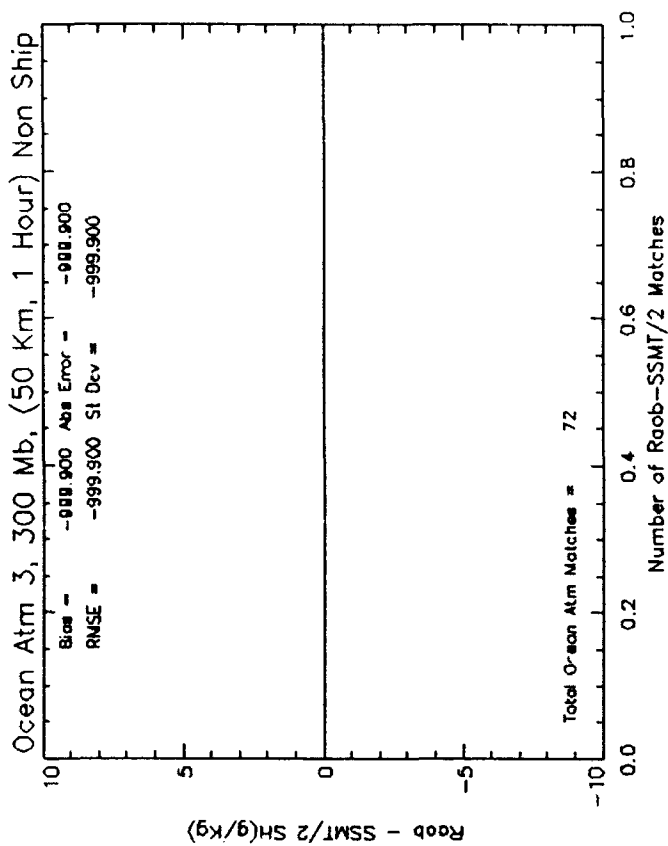
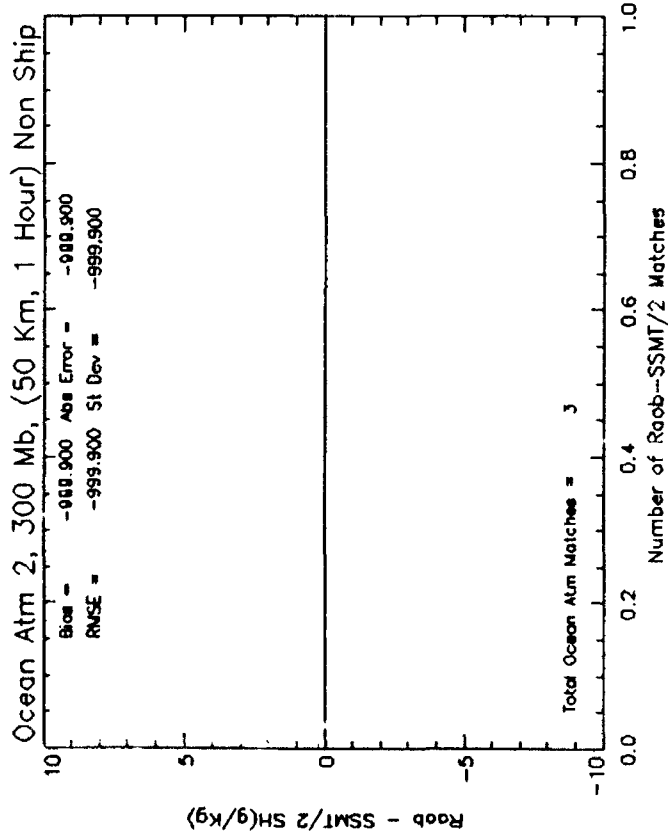


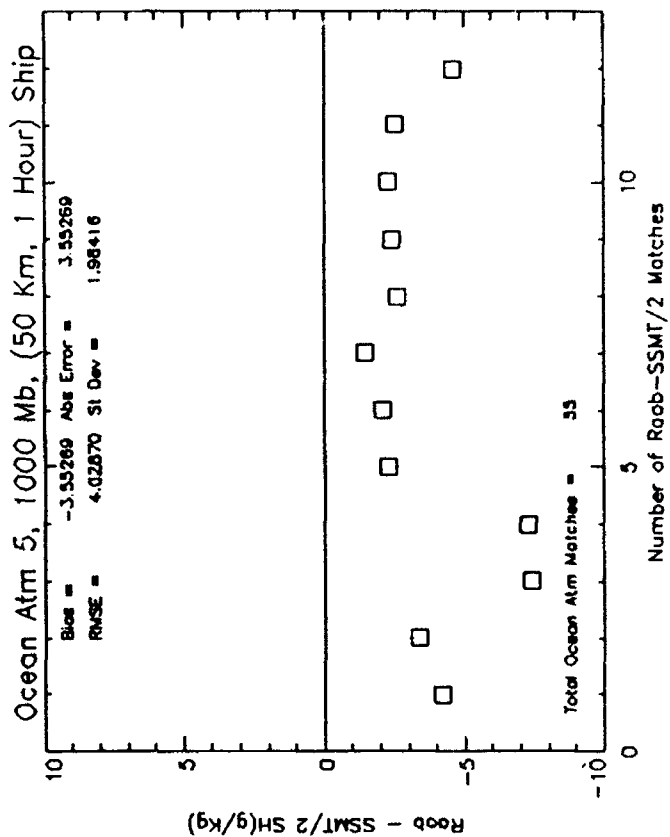
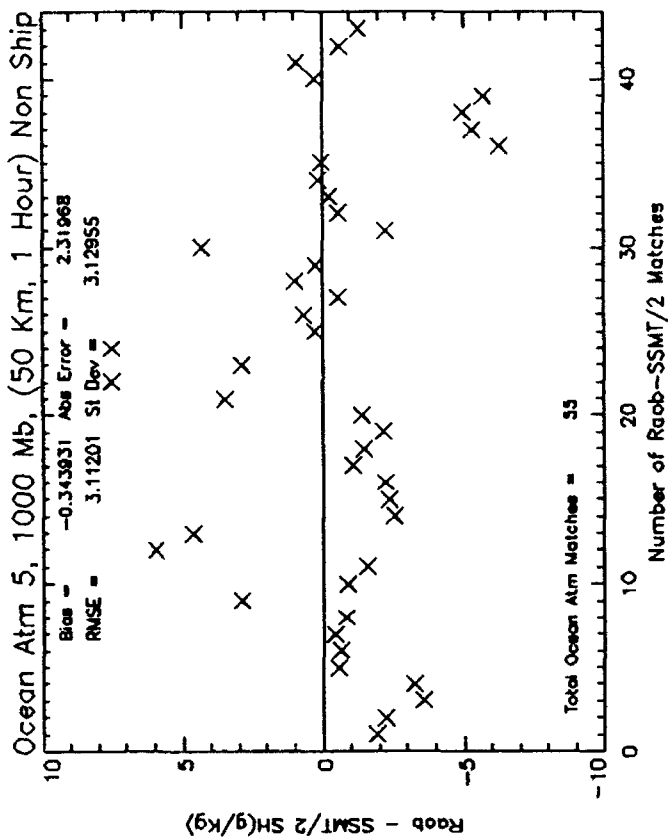
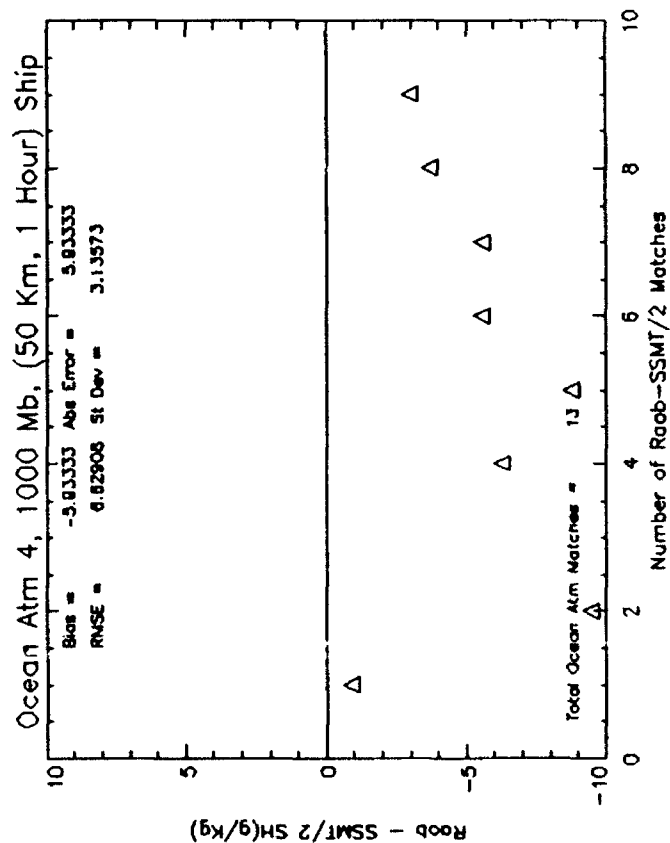
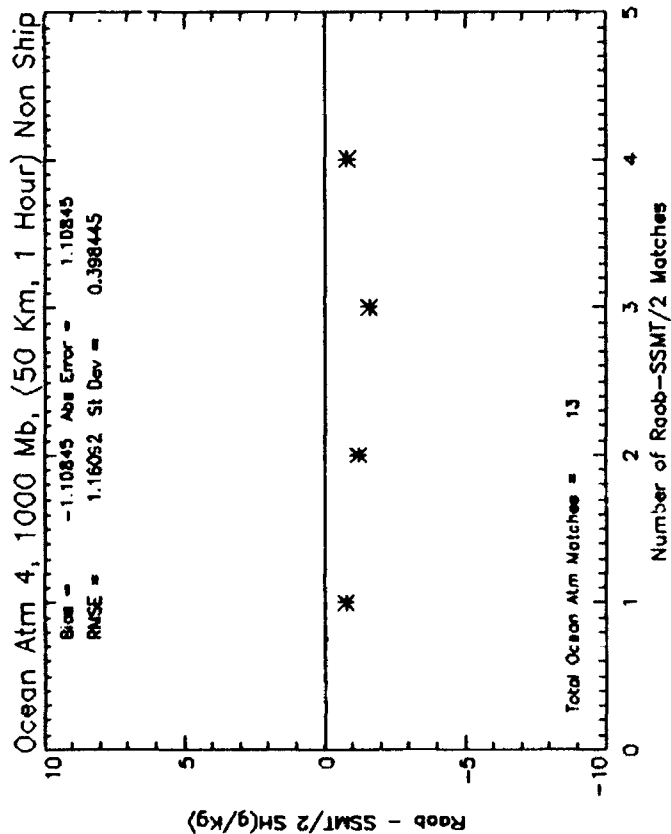
MANUFACTURED TO AIM STANDARDS  
BY APPLIED IMAGE, INC.

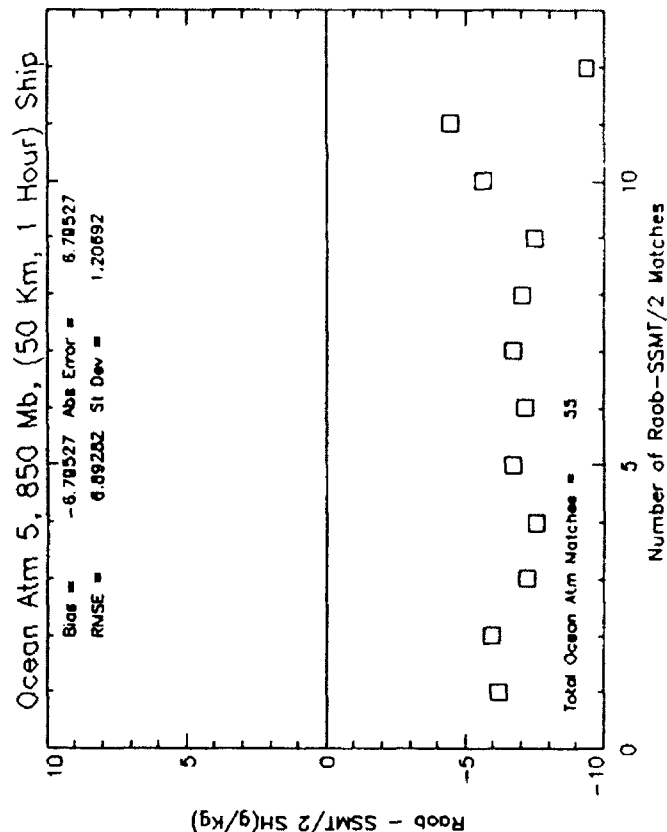
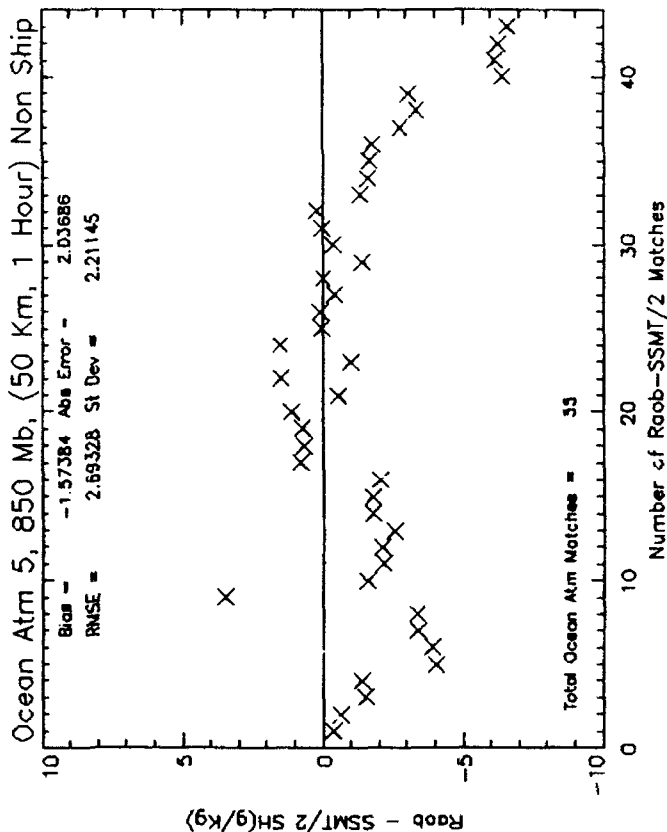
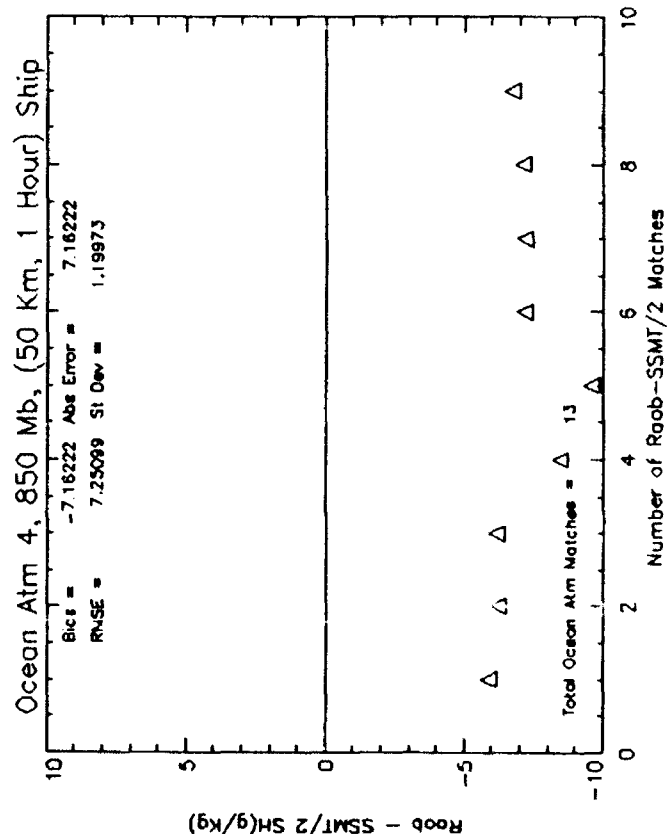
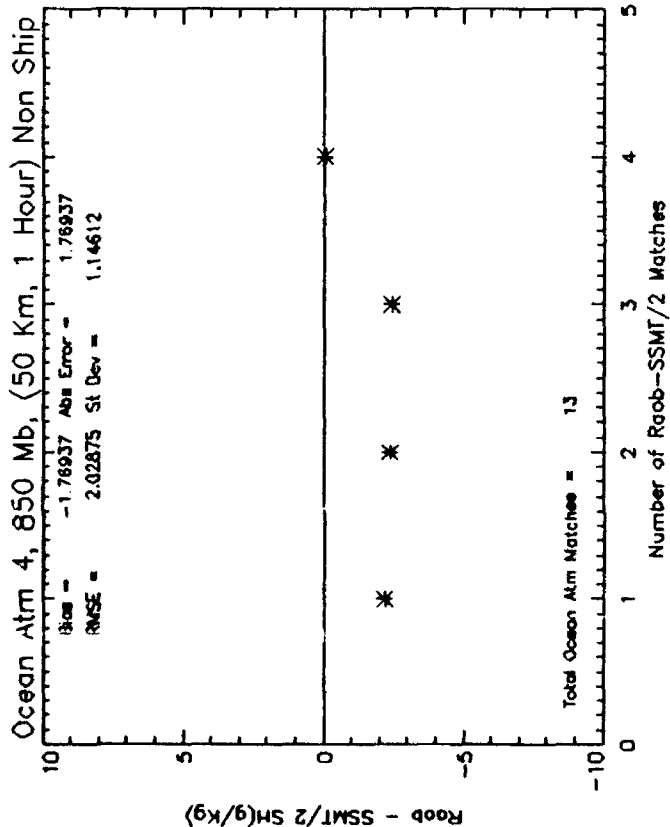


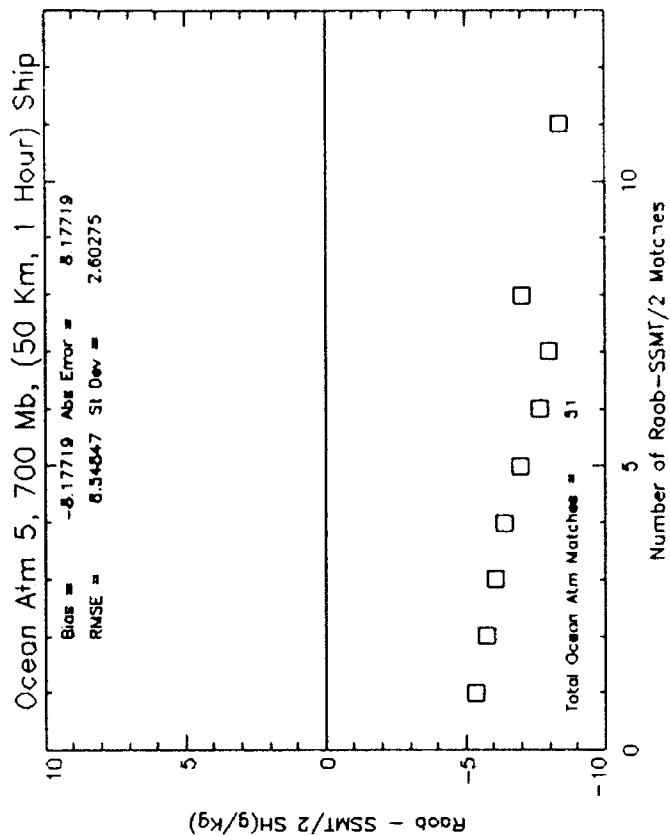
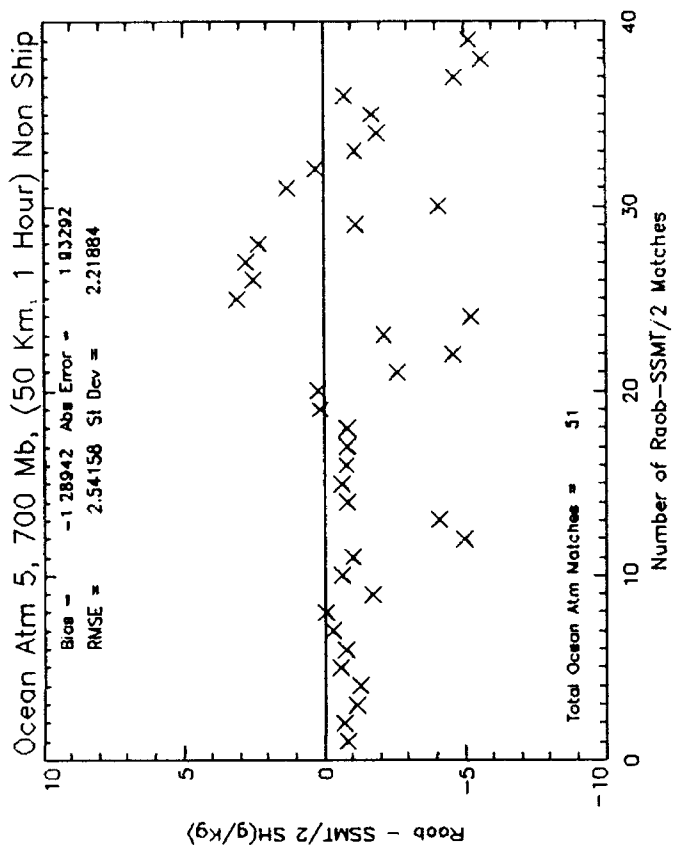
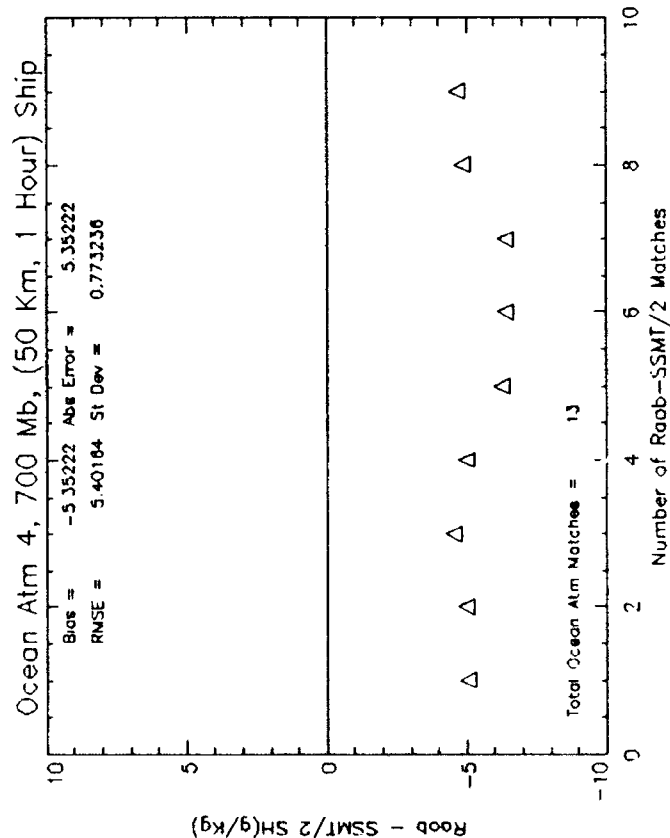
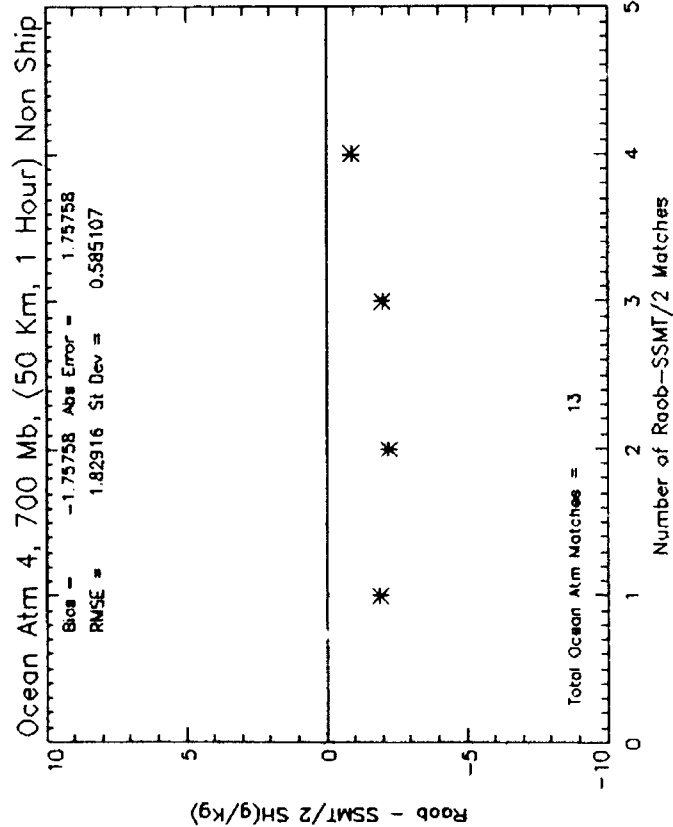


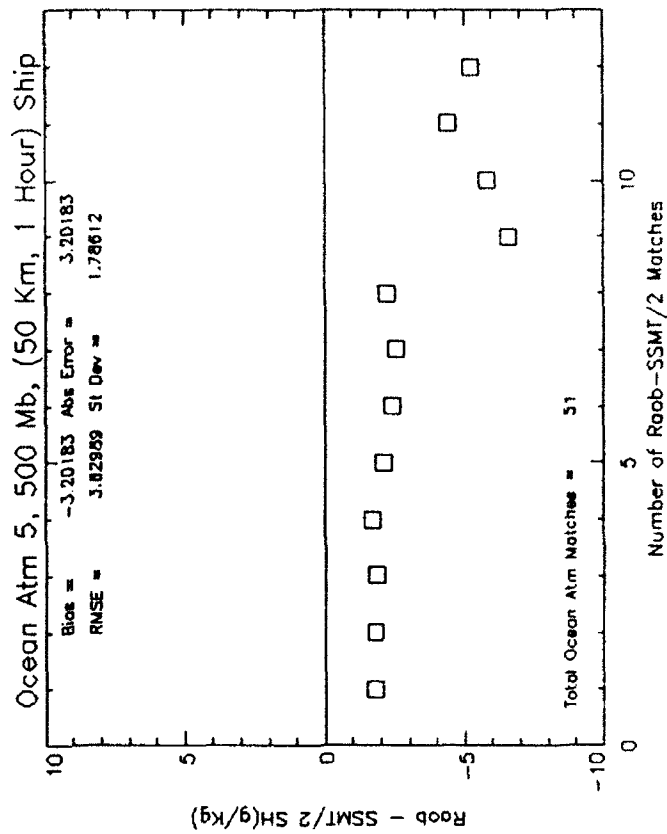
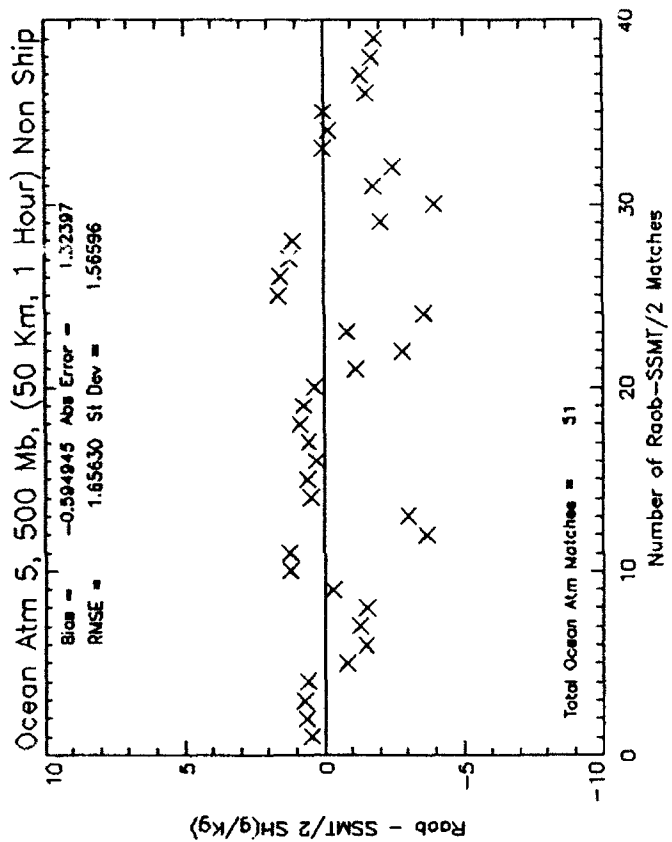
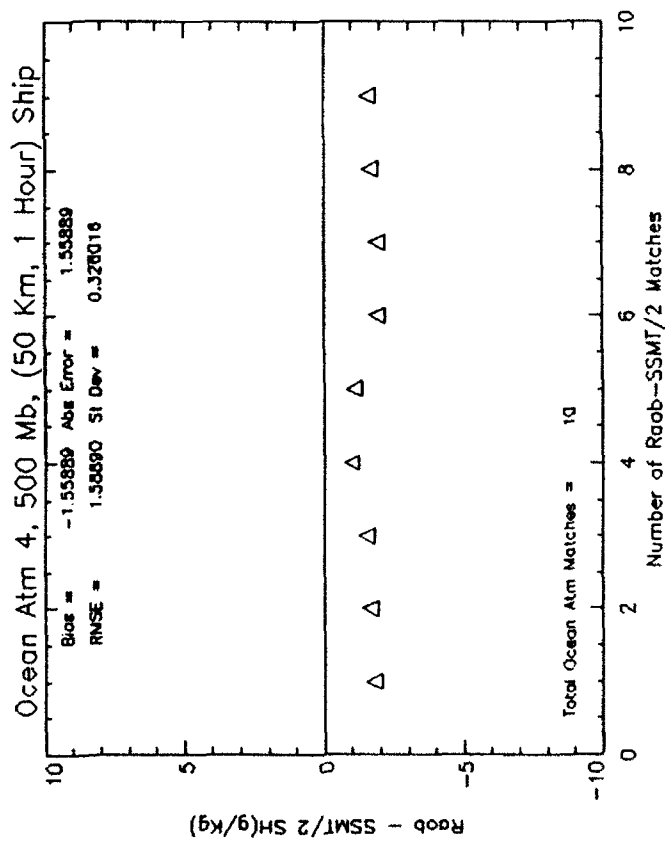
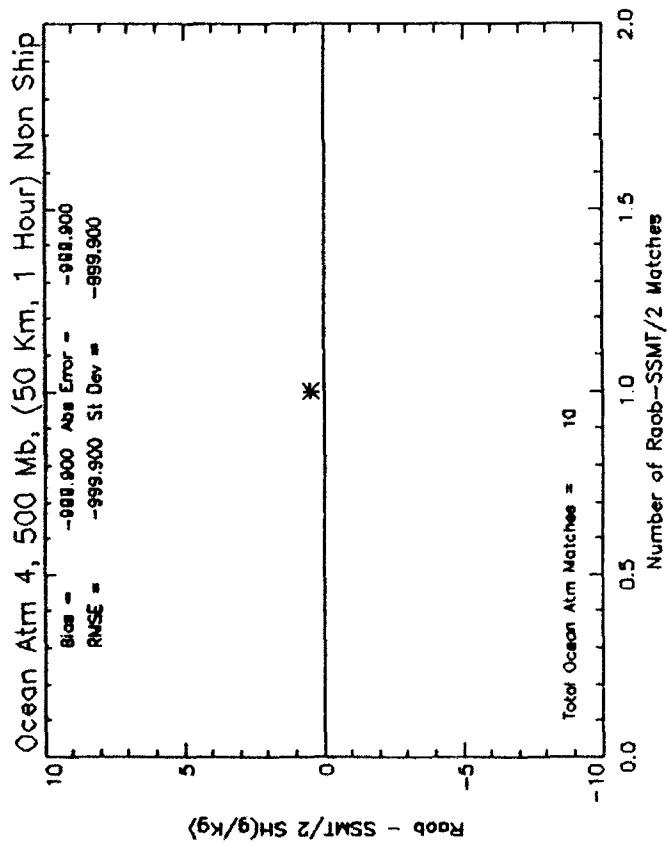


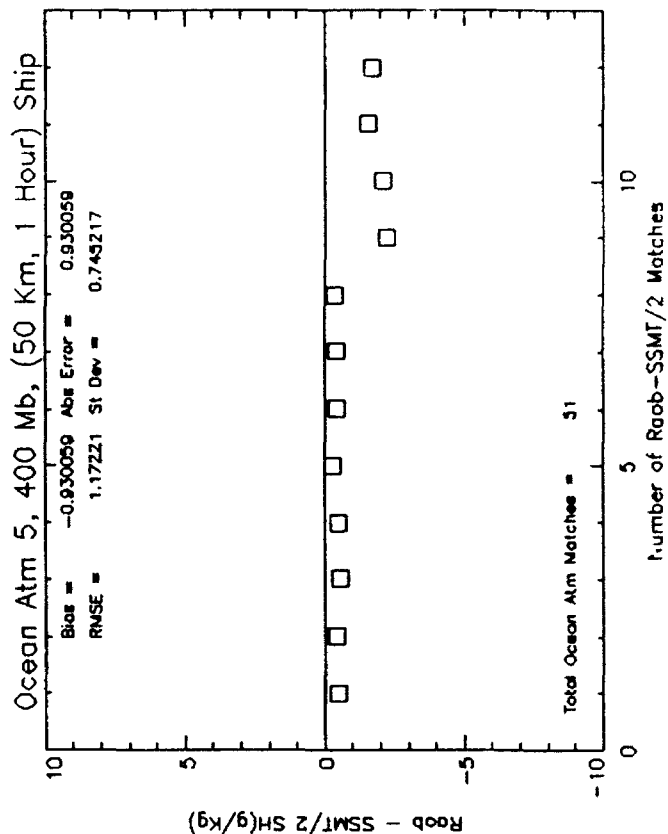
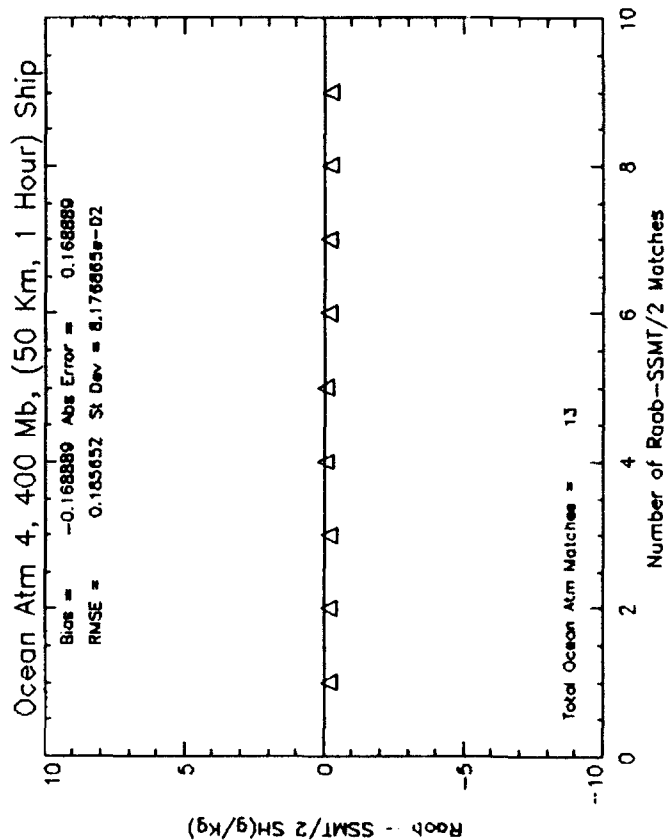
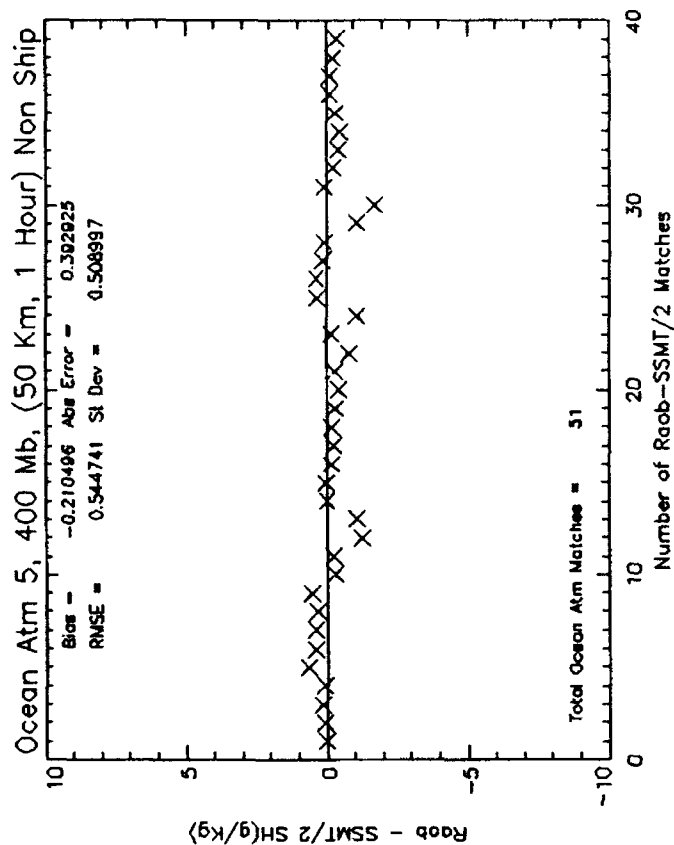
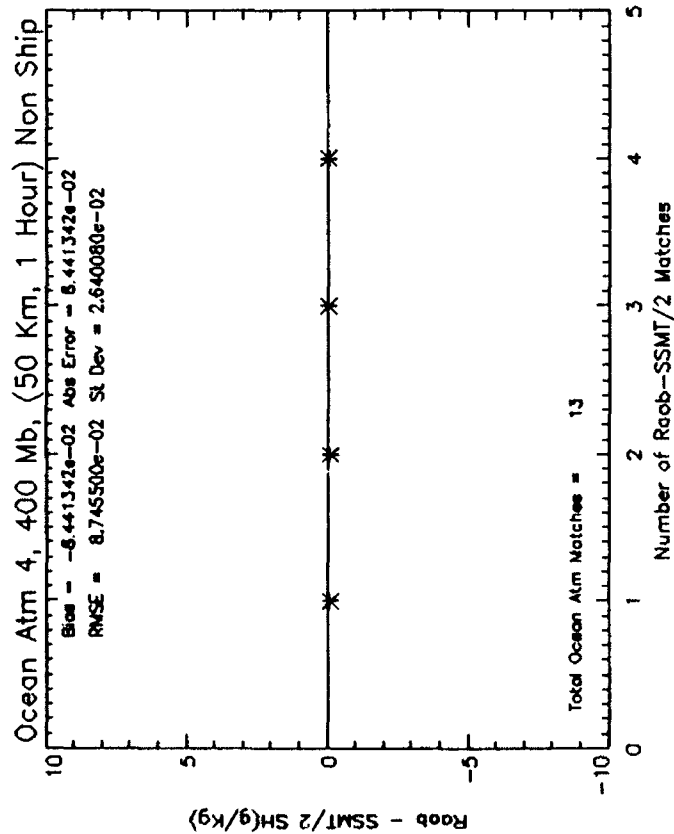


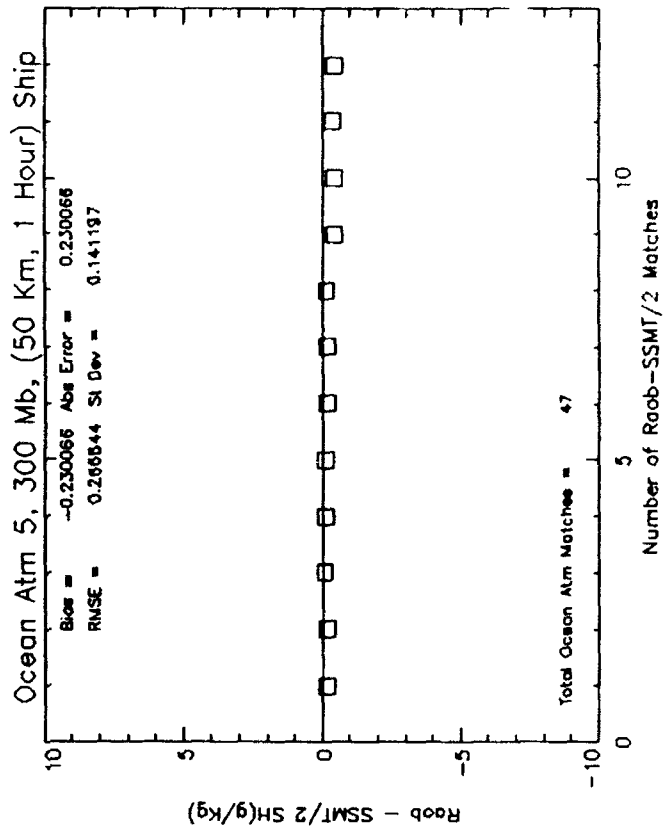
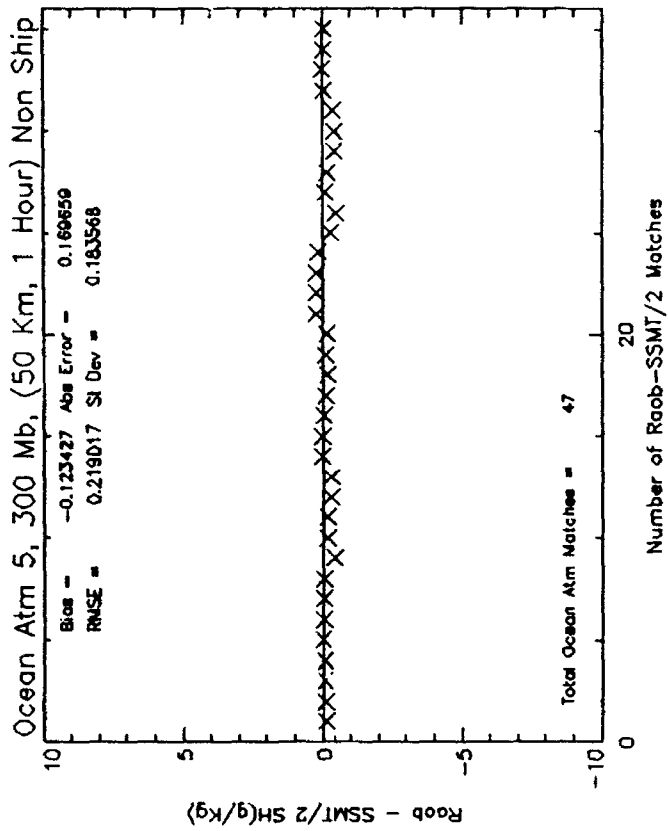
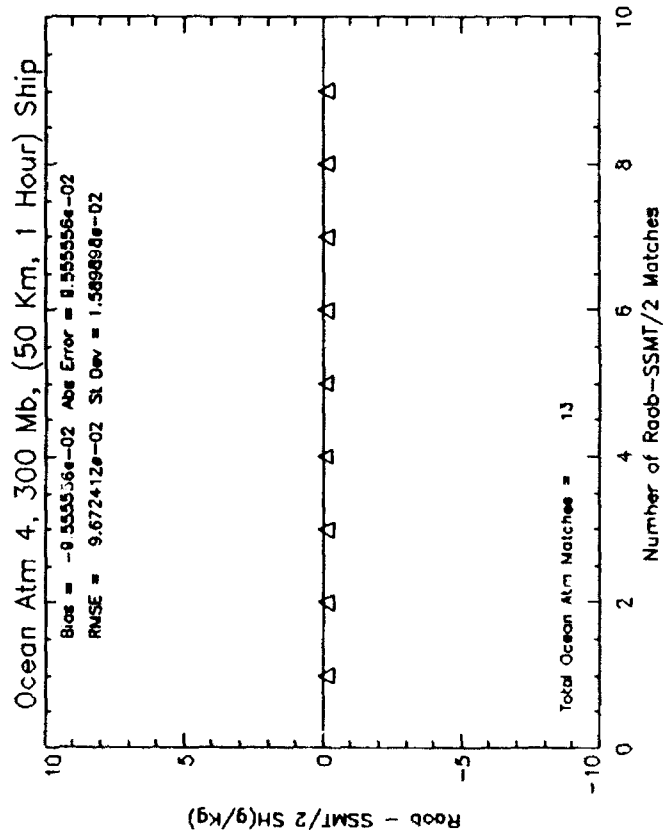
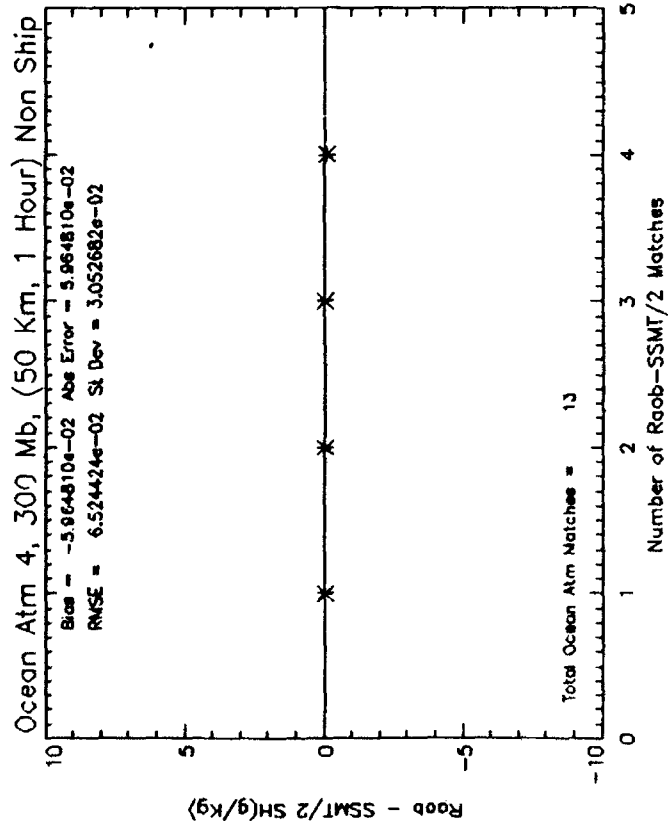












Appendix J. SSM/T-2 channel TB imagery and HIRAS model-generated fields.

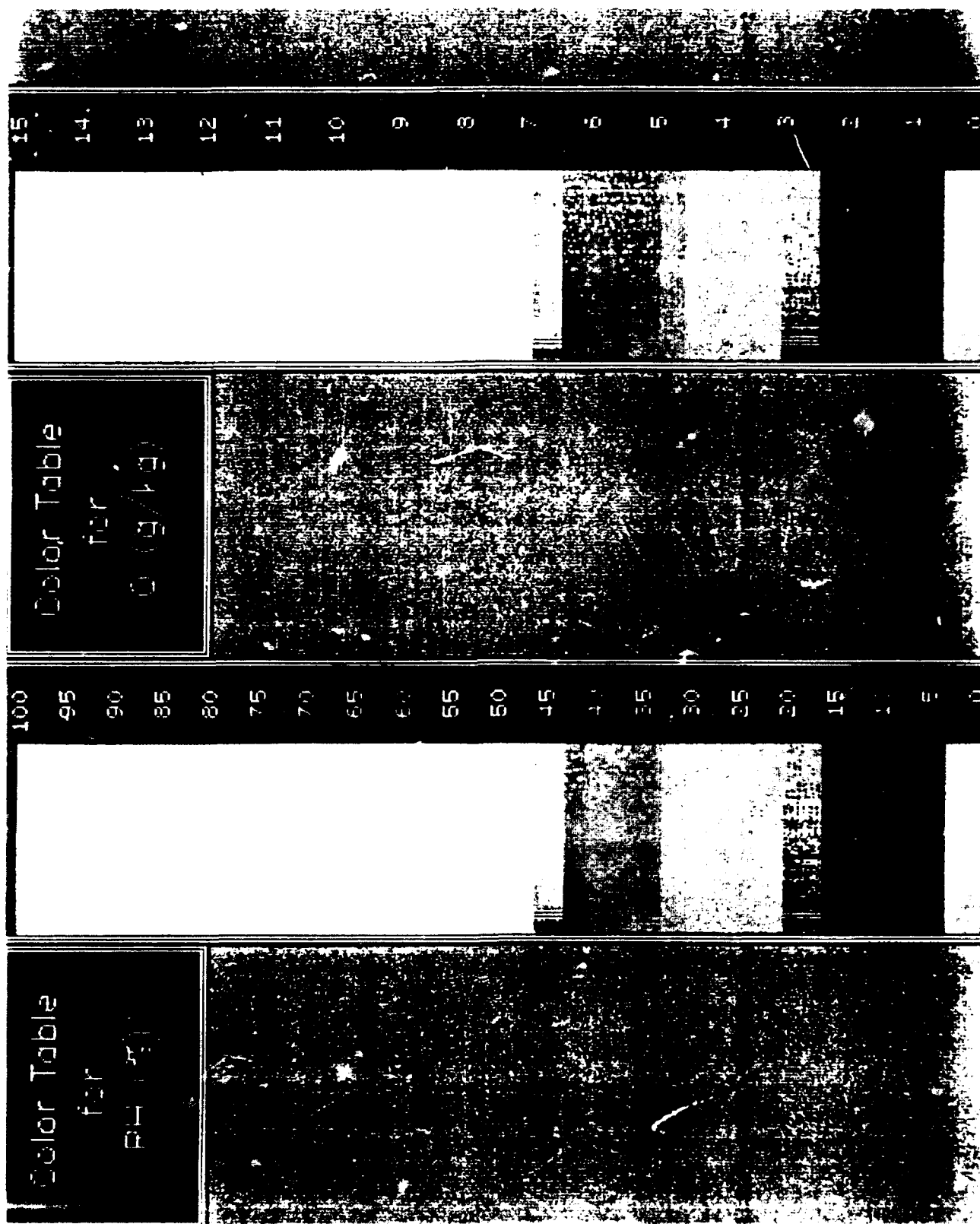
Key for RH color table

White = 100%; Red shades range from 95 - 80%; Yellow shades range from 80 - 60%; Green shades range from 50 - 35%; Blue shades range from 30 - 10%; Magenta shades range from 10 - 0%

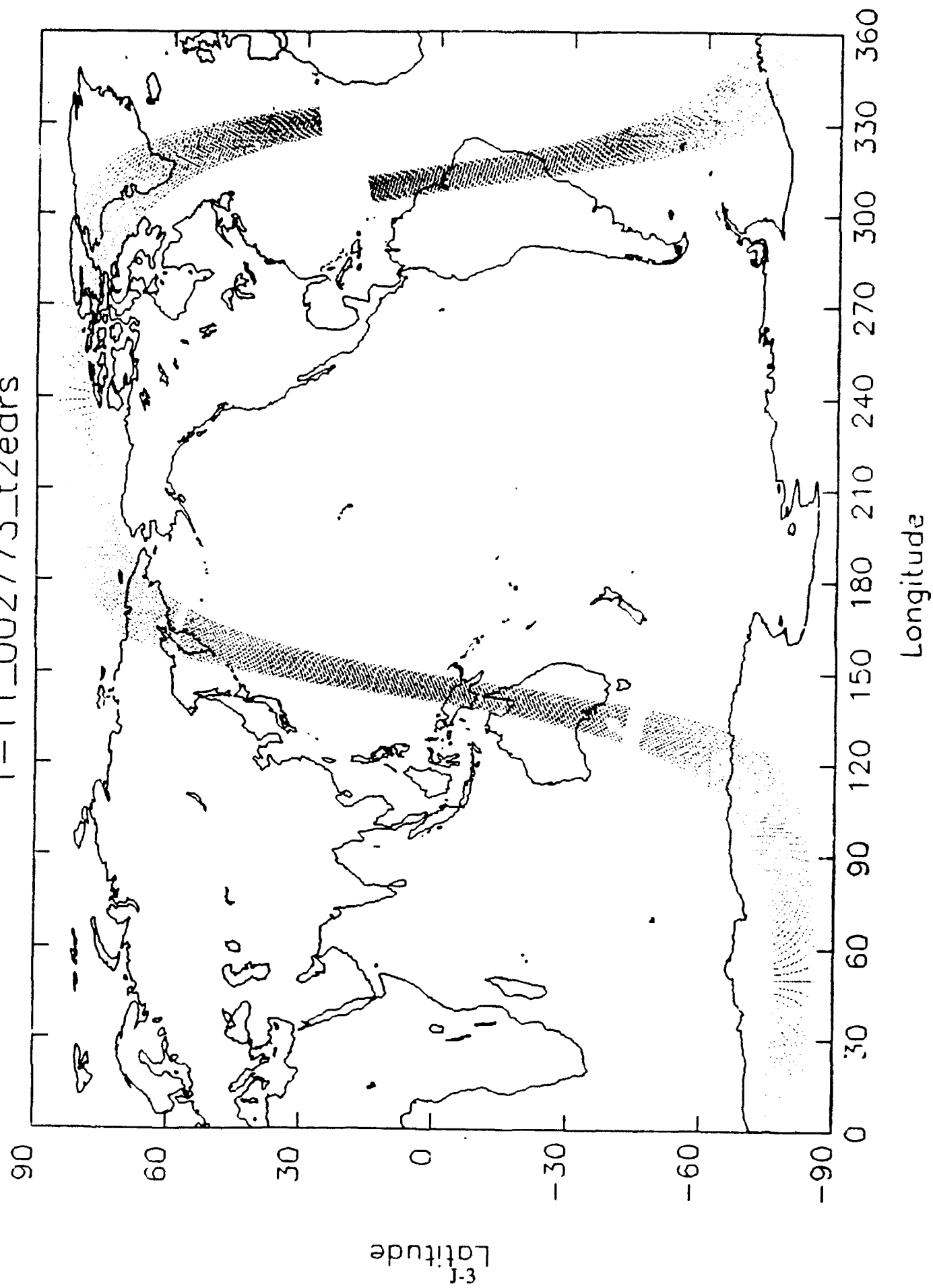
Key for Q color table

White = 15 g/kg; Red shades range from 14 - 12 g/kg; Yellow shades range from 12 - 8 g/kg; Green shades range from 7 - 5 g/kg; Blue shades range from 5 - 2 g/kg; Magenta shades range from 2 - 0 g/kg.

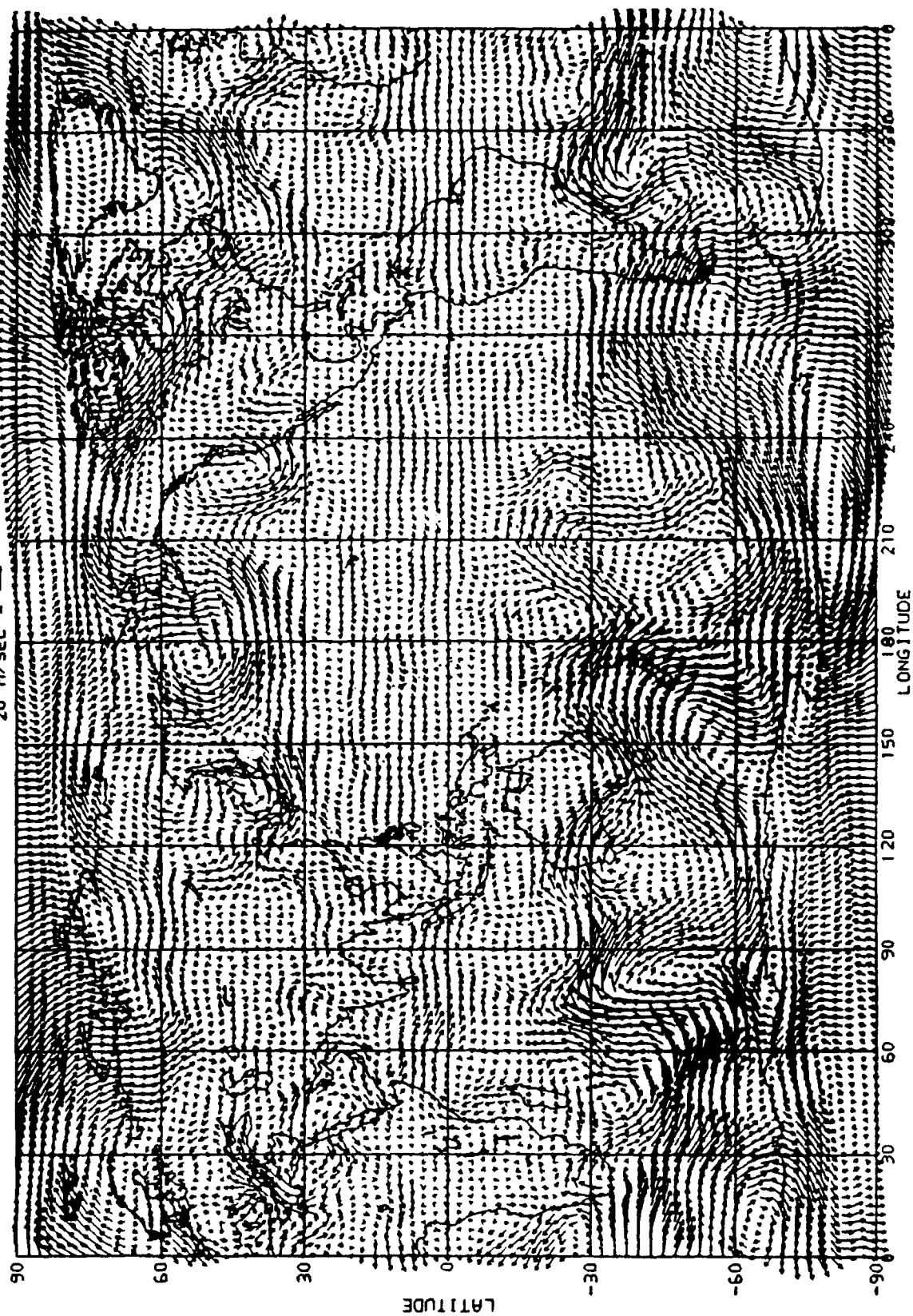




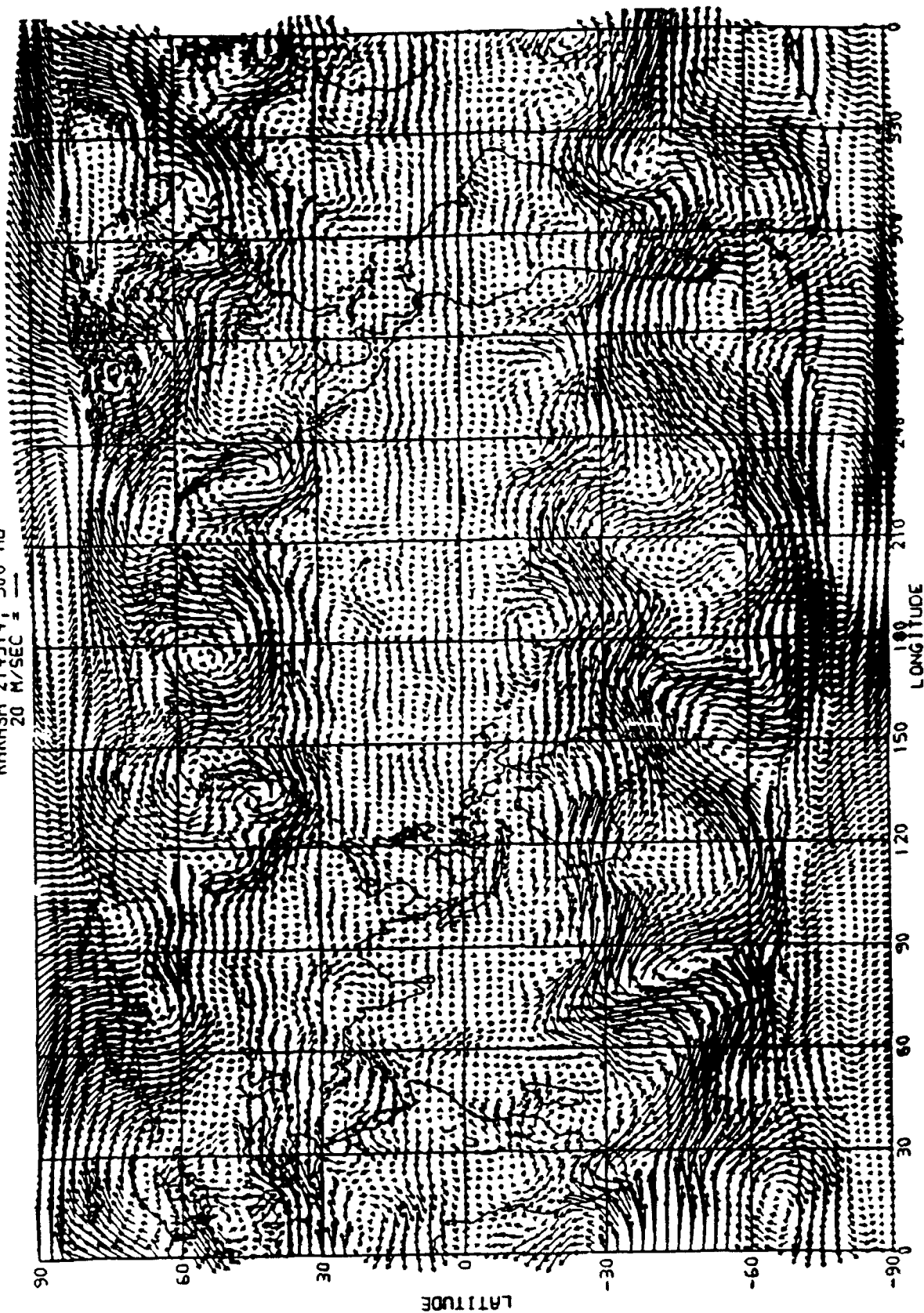
f-11\_002773\_t2edrs



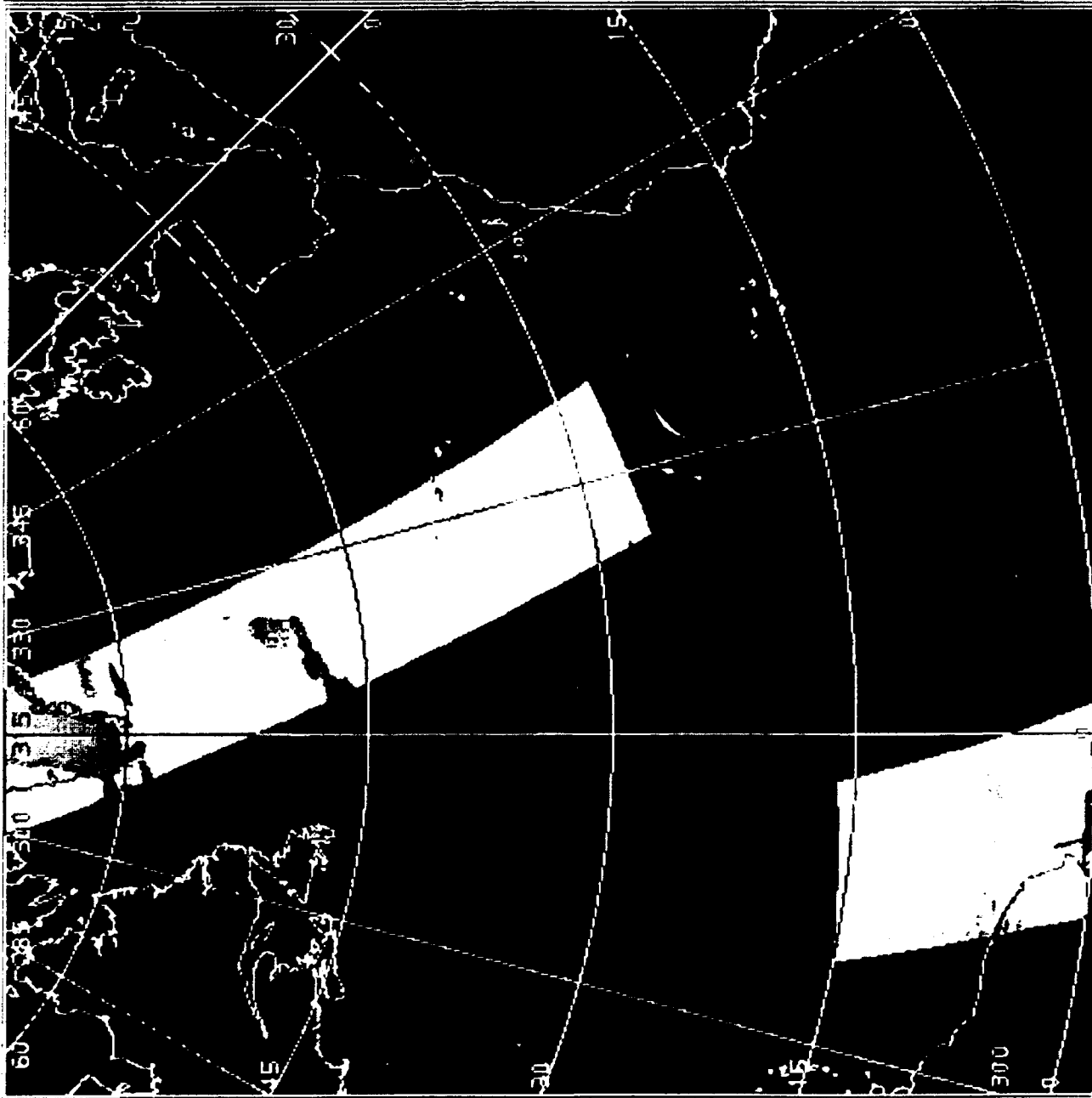
RHRASA 214314, 700 MB  
20 M/SEC = —



RHRASA 214314, 500 MB  
20 M/SEC

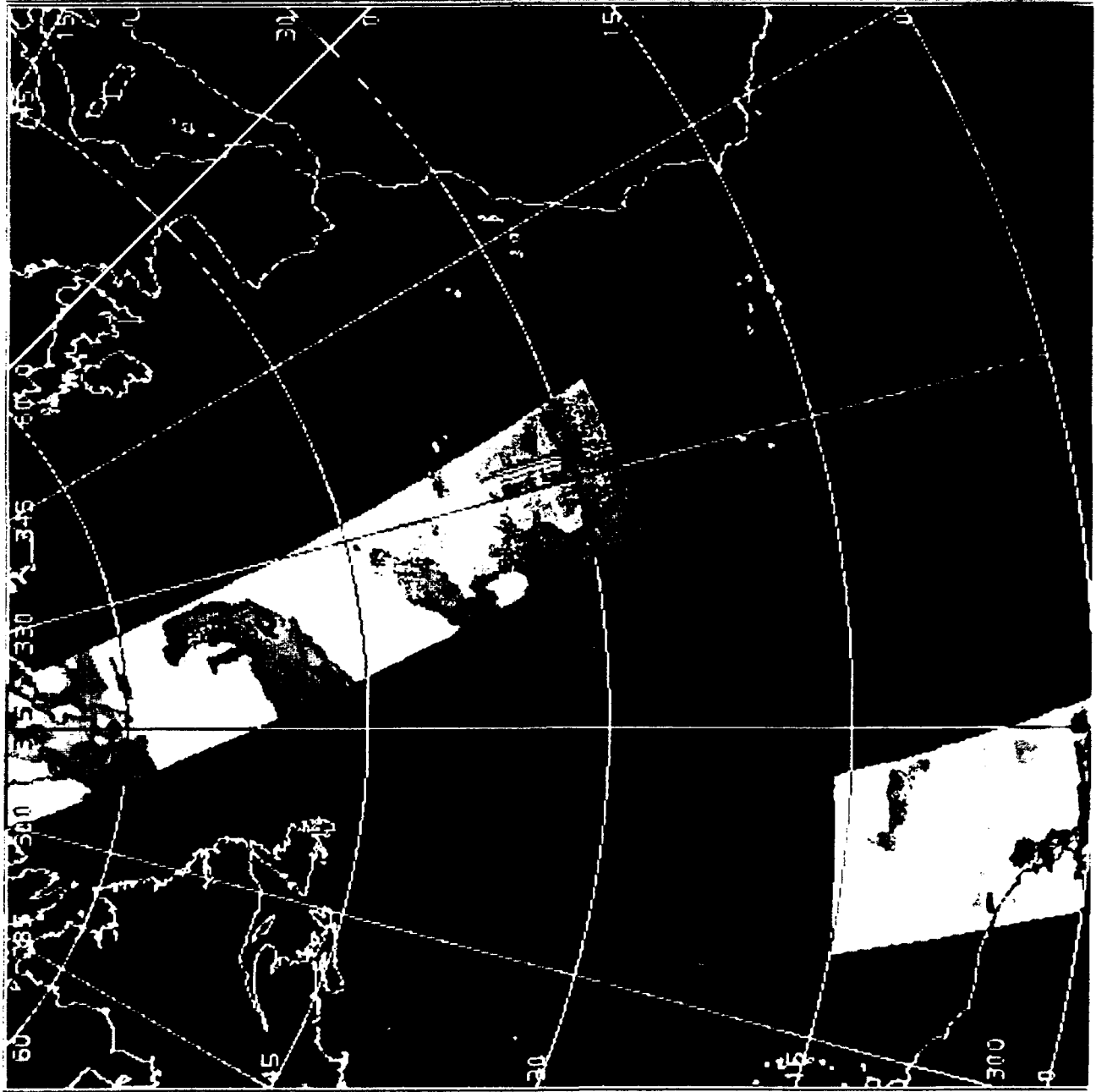


SSM/T2  
RH 250 MB  
F-11 002773





SSM/T2  
RH 700 MB  
F-11 0002773

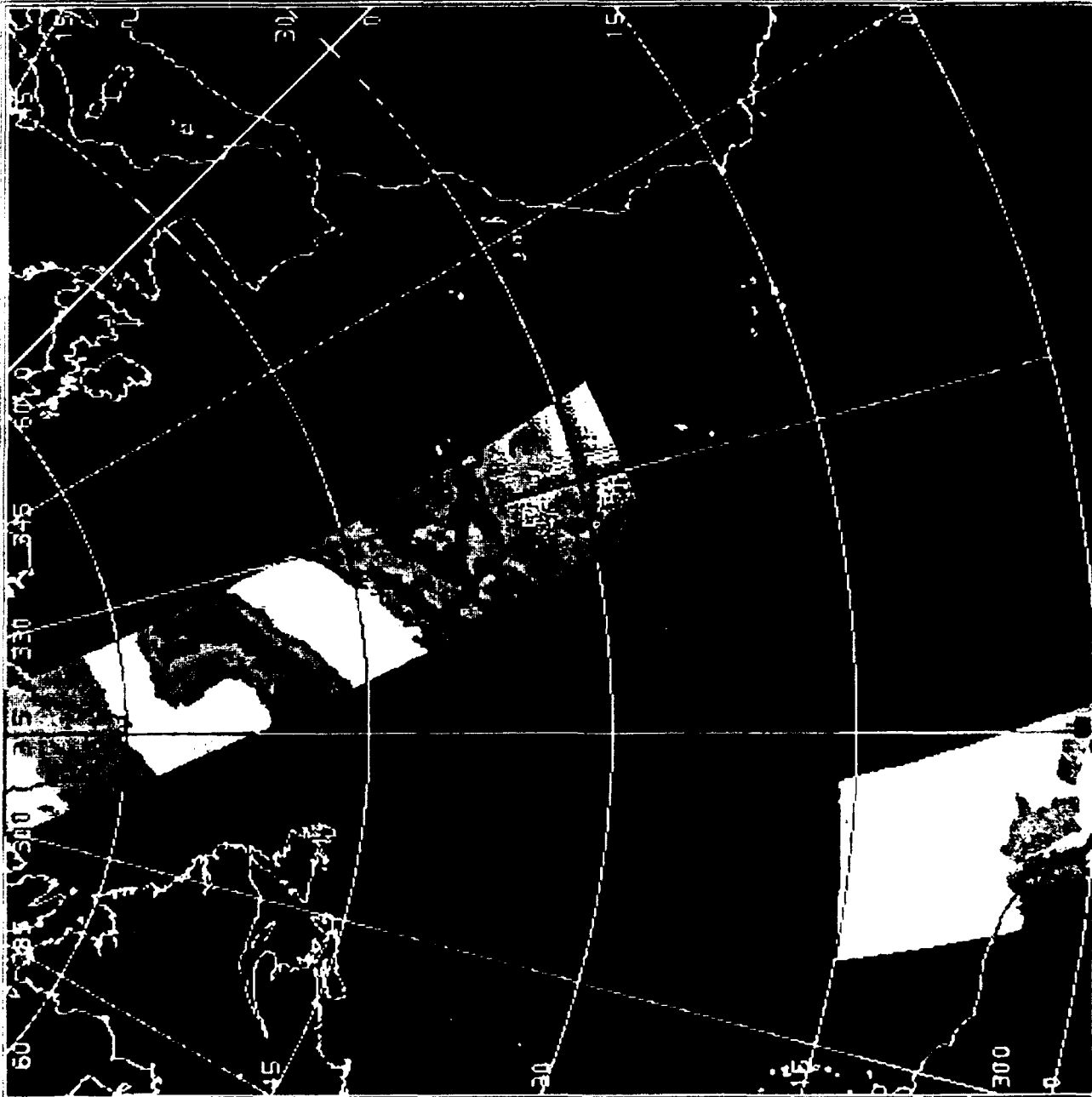


HIPAS  
PH 700 MB  
SHRASEC  
2-12-1



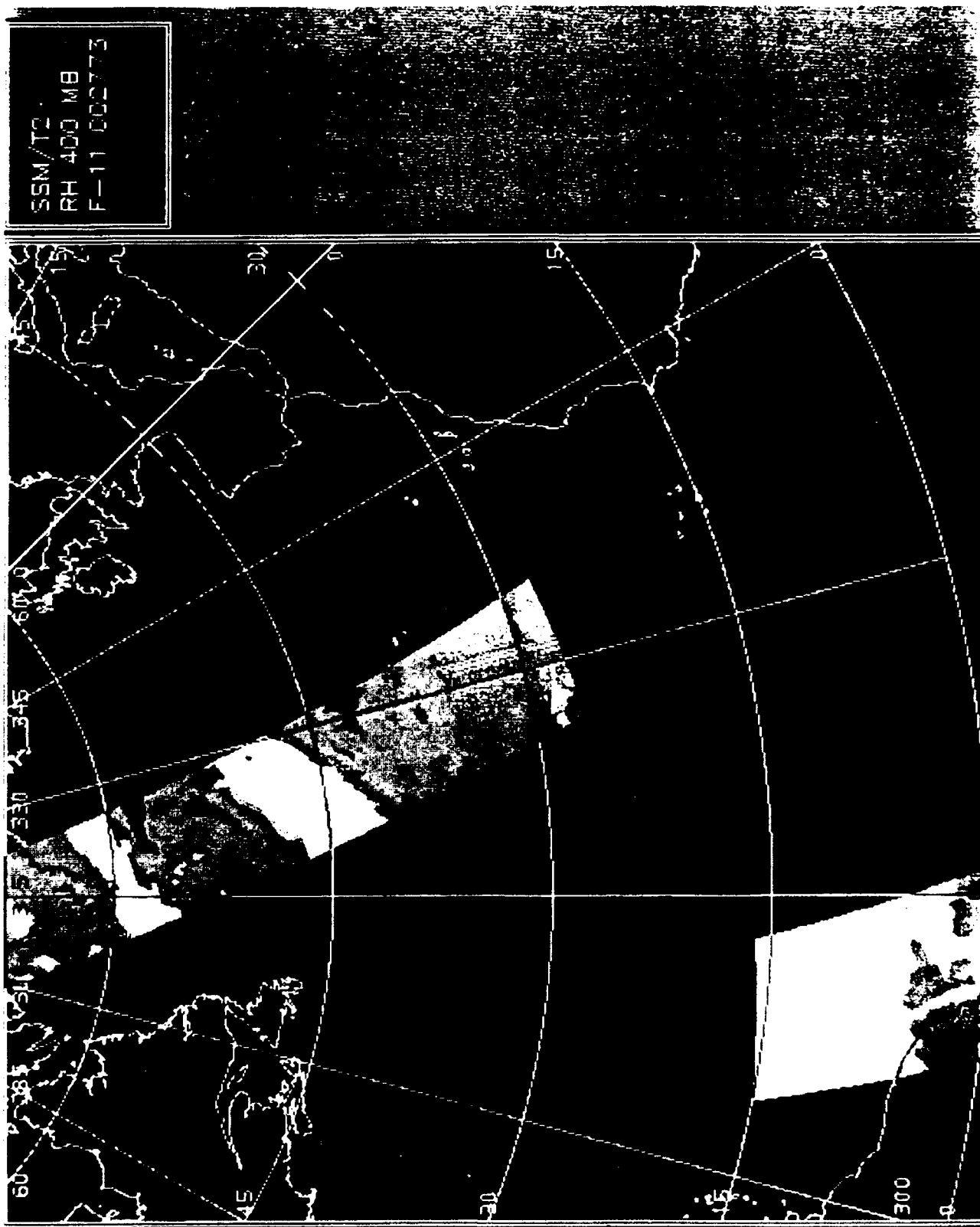


SSM/T2  
RH 500 MB  
F-11 002773



HIRAS  
RH 500 MB  
RHP434  
214314

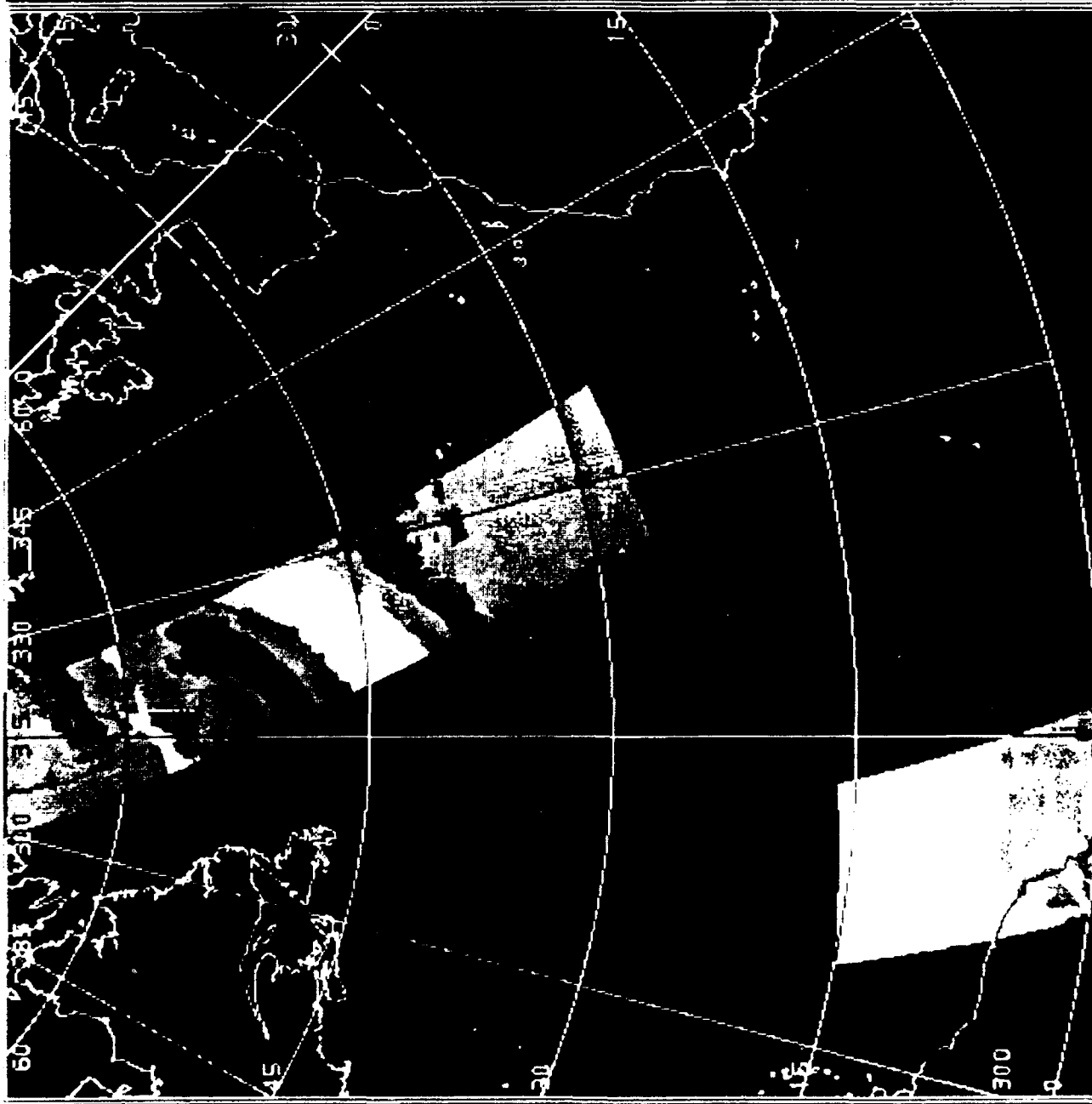




HIRAS  
RH 400 MB  
PHRASA  
214314



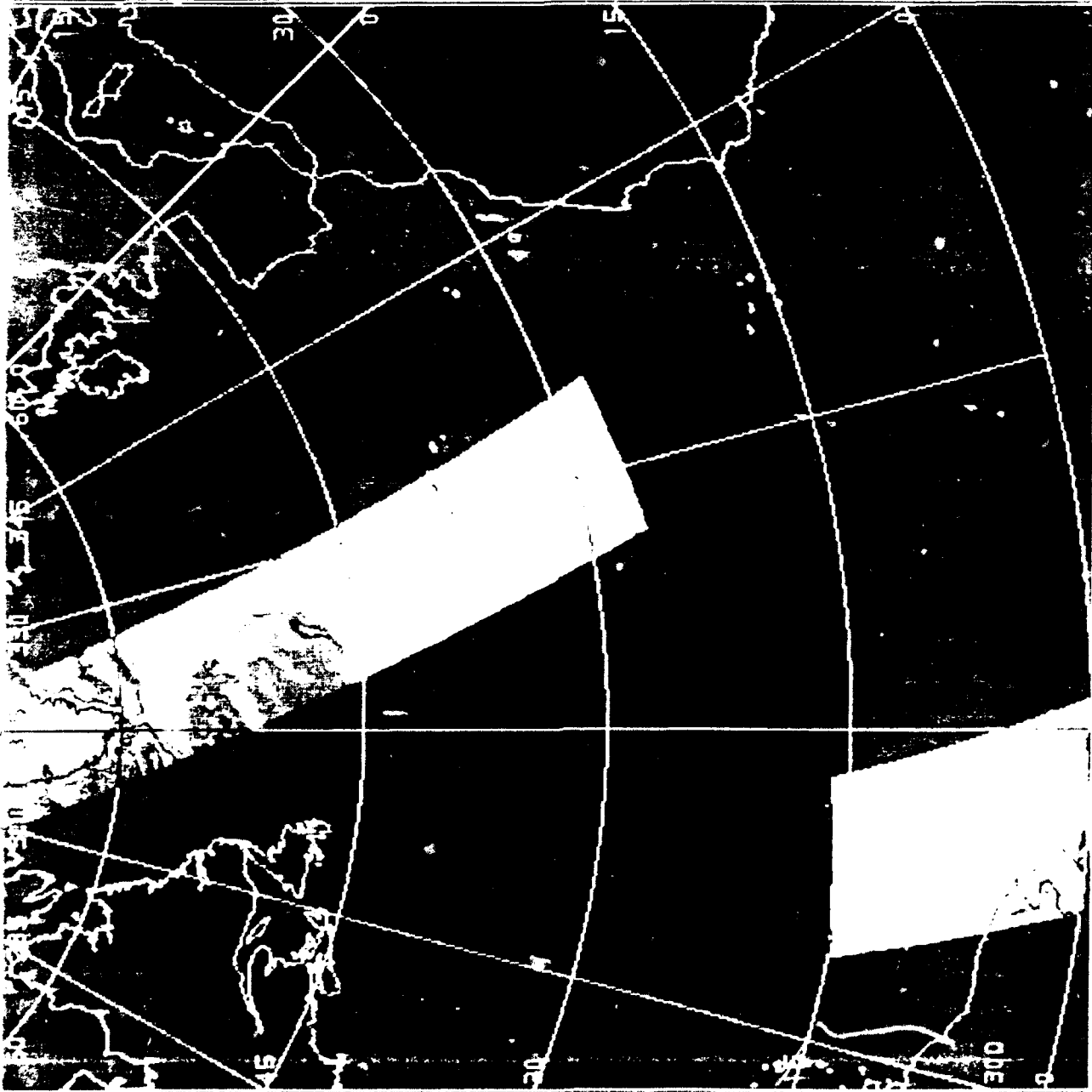
SSM/T2  
RH 300 MB  
F-11 002773



HIRAS  
PH 100 MB  
PHRASA  
C1211



SSM/T2  
Q 1000 MB  
F-11 DD2773

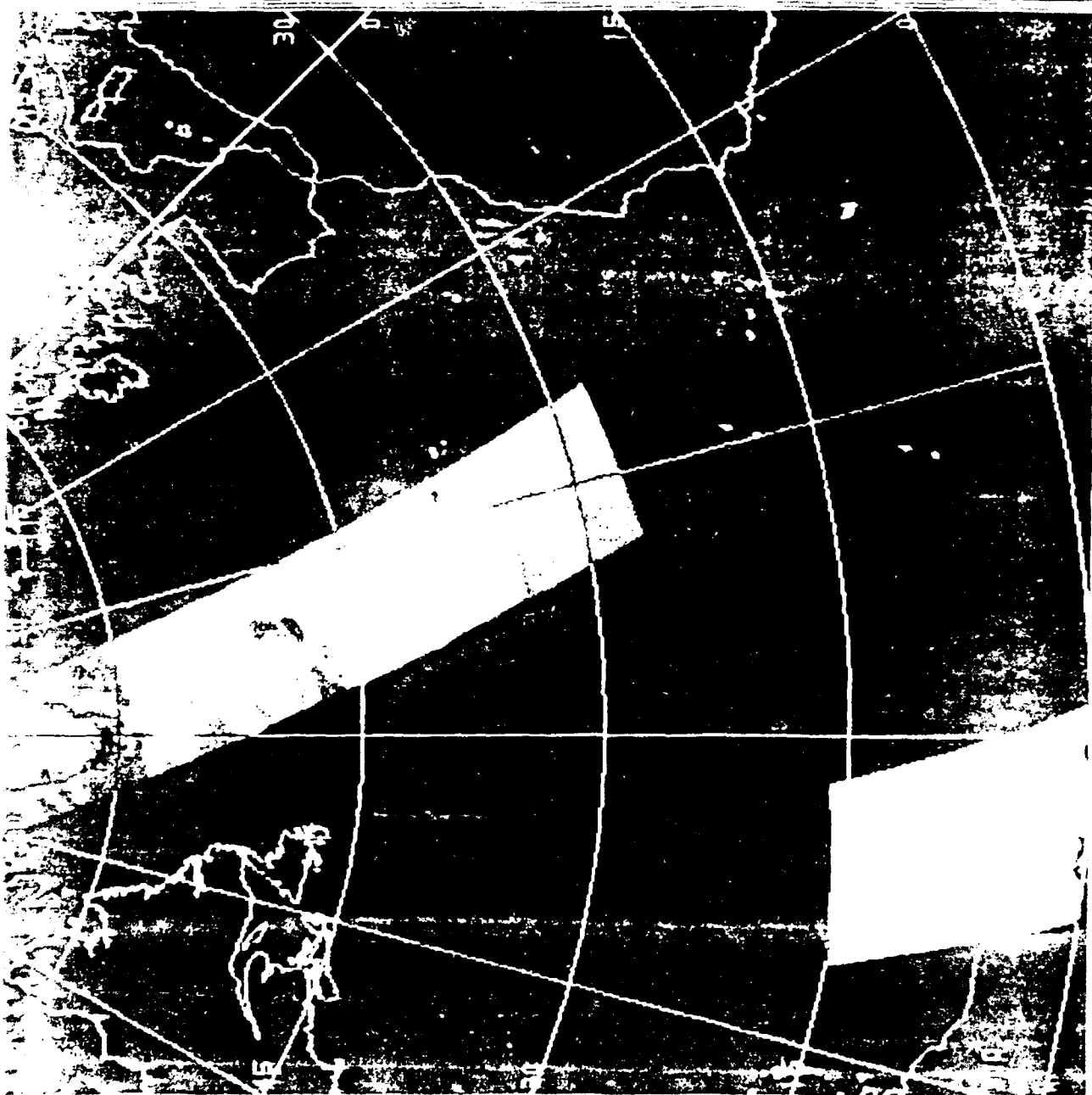


HRAS  
31000 ME  
HRASA  
214314



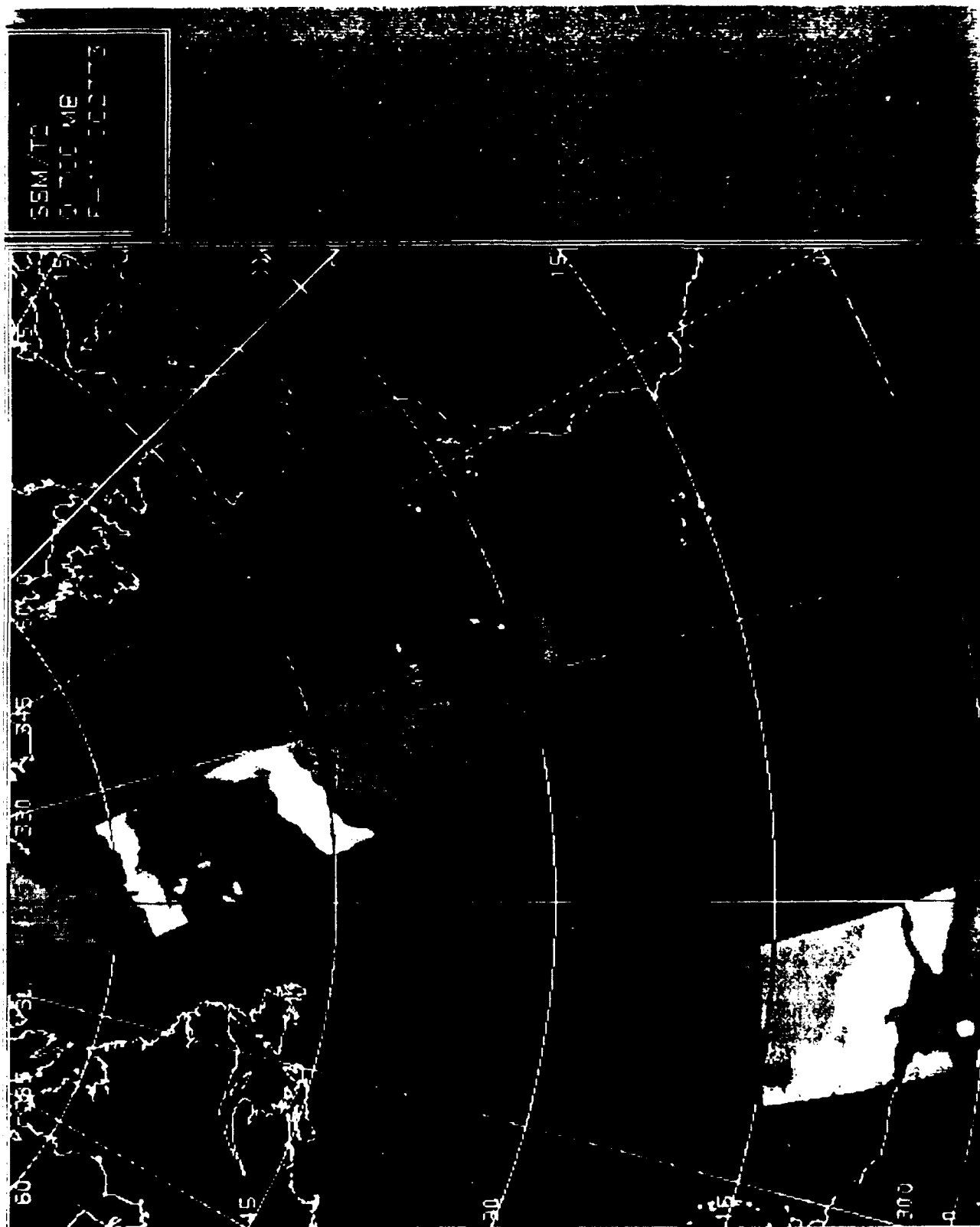


PC277



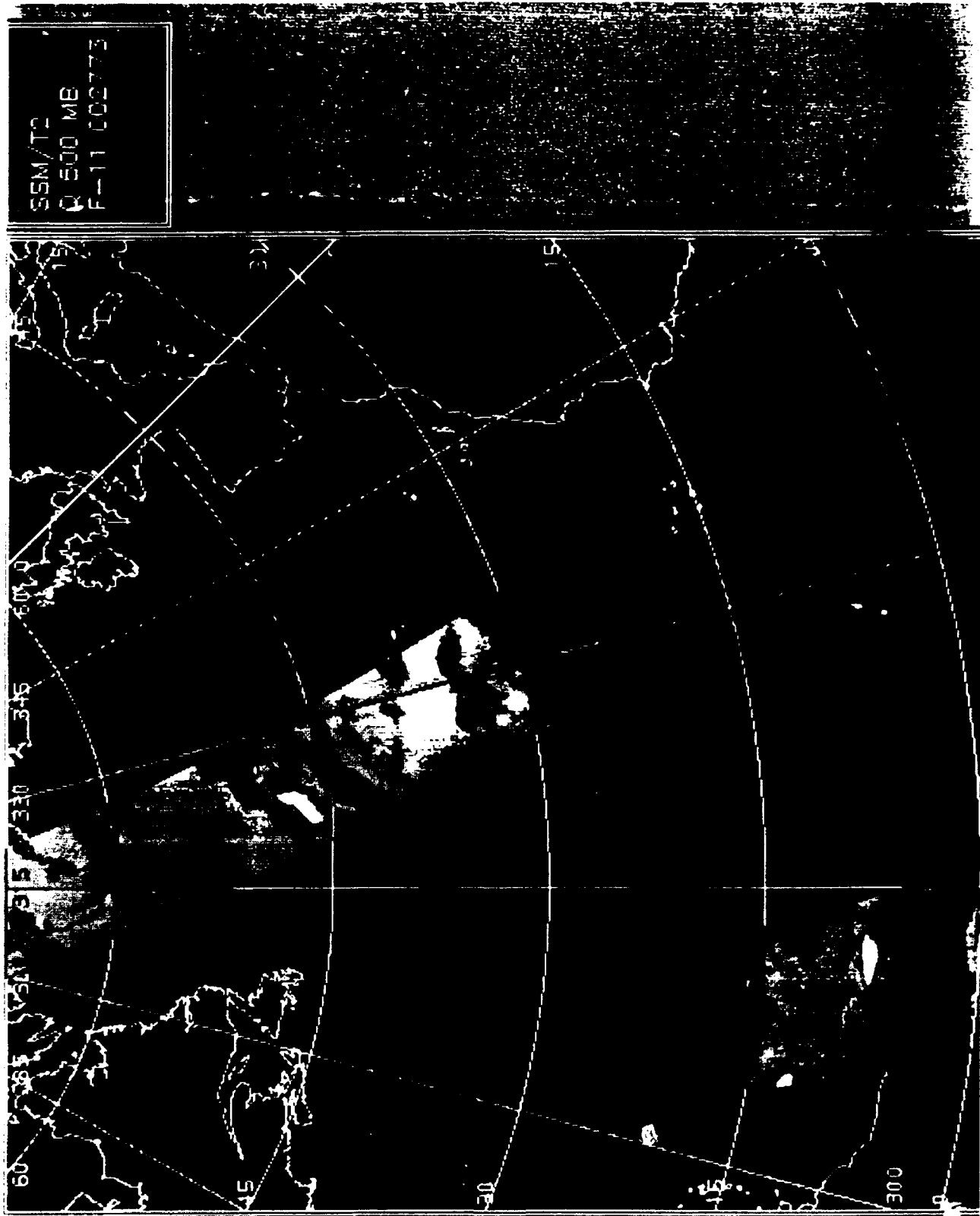
HIRAS  
Q 850 MB  
RHRASA  
214314







HIRAS  
0700 ME  
BHRASA  
214514



HIRAS  
O 500 MB  
RHR454  
214314





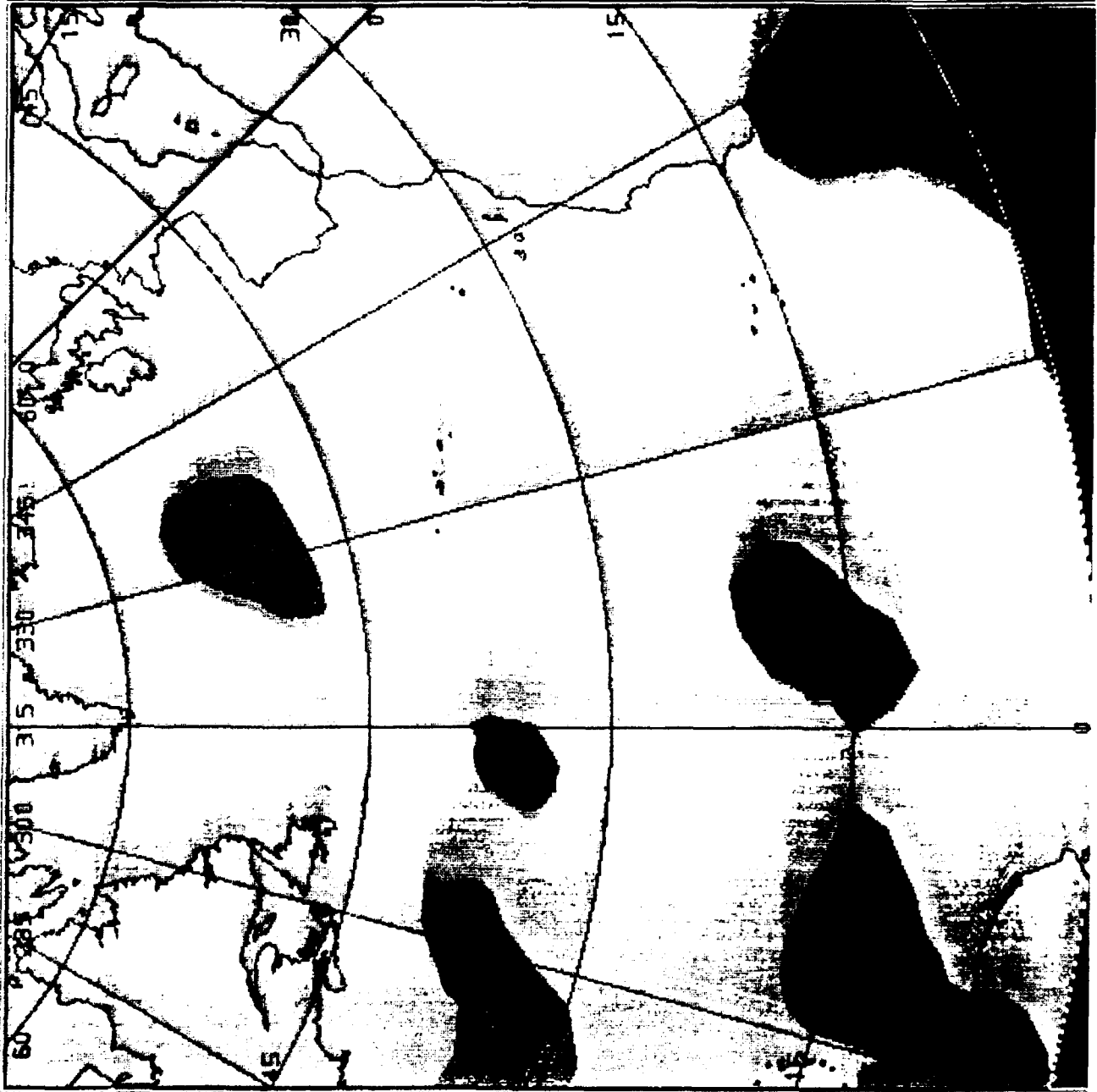
HIRAS  
Q 400 MB  
PHRASA  
214314



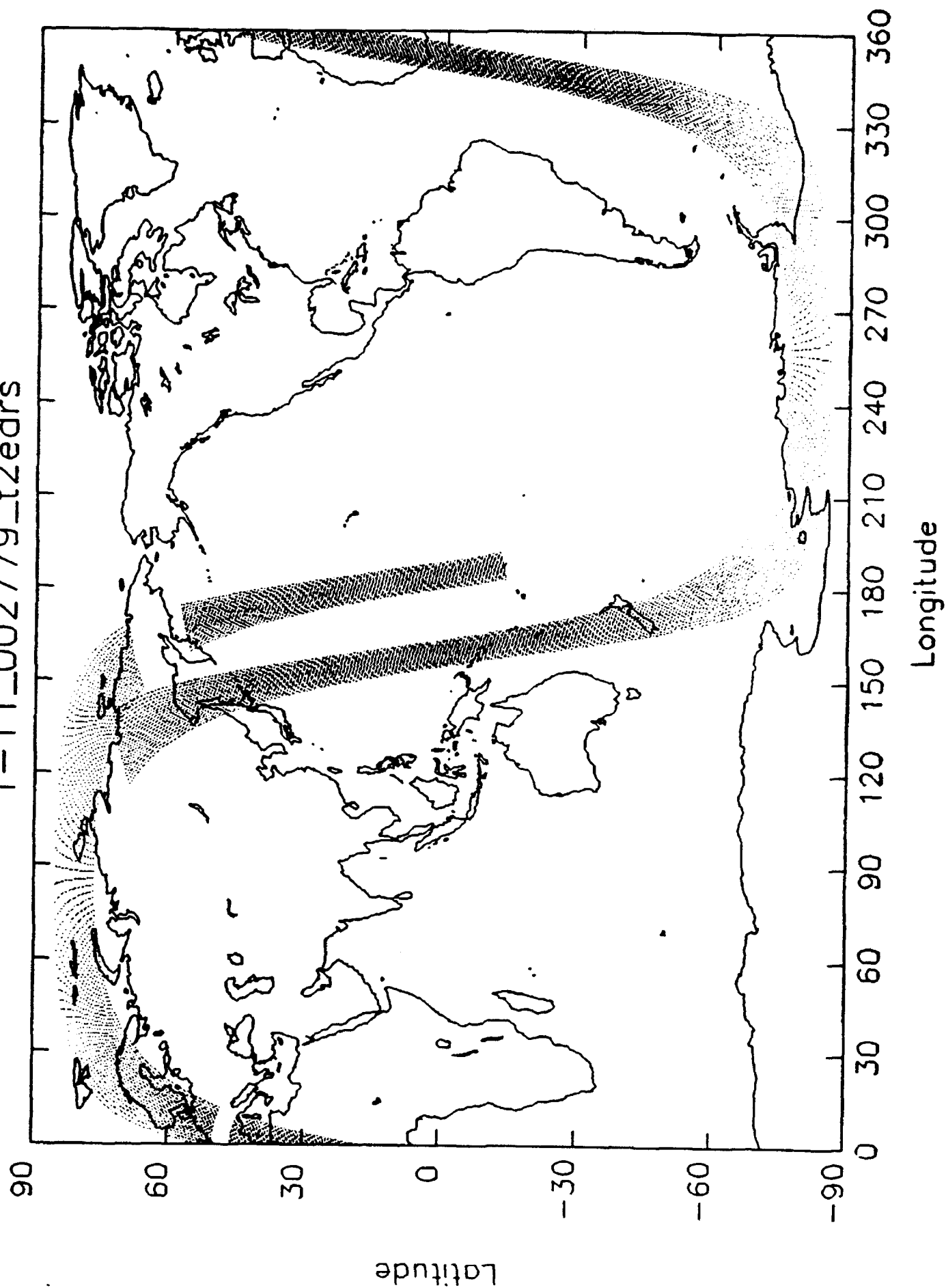




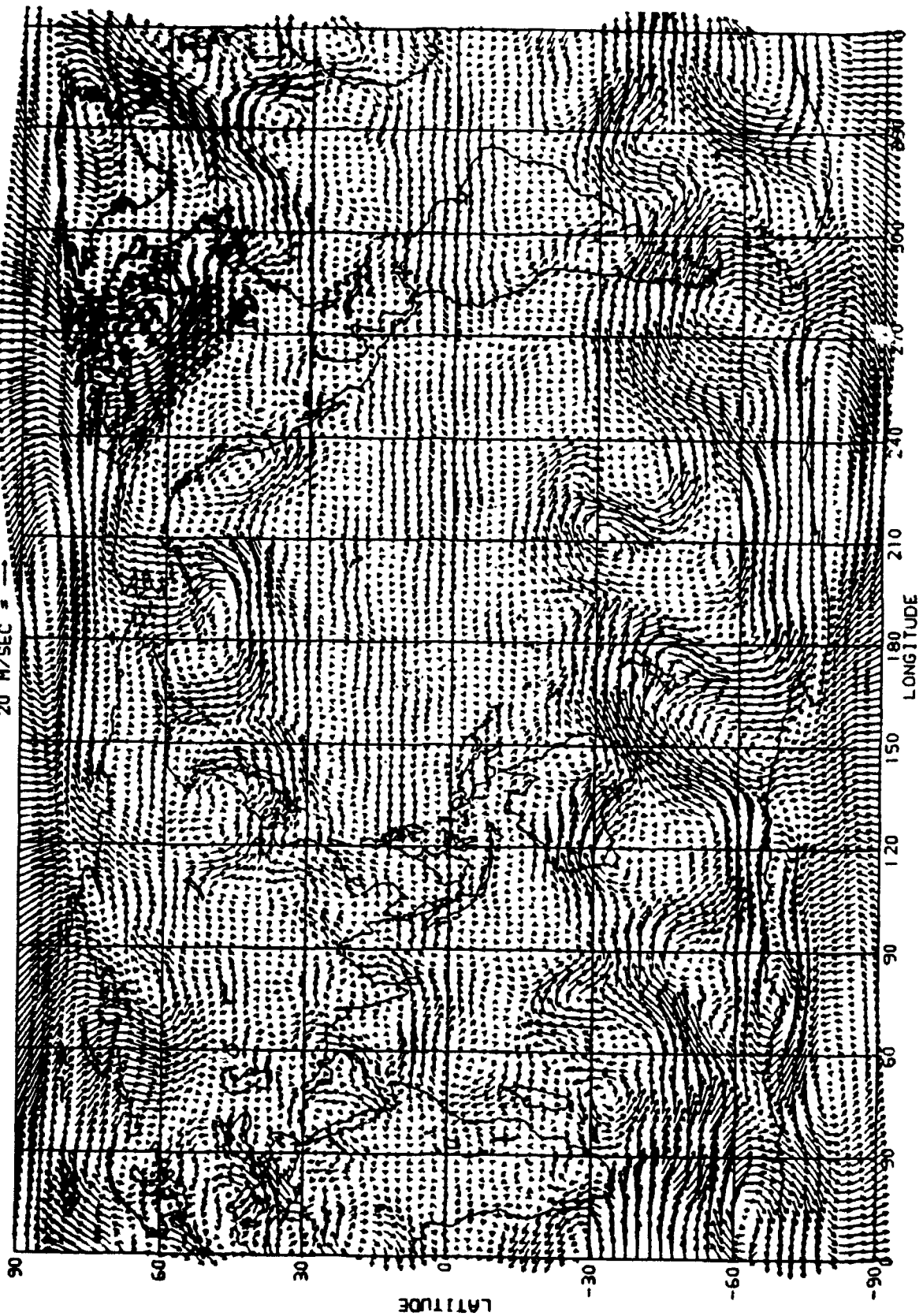
HIRAS  
Q 300 MB  
RHRASA  
214314



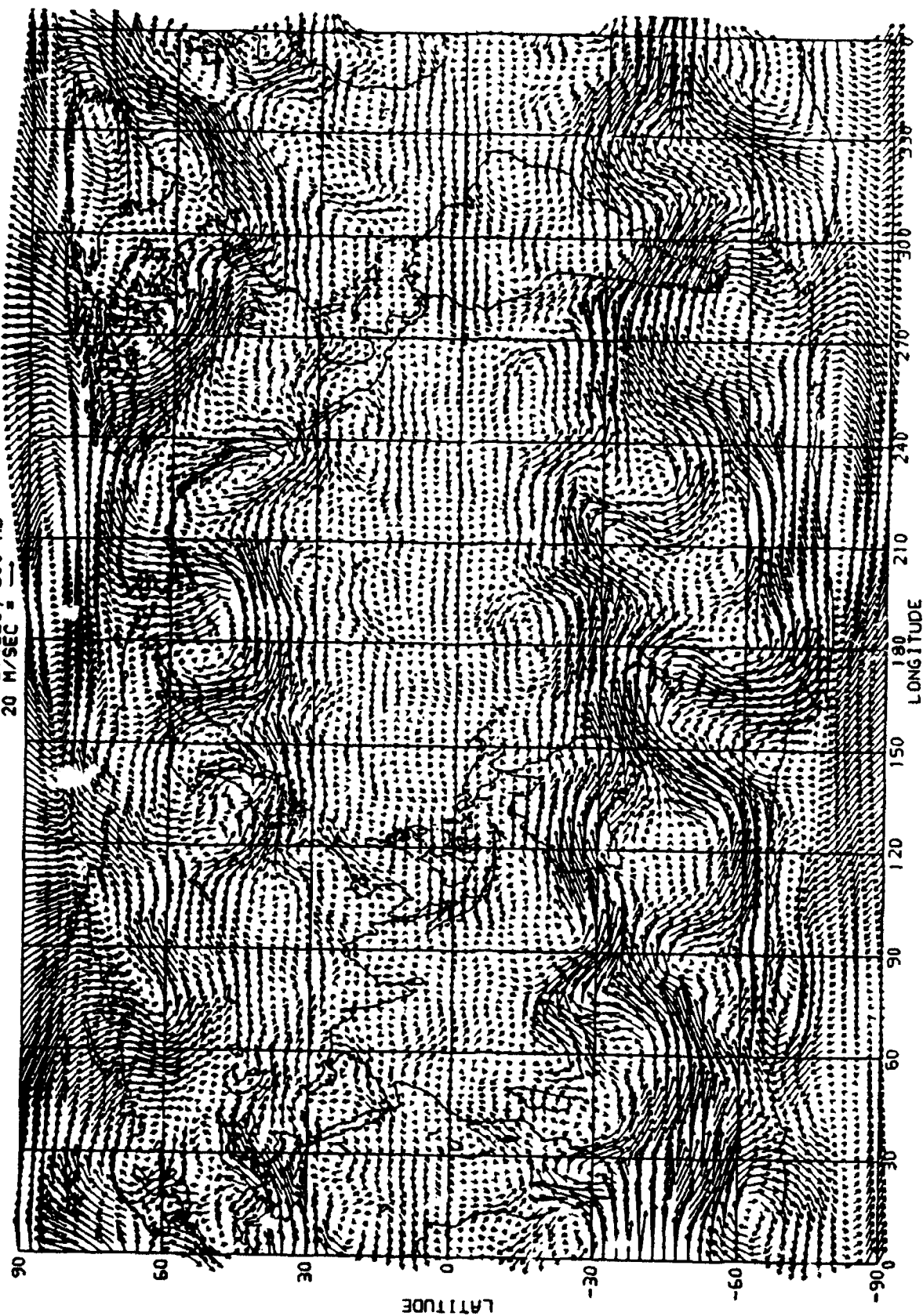
f-11\_002779\_t2edrs



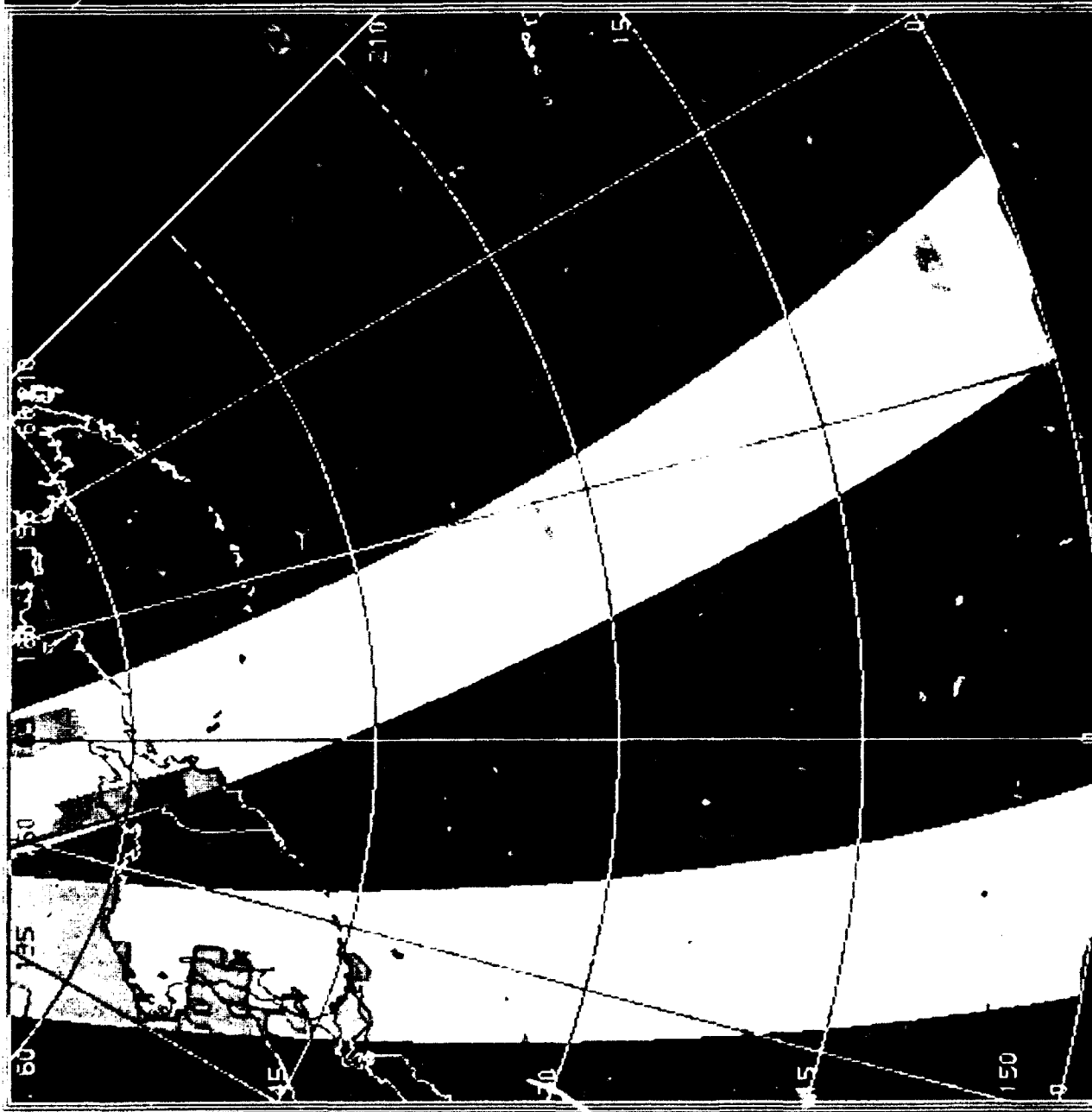
RHRASA 214326, 700 MB  
20 M/SEC —



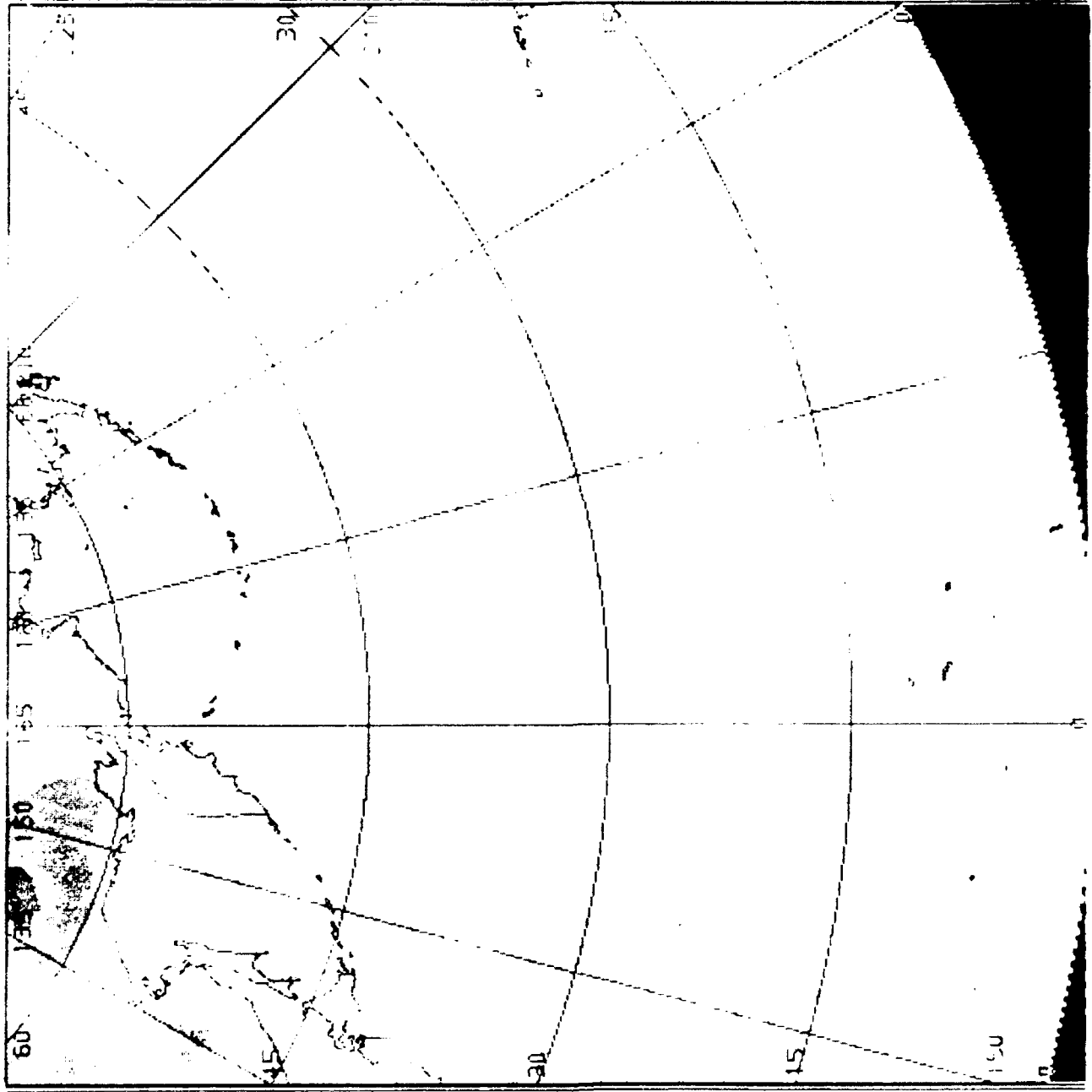
RHRASA 214326, 500 MB  
20 M/SEC



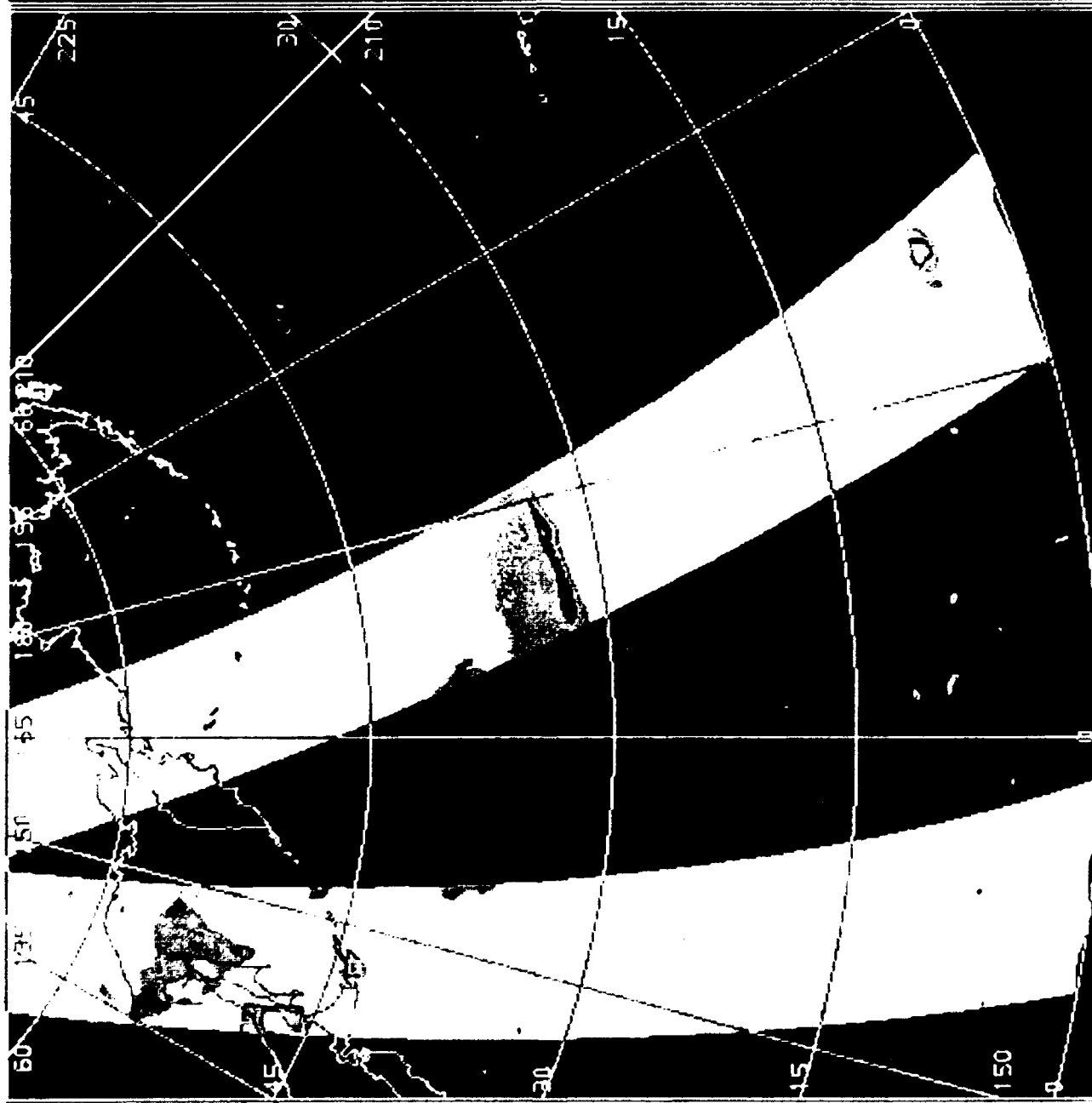
SSM/T2  
RH 1000 MB  
F-11 0002779



HIRAS  
RH 1000 MB  
RHRASA  
214326

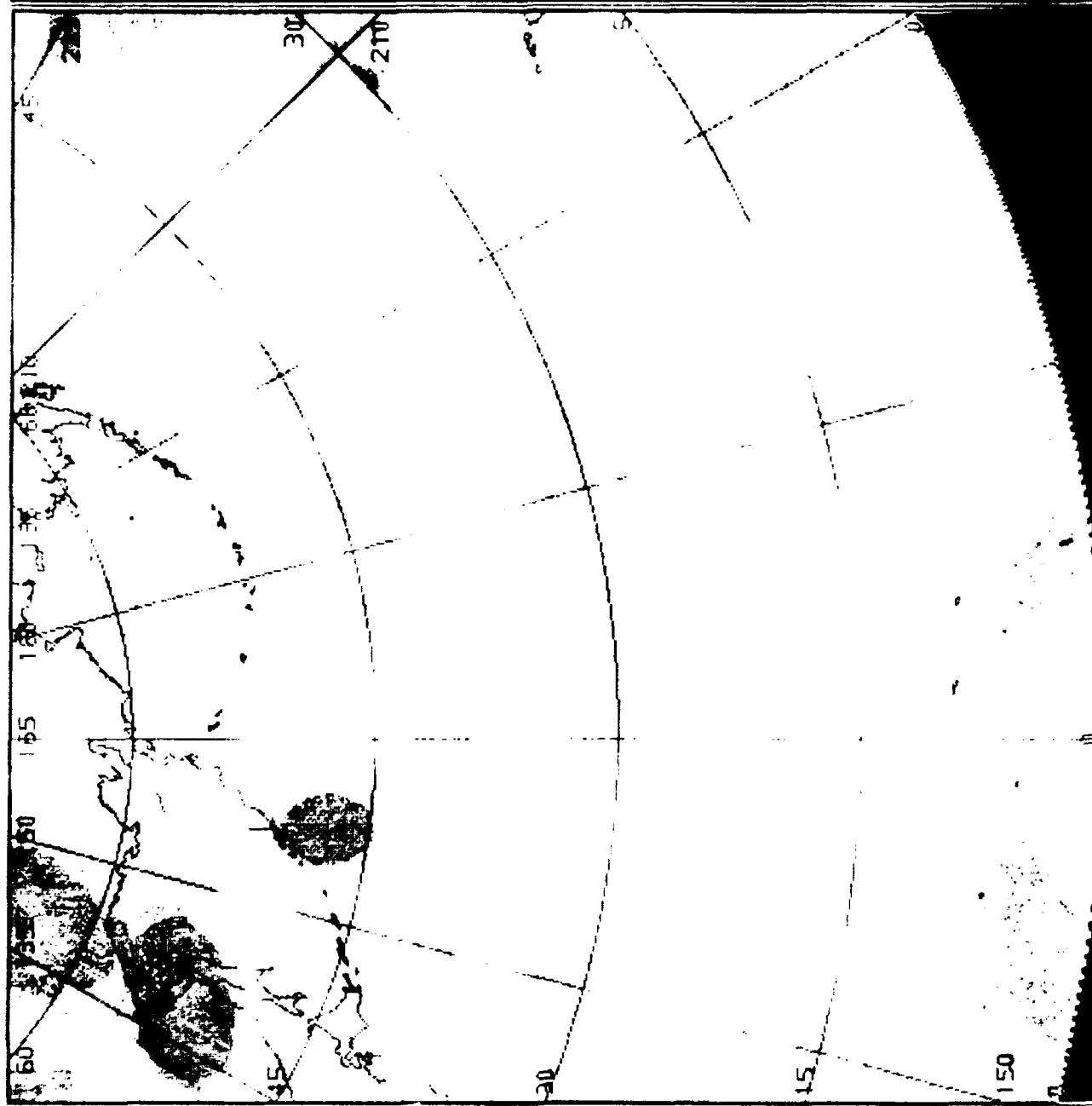


SSM/T2  
RH 850 MB  
F-11 002779

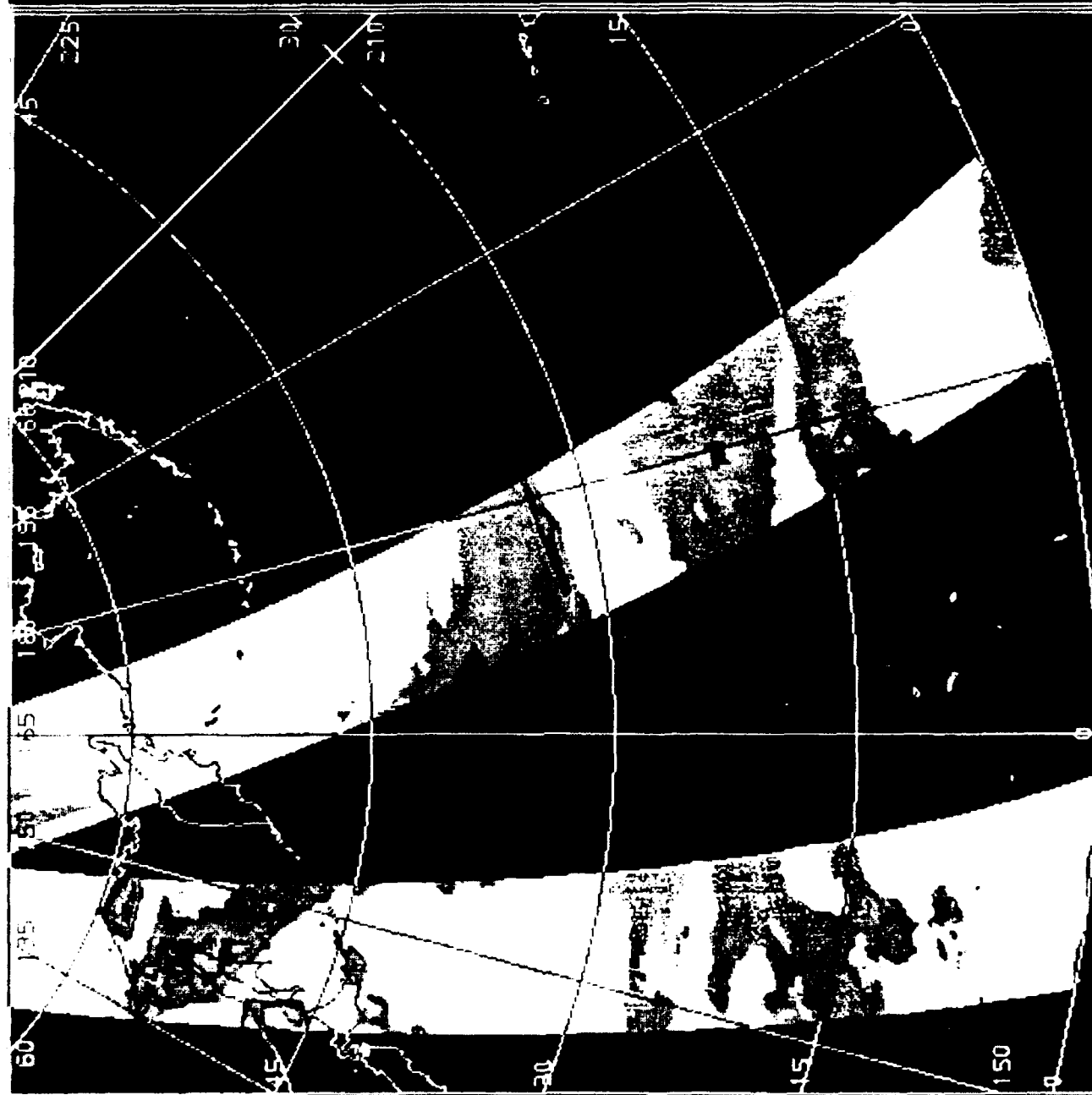




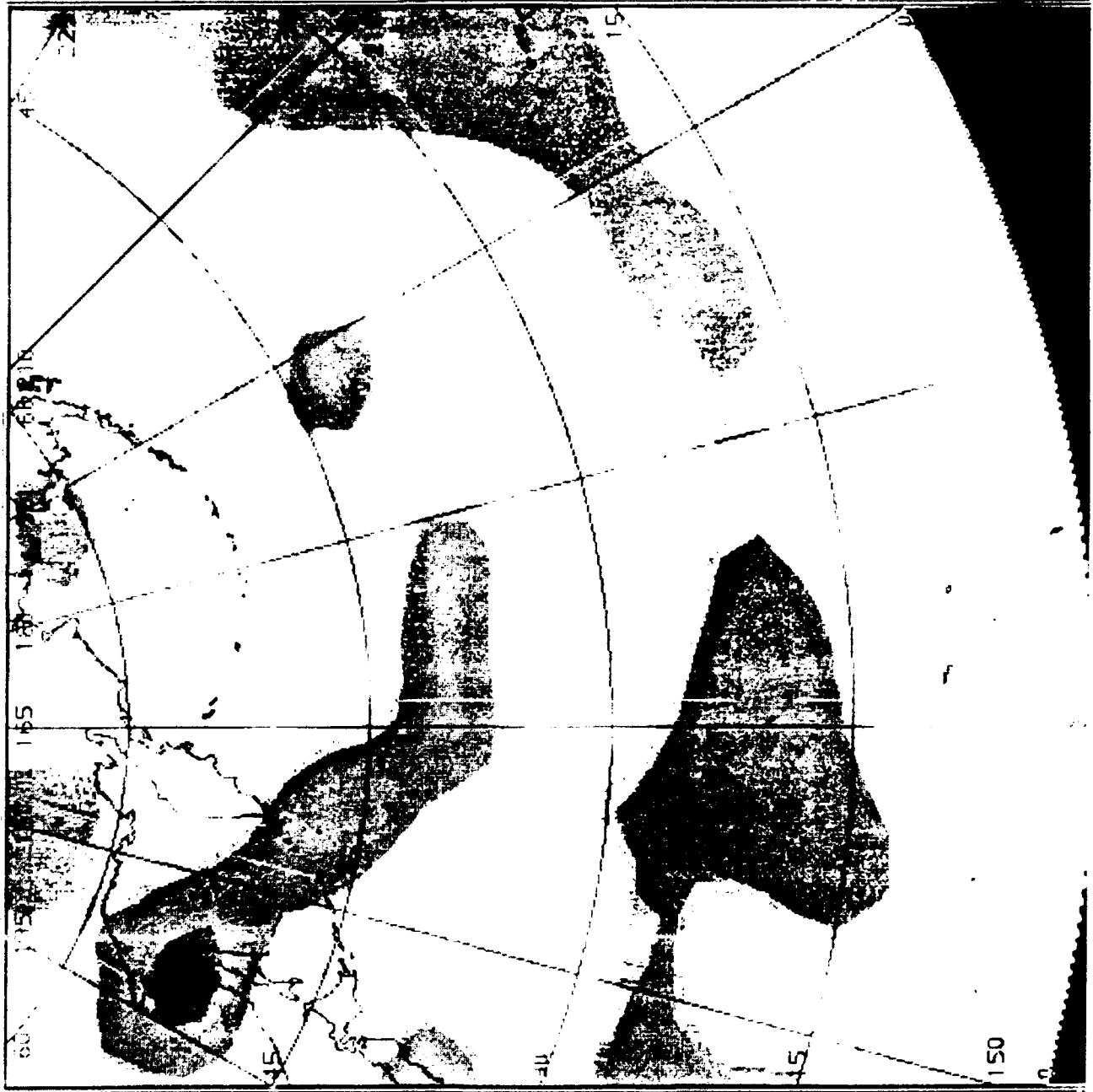
HIRAS  
RH 350 MB  
RHRASA  
214326



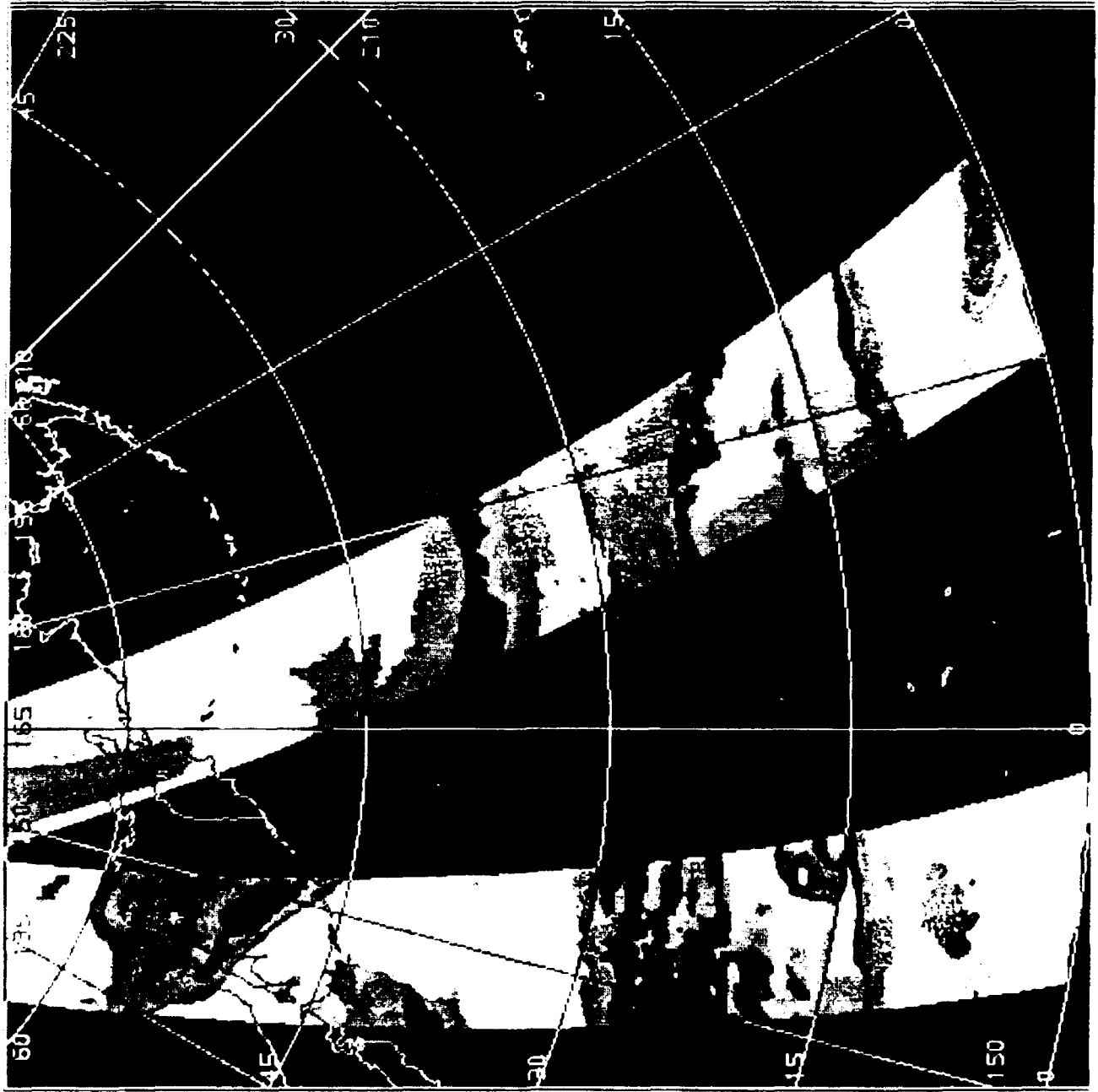
SSM/T2  
RH 700 MB  
F-11 002779



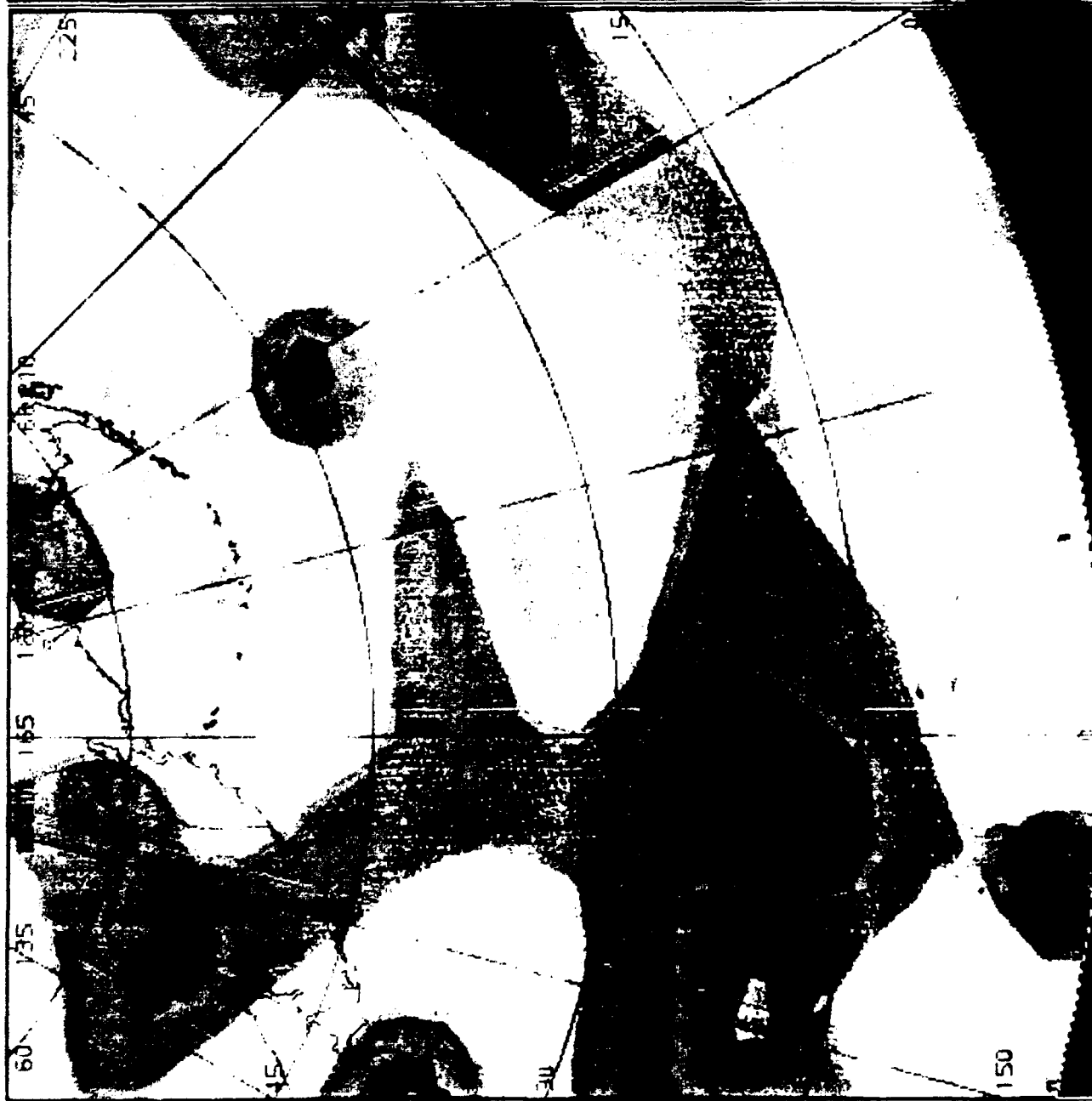
HIRAS  
RH 700 MB  
RHRASA  
214326



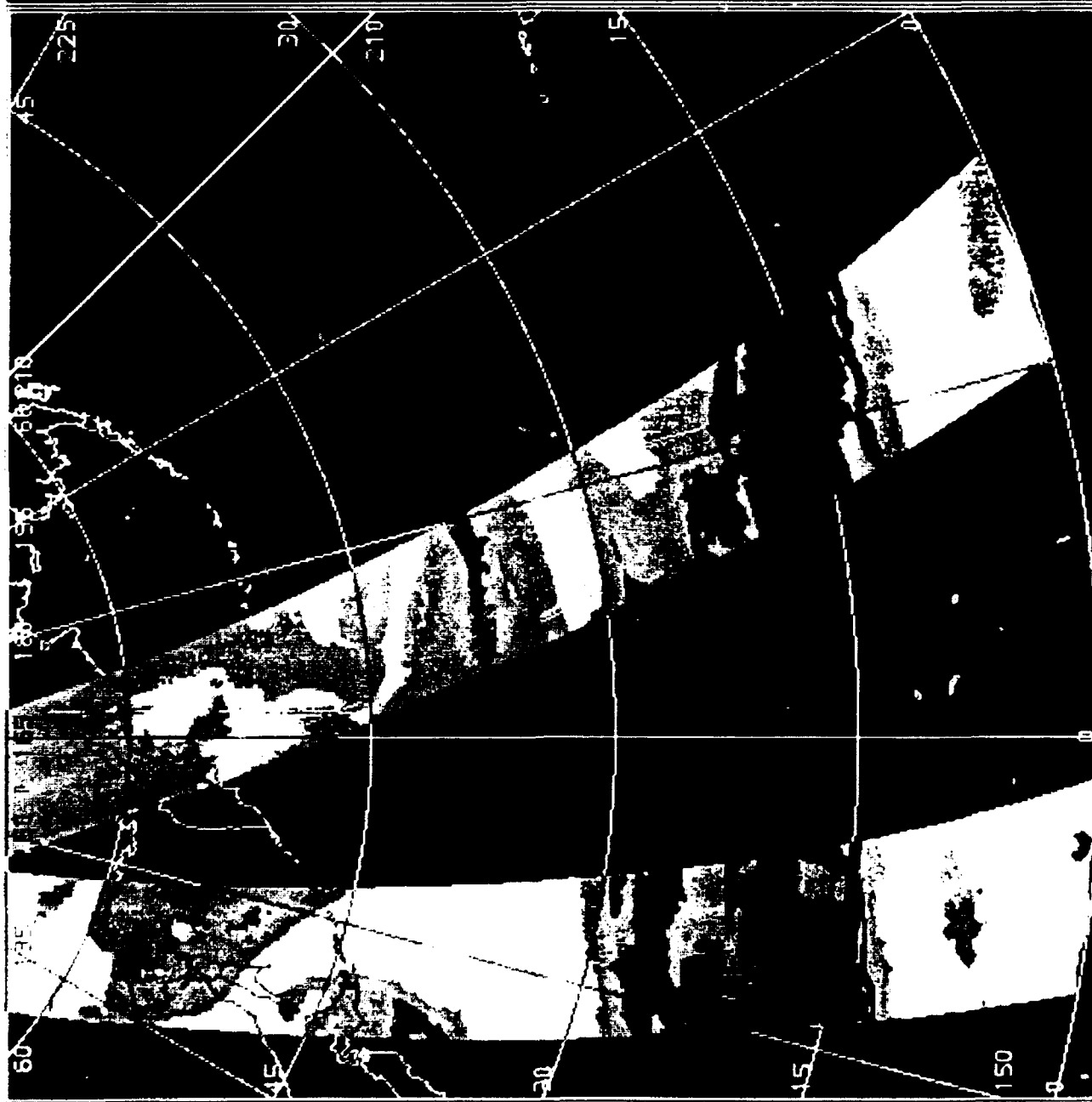
SSM/T2  
RH 500 MB  
F-11 002779



HIRAS  
RH 500 MB  
RHR434  
21432E



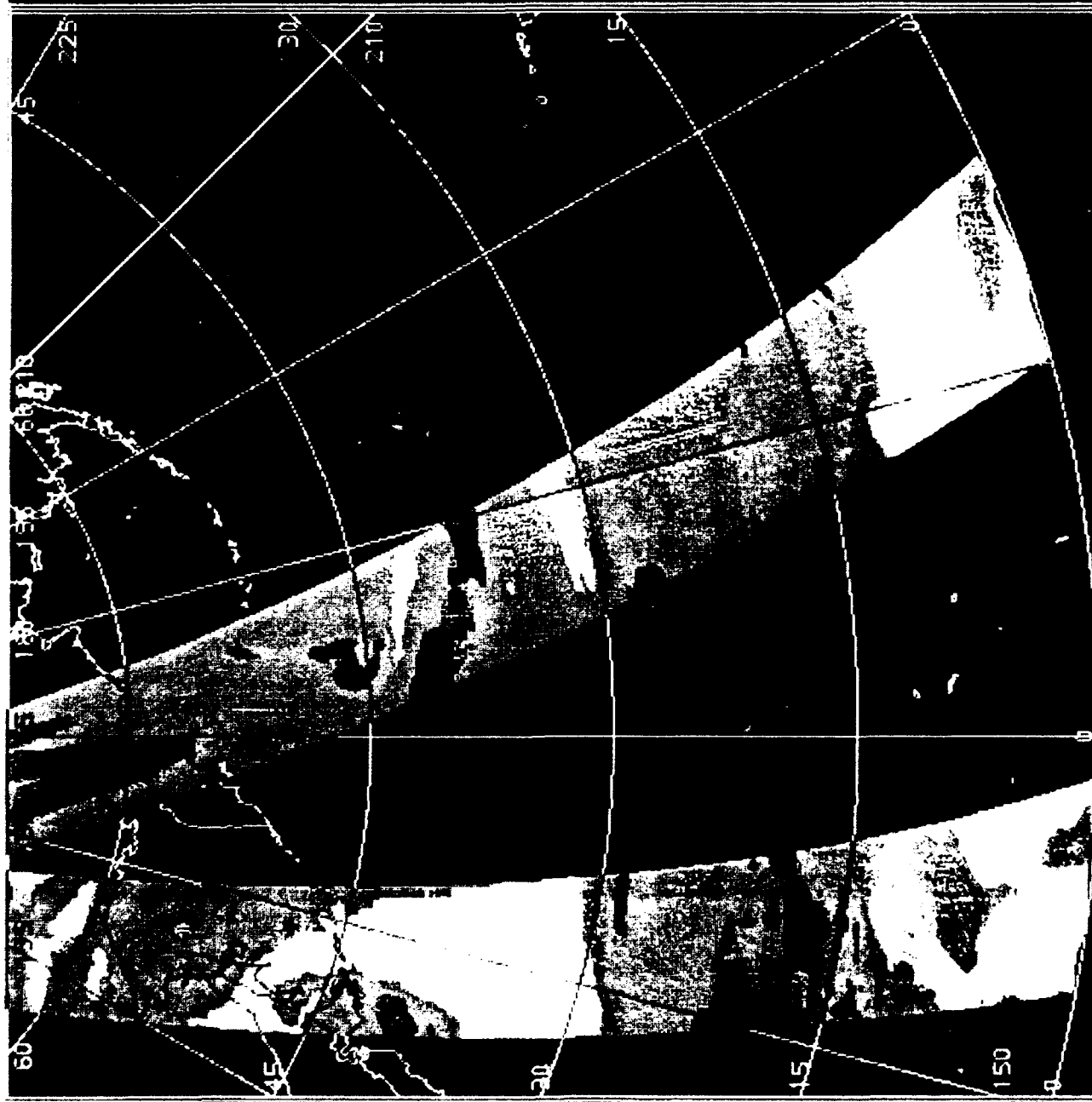
SSM/T2  
RH 400 MB  
F-11 002779



HIRAS  
RH 400 MB  
RHRASA  
214326



SSM/T2  
RH 300 MB  
F-11 002779

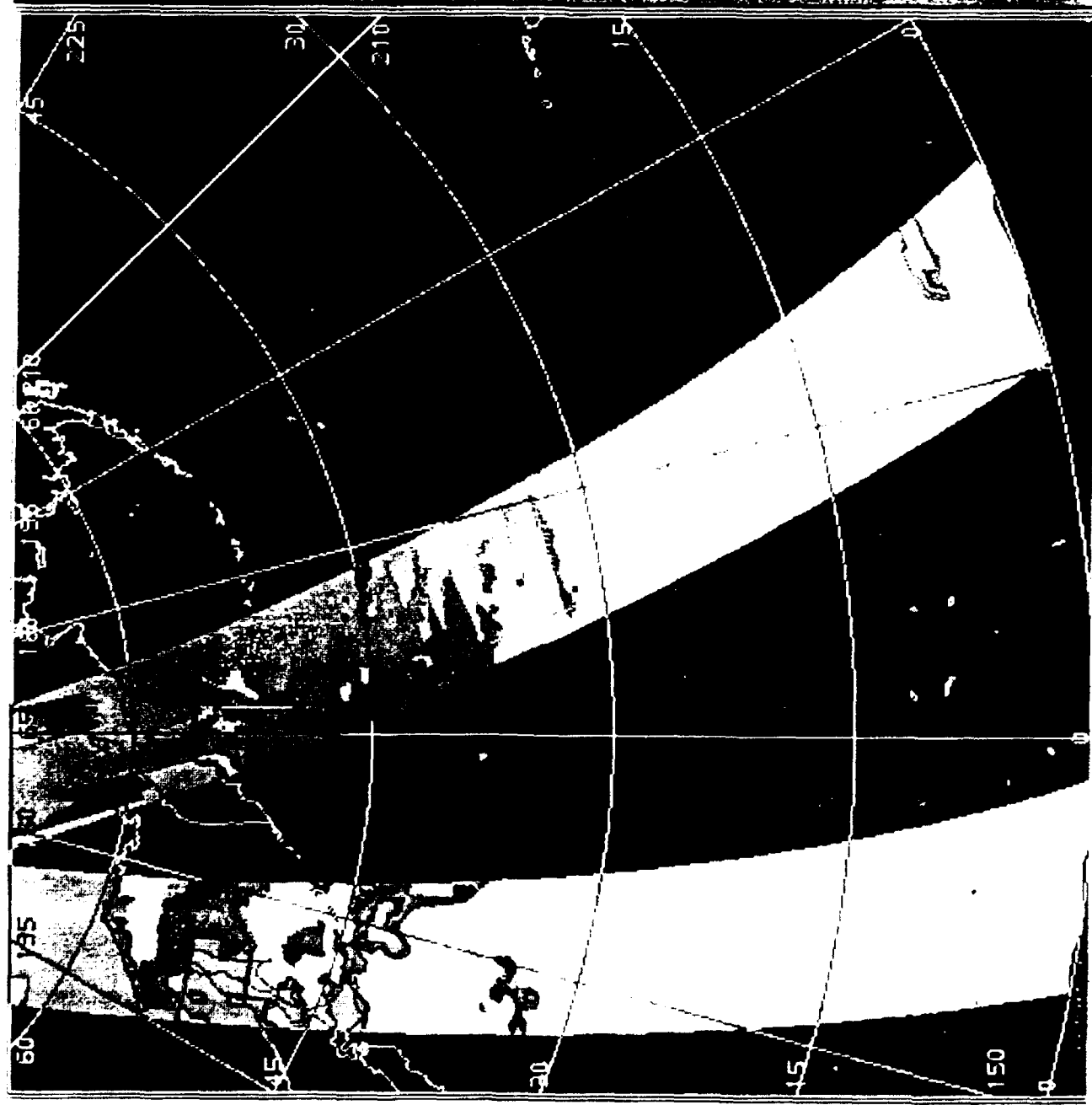




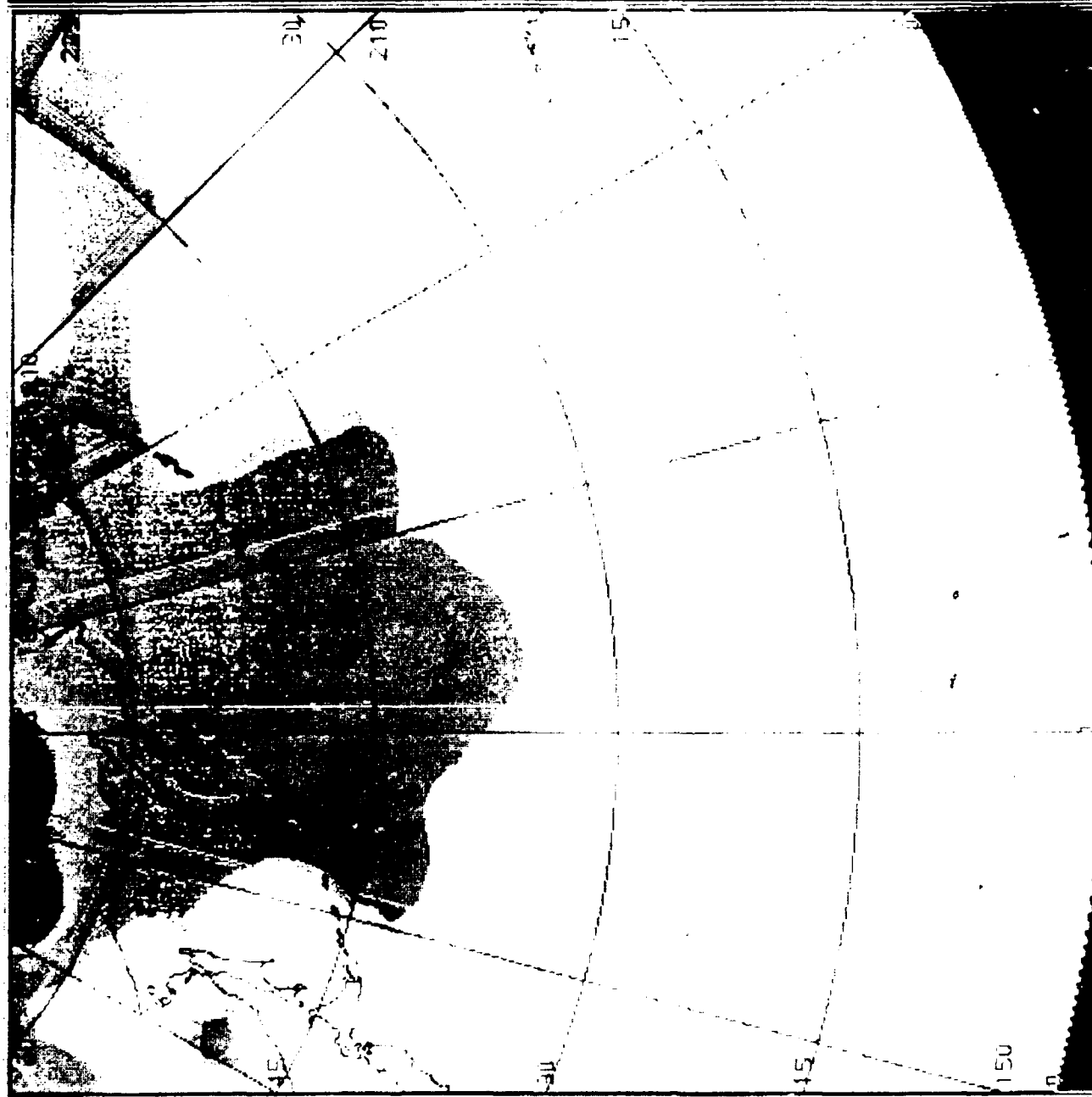
HIRAS  
RH 300 MB  
RHRASA  
214326



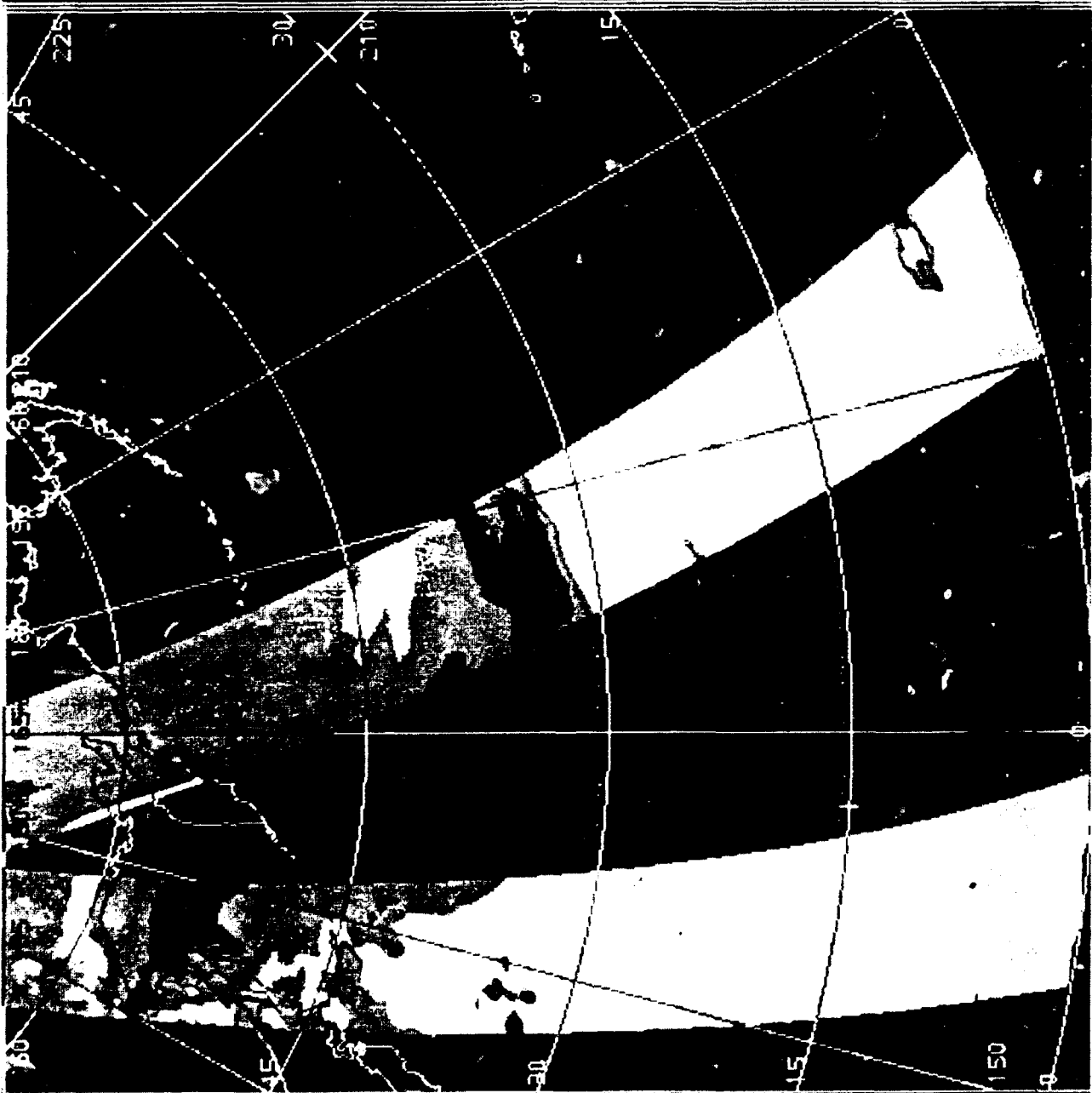
SSM/T2  
Q 1000 MB  
F-11 002779



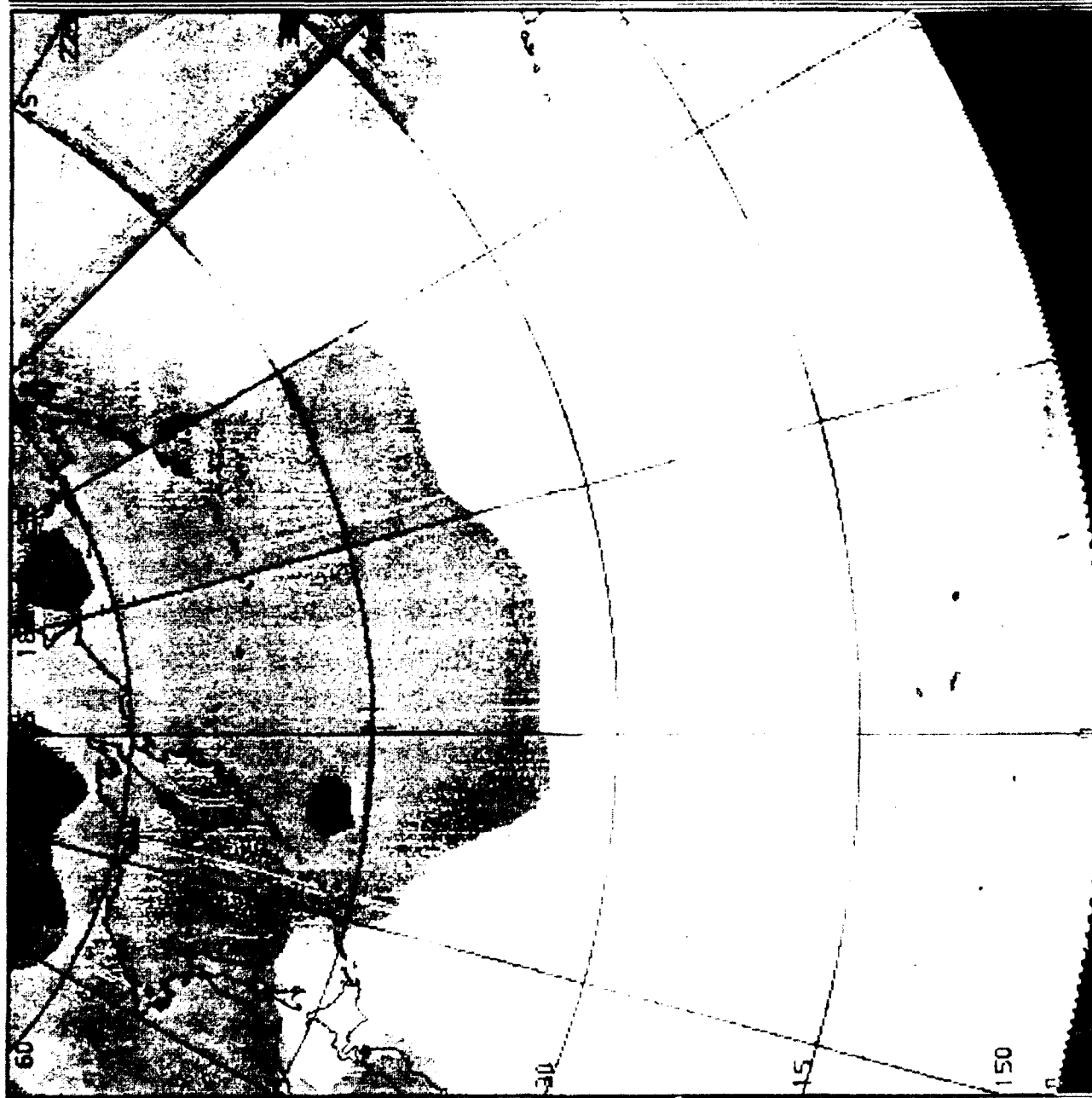
HIRAS  
O 1000 MB  
RHRASA  
214326



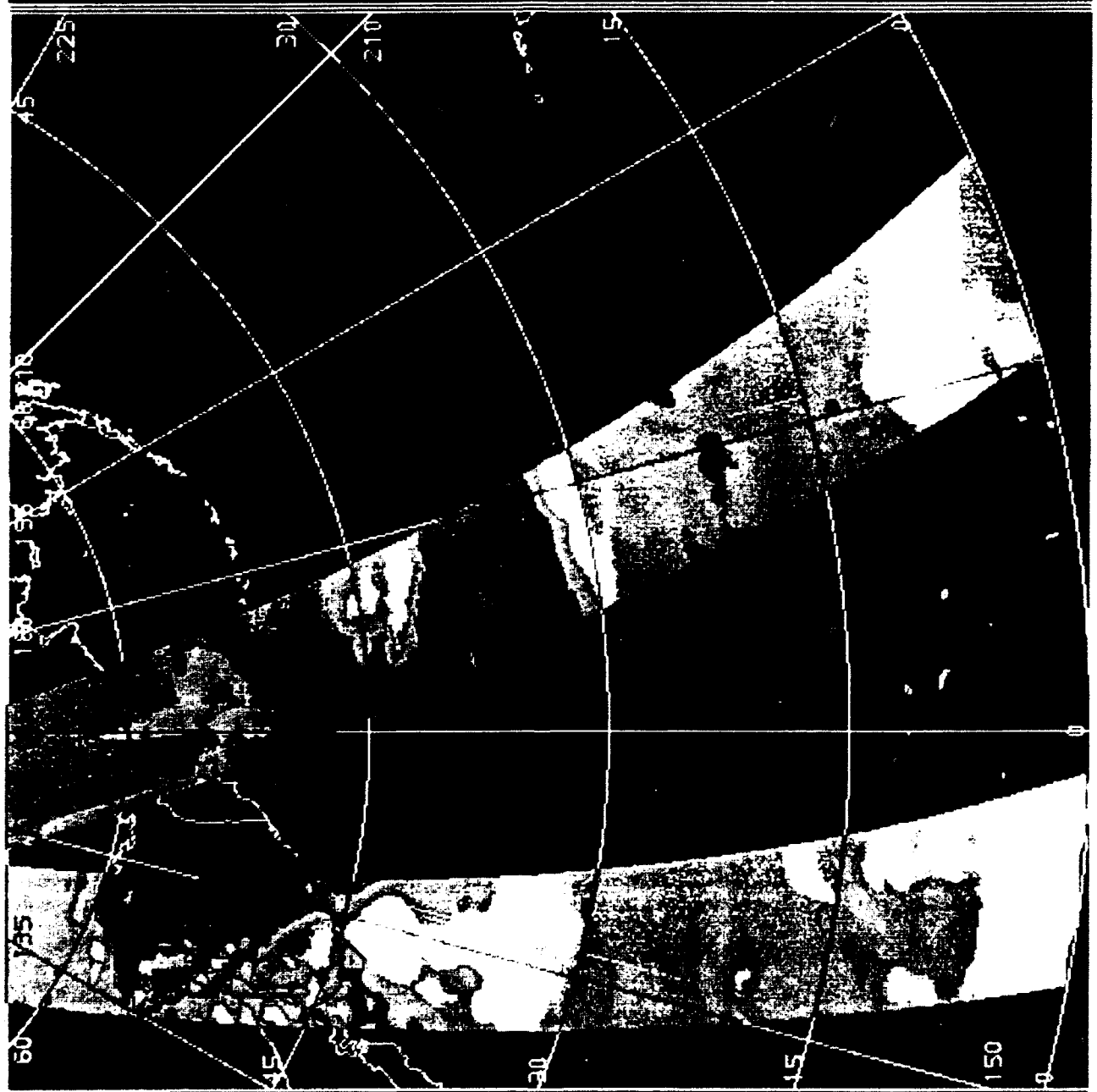
SSM/T2  
Q 850 MB  
F-11 002779



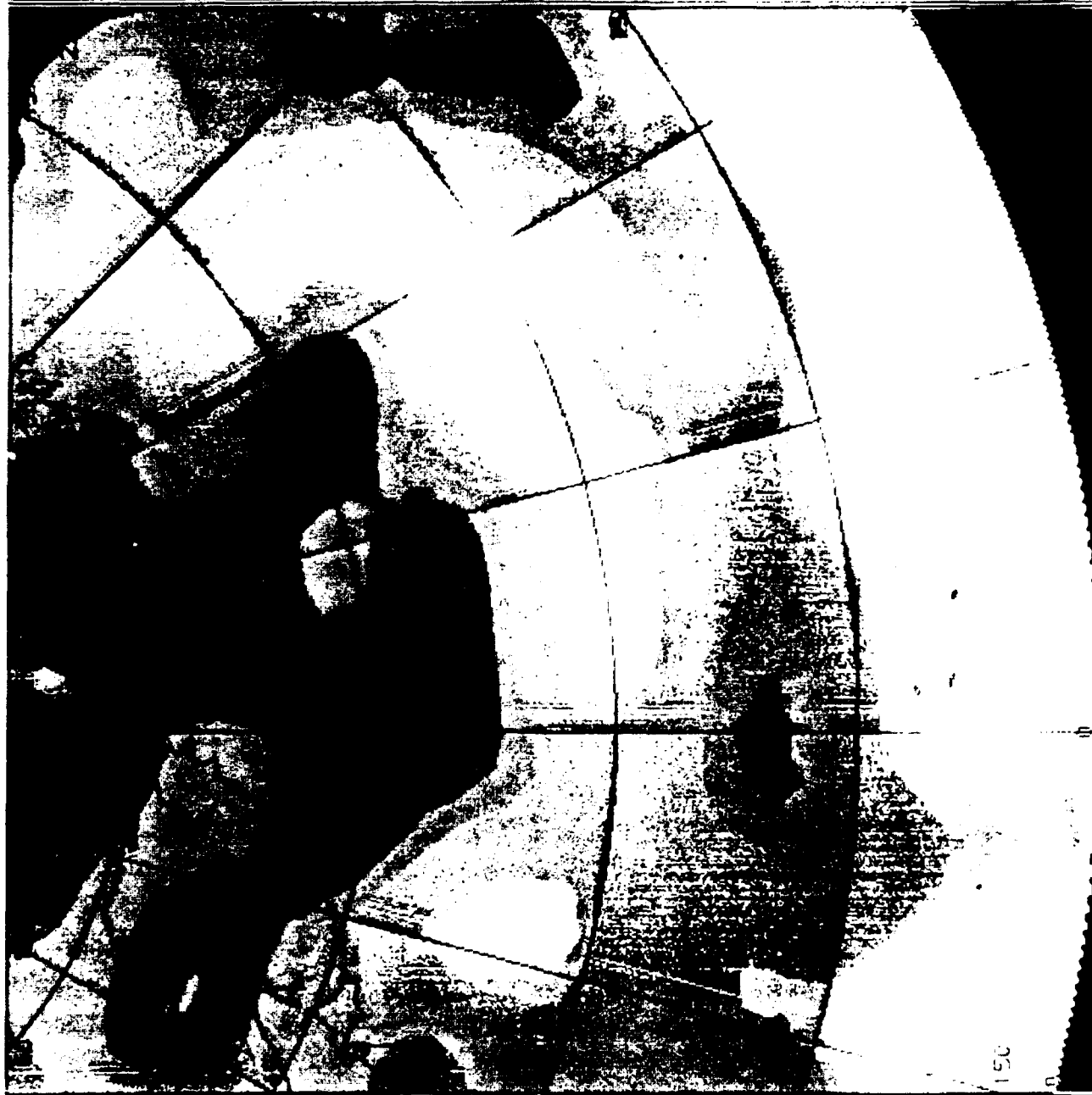
HIRAS  
O 850 MB  
RHRASA  
214326



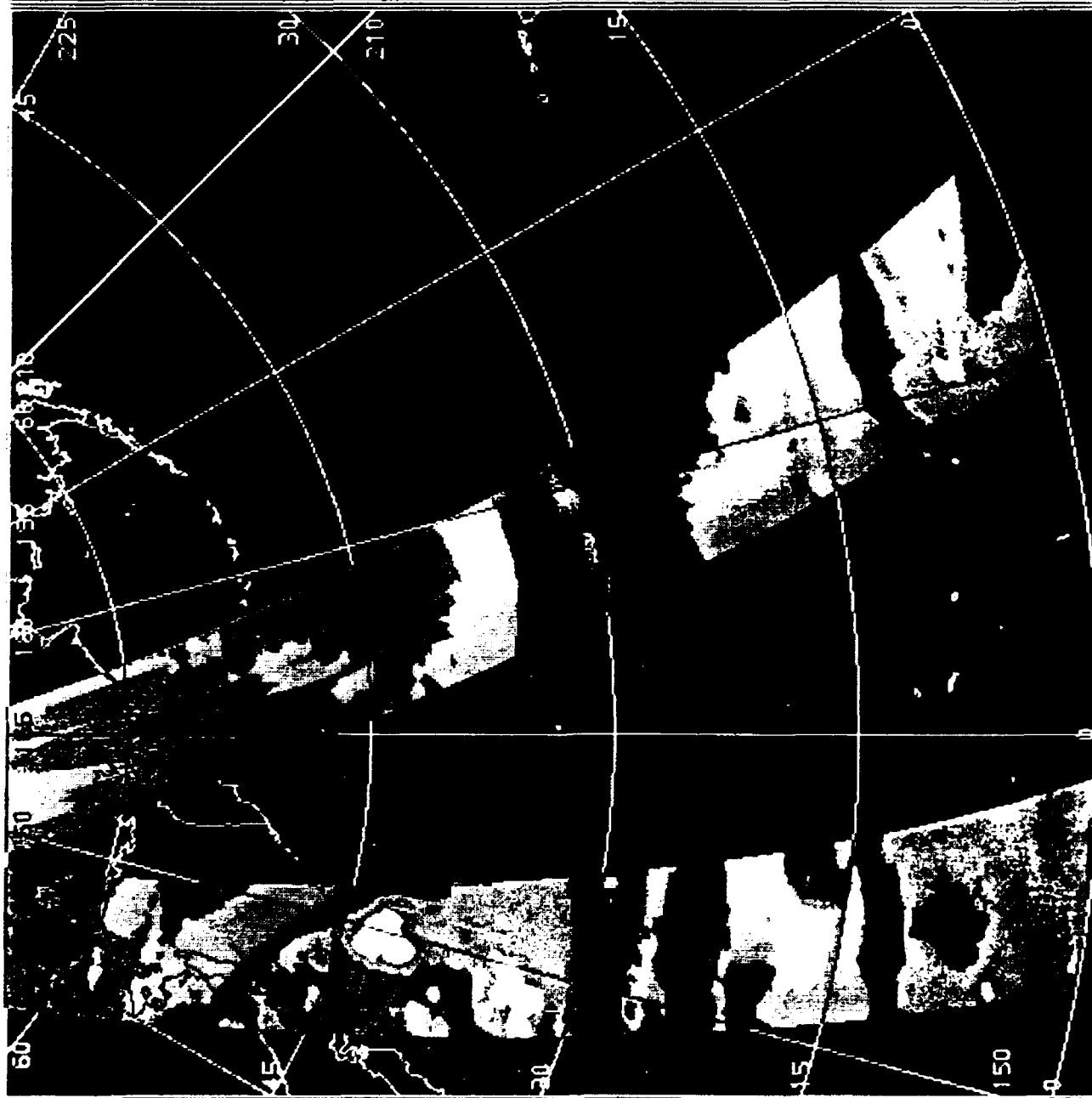
SSM/T2  
Q 700 MB  
F-11 002779



HIRAS  
C 700 MB  
RHRASA  
214328



SSM/T2  
Q 500 MB  
F-11 002779

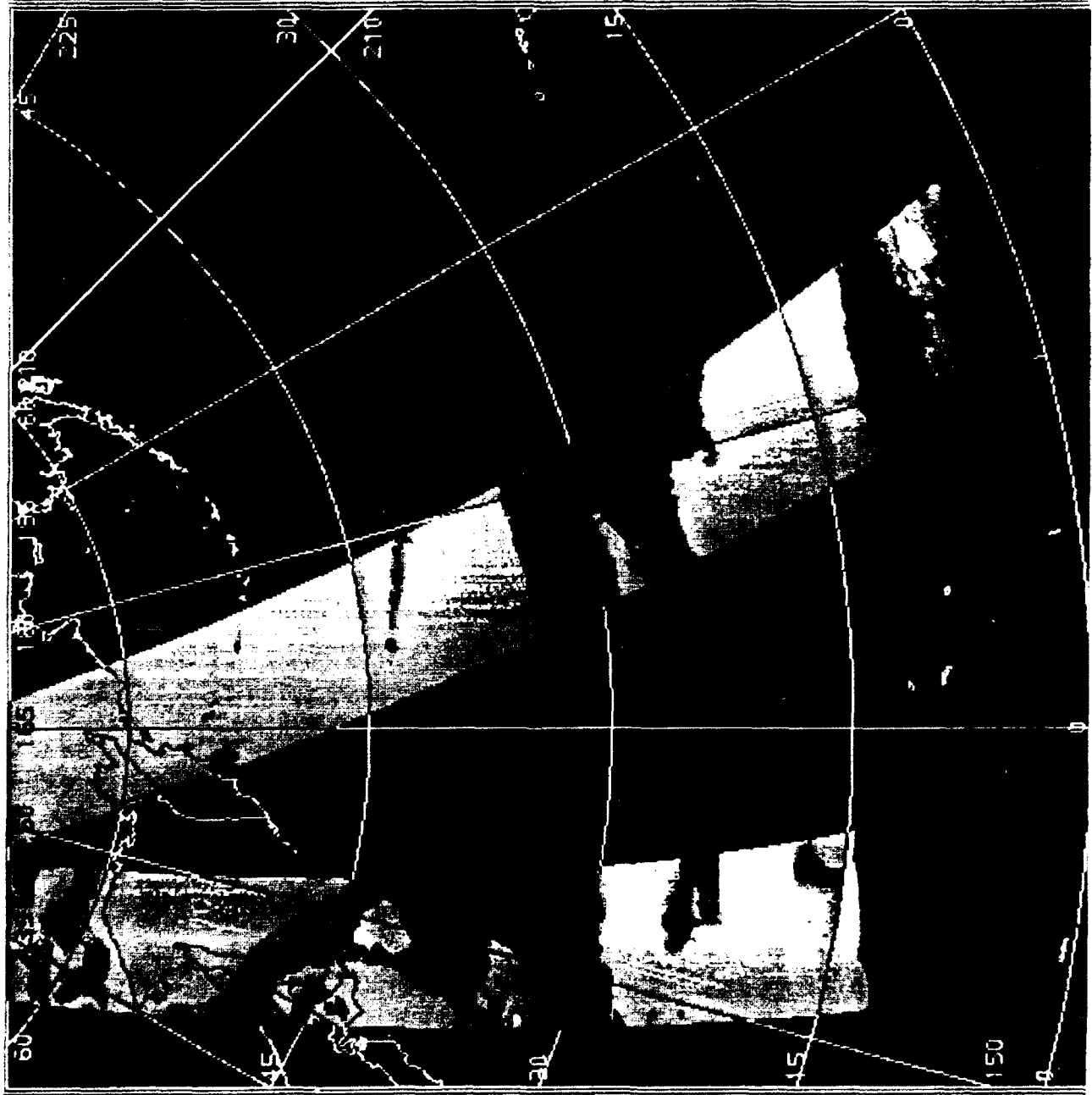




HIRAE  
0 500 MB  
RHAE  
2.4328



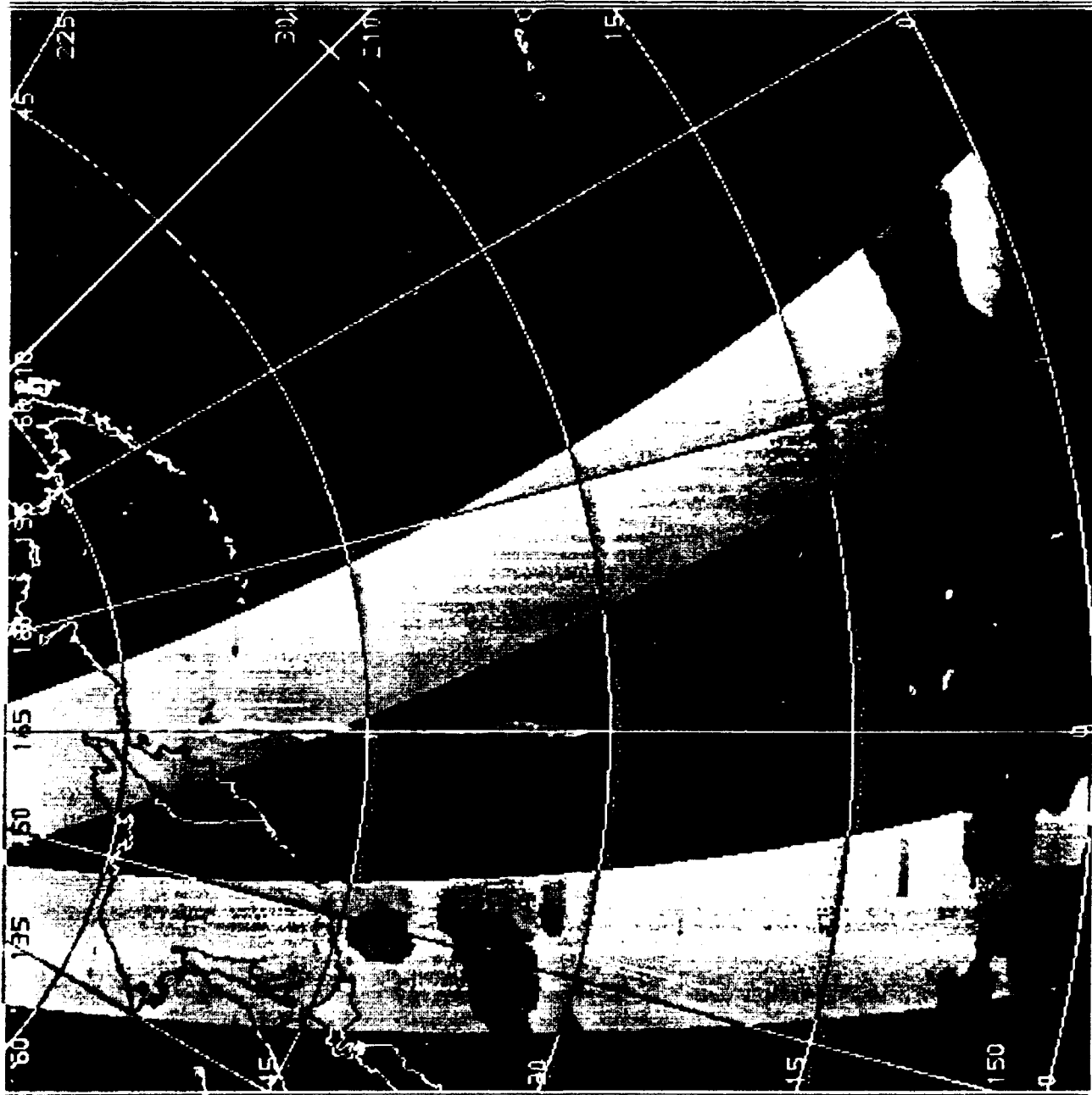
SSM/T2  
O 400 MB  
F-11 002779



HIRAS  
Q 400 MB  
PHRASA  
214326



SSM/T2  
O 300 MB  
F-11 002779



HIRAS  
O 300 MB  
RHR434  
214328

